PROGRESS TOWARD THE ENANTIOSELECTIVE TOTAL SYNTHESIS OF INELEGANOLIDE AND THE POLYCYCLIC NORCEMBRANOID DITERPENES AND CONSTRUCTION OF THE INELEGANOLOIDS

Thesis by

Robert Allen Craig II

In Partial Fulfillment of the Requirements for the Degree of

Doctor of Philosophy

California Institute of Technology

Pasadena, California

2015

(Defended May 11, 2015)

PROGRESS TOWARD THE ENANTIOSELECTIVE TOTAL SYNTHESIS OF INELEGANOLIDE AND THE POLYCYCLIC NORCEMBRANOID DITERPENES AND CONSTRUCTION OF THE INELEGANOLOIDS

VOLUME I

Thesis by

Robert Allen Craig II

In Partial Fulfillment of the Requirements for the Degree of

Doctor of Philosophy

California Institute of Technology

Pasadena, California

2015

(Defended May 11, 2015)

© 2015

Robert Allen Craig II

All Rights Reserved

To my parents,

for their unwavering support and encouragement

in my pursuit of education within and beyond the classroom and laboratory

Acknowledgements

I truly do not know how to begin. At this point in my life, at the culmination of 22 contiguous years of formal education, I find myself reflecting not only on my time in graduate school at Caltech, but also on the people who have helped mold and form the person I am today. Although I will always be a student, striving to learn and understand the world around me both within and beyond the laboratory, the conclusion of my doctoral studies presents a unique opportunity to acknowledge those without whom I could not have come so far.

Let me begin by acknowledging my advisor, mentor, and friend Professor Brian M. Stoltz. Throughout my doctoral studies, Brian has offered a tremendous amount of guidance. He has been the most instrumental teacher and mentor: helping to expand my ability to think critically about chemistry, develop experimental procedures to test hypotheses, and rationalize empirical data. His curiosity is endless, the scope of his interests is boundless, and his enthusiasm for science is truly infectious. He has always been respectful of circumstances beyond the walls of the laboratory and the things beyond our control. It is impossible to thank him enough to his support, mentorship, generosity, and kindness over the last 5 years.

Each of the remaining members of the thesis committee has had a profound impact on the development of my scientific interests. Professor Peter Dervan has been an impeccably organized thesis committee chairman. Each of our conversations about my published work, my ongoing research, and my research proposals has left me thinking about new avenues of investigation, new experiments to execute, and new problems to solve.

Professor Sarah Reisman has been a tremendous addition to my thesis committee. Her approach to organic chemistry has helped shaped the direction of my research countless times, whether through informal conversations or during questioning after formal presentations. I will always admire how thoroughly she knows our field and will forever be grateful for how thoughtful and invested she has been in my total synthetic efforts and for the motivation that her deep interest helped provide on the worst days. I could not be more thankful to have her as part of my committee.

The final member of my committee, Professor Bob Grubbs, and I have developed an excellent personal and professional relationship. I have a tremendous amount of respect for Bob not only for his past accomplishments, but also for the laboratory he continues to run and the excellent organometallic chemists that he graduates. His perspective on my proposal ideas and the realistic interdisciplinary application of those ideas, along with many conversations about the crossover between academic research and industrial application, have helped shaped my thinking about developing solutions to problems that can make a tangible impact on society. Beyond the hallowed halls of Crellin, Bob and I have shared a number of adventures into the mountains and on the forks of the San Gabriel river, chasing brown trout and the serenity of fly fishing. I have cherished these trips.

During my graduate studies, I was also highly involved in the administration of the Honor Code as it relates to graduate students, co-chairing the Graduate Honor Council (GHC) for 4 years. Having completed my B.S. at Davidson College, a community that relies heavily on a student-run honor code system, I knew I wanted to be involved in the honor system at Caltech before I arrived. Dr. Maggie Osburn and I were co-chairs of the Honor Council for my first two years on the job, with Matt Smarte joining for the next two years before I stepped down to complete my dissertation. I never imagined how much I would learn when I took the post. Together with the graduate Dean, Professor Joe Shepard, and the associate Dean, Felicia Hunt, I learned the ins and outs of academic administration and how to navigate the politics within an academic environment. I learned about the legal protections and legal liabilities that are associated with an Honor Code-based community. My time as co-chair also presented me with my first public speaking opportunity in front of a large crowd in a giant lecture hall. Through trial and error, my position helped me understand how to design a talk to connect with each member of a broad audience with variable academic and circumstantial backgrounds. The interpersonal interactions that I gained from interviewing the accused and character witnesses, speaking with irate professors, and presenting redesigned GHC bylaws to the provost, have taught me invaluable lessons about how to present arguments and how to adapt to the attitudes and assumptions of others during a heated conversation. My appreciation for the GHC, Joe, Felicia, Maggie, and Matt cannot be fully described, but

suffice it to say that I will always count my time with each of them among the most valuable of my graduate school career.

Another truly unexpected pleasure has been mentoring an undergraduate student in the laboratory. I expected mentoring a freshman undergraduate student would largely feel like a chore, having to teach them how to perform laboratory research while still maintaining a productive laboratory schedule of my own. The first time I met Benzi Estipona, however, I knew it would not be simply another burden on a hectic schedule. From our first meeting with Brian, Benzi was inquisitive, interested, and passionate, although a little reserved. Over the past year, Benzi has been an excellent student and really started to come out of his shell. He always comes to lab ready to work, excited to learn, and never afraid to ask questions. He has become a star on the lab softball team, although he may not always show up prepared for that! Benzi's future is tremendously bright. I am excited to see where he goes after Caltech and how he will choose to use his talents to make a difference in the world.

When Benzi started last year, it reminded me of when I first started at Caltech, having never previously worked in an organic chemistry laboratory. When I arrived, Dr. Russell Smith took me under his wing. For the next five months, we worked nonstop. He taught me everything I needed to know to progress toward becoming a competent chemist, from basic laboratory technique to comprehension of current literature. For a good portion of that time, we had to share his hood. I must say, you get to know someone pretty well when you share four feet of counter space all day, every day for months.

When Russell moved on to Johnson & Johnson only five months after I started in lab, my hoodmate, Dr. Jeff Holder, quickly became my mentor. The two of us worked side by side for almost my whole time at Caltech. He is an exceptional chemist. He continued what Russell had started, teaching me about laboratory technique and how to broadly think about chemistry, how to think about reactivity and mechanism, how to design new experiments, and how to rigorously test hypotheses. To Russell and Jeff, I cannot say thank you enough; without you two, I would not have made it nearly as far, nor would I have enjoy graduate school nearly as much.

I also need to thank all of the members of my class within the Stoltz lab for all of the learning we have done together and patience and kindness you have shown me over

the years: Yiyang Liu, Christopher Haley, Chung Whan Lee, and especially Doug Duquette and Corey Reeves. Doug, Corey, and I have shared a number of adventures over the years, including weekend surf trips, inventing a Frisbee golf course around Caltech's campus, and planning the most memorable Halloween party ever to be thrown. Corey and I made fast friends on our perspective visit to Caltech all those years ago and we have never looked back. Thank you both for your friendship and support over the last five years. Through thick and thin, you have both been tremendous friends.

I wish there were time to thank every Stoltz group member, past and present, for his or her helpful discussions, thoughtfulness, and contribution to my development as a chemist, but unfortunately, I cannot. I do want to mention a few of them by name, and there are surely some names that should be here that I will miss, but please forgive me. Professor Hosea Nelson has been another tremendous mentor. He has a brilliant scientific mind and will undoubtedly have a successful career in academia, starting his lab on July 1st, 2015, at UCLA. To Dr. Alex "Rookie" Goldberg, Dr. Hideki Shimizu, Dr. Chris Henry, Dr. Florian Vogt, Dr. Chris Gilmore, Dr. Pam Tadross, Dr. Marc Liniger, Dr. Hendrik "Jimmy" Klare, Dr. Christian Eidamshaus, Dr. Doug Behenna, and Dr. Jonny Gordon, thank you all for your mentorship and guidance. I am looking forward to seeing most of you this summer in Europe! To the younger students I have had the pleasure to work with, especially Beau Pritchett, Nick O'Connor, Katerina Korch, Seojung Han, Steve Loskot, and Austin Wright, thank you for all of the insightful conversations and I wish you all best throughout the rest of your time at Caltech.

Beyond the Stoltz lab, many thanks to the members past and present of the Reisman and Grubbs labs for supporting the excellent collaborative atmosphere that is characteristic of the chemistry department at Caltech. I especially want to acknowledge Dr. Jay Codelli, Dr. Roger Nani, Dr. Jake Cha, Nick Cowper, and Dr. Myles Herbert for their willingness to answer my questions and help me solve problems along the way. I must also thank Dr. Scott Virgil for his patience and seemingly endless wisdom and insight.

I also want to thank the staff at Caltech, without whom my dissertation would not have been possible. Personally, the most significant member of the staff during my time here has been Dr. Dave VanderVelde in the NMR laboratory. Natural product synthesis

has necessitated that I become an expert in NMR analysis of small quantities of often impure samples. Dave has taught me countless types of experiments, helped me analyzed complicated data sets for hours, and a huge amount of credit is due to him to the advancement of my total synthetic efforts.

I also want to thank Joe Drew and all of the chemistry stockroom staff, Rick Gerhart for helping repair glassware, Dr. Mike Takase and Larry Henling for X-ray crystal structure determination, Dr. Mona Shahgholi and Naseem for their help obtaining HRMS data, Tony, for all his help on the third floor of Schlinger, as well as Agnes Tong, Lynne Martinez, and Anne Penny for their help with administrative duties.

It is not only people at Caltech that have shaped my Ph.D., but also all of the mentors and teachers that have come before my graduates studies and encouraged me to constantly pursue education. Among this group, I must thank the most influential teachers of my early schooling, at Westtown School, from Pre-K through 12th grade, including T. Peg, my afterschool care teacher and godmother, T. Tim and T. Terry Jamieson, who ran many of the lower and middle school canoe and field trips, T. Greg, my 9th grade advisor and golf coach, T. Kwesi Koomson, my Calculus A/B and Calculus B/C teacher, T. Jonathan Ogle, my 10th grade English teacher, T. Eric Mayer, my 11th grade world religions teacher, and T. Chris Benbow, my 11th and 12th grade advisor (for those you unfamiliar with Quaker school, we addressed everyone as "Teacher"). Each of these classes or activities had a profound impact on my educational interests and my choices both personal and educational.

I also want to thank Davidson College professors of religion Dr. Greg Snyder and Dr. W. Trent Foley, whose classes entitled "The Gnostic Gospels" and "Religion and Racism" incorporated some of the most thought-provoking and enthralling discussions and lectures I have ever had the pleasure to attend. I also want to thank Dr. Gregory Webster and Dr. Cynthia Pommerening, my summer internship advisors at Abbott Laboratories, for their guidance and patience as I learned about pharmaceutical and analytical science in an industrial setting. I must also thank Dr. David Brown, my academic advisor at Davidson, for his guidance and encouragement, as well as Davidson Chemistry professors and Caltech alumni Dr. Felix Carroll and Dr. David Blauch. Without these three, I never would have dreamed of coming to Caltech for my doctoral

studies. Without their help, without coming out to California, without coming to Caltech, without trying to pad my CV for funding applications, I never would have met Ms. Jennifer Rohrs.

I am unsure I would have made it all the way through Caltech with all of my marbles if not for Jen. We met at a conference at USC run by the NIH on the physical science in oncology and the rest, they say, is history. A doctoral student in the biomedical engineering department at USC, having someone to talk with about the frustrations of lab work and having someone to forget the frustrations of lab work with has been invaluable. Her constant loving support, tolerance of the long hours, encouragement, sense of humor, and generosity cannot be put into words. To Jen, from the bottom of my heart, thank you and I love you.

Lastly, I would be remiss if I didn't acknowledge all of the friends, past and present, all over the world, and family who have helped me develop into the scientist and person I am today. Firstly, to my parents, Dr. Robert Allen Craig and Dr. Ross Ann Craig, thank you both for your encouragement and support. There have been days that without you both, I know I would not be where I am today. Nothing I can write here will ever comprehensively describe the gratefulness I have for everything you have both given to me. Thanks also go to my late grandfather, John H. Jenny, for everything he taught me in our time together and through his writings. His guidance and outlook on life has undoubtedly helped shape lens through which I see the world.

I must thank my long-time friends and second family, the Turner's, from back home in Chadds Ford, PA. Steve Turner and I went through 13 years of Westtown together and have been best friends for literally multiple decades (I guess we are getting old!). It was his friendship that brought me out of my quiet, reserved shell in middle school. Along with his parents, John and Janice, sister Laura and Brother-in-Law Will Igoe, they taught me not only the meaning of a good work ethic, but also how to take time away from work, how enjoy life, how to play, how to laugh at the little things and enjoy every day together. Their generosity and guidance has played a large part in molding me into the person I am today.

Additionally, many thanks to family friends past and present. To Dr. Howard Borin, my pediatrician and long-time family friend, thank you for all of your guidance and

support. Also, to Tom and Donna Wells, Donna Colton, and Richard and Doreen Browning, thank you for all you have shared with me. And to all those at Camp Miniwanca and the American Youth Foundation, thank you for playing such a significant role in my formative years and shaping my appreciation for leading a balanced life.

I must also thank all of my Davidson friends, including all of the members of the Davidson Chapter of Sigma Phi Epsilon as well as the members of the Davidson Crew Team. Among them, Erich and Caroline Kreutzer, David Suich, John Jertson, Max Simonsen, Will Branch, and the Shaw brothers, Walker and Max. The friendship of each of them through my time at Davidson and beyond has helped support me on the worst days and formed some of the happiest memories of my life on the best. To each and every one of them, thank you.

Finally, I want to acknowledge my friend and roommate, soon-to-be Dr. John "Sleevie" Steeves. Sleevie, a graduate student in Aerospace here at Caltech, has been instrumental in my success at Caltech. We have lived together for the last four years and have had many adventures. From Thanksgiving in Carmel with Erich, Caroline, and David, to San Diego, Coachella, Phoenix with a gaggle of Canadians, and St. Patrick's Day celebrations, we have enjoyed countless laughs. It has been a pleasure and a privilege to have Sleevie as my roommate. He is a brilliant engineer, scientist, and scholar. I wish him the best of luck at JPL and throughout the rest of his career. I cannot wait to see where he will be and what he will have done in the next twenty years.

Caltech has been a wonderful place to learn and for that, I will forever be grateful. Although my education will never cease, and my hunger to learn will never be satiated, it is time to move to the next phase of my career and my life. Lastly, I would like to leave you with two simple phrases by which you may live, survive, and proposer. One comes from one of the greatest and brightest men in this history of the United States, Benjamin Franklin, and another from a man of tremendous work ethic and integrity for whom my respect will never fade, Robert Briggs, the grandfather of my closest friend, Steve Turner. The truth contained within these words will never steer you wrong and they are words I have and will continue to live by for the rest of my life:

"If at first you don't succeed, try, try again." – Benjamin Franklin

"If you roll up your sleeves, you will never lose your shirt." – Robert Briggs

Abstract

Ineleganolide, horiolide, kavaranolide, sinulochmodin C, scabrolide A, scabrolide B, and yonarolide are related polycyclic furanobutenolide norcembranoid natural products that exhibit potent biological activity, and feature highly oxygenate carbocyclic scaffolds with complex stereochemical frameworks. Herein, we describe a unified synthetic approach toward ineleganolide and the related furanobutenolide norcembranoids. Assembly of the tetracyclic scaffold of ineleganolide is accomplished in a convergent manner from (*R*)-carvone and an enantioenriched *cis*-1,3-cyclopentenediol fragment, which is constructed by a key enantioselective allylic alkylation. From the combined product of the two major fragments, we employ a tandem intramolecular cyclopropanation/Cope rearrangement to furnish the cycloheptene carbocyclic core characteristic of ineleganolide.

Synthetic manipulations of this carbocyclic core are extensively investigated; several constitutional isomers of ineleganolide are synthesized through these studies. Many approaches are explored to assist in the completion of the synthesis. Computational studies inform our understanding of the conformational bias of late-stage intermediates. The retroaldol-aldol carbocyclic isomerization from the core of ineleganolide to the core of sinulochmodin C is also investigated.

Additionally, our work on the (3 + 2) cycloadditions of heterocumulenes with donor–acceptor cyclopropanes and with *N*–H- and *N*–sulfonyl aziridines is disclosed. The exploration of substrate scope, reaction mechanism, and the enantiospecific formation of heterocyclic products in investigated.

TABLE OF CONTENTS

Acknowledgements v
Abstract xii
Table of Contents xiii
List of Figures xxii
List of Schemes xxxviii
List of Tables xlvii
List of Abbreviations liii

CHAPTER 1 ***1***
Furanobutenolide Cembranoid and Norcembranoid Natural Products: Biosynthetic Connections and Synthetic Efforts

1.1 Introduction 1
1.2 Statement of Purpose 3
1.3 Polycyclic Furanobutenolide Cembranoids and Norcembranoids 3
1.4 Brief Summary of Biosynthetic Connections 5
1.4.1 Biosynthesis of Polycyclic Furanobutenolide Cembranoids 6
1.4.2 Biosynthesis of Polycyclic Furanobutenolide Norcembranoids 10
1.5 Synthetic Studies Toward Polycyclic Cembranoids and Norcembranoids 13
1.5.1 Synthetic Efforts Toward Bielschowskysin (BSK, **6**) 14
1.5.1.1 Photo [2 + 2] Approaches to Bielschowskysin 14
1.5.1.2 Non-Photochemical Approaches to Bielschowskysin 25
1.5.2 Synthetic Efforts Toward Verrillin (**13**) 28
1.5.3 Synthetic Efforts Toward Havellockate (**14**) 29
1.5.4 Synthetic Efforts Toward Intricarene (**7**) 33
1.5.5 Synthetic Efforts Toward Rameswaralide (**8**) 36
1.5.6 Synthetic Efforts Toward Rameswaralide (**8**), Mandapamates (**17**–**19**), and Plumarellides (**15**–**16**) 41
1.5.7 Synthetic Efforts Toward Mandapamates (**17**–**19**), Plumarellides (**15**–**16**), and Dissectolide (**22**) 45
1.5.7 Synthetic Efforts Toward Yonarolide (**25**) 47
1.5.8 Synthetic Efforts Toward Ineleganolide (**9**) and Sinculochmodin C (**10**) 48

1.6 Conclusion 53
1.7 Notes and References 55

CHAPTER 2 ***61***
Enantioselective Synthesis of a Hydroxymethyl-cis-1,3-cyclopentenediol Building Block

2.1 Introduction 61
2.2 Retrosynthetic Analysis 62
2.3 Intramolecular Aldol Cyclization 63
2.4 Intramolecular Wittig Cyclization 64
2.5 Completion of Hydroxymethyl-*cis*-1,3-cyclopentenediol **262** 68
2.6 Conclusion 69
2.7 Experimental Methods and Analytical Data 70
2.7.1 Materials and Methods 70
2.7.2 Experimental Procedures 72
2.7.3 Ligand Synthesis 87
2.7.4 Ligand Screen in Palladium-Catalyzed Intermolecular Enantioselective Allylic Alkylation 91
2.8 Notes and References 93

APPENDIX 1 ***98***
Synthetic Summary for Chapter 2

APPENDIX 2 ***100***
Spectra Relevant to Chapter 2

APPENDIX 3 ***132***
Alternative Construction of Hydroxymethyl-cis-1,3-cyclopentenediol Building Block by Ring-Closing Metathesis

A3.1 Alternative Approach to 1,3-*cis*-Cyclopentenediol Building Block 132
A3.2 Synthesis of Diethyl Ketal Analog 133
A3.3 Attempted Deprotection of Kinetic Enol Ether Byproducts 134
A3.4 Exploration of Diastereoselective Vinyl Addition 135

A3.5 Ring-Closing Metathesis 136
A3.6 1,3-Allylic Transposition of Bicyclic Cyclopentenes 137
A3.7 Experimental Methods and Analytical Data 140
A3.7.1 Materials and Methods 140
A3.7.2 Experimental Procedures 141
A3.8 Notes and References 153

APPENDIX 4 ***155***
Spectra Relevant to Appendix 3

CHAPTER 3 ***171***
Progress Toward the Asymmetric Total Syntheses of the Furanobutenolide Norcembranoid Diterpene Natural Products

3.1 Introduction 171
3.2 Retrosynthetic Analysis 174
3.3 Enantioselective Construction of Cyclopentenediol Building Block 176
3.4 Synthesis of the Norcembranoid Diterpene Carbocyclic Core 178
3.5 Synthetic Advancement Toward *ent*-Ineleganolide 181
3.6 Alternative Retrosynthetic Strategy 183
3.7 Redox Advancement Toward *ent*-Ineleganolide 187
3.8 Computational Studies of Conformational Limitations 193
3.9 Experimental Methods and Analytical Data 198
3.9.1 Materials and Methods 198
3.9.2 Experimental Procedures 199
3.10 Notes and References 229

APPENDIX 5 ***238***
Synthetic Summary for Chapter 3

APPENDIX 6 ***241***
Spectra Relevant to Chapter 3

APPENDIX 7 ***290***
X-Ray Crystallography Reports Relevant to Chapter 3

A7.1 X-Ray Crystal Structure Analysis of Diene **324**..... 291
A7.2 X-Ray Crystal Structure Analysis of Isoineleganolide A (**328**).. 305
A7.3 X-Ray Crystal Structure Analysis of Bromide **346**..... 320
A7.4 X-Ray Crystal Structure Analysis of Diketone **347**..... 335
A7.5 X-Ray Crystal Structure Analysis of Hemiketal **350.**..... 350
A7.6 Notes and References..... 365

APPENDIX 8 ***366***
Alternative Synthetic Strategies Toward Ineleganolide

A8.1 Alternative Synthesis of Acid Coupling Partner..... 366
A8.2 Olefin Isomerization of [6,7,5,5]-Tetracyclic Diene..... 367
A8.3 Redox Advancement of [6,7,5,5]-Tetracyclic Diene 369
A8.4 Olefin Isomerization of Isoineleganolide A (**328**)..... 370
A8.5 Nucleophilic Epoxide Opening of Isoineleganolide A (**328**) 370
A8.6 Experimental Methods and Analytical Data 374
A8.6.1 Materials and Methods 374
A8.6.2 Experimental Procedures 375
A8.7 X-Ray Crystallography Reports 376
A8.7.1 X-Ray Crystal Structure Analysis of Chloride **367** 376
A8.7.2 X-Ray Crystal Structure Analysis of Fluoride **369**..... 391
A8.8 Notes and References..... 406

CHAPTER 4 ***408***
Revised Plan for the Synthesis of Ineleganolide: Alternative Advancement Toward the Asymmetric Total Synthesis of Ineleganolide by Late-Stage Oxidation State Manipulation

4.1 Revised Retrosynthetic Analysis – Conjugate Reduction 408
4.2 Exploration of Conjugate Reduction Pathway 409
4.3 Revised Retrosynthetic Analysis – 1,2-Reduction..... 414
4.4 Exploration of 1,2-Reduction Pathway..... 415
4.5 Retrosynthetic Analysis — Late-Stage Reduction 422
4.6 Exploration of Enedione Synthesis 423

4.7 New Approach toward Ineleganolide 428
4.8 Conclusion 429
4.9 Experimental Methods and Analytical Data 432
4.9.1 Materials and Methods 432
4.9.2 Experimental Procedures 433
4.10 Notes and References 477

APPENDIX 9 ***483***
Synthetic Summary for Chapter 4

APPENDIX 10 ***487***
Spectra Relevant to Chapter 4

APPENDIX 11 ***554***
X-Ray Crystallography Reports Relevant to Chapter 4

A11.1 X-Ray Crystal Structure Analysis of Epoxide **371** 555
A11.2 X-Ray Crystal Structure Analysis of 2*H*-Ineleganolide (**373**). 570
A11.3 X-Ray Crystal Structure Analysis of Diketone **375.** 594
A11.4 Notes and References 608

CHAPTER 5 ***609***
Lewis Acid Mediated (3+2) Cycloadditions of Donor–Acceptor Cyclopropanes with Heterocumulenes

5.1 Introduction 609
5.2 Initial Reaction Development Using Allyl and Alkyl Isothiocyanates 610
5.3 Unambiguous Structural Assignment of Heterocyclic Products 611
5.4 Carbodiimides as Competent Cycloaddition Partners 612
5.5 Use of Isocyanates Under Modified Conditions 613
5.6 Enantiospecific (3 + 2) Cycloaddition 614
5.7 Conclusion 616
5.8 Experimental Methods and Analytical Data 617
5.8.1 Materials and Methods 617
5.8.2 General Experimental Procedures 618

5.8.3 Cyclopropane Characterization Data 623
5.8.4 Thioimidate Characterization Data 628
5.8.5 Amidine Characterization Data 637
5.8.6 Lactam Characterization Data 643
5.9 Notes and References 647

APPENDIX 12 ***651***
Spectra Relevant to Chapter 5

APPENDIX 13 ***712***
X-Ray Crystallography Reports Relevant to Chapter 5

A13.1 X-Ray Crystal Structure Analysis of Thioimidate **440**. 713
A13.2 X-Ray Crystal Structure Analysis of Amidine **(*R*)-450•HBr**. 724

CHAPTER 6 ***774***
Stereoselective Lewis Acid Mediated (3 + 2) Cycloadditions of N-H- and N-Sulfonylaziridines with Heterocumulenes

6.1 Introduction 774
6.2 Initial Reaction Development 776
6.3 Exploration of 2-Aziridine and Heterocumulene Substitution 777
6.4 Effect of Aziridine *N*-Substitution 779
6.5 Extension of Heterocumulene Scope 780
6.6 Cycloaddition of Disubstituted *N*-Sulfonylaziridines 780
6.7 Development of a Stereoselective (3 + 2) Cycloaddition 782
6.8 Isothiocyanate Substitution in Stereoselective (3 + 2) Cycloaddition 783
6.9 Effect of Aziridine *N*-Substitution on Transfer of Chiral Information 784
6.10 Proposed Mechanism of Stereoselective (3 + 2) Cycloaddition 785
6.11 Cycloaddition of a Diester Aziridine 786
6.12 Deprotection of *N*-Sulfonyl Heterocycles 787
6.13 Conclusion 788
6.14 Experimental Methods and Analytical Data 789
6.14.1 Materials and Methods 789
6.14.2 General Experimental Procedures 790
6.14.3 Aziridine Synthesis and Characterization Data 794

6.14.4 Iminothiazolidine Synthesis and Characterization Data 811
6.14.5 Iminoimidazolidine Synthesis and Characterization Data 833
6.14.6 Preparation of Thioxoimidazolidine **550** 839
6.14.7 Stereoselective (3 + 2) Cycloaddition with Diphenylcarbodiimide 841
6.14.8 (3 + 2) Cycloaddition Byproduct Characterization Data 842
6.14.9 Deprotection of Iminothiazolidines **(*S*)-499** and **(*S*)-522** 843
6.14.9.1 Desulfonylation of Tosylthiazolidine **(*S*)-499** 843
6.14.9.2 Desulfonylation of (*p*-Nosyl)thiazolidine **(*S*)-522** 844
6.14.9.3 Deallylation of Tosylthiazolidine **(*S*)-499** 845
6.14.10 Control Reaction Experimental Procedures 846
6.14.10.1 Lewis Acid Control 846
6.14.10.2 Isomerization of Disubstituted Aziridine **540** 846
6.14.10.3 Isomerization of Disubstituted Aziridine **537** 848
6.14.10.4 Racemization of Aziridine Starting Material **(*R*)-498** 849
6.14.10.5 Racemization of Product **(*S*)-499** 849
6.14.10.6 Isomerization of *trans*-Disubstituted Thiazolidine Product **541** 850
6.14.10.7 Isomerization of *cis*-Disubstituted Thiazolidine Product **542** 851
6.15 Notes and References 852

APPENDIX 14 ***861***
Spectra Relevant to Chapter 6

APPENDIX 15 ***951***
X-Ray Crystallography Reports Relevant to Chapter 6

A15.1 X-Ray Crystal Structure Analysis of Thiazolidine **(*S*)-522**. 952
A15.2 X-Ray Crystal Structure Analysis of Thiazolidine **536** 975
A15.3 X-Ray Crystal Structure Analysis of Imidazolidinium **590•($ZnBr_3$•MeOH)**. 991
A15.4 X-Ray Crystal Structure Analysis of Imidazolidine **550** 1010
A15.5 X-Ray Crystal Structure Analysis of Oxazolidine **591**. 1028

APPENDIX 16 ***1047***
Synthesis of Functionalized Thiouracils as G Protein-Coupled Receptor Agonists

A16.1 Introduction 1047
A16.2 Retrosynthetic Analysis 1048
A16.3 Synthesis of a Functionalized Thiouracil 1048
A16.4 Experimental Methods and Analytical Data 1052
A16.4.1 Materials and Methods 1052
A16.4.2 Experimental Procedures 1053
A16.5 Notes and References 1058

APPENDIX 17 ***1061***
Spectra Relevant to Appendix 16

APPENDIX 18 ***1064***
Notebook Cross-Reference for New Compounds

A18.1 Contents 1064
A18.2 Notebook Cross-Reference Tables 1065

Comprehensive Bibliography 1075

Index 1099

About the Author 1105

LIST OF FIGURES

CHAPTER 1

Furanobutenolide Cembranoid and Norcembranoid Natural Products: Biosynthetic Connections and Synthetic Efforts

Figure 1.1.1. Characteristic Macrocyclic Furanobutenolide Cembranoids and Norcembranoids.....2

Figure 1.1.2. Characteristic Polycyclic Furanobutenolide Cembranoids and Norcembranoids.....3

Figure 1.3.1. Cembranoids and Norcembranoid Macrocyclic Scaffolds 4

Figure 1.3.2. Polycyclic Cembranoid Furanobutenolide Natural Products.....5

Figure 1.3.3. Polycyclic Norcembranoid Furanobutenolide Natural Products 5

Figure 1.4.1.1. Structural Comparison of Havellockate (**14**) and Rameswaralide (**8**) to Plumarellide (**15**) and Mandapamate (**17**)..... 10

Figure 1.4.2.1. Sinuleptolide (**4**) and 5-Episinuleptolide (**5**)..... 10

Figure 1.5.6.1. Mandapamate and Plumarellide Natural Products..... 43

CHAPTER 2

Enantioselective Synthesis of a Hydroxymethyl-cis-1,3-cyclopentenediol Building Block

Figure 2.1.1. Representative Natural Products Possessing *cis*-1,3-Cyclopentanediol Scaffold..... 62

Figure 2.4.1. Decomposition of NaOBr Stock Solution..... 66

Figure 2.4.2. Improved Technique for Conversion of Vinyl Chloride **258** to α-Bromoketone **259**..... 68

APPENDIX 2

Spectra Relevant to Chapter 2

Figure A2.1. ^{1}H NMR (500 MHz, $CDCl_3$) of compound **250**..... 101

Figure A2.2. Infrared spectrum (thin film/NaCl) of compound **250**. 102

Figure A2.3. ^{13}C NMR (126 MHz, $CDCl_3$) of compound **250**..... 102

Figure A2.4. ^{1}H NMR (500 MHz, $CDCl_3$) of compound **271**..... 103

Figure A2.5. Infrared spectrum (thin film/NaCl) of compound **271**. 104

Figure A2.6. ^{13}C NMR (126 MHz, $CDCl_3$) of compound **271**..... 104

Figure A2.7. ^{1}H NMR (500 MHz, $CDCl_3$) of compound **272**..... 105

Figure A2.8. Infrared spectrum (thin film/NaCl) of compound **272**. 106

Figure A2.9. ^{13}C NMR (126 MHz, $CDCl_3$) of compound **272**..... 106

Figure A2.10. ^{1}H NMR (500 MHz, $CDCl_3$) of compound **273**. 107
Figure A2.11. Infrared spectrum (thin film/NaCl) of compound **273**. 108
Figure A2.12. ^{13}C NMR (126 MHz, $CDCl_3$) of compound **273**. 108
Figure A2.13. ^{1}H NMR (500 MHz, $CDCl_3$) of compound **257**. 109
Figure A2.14. Infrared spectrum (thin film/NaCl) of compound **257**. 110
Figure A2.15. ^{13}C NMR (126 MHz, $CDCl_3$) of compound **257**. 110
Figure A2.16. ^{1}H NMR (300 MHz, $CDCl_3$) of compound **253**. 111
Figure A2.17. Infrared spectrum (thin film/NaCl) of compound **253**. 112
Figure A2.18. ^{13}C NMR (76 MHz, $CDCl_3$) of compound **253**. 112
Figure A2.19. ^{1}H NMR (500 MHz, $CDCl_3$) of compound **258**. 113
Figure A2.20. Infrared spectrum (thin film/NaCl) of compound **258**. 114
Figure A2.21. ^{13}C NMR (126 MHz, $CDCl_3$) of compound **258**. 114
Figure A2.22. ^{1}H NMR (300 MHz, $CDCl_3$) of compound **260**. 115
Figure A2.23. Infrared spectrum (thin film/NaCl) of compound **260**. 116
Figure A2.24. ^{13}C NMR (126 MHz, $CDCl_3$) of compound **260**. 116
Figure A2.25. ^{1}H NMR (500 MHz, $CDCl_3$) of compound **275**. 117
Figure A2.26. Infrared spectrum (thin film/NaCl) of compound **275**. 118
Figure A2.27. ^{13}C NMR (126 MHz, $CDCl_3$) of compound **275**. 118
Figure A2.28. 2-D ^{1}H NOESY (500 MHz, $CDCl_3$) of compound **275**. 119
Figure A2.29. ^{1}H NMR (500 MHz, $CDCl_3$) of compound **262**. 120
Figure A2.30. Infrared spectrum (thin film/NaCl) of compound **262**. 121
Figure A2.31. ^{13}C NMR (126 MHz, $CDCl_3$) of compound **262**. 121
Figure A2.32. ^{1}H NMR (500 MHz, $CDCl_3$) of compound **276**. 122
Figure A2.33. Infrared spectrum (thin film/NaCl) of compound **276**. 123
Figure A2.34. ^{13}C NMR (126 MHz, $CDCl_3$) of compound **276**. 123
Figure A2.35. ^{19}F NMR (282 MHz, $CDCl_3$) of compound **276**. 124
Figure A2.36. ^{1}H NMR (500 MHz, $CDCl_3$) of compound **277**. 125
Figure A2.37. Infrared spectrum (thin film/NaCl) of compound **277**. 126
Figure A2.38. ^{13}C NMR (126 MHz, $CDCl_3$) of compound **277**. 126
Figure A2.39. ^{19}F NMR (282 MHz, $CDCl_3$) of compound **277**. 127
Figure A2.40. ^{1}H NMR (500 MHz, C_6D_6) of compound **279**. 128
Figure A2.41. Infrared spectrum (thin film/NaCl) of compound **279**. 129
Figure A2.42. ^{13}C NMR (126 MHz, C_6D_6) of compound **279**. 129
Figure A2.43. ^{19}F NMR (282 MHz, C_6D_6) of compound **279**. 130
Figure A2.44. ^{31}P NMR (121 MHz, C_6D_6) of compound **279**. 131

APPENDIX 4

Spectra Relevant to Appendix 3

Figure A4.1. ^{1}H NMR (300 MHz, $CDCl_3$) of compound **287**..... 156
Figure A4.2. ^{1}H NMR (300 MHz, $CDCl_3$) of compound **288**..... 157
Figure A4.3. ^{1}H NMR (300 MHz, $CDCl_3$) of compound **289**..... 158
Figure A4.4. ^{1}H NMR (300 MHz, $CDCl_3$) of compound **290**..... 159
Figure A4.5. ^{1}H NMR (300 MHz, $CDCl_3$) of compound **291**..... 160
Figure A4.6. ^{1}H NMR (300 MHz, $CDCl_3$) of compound **296**..... 161
Figure A4.7. ^{1}H NMR (300 MHz, $CDCl_3$) of compound **297**..... 162
Figure A4.8. ^{1}H NMR (300 MHz, $CDCl_3$) of compound **298**..... 163
Figure A4.9. ^{1}H NMR (300 MHz, $CDCl_3$) of compound **299**..... 164
Figure A4.10. ^{1}H NMR (300 MHz, $CDCl_3$) of compound **302**..... 165
Figure A4.11. ^{1}H NMR (300 MHz, $CDCl_3$) of compound **303**..... 166
Figure A4.12. ^{1}H NMR (300 MHz, $CDCl_3$) of compound **306**..... 167
Figure A4.13. ^{1}H NMR (300 MHz, $CDCl_3$) of compound **307**..... 168
Figure A4.14. ^{1}H NMR (300 MHz, $CDCl_3$) of compound **311**..... 169
Figure A4.15. ^{1}H NMR (300 MHz, $CDCl_3$) of compound **313**..... 170

CHAPTER 3

Progress Toward the Asymmetric Total Syntheses of the Furanobutenolide Norcembranoid Diterpene Natural Products

Figure 3.1.1. Polycyclic Furanobutenolide Norcembranoid Diterpenes..... 172
Figure 3.4.1. Three-Dimensional Structure of Diene **324**..... 180
Figure 3.8.1. Free Energy Diagram Based on Computed Ground State Energies 195

APPENDIX 6

Spectra Relevant to Chapter 3

Figure A6.1. ^{1}H NMR (500 MHz, $CDCl_3$) of compound **354**..... 242
Figure A6.2. Infrared spectrum (thin film/NaCl) of compound **354**. 243
Figure A6.3. ^{13}C NMR (126 MHz, $CDCl_3$) of compound **354**..... 243
Figure A6.4. ^{1}H NMR (300 MHz, $CDCl_3$) of compound ***ent*-322**. 244
Figure A6.5. Infrared spectrum (thin film/NaCl) of compound ***ent*-322**. 245
Figure A6.6. ^{13}C NMR (76 MHz, $CDCl_3$) of compound ***ent*-322**..... 245
Figure A6.7. ^{1}H NMR (500 MHz, $CDCl_3$) of compound **323**..... 246

Figure A6.8. Infrared spectrum (thin film/NaCl) of compound **323**. 247
Figure A6.9. ^{13}C NMR (126 MHz, $CDCl_3$) of compound **323**. 247
Figure A6.10. ^{1}H NMR (600 MHz, $CDCl_3$) of compound ***ent*-320**. 248
Figure A6.11. Infrared spectrum (thin film/NaCl) of compound ***ent*-320**. 249
Figure A6.12. ^{13}C NMR (126 MHz, $CDCl_3$) of compound ***ent*-320**. 249
Figure A6.13. ^{1}H NMR (500 MHz, $CDCl_3$) of compound **324**. 250
Figure A6.14. Infrared spectrum (thin film/NaCl) of compound **324**. 251
Figure A6.15. ^{13}C NMR (126 MHz, $CDCl_3$) of compound **324**. 251
Figure A6.16. ^{1}H NMR (600 MHz, $CDCl_3$) of compound **325**. 252
Figure A6.17. Infrared spectrum (thin film/NaCl) of compound **325**. 253
Figure A6.18. ^{13}C NMR (126 MHz, $CDCl_3$) of compound **325**. 253
Figure A6.19. ^{1}H NMR (600 MHz, $CDCl_3$) of compound **328**. 254
Figure A6.20. Infrared spectrum (thin film/NaCl) of compound **328**. 255
Figure A6.21. ^{13}C NMR (126 MHz, $CDCl_3$) of compound **328**. 255
Figure A6.22. ^{1}H NMR (600 MHz, $CDCl_3$) of compound **329**. 256
Figure A6.23. Infrared spectrum (thin film/NaCl) of compound **329**. 257
Figure A6.24. ^{13}C NMR (126 MHz, $CDCl_3$) of compound **329**. 257
Figure A6.25. ^{1}H NMR (400 MHz, $CDCl_3$) of compound **331**. 258
Figure A6.26. Infrared spectrum (thin film/NaCl) of compound **331**. 259
Figure A6.27. ^{13}C NMR (101 MHz, $CDCl_3$) of compound **331**. 259
Figure A6.28. ^{1}H NMR (500 MHz, $CDCl_3$) of compound **336**. 260
Figure A6.29. Infrared spectrum (thin film/NaCl) of compound **336**. 261
Figure A6.30. ^{13}C NMR (126 MHz, $CDCl_3$) of compound **336**. 261
Figure A6.31. ^{1}H NMR (500 MHz, $CDCl_3$) of compound **337-A**. 262
Figure A6.32. Infrared spectrum (thin film/NaCl) of compound **337-A**. 263
Figure A6.33. ^{13}C NMR (126 MHz, $CDCl_3$) of compound **337-A**. 263
Figure A6.34. ^{1}H NMR (500 MHz, $CDCl_3$) of compound **337-B**. 264
Figure A6.35. Infrared spectrum (thin film/NaCl) of compound **337-B**. 265
Figure A6.36. ^{13}C NMR (126 MHz, $CDCl_3$) of compound **337-B**. 265
Figure A6.37. ^{1}H NMR (400 MHz, $CDCl_3$) of compound **338**. 266
Figure A6.38. Infrared spectrum (thin film/NaCl) of compound **338**. 267
Figure A6.39. ^{13}C NMR (101 MHz, $CDCl_3$) of compound **338**. 267
Figure A6.40. ^{1}H NMR (400 MHz, $CDCl_3$) of compound ***ent*-335**. 268
Figure A6.41. Infrared spectrum (thin film/NaCl) of compound ***ent*-335**. 269
Figure A6.42. ^{13}C NMR (101 MHz, $CDCl_3$) of compound ***ent*-335**. 269

Figure A6.43. ^{1}H NMR (400 MHz, $CDCl_3$) of compound **340**. 270
Figure A6.44. Infrared spectrum (thin film/NaCl) of compound **340**. 271
Figure A6.45. ^{13}C NMR (101 MHz, $CDCl_3$) of compound **340**. 271
Figure A6.46. ^{1}H NMR (600 MHz, $CDCl_3$) of compound **341**. 272
Figure A6.47. Infrared spectrum (thin film/NaCl) of compound **341**. 273
Figure A6.48. ^{13}C NMR (126 MHz, $CDCl_3$) of compound **341**. 273
Figure A6.49. ^{1}H NMR (400 MHz, $CDCl_3$) of compound **344**. 274
Figure A6.50. Infrared spectrum (thin film/NaCl) of compound **344**. 275
Figure A6.51. ^{13}C NMR (101 MHz, $CDCl_3$) of compound **344**. 275
Figure A6.52. ^{1}H NMR (500 MHz, $CDCl_3$) of compound **345**. 276
Figure A6.53. Infrared spectrum (thin film/NaCl) of compound **345**. 277
Figure A6.54. ^{13}C NMR (126 MHz, $CDCl_3$) of compound **345**. 277
Figure A6.55. ^{1}H NMR (600 MHz, $CDCl_3$) of compound **346**. 278
Figure A6.56. Infrared spectrum (thin film/NaCl) of compound **346**. 279
Figure A6.57. ^{13}C NMR (126 MHz, $CDCl_3$) of compound **346**. 279
Figure A6.58. ^{1}H NMR (500 MHz, $CDCl_3$) of compound **347**. 280
Figure A6.59. Infrared spectrum (thin film/NaCl) of compound **347**. 281
Figure A6.60. ^{13}C NMR (126 MHz, $CDCl_3$) of compound **347**. 281
Figure A6.61. ^{1}H NMR (500 MHz, $CDCl_3$) of compound **349/350**. 282
Figure A6.62. Infrared spectrum (thin film/NaCl) of compound **349/350**. 283
Figure A6.63. ^{13}C NMR (126 MHz, $CDCl_3$) of compound **349/350**. 283
Figure A6.64. ^{1}H NMR (600 MHz, $CDCl_3$) of compound ***ent*-313**. 284
Figure A6.65. Infrared spectrum (thin film/NaCl) of compound ***ent*-313**. 285
Figure A6.66. ^{13}C NMR (126 MHz, $CDCl_3$) of compound ***ent*-313**. 285
Figure A6.67. ^{1}H NMR (500 MHz, $CDCl_3$) of compound **351**. 286
Figure A6.68. Infrared spectrum (thin film/NaCl) of compound **351**. 287
Figure A6.69. ^{13}C NMR (126 MHz, $CDCl_3$) of compound **351**. 287
Figure A6.70. ^{1}H NMR (500 MHz, $CDCl_3$) of compound **352**. 288
Figure A6.71. Infrared spectrum (thin film/NaCl) of compound **352**. 289
Figure A6.72. ^{13}C NMR (126 MHz, $CDCl_3$) of compound **352**. 289

APPENDIX 7

X-Ray Crystallography Reports Relevant to Chapter 3

Figure A7.1.1. X-Ray Crystal Structure of Diene **324**. 291
Figure A7.2.1. X-Ray Crystal Structure of Isoineleganolide A (**328**). 305

Figure A7.3.1. X-Ray Crystal Structure of Bromide **346**. 320
Figure A7.4.1. X-Ray Crystal Structure of Diketone **347**. 335
Figure A7.5.1. X-Ray Crystal Structure of Hemiketal **350**. 350

APPENDIX 8
Alternative Synthetic Strategies Toward Ineleganolide

Figure A8.7.1.1. X-Ray Crystal Structure of Chloride **367**. 376
Figure A8.7.2.1. X-Ray Crystal Structure of Fluoride **369**. 391

CHAPTER 4
Revised Plan for the Synthesis of Ineleganolide: Alternative Advancement Toward the Asymmetric Total Synthesis of Ineleganolide by Late-Stage Oxidation State Manipulation

Figure 4.2.1. Computational Evaluation of Conformational Isomers of 2*H*-Ineleganolide 412
Figure 4.8.1. The Synthetic Natural Product-Like Ineleganoloids 431

APPENDIX 9
Synthetic Summary for Chapter 4

Figure A.9.1. Characteristic Examples of the Synthetic Natural Product-Like Ineleganoloids 486

APPENDIX 10
Spectra Relevant to Chapter 4

Figure A10.1. ^{1}H NMR (500 MHz, $CDCl_3$) of compound **372**. 488
Figure A10.2. Infrared spectrum (thin film/NaCl) of compound **372**. 489
Figure A10.3. ^{13}C NMR (126 MHz, $CDCl_3$) of compound **372**. 489
Figure A10.4. ^{1}H NMR (600 MHz, $CDCl_3$) of compound **371**. 490
Figure A10.5. Infrared spectrum (thin film/NaCl) of compound **371**. 491
Figure A10.6. ^{13}C NMR (126 MHz, $CDCl_3$) of compound **371**. 491
Figure A10.7. ^{1}H NMR (600 MHz, $CDCl_3$) of compound **374**. 492
Figure A10.8. Infrared spectrum (thin film/NaCl) of compound **374**. 493
Figure A10.9. ^{13}C NMR (126 MHz, $CDCl_3$) of compound **374**. 493
Figure A10.10. ^{1}H NMR (500 MHz, $CDCl_3$) of compound **373**. 494
Figure A10.11. Infrared spectrum (thin film/NaCl) of compound **373**. 495

Figure A10.12. ^{13}C NMR (126 MHz, $CDCl_3$) of compound **373**. 495
Figure A10.13. ^{1}H NMR (600 MHz, $CDCl_3$) of compound **375** 496
Figure A10.14. Infrared spectrum (thin film/NaCl) of compound **375**. 497
Figure A10.15. ^{13}C NMR (126 MHz, $CDCl_3$) of compound **375**. 497
Figure A10.16. ^{1}H NMR (400 MHz, $CDCl_3$) of compound **376** 498
Figure A10.17. Infrared spectrum (thin film/NaCl) of compound **376**. 499
Figure A10.18. ^{13}C NMR (101 MHz, $CDCl_3$) of compound **376**. 499
Figure A10.19. ^{1}H NMR (400 MHz, $CDCl_3$) of compound **377** 500
Figure A10.20. Infrared spectrum (thin film/NaCl) of compound **377**. 501
Figure A10.21. ^{13}C NMR (101 MHz, $CDCl_3$) of compound **377**. 501
Figure A10.22. ^{1}H NMR (400 MHz, $CDCl_3$) of compound **378** 502
Figure A10.23. Infrared spectrum (thin film/NaCl) of compound **378**. 503
Figure A10.24. ^{13}C NMR (101 MHz, $CDCl_3$) of compound **378**. 503
Figure A10.25. ^{1}H NMR (600 MHz, $CDCl_3$) of compound **383** 504
Figure A10.26. Infrared spectrum (thin film/NaCl) of compound **383**. 505
Figure A10.27. ^{13}C NMR (126 MHz, $CDCl_3$) of compound **383**. 505
Figure A10.28. ^{1}H NMR (600 MHz, $CDCl_3$) of compound **384** 506
Figure A10.29. Infrared spectrum (thin film/NaCl) of compound **384**. 507
Figure A10.30. ^{13}C NMR (126 MHz, $CDCl_3$) of compound **384**. 507
Figure A10.31. ^{1}H NMR (600 MHz, $CDCl_3$) of compound **385** 508
Figure A10.32. Infrared spectrum (thin film/NaCl) of compound **385**. 509
Figure A10.33. ^{13}C NMR (126 MHz, $CDCl_3$) of compound **385**. 509
Figure A10.34. ^{1}H NMR (400 MHz, $CDCl_3$) of compound **389** 510
Figure A10.35. Infrared spectrum (thin film/NaCl) of compound **389**. 511
Figure A10.36. ^{13}C NMR (101 MHz, $CDCl_3$) of compound **389**. 511
Figure A10.37. ^{1}H NMR (400 MHz, $CDCl_3$) of compound **390** 512
Figure A10.38. Infrared spectrum (thin film/NaCl) of compound **390**. 513
Figure A10.39. ^{13}C NMR (101 MHz, $CDCl_3$) of compound **390**. 513
Figure A10.40. ^{1}H NMR (400 MHz, $CDCl_3$) of compound **391** 514
Figure A10.41. Infrared spectrum (thin film/NaCl) of compound **391**. 515
Figure A10.42. ^{13}C NMR (101 MHz, $CDCl_3$) of compound **391**. 515
Figure A10.43. ^{1}H NMR (400 MHz, $CDCl_3$) of compound **393** 516
Figure A10.44. Infrared spectrum (thin film/NaCl) of compound **393**. 517
Figure A10.45. ^{13}C NMR (101 MHz, $CDCl_3$) of compound **393**. 517
Figure A10.46. ^{1}H NMR (400 MHz, $CDCl_3$) of compound **396** 518

Figure A10.47. Infrared spectrum (thin film/NaCl) of compound **396**. 519
Figure A10.48. ^{13}C NMR (101 MHz, $CDCl_3$) of compound **396**. 519
Figure A10.49. ^{1}H NMR (400 MHz, $CDCl_3$) of compound **394**. 520
Figure A10.50. Infrared spectrum (thin film/NaCl) of compound **394**. 521
Figure A10.51. ^{13}C NMR (101 MHz, $CDCl_3$) of compound **394**. 521
Figure A10.52. ^{1}H NMR (400 MHz, $CDCl_3$) of compound **397**. 522
Figure A10.53. Infrared spectrum (thin film/NaCl) of compound **397**. 523
Figure A10.54. ^{13}C NMR (101 MHz, $CDCl_3$) of compound **397**. 523
Figure A10.55. ^{1}H NMR (400 MHz, $CDCl_3$) of compound **399**. 524
Figure A10.56. Infrared spectrum (thin film/NaCl) of compound **399**. 525
Figure A10.57. ^{13}C NMR (101 MHz, $CDCl_3$) of compound **399**. 525
Figure A10.58. ^{1}H NMR (400 MHz, C_6D_6) of compound **401**. 526
Figure A10.59. Infrared spectrum (thin film/NaCl) of compound **401**. 527
Figure A10.60. ^{13}C NMR (101 MHz, C_6D_6) of compound **401**. 527
Figure A10.61. ^{1}H NMR (400 MHz, $CDCl_3$) of compound **403**. 528
Figure A10.62. Infrared spectrum (thin film/NaCl) of compound **403**. 529
Figure A10.63. ^{13}C NMR (101 MHz, $CDCl_3$) of compound **403**. 529
Figure A10.64. ^{1}H NMR (400 MHz, $CDCl_3$) of compound **404**. 530
Figure A10.65. Infrared spectrum (thin film/NaCl) of compound **404**. 531
Figure A10.66. ^{13}C NMR (101 MHz, $CDCl_3$) of compound **404**. 531
Figure A10.67. ^{1}H NMR (400 MHz, $CDCl_3$) of compound **405**. 532
Figure A10.68. Infrared spectrum (thin film/NaCl) of compound **405**. 533
Figure A10.69. ^{13}C NMR (101 MHz, $CDCl_3$) of compound **405**. 533
Figure A10.70. ^{1}H NMR (400 MHz, $CDCl_3$) of compound **406**. 534
Figure A10.71. Infrared spectrum (thin film/NaCl) of compound **406**. 535
Figure A10.72. ^{13}C NMR (101 MHz, $CDCl_3$) of compound **406**. 535
Figure A10.73. ^{1}H NMR (400 MHz, $CDCl_3$) of compound **407**. 536
Figure A10.74. Infrared spectrum (thin film/NaCl) of compound **407**. 537
Figure A10.75. ^{13}C NMR (101 MHz, $CDCl_3$) of compound **407**. 537
Figure A10.76. ^{1}H NMR (400 MHz, $CDCl_3$) of compound **408**. 538
Figure A10.77. Infrared spectrum (thin film/NaCl) of compound **408**. 539
Figure A10.78. ^{13}C NMR (101 MHz, $CDCl_3$) of compound **408**. 539
Figure A10.79. ^{1}H NMR (600 MHz, $CDCl_3$) of compound **412**. 540
Figure A10.80. Infrared spectrum (thin film/NaCl) of compound **412**. 541
Figure A10.81. ^{13}C NMR (126 MHz, $CDCl_3$) of compound **412**. 541

Figure A10.82. ^{1}H NMR (400 MHz, $CDCl_3$) of compound **413**..... 542
Figure A10.83. Infrared spectrum (thin film/NaCl) of compound **413**. 543
Figure A10.84. ^{13}C NMR (101 MHz, $CDCl_3$) of compound **413**..... 543
Figure A10.85. ^{1}H NMR (400 MHz, $CDCl_3$) of compound **415**..... 544
Figure A10.86. Infrared spectrum (thin film/NaCl) of compound **415**. 545
Figure A10.87. ^{13}C NMR (101 MHz, $CDCl_3$) of compound **415**..... 545
Figure A10.88. ^{1}H NMR (400 MHz, $CDCl_3$) of compound **416**..... 546
Figure A10.89. Infrared spectrum (thin film/NaCl) of compound **416**. 547
Figure A10.90. ^{13}C NMR (101 MHz, $CDCl_3$) of compound **416**..... 547
Figure A10.91. ^{1}H NMR (400 MHz, $CDCl_3$) of compound **420**..... 548
Figure A10.92. Infrared spectrum (thin film/NaCl) of compound **420**. 549
Figure A10.93. ^{13}C NMR (101 MHz, $CDCl_3$) of compound **420**..... 549
Figure A10.94. ^{1}H NMR (400 MHz, $CDCl_3$) of compound **422**..... 550
Figure A10.95. Infrared spectrum (thin film/NaCl) of compound **422**. 551
Figure A10.96. ^{13}C NMR (101 MHz, $CDCl_3$) of compound **422**..... 551
Figure A10.97. ^{1}H NMR (400 MHz, $CDCl_3$) of compound **423**..... 552
Figure A10.98. Infrared spectrum (thin film/NaCl) of compound **423**. 553
Figure A10.99. ^{13}C NMR (101 MHz, $CDCl_3$) of compound **423**..... 553

APPENDIX 11

X-Ray Crystallography Reports Relevant to Chapter 4

Figure A11.1.1. X-Ray Crystal Structure of Epoxide **371**..... 555
Figure A11.2.1. X-Ray Crystal Structure of 2*H*-Ineleganolide (**373**)..... 570
Figure A11.3.1. X-Ray Crystal Structure of Diketone **375**..... 594

CHAPTER 5

Lewis Acid Mediated (3+2) Cycloadditions of Donor–Acceptor Cyclopropanes with Heterocumulenes

Figure 5.6.1. Determination of Absolute Configuration..... 615

APPENDIX 12

Spectra Relevant to Chapter 5

Figure A12.1. ^{1}H NMR (500 MHz, $CDCl_3$) of compound **483**. 652
Figure A12.2. Infrared spectrum (thin film/NaCl) of compound **483**. 653
Figure A12.3. ^{13}C NMR (126 MHz, $CDCl_3$) of compound **483**. 653
Figure A12.4. ^{1}H NMR (500 MHz, $CDCl_3$) of compound **485**. 654
Figure A12.5. Infrared spectrum (thin film/NaCl) of compound **485**. 655
Figure A12.6. ^{13}C NMR (126 MHz, $CDCl_3$) of compound **485**. 655
Figure A12.7. ^{1}H NMR (500 MHz, $CDCl_3$) of compound **433**. 656
Figure A12.8. Infrared spectrum (thin film/NaCl) of compound **433**. 657
Figure A12.9. ^{13}C NMR (126 MHz, $CDCl_3$) of compound **433**. 657
Figure A12.10. ^{1}H NMR (500 MHz, $CDCl_3$) of compound **434**. 658
Figure A12.11. Infrared spectrum (thin film/NaCl) of compound **434**. 659
Figure A12.12. ^{13}C NMR (126 MHz, $CDCl_3$) of compound **434**. 659
Figure A12.13. ^{1}H NMR (500 MHz, $CDCl_3$) of compound **435**. 660
Figure A12.14. Infrared spectrum (thin film/NaCl) of compound **435**. 661
Figure A12.15. ^{13}C NMR (126 MHz, $CDCl_3$) of compound **435**. 661
Figure A12.16. ^{1}H NMR (500 MHz, $CDCl_3$) of compound **436**. 662
Figure A12.17. Infrared spectrum (thin film/NaCl) of compound **436**. 663
Figure A12.18. ^{13}C NMR (126 MHz, $CDCl_3$) of compound **436**. 663
Figure A12.19. ^{1}H NMR (500 MHz, $CDCl_3$) of compound **437**. 664
Figure A12.20. Infrared spectrum (thin film/NaCl) of compound **437**. 665
Figure A12.21. ^{13}C NMR (126 MHz, $CDCl_3$) of compound **437**. 665
Figure A12.22. ^{1}H NMR (500 MHz, $CDCl_3$) of compound **438**. 666
Figure A12.23. Infrared spectrum (thin film/NaCl) of compound **438**. 667
Figure A12.24. ^{13}C NMR (126 MHz, $CDCl_3$) of compound **438**. 667
Figure A12.25. ^{1}H NMR (500 MHz, $CDCl_3$) of compound **439**. 668
Figure A12.26. Infrared spectrum (thin film/NaCl) of compound **439**. 669
Figure A12.27. ^{13}C NMR (126 MHz, $CDCl_3$) of compound **439**. 669
Figure A12.28. ^{1}H NMR (500 MHz, $CDCl_3$) of compound **440**. 670
Figure A12.29. Infrared spectrum (thin film/NaCl) of compound **440**. 671
Figure A12.30. ^{13}C NMR (126 MHz, $CDCl_3$) of compound **440**. 671
Figure A12.31. ^{1}H NMR (500 MHz, $CDCl_3$) of compound **441**. 672
Figure A12.32. Infrared spectrum (thin film/NaCl) of compound **441**. 673
Figure A12.33. ^{13}C NMR (126 MHz, $CDCl_3$) of compound **441**. 673

Figure A12.34. ^{1}H NMR (500 MHz, $CDCl_3$) of compound **442**..... 674
Figure A12.35. Infrared spectrum (thin film/NaCl) of compound **442**. 675
Figure A12.36. ^{13}C NMR (126 MHz, $CDCl_3$) of compound **442**..... 675
Figure A12.37. ^{1}H NMR (500 MHz, $CDCl_3$) of compound **443**..... 676
Figure A12.38. Infrared spectrum (thin film/NaCl) of compound **443**. 677
Figure A12.39. ^{13}C NMR (126 MHz, $CDCl_3$) of compound **443**..... 677
Figure A12.40. ^{1}H NMR (500 MHz, $CDCl_3$) of compound **444**..... 678
Figure A12.41. Infrared spectrum (thin film/NaCl) of compound **444**. 679
Figure A12.42. ^{13}C NMR (126 MHz, $CDCl_3$) of compound **444**..... 679
Figure A12.43. ^{1}H NMR (500 MHz, $CDCl_3$) of compound **445**..... 680
Figure A12.44. Infrared spectrum (thin film/NaCl) of compound **445**. 681
Figure A12.45. ^{13}C NMR (126 MHz, $CDCl_3$) of compound **445**..... 681
Figure A12.46. ^{1}H NMR (500 MHz, $CDCl_3$) of compound **448**..... 682
Figure A12.47. Infrared spectrum (thin film/NaCl) of compound **448**. 683
Figure A12.48. ^{13}C NMR (126 MHz, $CDCl_3$) of compound **448**..... 683
Figure A12.49. ^{1}H NMR (400 MHz, $CDCl_3$) of compound **450**..... 684
Figure A12.50. Infrared spectrum (thin film/NaCl) of compound **450**. 685
Figure A12.51. ^{13}C NMR (101 MHz, $CDCl_3$) of compound **450**..... 685
Figure A12.52. ^{1}H NMR (400 MHz, $CDCl_3$) of compound **451**..... 686
Figure A12.53. Infrared spectrum (thin film/NaCl) of compound **451**. 687
Figure A12.54. ^{13}C NMR (101 MHz, $CDCl_3$) of compound **451**..... 687
Figure A12.55. ^{1}H NMR (500 MHz, $CDCl_3$) of compound **452**..... 688
Figure A12.56. Infrared spectrum (thin film/NaCl) of compound **452**. 689
Figure A12.57. ^{13}C NMR (126 MHz, $CDCl_3$) of compound **452**..... 689
Figure A12.58. ^{1}H NMR (500 MHz, $CDCl_3$) of compound **453**..... 690
Figure A12.59. Infrared spectrum (thin film/NaCl) of compound **453**. 691
Figure A12.60. ^{13}C NMR (126 MHz, $CDCl_3$) of compound **453**..... 691
Figure A12.61. ^{1}H NMR (500 MHz, $CDCl_3$) of compound **454**..... 692
Figure A12.62. Infrared spectrum (thin film/NaCl) of compound **454**. 693
Figure A12.63. ^{13}C NMR (126 MHz, $CDCl_3$) of compound **454**..... 693
Figure A12.64. ^{1}H NMR (500 MHz, $CDCl_3$) of compound **455**..... 694
Figure A12.65. Infrared spectrum (thin film/NaCl) of compound **455**. 695
Figure A12.66. ^{13}C NMR (126 MHz, $CDCl_3$) of compound **455**..... 695
Figure A12.67. ^{1}H NMR (500 MHz, $CDCl_3$) of compound **456**..... 696
Figure A12.68. Infrared spectrum (thin film/NaCl) of compound **456**. 697

Figure A12.69. ^{13}C NMR (126 MHz, $CDCl_3$) of compound **456**. 697
Figure A12.70. ^{1}H NMR (400 MHz, DMSO-d_6, 80 °C) of compound **457**. 698
Figure A12.71. Infrared spectrum (thin film/NaCl) of compound **457**. 699
Figure A12.72. ^{13}C NMR (101 MHz, DMSO-d_6, 80 °C) of compound **457**. 699
Figure A12.73. ^{1}H NMR (500 MHz, $CDCl_3$) of compound **459**. 700
Figure A12.74. Infrared spectrum (thin film/NaCl) of compound **459**. 701
Figure A12.75. ^{13}C NMR (126 MHz, $CDCl_3$) of compound **459**. 701
Figure A12.76. ^{1}H NMR (500 MHz, $CDCl_3$) of compound **460**. 702
Figure A12.77. Infrared spectrum (thin film/NaCl) of compound **460**. 703
Figure A12.78. ^{13}C NMR (126 MHz, $CDCl_3$) of compound **460**. 703
Figure A12.79. ^{1}H NMR (500 MHz, $CDCl_3$) of compound **461**. 704
Figure A12.80. Infrared spectrum (thin film/NaCl) of compound **461**. 705
Figure A12.81. ^{13}C NMR (126 MHz, $CDCl_3$) of compound **461**. 705
Figure A12.82. ^{1}H NMR (500 MHz, $CDCl_3$) of compound **462**. 706
Figure A12.83. Infrared spectrum (thin film/NaCl) of compound **462**. 707
Figure A12.84. ^{13}C NMR (126 MHz, $CDCl_3$) of compound **462**. 707
Figure A12.85. ^{1}H NMR (500 MHz, $CDCl_3$) of compound **463**. 708
Figure A12.86. Infrared spectrum (thin film/NaCl) of compound **463**. 709
Figure A12.87. ^{13}C NMR (126 MHz, $CDCl_3$) of compound **463**. 709
Figure A12.88. ^{1}H NMR (500 MHz, $CDCl_3$) of compound **464**. 710
Figure A12.89. Infrared spectrum (thin film/NaCl) of compound **464**. 711
Figure A12.90. ^{13}C NMR (126 MHz, $CDCl_3$) of compound **464**. 711

APPENDIX 13

X-Ray Crystallography Reports Relevant to Chapter 5

Figure A13.1.1. X-Ray Crystal Structure of Thioimidate **440**. 713
Figure A13.2.1. X-Ray Crystal Structure of Amidine **(*R*)-450•HBr**. 724

APPENDIX 14

Spectra Relevant to Chapter 6

Figure A14.1. ^{1}H NMR (500 MHz, $CDCl_3$) of compound **568**. 862
Figure A14.2. Infrared spectrum (thin film/NaCl) of compound **568**. 863
Figure A14.3. ^{13}C NMR (126 MHz, $CDCl_3$) of compound **568**. 863

Figure A14.4. ^{1}H NMR (500 MHz, $CDCl_3$) of compound **570**. 864
Figure A14.5. Infrared spectrum (thin film/NaCl) of compound **570**. 865
Figure A14.6. ^{13}C NMR (126 MHz, $CDCl_3$) of compound **570**. 865
Figure A14.7. ^{1}H NMR (500 MHz, $CDCl_3$) of compound **572**. 866
Figure A14.8. Infrared spectrum (thin film/NaCl) of compound **572**. 867
Figure A14.9. ^{13}C NMR (126 MHz, $CDCl_3$) of compound **572**. 867
Figure A14.10. ^{1}H NMR (500 MHz, $CDCl_3$) of compound **574**. 868
Figure A14.11. Infrared spectrum (thin film/NaCl) of compound **574**. 869
Figure A14.12. ^{13}C NMR (126 MHz, $CDCl_3$) of compound **574**. 869
Figure A14.13. ^{1}H NMR (500 MHz, $CDCl_3$) of compound **581**. 870
Figure A14.14. Infrared spectrum (thin film/NaCl) of compound **581**. 871
Figure A14.15. ^{13}C NMR (126 MHz, $CDCl_3$) of compound **581**. 871
Figure A14.16. ^{1}H NMR (500 MHz, $CDCl_3$) of compound **582**. 872
Figure A14.17. Infrared spectrum (thin film/NaCl) of compound **582**. 873
Figure A14.18. ^{13}C NMR (126 MHz, $CDCl_3$) of compound **582**. 873
Figure A14.19. Infrared spectrum (thin film/NaCl) of compound **537**. 874
Figure A14.20. ^{1}H NMR (500 MHz, $CDCl_3$) of compound **540**. 875
Figure A14.21. Infrared spectrum (thin film/NaCl) of compound **540**. 876
Figure A14.22. ^{13}C NMR (126 MHz, $CDCl_3$) of compound **540**. 876
Figure A14.23. Infrared spectrum (thin film/NaCl) of compound **549**. 877
Figure A14.24. ^{1}H NMR (500 MHz, $CDCl_3$) of compound **499**. 878
Figure A14.25. Infrared spectrum (thin film/NaCl) of compound **499**. 879
Figure A14.26. ^{13}C NMR (126 MHz, $CDCl_3$) of compound **499**. 879
Figure A14.27. ^{1}H NMR (500 MHz, $CDCl_3$) of compound **503**. 880
Figure A14.28. Infrared spectrum (thin film/NaCl) of compound **503**. 881
Figure A14.29. ^{13}C NMR (126 MHz, $CDCl_3$) of compound **503**. 881
Figure A14.30. ^{1}H NMR (500 MHz, $CDCl_3$) of compound **504**. 882
Figure A14.31. Infrared spectrum (thin film/NaCl) of compound **504**. 883
Figure A14.32. ^{13}C NMR (126 MHz, $CDCl_3$) of compound **504**. 883
Figure A14.33. ^{1}H NMR (500 MHz, $CDCl_3$) of compound **505**. 884
Figure A14.34. Infrared spectrum (thin film/NaCl) of compound **505**. 885
Figure A14.35. ^{13}C NMR (126 MHz, $CDCl_3$) of compound **505**. 885
Figure A14.36. ^{1}H NMR (500 MHz, $CDCl_3$) of compound **506**. 886
Figure A14.37. Infrared spectrum (thin film/NaCl) of compound **506**. 887
Figure A14.38. ^{13}C NMR (126 MHz, $CDCl_3$) of compound **506**. 887

Figure A14.39. ^{1}H NMR (500 MHz, $CDCl_3$) of compound **507**..... 888
Figure A14.40. Infrared spectrum (thin film/NaCl) of compound **507**. 889
Figure A14.41. ^{13}C NMR (126 MHz, $CDCl_3$) of compound **507**..... 889
Figure A14.42. ^{1}H NMR (500 MHz, $CDCl_3$) of compound **508**..... 890
Figure A14.43. Infrared spectrum (thin film/NaCl) of compound **508**. 891
Figure A14.44. ^{13}C NMR (126 MHz, $CDCl_3$) of compound **508**..... 891
Figure A14.45. ^{1}H NMR (500 MHz, $CDCl_3$) of compound **509**..... 892
Figure A14.46. Infrared spectrum (thin film/NaCl) of compound **509**. 893
Figure A14.47. ^{13}C NMR (126 MHz, $CDCl_3$) of compound **509**..... 893
Figure A14.48. ^{1}H NMR (500 MHz, $CDCl_3$) of compound **510**..... 894
Figure A14.49. Infrared spectrum (thin film/NaCl) of compound **510**. 895
Figure A14.50. ^{13}C NMR (126 MHz, $CDCl_3$) of compound **510**..... 895
Figure A14.51. ^{1}H NMR (500 MHz, $CDCl_3$) of compound **511**..... 896
Figure A14.52. Infrared spectrum (thin film/NaCl) of compound **511**. 897
Figure A14.53. ^{13}C NMR (126 MHz, $CDCl_3$) of compound **511**..... 897
Figure A14.54. ^{1}H NMR (500 MHz, $CDCl_3$) of compound **512**..... 898
Figure A14.55. Infrared spectrum (thin film/NaCl) of compound **512**. 899
Figure A14.56. ^{13}C NMR (126 MHz, $CDCl_3$) of compound **512**..... 899
Figure A14.57. ^{1}H NMR (500 MHz, $CDCl_3$) of compound **513**..... 900
Figure A14.58. Infrared spectrum (thin film/NaCl) of compound **513**. 901
Figure A14.59. ^{13}C NMR (126 MHz, $CDCl_3$) of compound **513**..... 901
Figure A14.60. ^{1}H NMR (500 MHz, $CDCl_3$) of compound **514**..... 902
Figure A14.61. Infrared spectrum (thin film/NaCl) of compound **514**. 903
Figure A14.62. ^{13}C NMR (126 MHz, $CDCl_3$) of compound **514**..... 903
Figure A14.63. ^{1}H NMR (500 MHz, $CDCl_3$) of compound **515**..... 904
Figure A14.64. Infrared spectrum (thin film/NaCl) of compound **515**. 905
Figure A14.65. ^{13}C NMR (126 MHz, $CDCl_3$) of compound **515**..... 905
Figure A14.66. ^{1}H NMR (500 MHz, $CDCl_3$) of compound **516**..... 906
Figure A14.67. Infrared spectrum (thin film/NaCl) of compound **516**. 907
Figure A14.68. ^{13}C NMR (126 MHz, $CDCl_3$) of compound **516**..... 907
Figure A14.69. ^{1}H NMR (500 MHz, $CDCl_3$) of compound **(*S*)-546**. 908
Figure A14.70. Infrared spectrum (thin film/NaCl) of compound **(*S*)-546**..... 909
Figure A14.71. ^{13}C NMR (126 MHz, $CDCl_3$) of compound **(*S*)-546**. 909
Figure A14.72. ^{1}H NMR (500 MHz, $CDCl_3$) of compound **518**..... 910
Figure A14.73. Infrared spectrum (thin film/NaCl) of compound **518**. 911

Figure A14.74. ^{13}C NMR (126 MHz, $CDCl_3$) of compound **518**. 911
Figure A14.75. ^{1}H NMR (500 MHz, $CDCl_3$) of compound **519**. 912
Figure A14.76. Infrared spectrum (thin film/NaCl) of compound **519**. 913
Figure A14.77. ^{13}C NMR (126 MHz, $CDCl_3$) of compound **519**. 913
Figure A14.78. ^{1}H NMR (500 MHz, $CDCl_3$) of compound **522**. 914
Figure A14.79. Infrared spectrum (thin film/NaCl) of compound **522**. 915
Figure A14.80. ^{13}C NMR (126 MHz, $CDCl_3$) of compound **522**. 915
Figure A14.81. ^{1}H NMR (500 MHz, $CDCl_3$) of compound **523**. 916
Figure A14.82. Infrared spectrum (thin film/NaCl) of compound **523**. 917
Figure A14.83. ^{13}C NMR (126 MHz, $CDCl_3$) of compound **523**. 917
Figure A14.84. ^{1}H NMR (500 MHz, $CDCl_3$) of compound **524**. 918
Figure A14.85. Infrared spectrum (thin film/NaCl) of compound **524**. 919
Figure A14.86. ^{13}C NMR (126 MHz, $CDCl_3$) of compound **524**. 919
Figure A14.87. ^{1}H NMR (500 MHz, $CDCl_3$) of compound **525**. 920
Figure A14.88. Infrared spectrum (thin film/NaCl) of compound **525**. 921
Figure A14.89. ^{13}C NMR (126 MHz, $CDCl_3$) of compound **525**. 921
Figure A14.90. ^{1}H NMR (500 MHz, $CDCl_3$) of compound **530•HCl**. 922
Figure A14.91. Infrared spectrum (thin film/NaCl) of compound **530•HCl**. 923
Figure A14.92. ^{13}C NMR (126 MHz, $CDCl_3$) of compound **530•HCl**. 923
Figure A14.93. ^{1}H NMR (500 MHz, $CDCl_3$) of compound **531**. 924
Figure A14.94. Infrared spectrum (thin film/NaCl) of compound **531**. 925
Figure A14.95. ^{13}C NMR (126 MHz, $CDCl_3$) of compound **531**. 925
Figure A14.96. ^{1}H NMR (500 MHz, $CDCl_3$) of compound **532**. 926
Figure A14.97. Infrared spectrum (thin film/NaCl) of compound **532**. 927
Figure A14.98. ^{13}C NMR (126 MHz, $CDCl_3$) of compound **532**. 927
Figure A14.99. ^{1}H NMR (500 MHz, $CDCl_3$) of compound **533**. 928
Figure A14.100. Infrared spectrum (thin film/NaCl) of compound **533**. 929
Figure A14.101. ^{13}C NMR (126 MHz, $CDCl_3$) of compound **533**. 929
Figure A14.102. ^{1}H NMR (500 MHz, $CDCl_3$) of compound **534**. 930
Figure A14.103. Infrared spectrum (thin film/NaCl) of compound **534**. 931
Figure A14.104. ^{13}C NMR (126 MHz, $CDCl_3$) of compound **534**. 931
Figure A14.105. ^{1}H NMR (500 MHz, $CDCl_3$) of compound **536**. 932
Figure A14.106. Infrared spectrum (thin film/NaCl) of compound **536**. 933
Figure A14.107. ^{13}C NMR (126 MHz, $CDCl_3$) of compound **536**. 933
Figure A14.108. ^{1}H NMR (500 MHz, $CDCl_3$) of compound **538**. 934

Figure A14.109. Infrared spectrum (thin film/NaCl) of compound **538**. 935
Figure A14.110. ^{13}C NMR (126 MHz, $CDCl_3$) of compound **538**. 935
Figure A14.111. ^{1}H NMR (500 MHz, $CDCl_3$) of compound **541**. 936
Figure A14.112. Infrared spectrum (thin film/NaCl) of compound **541**. 937
Figure A14.113. ^{13}C NMR (126 MHz, $CDCl_3$) of compound **541**. 937
Figure A14.114. ^{1}H NMR (500 MHz, $CDCl_3$) of compound **542**. 938
Figure A14.115. Infrared spectrum (thin film/NaCl) of compound **542**. 939
Figure A14.116. ^{13}C NMR (126 MHz, $CDCl_3$) of compound **542**. 939
Figure A14.117. ^{1}H NMR (500 MHz, $CDCl_3$) of compound **544**. 940
Figure A14.118. Infrared spectrum (thin film/NaCl) of compound **544**. 941
Figure A14.119. ^{13}C NMR (126 MHz, $CDCl_3$) of compound **544**. 941
Figure A14.120. ^{1}H NMR (500 MHz, $CDCl_3$) of compound **590•HCl**. 942
Figure A14.121. Infrared spectrum (thin film/NaCl) of compound **590•HCl**. 943
Figure A14.122. ^{13}C NMR (126 MHz, $CDCl_3$) of compound **590•HCl**. 943
Figure A14.123. ^{1}H NMR (300 MHz, $CDCl_3$) of compound **550**. 944
Figure A14.124. Infrared spectrum (thin film/NaCl) of compound **550**. 945
Figure A14.125. ^{13}C NMR (126 MHz, $CDCl_3$) of compound **550**. 945
Figure A14.126. Infrared spectrum (thin film/NaCl) of compound **592**. 946
Figure A14.127. ^{1}H NMR (500 MHz, $CDCl_3$) of compound **593**. 947
Figure A14.128. Infrared spectrum (thin film/NaCl) of compound **593**. 948
Figure A14.129. ^{13}C NMR (126 MHz, $CDCl_3$) of compound **593**. 948
Figure A14.130. ^{1}H NMR (500 MHz, $CDCl_3$) of compound **(*S*)-552**. 949
Figure A14.131. Infrared spectrum (thin film/NaCl) of compound **(*S*)-552**. 950
Figure A14.132. ^{13}C NMR (126 MHz, $CDCl_3$) of compound **(*S*)-552**. 950

APPENDIX 15

X-Ray Crystallography Reports Relevant to Chapter 6

Figure A15.1. X-Ray Crystal Structure of Thiazolidine **(*S*)-522**. 952
Figure A15.2. X-Ray Crystal Structure of Thiazolidine **536**. 975
Figure A15.3. X-Ray Crystal Structure of Imidazolidinium **590•($ZnBr_3$•MeOH)**. 991
Figure A15.4. X-Ray Crystal Structure of Imidazolidine **550**. 1010
Figure A15.5. X-Ray Crystal Structure of Oxazolidine **591**. 1028

APPENDIX 16

Synthesis of Functionalized Thiouracils as G Protein-Coupled Receptor Agonists

Figure A16.1.1. Computationally-Validated Bitter Taste GPCR Agonists..... 1048

APPENDIX 17

Spectra Relevant to Appendix 16

Figure A17.1. ^{1}H NMR (400 MHz, $CDCl_3$) of compound **597**..... 1062

Figure A17.2. Infrared spectrum (thin film/NaCl) of compound **597**. 1063

Figure A17.3. ^{13}C NMR (101 MHz, $CDCl_3$) of compound **597**..... 1063

LIST OF SCHEMES

CHAPTER 1

Furanobutenolide Cembranoid and Norcembranoid Natural Products: Biosynthetic Connections and Synthetic Efforts

Scheme 1.4.1.1. Biosynthetic Proposal for the Construction of Bielschowskysin (BSK, **6**).....6

Scheme 1.4.1.2. Proposed Biosynthesis of Verrillin (**13**) 7

Scheme 1.4.1.3. Biosynthetic Speculation Concerning the Formation of Intricarene (**7**) 8

Scheme 1.4.1.4. Proposed Biosynthetic Construction of the Plumarellides and Mandapamates 9

Scheme 1.4.2.1. Proposed Biosynthesis of Ineleganolide (**9**), Horiolide (**20**), and Kavaranolide (**21**) .. 11

Scheme 1.4.2.2. Biosynthetic Formation of Sinulochmodin C (**10**), Scabrolide B (**23**), Scabrolide A (**24**), and Yonarolide (**25**) 12

Scheme 1.4.2.3. Biosynthetic Conjectures for the Formation of Dissectolide A (**22**) 13

Scheme 1.5.1.1.1. Retrosynthetic Analysis of BSK Employing Photo-Induced [2 + 2] 14

Scheme 1.5.1.1.2. Copper-Catalyzed Light-Induced [2 + 2] Cycloaddition (Ghosh) 15

Scheme 1.5.1.1.3. Tandem Inversion of Configuration at C(8) and C(10) with Core Cyclobutane **52** (Ghosh)..... 16

Scheme 1.5.1.1.4. Retrosynthetic Strategy Employed by Sulikowski 16

Scheme 1.5.1.1.5. Model System for Intramolecular Butenolide [2 + 2] Cycloaddition (Sulikowski) .. 17

Scheme 1.5.1.1.6. Intramolecular [2 + 2] Cycloaddition with Elaborated Butenolide (Sulikowski)..... 18

Scheme 1.5.1.1.7. Mulzer's Retrosynthesis of BSK Employing an Allene [2 + 2] Cycloaddition 18

Scheme 1.5.1.1.8. Allene [2 + 2] Cycloaddition (Mulzer)..... 19

Scheme 1.5.1.1.9. Unexpected Cyclooctane Product Formation (Mulzer)..... 19

Scheme 1.5.1.1.10. Nicolaou's Macrocyclic [2 + 2] Cycloaddition Strategy and Model Macrocycle Synthesis 20

Scheme 1.5.1.1.11. Stereochemical Outcome of Macrocyclic [2 + 2] Cycloaddition (Nicolaou)..... 21

Scheme 1.5.1.1.12. Lear's Macrocyclic Tandem [2 + 2] and [4 + 2] Cycloaddition Strategy..... 22

Scheme 1.5.1.1.13. Planned Tandem [2 + 2] and [4 + 2] Cycloaddition in the Forward Sense (Lear)..... 22

Scheme 1.5.1.1.14. Model System Studies on Allene Cycloaddition with a Butenolide (Lear)..... 23

Scheme 1.5.1.1.15. Model System Studies on Allene Cycloaddition with a Butenolide (Lear)..... 23

Scheme 1.5.1.1.16. Alternative Retrosynthetic Analysis of Cyclobutane Moiety of BSK (**6**, Mulzer) ... 24

Scheme 1.5.1.1.17. Limitations of Targeted [2 + 2] Cycloaddition (Mulzer) 25

Scheme 1.5.1.2.1. Mulzer's 3rd Generation Retrosynthetic Analysis of BSK (**6**) 25

Scheme 1.5.1.2.2. Advancement of Enantioenriched Cyclobutanol **(+)-92** Toward BSK (Mulzer) 26
Scheme 1.5.1.2.3. Stoltz's Retrosynthetic Analysis of BSK Core Scaffold **97** 27
Scheme 1.5.1.2.4. Synthesis and Exploration of Cyclopropane Intermediate **101** (Stoltz) 27
Scheme 1.5.2.1. Retrosynthetic Analysis of Verrillin (Theodorakis) 28
Scheme 1.5.2.2. Theodorakis' Synthetic Approach Toward Verrillin (**13**) 29
Scheme 1.5.3.1. Mehta's Retrosynthetic Analysis of Havellockate (**14**) 29
Scheme 1.5.3.2. Construction of the Havellockate Core (Mehta) 30
Scheme 1.5.3.3. Barriault's Retrosynthesis of Havellockate (**14**) 31
Scheme 1.5.3.4. Synthesis of Elaborated Core Tetracycle of Havellockate (**14**, Barriault) 32
Scheme 1.5.3.5. Scheme 1.5.3.5. Alternative Synthetic Approach
Toward Havellockate (**14**, Barriault) 33
Scheme 1.5.4.1. Proposed Biosynthesis of Intricarene (**7**) 33
Scheme 1.5.4.2. Synthesis of Common Intermediate Vinyl Iodide **137** (Pattenden and Trauner) 34
Scheme 1.5.4.3. Completion of the Asymmetric Total Synthesis of
Bipinnatin J (**26**, Pattenden and Trauner) 35
Scheme 1.5.4.4. Biomimetic Syntheses of Intricarene (**7**) from
Bipinnatin J (**26**, Pattenden and Trauner) 35
Scheme 1.5.5.1. Mehta's Retrosynthetic Analysis of Rameswaralide (**8**) 36
Scheme 1.5.5.2. Synthesis of Corey Lactone Derivative **151** (Mehta) 37
Scheme 1.5.5.3. Synthesis of Bicyclic Metathesis Substrates **153** and **154** (Mehta) 37
Scheme 1.5.5.4. Construction of the Rameswaralide Tricyclic Core (Mehta) 38
Scheme 1.5.5.5. Srikrishna's Proposed Construction of Two Rameswaralide
Cores from a Common Intermediate 38
Scheme 1.5.5.6. Synthesis of the [6,7]-Bicyclic Core of Rameswaralide (Srikrishna) 39
Scheme 1.5.5.7. Formation of the [5,7]-Bicyclic Core of Rameswaralide (Srikrishna) 39
Scheme 1.5.5.8. Trost's Retrosynthetic Approach Toward Rameswaralide Core **166** 40
Scheme 1.5.5.9. Trost's Construction of the Rameswaralide Tricyclic Scaffold (Trost) 41
Scheme 1.5.6.1. Substrates for Exploration of Proposed Biosynthesis (Pattenden) 42
Scheme 1.5.6.2. Synthesis of the Mandapamate and Rameswaralide Core Scaffolds (Pattenden) 43
Scheme 1.5.6.3. Formation of Rameswaralide Core from Diol **179** (Pattenden) 43
Scheme 1.5.6.4. Synthesis of Unexpected Novel Cembranoid Core (Pattenden) 44
Scheme 1.5.6.5. Alternative Proposal for Biosynthesis of Mandapamates and Plumarellides 45
Scheme 1.5.7.1. Retrosynthesis of Common Carbocyclic Core (Mehta) 45
Scheme 1.5.7.2. Synthesis of Macrocyclic Diene **195** (Mehta) 46
Scheme 1.5.7.3. Construction of Tricycle **202** by Diels–Alder Cycloaddition (Mehta) 47

Scheme 1.5.8.1. Retrosynthetic Analysis of Yonarolide (**25**, Ito) 47
Scheme 1.5.8.2. Diels–Alder Cycloaddition of Butenolide **206** (Ito) 48
Scheme 1.5.8.3. Synthesis of the Yonarolide Core by Tandem
Isomerization-Aldol Cyclization (Ito) 48
Scheme 1.5.9.1. Biomimetic Semisynthesis of Ineleganolide (**9**)
and Sinulochmodin C (**10**, Pattenden) 49
Scheme 1.5.9.2. Attempted Biomimetic Semisynthesis of Additional Norcembranoids (Pattenden) 50
Scheme 1.5.9.3. Vanderwal's Retrosynthetic Analysis of Ineleganolide (**9**) 50
Scheme 1.5.9.4. Synthesis of Enantioenriched Cyclopentenone **(+)218** (Vanderwal) 51
Scheme 1.5.9.5. Construction of Ketofurans **221** and **222** (Vanderwal) 51
Scheme 1.5.9.6. Completion of Tricyclic Coupling Partner (Vanderwal) 51
Scheme 1.5.9.7. Asymmetric Synthesis of Complimentary Cyclohexenone **(+)-213** (Vanderwal) 52
Scheme 1.5.9.8. Coupling of Ineleganolide Fragments (Vanderwal) 52
Scheme 1.5.9.9. Alternative Advancement Toward Ineleganolide (Vanderwal) 53

CHAPTER 2

Enantioselective Synthesis of a Hydroxymethyl-cis-1,3-cyclopentenediol Building Block

Scheme 2.2.1. Retrosynthetic Analysis of *cis*-1,3-Cyclopentenediol **241** 63
Scheme 2.3.1. Enantioselective Allylic Alkylation and Elaboration of
Cyclohexanone and Dioxanone Substrates 63
Scheme 2.4.1. Proposed Construction of Cyclopentenone **250** Using
Intramolecular Wittig Cyclization 64
Scheme 2.4.2. Construction of Enone **250** by Epoxidation of Chloroallylketone **254** 65
Scheme 2.4.3. Construction of Enone **250** by Oxidative Bromination of Chloroallylketone **254** 65
Scheme 2.4.4. Synthetic Route Enabled by the Crucial Choice of the Cyclohexyl Ketal Group 67
Scheme 2.5.1. Synthetic Advancement Toward the Desired Hydroxylmethyl-
cis-1,3-Cyclopentenediol Framework 69

APPENDIX 1

Synthetic Summary for Chapter 2

Scheme A1.1. Synthetic Summary for Construction of *cis*-1,3-Cyclopentenediol **262** 99

APPENDIX 3

Alternative Construction of Hydroxymethyl-cis-1,3-cyclopentenediol Building Block by Ring-Closing Metathesis

Scheme A3.1.1. Alternative Retrosynthetic Analysis of Hydroxymethyl-*cis*-1,3-cyclopentenediol Building Block **241**. 133
Scheme A3.2.1. Ketal Substrates for Exploration of Diastereoselective Addition. 133
Scheme A3.2.2. Synthesis of Diethyl Ketal Allylic Alkylation Product **291**. 134
Scheme A3.5.1. Ring-Closing Metathesis of Allyl Dioxanones. 137
Scheme A3.6.1. Attempted 1,3-Allylic Transposition of Bicyclic Acetonide **306**. 138
Scheme A3.6.2. Isomerization of Acetonide **306**. 138

CHAPTER 3

Progress Toward the Asymmetric Total Syntheses of the Furanobutenolide Norcembranoid Diterpene Natural Products

Scheme 3.1.1. Postulated Biosynthetic Conversion of Ineleganolide (**9**) to Kavaranolide (**21**)..... 173
Scheme 3.1.2. Postulated Biosynthetic and Proposed Synthetic Relationship of [7,6]-Norcembranoids 173
Scheme 3.2.1. Retrosynthetic Analysis of Ineleganolide (**9**) and Scabrolide A (**10**) 174
Scheme 3.2.2. Retrosynthetic Analysis of Divergent Tetracyclic Diol **314** 176
Scheme 3.3.1. Synthesis of Hydroxymethyl-1,3-cis-cyclopentenediol Building Block 177
Scheme 3.4.1. Completion of Building Blocks 178
Scheme 3.4.2. Fragment Coupling and Synthesis of Cyclopropanation Precursor 179
Scheme 3.4.3. Construction of Tetracycle **324** by Tandem Cyclopropanation-Cope Rearrangement 179
Scheme 3.4.4. Diastereoselective 1,2-Reduction of Enone Byproduct **325** 181
Scheme 3.5.1. Advancement of Diene **324** and Formation of Isoineleganolide A (**328**) 181
Scheme 3.5.2. Hypothesized Completion of Ineleganolide 182
Scheme 3.5.3. Isomerization of Isoineleganolide A (**328**) to Isoineleganolide B (**331**) 183
Scheme 3.6.1. Alternative Retrosynthetic Disconnection of Divergent Intermediate **314** 183
Scheme 3.6.2. Construction of Methyl Ketone **338** 184
Scheme 3.6.3. Advancement of Silyl Ether **338** 185
Scheme 3.6.4. Fragment Coupling with Methyl Ketone Diol ***ent*-335** 185
Scheme 3.6.5. Formation of Pyrazole **341** 186
Scheme 3.6.6. Attempted Stepwise Formation of ***ent*-316** from Diazoester **340** 186

Scheme 3.7.1. Originally Hypothesized Completion of ent-Ineleganolide (***ent*-9**) 187
Scheme 3.7.2. Reactivity of Isoineleganolide A (**328**) with $In(OTF)_3$ in Stabilized $CHCl_3$ 188
Scheme 3.7.3. Formation of Requisite 1,4-Diketone Oxidation Pattern 188
Scheme 3.7.4. Reductive Furan Opening 190
Scheme 3.7.5. Core Isomerization of Divergent Intermediate Diol **349** 191
Scheme 3.7.6. Selective Dehydration of Diol **349** 192
Scheme 3.7.7. Intended Completion of ent-Ineleganolide (***ent*-9**)
through Vinylogous Diketone **330** 192
Scheme 3.7.8. Attempted Functionalization of Isoineleganolide C (***ent*-313**) by C–H Oxidation 193
Scheme 3.8.1. Consideration of Three-Dimensional Structures of Late-Stage Intermediates 194

APPENDIX 5

Synthetic Summary for Chapter 3

Scheme A.5.1. Construction of cis-1,3-Cyclopentenediol ***ent*-322** 239
Scheme A.5.2. Construction of the Tetracyclic Core and Isomers of *ent*-Ineleganolide (***ent*-9**) 239
Scheme A.5.3. Synthesis of Alternative cis-1,3-Cyclopentenediol ***ent*-335** 240
Scheme A.5.4. Advancement of Methyl Ketone Fragment ***ent*-335** 240

APPENDIX 8

Alternative Synthetic Strategies Toward Ineleganolide

Scheme A.8.1.1. Synthesis of Acid ***ent*-321** Using Isopropyl Acetate 366
Scheme A.8.2.1. 1,3-Allylic Transposition of Alcohol **324** 369
Scheme A.8.3.1. Attempted 1,4-Reduction of Enone **324** with Wilkinson's Catalyst 369
Scheme A.8.3.2. Attempted Oxidation of Doubly Allylic C–H Bonds 369
Scheme A.8.4.1. Attempted Olefin Isomerization of Enone **328** 370
Scheme A.8.5.1. Nucleophilic Opening of Epoxide **328** 371
Scheme A.8.5.2. Nucleophilic Opening of Epoxide **328** with Halogen Ions 372
Scheme A.8.5.3. Kornblum Oxidation of Halogenated Furanopentacycles 373

CHAPTER 4

Revised Plan for the Synthesis of Ineleganolide: Alternative Advancement Toward the Asymmetric Total Synthesis of Ineleganolide by Late-Stage Oxidation State Manipulation

Scheme 4.1.1. Adapted Retrosynthetic Analysis of ent-Ineleganolide with Late-Stage Oxidation 409
Scheme 4.2.1. Conjugate Reduction of Diene **324** 409
Scheme 4.2.2. Unsuccessful Epoxide Rearrangement of Epoxide **371** 410
Scheme 4.2.3. Attempted Kornblum Oxidation of Epoxide **371** 410
Scheme 4.2.4. Sequential Reductive Epoxide Opening and Carbinol Oxidation 411
Scheme 4.2.5. Attempted C(5) Oxidation by C–H Activation 413
Scheme 4.2.6. Representative Reaction Conditions for Attempted C(4)–C(5) Oxidation 414
Scheme 4.2.7. Advancement of Tetracycle **372** by Diastereoselective C(3) Reduction 414
Scheme 4.3.1. Retrosynthetic Analysis of ent-Ineleganolide Employing a 1,2-Reduction 415
Scheme 4.4.1. 1,2-Reduction of Enone **328** 416
Scheme 4.4.2. Attempted Epoxide Rearrangement 416
Scheme 4.4.3. Silyl Ether Formation with Unexpected Olefin Isomerization 417
Scheme 4.4.4. Assessment of Configurational Stability of Unsaturated Lactone Moiety 417
Scheme 4.4.5. Reductive Epoxide Opening of Isomeric Silyl Ethers 418
Scheme 4.4.6. Silyl Enol Ether Formation from Ketone **397** 419
Scheme 4.4.7. Attempted Formation of TMS Enol Ether of Ketone **401** 419
Scheme 4.4.8. Lactol Formation 421
Scheme 4.4.9. Advancement of Lactol **403** 422
Scheme 4.5.1. Retrosynthetic Analysis of *ent*-Ineleganolide Employing Late-Stage Reduction 423
Scheme 4.6.1. Oxidation of 1,4-Diketone **347** 423
Scheme 4.6.2. Reduction of Vinylogous Diketone **412** 424
Scheme 4.6.3. Dienol Ether Formation 425
Scheme 4.6.4. Attempted Reductive Epoxide Opening of Disilyl Enol Ether of Enone **328** 425
Scheme 4.6.5. Attempted Reductive Epoxide Opening of Dienol Ether **416** 426
Scheme 4.6.6. Construction of α-Bromolactone **420** 426
Scheme 4.6.7. Oxidation of Isoineleganolide A (**328**) to Cycloheptadiene **422** 427
Scheme 4.6.8. Formation of Cycloheptatrienone **423** 428
Scheme 4.7.1. Redesigned Retrosynthetic Strategy Toward *ent*-Ineleganolide (***ent*-9**) 429
Scheme 4.8.1. Asymmetric Allylic Alkylation Stereoselectively Determines All Remaining Chiral Information 430

APPENDIX 9

Synthetic Summary for Chapter 4

Scheme A.9.1. Synthesis of 2*H*-Ineleganolide (**273**) Through Conjugate Reduction of Diene **324**... 484
Scheme A.9.2. Formation of Translactonized Polycycle **378** 484
Scheme A.9.3. 1,2-Reduction of Isoineleganolide A (**328**) and Subsequent Silyl Ether Formation with Concomitant Olefin Isomerization 484
Scheme A.9.4. Advancement of Isomeric Allylic Silyl Ether **389** and Unsaturated Lactone **390** 485
Scheme A.9.5. Construction and Transformation of Lactol **403** 485
Scheme A.9.6. Oxidative Desaturation of Isoineleganolide A (**328**)..... 485

CHAPTER 5

Lewis Acid Mediated (3+2) Cycloadditions of Donor–Acceptor Cyclopropanes with Heterocumulenes

Scheme 5.2.1. Substrate Scope of Isothiocyanate (3 + 2) Cycloaddition 610
Scheme 5.3.1. Structural Reassignment of Li's Aryl Isothiocyanate (3 + 2) Products 612
Scheme 5.4.1. Substrate Scope of Carbodiimide (3 + 2) Cycloaddition 613
Scheme 5.5.1. Substrate Scope of Isocyanate (3 + 2) Cycloaddition 614
Scheme 5.6.1. Investigations into the Stereochemical Outcome of the (3 + 2) Cycloaddition..... 615
Scheme 5.6.2. Proposed Mechanism for (3 + 2) Cycloaddition 616

CHAPTER 6

Stereoselective Lewis Acid Mediated (3 + 2) Cycloadditions of N-H- and N-Sulfonylaziridines with Heterocumulenes

Scheme 6.3.1. Substrate Scope of Isothiocyanate (3 + 2) Cycloadditions..... 778
Scheme 6.3.2. (3 + 2) Cycloaddition with 2-Alkylaziridine **517**..... 779
Scheme 6.5.1. Substrate Scope of Carbodiimide (3 + 2) Cycloaddition 780
Scheme 6.6.1. Diastereoselective (3 + 2) Cycloaddition with Aziridine **535**..... 781
Scheme 6.6.2. Diastereoselective (3 + 2) Cycloaddition with Aziridine **537**..... 781
Scheme 6.6.3. (3 + 2) Cycloaddition with Aziridine **540** 782
Scheme 6.8.1. Substrate Scope of Stereoselective Isothiocyanate (3 + 2) Cycloaddition..... 784
Scheme 6.10.1. Proposed General Reaction Mechanism for Stereoselective (3 + 2) Cycloaddition 786

Scheme 6.11.1. (3 + 2) Cycloaddition with Diester Aziridine **549** 786
Scheme 6.12.1. Desulfonylation and Deallylation of Iminothiazolidine Products..... 787

APPENDIX 16

Synthesis of Functionalized Thiouracils as G Protein-Coupled Receptor Agonists

Scheme A.16.2.1. Retrosynthetic Analaysis of PEGylated Thiouracil 1048
Scheme A.16.3.1. Saponification of Lactone **600**..... 1049
Scheme A.16.3.2. Attempted Condensation of Carboxylate Salt **601** onto Meldrum's Acid (**602**) 1049
Scheme A.16.3.3. β-Ketoester Formation from Carboxylate Salt **601** 1049
Scheme A.16.3.4. Synthetic Access to Alkyne **610** 1050
Scheme A.16.3.5. Construction of β-Ketoester **613**..... 1050
Scheme A.16.3.6. Thiouracil Formation..... 1051
Scheme A.16.3.7. Attempted PEGylation of Thiouracil **597** by Click Reaction 1051

LIST OF TABLES

APPENDIX 3

Alternative Construction of Hydroxymethyl-cis-1,3-cyclopentenediol Building Block by Ring-Closing Metathesis

Table A3.3.1. Enolization of Ketodioxanone **292** 135
Table A3.3.2. Attempted Deprotection of Undesired Kinetic Silyl Enol 135
Table A3.4.1. Effect of Ketal Identity on Diastereoselective Grignard Addition 136
Table A3.6.1. 1,3-Allylic Transposition of Vinyl Chloride **312** 139

APPENDIX 7

X-Ray Crystallography Reports Relevant to Chapter 3

Table A7.1.1. Experimental Details for X-Ray Structure Determination of Diene **324** 292
Table A7.1.2. Crystal Data and Structure Refinement for Diene **324** 293
Table A7.1.3. Atomic coordinates (x 10^4) and equivalent isotropic displacement parameters (Å^{2}x 10^3) for Diene **324** 294
Table A7.1.4. Bond lengths [Å] and angles [°] for Diene **324** 295
Table A7.1.5. Anisotropic displacement parameters (Å^{2}x10^3) for Diene **324** 300
Table A7.1.6. Hydrogen coordinates (x10^4) and isotropic displacement parameters (Å^{2}x10^3) for Diene **324** 301
Table A7.1.7. Torsion angles [°] for Diene **324** 302
Table A7.1.8. Hydrogen bonds for Diene **324** [Å and °]. 304
Table A7.2.1. Experimental Details for X-Ray Structure Determination of Isoineleganolide A (**328**) 306
Table A7.2.2. Crystal Data and Structure Refinement for Isoineleganolide A (**328**) 307
Table A7.2.3. Atomic coordinates (x 10^4) and equivalent isotropic displacement parameters (Å^{2}x 10^3) for Isoineleganolide A (**328**) 308
Table A7.2.4. Bond lengths [Å] and angles [°] for Isoineleganolide A (**328**) 309
Table A7.2.5. Anisotropic displacement parameters (Å^{2}x10^3) for Isoineleganolide A (**328**) 314
Table A7.2.6. Hydrogen coordinates (x10^4) and isotropic displacement parameters (Å^{2}x10^3) for Isoineleganolide A (**328**) 315
Table A7.2.7. Torsion angles [°] for Isoineleganolide A (**328**) 316
Table A7.2.8. Hydrogen bonds for Isoineleganolide A (**328**) [Å and °]. 319

Table A7.3.1. Experimental Details for X-Ray Structure Determination of Bromide **346** 321
Table A7.3.2. Crystal Data and Structure Refinement for Bromide **346** 322
Table A7.3.3. Atomic coordinates (x 10^4) and equivalent isotropic displacement parameters ($Å^2$x 10^3) for Bromide **346** 323
Table A7.3.4. Bond lengths [Å] and angles [°] for Bromide **346** 324
Table A7.3.5. Anisotropic displacement parameters ($Å^2$x10^3) for Bromide **346** 329
Table A7.3.6. Hydrogen coordinates (x10^4) and isotropic displacement parameters ($Å^2$x10^3) for Bromide **346** 330
Table A7.3.7. Torsion angles [°] for Bromide **346** 331
Table A7.3.8. Hydrogen bonds for Bromide **346** [Å and °]. 334
Table A7.4.1. Experimental Details for X-Ray Structure Determination of Diketone **347** 336
Table A7.4.2. Crystal Data and Structure Refinement for Diketone **347** 337
Table A7.4.3. Atomic coordinates (x 10^4) and equivalent isotropic displacement parameters ($Å^2$x 10^3) for Diketone **347** 338
Table A7.4.4. Bond lengths [Å] and angles [°] for Diketone **347** 339
Table A7.4.5. Anisotropic displacement parameters ($Å^2$x10^3) for Diketone **347** 344
Table A7.4.6. Hydrogen coordinates (x10^4) and isotropic displacement parameters ($Å^2$x10^3) for Diketone **347** 345
Table A7.4.7. Torsion angles [°] for Diketone **347** 346
Table A7.4.8. Hydrogen bonds for Diketone **347** [Å and °]. 349
Table A7.5.1. Experimental Details for X-Ray Structure Determination of Hemiketal **350** 351
Table A7.5.2. Crystal Data and Structure Refinement for Hemiketal **350** 352
Table A7.5.3. Atomic coordinates (x 10^4) and equivalent isotropic displacement parameters ($Å^2$x 10^3) for Hemiketal **350** 353
Table A7.5.4. Bond lengths [Å] and angles [°] for Hemiketal **350** 354
Table A7.5.5. Anisotropic displacement parameters ($Å^2$x10^3) for Hemiketal **350** 359
Table A7.5.6. Hydrogen coordinates (x10^4) and isotropic displacement parameters ($Å^2$x10^3) for Hemiketal **350** 360
Table A7.5.7. Torsion angles [°] for Hemiketal **350** 361
Table A7.5.8. Hydrogen bonds for Hemiketal **350** [Å and °] 364

APPENDIX 8

Alternative Synthetic Strategies Toward Ineleganolide

Table A8.2.1. Attempted Olefin Isomerization 368

Table A8.7.1.1. Experimental Details for X-Ray Structure Determination of Chloride **367** 377
Table A8.7.1.2. Crystal Data and Structure Refinement for Chloride **367** 378
Table A8.7.1.3. Atomic coordinates (x 10^4) and equivalent isotropic displacement parameters ($Å^2$x 10^3) for Chloride **367** 379
Table A8.7.1.4. Bond lengths [Å] and angles [°] for Chloride **367** 380
Table A8.7.1.5. Anisotropic displacement parameters ($Å^2$x10^3) for Chloride **367** 385
Table A8.7.1.6. Hydrogen coordinates (x10^4) and isotropic displacement parameters ($Å^2$x10^3) for Chloride **367** 386
Table A8.7.1.7. Torsion angles [°] for Chloride **367** 387
Table A8.7.1.8. Hydrogen bonds for Chloride **367** [Å and °]. 390
Table A8.7.2.1. Experimental Details for X-Ray Structure Determination of Fluoride **369** 392
Table A8.7.2.2. Crystal Data and Structure Refinement for Fluoride **369** 393
Table A8.7.2.3. Atomic coordinates (x 10^4) and equivalent isotropic displacement parameters ($Å^2$x 10^3) for Fluoride **369** 394
Table A8.7.2.4. Bond lengths [Å] and angles [°] for Fluoride **369** 395
Table A8.7.2.5. Anisotropic displacement parameters ($Å^2$x10^3) for Fluoride **369** 400
Table A8.7.2.6. Hydrogen coordinates (x10^4) and isotropic displacement parameters ($Å^2$x10^3) for Fluoride **369** 401
Table A8.7.2.7. Torsion angles [°] for Fluoride **369** 402
Table A8.7.2.8. Hydrogen bonds for Fluoride **369** [Å and °] 405

CHAPTER 4

Revised Plan for the Synthesis of Ineleganolide: Alternative Advancement Toward the Asymmetric Total Synthesis of Ineleganolide by Late-Stage Oxidation State Manipulation

Table 4.6.1. Comparison of ^{13}C NMR Shifts of Enone **328** and Diene **422** 427

APPENDIX 11

X-Ray Crystallography Reports Relevant to Chapter 4

Table A11.1.1. Experimental Details for X-Ray Structure Determination of Epoxide **371** 556
Table A11.1.2. Crystal Data and Structure Refinement for Epoxide **371** 557
Table A11.1.3. Atomic coordinates (x 10^4) and equivalent isotropic displacement parameters ($Å^2$x 10^3) for Epoxide **371** 558

Table A11.1.4. Bond lengths [Å] and angles [°] for Epoxide **371** 559
Table A11.1.5. Anisotropic displacement parameters ($Å^2x10^3$) for Epoxide **371** 564
Table A11.1.6. Hydrogen coordinates ($x10^4$) and isotropic displacement parameters ($Å^2x10^3$) for Epoxide **371** 565
Table A11.1.7. Torsion angles [°] for Epoxide **371** 566
Table A11.1.8. Hydrogen bonds for Epoxide **371** [Å and °]. 569
Table A11.2.1. Experimental Details for X-Ray Structure Determination of 2*H*-Ineleganolide (**373**) 571
Table A11.2.2. Crystal Data and Structure Refinement for 2*H*-Ineleganolide (**373**) 572
Table A11.2.3. Atomic coordinates ($x\ 10^4$) and equivalent isotropic displacement parameters ($Å^2x\ 10^3$) for 2*H*-Ineleganolide (**373**) 573
Table A11.2.4. Bond lengths [Å] and angles [°] for 2*H*-Ineleganolide (**373**) 575
Table A11.2.5. Anisotropic displacement parameters ($Å^2x10^3$) for 2*H*-Ineleganolide (**373**) 585
Table A11.2.6. Hydrogen coordinates ($x10^4$) and isotropic displacement parameters ($Å^2x10^3$) for 2*H*-Ineleganolide (**373**) 587
Table A11.2.7. Torsion angles [°] for 2*H*-Ineleganolide (**373**) 589
Table A11.2.8. Hydrogen bonds for 2*H*-Ineleganolide (**373**) [Å and °]. 593
Table A11.3.1. Experimental Details for X-Ray Structure Determination of Diketone **375** 595
Table A11.3.2. Crystal Data and Structure Refinement for Diketone **375** 596
Table A11.3.3. Atomic coordinates ($x\ 10^4$) and equivalent isotropic displacement parameters ($Å^2x\ 10^3$) for Diketone **375** 597
Table A11.3.4. Bond lengths [Å] and angles [°] for Diketone **375** 598
Table A11.3.5. Anisotropic displacement parameters ($Å^2x10^3$) for Diketone **375** 603
Table A11.3.6. Hydrogen coordinates ($x10^4$) and isotropic displacement parameters ($Å^2x10^3$) for Diketone **375** 604
Table A11.3.7. Torsion angles [°] for Diketone **375** 605
Table A11.3.8. Hydrogen bonds for Diketone **375** [Å and °]. 607

APPENDIX 13

X-Ray Crystallography Reports Relevant to Chapter 5

Table A13.1.1. Crystal Data and Structure Refinement for Thioimidate **440** 714
Table A13.1.2. Atomic coordinates ($x\ 10^4$) and equivalent isotropic displacement parameters ($Å^2x\ 10^3$) for Thioimidate Thioimidate **440** 716
Table A13.1.3. Bond lengths [Å] and angles [°] for Thioimidate **440** 717
Table A13.1.4. Anisotropic displacement parameters ($Å^2x10^3$) for Thioimidate **440** 722

Table A13.1.5. Hydrogen coordinates (x10^3) and isotropic displacement parameters (Å^{2}x10^3) for Thioimidate **440** 723
Table A13.2.1. Crystal Data and Structure Refinement for Amidine **(*R*)-450•HBr** 725
Table A13.2.2. Atomic coordinates (x 10^4) and equivalent isotropic displacement parameters (Å^{2}x 10^3) for Amidine **(*R*)- 450•HBr** 727
Table A13.2.3. Bond lengths [Å] and angles [°] for Amidine **(*R*)- 450•HBr** 733
Table A13.2.4. Anisotropic displacement parameters (Å^{2}x10^3) for Amidine **(*R*)- 450•HBr** 762
Table A13.2.5. Hydrogen coordinates (x10^3) and isotropic displacement parameters (Å^{2}x10^3) for Amidine **(*R*)- 450•HBr** 768

CHAPTER 6

Stereoselective Lewis Acid Mediated (3 + 2) Cycloadditions of N-H- and N-Sulfonylaziridines with Heterocumulenes

Table 6.2.1. Optimization of Reaction Conditions 776
Table 6.4.1. *N*-Substitution Scope of Isothiocyanate (3 + 2) Cycloaddition 779
Table 6.7.1. Optimization of Stereoselective Reaction Conditions 783
Table 6.9.1. N-Substitution Scope of Stereoselective Isothiocyanate (3 + 2) Cycloaddition 785

APPENDIX 15

X-Ray Crystallography Reports Relevant to Chapter 6

Table A15.1.1. Experimental Details for X-Ray Structure Determination of Thiazolidine **(*S*)-522** 953
Table A15.1.2. Crystal Data and Structure Refinement for Thiazolidine **(*S*)-522** 953
Table A15.1.3. Atomic coordinates (x 10^4) and equivalent isotropic displacement parameters (Å^{2}x 10^3) for Thioimidate Thiazolidine **(*S*)-522** 955
Table A15.1.4. Bond lengths [Å] and angles [°] for Thiazolidine **(*S*)-522** 958
Table A15.1.5. Anisotropic displacement parameters (Å^{2}x10^3) for Thiazolidine **(*S*)-522** 970
Table A15.1.6. Hydrogen coordinates (x10^3) and isotropic displacement parameters (Å^{2}x10^3) for Thiazolidine **(*S*)-522** 973
Table A15.2.1. Experimental Details for X-Ray Structure Determination of Thiazolidine **536** 976
Table A15.2.2. Crystal Data and Structure Refinement for Thiazolidine **536** 977
Table A15.2.3. Atomic coordinates (x 10^4) and equivalent isotropic displacement parameters (Å^{2}x 10^3) for Thioimidate Thiazolidine **536** 978
Table A15.2.4. Bond lengths [Å] and angles [°] for Thiazolidine **536** 980

Table A15.2.5. Anisotropic displacement parameters ($Å^2x10^3$) for Thiazolidine **536** 987
Table A15.2.6. Hydrogen coordinates ($x10^4$) and isotropic displacement parameters ($Å^2x10^3$) for Thiazolidine **536** 989
Table A15.3.1. Experimental Details for X-Ray Structure Determination of Imidazolidinium **590•($ZnBr_3$•MeOH)** 992
Table A15.3.2. Crystal Data and Structure Refinement for Imidazolidinium **590•($ZnBr_3$•MeOH)** 993
Table A15.3.3. Atomic coordinates ($x\ 10^4$) and equivalent isotropic displacement parameters ($Å^2x\ 10^3$) for Thioimidate Imidazolidinium **590•($ZnBr_3$•MeOH)** 995
Table A15.3.4. Bond lengths [Å] and angles [°] for Imidazolidinium **590•($ZnBr_3$•MeOH)** 997
Table A15.3.5. Anisotropic displacement parameters ($Å^2x10^3$) for Imidazolidinium **590•($ZnBr_3$•MeOH)** 1005
Table A15.3.6. Hydrogen coordinates ($x10^4$) and isotropic displacement parameters ($Å^2x10^3$) for Imidazolidinium **590•($ZnBr_3$•MeOH)** 1007
Table A15.3.7. Hydrogen bonds for Imidazolidinium **590•($ZnBr_3$•MeOH)** [Å and °]. 1009
Table A15.4.1. Experimental Details for X-Ray Structure Determination of Imidazolidine **550** 1011
Table A15.4.2. Crystal Data and Structure Refinement for Imidazolidine **550** 1012
Table A15.4.3. Atomic coordinates ($x\ 10^4$) and equivalent isotropic displacement parameters ($Å^2x\ 10^3$) for Thioimidate Imidazolidine **550** 1013
Table A15.4.4. Bond lengths [Å] and angles [°] for Imidazolidine **550** 1015
Table A15.4.5. Anisotropic displacement parameters ($Å^2x10^3$) for Imidazolidine **550** 1024
Table A15.4.6. Hydrogen coordinates ($x10^4$) and isotropic displacement parameters ($Å^2x10^3$) for Imidazolidine **550** 1026
Table A15.5.1. Experimental Details for X-Ray Structure Determination of Oxazolidine **591** 1029
Table A15.5.2. Crystal Data and Structure Refinement for Oxazolidine **591** 1030
Table A15.5.3. Atomic coordinates ($x\ 10^4$) and equivalent isotropic displacement parameters ($Å^2x\ 10^3$) for Thioimidate Oxazolidine **591** 1032
Table A15.5.4. Bond lengths [Å] and angles [°] for Oxazolidine **591** 1034
Table A15.5.5. Anisotropic displacement parameters ($Å^2x10^3$) for Oxazolidine **591** 1043
Table A15.5.6. Hydrogen coordinates ($x10^4$) and isotropic displacement parameters ($Å^2x10^3$) for Oxazolidine **591** 1045

APPENDIX 18

Notebook Cross-Reference for New Compounds

Table A18.2.1. Notebook Cross-Reference for Compounds in Chapter 2 1065
Table A18.2.2. Notebook Cross-Reference for Compounds in Appendix 3..... 1066
Table A18.2.3. Notebook Cross-Reference for Compounds in Chapter 3 1067
Table A18.2.4. Notebook Cross-Reference for Compounds in Chapter 4 1068
Table A18.2.5. Notebook Cross-Reference for Compounds in Chapter 5 1070
Table A18.2.6. Notebook Cross-Reference for Compounds in Chapter 6 1072
Table A18.2.7. Notebook Cross-Reference for Compounds in Appendix 16..... 1074

LIST OF ABBREVIATIONS

Å	Ångstrom
λ	wavelength
μ	micro
μwaves	microwave irradiation
$[\alpha]_D$	specific rotation at wavelength of sodium D line
[H]	reduction
[O]	oxidation
°C	degrees Celsius
Ac	acetyl
acac	acetylacetonate
AcOH	acetic acid
APCI	atmospheric pressure chemical ionization
app	apparent
aq	aqueous
Ar	aryl
atm	atmosphere
B3LYP	3-parameter hybrid Becke exchange/ Lee–Yang–Parr correlation functional
Bn	benzyl
Boc	*tert*-butyloxycarbonyl
bp	boiling point
br	broad
Bu	butyl
Bz	benzoyl

c	concentration for specific rotation measurements
ca.	about (Latin circa)
calc'd	calculated
cat	catalytic
CCDC	Cambridge Crystallographic Data Centre
CDI	1,1'-carbonyldiimidazole
cf.	compare (Latin confer)
CI	chemical ionization
cm^{-1}	wavenumber(s)
cod	1,5-cyclooctadiene
comp	complex
Cp	cyclopentadienyl
Cy	cyclohexyl
d	doublet
D	deuterium
dba	dibenzylideneacetone
DBU	1,8-diazabicyclo[5.4.0]undec-7-ene
DCE	1,2-dichloroethane
DDQ	2,3-dichloro-5,6-dicyano-*p*-benzoquinone
dec	decomposition
DFT	density functional theory
DIBAL	diisobutylaluminum hydride
DMA	*N*,*N*-dimethylacetamide
DMAD	dimethyl acetylenedicarboxylate
DMAP	4-dimethylaminopyridine
dmdba	bis(3,5-dimethoxybenzylidene)acetone
DMDO	dimethyldioxirane

DME	1,2-dimethoxyethane
DMF	*N*,*N*-dimethylformamide
DMP	Dess–Martin periodinane
DMSO	dimethyl sulfoxide
dr	diastereomeric ratio
e.g.	for example (Latin exempli gratia)
E_A	activation energy
EC_{50}	median effective concentration (50%)
EDC	*N*-(3-dimethylaminopropyl)-*N*'-ethylcarbodiimide
ee	enantiomeric excess
EI+	electron impact
equiv	equivalent
ESI	electrospray ionization
Et	ethyl
EtOAc	ethyl acetate
FAB	fast atom bombardment
FID	flame ionization detector
g	gram(s)
GC	gas chromatography
gCOSY	gradient-selected correlation spectroscopy
h	hour(s)
$h\nu$	light
HBPin	4,4,5,5-tetramethyl-1,3,2-dioxaborolane; pinacolborane
HFIP	1,1,1,3,3,3-hexafluoro-2-propanol
HMDS	1,1,1,3,3,3-hexamethyldisilazane
HMPA	hexamethylphosphoramide
HPLC	high-performance liquid chromatography

HRMS	high-resolution mass spectroscopy
Hz	hertz
i.e.	that is (Latin id est)
IBX	2-iodoxybenzoic acid
IC_{50}	median inhibition concentration (50%)
IMDA	Intramolecular Diels–Alder reaction
IPA	isopropanol, 2-propanol
i-Pr	isopropyl
IR	infrared (spectroscopy)
IRC	intrinsic reaction coordinate
J	coupling constant
K	Kelvin(s) (absolute temperature)
kcal	kilocalorie
KHMDS	potassium hexamethyldisilazide
L	liter; ligand
LDA	lithium diisopropylamide
lit.	literature value
m	multiplet; milli
m	meta
M	metal; molar; molecular ion
m/*z*	mass to charge ratio
m-CPBA	*meta*-chloroperoxybenzoic acid
Me	methyl
mg	milligram(s)
MHz	megahertz
min	minute(s)
MM	mixed method

MMPP	magnesium monoperoxyphthalate
mol	mole(s)
MOM	methoxymethyl
mp	melting point
Ms	methanesulfonyl (mesyl)
MS	molecular sieves
MVK	methyl vinyl ketone
n	nano
N	normal
nbd	norbornadiene
NBS	*N*-bromosuccinimide
n-Bu	butyl
NMO	*N*-methylmorpholine *N*-oxide
NMR	nuclear magnetic resonance
NOE	nuclear Overhauser effect
NOESY	nuclear Overhauser enhancement spectroscopy
Nosyl	nitrobenzenesulfonyl
Nu	nucleophile
o	ortho
p	para
PCC	pyridinium chlorochromate
Pd/C	palladium on carbon
PDC	pyridinium dichromate
Ph	phenyl
pH	hydrogen ion concentration in aqueous solution
PHOX	phosphinooxazoline ligand
Piv	pivaloyl

p*Ka*	p*K* for association of an acid
pmdba	bis(4-methoxybenzylidene)acetone
ppm	parts per million
PPTS	pyridinium *p*-toluenesulfonate
Pr	propyl
PTU	*n*-Propylthiouracil
Py	pyridine
q	quartet
R	generic for any atom or functional group
Ref.	reference
R_f	retention factor
s	singlet or strong or selectivity factor
sat.	saturated
Selectfluor	1-chloromethyl-4-fluoro-1,4-diazoniabicyclo[2.2.2]octane bis(tetrafluoroborate)
SFC	supercritical fluid chromatography
S_N2	second-order nucleophilic substitution
S_N2'	nucleophilic substitution with allylic rearrangement
sp	sparteine
sp.	species
t	triplet
TBAF	tetrabutylammonium fluoride
TBAI	tetrabutylammonium iodide
TBAT	tetrabutylammonium difluorotriphenylsilicate
TBDPS	*tert*-butyldiphenylsilyl
TBHP	*tert*-butyl hydroperoxide

TBME	*tert*-butyl methyl ether
TBS	*tert*-butyldimethylsilyl
t-Bu	*tert*-butyl
TES	triethylsilyl
Tf	trifluoromethanesulfonyl (triflyl)
TFA	trifluoroacetic acid
TFAA	trifluoroacetic anhydride
TFE	2,2,2-trifluoroethanol
THF	tetrahydrofuran
TIPS	triisopropylsilyl
TLC	thin-layer chromatography
TMEDA	*N*,*N*,*N'*,*N'*-tetramethylethylenediamine
TMS	trimethylsilyl
TOF	time-of-flight
Tol	tolyl
t_R	retention time
Ts	*p*-toluenesulfonyl (tosyl)
UV	ultraviolet
v/*v*	volume to volume
$VO(acac)_2$	vanadyl acetoacetonate
w	weak
w/*v*	weight to volume
X	anionic ligand or halide

CHAPTER 1

Furanobutenolide Cembranoid and Norcembranoid Natural Products: Biosynthetic Connections and Synthetic Efforts

1.1 Introduction

The cembranoid natural products are a vast family of marine and terrestrial diterpene natural products found throughout the world. This structurally diverse and highly oxygenated class of metabolites is produced in vast numbers by an array of gorgonian octocorals and soft coral species. Considering the relatively few marine fauna that prey upon gorgonian and soft corals, it has been hypothesized that marine cembranoids serve to defend against competing and/or predatory organisms.[1] Indeed, the isolation and investigation of the biological activity of cembranoids has led to the discovery of a vast range of structurally diverse, biologically active compounds possessing potent cytotoxicity.[2]

Among the most biologically active members of the cembranoids is the subclass of furanobutenolides, including the macrocyclic furanobutenolide C_{20}-cembranoids lophotoxin (**1**), bipinnatin D (**2**), and bipinnatin I (**3**) as well as the C_{19}-norcembranoids

sinuleptolide (**4**) and 5-episinuleptolide (**5**, Figure 1.1.1). Lophotoxin is a potent neurotoxin, functioning as an irreversible antagonist of the nicotinic acetylcholine receptor.[3] Alternatively, bipinnatin D (**2**) is active against P-388 murine leukemia in vitro[4] and bipinnatin I (**3**) is strongly cytotoxic (μM GI_{50}) against a variety of cancer cell lines including variants of melanoma and colon cancer.[5] The norcembranoids sinuleptolide (**4**) and 5-episinuleptolide (**5**) also possess antitumor and cytotoxic properties toward human KB human oral epidermoid cells, Hepa59T/VGH human liver carcinoma cells, and a panel of squamous cell carcinomas (μM IC_{50}).[6]

Figure 1.1.1. Characteristic Macrocyclic Furanobutenolide Cembranoids and Norcembranoids

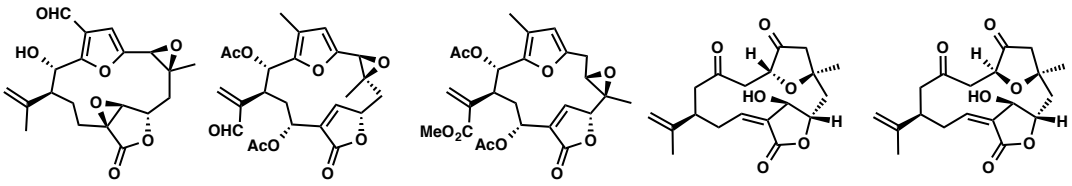

Among the vast numbers of macrocyclic furanobutenolides are a small subset of congested, stereochemically complex, and extensively oxygenated polycyclic diterpenes and norditerpenes (Figure 1.1.2). Example polycyclic diterpenes include bielschowskysin (BSK, **6**), the cytotoxic cyclobutanoid that is highly active against EKVX nonsmall cell lung cancer (GI_{50} < 0.01 μM),[7] as well as the mildly cytotoxic intricarene (**7**)[8] and rameswaralide (**8**).[9] The polycyclic norcembranoid diterpenes are highlighted by the antileukemic ineleganolide (**9**)[10] and the isomeric sinulochmodin C (**10**),[11] which are both highly compact, cycloheptanone-derived ketofurans. The beauty and complexity of these structures, paired with their pertinent and variable bioactivity, has and continues to entice synthetic chemists to pursue their syntheses and further explore the biological activities of these scarce natural products.

Figure 1.1.2. Characteristic Polycyclic Furanobutenolide Cembranoids and Norcembranoids

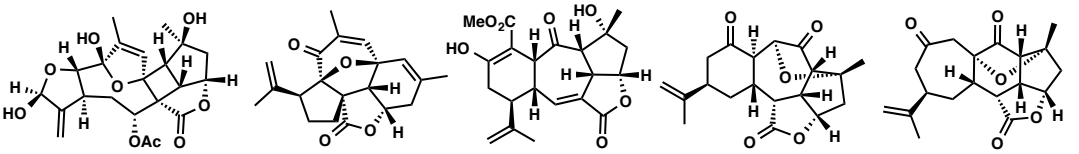

Bielschowskysin (BSK, 6) ***Intricarene (7)*** ***Rameswaralide (8)*** ***Ineleganolide (9)*** ***Sinulochmodin C (10)***

1.2 Statement of Purpose

The purpose of this review is not to present a comprehensive catalog of the literature surrounding the cembranoid family of natural products.[12] A tremendous amount of research has been performed previously by Trauner[13] and Pattenden,[1a,14] among others,[2c,15] to compile a series of scholarly works covering the known members of the cembranoid natural products, their biological activity, and the elaborate details of their biosynthetic relationships. Rather, the focus of this chapter will be on the polycyclic furanobutenolide members of the cembranoid natural product family and the array of approaches taken toward their syntheses. Including semisynthetic studies and de novo synthetic efforts, we have gathered this body of knowledge to gain insight into the reactivity and constraints of these compact and highly oxygenated polycyclic structures.

1.3 Polycyclic Furanobutenolide Cembranoids and Norcembranoids

The polycyclic furanobutenolide natural products can be separated into two categories: cembranoid and norcembranoid (Figure 1.3.1). The former is derived from macrocyclic furanobutenolide scaffold **11**, which is derived from the linear tetraisoprene geranylgeranyl diphosphate and has retained all 20 carbons.[1a] Comparatively, the norcembranoid furanobutenolide natural products are based on macrocyclic lactone precursors related to furan **12**, which contains only 19 carbons. It has been postulated that the loss of C(18) in vivo typically occurs by oxidation and subsequent hydrolysis.[1a]

The absolute stereochemistry of the polycyclic cembranoids is biosynthetically derived from oxygenated derivatives of scaffolds **11** and **12**, which contain the isopropenyl and butenolide groups in the C(1)-(*R*)- and C(10)-(*S*)-configurations, respectively, as drawn.[11,16]

Figure 1.3.1. Cembranoid and Norcembranoid Macrocyclic Scaffolds

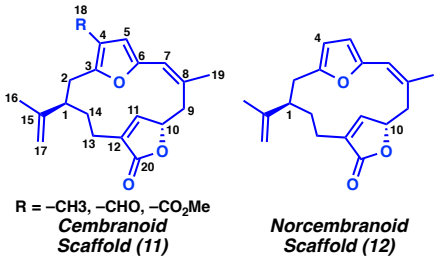

There are 10 polycyclic furanobutenolide cembranoids, including macrocycles BSK (**6**) and verrillin (**13**), polycycles intricarene (**7**), rameswaralide (**8**), havellockate (**14**), and the closely related plumarellides and mandapamates (**15**–**19**, Figure 1.3.2). Decorated by a variety of oxygenation states and patterns, these furanobutenolide diterpenes display a variety of complex, highly compact, stereochemically dense architectures. In a similar fashion, the biosynthetically related furanobutenolide norcembranoids include ineleganolide (**9**), horiolide (**20**), kavaranolide (**21**) all possess a central heptacycle. In comparison, the remaining members of the polycyclic furanobutenolide norcembranoids dissectolide (**22**), sinulochmodin C (**10**), scabrolide B (**23**), scabrolide A (**24**), and yonarolide (**25**) are all constructed around a central 6-membered carbocycle with a cycloheptanone ring decorating the peripheral structure.

Figure 1.3.2. Polycyclic Cembranoid Furanobutenolide Natural Products

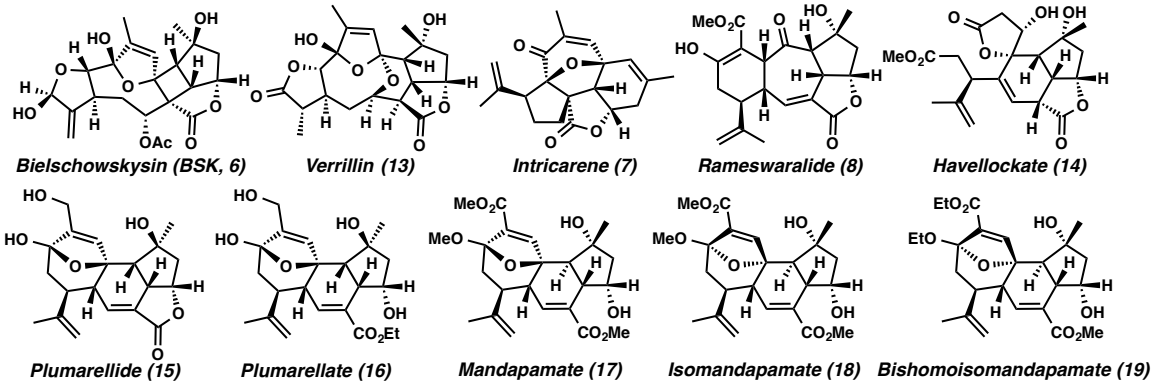

Figure 1.3.3. Polycyclic Norcembranoid Furanobutenolide Natural Products

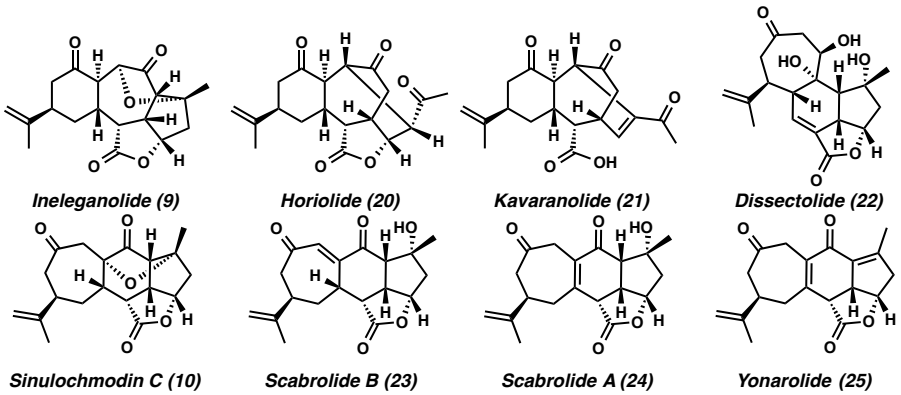

1.4 Brief Summary of Biosynthetic Connections

Despite the breadth of complexity found within the family of polycyclic furanobutenolide diterpenes and norditerpenes, these natural products are typically co-isolated with (and hypothesized to be derived from) the more simplified furanobutenolide macrocycles. Before discussing synthetic strategies, it is critical to establish the context of the interconnected nature of these polycycles derived from the postulated biosynthetic routes. While the comprehensive review of the biosynthesis of the cembranoid and norcembranoid natural products can be found elsewhere,[1a,13,14,15] a brief overview of postulated biosynthetic routes to these molecules is presented before exploring the in vitro approaches toward the same targets.

1.4.1 Biosynthesis of Polycyclic Furanobutenolide Cembranoids

Bielschowskysin (BSK, **6**) is a rare cyclobutane-containing cembranoid that is highly biologically active, showing excellent cytotoxicity against EKVX nonsmall cell lung cancer (GI_{50} < 0.01 μM) and CAKI-1 renal cancer (GI_{50} = 0.51 μM) as well as antiplasmodial activity.[7] The majority of synthetic efforts toward entry into the polycyclic cembranoids have focused on the synthesis of BSK, owing the attention to its unique carbocyclic scaffold paired with its bioactivity profile (vida supra). Biosynthetically, BSK is believed to be derived from bipinnatin J (**26**, Scheme 1.4.1.1).[1a,13] Oxidation at C(13) and C(16) followed by intramolecular lactolization would provide acetate **27**. Oxidation of the $\Delta_{7,8}$ bond would afford epoxide **28** and subsequent doubly vinylogous transposition across the furan ring would furnish hydroxyfuran **29**. Butenolide **29** is then positioned to undergo a light-induced [2 + 2] cycloaddition to construct the characteristic cyclobutane ring and complete BSK (**6**).

*Scheme 1.4.1.1. Biosynthetic Proposal for the Construction of Bielschowskysin (BSK, **6**)*

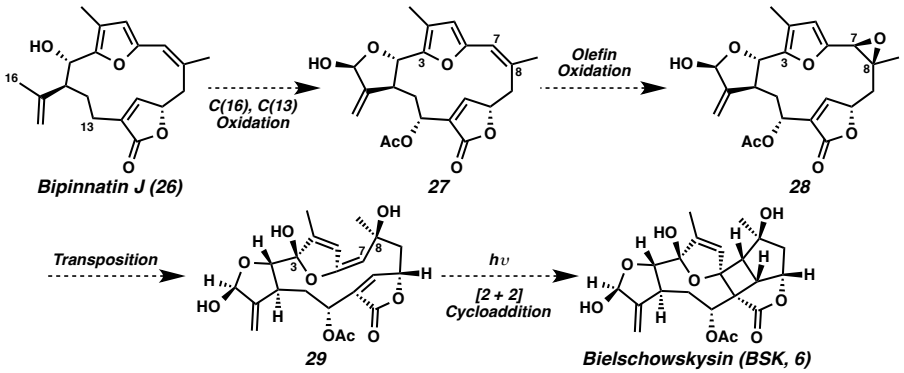

The furanobutenolide verrillin (**13**),[17] similarly based around a central ether-bridged macrocycle, is also likely derived from bipinnatin J (**26**, Scheme 1.4.1.2).[1a,13] Alternative oxidation of butenolide **26** would not only oxidizes C(13) and the isopropenyl group, but also set the epimeric stereochemistry at C(8) compared to BSK and accomplish the

oxidative opening of the furan ring. Intramolecular Michael addition within vinylogous diketone **30** would construct the C(7)–C(11) bond, furnishing polycycle **31** after transposition of the acetate group to reveal an oxyanion at C(13). Ultimately, sequential ketalization of diol **31** through the vinylogous diketone system and hydrolysis of the enol acetate moiety would provide verrillin (**13**).

*Scheme 1.4.1.2. Biosynthesis of Verrillin (**13**)*

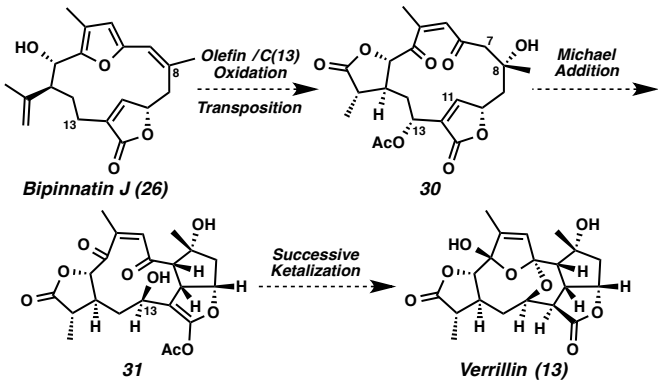

Bipinnatin J also likely serves as the biosynthetic precursor for the contrasting pentacyclic cytotoxic cembranoid intricarene (**7**).[1a,8,13,18] Oxidative cleavage of the furan ring affords homoallylic alcohol **32** (Scheme 1.4.1.3). Equilibration of alcohol **32** through hemiketal **33** would access oxocarbenium **34**. The charge separated aromatic ring within macrocycle **34** is proposed to participate in an intramolecular [5 + 2] cycloaddition, forming the furan-bridged cycloheptenone ring and completing the biosynthesis of intricarene (**7**).

*Scheme 1.4.1.3. Biosynthetic Speculation Concerning the Formation of Intricarene (**7**)*

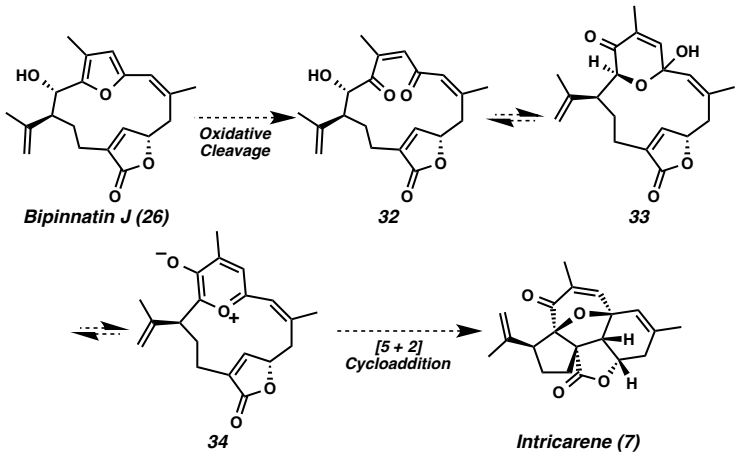

Bipinnatin J (**26**), however, is not the progenitor of every polycyclic cembranoid. Macrocycle **35**, which in comparison to bipinnatin J is oxidized at C(18) rather than C(2) and has an extra unit of unsaturation between C(13) and C(14), is the proposed precursor to the hemolytic cembranoids plumarellide (**15**) and plumarellate (**16**, Scheme 1.4.1.4.A).[1a,13,19] Oxidation across the $\Delta_{7,8}$ bond followed by olefin transposition would afford intermediate hemiketal **36**. Diene **36** could proceed through an intramolecular [4 + 2] cycloaddition with the transannular enol moiety to construct the central cyclohexene ring and complete plumarellide (**15**). Ethanolysis of the lactone by ethanol would provide the tetracyclic derivative plumarellate (**16**).

Scheme 1.4.1.4. Proposed Biosynthetic Construction of the Plumarellides and Mandapamates

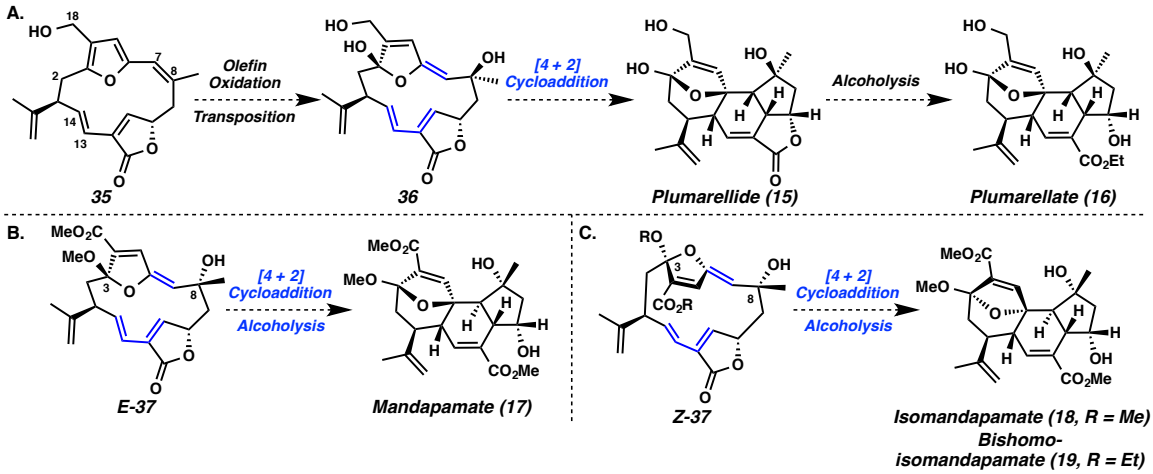

Analogs of the plumarellides, the cembranoid natural products mandapamate (**17**)[20] and isomandapamate (**18**),[21] and bishomoisomandapamate (**19**),[22] are expected to arise from a related biosynthetic route (Scheme 1.4.1.4.B and 1.4.1.4.C).[1a,13,20,21] Each of these three natural products would be formed from a derivative of macrocycle **37**, a C(8) epimeric analog of intermediate **36**, that has been oxidized to the acid oxidation state at C(18), and possesses methyl ketal rather than a hemiketal at the furan ring (i.e., C(3)). Mandapamate (**17**) would be constructed by the intramolecular [4 + 2] cycloaddition for the *E*-enol isomer of **37** (Scheme 1.4.1.4.B). Isomandapamate (**18**, R = Me) and bisohomoisomandapamate (**19**, R = Et) would be formed in an analogous manner from the *Z*-enol isomer of ketal **37** (Scheme 1.4.1.4.C).

The biosynthetic formation of the remaining two members of the polycyclic cembranoid natural product family remains unclear. Havellockate (**14**) contains a related tricyclic core to the plumarellides and the mandapamates that is flanked by a spirocyclic butyrolatone whose relative stereochemistry was unambiguously established upon initial isolation (Figure 1.4.1.1).[23] Comparatively, the cytotoxic diterpenoid rameswaralide (**8**) is also characterized by a unique cembranoid scaffold, containing a central 4-

cycloheptenone.[9,24] Both havellockate (**14**) and rameswaralide (**8**) bear similarities to the plumarellides and the mandapamates, although they are both epimeric at C(8) compared to the former and epimeric at C(7) compared to the later. Multiple biosynthetic proposals have been described, hypothesizing that havellockate (**14**) and rameswaralide (**8**) may arise either from the cyclization cembranoids related to macrocycles **36** and **37** with the proper C(8) stereochemistry or from rearrangement cascades directly forming the plumarellides and mandapamates.[1a,13,24,25]

*Figure 1.4.1.1. Structural Comparison of Havellockate (**14**) and Rameswaralide (**8**) to Plumarellide (**15**) and Mandapamate (**17**)*

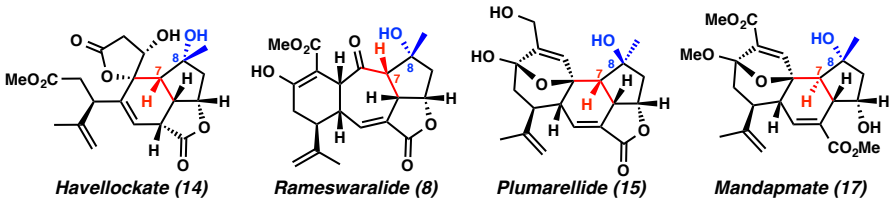

1.4.2 Biosynthesis of Polycyclic Furanobutenolide Norcembranoids

The furanobutenolide norcembranoid natural products are exclusively found in soft corals of the genus *Sinularia*.[1a,14] The progenitors of all of these C_{19} natural products are speculated to be the sinuleptolides (**4** and **5**), being epimeric at C(5) and likely in equilibrium via epimerization in vivo (Figure 1.4.2.1).[1,11,14] The biosynthetic derivation of macrocyclic cembranoids to the antitumor norcembranoids sinuleptolide (**4**) and 5-episinuleptolide (**5**) has been described in detail elsewhere and will not be discussed here.[1,6,14]

*Figure 1.4.2.1. Sinuleptolide (**4**) and 5-Episinuleptolide (**5**)*

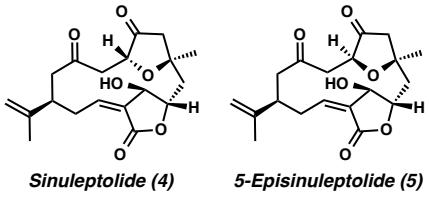

The biosynthesis of the antileukemic norditerpenoid ineleganolide (**9**)[10] and the related cycloheptanone natural products horiolide (**20**)[26] and kavaranolide (**21**)[27] are proposed to arise from ketofuran **38**, which is formed after the intramolecular Michael addition of 5-episinuleptolide (**5**) and sequential dehydration (Scheme 1.4.2.1).[1a,14] Subsequent 5-exo-trig Michael addition would forge the C(7)–C(19) bond and complete ineleganolide (**9**).

*Scheme 1.4.2.1. Biosynthesis of Ineleganolide (**9**), Horiolide (**20**), and Kavaranolide (**21**)*

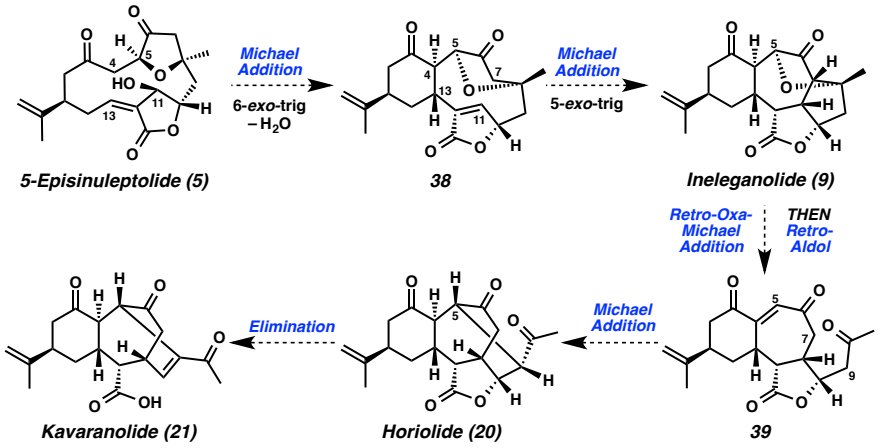

Ineleganolide could subsequently undergo a retro-oxa-Michael addition, opening the ketofuran ring, followed by a retro-Michael addition to provide methyl ketone intermediate **39**. Considering ketone **39** has yet to be isolated and described from natural sources, it is proposed to rapidly undergo an intramolecular Michael addition to construct the C(5)–C(9) bond and furnish horiolide (**20**). Ultimately, isomerization of horiolide by elimination of the β-acetoxy group would generate the unsaturated methyl ketone found within kavaranolide (**21**).

In a similar fashion, 5-episinuleptolide (**5**) could serve as the biosynthetic progenitor to sinulochmodin C (**10**),[11] scabrolide B (**23**),[6d] scabrolide A (**24**),[6d] and yonarolide (**25**, Scheme 1.4.2.2).[28] The biosynthesis would begin with a 7-*exo*-trig

intramolecular Michael cyclization to construct the characteristic peripheral cycloheptanone ring of these related norcembranoids and furnish intermediate **40** after dehydration. Ketofuran **40** would furnish sinulochmodin C (**10**) after a second Michael addition to construct the bond between C(7) and C(11).

*Scheme 1.4.2.2. Biosynthetic Formation of Sinulochmodin C (**10**), Scabrolide B (**23**), Scabrolide A (**24**), and Yonarolide (**25**)*

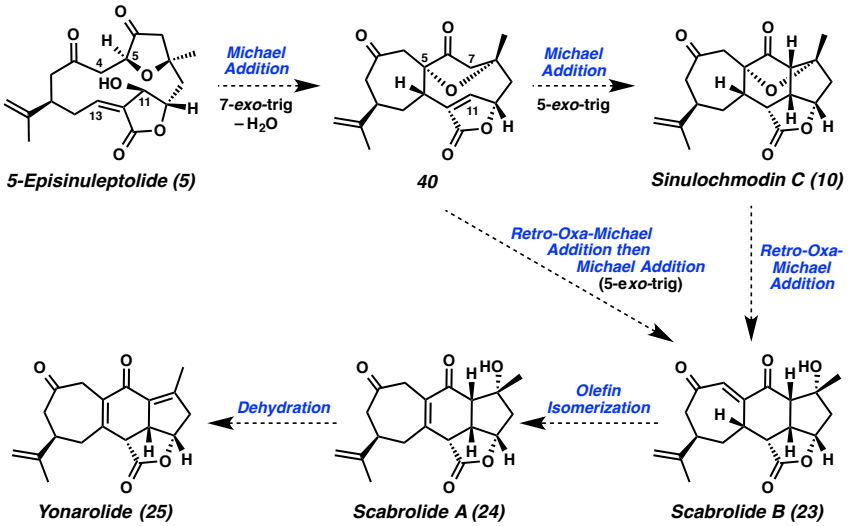

Scabrolide B (**23**) could be biosynthetically produced by one of two possible routes. First, scabrolide B could be formed after a retro-oxa-Michel addition from sinulochmodin C (**10**). Alternatively, direct conversion of biosynthetic intermediate **40** to scabrolide B could occur by a retro-oxa-Michael addition and subsequent intramolecular Michael addition. From scabrolide B (**23**), olefin isomerization from a trisubstituted vinylogous diketone to a tetrasubstituted enone would furnish scabrolide A (**24**). Ultimately, sequential dehydration would provide the dienone norcembranoid yonarolide (**25**).

The exact biosynthetic process for the construction of the remaining member of the polycyclic norcembranoids, dissectolide A (**22**), is less clear.[29] Two plausible biosynthetic routes have been postulated (Scheme 1.4.2.3).[1,14] The core [7,6,5,5]-tetracyclic structure

bears remarkable similarity to the mandapamate and plumarellide cembranoids (see Scheme 1.4.1.4), perhaps suggesting that intermediate **41**, with the $\Delta_{13,14}$ bond in the *trans* configuration, undergoes a [4 + 2] cycloaddition with the C(6)–C(7) enol tautomer of the ketofuran ring to directly construct the central cyclohexene moiety of tetrahydrofuran **42**. Macrocycle **41** could alternatively proceed to intermediate furan **42** in a stepwise manner through a Michael addition between C(7) and C(11) and subsequent vinylogous aldol cyclization of the resultant enolate to construct the C(14)–C(6) bond. Proposed intermediate **42** would then only need to undergo the hydrolytic opening of the furan ring in an S_N2 fashion to complete the biosynthesis of dissectolide A (**22**).

*Scheme 1.4.2.3. Biosynthetic Conjectures for the Formation of Dissectolide A (**22**)*

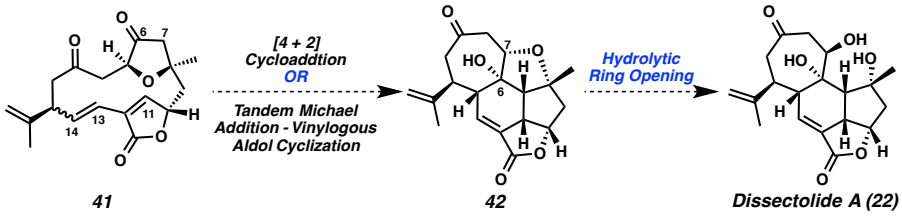

1.5 Synthetic Studies Toward Polycyclic Cembranoids and Norcembranoids

A testament to the synthetic challenge of accessing the complex structures of the polycyclic furanobutenolide cembranoid and norcembranoid natural products is that the syntheses of only a handful of members of this family have been completed. This article will explore the literature concerning the synthetic efforts toward the polycyclic furanobutenolide cembranoid and norcembranoid natural products in an effort to condense the knowledge surrounding these natural products and explore the limitations around the construction and the synthetic manipulations of their polycyclic scaffolds.

1.5.1 Synthetic Efforts Toward Bielschowskysin (BSK, 6)

Bielschowskysin (BSK, **6**) has been the most studied member of either the polycyclic cembranoid or norcembranoid family of natural products, piquing the interest of the scientific community with its unique cyclobutane scaffold and potent biological activity.[7] Six different research groups have reported synthetic studies toward BSK, five of them employing a light-induce cyclobutane formation. While the total synthesis of BSK has not yet been reported, a tremendous amount of work toward the functionalization of the BSK scaffold has been accomplished. Because of this large body of literature, this chapter will be limited to a brief summary of each approach taken and the limitations that prevented each method from advancement to BSK.

1.5.1.1 Photo [2 + 2] Approaches to Bielschowskysin

The majority of approaches toward the synthesis of BSK have hinged on a photo-induced [2 + 2] cycloaddition to construct the characteristic fused cyclobutane moiety. In that sense, there are two directions to retrosynthetically disconnect the central cyclobutane within building block **43** (Scheme 1.5.1.1.1). The most commonly employed retrosynthetic disconnection of the four-membered carbocycle has been along the axis of the [4,5]-bicycle (Pathway A, green arrow) to furnish retron **44**.

Scheme 1.5.1.1.1. Retrosynthetic Analysis of BSK Employing Photo-Induced [2 + 2]

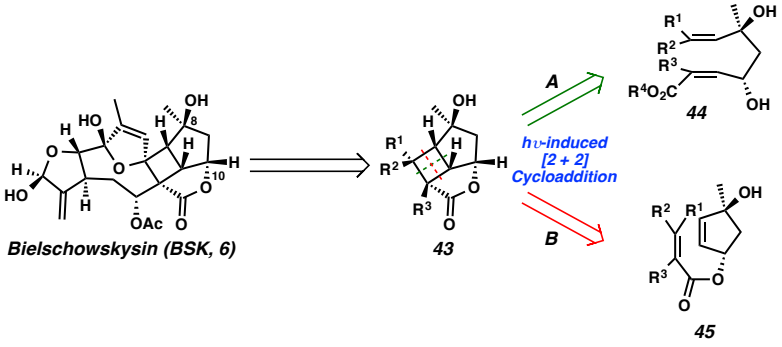

The utility of this synthetic approach was explored by Ghosh and coworkers.[30] Early synthetic studies to explore the planned copper-catalyzed [2 + 2] photocycloaddition were performed on a model system that was available in an enantiopure fashion after three synthetic transformations from a known reported derivative of α-D-glucofuranose (Scheme 1.5.1.1.2.A). Copper(I) triflate-catalyzed [2 + 2] cycloaddition of 1,6-diene **46** proceeded smoothly to furnish cyclobutane **47** in 75% yield as a single diastereomer. The cycloaddition is hypothesized to proceed exclusively through the copper-coordinated intermediate **48**, accounting for the observed stereoselectivity. Attempting to extend the developed cycloaddition to a functionalized system more closely related to BSK, Ghosh and coworkers synthesized allylic alcohol **49** (Scheme 1.5.1.1.2.B). Under the same copper-catalyzed light-induced [2 + 2] cycloaddition conditions, cyclobutane **50** was isolated in a comparable 66% yield. Unfortunately, while the substrate has dictated the formation of many of the stereocenters as required for BSK, the configuration at C(8) and C(10) were epimeric to those found in BSK.

Scheme 1.5.1.1.2. Cooper-Catalyzed Light-Induced [2 + 2] Cycloaddition (Ghosh)

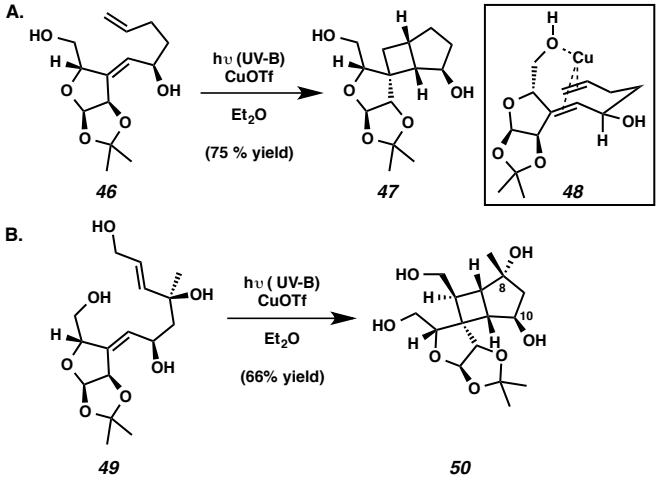

The development of a method for the tandem epimerization of C(8) and C(10) was procured on the closely related allylic alcohol **51** (Scheme 1.5.1.1.3). Photocycloaddition again under copper(I)-catalyzed conditions produced cyclobutane **52** in 78% yield. A five step redox procedure from *trans*-1,3-cyclopentanediol **52** accomplished the inversion of configuration at both C(8) and C(10) by a tandem oxidation-elimination pathway, setting their relative stereochemistry as required for BSK. To date, protected *trans*-diol **53** represents the most advanced published compound produced by Ghosh and coworkers in their work toward BSK.

*Scheme 1.5.1.1.3. Tandem Inversion of Configuration at C(8) and C(10) with Core Cyclobutane **52** (Ghosh)*

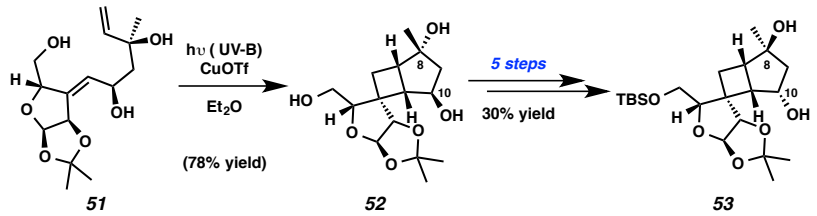

Sulikowski and coworkers also envisioned accessing BSK by a similar retrosynthetic strategy (Scheme 1.5.1.1.4).[31] Simplifying BSK to scaffold **54**, they planned to construct the core central cyclobutane through an intramolecular [2 + 2] photocycloaddition of dibutenolide **55**. Diastereoselective control of this cycloaddition depends on both the geometry of the exocyclic olefin as well as the steric encumbrance of the butenolide-substituted olefin cycloaddition partners.

Scheme 1.5.1.1.4. Retrosynthetic Strategy Employed by Sulikowski

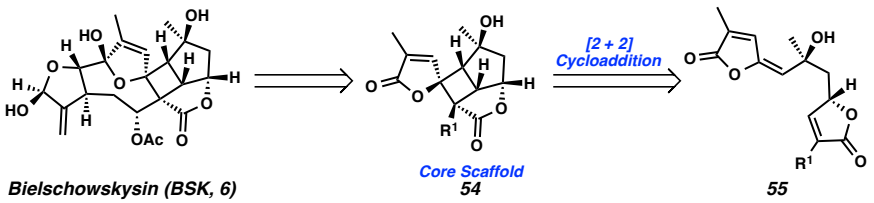

Development of the reaction conditions for the desired photochemical [2 + 2] cycloaddition began with the model butenolide **56**, where the steric congestion at the butenolide cycloaddition partner was reduced from optimal (Scheme 1.5.1.1.5). Lactone **56** was available in an enantiospecific fashion from (–)-malic acid. Intramolecular cycloaddition of enoate **56** proceeded smoothly, furnishing spirocycle **57** in 50% yield as a single diastereomer. UV light was not required in order to induce the desired cycloaddition and the choice of acetone for the solvent was critical for the minimization of impurity formation. The stereoselective formation of cyclobutane **57** accomplished solely by substrate control to provide the desired scaffold that mirrors the relative stereochemistry found in BSK (**6**).

Scheme 1.5.1.1.5. Model System for Intramolecular Butenolide [2 + 2] Cycloaddition (Sulikowski)

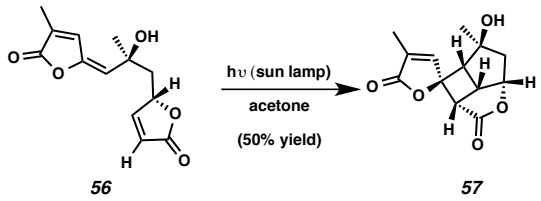

56 ***57***

Having succeeded in selectively forming the tetracyclic scaffold of BSK, Sulikowski and coworkers turned their attention to the construction of a more densely functionalized cyclobutane for synthetic advancement toward BSK. Thus the [2 + 2] cycloaddition of substrate **58** was explored, where the butenolide cycloaddition partner has been functionalized with a side chain produced in an enantiospecific fashion from D-glyceraldhyde (Scheme 1.5.1.1.6). Fully elaborated butenolide underwent a visible light-induced [2 + 2] cycloaddition to provide cyclobutane **59** in 81% yield over two steps after the removal of the benzyl ether by hydrogenolysis. Pleasingly, like cyclobutane **57**, cycloaddition adduct **59** was produced as a single diastereomer. Spirocycle **59** contains

the fully elaborated fused cyclobutane polycyclic portion of BSK and represents the most advanced intermediate detailed by the Sulikowski group to date.

Scheme 1.5.1.1.6. Intramolecular [2 + 2] Cycloaddition with Elaborated Butenolide (Sulikowski)

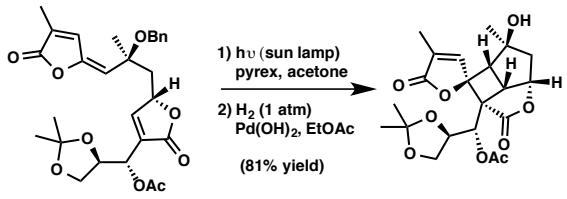

58 ***59***

Mulzer and coworkers envisioned accomplishing the construction of the cyclobutane moiety from an even more functionalized, late-stage synthetic intermediate.[32] Access to BSK (**6**) was planned by the late-stage oxidation of exocyclic olefin **60** (Scheme 1.5.1.1.7). Construction of the central macrocycle would be accomplished by an intramolecular Heck reaction of vinyl bromide **61**. Olefin **61** would be constructed by an intramolecular light-mediated [2 + 2] cycloaddition of allene **62** to construct the characteristic 4-membered carbocycle.

Scheme 1.5.1.1.7. Mulzer's Retrosynthesis of BSK Employing an Allene [2 + 2] Cycloaddition

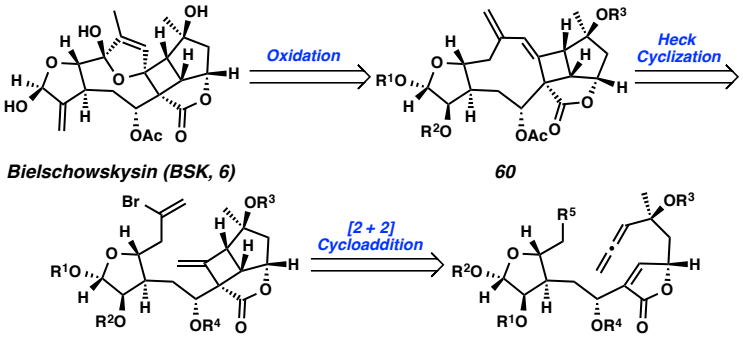

Bielschowskysin (BSK, 6) ***60*** ***61*** ***62***

Asymmetric access to late-stage allene **62** was achieved in an enantiospecific fashion, in a similar fashion to other synthetic approaches, beginning with (–)-malic acid and α-D-ribofuranose (Scheme 1.5.1.1.8). The allene moiety was generated by the

homologation of a terminal alkyne and carried through a number of synthetic transformations to access to butenolide **63**. Intramolecular [2 + 2] cycloaddition induced by UV-C light in cyclohexane provided cyclobutane **64** as a single diastereomer, furnishing the stereochemistry around the periphery of the cyclobutane as required for BSK.

Scheme 1.5.1.1.8. Allene [2 + 2] Cycloaddition (Mulzer)

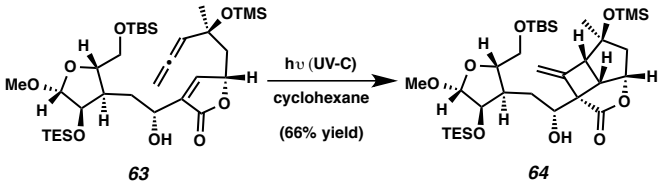

63 ***64***

Subsequently, the construction of the central macrocycle would be necessary in order to progress toward BSK. Unfortunately, under Heck cyclization conditions, desired cyclononene **67** was not isolated (Scheme 1.5.1.1.9). Surprisingly, Mulzer and coworkers observed a cyclization to produce cyclooctane **66**, which has undergone a concomitant acetoxylation of the 1,1-disubstituted olefin to provide a neopentyl acetate. Although this type of reactivity had previously been unknown for a 1,1-disubsitited olefin, the direct advancement of vinyl bromide **65** toward BSK was thwarted. While Mulzer and coworkers continue to explore the utility of cyclooctane **66** as a synthetic intermediate en route to BSK, they have pursued a series of alternative retrosynthetic strategies in their pursuit of the total synthesis of BSK (vide infra).

Scheme 1.5.1.1.9. Unexpected Cyclooctane Product Formation (Mulzer)

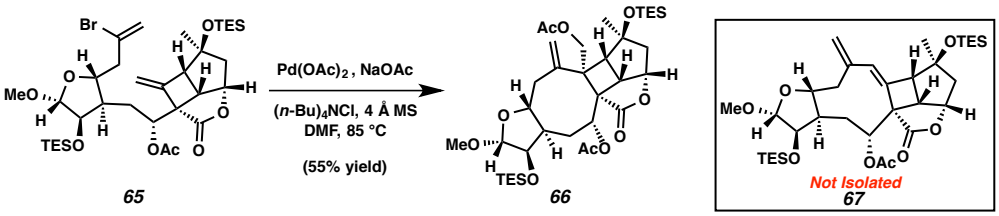

65 ***66*** ***67***

In comparison to Mulzer's planned late-stage formation of the central macrocycle after construction of the cyclobutane moiety, Nicolaou and coworkers explored the potential to accomplish the formation of the 4-membered carbocycle after completion of the macrocyclic scaffold in a manner reminiscent of the proposed biosynthesis of BSK (see Scheme 1.4.1.1).[33] Retrosynthetically, BSK was simplified to a model core scaffold **68**, retaining the required functionalization or providing a functional group handle at C(2), C(3), and C(8) (Scheme 1.5.1.1.10.A). Synthesis of polycycle **68** would be accomplished by the transannular photochemical [2 + 2] cycloaddition of alkene **69**.

Scheme 1.5.1.1.10. Nicolaou's Macrocyclic [2 + 2] Cycloaddition Strategy and Model Macrocycle Synthesis

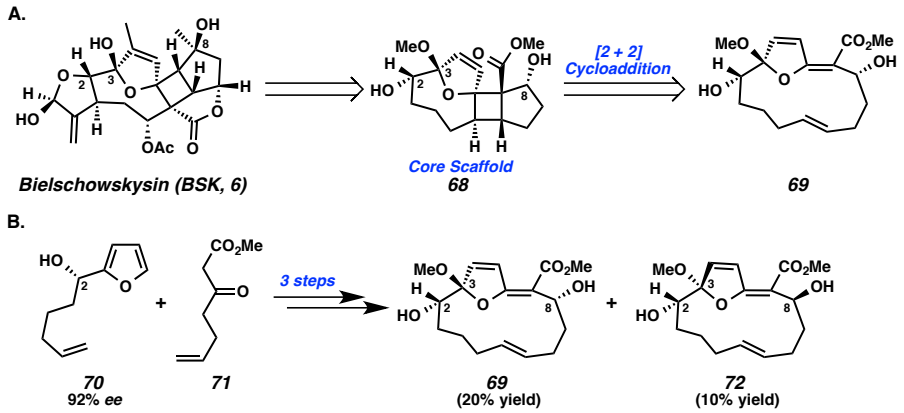

Enantioselective synthesis of the macrocyclic cycloaddition precursor **69** began with the coupling of furan **70** and β-ketoester **71** (Scheme 1.5.1.1.10.B). Furanyl alcohol **70** was produced with 92% enantiomeric excess (*ee*) by asymmetric reduction of the corresponding α-ketofuran precursor. Over the following three synthetic transformations, the (*S*)-configuration at C(2) dictated the stereochemistry at the remaining chiral centers, furnishing desired diastereomer **69** in 20% yield from alcohol **70** with the minor diastereomer **72** also possessing an *anti* relationship between the C(3)-methoxy and C(8)-hydroxyl moieties.

The potential of both furan macrocycles **69** and **72** to undergo an intramolecular [2 + 2] photocycloaddition was subsequently explored. Furan **69**, when exposed to UV-B light in either benzene or chloroform, produced cyclobutane **68** in high yield as a single diastereomer (Scheme 1.5.1.1.11.A). The new fused carbocycle contained the desired relative stereochemistry, furnishing the spirocyclic furan as found in BSK. Under identical photocyclization conditions, diastereomeric macrocycle **72** produced carbocycle **73** as the sole product (Scheme 1.5.1.1.11.B). The relative stereochemistry of furan **72** dictated enantiomeric formation of the stereocenters on the periphery of the cyclobutane in comparison to polycycle **68**, constructing the spirocyclic furan in the opposite and undesirable sense for advancement toward BSK. Although cyclobutane contains the proper spirocycle relative to BSK and a series of functional group handles, the Nicolaou group has not disclosed any further studies to date concerning its advancement toward BSK.

Scheme 1.5.1.1.11. Stereochemical Outcome of Macrocyclic [2 + 2] Cycloaddition (Nicolaou)

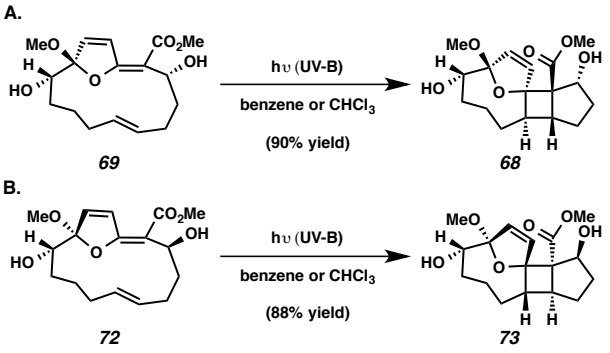

By a comparative approach toward BSK, Lear and coworkers additionally envisioned late-stage construction of the cyclobutane moiety from a fully elaborated macrocyclic precursor **74** by a tandem [2 + 2]-oxidative [4 + 2] cycloaddition (Scheme 1.5.1.1.12).[34] Allene **74** would be generated from alkyne **75** after oxidation of the C(8)

hydroxyl group and subsequent isomerization. In the forward sense, allene **74** would proceed toward BSK by first undergoing a light-induced [2 + 2] cycloaddition to furnish cyclobutane intermediate **76** (Scheme 1.5.1.1.13). Diene **76** would then undergo a photochemical [4 + 2] cycloaddition with singlet oxygen to construct peroxide **77**. Homolytic cleavage of the peroxide bond by cobalt(II) would result in the formation of elaborated BSK scaffold **78**.

Scheme 1.5.1.1.12. Lear's Macrocyclic Tandem [2 + 2] and [4 + 2] Cycloaddition Strategy

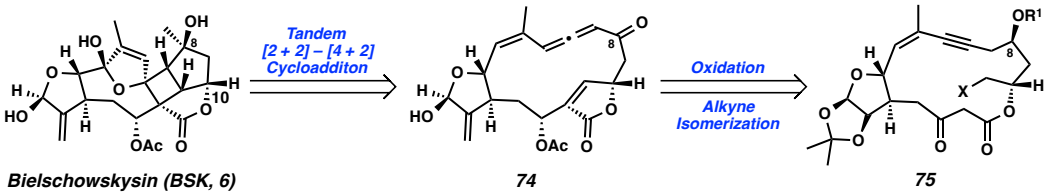

Scheme 1.5.1.1.13. Planned Tandem [2 + 2] and [4 + 2] Cycloaddition in the Forward Sense (Lear)

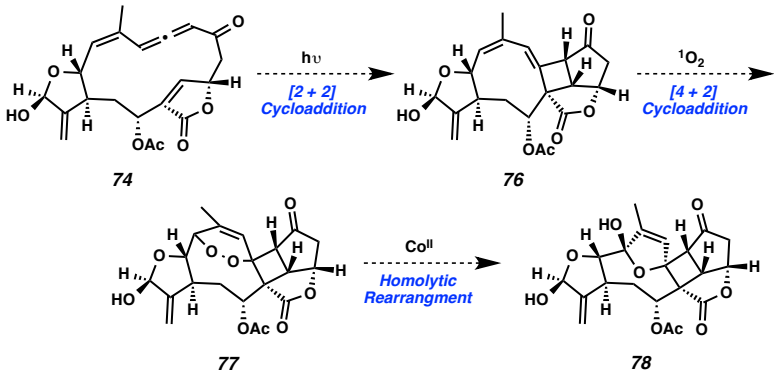

Initial exploration of the planned tandem cycloaddition strategy focused on the potential to accomplish the [2 + 2] cycloaddition of a tethered allene and butenolide system. Model allene **79** was available in an enantiospecific fashion from (–)-malic acid in 10 synthetic steps, constructing the allene moiety by a homologation of an alkyne (Scheme 1.5.1.1.14). Irradiation of allene with UV light in a 1:1 mixture of hexane and dichloromethane furnished the desired cyclobutane tricycle (**80**) in 70% yield as a single diastereomer. In a similar fashion to other methods, the use of enantioenriched (–)-malic

acid as the starting material has endowed the cyclobutane tricycle with both the relative and absolute stereochemistry as required for BSK. These initial studies concerning the formation of allene **79** and its success in a [2 + 2] cycloaddition as desired informed the aforementioned synthetic strategy of Mulzer and coworkers (see Scheme 1.5.1.1.7).[32]

Scheme 1.5.1.1.14. Model System Studies on Allene Cycloaddition with a Butenolide (Lear)

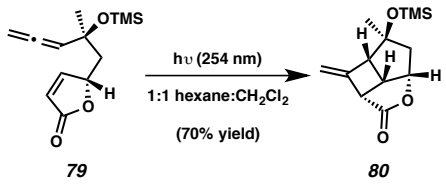

With this result in hand, Lear and coworkers aimed to construct the fully elaborated system and test the efficacy of the proposed tandem [2 + 2] and [4 + 2] cycloaddition. Enantiospecific access to macrocycle **81** was achieved from (–)-malic acid paired with a known derivative of α-D-glucofuranose (Scheme 1.5.1.1.15). The central macrocycle was stitched together using a Sonogashira coupling and subsequent macrolactonization. Unfortunately, progress toward BSK was halted at intermediate **81** because cyclization between the primary chloride and the α-position of the β-ketoester could not be achieved. Without the ability to form the butenolide moiety, the tandem oxidative cycloaddition cascade could not be investigated.

Scheme 1.5.1.1.15. Model System Studies on Allene Cycloaddition with a Butenolide (Lear)

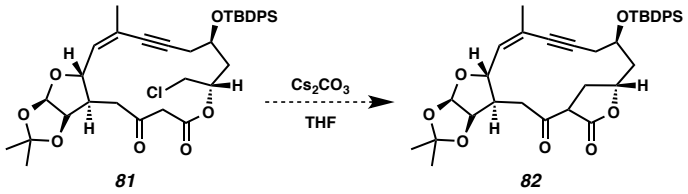

Although these synthetic approaches toward BSK had provided numerous methods for the synthesis of cyclobutane-centered polycycles, the total synthesis of BSK remained

elusive. As a result, Mulzer and coworkers developed an alternative retrosynthetic strategy for the construction of the BSK core **83** (Scheme 1.5.1.1.16).[35] Rather than bisecting the cyclobutane along the axis of the [4,5]-bicycle like each of the previous synthetic approaches, they envisioned accessing the 4-membered carbocycle by an intramolecular photo-induced [2 + 2] cycloaddition between an α,β-unsaturated ester and a cyclopentenyl olefin.

*Scheme 1.5.1.1.16. Alternative Retrosynthetic Analysis of Cyclobutane Moiety of BSK (**6**, Mulzer)*

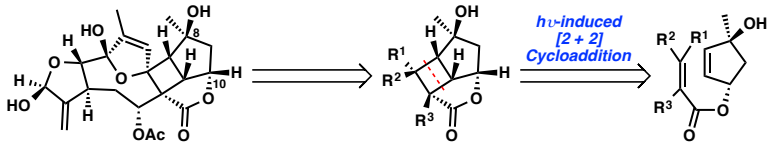

Investigation of the desired [2 + 2] cycloaddition began with the assessment of a cyclopentene diol (**85**) in a [2 + 2] photocycloaddition (Scheme 1.5.1.1.17.A). Cyclopentene **85** underwent [2 + 2] cycloaddition with maleic anhydride in the presence of UV-A light, furnishing cyclobutane **86**. Unfortunately, nearly every attempt to construct functionalized tricycle **87** was unsuccessful, including systems containing an ester conjugated with substituted allenes, ketenes, ketene acetals, ketene iminium salts, aryl groups, and butenolides in the presence of either a sun lamp, UV-A, or UV-B light or under thermal conditions (Scheme 1.5.1.1.17.B). Successful [2 + 2] cycloaddition could only be accomplished with allene **89** generating tetrahydrofuran **90** in 60% yield (Scheme 1.5.1.1.17.C). Rather than explore the advancement of tricycle **90** toward BSK, the authors chose to explore an alternative route through which the cyclobutane moiety was purchased from commercial sources.

Scheme 1.5.1.1.17. Limitations of Targeted [2 + 2] Cycloaddition (Mulzer)

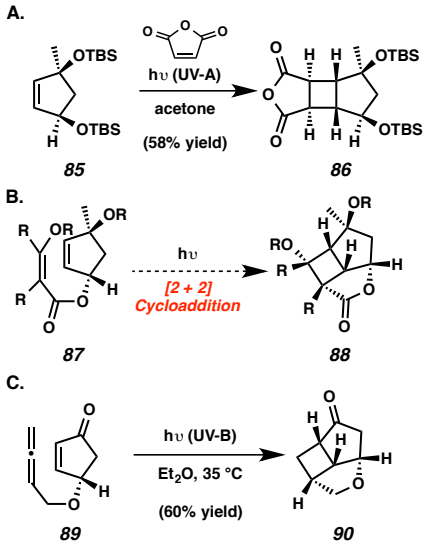

1.5.1.2 Non-Photochemical Approaches to Bielschowskysin

In the face of the challenges encountered in their efforts toward BSK (**6**), Mulzer and coworkers designed a 3rd generation synthetic strategy toward BSK hinging on the production of core scaffold **91** from a cyclobutane-containing feedstock (**93**, Scheme 1.5.1.2.1).[35,36] Enantioselective access to tricycle **91** was envisioned from cyclobutanol **(+)-92**. Bicycle **(+)-92** could be synthesized over four steps from racemic ketone **93** by a classical resolution. Thus the cyclobutane moiety within BSK was available from commercially available ketone **93**.

*Scheme 1.5.1.2.1. Mulzer's 3rd Generation Retrosynthetic Analysis of BSK (**6**)*

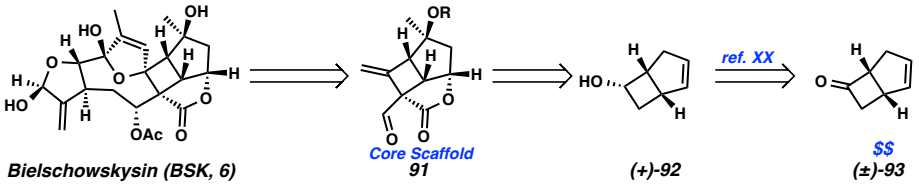

Cyclobutanol **(+)-92** was advanced toward BSK through a series of stereoselective alkylations and redox manipulations over 16 steps to furnish the enantioenriched tricyclic core of BSK (**91**) in 11% overall yield (Scheme 1.5.1.2.2.A). Unfortunately, the

advancement of aldehyde **91** toward BSK was found to be infeasible. Attempts to functionalize the 1,1-disubstitued olefin with carbon nucleophiles in a productive manner failed. As a result, intermediate **95**, encountered en route to aldehyde **91**, was utilized for further elaboration (Scheme 1.5.1.2.2.B). From cyclobutane **95**, installation of the spirocyclic furan was accomplished as desired for BSK and the complimentary furan was synthesized in an enantiospecific fashion from α-D-glucofuranose and installed by a chromium(II)-mediated coupling, furnishing polycycle **96** in 13% yield over eight steps. Although Mulzer and coworkers envision advancement of ketal **96** to BSK over a few additional synthetic transformations, and they briefly explored an additional strategy for the formation of core **91** by a ring contraction strategy without any success,[32b] they have instead chosen to actively pursue their light-induced [2 + 2] cycloaddition strategy for continued efforts toward BSK (see Scheme 1.5.1.1.8).

Scheme 1.5.1.2.2. Advancement of Enantioenriched Cyclobutanol ***(+)-92*** *Toward BSK (Mulzer)*

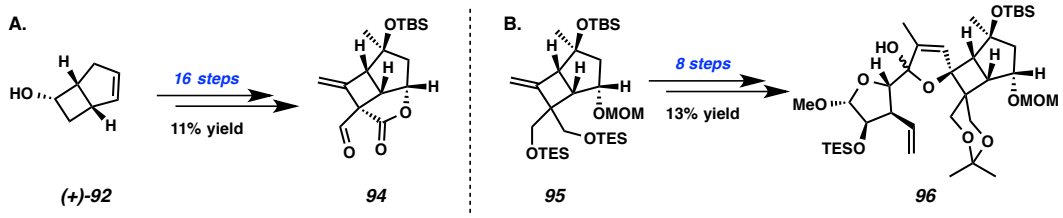

The final strategy for the synthesis of BSK presented in the literature to date is a cyclopropane fragmentation-Michael addition strategy developed by Stoltz and coworkers.[37] Access to BSK (**6**) was envisioned through the highly functionalized core cyclobutane-centered polycycle **97** (Scheme 1.5.1.2.3). Construction of the cyclobutane was planned through an intramolecular Michael addition of enolate **98** into the extended oxocarbenium fragment. Generation of charge-separated intermediate would be achieved by the fragmentation of cyclopropane **99**.

Scheme 1.5.1.2.3. Stoltz's Retrosynthetic Analysis of BSK Core Scaffold ***97***

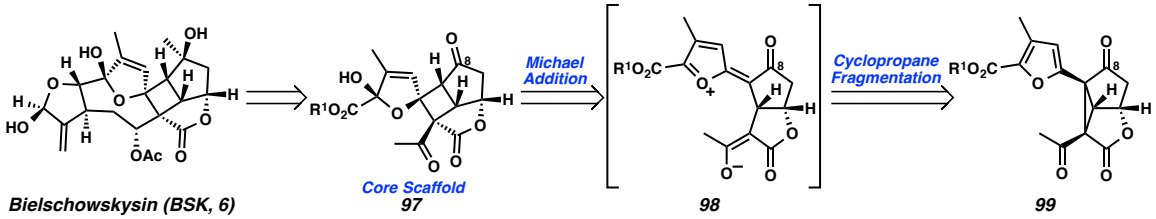

Investigation of the planned cyclopropane fragmentation began with the enantioselective synthesis of furan-substituted cyclopentenediol **100** by palladium-catalyzed aerobic oxidative kinetic resolution (Scheme 1.5.1.2.4). By this method, diol **100** was accessible in 93% *ee*. Cyclopropane **101** was then synthesized from diol **100** in 29% yield over four steps. Unfortunately, advancement of the cyclopropane was plagued by nonproductive translactonization after liberation of the free hydroxyl group at C(8) independent of the identity of and conditions used to remove the protecting group. For example, saponification of acetate **101** results in translactonization, liberating a free hydroxyl at C(10), which underwent oxidation by DMP and after cyclopropane fragmentation, regenerated the bicyclic lactone scaffold as ketal **102**. Ultimately, like all of the other synthetic methods disclosed to date, Stoltz and coworkers were not successful in the completion of their efforts toward BSK (**6**), as they were unable to develop conditions for the successful advancement of any cyclopropane scaffold related to **101** to the desired cyclobutane intermediate. Bicyclic lactone **102**, however, could still be employed as an intermediate toward the total synthesis of verrillin (**13**).

Scheme 1.5.1.2.4. Synthesis and Exploration of Cyclopropane Intermediate ***101*** *(Stoltz)*

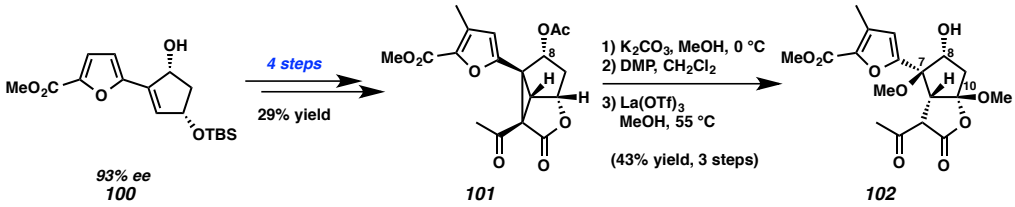

1.5.2 *Synthetic Efforts Toward Verrillin (13)*

The total synthesis of the closely related macrocycle verrillin (**13**) has only been attempted by Theodorakis and coworkers (Scheme 1.5.2.1).[38] Retrosynthetically, they envisioned completion of verrillin (**13**) by late-stage oxidation of furan **103** to complete the sequential bridging ketals and the second lactone from the isopropenyl side chain. Convergent assembly of furan **103** would be accomplished by the coupling of three components: aldehyde **104**, furan **105** and *cis*-1,3-cyclopentenediol **106**. The relative stereochemistry throughout the synthesis would be derived from the stereochemistry of the 1,3-*cis*-cyclopentenediol building block.

Scheme 1.5.2.1. Retrosynthetic Analysis of Verrillin (Theodorakis)

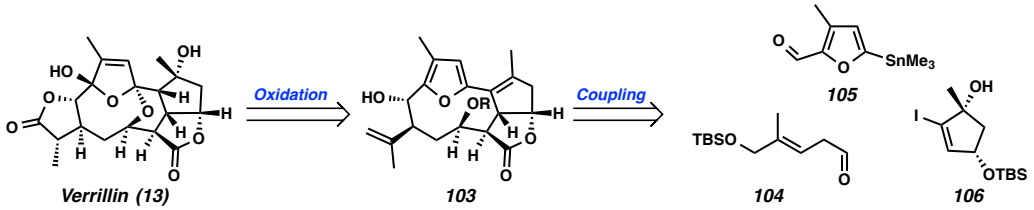

Theodorakis and coworkers pursued the synthesis of racemic verrillin (**13**) beginning with furanyl alcohol **107**. Conversion of furan **107** to racemic vinyl iodide **106** was accomplished in 21% yield over 4 steps (Scheme 1.5.2.2). Eschenmoser–Claisen rearrangement from tertiary alcohol **106** with amide acetal **108** followed by removal of the TBS ether with concomitant lactonization provided bicycle **109**. Addition of lactone **109** into aldehyde **104** provided alcohol **110** as a 1.7:1 mixture of diastereomers at C(13) in favor the desired diastereomer as shown. After protecting group manipulation, vinyl iodide **111** was coupled with furanyl stannane **105**. Subsequent Appel halogenation provided bromide **112**, which could be cyclized to provide macrocycle **113** in 39% isolated yield, although **113** was produced in a 4:1 ratio of diastereomers in favor of the

desired *anti* configuration between C(1) and C(2) as required for verrillin (**13**). The completion of the furanyl core of the natural product marked the end of the only reported synthetic studies toward the total synthesis of verrillin.

*Scheme 1.5.2.2. Theodorakis' Synthetic Approach Toward Verrillin (**13**)*

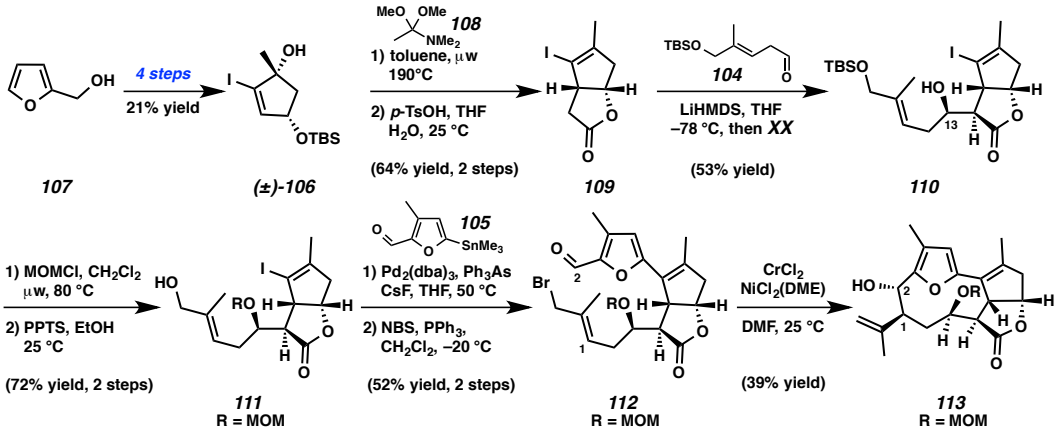

1.5.3 *Synthetic Efforts Toward Havellockate (14)*

Havellockate (**14**), which contains the same C(8)/C(10) relative stereochemistry found in verrillin (**13**), has been targeted by two laboratories through two distinct synthetic strategies. Mehta and coworkers disclosed the first synthetic studies toward havellockate in 2001.[39] They envisioned access to havellockate (**14**) could be achieved through tetracycle **114** after addition of the isopropenyl side chain and ultimate oxidation (Scheme 1.5.3.1). Spirocyclic lactone **114** would in turn be derived from the oxidation of spirocyclic furan **115**.

*Scheme 1.5.3.1. Mehta's Retrosynthetic Analysis of Havellockate (**14**)*

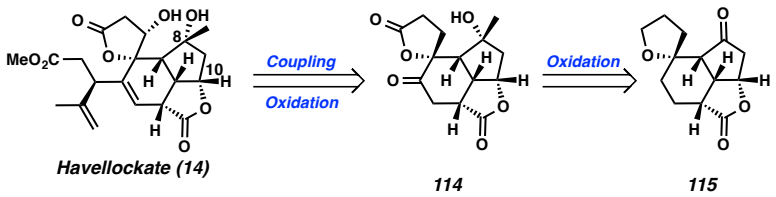

Targeting core tetracycle **115**, synthetic advancement toward racemic havellockate (**14**) was pursued from ketal **116** (Scheme 1.5.3.2). Synthesis of *cis*-1,3-cyclopentanediol **117** was achieved after eight synthetic transformations comprised mainly of a series of stereoselective redox manipulations in 16% overall yield. Baeyer–Villager oxidation of ketone **117** furnished lactone **118** as a single product. Reductive opening of lactone **118** followed by sequential selective silyl ether formation and oxidation furnished enone **119**. Formation of the targeted spirocyclic furan was accomplished after 1,2-addition of a vinyl nucleophile into the enone, allylic alkylation of the resultant tertiary alcohol, and ring-closing metathesis to provide spirocycle **120** in 49% yield over three steps. Silyl ether cleavage, oxidation, and olefin isomerization supplied aldehyde **121**, which was globally hydrogenated and oxidized afforded tetrahydrofuran **115**, the targeted core polycycle of havellockate (**14**) with the proper stereochemistry installed at each ring junction. Mehta and coworkers did not advance furan **115** further toward havellockate.

Scheme 1.5.3.2. Construction of the Havellockate Core (Mehta)

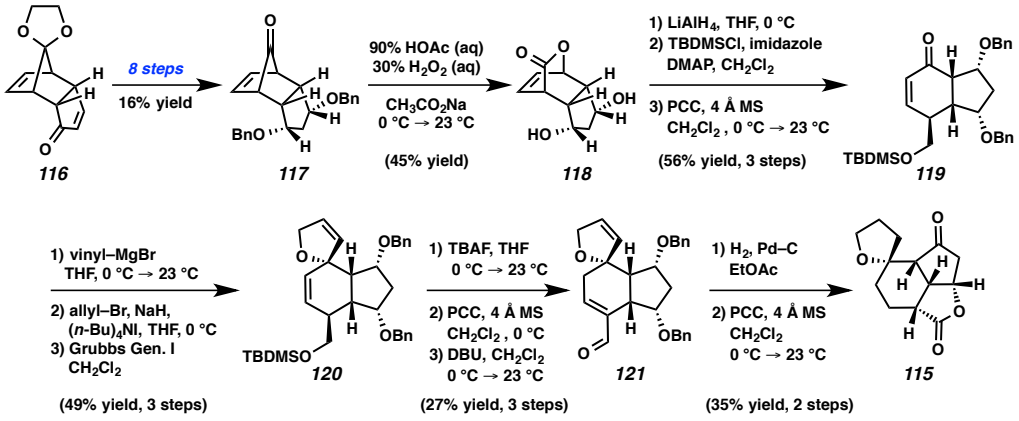

More recently, in 2010, Barriault and workers disclosed their progress toward the racemic total synthesis of havellockate.[40] Access to havellockate (**14**) was envisioned through enone **122** after formation of the spirocyclic lactone moiety (Scheme 1.5.3.3).

Enone **122** would be available from bicycle **123** after oxidation and functionalization of the cyclohexene. Bicycle **123** would in turn be formed through a Diels–Alder cycloaddition of diene **124**.

*Scheme 1.5.3.3. Barriault's Retrosynthesis of Havellockate (**14**)*

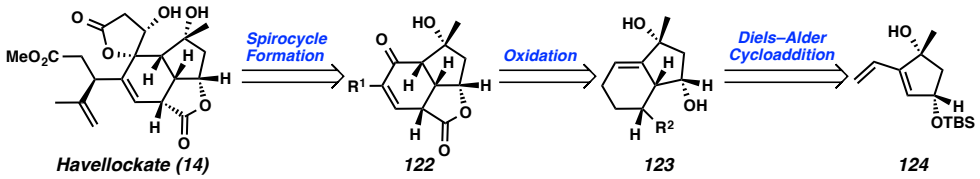

In the forward sense, furanyl alcohol **107** was advanced to racemic *cis*-1,3-cyclopentenediol **124** over five steps in 10% overall yield. Hydroxyl-directed Diels–Alder cycloaddition of diene **124** with acrolein in the presence of excess magnesium(II) bromide followed by global reduction furnished cyclohexanol **125**. Oxidation of polyol **125** furnished silyl ether **126** after concomitant lactonization. Addition of a vinyl nucleophile to ketone **126** followed by the addition of acetic anhydride provided acetate **127** in 42% yield. Ozonolysis, aldol condensation, and ultimate silyl ether cleavage provided spirocycle **128** after in situ translactonization. Tetracycle **128** is the fully elaborated core of havellockate lacking the appropriate oxidation state and the isopropenyl side chain flanking the cyclohexane as well as the β-hydroxyl group within the spirocyclic lactone.

*Scheme 1.5.3.4. Synthesis of Elaborated Core Tetracycle of Havellockate (**14**, Barriault)*

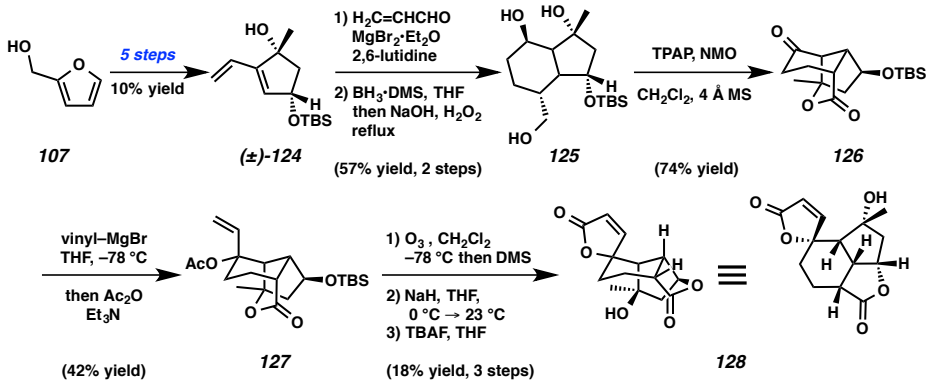

While direct advancement of tetracycle **128** toward havellockate (**14**) proved unfruitful, cyclohexanone **126** proved amenable to functionalization of the cyclohexane (Scheme 1.5.3.5). Two-step oxidative desaturation of cyclohexanone **126** furnished enone **129** in 34% yield. Stille coupling of stannane **130** with the vinyl iodide of enone **129** afforded diene **131**. Installation of the spirocyclic dihydrofuran was accomplished by a method derived from Mehta and coworkers (see Scheme 1.5.3.2) to provide alcohol **132** after PMB ether cleavage in 44% yield over four steps. Vinylation of allylic alcohol **132** followed by Claisen rearrangement furnished aldehyde **133** in 53% yield as a 1:1 mixture of C(1) diastereomers. The successful installation of the isopropenyl side chain produced another late-stage, highly functionalized intermediate that stands as the Barriault laboratory's most advanced intermediate en route to havellockate (**14**).

*Scheme 1.5.3.5. Alternative Synthetic Approach Toward Havellockate (**14**, Barriault)*

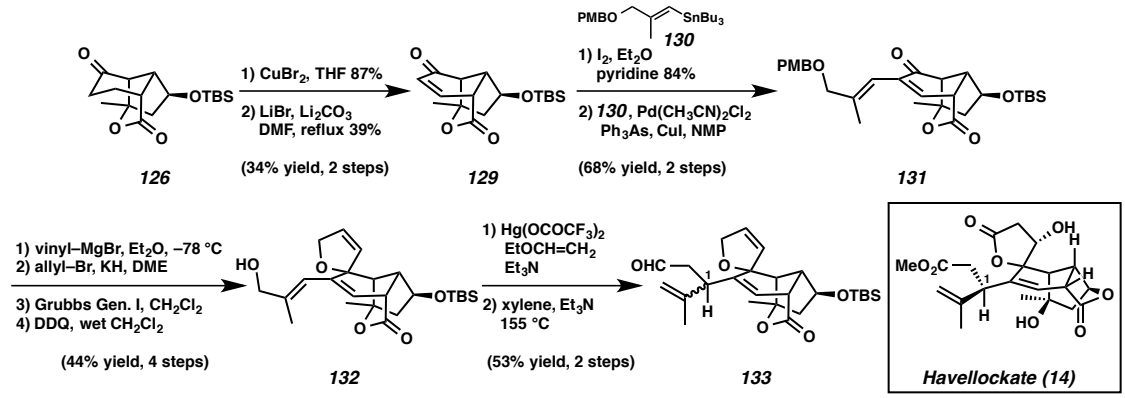

1.5.4 *Synthetic Efforts Toward Intricarene (7)*

The biomimetic asymmetric total synthesis of intricarene (**7**) was accomplished by both the Pattenden[18b,c] and Trauner[18] laboratories in 2013, representing two of the rare examples of a completed synthesis of a member of the polycyclic furanobutenolide cembranoid and norcembranoid natural family. The biosynthesis of intricarene (**7**) had been proposed from bipinnatin J (**26**, Scheme 1.5.4.1). Oxidative cleavage of the furan moiety followed by isomerization would produce the hypothesized biosynthetic intermediate **34**. Subsequent dipolar [5 + 2] cycloaddition would then complete the construction of intricarene (**7**). In order to confirm this speculated biosynthetic pathway, which has been explored computationally as well,[41] both Pattenden and Trauner sought initially to complete the asymmetric total synthesis of bipinnatin J (**26**).

*Scheme 1.5.4.1. Proposed Biosynthesis of Intricarene (**7**)*

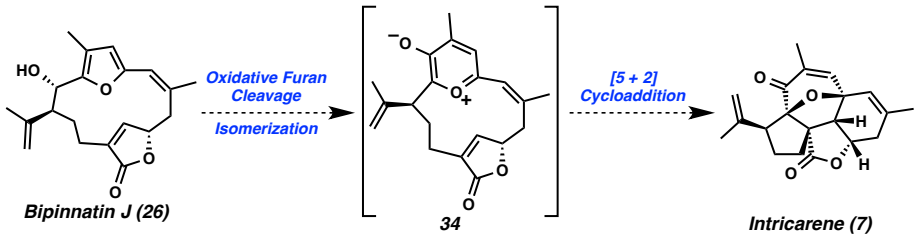

Both laboratories took similar routes toward the asymmetric total synthesis of bipinnatin J (**26**). Pattenden and coworkers began their enantiospecific synthesis with epoxide **134**, which was available five steps from (+)-glycidol (Scheme 1.5.4.2.A). Coupling of epoxide **134** with selenide **135** provided alkene **136** in 60% yield. Sequential lactonization, selenide oxidation and elimination, and silyl ether cleavage furnished vinyl iodide **137** in 62% yield over three steps. Alternatively, Trauner and coworkers pursued the enantioselective synthesis of bipinnatin J (**26**) beginning with alkyne **138**, which was available in with 92% *ee* after the asymmetric 1,2-reduction of the ketone precursor (Scheme 1.5.4.2.B). Conversion of silyl alkyne **138** into alkynoate **139** was accomplished in four steps in high yield. Butenolide **141** was formed from ester **139** through a ruthenium-catalyzed Alder ene reaction, followed by olefination of the resultant aldehyde to furnish lactone **141**. Redox manipulation of ester **141** again provided vinyl iodide **137**.

*Scheme 1.5.4.2. Synthesis of Common Intermediate Vinyl Iodide **137** (Pattenden and Trauner)*

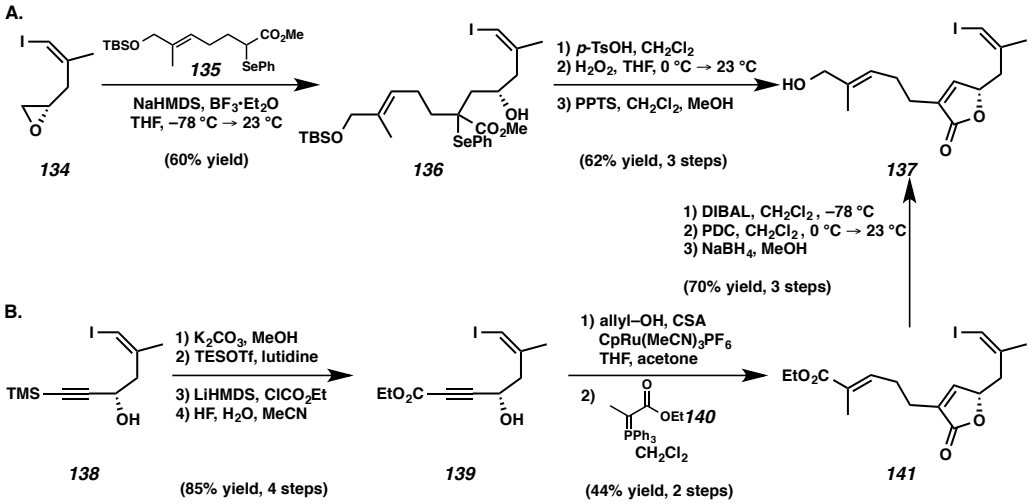

Advancement of iodide **137** was accomplished by both Pattenden (Scheme 1.5.4.3.A) and Trauner (Scheme 1.5.4.3.B) in nearly identical fashion. Stille coupling of

iodide **137** and furfural stannane **105** and subsequent Appel halogenation of the primary allylic alcohol produced allylic bromide **142**. Chromium(II)-mediated macrocycle formation was then employed to couple the allylic bromide and furanyl aldehyde to complete the asymmetric synthesis of bipinnatin J (**26**).

*Scheme 1.5.4.3. Completion of the Asymmetric Total Synthesis of Bipinnatin J (**26**, Pattenden and Trauner)*

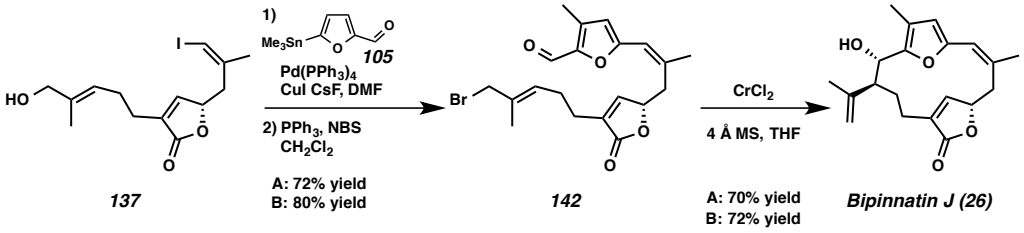

With the asymmetric total synthesis of bipinnatin J (**26**), both Pattenden (Scheme 1.5.4.4.A) and Trauner (Scheme 1.5.4.4.B) turned their attention to the investigation of the biomimetic synthesis of intricarene (**7**). Pattenden and coworkers proceeded with the vanadium-catalyzed epoxidation of allylic alcohol **26** followed by acetylation of the resultant hemiketal to provide enone **143** in 30% yield from polycycle **26**. Alternatively, Trauner and coworkers accomplished the epoxidation of furan **26** with *m*-CPBA. Acetylation of the intermediate hemiketal furnished enone **143** in an improved 81% yield from bipinnatin J (**26**).

*Scheme 1.5.4.4. Biomimetic Syntheses of Intricarene (**7**) from Bipinnatin J (**26**, Pattenden and Trauner)*

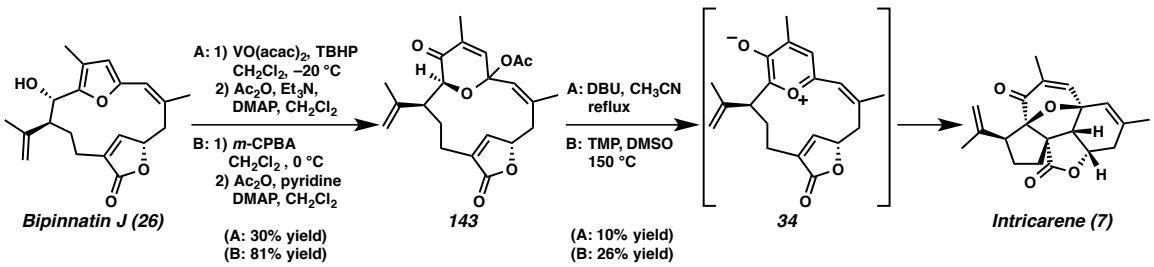

Advancement of acetate **143** was accomplished under basic conditions. Pattenden and coworkers found that exposure of ketal **143** to DBU in refluxing acetonitrile furnished intricarene (**7**) in 10% yield, proposing the reaction proceeded through intermediate dipole **34** and ultimate [5 + 2] cycloaddition. Similarly, Trauner and coworkers found that in the presence of TMP in DMSO at 150 °C, acetate **143** was converted to intricarene (**7**) in 26 % yield, again invoking the intermediacy of the same charge separated and speculated biosynthetic precursor **34**. These studies led the authors to conclude that the biosynthetic speculations surrounding the formation of intricarene (**7**) from macrocycle **34** are likely correct and the production of intricarene likely happens spontaneously in vivo directly from bipinnatin J (**26**).

1.5.5 *Synthetic Efforts Toward Rameswaralide (8)*

Several approaches to the core structure of rameswaralide (**8**) have been described, although the synthesis of rameswaralide itself has not yet been achieved. Mehta and coworkers envisioned access to rameswaralide (**8**) through core tricycle **144** after Diels–Alder cycloaddition (Scheme 1.5.5.1).[42] Cycloheptenone **144** would in turn be synthesized by a ring-closing metathesis from diene **145**. Access to enone **145** would be accomplished by the functionalization of bicyclic lactone **146**, a derivative of the Corey lactone.

*Scheme 1.5.5.1. Mehta's Retrosynthetic Analysis of Rameswaralide (**8**)*

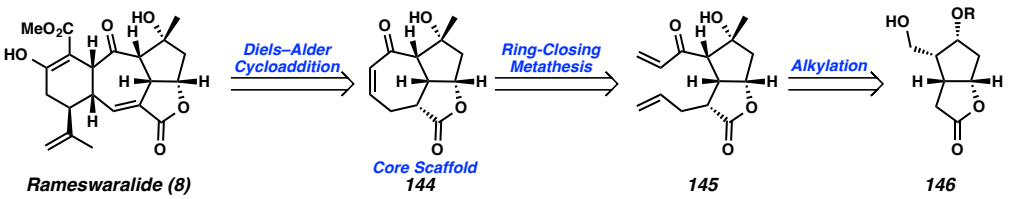

The pursuit of (±)-rameswaralide was accomplished from bicyclic ketone **148**, which was available from acetate **147** in 49% yield over six steps (Scheme 1.5.5.2). Baeyer–Villager oxidation of ketone **148** provided lactone **149** as a single product in excellent yield. Silyl ether cleavage and subsequent iodolactonization furnished bicyclic iodide **150**. Global silyl ether formation followed by reduction of the secondary iodide provided lactone **151** in 85% yield over two steps from halide **150**.

*Scheme 1.5.5.2. Synthesis of Corey Lactone Derivative **151** (Mehta)*

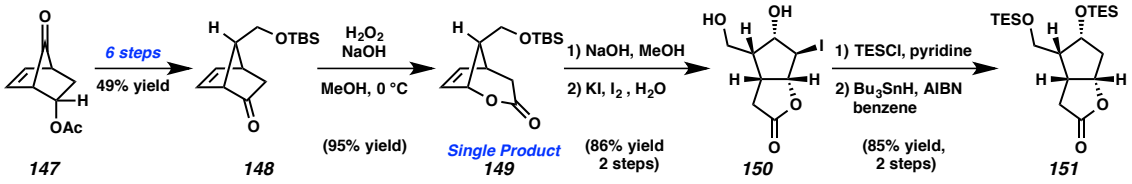

Advancement of lactone **151** was then accomplish by alkylation with either allyl or propargyl bromide (Scheme 1.5.5.3). Sequential selective primary silyl ether cleavage and oxidation of the resultant primary alcohol provided intermediate bicycle **152** as a single diastereomer independent of the identity of the α-lactone substituent. Addition of an vinyl nucleophile to aldehyde **152** followed by oxidation of the intermediate secondary alcohol provided allyl-substituted lactone **153** and propargyl-substituted lactone **154** in 47% and 41% yield, respectively, over five steps from bicycle **152**.

*Scheme 1.5.5.3. Synthesis of Bicyclic Metathesis Substrates **153** and **154** (Mehta)*

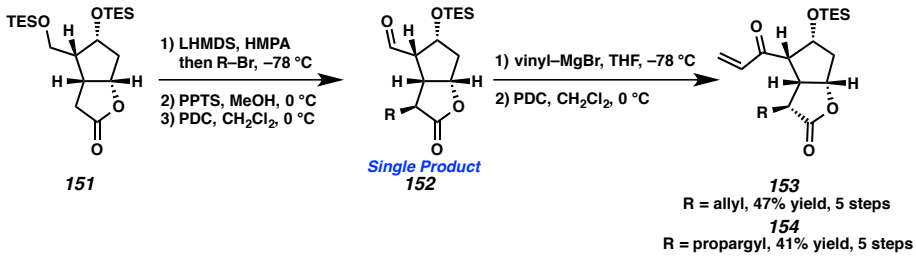

Pleasingly, exposure of allylic bicycle **153** to Grubbs generation II catalyst smoothly furnished tricycle **155**, completing the core scaffold of rameswaralide (Scheme

1.5.5.4.A). Unfortunately, all attempts to advance dienophile **155** toward rameswaralide through a Diels–Alder cycloaddition were unfruitful. In an attempt to alternatively access rameswaralide, Mehta and coworkers sought to complete the more extensively functionalized core of rameswaralide (**156**) by the enyne metathesis of alkyne **154** (Scheme 1.5.5.4.B). Unfortunately, this synthetic approach could not be successfully employed for the formation of the characteristic 7-membered ring integral to the carbocyclic scaffold of rameswaralide.

Scheme 1.5.5.4. Construction of the Rameswaralide Tricyclic Core (Mehta)

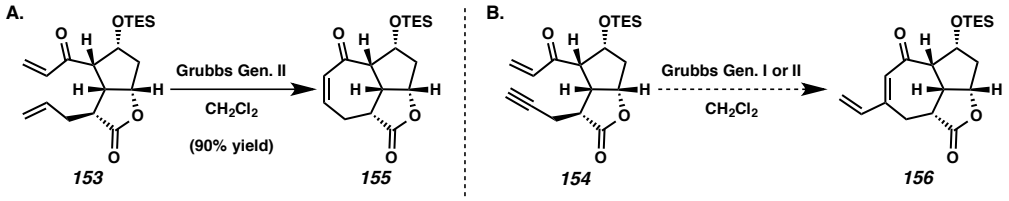

Comparatively, Srikrishna and coworkers envisioned the use of a ring-closing metathesis to access two different rameswaralide core bicycles **157** and **158** (Scheme 1.5.5.5).[43] The [6,7]-core scaffold **157** would arise directly from olefin **159** by ring-closing metathesis. Alternatively, synthetic access to [5,7]-core scaffold **158** was also envisioned from olefin **159** after ring contraction and subsequent ring-closing metathesis.

Scheme 1.5.5.5. Srikrishna's Proposed Construction of Two Rameswaralide Cores from a Common Intermediate

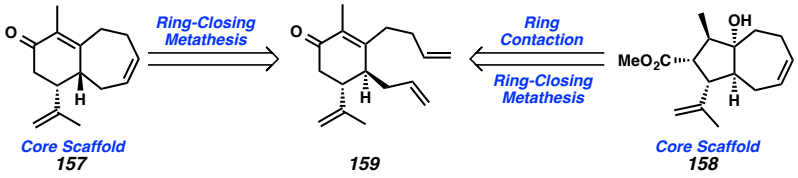

The enantiospecific synthesis of the [6,7]-bicyclic core of rameswaralide (**157**) began with the alkylation of (*R*)-carvone (**160**) with allyl bromide to provide *anti* product **161** in 12% yield as the minor diastereomer (Scheme 1.5.5.6). Sequential 1,2-addition of

butenyl bromide **162** in the presence of lithium metal and oxidative 1,3-allylic transposition of the intermediate tertiary alcohol provided enone **163** in 80% yield over two steps. Ring-closing metathesis of tetraene **163** furnished **157** in 98% yield as the core [6,7]-bicycle of rameswaralide, possessing the proper relative *anti* configuration between the isopropenyl substituent and the fused cycloheptene.

Scheme 1.5.5.6. Synthesis of the [6,7]-Bicyclic Core of Rameswaralide (Srikrishna)

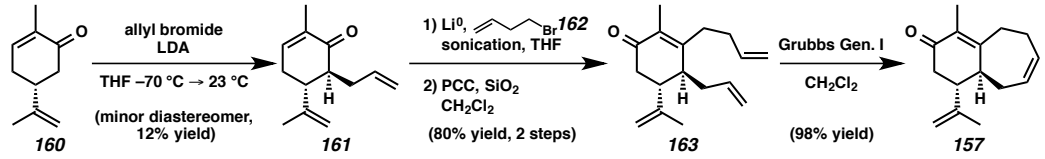

Construction of the complimentary [5,6]-bicyclic core of rameswaralide began with the diastereoselective reduction and sequential diastereo- and chemoselective epoxidation to provide alcohol **164** in 62% yield over two steps (Scheme 1.5.5.7). Oxidation of secondary alcohol followed by a Favorskii-type ring contraction produced cyclopentane **165**. Ultimate ring-closing metathesis furnished bicyclic cycloheptene **158** in 95% yield from cyclopentanol **165**. Although the core carbocyclic scaffold of the cycloheptene **158** contains a portion of the core bicyclic structure of rameswaralide (**8**), the substitution and oxidation pattern would need to be greatly altered in order to utilize bicycle **158** in total synthetic efforts toward the natural product.

Scheme 1.5.5.7. Formation of the [5,7]-Bicyclic Core of Rameswaralide (Srikrishna)

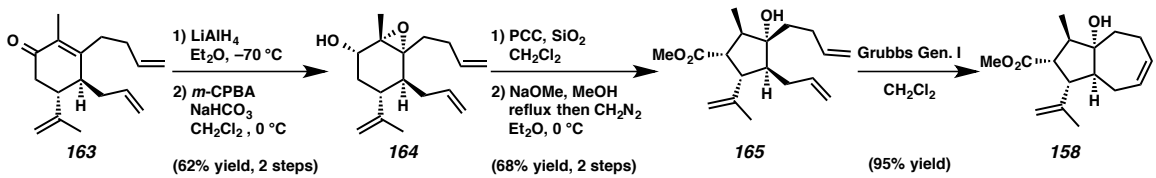

A third approach to the core scaffold of rameswaralide (**8**) was disclosed by Trost and coworkers.[44] Synthetic access to core tricycle **166** would be accomplished by an acyl

radical cyclization and epoxidation of selenide **167** (Scheme 1.5.5.8). Acylselenide **167** would be produced by the acylation of secondary alcohol **168**. Construction of bicycle **168** could be achieved by the intramolecular [5 + 2] cycloaddition of allylic cyclopropane **169**.

Scheme 1.5.5.8. Trost's Retrosynthetic Approach Toward Rameswaralide Core ***166***

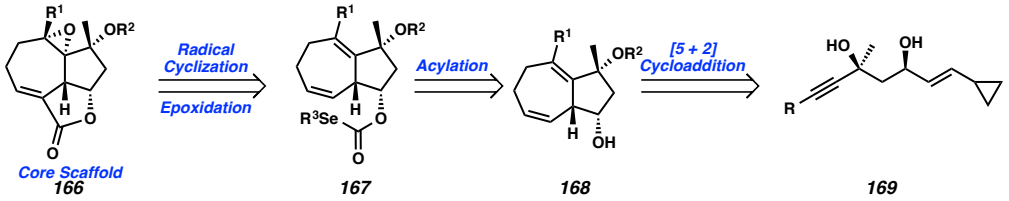

Synthesis of the racemic core tricycle of rameswaralide commenced with known cyclopropane **170** (Scheme 1.5.5.9). Stereoselective 1,2-reduction of enone **170** furnished *syn*-1,3-diol **171** in a 20:1 diastereomeric ratio in favor of the desired product as shown. Subsequent ruthenium-catalyzed intramolecular [5 + 2] cycloaddition provided cycloheptadiene **172** in 73% yield. Acylselenide **173** was then formed over two steps from secondary alcohol **172** in high yield. Reductive radical cyclization of acylselenide **173** furnished tricycle **174** in 88% yield. Epoxidation of allylic alcohol **174** provided tetracycle **175**, which was advanced to sulfoxide **176** over two steps. Ultimately, elimination of sulfoxide **176** by heating in toluene at 90 °C provided two isomeric forms of the desired core of rameswaralide, **177** and **178**, although further progress toward the natural product itself has not been disclosed at this stage.

Scheme 1.5.5.9. Trost's Construction of the Rameswaralide Tricyclic Scaffold (Trost)

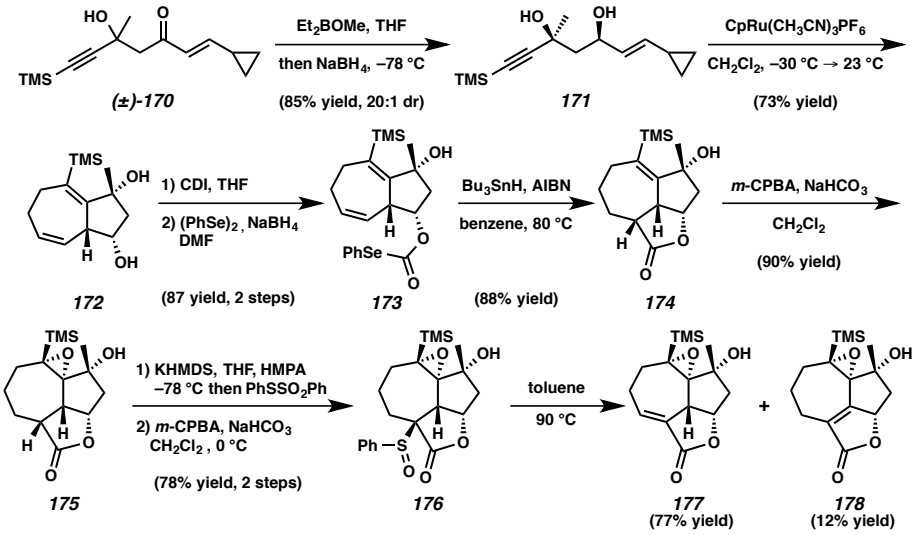

1.5.6 *Synthetic Efforts Toward Rameswaralide (8), Mandapamates (17–19), and Plumarellides (15–16)*

Pattenden and coworkers also developed synthetic access to the core of rameswarellide during their pursuit of a unified biomimetic approach to the mandapamates and plumarellides.[45] The mandapamates (**17**–**19**) and plumarellides (**15** and **16**) share a common carbocyclic scaffold (Figure 1.5.6.1). Although they are varied to a different extent in overall oxidation state and relative configuration at the spirocyclic furan ring juncture, Pattenden and coworkers sought to test their biosynthetic hypotheses for the construction of each of these 5 natural products through related mechanisms.

Figure 1.5.6.1. Mandapamate and Plumarellide Natural Products

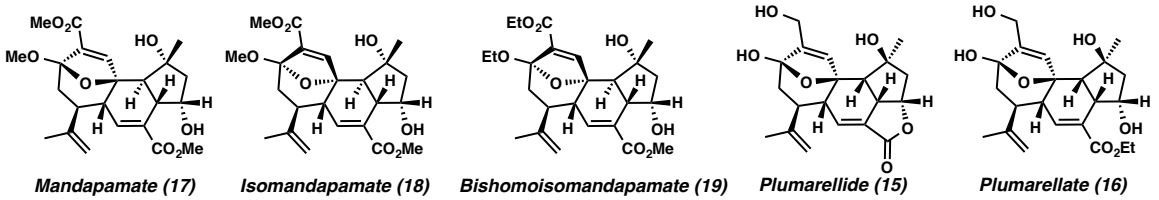

Hypothesizing that each of the mandapamates and plumarellides arises in vivo from the corresponding macrocyclic precursor by an intramolecular [4 + 2] cycloaddition (e.g.,

macrocycle **35** to plumarellide (**15**), Scheme 1.5.6.1), Pattenden and coworkers designed a series of model substrates (**179–182**) to explore the propensity of related systems to construct the desired carbocyclic scaffold. Acyclic diastereomeric diols **179** and **180** were synthesized through an asymmetric dihydroxylation route while macrocyclic ester **181** and acetate **182** were each constructed in an enantiospecific fashion from (–)-malic acid.

Scheme 1.5.6.1. Substrates for Exploration of Proposed Biosynthesis (Pattenden)

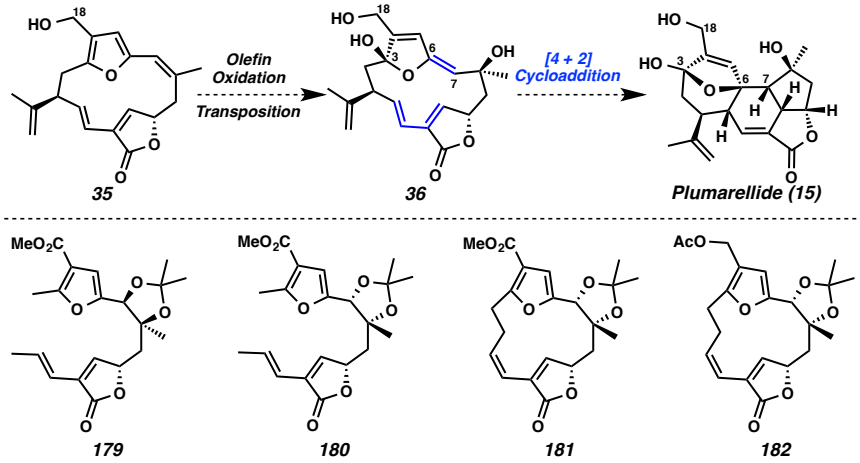

Exposure of acetonide **180** to TFA resulted in the cleavage of the ketal and subsequent intramolecular rearrangement (Scheme 1.5.6.2). Based on the isolated products, Pattenden and coworkers hypothesize that under the reaction conditions, furan **180** proceeds through intermediate **183** en route to allylic cation **184** after intramolecular cyclization. Cation **184** would then undergo nucleophilic attack from either C(6) or C(5) of the furan ring to furnish cyclohexene **185** or cycloheptene **186**, respectively. Cyclohexene **183**, the minor product, represents the core structure of the mandapamates with the lactone found in plumerallide still intact. Pentacycle **185** is epimeric to the plumarellide core, however, at C(8). The unexpected major product, tetracycle **186**, is

the core structure of rameswaralide (**8**), containing all of the required relative stereochemistry.

Scheme 1.5.6.2. Synthesis of the Mandapamate and Rameswaralide Core Scaffolds (Pattenden)

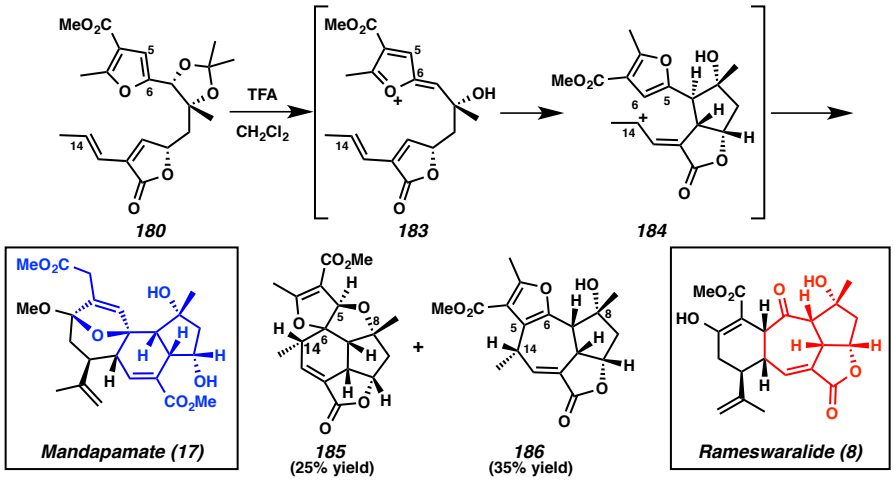

In an effort to construct the plumarellide core, diastereomeric diol **179** was subjected to identical reaction conditions (Scheme 1.5.6.3). Surprisingly, the only observed product was the C(7) and C(8) diastereomer of the rameswaralide core **189**. This empirical evidence suggests that the influence of C(8) stereochemistry is critical for the productive formal intramolecular cycloaddition of the nonmacrocyclic substrates **179** and **180**.

*Scheme 1.5.6.3. Formation of Rameswaralide Core from Diol **179** (Pattenden)*

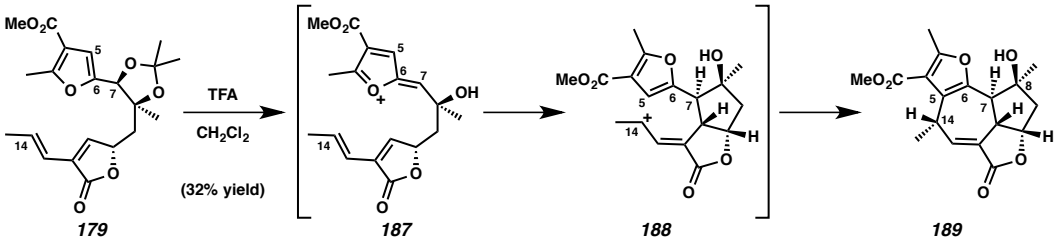

Macrocyclic substrates **181** and **182** were then exposed to aqueous TFA and both selectively furnished unexpected tetracycle **192** as the sole product without any trace of the desired plumarellide scaffold **193** (Scheme 1.5.6.4). Tetracycle **192** is proposed to

arise from the formal cycloaddition between C(4) and C(5) of the vinylogous diketone moiety and the 1,3-diene between C(11) and C(14). Plumarellide core **193**, the expected product, would have been produced by the proposed biomimetic [4 + 2] cycloaddition between the olefin at C(6) and C(7) of macrocycle **190** with the diene moiety before isomerization to vinylogous diketone **191**.

Scheme 1.5.6.4. Synthesis of Unexpected Novel Cembranoid Core (Pattenden)

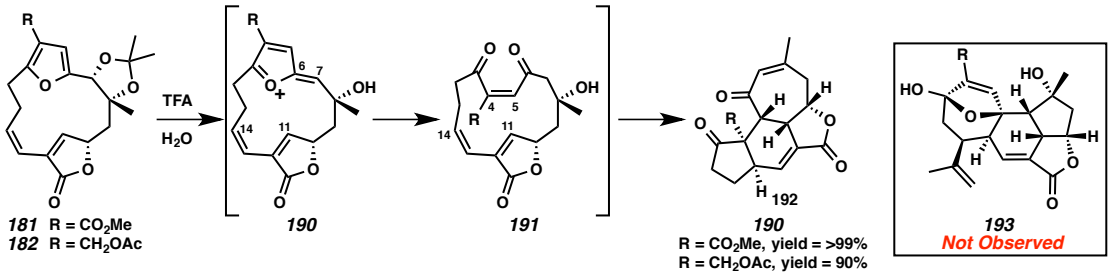

Although these results did not disprove the originally proposed biosynthesis of the mandapamates and plumarellides, Pattenden and coworkers began exploring alternative biosynthetic pathways for the formation of these two natural product families. One such alternative, considering the biosynthesis of plumarellide, for example, would begin with macrocyclic cembranoid **35** (Scheme 1.5.6.5). Oxidation of the olefin between C(7) and C(8) followed by olefin transposition and intramolecular Michael addition would provide intermediate ketal **194**. Subsequent vinylogous aldol addition would complete plumarellide. Although the exact biosynthesis of the mandapamates and plumarellides remains unknown, the work done by Pattenden and workers has provided a wealth of information about the chemistry of the furanobutenolide cembranoid natural products.

Scheme 1.5.6.5. Alternative Proposal for Biosynthesis of Mandapamates and Plumarellides

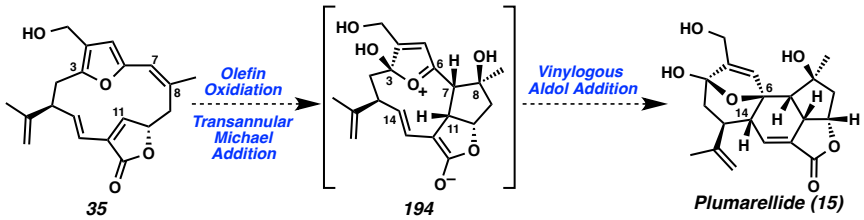

1.5.7 *Synthetic Efforts Toward Mandapamates (17–19), Plumarellides (15–16), and Dissectolide (22)*

The only other work toward the mandapamates and plumarellides was carried out by Mehta and coworkers in their pursuit of a unified strategy to the carbocyclic core of both families of cembranoids as well as the furanobutenolide norcembranoid dissectolide (**22**, Scheme 1.5.7.1).[46] Synthetic access to the common [7,6,5]-carbocyclic core **195** was envisioned through the intramolecular Diels–Alder cycloaddition of diene **196**. Vinylogous diketone **196** would in turn be synthesized by the oxidative cleavage of furan **197**.

Scheme 1.5.7.1. Retrosynthesis of Common Carbocyclic Core (Mehta)

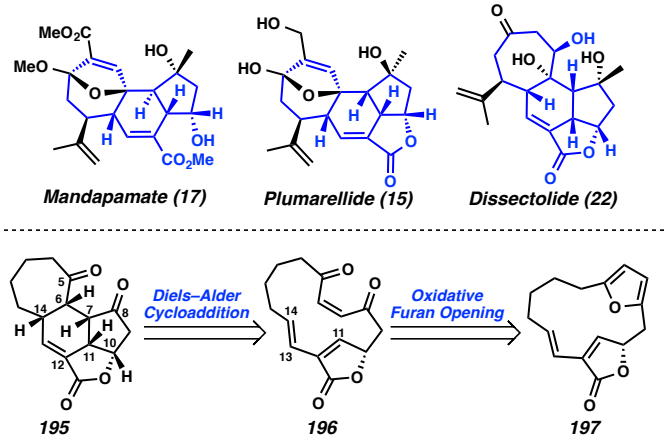

Synthetic advancement began with furfural derivative **198** (Scheme 1.5.7.2). Coupling of alkyl zinc **199** followed by nucleophilic addition of bromide **200** into the aldehyde moiety provided butenolide **201** in 47% yield over two steps. Sequential

reduction, Stille coupling, and ring-closing metathesis yielded macrocycle **202** in 14% yield over three steps. This synthetic route only provides access to the *cis*-macrocyclic product **202** with no trace to *trans*-macrocycle **197**.

*Scheme 1.5.7.2. Synthesis of Macrocyclic Diene **202** (Mehta)*

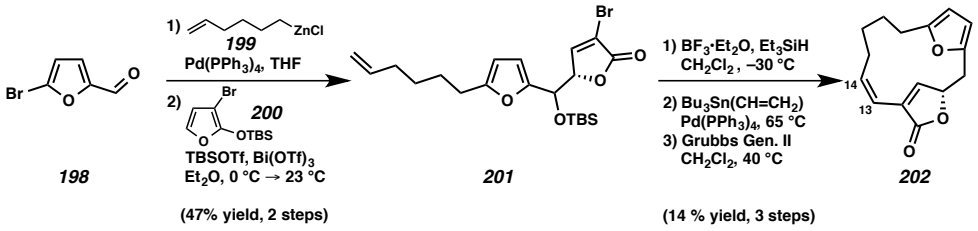

Advancement of *cis*-macrocycle **202** by oxidative cleavage of the furan moiety provided *cis*-vinylogous diketone **203** in excellent yield (Figure 1.5.7.3). Diene **202** was then heated in toluene in order to induce an intramolecular Diels–Alder cycloaddition. Under the reaction conditions, the *cis*-dienophile isomerized to the *trans*-vinylogous diketone, as evidenced by the resulting *trans*-stereochemistry in tricycle **204**, which was isolated as the sole product from diene **203** after in situ opening of the lactone. Tricycle **205** represents the most advanced intermediate synthetized by Mehta and coworkers.

Unfortunately, core scaffold **205** possesses the improper relative stereochemistry at C(7) in comparison to plumarellide (**15**) and dissectolide (**22**) and at C(11) as required for all three natural products (i.e., **15**, **17**, and **22**). While the epimerization of configuration at C(7) can easily be envisioned, the correction of the *anti*-relationship between C(11) and C(14) to the desired *syn* configuration would be nontrival. This *anti*-relationship is dictated by the *cis*-configuration of the $\Delta_{13,14}$ bond formed during the macrocyclization of lactone **202** by ring-closing metathesis. As such, alternative formation of macrocycle **202** would need to be established in order for this synthetic route to warrant further exploration in pursuit of the polycyclic furanobutenolide natural products.

*Scheme 1.5.7.3. Construction of Tricycle **205** by Diels–Alder Cycloaddition (Mehta)*

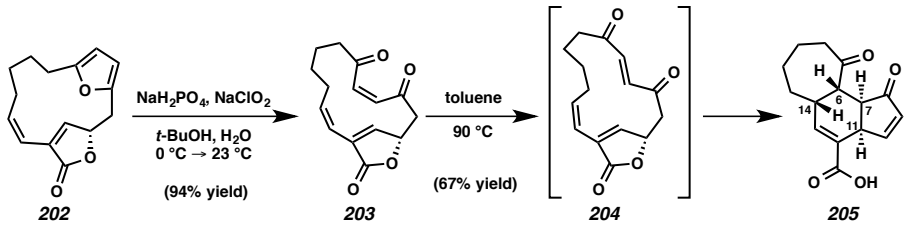

1.5.8 *Synthetic Efforts Toward Yonarolide (25)*

The synthesis of yonarolide (**25**) has only been studied by Ito and coworkers in their development of a strategy for the construction of the tricyclic portion if its core scaffold (**203**, Scheme 1.5.8.1).[47] Cyclopentene **206** would be formed after intramolecular aldol condensation of methyl ketone **207**. Synthesis of bicyclic cyclohexenone **207** would be constructed by the Diels–Alder cycloaddition of bisenol ether **208** and butenolide **209**.

*Scheme 1.5.8.1. Retrosynthetic Analysis of Yonarolide (**25**, Ito)*

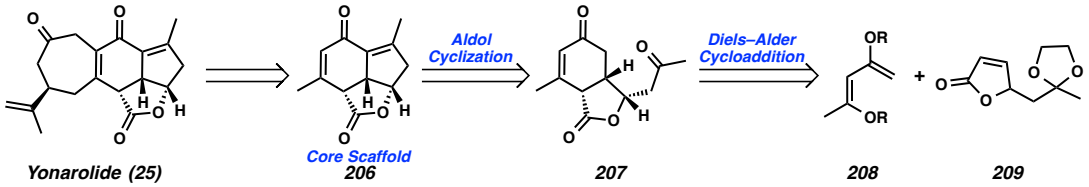

In the forward sense, Ito and coworkers pursued the racemic synthesis of the core structure of yonarolide beginning with butenolide **209**, which was available from β-ketoester **210** in 65% yield over four steps. Diels–Alder cycloaddition of dienol ether **211** with butenolide **209** proceeded smoothly in the presence of trimethylaluminum and bis(trifluoromethanesulfonyl)methane. Subsequent ketal cleavage provided methyl ketone **212** in 52% yield over two steps from unsaturated lactone **209**.

*Scheme 1.5.8.2. Diels–Alder Cycloaddition of Butenolide **209** (Ito)*

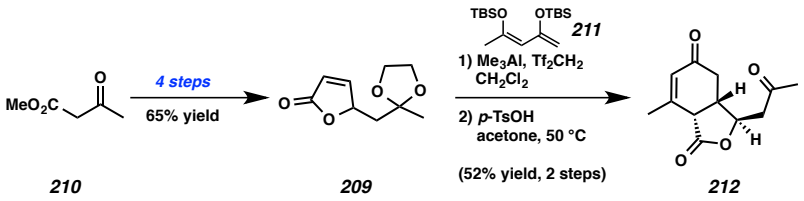

Although methyl ketone **212** contained the wrong relative stereochemistry at the lactone carbinol, exposure of the substrate to TFA in toluene at elevated temperature resulted in the isomerization of configuration at this stereocenter (likely through a retro-conjugate addition and cyclization pathway) and induced the desired aldol condensation to furnish the yonarolide core (**206**) in 55% yield (Scheme 1.5.8.3). No trace of undesired core **213** was observed. By this synthetic route, Ito and coworkers showed the viability of their retrosynthetic strategy for accessing the core of yonarolide (**206**), however, the employment of this method in further advancement toward yonarolide has not yet been disclosed.

Scheme 1.5.8.3. Synthesis of the Yonarolide Core by Tandem Isomerization-Aldol Cyclization (Ito)

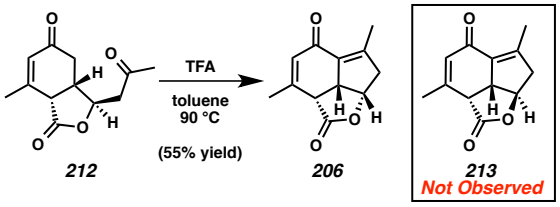

1.5.9 *Synthetic Efforts Toward Ineleganolide (9) and Sinulochmodin C (10)*

Three different methods for the total synthesis of ineleganolide (**9**) have been disclosed in the literature. The first example was presented by Moeller and coworkers, however, the studies on their model system failed to generate even the bicyclic core of ineleganolide.[48] The second was a biomimetic, semisynthetic approach taken by Pattenden and coworkers toward both ineleganolide (**9**) and sinulochmodin C (**10**,

Scheme 1.5.9.1).[49] Previously, Pattenden and coworkers had postulated the biosynthesis of both ineleganolide (**9**) and sinulochmodin C (**10**) occurred through sequential transannular Michael additions from 5-episinuleptolide (**5**, see Schemes 1.4.2.1 and 1.4.2.2).[1a,14]

*Scheme 1.5.9.1. Biomimetic Semisynthesis of Ineleganolide (**9**) and Sinulochmodin C (**10**, Pattenden)*

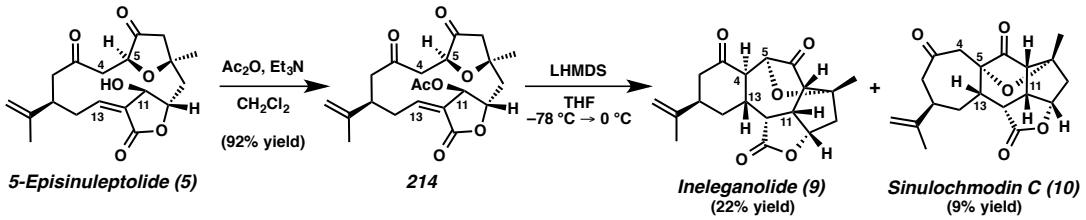

To explore this hypothesis, the authors took a portion of 5-episinuleptolide (**5**) isolated from the natural source for exploratory semisynthetic studies. It is noteworthy that, to date, there are no reports of the total synthesis of 5-episinuleptolide. Acetylation of secondary alcohol **214** was accomplished in 92% yield using standard conditions. Exposure of acetate **214** to LHMDS over an extended reaction time, warming to 0 °C furnished both ineleganolide (**9**) and sinulochmodin C (**10**) as predicted in 22% yield and 9% yield, respectively.

Additionally, Pattenden and coworkers sought to accomplish the biomimetic semisynthesis of another norcembranoid diterpene natural product horiolide (**20**)[26] by exposure of acetate **214** to modified strongly basic conditions (Scheme 1.5.9.2). Despite their efforts, only novel norcembranoid derivative **215** was isolated as a product of the reaction. No trace of either horiolide (**20**) or kavaranolide (**21**), which has only been isolated and described since the publication of Pattenden's work,[27] was detected.

Scheme 1.5.9.2. Attempted Biomimetic Semisynthesis of Additional Norcembranoids (Pattenden)

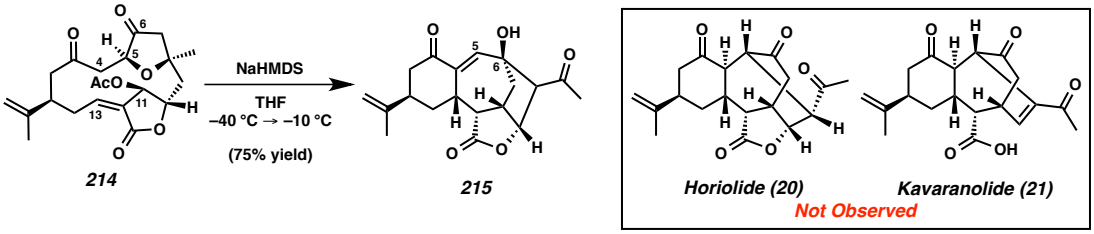

The second example of the synthetic pursuit of ineleganolide comes from the Vanderwal laboratory and their work toward the asymmetric total synthesis of the natural product.[50] Retrosynthetically, access to ineleganolide (**9**) was envisioned after construction of the central heptacycle by cyclization of tetracycle **216** (Scheme 1.5.9.3). Ketofuran **216** would in turn be synthesized from desmethylcarvone (**217**) and tricycle **218** after intermolecular Michael addition.

*Scheme 1.5.9.3. Vanderwal's Retrosynthetic Analysis of Ineleganolide (**9**)*

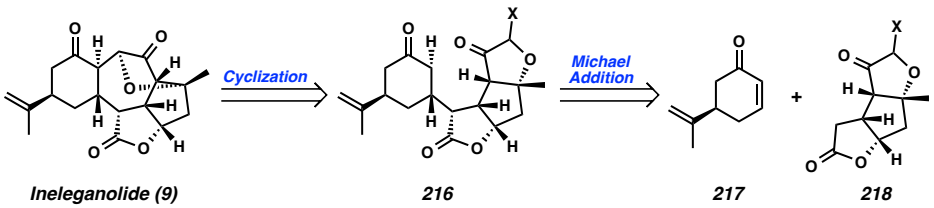

For the purpose of synthetic development, the enantiomer *ent*-ineleganolide (***ent*-9**) was targeted. Advancement toward the natural product began with the asymmetric deprotonation and subsequent rearrangement of epoxide **219** to furnish *cis*-1,3-cyclopentenediol **221** in 79% yield with 89% *ee* (Scheme 1.5.9.4). Oxidation of allylic alcohol **(+)-221** with PCC provided the cyclopentenone building block **(+)-222** in 97% yield.

*Scheme 1.5.9.4. Synthesis of Enantioenriched Cyclopentenone **(+)-222** (Vanderwal)*

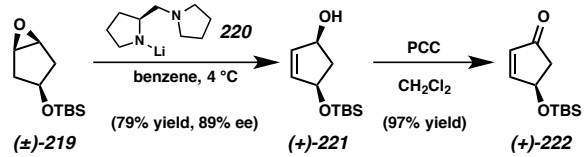

Advancement of enantioenriched cyclopentenone **(+)-222** proceeded with the 1,2-addition of methyl lithium into the conjugated system (Scheme 1.5.9.5). Alkylation of the resultant tertiary alcohol and cleavage of the silyl ether provided propargyl alcohol **223** in 87% yield over three steps from enone **(+)-222**. Functionalization of secondary alcohol **223** with ethyl vinyl ether in the presence of NBS provided bromide **224** in 87% yield as a 1:1 mixture of diastereomers. Radical cascade cyclization of cyclopentene **224** furnished tricycles **225** and **226** in a 1:1 mixture after sequential ozonolysis in a combined 78% yield over two steps.[51]

*Scheme 1.5.9.5. Construction of Ketofurans **225** and **226** (Vanderwal)*

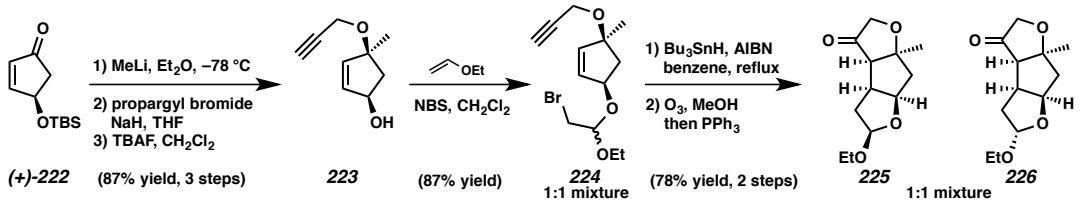

Fortuitous equilibration of epimers **225** and **226** toward lactol **226** in a 19:1 ratio enabled the triflation of the ketofuran moiety and efficient advancement of material, as epimer **225** would not undergo this desired transformation (Scheme 1.5.9.6). Oxidation of acetal **227** to lactone **228** provided the desired tricyclic coupling partner in 88% yield.

Scheme 1.5.9.6. Completion of Tricyclic Coupling Partner (Vanderwal)

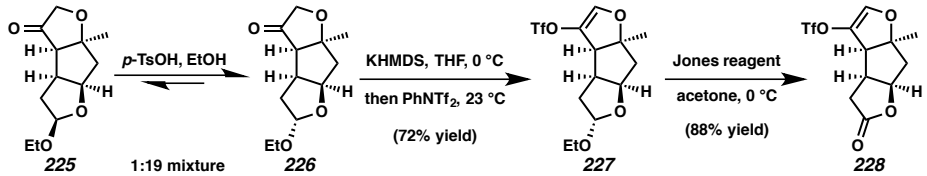

The asymmetric synthesis of complimentary enone **(+)-217** began with racemic cyclohexanone **229** (Scheme 1.5.9.7). Diastereoselective reduction of the carbonyl followed by enzymatic acetylation provided both alcohol **(+)-230** and acetate **(+)-231** in greater than 95% *ee*.[52] Advancement of desired diastereomer **(+)-231** was accomplished by saponification and oxidation of the intermediate secondary alcohol. Oxidative desaturation of the resultant cyclohexanone was accomplished over two steps to provide enone **(+)-217** in 69% yield from acetate **(+)-231** as the complimentary coupling partner.

*Scheme 1.5.9.7. Asymmetric Synthesis of Complimentary Cyclohexenone **(+)-217** (Vanderwal)*

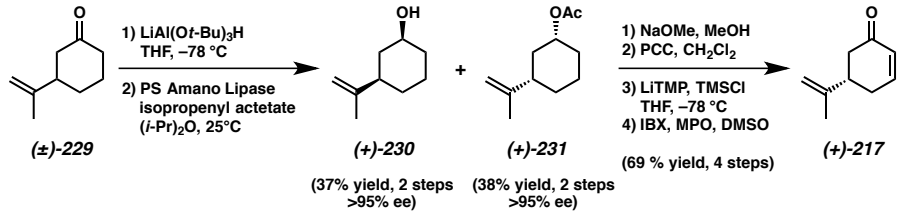

Coupling of the two fragments of ineleganolide was accomplished using a Mukaiyama–Michael addition, beginning with formation of the silyl enol ether of lactone **228** (Scheme 1.5.9.8). Subsequent exposure of the intermediate enol ether to enone **(+)-217** in the presence of lanthanum(III) triflate induced the planned Mukaiyama-Michael addition, providing tetracycle **232** in 91% yield in high diastereoselectivity as the undesired epimer at the α-position of the lactone moiety. Despite screening a variety of conditions, Vanderwal and coworkers were unable to accomplish the desired epimerization to furnish tetracycle **233**.

Scheme 1.5.9.8. Coupling of Ineleganolide Fragments (Vanderwal)

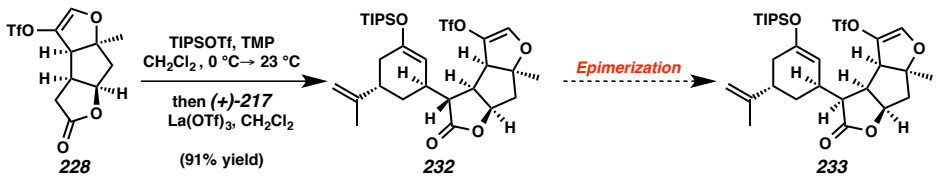

Exploring alternative approaches toward *ent*-ineleganolide (***ent*-9**), tetracycle **232** would be advanced by saponification of the lactone moiety, followed by protection of the secondary alcohol and carboxylic acid to furnish ketone **234** in 45% yield over three steps (Scheme 1.5.9.9). Bromination of silyl enol ether **234** with NBS furnished α-bromoketone **235** as a mixture of diastereomers. Unfortunately, samarium(II) iodide-mediated cyclization conditions failed to produce desired ketofuran **237**, forming instead tetrahydrofuran **236** in high yield. Despite attempting a number of alternative routes, Vanderwal and coworkers were unable to complete the total synthesis of *ent*-ineleganolide (***ent*-9**).

Scheme 1.5.9.9. Alternative Advancement Toward Ineleganolide (Vanderwal)

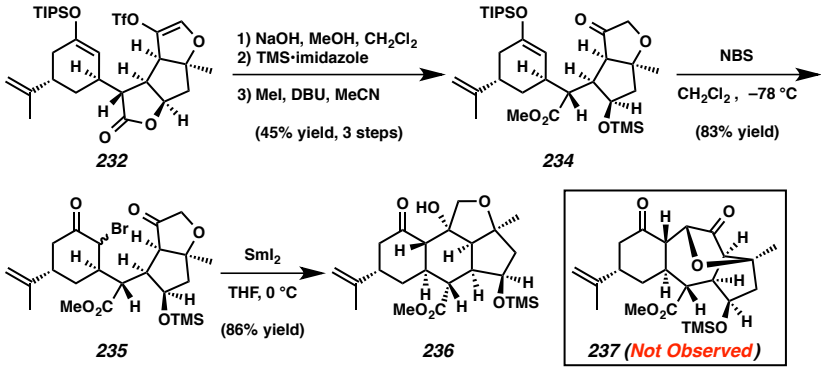

1.6 Conclusion

The synthetic efforts toward ineleganolide are a tremendous representation of the pattern of successes and failures around the synthetic studies of the furanobutenolide cembranoid and norcembranoid natural products. The extremely limited examples of completed syntheses of members of this natural product family have been exclusively biomimetic synthetic or semisynthetic studies. Not a *single* de novo synthesis of a furanobutenolide cembranoid and norcembranoid has been completed to date. A number of studies toward the synthesis of cembranoid and norcembranoid carbocyclic scaffolds

have been disclosed, revealing valuable information about the chemistry of these core structures. The fact that not one of these synthetic routes has yielded the targeted natural product, however, highlights the need for further investigations. The continued investigation of these elegant, biologically active, stererogenically complex, and highly oxygenated family of natural products will require the development of new synthetic methods for the synthetic manipulations of compact and highly oxidized polycycles. Success in this area and completion of the syntheses of the polycyclic furanobutenolide cembranoids and norcembranoids will benefit not only other areas of synthetic chemistry through methodological development, but also medicinal chemistry and chemical biology, providing access to these scarce bioactive compounds for complete biological evaluation.

1.7 Notes and References

1. (a) Li, Y.; Pattenden, G. *Nat. Prod. Rep.* **2011**, *28*, 1269–1310. (b) Marrero, J.; Rodríguez I. I.; Rodríguez, A. D. *Compr. Nat. Prod. II* **2010**, *2*, 363–428. (c) Weinheimer, A. J.; Chang, C. W. J.; Matson, J. A. *Fortschr. Chem. Org. Naturst.* **1979**, *36*, 285–387.

2. (a) Montaser, R.; Luesch, H. *Future Med. Chem.* **2011**, *3*, 1475–1489. (b) Berrue, F.; Kerr, R. G. *Nat. Prod. Rep.* **2009**, *26*, 681–710. (c) Kamel, H. N.; Slattery, M. *Pharm. Biol.* **2005**, *43*, 253–269.

3. (a) Abramson, S. N.; Trischman, J. A.; Tapiolas, D. M.; Harold, E. E.; Fenical, W.; Taylor, P. *J. Med. Chem.* **1991**, *34*, 1798–1804. (b) Fenical, W.; Okuda, R. K.; Bandurraga, M. M.; Culver, P.; Jacobs, R. S. *Science* **1981**, *212*, 1512–1514. (c) Culver, P.; Jacobs, R. S. *Toxicon* **1981**, *19*, 825–830.

4. Wright, A. E.; Burres, N. S.; Schulte, G. K. *Tetrahedron Lett.* **1989**, *30*, 3491–3494.

5. Rodríguez, A. D.; Shi, J.-G.; Huang, S. D. *J. Nat. Prod.* **1999**, *62*, 1228–1237.

6. (a) Liang, C.-H.; Wang, G.-H.; Chou, T.-H.; Wang, S.-H.; Lin, R.-J.; Chan, L.-P.; So, E. C.; Sheu, J.-H. *Biochim. Biophys. Acta* **2012**, *1820*, 1149–1157. (b) Yang, B.; Zhou, X.-F.; Lin, X.-P.; Liu, J.; Peng, Y.; Yang, X.-W.; Liu, Y. *Curr. Org. Chem.* **2012**, *16*, 1512–1539. (c) Ahmed, A. F.; Shiue, R.-T.; Wang, G.-H.; Dai, C.-F.; Kuo, Y.-H.; Sheu, J.-H. *Tetrahedron* **2003**, *59*, 7337–7344. (d) Sheu, J.-H.; Ahmed, A. F.; Shiue, R.-T.; Dai, C.-F.; Kuo, Y.-H. *J. Nat. Prod.* **2002**, *65*, 1904–1908.

7. Marrero, J.; Rodríguez, A. D.; Baran, P.; Raptis, R. G.; Sánchez, J. A.; Ortega-Barria, E.; Capson, T. L. *Org. Lett.* **2004**, *6*, 1661–1664.

8. Marrero, J.; Rodríguez, A. D.; Barnes, C. L. *Org. Lett.* **2005**, *7*, 1877–1880.

9. Faulkner, J. D.; Venkateswarlue, Y. Rameswaralide and Rameswaralide Derivatives. U.S. Patent 6300371, May 18, 2000.

10. Duh, C.-Y.; Wang, S.-K.; Chia, M.-C.; Chiang, M. Y. *Tetrahedron Lett.* **1999**, *40*, 6033–6035.

11. Tseng, Y.-J.; Ahmed, A. F.; Dai, C.-F.; Chiang, M. Y.; Sheu, J.-H. *Org. Lett.* **2005**, *7*, 3813–3816.

12. For general reviews on marine natural products, see: Blunt, J. W.; Copp, B. R.; Keyzers, R. A.; Munro, M. H. G.; Prinsep, M. R. *Nat. Prod. Rep.* **2015**, *32*, 116–211 and all preceeding reviews in this annual series from *Nat. Prod. Rep.*

13. Roethle, P. A.; Trauner, D. *Nat. Prod. Rep.* **2008**, *25*, 298–317.

14. Li, Y.; Pattenden, G. *Nat. Prod. Rep.* **2011**, *28*, 429–440.

15. (a) Rodríguez, A. D. *Tetrahedron* **1995**, *51*, 4571–4618. (b) Tius, M. A. *Chem. Rev.* **1988**, *88*, 719–732.

16. The initial studies to determine the absolute stereochemistry of the cembranoid diterpenes were performed on rubifolide (**11**, R = CH_3) and confirmed by subsequent studies on other members of the family, see: (a) Dorta, E.; Diaz-Marrero, A. R.; Brito, I.; Cueto, M.; D'Croz, L.; Darias, J. *Tetrahedron* **2007**, *63*, 9057–9062. (b) Gutierrez, M.; Capson, T. L.; Guzman, H. M.; Gonzalez, J.; Ortega-Barria, E.; Quinoa, E.; Riguera, R. *J. Nat. Prod.* **2005**, *68*, 614–616. (c) Marshall, J. A.; Sehon, C. A. *J. Org. Chem.* **1997**, *62*, 4313–4320.

17. Rodríguez, A. D.; Shi, Y.-P. *J. Org. Chem.* **2000**, *65*, 5839–5842.

18. (a) Roethle, P. A.; Hernandez, P. T.; Trauner, D. *Org. Lett.* **2006**, *8*, 5901–5904. (b) Tang, B.; Bray, C. D.; Pattenden, G. *Tetrahedron Lett.* **2006**, *47*, 6401–6404. (c) Tang, B.; Bray, C. D.; Pattenden, G. *Org. Biomol. Chem.* **2009**, *7*, 4448–4457.

19. Stonik, V. A.; Kapustina, I. I.; Kalinovsky, A. I.; Dmitrenok, P. S.; Grebnev, B. B. *Tetrahedron Lett.* **2002**, *43*, 315–317.

20. Venkateswarlu, Y.; Biabani, M. F.; Reddy, M. V. R.; Rao, T. P.; Kunwar, A. C.; Faulkner, D. J. *Tetrahedron Lett.* **1994**, *35*, 2249–2252.

21. Anjaneyulu, A. S.; Sagar, K. S.; Venugopal, M. J. *Tetrahedron* **1995**, *51*, 10997–11010.

22. Ammanamanchi; Anjaneyulu, S. R.; Sarada, P. *J. Chem. Res. (S)* **1999**, 600–601.

23. Anjaneyulu, A. S.; Venugopal, M. J.; Sarada, P.; Clardy, J.; Lobkovsky, E. *Tetrahedron Lett.* **1998**, *39*, 139–142.

24. For isolation of rameswaralide (**8**) and initial biosynthetic speculation, see: Ramesh, P.; Reddy, N. S.; Venkateswarlu, Y.; Reddy, M. V. R.; Faulkner, D. J. *Tetrahedron Letters* **1998**, *39*, 8217–8220.

25. Pattenden, G.; Winne, J. M. *Tetrahedron Lett.* **2009**, *50*, 7310–7313.

26. Radhika, P.; Subba Rao, P. V.; Anjaneyulu, V.; Asolkar, R. N.; Laatsch, H. *J. Nat. Prod.* **2002**, *65*, 737–739.

27. Lillsunde, K.-E.; Festa, C.; Adel, H.; de Marino, S.; Lombardi, V.; Tilvi, S.; Nawrot, D.; Zampella, A.; D'Souza, L.; D'Auria, M.; Tammela, P. *Marine Drugs* **2014**, *12*, 4045–4068.

28. Iguchi, K.; Kajiyama, K.; Yamada, Y. *Tetrahedron Lett.* **1995**, *36*, 8807–8808.

29. Kobayashi, M.; Appa Rao, K. M. C.; Krishna, M. M.; Anjaneyulu, V. *J. Chem. Res. (S)* **1995**, 188–189.

30. (a) Jana, A.; Mondal, S.; Ghosh, S. *Org. Biomol. Chem.* **2015**, *13*, 1846–1859. (b) Jana, A.; Mondal, S.; Hossain, M. F.; Ghosh, S. *Tetrahedron Lett.* **2012**, *53*, 6830–6833.

31. (a) Townsend, S. D.; Sulikowski, G. A. *Org. Lett.* **2013**, *15*, 5096–5098. (b) Doroh, B.; Sulikowski, G. A. *Org. Lett.* **2006**, *8*, 903–906.

32. (a) Himmelbauer, M.; Farcet, J.-B.; Gagnepain, J.; Mulzer, J. *Org. Lett.* **2013**, *15*, 3098–3101. (b) Himmelbauer, M.; Farcet, J.-B.; Gagnepain, J.; Mulzer, J. *Eur. J. Org. Chem.* **2013**, 8214–8244.

33. Nicolaou, K. C.; Adsool, V. A.; Hale, C. R. H. *Angew. Chem., Int. Ed.* **2011**, *50*, 5149–5152.

34. (a) Yang, E. G.; Sekar, K.; Lear, M. J. *Tetrahedron Lett.* **2013**, *54*, 4406–4408. (b) Miao, R.; Gramani, S. G.; Lear, M. J. *Tetrahedron Lett.* **2009**, *50*, 1731–1733.

35. Farcet, J.-B.; Himmelbauer, M.; Mulzer, J. *Eur. J. Org. Chem.* **2013**, 4379–4398.

36. (a) Farcet, J.-B.; Himmelbauer, M.; Mulzer, J. *Eur. J. Org. Chem.* **2013**, 8245–8252. (b) Farcet, J.-B.; Himmelbauer, M.; Mulzer, J. *Org. Lett.* **2012**, *14*, 2195–

2197.

37. Meyer, M. E.; Phillips, J. H.; Ferreira, E. M.; Stoltz, B. M. *Tetrahedron* **2013**, *69*, 7627–7635.

38. Saitman, A.; Theodorakis, E. A. *Org. Lett.* **2013**, *15*, 2410–2413.

39. Mehta, G.; Kumaran, R. S. *Tetrahedron Lett.* **2001**, *42*, 8097–8100.

40. Beingessner, R. L.; Farand, J. A.; Barriault, L. *J. Org. Chem.* **2010**, *75*, 6337–6346.

41. Wang, S. C.; Tantillo, D. J. *J. Org. Chem.* **2008**, *73*, 1516–1523.

42. Mehta, G.; Lakshminath, S. *Tetrahedron Lett.* **2006**, *47*, 327–330.

43. Srikrishna, A.; Dethe, D. H. *Org. Lett.* **2004**, *6*, 165–168.

44. Trost, B. M.; Nguyen, H. M.; Koradin, C. *Tetrahedron Lett.* **2010**, *51*, 6232–6235.

45. (a) Li, Y.; Palframan, M. J.; Pattenden, G.; Winne, J. M. *Tetrahedron* **2014**, *70*, 7229–7240. (b) Palframan, M. J.; Pattenden, G. *Tetrahedron Lett.* **2013**, *54*, 324–328. (c) Li, Y.; Pattenden, G. *Tetrahedron Lett.* **2011**, *52*, 2088–2092. (d) Pattenden, G.; Winne, J. M. *Tetrahedron Lett.* **2010**, *51*, 5044–5047. (e) Pattenden, G.; Winne, J. M. *Tetrahedron Lett.* **2009**, *50*, 7310–7313.

46. Vasamsetty, L.; Khan, F. A.; Mehta, G. *Tetrahedron Lett.* **2014**, *55*, 7068–7071.

47. Ueda, Y.; Abe, H.; Iguchi, K.; Ito, H. *Tetrahedron Lett.* **2011**, *52*, 3379–3381.

48. (a) Tang, F.; Moeller, K. D. *Tetrahedron* **2009**, *65*, 10863–10875. (b) Tang, F.; Moeller, K. D. *J. Am. Chem. Soc.* **2007**, *129*, 12414–12415.

49. Li, Y.; Pattenden, G. *Tetrahedron* **2011**, *67*, 10045–10052.

50. Horn, E. J. Studies Toward the Synthesis of Ineleganolide. Ph.D. dissertation, University of California at Irvine, Irvine, CA, 2014.

51. (a) Jasperse, C. P.; Curran, D. P.; Fevig, T. L. *Chem. Rev.* **1991**, *91*, 1237–1286. (b) Curran, D. P.; Rakiewicz, D. M. *J. Am. Chem. Soc.* **1985**, *107*, 1448–1449.

52. Sarakinos, G.; Corey, E. J. *Org. Lett.* **1999**, *1*, 811–814.

CHAPTER 2

Enantioselective Synthesis of a Hydroxymethyl-cis-1,3-cyclopentenediol Building Block†

2.1 Introduction

Functionalized cyclopentanol frameworks are an important structural motif in organic chemistry. Scaffolds of this type are found in many biologically active natural products,[1] pharmaceuticals,[2] and nucleoside analogs.[3] In particular, *cis*-1,3-cyclopentanediols (**238**) have been extensively employed in the synthesis of medicinally relevant natural and non-natural compounds (Figure 2.1.1).[3,4] For example, the biologically active prostaglandin (e.g., **239** and **240**),[2,5] furanocembranoid diterpene (e.g., **8** and **13**), and norcembranoid diterpene families of natural products (e.g., **9** and **10**)[1d,6] all contain the *cis*-1,3-cyclopentanediol motif.

Typically, enantioenriched carbocycles of this type have been accessed by kinetic enzymatic[7] or classical[8] resolutions. The utility of *cis*-1,3-cyclopentanediols that contain

† This work was performed in collaboration with Dr. Jennifer L. Roizen, Dr. Russell C. Smith, and Dr. Amanda C. Jones, all alumni of the Stoltz group. Additionally, this work has been published and adapted with permission from Craig, R. A., II; Roizen, J. L.; Smith, R. C.; Jones, A. C.; Stoltz, B. M. *Org. Lett.* **2012**, *14*, 5716–5719. Copyright 2012 American Chemical Society.

a tertiary alcohol is severely limited due to the challenges associated with the stereocontrolled formation of such chiral centers. Literature examples of the asymmetric synthesis of this moiety are limited to substrate-controlled diastereoselective alkylation[4b] or asymmetric oxidation of prochiral substrates.[9] To the best of our knowledge, the enantioselective synthesis of the *cis*-1,3-cyclopentanediol scaffold has not been accomplished through asymmetric alkylation. As such, in concert with our research program dedicated to the development and application of the palladium-catalyzed asymmetric allylic alkylation,[10] we developed an efficient and general route for the enantioselective synthesis of *cis*-1,3-cyclopentanediol building block **238**.

Figure 2.1.1. Representative Natural Products Possessing cis-1,3-Cyclopentanediol Scaffold

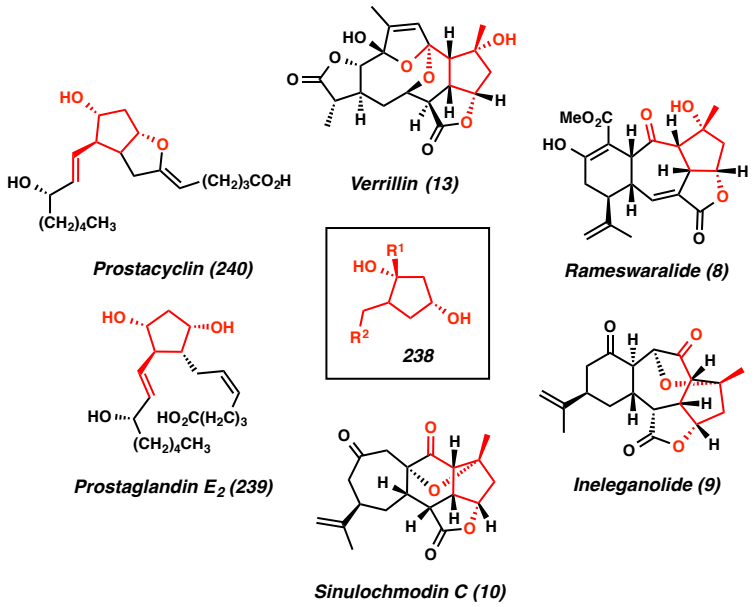

2.2 Retrosynthetic Analysis

We envisioned that a catalytic asymmetric preparation of a *cis*-1,3-cyclopentanediol core (**238**) with additional functional handles would serve as an enabling technology for various total synthetic efforts. Specifically, we targeted diol **241**, which can be synthesized from cyclopentenone **242** following diastereoselective reduction and ketal

cleavage (Scheme 2.2.1). Intramolecular cyclization of dioxanone **243** would afford cyclopentenone **242**. In turn, chiral dioxanone **243** would be prepared by palladium-catalyzed asymmetric allylic alkylation of silyl enol ether **244**.

*Scheme 2.2.1. Retrosynthetic Analysis of cis-1,3-Cyclopentenediol **241***

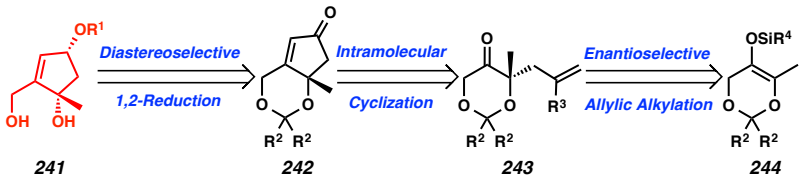

2.3 Intramolecular Aldol Cyclization

Our synthetic approach to *cis*-1,3-cyclopentenediol **241** was inspired by our previous report of the synthesis of related enone **247** (Scheme 2.3.1.A).[10a–b,e] The palladium-catalyzed asymmetric alkylation of enol ether **245** afforded allyl ketone **246** in 95% yield with 87% ee. Wacker oxidation of the allyl fragment to the intermediate methyl ketone followed by intramolecular aldol condensation generated cyclopentenone **247** in 73% yield over two steps from allylic alkylation product **246**.

Scheme 2.3.1. Enantioselective Allylic Alkylation and Elaboration of Cyclohexanone and Dioxanone Substrates

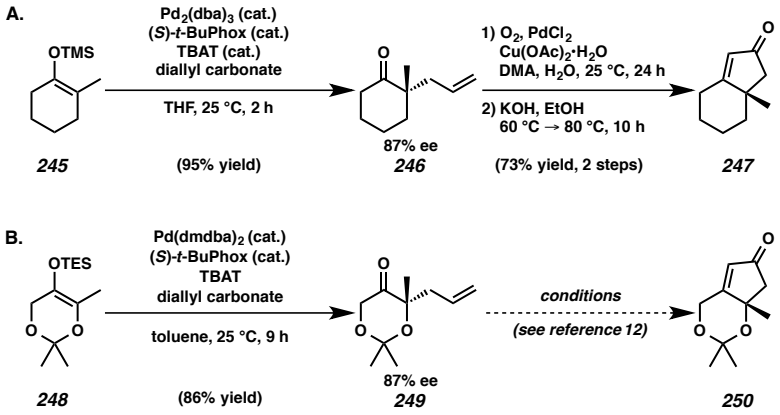

Similarly, acetonide **248** was converted to chiral ketal **249** in 86% yield and 87% ee through the enantioselective allylic alkylation procedure developed by our group

(Scheme 2.3.1.B).[11] However, employment of the sequential Wacker oxidation–intramolecular aldol cyclization conditions were found to be ineffective for the preparation cyclopentenone ketal **250**. Despite extensive exploration of alternative conditions for this transformation, formation of enone **250** was never observed by this approach.[12]

2.4 Intramolecular Wittig Cyclization

Faced with this challenge, we envisioned preparation of cyclopentenone **250** by an intramolecular Wittig cyclization (Scheme 2.4.1).[13] The introduction of an oxidized allyl fragment during the alkylation event to generate ketone **251** could facilitate the olefinic oxidation. Subsequent nucleophilic substitution with a phosphine would generate Wittig precursor **252**. Exposure to basic conditions could generate the phosphonium ylide, thereby enabling an intramolecular Wittig cyclization to form cyclopentenone **250**.

*Scheme 2.4.1. Proposed Construction of Cyclopentenone **250** Using Intramolecular Wittig Cyclization*

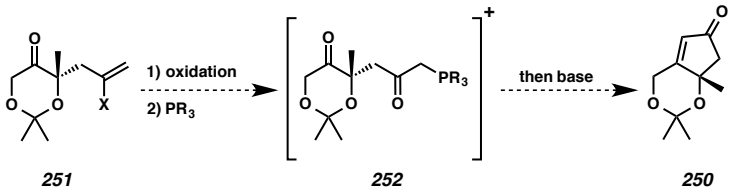

To explore this pathway, we began with chloroallylketone **254**, which was prepared by palladium-catalyzed asymmetric allylic alkylation in 82% yield and 91% ee by a known procedure (Scheme 2.4.2).[14] Epoxidation of ketone **254** with *m*-CPBA generated intermediate epoxide **255**. Nucleophilic epoxide opening then formed the α-phosphinoketone in situ, enabling the construction of enone **250** by intramolecular Wittig cyclization. Although the yield for the two-step sequence was low and varied unpredictably, desired cyclopentenone **250** could be isolated in small quantities.

*Scheme 2.4.2. Construction of Enone **250** by Epoxidation of Chloroallylketone **254***

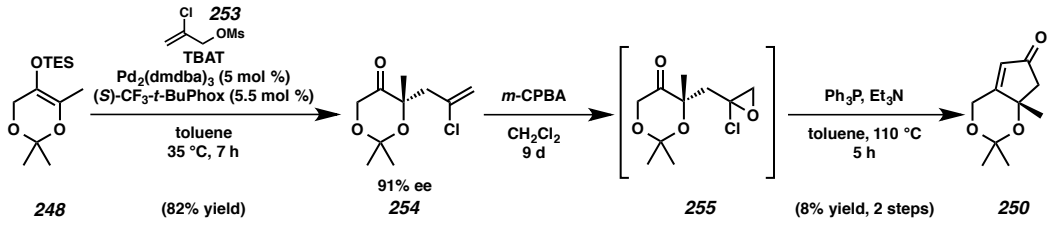

Having accomplished a proof of principle, we turned our attention to optimization. Despite the fact that a variety of epoxidation conditions had been screened,[15] the synthesis of intermediate **255** proved difficult and remained low yielding. The Wittig cyclization had similar constraints, furnishing cyclopentenone **250** in variable, unsatisfactory yields.

In spite of these failed attempts, we remained inspired by the successful isolation of the desired enone **250**. As an alternative, we decided to explore the synthesis of other Wittig cyclization precursors. One appealing option was to target intermediate α-bromoketone **256** (Scheme 2.4.3).[13] Oxidative bromination of vinyl chloride **254** with NaOBr in AcOH resulted in the formation of intermediate bromide **256**. In situ displacement of the bromide by triphenylphosphine and subsequent intramolecular Wittig cyclization furnished cyclopentenone **250** with no erosion of enantiomeric excess, albeit in unpredictable yields.

*Scheme 2.4.3. Construction of Enone **250** by Oxidative Bromination of Chloroallylketone **254***

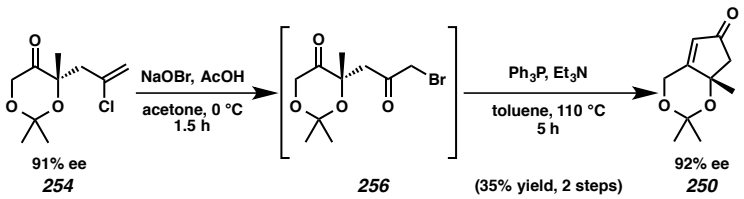

Synthetic advancement of dioxanone **254** through α-bromoketone **256** was plagued by vast inconsistencies, and optimization proved difficult. The two-step sequence offered

a range of yields from 0% to 82%. A variety of oxidative bromination conditions were attempted,[15] yet consistent yields could not be achieved. Importantly, when intermediate **256** was successfully formed,[16] conversion to cyclopentenone **250** could be reproducibly achieved with moderate success, indicating that the oxidative bromination was the problematic step in the sequence.

Upon closer inspection of the oxidative α-bromination procedure, we identified two possible sources of inconsistency. First, we suspected that exposure of substrate **254** and intermediate **256** to acetic acid was causing the ketal cleavage of both compounds throughout the reaction, resulting in decomposition. Direct observation of this hypothesis was challenging, as the cleavage of the acetonide simply generated additional quantities of the reaction solvent, acetone. An additional source of variability arose as the scale of the reaction was increased. During prolonged reaction times, a consequence of operating on greater scale (ca. 2 h), the bright yellow NaOBr solution suspended over the reaction flask in an addition funnel (Figure 2.4.1.A) decomposes due to the acetic acid vapors in the reaction headspace (Figure 2.4.1.B). This decomposition hinders reproducibility and lowers the reaction yield.

Figure 2.4.1. Decomposition of NaOBr Stock Solution

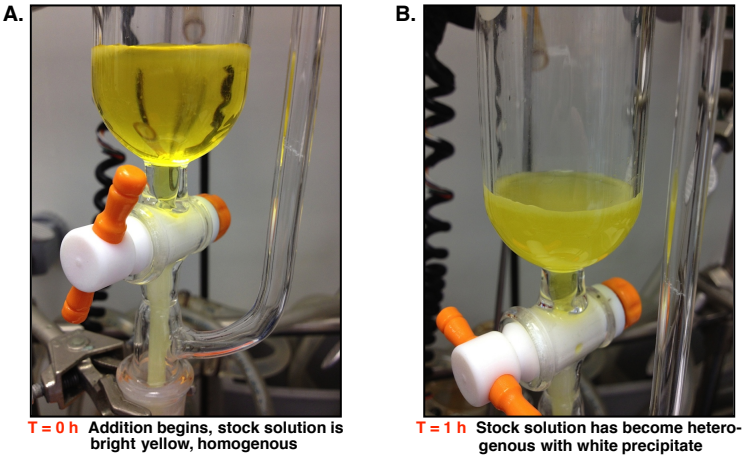

In order to address these concerns, we first sought to alter the ketal. The introduction of additional steric bulk was hypothesized to impart additional stability to the protecting group and thus its tolerance to the oxidative bromination conditions. Gratifyingly, the selection of the cyclohexyl ketal proved to have no deleterious effects on the asymmetric allylic alkylation of enol ether **257** (Scheme 2.4.4).[17] Under optimized conditions,[18] chloroallylketone **258** was generated in a greatly improved 82% yield and increased 92% ee in comparison to acetonide allylic alkylation product **254**.

Scheme 2.4.4. Synthetic Route Enabled by the Crucial Choice of the Cyclohexyl Ketal Group

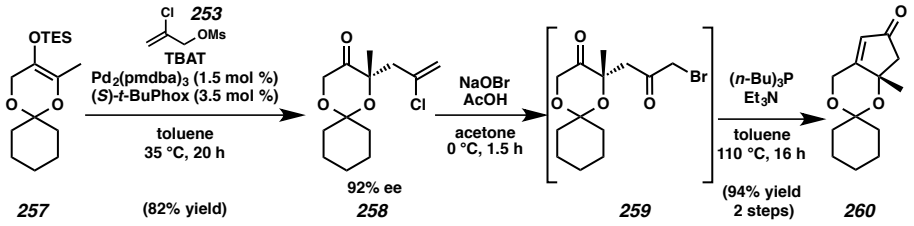

With vinyl chloride **258** in hand, we set about developing an improved procedure for the formation of α-bromoketone **259**. In order to avoid suspending the NaOBr stock solution over the headspace of the reaction for any prolonged period, we divided vinyl chloride **258** into equal portions in a solution of acetone and AcOH among a series of vials cooled to 0 °C (Figure 2.4.2.A). The addition of NaOBr was then accomplished dropwise from a needleless plastic syringe, adding one drop (ca. 40 μL) of the bright yellow stock solution to each vial every 30 seconds.[19] As the addition commences, the transparent colorless solution of vinyl chloride **258** immediately took the bright yellow color of the NaOBr stock solution (Figure 2.4.2.B). As the addition proceeded, the vials progressed through light orange (Figure 2.4.2.C) to deep red-orange (Figure 2.4.2.D) at the completion of the addition. Attempts to convert cyclohexyl ketal **258** to α-bromoketone **259** employing this procedure were met with consistent success and

complete conversion could be reliably accomplished under optimized conditions, affording bromide **259** in nearly quantitative yield.[20]

*Figure 2.4.2. Improved Technique for Conversion of Vinyl Chloride **258** to α-Bromoketone **259***

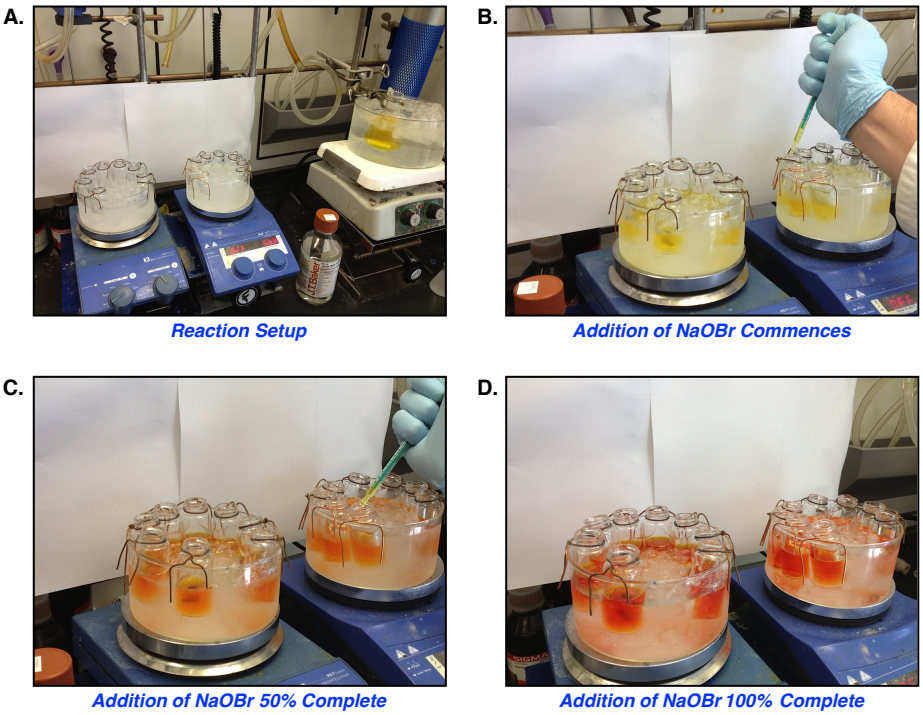

With α-bromoketone **259** in hand, the silica sensitive intermediate was immediately advanced as a crude oil to cyclopentenone **260**. Application of standard conditions for this transformation afforded enone **260**, albeit in 35–40% yield.[21] Modification of these conditions, including the use of $(n\text{-Bu})_3\text{P}$, enabled the conversion of bromide **259** to the desired cyclopentenone **260** in 94% yield over two steps from chloroallylketone **258**.

2.5 Completion of Hydroxymethyl-*cis*-1,3-cyclopentenediol 262

With the establishment of a scalable, reliable route for the production of cyclopentenone **260**, we sought to advance toward the desired *cis*-1,3-cyclopentenediol **241**. Diastereoselective 1,2-reduction of enone **260** with diisobutylaluminum hydride (DIBAL) smoothly furnished allylic alcohol **261** in excellent yield as a single

diastereomer (Scheme 2.5.1).[22] Sequential benzoylation of alcohol **261** and fumaric acid-mediated ketal cleavage yielded provided alcohol **262**, a surrogate for the targeted cyclopentene **241**. This three-step transformation from cyclopentenone **260** not only provided *cis*-1,3-cyclopentenediol building block **262** in 97% yield but also proved to be scalable, allowing access the desired product in multi-gram quantities.[23]

Scheme 2.5.1. Synthetic Advancement Toward the Desired Hydroxylmethyl-cis-1,3-Cyclopentenediol Framework

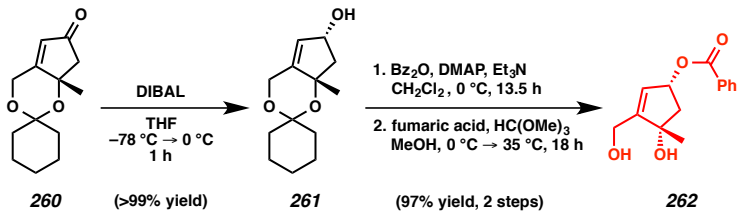

2.6 Conclusion

In summary, this chapter discloses a highly efficient and scalable route for the construction of a *cis*-1,3-cyclopentenediol building block, enabling access to such frameworks found in a variety of natural products and analogs. The enantioselective palladium-catalyzed allylic alkylation has been used effectively to generate the desired chiral tertiary alcohol stereocenter. Judicious choice of the ketal protecting group, along with an improved procedure for the formation of the requisite α-bromoketone intermediate, allowed for successful optimization of the diastereoselective formation of the *cis*-1,3-diol framework, generating diol **262** in 91% yield over 5 steps from allylic alkylation product **258**. Efforts are currently underway to employ this building block in the synthesis of members of the norcembranoid diterpene family of natural products.

2.7 Experimental Methods and Analytical Data

2.7.1 Materials and Methods

Unless stated otherwise, reactions were performed at ambient temperature (23 °C) in flame-dried glassware under an argon atmosphere using dry, deoxygentated solvents (distilled or passed over a column of activated alumina)[24] stirring with a Teflon®-coated magnetic stirring bar. Commercially available reagents were used as received unless otherwise noted. TBAT was triturated with bench-top EtOAc (25 g batches, 2 x 100 mL washes) under a cone of argon, dried in vacuo (ca. 0.30 torr) for 24 hours, and then stored in a nitrogen-filled glovebox. Et_3N was distilled from calcium hydride immediately prior to use. MeOH was distilled from magnesium methoxide immediately prior to use. Reagent grade acetone was obtained from Sigma-Aldrich and used as received. Purified H_2O was obtained using a Barnstead NANOpure Infinity UV/UF system. 4 Å molecular sieves were oven-dried at 120 °C for a minimum of 24 h and cooled in a desiccator to ambient temperature immediately prior to use. (*S*)-*t*-BuPhox (**263**),[10a,25] (*S*)-5,5-diphenyl-*i*-PrPhox (**264**), [26] (*R*)-5,5-dimethyl-*i*-PrPhox (**265**), [27] 2-bromo-5-(trifluoromethyl)-benzoyl chloride (**266**), [28] (*R*)-3-amino-2,4-dimethylpentan-2-ol hydrogen chloride (**267**),[26,27] bis(4-(trifluoromethyl)phenyl)phosphine oxide (**268**),[28] and tris(4,4'-methoxydibenzylideneacetone)-dipalladium(0) ($Pd_2(pmdba)_3$)[29] were prepared by known methods. Reactions requiring external heat were modulated to the specified temperatures using an IKAmag temperature controller. Thin-layer chromatography (TLC) was performed using E. Merck silica gel 60 F254 precoated plates (250 nm) and visualized by UV fluorescence quenching, potassium permanganate, or *p*-anisaldehyde staining. Silicycle SiliaFlash P60 Academic Silica gel (particle size 40-63 nm) was used for flash

chromatography. ^{1}H and ^{13}C NMR spectra were recorded on a Varian Inova 500 (500 MHz and 126 MHz, respectively) and a Varian Mercury 300 spectrometer (300 MHz and 76 MHz, respectively) and are reported in terms of chemical shift relative to residual $CHCl_3$ (in $CDCl_3$, δ 7.26 and δ 77.16, respectively) or C_6D_5H (in C_6D_6, δ 7.16 and δ 128.06, respectively). ^{19}F and ^{31}P NMR spectra were recorded on a Varian Mercury 300 spectrometer (282 MHz and 121 MHz, respectively) and are reported in terms of absolute chemical shift according to IUPAC standard recommendations from $CFCl_3$ and H_3PO_4, respectively.[30] Data for ^{1}H NMR spectra are reported as follows: chemical shift (δ ppm) (multiplicity, coupling constant (Hz), integration). Infrared (IR) spectra were recorded on a Perkin Elmer Paragon 1000 Spectrometer and are reported in frequency of absorption (cm^{-1}). Analytical chiral gas chromatography was performed with an Agilent 6850 GC using a G-TA (30 m x 0.25 cm) column (1.0 mL/minute carrier gas flow). Analytical chiral HPLC was performed with an Agilent 1100 Series HPLC utilizing a Chiralcel OB-H column (4.6 mm x 25 cm) obtained from Daicel Chemical Industries, Ltd. with visualization at 254 nm. High resolution mass spectra (HRMS) were obtained from the Caltech Mass Spectral Facility using a JEOL JMS-600H High Resolution Mass Spectrometer in fast atom bombardment (FAB+) or electron ionization (EI+) mode or acquired using an Agilent 6200 Series TOF with an Agilent G1978A Multimode source in atmospheric pressure chemical ionization (APCI) or mixed (MultiMode ESI/APCI) ionization mode. Optical rotations were measured on a Jasco P-2000 polarimeter using a 100 mm path length cell at 589 nm.

2.7.2 Experimental Procedures

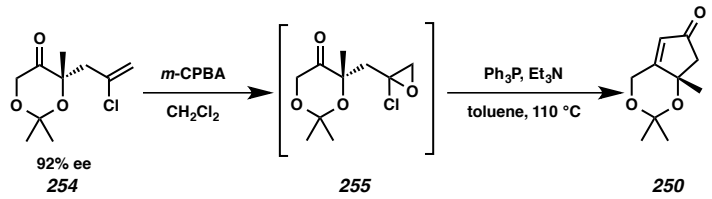

Cyclopentenone Acetonide 250: A solution of chloroallylketone **254** (0.157 g, 0.72 mmol, 1.00 equiv) in CH_2Cl_2 (4.5 mL) was distributed evenly among three oven-dried one-dram vials. Solid *m*-CPBA (0.252 g, 1.46 mmol, 2.00 equiv) was divided into three equal portions and added to each vial. After 9 days, the reaction vessels were simultaneously cooled to 0 °C, filtered individually through celite plugs, rinsing with pentane. The organics were then combined, concentrated in vacuo (>300 torr) and purified immediately by column chromatography (5% Et_2O in pentane eluent) to afford volatile intermediate epoxide **255** (0.051 g, 30 % yield) as a pale yellow oil which was immediately carried onto the sequential reaction.[31]

Epoxide **255** (0.051 g, 0.22 mmol, 1.00 equiv) was added as a solution in toluene (2.5 mL) to a Schlenk flask. Upon the subsequent addition of Ph_3P (0.123 g, 0.47 mmol, 2.15 equiv) as a solid at ambient temperature, the reaction immediately turned bright yellow. The mixture was allowed to stir for 1 h, at which time the addition of Et_3N (0.13 mL, 0.91 mmol, 4.15 equiv) was accomplished dropwise. The reaction vessel was immediately sealed with a Teflon® stopcock and introduced to a preheated 110 °C bath. After 4.5 h, the reaction was removed from the bath, cooled to ambient temperature (ca. 23 °C), and purified by silica gel column chromatography (5%→10% Et_2O in pentane eluent) to furnish volatile cyclopentenone acetonide **250** (0.008 g, 20% yield) as a yellow oil: R_f = 0.29 (1:1 Et_2O:Hexanes eluent); ^1H NMR (500 MHz, $CDCl_3$) δ 5.91 (t, J = 1.7,

1H), 4.95–4.81 (m, 2H), 2.60 (d, J = 17.7, 1H), 2.47 (d, J = 17.7, 1H), 1.62 (s, 3H), 1.42 (s, 3H), 1.37 (s, 3H); ^{13}C NMR (126 MHz, $CDCl_3$) δ 203.4, 175.9, 125.4, 100.8, 77.8, 60.9, 53.5, 30.2, 28.6, 25.4; IR (Neat Film, NaCl) 3072, 2991, 2937, 2861, 1723, 1639, 1445, 1408, 1382, 1372, 1349, 1316, 1267, 1226, 1200, 1169, 1139, 1094, 1060, 1010, 983, 952, 920, 903, 848, 831, 772, 752 cm^{-1}; HRMS (EI+) *m/z* calc'd for $C_{10}H_{14}O_3$ $[M\bullet]^+$:182.0943, found 182.0941; $[\alpha]_D^{23.6}$ –19.8° (*c* 1.53, $CHCl_3$).

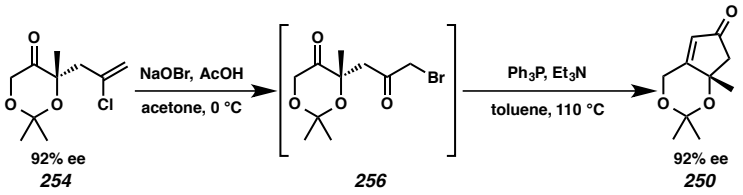

Cyclopentenone Acetonide 250: To a stirred solution of NaOH (0.942 g, 23.6 mmol, 17.2 equiv) in H_2O (12 mL) at 0 °C (ice/H_2O bath) was added Br_2 (0.40 mL, 7.81 mmol, 5.70 equiv) dropwise through a needleless plastic syringe. The resulting yellow solution of NaOBr was stirred for 30 minutes at 0 °C.

A flask was charged with a solution of chloroallylketone **254** (0.300 g, 1.37 mmol, 1.00 equiv), acetone (12 mL), and acetic acid (7.10 mL, 124 mmol, 90.5 equiv). The colorless solution was cooled to 0 °C (ice/H_2O bath). The reaction was treated with NaOBr (8.20 mL, 5.44 mmol, 4.00 equiv) dropwise using a needleless plastic syringe over 1 h. At the completion of the addition, the reaction progress was monitored by TLC (1:1 Et_2O:Hexanes eluent). If the reaction was not immediately complete, further addition of NaOBr (up to 1 mL) was carried out at the same rate. Upon complete consumption of the starting material as determined by TLC, the reaction mixture was diluted with CH_2Cl_2 (10 mL) and H_2O (5 mL), followed by dropwise addition of a solution of K_2CO_3 (5.000 g)

and $Na_2S_2O_3 \bullet 5H_2O$ (2.084 g) in H_2O (10 mL). Quenching resulted in the vigorous evolution of gas and the dissipation of the orange color, affording two colorless phases. The aqueous layer was further diluted with H_2O (15 mL) and extracted with CH_2Cl_2 (3 x 25 mL). Combined organic layers were dried over $MgSO_4$ for 1 minute, filtered, and concentrated under reduced pressure until around 2 mL of solution remained. The solution was diluted with heptane (10 mL), and the reaction was concentrated under reduced pressure until around 0.6 mL of solution remained. The reaction was quickly purified through an SiO_2 plug (10% Et_2O in hexanes eluent) and partially concentrated under reduced pressure to give the desired α-bromoketone **256** as a yellow solution, which was promptly diluted with anhydrous toluene (1 mL) and immediately employed.[32]

A 250 mL Schlenk flask and stir bar was charged with powdered Ph_3P (0.893 g, 3.40 mmol, 2.48 equiv) and toluene (10 mL). The colorless solution was treated dropwise with the solution of α-bromoketone **256** and rinsed with additional toluene (4 mL). The colorless solution was then treated dropwise with Et_3N (0.29 mL, 2.08 mmol, 1.50 equiv). The reaction vessel was immediately sealed with a Teflon® stopcock and introduced to a preheated 110 °C bath. After 5 h, the reaction was removed from the bath, cooled to ambient temperature, and purified directly by column chromatography (25%→50% Et_2O in pentane eluent) to furnish the volatile cyclopentenone acetonide **250** (0.205 g, 82% yield) as a yellow oil.[33] See above for characterization data. Additionally, the enantiomeric excess of enone **250** generated by this procedure was determined by analytical chiral HPLC (Chiralcel OB-H column, 3:7 *i*-PrOH:Hexanes, 1 mL/minute, major retention time: 12.7 minutes, minor retention time: 16.5 minutes, 92% ee).

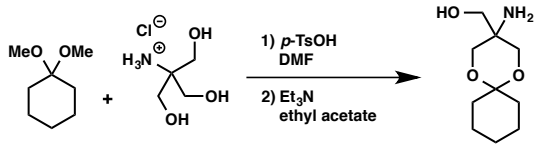

269 *270* *271*

Aminoalcohol 271: To a suspension of Trizma•HCl (**270**, 45.0 g, 286 mmol, 1.00 equiv) in DMF (365 mL) were added cyclohexanone dimethyl ketal (**269**, 50.0 mL, 329 mmol, 1.15 equiv) and *p*-toluenesulfonic acid monohydrate (*p*-TsOH, 1.63 g, 8.57 mmol, 0.03 equiv) in one portion with stirring. After 17 h, a distillation apparatus was attached directly to the reaction flask and the volatiles were distilled off (75 °C/6 torr). The semisolid residue was triturated with Et_2O (700 mL) until white solid precipitated. The resulting heterogeneous solution was filtered, washed with EtOAc (4 x 100 mL), and dried under high vacuum (0.50 torr) to afford a white solid.

To a portion of the resulting crude white solid (19.7 g, 82.9 mmol, 1.00 equiv) as a suspension in EtOAc (276 mL) was added Et_3N (13.9 mL, 99.4 mmol, 1.20 equiv) dropwise with stirring. After 11 h, the reaction mixture was filtered, the solids washed with EtOAc (4 x 20 mL) and resuspended in EtOAc (150 mL) to which Et_3N (5.0 mL, 35.9 mmol) was added dropwise. The suspension was stirred for 48 h and then filtered and the solids were washed with EtOAc (4 x 120 mL). Combined organic filtrate was concentrated in vacuo to give aminoalcohol **271** (16.68 g, 94% yield from **270**) as a white solid: R_f = 0.17 (1:4 MeOH:CH_2Cl_2 eluent); ^{1}H NMR (500 MHz, $CDCl_3$) δ 3.80 (d, *J* = 11.9 Hz, 2H), 3.54 (d, *J* = 11.9 Hz, 2H), 3.49 (s, 2H), 1.87–1.64 (m, 7H), 1.59–1.52 (m, 2H), 1.52–1.46 (m, 2H), 1.42 (q, *J* = 6.0 Hz, 2H); ^{13}C NMR (126 MHz, $CDCl_3$) δ 98.7, 66.5, 65.2, 50.7, 34.0, 31.0, 25.8, 22.7; IR (Neat Film, NaCl) 3350, 3294, 2937, 2857,

1618, 1448, 1331, 1284, 1255, 1160, 1087, 918 cm^{-1}; HRMS (MM: ESI-APCI) *m/z* calc'd for $C_{10}H_{20}NO_3$ $[M+H]^+$: 202.1438, found 202.1434.

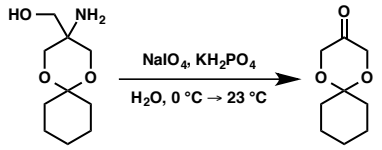

271 *272*

Dioxanone 272: Aminoalcohol **271** (14.7 g, 73.0 mmol, 1.00 equiv) was dissolved in a solution of KH_2PO_4 (11.9 g, 87.6 mmol, 1.20 equiv) in H_2O (243 mL) and cooled to 0 °C (ice/H_2O bath). To the resultant stirred homogenous solution was added a solution of $NaIO_4$ (15.6 g, 73.0 mmol, 1.00 equiv) in H_2O (243 mL) dropwise over 2.5 h through a 250 mL additional funnel. The reaction was then allowed to stir at temperature for 40 minutes before being allowed to warm to ambient temperature. The starting material was consumed after an additional 4 h as determined by TLC (1:4 MeOH:CH_2Cl_2 eluent). $Na_2S_2O_3$•$5H_2O$ (18.1 g, 73.0 mmol, 1.00 equiv) was then immediately added in one portion. The solution was allowed to stir for 40 minutes at which time the reaction mixture was extracted with CH_2Cl_2 (11 x 150 mL). Combined organic layers were dried over Na_2SO_4, filtered, and concentrated in vacuo (26 °C/100 torr) to afford dioxanone **272** (12.4 g, >99% yield) as a pale yellow oil. This compound was carried to the next step without further purification: R_f = 0.80 (1:4 MeOH:CH_2Cl_2 eluent); ^{1}H NMR (500 MHz, $CDCl_3$) δ 4.12 (s, 4H), 1.72–1.65 (m, 4H), 1.59–1.51 (m, 4H), 1.44–1.35 (m, 2H); ^{13}C NMR (126 MHz, $CDCl_3$) δ 208.3, 100.0, 66.7, 32.6, 25.3, 22.9; IR (Neat Film, NaCl) 2937, 2862, 1751, 1448, 1435, 1425, 1369, 1338, 1281, 1263, 1239, 1200, 1162, 1146,

1118, 1079, 1058, 1028, 922, 847, 825 cm^{-1}; HRMS (EI+) *m/z* calc'd for $C_9H_{14}O_3$ $[M\bullet]^+$: 170.0943, found 170.0961.

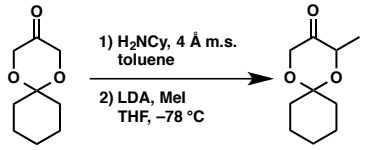

272 *273*

Methyldioxanone 273: A solution of dioxanone **272** (12.4 g, 73.0 mmol, 1.00 equiv) in toluene (243 mL) was charged with 4 Å molecular sieves (14.9 g, 1.20 equiv by mass) and cyclohexylamine (16.2 mL, 142 mmol, 1.94 equiv). After 13 h, the reaction mixture was filtered over celite, rinsing with toluene, and concentrated in vacuo to give the crude cyclohexylimine.

In a separate three-neck flask with an internal temperature probe, a solution of freshly prepared lithium diisopropylamine (LDA, 0.60 M in THF, 1.00 equiv) was cooled to –78 °C (dry ice/*i*-PrOH bath). To the solution of LDA was added crude cyclohexylimine as a solution in THF (73 mL) dropwise through a cannula with an overpressure of argon. After 5 minutes, the reaction flask was introduced to a –15 °C bath (ice/MeOH) and after 1.75 h was cooled back to –78 °C. To the reaction mixture was then added methyl iodide (4.77 mL, 76.7 mmol, 1.05 equiv) at a rate of 2.00 mL/h with a syringe pump, ensuring the internal temperature did not exceed –70 °C. Upon completion of addition, the reaction was allowed to stir for 30 minutes before being allowed to slowly warm to ambient temperature. Upon reaching ambient temperature, the reaction was quenched with saturated aqueous NH_4Cl (150 mL) and stirred for 14 h. The reaction mixture was then extracted with Et_2O (4 x 150 mL). Combined organic layers were then

washed with H_2O (50 mL), brine (50 mL), dried over Na_2SO_4, filtered, and concentrated in vacuo to afford an orange-tan oil. Purification of this residue by flash chromatography (10% Et_2O in hexanes eluent) furnished methyldioxanone **273** (9.77 g, 73% yield) as a clear, colorless oil: R_f = 0.30 (1:9 Et_2O:Hexanes eluent); ^1H NMR (500 MHz, $CDCl_3$) δ 4.38 (qd, *J* = 6.8, 1.5 Hz, 1H), 4.28 (dd, *J* = 17.2, 1.5 Hz, 1H), 4.02 (d, *J* = 17.2 Hz, 1H), 1.84–1.76 (m, 1H), 1.76–1.66 (m, 3H), 1.62–1.54 (m, 4H), 1.47–1.39 (m, 2H), 1.31 (d, *J* = 6.7 Hz, 3H); ^{13}C NMR (126 MHz, $CDCl_3$) δ 210.4, 100.8, 70.8, 66.3, 33.3, 33.0, 25.4, 23.1, 23.0, 14.4; IR (Neat Film, NaCl) 2935, 2859, 1748, 1447, 1365, 1339, 1278, 1255, 1164, 1151, 1133, 1118, 1072, 1045, 991, 928, 846, 825 cm^{-1}; HRMS (EI+) *m/z* calc'd for $C_{10}H_{16}O_3$ $[M\bullet]^+$: 184.1100, found 184.1129.

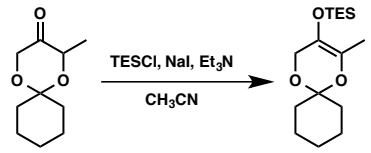

273 *257*

Silyl enol ether 257: A 250 mL round bottom was soaked in a 20:1 *i*-PrOH:toluene bath saturated with KOH for 12 h, rinsed with deionized H_2O, acetone, and allowed to dry. To a solution of methyldioxanone **273** (9.77 g, 53.0 mmol, 1.00 equiv) in CH_3CN (88 mL) in a flame-dried 250 mL base-bathed round bottom flask with stir bar were added sodium iodide (10.3 g, 68.9 mmol, 1.30 equiv) in a single portion and Et_3N (11.8 mL, 84.8 mmol, 1.60 equiv) dropwise with stirring. After 5 minutes, triethylsilyl chloride (TESCl, 11.6 mL, 68.9 mmol, 1.30 equiv) was added dropwise. After 18 h, consumption of starting material was complete as determined by TLC (1:9 Et_2O:Hexanes eluent) and the reaction mixture was extracted with pentane (4 x 250 mL). Combined organic layers were washed

with H_2O (100 mL), brine (100 mL), dried over Na_2SO_4, filtered, and concentrated in vacuo to produce a yellow oil. Purification of this residue by flash chromatography (1.0% Et_2O / 0.5% Et_3N in hexanes eluent) on base–treated silica furnished silyl enol ether **257** (8.68 g, 55% yield) as a faintly pink, clear oil: R_f = 0.31 (1:19 Et_2O:Hexanes eluent); ^1H NMR (500 MHz, $CDCl_3$) δ 4.03 (q, *J* = 2.0 Hz, 2H), 1.78 (t, *J* = 2.0 Hz, 3H), 1.74–1.69 (m, 4H), 1.58–1.50 (m, 4H), 1.45–1.38 (m, 2H), 0.98 (t, *J* = 8.0 Hz, 9H), 0.64 (q, *J* = 8.0 Hz, 6H); ^{13}C NMR (126 MHz, $CDCl_3$) δ 134.1, 125.7, 98.5, 60.4, 33.0, 25.7, 22.8, 14.0, 6.8, 5.5; IR (Neat Film, NaCl) 2953, 2937, 2877, 1718, 1448, 1412, 1395, 1362, 1289, 1253, 1219, 1203, 1154, 1133, 1096, 1055, 1012, 946, 923, 866, 848, 830, 745 cm^{-1}; HRMS (MM: ESI-APCI) *m/z* calc'd for $C_{16}H_{31}O_3Si$ $[M+H]^+$: 299.2037, found 299.2031.

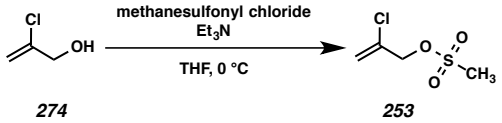

274 *253*

Chloroallylmesylate 253: A flask was charged with 2-chloroallyl alcohol (**274**, 4.78 mL, 60.0 mmol, 1.00 equiv), THF (120 mL), and Et_3N (17.2 mL, 120 mmol, 2.00 equiv) and cooled to 0 °C (ice/H_2O bath) with stirring. To the solution was added methanesulfonyl chloride (6.96 mL, 90.0 mmol, 1.50 equiv) dropwise. After 2 h, the reaction was quenched with saturated aquesous $NaHCO_3$ (120 mL). The reaction mixture was warmed to ambient temperature and extracted with Et_2O (3 x 180 mL). Combined organic layers were washed with 1 N HCl (120 mL), saturated $NaHCO_3$ (120 mL), brine (120 mL), dried over $MgSO_4$, filtered, and concentrated in vacuo to provide a crude tan oil. The residue was purified by bulb-to-bulb distillation using a Kügelrohr apparatus (150 °C/3.5 torr) to furnish chloroallylmesylate **253** (9.69 g, 95% yield) as a clear, colorless oil: R_f =

0.34 (2:1 EtOAc:Hexanes eluent); ^{1}H NMR (300 MHz, $CDCl_3$) δ 5.65 (d, *J* = 0.5 Hz, 1H), 5.55 (d, *J* = 0.5 Hz, 1H), 4.77 (s, 2H), 3.10 (s, 3H); ^{13}C NMR (76 MHz, $CDCl_3$) δ 134.3, 117.9, 71.1, 38.6; IR (Neat Film, NaCl) 3652, 3570, 3267, 3119, 3033, 2943, 2523, 2310, 2089, 1832, 1639, 1454, 1415, 1360, 1175, 1010, 923, 830, 757 cm^{-1}; HRMS (EI+) *m/z* calc'd for $C_4H_7{}^{35}ClO_3S$ $[M\bullet]^+$: 169.9804, found 169.9811.

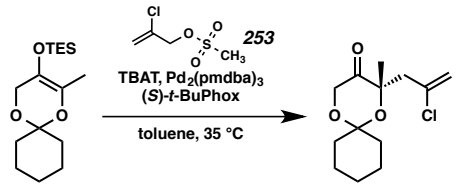

Chloroallyl ketal 258: A 500 mL Schlenk flask was soaked in a 20:1 *i*-PrOH:toluene bath saturated with KOH for 12 h, rinsed with deionized H_2O, acetone, and allowed to dry. To a flame-dried 500 mL base-bathed Schlenk flask in a nitrogen-filled glovebox were charged $Bu_4NPh_3SiF_2$ (TBAT, 7.53 g, 13.9 mmol, 1.00 equiv), $Pd_2(pmdba)_3$ (230 mg, 0.21 mmol, 0.015 equiv), (*S*)-*t*-BuPhox (190 mg, 0.49 mmol, 0.035 equiv), and toluene (280 mL, 0.0015 M in Pd). The reaction vessel was immediately removed from the glovebox, introduced to an argon atmosphere and placed in a preheated 35 °C bath with stirring. After 20 minutes, a yellow-brown solution was observed. Chloroallylmesylate **253** (2.85 g, 16.7 mmol, 1.20 equiv) was added quickly dropwise affording a blue-green solution. After 3 minutes, silyl enol ether **257** (4.16 g, 13.9 mmol, 1.00 equiv) was added quickly dropwise over 3 minutes. The resultant blue-green reaction mixture was allowed to stir for 20 h. The resultant yellow-brown reaction was then allowed to cool to ambient temperature, filtered through a pad of SiO_2 using hexanes as the eluent to remove toluene, at which time separate fractions were collected, eluting

with Et_2O, to isolate the volatile reaction products. The filtrate was concentrated in vacuo to furnish a bright yellow oil which was subsequently purified by flash chromatography (1%→3%→5% Et_2O in hexanes eluent) to afford volatile chloroallyl ketal **258** (2.95 g, 82% yield) as a clear, colorless oil: R_f = 0.41 (19:1 Et_2O:Pentane eluent); ^1H NMR (500 MHz, $CDCl_3$) δ 5.30 (d, *J* = 1.1 Hz, 1H), 5.23 (q, *J* = 0.8 Hz, 1H), 4.36 (d, *J* = 17.9 Hz, 1H), 4.20 (d, *J* = 17.9 Hz, 1H), 2.87 (dd, *J* =14.6, 0.9 Hz, 1H), 2.74 (d, *J* = 14.6 Hz, 1H), 1.84–1.76 (m, 2H), 1.76–1.69 (m, 2H), 1.66–1.58 (m, 2H), 1.57–1.50 (m, 2H), 1.47 (s, 3H), 1.45–1.41 (m, 1H), 1.41–1.36 (m, 1H); ^{13}C NMR (126 MHz, $CDCl_3$) δ 210.2, 137.1, 116.9, 100.5, 81.1, 66.5, 48.2, 36.2, 35.0, 25.3, 25.2, 23.1, 23.0; IR (Neat Film, NaCl) 2937, 2862, 1743, 1635, 1447, 1364, 1332, 1280, 1258, 1245, 1172, 1159, 1113, 1052, 1005, 943, 889, 826 cm^{-1}; HRMS (APCI) *m/z* calc'd for $C_{13}H_{20}{}^{35}ClO_3$ $[M+H]^+$: 259.1095, found 259.1092; 92% *ee* (analytical chiral GC, G-TA column, 120 °C isotherm, major retention time: 53.209 min, minor retention time: 52.075 min); $[\alpha]_D^{25.0}$ –75.8° (*c* 1.41, $CHCl_3$).

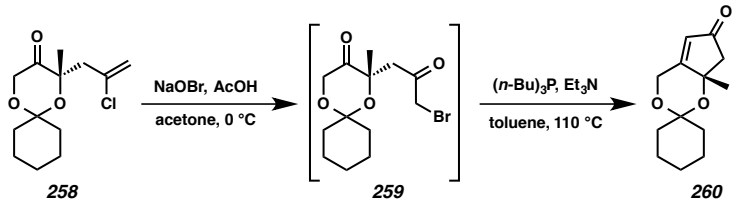

Cyclopentenone Cyclohexyl Ketal 260: To a stirred solution of NaOH (3.25 g, 81.2 mmol, 18.0 equiv) in H_2O (54 mL) at 0 °C (ice/H_2O bath) was added Br_2 (1.39 mL, 27.1 mmol, 6.00 equiv) dropwise through a needleless plastic syringe. The resulting yellow solution of NaOBr was stirred for 3 h at 0 °C.

A solution of chloroallyl ketal **258** (1.17 g, 4.51 mmol, 1.00 equiv) in acetone (45 mL) was distributed equally to eight 20 mL scintillation vials with stir bars. Each vial was capped loosely with a septum and cooled to 0 °C open to air. AcOH (23.2 mL, 406 mmol, 90.0 equiv) was distributed between the eight reaction vessels in a dropwise fashion. After 5 minutes, addition of NaOBr (28.0 mL, ca. 3.0 equiv) was accomplished by adding one drop (ca. 40 μL) every 30 seconds to each reaction vessel through a needleless 1 mL plastic syringe.[34] Upon completion of addition (approximately 80 minutes), the bright orange reactions were allowed to stir for 10 minutes, at which time the consumption of starting material was complete as determined by TLC (1:4 EtOAc:Hexanes eluent). If the consumption of starting material was determined incomplete, additional NaOBr (2.00 mL, ca. 0.21 equiv) was added by the previously specified procedure and allowed to react for a maximum of 5 additional minutes. The reactions were then diluted with CH_2Cl_2 at 0 °C, quickly combined in a separatory funnel with additional CH_2Cl_2 (100 mL total), and carefully quenched with a solution of $Na_2S_2O_3 \bullet 5H_2O$ (11.2 g, 45.1 mmol, 10.0 equiv) and K_2CO_3 (12.5 g, 90.2 mmol, 20.0 equiv) in H_2O (54 mL). Quenching resulted in the vigorous evolution of gas and the dissipation of the orange color, affording a cloudy, white organic layer. The aqueous layer was washed with CH_2Cl_2 (3 x 100 mL). The combined organic layers were dried over $MgSO_4$ for 1 minute, filtered, concentrated in vacuo, and azeotroped with heptane (4 x 30 mL) to ensure thorough removal of AcOH and afford crude bromide **259** (1.440 g, >99% yield) as a white, viscous, opaque oil which was immediately subjected to the subsequent reaction conditions without further purification.[35]

To a clear, colorless solution of neat (*n*-Bu)$_3$P (2.25 mL, 9.02 mmol, 2.00 equiv) in toluene (30 mL) in a Schlenk flask was added crude bromide **259** (1.440g, 4.51 mmol, 1.00 equiv) as a solution in toluene (15 mL) dropwise affording a clear, gold solution. After 90 minutes Et_3N (0.94 mL, 6.77 mmol, 1.50 equiv) was added dropwise, generating white precipitate on the first drops. The reaction was allowed to stir for 5 minutes, after which the vessel was sealed with a Teflon® stopcock and introduced to a preheated 110 °C bath. The reaction solution was allowed to stir vigorously for 16 h, after which the dark brown reaction mixture was removed from the bath and allowed to cool to ambient temperature with stirring. The vessel was then opened to the atmosphere in a well-ventilated fume hood and allowed to stir for an additional hour. The reaction mixture was filtered through a pad of SiO_2 using hexanes to remove toluene at which time separate fractions were collected, eluting with Et_2O, to isolate the volatile reaction products. The filtrate was concentrated in vacuo (>100 torr) and the resultant dark brown oil was purified by column chromatography (40% Et_2O in hexanes eluent) to furnish the volatile cyclopentenone cyclohexyl ketal **260** (0.939 mg, 94% yield) as a light yellow oil: R_f = 0.28 (2:3 Et_2O:Hexanes eluent); ^{1}H NMR (300 MHz, $CDCl_3$) δ 5.92–5.82 (m, 1H), 4.95–4.76 (m, 2H), 2.60 (app d, *J* = 17.6 Hz, 1H), 2.46 (app d, *J* = 17.7 Hz, 1H), 1.92–1.62 (m, 2H), 1.60 (s, 3H), 1.57–1.15 (m, 8H); ^{13}C NMR (126 MHz, $CDCl_3$) δ 203.4, 176.4, 125.0, 101.0, 77.3, 60.2, 53.4, 39.0, 34.3, 28.7, 25.1, 23.4, 22.9; IR (Neat Film, NaCl) 3509, 3419, 2936, 2857, 1717, 1639, 1446, 1408, 1366, 1286, 1235, 1198, 1147, 1096, 1081, 1035, 984, 933, 855, 755 cm^{-1}; HRMS (EI+) *m/z* calc'd for $C_{13}H_{18}O_3$ $[M\bullet]^+$: 222.1256, found 222.1262; $[\alpha]_D^{25.0}$ –55.9° (*c* 13.02, $CHCl_3$).

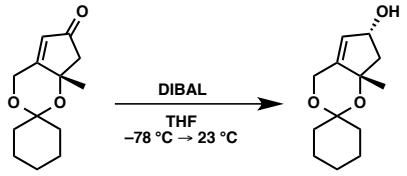

260 ***261***

Allylic Alcohol 261: To a pale yellow solution of cyclopentenone cyclohexyl ketal **260** (840 mg, 3.78 mmol, 1.00 equiv) in THF (38 mL) at –78 °C (*i*-PrOH/dry ice bath) was added a solution of DIBAL (1.35 mL, 7.56 mmol, 2.00 equiv) in THF (7.6 mL) dropwise. After 30 minutes, the gold reaction mixture was removed from the bath and allowed to warm slowly. After an additional 30 minutes, the consumption of starting material was complete as determined by TLC (1:4 EtOAc:Hexanes eluent) and the reaction mixture was cooled to 0 °C (ice/H_2O bath). The reaction was subsequently quenched with a 1:1 solution of saturated aqueous NH_4Cl and saturated aqueous Rochelle salt (35 mL) dropwise, vigorously evolving gas on the first drops. The mixture was then diluted with CH_2Cl_2 (250 mL) and H_2O (30 mL). The aqueous layer was then extracted with CH_2Cl_2 (3 x 60 mL). The combined organics were dried over Na_2SO_4, filtered, and concentrated in vacuo to provide crude allylic alcohol **261** (0.848 g, >99% yield), which was used without further purification.

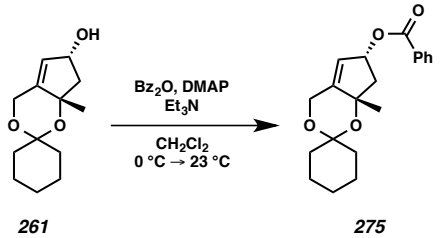

261 ***275***

Benzoylated Alcohol 275: To a stirred solution of crude allylic alcohol **261** (2.05 g, 9.14 mmol, 1.00 equiv) in CH_2Cl_2 (183 mL) were added 4-(dimethylamino)pyridine (DMAP,

2.233 g, 18.3 mmol, 2.00 equiv) and Et_3N (10.2 mL, 73.1 mmol, 8.00 equiv). The light yellow reaction mixture was cooled to 0 °C (ice/H_2O bath) at which time benzoic anhydride (Bz_2O, 4.135 g, 18.28 mmol, 2.00 equiv) was added in one portion. After 30 minutes, the reaction was removed from the bath and allowed to warm to ambient temperature. After an additional 13 h, at which time the consumption of starting material was complete as determined by TLC (3:2 EtOAc:Hexanes eluent), the reaction was again cooled to 0 °C (ice/H_2O bath) and quenched with saturated aqueous NH_4Cl (150 mL). The biphasic solution was further diluted with CH_2Cl_2 (240 mL) and H_2O (200 mL). The organics were separated and the aqueous was extracted with CH_2Cl_2 (2 x 240 mL). The combined organics were washed with saturated NH_4Cl (5 x 500 mL), dried over Na_2SO_4, filtered, and concentrated in vacuo to afford benzoylated alcohol **275** (3.002 g, >99% yield) as a light gold oil that was typically utilized without further purification. A characterization sample of benzoylated alcohol **275** was obtained through purification by column chromatography (1% Et_3N in CH_2Cl_2 eluent) to afford a clear colorless oil: R_f = 0.63 (1:4 EtOAc:Hexanes eluent); ^{1}H NMR (500 MHz, $CDCl_3$) δ 8.03 (dt, *J* = 8.2, 1.0 Hz, 2H), 7.55 (td, *J* = 7.4, 1.3 Hz, 1H), 7.43 (td, *J* = 7.6, 1.1 Hz, 2H), 5.79 (ddq, *J* = 6.9, 3.8, 1.8 Hz, 1H), 5.64 (q, *J* = 1.6 Hz, 1H), 4.74–4.58 (m, 2H), 2.67 (dd, *J* = 12.7, 6.8 Hz, 1H), 2.12 (dd, *J* = 12.7, 6.7 Hz, 1H), 2.06–1.93 (m, 1H), 1.74–1.51 (m, 6H), 1.48 (s, 3H), 1.46–1.34 (m, 2H), 1.33–1.21 (m, 1H); ^{13}C NMR (126 MHz, $CDCl_3$) δ 166.5, 147.1, 133.1, 130.3, 129.7, 128.4, 121.5, 100.6, 80.6, 76.6, 59.7, 49.4, 38.9, 34.8, 28.8, 25.4, 23.6, 23.1; IR (Neat Film, NaCl) 2934, 2858, 1719, 1450, 1367, 1266, 1110, 1095, 1026, 984, 712 cm^{-1}; HRMS (MM: ESI-APCI) *m/z* calc'd for $C_{20}H_{25}O_4$ $[M+H]^+$: 329.1747, found 329.1745; $[\alpha]_D^{25.0}$ +48.7° (*c* 6.09, $CHCl_3$).

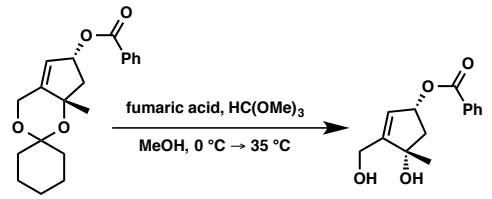

275 ***262***

Diol 262: To a flask containing benzoylated alcohol **275** (1.12 g, 3.40 mmol, 1.00 equiv) were added MeOH (68 mL) and $HC(OMe)_3$ (3.35 mL, 30.6 mmol, 9.00 equiv). The reaction mixture was cooled to 0 °C (ice/H_2O bath) with stirring, at which time the addition of fumaric acid (0.988 g, 8.51 mmol, 2.50 equiv) was accomplished in one portion. After 10 minutes, the reaction was removed from the cold bath and immediately introduced to a preheated 35 °C bath. After 18 h, the consumption of starting material was complete as determined by TLC (1:4 EtOAc:Hexanes eluent) and the reaction was allowed to cool to ambient temperature (ca. 23 °C). The reaction mixture was diluted with EtOAc (150 mL) and poured over saturated aqueous $NaHCO_3$ (150 mL). The organics were separated and the aqueous was extracted with EtOAc (3 x 150 mL). Combined organic layers were washed with brine (100 mL), dried over $MgSO_4$ for 2 minutes, filtered, and concentrated in vacuo to generate a yellow oil. The crude residue was then purified by column chromatography (50% EtOAc in hexanes eluent) to afford diol **262** (0.816 g, 97% yield) as a pale yellow oil: R_f = 0.18 (1:1 EtOAc:Hexanes eluent); ^{1}H NMR (500 MHz, $CDCl_3$) δ 8.03–7.94 (m, 2H), 7.54–7.47 (m, 1H), 7.41–7.35 (m, 2H), 5.85 (q, *J* = 1.7 Hz, 1H), 5.66 (ddq, *J* = 7.8, 3.8, 1.8 Hz, 1H), 4.39 (td, *J* = 14.5, 1.7 Hz, 1H), 4.31 (td, *J* = 14.6, 1.3 Hz, 1H), 3.29 (bs, 2H), 2.64 (dd, *J* = 14.2, 7.3 Hz, 1H), 2.17 (dd, J = 14.2, 4.2 Hz, 1H), 1.39 (s, 3H); ^{13}C NMR (126 MHz, $CDCl_3$) δ 166.6, 153.2, 133.2, 130.1, 129.7, 128.4, 125.6, 81.2, 76.3, 58.8, 48.3, 26.6; IR (Neat Film, NaCl) 3400, 2971, 1713, 1694, 1451, 1315, 1273, 1111, 1070, 1026, 952, 712 cm^{-1}; HRMS

(FAB+) *m/z* calc'd for $C_{14}H_{17}O_4$ $[M+H]^+$: 249.1127, found 249.1132; $[\alpha]_D^{25.0}$ 115.1° (*c* 6.90, $CHCl_3$).

2.7.3 Ligand Synthesis

The synthesis of (*R*)-CF_3-5,5-dimethyl-*i*-PrPhox proceeded as follows:

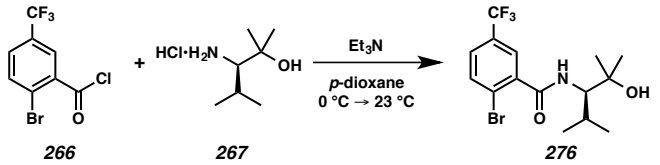

266 *267* *276*

Amide 276:[36] To a stirred solution of the hydrogen chloride salt of aminoalcohol **267** (1.00 g, 5.96 mmol, 1.00 equiv) in *p*-dioxane (20 mL) was added Et_3N (2.50 mL, 17.9 mmol, 3.00 equiv). The reaction mixture was then cooled to 0 °C (ice/H_2O bath) followed by the addition of acid chloride **266** (1.971 g, 6.86 mmol, 1.15 equiv) as a solution in *p*-dioxane (13 mL) slowly dropwise. After 15 minutes, the reaction was removed from the cooling bath and allowed to warm to ambient temperature (ca. 23 °C). After 4 h, the consumption of starting material was complete as determined by TLC (1:9 MeOH:CH_2Cl_2 eluent). The reaction mixture was concentrated in vacuo, dissolved in Et_2O and filtered through a pad of silica gel, eluting the product with Et_2O. The filtrate was then concentrated in vacuo and the crude white solid residue was purified by silica gel column chromatography (20% acetone in hexanes eluent) to provide amide **276** (1.79 g, 79% yield) as an amorphous white solid: R_f = 0.20 (1:4 Acetone:Hexanes eluent); ^{1}H NMR ($CDCl_3$, 500 MHz) δ 7.78–7.71 (m, 2H), 7.52 (ddt, *J* = 8.3, 2.3, 0.7 Hz, 1H), 6.40 (d, *J* = 10.3 Hz, 1H), 4.03 (dd, *J* = 10.1, 2.6 Hz, 1H), 2.27 (dtd, *J* = 13.7, 6.8, 2.6 Hz, 1H),

1.37 (s, 3H), 1.34 (s, 3H), 1.08 (d, J = 6.8 Hz, 3H), 1.00 (d, J = 6.8 Hz, 3H); ^{13}C NMR ($CDCl_3$, 126 MHz) δ 167.0, 139.4, 134.3, 130.4 (q, J = 33.5 Hz), 127.7 (q, J = 3.6 Hz), 126.6 (q, J = 3.8 Hz), 123.5 (q, J = 272.3 Hz), 123.2 (q, J = 1.5 Hz), 73.8, 60.9, 29.9, 28.8, 27.7, 22.5, 17.2; ^{19}F NMR ($CDCl_3$, 282 MHz) δ –62.8 (s); IR (Neat Film, NaCl) 3413, 3299, 2964, 1638, 1540, 1332, 1311, 1173, 1132, 1080, 1033, 828 cm^{-1}; HRMS (MM: ESI-APCI) *m/z* calc'd for $C_{15}H_{20}O_2{}^{79}BrF_3N$ $[M+H]^+$: 382.0624, found 382.0633; $[\alpha]_D^{25.0}$ –3.9° (*c* 0.895, $CHCl_3$).

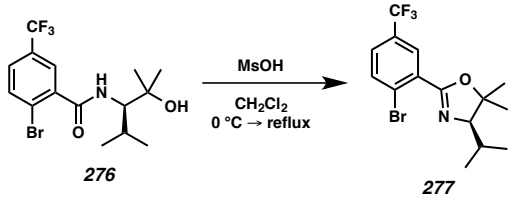

276 *277*

Oxazoline 277:[36] To a solution of amide **276** (1.41 g, 3.70 mmol, 1.00 equiv) in CH_2Cl_2 (93 mL) at 0 °C (ice/H_2O bath) was added methanesulfonic acid (MsOH, 1.44 mL, 22.2 mmol, 6.00 equiv) dropwise over 10 minutes. The flask was subsequently removed from the cooling bath, topped with a reflux condenser, and introduced to a preheated 50 °C bath. After 17 h, the consumption of starting material was complete as determined by TLC (1:4 Acetone:Hexanes eluent). The refluxing solution was removed from the heating bath and allowed to cool to ambient temperature (ca. 23 °C). The yellow reaction mixture was then diluted with CH_2Cl_2 (100 mL) and poured onto saturated aqueous $NaHCO_3$ (100 mL). The organics were separated and washed with H_2O (40 mL), brine (40 mL), dried over $MgSO_4$, filtered and concentrated in vacuo. The crude gold oil was purified by silica gel column chromatography (5%→10% acetone in Hexanes eluent) to provide oxazoline **277** (1.18 g, 87% yield) as a pale yellow oil: R_f = 0.42 (1:9 Et_2O:Hexanes eluent); ^{1}H

NMR ($CDCl_3$, 500 MHz) δ 7.92–7.88 (m, 1H), 7.77–7.72 (m, 1H), 7.52–7.46 (m, 1H), 3.53 (d, *J* = 8.1 Hz, 1H), 1.94 (dhept, *J* = 8.0, 6.6 Hz, 1H), 1.56 (s, 3H), 1.45 (s, 3H), 1.16 (d, *J* = 6.5 Hz, 3H), 1.05 (d, *J* = 6.6 Hz, 3H); ^{13}C NMR ($CDCl_3$, 126 MHz) δ 160.4, 134.6, 131.6, 129.8 (q, *J* = 33.4 Hz), 128.4 (q, *J* = 3.8 Hz), 127.9 (q, *J* = 3.6 Hz), 126.1 (q, *J* = 1.7 Hz), 123.5 (q, *J* = 272.8 Hz), 88.2, 81.0, 29.4, 29.2, 21.4, 21.3, 20.7; ^{19}F NMR ($CDCl_3$, 282 MHz) δ –62.8 (s); IR (Neat Film, NaCl) 2973, 1652, 1608, 1472, 1343, 1306, 1173, 1133, 1077, 1028, 830 cm^{-1}; HRMS (MM: ESI-APCI) *m/z* calc'd for $C_{15}H_{18}O^{79}BrF_3N$ $[M+H]^+$: 364.0518, found 364.0535; $[\alpha]_D^{25.0}$ +33.1° (*c* 6.050, $CHCl_3$).

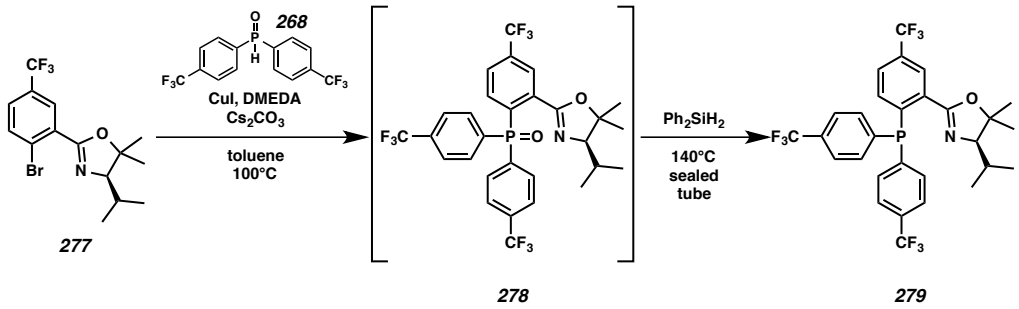

CF_3-(*R*)-5,5-dimethyl-*i*-PrPhox (279):[37] To a multineck reaction vessel fitted with a reflux condenser were added CuI (377 mg, 1.98 mmol, 1.00 equiv) and phosphine oxide **268** (870 mg, 2.57 mmol, 1.30 equiv) as solids. The reaction vessel was then evacuated and backfilled with argon (3 x 5 minute cycles). Toluene (8 mL) was then added and stirring commenced. *N*,*N*'-Dimethylethylenediamine (DMEDA, 0.64 mL, 5.94 mmol, 3.00 equiv) was then added dropwise causing the yellow heterogeneous reaction mixture to become dark green and homogeneous. After 20 minutes, oxazoline **277** (721 mg, 1.98 mmol, 1.00 equiv) was added as a neat oil dropwise followed by Cs_2CO_3 (2.39 g, 7.33 mmol, 3.70 equiv) as a solid in single portion. The reaction vessel was then introduced to a preheated 110 °C bath. After 20 h, the consumption of starting material was complete

as determined by TLC (1:9 Et_2O:Hexanes eluent). The refluxing solution was removed from the heating bath and allowed to cool to ambient temperature (ca. 23 °C). The crude reaction mixture was concentrated in vacuo and the crude brown solid was purified by silica gel column chromatography (25%→50% EtOAc in hexanes eluent) to provide phosphine oxide **278** (778 mg, 63% yield) as an amorphous white solid that was carried directly into the next transformation.

Solid phosphine oxide **278** (778 mg, 1.25 mmol, 1.00 equiv) was added to a sealable pressure vessel, which was then evacuated and backfilled with argon (3 x 5 minute cycles). To the flask was then added Ph_2SiH_2 (1.63 mL, 8.76 mmol, 7.00 equiv) with stirring. The reaction vessel, containing a homogeneous yellow solution, was then sealed and introduced to a preheated 140 °C bath. After 48 h, the consumption of starting material was complete as determined by TLC (1:1 EtOAc:Hexanes eluent). The refluxing solution was removed from the heating bath and allowed to cool to ambient temperature (ca. 23 °C). The crude reaction mixture was directly purified by silica gel column chromatography (20% CH_2Cl_2 in hexanes eluent) to furnish CF_3-(*R*)-5,5-dimethyl-*i*-PrPhox (**279**, 614 mg, 81% yield) as an amorphous white solid: R_f = 0.27 (1:4 CH_2Cl_2:Hexanes eluent); ^{1}H NMR (C_6D_6, 500 MHz) δ 8.57 (dd, *J* = 3.3, 2.0 Hz, 1H), 7.41–7.36 (m, 4H), 7.21–7.15 (m, 4H), 7.10 (dd, *J* = 8.2, 2.0 Hz, 1H), 6.78 (dd, *J* = 8.0, 3.0 Hz, 1H), 3.22 (d, *J* = 8.4 Hz, 1H), 1.55 (ddt, *J* = 13.0, 8.3, 6.5 Hz, 1H), 1.21 (s, 3H), 1.08 (s, 3H), 0.99 (d, *J* = 6.5 Hz, 3H), 0.75 (d, *J* = 6.5 Hz, 3H); ^{13}C NMR (C_6D_6, 126 MHz) δ 159.1 (d, *J* = 4.0 Hz), 143.5 (t, *J* = 14.8 Hz), 142.7 (d, *J* = 30.6 Hz), 134.5 (dd, *J* = 21.3, 15.7 Hz), 133.7 (d, *J* = 19.5 Hz), 131.1 (q, *J* = 33.1 Hz), 131.0 (dq, *J* = 32.3, 4.4 Hz), 127.1 (q, *J* = 3.6 Hz), 126.4–126.1 (m), 125.5 (dp, *J* = 7.5, 3.8 Hz), 124.8 (dq, *J* =

272.0, 3.3 Hz), 124.4 (q, J = 272.6 Hz), 87.2, 81.7 (d, J = 1.5 Hz), 29.1, 28.8, 21.1, 20.8, 20.8 (d, J = 1.8 Hz); ^{19}F NMR (C_6D_6, 282 MHz) δ –62.6 (s), –62.9 (s); ^{31}P NMR (C_6D_6, 121 MHz) δ –7.1 (s); IR (Neat Film, NaCl) 2974, 1652, 1606, 1397, 1323, 1165, 1128, 1060, 1017, 832, 756 cm^{-1}; HRMS (FAB+) *m/z* calc'd for $C_{29}H_{26}OF_9NP$ $[M+H]^+$: 606.1608, found 606.1585; $[\alpha]_D^{25.0}$ +9.5° (*c* 3.200, $CHCl_3$).

2.7.4 Ligand Screen in Palladium-Catalyzed Intermolecular Enantioselective Allylic Alkylation

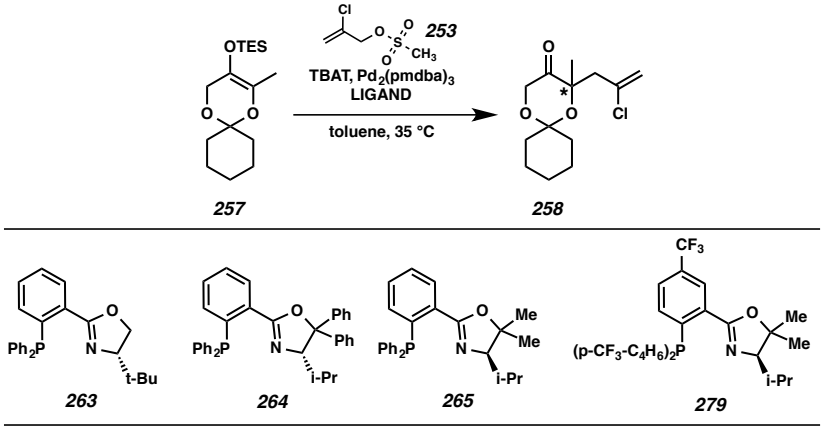

Entry	Ligand	Starting Material	Cost per gram ($) S - Enantiomer	R	Product Enantiomer [a]	Product ee (%) [b]
1	***263***	***tert*-Leucine**	33	351	***S***	92
2	***264***	**Valine**	0.60	6	***S***	90
3	***265***	**Valine**	0.60	6	***R***	89
4	***279***	**Valine**	0.60	6	***R***	91

[a] Configuration at chiral center of product **258**. [b] measured by analytical chiral GC

General Procedure for Ligand Screen

A 20 mL scintillation vial was soaked in a 20:1 *i*-PrOH:toluene bath saturated with KOH for 12 h, rinsed with deionized H_2O, acetone, and allowed to dry in a 120 °C oven for an additional 12 h. To this oven-dried 20 mL scintillation vial in a nitrogen-filled glovebox were charged $Bu_4NPh_3SiF_2$ (TBAT, 216 mg, 0.40 mmol, 1.00 equiv), $Pd_2(pmdba)_3$ (7 mg, 0.006 mmol, 0.015 equiv), ligand (0.014 mmol, 0.035 equiv), and toluene (8.0 mL). The reaction vessel immediately placed a into preheated 35 °C heating

block with stirring. After 20 minutes, a yellow-brown solution was observed. Chloroallylmesylate **253** (82 mg, 0.48 mmol, 1.20 equiv) was added quickly dropwise affording a blue-green solution. After 3 minutes, silyl enol ether **257** (120 mg, 0.40 mmol, 1.00 equiv) was added quickly dropwise. The resultant blue-green reaction mixture was allowed to stir for 20 h, at which time the consumption of starting material was complete as determined by TLC (1:19 Et_2O:Hexanes eluent). The resultant yellow-brown reaction was then allowed to cool to ambient temperature (ca. 23 °C), filtered through a pad of SiO_2 using hexanes as the eluent to remove toluene, at which time separate fractions were collected, eluting with Et_2O, to isolate the volatile reaction products. The filtrate was concentrated in vacuo to a bright yellow oil which was subsequently purified by flash chromatography (1%→3%→5% Et_2O in hexanes eluent) to afford volatile chloroallyl ketal **258** as a clear, colorless oil. The yield of each reaction was not determined. The *ee* of each product was determined by analytical chiral GC (G-TA column, 120 °C isotherm, major retention time: 53.209 min, minor retention time: 52.075 min).

2.8 Notes and References

1. For selected examples, see: (a) Herdewijn, P.; Balzarini, J.; De Clercq, E.; Vanderhaeghe, H. *J. Med. Chem.* **1985**, *28*, 1385–1386. (b) King, S. B.; Ganem, B. *J. Am. Chem. Soc.* **1991**, *113*, 5089–5090. (c) Ono, M.; Nishimura, K.; Tsubouchi, H.; Nagaoka, Y.; Tomioka, K. *J. Org. Chem.* **2001**, *66*, 8199–8203. (d) Kamel, H. N.; Slattery, M. *Pharm. Biol.* **2005**, *43*, 253–269.

2. Collins, P. W.; Djuric, S. W. *Chem. Rev.* **1993**, *93*, 1533–1564.

3. (a) Perigaud, C.; Gosselin, G.; Imbach, J. L. *Nucleosides Nucleotides* **1992**, *11*, 903–945. (b) Boyer, S. J.; Leahy, J. W. *J. Org. Chem.* **1997**, *62*, 3976–3980.

4. (a) Bisacchi, G. S.; Chao, S. T.; Bachard, C.; Daris, J. P.; Innaimo, S.; Jacobs, G. A.; Kocy, O.; Lapointe, P.; Martel, A.; Merchant, Z. Slusarchyk, W. A.; Sundeen, J. E.; Young, M. G.; Colonno, R.; Zahler, R. *Bioorg. Med. Chem. Lett.* **1997**, *7*, 127–132. (b) Tsuna, K.; Noguchi, N.; Nakada, M. *Angew. Chem., Int. Ed.* **2011**, *50*, 9452–9455.

5. Corey, E. J.; Weinshenker, N. M.; Schaaf, T. K.; Huber, W. *J. Am. Chem. Soc.* **1969**, *91*, 5675–5677.

6. (a) Roethle, P. A.; Trauner, D. *Nat. Prod. Rep.* **2008**, *25*, 298–317. (b) Li, Y.; Pattenden, G. *Nat. Prod. Rep.* **2011**, *28*, 1269–1310.

7. (a) Nakashima, H.; Sato, M.; Taniguchi, T.; Ogasawara, K. *Tetrahedron Lett.* **2000**, *41*, 2639–2642. (b) Audran, G.; Acherar, S.; Monti, H. *Eur. J. Org. Chem.* **2003**, 92–98.

8. Corey, E. J.; Schaaf, T. K.; Huber, W.; Koelliker, U.; Weinshenker, N. M. *J. Am. Chem. Soc.* **1970**, *92*, 397–398.

9. Niidu, A.; Paju, A.; Eek, M.; Müürisepp, A.-M.; Pehk, T.; Lopp, M. *Tetrahedron: Asymmetry* **2006**, *17*, 2678–2683.

10. (a) Behenna, D. C.; Stoltz, B. M. *J. Am. Chem. Soc.* **2004**, *126*, 15044–15045. (b) McFadden, R. M.; Stoltz, B. M. *J. Am. Chem. Soc.* **2006**, *128*, 7738–7739. (c) Mohr, J. T.; Stoltz, B. M. *Chem. Asian J.* **2007**, *2*, 1476–1491. (d) Enquist, Jr., J. A.; Stoltz, B. M. *Nature* **2008**, *453*, 1228–1231. (e) Day, J. J.; McFadden, R. M.; Virgil, S. C.; Kolding, H.; Alleva, J. L.; Stoltz, B. M. *Angew. Chem., Int. Ed.* **2011**, *50*, 6814–6818.

11. Seto, M.; Roizen, J. L.; Stoltz, B. M. *Angew. Chem., Int. Ed.* **2008**, *47*, 6873–6876.

12. A variety of conditions were found to be ineffective in the formation of desired product **250** including: KOH/xylenes/110 °C, NaH/110 °C, $Ba(OH)_2 \bullet 8H_2O/H_2O$/methoxyethanol, LDA/THF/–78 °C, NaO*t*-Bu/HO*t*-Bu, KF/18-crown-6/xylenes, TMSOTf/EtN(*i*-Pr)$_2$/0 °C then TBAF.

13. (a) Trost, B. M.; Curran, D. P. *J. Am. Chem. Soc.* **1980**, *102*, 5699–5700. (b) VanBrunt, M. P.; Ambenge, R. O.; Weinreb, S. M. *J. Org. Chem.* **2003**, *68*, 3323–3326.

14. The procedure for the conversion of silyl enol ether **248** to chloroallylketone **254** with the associated characterization data has been reported by our group, see reference 11, and: Roizen, J. L. Progress Toward an Enantioselective Total Synthesis of Ineleganolide. Ph.D. dissertation, California Institute of Technology, Pasadena, CA, 2010.

15. For full details and optimized procedure, see section 2.7.2.

16. Determined by ^{1}H NMR studies of the crude mixture.

17. For details concerning the synthesis of silyl enol ether **257**, see Section 2.7.2.

18. Optimized conditions for the transformation of silyl enol ether **257** to chloroallylketone **258** are displayed in Scheme 2.4.4. For full details, see Section 2.7.2.

19. For the experimental procedure and full details, see Section 2.7.2.

20. This transformation has been performed on scales up to 1.40 g of starting material **258**. For full details, see Section 2.7.2.

21. See Scheme 2.4.3. Also, see reference 13.

22. Only one diastereomer is observed as a product. The stereochemistry of the reduction has been confirmed by NOE studies of alcohol **261** after benzoylation. See Section 2.7.2. and Appendix 1.

23. This transformation has been performed on scales up to 3.30 g of starting material **260**. For full details, see Section 2.7.2.

24. Pangborn, A. B.; Giardello, M. A.; Grubbs, R. H.; Rosen, R. K.; Timmers, F. J. *Organometallics* **1996**, *15*, 1518–1520.

25. (a) Peer, M.; de Jong, J. C.; Kiefer, M.; Langer, T.; Rieck, H.; Schell, H.; Sennhenn, P.; Sprinz, J.; Steinhagen, H.; Wiese, B.; Helmchen, G. *Tetrahedron* **1996**, *52*, 7547–7583. (b) Krout, M. R.; Mohr, J. T.; Stoltz, B. M. *Org. Synth.* **2009**, *86*, 181–193.

26. Bélanger, E.; Pouliot, M.-F.; Courtemanche, M.-A.; Paquin, J.-F. *J. Org. Chem.* **2012**, *77*, 317–331.

27. Bélanger, E.; Pouliot, M.-F.; Paquin, J.-F. *Org. Lett.* **2009**, *11*, 2201–2204.

28. White, D. E.; Stewart, I. C.; Grubbs, R. H.; Stoltz, B. M. *J. Am. Chem. Soc.* **2008**, *130*, 810–811.

29. (a) Ukai, T.; Kawazura, H.; Ishii, Y.; Bonnet, J. J.; Ibers, J. A. *J. Organomet. Chem.* **1974**, *65*, 253–266. (b) Fairlamb, I. J. S.; Kapdi, A. R.; Lee, A. F. *Org. Lett.* **2004**, *6*, 4435–4438.

30. (a) Harris, R. K.; Becker, E. D.; Cabral de Menezes, S. M.; Granger, P.; Hoffman, R. E.; Zilm, K. W. *Pure Appl. Chem.* **2008**, *80*, 59–84. (b) Harris, R. K.; Becker, E. D.; Cabral de Menezes, S. M.; Goodfellow, R.; Granger, P. *Pure Appl. Chem.* **2001**, *73*, 1795–1818.

31. The epoxidizing conditions tested include: Oxone®, magnesium monoperoxyphthalate hydrate (MMPP•$6H_2O$), *t*-BuOOH/SiO_2, *t*-BuOOH/$VO(acac)_2$, *m*-CPBA, *m*-CPBA/Jacobsen's catalyst.

32. A variety of conditions were found to be ineffective in the formation of the desired brominated product including: NaOH/Br_2/$CeCl_3$, $Ca(OH)_2$/Br_2, Selectfluor/KBr, LiBr/$NaIO_4$/AcOH.

33. Repetition of this procedure provided cyclopentenone **250** in yields ranging from 0 to 82%.

34. It was observed that slow addition via addition funnel of the bright yellow, transparent NaOBr solution into the reaction mixture resulted in clouding and discoloration of solution remaining in the funnel. We believed that the vapors in the headspace of the reaction vessel were facilitating this apparent decomposition and lowering the yield in the process.

35. Although storage of this intermediate in a benzene matrix is possible for extended periods, purification by silica gel chromatography results in moderate decomposition.

36. Procedure adapted from reference 26.

37. Procedure adapted from: McDougal, N. T.; Streuff, J.; Mukherjee, H.; Virgil, S. C.; Stoltz, B. M. *Tetrahedron Lett*. **2010**, *51*, 5550–5554.

APPENDIX 1

Synthetic Summary for Chapter 2:

Enantioselective Synthesis of a

Hydroxymethyl-cis-1,3-cyclopentenediol Building Block

Scheme A1.1. Synthetic Summary for Construction of cis-1,3-Cyclopentenediol ***262***

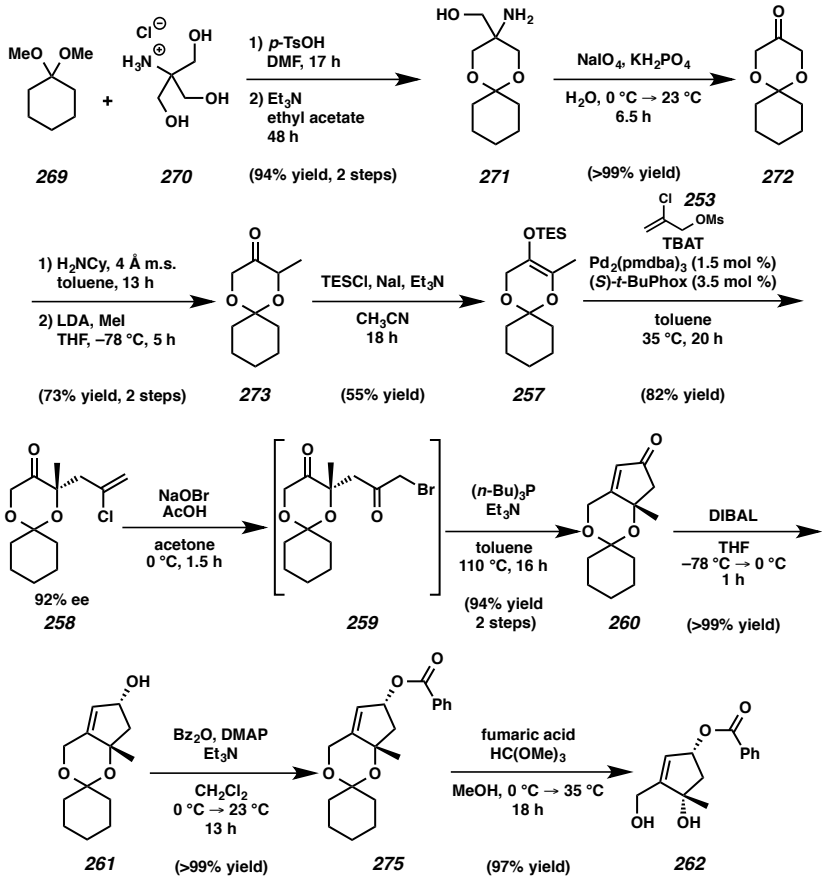

APPENDIX 2

Spectra Relevant to Chapter 2:

Enantioselective Synthesis of a

Hydroxymethyl-cis-1,3-cyclopentenediol Building Block

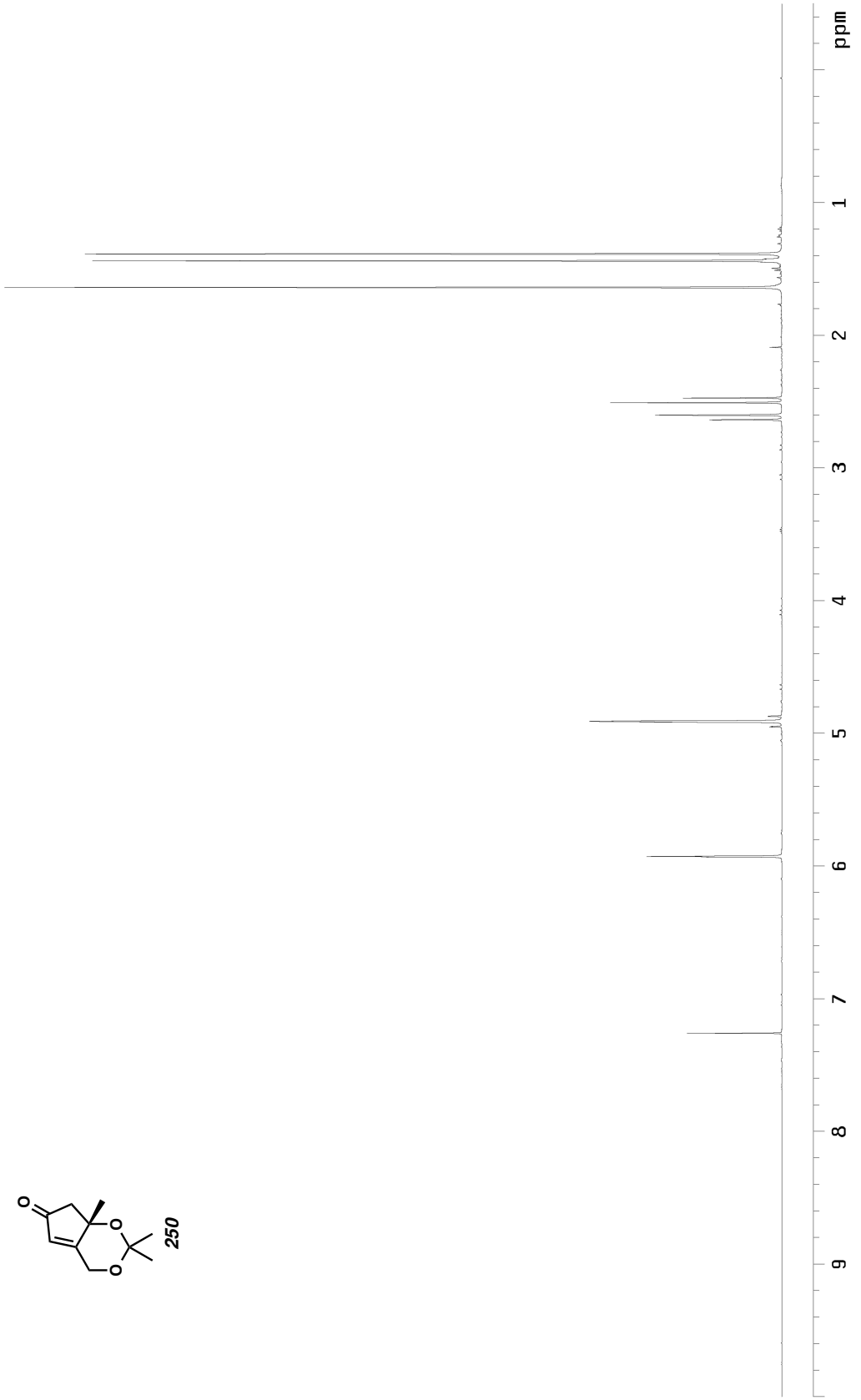

Figure A2.1. ^{1}H NMR (500 MHz, $CDCl_3$) of compound **250**.

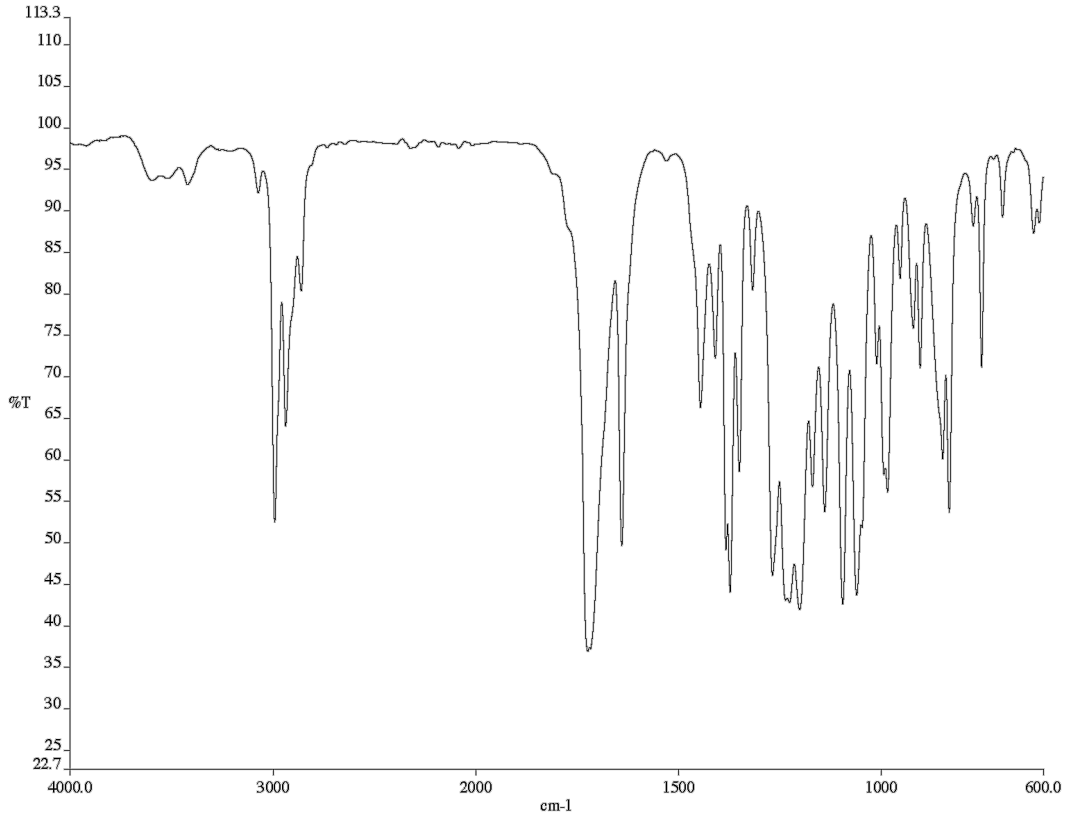

Figure A2.2. Infrared spectrum (Thin Film, NaCl) of compound **250**.

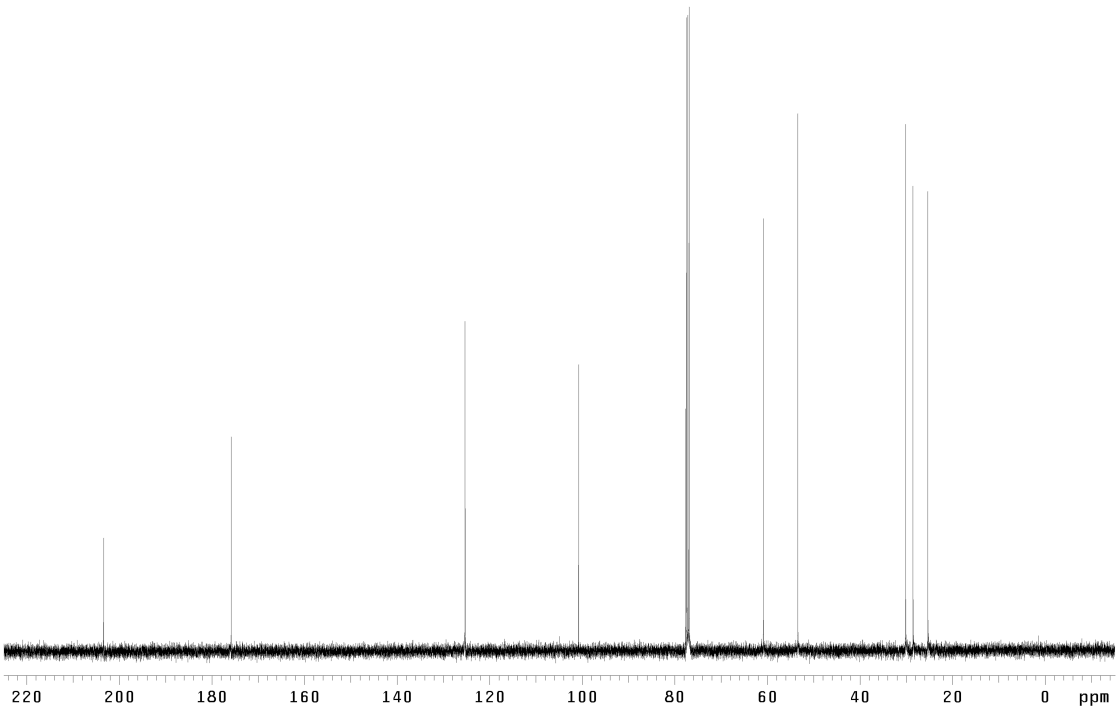

Figure A2.3. ^{13}C NMR (126 MHz, $CDCl_3$) of compound **250**.

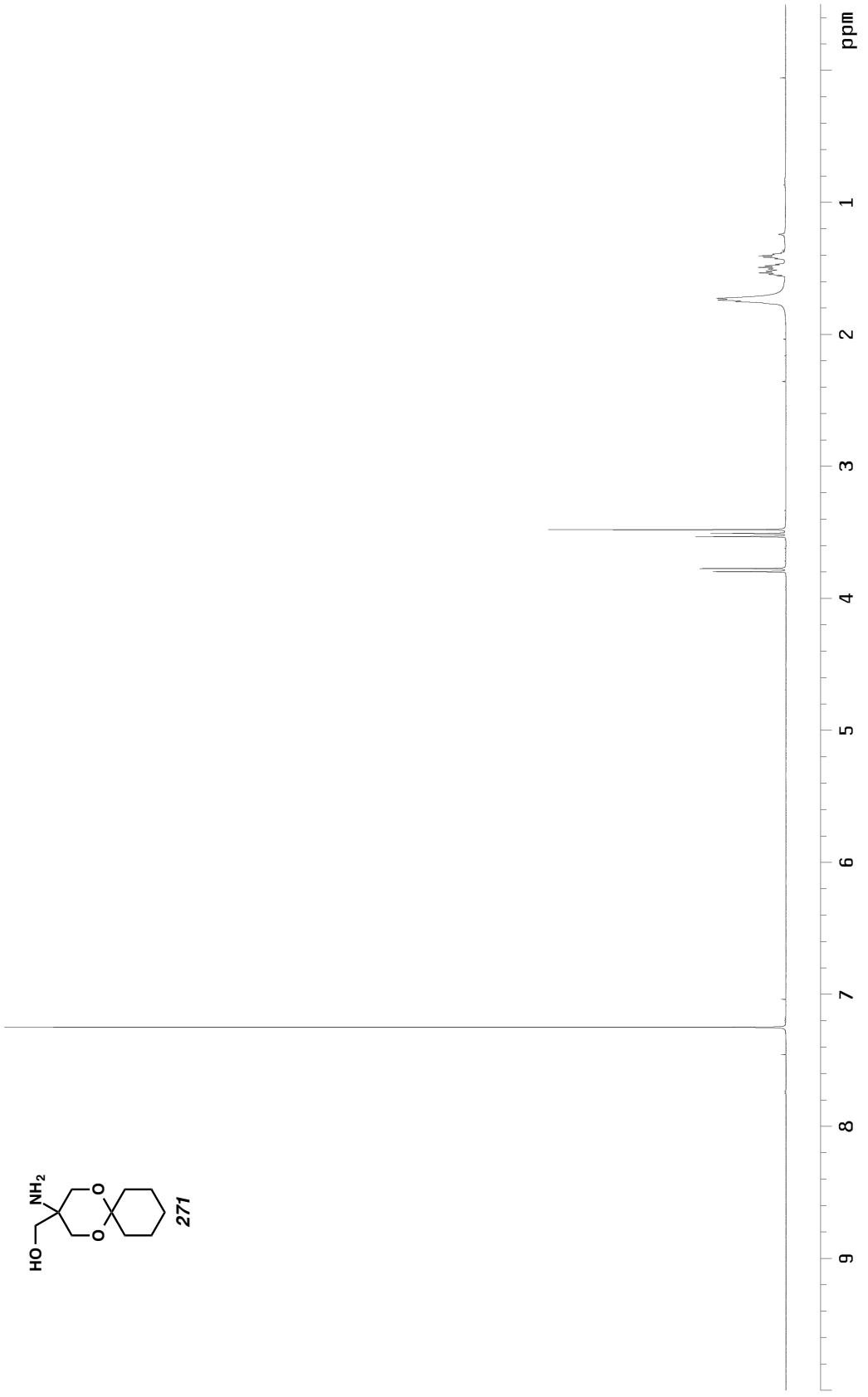

Figure A2.4. ^{1}H NMR (500 MHz, $CDCl_3$) of compound **271**.

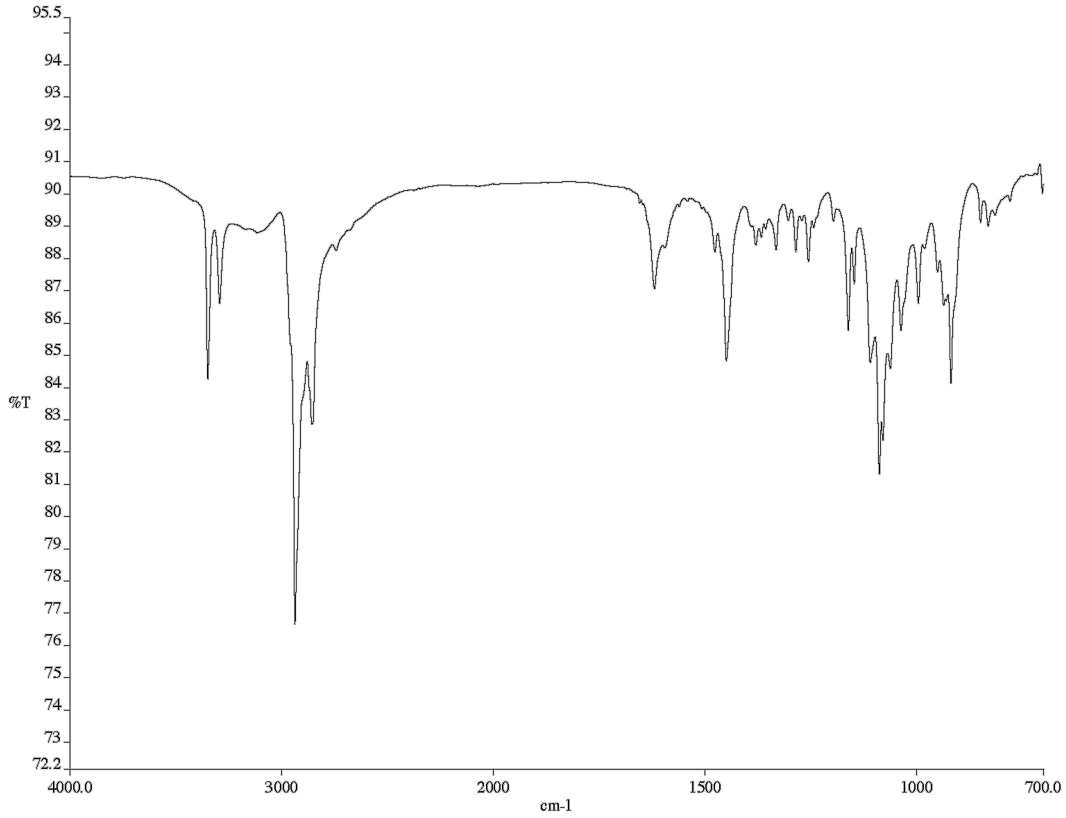

Figure A2.5. Infrared spectrum (Thin Film, NaCl) of compound **271**.

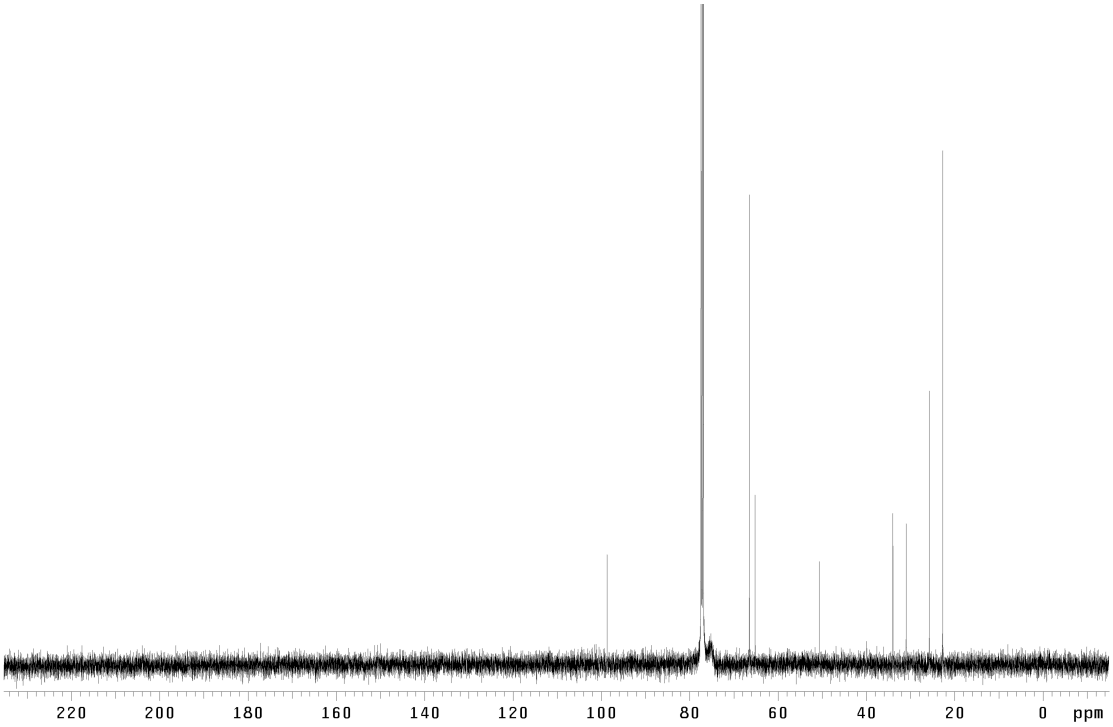

Figure A2.6. ^{13}C NMR (126 MHz, $CDCl_3$) of compound **271**.

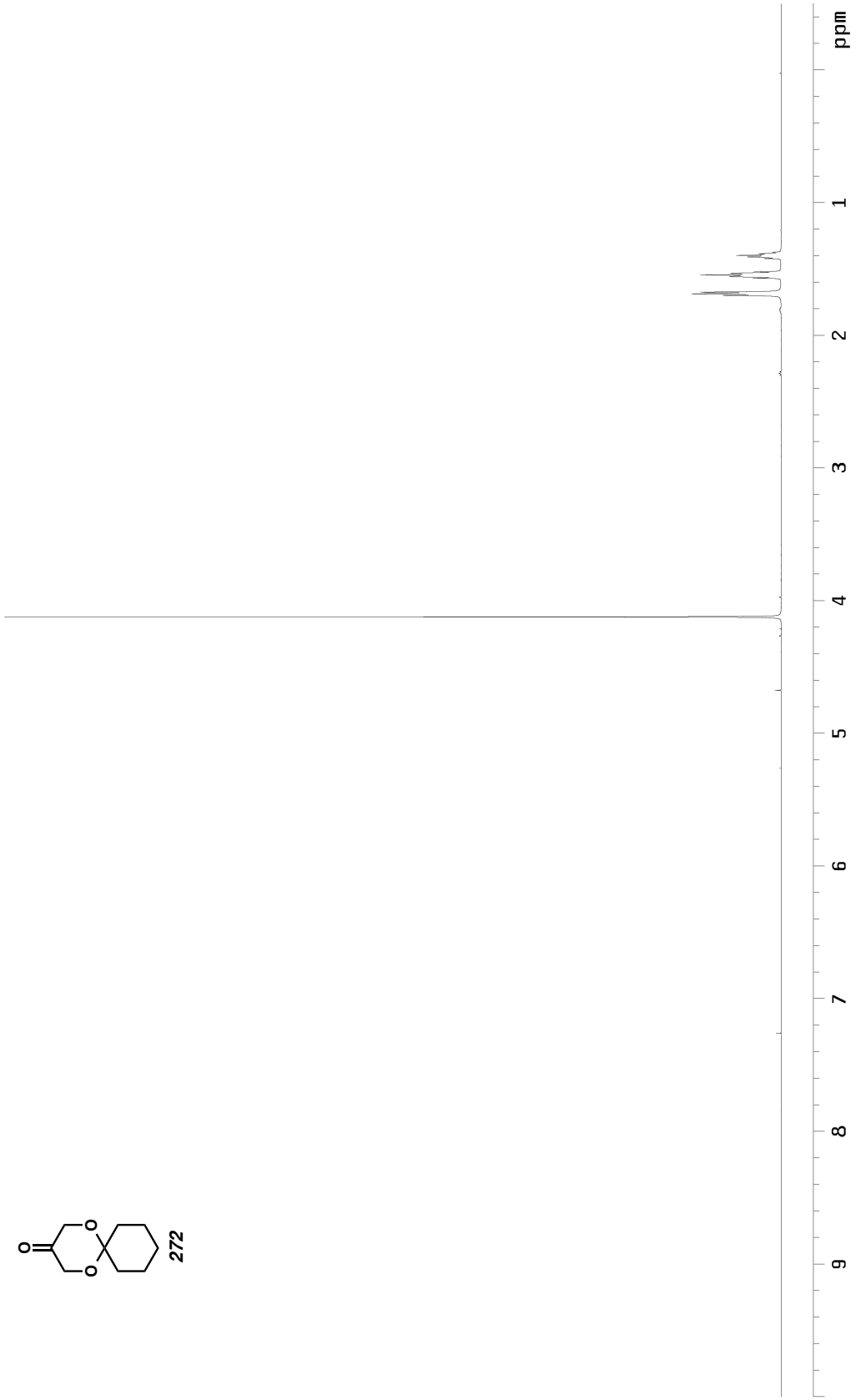

Figure A2.7. ^{1}H NMR (500 MHz, $CDCl_3$) of compound **272**.

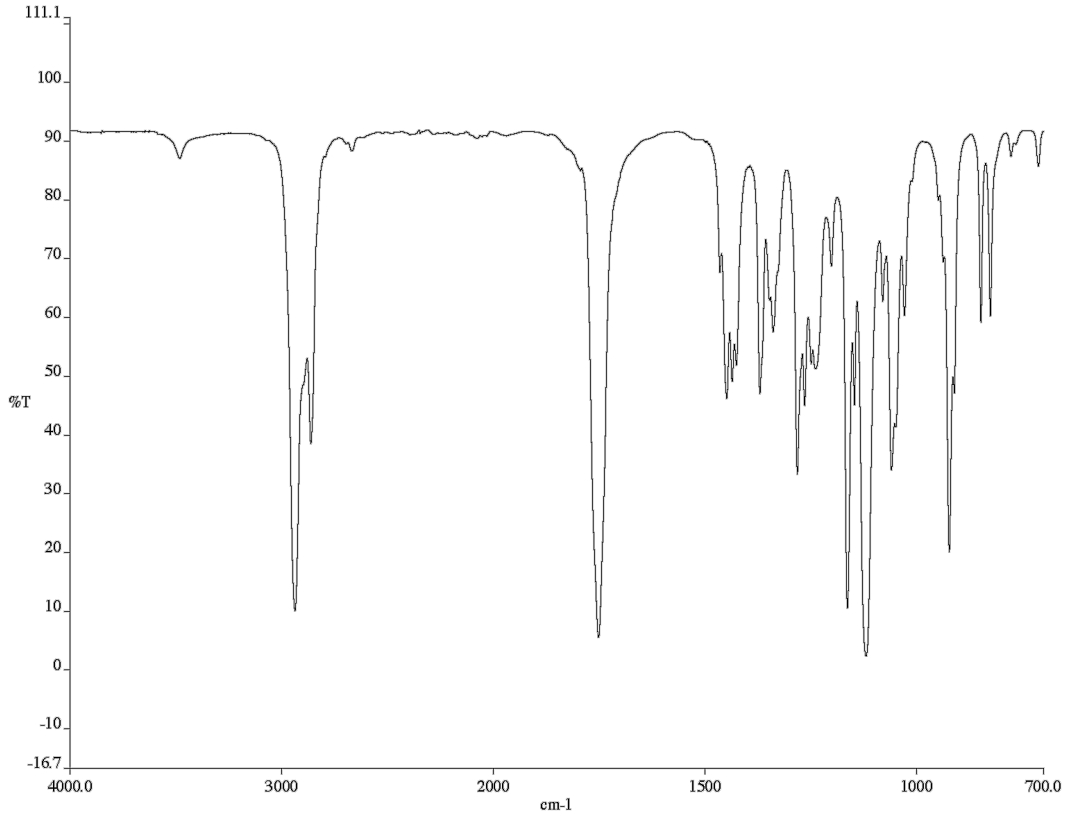

Figure A2.8. Infrared spectrum (Thin Film, NaCl) of compound **272**.

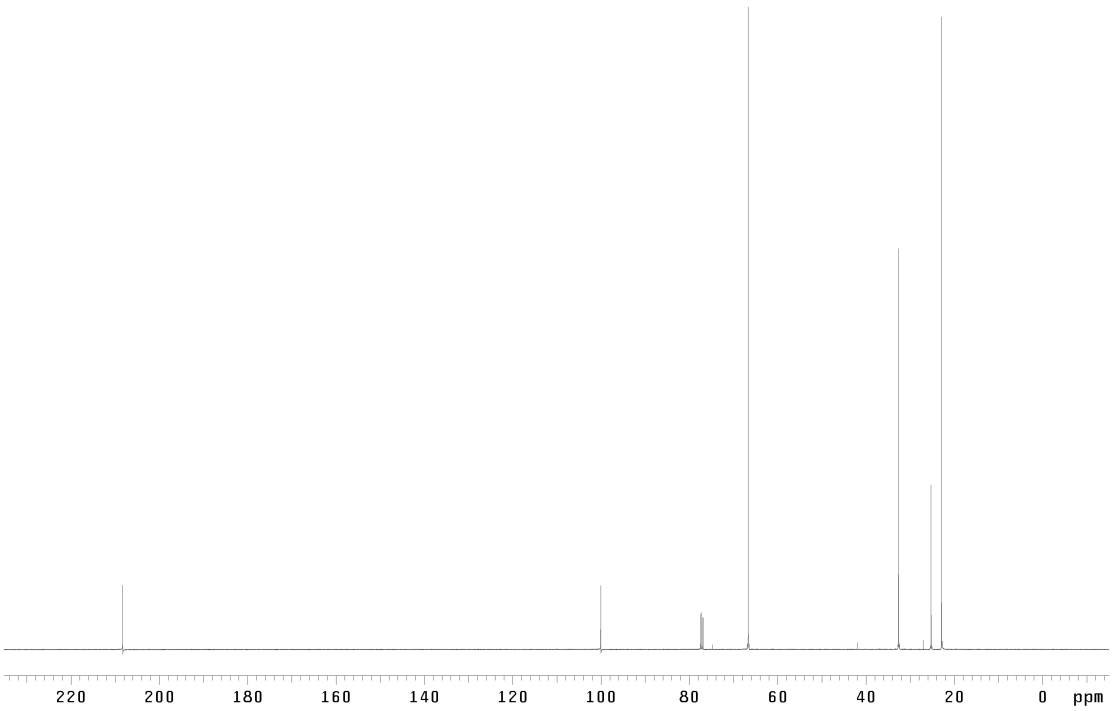

Figure A2.9. ^{13}C NMR (126 MHz, $CDCl_3$) of compound **272**.

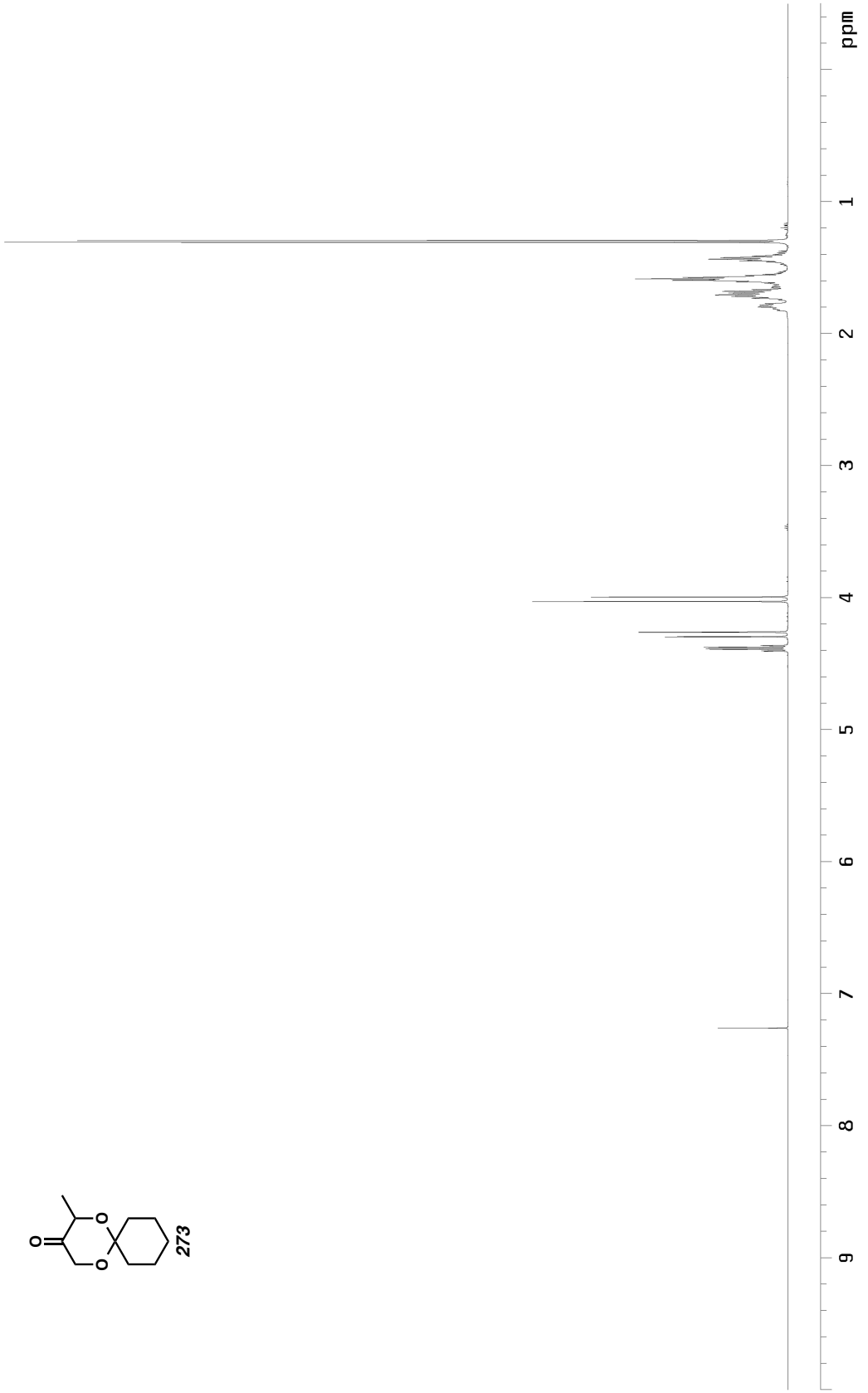

Figure A2.10. ^{1}H NMR (500 MHz, $CDCl_3$) of compound **273**.

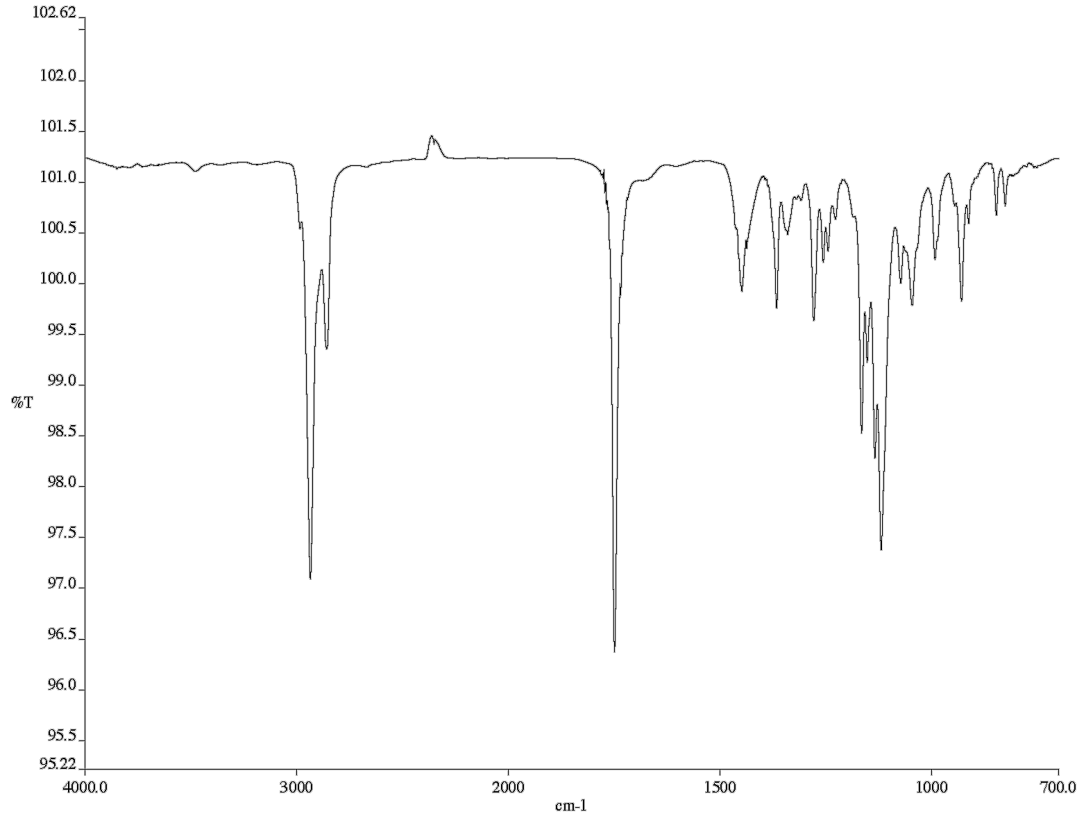

Figure A2.11. Infrared spectrum (Thin Film, NaCl) of compound **273**.

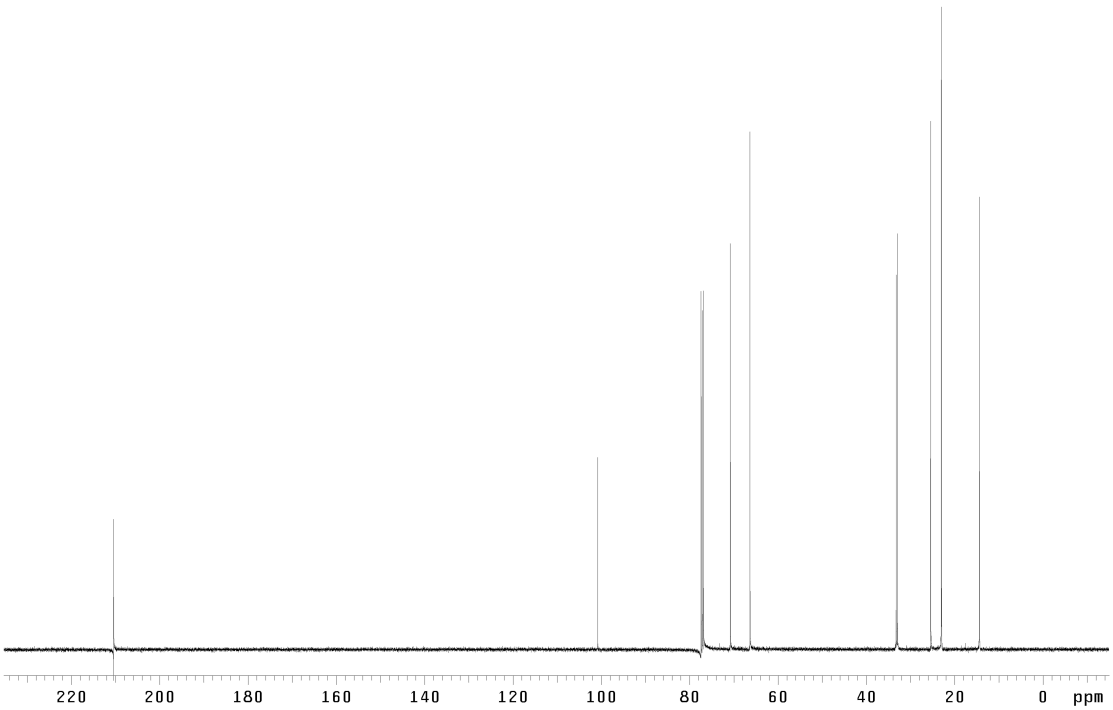

Figure A2.12. ^{13}C NMR (126 MHz, $CDCl_3$) of compound **273**.

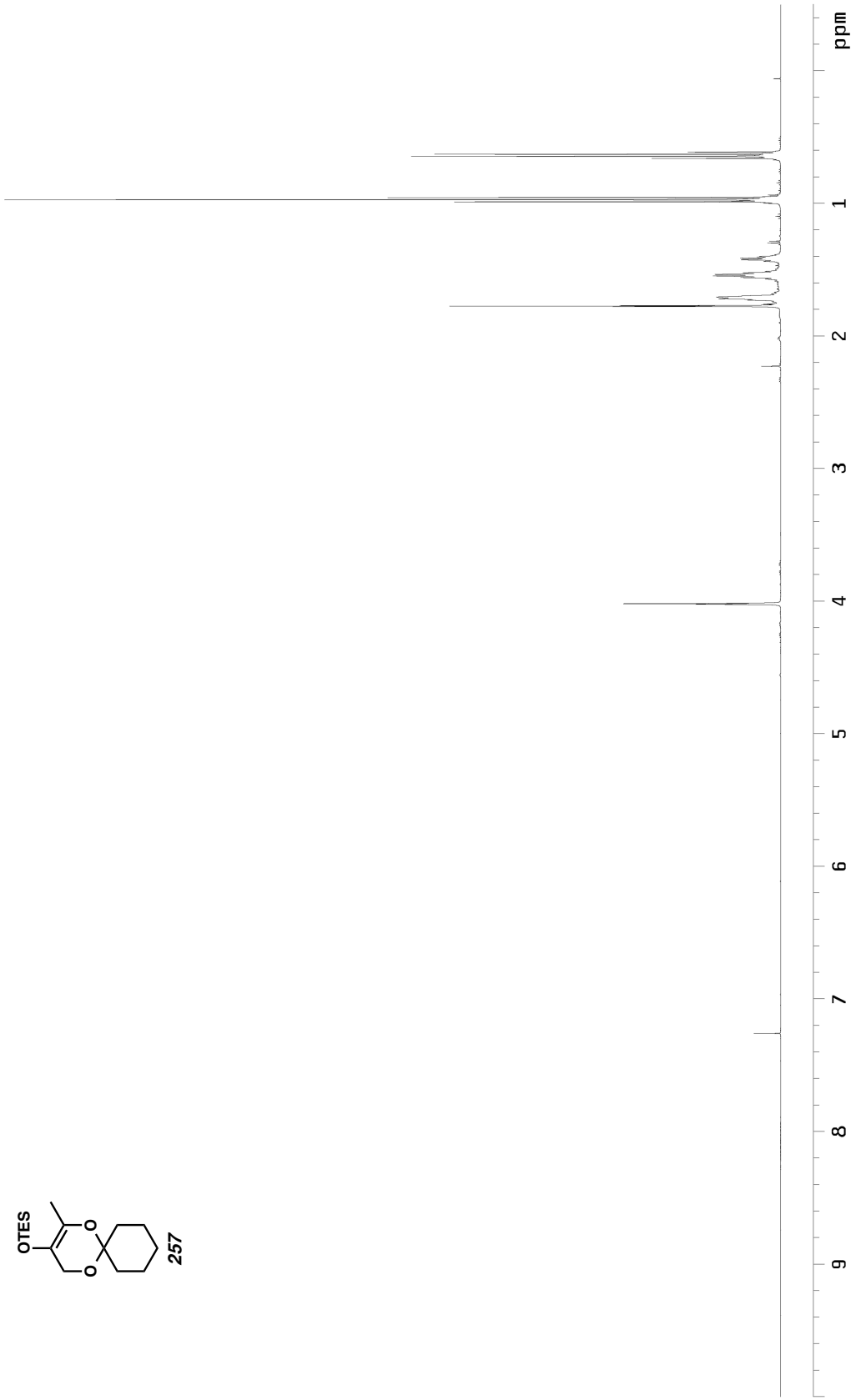

Figure A2.13. ^{1}H NMR (500 MHz, $CDCl_3$) of compound **257**.

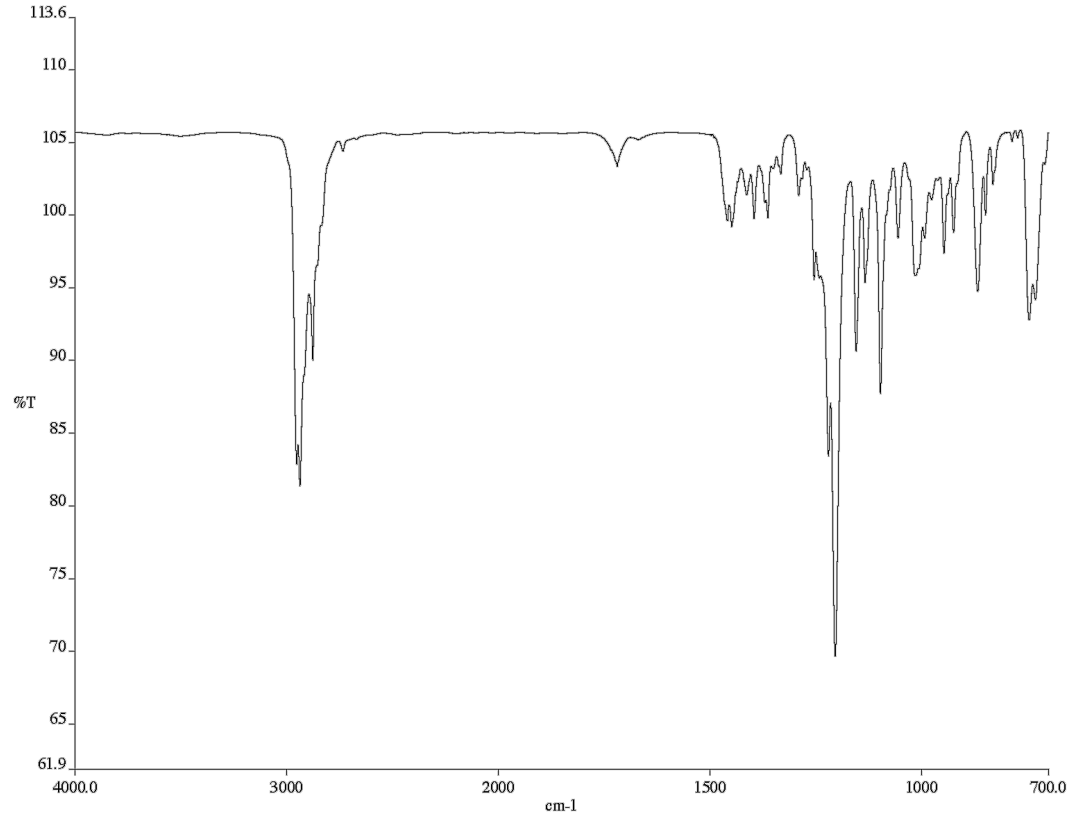

Figure A2.14. Infrared spectrum (Thin Film, NaCl) of compound **257**.

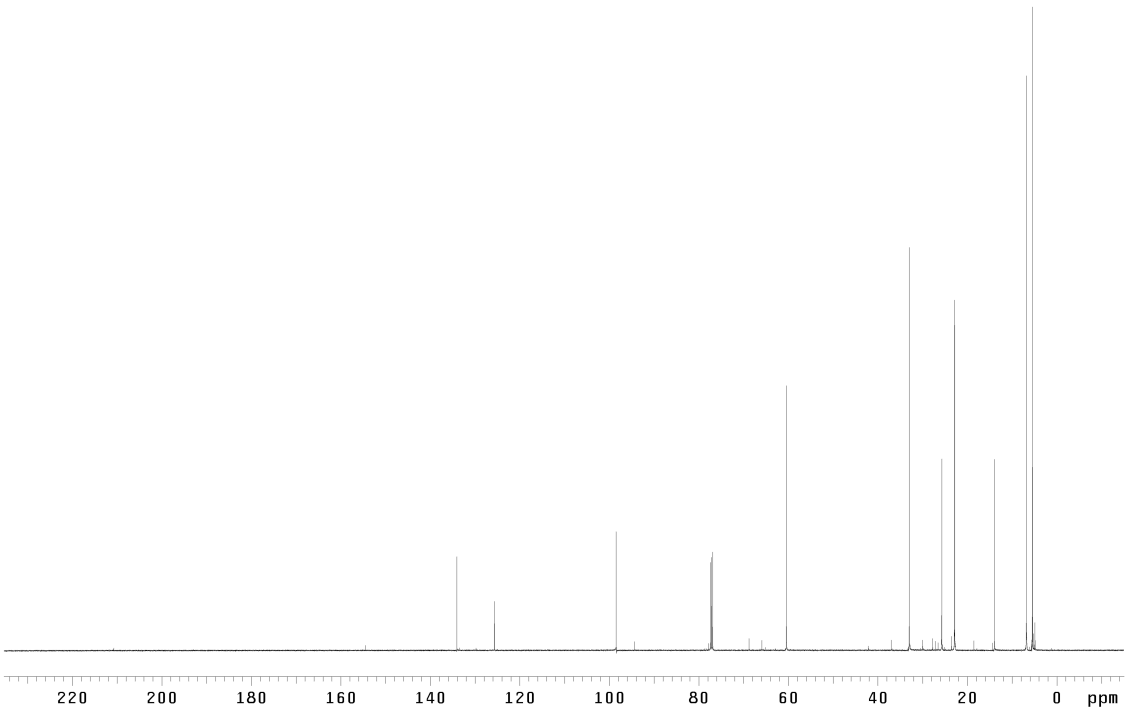

Figure A2.15. ^{13}C NMR (126 MHz, $CDCl_3$) of compound **257**.

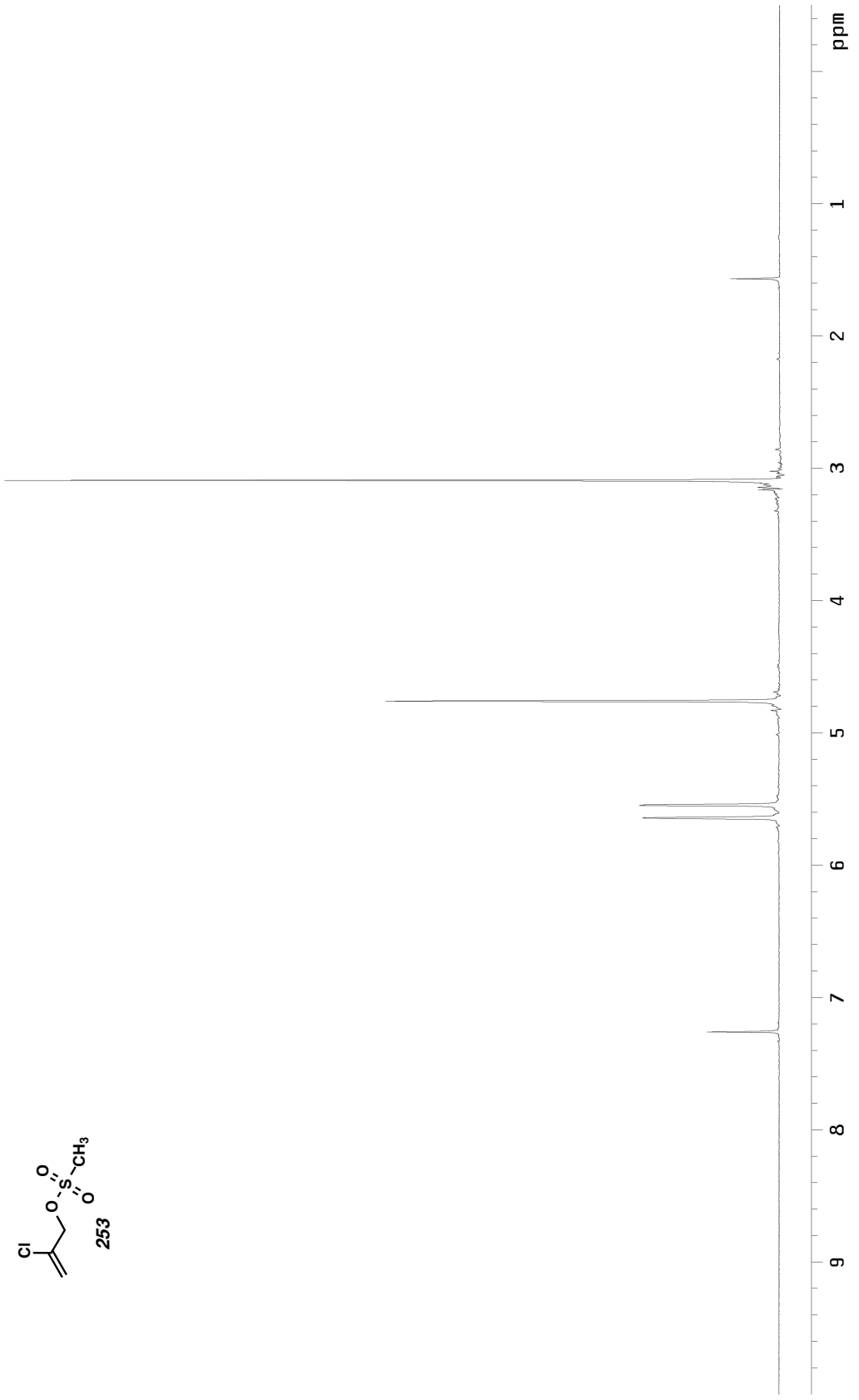

Figure A2.16. ^{1}H NMR (300 MHz, $CDCl_3$) of compound **253**.

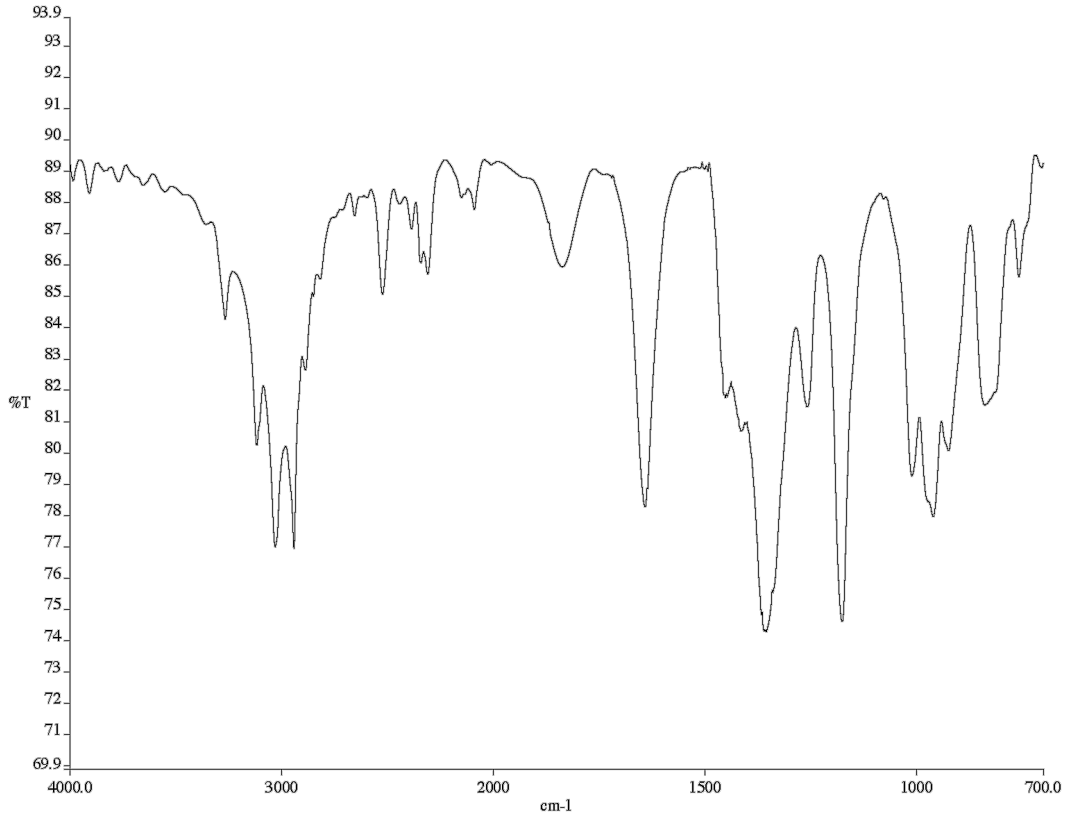

Figure A2.17. Infrared spectrum (Thin Film, NaCl) of compound **253**.

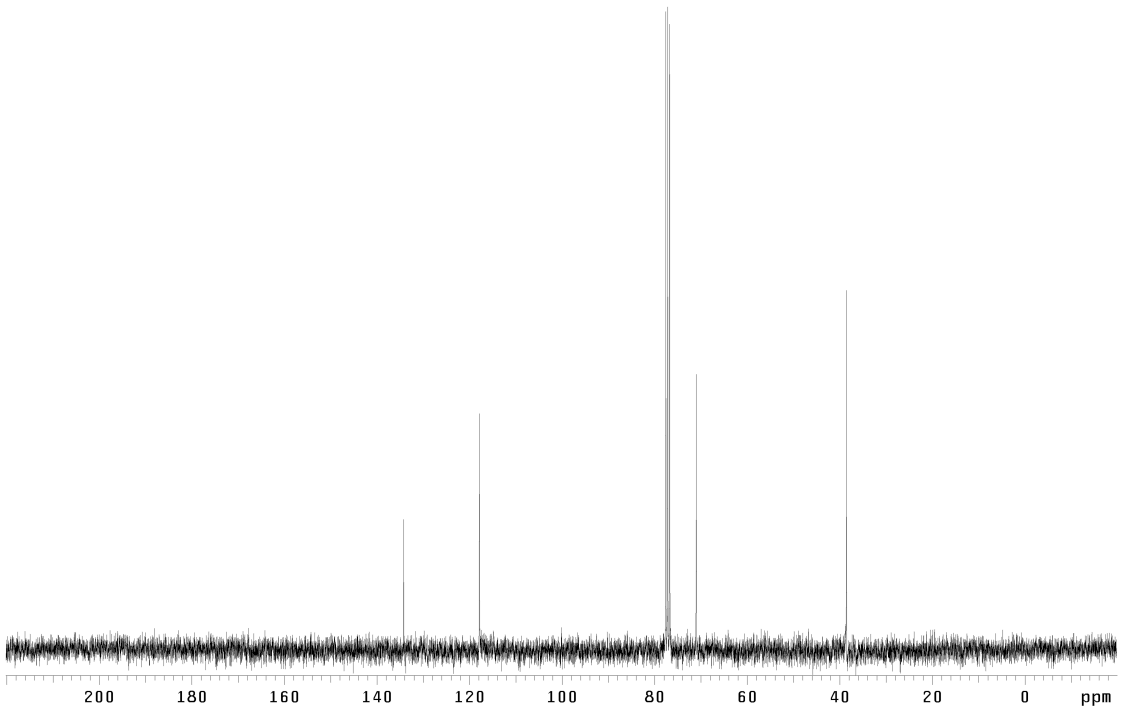

Figure A2.18. ^{13}C NMR (76 MHz, $CDCl_3$) of compound **253**.

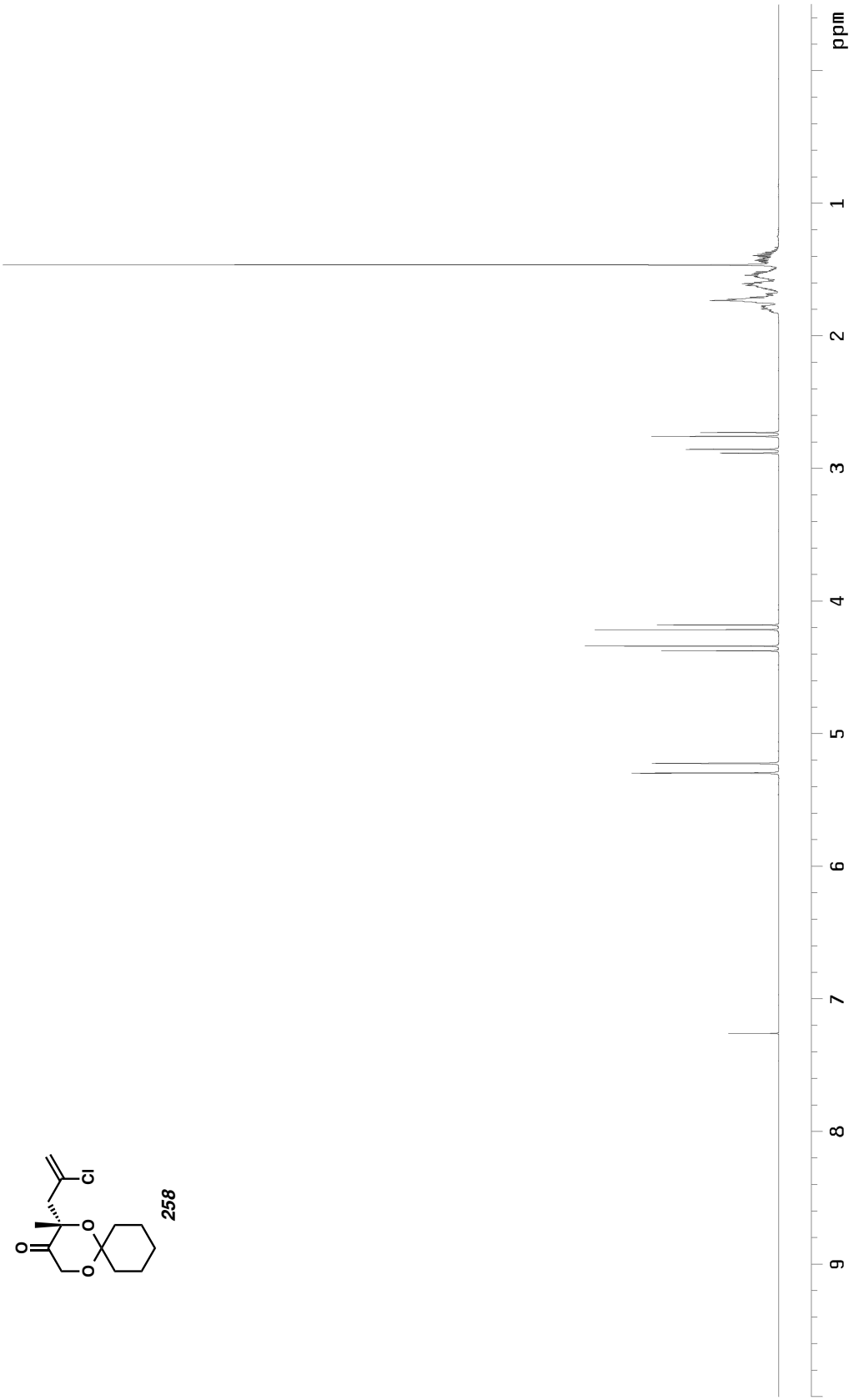

Figure A2.19. ^{1}H NMR (500 MHz, $CDCl_3$) of compound **258**.

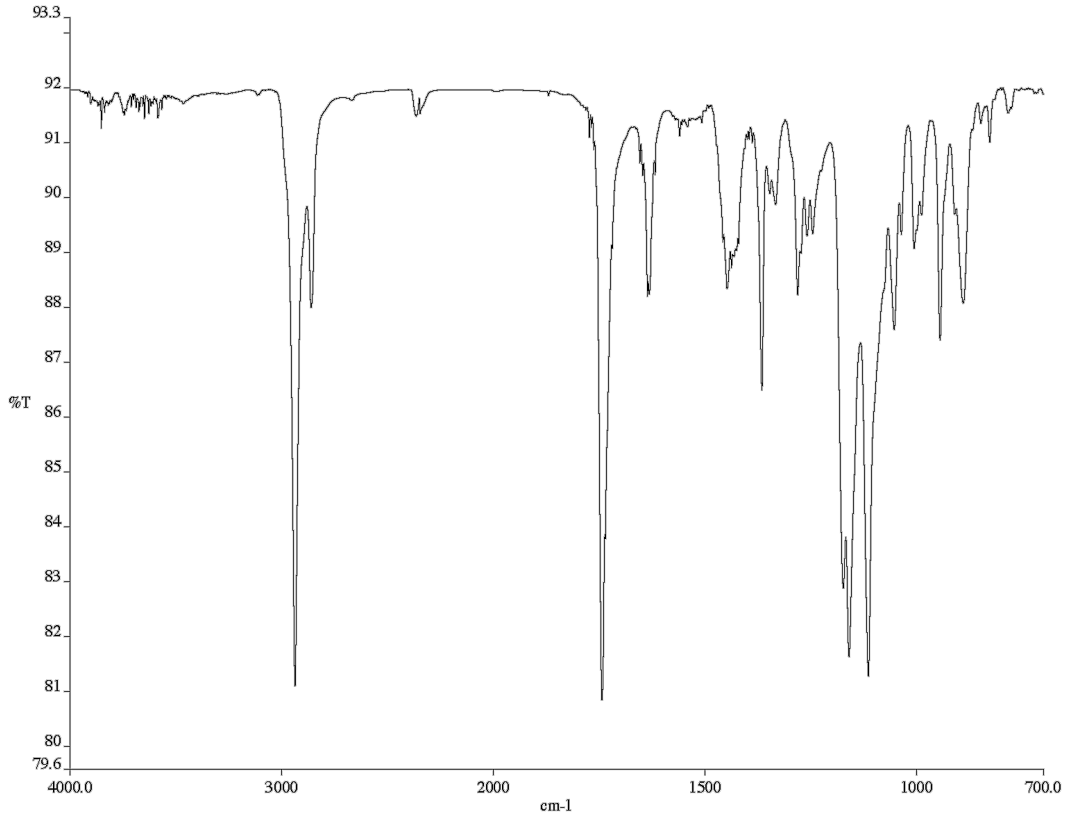

Figure A2.20. Infrared spectrum (Thin Film, NaCl) of compound **258**.

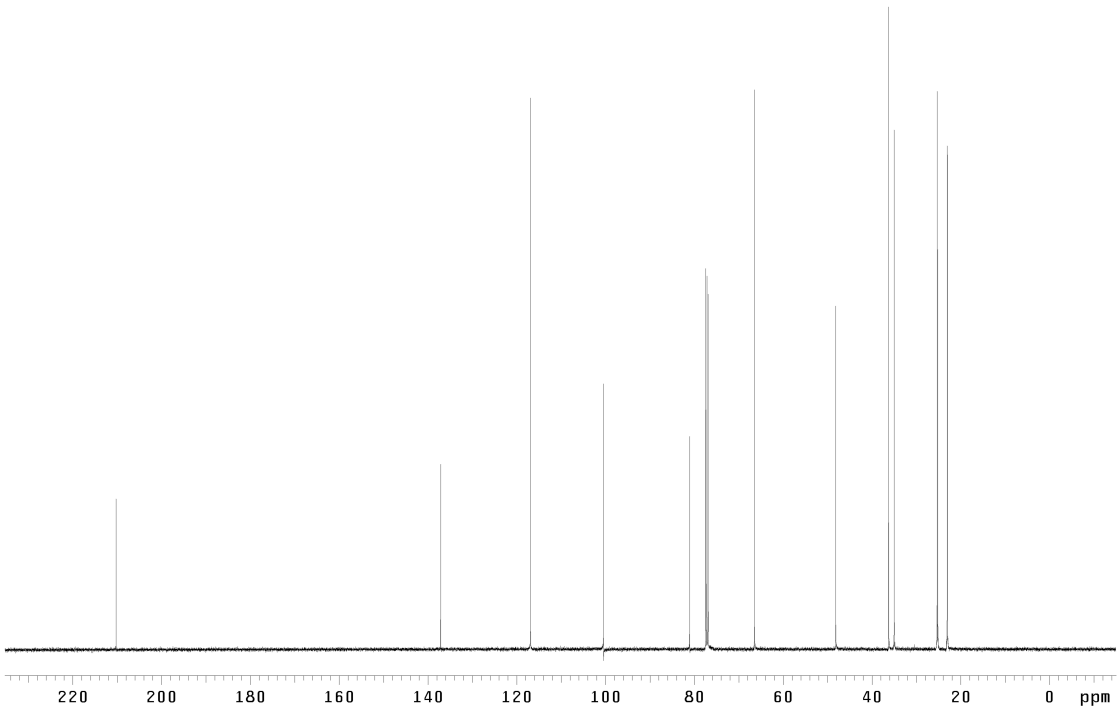

Figure A2.21. ^{13}C NMR (126 MHz, $CDCl_3$) of compound **258**.

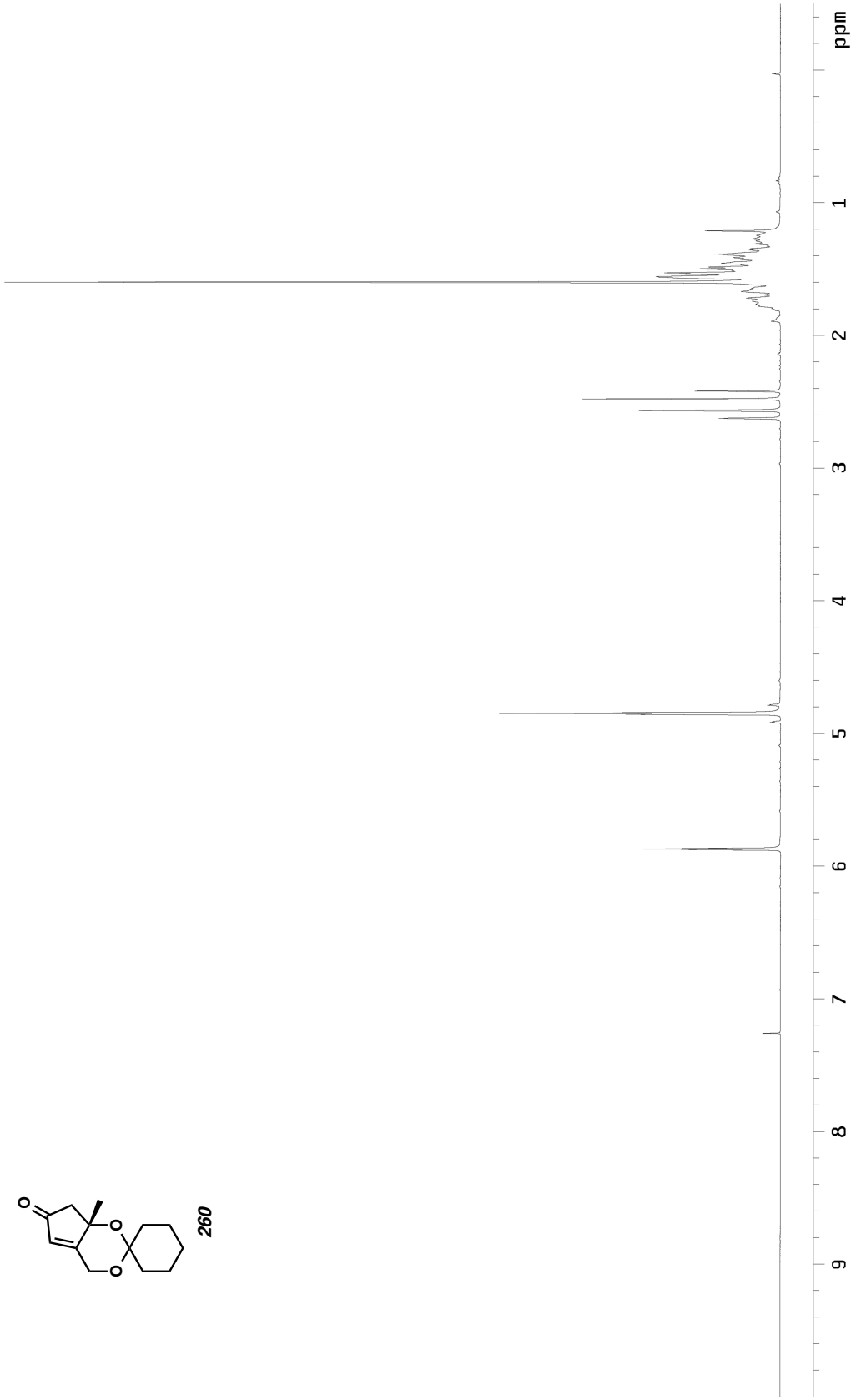

260

Figure A2.22. ^{1}H NMR (300 MHz, $CDCl_3$) of compound **260**.

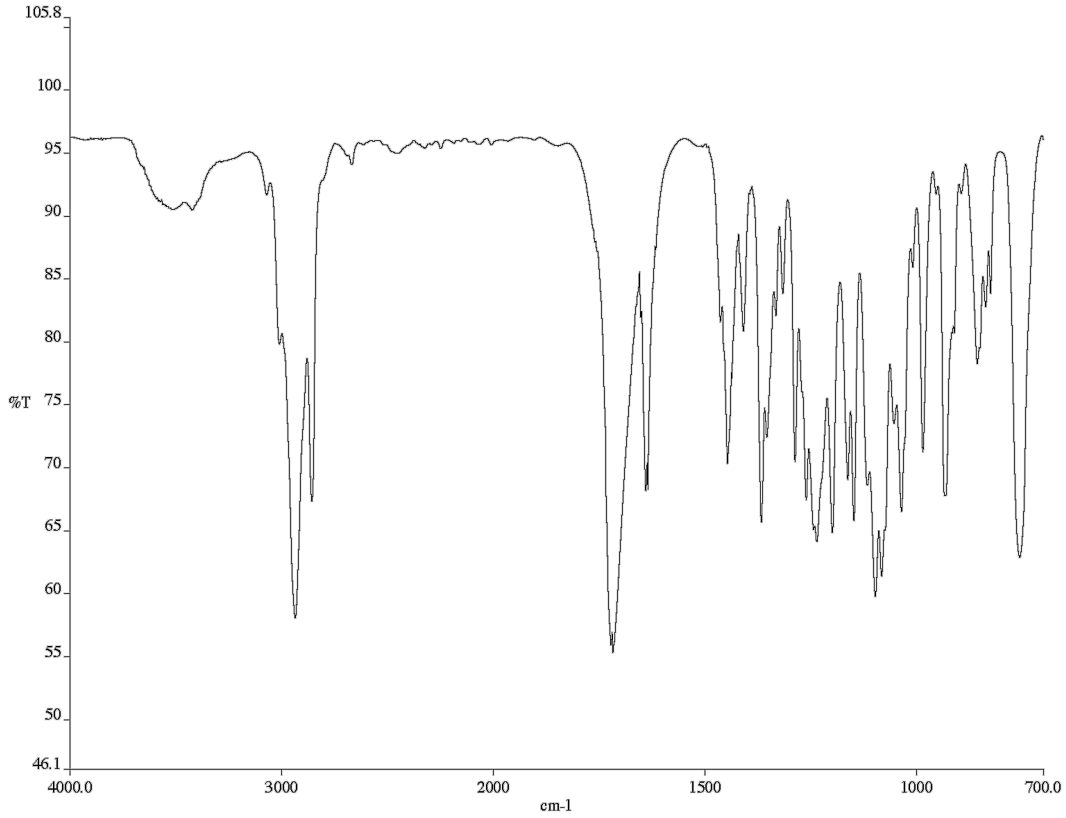

Figure A2.23. Infrared spectrum (Thin Film, NaCl) of compound **260**.

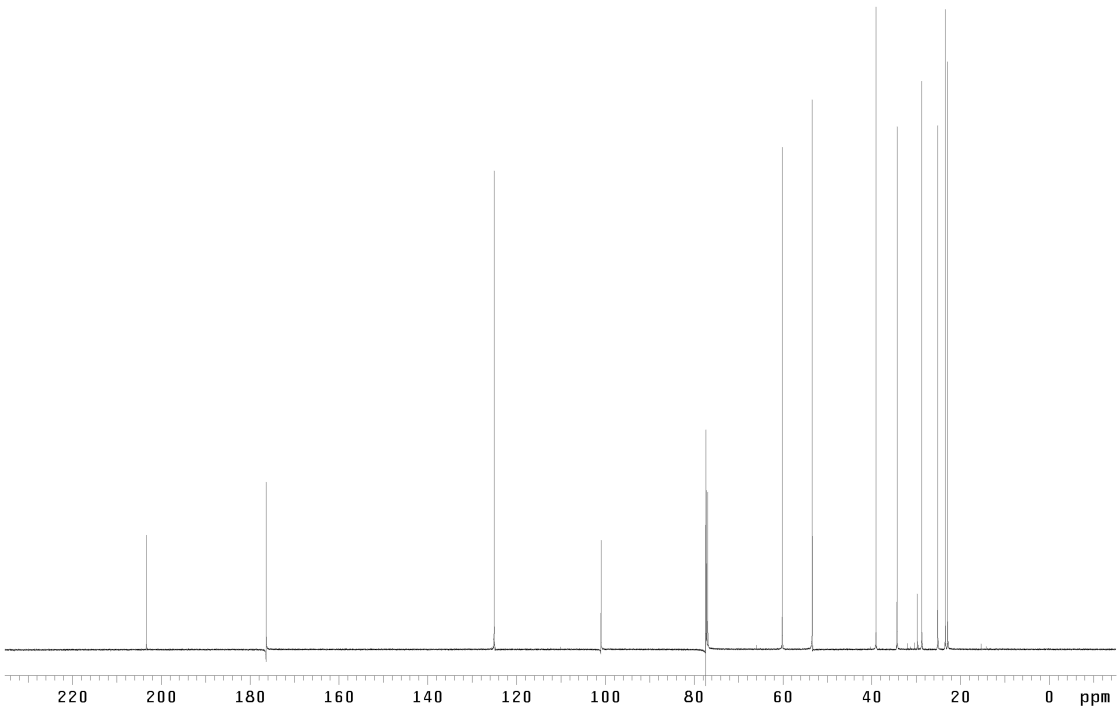

Figure A2.24. ^{13}C NMR (126 MHz, $CDCl_3$) of compound **260**.

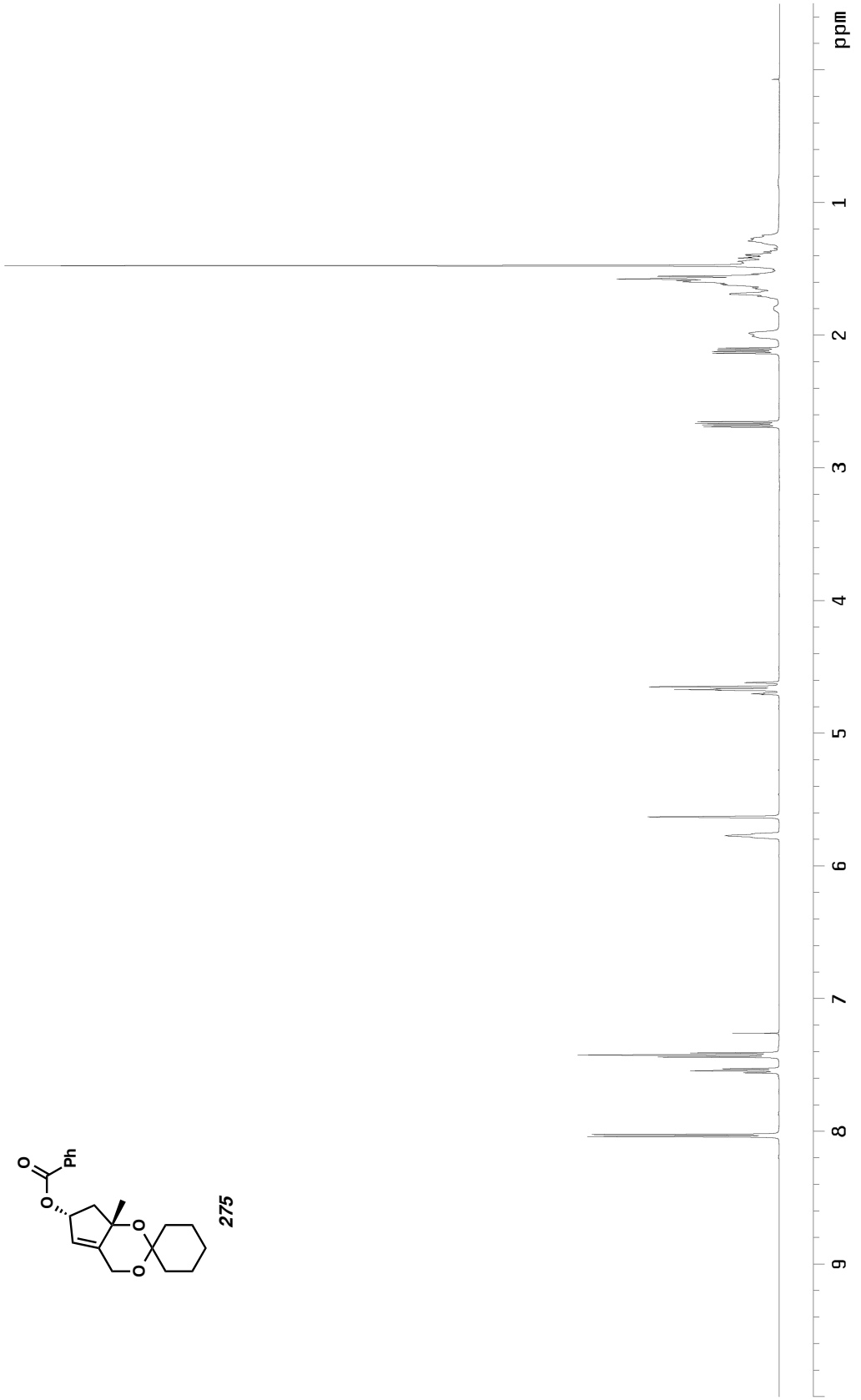

Figure A2.25. ^{1}H NMR (500 MHz, $CDCl_3$) of compound **275**.

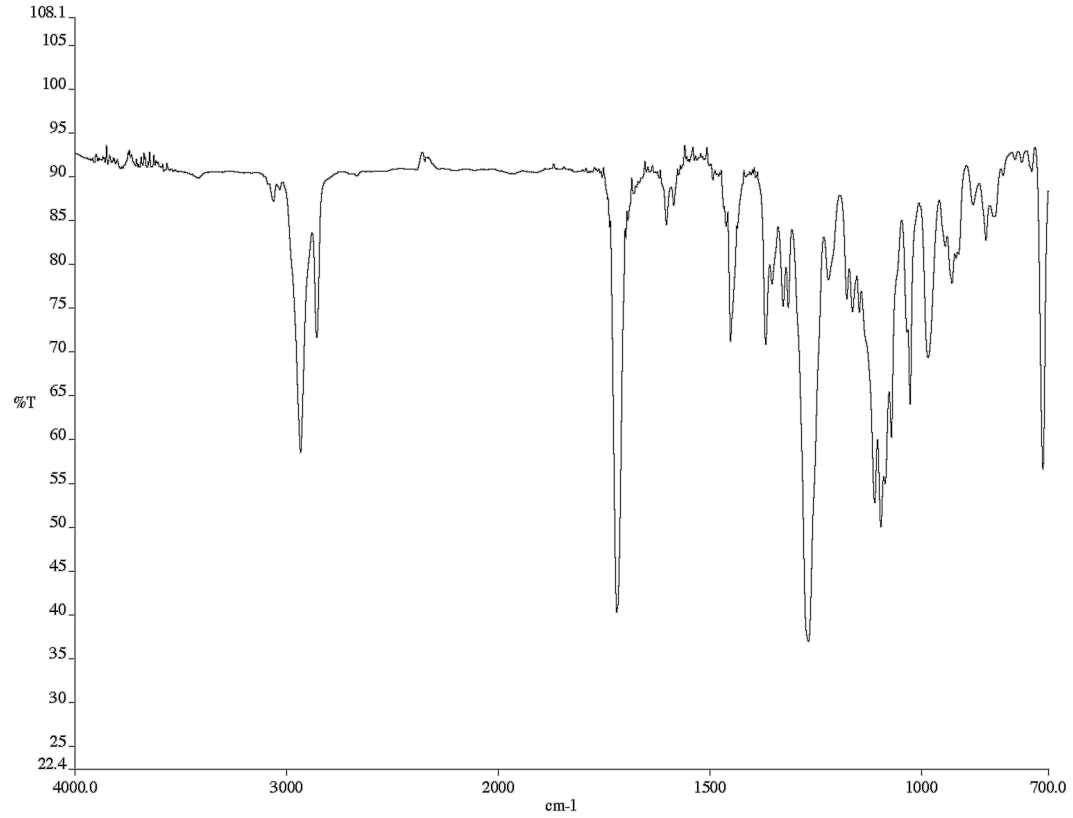

Figure A2.26. Infrared spectrum (Thin Film, NaCl) of compound **275**.

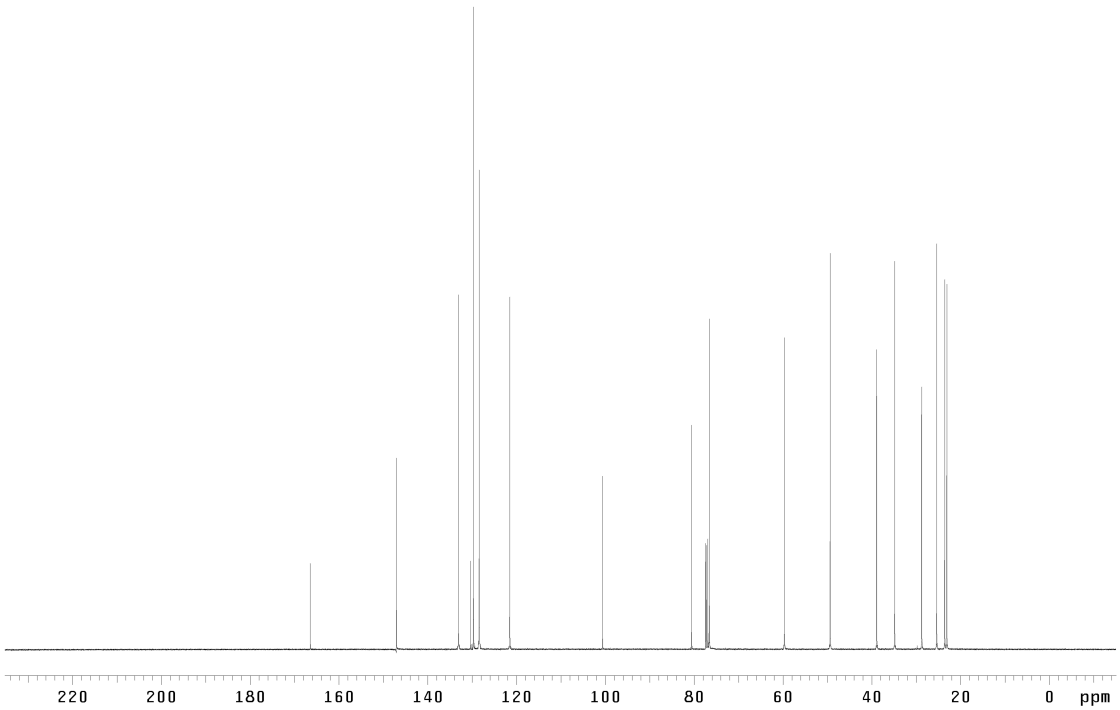

Figure A2.27. ^{13}C NMR (126 MHz, $CDCl_3$) of compound **275**.

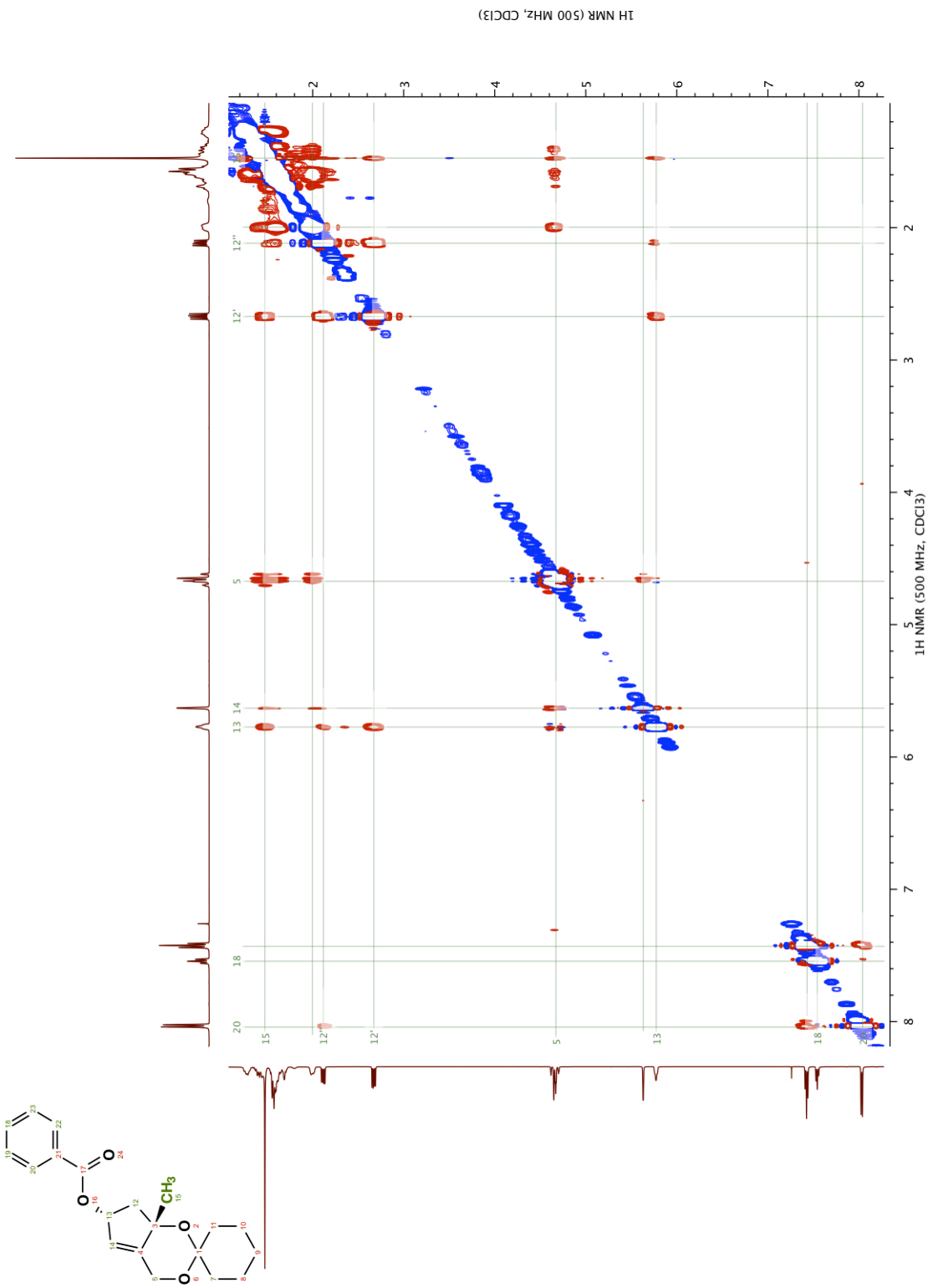

Figure A2.28. 2-D ^{1}H NOESY (500 MHz, $CDCl_3$) of compound **275**.

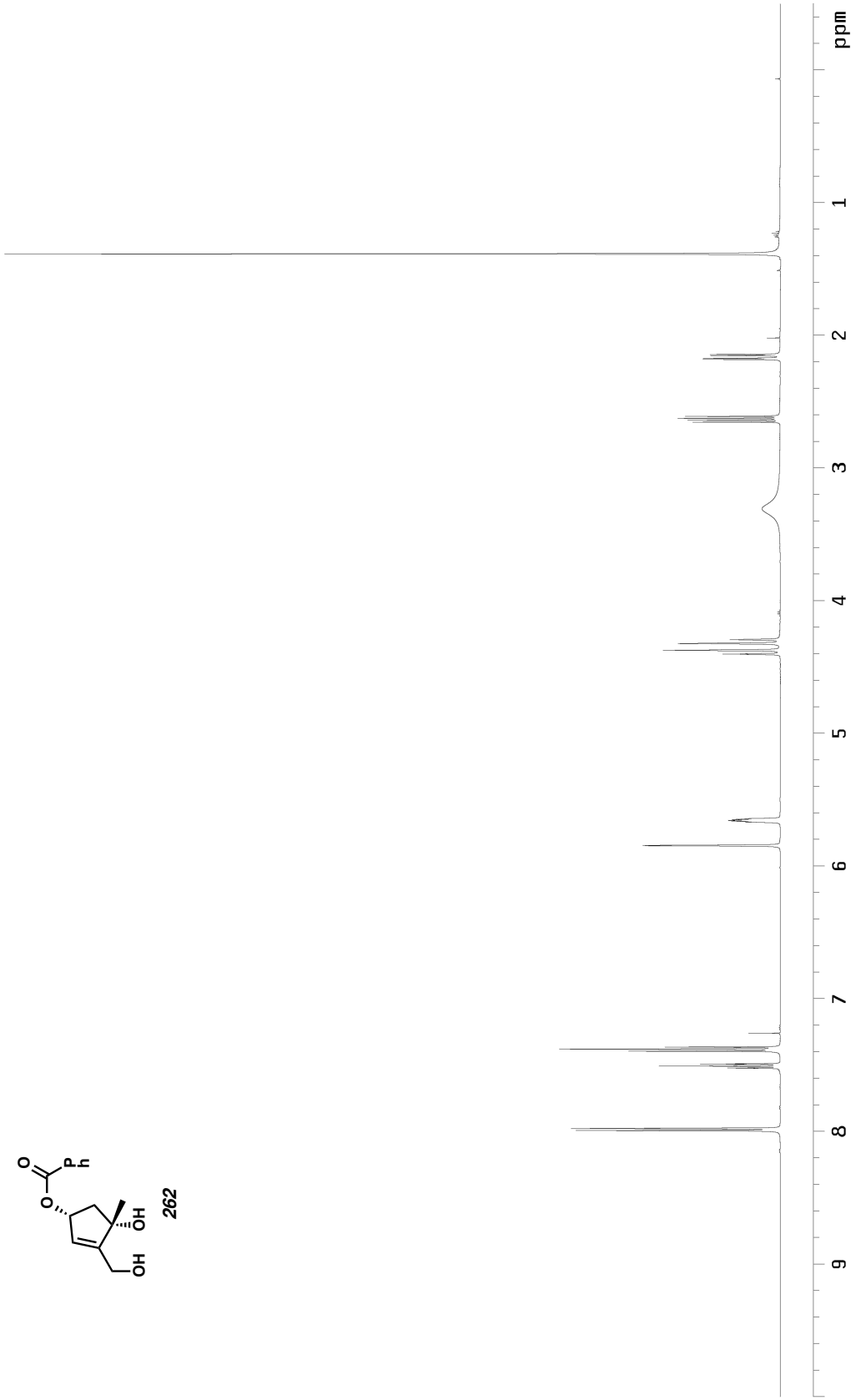

Figure A2.29. ^{1}H NMR (500 MHz, $CDCl_3$) of compound **262**.

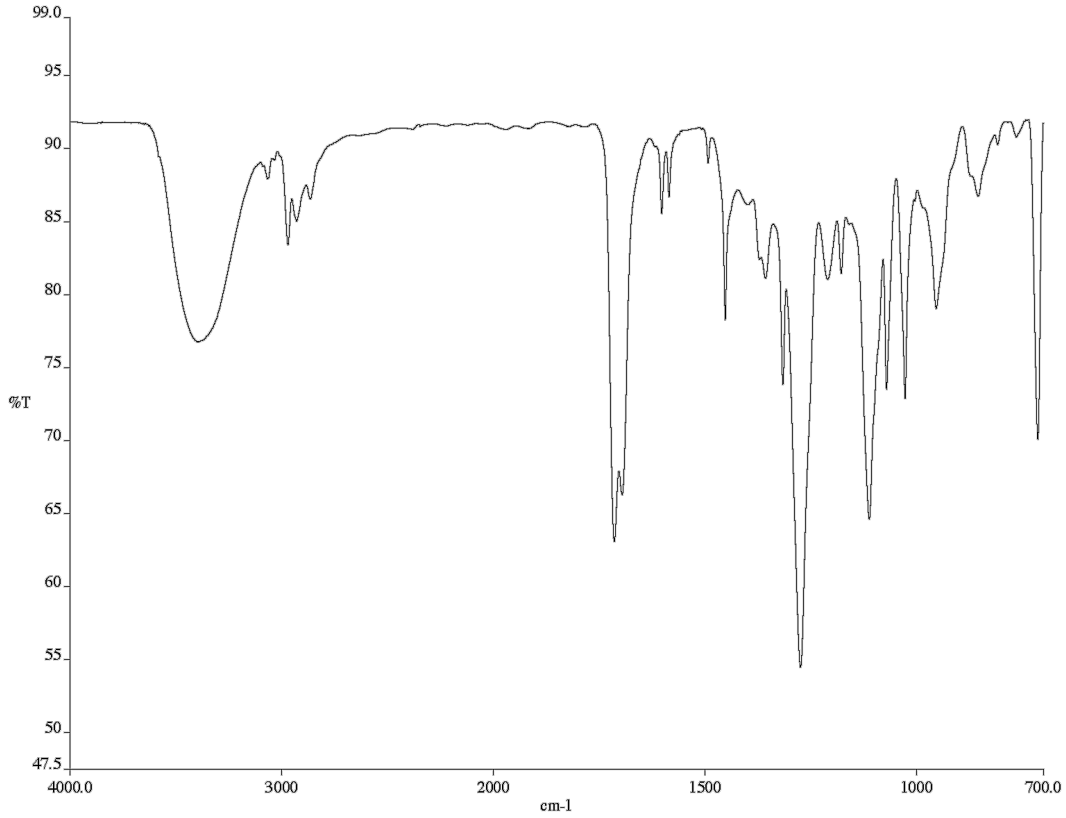

Figure A2.30. Infrared spectrum (Thin Film, NaCl) of compound **262**.

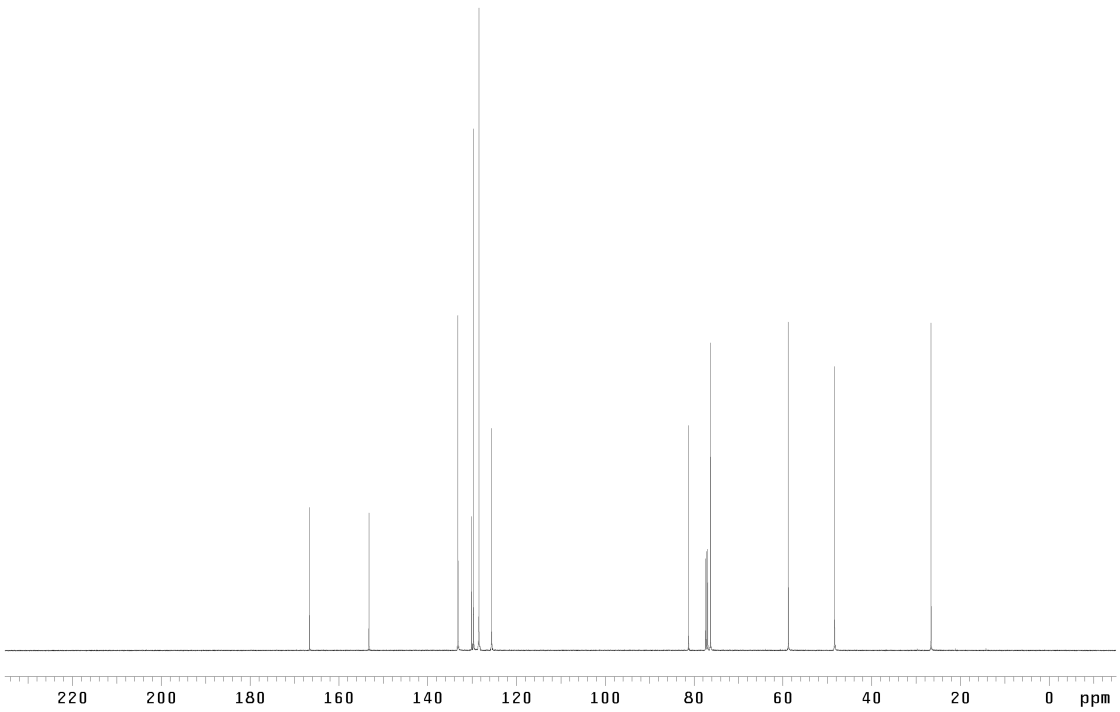

Figure A2.31. ^{13}C NMR (126 MHz, $CDCl_3$) of compound **262**.

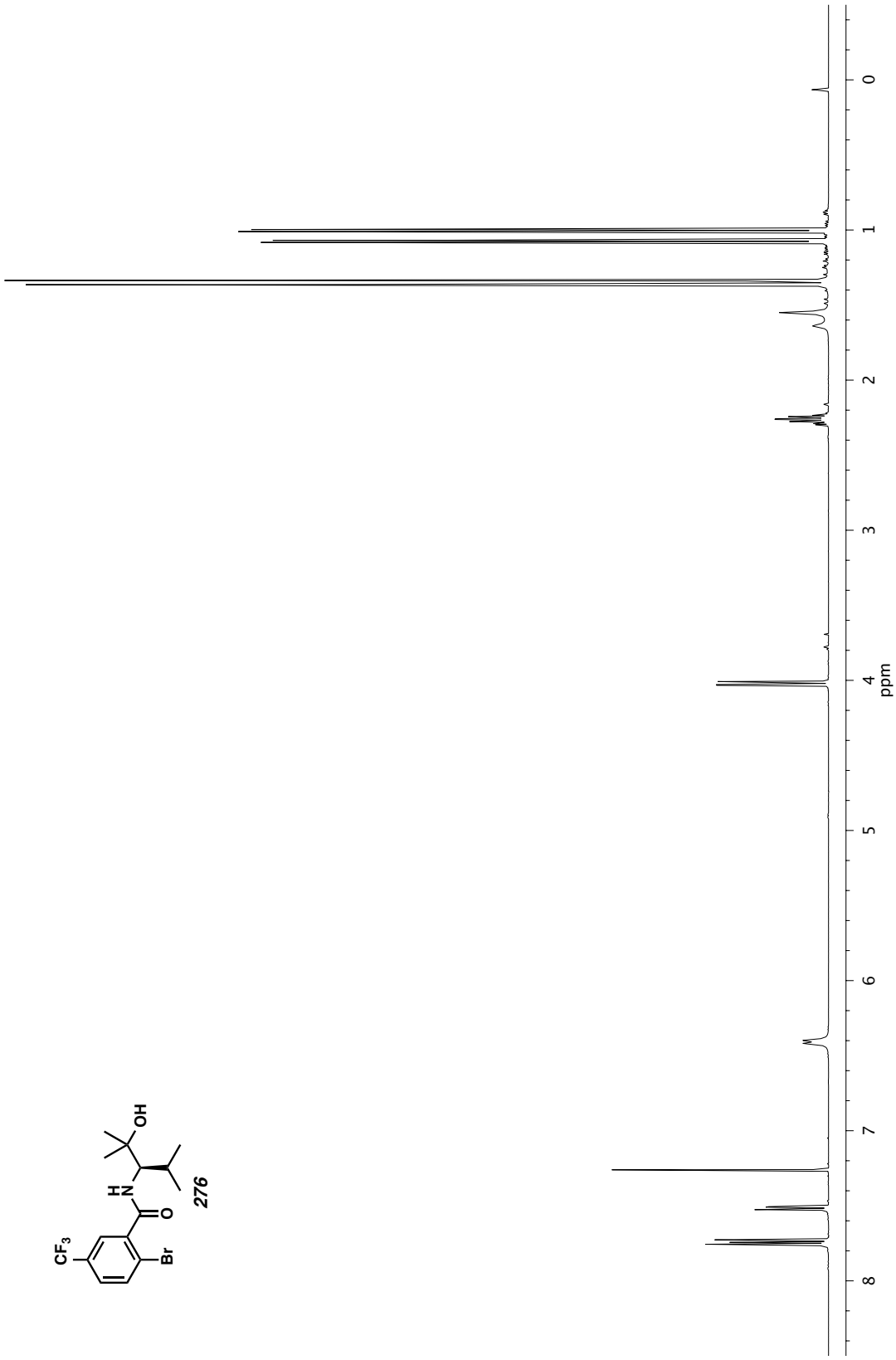

Figure A2.32. ^{1}H NMR (500 MHz, $CDCl_3$) of compound **276**.

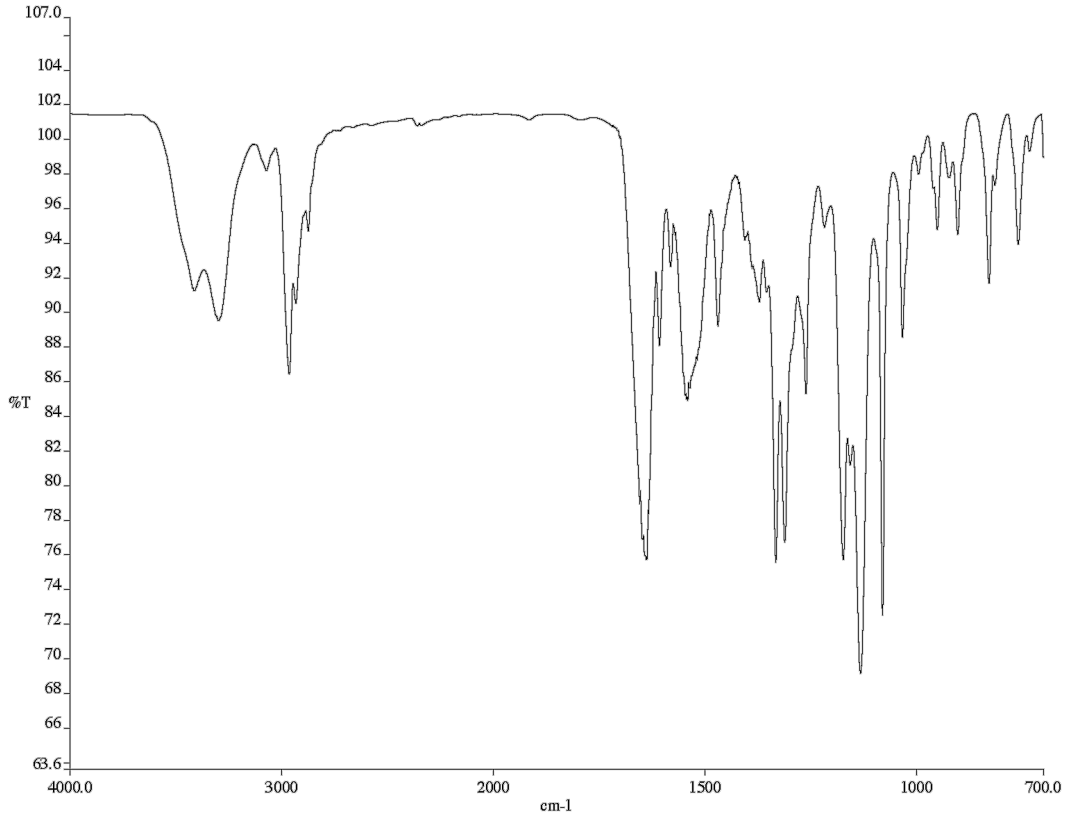

Figure A2.33. Infrared spectrum (Thin Film, NaCl) of compound **276**.

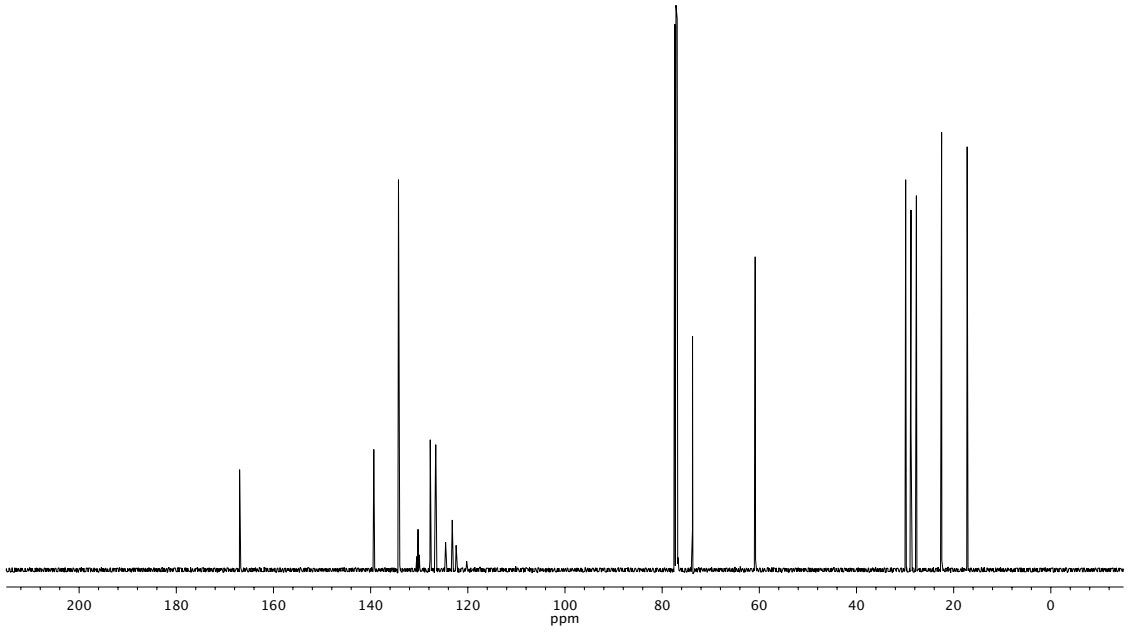

Figure A2.34. ^{13}C NMR (126 MHz, $CDCl_3$) of compound **276**.

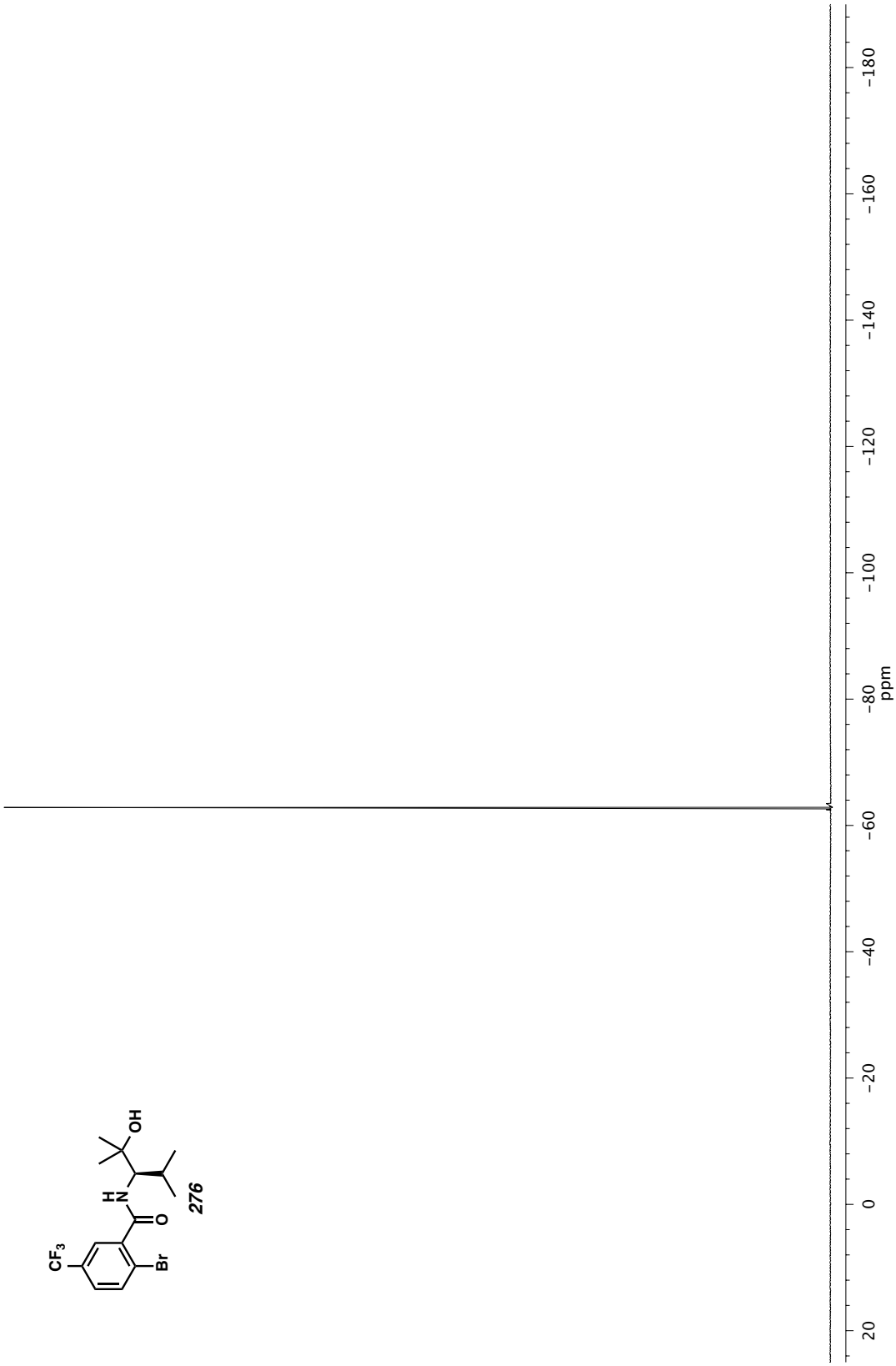

Figure A2.35. ^{19}F NMR (282 MHz, $CDCl_3$) of compound **276**.

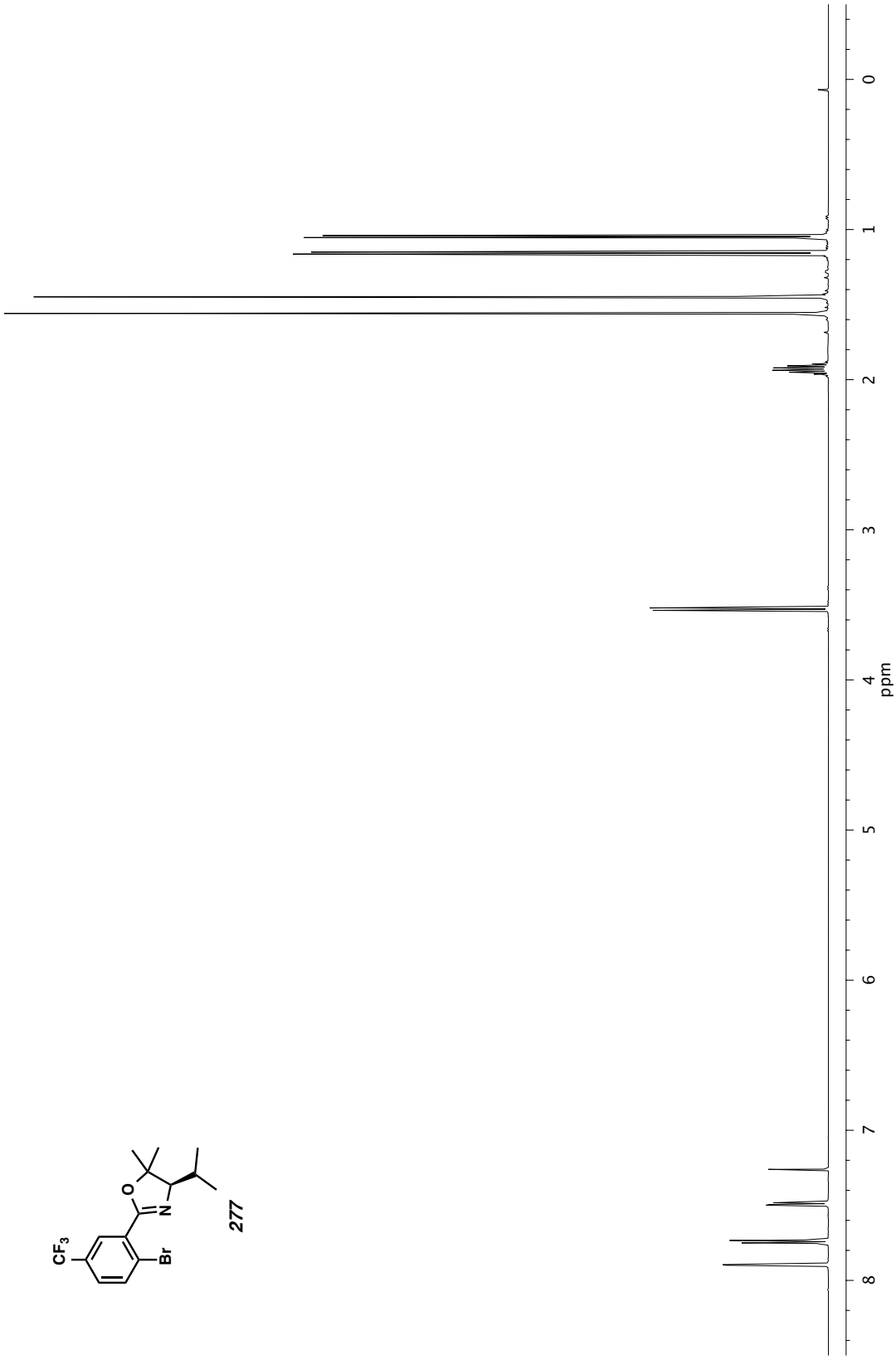

Figure A2.36. ^{1}H NMR (500 MHz, $CDCl_3$) of compound **277**.

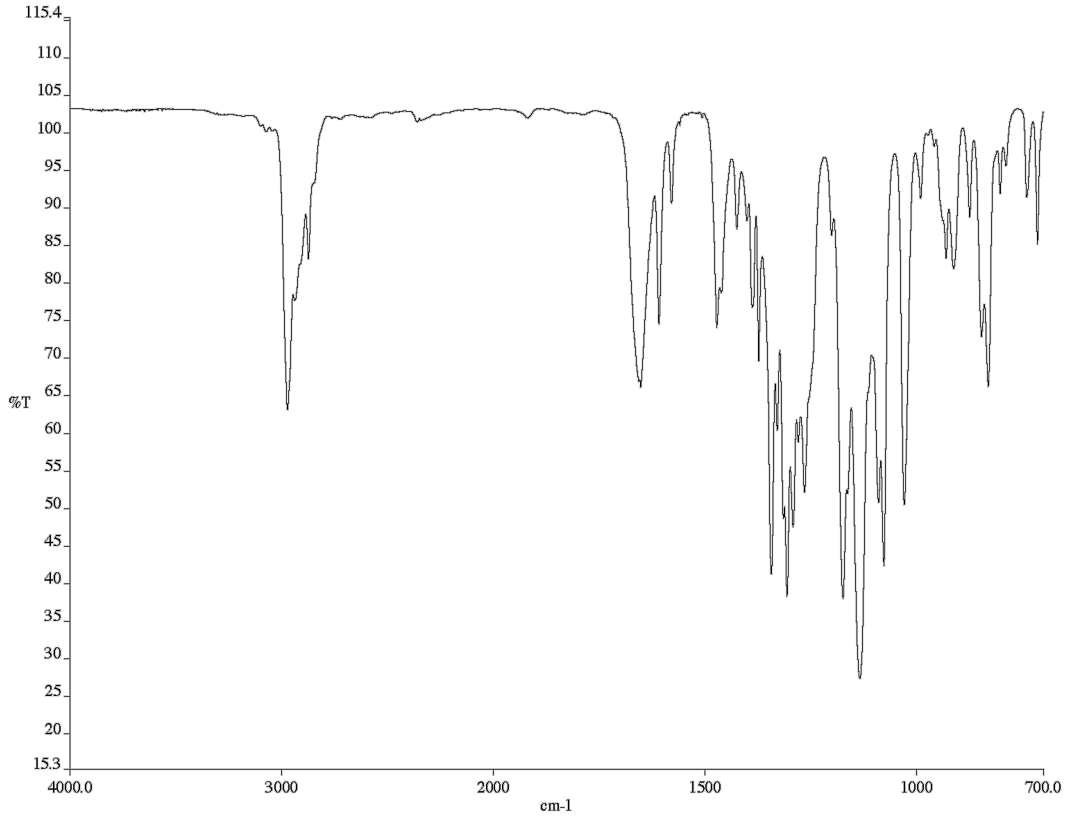

Figure A2.37. Infrared spectrum (Thin Film, NaCl) of compound **277**.

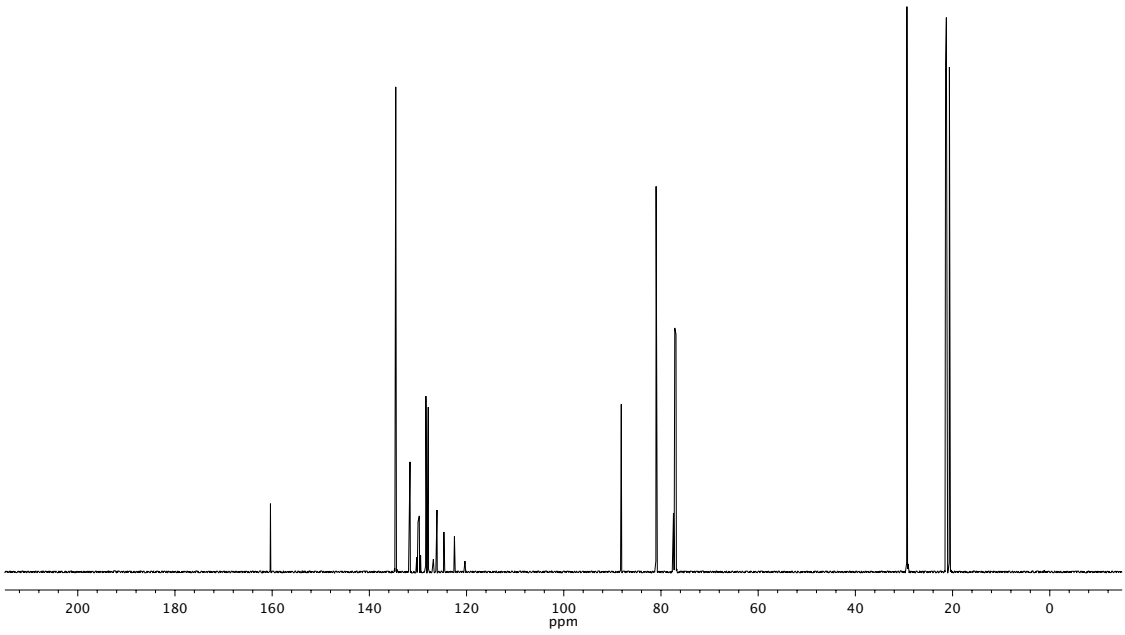

Figure A2.38. ^{13}C NMR (126 MHz, $CDCl_3$) of compound **277**.

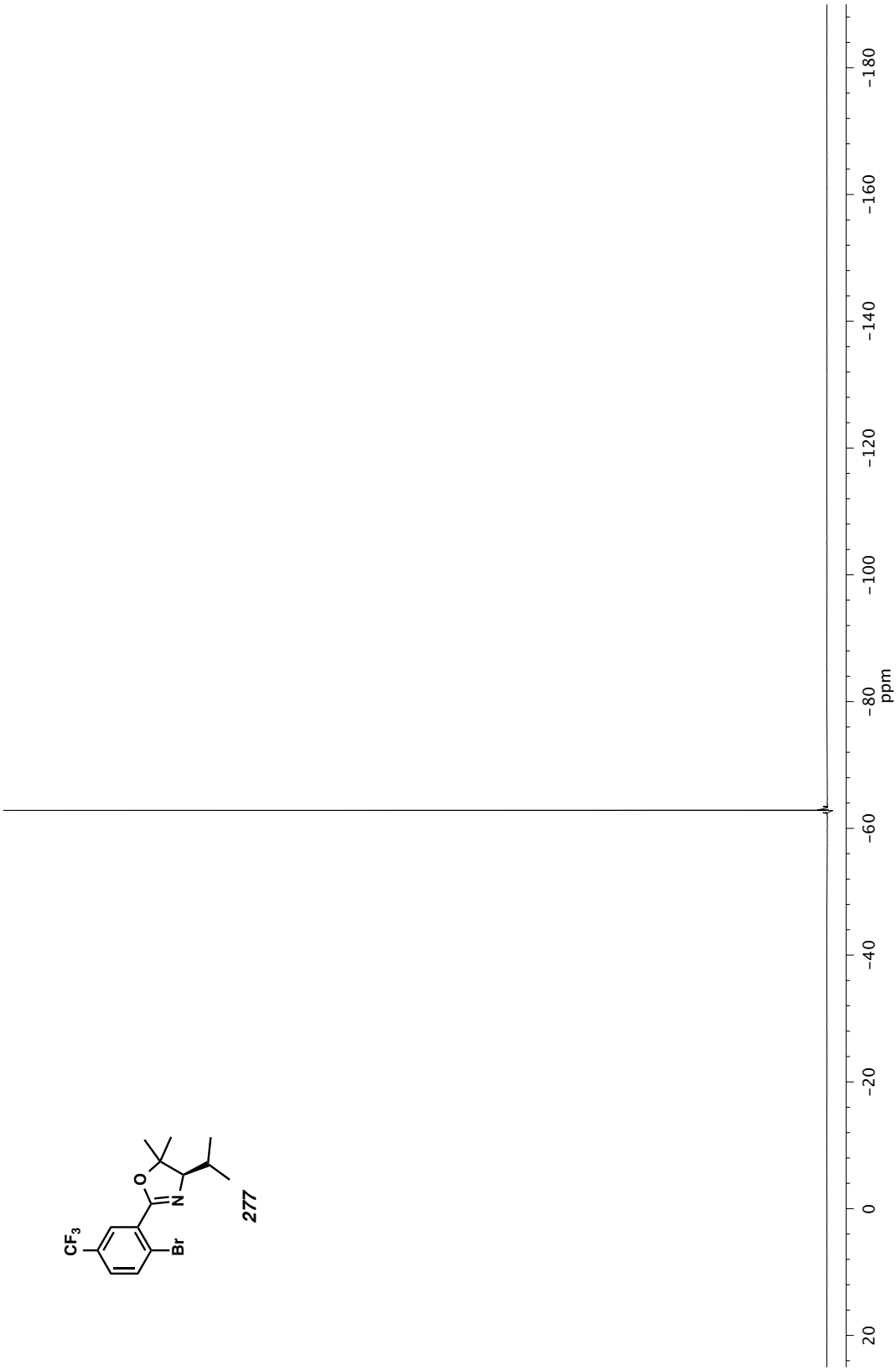

Figure A2.39. ^{19}F NMR (282 MHz, $CDCl_3$) of compound **277**.

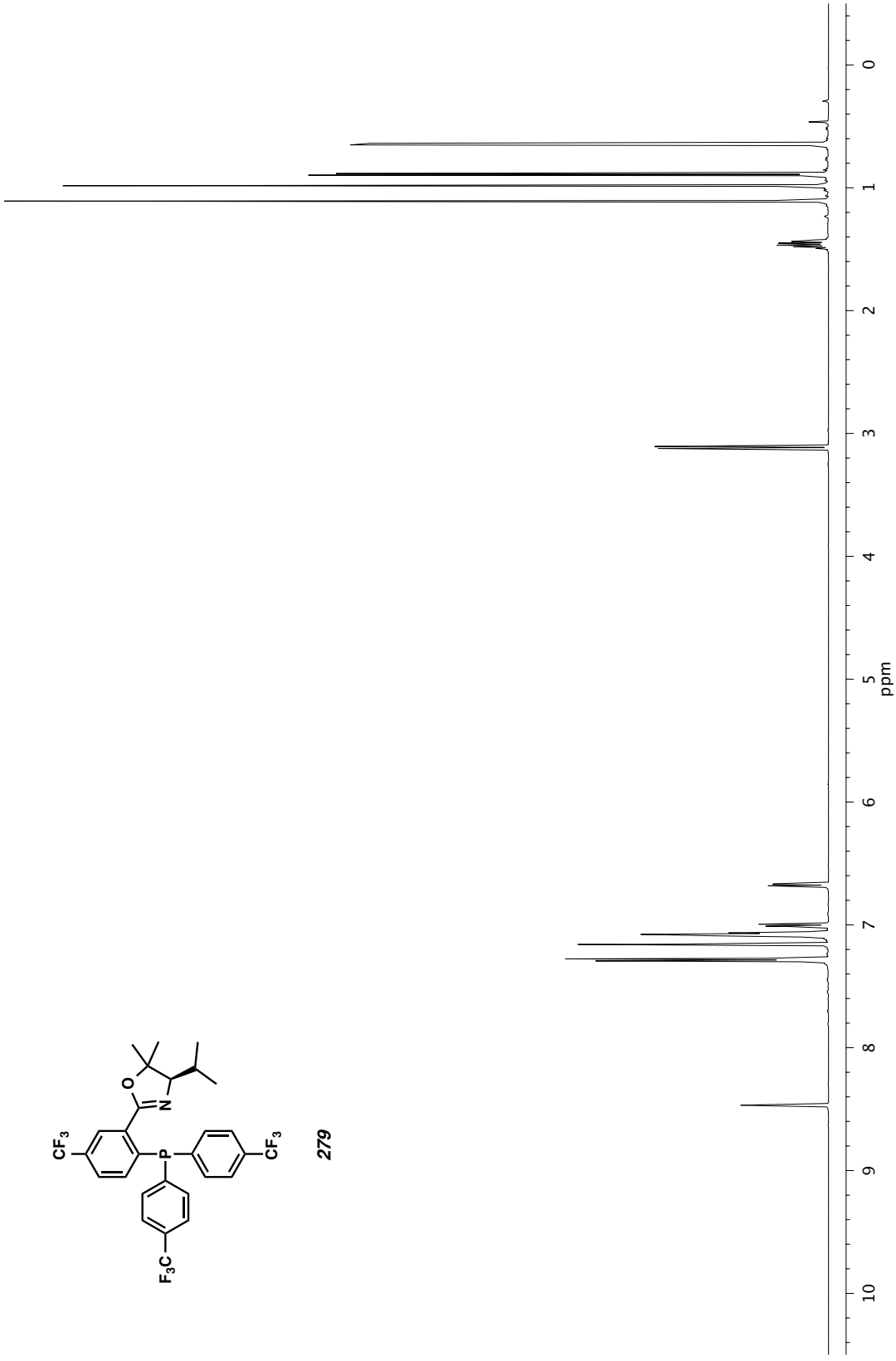

279

Figure A2.40. ^{1}H NMR (500 MHz, C_6D_6) of compound **279**.

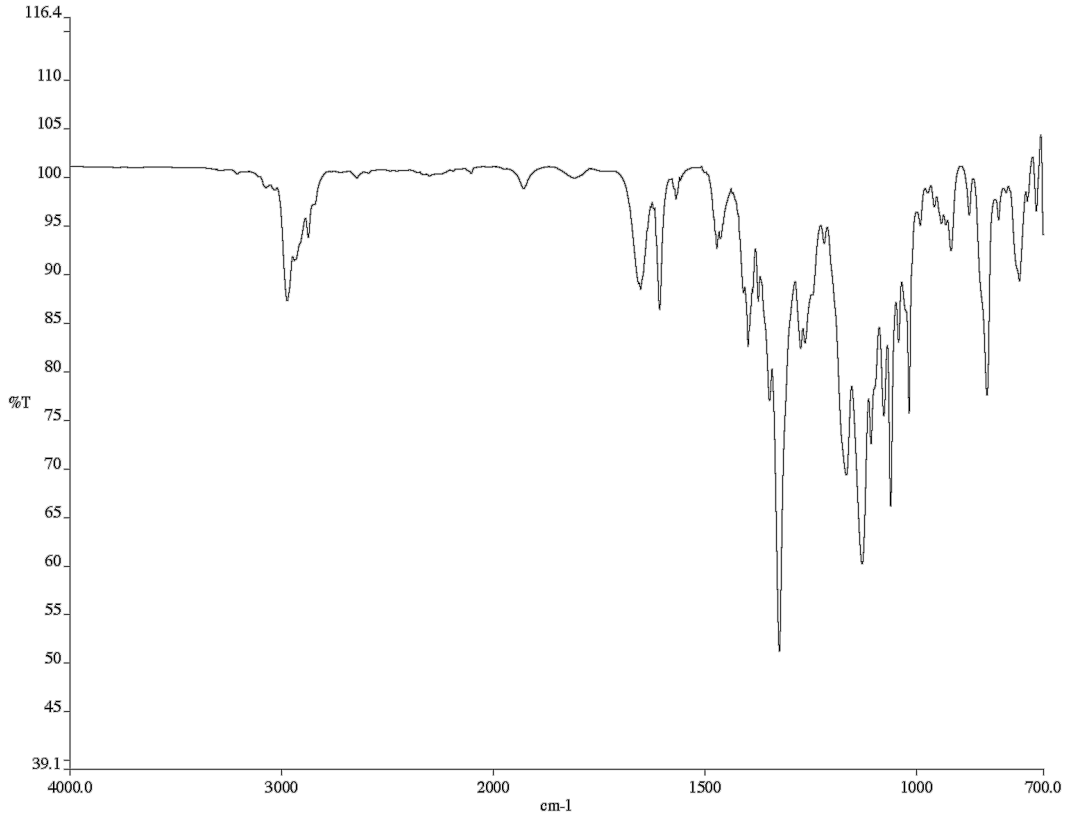

Figure A2.41. Infrared spectrum (Thin Film, NaCl) of compound **279**.

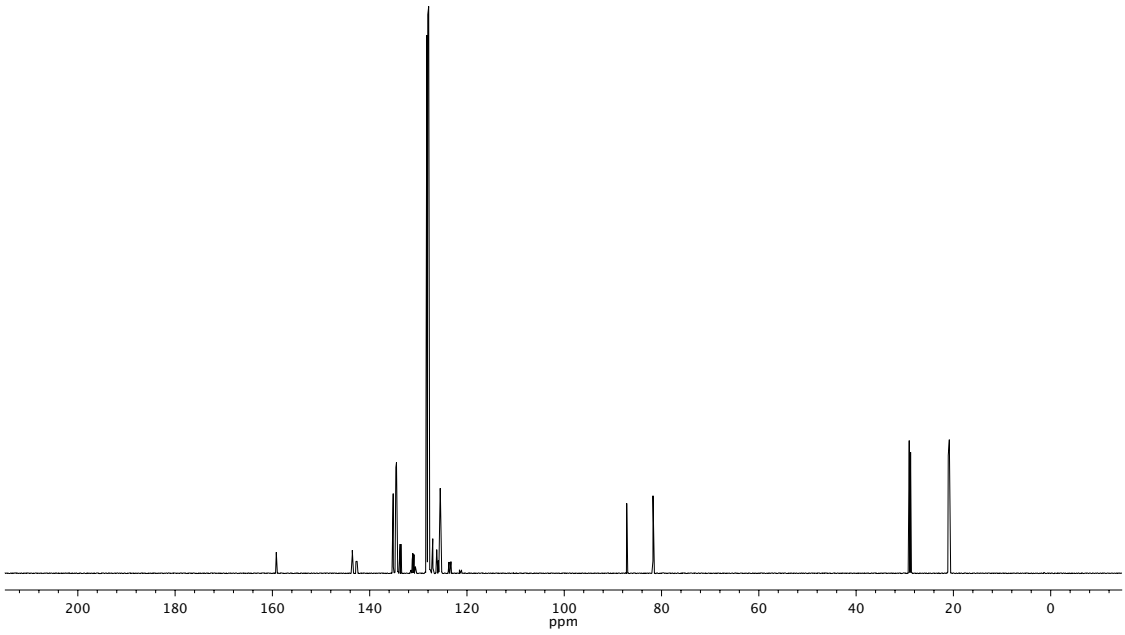

Figure A2.42. ^{13}C NMR (126 MHz, C_6D_6) of compound **279**.

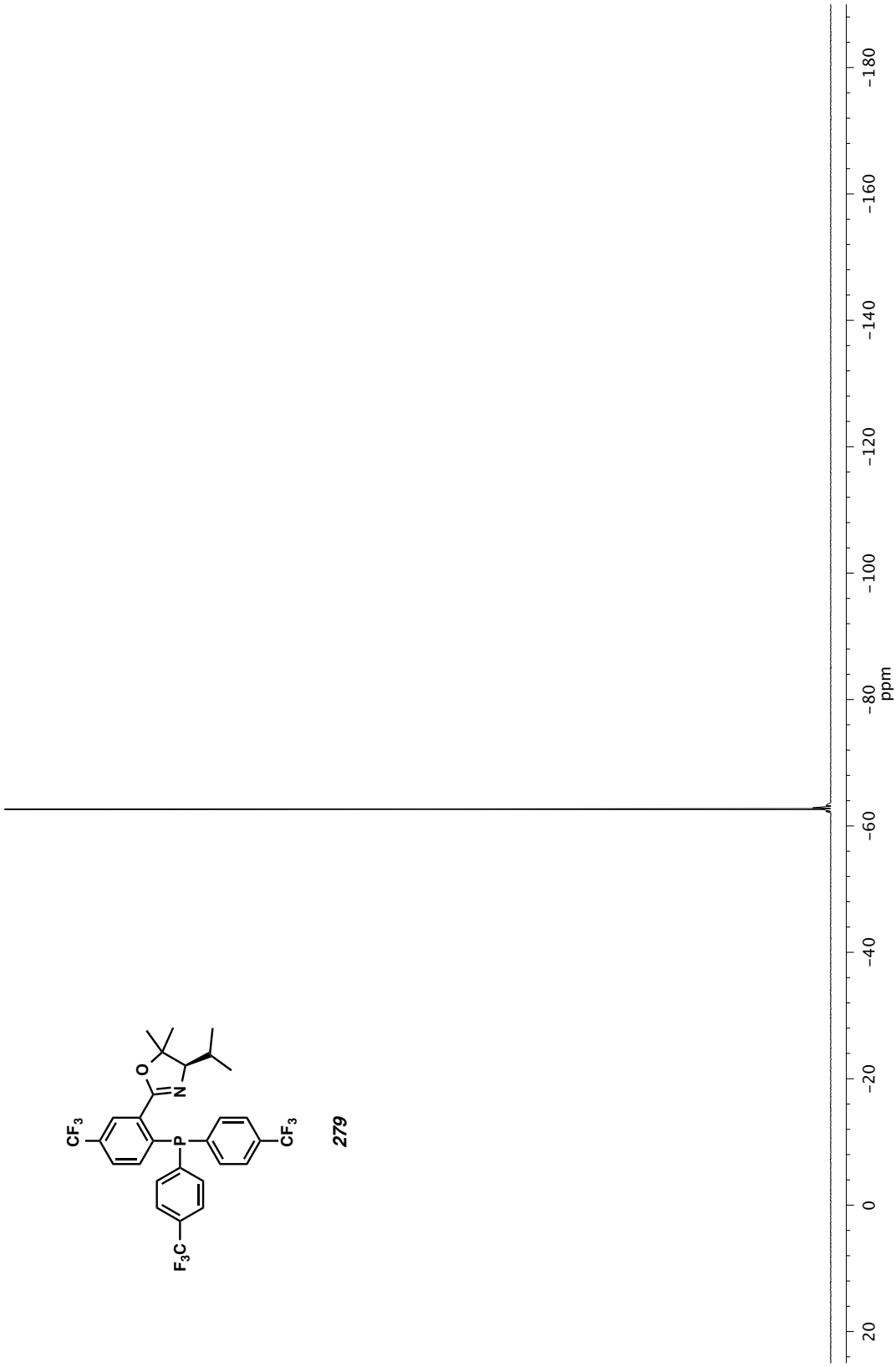

279

Figure A2.43. ^{19}F NMR (282 MHz, C_6D_6) of compound **279**.

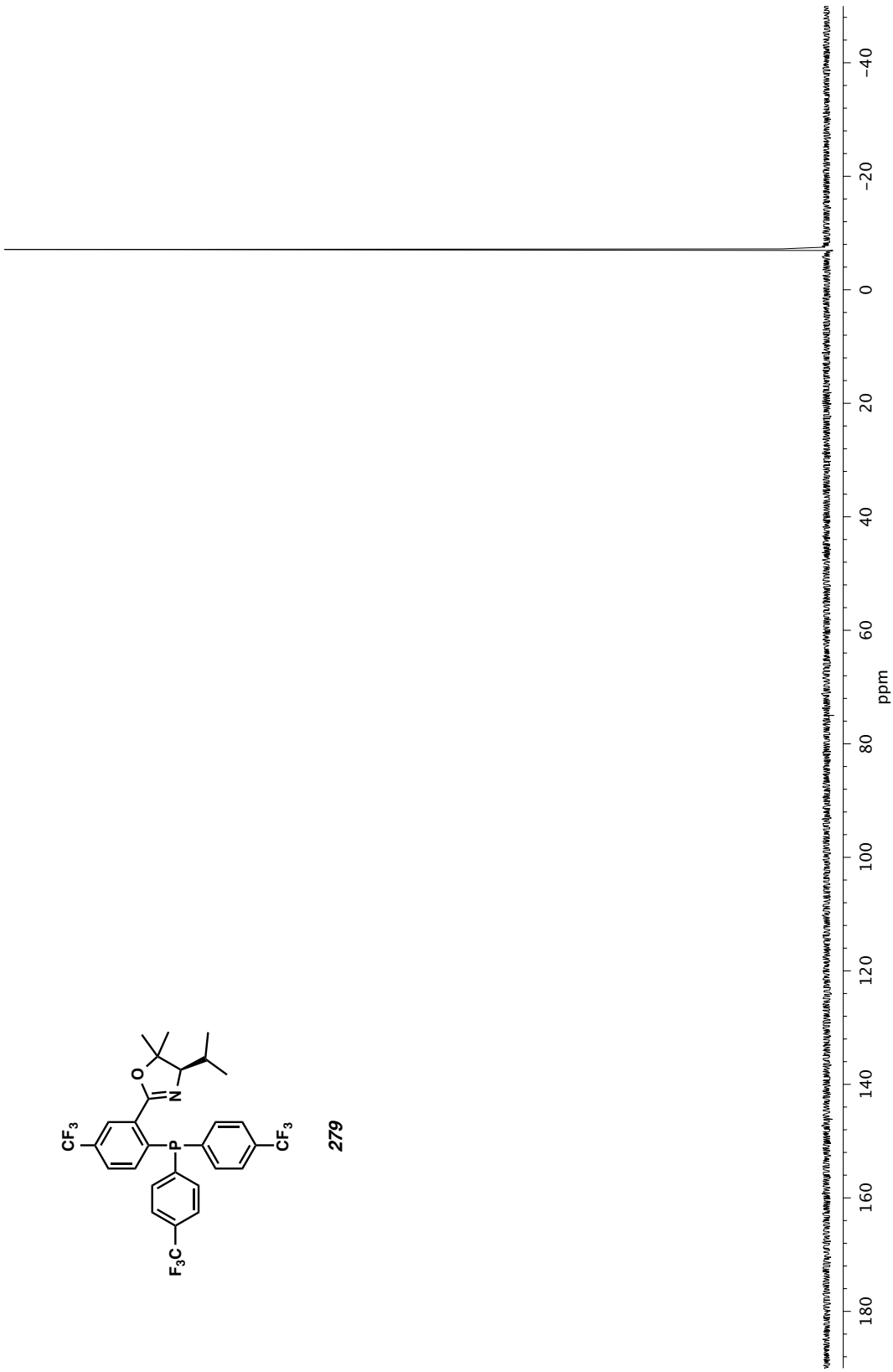

279

Figure A2.44. ^{31}P NMR (121 MHz, C_6D_6) of compound **279**.

APPENDIX 3

Alternative Construction of Hydroxymethyl-cis-1,3-cyclopentenediol Building Block by Ring-Closing Metathesis

A3.1 Alternative Approach to 1,3-*cis*-Cyclopentenediol Building Block

During the development of the ultimately successful and highly efficient route to hydroxymethyl-*cis*-1,3-cyclopentenediol building block **241** through intramolecular Wittig cyclization,[1] we concurrently investigated an alternative procedure (Scheme A3.1.1). Retrosynthetically, we envisioned access to cyclopentenediol **241** through the same key cyclopentenone intermediate **242**. Bicycle **242** would be accessed by the 1,3-allylic transposition of tertiary alcohol **280**. Cyclopentenol **280**, in turn, could be constructed by a ring-closing metathesis from vinyl alcohol **281**. Synthesis of vinyl alcohol **281** was envisioned to be accomplished by the 1,2-addition of a vinyl group into ketone **243**. Although the stereochemistry of the 1,2-vinyl addition is ultimately inconsequential for the synthesis of cyclopentenone **242**, we hypothesized that only *syn*-**281** will only undergo productive ring-closing metathesis to form the *cis*-fused [5,6]-bicycle **280**. Thus, we planned to accomplish the vinyl addition into ketone **243** in a

diastereoselective fashion. Access to allyl dioxanone **243** would be accomplished in an asymmetric fashion through the enantioselective palladium-catalyzed allylic alkylation of enol ether **244**.

*Scheme A3.1.1. Alternative Retrosynthetic Analysis of Hydroxymethyl-*cis*-1,3-cyclopentenediol Building Block **241***

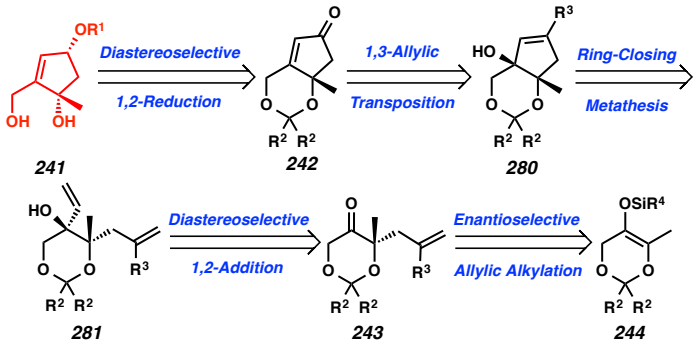

A3.2 Synthesis of Diethyl Ketal Analog

Exploration of the proposed synthetic route to access to hydroxymethyl-*cis*-1,3-cyclopentenediol **241** began with the evaluation of the influence of the identity of the ketal protecting group on the diastereoselective 1,2-addition of a vinyl nucleophile into dioxanone **243** (Scheme A3.2.1). We had previously established synthetic access to acetonide **283**[2] as well as cyclohexyl ketal **284**,[1] but had not explored the synthesis of diethyl ketal variant **285**.

Scheme A3.2.1. Ketal Substrates for Exploration of Diastereoselective Addition

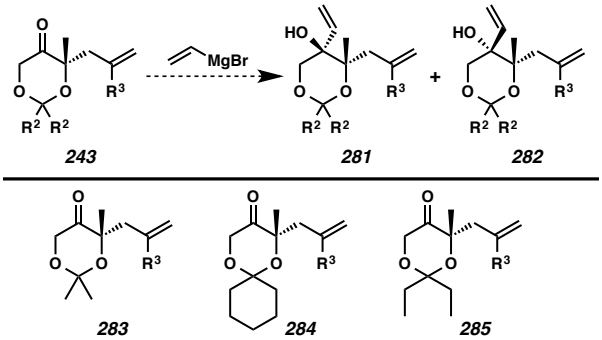

Synthesis of diethyl ketal **285** was accomplished by modification of the procedure employed for the synthesis of cyclohexyl ketal **284**,[1] beginning with the transketalization of 3,3-dimethoxypentane (**286**)[3] with the hydrogen chloride salt of amino alcohol **270** (Scheme A3.2.2). Exposure of the intermediate ammonium salt to excess Et_3N furnished aminoalcohol **287** in 19% yield over two steps. Subsequent oxidative cleavage of amine **287** using $NaIO_4$ provided ketodioxanone **288** in 67% yield. Ketone **288** was then alkylated by a two-step procedure beginning with cyclohexylimine formation followed by deprotonation using LDA to furnish methylated dioxanone **289** in 44% yield. Thermodynamic enolization of ketone **289** afforded enol ether **290** as the allylic alkylation substrate in 53% yield. Ultimately, palladium-catalyzed allylic alkylation of TES enol ether was smoothly accomplished using mesylate **253** as the external electrophile to furnish chloroallylketone **291** in 73% yield.[4]

*Scheme A3.2.2. Synthesis of Diethyl Ketal Allylic Alkylation Product **291***

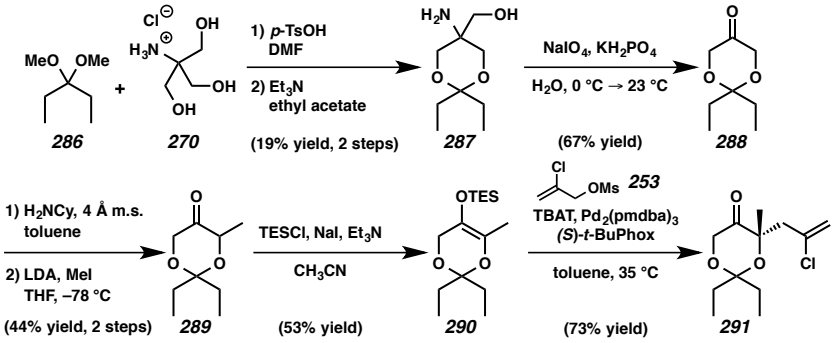

A3.3 Attempted Deprotection of Kinetic Enol Ether Byproducts

The formation of enol ether **290** from diethylketal **289**, as with the acetonide **291** and cyclohexyl ketal **273**, was complicated by the competing formation of the undesired kinetic silyl enol ether **294** (Table A3.3.1). In order to improve the overall yield of thermodynamic enol ether **293**, we attempted to develop conditions for the deprotection

silyl enol ether **295** back to ketone **273** (Table A3.3.2). Unfortunately, even using the more robust cyclohexyl ketal **295**, we were never able to accomplish the removal of the TES group. The majority of reaction conditions screened resulted in cleavage of the ketal group or complete decomposition of the reactant. No trace of ketone **273** was observed.

*Table A3.3.1. Enolization of Ketodioxanone **292***

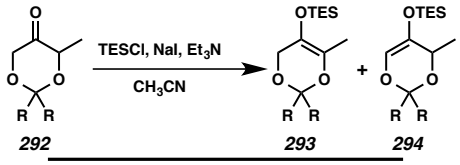

292 ***293*** ***294***

Ketone	*R,R*	*Yield 293 (%) [a]*
291	*Me,Me*	*77*
285	*Et,Et*	*53*
273	*$(CH_2)_5$*	*55*

[a] Isolated Yield.

Table A3.3.2. Attempted Deprotection of Undesired Kinetic Silyl Enol

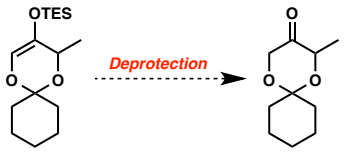

295 ***273***

Entry	*Conditions*	*Result [a]*
1	TBAF, THF	Decomposition
2	TBAF, DMF	Ketal Cleavage
3	HF·pyridine, pyridine, THF	Ketal Cleavage
4	DBU, THF	No reaction
5	$ZnBr_2$, H_2O, CH_2Cl_2	Decomposition

[a] All results assessed by crude ^{1}H NMR.

A3.4 Exploration of Diastereoselective Vinyl Addition

Nevertheless, with the acetonide, diethyl, and cyclohexyl ketal variants of ketone **243** in hand, we explored the diastereoselectivity of nucleophilic vinyl addition (Table A3.4.1). The addition of the vinyl Grignard reagent directly into ketone **243** routinely produced a complex mixture of products. Alternatively, the use of $LaCl_3$•2LiCl as a stoichiometric additive facilitated nucleophilic addition the vinyl nucleophile, furnishing a mixture of *syn*-vinyl alcohol **281** and *anti*-vinyl alcohol **282**.[5] The nucleophilic addition

of the vinyl nucleophile into allyl acetonide **249** furnished a 1.2:1.0 mixture in favor of the undesired diastereomer *anti*-vinyl alcohol **297**.

Table A3.4.1. Effect of Ketal Identity on Diastereoselective Grignard Addition

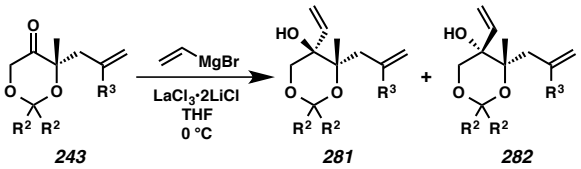

Ketone	R^2,R^2	R^3	syn	anti	syn:anti [a]
249	Me,Me	H	296	297	1.0:1.2
254	Me,Me	Cl	298	299	2.8:1.0
291	Et,Et	Cl	300	301	3.2:1.0
258	$(CH_2)_5$	Cl	302	303	2.9:1.0

Fortunately, switching from allylketone **249** to chloroallylketone **254** furnished *syn*-vinyl alcohol **298** as the major product in a 2.8:1.0 ratio with *anti*-vinyl alcohol **299**. Switching the identity the ketal to the diethyl ketal slightly improved the product ratio, while the cyclohexyl ketal variant provided an intermediate product ratio. Ultimately, we decided to explore the advancement of chloroallylalcohol **302**, because of the improved stability of the cyclohexyl ketal, along with allylalcohol **296**.

A3.5 Ring-Closing Metathesis

We were pleased to find the ruthenium-catalyzed ring-closing metathesis of *syn*-allylalcohol **296** proceeded smoothly to furnish bicyclic cyclopentene **305** in 95% yield (Scheme A3.5.1.A). Similarly, the cyclization of *syn*-chloroallylketone **298** could be accomplished under the same reaction conditions to provide vinyl chloride **306** in 89% yield (Scheme A3.5.1.B). As we hypothesized, the exposure of *anti*-chloroallylketone **299** provided no *trans*-fused product **307** even after prolonged exposure to the ruthenium-catalyzed conditions that were highly effective for the cyclization of its diastereomer (i.e., **298**, Scheme A3.5.1.C).[6]

Scheme A3.5.1. Ring-Closing Metathesis of Allyl Dioxanones

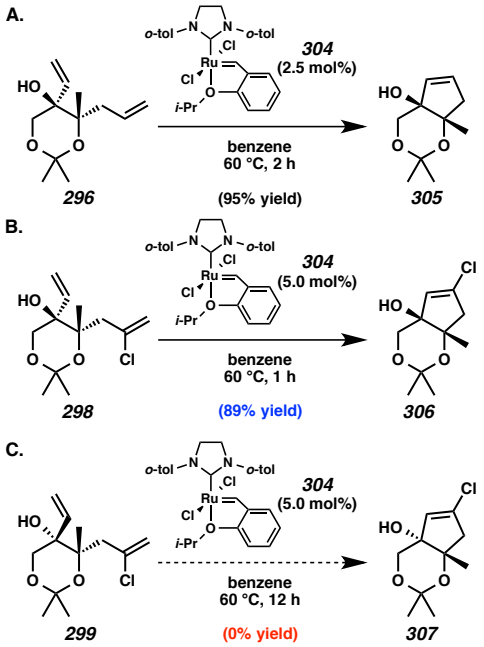

A3.6 1,3-Allylic Transposition of Bicyclic Cyclopentenes

With cyclopentenes **305** and **306** in hand, we began exploring the potential to accomplish a 1,3-allylic transposition and convert the allylic alcohols into the corresponding cyclopentenones. We began by exploring the potential to rearrange cyclopentene **305** to either allylic alcohol **308** under redox neutral conditions or cyclopentenone **309** employing oxidative 1,3-allylic transposition reaction manifolds (Scheme A3.6.1). Unfortunately, no trace of any allylic transposition product was observed employing SO_3•pyridine,[7] IBX,[8] or PCC.[9] In fact, we most typically observed decomposition of the substrate, most likely due to the labile nature of the acetonide protecting group.[6] One of the few isolable products we encountered was simply the result of an intramolecular transketalization in the presence of PCC to provide spirocyclic acetonide **311** (Scheme A3.6.2).[10] Without any success, we turned our attention to the vinyl chloride substrates.

*Scheme A3.6.1. Attempted 1,3-Allylic Transposition of Bicyclic Acetonide **305***

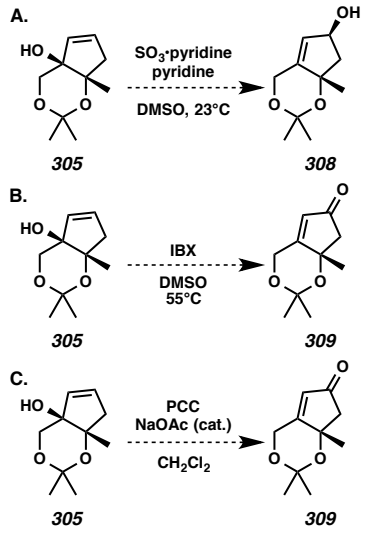

*Scheme A3.6.2. Isomerization of Acetonide **306***

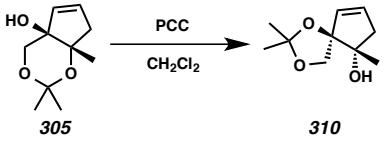

Having installed an oxidized allyl fragment earlier in the synthetic route with a chloroallyl electrophile to provide vinyl chloride **311**, we needed only to accomplish a 1,3-allylic transposition under redox neutral conditions to directly furnish bicyclic cyclopentenone **242** (Table A3.6.1). Under rhenium catalysis, the substrate protected with an acetonide ketal decomposed (Entries 1 and 2) and the cyclohexyl ketal variant failed to react (Entry 3).[11] Comparatively, the use of PCC (Entry 4)[9] and SO_3•pyridine (Entry 5)[7] failed to induce any reactivity at all, resulting in the quantitative recovery of starting material. Fortunately, we found that exposure of vinyl chloride **311** (R,R = $(CH_2)_5$, Entry 6) to SO_3•pyridine followed by a phosphate buffer produced traces of cyclopentenone.[12] Although we were encouraged by this result, we quickly discovered that scaling up the transformation failed to produce any isolable quantities of cyclopentenone **242**.

*Table A3.6.1. 1,3-Allylic Transposition of Vinyl Chloride **311***

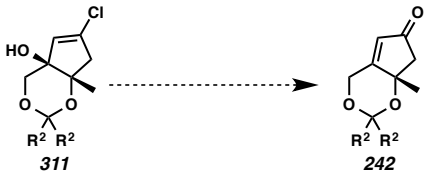

311 ***242***

Entry	*R,R*	*Reaction Conditions*	*Outcome*
1	*Me,Me*	ReO_3Me, Ph_3SiOH Et_2O, 0 °C	Decomposition
2	*Me,Me*	$ReO_3(OSiPh_3)$, Et_2O, 23 °C	Decomposition
3	*$(CH_2)_5$*	$ReO_3(OSiPh_3)$, Et_2O, 23 °C	No Reaction [a]
4	*$(CH_2)_5$*	PCC, Et_3N CH_2Cl_2, 50 °C	No Reaction [a]
5	*$(CH_2)_5$*	SO_3·pyridine, pyridine DMSO, 23 °C	No Reaction [a]
6	*$(CH_2)_5$*	SO_3·pyridine, pyridine DMSO, 23 °C then phosphate buffer, 60 °C	Trace ***242*** [b]

[a] Quantitative recovery of starting material. [b] Trace of enone **242** by LCMS, however no isolated product was obtained. Instead, mostly decomposition of vinyl chloride **312** was observed.

Despite our best attempts, we were unable to access the required cyclopentenone fragment **242** for further advancement toward the hydroxymethyl-*cis*-1,3-cyclopentenediol building block **241**. We did establish the substitution at the 2-position of the allyl fragment of allylic alkylation product **243** has a profound impact on the diastereoselective addition of a vinyl group in a 1,2-fashion into the carbonyl moiety. Additionally, we showed that only the *syn*-vinyl products undergo a ring-closing metathesis to build bicyclic cyclopentenes. Although these intermediates were not immediately useful for the purposes of our synthesis of *cis*-1,3-cyclopentadiol-containing natural products, these easily accessible, enantioenriched, highly oxygenated cyclopentene frameworks represent a new class of easily derivatizable synthetic building block.

A3.7 Experimental Methods and Analytical Data

A3.7.1 Materials and Methods

Unless stated otherwise, reactions were performed at ambient temperature (23 °C) in flame-dried glassware under an argon atmosphere using dry, deoxygentated solvents (distilled or passed over a column of activated alumina)[13] using a Teflon®-coated magnetic stirring bar. Commercially available reagents were used as received unless otherwise noted. Et_3N was distilled from calcium hydride immediately prior to use. Purified H_2O was obtained using a Barnstead NANOpure Infinity UV/UF system. 4 Å molecular sieves were oven-dried at 120 °C for a minimum of 24 h and cooled in a desiccator to ambient temperature immediately prior to use. (*S*)-*t*-BuPhox (**263**),[14] tris-(4,4'-methoxydibenzylideneacetone)-dipalladium(0) ($Pd_2(pmdba)_3$),[15] and LaCl3•2LiCl[5] were prepared by known methods. Reactions requiring external heat were modulated to the specified temperatures using an IKAmag temperature controller. Thin-layer chromatography (TLC) was performed using E. Merck silica gel 60 F254 precoated plates (250 nm) and visualized by UV fluorescence quenching, potassium permanganate, or *p*-anisaldehyde staining. Silicycle SiliaFlash P60 Academic Silica gel (particle size 40-63 nm) was used for flash chromatography. ^1H and ^{13}C NMR spectra were recorded on a Varian Mercury 300 spectrometer (300 MHz and 76 MHz, respectively) and are reported in terms of chemical shift relative to residual $CHCl_3$ (in $CDCl_3$, δ 7.26 and δ 77.16, respectively). Data for ^1H NMR spectra are reported as follows: chemical shift (δ ppm) (multiplicity, coupling constant (Hz), integration). Infrared (IR) spectra were recorded on a Perkin Elmer Paragon 1000 Spectrometer and are reported in frequency of absorption (cm^{-1}). High resolution mass spectra (HRMS) were acquired using an Agilent

6200 Series TOF with an Agilent G1978A Multimode source in atmospheric pressure chemical ionization (APCI) or mixed (MultiMode ESI/APCI) ionization mode or obtained from the Caltech Mass Spectral Facility using a JEOL JMS-600H High Resolution Mass Spectrometer in fast atom bombardment (FAB+) or electron ionization (EI+) mode. Optical rotations were measured on a Jasco P-2000 polarimeter using a 100 mm path length cell at 589 nm.

A3.7.2 Experimental Procedures

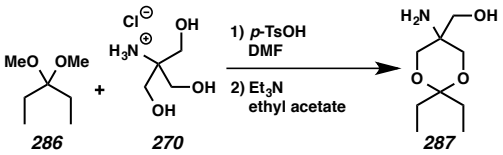

Aminoalcohol 287: To a suspension of Trizma•HCl (**270**, 11.8 g, 74.8 mmol, 1.00 equiv) in DMF (83 mL) were added 3-pentanone dimethyl ketal (**286**, 10.9 g, 82.3 mmol, 1.15 equiv) and *p*-toluenesulfonic acid monohydrate (*p*-TsOH, 427 mg, 2.24 mmol, 0.03 equiv) in one portion with stirring. After 17 h, a distillation apparatus was attached directly to the reaction flask and the volatiles were distilled off (75 °C/6 torr). The semisolid residue was triturated with Et_2O (700 mL) until white solid precipitated. The resulting heterogeneous solution was filtered, washed with EtOAc (4 x 75 mL), and dried under high vacuum (0.50 torr) to afford a white solid.

To the crude white solid as a suspension in EtOAc (300 mL) was added Et_3N (11.0 mL, 74.8 mmol, 1.00 equiv) dropwise with stirring. After 11 h, the reaction mixture was filtered and the solids washed with EtOAc (4 x 20 mL). The combined organic filtrate was concentrated in vacuo to give aminoalcohol **287** (2.72 g, 19% yield from **270**) as a white solid: R_f = 0.16 (4:1 CH_2Cl_2:MeOH eluent); ^{1}H NMR (300 MHz, $CDCl_3$) δ 3.82–

3.72 (m, 2H), 3.55–3.49 (m, 2H), 3.48 (s, 2H), 2.03 (s, 3H), 1.73 (app qd, J = 7.5, 2.7 Hz, 4H), 0.90 (app dt, J = 14.2, 7.5 Hz, 6H).

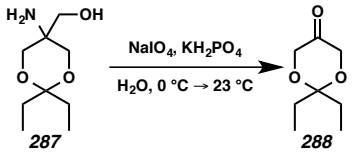

Dioxanone 288: Aminoalcohol **287** (2.72 g, 14.4 mmol, 1.00 equiv) was dissolved in a solution of KH_2PO_4 (3.91 g, 28.8 mmol, 2.00 equiv) in H_2O (48 mL) and cooled to 0 °C (ice/H_2O bath). To the resultant stirred homogenous solution was added a solution of $NaIO_4$ (3.07 g, 14.4 mmol, 1.00 equiv) in H_2O (48 mL) dropwise over 2 h through a 250 mL additional funnel. The reaction was then allowed to stir at temperature for 40 minutes before being allowed to warm to ambient temperature (ca. 23 °C). The starting material was consumed after an additional 16 h as determined by TLC (1:4 MeOH:CH_2Cl_2 eluent). $Na_2S_2O_3$•$5H_2O$ (3.57 g, 14.4 mmol, 1.00 equiv) was then immediately added in one portion. The solution was allowed to stir for 40 minutes at which time the reaction mixture was extracted with CH_2Cl_2 (11 x 75 mL). Combined organic layers were dried over Na_2SO_4, filtered, and concentrated in vacuo (26 °C/100 torr) to afford dioxanone **288** (1.53 g, 67% yield) as a pale yellow oil. This compound was carried on to the next step without further purification: R_f = 0.80 (1:4 MeOH:CH_2Cl_2 eluent); ^{1}H NMR (300 MHz, $CDCl_3$) δ 4.16 (s, 4H), 1.73 (q, J = 7.5 Hz, 4H), 0.92 (t, J = 7.5 Hz, 6H).

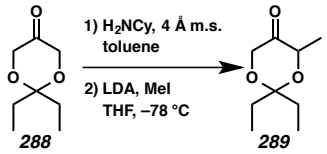

Methyldioxanone 289: To a solution of dioxanone **288** (1.15 g, 7.29 mmol, 1.00 equiv) in toluene (24 mL) were added 4 Å molecular sieves (1.14 g, 1.00 equiv by mass) and cyclohexylamine (1.62 mL, 14.1 mmol, 1.94 equiv). After 13 h, the reaction mixture was filtered through celite, rinsing with toluene, and concentrated in vacuo to give the crude cyclohexylimine.

In a separate three-neck flask with an internal temperature probe, a solution of freshly prepared lithium diisopropylamine (LDA, 0.60 M in THF, 1.00 equiv) was cooled to –78 °C (dry ice/*i*-PrOH bath). To the solution of LDA was added crude cyclohexylimine as a solution in THF (7.3 mL) dropwise through a cannula with an overpressure of argon. After 5 minutes, the reaction flask was the cooled to 0 °C (ice/H_2O bath) and after 1.75 h was cooled back to –78 °C. To the reaction mixture was then added methyl iodide (0.45 mL, 7.30 mmol, 1.00 equiv) at a rate of 2.00 mL/h with a syringe pump, ensuring the internal temperature did not exceed –70 °C. Upon completion of addition, the reaction was allowed to stir for 30 minutes before being allowed to slowly warm to ambient temperature. Upon reaching ambient temperature, the reaction was quenched with saturated NH_4Cl (100 mL) and stirred for 14 h. The reaction mixture was then extracted with Et_2O (4 x 50 mL). The combined organic layers were then washed with H_2O (25 mL), brine (25 mL), dried over Na_2SO_4, filtered, and concentrated in vacuo to afford an orange-tan oil. Purification of this residue by flash chromatography (10% Et_2O in hexanes eluent) furnished methyldioxanone **289** (547 mg, 44% yield) as a clear, colorless oil: R_f = 0.28 (9:1 hexanes:Et_2O eluent); ^{1}H NMR (300 MHz, $CDCl_3$) δ

4.41–4.33 (m, 1H), 4.27 (dd, *J* = 17.3, 1.4 Hz, 1H), 4.01 (d, *J* = 17.3 Hz, 1H), 1.82–1.62 (m, 4H), 1.30 (d, *J* = 6.7 Hz, 3H), 1.00–0.85 (m, 6H).

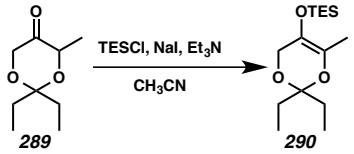

Silyl Enol Ether 290: A 50 mL round bottom was soaked in a 20:1 *i*-PrOH:toluene bath saturated with KOH for 12 h, rinsed with deionized H_2O, acetone, and allowed to dry. To a solution of methyldioxanone **289** (547 mg, 3.18 mmol, 1.00 equiv) in CH_3CN (5.3 mL) in a flame-dried 50 mL base-bathed round bottom flask with stir bar were added sodium iodide (619 mg, 4.13 mmol, 1.30 equiv) in a single portion and Et_3N (0.71 mL, 5.08 mmol, 1.60 equiv) dropwise with stirring. After 5 minutes, triethylsilyl chloride (TESCl, 0.69 mL, 4.13 mmol, 1.30 equiv) was added dropwise. After 18 h, consumption of starting material was complete as determined by TLC (1:9 Et_2O:Hexanes eluent) and the reaction mixture was extracted with pentane (4 x 100 mL). Combined organic layers were washed with H_2O (50 mL), brine (50 mL), dried over Na_2SO_4, filtered, and concentrated in vacuo to produce a yellow oil. Purification of this residue by flash chromatography (1.0% Et_2O / 0.5% Et_3N in hexanes eluent) on base-treated silica furnished silyl enol ether **290** (485 mg, 53% yield) as a faintly pink, clear oil: R_f = 0.28 (1:19 Et_2O:Hexanes eluent); ^1H NMR (300 MHz, $CDCl_3$) δ 4.02 (q, *J* = 2.0 Hz, 2H), 1.77 (t, *J* = 2.0 Hz, 3H), 1.21 (t, *J* = 7.0 Hz, 4H), 1.03–0.84 (m, 15H), 0.64 (qd, *J* = 7.8, 0.9 Hz, 6H).

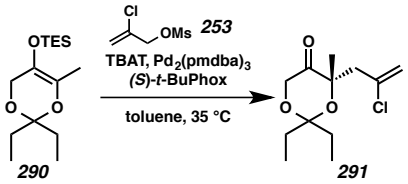

Chloroallyl Ketal 291: A 500 mL Schlenk flask was soaked in a 20:1 *i*-PrOH:toluene bath saturated with KOH for 12 h, rinsed with deionized H_2O, acetone, and allowed to dry. To a flame-dried 500 mL base-bathed Schlenk flask in a nitrogen-filled glovebox were charged $Bu_4NPh_3SiF_2$ (TBAT, 642 mg, 1.19 mmol, 1.00 equiv), $Pd_2(pmdba)_3$ (20 mg, 0.018 mmol, 0.015 equiv), (*S*)-*t*-BuPhox (16 mg, 0.042 mmol, 0.035 equiv), and toluene (12 mL, 0.003 M in Pd). The reaction vessel was immediately removed from the glovebox, placed under an argon atmosphere and introduced to a preheated 35 °C bath with stirring. After 20 minutes, a yellow-brown solution was observed. Chloroallylmesylate **253** (0.21 mL, 1.67 mmol, 1.40 equiv) was added quickly dropwise affording a blue-green solution. After 3 minutes, silyl enol ether **290** (340 mg, 1.19 mmol, 1.00 equiv) was added quickly dropwise over 3 minutes. The resultant blue-green reaction mixture was allowed to stir for 20 h. The resultant yellow-brown reaction was then allowed to cool to ambient temperature, filtered through a pad of SiO_2 using hexanes as the eluent to remove toluene, at which time separate fractions were collected, eluting with Et_2O, to isolate the volatile reaction products. The filtrate was concentrated in vacuo to a bright yellow oil which was subsequently purified by flash chromatography (1%→3%→5% Et_2O in pentane eluent) to afford volatile chloroallyl ketal **291** (2.95 g, 82% yield) as a clear, colorless oil: R_f = 0.35 (19:1 pentane:Et_2O eluent); ^{1}H NMR (300 MHz, $CDCl_3$) δ 5.30 (d, *J* = 1.1 Hz, 1H), 5.22 (dd, *J* = 1.1, 0.6 Hz, 1H), 4.35 (d, *J* = 18.2

Hz, 1H), 4.21 (d, *J* = 18.2 Hz, 1H), 2.87 (dd, *J* = 14.5, 0.9 Hz, 1H), 2.76 (d, *J* = 14.5 Hz, 1H), 1.81–1.63 (m, 4H), 1.46 (s, 3H), 0.92 (app td, *J* = 7.5, 5.9 Hz, 6H).

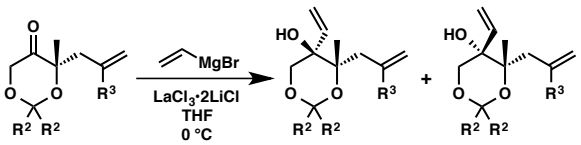

243 ***281*** ***282***

Ketone	*R²,R²*	*R³*	*syn*	*anti*	*syn:anti* [a]
249	*Me,Me*	*H*	*296*	*297*	*1.0:1.2*
254	*Me,Me*	*Cl*	*298*	*299*	*2.8:1.0*
291	*Et,Et*	*Cl*	*300*	*301*	*3.2:1.0*
258	*$(CH_2)_5$*	*Cl*	*302*	*303*	*2.9:1.0*

Example Procedure for the Addition of Vinyl–MgBr to Ketodioxanones

The following procedure was adapted from the literature.[5] To a solution of chloroallylketone **258** (80 mg, 0.31 mmol, 1.00 equiv) in THF (1.0 mL) was added LaCl3•2LiCl (0.52 mL, 0.60 M in THF, 0.31 mmol). The reaction mixture was then cooled to 0 °C (ice/H_2O bath). Vinyl magnesium bromide (0.50 mL, 0.68 M in THF, 1.10 equiv) was then added slowly dropwise over 4 minutes. After 20 minutes, consumption of starting material was complete as determined by TLC (1:9 Et_2O:Hexanes eluent). The reaction was immediately diluted with Et_2O (50 mL) and poured onto a mixture of H_2O (20 mL), brine (20 mL), and hexanes (30 mL). The organics were separated and the aqueous was extracted with Et_2O (2 x 50 mL). The combined organics were dried over $MgSO_4$, filtered, and concentrated in vacuo. The crude dark yellow oil was purified by silica gel column chromatography (20% Et_2O in hexanes eluent) to yield *syn*-vinyl alcohol **302** (77 mg, 87% yield) and *anti*-vinyl alcohol **303** (12 mg, 13% yield), both as a clear, colorless oils.

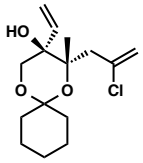

302

***syn*-Vinyl Chloroallylcyclohexyl Ketal 302**: R_f = 0.37 (1:4 Et_2O:Hexanes eluent); ^1H NMR (300 MHz, $CDCl_3$) δ 6.13 (ddd, *J* = 17.5, 11.0, 0.8 Hz, 1H), 5.50–5.22 (m, 4H), 3.82–3.70 (m, 2H), 2.87–2.73 (m, 1H), 2.45–2.33 (m, 2H), 1.99–1.93 (m, 1H), 1.80–1.71 (ddd, *J* = 19.4, 9.1, 4.4 Hz, 2H), 1.67–1.55 (m, 7H), 1.43 (s, 3H).

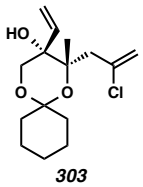

303

***anti*-Vinyl Chloroallylcyclohexyl Ketal 303**: R_f = 0.30 (1:4 Et_2O:Hexanes eluent); ^1H NMR (300 MHz, $CDCl_3$) δ 5.68 (ddd, *J* = 17.2, 10.5, 1.5 Hz, 1H), 5.55 (dd, *J* = 17.2, 2.3 Hz, 1H), 5.35–5.17 (m, 3H), 4.26 (dd, *J* = 11.9, 1.3 Hz, 1H), 3.33 (dd, *J* = 12.0, 1.5 Hz, 1H), 3.17 (d, *J* = 1.5 Hz, 1H), 3.02–2.90 (m, 1H), 2.26 (dd, *J* = 14.9, 0.9 Hz, 1H), 2.10–2.03 (m, 1H), 1.78–1.52 (m, 8H), 1.50 (s, 3H), 1.48–1.41 (m, 1H).

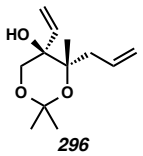

296

***syn*-Vinyl Allylacetonide 296**: R_f = 0.47 (1:4 Et_2O:Hexanes eluent); ^1H NMR (300 MHz, $CDCl_3$) δ 5.99–5.73 (m, 2H), 5.51 (dd, *J* = 17.3, 1.8 Hz, 1H), 5.27 (dd, *J* = 11.0, 1.8 Hz, 1H), 5.18–5.02 (m, 2H), 4.15 (d, *J* = 11.9 Hz, 1H), 3.48 (d, *J* = 11.9 Hz, 1H), 2.98 (d, *J* =

1.2 Hz, 1H), 2.82–2.69 (m, 1H), 2.14 (ddt, *J* = 14.8, 8.2, 1.1 Hz, 1H), 1.52 (s, 3H), 1.45 (s, 3H), 1.15 (s, 3H).

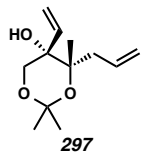

297

***anti*-Vinyl Allylacetonide 297**: R_f = 0.33 (1:4 Et_2O:Hexanes eluent); ^1H NMR (300 MHz, $CDCl_3$) δ 5.87 (dddd, *J* = 16.9, 10.4, 8.7, 5.8 Hz, 1H), 5.71 (ddd, *J* = 17.2, 10.7, 1.4 Hz, 1H), 5.54 (dd, *J* = 17.2, 2.1 Hz, 1H), 5.33–5.21 (m, 1H), 5.11–4.92 (m, 2H), 4.18 (d, *J* = 11.9 Hz, 1H), 3.36 (d, *J* = 12.0 Hz, 1H), 3.08 (d, *J* = 1.4 Hz, 1H), 2.57 (ddtd, *J* = 14.2, 5.8, 1.7, 0.8 Hz, 1H), 2.03 (ddt, *J* = 14.1, 8.7, 1.0 Hz, 1H), 1.47 (s, 3H), 1.42 (s, 3H), 1.33 (s, 3H).

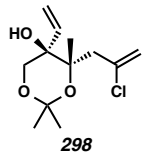

298

***syn*-Vinyl Chloroallylacetonide 298**: R_f = 0.31 (1:4 Et_2O:Hexanes eluent); ^1H NMR (300 MHz, $CDCl_3$) δ 5.95 (ddd, *J* = 17.4, 11.0, 0.9 Hz, 1H), 5.53–5.43 (m, 2H), 5.38 (t, *J* = 1.2 Hz, 1H), 5.30 (dd, *J* = 11.0, 1.4 Hz, 1H), 3.97 (d, *J* = 11.8 Hz, 1H), 3.63 (d, *J* = 11.8 Hz, 1H), 2.97–2.85 (m, 1H), 2.73 (d, *J* = 1.0 Hz, 1H), 2.41 (dd, *J* = 16.7, 1.0 Hz, 1H), 1.50 (s, 3H), 1.45 (s, 3H), 1.38 (s, 3H).

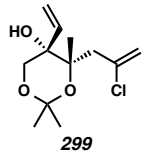

299

***anti*-Vinyl Chloroallylacetonide 299**: R_f = 0.19 (1:4 Et_2O:Hexanes eluent); ^1H NMR (300 MHz, $CDCl_3$) δ 5.68 (ddd, *J* = 17.2, 10.5, 1.5 Hz, 1H), 5.56 (dd, *J* = 17.2, 2.3 Hz, 1H), 5.32–5.25 (m, 2H), 5.19 (t, *J* = 0.9 Hz, 1H), 4.22 (d, *J* = 12.0 Hz, 1H), 3.35 (d, *J* = 12.0 Hz, 1H), 3.12 (d, *J* = 1.4 Hz, 1H), 2.93 (dd, *J* = 14.9, 1.4 Hz, 1H), 2.26 (dd, *J* = 14.9, 0.9 Hz, 1H), 1.51–1.47 (m, 6H), 1.45–1.38 (m, 3H).

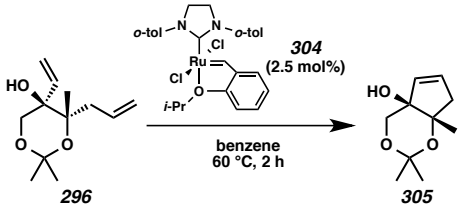

296 ***305***

Bicycle 305: To a stirred solution of *syn*-vinyl alcohol **296** (187 mg, 0.88 mmol, 1.00 equiv) in benzene (9.0 mL) was added ruthenium carbene **304** (13 mg, 0.022 mmol, 0.025 equiv). The reaction vessel was the introduced to a preheated 60 °C bath. After 2 h, consumption of starting material was complete as determined by TLC (1:4 Et_2O:Hexanes eluent). The reaction mixture was then removed form the heating bath and allowed to cool to ambient temperature (ca. 23 °C). The crude reaction mixture was then directly purified by silica gel column chromatography (10%→20% Et_2O in pentane eluent) to afford semi-volatile bicycle **305** (154 mg, 95% yield) as a clear, colorless oil: R_f = 0.25 (3:7 Et_2O:Hexanes eluent); ^1H NMR (300 MHz, $CDCl_3$) δ 5.89 (ddd, *J* = 6.0, 3.0, 1.8 Hz, 1H), 5.57–5.47 (m, 1H), 3.74–3.68 (m, 1H), 3.65 (d, *J* = 11.8 Hz, 1H), 2.60 (dt, *J* = 17.3,

2.3 Hz, 1H), 2.48–2.36 (m, 1H), 1.88 (d, *J* = 1.2 Hz, 1H), 1.41 (s, 3H), 1.36 (s, 3H), 1.28 (s, 3H).

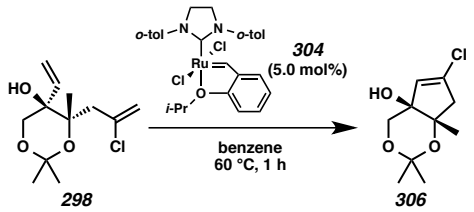

Bicycle 306: To a stirred solution of *syn*-vinyl alcohol **298** (284 mg, 1.15 mmol, 1.00 equiv) in benzene (12.0 mL) was added ruthenium carbene **304** (33 mg, 0.058 mmol, 0.05 equiv). The reaction vessel was the introduced to a preheated 60 °C bath. After 1 h, consumption of starting material was complete as determined by TLC (1:4 Et_2O:Hexanes eluent). The reaction mixture was then removed form the heating bath and allowed to cool to ambient temperature (ca. 23 °C). The crude reaction mixture was then directly purified by silica gel column chromatography (10%→20% Et_2O in pentane eluent) to supply bicycle **306** (242 mg, 89% yield) as a clear, colorless oil: R_f = 0.20 (3:7 Et_2O:Hexanes eluent); ^1H NMR (300 MHz, $CDCl_3$) δ 5.59 (t, *J* = 1.9 Hz, 1H), 3.79 (d, *J* = 12.0 Hz, 1H), 3.71 (d, *J* = 11.9 Hz, 1H), 2.86 (dd, *J* = 17.1, 1.8 Hz, 1H), 2.66 (dd, *J* = 17.1, 2.0 Hz, 1H), 2.02 (d, *J* = 1.7 Hz, 1H), 1.48–144 (s, 6H), 1.37 (s, 3H).

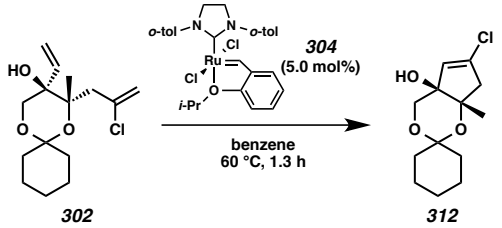

Chloride 312: To a stirred solution of *syn*-vinyl alcohol **302** (35 mg, 0.12 mmol, 1.00 equiv) in benzene (2.5 mL) was added ruthenium carbene **304** (3 mg, 0.006 mmol, 0.05 equiv). The reaction vessel was the introduced to a preheated 60 °C bath. After 1.3 h, consumption of starting material was complete as determined by TLC (1:4 Et_2O:Hexanes eluent). The reaction mixture was then removed form the heating bath and allowed to cool to ambient temperature (ca. 23 °C). The crude reaction mixture was then directly purified by silica gel column chromatography (10%→20% Et_2O in pentane eluent) to furnish volatile chloride **312** (154 mg, 95% yield) as a clear, colorless oil: R_f = 0.14 (2:3 Et_2O:Hexanes eluent); ^1H NMR (300 MHz, $CDCl_3$) δ 5.59 (t, *J* = 1.9 Hz, 1H), 3.78 (d, *J* = 11.8 Hz, 1H), 3.68 (d, *J* = 11.9 Hz, 1H), 2.85 (dd, *J* = 17.0, 1.8 Hz, 1H), 2.66 (dd, *J* = 17.0, 1.9 Hz, 1H), 2.01 (s, 1H), 1.88–1.76 (m, 1H), 1.75–1.64 (m, 1H), 1.61–1.51 (m, 5H), 1.54 (s, 3H), 1.45 (s, 3H).

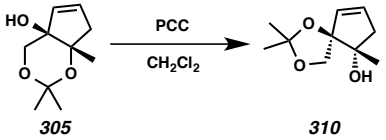

Acetonide 310: To a mixture of allylic alcohol **305** (35 mg, 0.19 mmol, 1.00 equiv) in CH_2Cl_2 (2.0 mL) was added PCC (123 mg, 0.57 mmol, 3.00 equiv) as a solid in a single portion. After 18 h, the consumption of starting material was complete as determined by TLC (2:3 Et_2O:Hexanes eluent). The reaction was filtered through a silica gel plug,

rinsing with Et_2O. The combined organics were concentrated in vacuo to provide acetonide **310**:[16] R_f = 0.26 (1:1 Et_2O:Hexanes eluent); ^1H NMR (300 MHz, $CDCl_3$) δ 5.76 (dd, *J* = 6.2, 2.7 Hz, 1H), 5.56 (dd, *J* = 5.4, 2.6 Hz, 1H), 4.25–4.12 (m, 1H), 3.73–3.55 (m, 1H), 3.35–3.21 (m, 1H), 2.43–2.30 (m, 1H), 2.27–2.12 (m, 1H), 1.25 (s, 3H), 1.22 (s, 3H), 1.19 (s, 3H).

A3.8 Notes and References

1. See Chapter 2, and: Craig, R. A., II; Roizen, J. L.; Smith, R. C.; Jones, A. C.; Stoltz, B. M. *Org. Lett.* **2012**, *14*, 5716–5719.

2. (a) Roizen, J. L. Progress Toward an Enantioselective Total Synthesis of Ineleganolide. Ph.D. dissertation. California Institute of Technology, 2010. (b) Seto, M.; Roizen, J. L.; Stoltz, B. M. *Angew. Chem., Int. Ed.* **2008**, *47*, 6873–6876.

3. Shi, Y. Catalytic Asymmetric Epoxidation. U.S. Patent 6348608 B1, 19 February 2002.

4. No racemic allylic alkylation of diethyl ketal **291** was performed, thus the enantiomeric excess of alkylation product **291** was not determined.

5. Krasovskiy, A.; Kopp, F.; Knochel, P. *Angew. Chem., Int. Ed.* **2006**, 45, 497–500.

6. Product formation was observed by both HPLC-MS and crude ^{1}H NMR.

7. Larson, K. K.; Sarpong, R. *J. Am. Chem. Soc.* **2009**, *131*, 13244–13245.

8. Shibuya, M.; Ito, S.; Takahashi, M.; Iwabuchi, Y. *Org. Lett.* **2004**, *6*, 4303–4306.

9. Corey, E. J.; Suggs, J. W. *Tetrahedron Lett.* **1975**, *16*, 2647–2650.

10. Structural assignment of acetonide **310** is only a tentative assignment, as the full data required for unambiguous structural assignment was not collected.

11. Morrill, C.; Grubbs, R. H. *J. Am. Chem. Soc.* **2005**, *127*, 2842–2843.

12. Cyclopentenone **242** generated by 1,3-allylic transposition using SO_3•pyridine followed by aqueous buffer was detectable by HPLC-MS, but not observed after reaction work-up by crude ^{1}H NMR.

13. Pangborn, A. B.; Giardello, M. A.; Grubbs, R. H.; Rosen, R. K.; Timmers, F. J. *Organometallics* **1996**, *15*, 1518–1520.

14. (a) Peer, M.; de Jong, J. C.; Kiefer, M.; Langer, T.; Rieck, H.; Schell, H.; Sennhenn, P.; Sprinz, J.; Steinhagen, H.; Wiese, B.; Helmchen, G. *Tetrahedron* **1996**, *52*, 7547–7583. (b) Behenna, D. C.; Stoltz, B. M. *J. Am. Chem. Soc.* **2004**, *126*, 15044–15045. (c) Krout, M. R.; Mohr, J. T.; Stoltz, B. M. *Org. Synth.* **2009**, *86*, 181–193.

15. (a) Ukai, T.; Kawazura, H.; Ishii, Y.; Bonnet, J. J.; Ibers, J. A. *J. Organomet. Chem.* **1974**, *65*, 253–266. (b) Fairlamb, I. J. S.; Kapdi, A. R.; Lee, A. F. *Org. Lett.* **2004**, *6*, 4435–4438.

16. The assignment of acetonide **310** in only tentative as high quality characterization data was not generated for this compound.

APPENDIX 4

Spectra Relevant to Appendix 3:

Alternative Construction of Hydroxymethyl-cis-

1,3-cyclopentenediol Building Block by Ring-Closing Metathesis

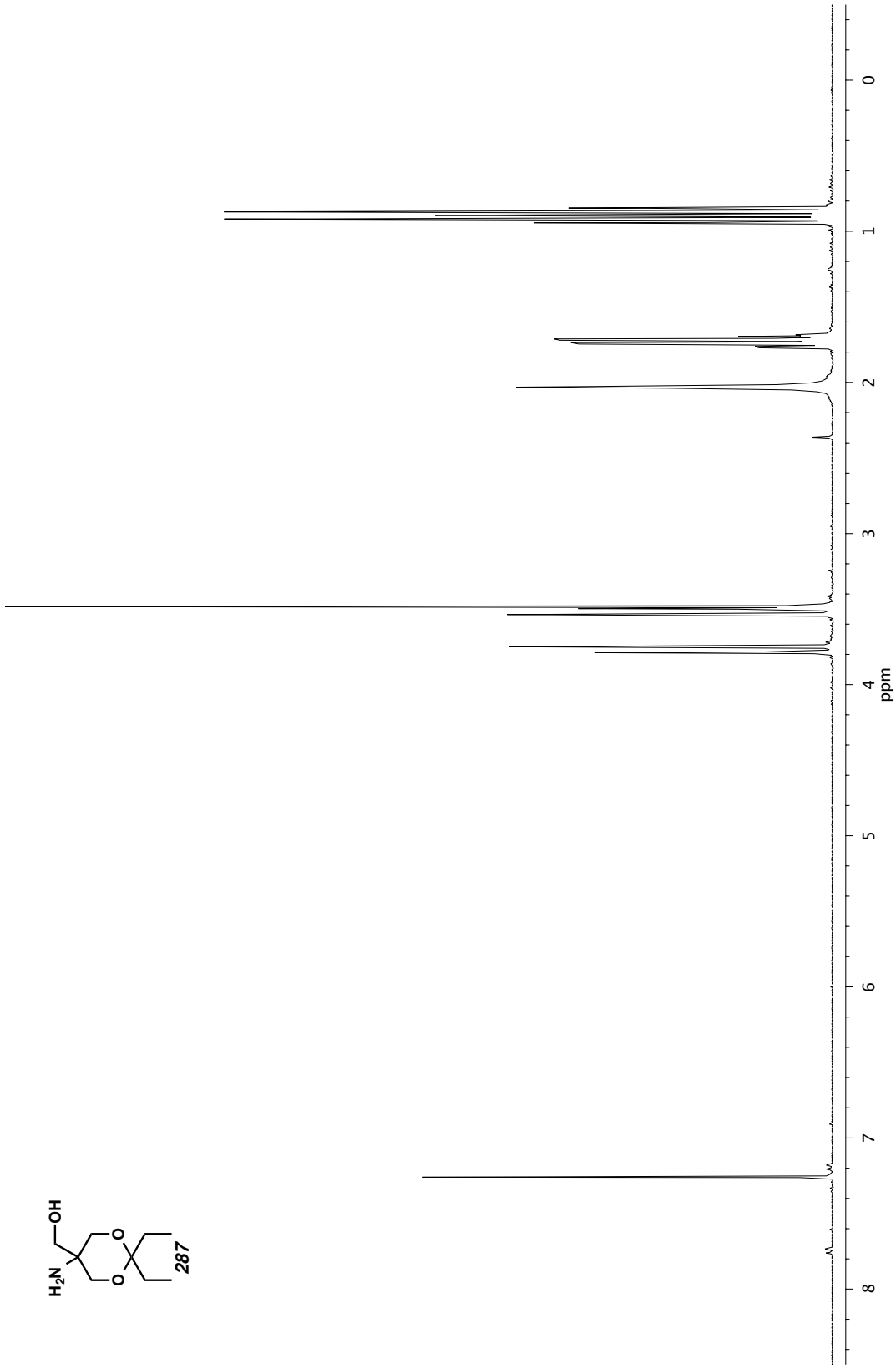

Figure A4.1. ^{1}H NMR (300 MHz, $CDCl_3$) of compound **287**.

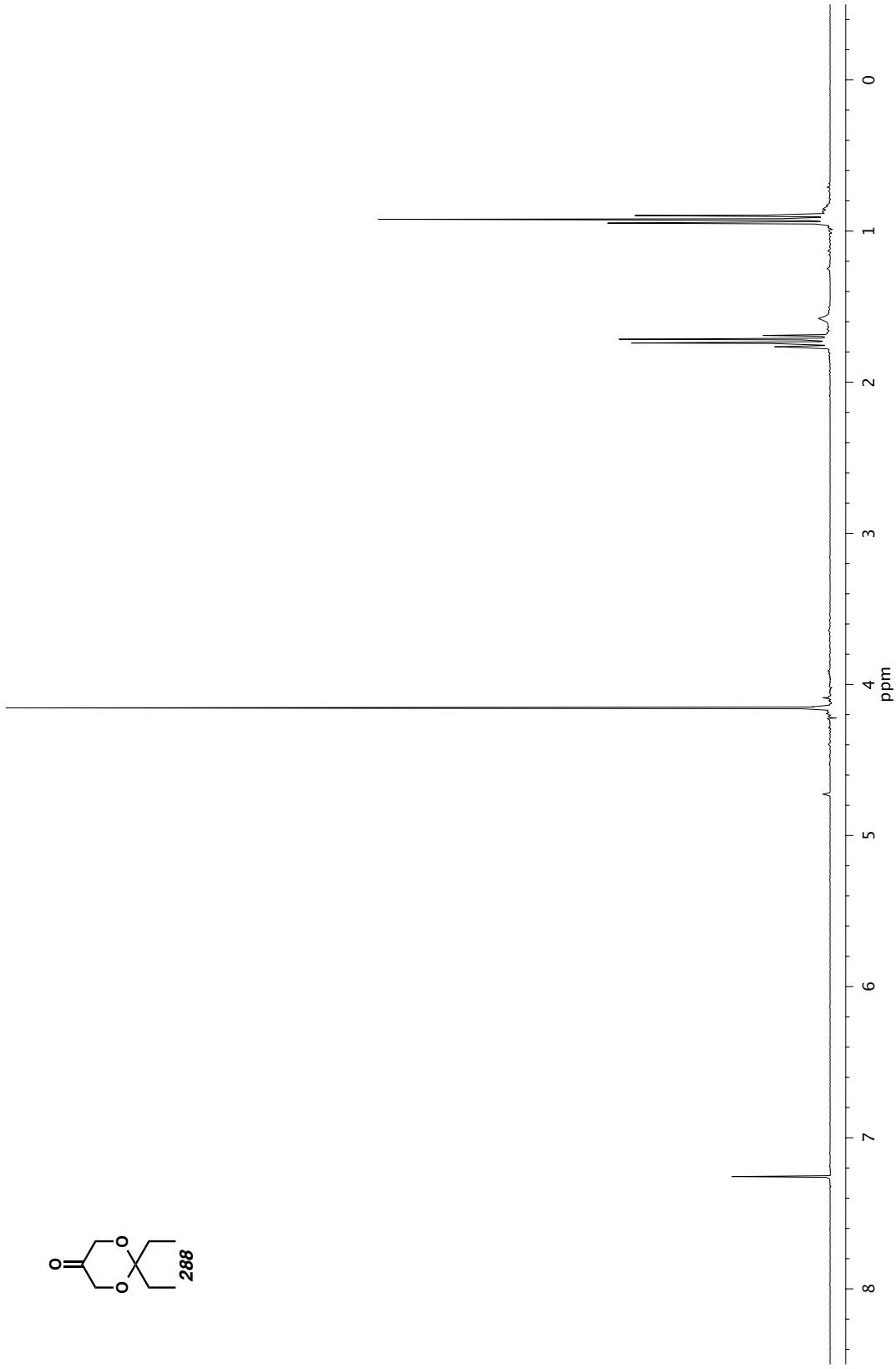

Figure A4.2. ^{1}H NMR (300 MHz, $CDCl_3$) of compound **288**.

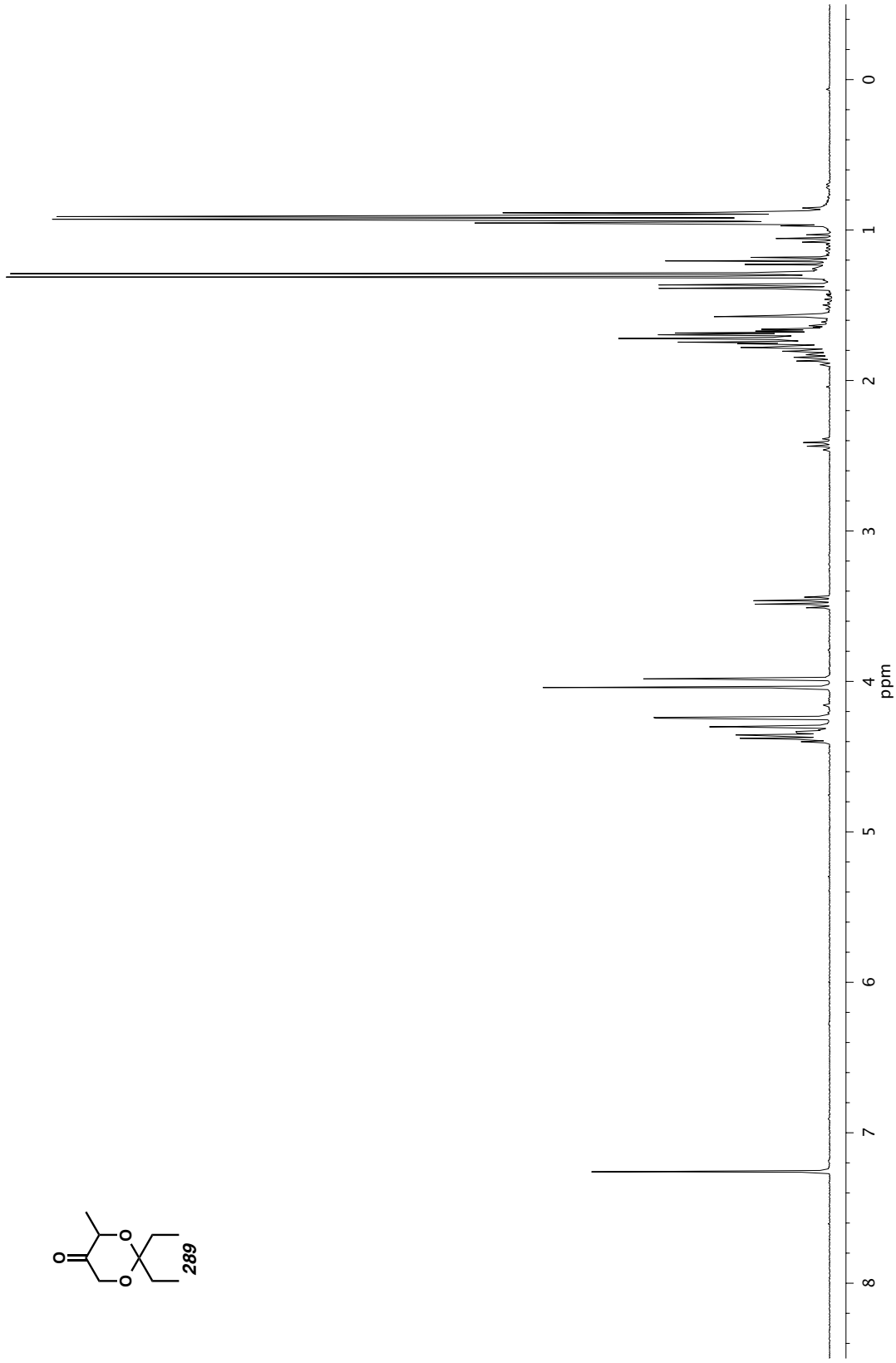

Figure A4.3. ^{1}H NMR (300 MHz, $CDCl_3$) of compound **289**.

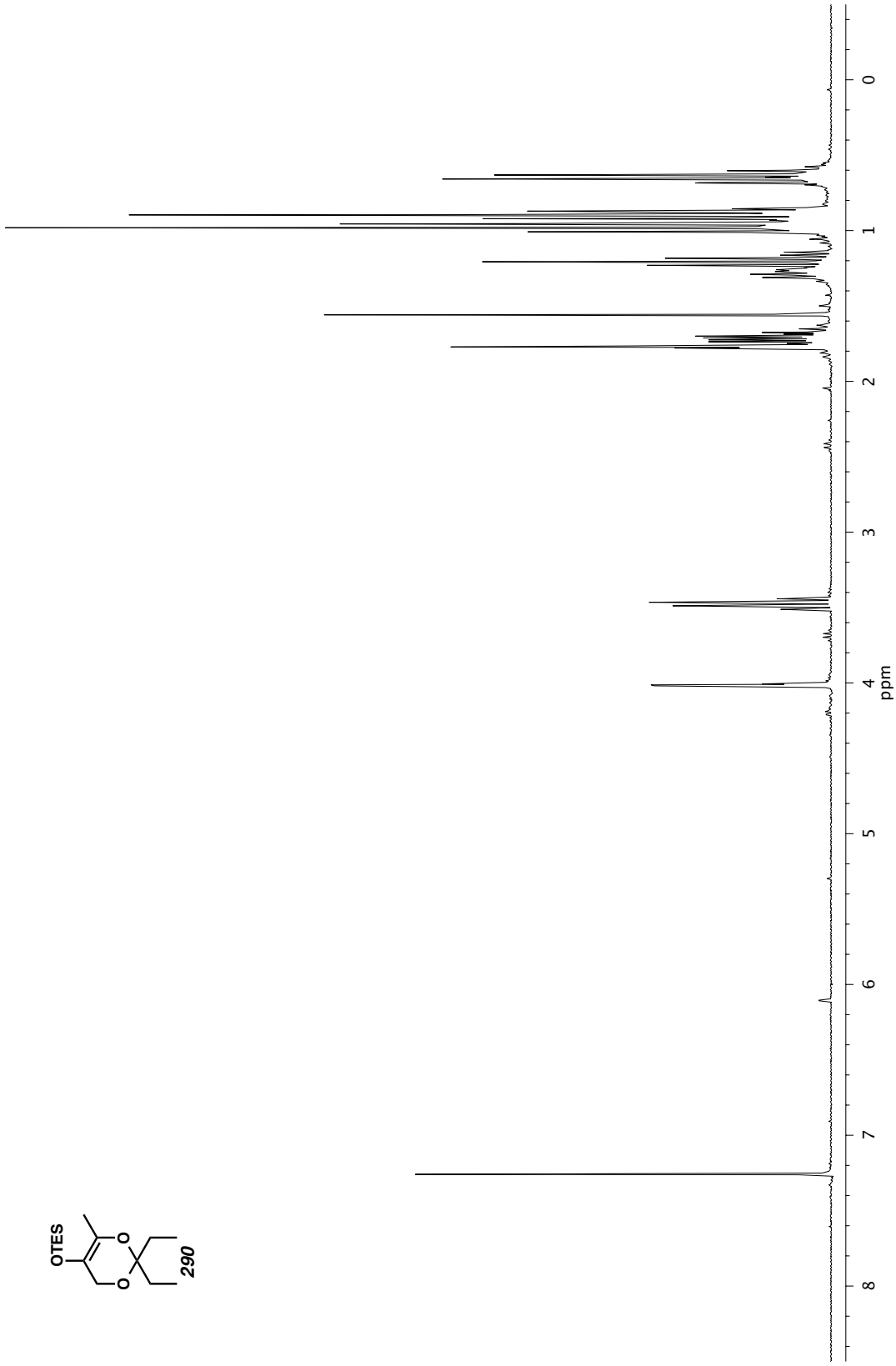

Figure A4.4. ^{1}H NMR (300 MHz, $CDCl_3$) of compound **290**.

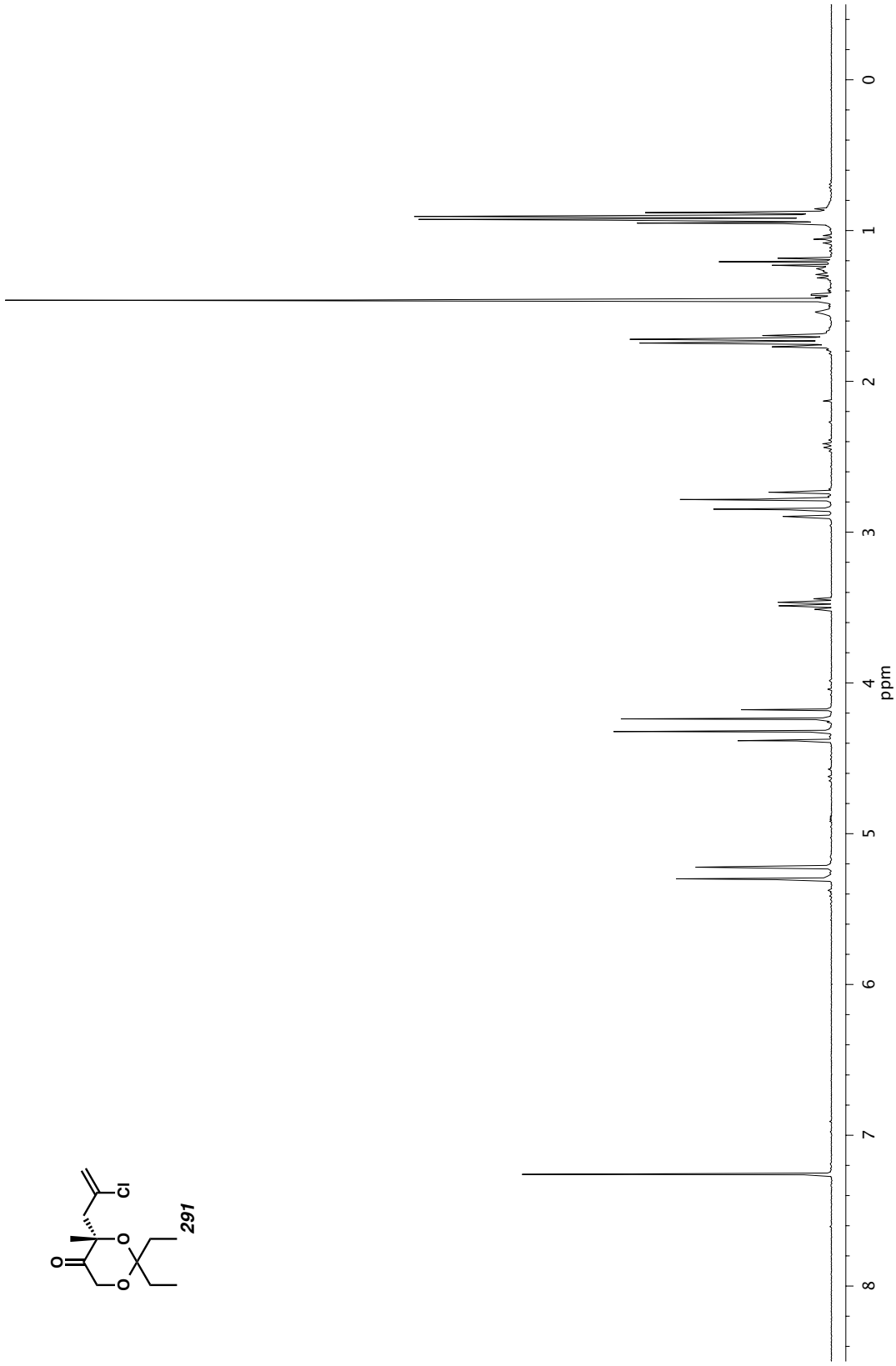

Figure A4.5. ^{1}H NMR (300 MHz, $CDCl_3$) of compound **291**.

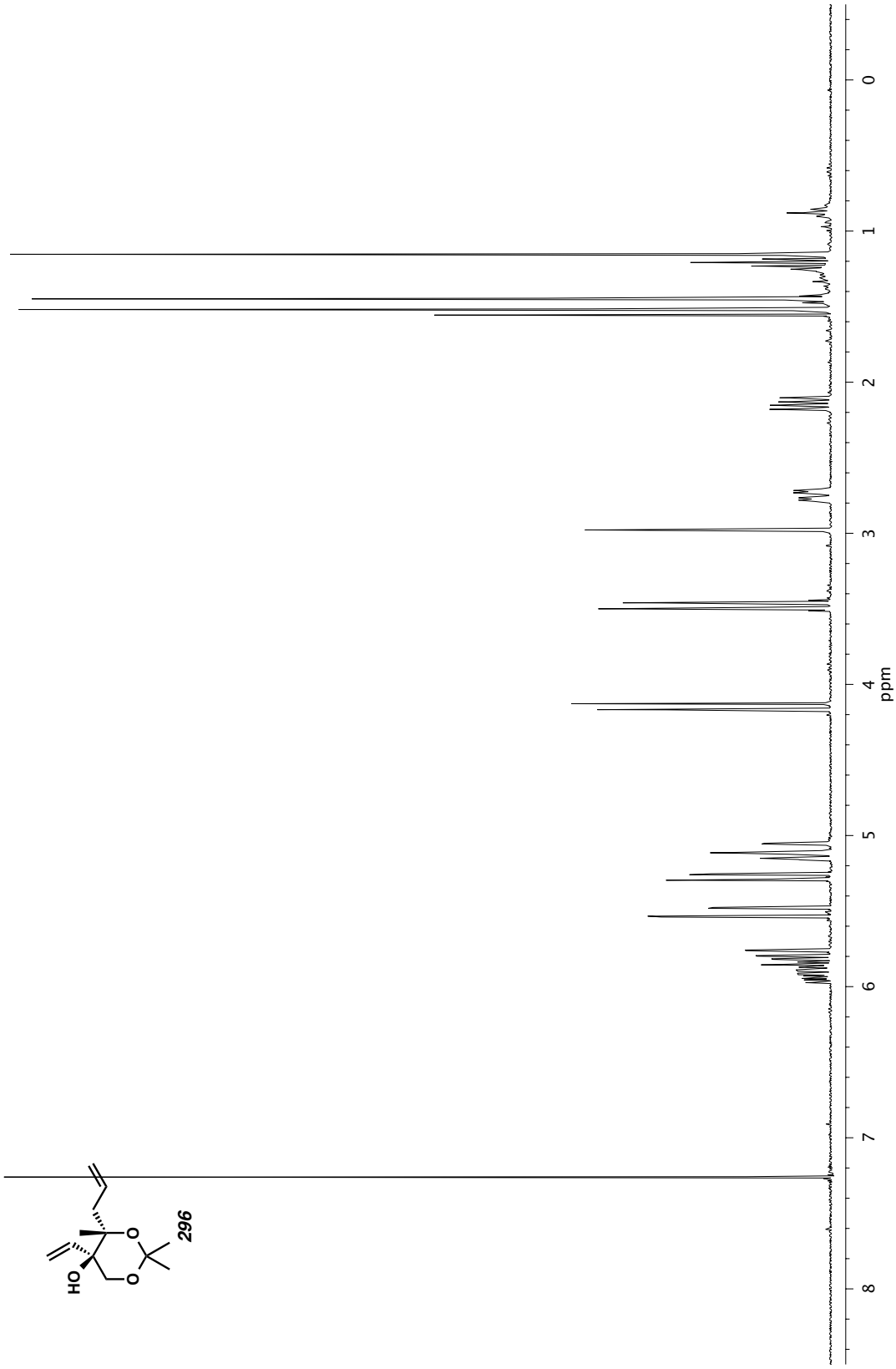

Figure A4.6. ^{1}H NMR (300 MHz, $CDCl_3$) of compound **296**.

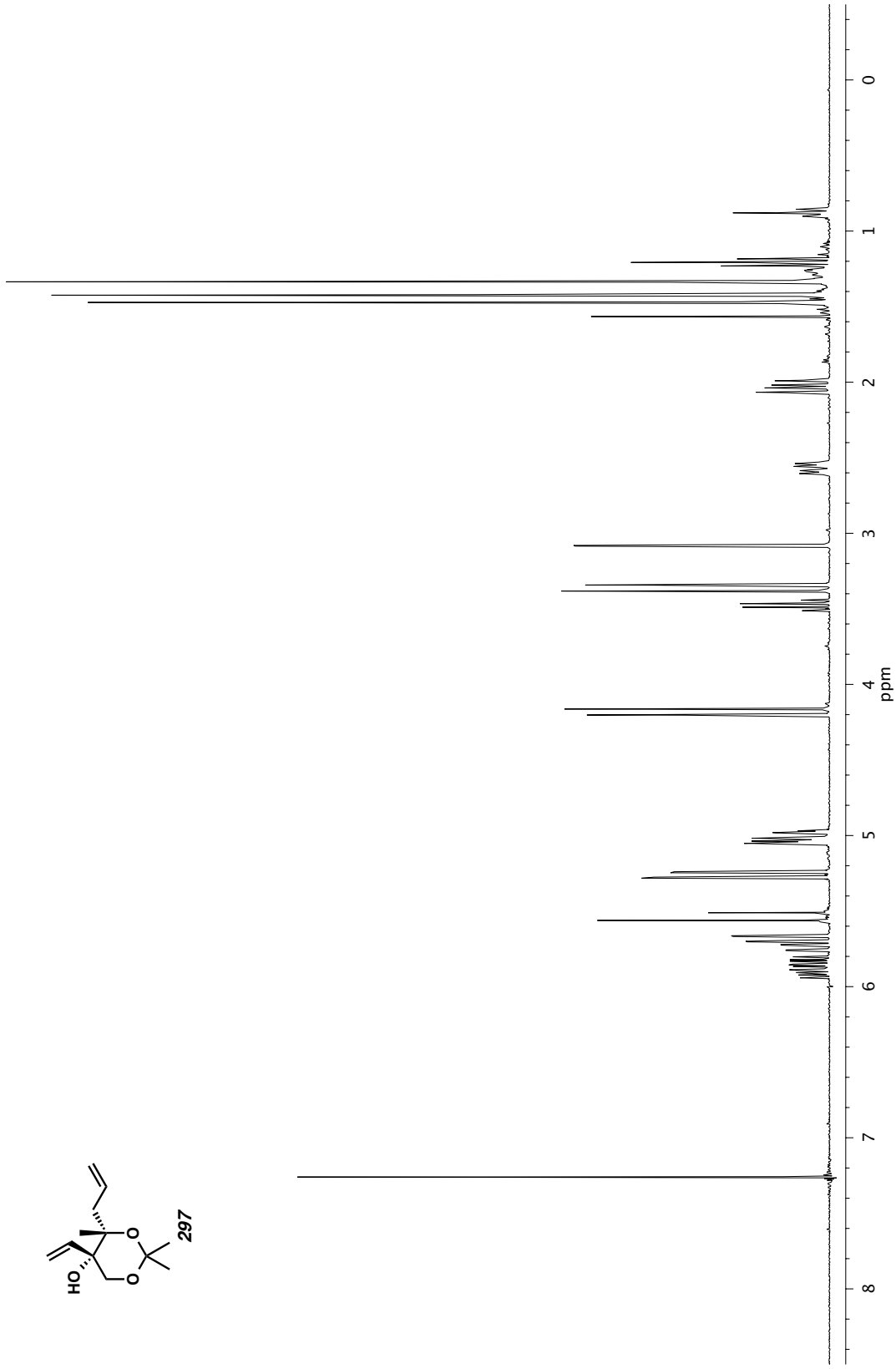

Figure A4.7. ^{1}H NMR (300 MHz, $CDCl_3$) of compound **297**.

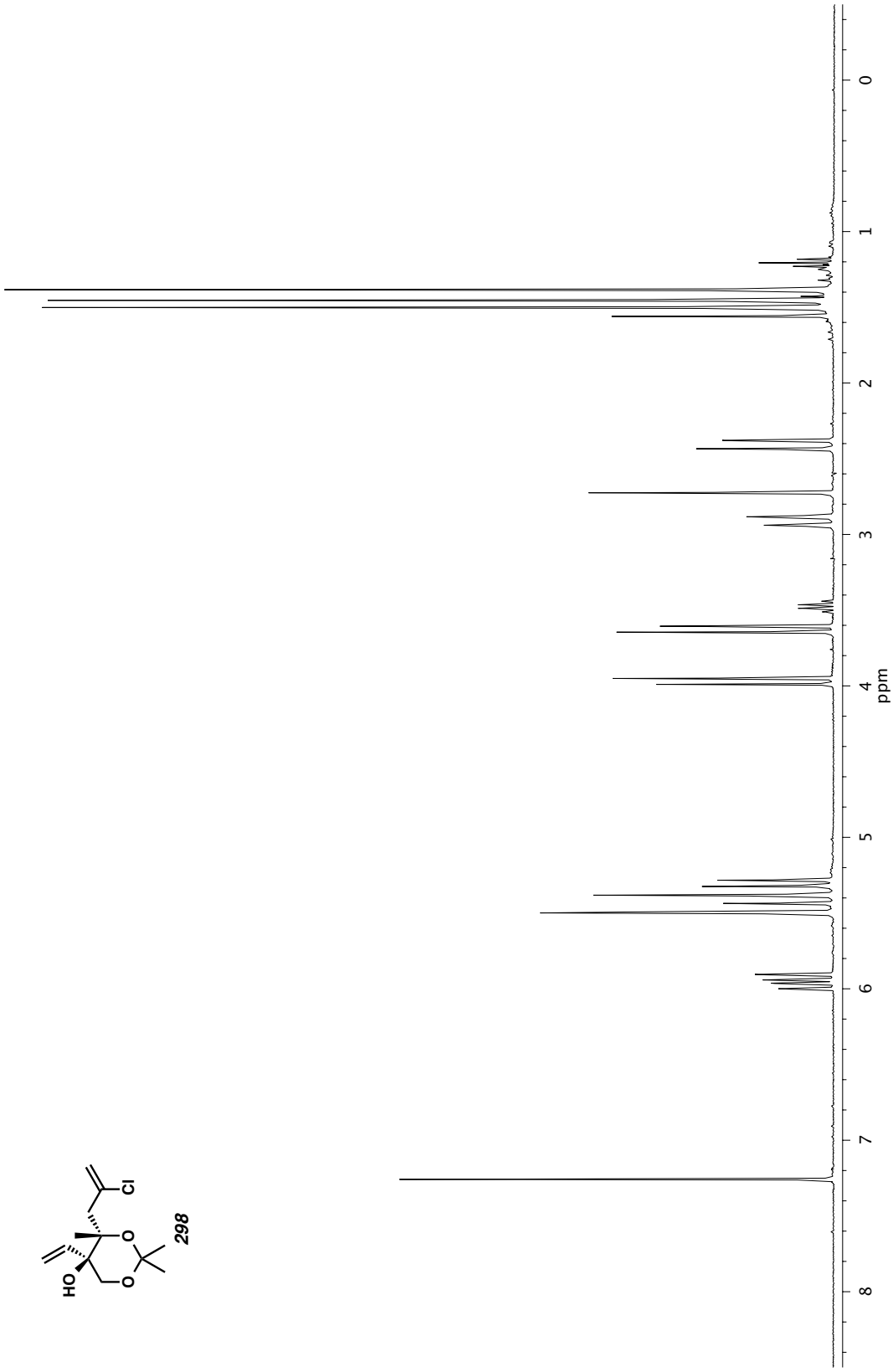

Figure A4.8. ^{1}H NMR (300 MHz, $CDCl_3$) of compound **298**.

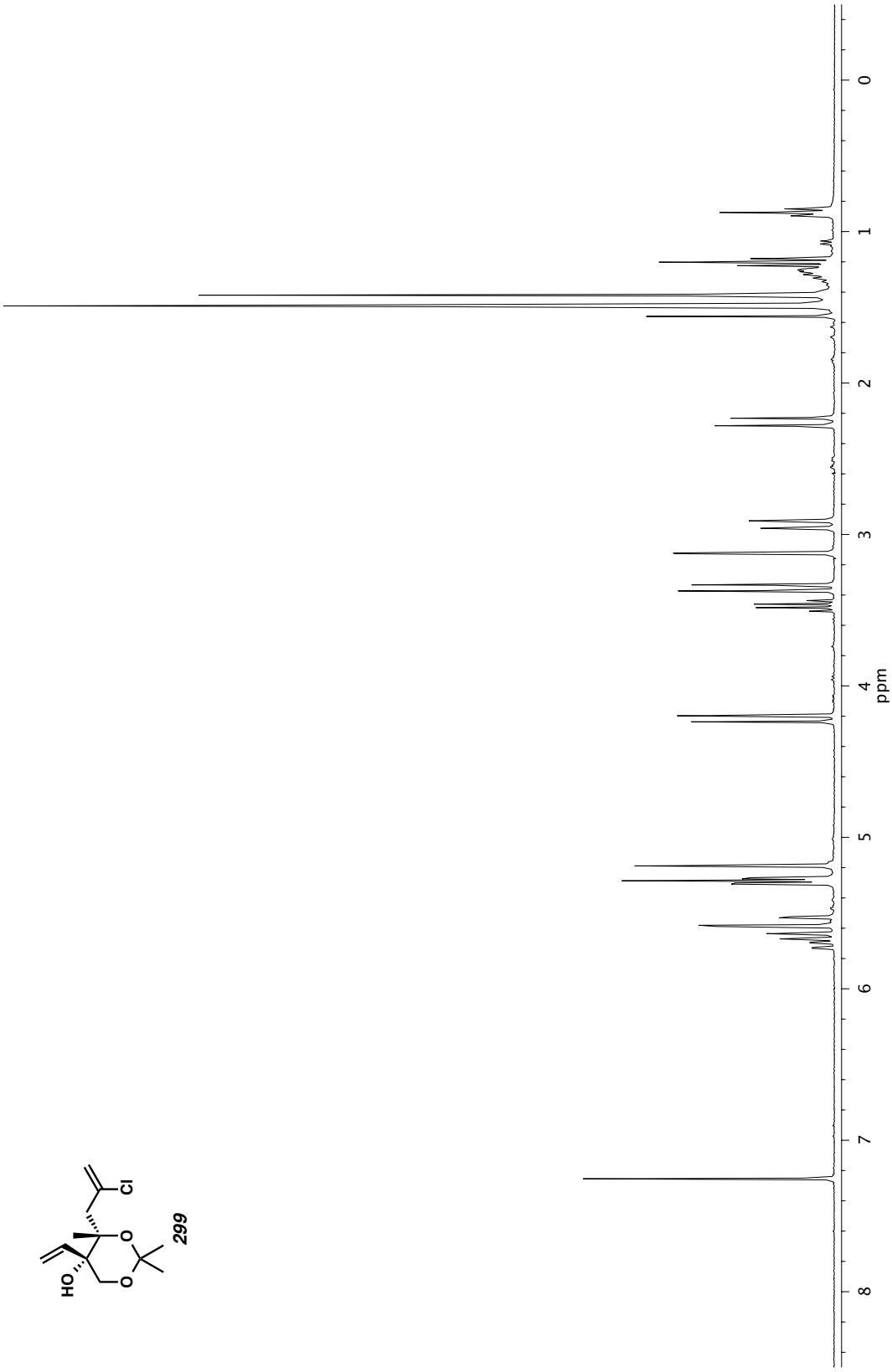

Figure A4.9. ^{1}H NMR (300 MHz, $CDCl_3$) of compound **299**.

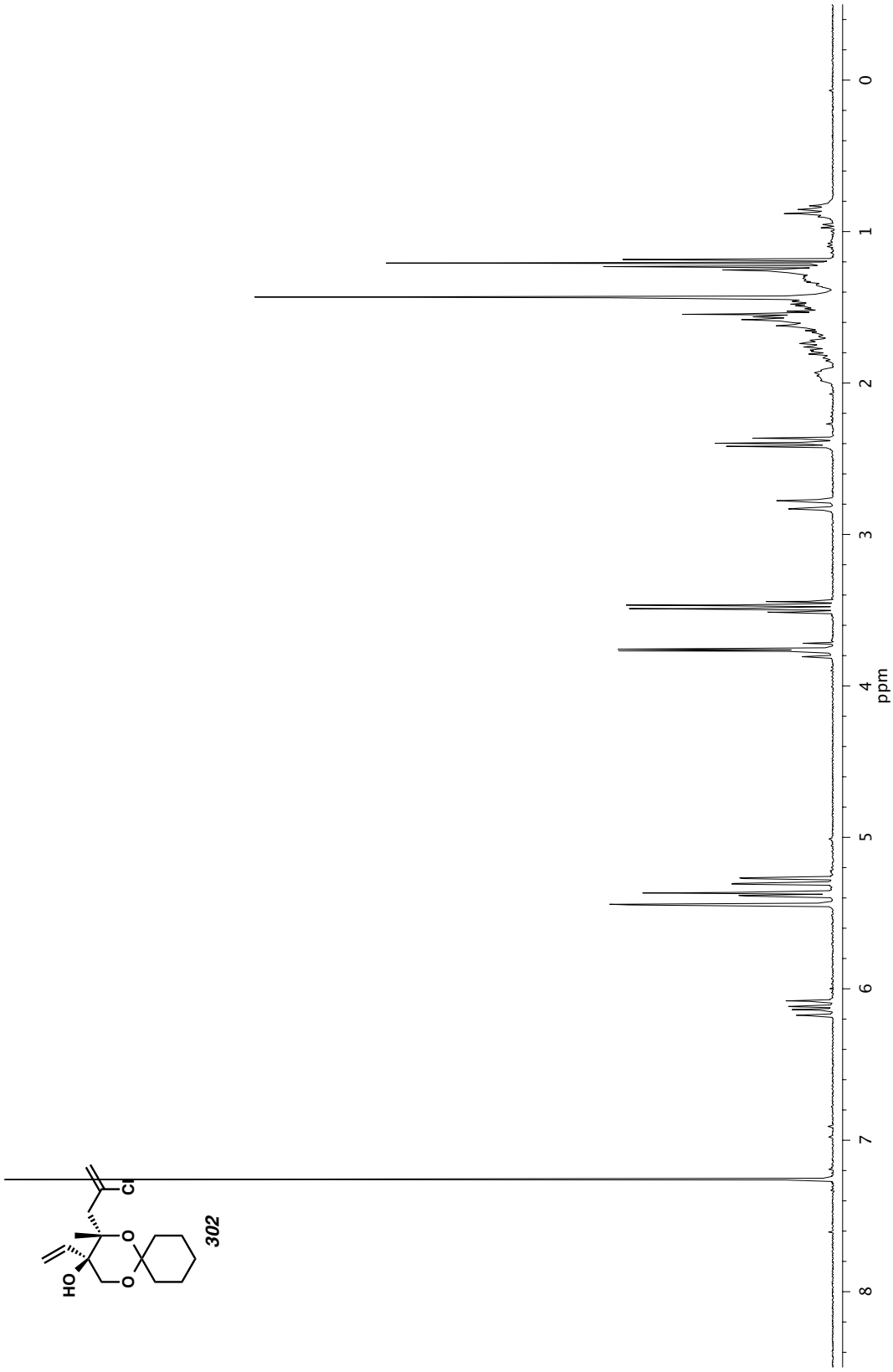

Figure A4.10. ^{1}H NMR (300 MHz, $CDCl_3$) of compound **302**.

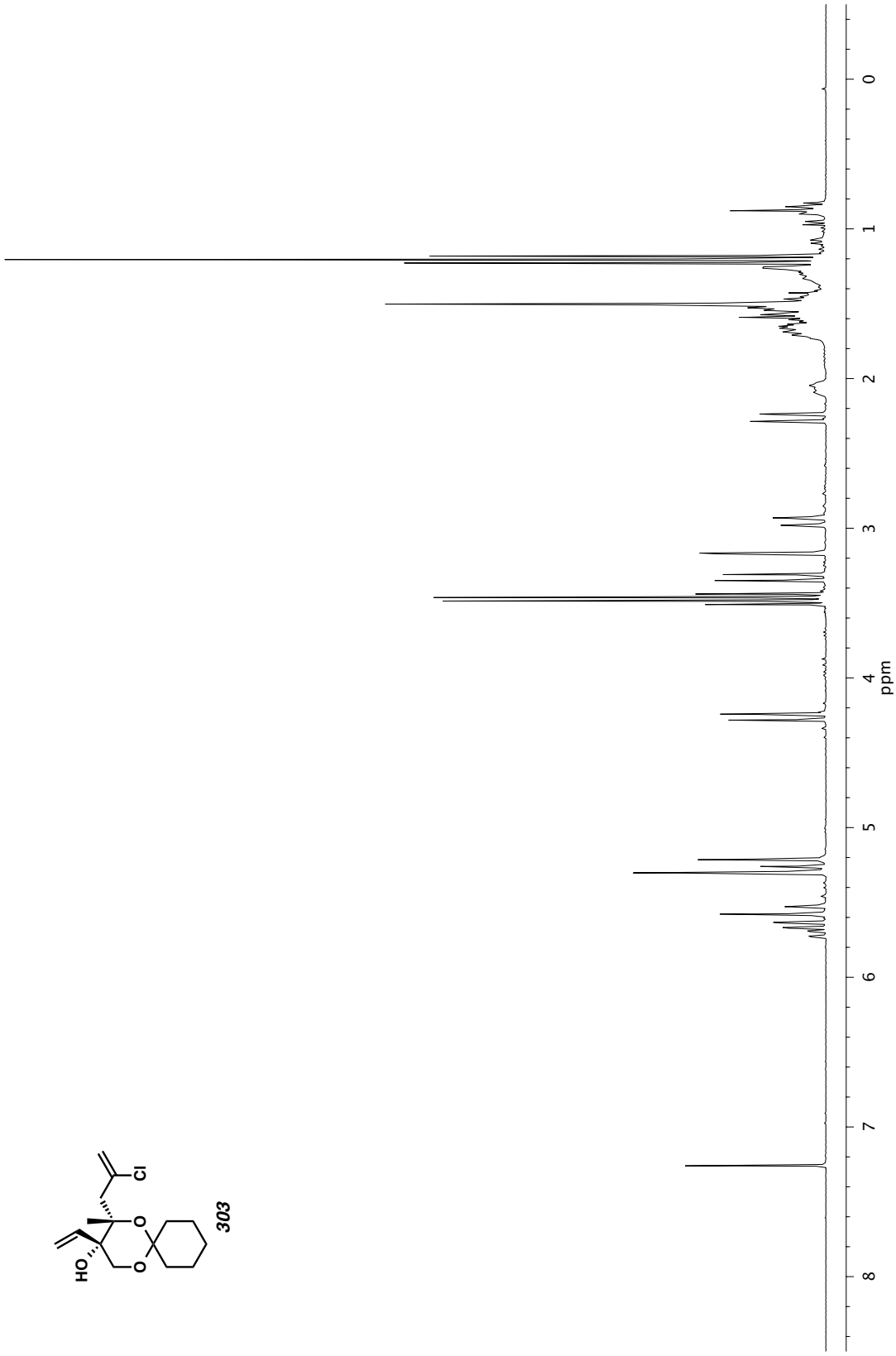

Figure A4.11. ^{1}H NMR (300 MHz, $CDCl_3$) of compound **303**.

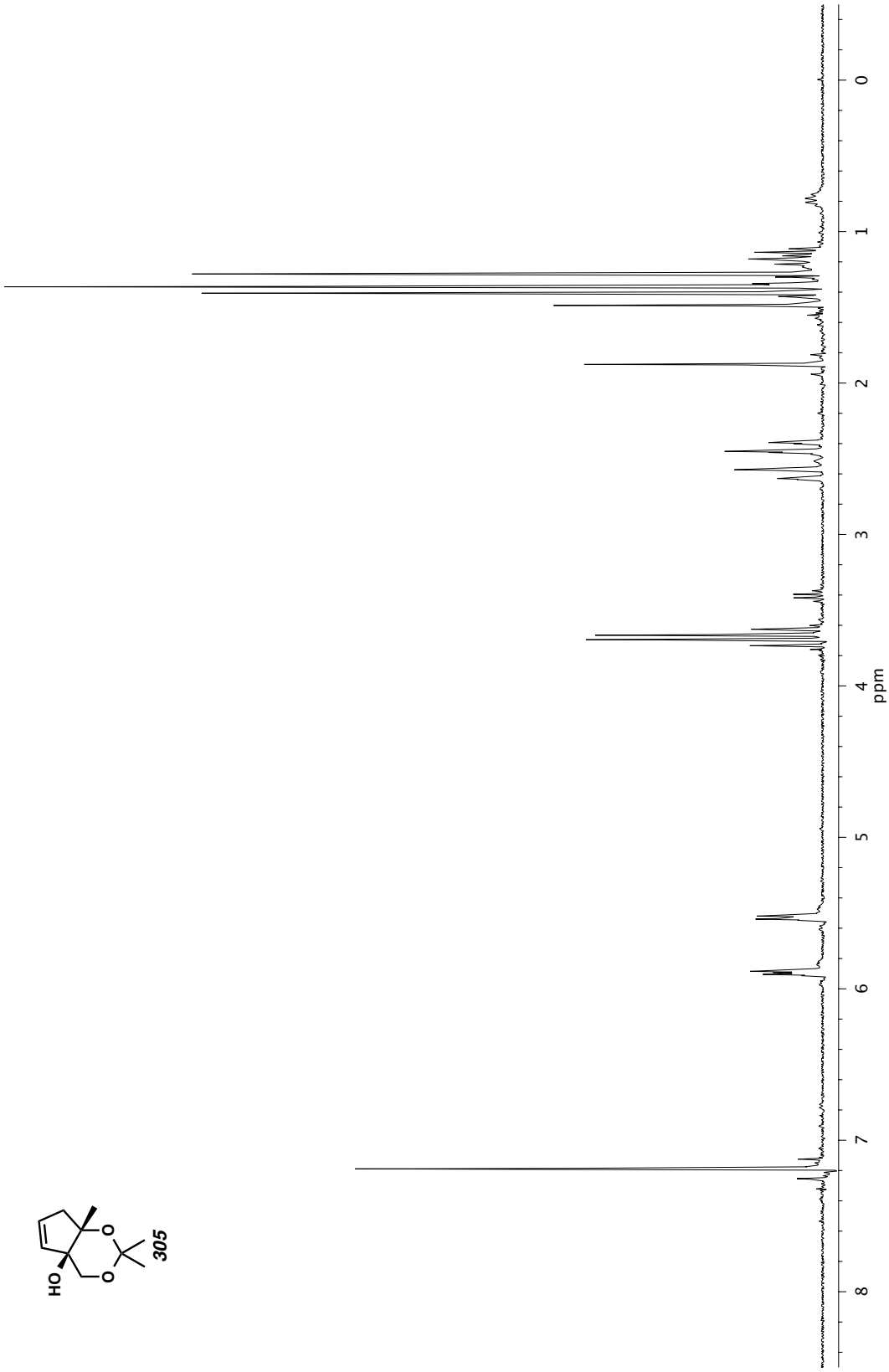

Figure A4.12. ^{1}H NMR (300 MHz, $CDCl_3$) of compound **305**.

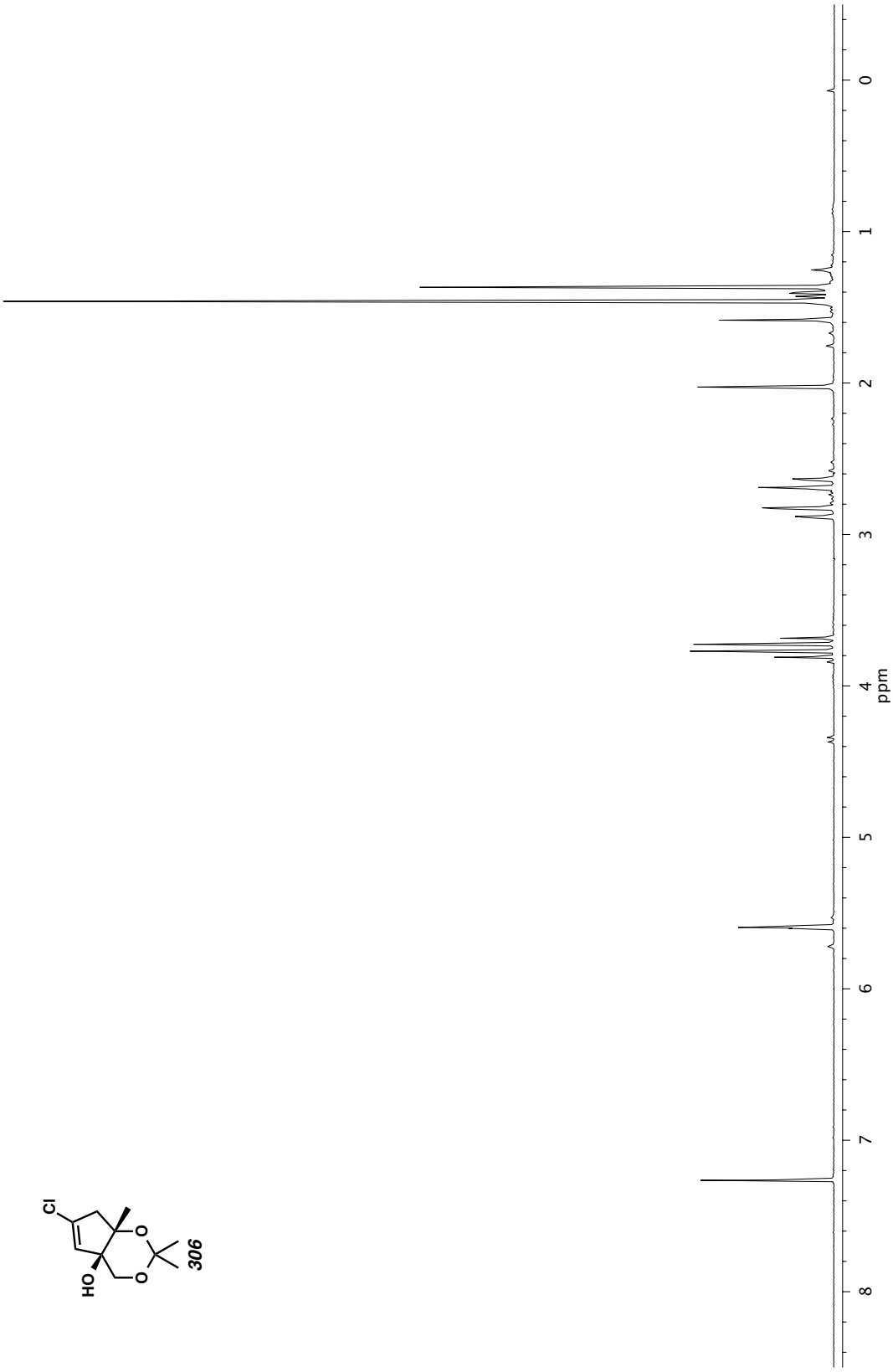

Figure A4.13. ^{1}H NMR (300 MHz, $CDCl_3$) of compound **306**.

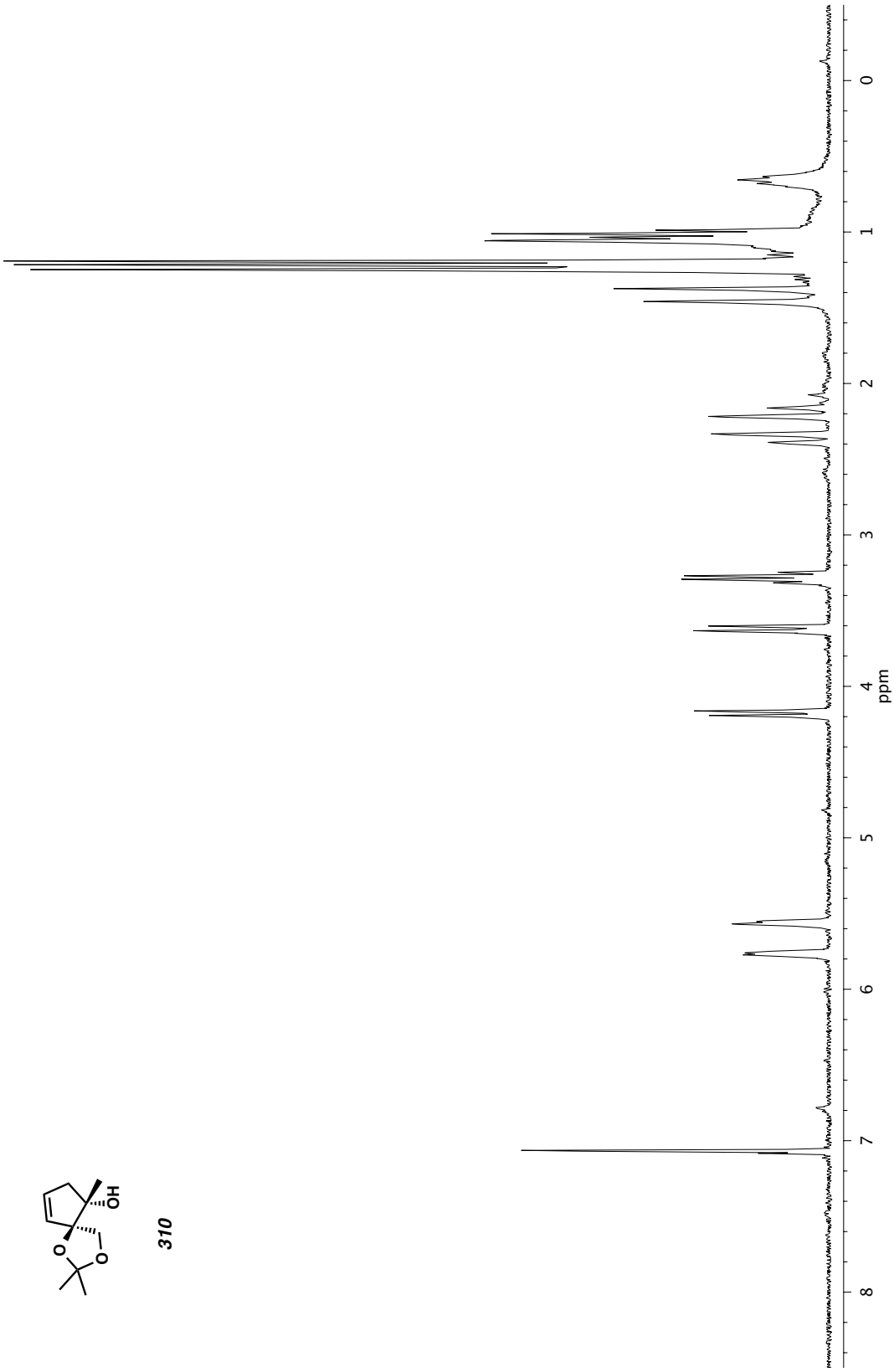

310

Figure A4.14. ^{1}H NMR (300 MHz, $CDCl_3$) of compound **310**.

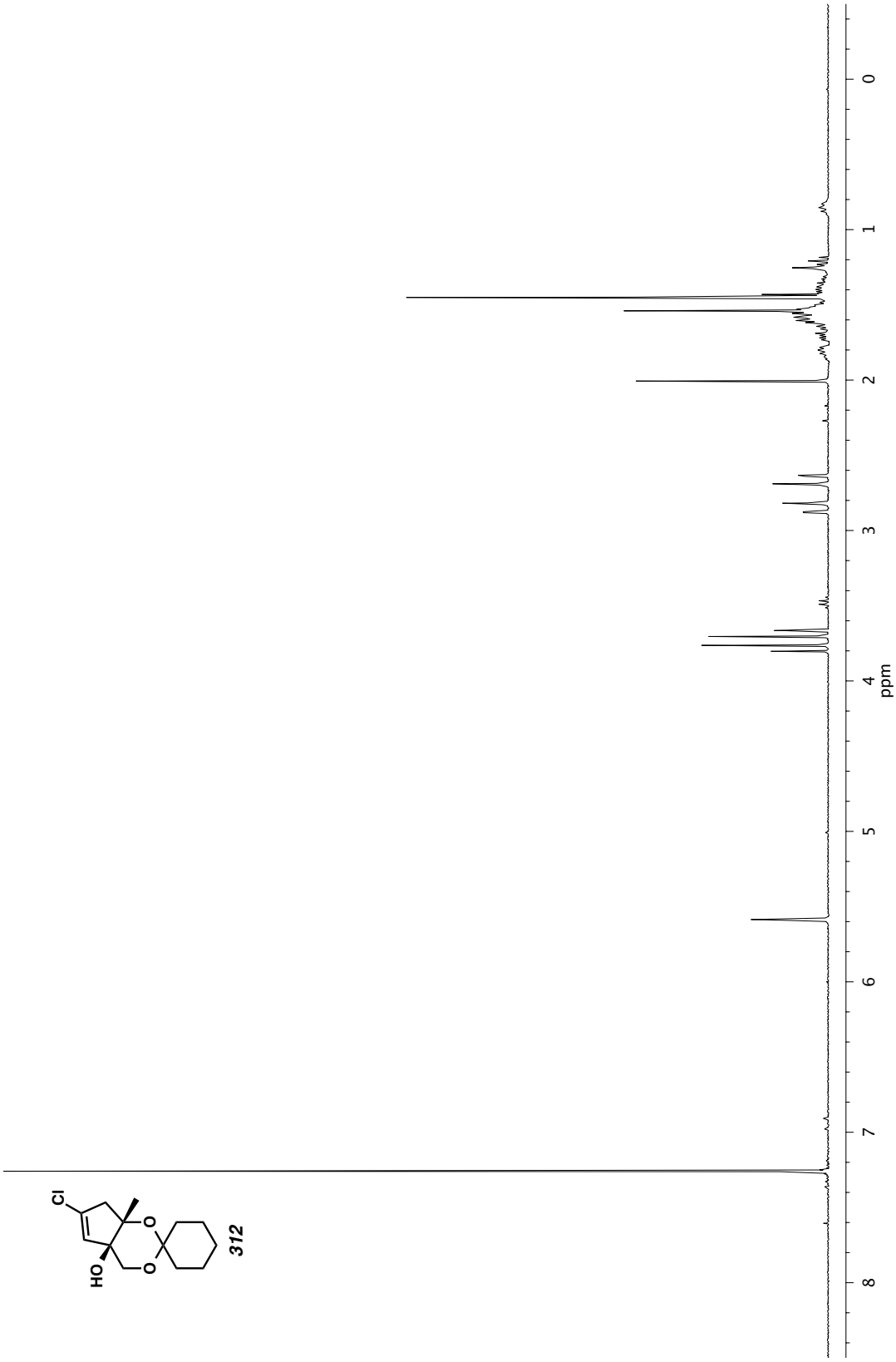

Figure A4.15. ^{1}H NMR (300 MHz, $CDCl_3$) of compound **312**.

CHAPTER 3

Progress Toward the Asymmetric Total Syntheses of the Furanobutenolide Norcembranoid Diterpene Natural Products

3.1 Introduction

Natural products produced by flora and fauna throughout the world have been successfully applied to the treatment of human ailments for centuries.[1] Modern synthetic chemistry has enabled the isolation, identification, and manufacturing of many of the most promising biologically active natural products for therapeutic application against a breadth of diseases including cancer,[1b,c, 2] malaria,[1b, 3] infectious bacteria,[1b,c, 4] and neurological diseases.[1b,2a, 5] Despite these successes, the need for more effective therapeutics for a variety of intractable ailments remains constant.[1c,6] Toward this end, the norcembranoid diterpenes remains a largely unexplored class of biologically active natural products.[7] Included within this natural product family is the compact and highly oxygenated antileukemic and antitumor ineleganolide (**9**)[8] as well as the closely related norcembranoid diterpenes horiolide (**20**),[9] kavaranolide (**21**),[10] sinulochmodin C (**10**),[11]

scabrolide B (**23**),[12] scabrolide A (**24**),[12] and yonarolide (**25**, Figure 3.1.1).[13] The total synthesis of any member of these polycyclic furanobutenolide norcembranoids has not been accomplished to date, although the syntheses of select members have been investigated[14] and the biomimetic semisynthesis of ineleganolide (**9**) and sinulochmodin C (**10**) has been disclosed.[15]

Figure 3.1.1. Polycyclic Furanobutenolide Norcembranoid Diterpenes

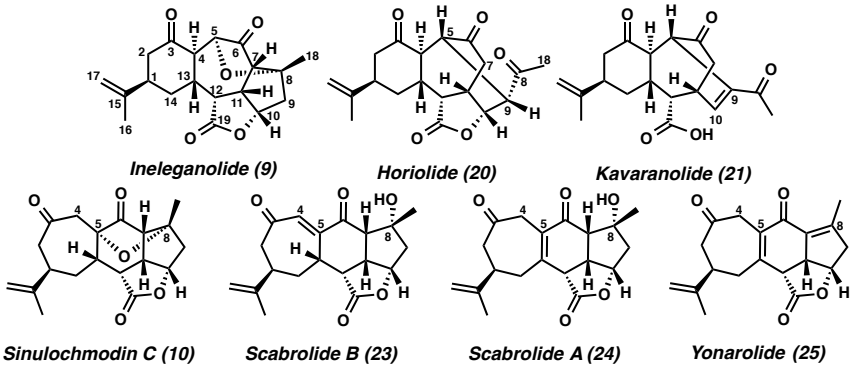

It has been proposed that ineleganolide (**9**) and sinulochmodin C (**10**) are the biosynthetic precursors to the other related polycyclic [6,7]- and [7,6]-fused norcembranoid diterpenes, respectively.[7a,b,10] Ineleganolide is believed to undergo a retro-oxa-Michael addition followed by a retroaldol cyclization to furnish intermediate triketone **39** (Scheme 3.1.1). Although ketone **39** has not been isolated, it is the postulated biosynthetic precursor of horiolide (**20**), undergoing an intramolecular Michael addition with the vinylogous diketone moiety to construct the transannular C–C bond. Horiolide (**20**) would then undergo a β-acetoxy elimination from the methyl ketone moiety to furnish kavaranolide (**21**).

*Scheme 3.1.1. Postulated Biosynthetic Conversion of Ineleganolide (**9**) to Kavaranolide (**21**)*

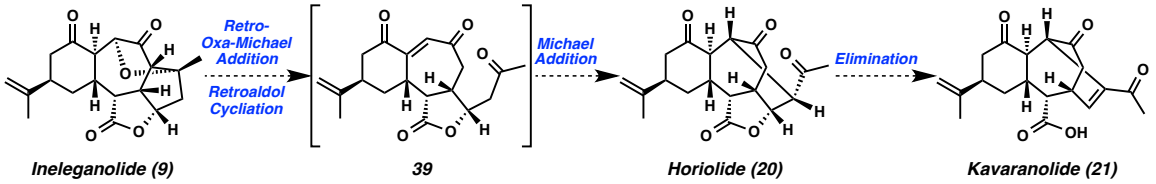

Sinulochmodin C (**10**), the constitutional isomer of ineleganolide (**9**), is the postulated biosynthetic precursor to each of the other related [7,6]-fused norcembranoid diterpenes furnishing scabrolide B (**23**) after undergoing a retro-oxa-Michael addition (Scheme 3.1.2). Olefin isomerization of vinylogous diketone **23** would furnish the tetrasubstitued enone scabrolide A (**24**). Finally, dehydration of tertiary alcohol **24** would afford bisenone yonarolide (**25**).

Scheme 3.1.2. Postulated Biosynthetic and Proposed Synthetic Relationship of [7,6]-Norcembranoids

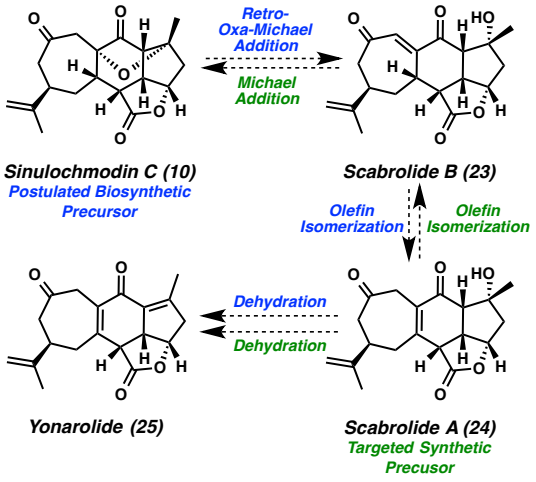

We were drawn to the unique furanobutenolide scaffold of these norcembranoid diterpenes and the challenge of designing a convergent synthetic pathway toward complex late-stage polycyclic intermediates from which divergent access to each of these six closely related natural products could be achieved. The synthesis would require careful design of redox manipulation, substrate-controlled diastereoselective

transformations, and intramolecular rearrangements to provide enantioselective synthetic access to these highly oxygenated, cycloheptanone-derived polycycles. Successful development of such a synthetic route would enable the thorough exploration of the biological activity of these largely untested members of the known antitumor and antileukimia norcembranoid diterpene natural product family. We targeted ineleganolide (**9**) and scabrolide A (**24**) as the intermediates through which we could access the remaining furanobutenolide norcembranoid diterpenes.

3.2 Retrosynthetic Analysis

Synthetic access to furanobutenolide norcembranoid diterpenes **20**, **21**, and **23**–**25** could be achieved through either ineleganolide (**9**) or scabrolide A (**24**) in a divergent fashion from a common, late-stage synthetic intermediate **314** (Scheme 3.2.1). Retrosynthetically, completion of the asymmetric total synthesis of ineleganolide (**9**) would be achieved by the olefin isomerization of enone **313** followed by intramolecular oxa-Michael addition (Scheme 3.2.1.A). Unsaturated diketone **313** could by synthesized after the selective dehydration of common intermediate diol **314**.

*Scheme 3.2.1. Retrosynthetic Analysis of Ineleganolide (**9**) and Scabrolide A (**24**)*

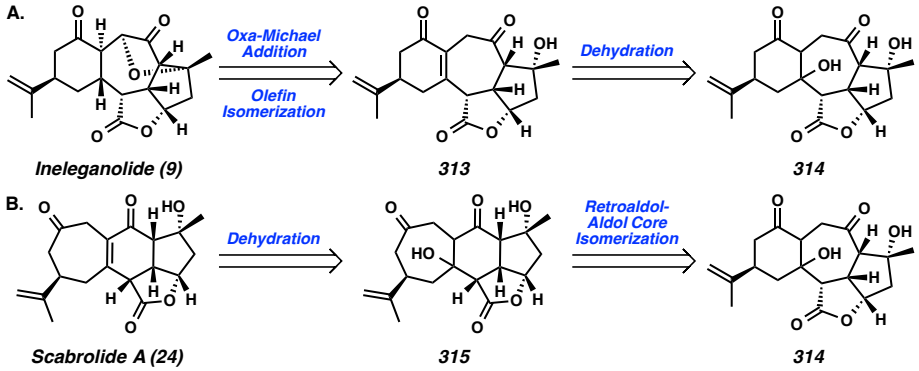

The enantioselective construction of scabrolide A (**24**) would be achieved through a synthetic method inspired by the biosynthetic formation of the polycyclic

furanobutenolide norcembranoids (**9**, **10**, **20**, **21**, **23–25**) from a common macrocyclic precursor through a sequential anionic cyclization cascade.[7a,b,15] Scabrolide A (**24**) would be accessed by dehydration of diol **315** (Scheme 3.2.1.B). Synthesis of [7,6,5,5]-tetracyclic diol **315** would require a carbocyclic core isomerization from common intermediate diol **314**. We envision accomplishing this transformation directly from [6,7,5,5]-tetracyclic diol **314** by a biosynthesis-inspired tandem retroaldol-aldol cyclization.

These divergent syntheses from [6,7,5,5]-tetracyclic diol **314** would be enabled by the concise, convergent enantioselective synthesis of the [6,7,5,5]-tetracyclic scaffold of ineleganolide (Scheme 3.2.2). Access to diol **314** would be achieved by selective olefin hydration of α,β-unsaturated lactone **316**. Diketone **316** would be constructed by the isomerization of epoxide **317** via *syn*-facial 1,2-hydride shift. Pentacycle **317** would be synthesized in a stereoselective fashion by hydroxyl-directed epoxidation of allylic alcohol **318**. Construction of the central cycloheptadiene within tetracycle **318** would be accomplished by the Cope rearrangement of divinylcyclopropane **319**, which would be synthesized by the intramolecular cyclopropanation of α-diazoester **320**. Cyclization precursor **320** would be assembled in a convergent fashion by the coupling of carboxylic acid **321** and 1,3-*cis*-cyclopentenediol **322**. Acid **321** is rapidly constructed from (*S*)-(+)-carvone. Consequently, our initial synthetic efforts focused on the construction of enantioenriched cyclopentenediol **322**.

Scheme 3.2.2. Retrosynthetic Analysis of Divergent Tetracyclic Diol ***314***

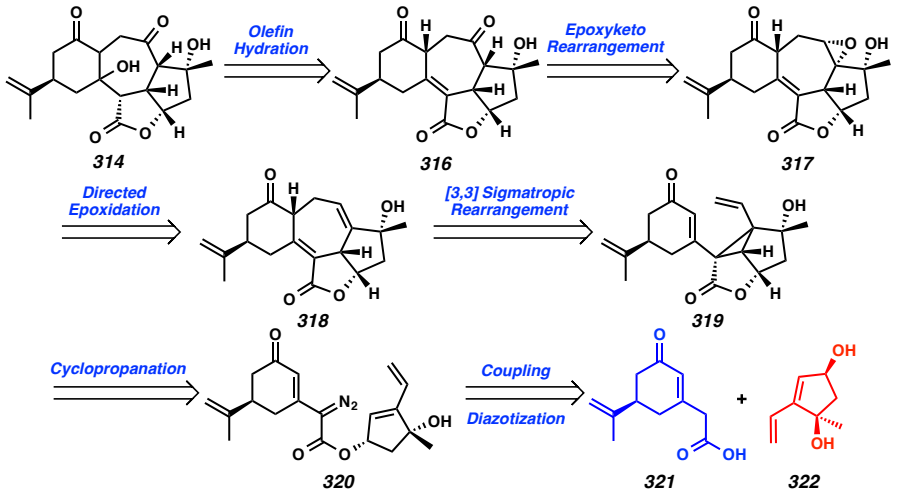

3.3 Enantioselective Construction of Cyclopentenediol Building Block

Enantioselective synthesis of the targeted polycyclic norcembranoid diterpene natural products requires the enantioselective construction of the common 1,3-*cis*-cyclopentenediol building block **322**. The isopropenyl stereocenter introduced from the chiral pool by the derivatization of the complimentary enantiomer of carvone to acid **321**. However, the remaining chiral information within each natural product will be relayed from the two stereocenters in this highly oxygenated cyclopentene. Thus, a highly enantioselective bond forming reaction is a compulsory feature of our route.

Previously, our group had disclosed the development of the enantioselective synthesis of a functionalized hydroxymethyl-1,3-*cis*-cyclopentenediol synthetic building block.[16] Selective formation of tetrasubstituted silyl enol ether **257** was accomplished in six steps from cyclohexanone dimethyl ketal (**269**) and amino alcohol hydrogen chloride salt **270** (Scheme 3.3.1). Intermolecular asymmetric palladium-catalyzed allylic alkylation of bicyclic enol ether **257** using chloroallylmesylate **258** as the external electrophile employing (*S*)-*t*-BuPhox (**263**), the more readily available enantiomer of the

chiral ligand, furnished (*S*)-chloroallylketone **258** in 82% yield and 92% ee.[17] For the purposes of synthetic development, (*S*)-chloroallylketone **258** was used as an intermediate in the opposite enantiomeric series from the natural occurring norcembranoid diterpenes. The synthesis of the enantiomerically matched norcembranoid diterpenes may be subsequently achieved using (*R*)-*t*-BuPhox[18] as well as Phox ligands derived (*R*)-valine, which have been shown to be comparably effective for the enantioselective formation of ketone **258**.[19]

Scheme 3.3.1. Synthesis of Hydroxymethyl-1,3-cis-cyclopentenediol Building Block

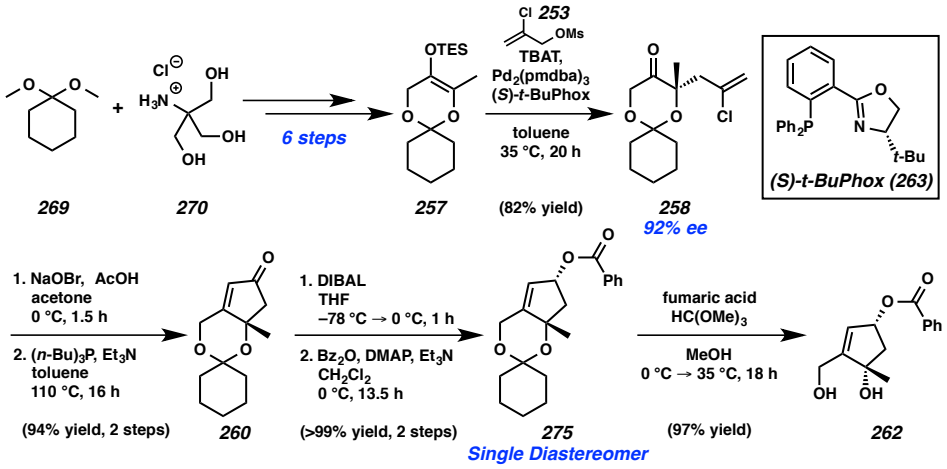

Advancement of chloroallylketone **258** through oxidative α-bromoketone formation and subsequent intramolecular Wittig olefination provided cyclopentenone **260** in 94% yield over two steps. Diastereoselective 1,2-reduction of enone **260** followed by benzoylation of the resultant secondary alcohol furnished allylic ester **275** in quantitative yield over two steps as a single diastereomer. Cleavage of the cyclohexyl ketal revealed primary alcohol **262** in 97% yield as the hydroxymethyl-1,3-*cis*-cyclopentenediol building block.

3.4 Synthesis of the Norcembranoid Diterpene Carbocyclic Core

Hydroxymethylcyclopentene **262** could then be advanced toward the norcembranoid diterpenes natural products beginning with oxidation of the primary alcohol with Dess–Martin periodinane (DMP, Scheme 3.4.1.A). Methylenation of the intermediate aldehyde and ultimate saponification of the benzoyl ester revealed the requisite diol fragment common to the norcembranoid diterpene natural product family (***ent*-322**) in 85% yield over three steps.

Scheme 3.4.1. Completion of Coupling Partners

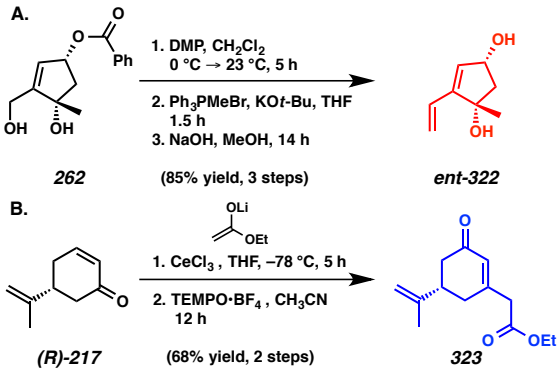

Synthesis of the complimentary coupling partner required for the synthesis of the enantiomeric norcembranoid diterpenes began with (*R*)-(–)-desmethylcarvone (**(*R*)-217**), which is available by a known procedure from (*R*)-(–) carvone.[20] Cerium-mediated 1,2-addition of the preformed lithium enolate of ethyl acetate into enone **(*R*)-217** followed by a 1,3-oxidative allylic transposition[21] provided ester **323** in 68% yield over two steps (Scheme 3.4.1.B).

Saponification of ethyl ester **323** provided acid coupling partner ***ent*-321** (Scheme 3.4.2). Coupling of crude acid ***ent*-321** and diol ***ent*-322** was accomplished using EDC•HCl with catalytic DMAP, requiring nearly a two-fold excess of acid ***ent*-321** to drive the reaction to completion relative to diol ***ent*-322**. Diazo transfer onto the

intermediate ester product using *p*-ABSA furnished α-diazoester ***ent*-320** in 75% yield from diol ***ent*-322**.

Scheme 3.4.2. Fragment Coupling and Synthesis of Cyclopropanation Precursor

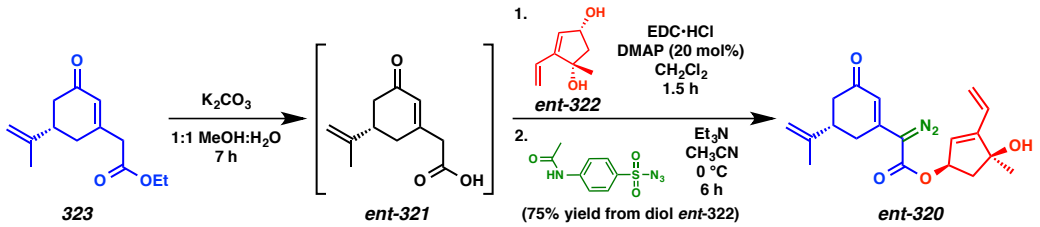

With α-diazoester ***ent*-320** in hand, we began investigating the potential to accomplish a chemoselective intramolecular cyclopropanation. Gratifyingly, exposure of diazo ***ent*-320** to 1 mol % Rh_2OAc_4 in dichloromethane at ambient temperature enabled a tandem cyclopropanation-Cope rearrangement cascade, furnishing cycloheptadiene **324** in 53% yield after in situ olefin isomerization from the unsaturated lactone ***ent*-318** to the corresponding tetrasubstituted enone (Scheme 3.4.3).[22] We were pleased to find diene **324** was a crystalline solid and its relative configuration was unambiguously established by single crystal X-ray diffraction (Figure 3.4.1), confirming the stereocenters at C(11) and C(12) were set as required for the norcembranoid diterpenes natural products and revealing the creased conformation of the central heptacycle.

*Scheme 3.4.3. Construction of Tetracycle **324** by Tandem Cyclopropanation-Cope Rearrangement*

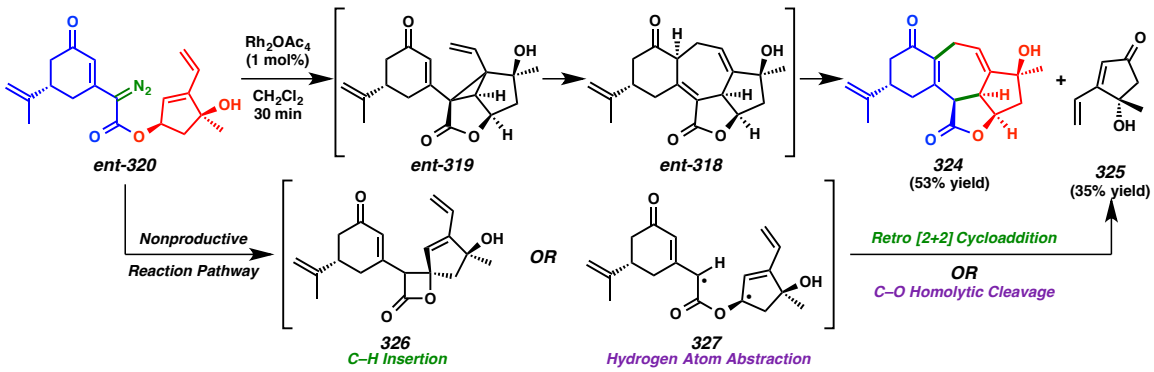

Figure 3.4.1. Three-Dimensional Structure of Diene ***324***

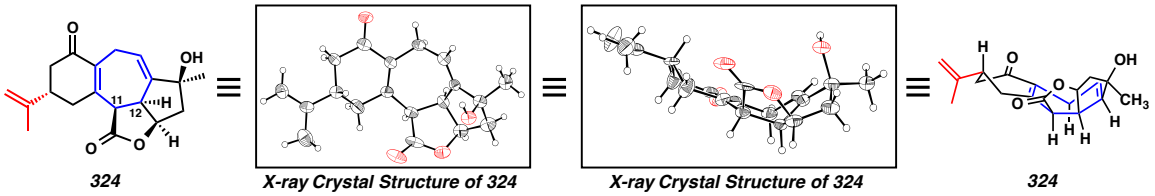

The only other product observed from this transformation is extended enone **325**, which was isolated in 35% yield. Despite our efforts to optimize this transformation further, screening a variety of rhodium catalysts as well as reaction conditions, we were never able to improve the ratio between desired tetracycle **324** and cyclopentenone byproduct **325**.[23] We hypothesize that the nonproductive reaction pathway proceeds from the metal carbenoid of α-diazoester ***ent*-320** through C–H insertion at or hydrogen abstraction from the allylic position of the cyclopentene fragment to furnish either intermediate β-lactone **326** or separated diradical **327**, respectively. Ultimately, retro-ketene [2+2]-cycloaddition from heterocycle **326** or radical recombination by homolytic cleavage of the ester C–O single bond within diradical **327** would furnish cyclopentenone **325**.

Enone byproduct **325** could be recycled through a diastereoselective 1,2-reduction with DIBAL at low temperature to provide *cis*-1,3-cyclopentenediol ***ent*-322**, albeit in low yield (Scheme 3.4.4). The unsatisfactory yield of this transformation is likely due to coordination of the product to the byproduct aluminum salts, preventing extraction of diol ***ent*-322** from the aqueous layer during purification. Other hydride sources like $NaBH_4$ and L-Selectride® failed to accomplish the reduction of enone **325** in a stereoselective fashion.

*Scheme 3.4.4. Diastereoselective 1,2-Reduction of Enone Byproduct **325***

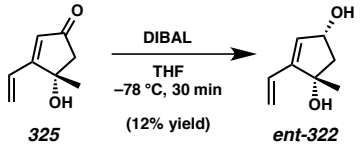

3.5 Synthetic Advancement Toward *ent*-Ineleganolide

Nevertheless, we were please to have efficient and convergent synthetic access to the tetracyclic carbocyclic core of the norcembranoid diterpenes and began advancing toward the targeted natural products. Hydroxyl-directed epoxidation of allylic alcohol **324** was accomplished in 85% yield using catalytic $VO(acac)_2$ (Scheme 3.5.1). Epoxytetracycle **328** was found to be a crystalline white solid and its configuration was unambiguously established by single crystal X-ray diffraction, confirming the success of the diastereoselective and chemoselective directed epoxidation. Considering examples of successful epoxyketo rearrangements in the presence of free hydroxyl groups are extremely rare in the literature,[24] conditions for the protection tertiary alcohol **328** were developed, affording silyl ether **329** in excellent yield at low temperature.

*Scheme 3.5.1. Advancement of Diene **324** and Formation of Isoineleganolide A (**328**)*

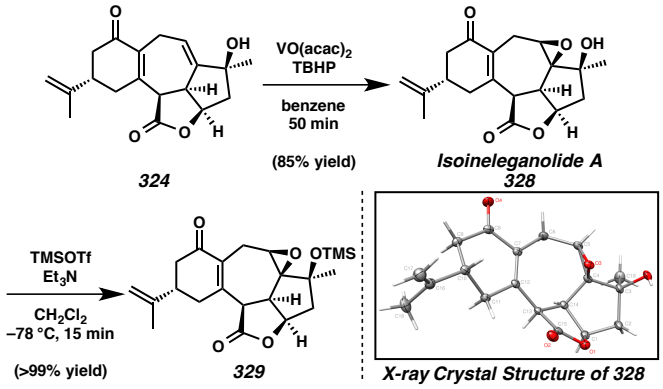

With two substrates in hand (**328** and **329**), we began screening reaction conditions known to effect epoxyketo rearrangements in the literature including reaction manifolds

mediated by protic acid, aprotic base, and, most commonly, Lewis acids.[24,25] We hypothesized that epoxide **328** would undergo epoxyketo rearrangement to not only furnish the necessary 1,4-diketone pattern required for the norcembranoid diterpenes, but would result in an equilibrium mixture of enone ***ent*-313** and vinylogous diketone **330** (Scheme 3.5.2). Intramolecular oxa-Michael addition of tertiary alcohol **330** into the vinylogous diketone system would then form the expected thermodynamically favored natural product ***ent*-9**, driving the equilibrium mixture toward vinylogous diketone and thus *ent*-ineleganolide. Unfortunately, even under the most commonly employed conditions in the literature using magnesium(II)-, aluminum (III)-, and boron-based Lewis acids, both epoxytetracycle **328** and silyl ether derivative **329** proved largely unreactive or simply decomposed.[26]

Scheme 3.5.2. Hypothesized Completion of Ineleganolide

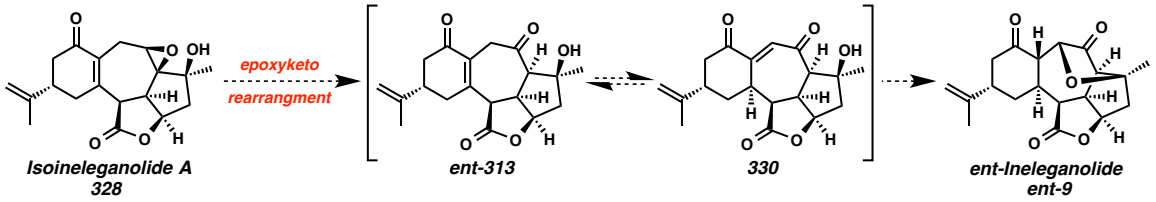

The only productive reactivity observed for either epoxytetracycle **328** or **329** was the isomerization of epoxyalcohol **328** to oxetane **331** using stoichiometric indium(III) triflate (Scheme 3.5.3). Bridged ether **331** is another isomeric form of *ent*-ineleganolide (***ent*-9**), although we did not envision isoineleganolide B (**331**) as immediately useful for completion of the asymmetric for either *ent*-ineleganolide or the remaining members of the norcembranoid diterpene natural product family.

*Scheme 3.5.3. Isomerization of Isoineleganolide A (**328**) to Isoineleganolide B (**331**)*

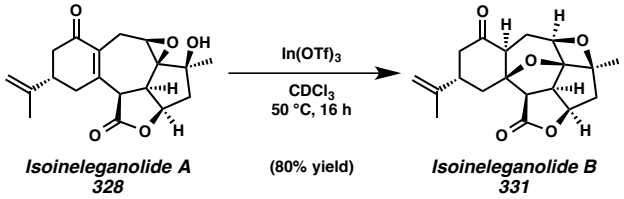

3.6 Alternative Retrosynthetic Strategy

In light of the difficulty encountered installing the transannular 1,4-dicarbonyl oxidation pattern that characterizes the norcembranoid diterpene natural product family from epoxytetracycle **328**, we reevaluated our synthetic strategy. Access to planned divergent intermediate **314** would be achieved by deprotection of enol ether **332** followed by olefin hydration of the unsaturated lactone moiety (Scheme 3.6.1). Construction of tetracyclic core **332** would be accomplished through an analogous Cope rearrangement from cyclopropane **333** that would be formed in turn after the intramolecular cyclopropanation of α-diazoester **334**. Cyclization precursor **334** would be assembled by the coupling carboxylic acid **321** with methyl ketone **335**.

*Scheme 3.6.1. Alternative Retrosynthetic Disconnection of Divergent Intermediate **314***

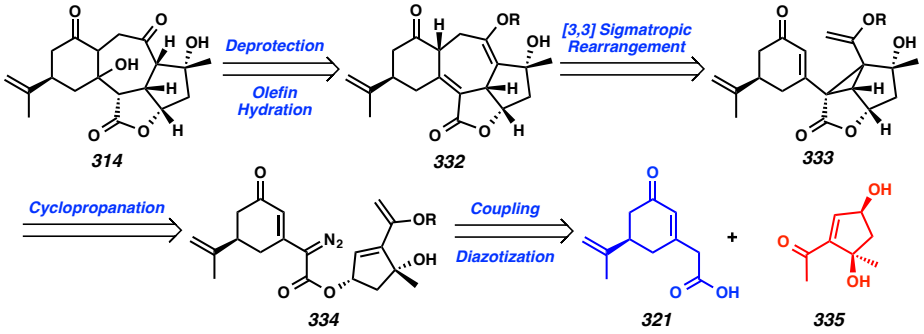

Having previously established synthetic access to acid ***ent*-321**, we turned our attention to the modification of the 1,3-cyclopentenediol synthetic route toward the complimentary methyl ketone ***ent*-335**. Diastereoselective reduction of cyclopentenone

260, silylation of the intermediate alcohol using TBSOTf, and removal of the cyclohexyl ketal under fumaric acid-mediated transketalization conditions furnished silyl ether **336** in 83% yield over three steps as a single diastereomer (Scheme 3.6.2). Oxidation of primary alcohol **336** with DMP to the intermediate aldehyde followed by the 1,2-addition of a methyl substituent into the enal system provided secondary alcohol **337** as a 1 to 1 mixture of diastereomers. This mixture of diastereomers is inconsequential as the allylic oxidation of the diastereomeric mixture of alcohol **337** furnished methyl ketone **338** in 89% yield.

*Scheme 3.6.2. Construction of Methyl Ketone **338***

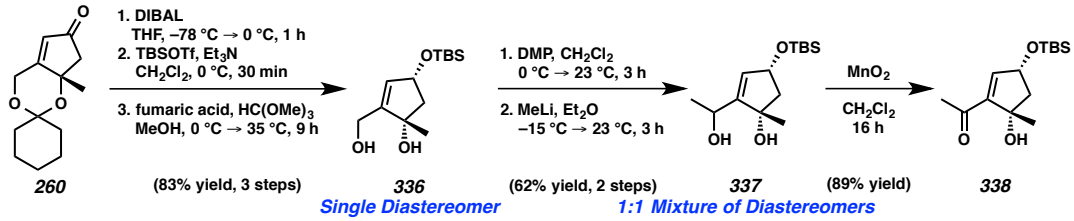

We next needed to convert methyl ketone into the corresponding enol ether for use in the desired Cope rearrangement. Unfortunately, all attempts to form a stable enol ether that would be orthogonal to the deprotection conditions needed for the requisite removal of the secondary TBS ether were unsuccessful (Scheme 3.6.3.A).[27] Alternatively, we reasoned that the formation of the enol ether from the methyl ketone moiety could be accomplished at a later stage. Thus, enone **339** was advanced by deprotection of the silyl ether using TBAF at ambient temperature for afford diol ***ent*-335** in 98% yield (Scheme 3.6.3.B).

Scheme 3.6.3. Advancement of Silyl Ether ***338***

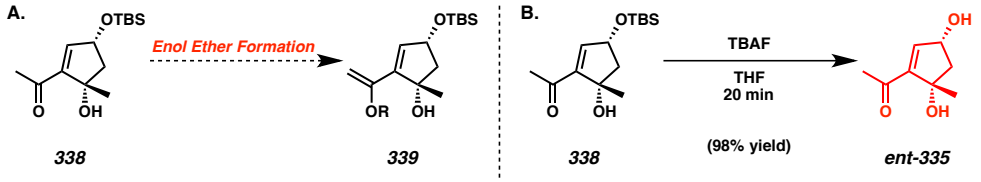

Saponification of ethyl ester **323** again revealed coupling partner ***ent*-321** (Scheme 3.6.4). Esterification of crude acid ***ent*-321** with diol ***ent*-335** was accomplished using catalytic DMAP in the presence of EDC•HCl, again requiring a 2-fold excess of acid ***ent*-321** to drive the reaction to completion relative to diol ***ent*-335**. Diazo transfer onto the intermediate ester product using *p*-ABSA furnished α-diazoester **340** in 65% yield from diol ***ent*-335**.

Scheme 3.6.4. Fragment Coupling with Methyl Ketone Diol ***ent-335***

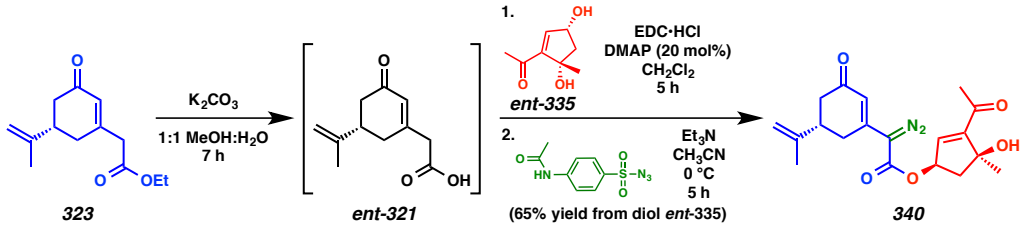

With α-diazoester **340** in hand, we sought to form the enol ether from the methyl ketone moiety and subsequently accomplish a tandem cyclopropanation-Cope rearrangement. Exposure of diazo **340** to a variety of base-mediated silyl enol ether forming conditions generated light sensitive, neon orange intermediates that quickly decomposed in the presence of silica or as neat crude oils. Exposure of diazoester **340** to TBSOTf and Et_3N at 0°C in the dark followed by immediate filtration through Florisil® and dilution of the crude oil with dichloromethane and the addition of catalytic $Rh_2(OAc)_4$ provided pyrazole **341** as the sole product in 38% yield over two steps (Scheme 3.6.5).

*Scheme 3.6.5. Formation of Pyrazole **341***

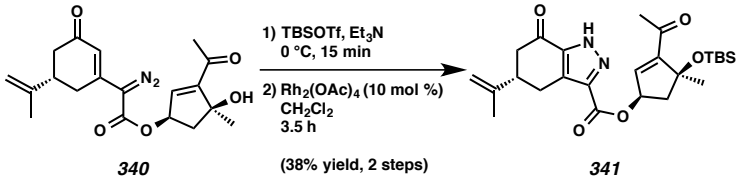

Without success in accomplishing the tandem cyclopropanation-Cope rearrangement, we began exploring the potential to accomplish the synthesis of the central heptacycle in a stepwise fashion. Intramolecular cyclopropanation of α-diazoester **340** onto the olefin of the enone system to access cyclopropane **342** proved somewhat challenging (Scheme 3.6.6.). While rhodium(II) dimers including $Rh_2(OAc)_4$ and $Rh_2(CF_3CO_2)_4$ were ineffective catalysts for the desired intramolecular cyclization, we were pleased to find that $Cu(tbs)_2$ (**343**) was able to catalyze the desired transformation, albeit in low yield over an extended reaction period.

*Scheme 3.6.6. Attempted Stepwise Formation of **ent-316** from Diazoester **340***

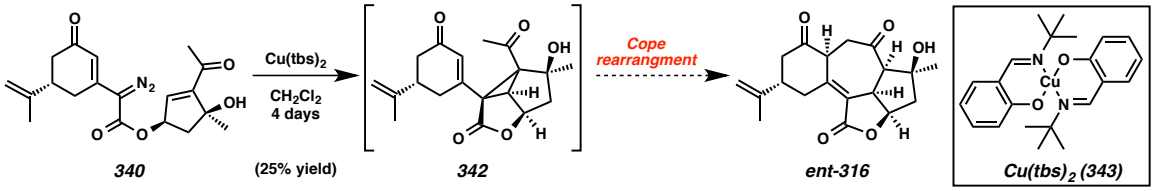

With cyclopropane in hand, we next needed to induce the Cope rearrangement to access ***ent*-316**. Unfortunately, formation of the silyl enol ether of methyl ketone **342** was unsuccessful as the TMS, TES, or TBS enol ethers using reaction conditions mediated by either weak ((*i*-Pr)$_2$NEt, Et_3N) or strong (LDA, LHMDS) bases. Additionally, the anionic 2-oxa-Cope rearrangement failed to proceed after subjecting cyclopropane **342** to LDA or LHMDS at –78 °C and warming to ambient temperature, only resulting in decomposition of the cyclopropane starting material.[28] Without a way to construct the desired [6,7,5,5]-tetracyclic core of the norcembranoid diterpenes

employing substrates derived from methyl ketone analog diol ***ent*-335**, we returned to our initial route to explore alternative methods for the advancement of our previously isolated epoxytetracycle **328** toward the norcembranoid diterpenes natural products.

3.7 Redox Advancement Toward *ent*-Ineleganolide

Although all attempts to effect the epoxyketo rearrangement of isoineleganolide A (**328**) to provide *ent*-ineleganolide (***ent*-9**) or any 1,4-diketone product had failed (Scheme 3.7.1), we sought to more thoroughly explore the reactivity of epoxide **328**. Having encountered the productive rearrangement of epoxytetracycle **328** to oxetane **331** (see Scheme 3.5.3), we set about characterizing the reactivity of epoxide **328** in the presence of indium(III) triflate on larger scale. To our surprised, simply switching the solvent from unstabilized $CDCl_3$ to $CHCl_3$, stabilized with 0.75% EtOH, caused oxetane **331** become a minor product (Scheme 3.7.2). Instead, ether **344** became the major product and was isolated in 70% yield,[29] with cycloheptatriene **345** as a third, minor product. Given the apparent propensity of the epoxide moiety within isoineleganolide A (**328**) to undergo nucleophilic opening at the least hindered position, we began exploring the potential to exploit this reactivity for the synthesis of the norcembranoid diterpenes natural products.

*Scheme 3.7.1. Originally Hypothesized Completion of ent-Ineleganolide (**ent-9**)*

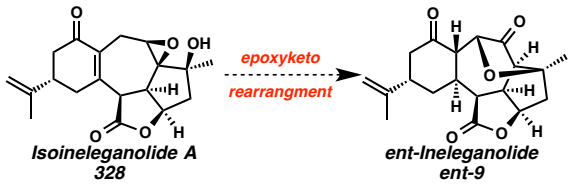

*Scheme 3.7.2. Reactivity of Isoineleganolide A (**328**) with $In(OTF)_3$ in Stabilized $CHCl_3$*

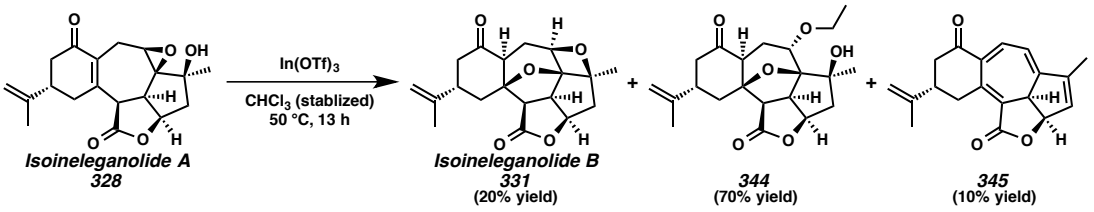

We quickly discovered that halogenated Lewis acids in nonpolar solvent systems containing a small amount to Lewis basic cosolvent could facilitate the opening of epoxide **328** with their halogen counterions.[30] Under optimized conditions, in a 4 to 1 mixture of toluene to THF, magnesium(II) bromide could accomplish the formation of furanopentacycle **346** in quantitative yield (Scheme 3.7.3.A). Bromide **346** proved to be a crystalline white solid whose relative and absolute configuration was unambiguously established by single crystal X-ray diffraction, proving not only the stereochemical result of the expected S_n2 opening of the epoxide, but also the concomitant intramolecular oxa-Michael addition and construction of the transannular ether bridge.

Scheme 3.7.3. Formation of Requisite 1,4-Diketone Oxidation Pattern

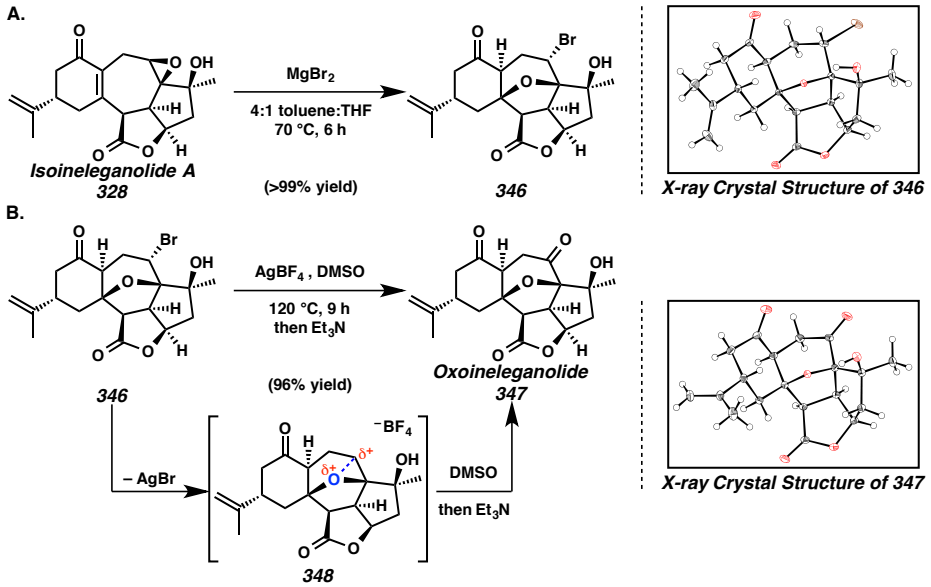

Installation of the requisite 1,4-diketone oxidation pattern from bromide **346** would depend on the ability to oxidize the newly installed secondary halide. The Kornblum oxidation is most routinely used for the oxidation of a halide to the ketone oxidation state, however this transformation is largely limited to the oxidation of primary or benzylic halides to the corresponding aldehydes or benzylic ketone.[31] Fortunately, initial attempts to oxidize bromide **346** proved fruitful.[32] Under optimized reaction conditions employing $AgBF_4$ in DMSO at 120 °C for 9 hours provided diketone **347** in 96% yield; this high yield exemplifies the thermodynamic stability of the product, being formed under harsh, Lewis acidic conditions in the presence of a nucleophilic solvent (Scheme 3.7.3.B). The stereochemical assignment of ketofuran **347** was unambiguously confirmed by single crystal X-ray diffraction.

We hypothesize that the oxidation of secondary bromide **346** to ketone **347** is facilitated by the fused heterocyclic ring structure of the central furan. The reaction proceeds initially by abstraction of the halide by the silver(I) salt to generate intermediate carbocation **348**. The ridged conformation of pentacycle **348** positions the furyl oxygen bridge appropriately to allow for the donation of electron density into the vacant p-orbital of the secondary carbocation. The stabilization of cation **348** by distribution of the positive charge largely prevents nonproductive reaction pathways and decomposition, allowing the nucleophilic addition of DMSO to occur smoothly and, after the addition of Et_3N, the formation of the desired product in excellent yield. This hypothesis is supported by the failed Kornblum oxidation of the reduced substrate in which the vicinal hydroxyl group to the bromide cannot form the transannular ether bridge (vide infra).

With the assembly of the desired 1,4-diketone skeleton complete, the selective reductive opening of furan bridge at the α-alkoxyketone bond (C(7), Scheme 3.7.4) was needed. The selective reduction of carbonyls oxidized at the α-position to the corresponding α-saturated carbonyl is routinely accomplished under single electron transfer conditions. We hypothesized that the rapid equilibration of the intermediate radical generated at C(7) under similar conditions would allow for the formation of the thermodynamically favorable *cis*-fused [7,5]-ring juncture. We were pleased to find that freshly formed SmI_2 could accomplish the desired selective reduction to furnish diol **349** in 85% yield.[33] The stereochemical configuration of the newly formed methine was established by single crystal X-ray diffraction of the crystalline hemiketal isomer **350**, confirming the formation of the desired epimer as required for the synthesis of the furanobutenolide norcembranoid natural products. The use of LiCl as an additive was essential for the high yield of this transformation, as the use of either H_2O or HMPA as an additive or the use of SmI_2 without an additive furnished a complex mixture of diol **349** and dehydrated forms of the desired product.

Scheme 3.7.4. Reductive Furan Opening

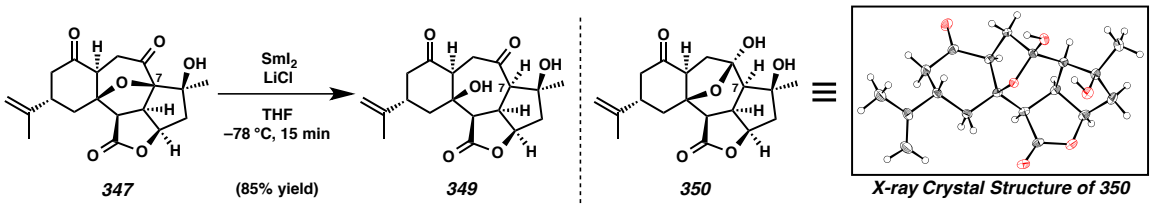

Fortuitously, diol **349** represents a form of the desired retron **316** in the enantiomeric series (see Scheme 3.2.1) for the planned retroaldol-aldol core isomerization to access the [7,6,5,5]-tetracyclic norcembranoid diterpenes (Scheme 3.7.5). Exposure of diol **349** to amine base (e.g., Et_3N, $(i\text{-}Pr)_2NEt$) in protic and aprotic

solvent failed to induce any reactivity. Alternatively, the use of hydroxide bases (e.g., NaOH, KOH) in H_2O or H_2O:MeOH blends resulted in the saponification of the lactone moiety.[34] Although the use of stronger bases (NaH, LHMDS, KHMDS) in THF at low temperature failed to induce any productive reactivity, the exposure of diol **349** to excess LDA at –78 °C effected a retroaldol-aldol pathway, as determined by the isomerization of configuration at C(4) and C(13).[35] Although we have not yet observed the formation of [7,6,5,5]-diol ***ent*-315**, we are optimistic that synthetic access to the [7,6,5,5]-norcembranoid diterpenes may still be achieved by this retroaldol-aldol core isomerization pathway.

*Scheme 3.7.5. Core Isomerization of Divergent Intermediate Diol **349***

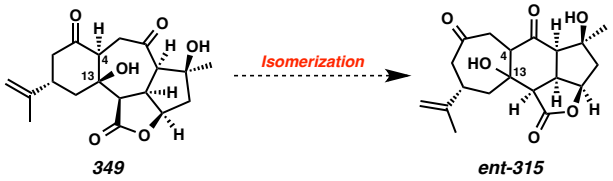

Complimentarily, diol **349** could be advanced toward *ent*-ineleganolide (***ent*-9**). Selective dehydration of tertiary alcohol **349** was achieved in CH_2Cl_2 using the acidic resin Amberlyst 15 (Scheme 3.7.6). Although the product of the desired dehydration (***ent*-313**) is the first to form, the extended reaction period required to accomplish the complete consumption of the starting material results the formation of undesired enone isoineleganolide D (**351**) and bisenone **352** as minor products. We were quite surprised to isolate isoineleganolide C (***ent*-313**) from the reaction mixture as we had expected product ***ent*-313** to spontaneously proceed to *ent*-ineleganolide (***ent*-9**) (see Scheme 3.5.2). Nevertheless, we began exploring reaction conditions to induce the desired isomerization.

Scheme 3.7.6. Selective Dehydration of Diol ***349***

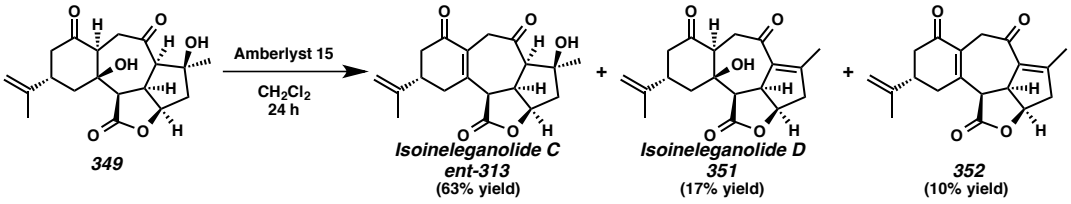

We hypothesized that under olefin isomerization conditions, isoineleganolide C (***ent*-313**) would proceed through vinylogous diketone **330** and then undergo a spontaneous intramolecular oxa-Michael addition to complete the total synthesis of *ent*-ineleganolide (***ent*-9**, Scheme 3.7.7). Unfortunately, isoineleganolide C (***ent*-313**) proved to be a somewhat unstable, intractable intermediate. Exposure of enone ***ent*-313** to protic acid-, protic base-, aprotic base-, and an assortment of transition metal-mediated as well as thermal olefin isomerization conditions failed to provide a single isolable product.[36]

*Scheme 3.7.7. Intended Completion of ent-Ineleganolide (***ent-9***) through Vinylogous Diketone* ***330***

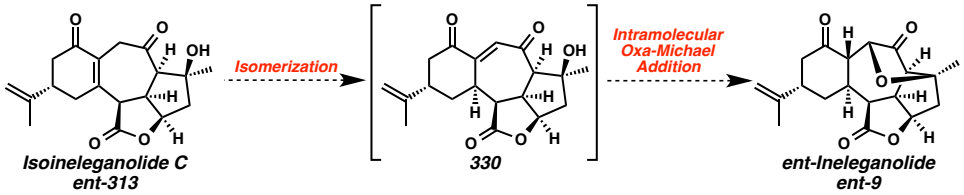

Additionally, redox advancement of isoineleganolide C (***ent*-313**) proved futile. Direct formation of the requisite ketofuran ring by C–H oxidation through α-bromination[37] or under Suárez conditions[38] was complicated by the reactivity of the cyclohexanone system and the isopropenyl moiety under the reaction conditions and ultimately unsuccessful (Scheme 3.7.8). Additionally, cyclohexanone ***ent*-313** was unreactive to the conjugate reduction by the nucleophilic addition of hydride through transition metal catalysis and the 1,4-reduction could not be selectively accomplished using samarium(II) iodide. Comparatively, the isomerization of enone ***ent*-313** could not

be facilitated by the 1,2-reduction of the cyclohexanone system as the selective reduction of the enone carbonyl could not be achieved in the presence of the cycloheptanone.[39]

*Scheme 3.7.8. Attempted Functionalization of Isoineleganolide C (**ent-313**) by C–H Oxidation*

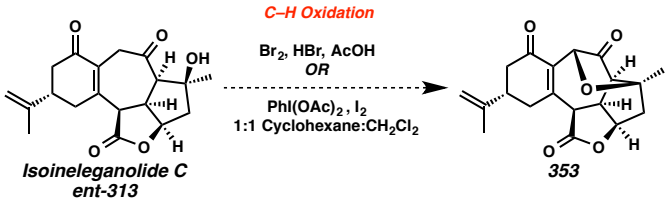

3.8 Computational Studies of Conformational Limitations

The empirical evidence surrounding isoineleganolide C (***ent*-313**) and its obstinate nature suggests the barrier for isomerization of the enone system to the ketofuran ring is a more complex transformation than simply assessing the thermodynamic equilibrium between tetrasubstituted enone ***ent*-313** and trisubstituted vinylogous diketone **330** (see Scheme 3.7.7). In order to assess the conformation of isoineleganolide C (***ent*-313**) in solution, we performed a series of two-dimensional ^{1}H NOE studies. We found that isoineleganolide C (***ent*-313**) in solution adopts a conformation that is highly related to the conformation of isoineleganolide A (**328**) in the solid state as determined by single crystal X-ray diffraction, wherein the central seven-membered ring is creased, bisecting the molecule (Schemes 3.8.1.A and 3.8.1.B). By analogy to the conformation of isoineleganolide A (**328**), the cyclohexanone ring of isoineleganolide C (***ent*-313**) is hypothesized to be in its most thermodynamically stable position when it has adopted a conformation in which the isopropenyl group is in the equatorial position.

Scheme 3.8.1. Consideration of Three-Dimensional Structures of Late-Stage Intermediates

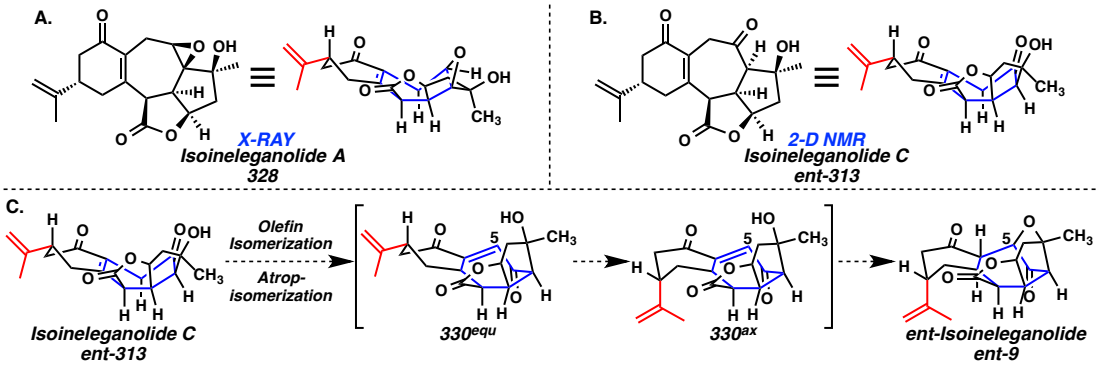

Considering the three-dimensional conformation of isoineleganolide C (***ent*-313**) in comparison to the conformation of *ent*-ineleganolide (***ent*-9**), observed by single crystal X-ray diffraction during the initial isolation,[8] we need to not only effect the isomerization of the olefin from the enone system into vinylogous diketone, but also accomplish the conformational isomerization of the central cycloheptenone ring. This conformational isomerization would induce the proximity between C(5) and the tertiary hydroxyl group required for intramolecular oxa-Michael addition. Ultimate equilibration of the cyclohexanone ring into the chair conformation, placing the isopropenyl group in the axial position, would furnish *ent*-ineleganolide (***ent*-9**) its observed, solid state conformation.

In order to quantitatively assess the energy landscape of the intermediates along the proposed isomerization route toward *ent*-ineleganolide (***ent*-9**) from isoineleganolide C (***ent*-313**), we performed a series of DFT ground state energy computations in vacuo using the 6-311+G** basis set.[40] All ground state energies were compared to the calculated ground state energy of ineleganolide in its preferred conformation (***ent*-9^{ax}**), as determined on its initial isolation by single crystal X-ray diffraction and confirmed herein by calculation of the ground state energies of the two cyclohexanone conformers (i.e.

ent*-9^{ax}** vs. ***ent*-9^{equ}**, Figure 3.8.1). The two conformers of isoineleganolide C in its isolated form, ***ent*-313^{equ}** and ***ent*-313^{ax}**, were calculated to be higher in energy than the natural product ***ent*-9^{ax}** by 0.8 and 2.1 kcal, respectively. This result implies that the most thermodynamically favorable conformation of isoineleganolide C (ent*-313**) is indeed closely related to the structure of isoineleganolide A (see Scheme 3.8.1.A vs. Scheme 3.8.1.B). This places the isopropenyl group of the cyclohexanone ring in the equatorial position in comparison to *ent*-ineleganolide (***ent*-9**), which finds increased thermodynamic stability with the saturated cyclohexanone moiety in the chair conformation, although the isopropenyl substituent is forced into the axial position.

Figure 3.8.1. Free Energy Diagram Based on Computed Ground State Energies

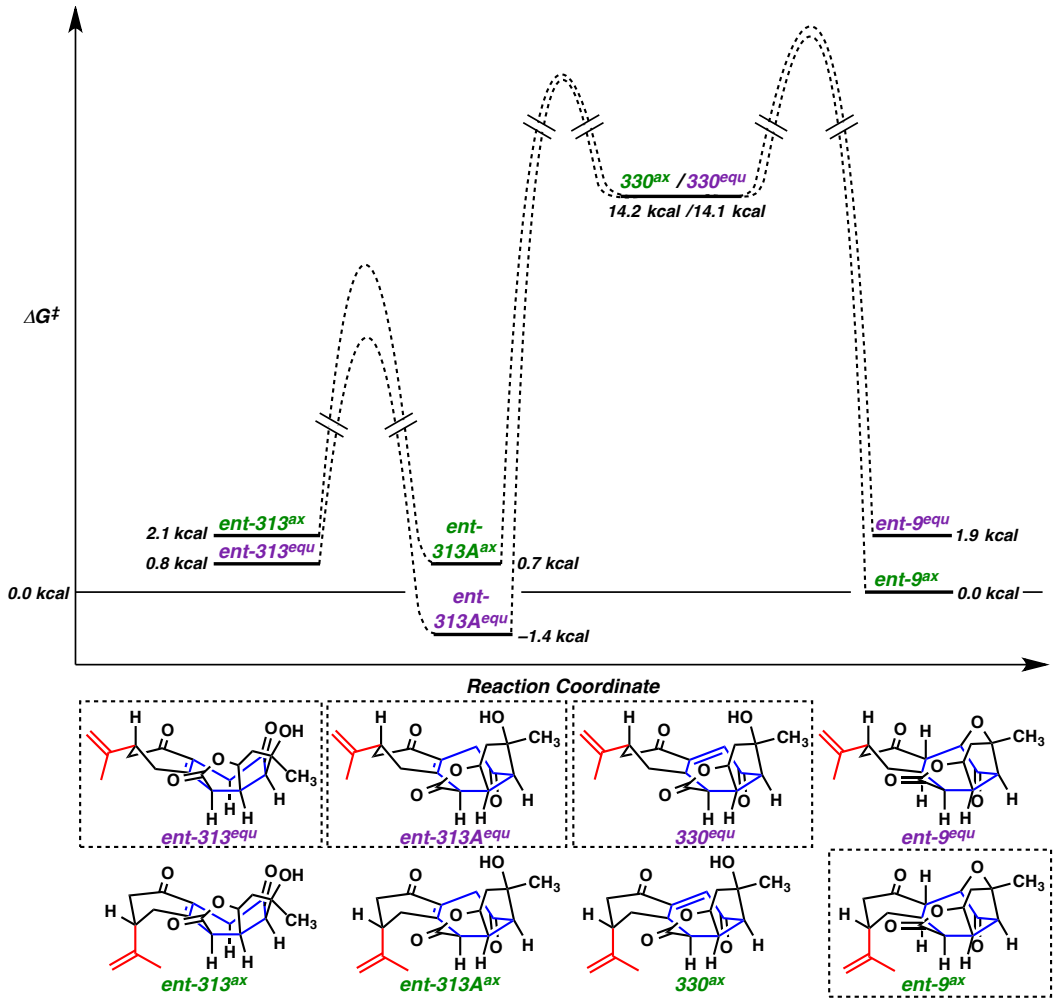

Conformational isomerization of the central heptacycle within ineleganolide C provides two enones, ***ent*-313A^{equ}** and ***ent*-313A^{ax}**, that are both lower in energy than ineleganolide C in its isolated conformation. In fact, ***ent*-313A^{equ}** was calculated to be the most thermodynamically stable compound within the set of isomers evaluated. This conformational isomer closely resembles that of ineleganolide and would be correctly positioned for the construction of the ketofuran ring by oxa-Michael addition after olefin isomerization or directly by C–H oxidation. Unfortunately, the lack of empirical evidence for the isolation of either ***ent*-313A^{equ}** or ***ent*-313A^{ax}** throughout our synthetic explorations and propensity of the isolated ineleganolide C (***ent*-313**) to undergo decomposition rather than productive isomerization or oxidation implies that the energy barrier to interconvert between the atropisomers of isoineleganolide C is greater than the energy required for the decomposition of the substrate.

In order to convert isoineleganolide C to *ent*-ineleganolide (***ent*-9**), we would need to accomplish an olefin isomerization, proceeding through vinylogous diketone **330**. Computation of the ground state energies of the two conformational isomers of conjugated diketone **330^{equ}** and **330^{ax}** reveals that this intermediate is significantly higher in energy than either ineleganolide C or ineleganolide. The energy gap between vinylogous diketone **330** and the highest energy conformation of ineleganolide C is still 12.0 kcal/mol. Considering the activation energy for this isomerization will make the energy cost even larger, decomposition of the substrate would likely occur before the direct conversion of isoineleganolide C (***ent*-313**) to *ent*-ineleganolide (***ent*-9**) by olefin isomerization through vinylogous diketone **330**. Armed with this knowledge, we began

exploring alternative synthetic pathways to complete the asymmetric total synthesis of *ent*-ineleganolide (***ent*-9**).

3.9 Experimental Methods and Analytical Data

3.9.1 Materials and Methods

Unless stated otherwise, reactions were performed at ambient temperature (23 °C) in flame-dried glassware under an argon atmosphere using dry, deoxygentated solvents (distilled or passed over a column of activated alumina)[41] stirring with a Teflon®-coated magnetic stirring bar. Commercially available reagents were used as received unless otherwise noted. Et_3N was distilled from calcium hydride immediately prior to use. MeOH was distilled from magnesium methoxide immediately prior to use. Purified H_2O was obtained using a Barnstead NANOpure Infinity UV/UF system. 4 Å molecular sieves were oven-dried at 120 °C for a minimum of 24 h and cooled in a desiccator to ambient temperature immediately prior to use. (*R*)-Desmethylcarvone (**(*R*)-217**),[20] $Cu(tbs)_2$ (**343**),[42] and TEMPO•BF_4[21] were prepared by known methods. Reactions requiring external heat were modulated to the specified temperatures using an IKAmag temperature controller. Thin-layer chromatography (TLC) was performed using E. Merck silica gel 60 F254 precoated plates (250 nm) and visualized by UV fluorescence quenching, potassium permanganate, or *p*-anisaldehyde staining. Silicycle SiliaFlash P60 Academic Silica gel (particle size 40-63 nm) was used for flash chromatography. ^1H and ^{13}C NMR spectra were recorded on a Varian Inova 600 (600 MHz and 151 MHz, respectively), Varian Inova 500 (500 MHz and 126 MHz, respectively), Bruker AV III HD spectrometer equipped with a Prodigy liquid nitrogen temperature cryoprobe (400 MHz and 101 MHz, respectively), or a Varian Mercury 300 spectrometer (300 MHz and 76 MHz, respectively) and are reported in terms of chemical shift relative to residual $CHCl_3$ (in $CDCl_3$, δ 7.26 and δ 77.16, respectively). Data for ^1H NMR spectra are

reported as follows: chemical shift (δ ppm) (multiplicity, coupling constant (Hz), integration). Infrared (IR) spectra were recorded on a Perkin Elmer Paragon 1000 Spectrometer and are reported in frequency of absorption (cm^{-1}). High resolution mass spectra (HRMS) were acquired using an Agilent 6200 Series TOF mass spectrometer with an Agilent G1978A Multimode source in atmospheric pressure chemical ionization (APCI) or mixed (MultiMode: ESI-APCI) ionization mode or were obtained from the Caltech Mass Spectral Facility using either a JEOL JMS-600H High Resolution Mass Spectrometer in fast atom bombardment (FAB+) or electron ionization (EI+) mode or an LCT Premier XE TOF mass spectrometer equipped with an electrospray ionization source (ES+). Optical rotations were measured on a Jasco P-2000 polarimeter using a 100 mm path length cell at 589 nm.

3.9.2 Experimental Procedures

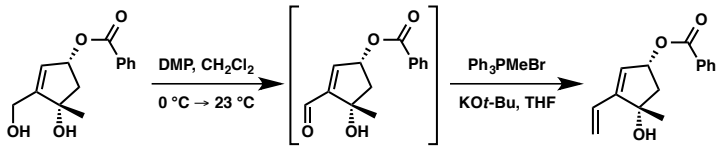

262 *353* *354*

Diene 354: To a pale yellow solution of diol **262** (241 mg, 0.97 mmol, 1.00 equiv) in CH_2Cl_2 (49 mL) at 0 °C (ice/H_2O bath) was added Dess–Martin periodinane (DMP, 823 mg, 1.94 mmol, 2.00 equiv) as a solid in one portion. After 3 h, the off-white heterogeneous reaction mixture was removed from the bath and allowed to warm to ambient temperature (ca. 23 °C). After an additional 2 h, the consumption of starting material was complete as determined by TLC (1:1 EtOAc:Hexanes eluent). The reaction was quenched by the addition of saturated aqueous $Na_2S_2O_3$ (100 mL) in one portion. The

biphasic mixture was allowed to stir for 10 minutes and subsequently poured into saturated $NaHCO_3$ (70 mL). The organics were separated and the aqueous layer was extracted with Et_2O (3 x 70 mL). The combined organic layers were washed with brine (50 mL), dried quickly over $MgSO_4$, filtered, and concentrated in vacuo to provide crude aldehyde **353**, which was immediately used without further purification.

To a round-bottom flask in an N_2-filled glovebox were charged Ph_3PMeBr (1.040 g, 2.91 mmol, 3.00 equiv) and KO*t*-Bu (294 mg, 2.62 mmol, 2.70 equiv) as solids followed by THF (97 mL). The bright yellow reaction mixture was then sealed with a rubber septum, removed from the glovebox, and placed under an argon atmosphere with stirring. After 2 h, a solution of crude aldehyde **353** in THF (3.00 mL) was added dropwise, causing the reaction mixture to become dark orange-brown. After 1.5 h, the consumption of starting material was complete as determined by TLC (3:7 EtOAc:Hexanes eluent). The reaction was poured onto a mixture of H_2O (90 mL) and Et_2O (30 mL). The organics were separated and the aqueous layer was extracted with Et_2O (3 x 30 mL). The combined organic layers were washed with brine (30 mL), dried over $MgSO_4$, filtered, and concentrated in vacuo. The crude dark brown residue was purified by silica gel column chromatography (40% Et_2O in hexanes eluent) to afford diene **354** (236 mg, >99% yield) as a pale yellow oil: R_f = 0.30 (2:3 Et_2O:Hexanes eluent); ^{1}H NMR ($CDCl_3$, 500 MHz) δ 8.04–7.99 (m, 2H), 7.56–7.51 (m, 1H), 7.41 (dddd, *J* = 7.6, 6.8, 1.5, 0.9 Hz, 2H), 6.35 (ddt, *J* = 17.8, 11.3, 0.7 Hz, 1H), 5.92 (d, *J* = 2.3 Hz, 1H), 5.80 (ddt, *J* = 17.8, 1.5, 0.6 Hz, 1H), 5.75–5.70 (m, 1H), 5.31 (ddd, *J* = 11.4, 1.6, 0.7 Hz, 1H), 2.73 (dd, *J* = 14.0, 7.3 Hz, 1H), 2.26 (dq, *J* = 6.6, 3.9, 3.0 Hz, 1H), 2.16 (ddd, *J* = 14.0, 4.7, 0.7 Hz, 1H), 1.48 (s, 3H); ^{13}C NMR ($CDCl_3$, 126 MHz) δ 166.5,

151.2, 133.1, 130.3, 129.7, 129.1, 128.4, 127.0, 119.2, 81.1, 76.0, 49.3, 26.9; IR (Neat Film, NaCl) 3447, 2973, 1714, 1451, 1355, 1315, 1271, 1177, 1111, 1070, 1026, 954, 858, 712 cm^{-1}; HRMS (APCI) *m/z* calc'd for $C_{15}H_{15}O_2$ $[M–OH]^+$: 227.1067, found 227.1064; $[\alpha]_D^{25.0}$ +126.9° (*c* 3.850, $CHCl_3$).

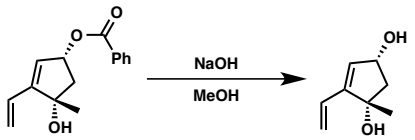

354 ***ent-322***

Diol *ent*-322: To a pale yellow solution of diene **354** (2.04 g, 8.33 mmol, 1.00 equiv) in distilled MeOH (167 mL) was added NaOH (16.7 mmol, 2.00 equiv) as a 0.50 M solution in distilled MeOH quickly dropwise over 5 mintues. After 14 h, the consumption of starting material was complete as determined by TLC (2:3 Et_2O:Hexanes eluent). The reaction was then concentrated to less than one-half of the original volume (ca. 70 mL) and then poured onto H_2O (150 mL). This homogeneous aqueous mixture was then extracted with 1:1 $CHCl_3$:*i*-PrOH (5 x 200 mL). The combined organic layers were dried over Na_2SO_4 for 1 h, filtered, and concentrated in vacuo. The crude off-white solid was then adsorbed onto Celite (6.0 g) and purified by silica gel column chromatography (75% EtOAc in hexanes eluent) to afford diol ***ent*-322** (1.11 g, 85% yield) as an amorphous white solid: R_f = 0.13 (1:5 EtOAc:CH_2Cl_2); ^{1}H NMR (300 MHz, $CDCl_3$) δ 6.30 (dd, *J* = 17.8, 11.3, 1H), 5.82 (d, *J* = 2.1, 1H), 5.73 (dd, *J* = 17.9, 1.7, 1H), 5.26 (dd, *J* = 11.2, 1.7, 1H), 4.65 (dd, *J* = 11.5, 5.1, 1H), 2.54 (dd, *J* = 13.6, 6.8, 1H), 1.85 (app dd, *J* = 13.6, 4.8, 2H), 1.68 (d, *J* = 6.6, 1H), 1.40 (s, 3H); ^{13}C NMR (76 MHz, $CDCl_3$) δ 149.5, 131.3, 129.5, 118.6, 81.3, 73.0, 53.1, 26.8; IR (Neat film, NaCl) 3287, 3252, 2968, 2930, 2873,

1587, 1481, 1445, 1370, 1341, 1316, 1124, 1088, 1056, 1032, 987, 945, 926 cm^{-1}; HRMS (EI+) *m/z* calc'd for $C_8H_{12}O_2$ $[M\bullet]^+$: 140.0837, found 140.0859; $[\alpha]_D^{25.0}$ +73.4° (*c* 0.600, MeOH).

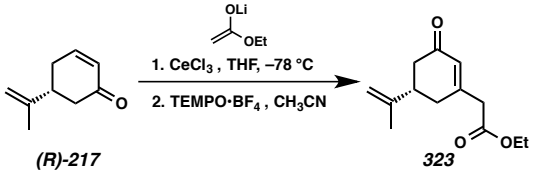

Ethyl Ester 323: To a flame-dried 250 mL round-bottom flask in an nitrogen-filled glovebox was charged anhydrous $CeCl_3$ (3.60 g, 14.6 mmol, 2.00 equiv). The flask was seal with a rubber septum, removed from the glovebox, placed under vacuum, and heated in an oil bath to 140 °C with vigorous stirring.[43] After 12 h the flask was removed from the oil bath, allowed to cool to ambient temperature (ca. 23 °C), placed under an atmosphere of argon, and charged with THF (49 mL). After 3.5 h, the reaction was cooled to –78 °C (*i*-PrOH/dry ice bath). (*R*)-Desmethylcarvone (**(*R*)-217**, 994 mg, 7.30 mmol) was then added as a solution in THF (7.3 mL) and stirred for 1 h. Simultaneously, in a separate flask, to a solution of LDA (0.80 M in THF, 2.22 equiv) at –78 °C was added anhydrous EtOAc (1.47 mL, 15.0 mmol, 2.06 equiv) as a solution in THF (10.0 mL) dropwise. After 40 m, to the solution of **(*R*)-217** was added the EtOAc solution dropwise via cannula transfer with an overpressure of argon over 1 h. Exactly 3 h after the completion of addition, the reaction was quenched at temperature with saturated NH_4Cl (24 mL) and warmed slowly to ambient temperature overnight. The reaction mixture was then filtered through a Celite plug, washing with 100% Et_2O. To the resulting solvent mixture was added H_2O (80 mL) and the aqueous layer was then

extracted with Et_2O (2 x 120 mL). The combined organic layers were washed with brine (60 mL), dried over $MgSO_4$, filtered, and concentrated in vacuo. The resultant crude orange-brown oil (1.64 g, >99% yield) was carried on without further purification.

To a solution of intermediate allylic alcohol (408 mg, 1.82 mmol) in CH_3CN (18 mL) was added TEMPO•BF_4 (664 mg, 2.73 mmol, 1.5 equiv) as a solid in one portion with stirring. Consumption of starting material was complete after 12 h, as determined by TLC (3:2 Et_2O:Hexanes eluent), and the reaction was diluted with Et_2O (125 mL), washed with H_2O (20 mL), brine (20 mL), dried over $MgSO_4$, filtered, and concentrated in vacuo. The crude orange-red oil was purified by silica gel column chromatography (40% Et_2O in hexanes eluent) to afford cyclohexenone ester **323** (275 mg, 68% yield) as an orange-tan oil: R_f = 0.26 (3:2 Et_2O:Hexanes eluent); ^{1}H NMR (500 MHz, $CDCl_3$) δ 5.93 (s, 1H), 4.79 (s, 1H), 4.75 (s, 1H), 4.14 (q, *J* = 7.1 Hz, 2H), 3.22 (s, 2H), 2.68 (ddd, *J* = 18.2, 9.5, 4.5 Hz, 1H), 2.49 (ddd, *J* = 16.3, 3.7, 1.1 Hz, 1H), 2.46–2.33 (m, 2H), 2.33–2.24 (m, 1H), 1.73 (s, 3H), 1.24 (t, *J* = 7.1 Hz, 3H); ^{13}C NMR (126 MHz, $CDCl_3$) δ 199.1, 169.2, 156.3, 146.0, 128.3, 110.8, 61.2, 43.2, 42.0, 41.7, 34.7, 20.4, 14.0; IR (Neat Film, NaCl) 2979, 1735, 1672, 1415, 1369, 1329, 1294, 1248, 1176, 1029, 891 cm^{-1}; HRMS (MM: ESI-APCI) *m/z* calc'd for $C_{13}H_{19}O_3$ $[M+H]^+$: 223.1329, found 223.1326; $[\alpha]_D^{25.0}$ +40.3° (*c* 3.400, $CHCl_3$).

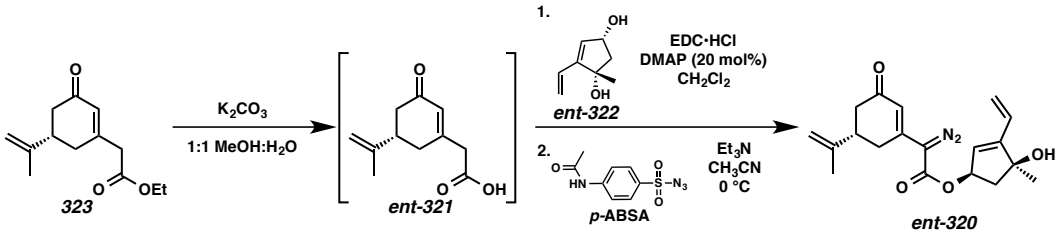

Diazoester *ent*-320: To a stirred solution of ethyl ester **323** (2.07 g, 9.32 mmol, 1.00 equiv) in MeOH (31 mL) and H_2O (31 mL) was added K_2CO_3 (5.16 g, 37.3 mmol, 4.00 equiv). After 7 h, the consumption of starting material was complete as determined by TLC (2:3 Et_2O:Hexanes eluent). The reaction mixture was cooled to 0 °C (ice/H_2O bath) and the pH was adjusted to between 1 and 2 by the careful addition of aqueous 1 N HCl (CAUTION: Vigorous gas evolution!). The reaction mixture was then poured onto a mixture of EtOAc (200 mL) and H_2O (100 mL). The organics were separated and the aqueous layer was extracted with EtOAc (3 x 200 mL). The combined organics were dried over Na_2SO_4, filtered and concentrated in vacuo. The crude dark orange oil of carboxylic acid ***ent*-321** (1.81 g, >99% yield) was carried on without further purification.

To a stirred solution of diol ***ent*-322** (119 mg, 0.85 mmol, 1.00 equiv) in CH_2Cl_2 (28 mL) were added a portion of crude carboxylic acid ***ent*-321** (330 mg, 1.70 mmol, 2.00 equiv) and EDC•HCl (326 mg, 1.70 mmol, 2.00 equiv). The orange reaction mixture was cooled to 0 °C (ice/H_2O bath) at which time DMAP (21 mg, 0.17 mmol, 0.20 equiv) was added in a single portion. After 30 minutes, the dark red-orange reaction mixture was removed from the cooling bath and allowed to warm to ambient temperature (ca. 23 °C). After 1 h, the consumption of starting material was complete as determined by TLC (3:1 EtOAc:Hexanes eluent). The reaction was quenched by the addition of 0.50 N HCl (8.0 mL) quickly dropwise with vigorous stirring. After 10 minutes, the heterogeneous solution was poured onto a mixture of EtOAc (100 mL) and H_2O (40 mL). The organics

were separated and washed with 0.50 N HCl (20 mL) followed by 5 wt % K_2CO_3 (3 x 30 mL), brine (30 mL), and saturated NH_4Cl (30 mL). The organics were then dried over $MgSO_4$, filtered, and concentrated in vacuo. The crude dark brown-orange oil of intermediate ester (269 mg, 0.85 mmol, >99% yield) was carried on without further purification.

Additionally, the combined K_2CO_3 washes were cooled to 0 °C (ice/H_2O bath) and the pH was adjusted to between 1 and 2 by the careful addition of aqueous 1 N HCl (CAUTION: Vigorous gas evolution!). The aqueous mixture was extracted with EtOAc (4 x 50 mL). The combined organics were dried over Na_2SO_4, filtered and concentrated in vacuo providing a recovered portion (60 mg) of excess carboxylic acid ***ent*-321**.

To a solution of crude ester (269 mg, 0.85 mmol, 1.00 equiv) in CH_3CN (8.5 mL) in the dark was added *p*-acetamidobenzenesulfonyl azide (*p*-ABSA, 226 mg, 0.94 mmol, 1.10 equiv) as a solid in one portion. The dark orange homogeneous reaction mixture was cooled to 0 °C (ice/H_2O bath). Et_3N (0.36 mL, 2.55 mmol, 3.00 equiv) was then added slowly dropwise. After 6 h, the consumption of starting material was complete as determined by TLC (1:4 EtOAc:CH_2Cl_2 eluent). The reaction was quenched by the addition of EtOAc (20 mL), removed from the cooling bath, and allowed warm to ambient temperature (ca. 23 °C). The reaction mixture was then concentrated in vacuo. The crude tan solid was the adsorbed onto Celite (2.0 g) and purified by silica gel column chromatography (20% EtOAc in CH_2Cl_2 eluent) to afford diazoester ***ent*-320** (218 mg, 75% yield from diol ***ent*-322**) as a dark yellow oil: R_f = 0.26 (1:4 EtOAc:CH_2Cl_2 eluent); ^{1}H NMR ($CDCl_3$, 600 MHz) δ 6.39 (d, *J* = 2.0 Hz, 1H), 6.32 (dd, *J* = 17.8, 11.4 Hz, 1H), 5.82 (s, 1H), 5.78 (s, 1H), 5.62 (ddd, *J* = 7.2, 4.8, 2.2 Hz, 1H), 5.34 (dd, *J* = 11.4, 1.6 Hz,

1H), 4.86 (t, *J* = 1.4 Hz, 1H), 4.80 (s, 1H), 2.78–2.71 (m, 1H), 2.70–2.64 (m, 2H), 2.53 (ddd, *J* = 16.1, 3.7, 1.4 Hz, 1H), 2.43 (ddd, *J* = 17.4, 10.9, 2.2 Hz, 1H), 2.34 (dd, *J* = 16.3, 13.0 Hz, 1H), 2.05 (dd, *J* = 14.0, 4.8 Hz, 1H), 1.78 (s, 3H), 1.45 (s, 3H); ^{13}C NMR ($CDCl_3$, 126 MHz) δ 197.2, 162.5, 151.7, 146.6, 145.9, 128.9, 126.0, 120.2, 119.6, 111.5, 80.8, 76.9, 67.3, 49.2, 41.8, 41.6, 31.7, 27.1, 20.5; IR (Neat Film, NaCl) 3406, 2971, 2102, 1708, 1645, 1579, 1377, 1328, 1250, 1222, 1140, 1061, 992, 952, 893, 744 cm^{-1}; HRMS (FAB+) *m/z* calc'd for $C_{19}H_{23}O_4N_2$ $[M+H]^+$: 343.1659, found 343.1634; $[\alpha]_D^{25.0}$ +233.5° (*c* 5.470, $CHCl_3$).

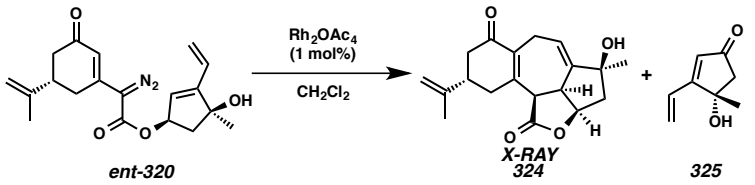

Diene 324 and Enone 325: To a stirred solution of diazoester ***ent*-320** (630 mg, 1.84 mmol, 1.00 equiv) in CH_2Cl_2 (184 mL) in an nitrogen-filled glovebox was added Rh_2OAc_4 (8 mg, 0.018 mmol, 0.01 equiv) at ambient temperature (ca. 30 °C). After 30 minutes, the consumption of starting material was complete as determined by TLC (1:4 EtOAc:CH_2Cl_2 eluent). The reaction mixture was then concentrated in vacuo and the yellow solid was purified by silica gel column chromatography (20% EtOAc in CH_2Cl_2 eluent) to afford diene **324** (306 mg, 53% yield) as a crystalline pale yellow solid and cyclopentenone **325** (89 mg, 35% yield) as an amorphous bright yellow solid.

Diene 324: Colorless, translucent X-ray quality crystals were obtained by slow diffusion of pentane into a solution of diene **324** in Et_2O, mp: 150–153 °C: R_f = 0.38 (1:4 EtOAc:CH_2Cl_2 eluent); ^{1}H NMR ($CDCl_3$, 500 MHz) δ 6.19 (dt, *J* = 8.6, 3.5 Hz, 1H), 4.81

(dd, *J* = 4.5, 3.9 Hz, 1H), 4.76 (td, *J* = 1.4, 0.7 Hz, 1H), 4.67 (td, *J* = 1.3, 0.7 Hz, 1H), 3.83–3.77 (m, 1H), 3.63–3.52 (m, 2H), 3.32–3.21 (m, 1H), 2.74–2.64 (m, 2H), 2.61 (ddd, *J* = 16.5, 4.0, 1.7 Hz, 1H), 2.44 (d, *J* = 15.5 Hz, 1H), 2.29 (dd, *J* = 16.5, 12.6 Hz, 1H), 2.15–2.06 (m, 1H), 1.95 (dd, *J* = 15.4, 4.0 Hz, 1H), 1.71 (dt, *J* = 1.3, 0.6 Hz, 3H), 1.38 (s, 3H); ^{13}C NMR ($CDCl_3$, 126 MHz) δ 198.2, 172.9, 149.2, 148.8, 146.3, 133.5, 128.1, 110.5, 82.2, 78.1, 49.6, 47.0, 45.9, 42.7, 40.0, 36.4, 27.8, 22.6, 20.8; IR (Neat Film, NaCl) 3435, 2923, 2853, 1761, 1661, 1443, 1377, 1263, 1148, 1106 cm^{-1}; HRMS (FAB+) *m/z* calc'd for $C_{19}H_{23}O_4$ $[M+H]^+$: 315.1596, found 315.1608; $[\alpha]_D^{25.0}$ +39.6° (*c* 0.680, $CHCl_3$).

Enone 325: R_f = 0.18 (1:4 EtOAc:CH_2Cl_2 eluent); ^{1}H NMR ($CDCl_3$, 600 MHz) δ 6.59 (dd, *J* = 17.7, 11.2 Hz, 1H), 6.10 (d, *J* = 17.7 Hz, 1H), 6.03 (s, 1H), 5.73 (d, *J* = 11.1 Hz, 1H), 2.62 (d, *J* = 2.3 Hz, 2H), 1.56 (s, 3H); ^{13}C NMR ($CDCl_3$, 126 MHz) δ 205.4, 174.7, 128.5, 127.7, 126.2, 77.1, 53.2, 27.4; IR (Neat Film, NaCl) 3400, 2970, 2927, 1687, 1599, 1408, 1373, 1261, 1233, 1195, 1064, 952, 864, 801 cm^{-1}; HRMS (EI+) *m/z* calc'd for $C_8H_{10}O_2$ $[M\bullet]^+$: 138.0681, found 138.0674; $[\alpha]_D^{25.0}$ +71.4° (*c* 0.900, $CHCl_3$).

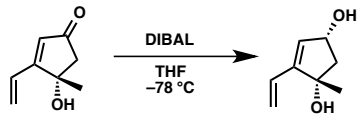

325 ***ent-322***
Single Diastereomer

Diol *ent*-322: To a stirred solution of enone **325** (50 mg, 0.36 mmol, 1.00 equiv) in THF (5.0 mL) at –78 °C (*i*-PrOH/dry ice bath) was added DIBAL (540 μL, 1 M in THF, 1.50 equiv) slowly dropwise. After 30 minutes, the consumption of starting material was complete as determined by TLC (1:4 EtOAc:CH_2Cl_2 eluent). The reaction was quenched

by the addition of $Na_2SO_4•(H_2O)_n$ (made by stirring anhydrous Na_2SO_4 with H_2O for 30 minutes prior to use). The reaction vessel was immediately removed from the cooling bath and allowed to warm to ambient temperature (ca. 23 °C) with stirring. After 15 minutes, the reaction was filtered, concentrated in vacuo, and the crude white solid was purified by silica gel column chromatography (75% EtOAc in hexanes eluent) to afford diol ***ent*-322** (6 mg, 12% yield) as an amorphous white solid and as a single diastereomer: characterization data match those reported above.

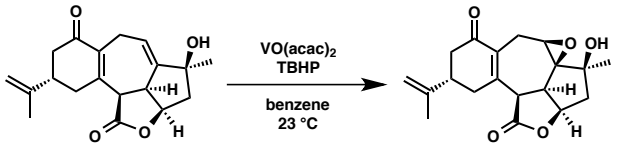

324 *X-RAY Isoineleganolide A 328*

Isoineleganolide A (328): To a pale yellow stirred solution of diene **324** (100 mg, 0.32 mmol, 1.00 equiv) in a vial open to air in benzene (10.7 mL) was added $VO(acac)_2$ (0.9 mg, 0.0032 mmol, 0.01 equiv). After 5 minutes, to this dark green solution was added *t*-butyl hydroperoxide (TBHP, 72 μL, 0.036 mmol, 1.10 equiv) as a 5 M solution in decane dropwise causing the reaction to immediately become deep ruby red. After 45 minutes, the reaction had lost all red color and become pale yellow. The consumption of starting material was complete as determined by TLC (1:4 EtOAc:CH_2Cl_2 eluent). The reaction was concentrated in vacuo and the crude tan solid was purified by silica gel column chromatography (25% EtOAc in CH_2Cl_2 eluent) to afford epoxide **328** (89 mg, 89% yield) as a white crystalline solid. Colorless, translucent X-ray quality crystals were obtained by slow diffusion of 1% benzene in heptane into a solution of epoxide **328** in EtOAc, mp: 272–275 °C: R_f = 0.22 (1:4 EtOAc:CH_2Cl_2 eluent); ^{1}H NMR ($CDCl_3$, 600 MHz) δ 4.84–4.80 (m, 2H), 4.74 (s, 1H), 3.75 (dd, *J* = 19.1, 6.1 Hz, 1H), 3.50–3.46 (m,

1H), 3.42–3.35 (m, 2H), 3.26 (ddd, *J* = 17.3, 3.9, 2.0 Hz, 1H), 2.78 (ddt, *J* = 14.3, 10.7, 3.9 Hz, 1H), 2.66 (ddd, *J* = 16.6, 3.9, 1.9 Hz, 1H), 2.48 (dt, *J* = 19.1, 2.0 Hz, 1H), 2.41 (m, 1H), 2.36 (m, 1H), 2.27 (dd, *J* = 16.5, 13.4 Hz, 1H), 2.10 (ddd, *J* = 17.3, 11.0, 3.8 Hz, 1H), 1.76 (d, *J* = 1.3 Hz, 3H), 1.35 (s, 3H); ^{13}C NMR ($CDCl_3$, 126 MHz) δ 198.8, 172.1, 148.7, 146.4, 129.9, 110.6, 79.9, 75.0, 70.2, 54.4, 50.2, 45.8, 43.6, 42.6, 39.8, 37.3, 26.7, 22.4, 20.9; IR (Neat Film, NaCl) 3479, 2965, 1767, 1647, 1625, 1369, 1233, 1154, 1102, 992, 975, 907 cm^{-1}; HRMS (FAB+) *m/z* calc'd for $C_{19}H_{23}O_5$ $[M+H]^+$: 331.1545, found 331.1540; $[\alpha]_D^{25.0}$ +161.3° (*c* 0.900, $CHCl_3$).

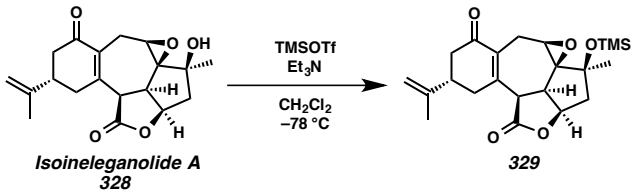

Silyl ether 329: To a stirred solution of isoineleganolide A (**328**, 3 mg, 0.009 mmol, 1.00 equiv) in CH_2Cl_2 (0.25 mL) at –78 °C (*i*-PrOH/dry ice bath) was added Et_3N (50 μL, 0.36 mmol, 40.0 equiv) dropwise. After 5 minutes, TMSOTf (8 μL, 0.045 mmol, 5.00 equiv) was added slowly dropwise. After 15 minutes, the consumption of starting material was complete as determined by TLC (1:4 EtOAc:CH_2Cl_2 eluent). The reaction was quenched by the addition of saturated $NaHCO_3$ (50 μL), removed from the cooling bath and allowed to warm to ambient temperature (ca. 23 °C). The reaction mixture was then filtered through a pad of SiO_2 (100% EtOAc eluent). The combined organics were then concentrated in vacuo to afford silyl ether **329** (3 mg, >99% yield) was as amorphous white solid: R_f = 0.50 (EtOAc eluent); ^{1}H NMR ($CDCl_3$, 600 MHz) δ 4.83 (qd, *J* = 4.0, 3.5, 1.5 Hz, 2H), 4.74 (d, *J* = 1.6 Hz, 1H), 3.76 (dd, *J* = 19.1, 6.2 Hz, 1H), 3.51–3.45 (m,

1H), 3.43–3.35 (m, 2H), 3.27 (ddd, *J* = 17.5, 3.9, 1.9 Hz, 1H), 2.79 (td, *J* = 14.4, 3.9 Hz, 1H), 2.67 (ddd, *J* = 16.6, 3.9, 1.9 Hz, 1H), 2.56–2.33 (m, 3H), 2.28 (dd, *J* = 16.6, 13.3 Hz, 1H), 2.14–2.05 (m, 1H), 1.77 (s, 3H), 1.36 (s, 3H), 0.07 (s, 9H); ^{13}C NMR ($CDCl_3$, 126 MHz) δ 198.8, 172.1, 148.7, 146.4, 129.9, 110.6, 79.9, 75.0, 70.2, 54.5, 50.2, 45.8, 43.7, 42.6, 39.8, 37.3, 26.8, 22.4, 20.9, 1.2; IR (Neat Film, NaCl) 2962, 1770, 1665, 1380, 1262, 1101, 1024, 799 cm^{-1}; HRMS (FAB+) *m/z* calc'd for $C_{22}H_{29}O_5Si$ [(M+H)–H-$_2$]$^+$: 401.1784, found 401.1798; $[\alpha]_D^{25.0}$ +1.4° (*c* 0.150, $CHCl_3$).

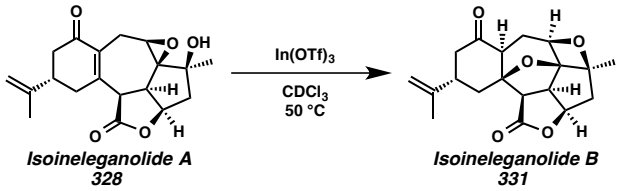

Isoineleganolide B (331):[44] To a stirred solution of isoineleganolide A (**328**, 5 mg, 0.015 mmol, 1.00 equiv) in $CDCl_3$ (0.60 mL) at ambient temperature (ca. 23 °C) was added $In(OTf)_3$ (20 mg, 0.036 mmol, 2.40 equiv) as a solid in one portion. The white suspension was stirred for 5 minutes and then introduced to a preheated 50 °C bath. After 12 h, the consumption of starting material was complete as determined by TLC (1:4 EtOAc:CH_2Cl_2 eluent). The reaction was directly purified by silica gel column chromatography (10% EtOAc in CH_2Cl_2 eluent) to provide isoineleganolide B (**331**, 4 mg, 80% yield) as an amorphous white solid: R_f = 0.78 (1:4 EtOAc:CH_2Cl_2 eluent); ^{1}H NMR ($CDCl_3$, 400 MHz) δ 5.31 (dd, *J* = 10.1, 6.0 Hz, 1H), 4.92–4.84 (m, 2H), 4.83–4.80 (s, 1H), 3.58 (t, *J* = 9.2 Hz, 1H), 3.25 (d, *J* = 9.2 Hz, 1H), 3.19–3.08 (m, 1H), 2.73 (d, *J* = 5.9 Hz, 1H), 2.69–2.56 (m, 2H), 2.45–2.12 (m, 4H), 2.02 (ddd, *J* = 14.8, 4.2, 2.1 Hz, 1H), 1.78–1.75 (m, 3H), 1.71 (ddd, *J* = 13.3, 10.2, 6.1 Hz, 1H), 1.35 (d, *J* = 1.2 Hz, 3H); ^{13}C

NMR ($CDCl_3$, 101 MHz) δ 204.8, 174.6, 145.6, 111.6, 94.0, 89.6, 79.0, 77.4, 77.1, 54.9, 54.6, 48.1, 46.4, 45.4, 41.3, 36.3, 26.3, 24.3, 20.3; IR (Neat Film, NaCl) 3485, 2963, 1767, 1721, 1410, 1260, 1243, 1209, 1142, 1034, 926, 798 cm^{-1}; HRMS (EI+) *m/z* calc'd for $C_{19}H_{22}O_5$ $[M\bullet]^+$: 330.1467, found 330.1491; $[\alpha]_D^{25.0}$ +10.4° (*c* 0.100, $CHCl_3$).

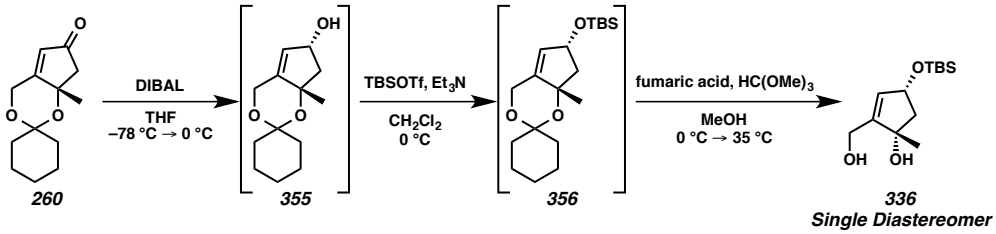

Diol 336: To a pale yellow solution of cyclopentenone **260** (918 mg, 4.13 mmol, 1.00 equiv) in THF (41 mL) at –78 °C (*i*-PrOH/dry ice bath) was added a solution of DIBAL (1.47 mL, 8.26 mmol, 2.00 equiv) in THF (8.3 mL) slowly dropwise over 15 minutes. After 30 minutes, the golden reaction mixture was removed from the bath and allowed to warm slowly. After an additional 30 minutes, the consumption of starting material was complete as determined by TLC (1:4 EtOAc:Hexanes eluent) and the reaction mixture was cooled to 0 °C (ice/H_2O bath). The reaction was subsequently quenched with a 1:1 solution of saturated aqueous NH_4Cl and saturated aqueous Rochelle's salt (40 mL) dropwise, vigorously evolving gas on the first drops. The mixture was then diluted with CH_2Cl_2 (250 mL) and H_2O (30 mL). The aqueous layer was then extracted with CH_2Cl_2 (3 x 75 mL). The combined organic layers were dried over Na_2SO_4, filtered, and concentrated in vacuo to provide crude allylic alcohol **355** (0.848 g, >99% yield), which was used without further purification.

To a stirred solution of crude allylic alcohol **355** (880 mg, 3.92 mmol, 1.00 equiv) in CH_2Cl_2 (39 mL) at 0 °C (ice/H_2O bath) was added Et_3N (1.09 mL, 7.84 mmol, 2.00

equiv). After 15 minutes, TBSOTf (0.99 mL, 4.31 mmol, 1.10 equiv) was added dropwise. After 30 minutes, the consumption of starting material was complete as determined by TLC (2:3 Et_2O:Hexanes eluent). The reaction mixture was diluted with CH_2Cl_2 (150 mL) and washed with H_2O (50 mL). The aqueous was extracted with CH_2Cl_2 (2 x 70 mL). The combined organic layers were dried over Na_2SO_4, filtered, and concentrated in vacuo to afford intermediate silyl ether alcohol **356** (1.33 g, >99% yield), which was used without further purification.

To a flask containing silyl ether **356** (1.33 g, 3.92 mmol, 1.00 equiv) were added MeOH (79 mL) and $HC(OMe)_3$ (3.86 mL, 35.3 mmol, 9.00 equiv). The reaction mixture was cooled to 0 °C (ice/H_2O bath) with stirring, at which time the addition of fumaric acid (1.14 g, 9.80 mmol, 2.50 equiv) was accomplished in one portion. After 10 minutes, the reaction was removed from the cold bath and immediately introduced to a preheated 35 °C oil bath. After 9 hours, the consumption of starting material was complete as determined by TLC (2:3 Et_2O:Hexanes eluent) and the reaction was removed from the heating bath and allowed to cool to ambient temperature (ca. 23 °C). The reaction mixture was diluted with EtOAc (150 mL) and poured onto saturated $NaHCO_3$ (125 mL). The organics were separated and the aqueous was extracted with EtOAc (2 x 125 mL). The combined organic layers were washed with brine (100 mL), dried over $MgSO_4$ for 2 minutes, filtered, and concentrated in vacuo to generate a yellow oil. The crude residue was then purified by silica gel column chromatography (50% EtOAc in hexanes eluent) to afford diol **336** (841 mg, 83% yield) as a pale yellow oil: R_f = 0.27 (1:1 EtOAc:Hexanes eluent); ^{1}H NMR ($CDCl_3$, 500 MHz) δ 5.60 (q, *J* = 1.7 Hz, 1H), 4.59 (ddt, *J* = 6.7, 4.7, 1.9 Hz, 1H), 4.30 (dt, *J* = 14.6, 1.7 Hz, 1H), 4.19 (dt, *J* = 15.0, 1.6 Hz,

1H), 3.67 (s, 2H), 2.38 (dd, J = 13.4, 6.9 Hz, 1H), 1.86 (dd, J = 13.4, 4.6 Hz, 1H), 1.26 (s, 3H), 0.86 (s, 9H), 0.05 (app d, J = 2.1 Hz, 6H); ^{13}C NMR ($CDCl_3$, 126 MHz) δ 150.5, 129.2, 80.9, 73.6, 58.4, 52.4, 26.3, 26.0, 18.3, –4.6, –4.6; IR (Neat Film, NaCl) 3367, 2929, 2857, 1472, 1362, 1256, 1089, 1017, 939, 901, 835, 776 cm^{-1}; HRMS (FAB+) *m/z* calc'd for $C_{13}H_{25}O_3Si$ $[(M+H)–H_2]^+$: 257.1573, found 257.1569; $[\alpha]_D^{25.0}$ +42.4° (*c* 10.550, $CHCl_3$).

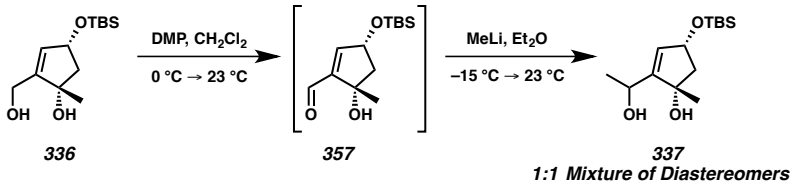

336 *357* *337*
1:1 Mixture of Diastereomers

Allylic alcohol 337: To a stirred solution of diol **336** (187 mg, 0.72 mmol, 1.00 equiv) in CH_2Cl_2 (36 mL) at 0 °C (ice/H_2O bath) was added DMP (611 mg, 1.44 mmol, 2.00 equiv) as a solid in a single portion. After 30 minutes, the reaction vessel was removed from the cooling bath and allowed to warm to ambient temperature (ca. 23 °C). After an additional 2.5 h, the consumption of starting material was complete as determined by TLC (1:1 EtOAc:Hexanes eluent). The reaction was quenched by the addition of saturated aqueous $Na_2S_2O_3$ (50 mL) with vigorous stirring. After 10 minutes, the reaction was diluted with CH_2Cl_2 (50 mL) and poured onto saturated aqueous $NaHCO_3$ (75 mL). The organics were separated and the aqueous was extracted with CH_2Cl_2 (2 x 80 mL). The combined organics were dried quickly over $MgSO_4$ (< 2 minutes), filtered, and concentrated in vacuo to afford crude aldehyde **357** (187 mg >99% yield), which was carried on without further purification.

To a stirred solution of crude aldehyde **357** (187 mg, 0.72 mmol, 1.00 equiv) in Et_2O (4.9 mL) at –15 °C (ice/MeOH bath) was added MeLi (1.92 mL, 1.5 M in Et_2O, 4.00 equiv) quickly dropwise. After 1.5 h, an additional portion of MeLi (0.96 mL, 1.5 M in Et_2O, 2.00 equiv) was added quickly dropwise and the reaction vessel was removed from the cooling bath and allowed to warm to ambient temperature (ca. 23 °C). After an additional 1.5 h, the consumption of starting material was complete as determined by TLC (1:1 EtOAc:Hexanes eluent). The reaction was quenched by the careful addition of saturated aqueous NH_4Cl (15 mL, CAUTION: Vigorous gas evolution!) with vigorous stirring. The biphasic reaction mixture was diluted with Et_2O (60 mL) and poured onto H_2O (30 mL). The organics were separated and the aqueous was extracted with Et_2O (2 x 60 mL). The combined organics were washed with brine (20 mL), dried over Na_2SO_4, filtered, and concentrated in vacuo. The crude golden oil was purified by silica gel column chromatography (60% Et_2O in hexanes eluent) to afford diol **337** (152 mg, 76% yield) as a pale yellow oil. For the purpose of characterization, a portion of each diastereomer was collected during purification.

Diol 337, Diastereomer A: R_f = 0.43 (3:1 Et_2O:Hexanes eluent); ^1H NMR ($CDCl_3$, 500 MHz) δ 5.59 (dd, *J* = 2.1, 1.4 Hz, 1H), 4.58 (ddt, *J* = 6.6, 4.5, 1.9 Hz, 1H), 4.48 (qt, *J* = 6.4, 1.7 Hz, 1H), 3.64 (s, 1H), 3.55 (s, 1H), 2.38 (dd, *J* = 13.4, 6.8 Hz, 1H), 1.89 (dd, *J* = 13.4, 4.5 Hz, 1H), 1.36 (d, *J* = 6.4 Hz, 3H), 1.34 (s, 3H), 0.87 (s, 9H), 0.06 (app d, *J* = 1.9 Hz, 6H); ^{13}C NMR ($CDCl_3$, 126 MHz) δ 152.6, 129.0, 81.9, 73.1, 63.7, 52.2, 26.5, 26.0, 21.8, 18.3, –4.5, –4.5; IR (Neat Film, NaCl) 3364, 2929, 2856, 1463, 1362, 1256, 1204, 1080, 1001, 940, 905, 835, 775 cm^{-1}; HRMS (FAB+) *m/z* calc'd for $C_{14}H_{27}O_3Si$ [(M+H)–H_2]$^+$: 271.1730, found 271.1728; $[\alpha]_D^{25.0}$ +54.9° (*c* 3.500, $CHCl_3$).

Diol 337, Diastereomer B: R_f = 0.35 (3:1 Et_2O:Hexanes eluent); ^1H NMR ($CDCl_3$, 500 MHz) δ 5.63 (dd, *J* = 2.1, 1.2 Hz, 1H), 4.59 (dddd, *J* = 6.6, 4.3, 2.2, 1.2 Hz, 2H), 2.94–2.76 (m, 1H), 2.68 (s, 1H), 2.33 (dd, *J* = 13.2, 6.5 Hz, 1H), 1.86 (dd, *J* = 13.2, 4.1 Hz, 1H), 1.41 (d, *J* = 6.6 Hz, 3H), 1.39 (s, 3H), 0.87 (s, 9H), 0.06 (s, 6H); ^{13}C NMR ($CDCl_3$, 126 MHz) δ 154.3, 129.0, 81.5, 73.2, 65.4, 52.9, 26.7, 26.0, 24.1, 16.3, –4.6; IR (Neat Film, NaCl) 3370, 2929, 2857, 1472, 1362, 1257, 1206, 1085, 1004, 939, 905, 836, 775 cm^{-1}; HRMS (FAB+) *m/z* calc'd for $C_{14}H_{27}O_3Si$ $[(M+H)–H_2]^+$: 271.1730, found 271.1735; $[\alpha]_D^{25.0}$ +61.4° (*c* 3.100 $CHCl_3$).

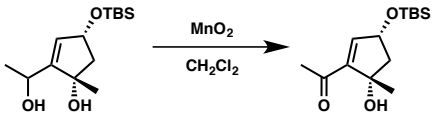

337 ***1:1 Mixture of Diastereomers*** ***338***

Methyl ketone 338: To a stirred solution of diol **337** (152 mg, 0.56 mmol, 1.00 equiv) as a 1:1 mixture of diastereomers in CH_2Cl_2 (3.8 mL) at ambient temperature (ca. 23 °C) was added MnO_2 (1.45 g, 16.7 mmol, 30.0 equiv) as a solid in a single portion. After 16 h, the consumption of starting material was complete as determined by TLC (1:1 EtOAc:Hexanes eluent). The reaction mixture was then filtered through a Celite plug, washing with CH_2Cl_2. The combined organics were concentrated in vacuo to provide methyl ketone **338** (134 mg, 89% yield) as a spectroscopically pure dark yellow oil: R_f = 0.24 (1:9 EtOAc:Hexanes eluent); ^1H NMR ($CDCl_3$, 400 MHz) δ 6.53 (d, *J* = 1.9 Hz, 1H), 4.76 (td, *J* = 7.1, 1.9 Hz, 1H), 2.41 (dd, *J* = 12.6, 7.0 Hz, 1H), 2.34 (s, 3H), 2.05–1.96 (m, 1H), 1.41 (d, *J* = 1.0 Hz, 3H), 0.90 (s, 9H), 0.11 (s, 3H), 0.09 (s, 3H); ^{13}C NMR ($CDCl_3$, 101 MHz) δ 198.8, 147.1, 146.1, 80.0, 73.0, 51.1, 28.2, 27.5, 25.9, 18.3, –4.4, –

4.6; IR (Neat Film, NaCl) 3534, 2929, 2857, 1667, 1472, 1362, 1275, 1259, 1094, 939, 914, 884, 836, 777 cm^{-1}; HRMS (FAB+) *m/z* calc'd for $C_{14}H_{25}O_3Si$ $[(M+H)–H_2]^+$: 269.1573, found 269.1584; $[\alpha]_D^{25.0}$ +114.7° (*c* 0.750, $CHCl_3$).

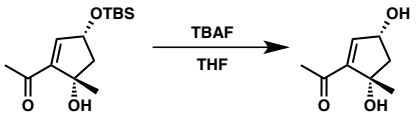

338 ***ent-335***

Methyl Ketone Diol *ent*-335: To a golden yellow stirred solution of methyl ketone **338** (200 mg, 0.78 mmol, 1.00 equiv) in THF (3.8 mL) at ambient temperature (ca. 23 °C) was added TBAF (0.92 mL, 1 M in THF, 1.20 equiv) dropwise. After 20 minutes, the consumption of starting material was complete as determined by TLC (3:7 EtOAc:Hexanes eluent). The orange-brown reaction mixture was then concentrated in vacuo and immediately purified by silica gel column chromatography (80% EtOAc in hexanes eluent) to furnish *cis*-1,3-cyclopentenediol ***ent*-335** (120 mg, 98% yield) as an amorphous white solid: R_f = 0.18 (3:1 EtOAc:Hexanes eluent); ^{1}H NMR ($CDCl_3$, 400 MHz) δ 6.63 (d, *J* = 2.0 Hz, 1H), 4.75 (ddd, *J* = 7.2, 6.1, 2.1 Hz, 1H), 2.49 (dd, *J* = 13.4, 7.2 Hz, 1H), 2.35 (s, 3H), 1.96 (dd, *J* = 13.4, 6.1 Hz, 1H), 1.43 (s, 3H); ^{13}C NMR ($CDCl_3$, 101 MHz) δ 199.0, 148.1, 145.0, 80.6, 72.9, 50.4, 27.9, 27.6; IR (Neat Film, NaCl) 3386, 2968, 1667, 1372, 1316, 1275, 1231, 1107, 1071, 958 cm^{-1}; HRMS (ES+) *m/z* calc'd for $C_8H_{11}O_2$ $[M–OH]^+$: 139.0759, found 139.0741; $[\alpha]_D^{25.0}$ +103.3° (*c* 0.650, $CHCl_3$).

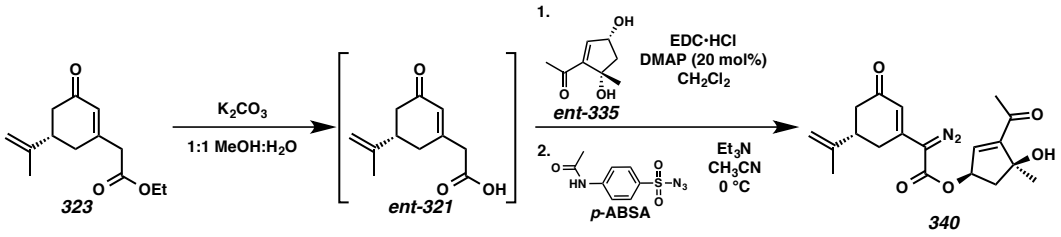

Methyl Ketone Diazoester 340: To a stirred solution of ethyl ester **323** (2.07 g, 9.32 mmol, 1.00 equiv) in MeOH (31 mL) and H_2O (31 mL) was added K_2CO_3 (5.16 g, 37.3 mmol, 4.00 equiv). After 7 h, the consumption of starting material was complete as determined by TLC (2:3 Et_2O:Hexanes eluent). The reaction mixture was cooled to 0 °C (ice/H_2O bath) and the pH was adjusted to between 1 and 2 by the careful addition of aqueous 1 N HCl (CAUTION: Vigorous gas evolution!). The reaction mixture was then poured onto a mixture of EtOAc (200 mL) and H_2O (100 mL). The organics were separated and the aqueous layer was extracted with EtOAc (3 x 200 mL). The combined organics were dried over Na_2SO_4, filtered and concentrated in vacuo. The crude dark orange oil of carboxylic acid ***ent*-321** (1.81 g, >99% yield) was carried on without further purification.

To a stirred solution of diol ***ent*-335** (76 mg, 0.49 mmol, 1.00 equiv) in CH_2Cl_2 (16 mL) were added a portion of crude carboxylic acid ***ent*-321** (190 mg, 0.98 mmol, 2.00 equiv) and EDC•HCl (188 mg, 0.98 mmol, 2.00 equiv). The orange reaction mixture was cooled to 0 °C (ice/H_2O bath) at which time DMAP (12 mg, 0.010 mmol, 0.20 equiv) was added in a single portion. After 30 minutes, the dark red-orange reaction mixture was removed from the cooling bath and allowed to warm to ambient temperature (ca. 23 °C). After 2.5 h, additional DMAP (12 mg, 0.010 mmol, 0.20 equiv) was added in a single portion. After an additional 2 h, the consumption of starting material was nearly complete as determined by TLC (1:1 EtOAc:Hexanes eluent). The crude reaction mixture was

concentrated in vacuo to approximately 25% of the original reaction volume and directly purified by silica gel column chromatography (50%→70%→90% EtOAc in hexanes eluent) to furnish a recovered portion of diol ***ent*-335** (11 mg, 14% yield) and the intermediate ester (125 mg, 77% yield), which was directly carried on to the next reaction.

To a portion of intermediate ester (57 mg, 0.17 mmol, 1.00 equiv) in CH_3CN (1.7 mL) in the dark was added *p*-acetamidobenzenesulfonyl azide (*p*-ABSA, 46 mg, 0.19 mmol, 1.10 equiv) as a solid in one portion. The dark orange homogeneous reaction mixture was cooled to 0 °C (ice/H_2O bath). Et_3N (71 μL, 0.51 mmol, 3.00 equiv) was then added slowly dropwise. After 5 h, the consumption of starting material was complete as determined by TLC (1:4 EtOAc:CH_2Cl_2 eluent). The reaction was quenched by the addition of EtOAc (20 mL), removed from the cooling bath, and allowed warm to ambient temperature (ca. 23 °C). The reaction mixture was then concentrated in vacuo. The crude tan solid was then adsorbed onto Celite (1.0 g) and purified by silica gel column chromatography (20% EtOAc in CH_2Cl_2 eluent) to afford diazoester **340** (51 mg, 65% yield from diol ***ent*-335**) as a dark yellow oil: R_f = 0.17 (1:4 EtOAc:CH_2Cl_2 eluent); ^{1}H NMR ($CDCl_3$, 400 MHz) δ 6.63 (d, *J* = 2.0 Hz, 1H), 6.45 (d, *J* = 2.0 Hz, 1H), 5.80 (ddd, *J* = 7.6, 6.6, 2.0 Hz, 1H), 4.89 (p, *J* = 1.5 Hz, 1H), 4.85–4.81 (m, 1H), 3.50 (s, 1H), 2.78 (tt, *J* = 11.1, 4.2 Hz, 1H), 2.69 (ddd, *J* = 17.4, 4.2, 1.4 Hz, 1H), 2.62 (dd, *J* = 13.5, 7.5 Hz, 1H), 2.59–2.53 (m, 1H), 2.47 (ddd, *J* = 17.3, 10.9, 2.2 Hz, 1H), 2.46–2.36 (m, 4H), 2.17 (dd, *J* = 13.5, 6.6 Hz, 1H), 1.80 (s, 3H), 1.51 (s, 3H); ^{13}C NMR ($CDCl_3$, 101 MHz) δ 198.2, 197.1, 162.3, 150.1, 146.0, 145.9, 139.5, 120.6, 111.6, 80.2, 75.6, 67.2, 46.7, 41.9, 41.6, 31.7, 28.3, 27.7, 20.6; IR (Neat Film, NaCl) 3454, 2967, 2104, 1709,

1652, 1580, 1377, 1274, 1223, 1136, 1048, 893, 741 cm^{-1}; HRMS (FAB+) *m/z* calc'd for $C_{19}H_{23}O_5N_2$ $[M+H]^+$: 359.1607, found 359.1598; $[\alpha]_D^{25.0}$ +164.2° (*c* 0.500, $CHCl_3$).

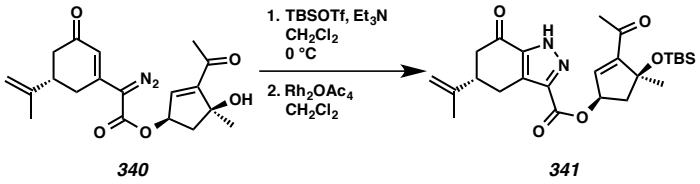

340 *341*

Pyrazole 341: In the dark, to a stirred solution of diazoester **340** (20 mg, 0.056 mmol, 1.00 equiv) in CH_2Cl_2 (0.56 mL) at 0 °C (ice/H_2O bath) was added Et_3N (78 μL, 0.56 mmol, 10.0 equiv) dropwise. After 5 minutes, TBSOTf (64 μL, 0.28 mmol, 5.00 equiv) was added dropwise. After an additional 15 minutes, the consumption of starting material was complete as determined by TLC (1:4 EtOAc:CH_2Cl_2 eluent). The deep red reaction mixture was filtered through a Florisil plug, washing with 100% EtOAc. The combined organics were concentrated in vacuo to afford a bright red oil that was immediately carried on to the next reaction.

In the dark, to a solution of the red oil in CH_2Cl_2 (5.6 mL) was added Rh_2OAc_4 (0.3 mg, 0.0006 mmol, 0.01 equiv) as a solid in one portion. After an additional 15 minutes, the consumption of starting material was complete as determined by IR spectroscopy (complete disappearance of diazo absorbance at ca. 2100 cm^{-1}). The reaction mixture was then poured onto H_2O (10 mL). The organics were separated and the aqueous was extracted with CH_2Cl_2 (3 x 25 mL). The combined organics were washed with brine (10 mL), dried over Na_2SO_4, filtered and concentrated in vacuo. The crude golden solid was purified by silica gel column chromatography (30%→50% EtOAc in CH_2Cl_2 eluent) to afford pyrazole **341** (10 mg, 38% yield) as an amorphous white solid: R_f = 0.30 (1:4

EtOAc:CH_2Cl_2 eluent); ^{1}H NMR ($CDCl_3$, 600 MHz) δ 6.59 (d, *J* = 2.0 Hz, 1H), 5.79 (ddd, *J* = 7.4, 6.6, 2.0 Hz, 1H), 4.89 (t, *J* = 1.4 Hz, 1H), 4.86 (q, *J* = 1.0 Hz, 1H), 3.32 (ddd, *J* = 16.3, 3.7, 1.3 Hz, 1H), 2.97–2.83 (m, 2H), 2.78–2.69 (m, 2H), 2.68–2.58 (m, 1H), 2.36 (s, 3H), 2.25 (dd, *J* = 13.0, 6.6 Hz, 1H), 1.82 (t, *J* = 1.1 Hz, 3H), 1.59 (s, 3H), 0.83 (s, 9H), 0.12 (s, 3H), 0.09 (s, 3H); ^{13}C NMR ($CDCl_3$, 126 MHz) δ 196.1, 189.2, 161.0, 152.4, 145.6, 136.6, 111.8, 81.8, 75.3, 49.9, 44.0, 43.5, 28.8, 28.5, 26.5, 25.7, 20.7, 18.0, –2.4, –2.5; IR (Neat Film, NaCl) 3207, 2928, 2856, 1688, 1464, 1367, 1259, 1167, 1101, 1006, 837, 776 cm^{-1}; HRMS (FAB+) *m/z* calc'd for $C_{25}H_{36}O_5N_2NaSi$ $[M+Na]^+$: 495.2286, found 495.2291; $[\alpha]_D^{25.0}$ +55.1° (*c* 0.135, $CHCl_3$).[45]

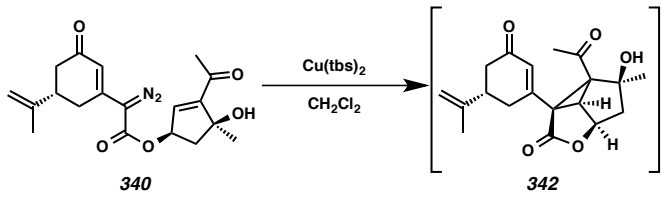

340 *342*

Cyclopropane 342: To a stirred solution of diazoester **340** (14 mg, 0.039 mmol, 1.00 equiv) in CH_2Cl_2 (3.9 mL) in a nitrogen-filled glovebox at ambient temperature (ca. 30 °C) was added $Cu(tbs)_2$ (1.6 mg, 0.004 mmol, 0.10 equiv) as a solid in one portion. After 4 days, although the starting material was not fully consumed as determined by TLC (1:4 EtOAc:CH_2Cl_2 eluent), the reaction was removed from the glovebox and concentrated in vacuo to approximately 25% of the original reaction volume. The crude reaction solution was directly purified by silica gel column chromatography (50% EtOAc in CH_2Cl_2 eluent) to afford cyclopropane **342** (4 mg, 29% yield, R_f = 0.21 (1:1 EtOAc:CH_2Cl_2 eluent)) which was directly carried on, although the subsequent reactions were not successful.[46]

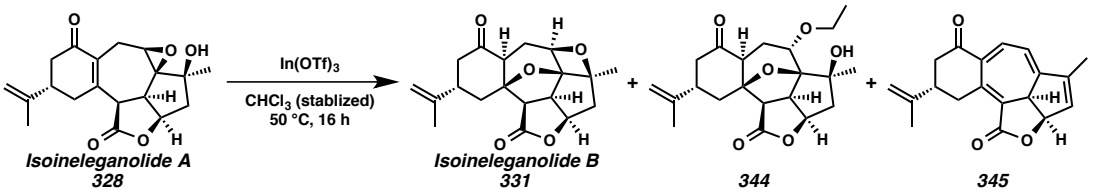

Isoineleganolide B (331), Ethyl Ether 344, and Cycloheptatriene 345: To a colorless stirred solution of isoineleganolide A (**328**, 10 mg, 0.30 mmol, 1.00 equiv) in $CHCl_3$ (stabilized with 0.75% EtOH, 1.0 mL) at ambient temperature (ca. 23 °C) was added $In(OTf)_3$ (40 mg, 0.71 mmol, 2.37 equiv). The white suspension was stirred for 5 minutes and then introduced to a preheated 50 °C bath. After 13 h, the consumption of starting material was complete as determined by TLC (1:4 EtOAc:CH_2Cl_2 eluent). The reaction was directly purified by silica gel column chromatography (10%→20% EtOAc in CH_2Cl_2 eluent) to provide isoineleganolide B (**331**, 2 mg, 20% yield) as an amorphous white solid, ethyl ether **344** (7 mg, 70% yield) as an amorphous white solid, and cycloheptatriene **345** (1 mg, 10% yield) as an amorphous white solid.

Isoineleganolide B (331): Characterization data match those reported above.

Ethyl ether 344: R_f = 0.39 (1:4 EtOAc:CH_2Cl_2 eluent); ^{1}H NMR ($CDCl_3$, 400 MHz) δ 4.88–4.76 (m, 3H), 3.79–3.65 (m, 2H), 3.59–3.44 (m, 2H), 3.15 (d, *J* = 9.2 Hz, 1H), 2.91 (ddt, *J* = 13.3, 5.6, 1.1 Hz, 1H), 2.65 (tt, *J* = 13.2, 3.7 Hz, 1H), 2.60–2.49 (m, 2H), 2.36–2.18 (m, 4H), 2.17–2.09 (m, 1H), 1.98 (ddd, *J* = 14.5, 3.7, 2.1 Hz, 1H), 1.79–1.73 (m, 3H), 1.30 (d, *J* = 1.2 Hz, 3H), 1.17 (t, *J* = 7.0 Hz, 3H); ^{13}C NMR ($CDCl_3$, 101 MHz) δ 206.7, 176.1, 146.2, 111.1, 95.5, 89.0, 79.6, 78.1, 69.3, 64.4, 55.4, 54.0, 48.5, 46.3, 45.7, 41.2, 36.8, 25.6, 24.7, 20.4, 15.7; IR (Neat Film, NaCl) 3490, 2965, 1767, 1717, 1447, 1357, 1262, 1178, 1107, 1025, 967, 895, 799, 758 cm^{-1}; HRMS (FAB+) *m/z* calc'd for $C_{21}H_{29}O_6$ $[M+H]^+$: 377.1964, found 377.1970; $[\alpha]_D^{25.0}$ +28.4° (*c* 0.200, $CHCl_3$).

Cycloheptatriene 345: R_f = 0.94 (1:4 EtOAc:CH_2Cl_2 eluent); ^{1}H NMR ($CDCl_3$, 500 MHz) δ 7.86 (d, *J* = 6.7 Hz, 1H), 6.46 (ddd, *J* = 6.7, 1.8, 0.6 Hz, 1H), 6.36 (t, *J* = 1.8 Hz, 1H), 5.48 (ddd, *J* = 7.2, 2.3, 1.1 Hz, 1H), 4.84 (t, *J* = 1.4 Hz, 1H), 4.76 (q, *J* = 1.0 Hz, 1H), 3.33 (dq, *J* = 6.8, 2.3 Hz, 2H), 2.93 (dd, *J* = 7.5, 1.9 Hz, 1H), 2.76–2.69 (m, 1H), 2.67–2.58 (m, 2H), 2.01 (t, *J* = 1.3 Hz, 3H), 1.81 (dd, *J* = 1.5, 0.8 Hz, 3H); ^{13}C NMR ($CDCl_3$, 126 MHz) δ 200.1, 166.1, 149.1, 146.2, 145.9, 143.5, 140.2, 138.1, 137.5, 117.4, 114.8, 111.3, 81.1, 44.8, 44.1, 38.7, 32.2, 21.1, 12.7; IR (Neat Film, NaCl) 2924, 2854, 1738, 1684, 1611, 1495, 1451, 1262, 1234, 1086, 1006, 827 cm^{-1}; HRMS (EI+) *m/z* calc'd for $C_{19}H_{18}O_3$ [M•]$^+$: 294.1256, found 294.1260; $[\alpha]_D^{25.0}$ –84.6° (*c* 0.100, $CHCl_3$).

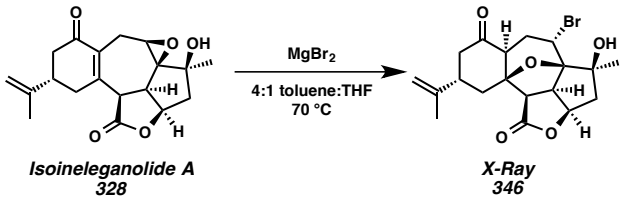

Bromide 346: To a stirred colorless solution of isoineleganolide A (**328**, 133 mg, 0.40 mmol, 1.00 equiv) in a mixture of toluene (27 mL) and THF (7 mL) in a nitrogen-filled glovebox was added $MgBr_2$ (370 mg, 2.01 mmol, 5.00 equiv) in a single portion. The reaction mixture was then sealed and heated to 70 °C. After 6 h, the consumption of starting material was complete as determined by TLC (1:4 EtOAc:CH_2Cl_2 eluent). The golden yellow solution was removed from the glovebox and concentrated in vacuo to approximately 25% of the original reaction volume. The reaction was then filtered through a silica gel plug, eluting the product with 20% EtOAc in CH_2Cl_2 to afford spectroscopically pure bromide **346** (166 mg, >99% yield) as a white crystalline solid. Colorless, translucent X-ray quality crystals were obtained by slow diffusion of 1%

benzene in heptane into a solution of bromide **346** in EtOAc, mp: 150–153 °C: R_f = 0.26 (1:19 EtOAc:CH_2Cl_2 eluent); ^{1}H NMR ($CDCl_3$, 600 MHz) δ 4.89 (dt, *J* = 9.1, 7.6 Hz, 1H), 4.84 (t, *J* = 1.5 Hz, 1H), 4.81 (s, 1H), 4.39 (dd, *J* = 11.3, 5.5 Hz, 1H), 3.74 (t, *J* = 9.2 Hz, 1H), 3.25 (d, *J* = 9.0 Hz, 1H), 3.08 (ddd, *J* = 14.1, 5.6, 1.4 Hz, 1H), 2.66 (tt, *J* = 13.2, 3.9 Hz, 1H), 2.56 (ddd, *J* = 13.2, 3.7, 2.0 Hz, 1H), 2.52 (d, *J* = 5.8 Hz, 1H), 2.36–2.27 (m, 2H), 2.22 (dd, *J* = 14.6, 12.9 Hz, 1H), 2.15 (m, 1H), 1.94 (m, 2H), 1.76 (d, *J* = 1.0 Hz, 3H), 1.49 (d, *J* = 1.2 Hz, 3H); ^{13}C NMR ($CDCl_3$, 126 MHz) δ 205.7, 175.2, 145.7, 111.2, 96.3, 88.9, 80.8, 77.5, 55.5, 55.4, 48.4, 46.2, 45.4, 41.5, 41.1, 36.7, 32.3, 26.6, 20.2; IR (Neat Film, NaCl) 3508, 2970, 1767, 1716, 1443, 1354, 1271, 1203, 1173, 1073, 1016, 755 cm^{-1}; HRMS (FAB+) *m/z* calc'd for $C_{19}H_{24}O_5{}^{79}Br$ $[M+H]^+$: 411.0807, found 411.0800; $[\alpha]_D^{25.0}$ +26.7° (*c* 1.150, $CHCl_3$).

Diketonefuranopentacycle 347: A reaction vessel in a nitrogen-filled glove box was charged with $AgBF_4$ (43 mg, 0.22 mmol, 3.00 equiv) followed by bromide **346** (30 mg, 0.073 mmol, 1.00 equiv) as a solution in DMSO (1.5 mL) with stirring. The reaction vessel was sealed and after 5 minutes the white suspension had become a completely homogenous, pale yellow solution. The reaction vessel was removed from the glovebox, and introduced to an argon atmosphere and a preheated 120 °C bath. After 9 h, the consumption of starting material was complete as determined by TLC (1:19 EtOAc:CH_2Cl_2 eluent). The dark brown, heterogeneous solution was removed from the

heating bath and allowed to cool to ambient temperature (ca. 23 °C). Once the temperature had equilibrated, Et_3N (0.30 mL, 2.15 mmol, 29.5 equiv) was added quickly dropwise with vigorous stirring. After 2 h, the reaction was filtered through a Celite plug, washing with EtOAc. The combined organics were diluted with EtOAc (30 mL) and washed with H_2O (4 x 20 mL). The combined aqueous layers were then extracted with EtOAc (3 x 20 mL). The combined organics were dried over $MgSO_4$, filtered, and concentrated in vacuo. The crude brown solid was purified by silica gel column chromatography (40% EtOAc in CH_2Cl_2 eluent) to furnish diketone **347** (24 mg, 96% yield) as a crystalline white solid. Colorless, translucent X-ray quality crystals were obtained by slow diffusion of 1% benzene in heptane into a solution of diketone **347** in ethyl acetate, mp: 270–273 °C: R_f = 0.40 (1:3 EtOAc:CH_2Cl_2 eluent); ^{1}H NMR ($CDCl_3$, 500 MHz) δ 4.89–4.84 (m, 2H), 4.83 (dd, *J* = 2.3, 1.2 Hz, 1H), 3.56 (t, *J* = 9.0 Hz, 1H), 3.44 (d, *J* = 9.1 Hz, 1H), 3.20 (d, *J* = 15.6 Hz, 1H), 3.07 (dt, *J* = 7.4, 1.0 Hz, 1H), 2.76 (tt, *J* = 13.2, 3.6 Hz, 1H), 2.61 (ddd, *J* = 13.0, 3.6, 2.1 Hz, 1H), 2.43–2.28 (m, 5H), 2.13 (ddd, *J* = 14.7, 3.6, 2.1 Hz, 1H), 1.77 (t, *J* = 1.0 Hz, 3H), 1.50 (d, *J* = 1.1 Hz, 3H); ^{13}C NMR ($CDCl_3$, 126 MHz) δ 204.9, 199.1, 174.6, 145.8, 111.4, 95.2, 90.8, 78.1, 77.5, 57.4, 54.4, 51.2, 46.1, 45.5, 41.0, 36.6, 34.9, 24.6, 20.4; IR (Neat Film, NaCl) 3484, 2965, 2923, 1766, 1732, 1204, 1172, 1071, 1032, 947, 754 cm^{-1}; HRMS (EI+) *m/z* calc'd for $C_{19}H_{22}O_6$ $[M\bullet]^+$: 346.1416, found 346.1403; $[\alpha]_D^{25.0}$ –30.8° (*c* 0.800, $CHCl_3$).

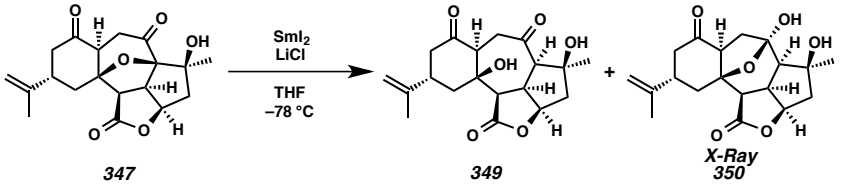

Diol tetracycle 349:

Preparation of a 0.07 M Stock Solution SmI_2

Into a Schlenk tube was added freshly filed samarium metal (150 mg, 1.00 mmol, 1.41 equiv). The reaction vessel was then thoroughly flame-dried, backfilled with argon, and allowed to cool to ambient temperature (ca. 23 °C). To the reaction vessel was then added THF (10.0 mL) that had previously been sparged with argon for 60 minutes and cooled to 0 °C (ice/H_2O bath) with stirring. EtI_2 (200 mg, 0.71 mmol, 1.00 equiv) was then added in separate 100 mg portions 30 minutes apart. After the addition of the second portion, the Schlenk tube was removed from the cooling bath, allowed to warm to ambient temperature, and the pale yellow solution was stirred overnight (ca. 14 h) causing the reaction to become deep blue, indicating the formation of SmI_2.

*Reduction of Vinlyogous Diketone **347***

A reaction vessel in a nitrogen-filled glovebox was charged with LiCl (49 mg, 1.15 mmol, 19.8 equiv), sealed, removed from the glovebox, and introduced to an argon atmosphere. To the reaction vessel was added a solution of diketone **347** (20 mg, 0.058 mmol, 1.00 equiv) in THF (26 mL) followed by *t*-BuOH (15 μL, 0.16 mmol, 1.23 equiv). The white suspension was then sparged with argon for 1 h, reducing the reaction volume to 20 mL. The reaction solution was then cooled to –78 °C (*i*-PrOH/dry ice bath) at which time SmI_2 (2.00 mL, 0.07 M in THF, 1.08 equiv) was added slowly dropwise over 5 minutes, dropping the SmI_2 solution down the sides of the reaction flask. After 15

minutes, the consumption of starting material was complete as determined by TLC (1:3 EtOAc:CH_2Cl_2 eluent). The reaction was quenched by the addition of saturated aqueous NH_4Cl (100 μL), immediately removed from the cooling bath, and allowed to warm to ambient temperature (23 °C). The yellow reaction mixture was filtered through a silica gel plug, eluting the product with 100% EtOAc. The organics were concentrated in vacuo and the crude pale yellow solid was purified by silica gel column chromatography (75%→85% EtOAc in CH_2Cl_2 eluent) to provide diol **349** (17 mg, 85% yield) as a crystalline white solid. Diol **349** was characterized as an inseparable, equilibrium mixture of free diol **349** and hemiketal **350**. Colorless, translucent X-ray quality crystals of hemiketal **350** were obtained by slow diffusion of 1% benzene in heptane into a solution of diol **349** in EtOAc, mp: 225–228 °C: R_f = 0.32 (3:1 EtOAc:CH_2Cl_2 eluent); ^{1}H NMR ($CDCl_3$, 500 MHz) δ 4.92 (dd, *J* = 7.0, 5.1 Hz, 1.00 H), 4.84 (dt, *J* = 2.8, 1.4 Hz, 2.28 H), 4.82–4.76 (m, 3.44 H), 3.63 (s, 0.95 H), 3.38 (tdd, *J* = 10.4, 7.0, 0.7 Hz, 0.99 H), 3.30 (d, J = 13.6 Hz, 1.23 H), 3.24 (d, *J* = 8.2 Hz, 1.23 H), 3.22–3.09 (m, 3.39 H), 3.02–2.95 (m, 2.16 H), 2.86–2.80 (m, 2.43 H), 2.76–2.55 (m, 8.89 H), 2.46 (dd, *J* = 14.0, 10.1 Hz, 1.00 H), 2.39–2.22 (m, 6.90 H), 2.19 (d, *J* = 10.3 Hz, 0.98 H), 2.15–2.09 (m, 1.16 H), 1.90 (dd, *J* = 15.3, 12.4 Hz, 1.03 H), 1.82–1.75 (m, 6.90 H), 1.72 (dd, *J* = 14.3, 12.1 Hz, 1.13 H), 1.53 (s, 2.90 H), 1.35 (d, *J* = 1.0 Hz, 3.61 H); ^{13}C NMR ($CDCl_3$, 126 MHz) δ 209.9, 209.1, 206.1, 174.8, 173.2, 146.5, 146.2, 111.0, 110.9, 105.6, 83.9, 81.2, 80.5, 79.3, 78.9, 75.0, 58.0, 54.4, 54.3, 52.2, 51.9, 47.6, 47.4, 46.4, 46.0, 45.6, 44.5, 42.7, 41.7, 41.1, 40.3, 38.2, 37.5, 36.1, 28.8, 24.8, 20.8, 20.7; IR (Neat Film, NaCl) 3358, 2921, 1752, 1711, 1689, 1358, 1261, 1182, 1098, 1026, 936, 896, 799, 756 cm^{-1}; HRMS (MM: ESI-APCI)

m/z calc'd for $C_{19}H_{23}O_6$ $[M–H]^-$: 347.1500, found 347.1509; $[\alpha]_D^{25.0}$ +3.1° (*c* 0.250, $CHCl_3$).

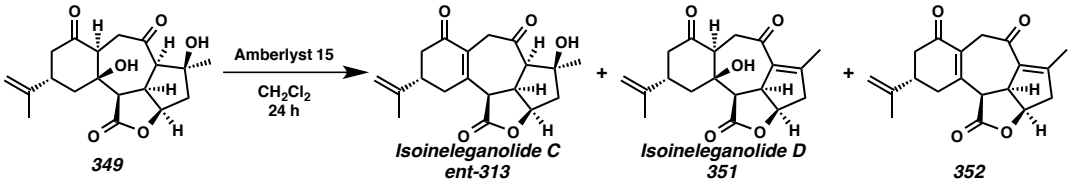

Isoineleganolide C (*ent*-313), Isoineleganolide D (351), and Dienone 352: To a heterogeneous mixture of diol **349** (30 mg, 0.086 mmol, 1.00 equiv) in CH_2Cl_2 (6.0 mL) was added Amberlyst® 15 (75 mg, 2.5 equiv by wt. to diol **349**) as a solid in one portion. After 24 h, the consumption of starting material was complete as determined by TLC (3:1 EtOAc:CH_2Cl_2 eluent). The heterogeneous, light yellow reaction mixture was filtered and the organics were concentrated in vacuo. The crude yellow solid was purified by silica gel column chromatography (30% EtOAc in CH_2Cl_2 eluent) to provide isoineleganolide C (***ent*-313**, 19 mg, 63% yield) as an amorphous yellow solid, isoineleganolide D (**351**, 5 mg, 17% yield) as an amorphous white solid, and dienone **352** (3 mg, 10% yield) as an amorphous white solid.

Isoineleganolide C (*ent*-313): R_f = 0.27 (2:3 EtOAc:CH_2Cl_2 eluent); ^{1}H NMR ($CDCl_3$, 600 MHz) δ 4.86 (dd, *J* = 2.3, 1.2 Hz, 1H), 4.80 (ddd, *J* = 7.0, 5.7, 2.6 Hz, 1H), 4.71–4.68 (m, 1H), 4.21 (d, *J* = 15.3 Hz, 1H), 3.91 (ddt, *J* = 7.4, 2.6, 1.3 Hz, 1H), 3.71 (dtd, *J* = 17.9, 2.8, 1.3 Hz, 1H), 3.31 (ddd, *J* = 13.2, 7.4, 5.8 Hz, 1H), 3.08 (dq, *J* = 15.3, 2.8 Hz, 1H), 2.91–2.83 (m, 1H), 2.78 (dp, *J* = 9.1, 4.5 Hz, 1H), 2.71 (ddd, *J* = 16.5, 4.5, 1.2 Hz, 1H), 2.53 (m, 1H), 2.48–2.41 (m, 1H), 2.41–2.35 (m, 1H), 2.26–2.22 (m, 1H), 1.79–1.78 (m, 3H), 1.30 (s, 3H); ^{13}C NMR ($CDCl_3$, 126 MHz) δ 207.9, 196.5, 172.1, 149.7, 145.6,

128.2, 111.3, 79.5, 78.2, 59.8, 51.0, 46.2, 43.0, 42.4, 39.7, 39.5, 33.8, 25.2, 21.3; IR (Neat Film, NaCl) 3458, 2960, 2923, 2854, 1767, 1709, 1662, 1438, 1377, 1262, 1139, 1038 cm^{-1}; HRMS (FAB+) *m/z* calc'd for $C_{19}H_{23}O_5$ $[M+H]^+$: 331.1545, found 331.1548; $[\alpha]_D^{25.0}$ –66.3° (*c* 0.275, $CHCl_3$).

Isoineleganolide D (351): R_f = 0.73 (3:1 EtOAc:CH_2Cl_2 eluent); ^1H NMR ($CDCl_3$, 500 MHz) δ 4.99 (t, *J* = 5.1 Hz, 1H), 4.83 (q, *J* = 1.5 Hz, 1H), 4.77 (s, 1H), 4.01 (bt, *J* = 7.0 Hz, 1H), 3.53 (dd, *J* = 14.3, 2.7 Hz, 1H), 3.22 (d, *J* = 8.6 Hz, 1H), 3.19 (t, J = 2.9 Hz, 1H), 2.95–2.77 (m, 3H), 2.77–2.64 (m, 2H), 2.54 (dd, *J* = 14.3, 10.9 Hz, 1H), 2.25 (t, *J* = 13.3 Hz, 1H), 2.19 (s, 3H) 1.77 (s, 3H), 1.69 (app t, *J* = 13.9 Hz, 1H); ^{13}C NMR ($CDCl_3$, 126 MHz) δ 205.1, 195.1, 175.0, 151.2, 146.5, 131.3, 110.7, 79.0, 76.3, 53.5, 53.2, 49.2, 46.2, 45.7, 42.8, 38.7, 37.9, 20.9, 16.3; IR (Neat Film, NaCl) 3355, 2922, 1750, 1712, 1679, 1626, 1372, 1260, 1184, 1017, 801 cm^{-1}; HRMS (MM: ESI-APCI) *m/z* calc'd for $C_{19}H_{23}O_5$ $[M+H]^+$: 331.1540, found 331.1539; $[\alpha]_D^{25.0}$ +10.5 ° (*c* 0.200, $CHCl_3$).

Dienone 352: R_f = 0.61 (2:3 EtOAc:CH_2Cl_2 eluent); ^1H NMR ($CDCl_3$, 500 MHz) δ 4.98 (td, *J* = 4.5, 1.1 Hz, 1H), 4.84 (td, *J* = 1.4, 0.7 Hz, 1H), 4.72 (q, *J* = 1.0 Hz, 1H), 4.16–4.08 (m, 2H), 3.76 (ddt, *J* = 7.4, 2.5, 1.2 Hz, 1H), 3.62 (dd, *J* = 18.1, 3.5 Hz, 1H), 3.14 (ddt, *J* = 13.6, 3.3, 2.4 Hz, 1H), 2.92–2.88 (m, 2H), 2.79–2.68 (m, 2H), 2.49–2.41 (m, 1H), 2.28–2.20 (m, 4H), 1.78 (dt, *J* = 1.2, 0.5 Hz, 3H); ^{13}C NMR ($CDCl_3$, 126 MHz) δ 196.4, 193.8, 172.1, 156.9, 149.0, 145.9, 131.4, 128.2, 110.8, 78.5, 50.4, 49.0, 45.7, 42.5, 39.8, 38.7, 34.3, 21.0, 16.7; IR (Neat Film, NaCl) 2924, 1767. 1674, 1622, 1435, 1377, 1259, 1158, 893, 754 cm^{-1}; HRMS (MM: ESI-APCI) *m/z* calc'd for $C_{19}H_{21}O_4$ $[M+H]^+$: 313.1434, found 313.1437; $[\alpha]_D^{25.0}$ +41.1° (*c* 0.250, $CHCl_3$).

3.10 Notes and References

1. (a) *Bioactive Natural Products: Detection, Isolation, and Structural Determination*; Colegate, S. M., Molyneux, R. J., Eds.; CRC Press: Boca Roton, 2008. (b) Newman, D. J.; Cragg, G. M.; Snader, K. M. *Nat. Prod. Rep.* **2000**, *17*, 215–234. (c) Grabley, S.; Thiericke, R. *Adv. Biochem. Eng. Biotechnol.* **1999**, *64*, 101–154. (d) Kapoor, L. D. *CRC Handbook of Ayurvedic Medicinal Plants*; CRC Press: Portland, 1990. (e) Chang, H.-M.; Bu, P. P.-H. *Pharmacology and Applications of Chinese Materia Medica*; World Scientific Publishing: Singapore, 1986, Vols. 1–2.

2. (a) Villa, F. A.; Gerwick, L. *Immunopharmacol. Immunotoxicol.* **2010**, *32*, 228–237. (b) Cragg, G. M.; Newman, D. J. Anticancer drug discovery and development from natural products. In *Bioactive Natural Products: Detection, Isolation, and Structural Determination*; Colegate, S. M., Molyneux, R. J., Eds.; CRC Press: Boca Roton, 2008; pp. 323–370. (c) Cragg, G. M. *Med. Res. Rev.* **1998**, *18*, 315–331.

3. (a) Mambu, L.; Grellier, P. Antimalarial Compounds from Traditionally Used Medicinal Plants. In *Bioactive Natural Products: Detection, Isolation, and Structural Determination*; Colegate, S. M., Molyneux, R. J., Eds.; CRC Press: Boca Roton, 2008; pp 491–530. (b) Gademann, K.; Kobylinska, J. *Chem. Rec.* **2009**, *9*, 187–198. (c) Mojab, F. *Avicenna J. Phytomed.* **2012**, *2*, 52–62.

4. (a) Jones, B.; Kazlauskas, R. J. *Nature Chem.* **2015**, *7*, 11–12. (b) Brown, D. G.; Lister, T.; May-Dracka, T. L. *Biorg. Med. Chem. Lett.* **2014**, *24*, 413–418. (c)

Von Nussbaum, F.; Brands, M.; Hinzen, B.; Weigand, S.; Häbich, D. *Angew. Chem., Int. Ed.* **2006**, *45*, 5072–5129.

5. (a) Choi, D.-Y.; Choi, H. *Arch. Pharm. Res.* **2014**, *38*, 139–170. (b) Fang, L.; Gou, S.; Fang, X.; Cheng, L.; Fleck, C. *Mini Rev. Med. Chem.* **2013**, *13*, 870–887. (c) Chen, X.; Decker, M. *Curr. Med. Chem.* **2013**, *20*, 1673–1685. (d) Magrone, T.; Marzulli, G.; Jirillo, E. *Curr. Pharm. Des.* **2012**, *18*, 34–42.

6. (a) Li, J. W.-H.; Vederas, J. C. *Science* **2009**, *325*, 161–165. (b) Ganesan, A. *Curr. Opin. Chem. Biol.* **2008**, *12*, 306–317. (c) Koehn, F. E.; Carter, G. T. *Nat. Rev. Drug Discov.* **2005**, *4*, 206–220. (d) Cragg, G. M.; Newman, D. J.; Snader, K. M. *J. Nat. Prod.* **1997**, *60*, 52–60.

7. (a) Li, Y.; Pattenden, G. *Nat. Prod. Rep.* **2011**, *28*, 1269–1310. (b) Li, Y.; Pattenden, G. *Nat. Prod. Rep.* **2011**, *28*, 429–440. (c) Montaser, R.; Luesch, H. *Future Med. Chem.* **2011**, *3*, 1475–1489. (d) Berrue, F.; Kerr, R. G. *Nat. Prod. Rep.* **2009**, *26*, 681–710. (e) Roethle, P. A.; Trauner, D. *Nat. Prod. Rep.* **2008**, *25*, 298–317. (f) Kamel, H. N.; Slattery, M. *Pharm. Biol.* **2005**, *43*, 253–269. (g) Rodríguez, A. D. *Tetrahedron* **1995**, *51*, 4571–4618. (h) Tius, M. A. *Chem. Rev.* **1988**, *88*, 719–732.

8. Duh, C.-Y.; Wang, S.-K.; Chia, M.-C.; Chiang, M. Y. *Tetrahedron Lett.* **1999**, *40*, 6033–6035.

9. Radhika, P.; Subba Rao, P. V.; Anjaneyulu, V.; Asolkar, R. N.; Laatsch, H. *J. Nat. Prod.* **2002**, *65*, 737–739.

10. Lillsunde, K.-E.; Festa, C.; Adel, H.; de Marino, S.; Lombardi, V.; Tilvi, S.; Nawrot, D.; Zampella, A.; D'Souza, L.; D'Auria, M.; Tammela, P. *Marine Drugs* **2014**, *12*, 4045–4068.

11. Tseng, Y.-J.; Ahmed, A. F.; Dai, C.-F.; Chiang, M. Y.; Sheu, J.-H. *Org. Lett.* **2005**, *7*, 3813–3816.

12. Sheu, J.-H.; Ahmed, A. F.; Shiue, R.-T.; Dai, C.-F.; Kuo, Y.-H. *J. Nat. Prod.* **2002**, *65*, 1904–1908.

13. Iguchi, K.; Kajiyama, K.; Yamada, Y. *Tetrahedron Lett.* **1995**, *36*, 8807–8808.

14. (a) Horn, E. J. Studies Toward the Synthesis of Ineleganolide. Ph.D. dissertation, University of California at Irvine, Irvine, CA, 2014. (b) Tang, F.; Moeller, K. D. *Tetrahedron* **2009**, *65*, 10863–10875. (c) Tang, F.; Moeller, K. D. *J. Am. Chem. Soc.* **2007**, *129*, 12414–12415. (d) Ueda, Y.; Abe, H.; Iguchi, K.; Ito, H. *Tetrahedron Lett.* **2011**, *52*, 3379–3381.

15. The biosynthetic speculations concerning the formation of ineleganolide (**9**) and sinulochmodin C (**10**) form a common macrocyclic precursor through a series of anionic intramolecular cyclizations were investigated and confirmed by the biomimetic semisynthesis, see: Li, Y.; Pattenden, G. *Tetrahedron* **2011**, *67*, 10045–10052.

16. Craig, R. A., II; Roizen, J. L.; Smith, R. C.; Jones, A. C.; Stoltz, B. M. *Org. Lett.* **2012**, *14*, 5716–5719.

17. For the intermolecular asymmetric palladium-catalyzed allylic alkylation of ketodioxanones, see: Seto, M.; Roizen, J. L.; Stoltz, B. M. *Angew. Chem., Int. Ed.* **2008**, *47*, 6873–6876.

18. Previously, (*R*)-*t*-BuPhox has been synthesized and used by our group in the enantioselective total synthesis of (+)-Liphagal, see: Day, J. J.; McFadden, R. M.; Virgil, S. C.; Kolding, H.; Alleva, J. L.; Stoltz, B. M. *Angew. Chem., Int. Ed.* **2011**, *50*, 6814–6818.

19. For full details, see Chapter 2, Section 2.7.4.

20. (a) Chen, L.; Deslongchamps, P. *Can. J. Chem.* **2005**, *83*, 728–740. (b) González, M. A.; Ghosh, S.; Rivas, F.; Fischer, D.; Theodorakis, E. A. *Tetrahedron Lett.* **2004**, *45*, 5039–5041. (c) Chen, J.; Marx, J. N. *Tetrahedron Lett.* **1997**, *38*, 1889–1892.

21. Shibuya, M.; Tomizawa, M.; Iwabuchi, Y. *J. Org. Chem.* **2008**, *73*, 4750–4752.

22. (a) Spangler, J. E.; Lian, Y.; Raikar, S. N.; Davies, H. M. L. *Org. Lett.* **2014**, *16*, 4794–4797. (b) Osler, J. D.; Unsworth, W. P.; Taylor, R. J. K. *Org. Biomol. Chem.* **2013**, *11*, 7587–7594. (c) Hudlicky, T.; Fan, R.; Reed, J. W.; Gadamasetti, K. G. *Org. React.* **2004**, *41*, 1–133. (d) Davies, H. M. L.; Stafford, D. G.; Doan, B. D.; Houser, J. H. *J. Am. Chem. Soc.* **1998**, *120*, 3326–3331. (e) Davies, H. M. L. *Tetrahedron* **1993**, *49*, 5203–5223. (f) Wong, H. N.; Hon, M. Y.; Tse, C. W.; Yip, Y. C.; Tanko, J.; Hudlicky, T. *Chem. Rev.* **1989**, *89*, 165–198. (g) Vogel, E. *Angew. Chem., Int. Ed.* **1963**, *2*, 1–11.

23. The rhodium sources evaluated included $Rh_2(OAc)_4$, $Rh_2(PhCO_2)_4$, $Rh_2(esp)_2$, $Rh_2(cap)_4$, $Rh_2(F_3CCO_2)_4$, and $Rh(oct)_4$ in CH_2Cl_2 from –20 °C to 40 °C. $Rh_2(cap)_4$ produced no product, resulting in quantitative recovery of diazoester ***ent*-320**. Under all other conditions, the ratio of diene **324** to enone **325** was consistent.

24. (a) Totobenazara, J.; Haroun, H.; Rémond, J.; Adil, K.; Dénès, F.; Lebreton, J.;

Gaulon-Nourry, C.; Gosselin, P. *Org. Biomol. Chem.* **2012**, *10*, 502–505. (b) Li, S.; Parish, E. J.; Webb, T.; Brodie, A. M. *Bioorg. Med. Chem. Lett.* **1997**, *7*, 403–408.

25. (a) Procopio, A.; Dalpozzo, R.; De Nino, A.; Nardi, M.; Sindona, G.; Tagarelli, A. *Synlett* **2004**, 2633–2635. (b) Karamé, I.; Tommasino, M. L.; Lemaire, M. *Tetrahedron Lett.* **2003**, *44*, 7687–7689. (c) Maruoka, K.; Murase, N.; Bureau, R.; Ooi, T.; Yamamoto, H. *Tetrahedron* **2001**, *50*, 3663–3672. (d) Ranu, B. C.; Jana, U. *J. Org. Chem.* **1998**, *63*, 8212–8216. (e) Marson, C. M.; Harper, S.; Walker, A. J.; Pickering, J.; Campbell, J.; Wrigglesworth, R.; Edge, S. J. *Tetrahedron* **1993**, *49*, 10339–10354. (f) Smith, J. G. *Synthesis* **1984**, 629–656. (g) Lee, K. H.; Ibuka, T.; Kim, S. H.; Vestal, B. R.; Hall, I. H.; Huang, E. S. *J. Med. Chem.* **1975**, *18*, 812–817.

26. A characteristic list of the conditions attempted to induce the desired epoxide isomerization: $H_2SO_4/CHCl_3$, $SiO_2/CHCl_3$, DBU/$CHCl_3$, KO*t*-Bu/THF, $Pd(CH_3CN)_2Cl_2$/benzene, $BF_3{\bullet}Et_2O/CHCl_3$, $In(OTf)_3/CHCl_3$, $Al(O\textit{i}\text{-}Pr)_3/CHCl_3$, $Ti(O\textit{i}\text{-}Pr)_4$/THF, $Zn(OTf)_2$/toluene, $Mg(OTf)_2$/toluene, $MgCl_2$/toluene, $MgBr_2$/toluene.

27. Conditions attempted to make enol ether of methyl ketone **338**: PMBCl/EtN(*i*-Pr)$_2$/CH_2Cl_2, PMBCl/TBAI/EtN(*i*-Pr)$_2$/CH_2Cl_2, PMBCl/LDA/CH_2Cl_2, MOMCl/ EtN(*i*-Pr)$_2$/CH_2Cl_2, methyl chloroformate/EtN(*i*-Pr)$_2$/CH_2Cl_2, pyrrolidine/$MgSO_4$/ toluene.

28. To our knowledge, there is no example of an anionic 2-oxy-Cope rearrangement in the literature, although the comparable 2-siloxy-Cope rearrangements have

been accomplished, see: (a) Vedejs, E.; Duncan, S. M. *J. Org. Chem.* **2000**, *65*, 6073–6081. (b) Hsu, D.-S.; Hsu, P.-Y.; Lee, Y.-C.; Liao, C.-C. *J. Org. Chem.* **2008**, *73*, 2554–2563.

29. The stereochemical assignment of ethyl ether **344** was accomplished by comparison to the unambiguous assignment of bromide **346** by single crystal X-ray analysis (vide infra).

30. The Lewis acids that accomplished the opening of epoxide **328** with their counterion include BF_3•Et_2O, $YbCl_3$, $MgCl_2$, $MgBr_2$, and MgI_2.

31. (a) Ly, T. W.; Liao, J.-H.; Shia, K.-S.; Liu, H.-J. *Synthesis* **2004**, 271–275. (b) Paisdor, B.; Kuck, D. *J. Org. Chem.* **1991**, *56*, 4753–4759. (c) Paritosh, D.; Byun, H.-S.; Engel, R. *Synth. Commun.* **1986**, *16*, 1343–1346. (d) Mancuso, A. J.; Swern, D. *Synthesis* **1981**, 165–185. (e) Kornblum, N.; Jones, W. J.; Anderson, G. J. *J. Am. Chem. Soc.* **1959**, *81*, 4113–4114.

32. The chloride analog of bromide **346** failed to undergo oxidation, resulting in the quantitative recovery of starting material. Alternatively, the iodide analog underwent oxidation, but provided diketone **347** in reduced yield. For further details and discussion, see appendix 8.

33. (a) Szostak, M.; Spain, M.; Procter, D. J. *J. Org. Chem.* **2014**, *79*, 2522–2537. (b) Egger, J.; Bretscher, P.; Freigang, S.; Kopf, M.; Carreira, E. M. *Angew. Chem., Int. Ed.* **2013**, *52*, 5382–5385. (c) Shoji, M.; Uno, T.; Kakeya, H.; Onose, R.; Shiina, I.; Osada, H.; Hayashi, Y. *J. Org. Chem.* **2005**, *70*, 9905–9915. (d) Yamaguchi, J.; Kakeya, H.; Uno, T.; Shoji, M.; Osada, H.; Hayashi, Y. *Angew. Chem., Int. Ed.* **2005**, *44*, 3110–3115. (e) Ready, J. M.; Reisman, S. E.; Hirata,

M.; Weiss, M. M.; Tamaki, K.; Ovaska, T. V.; Wood, J. L. *Angew. Chem. Int. Ed.* **2004**, *43*, 1270–1272. (f) Fuchs, J. R.; Mitchell, M. L.; Shabangi, M.; Flowers, R. A. *Tetrahedron Lett.* **1997**, *38*, 8157–8158. (g) Molander, G. A.; Hahn, G. *J. Org. Chem.* **1986**, *51*, 1135–1138. (h) Molander, G. A.; Hahn, G. *J. Org. Chem.* **1986**, *51*, 2596–2599.

34. Product formation assessed by ^{1}H NMR evaluation of the crude reaction product.

35. Exposure of diol **349** to LDA at low temperature induced an equilibrium between diol **349** and diastereomer **I** as determined by extensive ^{1}H NMR studies.

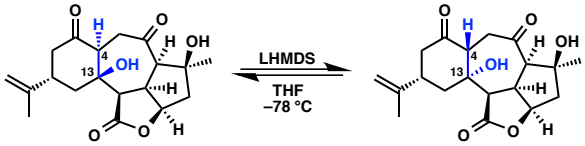

349 **I**

36. A characteristic list of the conditions attempted to induce the desired epoxide isomerization: DBU/CH_2Cl_2, $PdCl_2(CH_3CN)_2/CH_2Cl_2$, Grubbs Gen. II/MeOH, $RhCl_3 \bullet H_2O$/EtOH, LiHMDS/THF.

37. White, D. E.; Stewart, I. C.; Grubbs, R. H.; Stoltz, B. M. *J. Am. Chem. Soc.* **2008**, *130*, 810–811.

38. (a) Betancor, C.; Freire, R.; Pérez-Martín, I.; Prangé, T.; Suárez, E. *Tetrahedron* **2005**, *61*, 2803–2814. (b) Cornella, I.; Sestelo, J. P.; Mouriño, A.; Sarandeses, L. A. *J. Org. Chem.* **2002**, *67*, 4707–4714. (c) Paquette, L. A.; Sun, L.-Q.; Friedrich, D.; Savage, P. B. *J. Am. Chem. Soc.* **1997**, *119*, 8438–8450. (d) Dorta, R. L.; Francisco, C. G.; Hernández, R.; Salazar, J. A.; Suárez, E. *J. Chem. Res. (S)* **1990**, 240–241. (e) Concepción, J. I.; Francisco, C. G.; Hernández, R.; Salazar, J. A.; Suárez, E. *Tetrahedron Lett.* **1984**, *25*, 1953–1956.

39. The ketone moieties within enone could be reduced with hydride sources (e.g., $NaBH_4$, $Li(O\textit{t}\text{-}Bu)_3AlH$), but the reaction could not be performed chemo- or diastereoselectively.

40. Calculations were performed with Spartan '10 (Wavefunction, Inc., Irvine, CA). The in vacuo equilibrium geometry for each structure was calculated by a series of sequential calculations as follows: Hartree–Fock computation (equilibrium geometry, 3-21G basis set), DFT (equilibrium geometry, B3LYP/6-31G basis set), DFT (energy, B3LYP/6-311+G** basis set), DFT (equilibrium geometry, B3LYP/6-311+G** basis set). The error from these calculations is ±0.23 kcal/mol, thus all energy differences larger than 0.46 kcal/mol were considered significant. Except for molecular mechanics and semi-empirical models, the calculation methods used in Spartan have been documented in: Shao, Y.; Molnar, L. F.; Jung, Y.; Kussmann, J.; Ochsenfeld, C.; Brown, S. T.; Gilbert, A. T. B.; Slipchenko, L. V.; Levchenko, S. V.; O'Neill, D. P.; DiStasio, Jr., R. A.; Lochan, R. C.; Wang, T.; Beran, G. J. O.; Besley, N. A.; Herbert, J. M.; Lin, C. Y.; Van Voorhis, T.; Chien, S. H.; Sodt, A.; Steele, R. P.; Rassolov, V. A.; Maslen, P. E.; Korambath, P. P.; Adamson, R. D.; Austin, B.; Baker, J.; Byrd, E. F. C.; Dachsel, H.; Doerksen, R. J.; Dreuw, A.; Dunietz, B. D.; Dutoi, A. D.; Furlani, T. R.; Gwaltney, S. R.; Heyden, A.; Hirata, S.; Hsu, C-P.; Kedziora, G.; Khalliulin, R. Z.; Klunzinger, P. Lee, A. M.; Lee, M. S.; Liang, W. Z.; Lotan, I.; Nair, N.; Peters, B.; Proynov, E. I.; Pieniazek, P. A.; Rhee, Y. M.; Ritchie, J.; Rosta, E; Sherrill, C. D.; Simmonett, A. C.; Subotnik, J. E.; Woodcock, III, H. L.; Zhang, W.; Bell, A. T.; Chakraborty, A. K.; Chipman, D. M.; Keil, F. J.; Warshel, A.;

Hehre, W. J.; Schaefer, H. F.; Kong, J.; Krylov, A. I.; Gill, P. M. W.; Head-Gordon M. *Phys. Chem. Chem. Phys.* **2006**, *8*, 3172–3191.

41. Pangborn, A. B.; Giardello, M. A.; Grubbs, R. H.; Rosen, R. K.; Timmers, F. J. *Organometallics* **1996**, *15*, 1518–1520.

42. Voss, H.; Wannowius, K. J.; Elias, H. *J. Inorg. Nucl. Chem.* **1974**, *36*, 1402–1404.

43. Although we began with anhydrous $CeCl_3$, the drying procedure greatly increased the yield. It is likely increased surface area of the $CeCl_3$ after grinding due to stirring during the drying procedure that facilitated this yield increase.

44. The assignment of the structure of isoineleganolide B due to the fact that, while all of the predictive NMR experiments and empirical two-dimensional NMR data and mass spectral data indicate the oxetane structure is correct, some doubt still remains from the apparent O–H absorbance in the IR spectrum and the indication of an exchangeable proton on the molecule itself as deduced by two-dimensional NOE and DOSY experiments. Unfortunately, isoineleganolide B was not crystalline.

45. Only 20 lines appear in the ^{13}C spectrum of pyrazole **341**. Two are lost due to the symmetry of the TBS group. The remaining three carbons belong to the pyrazole ring and are broadened by the adjacent nitrogen atoms. Two of these three carbons, however, can be identified by two-dimensional ^{1}H–^{13}C gradient HMBC experiments and their approximate shifts are as follows: 146 ppm and 140 ppm.

46. For discussion of these failed reactions, see secton 3.6.

APPENDIX 5

Synthetic Summary for Chapter 3:

Progress Toward the Asymmetric Total Syntheses of the

Furanobutenolide Norcembranoid Diterpene Natural Products

Scheme A5.1. Construction of cis-1,3-Cyclopentenediol ***ent-322***

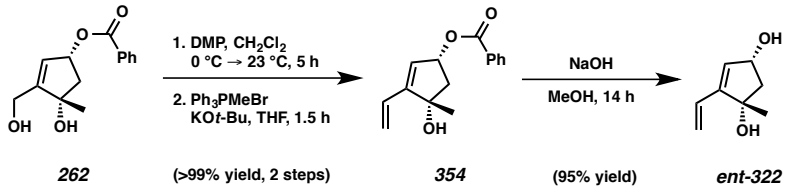

*Scheme A5.2. Construction of the Tetracyclic Core and Isomers of ent-Ineleganolide (****ent-9****)*

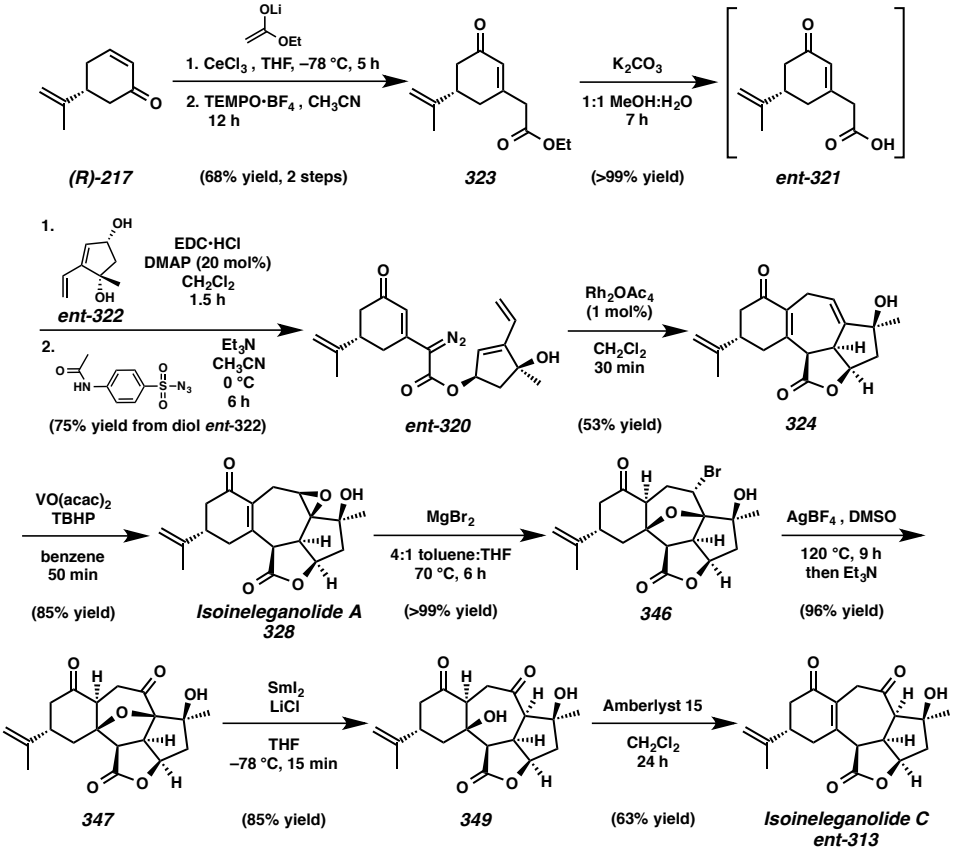

Scheme A5.3. Synthesis of Alternative cis-1,3-Cyclopentenediol ***ent-335***

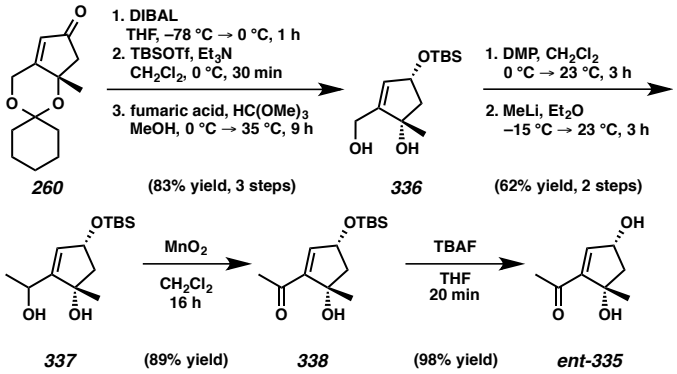

Scheme A5.4. Advancement of Methyl Ketone Fragment ***ent-335***

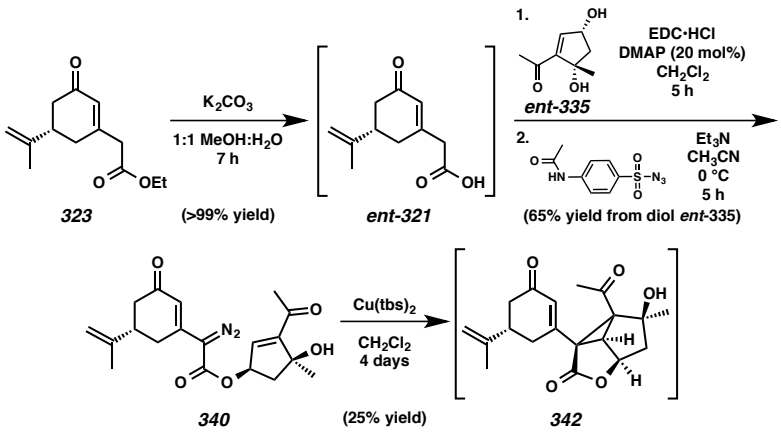

APPENDIX 6

Spectra Relevant to Chapter 3:

Progress Toward the Asymmetric Total Syntheses of the

Furanobutenolide Norcembranoid Diterpene Natural Products

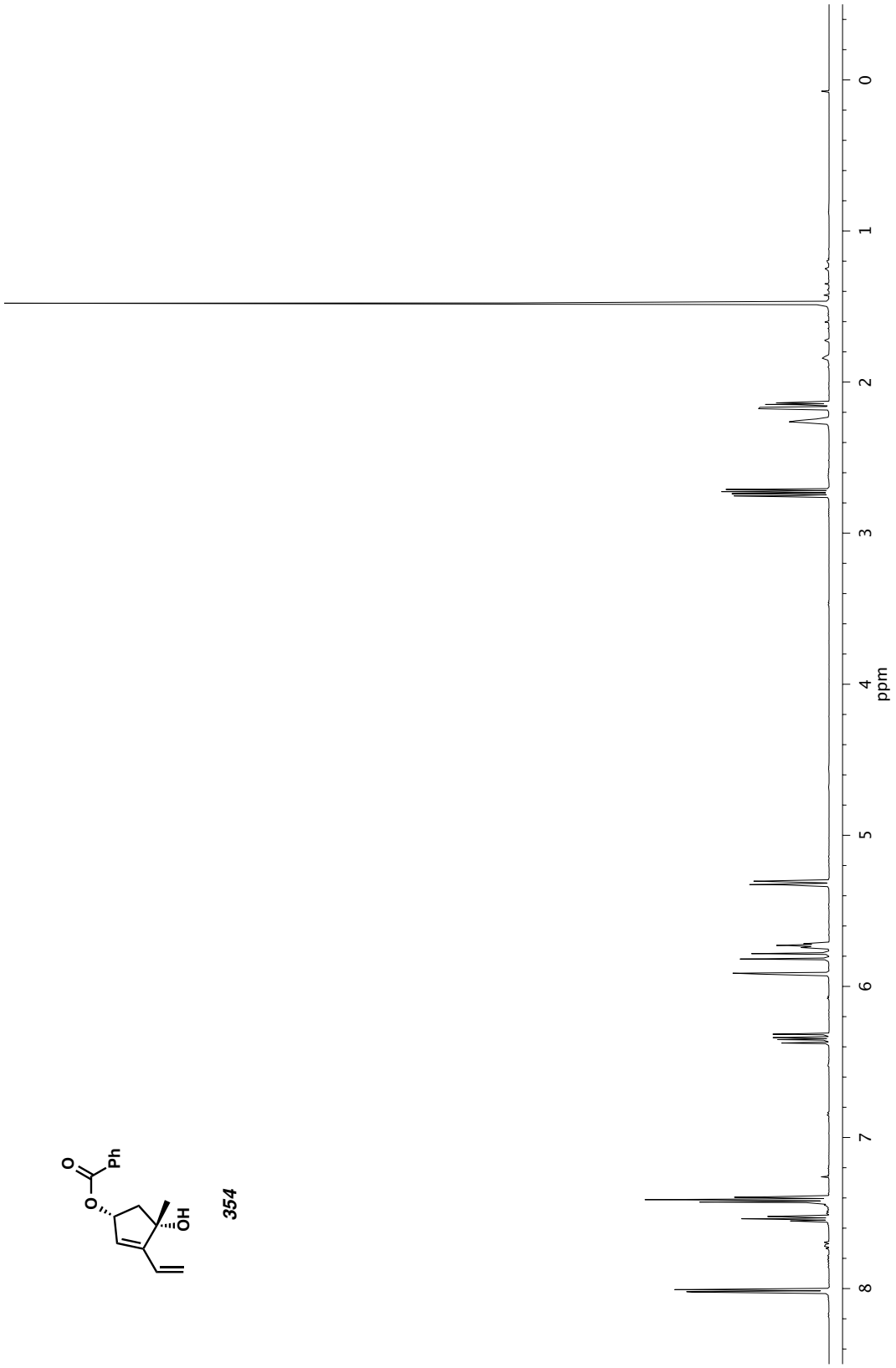

Figure A6.1. ^{1}H NMR (500 MHz, $CDCl_3$) of compound **354**.

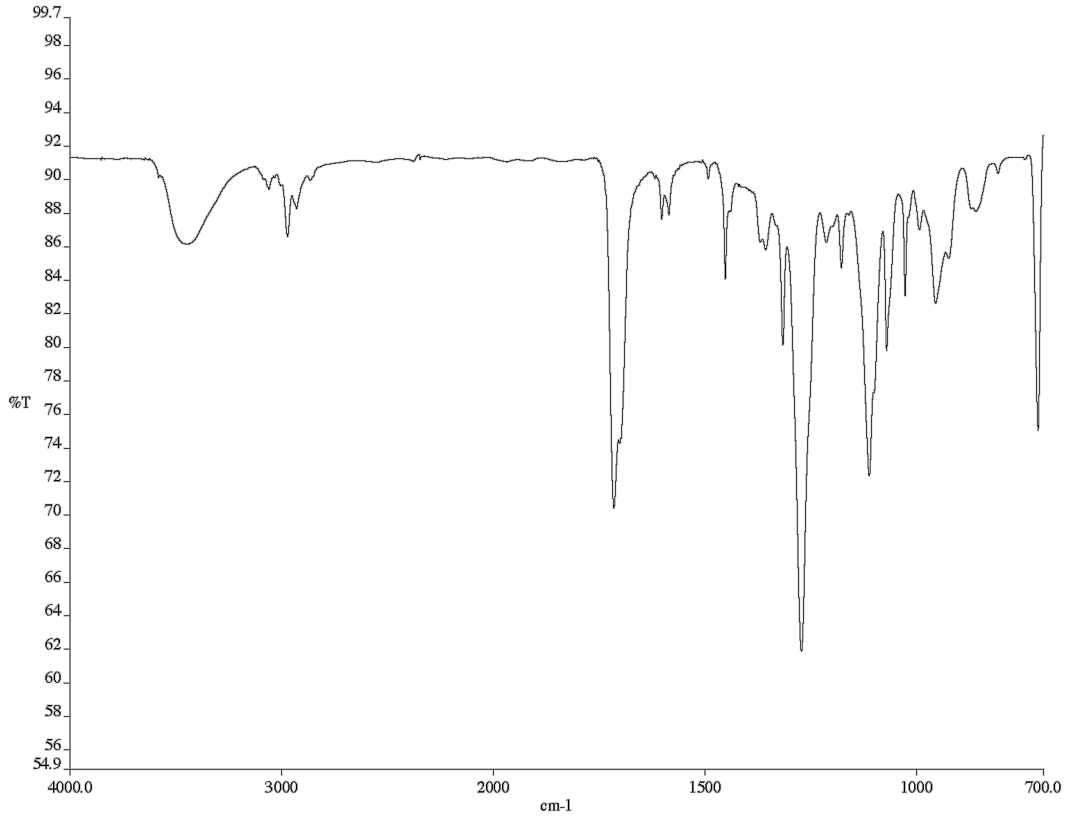

Figure A6.2. Infrared spectrum (Thin Film, NaCl) of compound **354**.

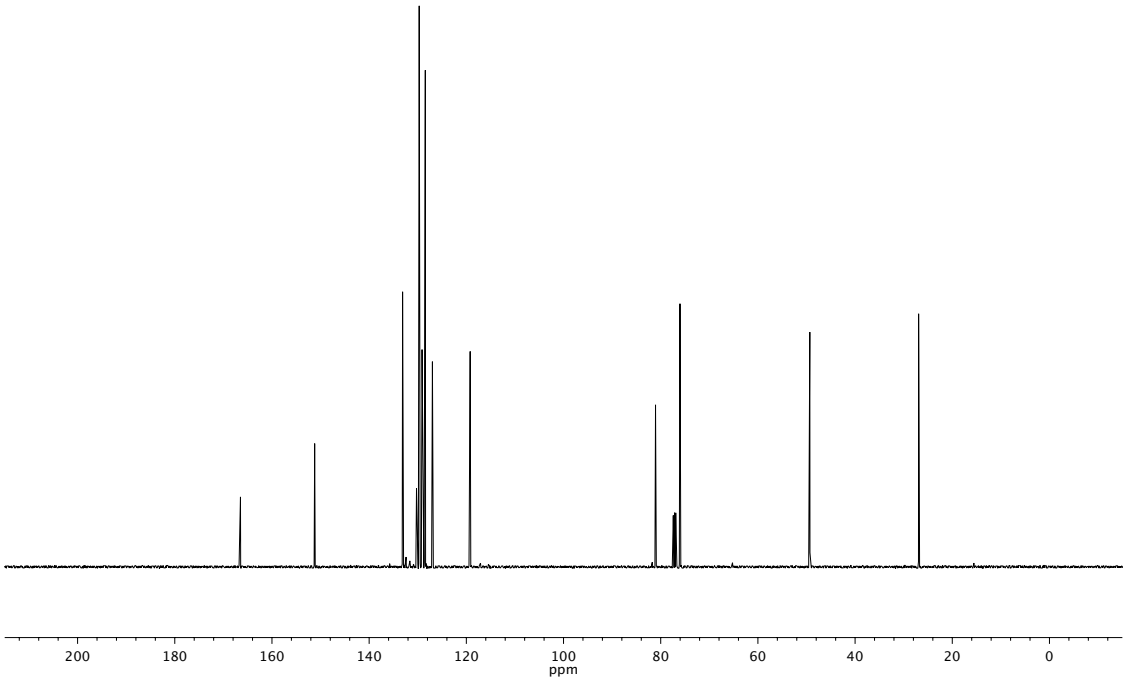

Figure A6.3. ^{13}C NMR (126 MHz, $CDCl_3$) of compound **354**.

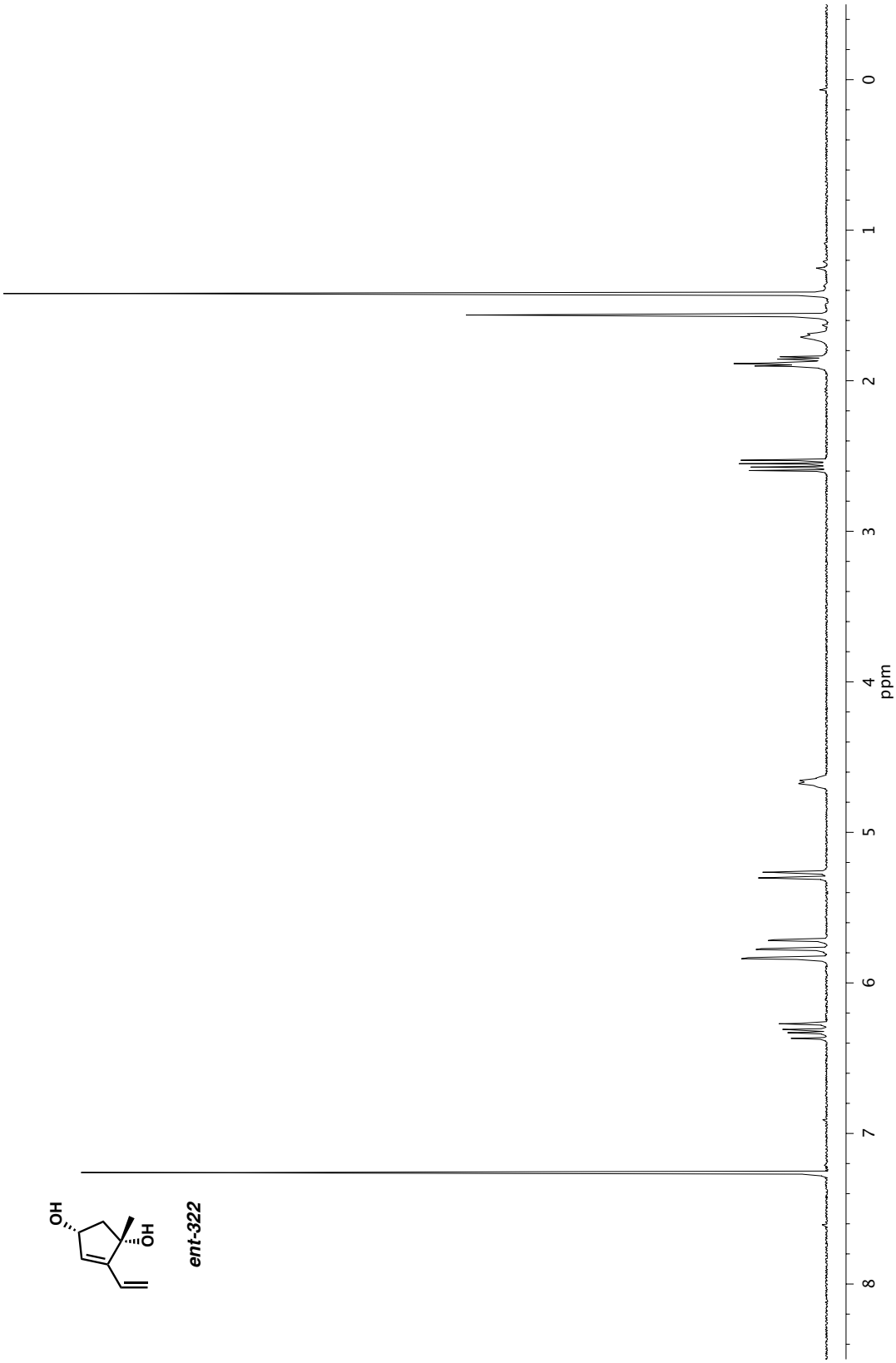

Figure A6.4. ^{1}H NMR (300 MHz, $CDCl_3$) of compound ***ent*-322**.

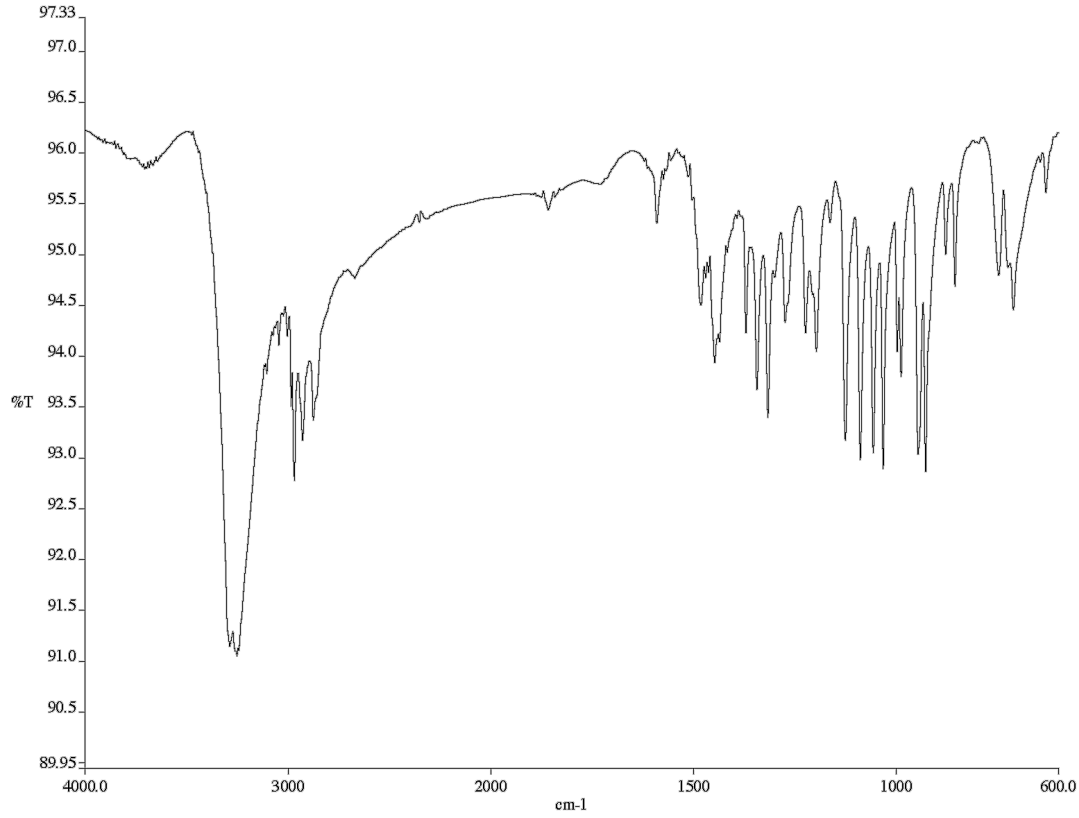

Figure A6.5. Infrared spectrum (Thin Film, NaCl) of compound ***ent*-322**.

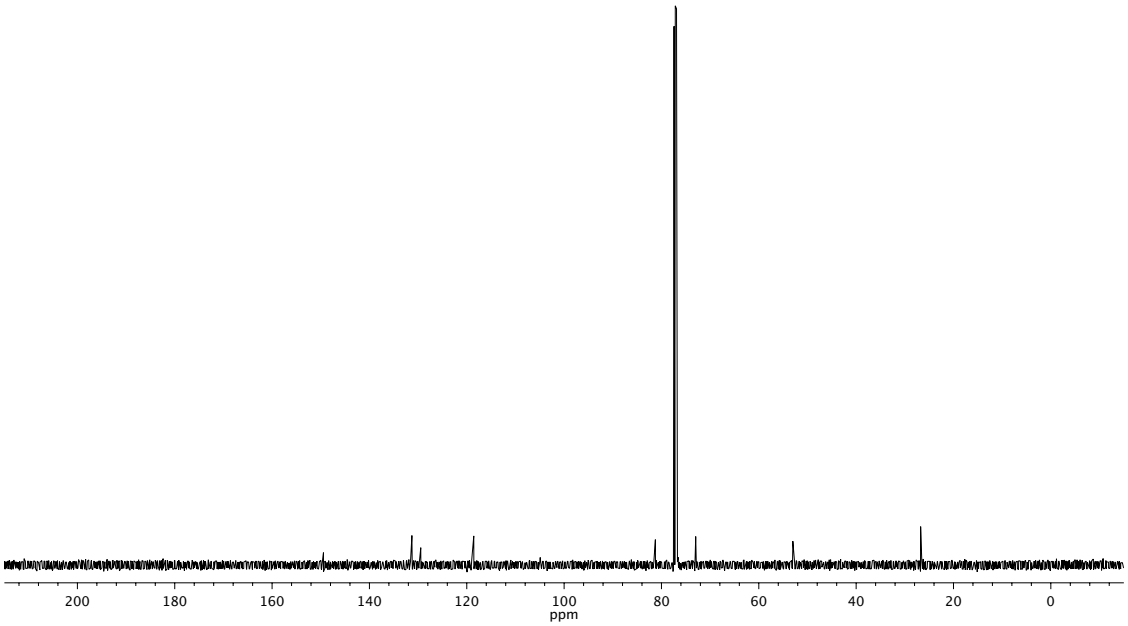

Figure A6.6. ^{13}C NMR (76 MHz, $CDCl_3$) of compound ***ent*-322**.

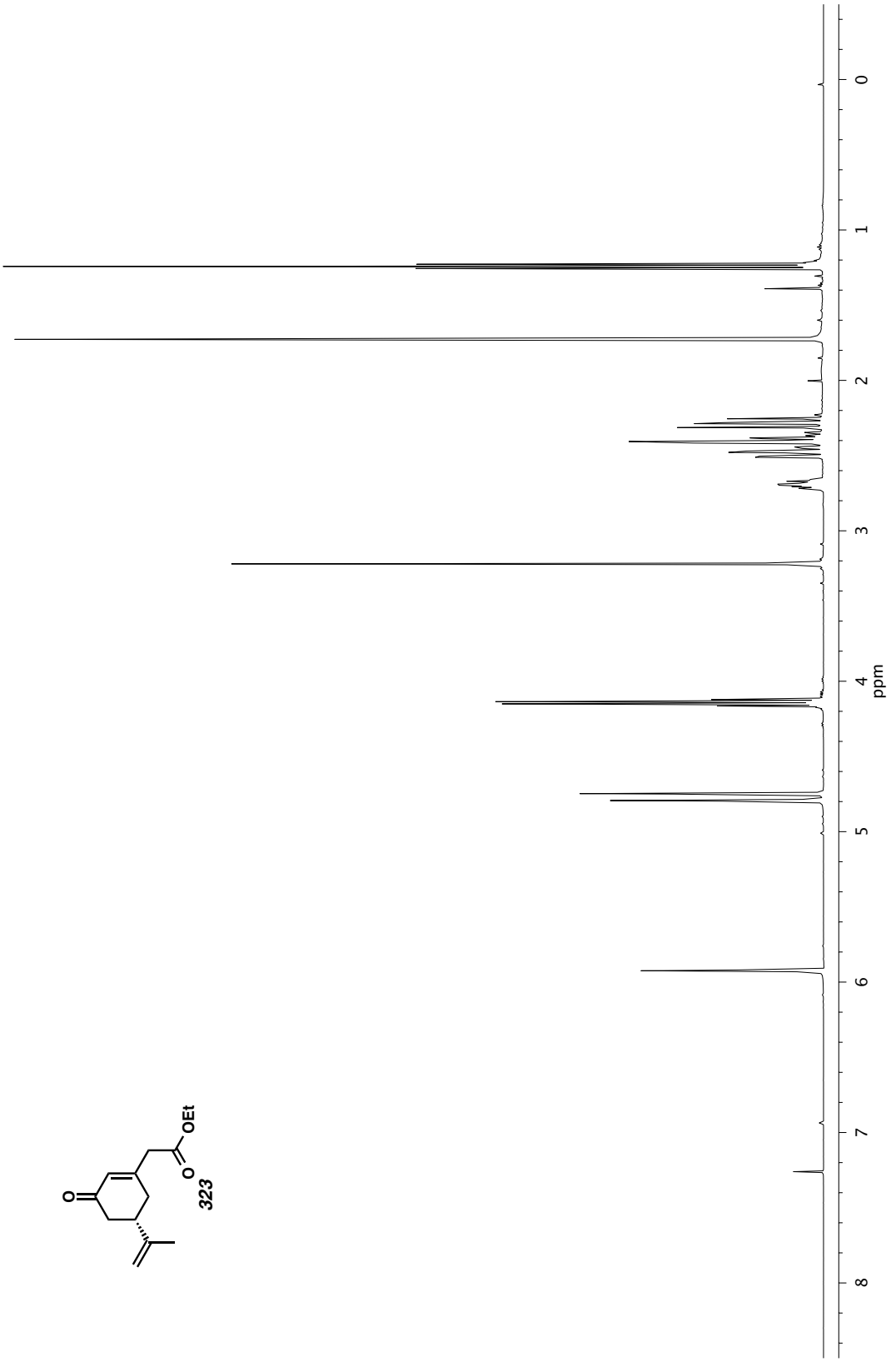

Figure A6.7. ^{1}H NMR (500 MHz, $CDCl_3$) of compound **323**.

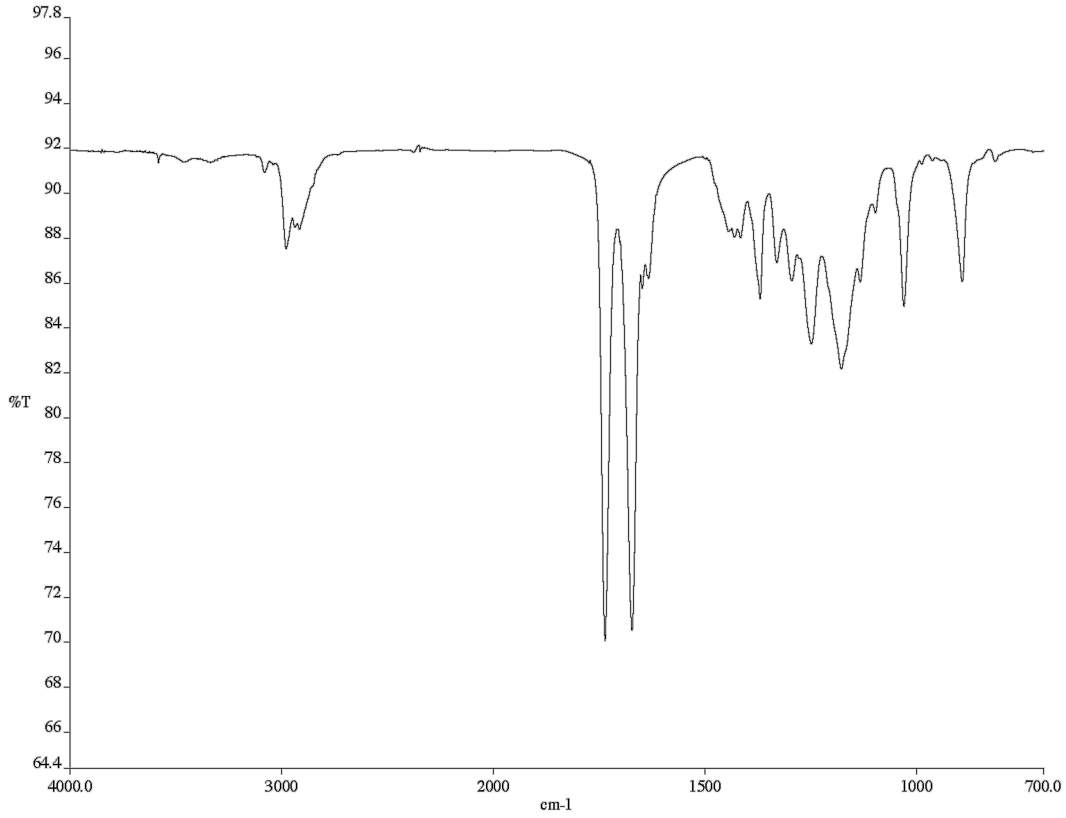

Figure A6.8. Infrared spectrum (Thin Film, NaCl) of compound **323**.

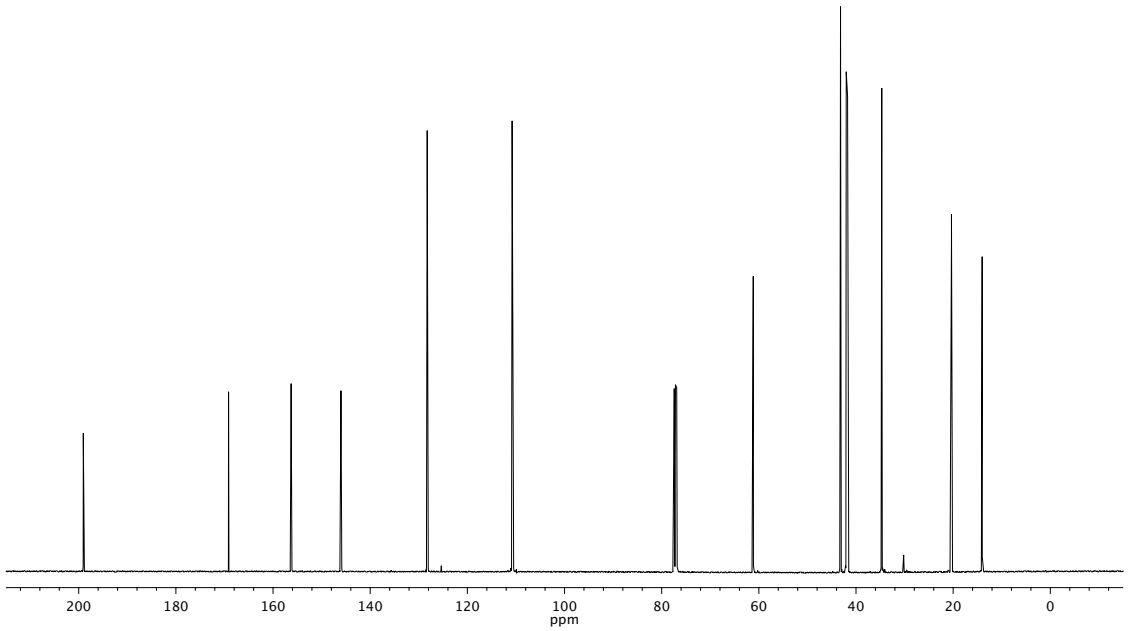

Figure A6.9. ^{13}C NMR (126 MHz, $CDCl_3$) of compound **323**.

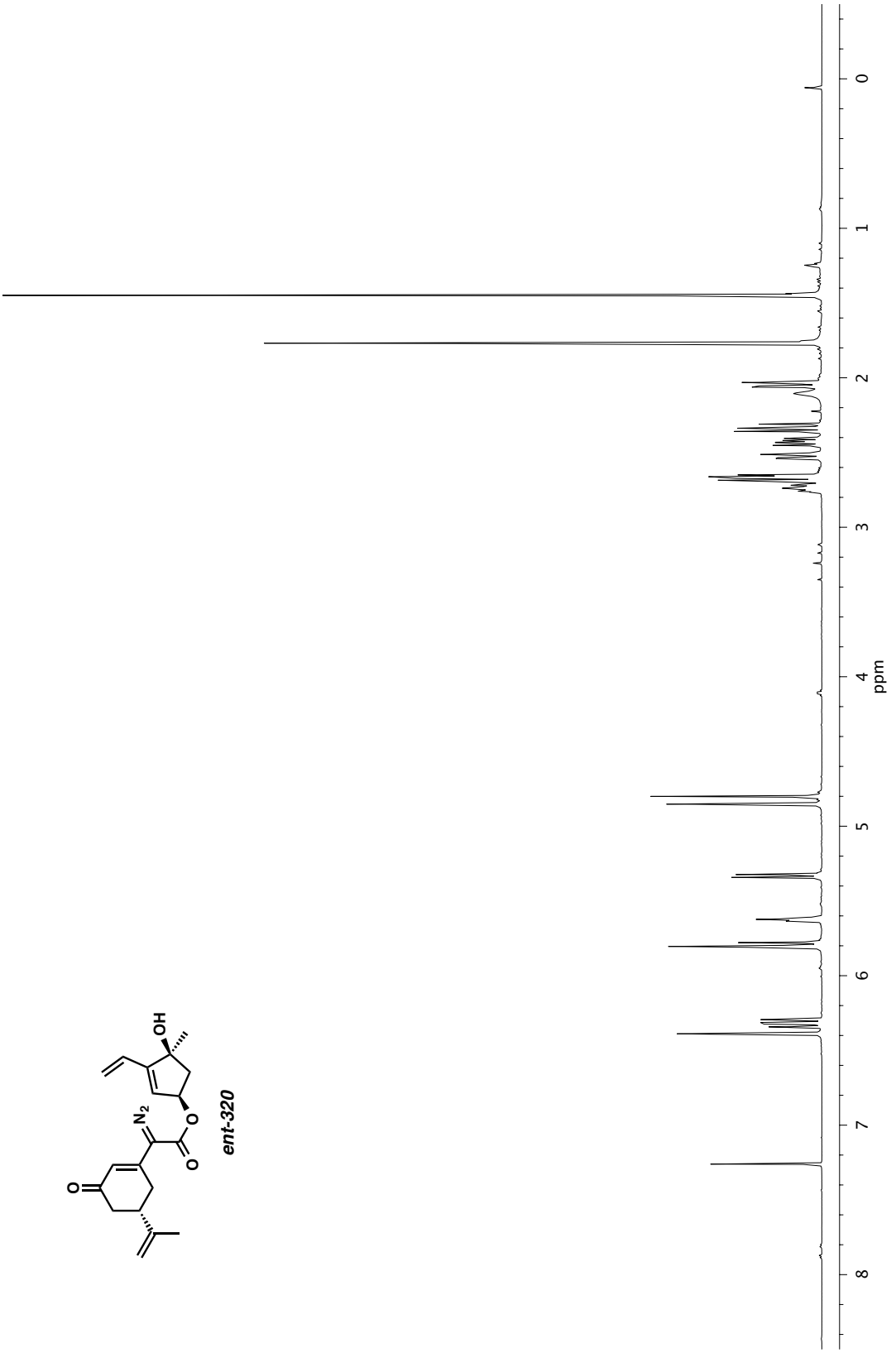

Figure A6.10. ^{1}H NMR (600 MHz, $CDCl_3$) of compound ***ent*-320**.

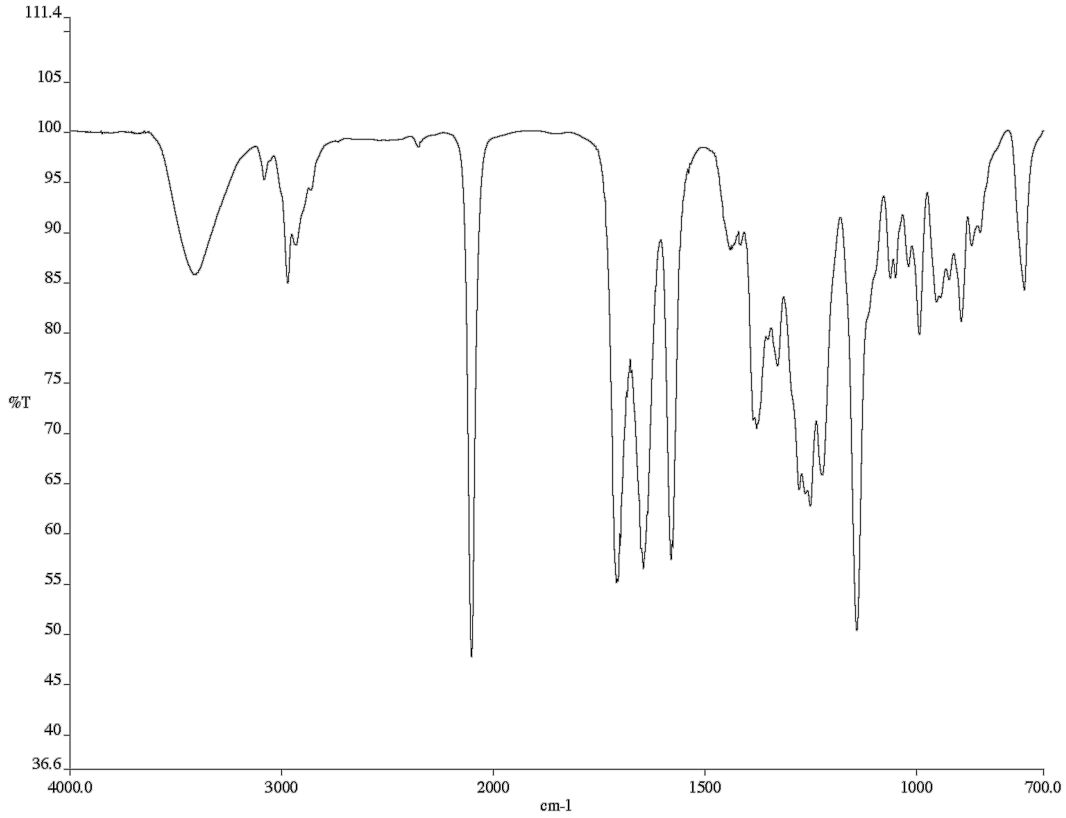

Figure A6.11. Infrared spectrum (Thin Film, NaCl) of compound ***ent*-320**.

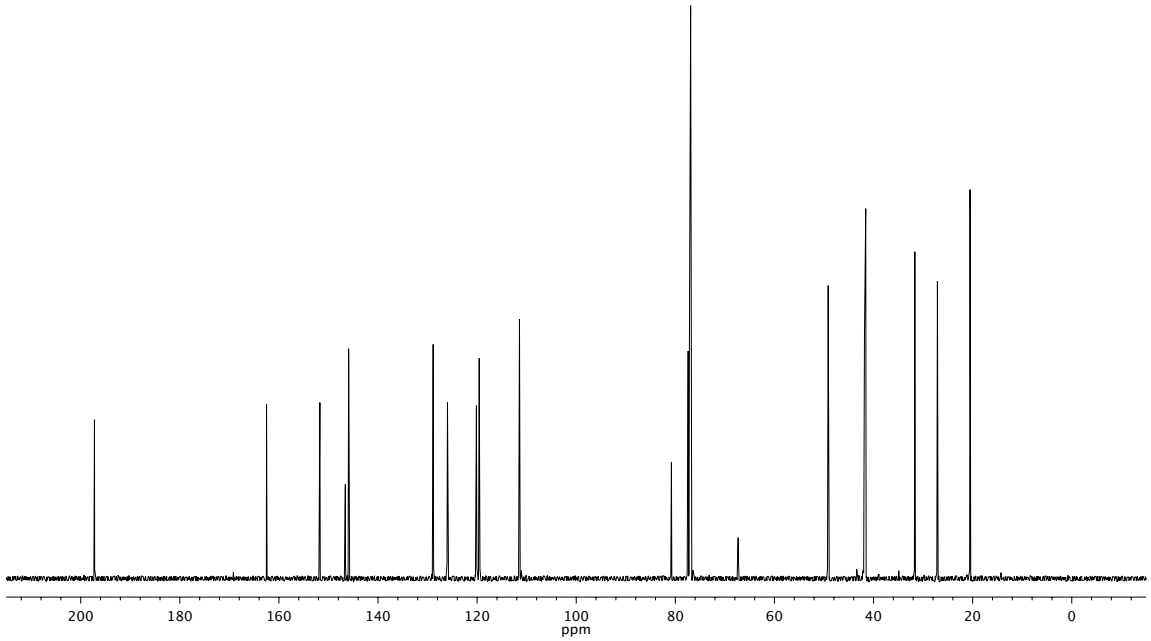

Figure A6.12. ^{13}C NMR (126 MHz, $CDCl_3$) of compound ***ent*-320**.

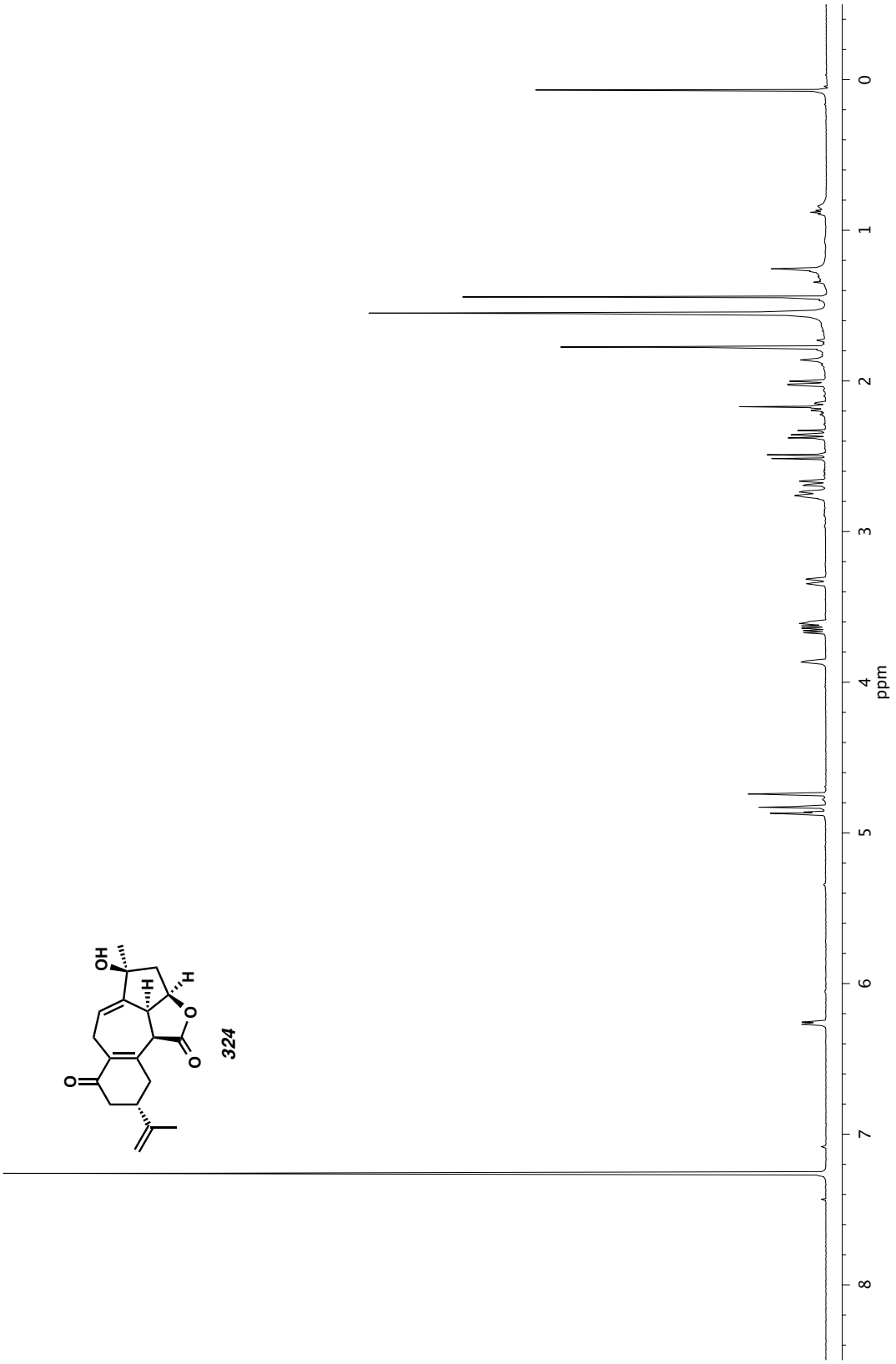

Figure A6.13. ^{1}H NMR (500 MHz, $CDCl_3$) of compound **324**.

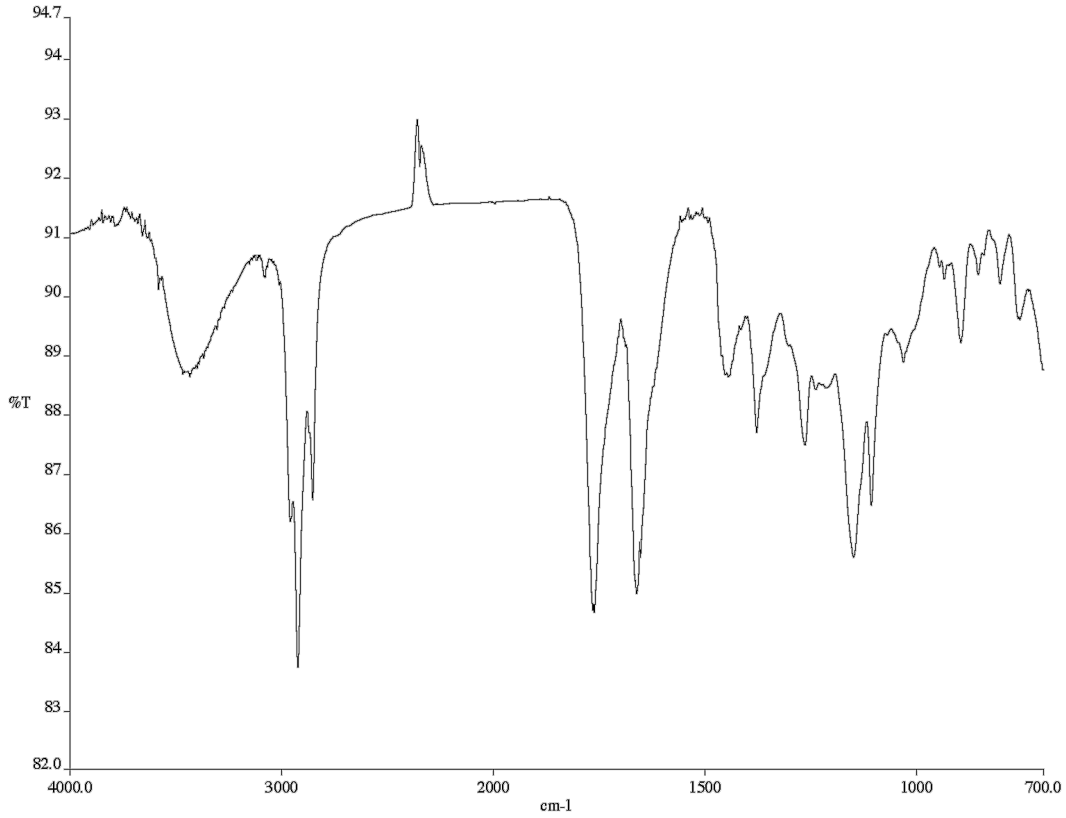

Figure A6.14. Infrared spectrum (Thin Film, NaCl) of compound **324**.

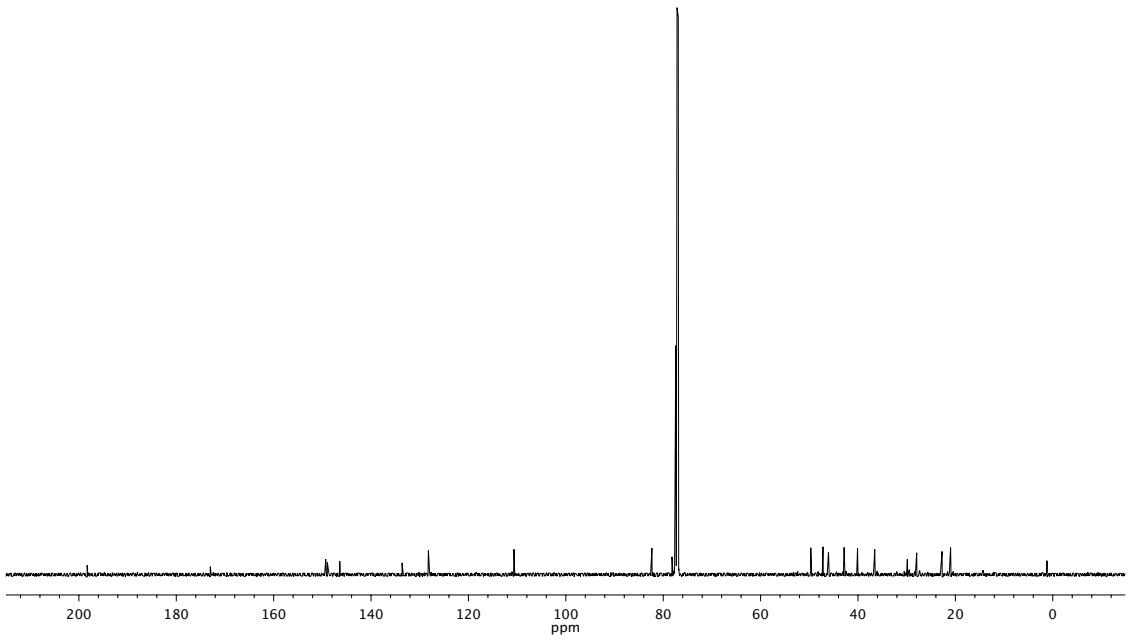

Figure A6.15. ^{13}C NMR (126 MHz, $CDCl_3$) of compound **324**.

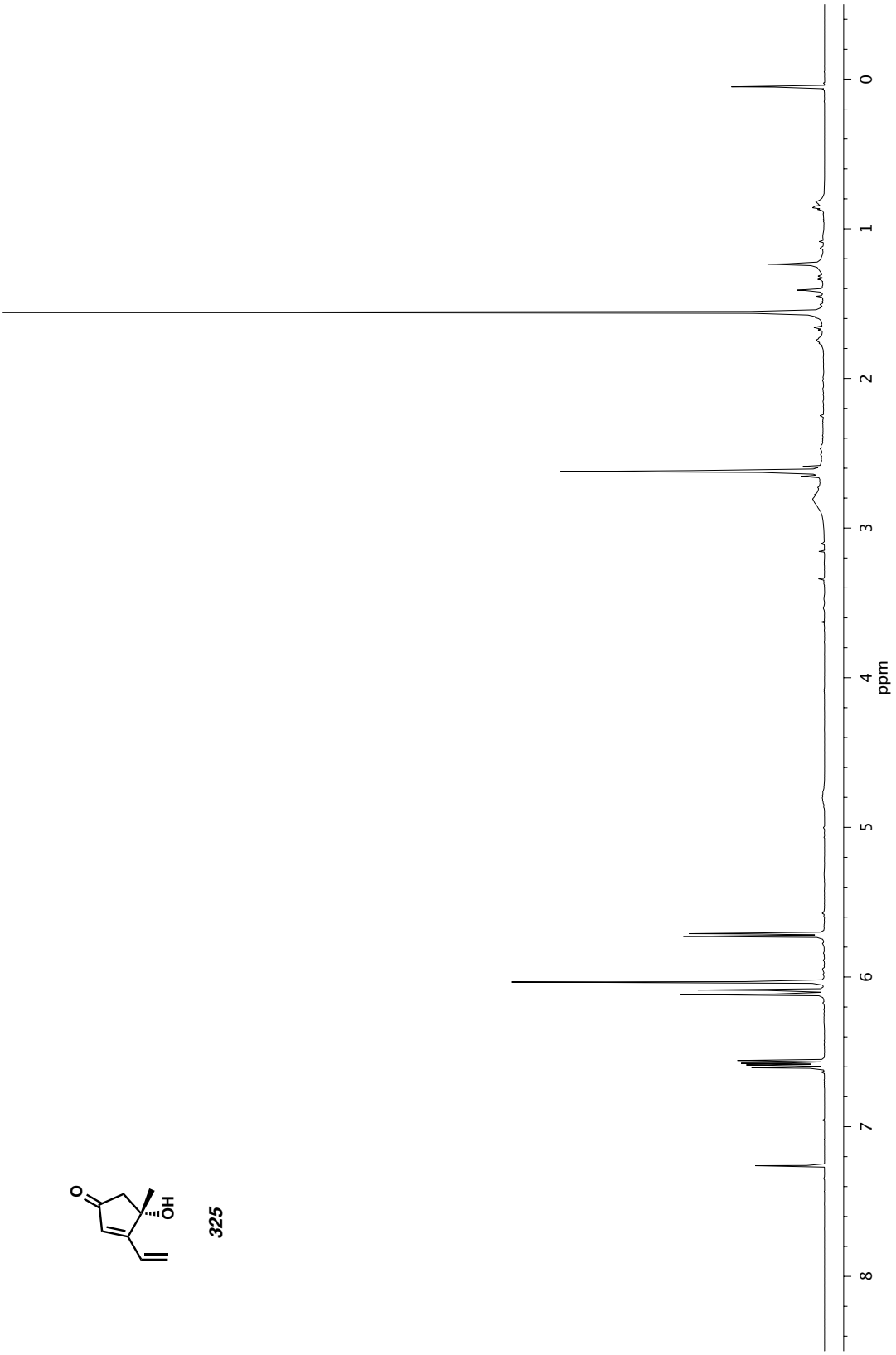

Figure A6.16. ^{1}H NMR (600 MHz, $CDCl_3$) of compound **325**.

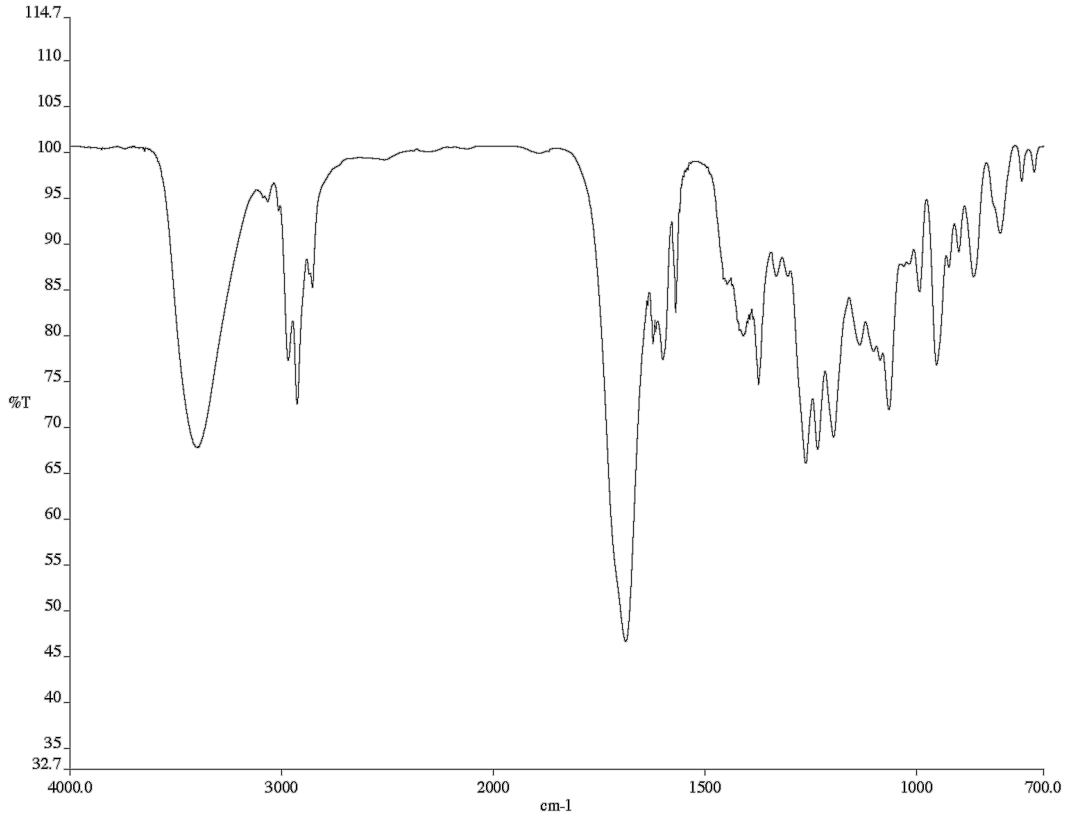

Figure A6.17. Infrared spectrum (Thin Film, NaCl) of compound **325**.

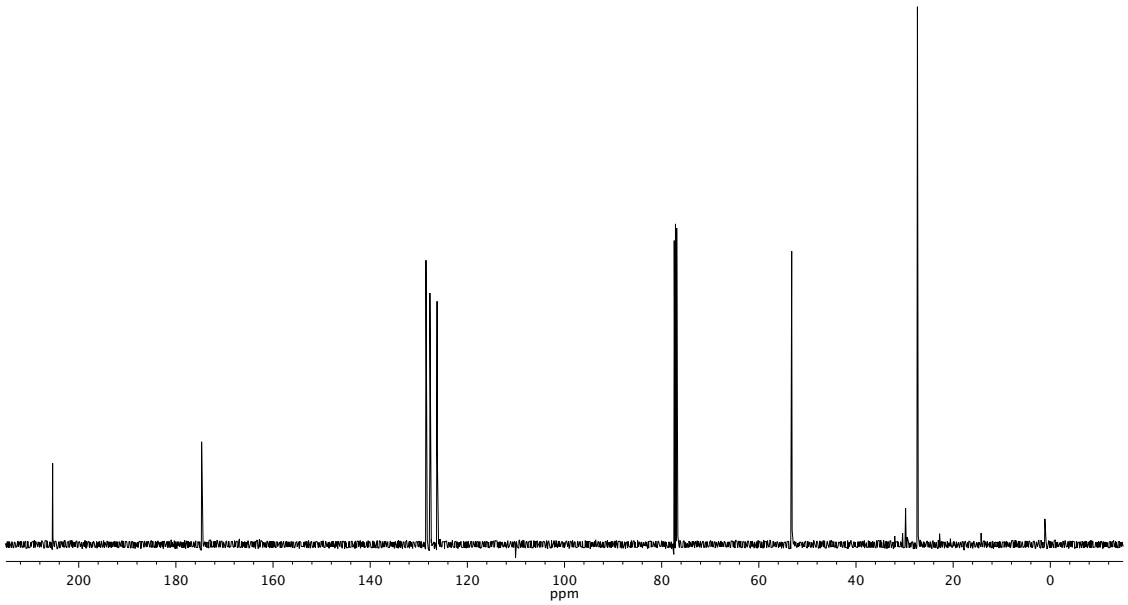

Figure A6.18. ^{13}C NMR (126 MHz, $CDCl_3$) of compound **325**.

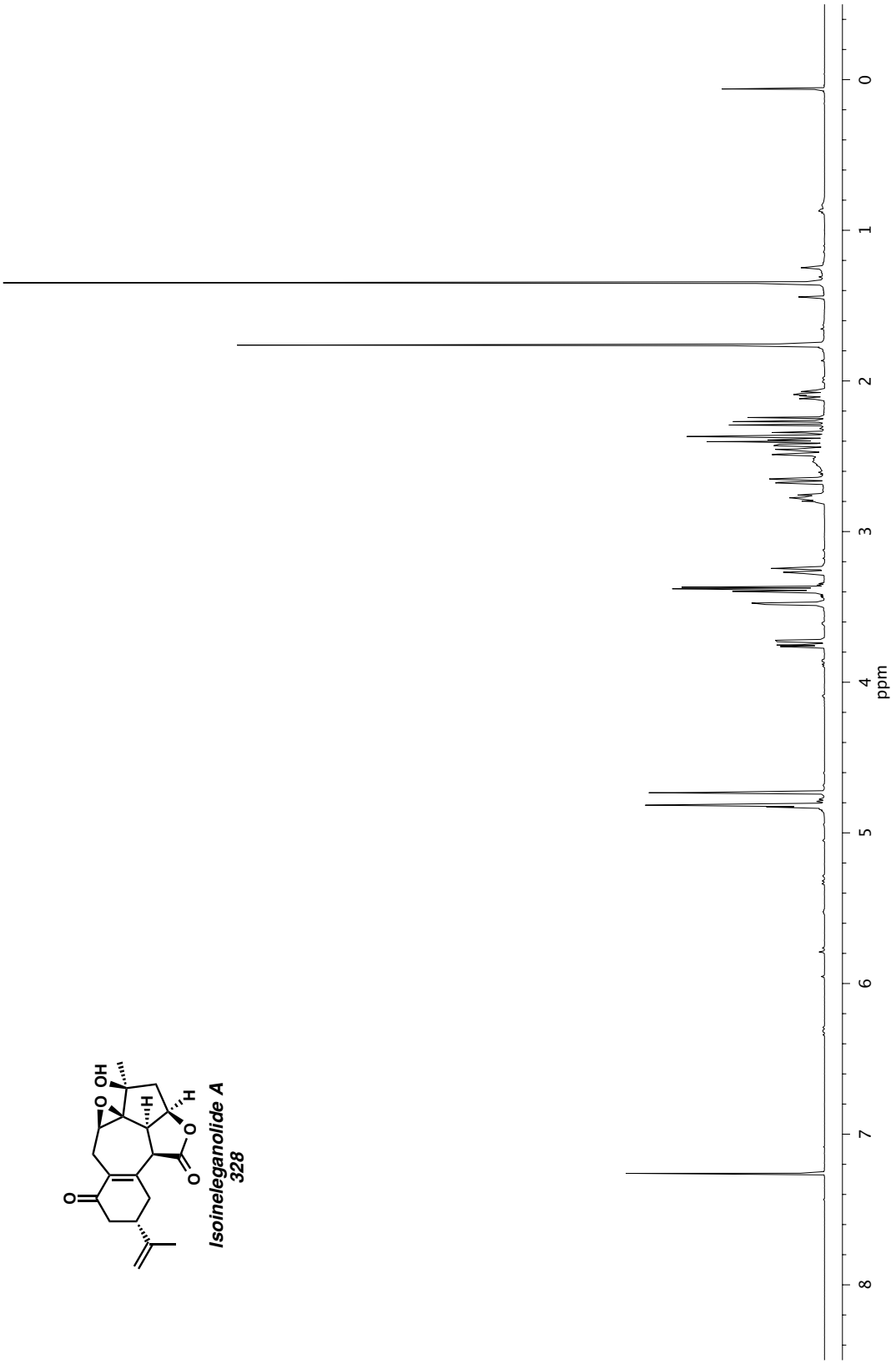

Figure A6.19. ^{1}H NMR (600 MHz, $CDCl_3$) of compound **328**.

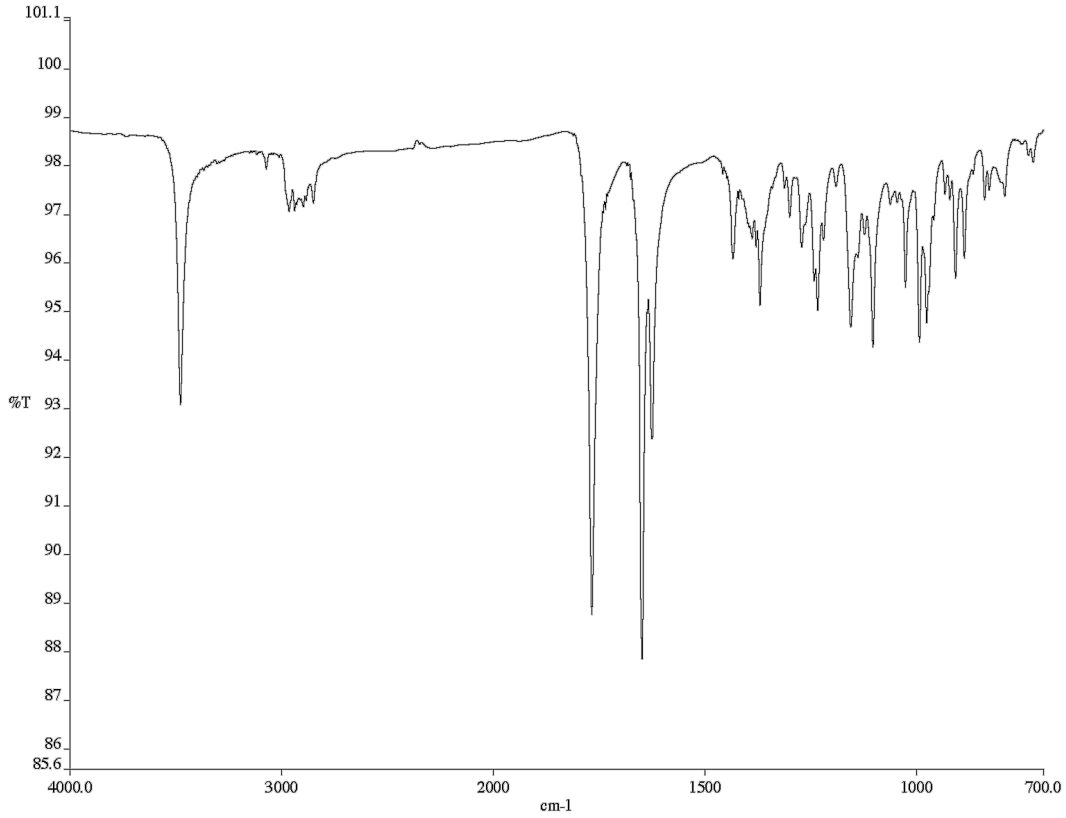

Figure A6.20. Infrared spectrum (Thin Film, NaCl) of compound **328**.

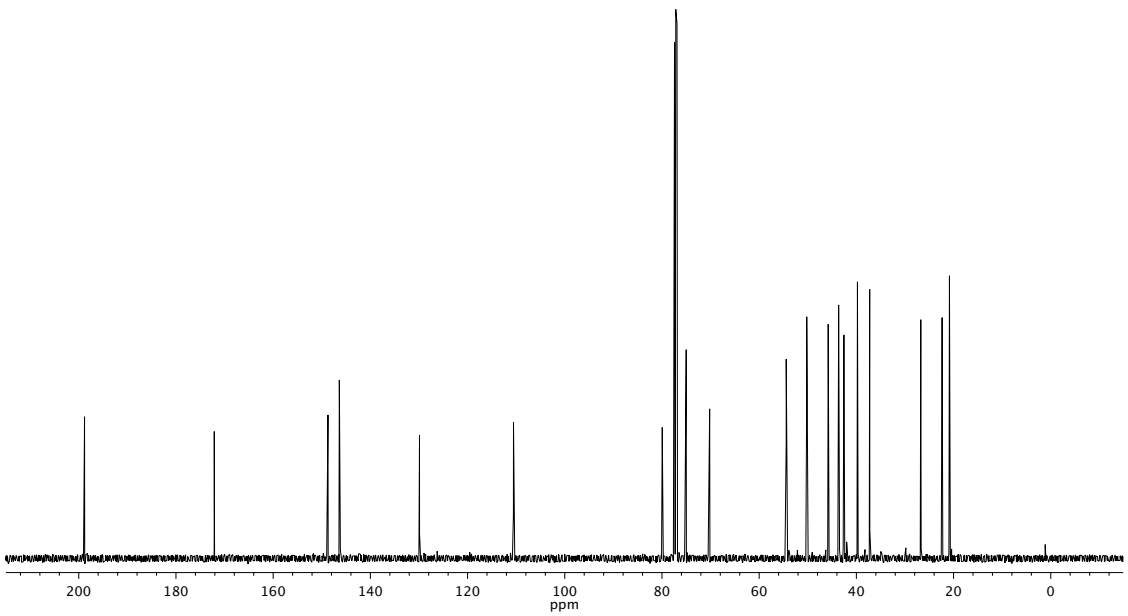

Figure A6.21. ^{13}C NMR (126 MHz, $CDCl_3$) of compound **328**.

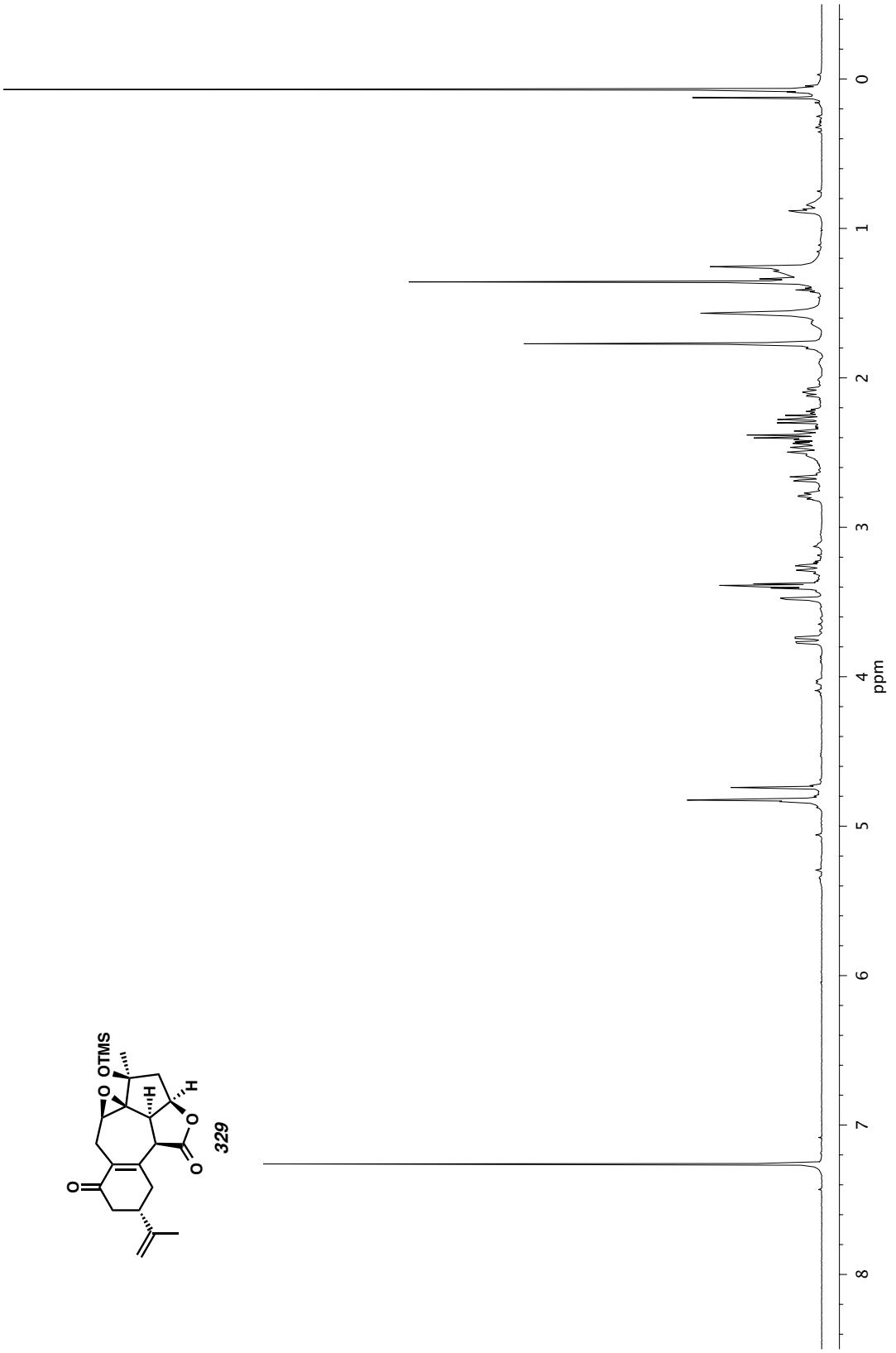

Figure A6.22. ^{1}H NMR (600 MHz, $CDCl_3$) of compound **329**.

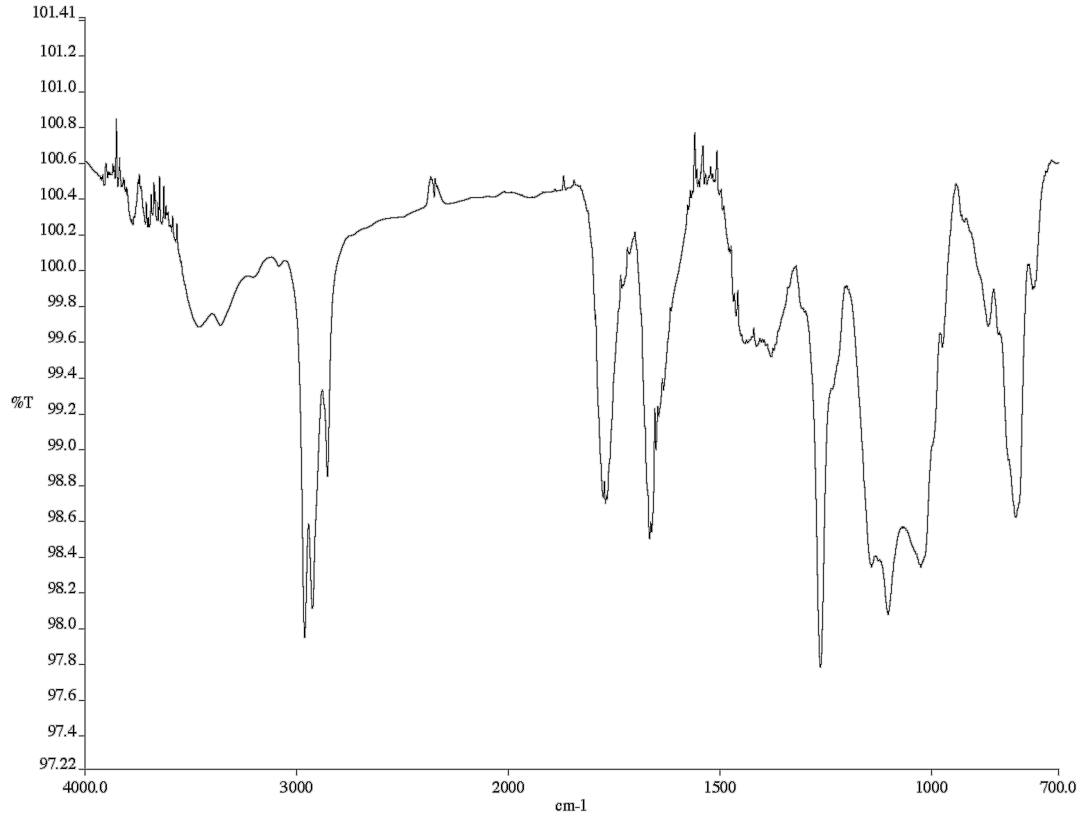

Figure A6.23. Infrared spectrum (Thin Film, NaCl) of compound **329**.

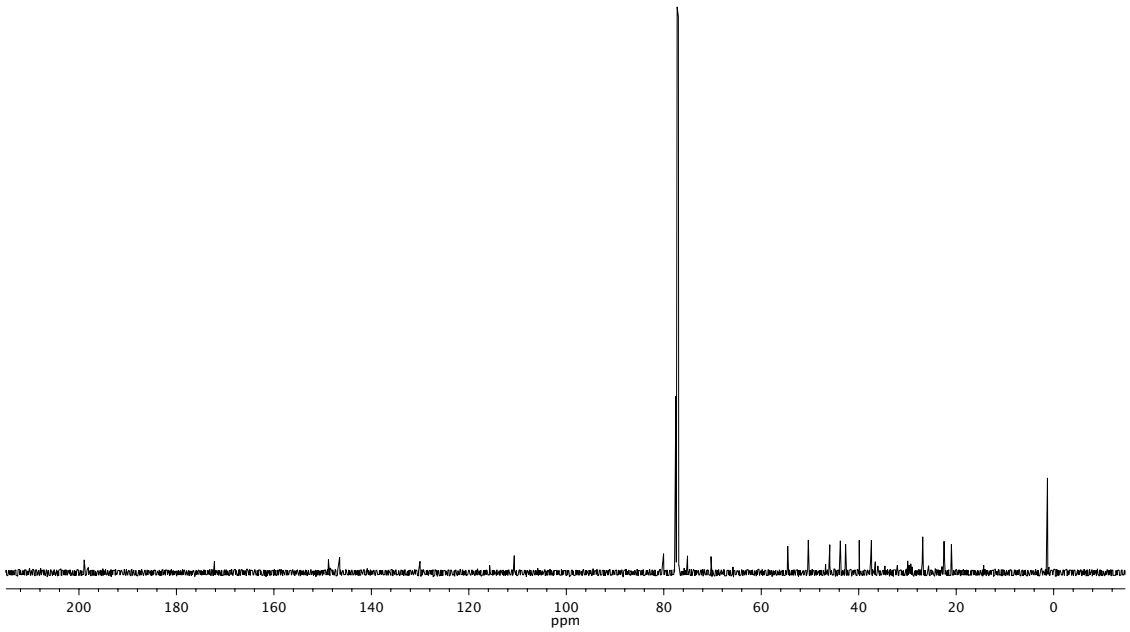

Figure A6.24. ^{13}C NMR (126 MHz, $CDCl_3$) of compound **329**.

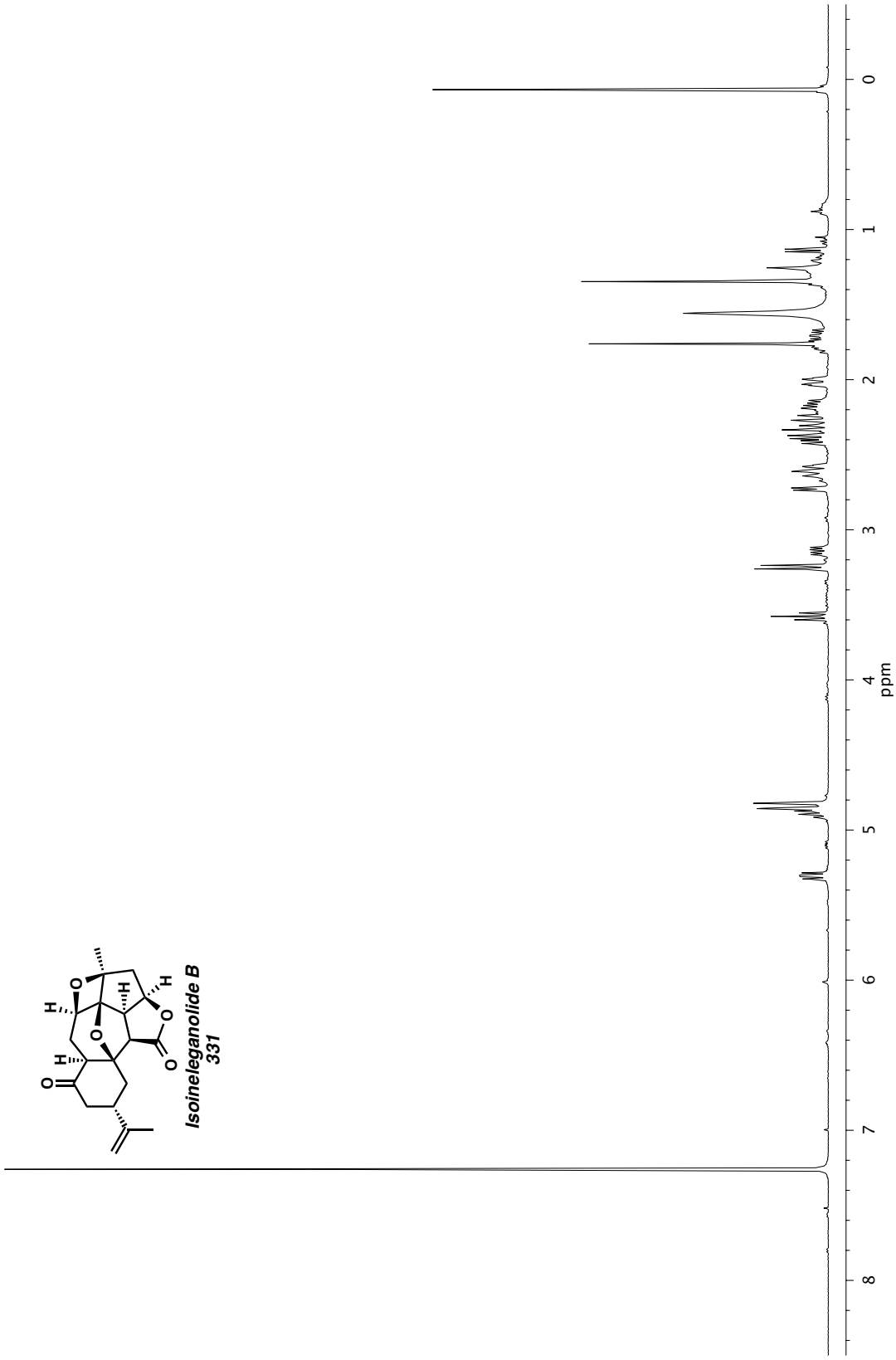

Figure A6.25. ^{1}H NMR (400 MHz, $CDCl_3$) of compound **331**.

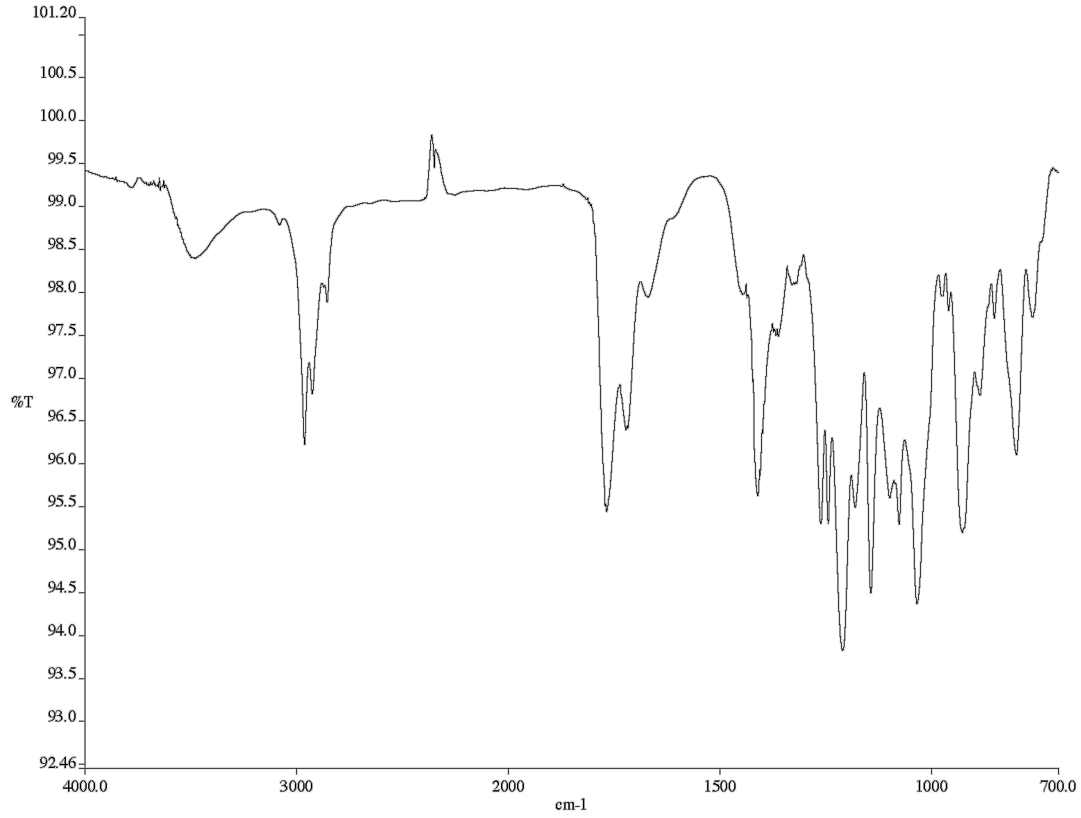

Figure A6.26. Infrared spectrum (Thin Film, NaCl) of compound **331**.

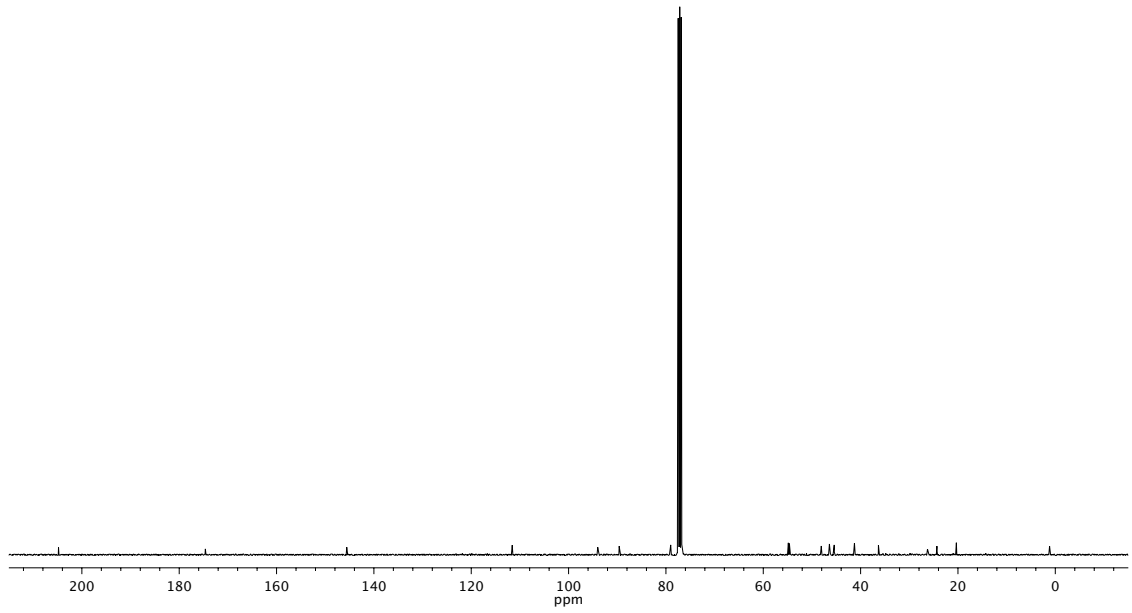

Figure A6.27. ^{13}C NMR (101 MHz, $CDCl_3$) of compound **331**.

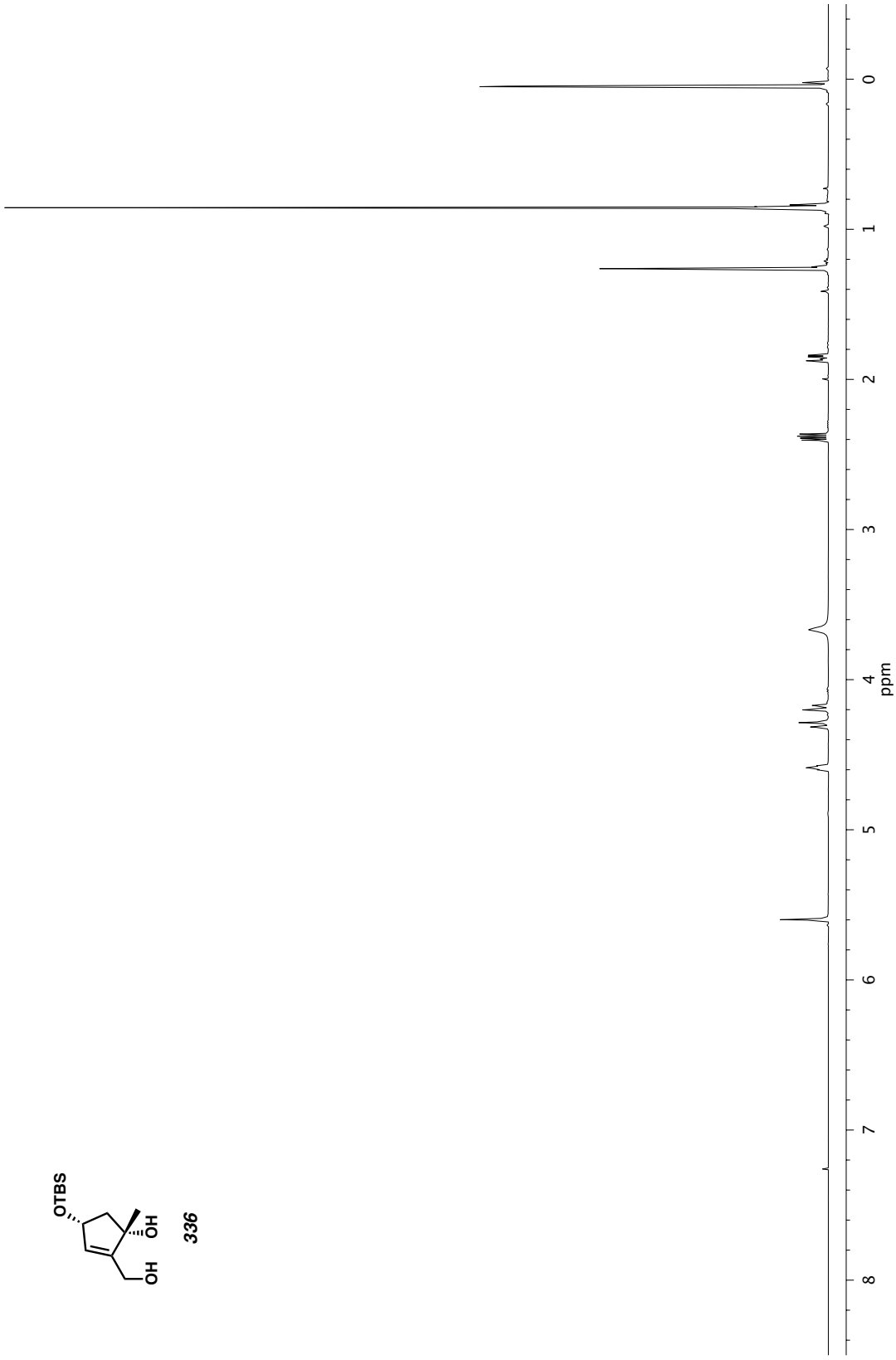

Figure A6.28. ^{1}H NMR (500 MHz, $CDCl_3$) of compound **336**.

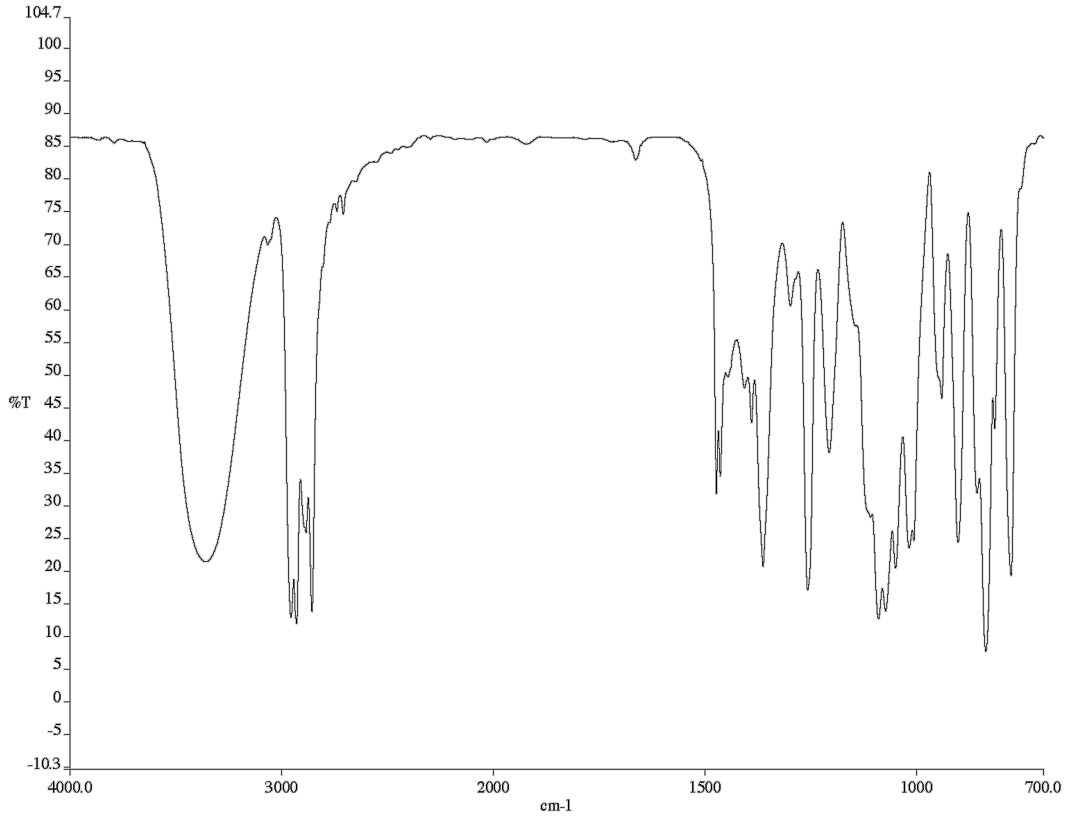

Figure A6.29. Infrared spectrum (Thin Film, NaCl) of compound **336**.

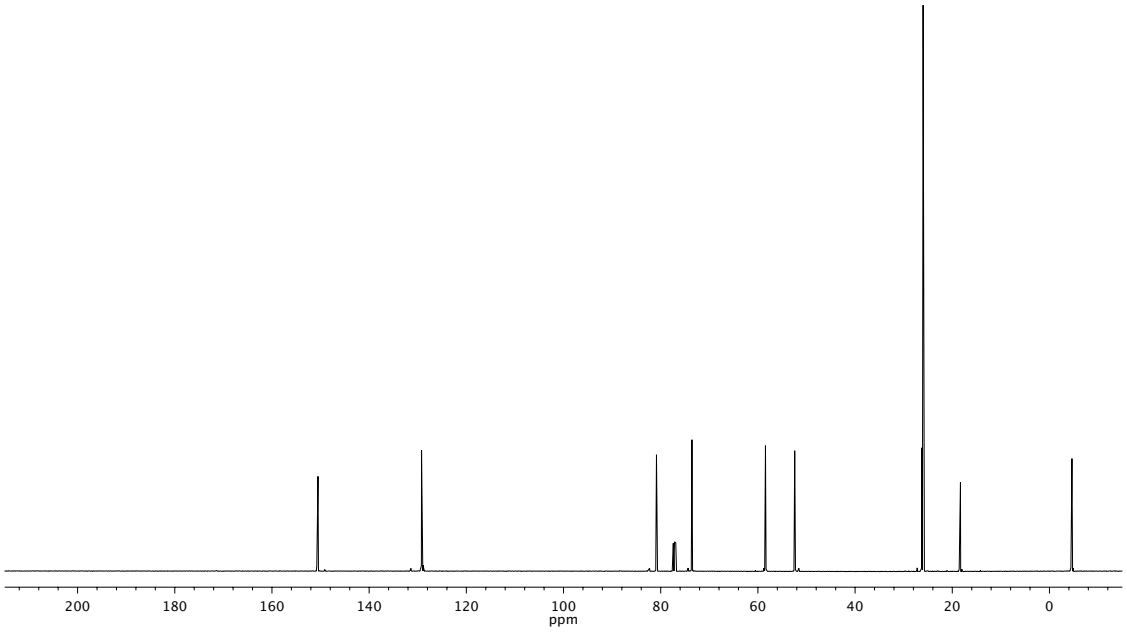

Figure A6.30. ^{13}C NMR (126 MHz, $CDCl_3$) of compound **336**.

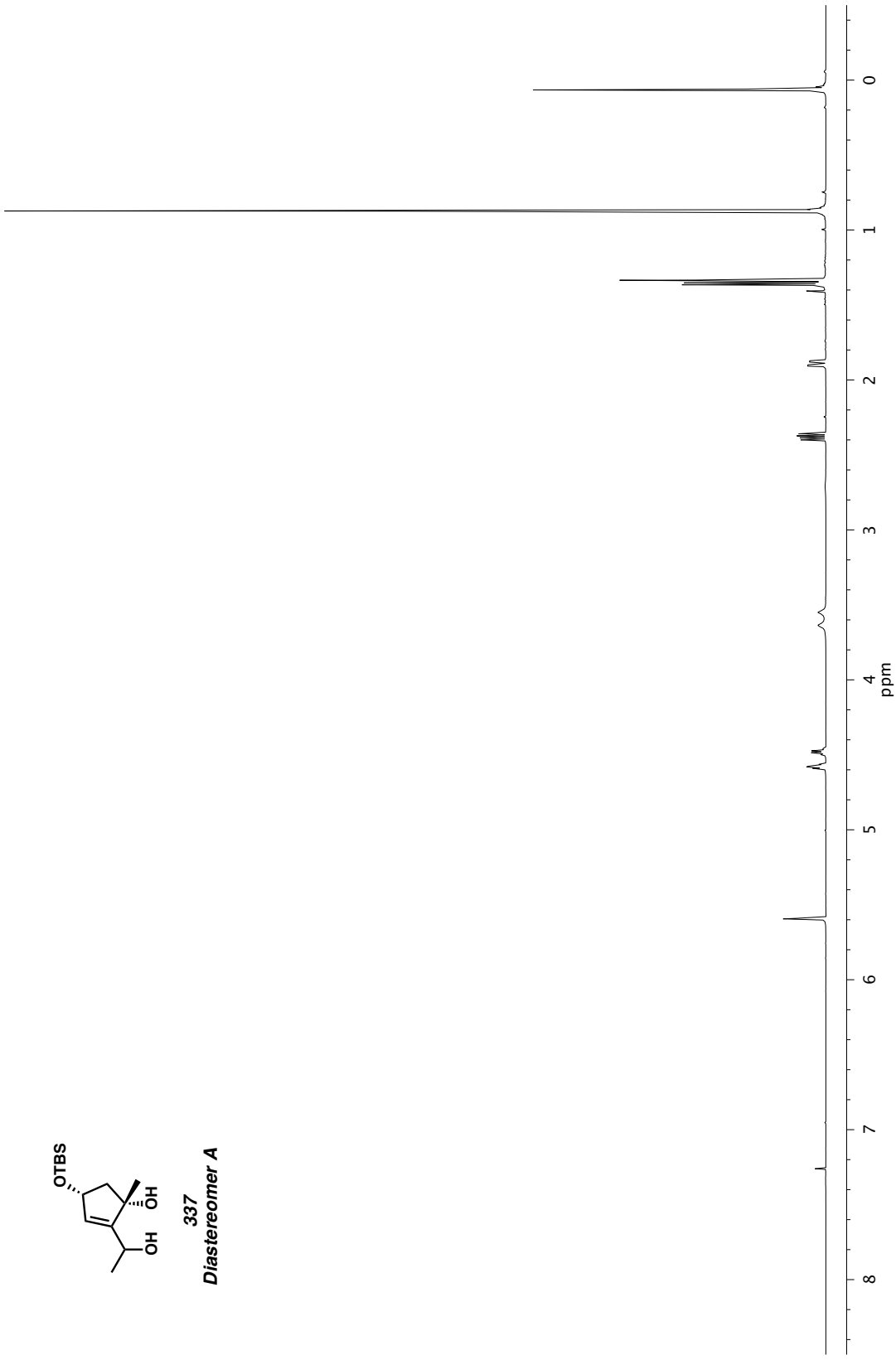

Figure A6.31. ^{1}H NMR (500 MHz, $CDCl_3$) of compound **337-A**.

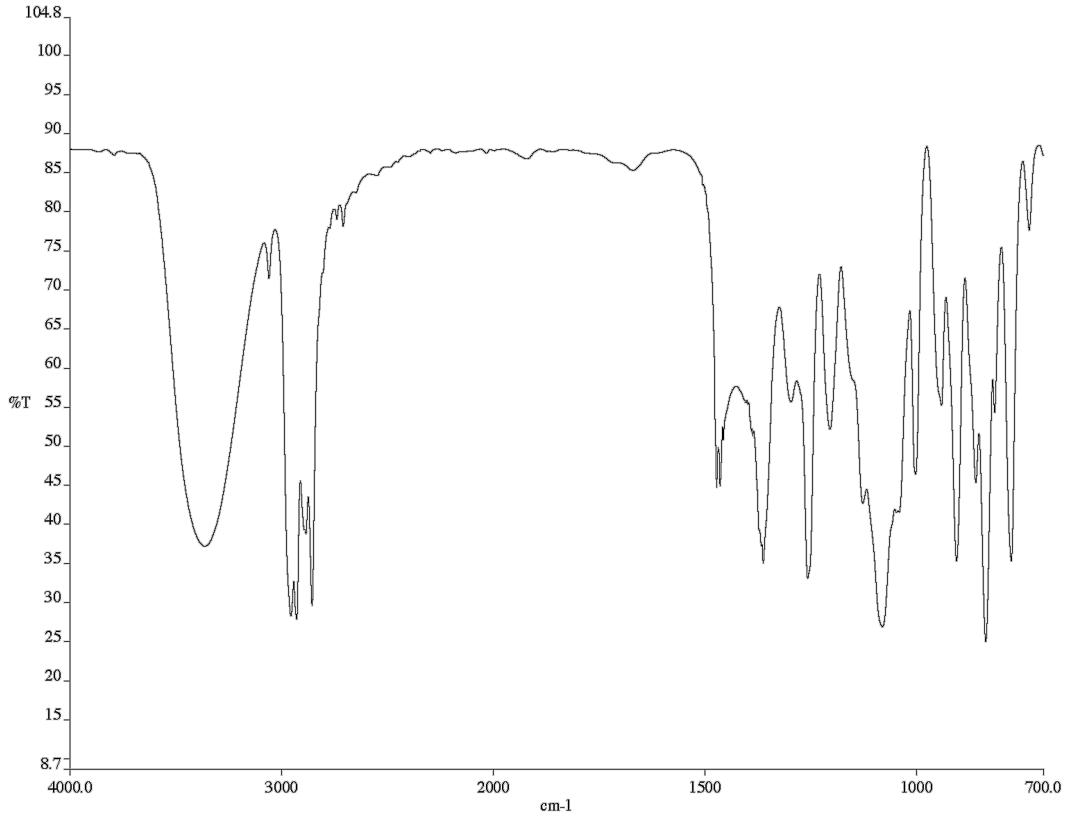

Figure A6.32. Infrared spectrum (Thin Film, NaCl) of compound **337-A**.

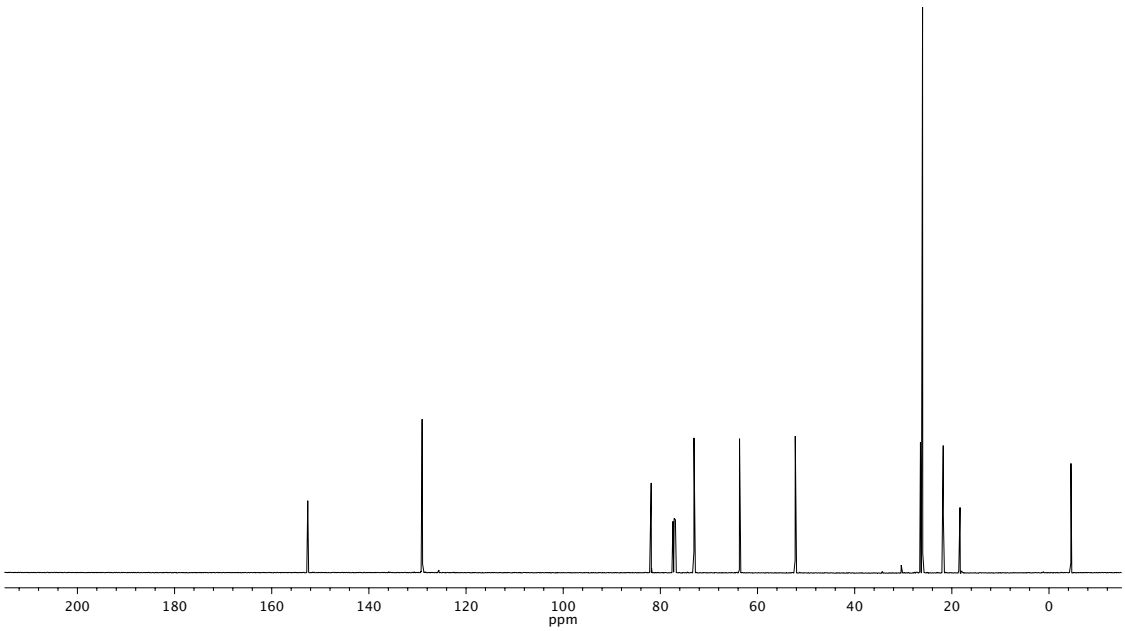

Figure A6.33. ^{13}C NMR (126 MHz, $CDCl_3$) of compound **337-A**.

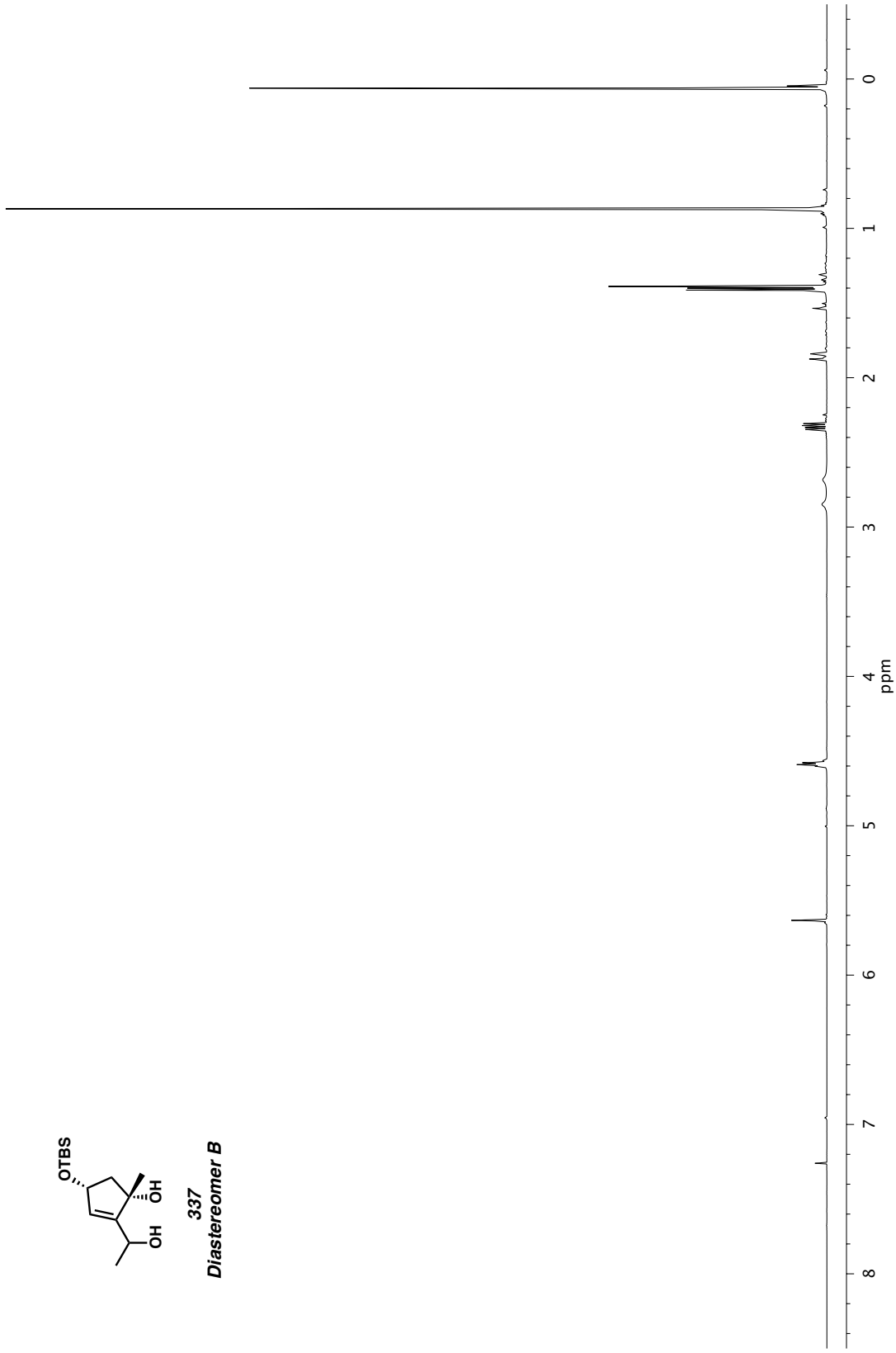

Figure A6.34. ^{1}H NMR (500 MHz, $CDCl_3$) of compound **337-B**.

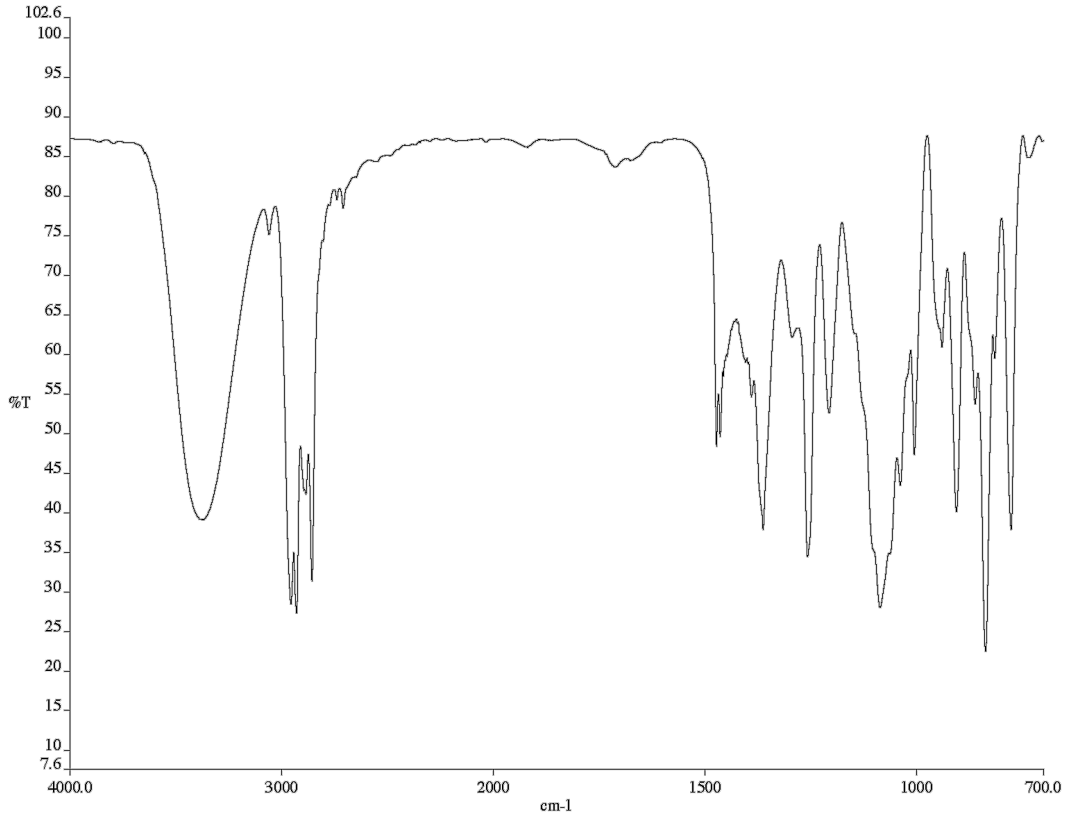

Figure A6.35. Infrared spectrum (Thin Film, NaCl) of compound **337-B**.

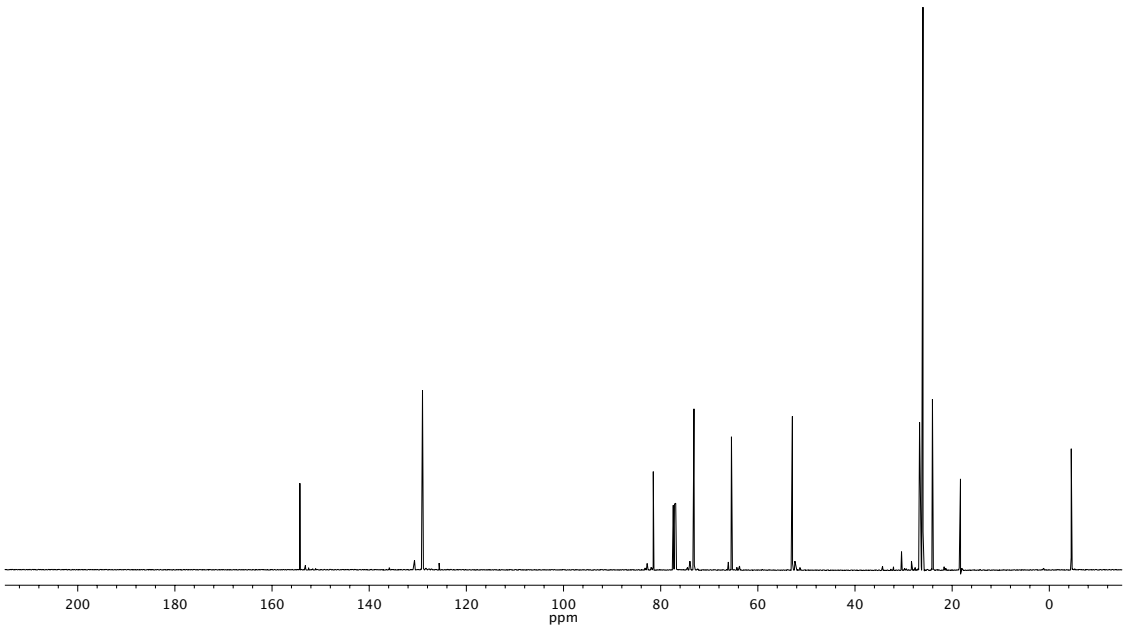

Figure A6.36. ^{13}C NMR (126 MHz, $CDCl_3$) of compound **337-B**.

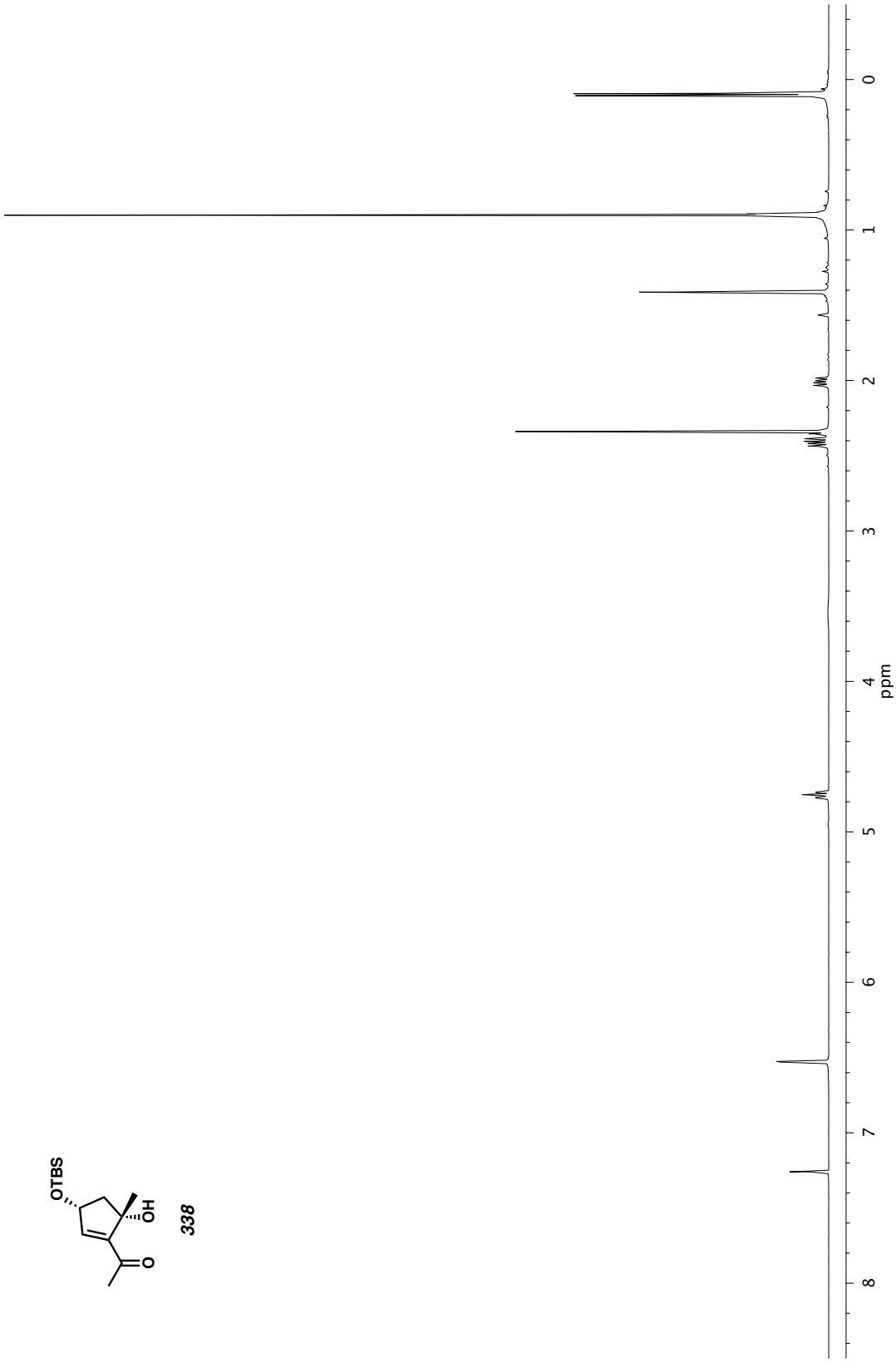

Figure A6.37. ^{1}H NMR (400 MHz, $CDCl_3$) of compound **338**.

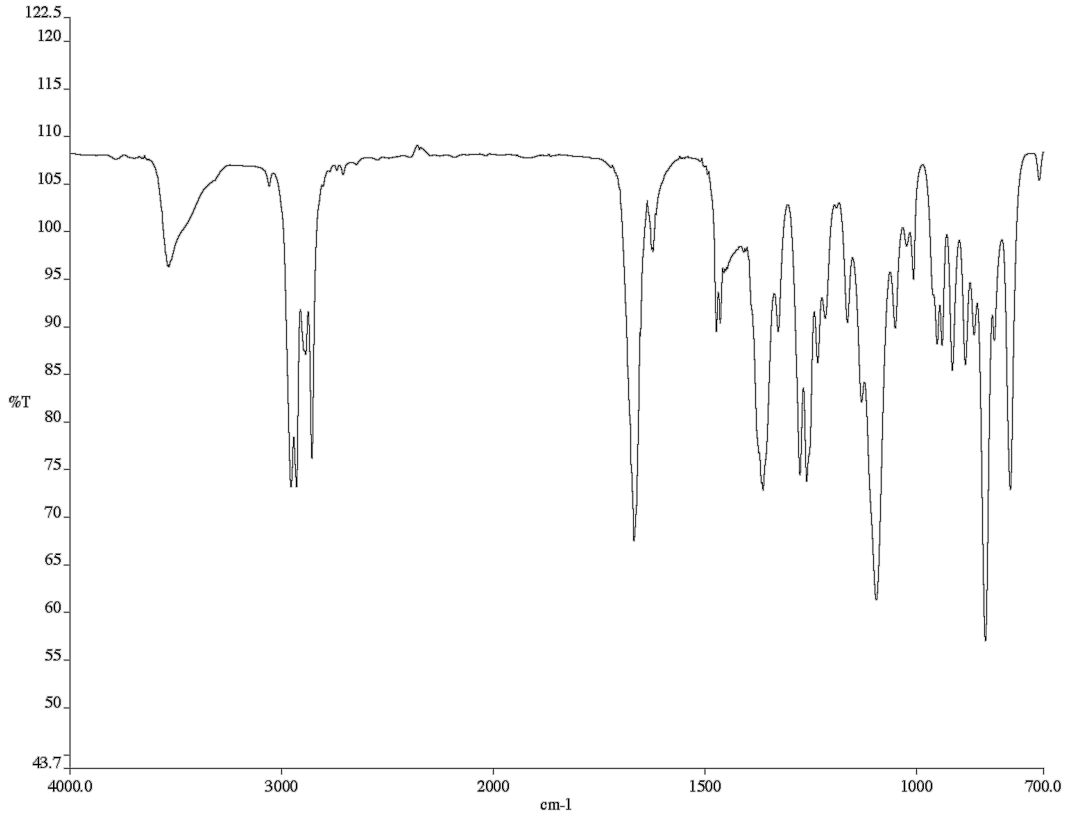

Figure A6.38. Infrared spectrum (Thin Film, NaCl) of compound **338**.

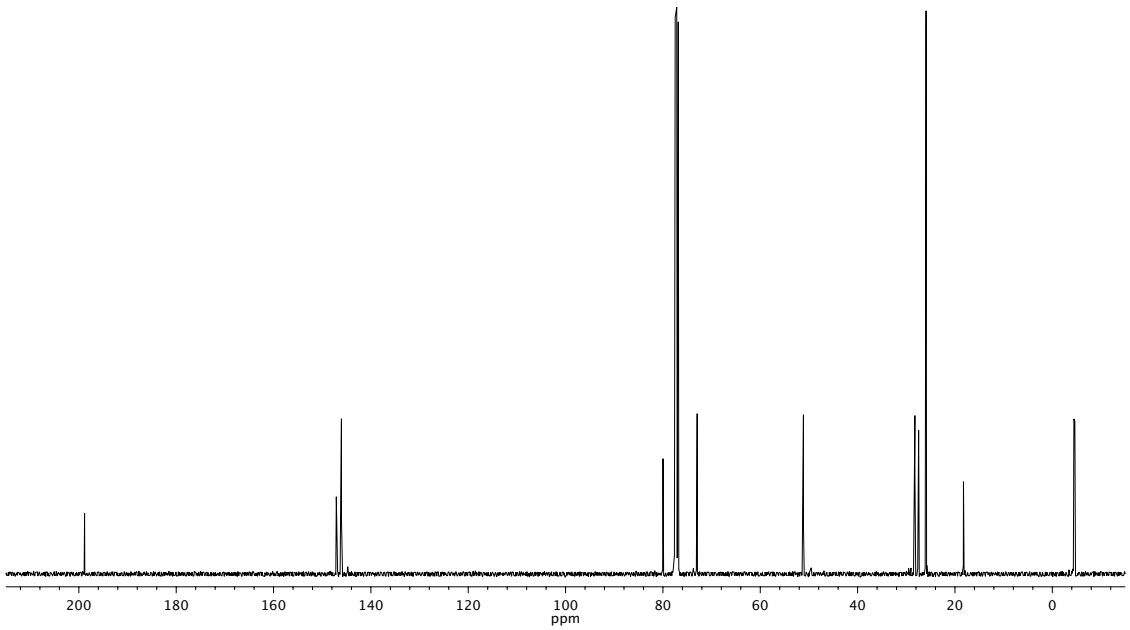

Figure A6.39. ^{13}C NMR (101 MHz, $CDCl_3$) of compound **338**.

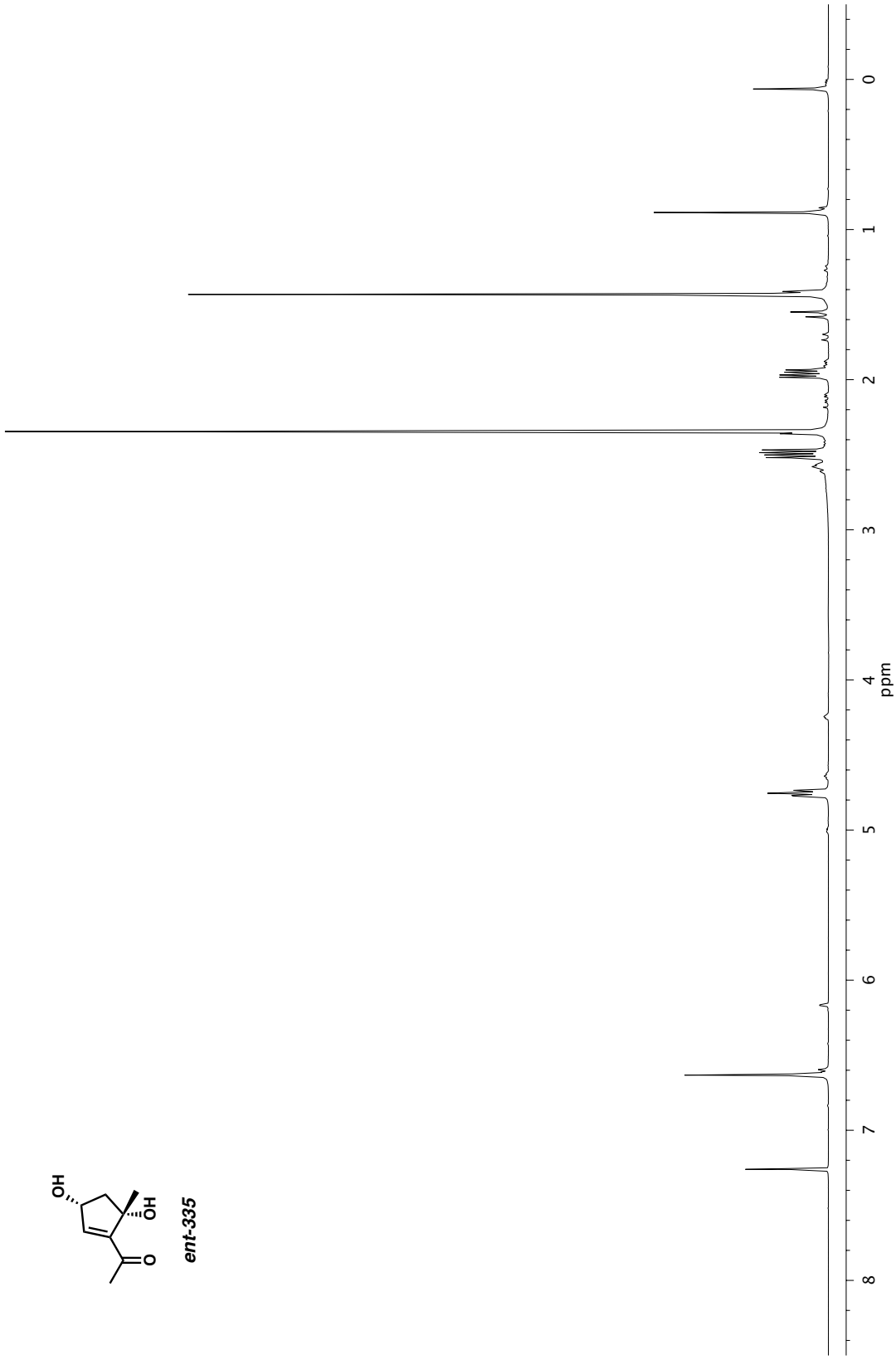

Figure A6.40. ^{1}H NMR (400 MHz, $CDCl_3$) of compound ***ent-335***.

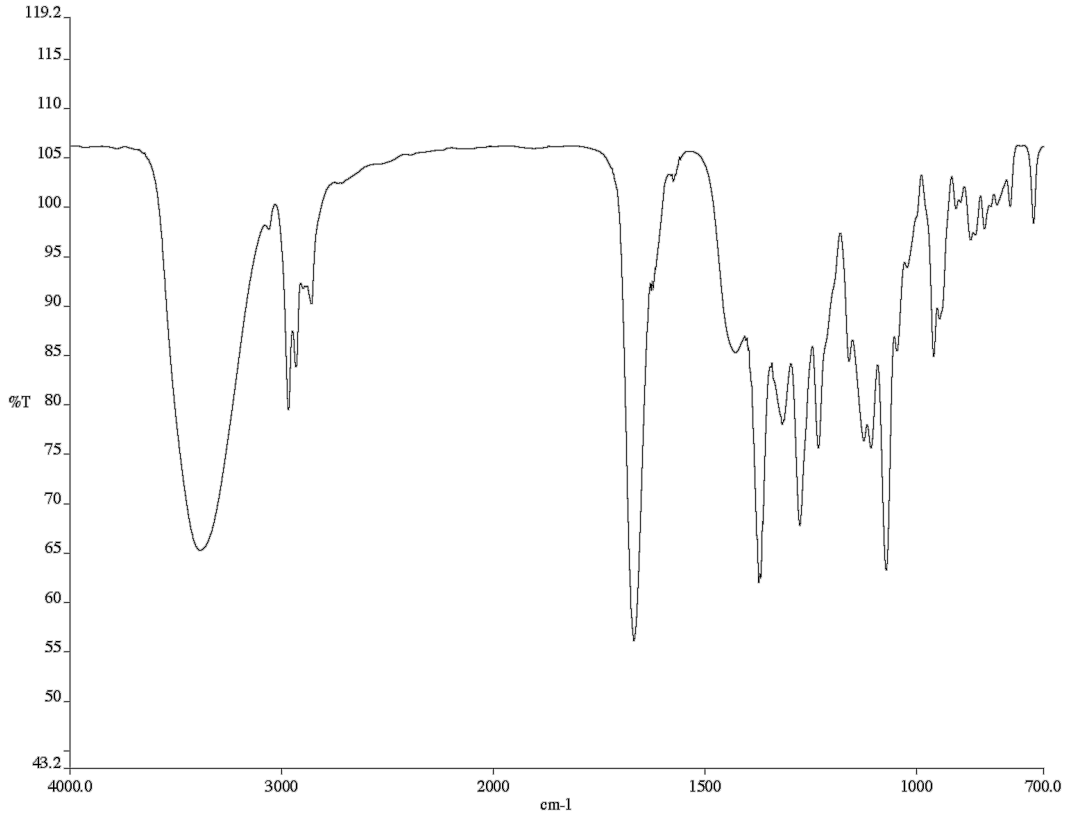

Figure A6.41. Infrared spectrum (Thin Film, NaCl) of compound ***ent*-335**.

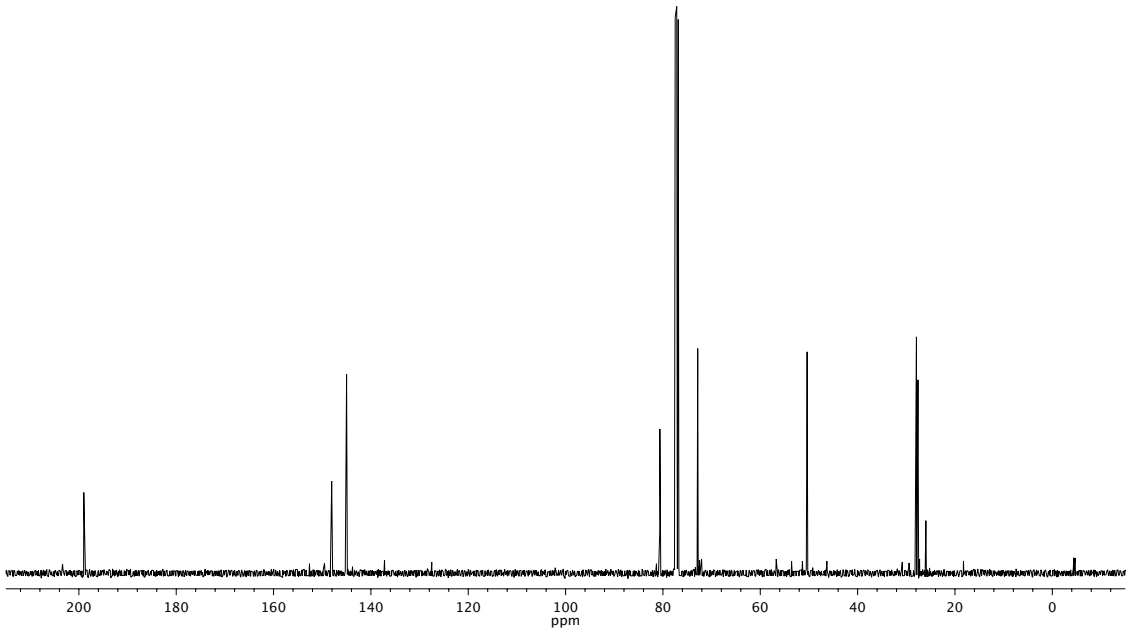

Figure A6.42. ^{13}C NMR (101 MHz, $CDCl_3$) of compound ***ent*-335**.

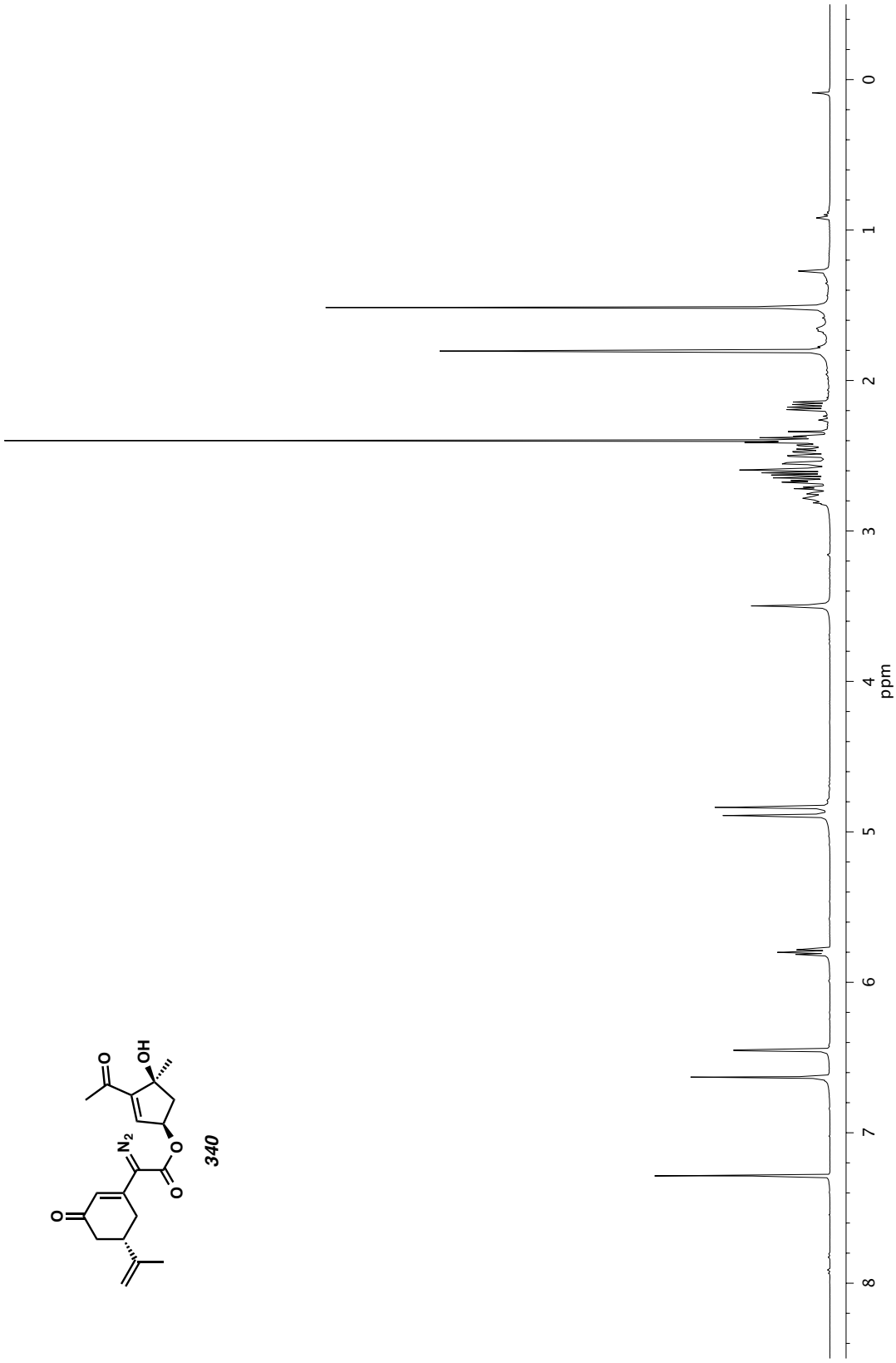

Figure A6.43. ^{1}H NMR (400 MHz, $CDCl_3$) of compound **340**.

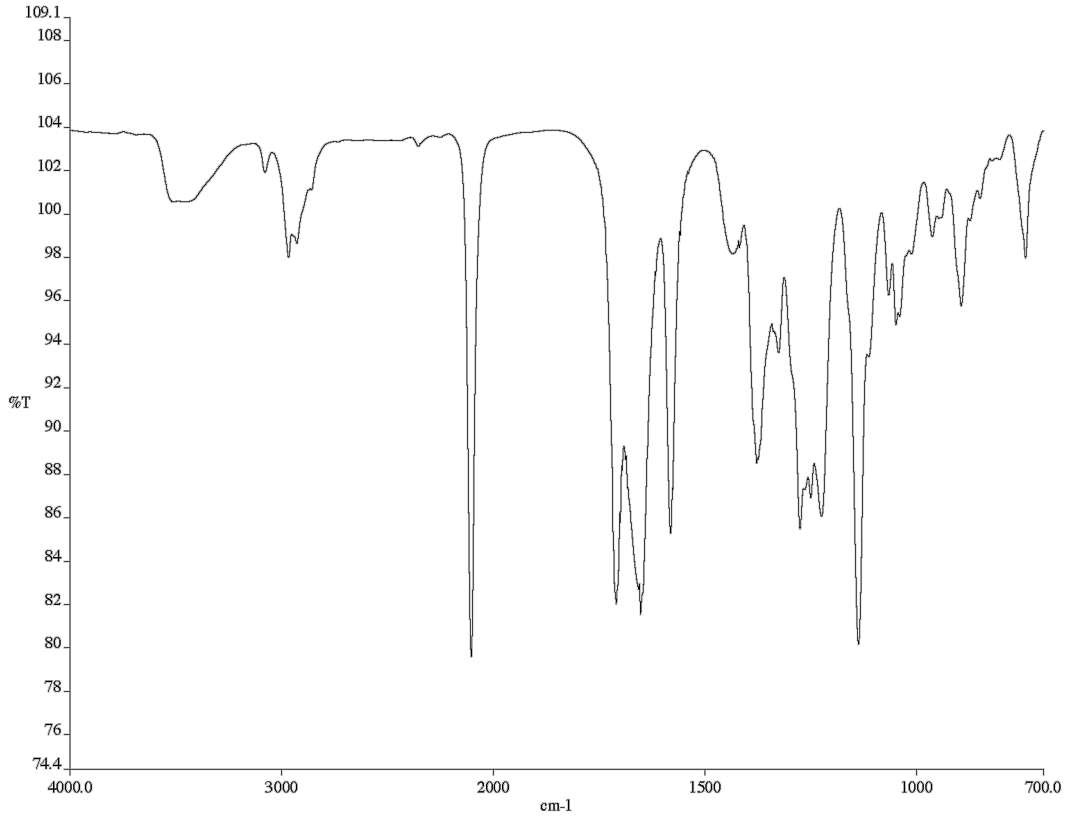

Figure A6.44. Infrared spectrum (Thin Film, NaCl) of compound **340**.

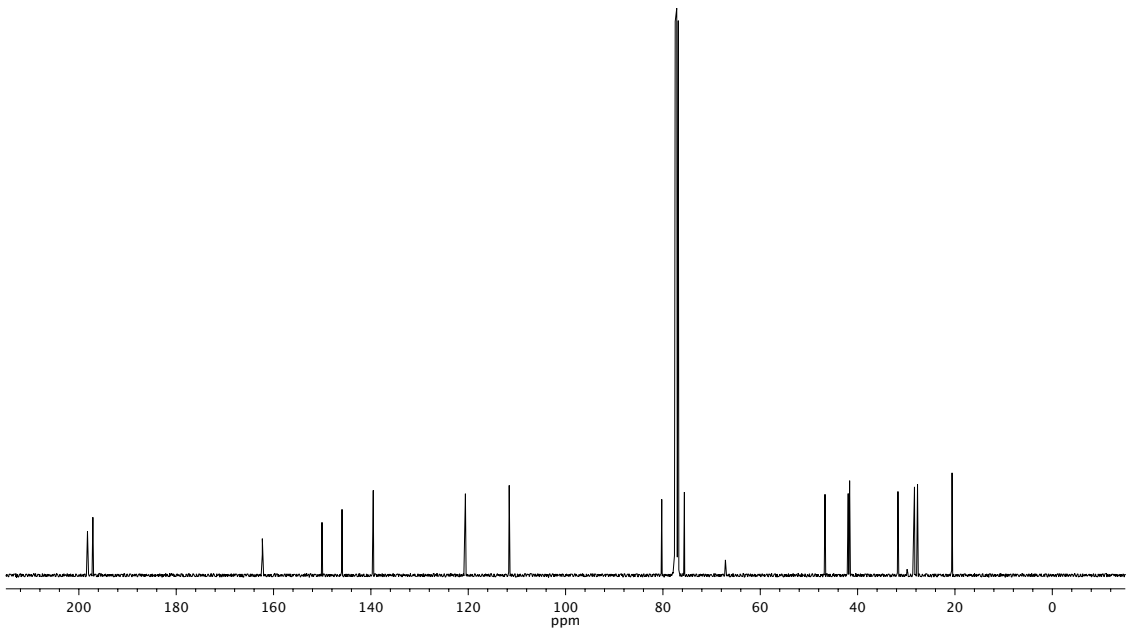

Figure A6.45. ^{13}C NMR (101 MHz, $CDCl_3$) of compound **340**.

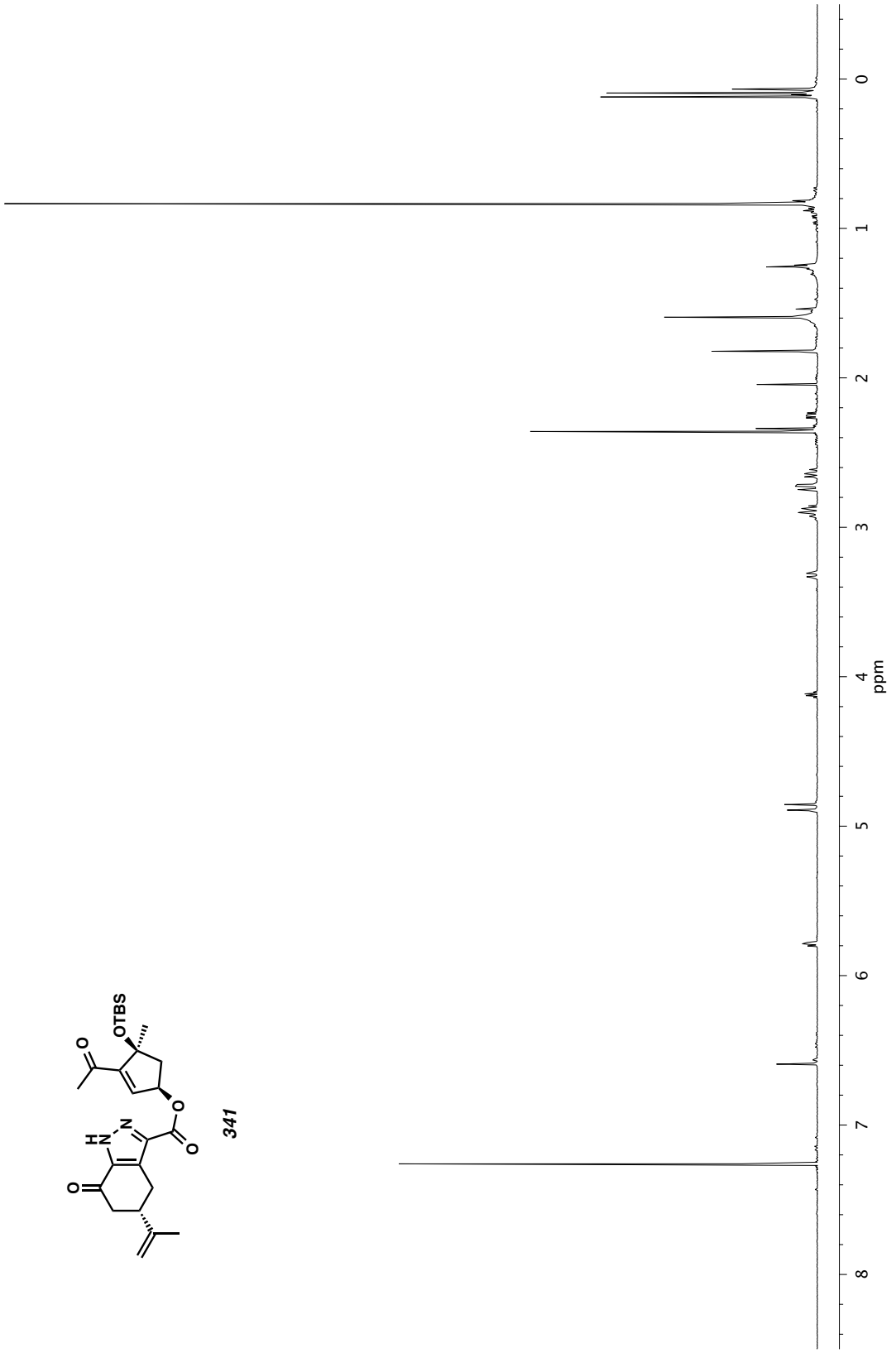

Figure A6.46. ^{1}H NMR (600 MHz, $CDCl_3$) of compound **341**.

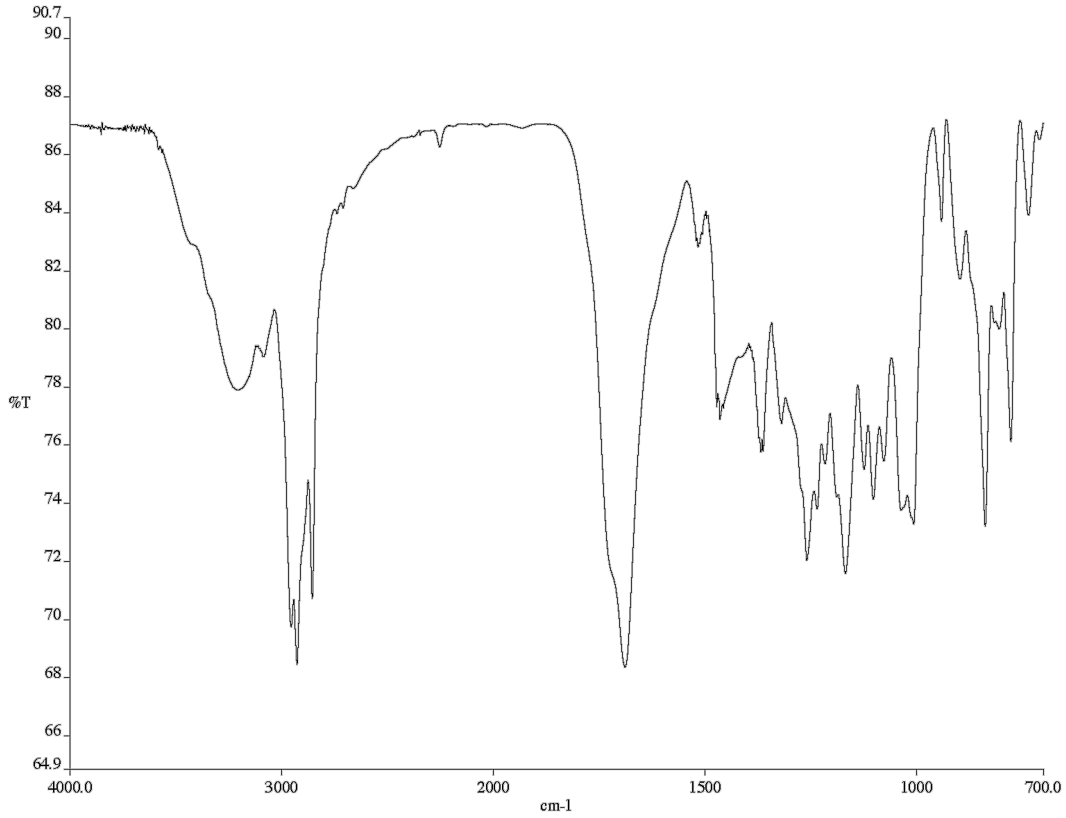

Figure A6.47. Infrared spectrum (Thin Film, NaCl) of compound **341**.

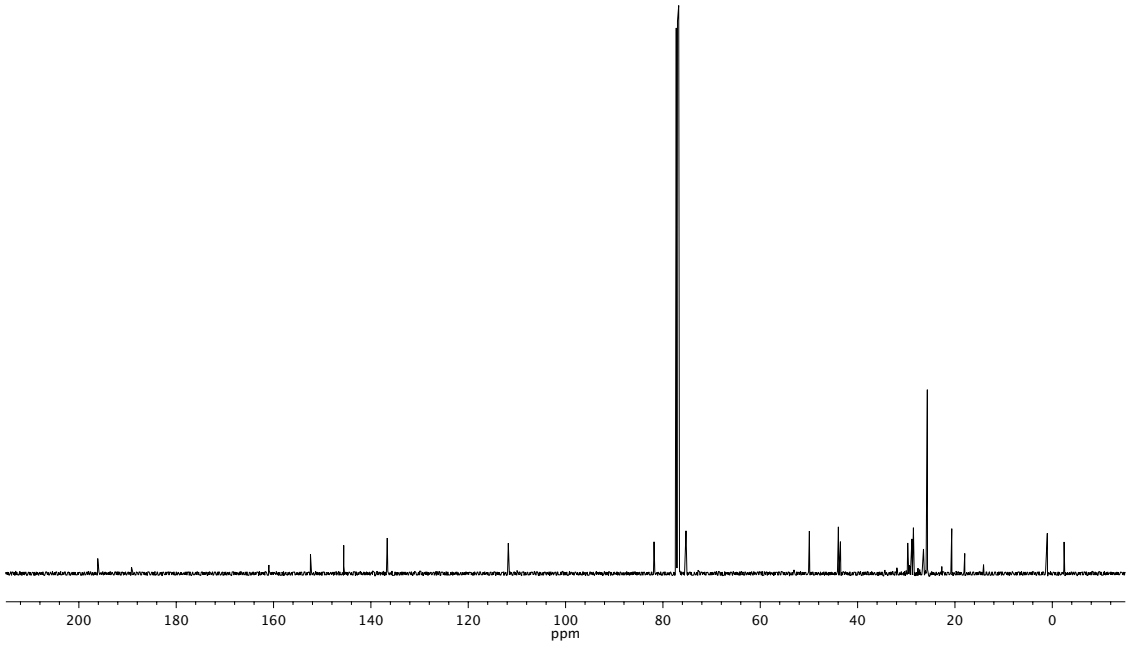

Figure A6.48. ^{13}C NMR (126 MHz, $CDCl_3$) of compound **341**.

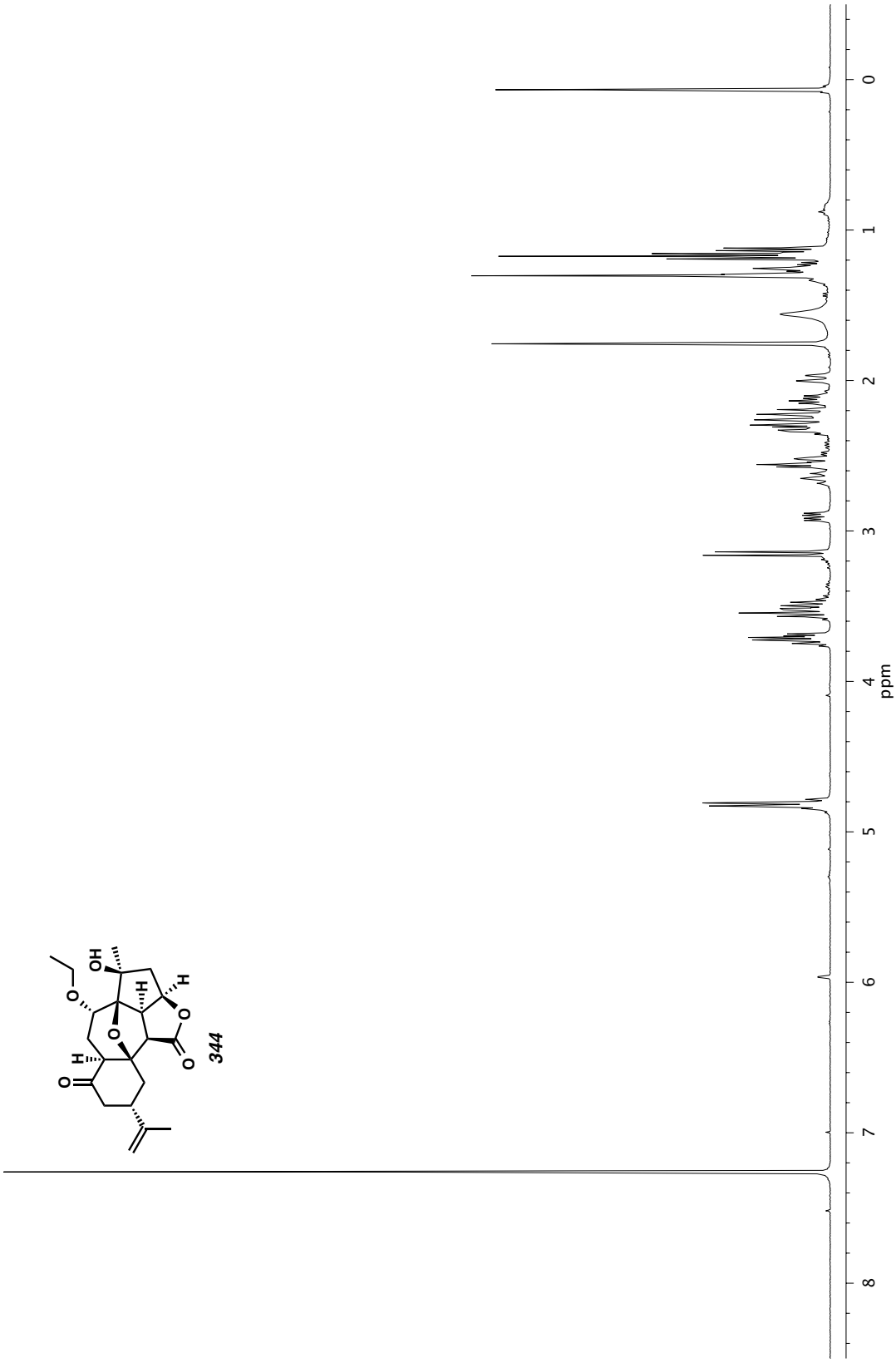

Figure A6.49. ^{1}H NMR (400 MHz, $CDCl_3$) of compound **344**.

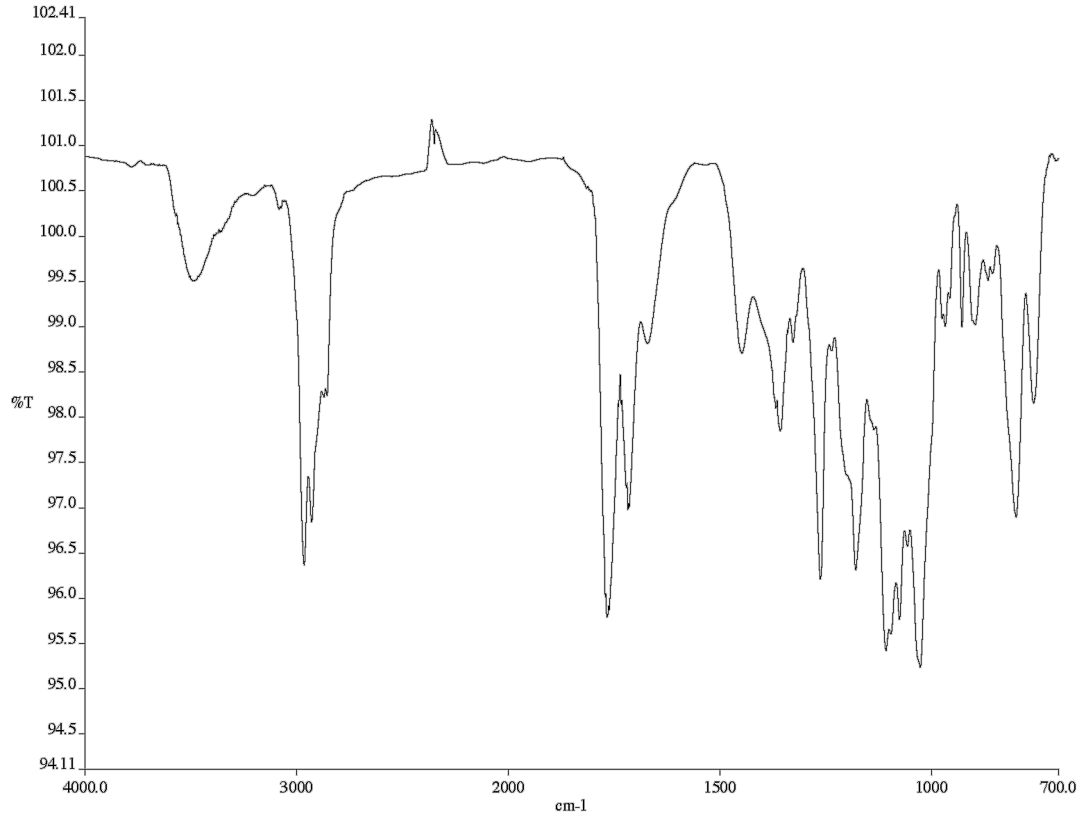

Figure A6.50. Infrared spectrum (Thin Film, NaCl) of compound **344**.

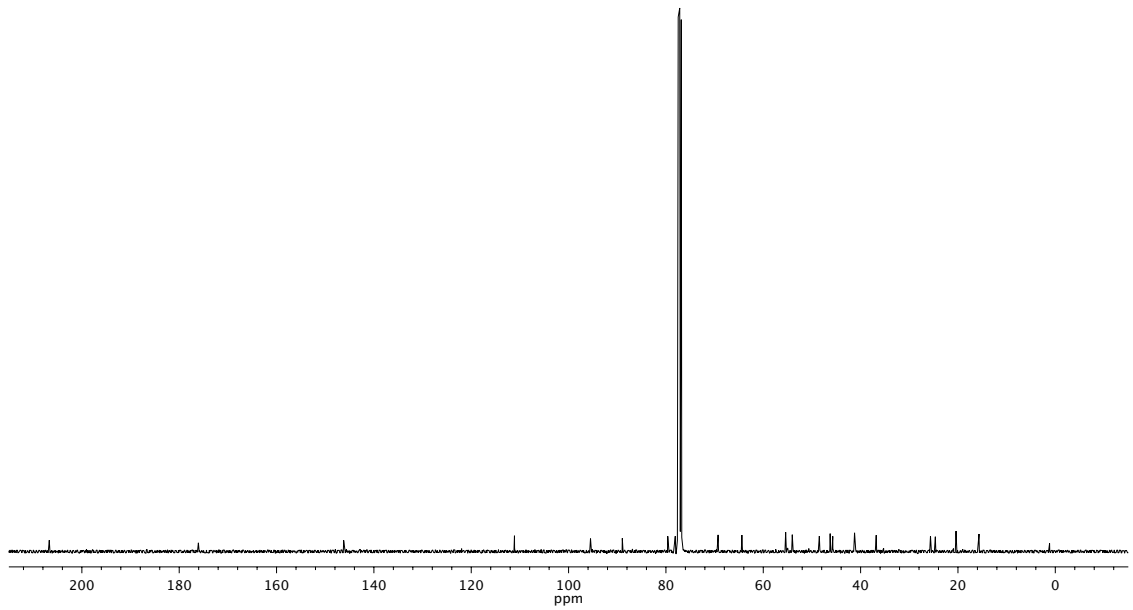

Figure A6.51. ^{13}C NMR (101 MHz, $CDCl_3$) of compound **344**.

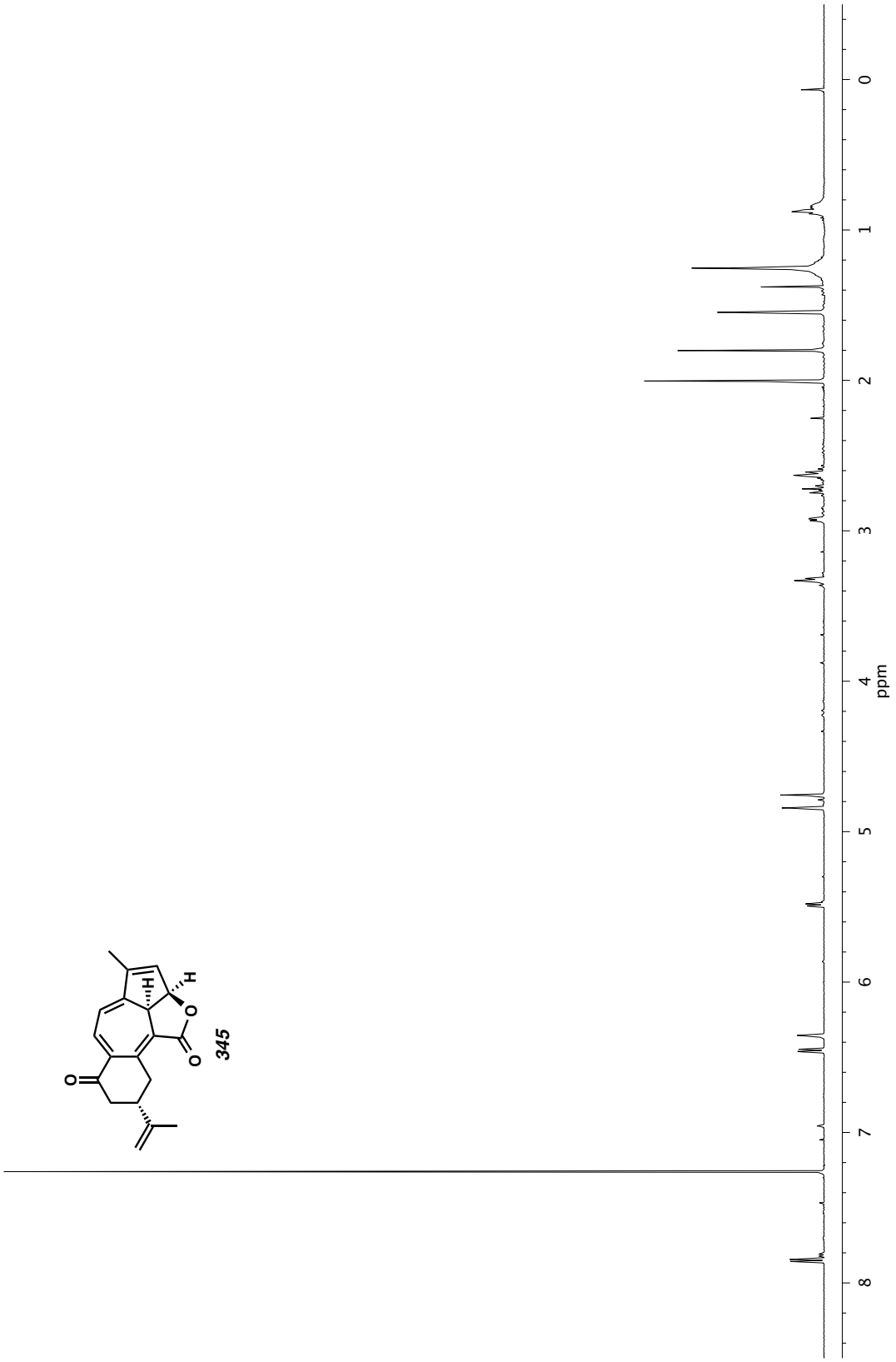

Figure A6.52. ^{1}H NMR (500 MHz, $CDCl_3$) of compound **345**.

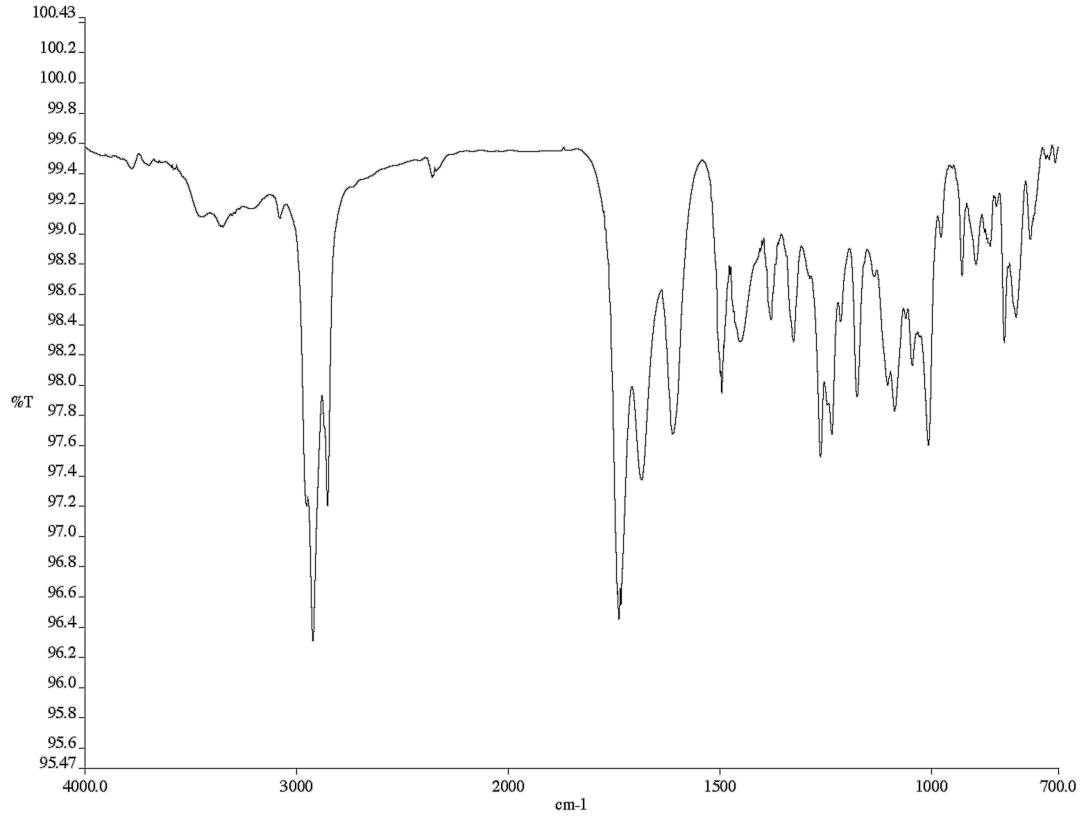

Figure A6.53. Infrared spectrum (Thin Film, NaCl) of compound **345**.

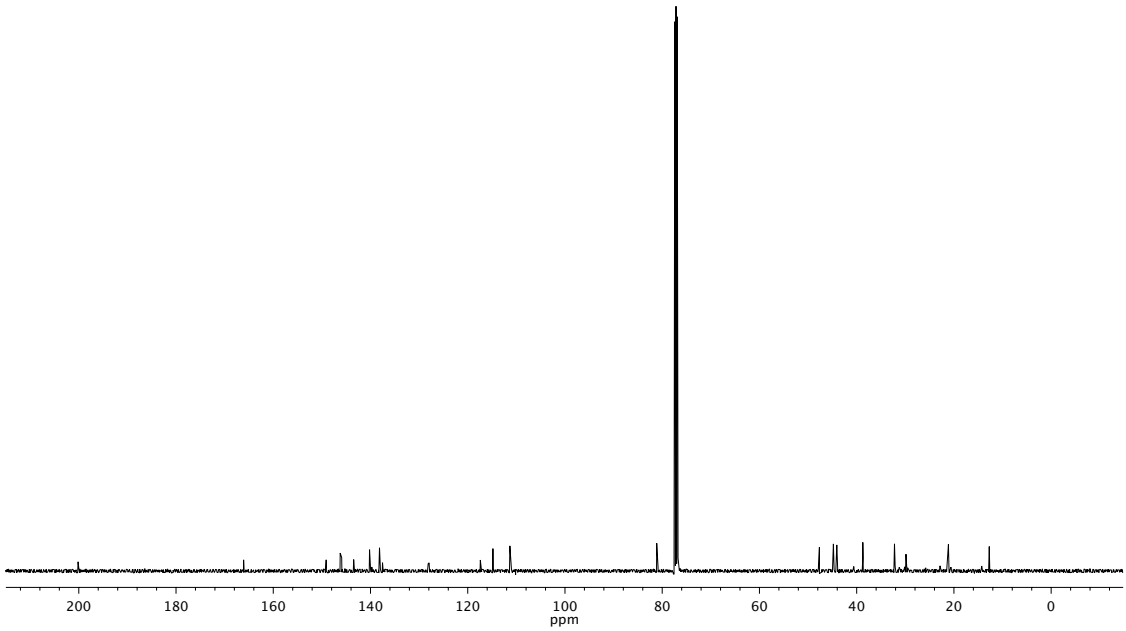

Figure A6.54. ^{13}C NMR (126 MHz, $CDCl_3$) of compound **345**.

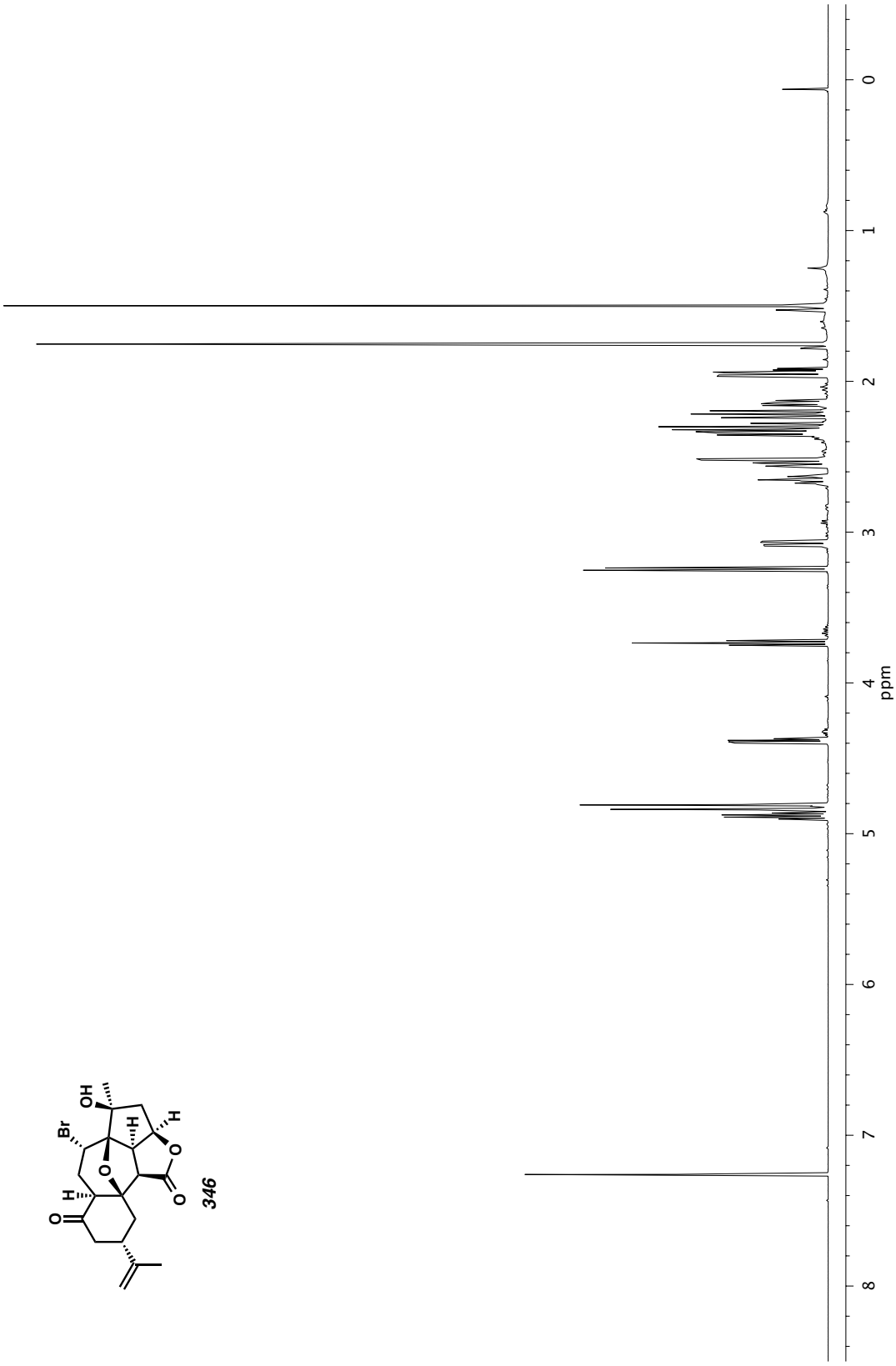

Figure A6.55. ^{1}H NMR (600 MHz, $CDCl_3$) of compound **346**.

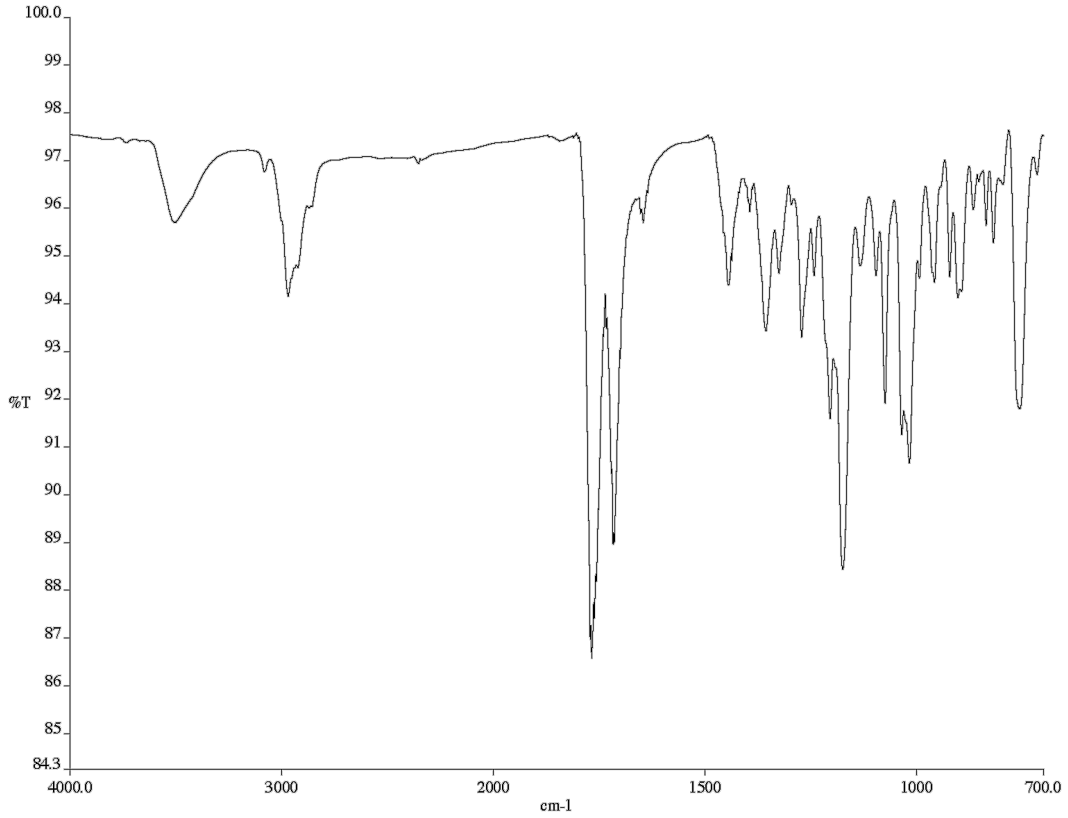

Figure A6.56. Infrared spectrum (Thin Film, NaCl) of compound **346**.

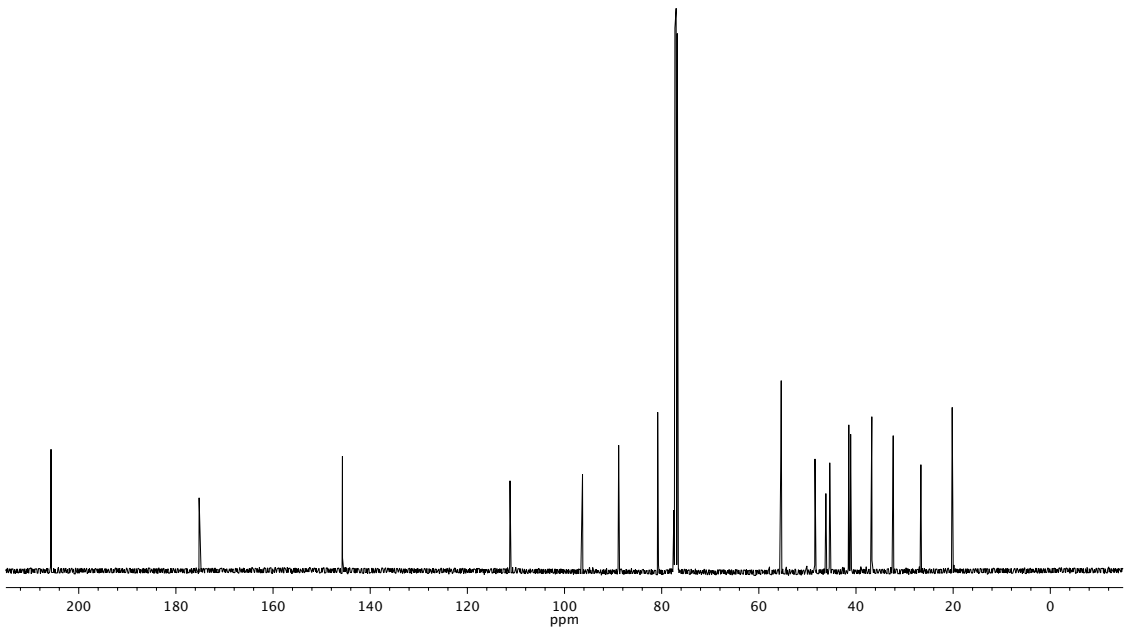

Figure A6.57. ^{13}C NMR (126 MHz, $CDCl_3$) of compound **346**.

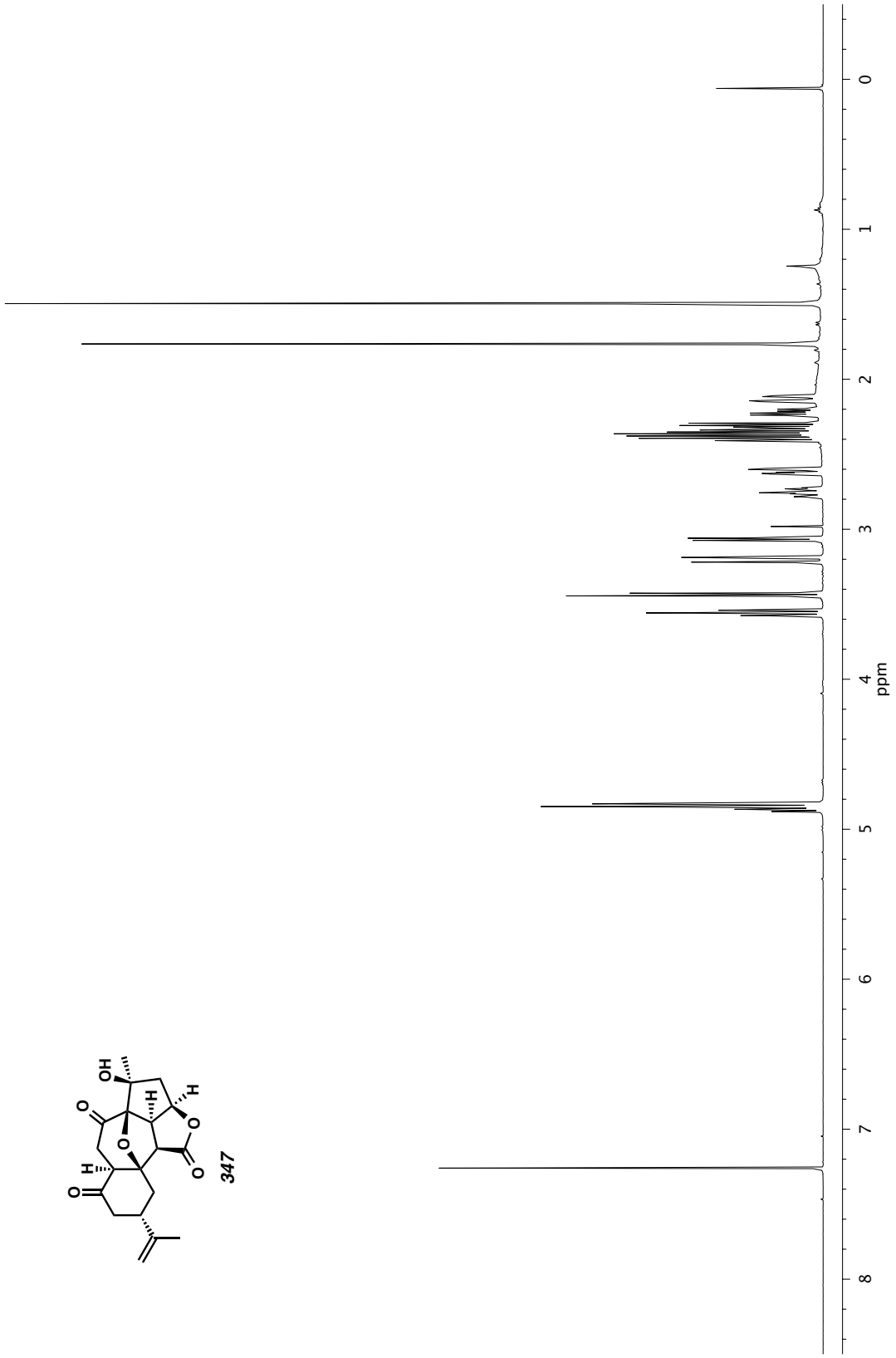

Figure A6.58. ^{1}H NMR (500 MHz, $CDCl_3$) of compound **347**.

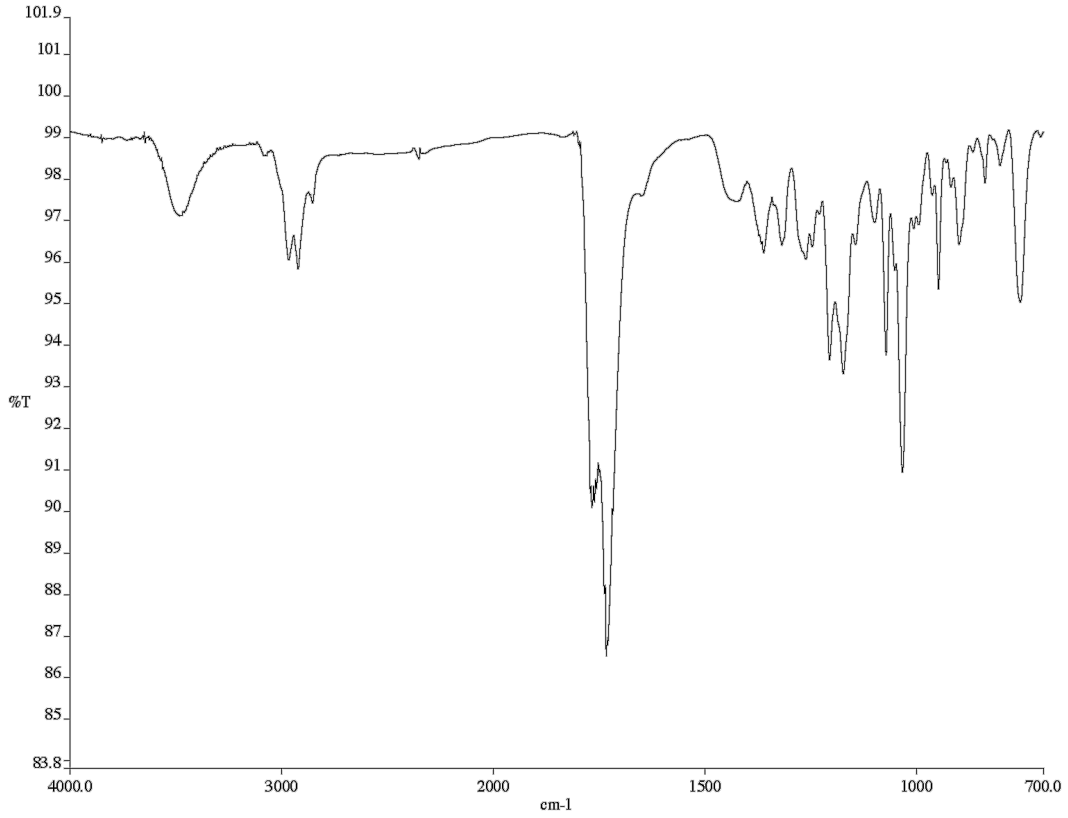

Figure A6.59. Infrared spectrum (Thin Film, NaCl) of compound **347**.

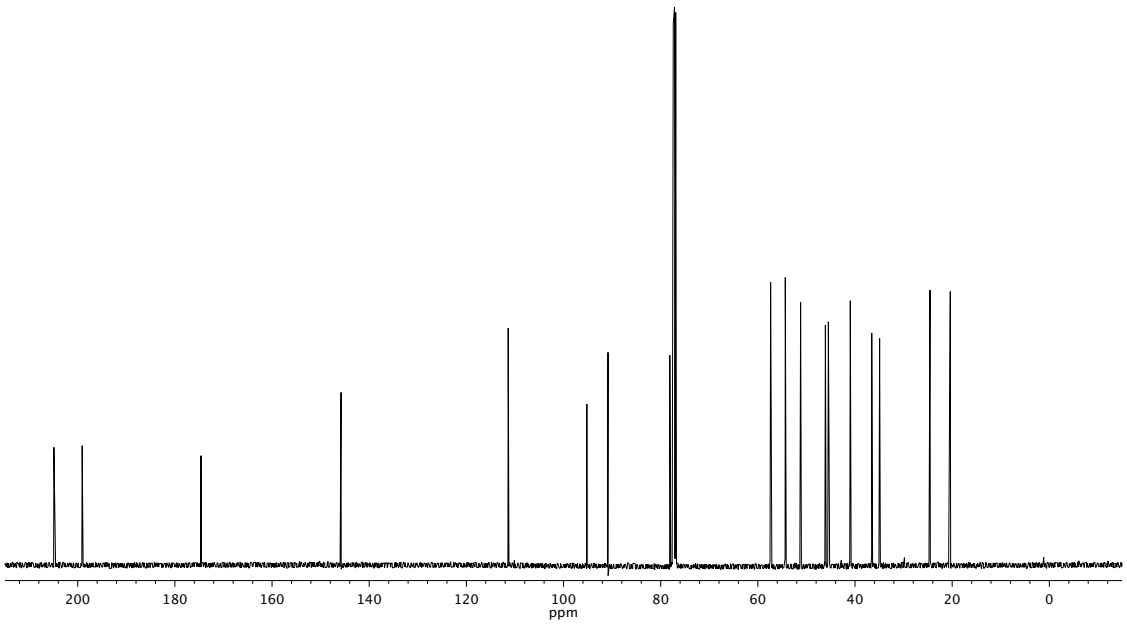

Figure A6.60. ^{13}C NMR (126 MHz, $CDCl_3$) of compound **347**.

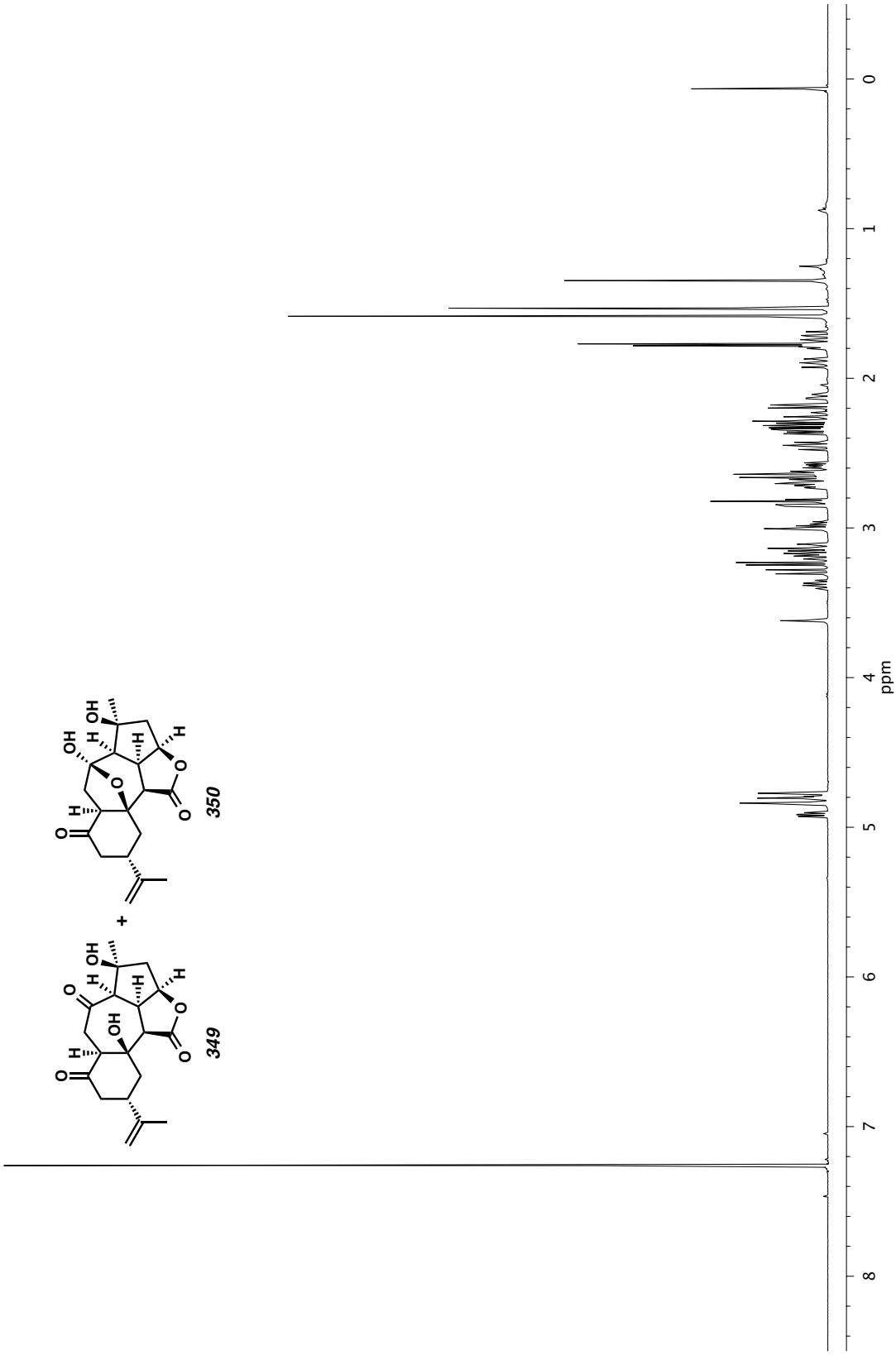

Figure A6.61. ^{1}H NMR (500 MHz, $CDCl_3$) of compound **349/350**.

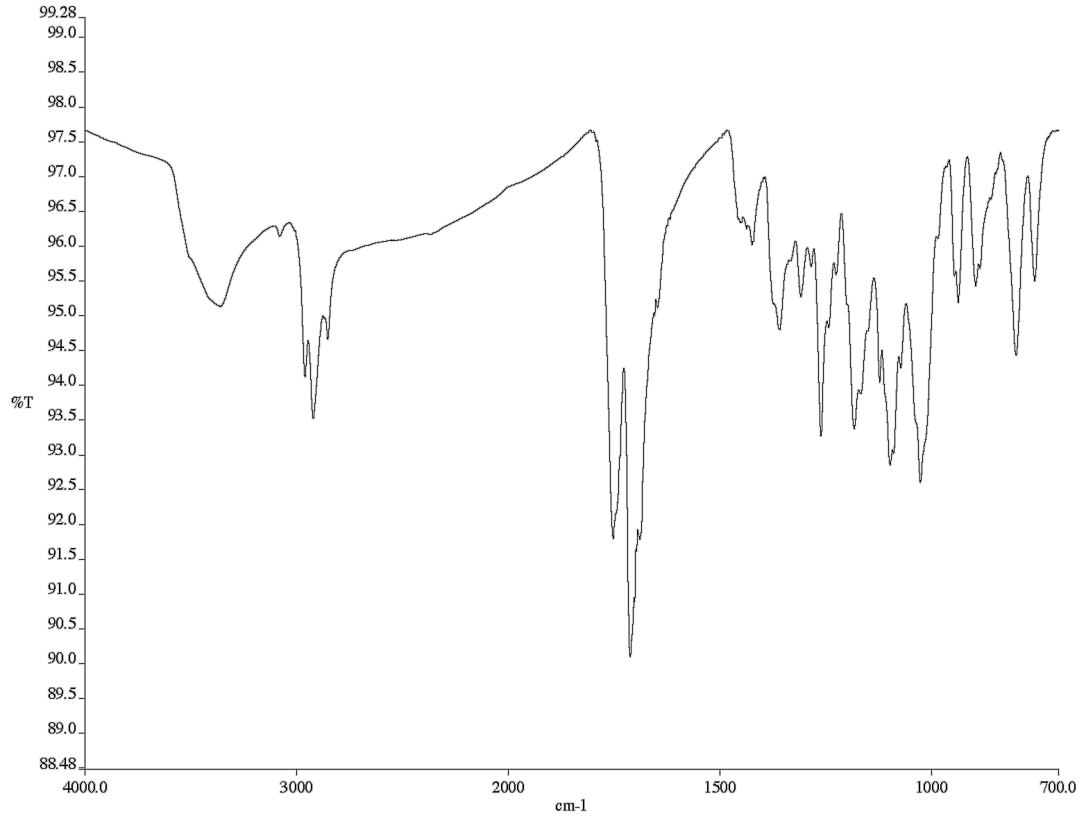

Figure A6.62. Infrared spectrum (Thin Film, NaCl) of compound **349/350**.

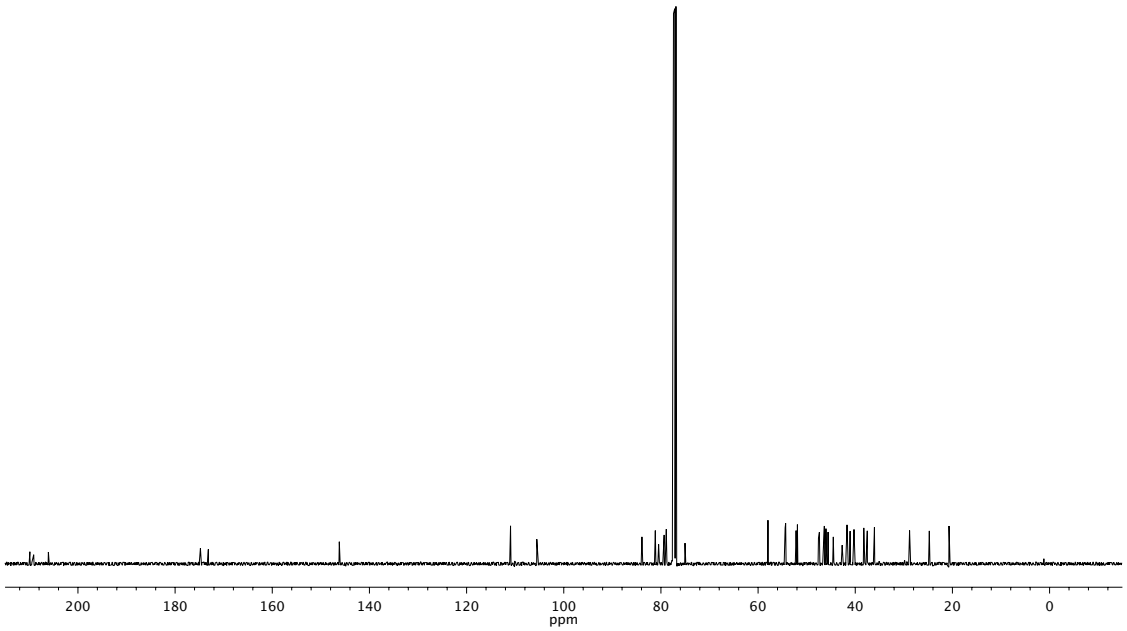

Figure A6.63. ^{13}C NMR (126 MHz, $CDCl_3$) of compound **349/350**.

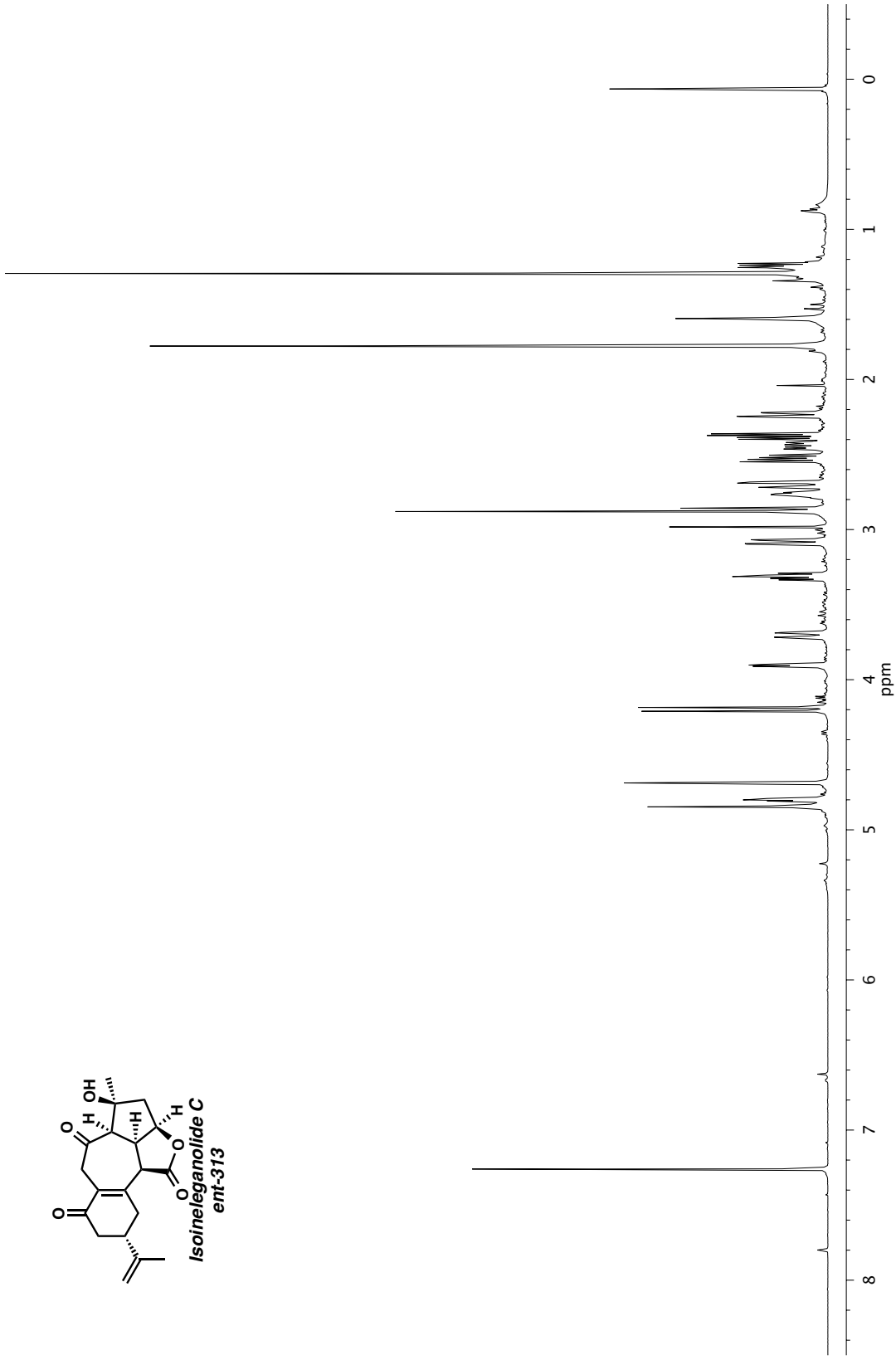

Figure A6.64. ^{1}H NMR (600 MHz, $CDCl_3$) of compound ***ent*-313**.

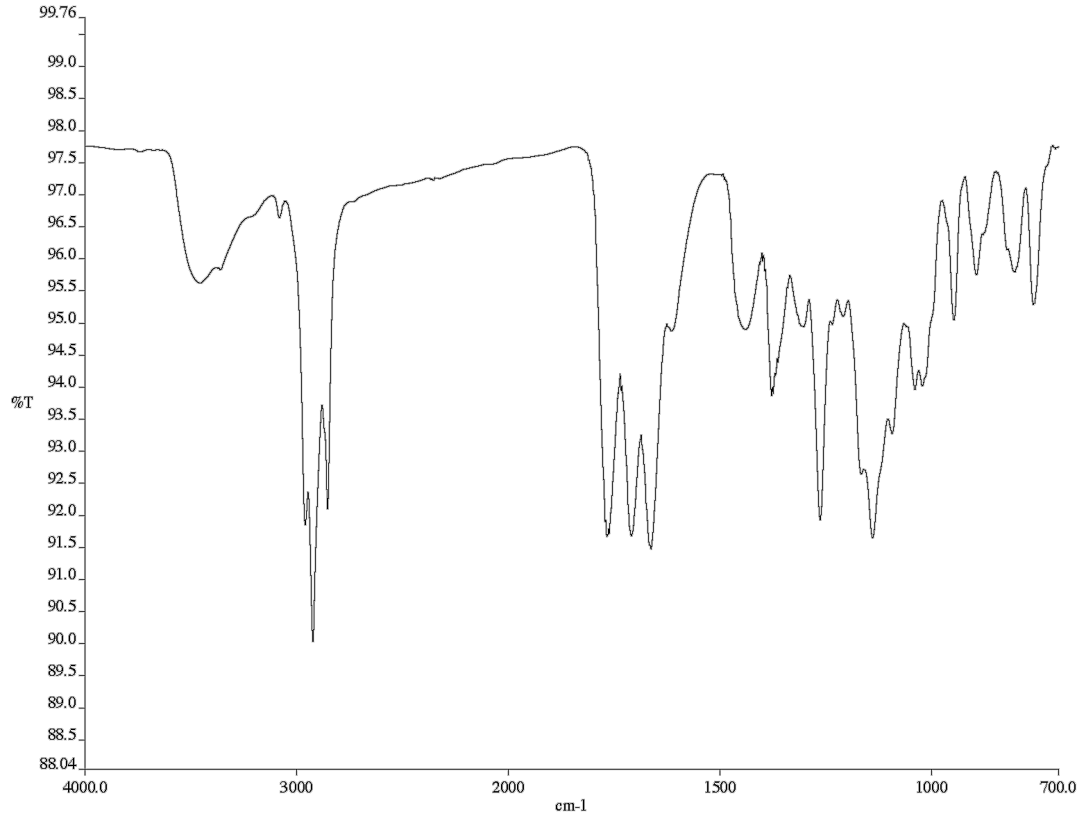

Figure A6.65. Infrared spectrum (Thin Film, NaCl) of compound ***ent*-313**.

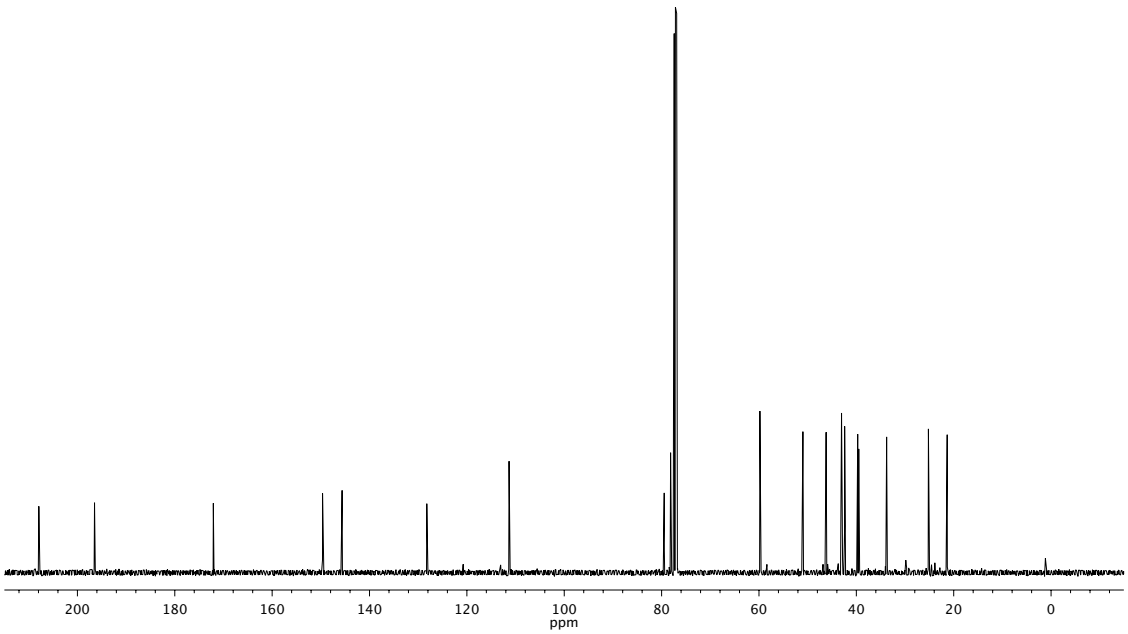

Figure A6.66. ^{13}C NMR (126 MHz, $CDCl_3$) of compound ***ent*-313**.

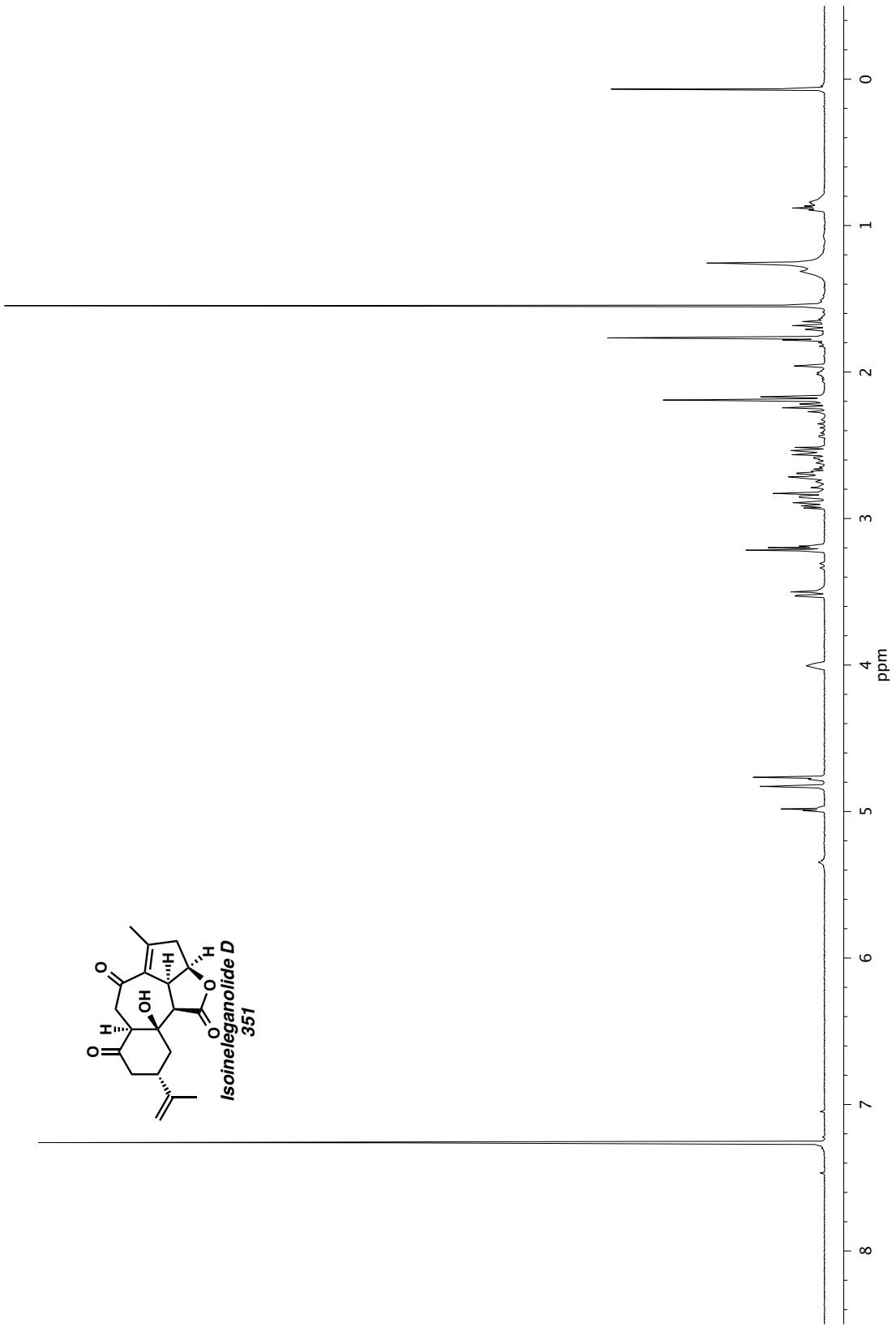

Figure A6.67. ^{1}H NMR (500 MHz, $CDCl_3$) of compound **351**.

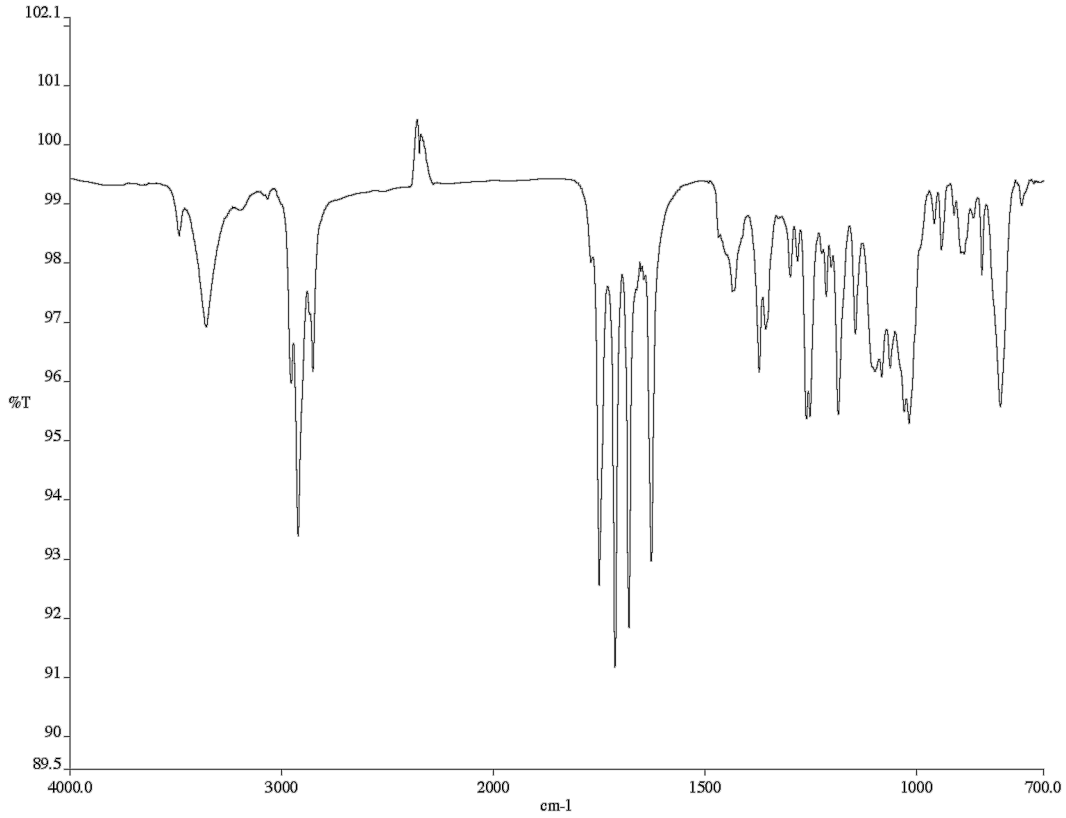

Figure A6.68. Infrared spectrum (Thin Film, NaCl) of compound **351**.

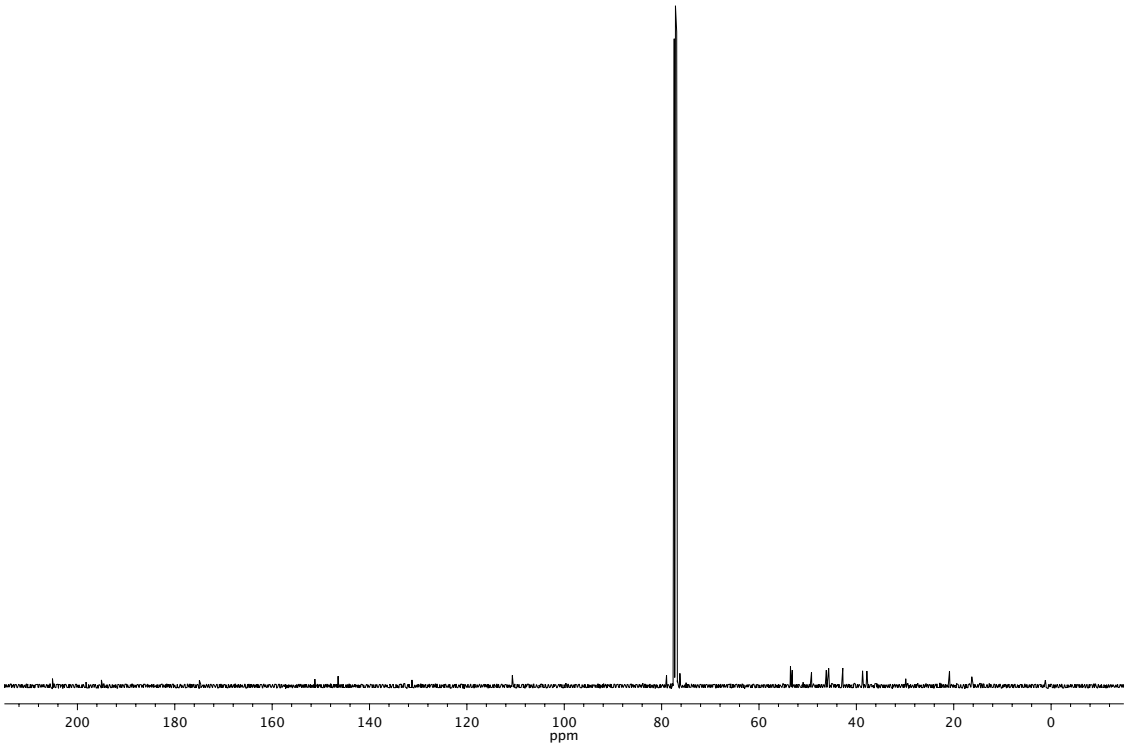

Figure A6.69. ^{13}C NMR (126 MHz, $CDCl_3$) of compound **351**.

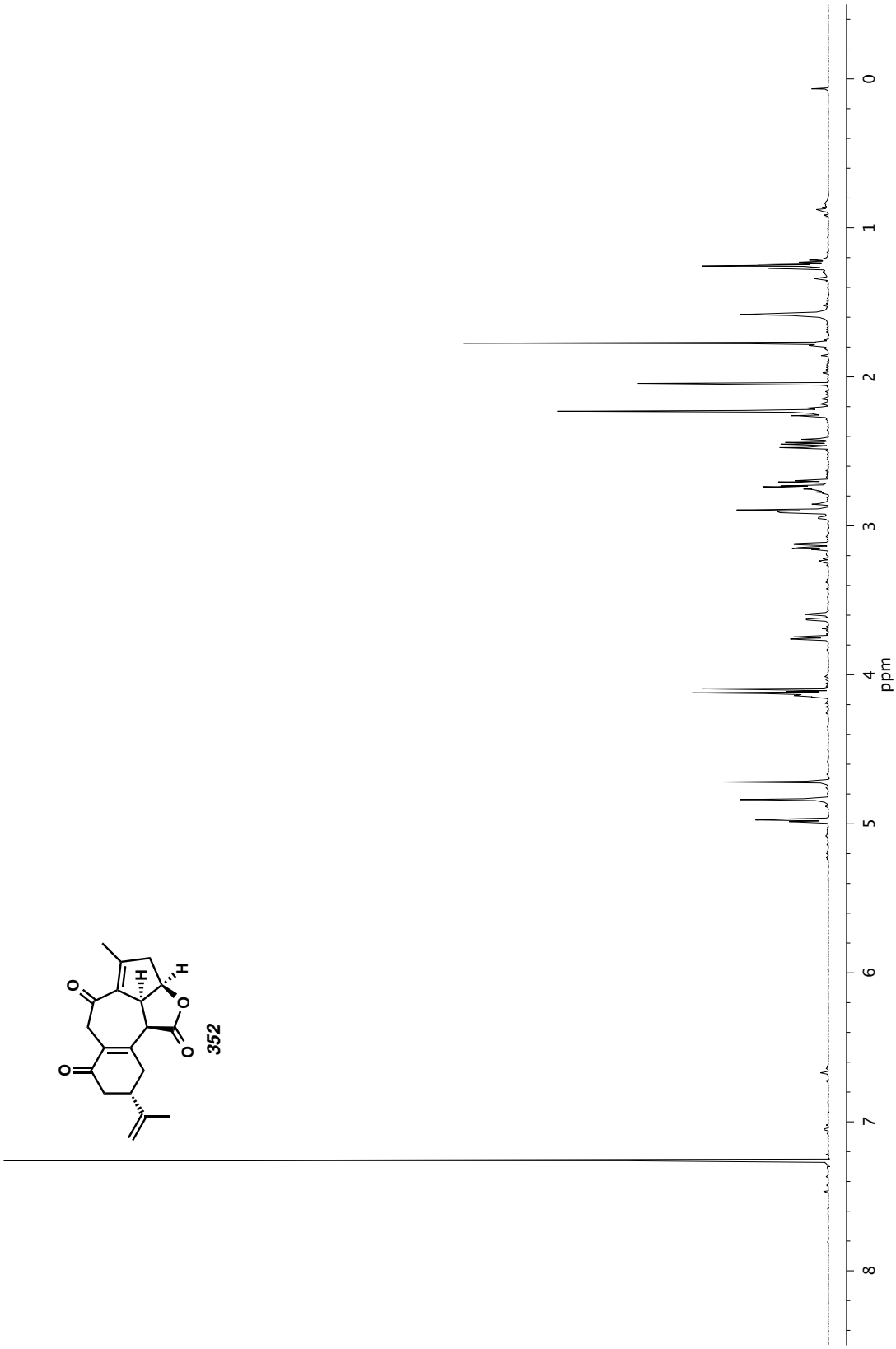

Figure A6.70. ^{1}H NMR (500 MHz, $CDCl_3$) of compound **352**.

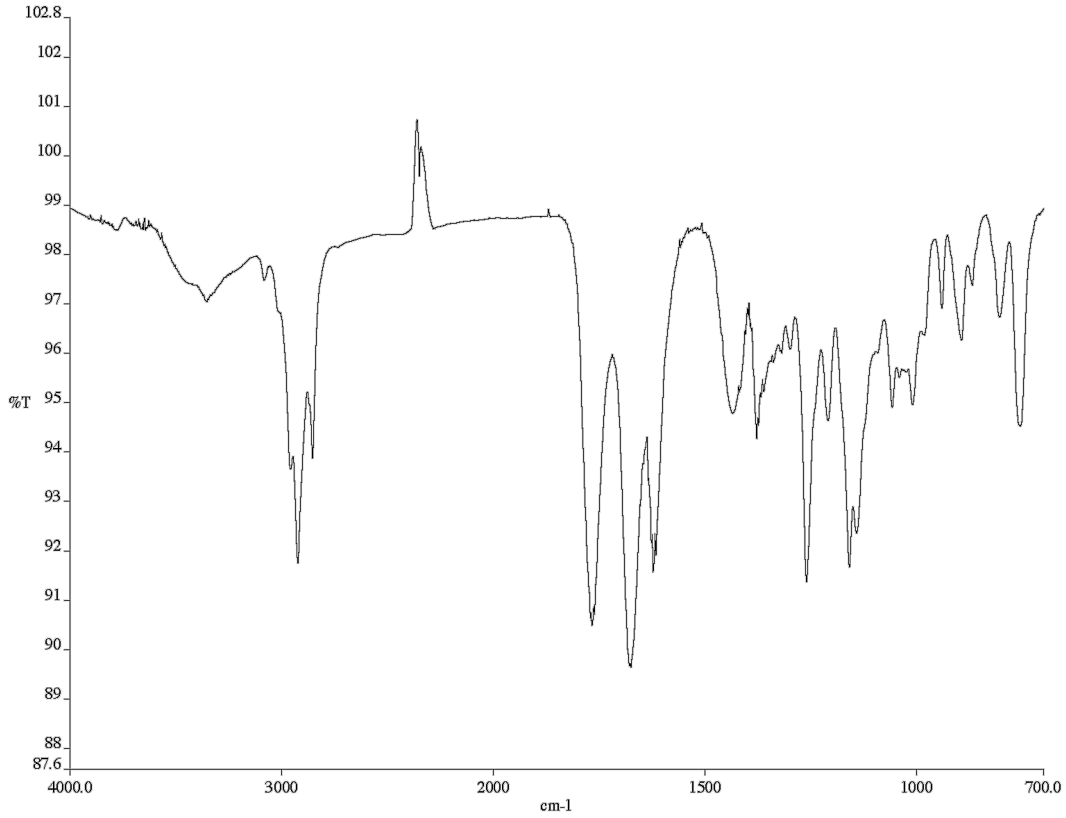

Figure A6.71. Infrared spectrum (Thin Film, NaCl) of compound **352**.

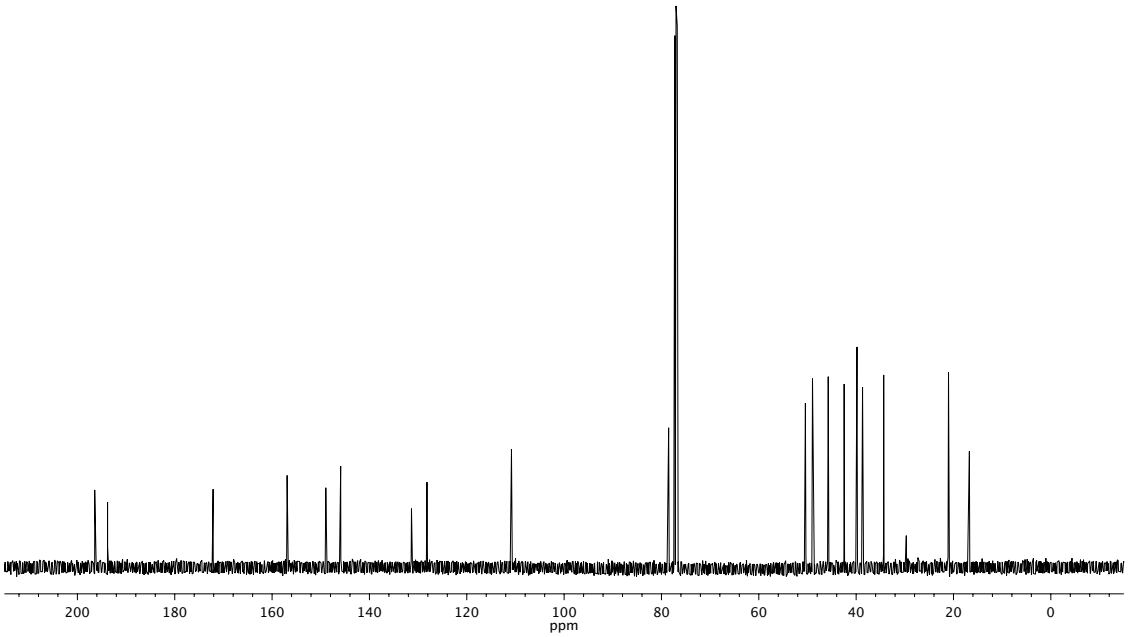

Figure A6.72. ^{13}C NMR (126 MHz, $CDCl_3$) of compound **352**.

APPENDIX 7

X-Ray Crystallography Reports Relevant to Chapter 3:

Progress Toward the Asymmetric Total Syntheses of the

Furanobutenolide Norcembranoid Diterpene Natural Products

A7.1 X-Ray Crystal Structure Analysis of Diene 324

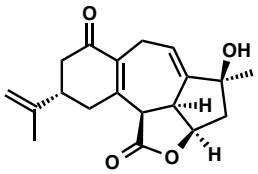

324

Contents

Table A7.1.1. Experimental Details

Table A7.1.2. Crystal Data

Table A7.1.3. Atomic Coordinates

Table A7.1.4. Full Bond Distances and Angles

Table A7.1.5. Anisotropic Displacement Parameters

Table A7.1.6. Hydrogen Atomic Coordinates

Table A7.1.7. Torsion Angles

Table A7.1.8. Hydrogen Bond Distances and Angle

Figure A7.1.1. X-Ray Crystal Structure of Diene ***324***

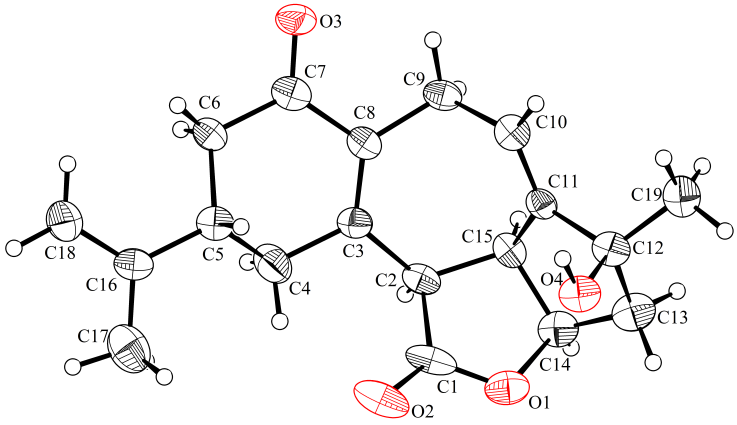

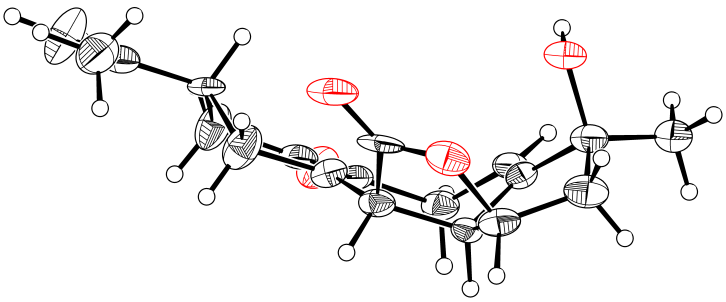

*Table A7.1.1. Experimental Details for X-Ray Structure Determination of Diene **324**.*

Low-temperature diffraction data (ϕ-and ω-scans) were collected on a Bruker AXS KAPPA APEX II diffractometer coupled to a APEX II CCD detector with graphite monochromated Mo K_α radiation (λ = 0.71073 Å) for the structure of diene **324**. The structure was solved by direct methods using SHELXS[1] and refined against F^2 on all data by full-matrix least squares with SHELXL-2014[2] using established refinement techniques.[3] All non-hydrogen atoms were refined anisotropically. All hydrogen atoms were included into the model at geometrically calculated positions and refined using a riding model. The isotropic displacement parameters of all hydrogen atoms were fixed to 1.2 times the U value of the atoms they are linked to (1.5 times for methyl groups).

Diene **324** crystallizes in the monoclinic space group $P2_1$ with one molecule in the asymmetric unit. The coordinates for the hydrogen atom bound to O4 was located in the difference Fourier synthesis and refined semi-freely with the help of a restraint on the O-H distance (0.84(4) Å). The crystal diffracted to 0.93 Å leading to low pond precision. The structure is sufficient to determine the relative stereochemistry of the molecule.

*Table A7.1.2. Crystal Data and Structure Refinement for Diene **324**.*

Caltech Identification code	rac01	
CCDC Deposition Number	1061010	
Empirical formula	C19 H22 O4	
Formula weight	314.36	
Temperature	100(2) K	
Wavelength	0.71073 Å	
Crystal system	Monoclinic	
Space group	$P2_1$	
Unit cell dimensions	a = 11.7563(19) Å	α= 90°.
	b = 5.3917(8) Å	β= 104.529(8)°.
	c = 12.861(2) Å	γ = 90°.
Volume	789.2(2) $Å^3$	
Z	2	
Density (calculated)	1.323 Mg/m^3	
Absorption coefficient	0.092 mm^{-1}	
F(000)	336	
Crystal size	0.500 x 0.100 x 0.050 mm^3	
Theta range for data collection	1.636 to 22.464°.	
Index ranges	$-12 \le h \le 11, -5 \le k \le 5, -13 \le l \le 13$	
Reflections collected	8970	
Independent reflections	2037 [R(int) = 0.0848]	
Completeness to theta = 22.464°	100.0 %	
Absorption correction	Semi-empirical from equivalents	
Refinement method	Full-matrix least-squares on F^2	
Data / restraints / parameters	2037 / 2 / 213	
Goodness-of-fit on F^2	1.016	
Final R indices [I>2sigma(I)]	R1 = 0.0505, wR2 = 0.1037	
R indices (all data)	R1 = 0.0898, wR2 = 0.1180	
Absolute structure parameter	0.4(10)	
Extinction coefficient	n/a	
Largest diff. peak and hole	0.181 and -0.210 $e.Å^{-3}$	

*Table A7.1.3. Atomic coordinates (x 10^4) and equivalent isotropic displacement parameters ($Å^2$x 10^3) for Diene **324**. U(eq) is defined as one third of the trace of the orthogonalized U^{ij} tensor.*

	x	y	z	U(eq)
O(1)	3461(4)	5365(8)	3878(3)	40(1)
C(1)	4556(7)	4881(12)	3816(5)	36(2)
O(2)	5025(4)	2972(8)	4167(3)	49(1)
C(2)	5051(5)	7063(10)	3307(5)	29(2)
C(3)	6016(6)	6448(10)	2746(5)	29(2)
C(4)	7038(6)	5073(14)	3464(5)	46(2)
C(5)	7733(5)	3556(10)	2834(5)	28(2)
C(16)	8739(6)	2141(10)	3541(5)	32(2)
C(17)	8632(7)	1281(13)	4544(6)	56(2)
C(18)	9737(6)	1587(14)	3197(6)	62(2)
C(6)	8111(6)	5325(13)	2068(6)	44(2)
C(7)	7114(6)	6803(11)	1381(5)	32(2)
O(3)	7222(4)	7704(8)	541(4)	44(1)
C(8)	6042(5)	7252(10)	1764(5)	27(2)
C(9)	5096(5)	8726(11)	995(5)	32(2)
C(10)	3886(5)	7674(10)	819(5)	31(2)
C(11)	3363(5)	7471(10)	1604(5)	26(2)
C(12)	2148(6)	6428(10)	1542(5)	32(2)
O(4)	2230(4)	3726(8)	1651(3)	36(1)
C(19)	1219(5)	7101(11)	538(5)	40(2)
C(13)	1888(6)	7406(13)	2568(5)	41(2)
C(14)	3051(6)	7757(11)	3367(5)	35(2)
C(15)	3927(5)	8399(10)	2713(5)	27(2)

*Table A7.1.4. Bond lengths [Å] and angles [°] for Diene **324**.*

O(1)-C(1)	1.336(8)
O(1)-C(14)	1.473(7)
C(1)-O(2)	1.201(8)
C(1)-C(2)	1.530(8)
C(2)-C(3)	1.526(8)
C(2)-C(15)	1.531(8)
C(2)-H(2)	1.0000
C(3)-C(8)	1.342(8)
C(3)-C(4)	1.513(9)
C(4)-C(5)	1.525(8)
C(4)-H(4A)	0.9900
C(4)-H(4B)	0.9900
C(5)-C(16)	1.506(8)
C(5)-C(6)	1.516(8)
C(5)-H(5)	1.0000
C(16)-C(18)	1.387(8)
C(16)-C(17)	1.406(8)
C(17)-H(17A)	0.9800
C(17)-H(17B)	0.9800
C(17)-H(17C)	0.9800
C(18)-H(18A)	0.9500
C(18)-H(18B)	0.9500
C(6)-C(7)	1.506(9)
C(6)-H(6A)	0.9900
C(6)-H(6B)	0.9900
C(7)-O(3)	1.221(7)
C(7)-C(8)	1.484(8)
C(8)-C(9)	1.515(8)
C(9)-C(10)	1.495(8)
C(9)-H(9A)	0.9900
C(9)-H(9B)	0.9900
C(10)-C(11)	1.311(7)
C(10)-H(10)	0.9500

Table A7.1.4. (cont'd)

C(11)-C(15)	1.499(8)
C(11)-C(12)	1.519(8)
C(12)-O(4)	1.465(7)
C(12)-C(19)	1.512(8)
C(12)-C(13)	1.522(8)
O(4)-H(4O)	0.83(3)
C(19)-H(19A)	0.9800
C(19)-H(19B)	0.9800
C(19)-H(19C)	0.9800
C(13)-C(14)	1.502(8)
C(13)-H(13A)	0.9900
C(13)-H(13B)	0.9900
C(14)-C(15)	1.524(8)
C(14)-H(14)	1.0000
C(15)-H(15)	1.0000

C(1)-O(1)-C(14)	110.9(5)
O(2)-C(1)-O(1)	120.2(6)
O(2)-C(1)-C(2)	129.2(7)
O(1)-C(1)-C(2)	110.5(6)
C(3)-C(2)-C(1)	116.3(5)
C(3)-C(2)-C(15)	121.1(5)
C(1)-C(2)-C(15)	101.7(5)
C(3)-C(2)-H(2)	105.5
C(1)-C(2)-H(2)	105.5
C(15)-C(2)-H(2)	105.5
C(8)-C(3)-C(4)	122.1(6)
C(8)-C(3)-C(2)	124.7(5)
C(4)-C(3)-C(2)	112.8(5)
C(3)-C(4)-C(5)	112.8(5)
C(3)-C(4)-H(4A)	109.0
C(5)-C(4)-H(4A)	109.0
C(3)-C(4)-H(4B)	109.0
C(5)-C(4)-H(4B)	109.0

Table A7.1.4. (cont'd)

H(4A)-C(4)-H(4B)	107.8
C(16)-C(5)-C(6)	113.4(5)
C(16)-C(5)-C(4)	113.3(5)
C(6)-C(5)-C(4)	107.0(5)
C(16)-C(5)-H(5)	107.6
C(6)-C(5)-H(5)	107.6
C(4)-C(5)-H(5)	107.6
C(18)-C(16)-C(17)	120.0(6)
C(18)-C(16)-C(5)	121.1(6)
C(17)-C(16)-C(5)	118.9(6)
C(16)-C(17)-H(17A)	109.5
C(16)-C(17)-H(17B)	109.5
H(17A)-C(17)-H(17B)	109.5
C(16)-C(17)-H(17C)	109.5
H(17A)-C(17)-H(17C)	109.5
H(17B)-C(17)-H(17C)	109.5
C(16)-C(18)-H(18A)	120.0
C(16)-C(18)-H(18B)	120.0
H(18A)-C(18)-H(18B)	120.0
C(7)-C(6)-C(5)	113.7(5)
C(7)-C(6)-H(6A)	108.8
C(5)-C(6)-H(6A)	108.8
C(7)-C(6)-H(6B)	108.8
C(5)-C(6)-H(6B)	108.8
H(6A)-C(6)-H(6B)	107.7
O(3)-C(7)-C(8)	120.9(6)
O(3)-C(7)-C(6)	119.5(6)
C(8)-C(7)-C(6)	119.5(6)
C(3)-C(8)-C(7)	118.7(5)
C(3)-C(8)-C(9)	126.7(5)
C(7)-C(8)-C(9)	114.5(5)
C(10)-C(9)-C(8)	114.5(5)
C(10)-C(9)-H(9A)	108.6
C(8)-C(9)-H(9A)	108.6

Table A7.1.4. (cont'd)

C(10)-C(9)-H(9B)	108.6
C(8)-C(9)-H(9B)	108.6
H(9A)-C(9)-H(9B)	107.6
C(11)-C(10)-C(9)	121.8(6)
C(11)-C(10)-H(10)	119.1
C(9)-C(10)-H(10)	119.1
C(10)-C(11)-C(15)	121.6(5)
C(10)-C(11)-C(12)	127.4(5)
C(15)-C(11)-C(12)	111.0(5)
O(4)-C(12)-C(19)	109.7(5)
O(4)-C(12)-C(11)	109.0(5)
C(19)-C(12)-C(11)	115.1(5)
O(4)-C(12)-C(13)	106.5(5)
C(19)-C(12)-C(13)	113.5(5)
C(11)-C(12)-C(13)	102.6(5)
C(12)-O(4)-H(4O)	106(5)
C(12)-C(19)-H(19A)	109.5
C(12)-C(19)-H(19B)	109.5
H(19A)-C(19)-H(19B)	109.5
C(12)-C(19)-H(19C)	109.5
H(19A)-C(19)-H(19C)	109.5
H(19B)-C(19)-H(19C)	109.5
C(14)-C(13)-C(12)	106.9(5)
C(14)-C(13)-H(13A)	110.4
C(12)-C(13)-H(13A)	110.4
C(14)-C(13)-H(13B)	110.4
C(12)-C(13)-H(13B)	110.4
H(13A)-C(13)-H(13B)	108.6
O(1)-C(14)-C(13)	109.5(5)
O(1)-C(14)-C(15)	104.8(5)
C(13)-C(14)-C(15)	106.0(5)
O(1)-C(14)-H(14)	112.0
C(13)-C(14)-H(14)	112.0
C(15)-C(14)-H(14)	112.0

Table A7.1.4. (cont'd)

C(11)-C(15)-C(14)	104.5(5)
C(11)-C(15)-C(2)	116.0(5)
C(14)-C(15)-C(2)	103.6(5)
C(11)-C(15)-H(15)	110.8
C(14)-C(15)-H(15)	110.8
C(2)-C(15)-H(15)	110.8

Symmetry transformations used to generate equivalent atoms:

*Table A7.1.5. Anisotropic displacement parameters ($Å^2x10^3$) for Diene **324**. The anisotropic displacement factor exponent takes the form: $-2\pi^2[h^2a^{*2}U^{11} + ... + 2hka^*b^*U^{12}]$.*

	U^{11}	U^{22}	U^{33}	U^{23}	U^{13}	U^{12}
O(1)	53(4)	37(3)	32(3)	-5(2)	14(3)	-10(3)
C(1)	74(6)	13(4)	16(4)	-6(3)	5(4)	-11(4)
O(2)	91(4)	20(2)	29(3)	-2(2)	3(3)	-6(3)
C(2)	43(4)	23(3)	20(3)	-3(3)	5(3)	-1(3)
C(3)	38(5)	22(3)	29(4)	0(3)	12(4)	3(3)
C(4)	54(5)	54(4)	32(4)	3(4)	10(4)	22(4)
C(5)	40(4)	11(3)	34(4)	-6(3)	9(4)	-4(3)
C(16)	43(5)	22(3)	30(4)	-2(3)	10(4)	-6(3)
C(17)	61(6)	46(4)	55(5)	-1(4)	5(4)	12(4)
C(18)	53(5)	70(5)	69(6)	30(5)	26(5)	32(5)
C(6)	40(5)	47(4)	48(4)	23(4)	14(4)	12(4)
C(7)	44(5)	17(3)	32(4)	-4(3)	7(4)	-6(3)
O(3)	50(3)	37(2)	48(3)	18(2)	20(3)	4(2)
C(8)	35(4)	16(3)	28(4)	-3(3)	5(3)	-1(3)
C(9)	42(5)	22(3)	30(4)	3(3)	9(4)	-3(3)
C(10)	37(4)	21(3)	33(4)	-6(3)	7(3)	-2(3)
C(11)	30(4)	17(3)	30(4)	3(3)	6(3)	2(3)
C(12)	42(5)	23(3)	32(4)	-4(3)	9(4)	-1(3)
O(4)	48(3)	23(2)	39(3)	-6(2)	14(3)	-6(2)
C(19)	40(4)	29(4)	48(5)	-3(3)	8(4)	-2(3)
C(13)	53(5)	35(4)	39(4)	-10(3)	18(4)	-4(4)
C(14)	49(5)	24(3)	35(4)	-7(3)	16(4)	2(3)
C(15)	33(4)	20(3)	25(4)	-6(3)	0(3)	-1(3)

*Table A7.1.6. Hydrogen coordinates ($x10^4$) and isotropic displacement parameters ($Å^2x10^3$) for Diene **324**.*

	x	y	z	U(eq)
H(2)	5428	8178	3918	35
H(4A)	6736	3951	3943	56
H(4B)	7570	6285	3921	56
H(5)	7183	2320	2392	34
H(17A)	9335	334	4894	84
H(17B)	7938	212	4441	84
H(17C)	8547	2697	4996	84
H(18A)	10348	627	3639	74
H(18B)	9810	2168	2519	74
H(6A)	8703	6486	2489	53
H(6B)	8493	4362	1594	53
H(9A)	5094	10436	1275	38
H(9B)	5297	8828	294	38
H(10)	3484	7139	119	37
H(4O)	2450(60)	3220(130)	1120(40)	54
H(19A)	1426	6385	-90	60
H(19B)	1170	8910	465	60
H(19C)	457	6445	589	60
H(13A)	1460	9002	2429	49
H(13B)	1398	6206	2846	49
H(14)	3016	9069	3907	42
H(15)	4056	10232	2706	33

*Table A7.1.7. Torsion angles [°] for Diene **324**.*

C(14)-O(1)-C(1)-O(2)	-178.0(5)
C(14)-O(1)-C(1)-C(2)	4.1(6)
O(2)-C(1)-C(2)-C(3)	28.0(9)
O(1)-C(1)-C(2)-C(3)	-154.4(5)
O(2)-C(1)-C(2)-C(15)	161.6(6)
O(1)-C(1)-C(2)-C(15)	-20.8(6)
C(1)-C(2)-C(3)-C(8)	132.6(6)
C(15)-C(2)-C(3)-C(8)	8.5(8)
C(1)-C(2)-C(3)-C(4)	-54.4(7)
C(15)-C(2)-C(3)-C(4)	-178.6(5)
C(8)-C(3)-C(4)-C(5)	-30.4(9)
C(2)-C(3)-C(4)-C(5)	156.4(5)
C(3)-C(4)-C(5)-C(16)	-178.9(5)
C(3)-C(4)-C(5)-C(6)	55.4(7)
C(6)-C(5)-C(16)-C(18)	-29.2(8)
C(4)-C(5)-C(16)-C(18)	-151.3(6)
C(6)-C(5)-C(16)-C(17)	153.7(6)
C(4)-C(5)-C(16)-C(17)	31.6(8)
C(16)-C(5)-C(6)-C(7)	-178.3(5)
C(4)-C(5)-C(6)-C(7)	-52.7(7)
C(5)-C(6)-C(7)-O(3)	-158.3(6)
C(5)-C(6)-C(7)-C(8)	24.8(8)
C(4)-C(3)-C(8)-C(7)	-0.8(8)
C(2)-C(3)-C(8)-C(7)	171.5(5)
C(4)-C(3)-C(8)-C(9)	-177.5(6)
C(2)-C(3)-C(8)-C(9)	-5.2(9)
O(3)-C(7)-C(8)-C(3)	-172.9(5)
C(6)-C(7)-C(8)-C(3)	3.9(8)
O(3)-C(7)-C(8)-C(9)	4.1(8)
C(6)-C(7)-C(8)-C(9)	-179.1(5)
C(3)-C(8)-C(9)-C(10)	-49.6(8)
C(7)-C(8)-C(9)-C(10)	133.6(5)
C(8)-C(9)-C(10)-C(11)	62.6(8)
C(9)-C(10)-C(11)-C(15)	3.1(9)

Table A7.1.7. (cont'd)

C(9)-C(10)-C(11)-C(12)	-179.5(5)
C(10)-C(11)-C(12)-O(4)	84.5(7)
C(15)-C(11)-C(12)-O(4)	-98.0(5)
C(10)-C(11)-C(12)-C(19)	-39.2(8)
C(15)-C(11)-C(12)-C(19)	138.4(5)
C(10)-C(11)-C(12)-C(13)	-162.9(6)
C(15)-C(11)-C(12)-C(13)	14.7(6)
O(4)-C(12)-C(13)-C(14)	86.9(6)
C(19)-C(12)-C(13)-C(14)	-152.3(5)
C(11)-C(12)-C(13)-C(14)	-27.5(6)
C(1)-O(1)-C(14)-C(13)	127.9(5)
C(1)-O(1)-C(14)-C(15)	14.6(6)
C(12)-C(13)-C(14)-O(1)	-81.9(6)
C(12)-C(13)-C(14)-C(15)	30.7(6)
C(10)-C(11)-C(15)-C(14)	-178.9(5)
C(12)-C(11)-C(15)-C(14)	3.4(6)
C(10)-C(11)-C(15)-C(2)	-65.5(7)
C(12)-C(11)-C(15)-C(2)	116.8(5)
O(1)-C(14)-C(15)-C(11)	95.2(5)
C(13)-C(14)-C(15)-C(11)	-20.6(6)
O(1)-C(14)-C(15)-C(2)	-26.7(5)
C(13)-C(14)-C(15)-C(2)	-142.5(5)
C(3)-C(2)-C(15)-C(11)	44.8(7)
C(1)-C(2)-C(15)-C(11)	-85.9(6)
C(3)-C(2)-C(15)-C(14)	158.7(5)
C(1)-C(2)-C(15)-C(14)	28.0(5)

Symmetry transformations used to generate equivalent atoms:

*Table A7.1.8. Hydrogen bonds for Diene **324** [Å and °].*

D-H...A	d(D-H)	d(H...A)	d(D...A)	<(DHA)
C(2)-H(2)...O(2)#1	1.00	2.65	3.309(7)	123.5
O(4)-H(4O)...O(3)#2	0.83(3)	2.28(3)	3.094(6)	165(7)
C(15)-H(15)...O(2)#3	1.00	2.44	3.167(7)	129.5

Symmetry transformations used to generate equivalent atoms:

#1 -x+1,y+1/2,-z+1 #2 -x+1,y-1/2,-z #3 x,y+1,z

A7.2 X-Ray Crystal Structure Analysis of Isoineleganolide A (328)

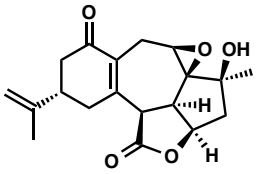

Isoineleganolide A
328

Contents

Table A7.2.1. Experimental Details

Table A7.2.2. Crystal Data

Table A7.2.3. Atomic Coordinates

Table A7.2.4. Full Bond Distances and Angles

Table A7.2.5. Anisotropic Displacement Parameters

Table A7.2.6. Hydrogen Atomic Coordinates

Table A7.2.7. Torsion Angles

Table A7.2.8. Hydrogen Bond Distances and Angles

*Figure A7.2.1. X-Ray Crystal Structure of Isoineleganolide A (**328**)*

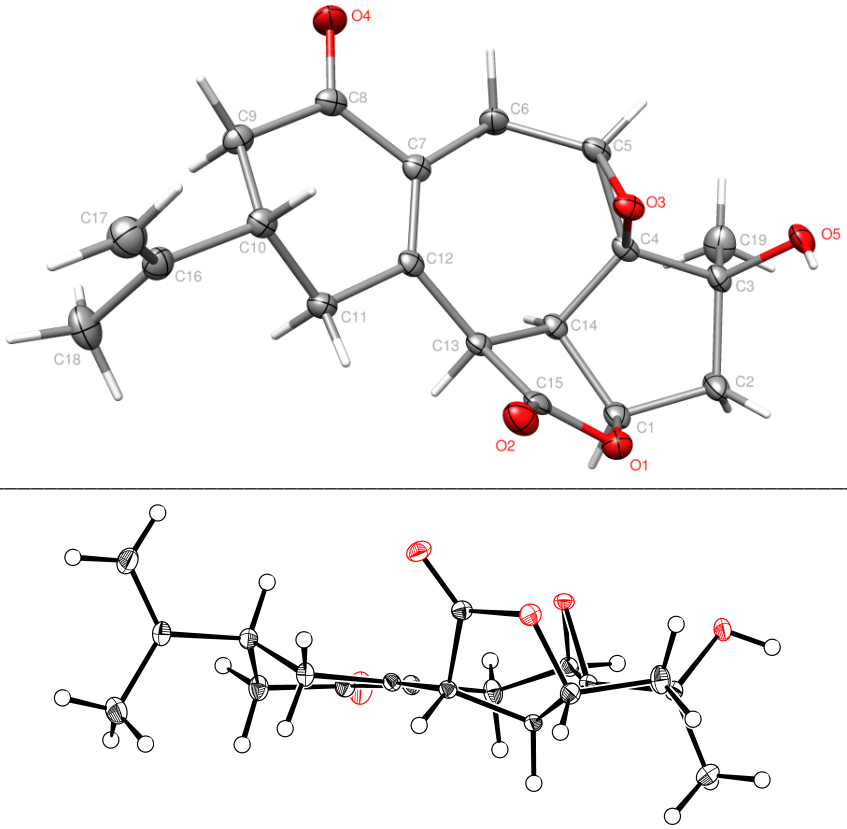

*Table A7.2.1. Experimental Details for X-Ray Structure Determination of Isoineleganolide A (**328**).*

Low-temperature diffraction data (ϕ-and ω-scans) were collected on a Bruker AXS KAPPA APEX II diffractometer coupled to a APEX II CCD detector with graphite monochromated Mo K_α radiation (λ = 0.71073 Å) for the structure of isoineleganolide A (**328**). The structure was solved by direct methods using SHELXS[1] and refined against F^2 on all data by full-matrix least squares with SHELXL-2014[2] using established refinement techniques.[3] All non-hydrogen atoms were refined anisotropically. Unless otherwise noted, all hydrogen atoms were included into the model at geometrically calculated positions and refined using a riding model. The isotropic displacement parameters of all hydrogen atoms were fixed to 1.2 times the U value of the atoms they are linked to (1.5 times for methyl groups).

Isoineleganolide A (**328**) crystallizes in the monoclinic space group $P2_1$ with one molecule in the asymmetric unit. The coordinates for the hydrogen atom bound to O4 was located in the difference Fourier synthesis and refined semi-freely with the help of a restraint on the O-H distance (0.84(4) Å).

*Table A7.2.2. Crystal Data and Structure Refinement for Isoineleganolide A (**328**).*

Caltech Identification code	rac03	
CCDC Deposition Number	853379 / 1061011	
Empirical formula	C19 H22 O5	
Formula weight	330.36	
Temperature	100(2) K	
Wavelength	0.71073 Å	
Crystal system	Monoclinic	
Space group	$P2_1$	
Unit cell dimensions	a = 6.9222(2) Å	α= 90°.
	b = 11.1470(4) Å	β= 94.070(2)°.
	c = 10.4409(4) Å	γ = 90°.
Volume	803.61(5) $Å^3$	
Z	2	
Density (calculated)	1.365 Mg/m^3	
Absorption coefficient	0.098 mm^{-1}	
F(000)	352	
Crystal size	0.500 x 0.450 x 0.200 mm^3	
Theta range for data collection	1.955 to 36.317°.	
Index ranges	$-11 \le h \le 11, -18 \le k \le 18, -17 \le l \le 17$	
Reflections collected	30117	
Independent reflections	7796 [R(int) = 0.0404]	
Completeness to theta = 25.242°	100.0 %	
Absorption correction	Semi-empirical from equivalents	
Max. and min. transmission	0.7475 and 0.6239	
Refinement method	Full-matrix least-squares on F^2	
Data / restraints / parameters	7796 / 2 / 222	
Goodness-of-fit on F^2	1.067	
Final R indices [I>2sigma(I)]	R1 = 0.0445, wR2 = 0.1109	
R indices (all data)	R1 = 0.0538, wR2 = 0.1198	
Absolute structure parameter	-0.5(3)	
Extinction coefficient	n/a	
Largest diff. peak and hole	0.732 and -0.318 $e.Å^{-3}$	

*Table A7.2.3. Atomic coordinates (x 10^4) and equivalent isotropic displacement parameters ($Å^2$x 10^3) for Isoineleganolide A (**328**). U(eq) is defined as one third of the trace of the orthogonalized U^{ij} tensor.*

	x	y	z	U(eq)
O(1)	6780(2)	3526(1)	2529(1)	17(1)
C(1)	6361(2)	3631(1)	3770(1)	13(1)
O(2)	6200(2)	2761(1)	4432(1)	18(1)
C(2)	6086(2)	4958(1)	4084(1)	11(1)
C(3)	6324(2)	5269(1)	5490(1)	11(1)
C(4)	4753(2)	4700(1)	6220(1)	14(1)
C(5)	5248(2)	4650(1)	7666(1)	12(1)
C(16)	3659(2)	4140(1)	8421(1)	15(1)
C(17)	1649(2)	4643(2)	8156(2)	23(1)
C(18)	4057(3)	3309(2)	9322(2)	21(1)
C(6)	5752(2)	5923(1)	8097(1)	14(1)
C(7)	7361(2)	6450(1)	7385(1)	14(1)
O(3)	8395(2)	7238(1)	7898(1)	22(1)
C(8)	7629(2)	6048(1)	6053(1)	12(1)
C(9)	9282(2)	6681(1)	5467(2)	16(1)
C(10)	10375(2)	6022(1)	4484(1)	13(1)
O(5)	10127(1)	4727(1)	4366(1)	13(1)
C(11)	9411(2)	5510(1)	3334(1)	11(1)
C(12)	10337(2)	5381(1)	2046(1)	13(1)
O(4)	12121(2)	4754(1)	2164(1)	18(1)
C(19)	10782(3)	6615(2)	1521(2)	25(1)
C(13)	8747(2)	4724(2)	1184(1)	18(1)
C(14)	6917(2)	4701(2)	1921(1)	14(1)
C(15)	7241(2)	5555(1)	3068(1)	12(1)

*Table A7.2.4. Bond lengths [Å] and angles [°] for Isoineleganolide A (**328**).*

O(1)-C(1)	1.3531(18)
O(1)-C(14)	1.462(2)
C(1)-O(2)	1.2007(19)
C(1)-C(2)	1.5291(19)
C(2)-C(3)	1.5070(18)
C(2)-C(15)	1.5255(19)
C(2)-H(2)	1.0000
C(3)-C(8)	1.3565(18)
C(3)-C(4)	1.5109(19)
C(4)-C(5)	1.5248(19)
C(4)-H(4A)	0.9900
C(4)-H(4B)	0.9900
C(5)-C(16)	1.509(2)
C(5)-C(6)	1.522(2)
C(5)-H(5)	1.0000
C(16)-C(18)	1.335(2)
C(16)-C(17)	1.508(2)
C(17)-H(17A)	0.9800
C(17)-H(17B)	0.9800
C(17)-H(17C)	0.9800
C(18)-H(18A)	0.9500
C(18)-H(18B)	0.9500
C(6)-C(7)	1.502(2)
C(6)-H(6A)	0.9900
C(6)-H(6B)	0.9900
C(7)-O(3)	1.2318(18)
C(7)-C(8)	1.485(2)
C(8)-C(9)	1.511(2)
C(9)-C(10)	1.508(2)
C(9)-H(9A)	0.9900
C(9)-H(9B)	0.9900
C(10)-C(11)	1.4490(19)
C(10)-O(5)	1.4582(18)

Table A7.2.4. (cont'd)

C(10)-H(10)	1.0000
O(5)-C(11)	1.4458(17)
C(11)-C(15)	1.5093(19)
C(11)-C(12)	1.5377(19)
C(12)-O(4)	1.4163(18)
C(12)-C(19)	1.521(2)
C(12)-C(13)	1.555(2)
O(4)-H(4O)	0.83(2)
C(19)-H(19A)	0.9800
C(19)-H(19B)	0.9800
C(19)-H(19C)	0.9800
C(13)-C(14)	1.528(2)
C(13)-H(13A)	0.9900
C(13)-H(13B)	0.9900
C(14)-C(15)	1.534(2)
C(14)-H(14)	1.0000
C(15)-H(15)	1.0000

C(1)-O(1)-C(14)	111.28(11)
O(2)-C(1)-O(1)	121.05(13)
O(2)-C(1)-C(2)	129.80(13)
O(1)-C(1)-C(2)	109.11(12)
C(3)-C(2)-C(15)	123.39(12)
C(3)-C(2)-C(1)	115.12(11)
C(15)-C(2)-C(1)	101.21(11)
C(3)-C(2)-H(2)	105.2
C(15)-C(2)-H(2)	105.2
C(1)-C(2)-H(2)	105.2
C(8)-C(3)-C(2)	126.34(12)
C(8)-C(3)-C(4)	122.11(12)
C(2)-C(3)-C(4)	111.24(11)
C(3)-C(4)-C(5)	113.28(11)
C(3)-C(4)-H(4A)	108.9
C(5)-C(4)-H(4A)	108.9

Table A7.2.4. (cont'd)

C(3)-C(4)-H(4B)	108.9
C(5)-C(4)-H(4B)	108.9
H(4A)-C(4)-H(4B)	107.7
C(16)-C(5)-C(6)	110.93(12)
C(16)-C(5)-C(4)	114.17(11)
C(6)-C(5)-C(4)	106.86(11)
C(16)-C(5)-H(5)	108.2
C(6)-C(5)-H(5)	108.2
C(4)-C(5)-H(5)	108.2
C(18)-C(16)-C(17)	121.95(15)
C(18)-C(16)-C(5)	120.53(14)
C(17)-C(16)-C(5)	117.47(13)
C(16)-C(17)-H(17A)	109.5
C(16)-C(17)-H(17B)	109.5
H(17A)-C(17)-H(17B)	109.5
C(16)-C(17)-H(17C)	109.5
H(17A)-C(17)-H(17C)	109.5
H(17B)-C(17)-H(17C)	109.5
C(16)-C(18)-H(18A)	120.0
C(16)-C(18)-H(18B)	120.0
H(18A)-C(18)-H(18B)	120.0
C(7)-C(6)-C(5)	112.36(12)
C(7)-C(6)-H(6A)	109.1
C(5)-C(6)-H(6A)	109.1
C(7)-C(6)-H(6B)	109.1
C(5)-C(6)-H(6B)	109.1
H(6A)-C(6)-H(6B)	107.9
O(3)-C(7)-C(8)	121.04(14)
O(3)-C(7)-C(6)	119.45(13)
C(8)-C(7)-C(6)	119.46(12)
C(3)-C(8)-C(7)	118.36(12)
C(3)-C(8)-C(9)	128.65(13)
C(7)-C(8)-C(9)	112.73(12)
C(10)-C(9)-C(8)	118.59(12)

Table A7.2.4. (cont'd)

C(10)-C(9)-H(9A)	107.7
C(8)-C(9)-H(9A)	107.7
C(10)-C(9)-H(9B)	107.7
C(8)-C(9)-H(9B)	107.7
H(9A)-C(9)-H(9B)	107.1
C(11)-C(10)-O(5)	59.64(9)
C(11)-C(10)-C(9)	122.14(12)
O(5)-C(10)-C(9)	118.60(12)
C(11)-C(10)-H(10)	115.1
O(5)-C(10)-H(10)	115.1
C(9)-C(10)-H(10)	115.1
C(11)-O(5)-C(10)	59.86(9)
O(5)-C(11)-C(10)	60.50(9)
O(5)-C(11)-C(15)	116.21(11)
C(10)-C(11)-C(15)	122.21(12)
O(5)-C(11)-C(12)	116.94(11)
C(10)-C(11)-C(12)	124.47(12)
C(15)-C(11)-C(12)	108.27(11)
O(4)-C(12)-C(19)	106.25(13)
O(4)-C(12)-C(11)	112.63(11)
C(19)-C(12)-C(11)	109.80(13)
O(4)-C(12)-C(13)	113.30(13)
C(19)-C(12)-C(13)	111.77(13)
C(11)-C(12)-C(13)	103.20(11)
C(12)-O(4)-H(4O)	108(2)
C(12)-C(19)-H(19A)	109.5
C(12)-C(19)-H(19B)	109.5
H(19A)-C(19)-H(19B)	109.5
C(12)-C(19)-H(19C)	109.5
H(19A)-C(19)-H(19C)	109.5
H(19B)-C(19)-H(19C)	109.5
C(14)-C(13)-C(12)	107.14(12)
C(14)-C(13)-H(13A)	110.3
C(12)-C(13)-H(13A)	110.3

Table A7.2.4. (cont'd)

C(14)-C(13)-H(13B)	110.3
C(12)-C(13)-H(13B)	110.3
H(13A)-C(13)-H(13B)	108.5
O(1)-C(14)-C(13)	108.36(13)
O(1)-C(14)-C(15)	103.16(10)
C(13)-C(14)-C(15)	107.59(12)
O(1)-C(14)-H(14)	112.4
C(13)-C(14)-H(14)	112.4
C(15)-C(14)-H(14)	112.4
C(11)-C(15)-C(2)	114.92(11)
C(11)-C(15)-C(14)	102.19(11)
C(2)-C(15)-C(14)	102.50(11)
C(11)-C(15)-H(15)	112.1
C(2)-C(15)-H(15)	112.1
C(14)-C(15)-H(15)	112.1

Symmetry transformations used to generate equivalent atoms:

*Table A7.2.5. Anisotropic displacement parameters ($Å^2x10^3$) for Isoineleganolide A (**328**). The anisotropic displacement factor exponent takes the form: $-2\pi^2[h^2a^{*2}U^{11} + ... + 2hka^*b^*U^{12}]$.*

	U^{11}	U^{22}	U^{33}	U^{23}	U^{13}	U^{12}
O(1)	17(1)	16(1)	18(1)	-5(1)	3(1)	-2(1)
C(1)	8(1)	13(1)	17(1)	-3(1)	0(1)	-2(1)
O(2)	16(1)	11(1)	26(1)	0(1)	2(1)	-1(1)
C(2)	7(1)	12(1)	13(1)	-1(1)	0(1)	0(1)
C(3)	9(1)	10(1)	13(1)	-1(1)	0(1)	1(1)
C(4)	12(1)	16(1)	14(1)	-1(1)	1(1)	-4(1)
C(5)	12(1)	10(1)	14(1)	0(1)	1(1)	1(1)
C(16)	16(1)	13(1)	16(1)	0(1)	3(1)	0(1)
C(17)	15(1)	23(1)	31(1)	4(1)	8(1)	3(1)
C(18)	24(1)	18(1)	20(1)	4(1)	3(1)	-2(1)
C(6)	16(1)	11(1)	15(1)	-1(1)	1(1)	1(1)
C(7)	13(1)	12(1)	17(1)	-3(1)	-1(1)	0(1)
O(3)	22(1)	19(1)	24(1)	-9(1)	3(1)	-7(1)
C(8)	11(1)	9(1)	15(1)	-1(1)	1(1)	0(1)
C(9)	15(1)	12(1)	20(1)	-3(1)	4(1)	-5(1)
C(10)	9(1)	11(1)	20(1)	-1(1)	0(1)	-1(1)
O(5)	11(1)	10(1)	18(1)	1(1)	-2(1)	1(1)
C(11)	8(1)	10(1)	16(1)	1(1)	0(1)	0(1)
C(12)	9(1)	14(1)	17(1)	1(1)	2(1)	1(1)
O(4)	8(1)	19(1)	25(1)	-3(1)	1(1)	2(1)
C(19)	30(1)	17(1)	29(1)	5(1)	10(1)	-1(1)
C(13)	10(1)	28(1)	15(1)	-2(1)	1(1)	1(1)
C(14)	9(1)	20(1)	14(1)	-1(1)	0(1)	0(1)
C(15)	8(1)	13(1)	14(1)	1(1)	0(1)	2(1)

*Table A7.2.6. Hydrogen coordinates (x10^4) and isotropic displacement parameters (Å^{2}x10^3) for Isoineleganolide A (**328**).*

	x	y	z	U(eq)
H(2)	4698	5133	3818	13
H(4A)	4519	3874	5897	17
H(4B)	3539	5160	6051	17
H(5)	6428	4140	7829	15
H(17A)	792	4315	8777	34
H(17B)	1155	4422	7285	34
H(17C)	1692	5519	8233	34
H(18A)	3058	3018	9819	25
H(18B)	5338	3009	9467	25
H(6A)	4587	6435	7960	17
H(6B)	6141	5920	9028	17
H(9A)	8762	7428	5061	19
H(9B)	10228	6922	6176	19
H(10)	11720	6319	4387	16
H(4O)	11890(40)	4050(20)	2350(30)	26
H(19A)	11784	7003	2089	37
H(19B)	9605	7106	1475	37
H(19C)	11245	6532	660	37
H(13A)	8498	5155	360	21
H(13B)	9165	3896	999	21
H(14)	5727	4906	1364	17
H(15)	6769	6385	2859	14

*Table A7.2.7. Torsion angles [°] for Isoineleganolide A (**328**).*

C(14)-O(1)-C(1)-O(2)	-179.60(13)
C(14)-O(1)-C(1)-C(2)	2.52(15)
O(2)-C(1)-C(2)-C(3)	23.4(2)
O(1)-C(1)-C(2)-C(3)	-158.97(11)
O(2)-C(1)-C(2)-C(15)	158.84(15)
O(1)-C(1)-C(2)-C(15)	-23.52(13)
C(15)-C(2)-C(3)-C(8)	-3.9(2)
C(1)-C(2)-C(3)-C(8)	120.54(15)
C(15)-C(2)-C(3)-C(4)	169.78(12)
C(1)-C(2)-C(3)-C(4)	-65.73(15)
C(8)-C(3)-C(4)-C(5)	-23.87(19)
C(2)-C(3)-C(4)-C(5)	162.09(11)
C(3)-C(4)-C(5)-C(16)	177.19(12)
C(3)-C(4)-C(5)-C(6)	54.15(15)
C(6)-C(5)-C(16)-C(18)	-106.25(16)
C(4)-C(5)-C(16)-C(18)	132.96(15)
C(6)-C(5)-C(16)-C(17)	71.09(16)
C(4)-C(5)-C(16)-C(17)	-49.70(18)
C(16)-C(5)-C(6)-C(7)	178.75(12)
C(4)-C(5)-C(6)-C(7)	-56.22(15)
C(5)-C(6)-C(7)-O(3)	-153.51(14)
C(5)-C(6)-C(7)-C(8)	28.95(18)
C(2)-C(3)-C(8)-C(7)	166.22(13)
C(4)-C(3)-C(8)-C(7)	-6.9(2)
C(2)-C(3)-C(8)-C(9)	-7.4(2)
C(4)-C(3)-C(8)-C(9)	179.48(14)
O(3)-C(7)-C(8)-C(3)	-173.25(14)
C(6)-C(7)-C(8)-C(3)	4.3(2)
O(3)-C(7)-C(8)-C(9)	1.4(2)
C(6)-C(7)-C(8)-C(9)	178.87(13)
C(3)-C(8)-C(9)-C(10)	-36.1(2)
C(7)-C(8)-C(9)-C(10)	149.96(13)
C(8)-C(9)-C(10)-C(11)	55.5(2)
C(8)-C(9)-C(10)-O(5)	-14.76(19)

Table A7.2.7. (cont'd)

C(9)-C(10)-O(5)-C(11)	112.51(14)
C(10)-O(5)-C(11)-C(15)	-113.83(13)
C(10)-O(5)-C(11)-C(12)	116.22(14)
C(9)-C(10)-C(11)-O(5)	-106.68(15)
O(5)-C(10)-C(11)-C(15)	104.08(14)
C(9)-C(10)-C(11)-C(15)	-2.6(2)
O(5)-C(10)-C(11)-C(12)	-104.06(14)
C(9)-C(10)-C(11)-C(12)	149.26(14)
O(5)-C(11)-C(12)-O(4)	-16.85(17)
C(10)-C(11)-C(12)-O(4)	54.41(19)
C(15)-C(11)-C(12)-O(4)	-150.44(12)
O(5)-C(11)-C(12)-C(19)	-135.03(13)
C(10)-C(11)-C(12)-C(19)	-63.77(18)
C(15)-C(11)-C(12)-C(19)	91.38(14)
O(5)-C(11)-C(12)-C(13)	105.68(13)
C(10)-C(11)-C(12)-C(13)	176.95(13)
C(15)-C(11)-C(12)-C(13)	-27.91(15)
O(4)-C(12)-C(13)-C(14)	131.35(13)
C(19)-C(12)-C(13)-C(14)	-108.65(15)
C(11)-C(12)-C(13)-C(14)	9.26(16)
C(1)-O(1)-C(14)-C(13)	133.46(12)
C(1)-O(1)-C(14)-C(15)	19.59(14)
C(12)-C(13)-C(14)-O(1)	-99.06(14)
C(12)-C(13)-C(14)-C(15)	11.85(17)
O(5)-C(11)-C(15)-C(2)	11.18(17)
C(10)-C(11)-C(15)-C(2)	-59.03(18)
C(12)-C(11)-C(15)-C(2)	145.14(12)
O(5)-C(11)-C(15)-C(14)	-98.98(13)
C(10)-C(11)-C(15)-C(14)	-169.19(13)
C(12)-C(11)-C(15)-C(14)	34.99(14)
C(3)-C(2)-C(15)-C(11)	54.29(18)
C(1)-C(2)-C(15)-C(11)	-76.18(13)
C(3)-C(2)-C(15)-C(14)	164.26(12)
C(1)-C(2)-C(15)-C(14)	33.79(12)

Table A7.2.7. (cont'd)

O(1)-C(14)-C(15)-C(11)	86.14(12)
C(13)-C(14)-C(15)-C(11)	-28.29(14)
O(1)-C(14)-C(15)-C(2)	-33.17(13)
C(13)-C(14)-C(15)-C(2)	-147.59(12)

Symmetry transformations used to generate equivalent atoms:

*Table A7.2.8. Hydrogen bonds for Isoineleganolide A (**328**) [Å and °].*

D-H...A	d(D-H)	d(H...A)	d(D...A)	<(DHA)
C(2)-H(2)...O(4)#1	1.00	2.43	3.2893(17)	143.6
C(6)-H(6A)...O(1)#2	0.99	2.55	3.4282(18)	147.3
C(10)-H(10)...O(2)#3	1.00	2.43	3.2055(18)	133.5
O(4)-H(4O)...O(3)#4	0.83(2)	2.04(2)	2.8276(19)	158(3)

Symmetry transformations used to generate equivalent atoms:

#1 x-1,y,z #2 -x+1,y+1/2,-z+1 #3 -x+2,y+1/2,-z+1

#4 -x+2,y-1/2,-z+1

A7.3 X-Ray Crystal Structure Analysis of Bromide 346

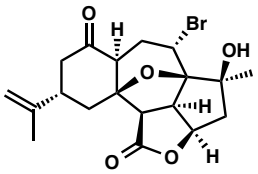

346

Contents

Table A7.3.1. Experimental Details

Table A7.3.2. Crystal Data

Table A7.3.3. Atomic Coordinates

Table A7.3.4. Full Bond Distances and Angles

Table A7.3.5. Anisotropic Displacement Parameters

Table A7.3.6. Hydrogen Atomic Coordinates

Table A7.3.7. Torsion Angles

Table A7.3.8. Hydrogen Bond Distances and Angles

*Figure A7.3.1. X-Ray Crystal Structure of Bromide **346***

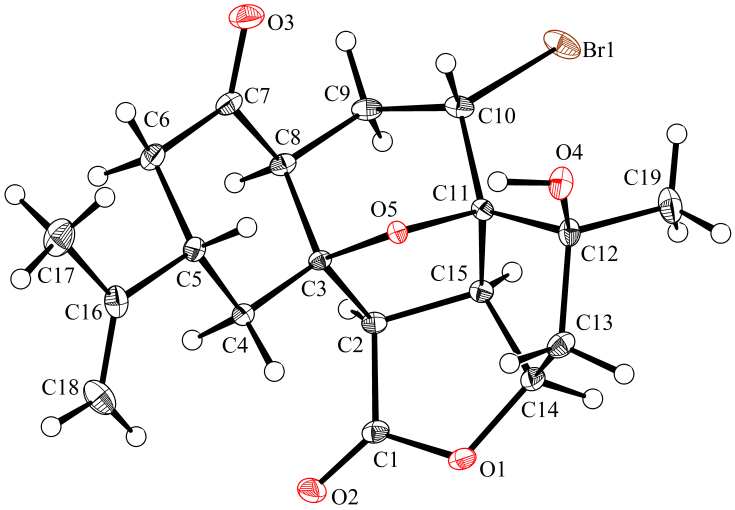

Table A7.3.1. Experimental Details for X-Ray Structure Determination of Bromide ***346****.*

Low-temperature diffraction data (ϕ-and ω-scans) were collected on a Bruker AXS KAPPA APEX II diffractometer coupled to a APEX II CCD detector with graphite monochromated Mo K_α radiation (λ = 0.71073 Å) for the structure of bromide **346**. The structure was solved by direct methods using SHELXS[1] and refined against F^2 on all data by full-matrix least squares with SHELXL-2014[2] using established refinement techniques.[3] All non-hydrogen atoms were refined anisotropically. Unless otherwise noted, all hydrogen atoms were included into the model at geometrically calculated positions and refined using a riding model. The isotropic displacement parameters of all hydrogen atoms were fixed to 1.2 times the U value of the atoms they are linked to (1.5 times for methyl groups).

Bromide **346** crystallizes in the orthorhombic space group $P2_12_12_1$ with one molecule in the asymmetric unit. The coordinates for the hydrogen atom bound to O4 was located in the difference Fourier synthesis and refined semi-freely with the help of a restraint on the O-H distance (0.84(4) Å).

*Table A7.3.2. Crystal Data and Structure Refinement for Bromide **346**.*

Caltech Identification code	rac10	
CCDC Deposition Number	1061013	
Empirical formula	C19 H23 Br O5	
Formula weight	411.28	
Temperature	100(2) K	
Wavelength	0.71073 Å	
Crystal system	Orthorhombic	
Space group	$P2_12_12_1$	
Unit cell dimensions	a = 7.6137(4) Å	α= 90°.
	b = 9.3584(5) Å	β= 90°.
	c = 24.1592(13) Å	γ = 90°.
Volume	1721.39(16) $Å^3$	
Z	4	
Density (calculated)	1.587 Mg/m^3	
Absorption coefficient	2.416 mm^{-1}	
F(000)	848	
Crystal size	0.500 x 0.450 x 0.100 mm^3	
Theta range for data collection	2.334 to 36.318°.	
Index ranges	$-12 \le h \le 12, -15 \le k \le 14, -39 \le l \le 40$	
Reflections collected	51998	
Independent reflections	8272 [R(int) = 0.0380]	
Completeness to theta = 25.242°	99.9 %	
Absorption correction	Semi-empirical from equivalents	
Max. and min. transmission	0.7478 and 0.5973	
Refinement method	Full-matrix least-squares on F^2	
Data / restraints / parameters	8272 / 1 / 231	
Goodness-of-fit on F^2	1.035	
Final R indices [I>2sigma(I)]	R1 = 0.0251, wR2 = 0.0613	
R indices (all data)	R1 = 0.0297, wR2 = 0.0625	
Absolute structure parameter	0.014(2)	
Extinction coefficient	n/a	
Largest diff. peak and hole	0.746 and -0.367 e.$Å^{-3}$	

*Table A7.3.3. Atomic coordinates (x 10^4) and equivalent isotropic displacement parameters ($Å^2$x 10^3) for Bromide **346**. U(eq) is defined as one third of the trace of the orthogonalized U^{ij} tensor.*

	x	y	z	U(eq)
O(1)	6345(1)	6209(1)	7159(1)	14(1)
C(1)	4823(2)	6108(2)	6871(1)	11(1)
O(2)	3840(2)	7103(1)	6827(1)	16(1)
C(2)	4583(2)	4619(1)	6642(1)	10(1)
C(3)	5114(2)	4473(2)	6017(1)	8(1)
O(5)	6928(1)	4038(1)	6041(1)	8(1)
C(4)	5024(2)	5837(2)	5681(1)	10(1)
C(5)	5590(2)	5618(2)	5077(1)	11(1)
C(6)	4489(2)	4411(2)	4820(1)	13(1)
C(7)	4584(2)	3064(2)	5155(1)	12(1)
O(3)	5000(2)	1919(1)	4955(1)	19(1)
C(8)	4104(2)	3212(2)	5760(1)	10(1)
C(9)	4411(2)	1846(2)	6093(1)	12(1)
C(10)	6347(2)	1653(1)	6251(1)	11(1)
Br(1)	6456(1)	-42(1)	6729(1)	19(1)
C(11)	7078(2)	3035(1)	6497(1)	8(1)
C(12)	9005(2)	3218(2)	6685(1)	11(1)
O(4)	10208(1)	3067(1)	6239(1)	14(1)
C(13)	8951(2)	4740(2)	6926(1)	14(1)
C(14)	7176(2)	4824(2)	7226(1)	12(1)
C(15)	5948(2)	3720(2)	6947(1)	10(1)
C(16)	5502(2)	6970(2)	4728(1)	15(1)
C(17)	5870(2)	6771(2)	4117(1)	22(1)
C(18)	5173(2)	8249(2)	4935(1)	20(1)
C(19)	9621(2)	2179(2)	7128(1)	18(1)

*Table A7.3.4. Bond lengths [Å] and angles [°] for Bromide **346**.*

O(1)-C(1)	1.3544(17)
O(1)-C(14)	1.4514(18)
C(1)-O(2)	1.1989(18)
C(1)-C(2)	1.5115(19)
C(2)-C(15)	1.5264(19)
C(2)-C(3)	1.5679(18)
C(2)-H(2)	1.0000
C(3)-O(5)	1.4409(14)
C(3)-C(4)	1.515(2)
C(3)-C(8)	1.5388(18)
O(5)-C(11)	1.4519(16)
C(4)-C(5)	1.5342(18)
C(4)-H(4A)	0.9900
C(4)-H(4B)	0.9900
C(5)-C(16)	1.522(2)
C(5)-C(6)	1.538(2)
C(5)-H(5)	1.0000
C(6)-C(7)	1.500(2)
C(6)-H(6A)	0.9900
C(6)-H(6B)	0.9900
C(7)-O(3)	1.2170(17)
C(7)-C(8)	1.5142(19)
C(8)-C(9)	1.527(2)
C(8)-H(8)	1.0000
C(9)-C(10)	1.5334(19)
C(9)-H(9A)	0.9900
C(9)-H(9B)	0.9900
C(10)-C(11)	1.5275(19)
C(10)-Br(1)	1.9635(13)
C(10)-H(10)	1.0000
C(11)-C(15)	1.5273(18)
C(11)-C(12)	1.5456(17)
C(12)-O(4)	1.4205(16)

Table A7.3.4. (cont'd)

C(12)-C(19)	1.520(2)
C(12)-C(13)	1.539(2)
O(4)-H(4O)	0.893(18)
C(13)-C(14)	1.5356(18)
C(13)-H(13A)	0.9900
C(13)-H(13B)	0.9900
C(14)-C(15)	1.5484(19)
C(14)-H(14)	1.0000
C(15)-H(15)	1.0000
C(16)-C(18)	1.322(2)
C(16)-C(17)	1.512(2)
C(17)-H(17A)	0.9800
C(17)-H(17B)	0.9800
C(17)-H(17C)	0.9800
C(18)-H(18A)	0.9500
C(18)-H(18B)	0.9500
C(19)-H(19A)	0.9800
C(19)-H(19B)	0.9800
C(19)-H(19C)	0.9800

C(1)-O(1)-C(14)	111.60(11)
O(2)-C(1)-O(1)	121.69(13)
O(2)-C(1)-C(2)	127.45(13)
O(1)-C(1)-C(2)	110.85(11)
C(1)-C(2)-C(15)	104.40(11)
C(1)-C(2)-C(3)	113.74(11)
C(15)-C(2)-C(3)	103.96(10)
C(1)-C(2)-H(2)	111.4
C(15)-C(2)-H(2)	111.4
C(3)-C(2)-H(2)	111.4
O(5)-C(3)-C(4)	107.61(10)
O(5)-C(3)-C(8)	106.18(10)
C(4)-C(3)-C(8)	114.06(11)
O(5)-C(3)-C(2)	103.45(10)

Table A7.3.4. (cont'd)

C(4)-C(3)-C(2)	115.53(11)
C(8)-C(3)-C(2)	109.04(10)
C(3)-O(5)-C(11)	106.78(9)
C(3)-C(4)-C(5)	112.61(11)
C(3)-C(4)-H(4A)	109.1
C(5)-C(4)-H(4A)	109.1
C(3)-C(4)-H(4B)	109.1
C(5)-C(4)-H(4B)	109.1
H(4A)-C(4)-H(4B)	107.8
C(16)-C(5)-C(4)	113.83(12)
C(16)-C(5)-C(6)	111.21(11)
C(4)-C(5)-C(6)	109.26(11)
C(16)-C(5)-H(5)	107.4
C(4)-C(5)-H(5)	107.4
C(6)-C(5)-H(5)	107.4
C(7)-C(6)-C(5)	111.86(11)
C(7)-C(6)-H(6A)	109.2
C(5)-C(6)-H(6A)	109.2
C(7)-C(6)-H(6B)	109.2
C(5)-C(6)-H(6B)	109.2
H(6A)-C(6)-H(6B)	107.9
O(3)-C(7)-C(6)	122.61(13)
O(3)-C(7)-C(8)	121.70(13)
C(6)-C(7)-C(8)	115.69(12)
C(7)-C(8)-C(9)	113.28(12)
C(7)-C(8)-C(3)	109.82(11)
C(9)-C(8)-C(3)	110.68(11)
C(7)-C(8)-H(8)	107.6
C(9)-C(8)-H(8)	107.6
C(3)-C(8)-H(8)	107.6
C(8)-C(9)-C(10)	112.12(11)
C(8)-C(9)-H(9A)	109.2
C(10)-C(9)-H(9A)	109.2
C(8)-C(9)-H(9B)	109.2

Table A7.3.4. (cont'd)

C(10)-C(9)-H(9B)	109.2
H(9A)-C(9)-H(9B)	107.9
C(11)-C(10)-C(9)	110.33(11)
C(11)-C(10)-Br(1)	116.09(9)
C(9)-C(10)-Br(1)	106.38(9)
C(11)-C(10)-H(10)	107.9
C(9)-C(10)-H(10)	107.9
Br(1)-C(10)-H(10)	107.9
O(5)-C(11)-C(15)	102.90(10)
O(5)-C(11)-C(10)	102.94(10)
C(15)-C(11)-C(10)	115.27(11)
O(5)-C(11)-C(12)	103.07(10)
C(15)-C(11)-C(12)	106.18(10)
C(10)-C(11)-C(12)	123.66(11)
O(4)-C(12)-C(19)	105.71(11)
O(4)-C(12)-C(13)	113.32(11)
C(19)-C(12)-C(13)	109.53(12)
O(4)-C(12)-C(11)	112.19(11)
C(19)-C(12)-C(11)	115.40(12)
C(13)-C(12)-C(11)	100.89(10)
C(12)-O(4)-H(4O)	108.7(15)
C(14)-C(13)-C(12)	104.44(11)
C(14)-C(13)-H(13A)	110.9
C(12)-C(13)-H(13A)	110.9
C(14)-C(13)-H(13B)	110.9
C(12)-C(13)-H(13B)	110.9
H(13A)-C(13)-H(13B)	108.9
O(1)-C(14)-C(13)	112.12(12)
O(1)-C(14)-C(15)	106.49(10)
C(13)-C(14)-C(15)	106.94(11)
O(1)-C(14)-H(14)	110.4
C(13)-C(14)-H(14)	110.4
C(15)-C(14)-H(14)	110.4
C(2)-C(15)-C(11)	105.75(10)

Table A7.3.4. (cont'd)

C(2)-C(15)-C(14)	104.71(11)
C(11)-C(15)-C(14)	104.51(10)
C(2)-C(15)-H(15)	113.6
C(11)-C(15)-H(15)	113.6
C(14)-C(15)-H(15)	113.6
C(18)-C(16)-C(17)	121.05(15)
C(18)-C(16)-C(5)	123.41(15)
C(17)-C(16)-C(5)	115.52(14)
C(16)-C(17)-H(17A)	109.5
C(16)-C(17)-H(17B)	109.5
H(17A)-C(17)-H(17B)	109.5
C(16)-C(17)-H(17C)	109.5
H(17A)-C(17)-H(17C)	109.5
H(17B)-C(17)-H(17C)	109.5
C(16)-C(18)-H(18A)	120.0
C(16)-C(18)-H(18B)	120.0
H(18A)-C(18)-H(18B)	120.0
C(12)-C(19)-H(19A)	109.5
C(12)-C(19)-H(19B)	109.5
H(19A)-C(19)-H(19B)	109.5
C(12)-C(19)-H(19C)	109.5
H(19A)-C(19)-H(19C)	109.5
H(19B)-C(19)-H(19C)	109.5

Symmetry transformations used to generate equivalent atoms:

*Table A7.3.5. Anisotropic displacement parameters ($Å^2x10^3$) for Bromide **346**. The anisotropic displacement factor exponent takes the form: $-2\pi^2[h^2a^{*2}U^{11} + ... + 2hka^*b^*U^{12}]$.*

	U^{11}	U^{22}	U^{33}	U^{23}	U^{13}	U^{12}
O(1)	15(1)	12(1)	13(1)	-4(1)	-2(1)	0(1)
C(1)	14(1)	12(1)	8(1)	-1(1)	3(1)	-1(1)
O(2)	21(1)	14(1)	13(1)	-2(1)	1(1)	5(1)
C(2)	10(1)	10(1)	9(1)	-1(1)	2(1)	0(1)
C(3)	7(1)	9(1)	9(1)	-2(1)	1(1)	0(1)
O(5)	7(1)	9(1)	8(1)	2(1)	1(1)	0(1)
C(4)	12(1)	10(1)	10(1)	-1(1)	-2(1)	0(1)
C(5)	11(1)	12(1)	9(1)	1(1)	-1(1)	0(1)
C(6)	15(1)	15(1)	10(1)	-1(1)	-2(1)	-1(1)
C(7)	11(1)	13(1)	11(1)	-3(1)	0(1)	-2(1)
O(3)	28(1)	15(1)	14(1)	-5(1)	2(1)	1(1)
C(8)	9(1)	12(1)	11(1)	-2(1)	1(1)	-2(1)
C(9)	13(1)	9(1)	14(1)	-2(1)	3(1)	-4(1)
C(10)	14(1)	9(1)	11(1)	0(1)	5(1)	-1(1)
Br(1)	27(1)	9(1)	22(1)	5(1)	8(1)	2(1)
C(11)	10(1)	8(1)	8(1)	1(1)	2(1)	1(1)
C(12)	10(1)	15(1)	8(1)	2(1)	1(1)	2(1)
O(4)	9(1)	23(1)	10(1)	1(1)	2(1)	2(1)
C(13)	11(1)	16(1)	13(1)	-3(1)	0(1)	-2(1)
C(14)	13(1)	13(1)	10(1)	-2(1)	0(1)	1(1)
C(15)	11(1)	10(1)	8(1)	0(1)	2(1)	0(1)
C(16)	12(1)	16(1)	15(1)	5(1)	-2(1)	-1(1)
C(17)	28(1)	25(1)	13(1)	6(1)	-1(1)	-5(1)
C(18)	21(1)	16(1)	24(1)	7(1)	3(1)	3(1)
C(19)	17(1)	23(1)	14(1)	6(1)	-1(1)	6(1)

*Table A7.3.6. Hydrogen coordinates (x10^4) and isotropic displacement parameters (Å^{2}x10^3) for Bromide **346**.*

	x	y	z	U(eq)
H(2)	3367	4256	6709	12
H(4A)	5792	6564	5854	13
H(4B)	3806	6206	5688	13
H(5)	6841	5293	5081	13
H(6A)	3250	4723	4792	16
H(6B)	4919	4217	4440	16
H(8)	2823	3441	5781	13
H(9A)	4023	1014	5872	15
H(9B)	3691	1877	6434	15
H(10)	7020	1439	5905	14
H(4O)	9730(30)	3450(20)	5936(8)	21
H(13A)	9934	4894	7188	16
H(13B)	9022	5464	6628	16
H(14)	7323	4596	7628	14
H(15)	5427	3016	7211	11
H(17A)	4884	6268	3944	33
H(17B)	6946	6209	4071	33
H(17C)	6019	7708	3942	33
H(18A)	5165	9063	4700	24
H(18B)	4944	8356	5320	24
H(19A)	9719	1219	6968	27
H(19B)	8772	2164	7432	27
H(19C)	10770	2482	7268	27

*Table A7.3.7. Torsion angles [°] for Bromide **346**.*

C(14)-O(1)-C(1)-O(2)	171.18(12)
C(14)-O(1)-C(1)-C(2)	-7.77(14)
O(2)-C(1)-C(2)-C(15)	-165.39(13)
O(1)-C(1)-C(2)-C(15)	13.48(14)
O(2)-C(1)-C(2)-C(3)	81.97(16)
O(1)-C(1)-C(2)-C(3)	-99.16(12)
C(1)-C(2)-C(3)-O(5)	92.31(12)
C(15)-C(2)-C(3)-O(5)	-20.60(12)
C(1)-C(2)-C(3)-C(4)	-25.01(14)
C(15)-C(2)-C(3)-C(4)	-137.92(11)
C(1)-C(2)-C(3)-C(8)	-155.00(11)
C(15)-C(2)-C(3)-C(8)	92.08(12)
C(4)-C(3)-O(5)-C(11)	162.08(10)
C(8)-C(3)-O(5)-C(11)	-75.41(12)
C(2)-C(3)-O(5)-C(11)	39.34(12)
O(5)-C(3)-C(4)-C(5)	64.07(13)
C(8)-C(3)-C(4)-C(5)	-53.44(13)
C(2)-C(3)-C(4)-C(5)	179.03(10)
C(3)-C(4)-C(5)-C(16)	179.64(10)
C(3)-C(4)-C(5)-C(6)	54.66(13)
C(16)-C(5)-C(6)-C(7)	179.13(11)
C(4)-C(5)-C(6)-C(7)	-54.39(15)
C(5)-C(6)-C(7)-O(3)	-126.40(14)
C(5)-C(6)-C(7)-C(8)	54.29(15)
O(3)-C(7)-C(8)-C(9)	6.81(18)
C(6)-C(7)-C(8)-C(9)	-173.87(11)
O(3)-C(7)-C(8)-C(3)	131.12(14)
C(6)-C(7)-C(8)-C(3)	-49.56(14)
O(5)-C(3)-C(8)-C(7)	-69.79(13)
C(4)-C(3)-C(8)-C(7)	48.54(14)
C(2)-C(3)-C(8)-C(7)	179.34(10)
O(5)-C(3)-C(8)-C(9)	56.02(13)
C(4)-C(3)-C(8)-C(9)	174.35(10)
C(2)-C(3)-C(8)-C(9)	-54.86(13)

Table A7.3.7. (cont'd)

C(7)-C(8)-C(9)-C(10)	79.81(14)
C(3)-C(8)-C(9)-C(10)	-44.03(14)
C(8)-C(9)-C(10)-C(11)	48.25(14)
C(8)-C(9)-C(10)-Br(1)	174.95(9)
C(3)-O(5)-C(11)-C(15)	-41.94(12)
C(3)-O(5)-C(11)-C(10)	78.19(11)
C(3)-O(5)-C(11)-C(12)	-152.22(10)
C(9)-C(10)-C(11)-O(5)	-62.73(12)
Br(1)-C(10)-C(11)-O(5)	176.18(7)
C(9)-C(10)-C(11)-C(15)	48.48(15)
Br(1)-C(10)-C(11)-C(15)	-72.60(13)
C(9)-C(10)-C(11)-C(12)	-178.32(11)
Br(1)-C(10)-C(11)-C(12)	60.60(14)
O(5)-C(11)-C(12)-O(4)	-52.81(14)
C(15)-C(11)-C(12)-O(4)	-160.63(12)
C(10)-C(11)-C(12)-O(4)	62.71(17)
O(5)-C(11)-C(12)-C(19)	-173.97(12)
C(15)-C(11)-C(12)-C(19)	78.21(15)
C(10)-C(11)-C(12)-C(19)	-58.45(17)
O(5)-C(11)-C(12)-C(13)	68.11(11)
C(15)-C(11)-C(12)-C(13)	-39.71(13)
C(10)-C(11)-C(12)-C(13)	-176.37(12)
O(4)-C(12)-C(13)-C(14)	159.21(11)
C(19)-C(12)-C(13)-C(14)	-83.03(13)
C(11)-C(12)-C(13)-C(14)	39.09(12)
C(1)-O(1)-C(14)-C(13)	115.35(12)
C(1)-O(1)-C(14)-C(15)	-1.29(14)
C(12)-C(13)-C(14)-O(1)	-141.44(11)
C(12)-C(13)-C(14)-C(15)	-25.07(14)
C(1)-C(2)-C(15)-C(11)	-123.39(11)
C(3)-C(2)-C(15)-C(11)	-3.91(13)
C(1)-C(2)-C(15)-C(14)	-13.32(12)
C(3)-C(2)-C(15)-C(14)	106.15(11)
O(5)-C(11)-C(15)-C(2)	26.87(13)

Table A7.3.7. (cont'd)

C(10)-C(11)-C(15)-C(2)	-84.37(13)
C(12)-C(11)-C(15)-C(2)	134.81(11)
O(5)-C(11)-C(15)-C(14)	-83.34(11)
C(10)-C(11)-C(15)-C(14)	165.42(11)
C(12)-C(11)-C(15)-C(14)	24.60(14)
O(1)-C(14)-C(15)-C(2)	9.44(13)
C(13)-C(14)-C(15)-C(2)	-110.61(12)
O(1)-C(14)-C(15)-C(11)	120.40(11)
C(13)-C(14)-C(15)-C(11)	0.35(14)
C(4)-C(5)-C(16)-C(18)	7.60(19)
C(6)-C(5)-C(16)-C(18)	131.52(15)
C(4)-C(5)-C(16)-C(17)	-174.03(12)
C(6)-C(5)-C(16)-C(17)	-50.10(16)

Symmetry transformations used to generate equivalent atoms:

*Table A7.3.8. Hydrogen bonds for Bromide **346** [Å and °].*

D-H...A	d(D-H)	d(H...A)	d(D...A)	<(DHA)
C(8)-H(8)...O(4)#1	1.00	2.31	3.1874(15)	146.5
O(4)-H(4O)...O(5)	0.893(18)	2.22(2)	2.7004(14)	113.4(17)
O(4)-H(4O)...O(3)#2	0.893(18)	2.19(2)	2.8908(16)	135.0(19)
C(15)-H(15)...O(1)#3	1.00	2.65	3.6389(17)	172.5
C(15)-H(15)...O(2)#3	1.00	2.54	3.3305(17)	136.0
C(19)-H(19A)...Br(1)	0.98	2.81	3.3248(17)	113.5

Symmetry transformations used to generate equivalent atoms:

#1 x-1,y,z #2 x+1/2,-y+1/2,-z+1 #3 -x+1,y-1/2,-z+3/2

A7.4 X-Ray Crystal Structure Analysis of Diketone 347

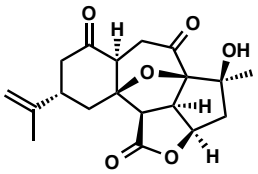

347

Contents

Table A7.4.1. Experimental Details

Table A7.4.2. Crystal Data

Table A7.4.3. Atomic Coordinates

Table A7.4.4. Full Bond Distances and Angles

Table A7.4.5. Anisotropic Displacement Parameters

Table A7.4.6. Hydrogen Atomic Coordinates

Table A7.4.7. Torsion Angles

Table A7.4.8. Hydrogen Bond Distances and Angles

*Figure A7.4.1. X-Ray Crystal Structure of Diketone **347***

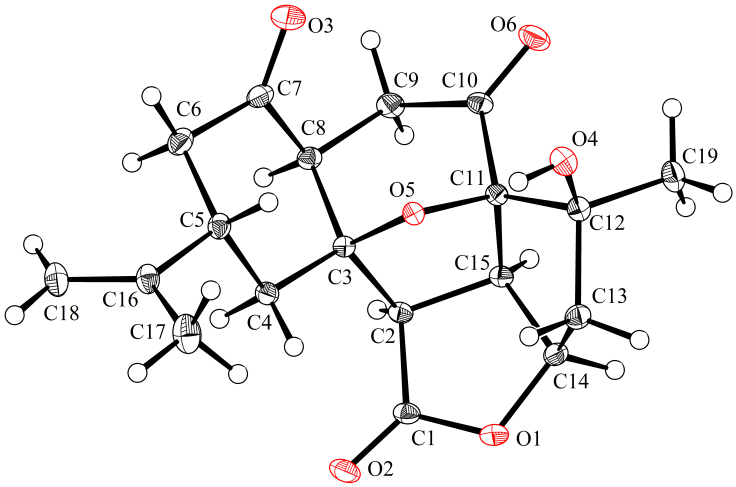

*Table A7.4.1. Experimental Details for X-Ray Structure Determination of Diketone **347**.*

Low-temperature diffraction data (ϕ-and ω-scans) were collected on a Bruker AXS KAPPA APEX II diffractometer coupled to a APEX II CCD detector with graphite monochromated Mo K_α radiation (λ = 0.71073 Å) for the structure of diketone **347**. The structure was solved by direct methods using SHELXS[1] and refined against F^2 on all data by full-matrix least squares with SHELXL-2014[2] using established refinement techniques.[3] All non-hydrogen atoms were refined anisotropically. Unless otherwise noted, all hydrogen atoms were included into the model at geometrically calculated positions and refined using a riding model. The isotropic displacement parameters of all hydrogen atoms were fixed to 1.2 times the U value of the atoms they are linked to (1.5 times for methyl groups).

Diketone **347** crystallizes in the orthorhombic space group $P2_12_12_1$ with one molecule in the asymmetric unit. The coordinates for the hydrogen atom bound to O4 was located in the difference Fourier synthesis and refined semi-freely with the help of a restraint on the O-H distance (0.84(4) Å). The chirality of the molecule cannot be reliably determined from the diffraction data. The molecule could be the wrong enantiomer or a mixture of both enantiomers.

*Table A7.4.2. Crystal Data and Structure Refinement for Diketone **347**.*

Caltech Identification code	rac06	
CCDC Deposition Number	1061012	
Empirical formula	C19 H22 O6	
Formula weight	346.36	
Temperature	100(2) K	
Wavelength	0.71073 Å	
Crystal system	Orthorhombic	
Space group	$P2_12_12_1$	
Unit cell dimensions	a = 8.2576(3) Å	α= 90°.
	b = 10.4049(4) Å	β= 90°.
	c = 19.0995(8) Å	γ = 90°.
Volume	1641.02(11) $Å^3$	
Z	4	
Density (calculated)	1.402 Mg/m^3	
Absorption coefficient	0.104 mm^{-1}	
F(000)	736	
Crystal size	0.450 x 0.350 x 0.100 mm^3	
Theta range for data collection	2.133 to 43.738°.	
Index ranges	$-16 \le h \le 14, -20 \le k \le 18, -37 \le l \le 37$	
Reflections collected	85501	
Independent reflections	12633 [R(int) = 0.0489]	
Completeness to theta = 25.242°	100.0 %	
Absorption correction	Semi-empirical from equivalents	
Max. and min. transmission	0.7487 and 0.7039	
Refinement method	Full-matrix least-squares on F^2	
Data / restraints / parameters	12633 / 1 / 231	
Goodness-of-fit on F^2	1.060	
Final R indices [I>2sigma(I)]	R1 = 0.0442, wR2 = 0.1107	
R indices (all data)	R1 = 0.0613, wR2 = 0.1176	
Absolute structure parameter	0.35(16)	
Extinction coefficient	n/a	
Largest diff. peak and hole	0.468 and -0.291 $e.Å^{-3}$	

*Table A7.4.3. Atomic coordinates (x 10^4) and equivalent isotropic displacement parameters ($Å^2$x 10^3) for Diketone **347**. U(eq) is defined as one third of the trace of the orthogonalized U^{ij} tensor.*

	x	y	z	U(eq)
O(1)	10548(1)	6025(1)	1279(1)	16(1)
C(1)	9704(1)	5326(1)	1747(1)	13(1)
O(2)	10382(1)	4599(1)	2142(1)	18(1)
C(2)	7892(1)	5564(1)	1681(1)	11(1)
C(3)	7159(1)	6320(1)	2311(1)	10(1)
O(5)	7376(1)	7644(1)	2113(1)	10(1)
C(4)	8008(1)	6121(1)	3008(1)	12(1)
C(5)	7310(1)	6968(1)	3590(1)	13(1)
C(16)	8277(1)	6778(1)	4253(1)	14(1)
C(17)	9841(2)	7514(1)	4288(1)	22(1)
C(18)	7820(2)	6000(1)	4772(1)	19(1)
C(6)	5484(1)	6699(1)	3661(1)	16(1)
C(7)	4701(1)	6954(1)	2966(1)	14(1)
O(3)	3728(1)	7814(1)	2870(1)	22(1)
C(8)	5303(1)	6116(1)	2362(1)	12(1)
C(9)	4451(1)	6481(1)	1677(1)	14(1)
C(10)	5157(1)	7655(1)	1315(1)	12(1)
O(6)	4336(1)	8392(1)	971(1)	20(1)
C(11)	6996(1)	7729(1)	1379(1)	10(1)
C(12)	8007(1)	8868(1)	1102(1)	12(1)
O(4)	7848(1)	9969(1)	1533(1)	15(1)
C(19)	7572(2)	9275(1)	359(1)	17(1)
C(13)	9732(1)	8287(1)	1121(1)	14(1)
C(14)	9514(1)	6892(1)	888(1)	13(1)
C(15)	7753(1)	6507(1)	1067(1)	10(1)

*Table A7.4.4. Bond lengths [Å] and angles [°] for Diketone **347**.*

O(1)-C(1)	1.3464(14)
O(1)-C(14)	1.4494(13)
C(1)-O(2)	1.2070(13)
C(1)-C(2)	1.5217(14)
C(2)-C(15)	1.5328(13)
C(2)-C(3)	1.5593(13)
C(2)-H(2)	1.0000
C(3)-O(5)	1.4396(12)
C(3)-C(4)	1.5185(13)
C(3)-C(8)	1.5501(13)
O(5)-C(11)	1.4381(11)
C(4)-C(5)	1.5318(13)
C(4)-H(4A)	0.9900
C(4)-H(4B)	0.9900
C(5)-C(16)	1.5101(15)
C(5)-C(6)	1.5397(15)
C(5)-H(5)	1.0000
C(16)-C(18)	1.3338(15)
C(16)-C(17)	1.5029(17)
C(17)-H(17A)	0.9800
C(17)-H(17B)	0.9800
C(17)-H(17C)	0.9800
C(18)-H(18A)	0.9500
C(18)-H(18B)	0.9500
C(6)-C(7)	1.5010(16)
C(6)-H(6A)	0.9900
C(6)-H(6B)	0.9900
C(7)-O(3)	1.2165(14)
C(7)-C(8)	1.5292(14)
C(8)-C(9)	1.5326(15)
C(8)-H(8)	1.0000
C(9)-C(10)	1.5204(15)
C(9)-H(9A)	0.9900

Table A7.4.4. (cont'd)

C(9)-H(9B)	0.9900
C(10)-O(6)	1.2150(13)
C(10)-C(11)	1.5255(13)
C(11)-C(15)	1.5379(13)
C(11)-C(12)	1.5436(13)
C(12)-O(4)	1.4169(13)
C(12)-C(19)	1.5238(14)
C(12)-C(13)	1.5477(14)
O(4)-H(4O)	0.797(17)
C(19)-H(19A)	0.9800
C(19)-H(19B)	0.9800
C(19)-H(19C)	0.9800
C(13)-C(14)	1.5296(15)
C(13)-H(13A)	0.9900
C(13)-H(13B)	0.9900
C(14)-C(15)	1.5462(14)
C(14)-H(14)	1.0000
C(15)-H(15)	1.0000

C(1)-O(1)-C(14)	111.90(8)
O(2)-C(1)-O(1)	120.92(10)
O(2)-C(1)-C(2)	127.58(10)
O(1)-C(1)-C(2)	111.48(8)
C(1)-C(2)-C(15)	103.94(8)
C(1)-C(2)-C(3)	113.59(7)
C(15)-C(2)-C(3)	103.82(7)
C(1)-C(2)-H(2)	111.7
C(15)-C(2)-H(2)	111.7
C(3)-C(2)-H(2)	111.7
O(5)-C(3)-C(4)	107.67(7)
O(5)-C(3)-C(8)	105.65(8)
C(4)-C(3)-C(8)	112.54(8)
O(5)-C(3)-C(2)	103.36(7)
C(4)-C(3)-C(2)	115.38(8)

Table A7.4.4. (cont'd)

C(8)-C(3)-C(2)	111.27(7)
C(11)-O(5)-C(3)	106.77(7)
C(3)-C(4)-C(5)	112.61(8)
C(3)-C(4)-H(4A)	109.1
C(5)-C(4)-H(4A)	109.1
C(3)-C(4)-H(4B)	109.1
C(5)-C(4)-H(4B)	109.1
H(4A)-C(4)-H(4B)	107.8
C(16)-C(5)-C(4)	109.53(8)
C(16)-C(5)-C(6)	114.87(8)
C(4)-C(5)-C(6)	109.15(8)
C(16)-C(5)-H(5)	107.7
C(4)-C(5)-H(5)	107.7
C(6)-C(5)-H(5)	107.7
C(18)-C(16)-C(17)	121.35(10)
C(18)-C(16)-C(5)	123.55(11)
C(17)-C(16)-C(5)	115.09(9)
C(16)-C(17)-H(17A)	109.5
C(16)-C(17)-H(17B)	109.5
H(17A)-C(17)-H(17B)	109.5
C(16)-C(17)-H(17C)	109.5
H(17A)-C(17)-H(17C)	109.5
H(17B)-C(17)-H(17C)	109.5
C(16)-C(18)-H(18A)	120.0
C(16)-C(18)-H(18B)	120.0
H(18A)-C(18)-H(18B)	120.0
C(7)-C(6)-C(5)	108.16(8)
C(7)-C(6)-H(6A)	110.1
C(5)-C(6)-H(6A)	110.1
C(7)-C(6)-H(6B)	110.1
C(5)-C(6)-H(6B)	110.1
H(6A)-C(6)-H(6B)	108.4
O(3)-C(7)-C(6)	123.18(10)
O(3)-C(7)-C(8)	121.40(10)

Table A7.4.4. (cont'd)

C(6)-C(7)-C(8)	115.28(9)
C(7)-C(8)-C(9)	110.70(9)
C(7)-C(8)-C(3)	106.90(8)
C(9)-C(8)-C(3)	111.54(8)
C(7)-C(8)-H(8)	109.2
C(9)-C(8)-H(8)	109.2
C(3)-C(8)-H(8)	109.2
C(10)-C(9)-C(8)	114.27(8)
C(10)-C(9)-H(9A)	108.7
C(8)-C(9)-H(9A)	108.7
C(10)-C(9)-H(9B)	108.7
C(8)-C(9)-H(9B)	108.7
H(9A)-C(9)-H(9B)	107.6
O(6)-C(10)-C(9)	122.61(9)
O(6)-C(10)-C(11)	124.53(10)
C(9)-C(10)-C(11)	112.67(8)
O(5)-C(11)-C(10)	107.03(7)
O(5)-C(11)-C(15)	103.75(7)
C(10)-C(11)-C(15)	109.36(8)
O(5)-C(11)-C(12)	105.34(7)
C(10)-C(11)-C(12)	123.33(8)
C(15)-C(11)-C(12)	106.36(8)
O(4)-C(12)-C(19)	107.12(8)
O(4)-C(12)-C(11)	111.75(8)
C(19)-C(12)-C(11)	113.94(8)
O(4)-C(12)-C(13)	112.79(8)
C(19)-C(12)-C(13)	110.36(9)
C(11)-C(12)-C(13)	100.94(8)
C(12)-O(4)-H(4O)	108.3(15)
C(12)-C(19)-H(19A)	109.5
C(12)-C(19)-H(19B)	109.5
H(19A)-C(19)-H(19B)	109.5
C(12)-C(19)-H(19C)	109.5
H(19A)-C(19)-H(19C)	109.5

Table A7.4.4. (cont'd)

H(19B)-C(19)-H(19C)	109.5
C(14)-C(13)-C(12)	104.80(8)
C(14)-C(13)-H(13A)	110.8
C(12)-C(13)-H(13A)	110.8
C(14)-C(13)-H(13B)	110.8
C(12)-C(13)-H(13B)	110.8
H(13A)-C(13)-H(13B)	108.9
O(1)-C(14)-C(13)	111.79(8)
O(1)-C(14)-C(15)	106.19(8)
C(13)-C(14)-C(15)	106.98(8)
O(1)-C(14)-H(14)	110.6
C(13)-C(14)-H(14)	110.6
C(15)-C(14)-H(14)	110.6
C(2)-C(15)-C(11)	105.24(7)
C(2)-C(15)-C(14)	105.35(7)
C(11)-C(15)-C(14)	104.72(8)
C(2)-C(15)-H(15)	113.5
C(11)-C(15)-H(15)	113.5
C(14)-C(15)-H(15)	113.5

Symmetry transformations used to generate equivalent atoms:

*Table A7.4.5. Anisotropic displacement parameters ($Å^2x10^3$) for Diketone **347**. The anisotropic displacement factor exponent takes the form: $-2\pi^2[h^2a^{*2}U^{11} + ... + 2hka^*b^*U^{12}]$.*

	U^{11}	U^{22}	U^{33}	U^{23}	U^{13}	U^{12}
O(1)	10(1)	18(1)	19(1)	1(1)	0(1)	3(1)
C(1)	12(1)	13(1)	12(1)	-3(1)	-1(1)	3(1)
O(2)	19(1)	20(1)	16(1)	0(1)	-3(1)	9(1)
C(2)	11(1)	10(1)	11(1)	-2(1)	-1(1)	1(1)
C(3)	10(1)	9(1)	10(1)	-1(1)	0(1)	0(1)
O(5)	11(1)	9(1)	10(1)	0(1)	-1(1)	-1(1)
C(4)	13(1)	13(1)	10(1)	-1(1)	-1(1)	2(1)
C(5)	15(1)	12(1)	11(1)	-1(1)	1(1)	0(1)
C(16)	20(1)	12(1)	10(1)	-1(1)	1(1)	0(1)
C(17)	28(1)	23(1)	15(1)	0(1)	-5(1)	-8(1)
C(18)	26(1)	18(1)	14(1)	3(1)	1(1)	-1(1)
C(6)	17(1)	16(1)	14(1)	-1(1)	4(1)	1(1)
C(7)	12(1)	12(1)	18(1)	0(1)	4(1)	0(1)
O(3)	21(1)	18(1)	27(1)	0(1)	3(1)	9(1)
C(8)	10(1)	11(1)	15(1)	0(1)	1(1)	-1(1)
C(9)	9(1)	16(1)	18(1)	1(1)	-3(1)	-3(1)
C(10)	10(1)	13(1)	14(1)	0(1)	-2(1)	1(1)
O(6)	14(1)	21(1)	26(1)	6(1)	-4(1)	2(1)
C(11)	9(1)	10(1)	10(1)	0(1)	-2(1)	-1(1)
C(12)	12(1)	11(1)	12(1)	0(1)	-1(1)	-2(1)
O(4)	18(1)	11(1)	15(1)	-1(1)	-2(1)	-2(1)
C(19)	19(1)	18(1)	13(1)	4(1)	-2(1)	-2(1)
C(13)	10(1)	16(1)	16(1)	1(1)	0(1)	-2(1)
C(14)	11(1)	16(1)	12(1)	0(1)	1(1)	1(1)
C(15)	10(1)	11(1)	10(1)	-2(1)	-2(1)	0(1)

*Table A7.4.6. Hydrogen coordinates (x10^4) and isotropic displacement parameters (Å^{2}x10^3) for Diketone **347**.*

	x	y	z	U(eq)
H(2)	7285	4750	1588	13
H(4A)	9174	6316	2952	14
H(4B)	7909	5208	3147	14
H(5)	7440	7884	3443	15
H(17A)	10447	7253	4705	33
H(17B)	9609	8436	4311	33
H(17C)	10487	7331	3869	33
H(18A)	8487	5902	5174	23
H(18B)	6826	5543	4740	23
H(6A)	5304	5794	3801	19
H(6B)	5007	7264	4024	19
H(8)	5077	5194	2471	14
H(9A)	4510	5741	1352	17
H(9B)	3293	6644	1777	17
H(4O)	8170(20)	9790(20)	1914(10)	22
H(19A)	6468	9622	352	25
H(19B)	7635	8529	47	25
H(19C)	8332	9937	199	25
H(13A)	10463	8753	798	16
H(13B)	10188	8329	1600	16
H(14)	9716	6805	374	15
H(15)	7139	6154	659	12

*Table A7.4.7. Torsion angles [°] for Diketone **347**.*

C(14)-O(1)-C(1)-O(2)	-176.30(10)
C(14)-O(1)-C(1)-C(2)	5.14(12)
O(2)-C(1)-C(2)-C(15)	-176.46(10)
O(1)-C(1)-C(2)-C(15)	1.98(10)
O(2)-C(1)-C(2)-C(3)	71.40(13)
O(1)-C(1)-C(2)-C(3)	-110.16(9)
C(1)-C(2)-C(3)-O(5)	87.64(9)
C(15)-C(2)-C(3)-O(5)	-24.57(9)
C(1)-C(2)-C(3)-C(4)	-29.62(12)
C(15)-C(2)-C(3)-C(4)	-141.83(8)
C(1)-C(2)-C(3)-C(8)	-159.41(8)
C(15)-C(2)-C(3)-C(8)	88.38(9)
C(4)-C(3)-O(5)-C(11)	163.62(7)
C(8)-C(3)-O(5)-C(11)	-75.92(8)
C(2)-C(3)-O(5)-C(11)	41.07(9)
O(5)-C(3)-C(4)-C(5)	60.78(10)
C(8)-C(3)-C(4)-C(5)	-55.23(11)
C(2)-C(3)-C(4)-C(5)	175.59(8)
C(3)-C(4)-C(5)-C(16)	-176.57(8)
C(3)-C(4)-C(5)-C(6)	56.88(11)
C(4)-C(5)-C(16)-C(18)	-98.21(13)
C(6)-C(5)-C(16)-C(18)	25.02(15)
C(4)-C(5)-C(16)-C(17)	80.52(12)
C(6)-C(5)-C(16)-C(17)	-156.25(10)
C(16)-C(5)-C(6)-C(7)	178.99(9)
C(4)-C(5)-C(6)-C(7)	-57.58(11)
C(5)-C(6)-C(7)-O(3)	-114.46(12)
C(5)-C(6)-C(7)-C(8)	61.17(12)
O(3)-C(7)-C(8)-C(9)	-3.01(14)
C(6)-C(7)-C(8)-C(9)	-178.72(8)
O(3)-C(7)-C(8)-C(3)	118.66(11)
C(6)-C(7)-C(8)-C(3)	-57.06(11)
O(5)-C(3)-C(8)-C(7)	-65.30(9)
C(4)-C(3)-C(8)-C(7)	51.92(10)

Table A7.4.7. (cont'd)

C(2)-C(3)-C(8)-C(7)	-176.81(8)
O(5)-C(3)-C(8)-C(9)	55.83(10)
C(4)-C(3)-C(8)-C(9)	173.05(8)
C(2)-C(3)-C(8)-C(9)	-55.68(11)
C(7)-C(8)-C(9)-C(10)	80.85(11)
C(3)-C(8)-C(9)-C(10)	-38.03(12)
C(8)-C(9)-C(10)-O(6)	-147.94(11)
C(8)-C(9)-C(10)-C(11)	36.97(12)
C(3)-O(5)-C(11)-C(10)	75.12(9)
C(3)-O(5)-C(11)-C(15)	-40.47(9)
C(3)-O(5)-C(11)-C(12)	-152.05(7)
O(6)-C(10)-C(11)-O(5)	131.33(11)
C(9)-C(10)-C(11)-O(5)	-53.70(11)
O(6)-C(10)-C(11)-C(15)	-116.89(12)
C(9)-C(10)-C(11)-C(15)	58.08(11)
O(6)-C(10)-C(11)-C(12)	9.15(16)
C(9)-C(10)-C(11)-C(12)	-175.88(9)
O(5)-C(11)-C(12)-O(4)	-48.50(10)
C(10)-C(11)-C(12)-O(4)	74.44(11)
C(15)-C(11)-C(12)-O(4)	-158.22(8)
O(5)-C(11)-C(12)-C(19)	-170.10(8)
C(10)-C(11)-C(12)-C(19)	-47.15(13)
C(15)-C(11)-C(12)-C(19)	80.18(10)
O(5)-C(11)-C(12)-C(13)	71.63(9)
C(10)-C(11)-C(12)-C(13)	-165.42(9)
C(15)-C(11)-C(12)-C(13)	-38.09(9)
O(4)-C(12)-C(13)-C(14)	158.08(8)
C(19)-C(12)-C(13)-C(14)	-82.15(10)
C(11)-C(12)-C(13)-C(14)	38.69(9)
C(1)-O(1)-C(14)-C(13)	106.34(10)
C(1)-O(1)-C(14)-C(15)	-9.99(11)
C(12)-C(13)-C(14)-O(1)	-141.52(8)
C(12)-C(13)-C(14)-C(15)	-25.67(10)
C(1)-C(2)-C(15)-C(11)	-117.99(8)

Table A7.4.7. (cont'd)

C(3)-C(2)-C(15)-C(11)	1.06(9)
C(1)-C(2)-C(15)-C(14)	-7.63(9)
C(3)-C(2)-C(15)-C(14)	111.42(8)
O(5)-C(11)-C(15)-C(2)	22.86(9)
C(10)-C(11)-C(15)-C(2)	-91.07(9)
C(12)-C(11)-C(15)-C(2)	133.69(8)
O(5)-C(11)-C(15)-C(14)	-87.95(8)
C(10)-C(11)-C(15)-C(14)	158.12(8)
C(12)-C(11)-C(15)-C(14)	22.89(9)
O(1)-C(14)-C(15)-C(2)	10.64(10)
C(13)-C(14)-C(15)-C(2)	-108.89(8)
O(1)-C(14)-C(15)-C(11)	121.37(8)
C(13)-C(14)-C(15)-C(11)	1.84(10)

Symmetry transformations used to generate equivalent atoms:

*Table A7.4.8. Hydrogen bonds for Diketone **347** [Å and °].*

D-H...A	d(D-H)	d(H...A)	d(D...A)	<(DHA)
C(2)-H(2)...O(3)#1	1.00	2.41	3.2731(13)	143.6
C(6)-H(6A)...O(6)#1	0.99	2.55	3.5149(15)	163.6
C(9)-H(9B)...O(1)#2	0.99	2.54	3.3451(13)	138.2
O(4)-H(4O)...O(2)#3	0.797(17)	2.171(17)	2.9477(12)	164.6(19)
C(19)-H(19A)...O(6)	0.98	2.48	3.0578(15)	117.7
C(14)-H(14)...O(6)#4	1.00	2.60	3.5664(14)	163.4

Symmetry transformations used to generate equivalent atoms:

#1 -x+1,y-1/2,-z+1/2 #2 x-1,y,z #3 -x+2,y+1/2,-z+1/2

#4 x+1/2,-y+3/2,-z

A7.5 X-Ray Crystal Structure Analysis of Hemiketal 350

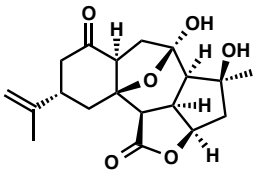

350

Contents

Table A7.5.1. Experimental Details

Table A7.5.2. Crystal Data

Table A7.5.3. Atomic Coordinates

Table A7.5.4. Full Bond Distances and Angles

Table A7.5.5. Anisotropic Displacement Parameters

Table A7.5.6. Hydrogen Atomic Coordinates

Table A7.5.7. Torsion Angles

Table A7.5.8. Hydrogen Bond Distances and Angles

*Figure A7.5.1. X-Ray Crystal Structure of Hemiketal **350***

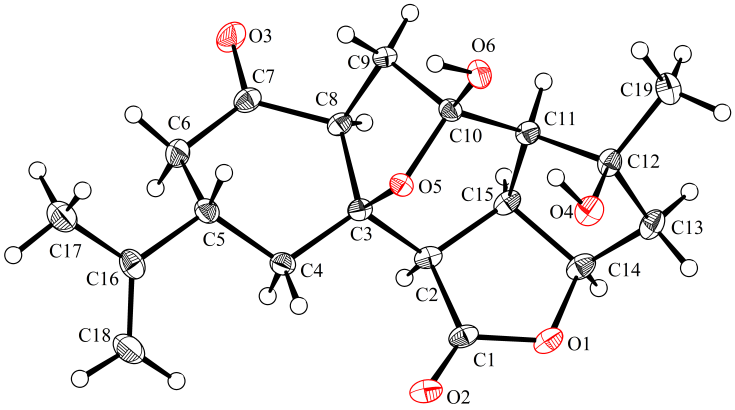

*Table A7.5.1. Experimental Details for X-Ray Structure Determination of Hemiketal **350**.*

Low-temperature diffraction data (ϕ-and ω-scans) were collected on a Bruker AXS KAPPA APEX II diffractometer coupled to a APEX II CCD detector with graphite monochromated Mo K_α radiation (λ = 0.71073 Å) for the structure of hemiketal **350** and on a Bruker AXS D8 VENTURE KAPPA diffractometer coupled to a PHOTON 100 CMOS detector with Cu K_α radiation (λ = 1.54178 Å) from an IμS micro-source for the structure of compound P15149 and P15156. The structure was solved by direct methods using SHELXS[1] and refined against F^2 on all data by full-matrix least squares with SHELXL-2014[2] using established refinement techniques.[3] All non-hydrogen atoms were refined anisotropically. Unless otherwise noted, all hydrogen atoms were included into the model at geometrically calculated positions and refined using a riding model. The isotropic displacement parameters of all hydrogen atoms were fixed to 1.2 times the U value of the atoms they are linked to (1.5 times for methyl groups).

Hemiketal **350** crystallizes in the orthorhombic space group $P2_12_12_1$ with one molecule in the asymmetric unit. The coordinates for all hydrogen atoms were located in the difference Fourier synthesis and refined freely.

*Table A7.5.2. Crystal Data and Structure Refinement for Hemiketal **350**.*

Caltech Identification code	p15156cu	
CCDC Deposition Number	1061009	
Empirical formula	C19 H24 O6	
Formula weight	348.38	
Temperature	100 K	
Wavelength	1.54178 Å	
Crystal system	Orthorhombic	
Space group	$P2_12_12_1$	
Unit cell dimensions	a = 8.2463(2) Å	α= 90°
	b = 10.3683(3) Å	β= 90°
	c = 19.3151(5) Å	γ = 90°
Volume	1651.44(8) $Å^3$	
Z	4	
Density (calculated)	1.401 Mg/m^3	
Absorption coefficient	0.859 mm^{-1}	
F(000)	744	
Crystal size	0.16 x 0.09 x 0.08 mm^3	
Theta range for data collection	4.578 to 79.097°.	
Index ranges	$-10 \le h \le 10, -13 \le k \le 13, -24 \le l \le 24$	
Reflections collected	40519	
Independent reflections	3557 [R(int) = 0.0399]	
Completeness to theta = 67.000°	100.0 %	
Absorption correction	Semi-empirical from equivalents	
Max. and min. transmission	1.0000 and 0.8788	
Refinement method	Full-matrix least-squares on F^2	
Data / restraints / parameters	3557 / 0 / 322	
Goodness-of-fit on F^2	1.070	
Final R indices [I>2sigma(I)]	R1 = 0.0252, wR2 = 0.0607	
R indices (all data)	R1 = 0.0268, wR2 = 0.0619	
Absolute structure parameter	0.03(4)	
Extinction coefficient	n/a	
Largest diff. peak and hole	0.170 and -0.183 e.$Å^{-3}$	

*Table A7.5.3. Atomic coordinates (x 10^4) and equivalent isotropic displacement parameters ($Å^2$x 10^3) for Hemiketal **350**. U(eq) is defined as one third of the trace of the orthogonalized U^{ij} tensor.*

	x	y	z	U(eq)
O(1)	23254(14)	24829(11)	25005(6)	192(2)
O(2)	33537(15)	14564(11)	34069(6)	209(3)
O(3)	100576(16)	50516(12)	31547(7)	248(3)
O(4)	42360(16)	11573(11)	13350(6)	193(2)
O(5)	67107(13)	18290(10)	24612(5)	128(2)
O(6)	75229(14)	16546(12)	13315(6)	180(2)
C(1)	34786(19)	23022(15)	29832(8)	161(3)
C(2)	48069(19)	33135(15)	29051(8)	144(3)
C(3)	65329(19)	27942(14)	29950(7)	133(3)
C(4)	68360(20)	21649(15)	36942(8)	158(3)
C(5)	86350(20)	19583(16)	38463(8)	165(3)
C(6)	94700(20)	32790(17)	38913(9)	202(3)
C(7)	91720(20)	41371(16)	32757(8)	168(3)
C(8)	77580(20)	38877(15)	27971(8)	148(3)
C(9)	83759(19)	34565(16)	20787(8)	164(3)
C(10)	70447(19)	25448(15)	18354(7)	139(3)
C(11)	55282(19)	32674(15)	15786(8)	140(3)
C(12)	43210(20)	24883(15)	11226(8)	161(3)
C(13)	26650(20)	30857(16)	12851(9)	194(3)
C(14)	27380(20)	35427(16)	20304(9)	181(3)
C(15)	45172(19)	38751(14)	21820(8)	146(3)
C(16)	89610(20)	11948(16)	45052(8)	190(3)
C(17)	106770(30)	7743(19)	46225(10)	250(4)
C(18)	77930(30)	8900(20)	49571(9)	270(4)
C(19)	47170(20)	25661(18)	3518(9)	218(3)

*Table A7.5.4. Bond lengths [Å] and angles [°] for Hemiketal **350**.*

O(1)-C(1)	1.345(2)
O(1)-C(14)	1.466(2)
O(2)-C(1)	1.204(2)
O(3)-C(7)	1.220(2)
O(4)-H(4)	0.86(3)
O(4)-C(12)	1.4414(18)
O(5)-C(3)	1.4443(17)
O(5)-C(10)	1.4448(18)
O(6)-H(6)	0.88(3)
O(6)-C(10)	1.3982(18)
C(1)-C(2)	1.524(2)
C(2)-H(2)	0.97(2)
C(2)-C(3)	1.532(2)
C(2)-C(15)	1.532(2)
C(3)-C(4)	1.520(2)
C(3)-C(8)	1.566(2)
C(4)-H(4A)	0.98(2)
C(4)-H(4B)	0.97(2)
C(4)-C(5)	1.528(2)
C(5)-H(5)	1.00(2)
C(5)-C(6)	1.535(2)
C(5)-C(16)	1.523(2)
C(6)-H(6A)	0.99(3)
C(6)-H(6B)	0.96(3)
C(6)-C(7)	1.505(2)
C(7)-C(8)	1.510(2)
C(8)-H(8)	1.01(2)
C(8)-C(9)	1.544(2)
C(9)-H(9A)	0.94(2)
C(9)-H(9B)	0.96(2)
C(9)-C(10)	1.523(2)
C(10)-C(11)	1.540(2)
C(11)-H(11)	0.97(2)

Table A7.5.4. (cont'd)

C(11)-C(12)	1.556(2)
C(11)-C(15)	1.565(2)
C(12)-C(13)	1.531(2)
C(12)-C(19)	1.526(2)
C(13)-H(13A)	1.00(2)
C(13)-H(13B)	1.01(3)
C(13)-C(14)	1.517(2)
C(14)-H(14)	0.99(2)
C(14)-C(15)	1.535(2)
C(15)-H(15)	0.98(2)
C(16)-C(17)	1.497(3)
C(16)-C(18)	1.338(3)
C(17)-H(17A)	0.98(3)
C(17)-H(17B)	1.00(3)
C(17)-H(17C)	0.99(3)
C(18)-H(18A)	0.97(3)
C(18)-H(18B)	0.99(3)
C(19)-H(19A)	1.00(3)
C(19)-H(19B)	0.97(2)
C(19)-H(19C)	1.00(3)

C(1)-O(1)-C(14)	111.70(12)
C(12)-O(4)-H(4)	103.7(18)
C(3)-O(5)-C(10)	105.11(11)
C(10)-O(6)-H(6)	109.4(16)
O(1)-C(1)-C(2)	110.10(13)
O(2)-C(1)-O(1)	120.81(14)
O(2)-C(1)-C(2)	129.06(15)
C(1)-C(2)-H(2)	105.4(13)
C(1)-C(2)-C(3)	114.51(12)
C(1)-C(2)-C(15)	103.87(13)
C(3)-C(2)-H(2)	109.7(13)
C(3)-C(2)-C(15)	112.45(12)
C(15)-C(2)-H(2)	110.5(12)

Table A7.5.4. (cont'd)

O(5)-C(3)-C(2)	104.89(12)
O(5)-C(3)-C(4)	108.66(12)
O(5)-C(3)-C(8)	105.18(11)
C(2)-C(3)-C(8)	108.50(12)
C(4)-C(3)-C(2)	113.85(13)
C(4)-C(3)-C(8)	114.93(13)
C(3)-C(4)-H(4A)	109.1(13)
C(3)-C(4)-H(4B)	107.6(13)
C(3)-C(4)-C(5)	112.99(13)
H(4A)-C(4)-H(4B)	105.8(18)
C(5)-C(4)-H(4A)	110.7(13)
C(5)-C(4)-H(4B)	110.3(13)
C(4)-C(5)-H(5)	110.4(12)
C(4)-C(5)-C(6)	108.74(13)
C(6)-C(5)-H(5)	107.1(12)
C(16)-C(5)-C(4)	113.91(13)
C(16)-C(5)-H(5)	106.8(12)
C(16)-C(5)-C(6)	109.71(13)
C(5)-C(6)-H(6A)	110.0(15)
C(5)-C(6)-H(6B)	112.6(14)
H(6A)-C(6)-H(6B)	108(2)
C(7)-C(6)-C(5)	114.17(13)
C(7)-C(6)-H(6A)	105.2(14)
C(7)-C(6)-H(6B)	106.8(14)
O(3)-C(7)-C(6)	120.88(15)
O(3)-C(7)-C(8)	118.57(15)
C(6)-C(7)-C(8)	120.55(14)
C(3)-C(8)-H(8)	112.3(13)
C(7)-C(8)-C(3)	118.21(13)
C(7)-C(8)-H(8)	103.8(12)
C(7)-C(8)-C(9)	110.18(13)
C(9)-C(8)-C(3)	102.86(12)
C(9)-C(8)-H(8)	109.4(12)
C(8)-C(9)-H(9A)	113.1(13)

Table A7.5.4. (cont'd)

C(8)-C(9)-H(9B)	109.8(12)
H(9A)-C(9)-H(9B)	111.1(18)
C(10)-C(9)-C(8)	102.66(12)
C(10)-C(9)-H(9A)	112.2(13)
C(10)-C(9)-H(9B)	107.6(12)
O(5)-C(10)-C(9)	101.42(11)
O(5)-C(10)-C(11)	111.38(12)
O(6)-C(10)-O(5)	107.28(12)
O(6)-C(10)-C(9)	114.91(13)
O(6)-C(10)-C(11)	109.02(12)
C(9)-C(10)-C(11)	112.51(13)
C(10)-C(11)-H(11)	106.9(12)
C(10)-C(11)-C(12)	116.72(13)
C(10)-C(11)-C(15)	112.86(12)
C(12)-C(11)-H(11)	106.0(12)
C(12)-C(11)-C(15)	106.84(12)
C(15)-C(11)-H(11)	106.9(12)
O(4)-C(12)-C(11)	111.53(12)
O(4)-C(12)-C(13)	106.61(13)
O(4)-C(12)-C(19)	109.78(13)
C(13)-C(12)-C(11)	104.15(12)
C(19)-C(12)-C(11)	112.81(13)
C(19)-C(12)-C(13)	111.68(14)
C(12)-C(13)-H(13A)	109.2(12)
C(12)-C(13)-H(13B)	112.6(14)
H(13A)-C(13)-H(13B)	107.3(18)
C(14)-C(13)-C(12)	106.59(13)
C(14)-C(13)-H(13A)	109.6(12)
C(14)-C(13)-H(13B)	111.5(14)
O(1)-C(14)-C(13)	110.16(13)
O(1)-C(14)-H(14)	106.1(12)
O(1)-C(14)-C(15)	105.79(13)
C(13)-C(14)-H(14)	113.8(12)
C(13)-C(14)-C(15)	106.81(13)

Table A7.5.4. (cont'd)

C(15)-C(14)-H(14)	113.8(12)
C(2)-C(15)-C(11)	116.28(12)
C(2)-C(15)-C(14)	103.75(13)
C(2)-C(15)-H(15)	110.5(13)
C(11)-C(15)-H(15)	109.8(13)
C(14)-C(15)-C(11)	106.05(13)
C(14)-C(15)-H(15)	110.1(13)
C(17)-C(16)-C(5)	116.41(14)
C(18)-C(16)-C(5)	122.73(16)
C(18)-C(16)-C(17)	120.85(16)
C(16)-C(17)-H(17A)	110.5(17)
C(16)-C(17)-H(17B)	111.6(16)
C(16)-C(17)-H(17C)	113.0(17)
H(17A)-C(17)-H(17B)	108(2)
H(17A)-C(17)-H(17C)	107(2)
H(17B)-C(17)-H(17C)	106(2)
C(16)-C(18)-H(18A)	118.5(17)
C(16)-C(18)-H(18B)	121.4(15)
H(18A)-C(18)-H(18B)	120(2)
C(12)-C(19)-H(19A)	110.0(13)
C(12)-C(19)-H(19B)	112.3(13)
C(12)-C(19)-H(19C)	108.5(14)
H(19A)-C(19)-H(19B)	107(2)
H(19A)-C(19)-H(19C)	110.7(19)
H(19B)-C(19)-H(19C)	108(2)

Symmetry transformations used to generate equivalent atoms:

*Table A7.5.5. Anisotropic displacement parameters ($Å^2x10^3$) for Hemiketal **350**. The anisotropic displacement factor exponent takes the form: $-2\pi^2[h^2a^{*2}U^{11} + ... + 2hka^*b^*U^{12}]$.*

	U^{11}	U^{22}	U^{33}	U^{23}	U^{13}	U^{12}
O(1)	128(5)	177(5)	271(6)	6(5)	5(4)	-21(4)
O(2)	179(6)	197(6)	252(6)	19(5)	52(5)	-36(5)
O(3)	222(6)	220(6)	303(6)	33(5)	-55(5)	-112(5)
O(4)	199(6)	118(5)	262(6)	16(4)	-21(5)	1(5)
O(5)	152(5)	113(5)	118(4)	-14(4)	9(4)	2(4)
O(6)	166(5)	232(6)	140(5)	-24(4)	2(4)	80(5)
C(1)	127(7)	149(7)	207(7)	-50(6)	50(6)	-1(6)
C(2)	135(7)	116(7)	181(7)	-30(6)	35(6)	-11(6)
C(3)	136(7)	125(6)	138(6)	-33(5)	18(5)	-20(6)
C(4)	172(7)	169(7)	134(6)	-10(6)	17(6)	-33(6)
C(5)	190(7)	183(7)	123(6)	-9(6)	4(6)	-19(6)
C(6)	199(8)	226(8)	183(7)	-1(6)	-43(6)	-58(7)
C(7)	146(7)	161(7)	197(7)	-35(6)	14(6)	-22(6)
C(8)	130(7)	136(7)	177(7)	-3(6)	0(6)	-30(6)
C(9)	122(7)	212(8)	159(7)	38(6)	13(6)	-24(7)
C(10)	134(7)	158(7)	124(6)	9(6)	15(5)	29(6)
C(11)	125(7)	121(7)	174(7)	17(6)	1(6)	15(6)
C(12)	156(7)	126(7)	201(7)	19(6)	-31(6)	15(6)
C(13)	138(7)	177(7)	266(8)	15(7)	-45(6)	10(6)
C(14)	122(7)	144(7)	277(8)	21(6)	9(6)	23(6)
C(15)	109(7)	100(6)	230(7)	-7(6)	7(6)	20(6)
C(16)	256(9)	179(7)	134(7)	-28(6)	-16(6)	0(7)
C(17)	276(9)	280(9)	193(8)	38(7)	11(7)	41(8)
C(18)	308(10)	323(10)	178(8)	56(7)	30(7)	22(8)
C(19)	241(9)	227(8)	186(7)	18(7)	-40(7)	21(7)

*Table A7.5.6. Hydrogen coordinates (x10^4) and isotropic displacement parameters (Å^{2}x10^3) for Hemiketal **350**.*

	x	y	z	U(eq)
H(4)	5230(40)	900(30)	1322(13)	38(7)
H(6)	8360(30)	1210(20)	1486(12)	34(6)
H(2)	4580(30)	3950(20)	3257(11)	19(5)
H(4A)	6250(30)	1350(20)	3715(11)	24(5)
H(4B)	6350(30)	2710(20)	4045(11)	21(5)
H(5)	9160(30)	1480(20)	3459(10)	19(5)
H(6A)	9050(30)	3760(20)	4292(13)	36(6)
H(6B)	10620(30)	3210(20)	3943(12)	28(6)
H(8)	7220(30)	4750(20)	2755(11)	19(5)
H(9A)	8530(30)	4150(20)	1771(11)	21(5)
H(9B)	9350(30)	2960(19)	2130(10)	14(4)
H(11)	5910(30)	3980(20)	1292(10)	17(5)
H(13A)	2480(30)	3840(20)	972(11)	18(5)
H(13B)	1740(30)	2460(20)	1210(12)	33(6)
H(14)	1970(30)	4250(20)	2137(10)	16(5)
H(15)	4670(30)	4810(20)	2186(11)	22(5)
H(17A)	11020(30)	170(30)	4263(14)	43(7)
H(17B)	10810(30)	340(20)	5083(13)	37(7)
H(17C)	11460(40)	1500(30)	4620(14)	48(8)
H(18A)	8080(30)	390(30)	5363(14)	39(7)
H(18B)	6650(30)	1110(30)	4869(13)	37(7)
H(19A)	5790(30)	2140(20)	258(12)	32(6)
H(19B)	4800(30)	3450(20)	190(12)	27(6)
H(19C)	3830(30)	2130(20)	88(12)	29(6)

*Table A7.5.7. Torsion angles [°] for Hemiketal **350**.*

O(1)-C(1)-C(2)-C(3)	-138.72(13)
O(1)-C(1)-C(2)-C(15)	-15.70(16)
O(1)-C(14)-C(15)-C(2)	-20.00(15)
O(1)-C(14)-C(15)-C(11)	103.00(14)
O(2)-C(1)-C(2)-C(3)	43.2(2)
O(2)-C(1)-C(2)-C(15)	166.23(16)
O(3)-C(7)-C(8)-C(3)	-174.28(15)
O(3)-C(7)-C(8)-C(9)	67.94(19)
O(4)-C(12)-C(13)-C(14)	86.84(15)
O(5)-C(3)-C(4)-C(5)	77.86(15)
O(5)-C(3)-C(8)-C(7)	-114.56(14)
O(5)-C(3)-C(8)-C(9)	7.03(15)
O(5)-C(10)-C(11)-C(12)	-84.55(15)
O(5)-C(10)-C(11)-C(15)	39.79(17)
O(6)-C(10)-C(11)-C(12)	33.65(18)
O(6)-C(10)-C(11)-C(15)	157.99(12)
C(1)-O(1)-C(14)-C(13)	126.20(14)
C(1)-O(1)-C(14)-C(15)	11.11(16)
C(1)-C(2)-C(3)-O(5)	60.00(15)
C(1)-C(2)-C(3)-C(4)	-58.66(17)
C(1)-C(2)-C(3)-C(8)	172.01(12)
C(1)-C(2)-C(15)-C(11)	-94.84(15)
C(1)-C(2)-C(15)-C(14)	21.15(15)
C(2)-C(3)-C(4)-C(5)	-165.66(13)
C(2)-C(3)-C(8)-C(7)	133.63(14)
C(2)-C(3)-C(8)-C(9)	-104.78(13)
C(3)-O(5)-C(10)-O(6)	169.22(12)
C(3)-O(5)-C(10)-C(9)	48.36(14)
C(3)-O(5)-C(10)-C(11)	-71.54(14)
C(3)-C(2)-C(15)-C(11)	29.52(18)
C(3)-C(2)-C(15)-C(14)	145.52(12)
C(3)-C(4)-C(5)-C(6)	63.83(16)
C(3)-C(4)-C(5)-C(16)	-173.48(13)
C(3)-C(8)-C(9)-C(10)	21.03(15)

Table A7.5.7. (cont'd)

C(4)-C(3)-C(8)-C(7)	4.9(2)
C(4)-C(3)-C(8)-C(9)	126.49(13)
C(4)-C(5)-C(6)-C(7)	-52.59(18)
C(4)-C(5)-C(16)-C(17)	170.32(14)
C(4)-C(5)-C(16)-C(18)	-8.8(2)
C(5)-C(6)-C(7)-O(3)	-161.18(16)
C(5)-C(6)-C(7)-C(8)	19.3(2)
C(6)-C(5)-C(16)-C(17)	-67.52(19)
C(6)-C(5)-C(16)-C(18)	113.37(19)
C(6)-C(7)-C(8)-C(3)	5.3(2)
C(6)-C(7)-C(8)-C(9)	-112.51(17)
C(7)-C(8)-C(9)-C(10)	147.92(13)
C(8)-C(3)-C(4)-C(5)	-39.64(18)
C(8)-C(9)-C(10)-O(5)	-42.13(14)
C(8)-C(9)-C(10)-O(6)	-157.47(12)
C(8)-C(9)-C(10)-C(11)	76.97(15)
C(9)-C(10)-C(11)-C(12)	162.34(13)
C(9)-C(10)-C(11)-C(15)	-73.31(16)
C(10)-O(5)-C(3)-C(2)	79.80(13)
C(10)-O(5)-C(3)-C(4)	-158.10(12)
C(10)-O(5)-C(3)-C(8)	-34.56(14)
C(10)-C(11)-C(12)-O(4)	34.69(18)
C(10)-C(11)-C(12)-C(13)	149.29(13)
C(10)-C(11)-C(12)-C(19)	-89.42(16)
C(10)-C(11)-C(15)-C(2)	-19.82(19)
C(10)-C(11)-C(15)-C(14)	-134.52(14)
C(11)-C(12)-C(13)-C(14)	-31.21(16)
C(12)-C(11)-C(15)-C(2)	109.78(14)
C(12)-C(11)-C(15)-C(14)	-4.92(15)
C(12)-C(13)-C(14)-O(1)	-85.69(15)
C(12)-C(13)-C(14)-C(15)	28.74(16)
C(13)-C(14)-C(15)-C(2)	-137.36(13)
C(13)-C(14)-C(15)-C(11)	-14.36(16)
C(14)-O(1)-C(1)-O(2)	-178.78(14)

Table A7.5.7. (cont'd)

C(14)-O(1)-C(1)-C(2)	2.96(17)
C(15)-C(2)-C(3)-O(5)	-58.27(15)
C(15)-C(2)-C(3)-C(4)	-176.92(12)
C(15)-C(2)-C(3)-C(8)	53.75(16)
C(15)-C(11)-C(12)-O(4)	-92.67(15)
C(15)-C(11)-C(12)-C(13)	21.93(15)
C(15)-C(11)-C(12)-C(19)	143.23(13)
C(16)-C(5)-C(6)-C(7)	-177.78(14)
C(19)-C(12)-C(13)-C(14)	-153.25(14)

Symmetry transformations used to generate equivalent atoms:

*Table A7.5.8. Hydrogen bonds for Hemiketal **350** [Å and °].*

D-H...A	d(D-H)	d(H...A)	d(D...A)	<(DHA)
O(4)-H(4)...O(6)	0.86(3)	2.04(3)	2.7591(18)	140(2)
O(6)-H(6)...O(3)#1	0.88(3)	1.90(3)	2.7799(17)	172(2)
C(2)-H(2)...O(4)#2	0.97(2)	2.61(2)	3.3870(19)	138.0(16)
C(4)-H(4A)...O(2)	0.98(2)	2.46(2)	3.015(2)	115.7(16)
C(8)-H(8)...O(4)#2	1.01(2)	2.58(2)	3.324(2)	130.9(15)
C(9)-H(9B)...O(1)#3	0.96(2)	2.60(2)	3.506(2)	156.9(16)
C(15)-H(15)...O(2)#2	0.98(2)	2.62(2)	3.397(2)	136.0(17)
C(15)-H(15)...O(5)#2	0.98(2)	2.48(2)	3.2986(18)	141.5(17)
C(19)-H(19A)...O(6)	1.00(3)	2.57(2)	3.135(2)	115.5(16)

Symmetry transformations used to generate equivalent atoms:

#1 -x+2,y-1/2,-z+1/2 #2 -x+1,y+1/2,-z+1/2 #3 x+1,y,z

A7.6 Notes and References

1. Sheldrick, G. M. *Acta Cryst*. **1990**, A46, 467–473.

2. Sheldrick, G. M. *Acta Cryst*. **2008**, A64, 112–122.

3. Müller, P. *Crystallography Reviews* **2009**, *15*, 57–83.

APPENDIX 8

Alternative Synthetic Strategies Toward Ineleganolide

A8.1 Alternative Synthesis of Acid Coupling Partner

Coupling partner ***ent*-321** was available after three synthetic transformations from literature known (*R*)-(–)-desmethylcarvone (**(*R*)-217**).[1] In an effort to improve the overall transformation of enone **(*R*)-217** to acid ***ent*-321**, we sought to improve the synthesis of intermediate ester **358**.

*Scheme A8.1.1. Synthesis of Acid **ent-321** Using Isopropyl Acetate*

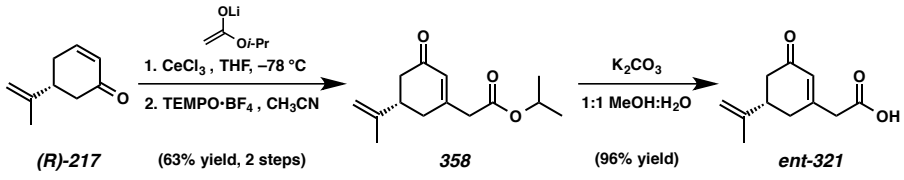

The ethyl analog of ester **358** could be accessed in 68% yield over two steps form enone **(*R*)-217**.[2] We hypothesized that the introduction of additional steric bulk at the ester position would impart greater stability to the substrate and thus improve the tolerance to oxidative 1,3-allylic transposition conditions, subsequently improving the

isolated yield of the intermediate ester **358**. Introduction of increased steric bulk was accomplished directly by the 1,2-addition of the lithium enolate of isopropyl acetate into (*R*)-(–)-desmethylcarvone (**(*R*)-(217)**, Scheme A8.1.1). Oxidative 1,3-allylic transposition of the intermediate tertiary alcohol provided isopropyl ester in 63% yield over two steps. Although the yield was not improved compared to the analogous ethyl ester series (see Chapter 3)[2] and we ultimately chose not to pursue the syntheses of isopropyl ester **358** for the large scale advancement of material, ester **358** could be efficiently saponified to provide acid coupling ***ent*-321** partner in 96% yield. With acid coupling partner ***ent*-321** in hand, we were able to advance through the synthetic route and explore the reactivity of the tetracyclic core of the norcembranoid diterpenes natural products.

A8.2 Olefin Isomerization of [6,7,5,5]-Tetracyclic Diene

Advancement toward the norcembranoid diterpene natural products began with an evaluation of the reactivity profile of tetracyclic diene **324**, the first intermediate developed with complete core of the norcembranoid diterpenes. We wanted to explore the potential to isomerize 1,4-diene **324** into the extended conjugated system within 1,3-diene **359**. This would accomplish the transposition the oxidation state onto C(5) as necessary of the synthesis of *ent*-ineleganolide (***ent*-9**).

Table A8.2.1. Attempted Olefin Isomerization

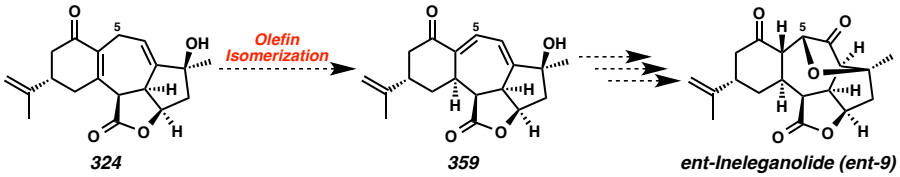

324 *359* ***ent-Ineleganolide (ent-9)***

Entry	*Conditions*	*Result* [a]
1	KO*t*-Bu, THF	Decomposition
2	DBU, $CHCl_3$	Decomposition
3	$RhCl_3 \cdot H_2O$, K_2CO_3, EtOH, 60 °C	Decomposition
4	HCl, Et_2O	Decomposition
5	toluene, 80 °C	No reaction
6	HO*t*-Bu, benzene, 60 °C	Decomposition

a: All results assessed by crude ^{1}H NMR

Unfortunately, standard conditions for olefin isomerization failed to produce any desired reactivity (Table A8.2.1). Diene **324** was largely unstable to the reaction conditions tested, save the sole addition of thermal energy in toluene (Entry 5). Under these conditions, diene **324** was completely unreactive. We did find, however, that in the presence of palladium dichloride bis(acetonitrile) in benzene at 60 °C, diene **324** underwent an unexpected isomerization (Scheme A8.2.1). Rather than isomerizing the enone olefin into conjugation, palladium(II) facilitated the transposition of the tertiary allylic alcohol into a 1:1 mixture of the secondary alcohol diastereomers **360** and **361**, forming cycloheptatriene **345** as a byproduct. The structural assignment of diastereomers **360** and **361** was accomplished by extensive two-dimensional ^{1}H and ^{13}C NMR studies. To our knowledge, this is the first example of the 1,3-transposition of an allylic alcohol by palladium(II). Unfortunately, the unoptimized transformation was low yielding and was not pursued further for advancement toward *ent*-ineleganolide (***ent*-9**) and the remaining furanobutenolide norcembranoid diterpenes.

*Scheme A8.2.1. 1,3-Allylic Transposition of Alcohol **324***

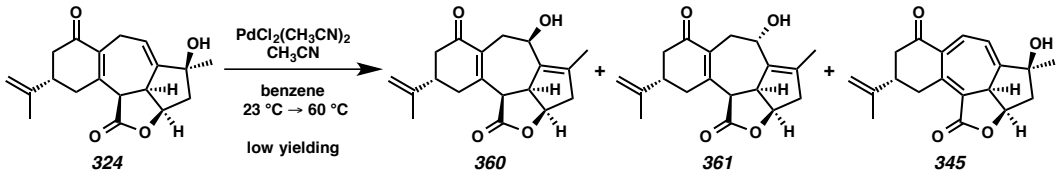

A8.3 Redox Advancement of [6,7,5,5]-Tetracyclic Diene

We briefly explored the potential to advance diene core **324** by redox manipulation. Conjugate reduction of enone **324** using dimethylphenylsilane in the presence of Wilkinson's catalyst failed to produce any isolable product, resulting in complete decomposition of the staring material (Scheme A8.3.1). Attempted oxidative advancement of diene **324** was met with similar results (Scheme A8.3.2). Although the double allylic C–H bonds appear poised for facile C–H oxidation, the use of typically efficient palladium-catalyzed C–H acetoxylation conditions caused decomposition of the substrate.[3]

*Scheme A8.3.1. Attempted 1,4-Reduction of Enone **324** with Wilkinson's Catalyst*

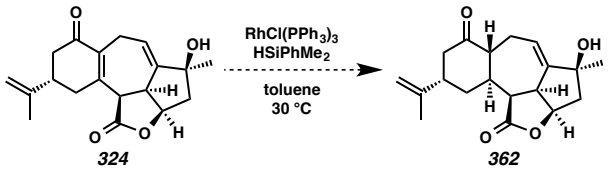

Scheme A8.3.2. Attempted Oxidation of Doubly Allylic C–H Bonds

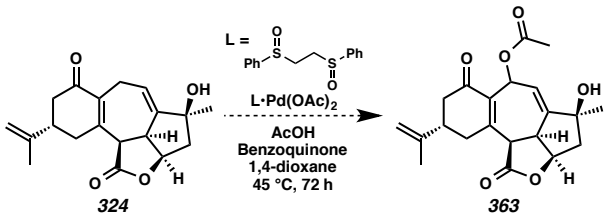

A8.4 Olefin Isomerization of Isoineleganolide A (328)

Without successfully developing any productive alternative advancement procedures from diene **324** toward the norcembranoid diterpenes, we turned our attention to the exploration of the reactivity of isoineleganolide A (**328**, Scheme A8.4.1). We began by applying the isomerization conditions that had proven productive for diene **324** to see if they would induce the desired isomerization of enone **328** in the absence of the allylic alcohol moiety. Unfortunately, epoxide **328** underwent a slow decomposition under the reaction conditions, failing to provide any isolable products.

*Scheme A8.4.1. Attempted Olefin Isomerization of Enone **328***

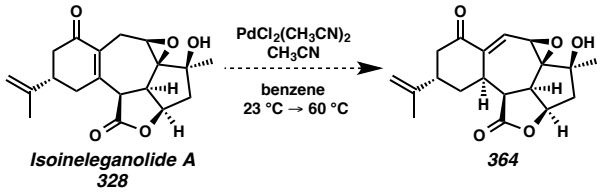

A8.5 Nucleophilic Epoxide Opening of Isoineleganolide A (328)

We envisioned advancing isoineleganolide A (**328**) instead by the nucleophilic opening of the epoxide moiety. While the opening of the strained heterocycle with a sulfur nucleophile failed (Scheme A8.5.1),[4] the opening of epoxide **328** with an oxygen nucleophile was indeed successful, furnishing furan **366** on small scale.[5] Unfortunately, the efficacy of the reaction could not be maintained as scale increased, thus we sought alternative methods for the ring opening of epoxytetracycle **328**.

Scheme A8.5.1. Nucleophilic Opening of Epoxide ***328***

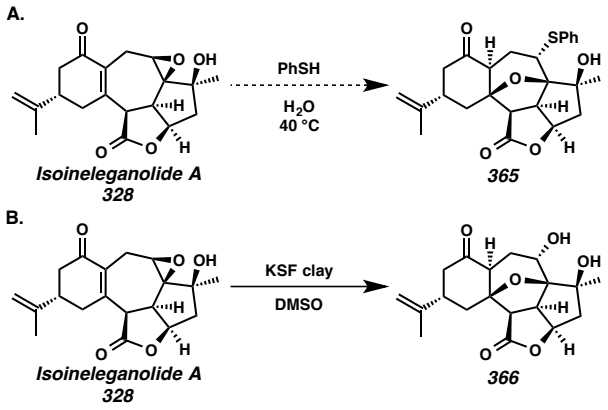

During our exploration of the potential of isoineleganolide A (**328**) to undergo an epoxyketo rearrangement, we discovered that halogenated Lewis acids would regularly accomplish the nucleophilic opening of the epoxide moiety with their halogen counterion.[6] While we used the product of nucleophilic opening by bromide for our optimize synthetic route, we found that epoxide **328** could smoothly be opened by Lewis acids with other halogen counterions. Both $MgCl_2$ and $YbCl_3$ under the same reaction conditions furnished chloride **367** (Scheme A8.5.2.A). This reactivity could be duplicated using TMSCl in the presence of zinc metal to furnish the identical product (**367**, Scheme A8.5.2.B).[7] The structural assignment of chloride **367** was unambiguously established by single crystal X-ray diffraction.

*Scheme A8.5.2. Nucleophilic Opening of Epoxide **328** with Halogen Ions*

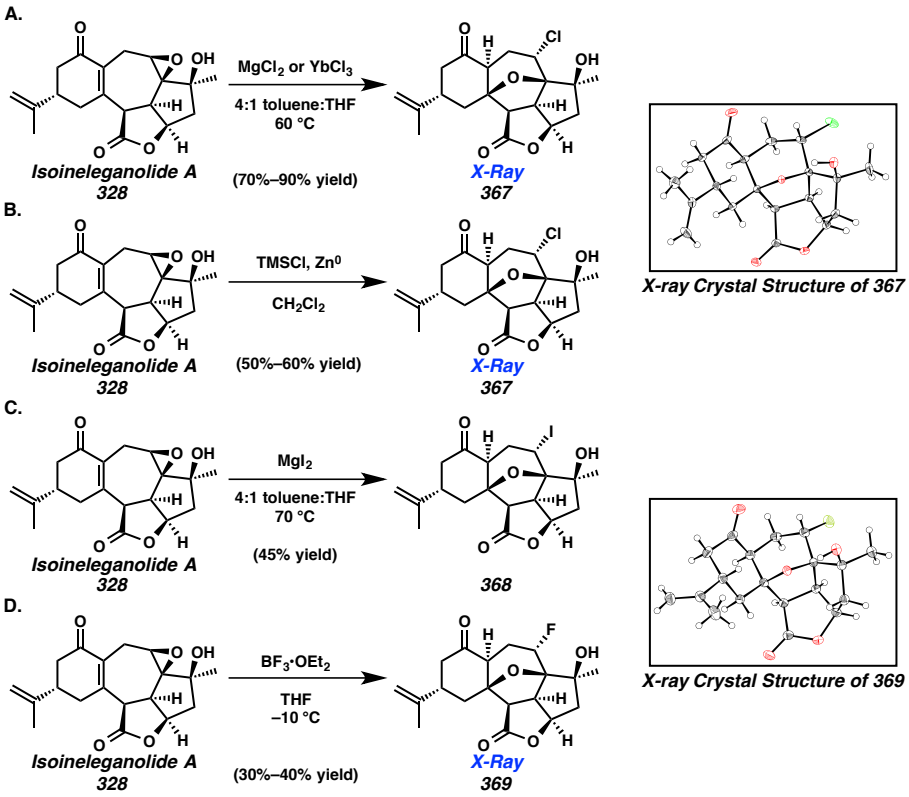

The opening of epoxide **328** could also be accomplished with MgI_2 in a mixed toluene and THF solvent system, providing iodide **368** in 45% yield (Scheme A8.5.2.C). Surprisingly, the formation of the analogous fluoride **369** was achieved by the exposure of epoxide **328** to superstoichiometric BF_3•Et_2O in THF at cold temperatures (Scheme A8.5.2.D). We were able to unambiguously establish the structural assignment of unexpected fluoride **369** by single crystal X-ray diffraction. Although the nucleophilic transfer of a fluoride anion from BF_3•Et_2O is rare, it has been shown previously to occur in the presence of a Lewis basic solvent to accomplish epoxide opening.[8]

We next explored the potential to advance the halogenated furanopentacycles by Kornblum oxidation.[9] Exposure of chloride **367** to excess $AgBF_4$ in DMSO at elevated temperature over 24 h failed to provide any trace of diketone **347**, resulting in the

quantitative recovery of staring material (Scheme A8.5.3.A). Contrastingly, iodide **368** underwent the desired oxidation to provide 1,4-diketone **347**,[10] albeit in a reduced 60% yield in comparison to the bromide analog employed in our optimized synthetic route (Scheme A8.5.3.B).[6]

Scheme A8.5.3. Kornblum Oxidation of Halogenated Furanopentacycles

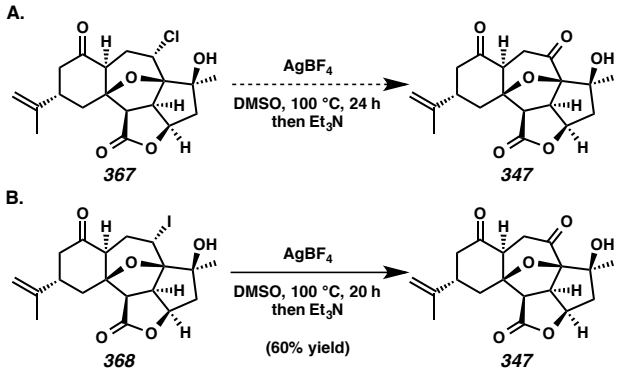

Although the exploration of the reactivity profile of diene **324** and epoxide **328** was largely unfruitful, the information gleaned form these studies contributed to the development of an optimized route for progression toward the norcembranoid diterpene natural products.

A8.6 Experimental Methods and Analytical Data

A8.6.1 Materials and Methods

Unless stated otherwise, reactions were performed at ambient temperature (23 °C) in flame-dried glassware under an argon atmosphere using dry, deoxygentated solvents (distilled or passed over a column of activated alumina)[11] using a Teflon®-coated magnetic stirring bar. Commercially available reagents were used as received unless otherwise noted. Reactions requiring external heat were modulated to the specified temperatures using an IKAmag temperature controller. Thin-layer chromatography (TLC) was performed using E. Merck silica gel 60 F254 precoated plates (250 nm) and visualized by UV fluorescence quenching, potassium permanganate, or *p*-anisaldehyde staining. Silicycle SiliaFlash P60 Academic Silica gel (particle size 40-63 nm) was used for flash chromatography. ^{1}H and ^{13}C NMR spectra were recorded on a Varian Inova 500 (500 MHz and 126 MHz, respectively) and are reported in terms of chemical shift relative to residual $CHCl_3$ (in $CDCl_3$, δ 7.26 and δ 77.16, respectively). Data for ^{1}H NMR spectra are reported as follows: chemical shift (δ ppm) (multiplicity, coupling constant (Hz), integration). Infrared (IR) spectra were recorded on a Perkin Elmer Paragon 1000 Spectrometer and are reported in frequency of absorption (cm^{-1}). High resolution mass spectra (HRMS) were obtained from the Caltech Mass Spectral Facility using a JEOL JMS-600H High Resolution Mass Spectrometer in fast atom bombardment (FAB+) ionization mode. Optical rotations were measured on a Jasco P-2000 polarimeter using a 100 mm path length cell at 589 nm.

A8.6.2 Experimental Procedures

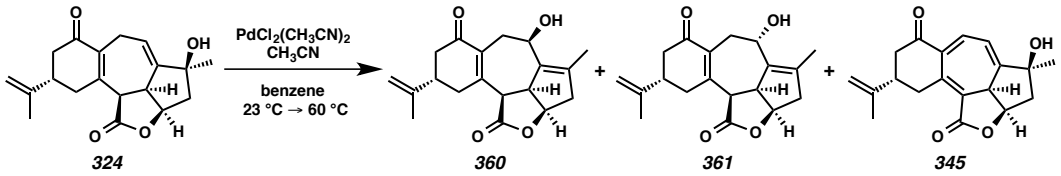

Allylic Alcohol 360, Allylic Alcohol 361, and Cycloheptatriene 345: To a stirred solution diene **324** (15 mg, 0.070 mmol, 1.00 equiv) in a mixture of benzene (5.0 mL) and CH_3CN (5.0 μL) was added $PdCl_2(CH_3CN)_2$ (0.6 mg, 0.0024 mmol, 0.05 equiv) as a solid in a single portion. After 2 minutes, the homogeneous golden solution was introduced to a preheated 50 °C bath. After 18 h, the consumption of starting material was complete as determined by TLC (1:4 EtOAc:CH_2Cl_2 eluent). The brown reaction mixture was then removed from the heating bath and allowed to cool to ambient temperature (ca. 23 °C). The reaction mixture was then filtered through a short silica gel plug, rinsing with 50% EtOAc in CH_2Cl_2 eluent. The combined organics were then concentrated in vacuo and the crude brown residue was dissolved in CH_3CN and purified by reverse phase HPLC to provide allylic alcohol **360** (1.5 mg, 10% yield), allylic alcohol **361** (1.5 mg, 10% yield), and cycloheptatriene **345** (1.5 mg, 10% yield):

Allylic Alcohol 360: $R_f = 0.23$ (1:9 EtOAc:CH_2Cl_2 eluent).

Allylic Alcohol 361: $R_f = 0.23$ (1:9 EtOAc:CH_2Cl_2 eluent).

Cycloheptatriene 345: $R_f = 0.94$ (1:4 EtOAc:CH_2Cl_2 eluent); Characterization data match those reported above, see chapter 3, section 3.9.2.

A8.7 X-Ray Crystallography Reports

A8.7.1 X-Ray Crystal Structure Analysis of Chloride 367

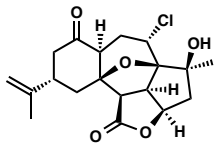

367

Contents

Table A8.7.1.1. Experimental Details

Table A8.7.1.2. Crystal Data

Table A8.7.1.3. Atomic Coordinates

Table A8.7.1.4. Full Bond Distances and Angles

Table A8.7.1.5. Anisotropic Displacement Parameters

Table A8.7.1.6. Hydrogen Atomic Coordinates

Table A8.7.1.7. Torsion Angles

Table A8.7.1.8. Hydrogen Bond Distances and Angles

*Figure A8.7.1.1. X-Ray Crystal Structure of Chloride **367***

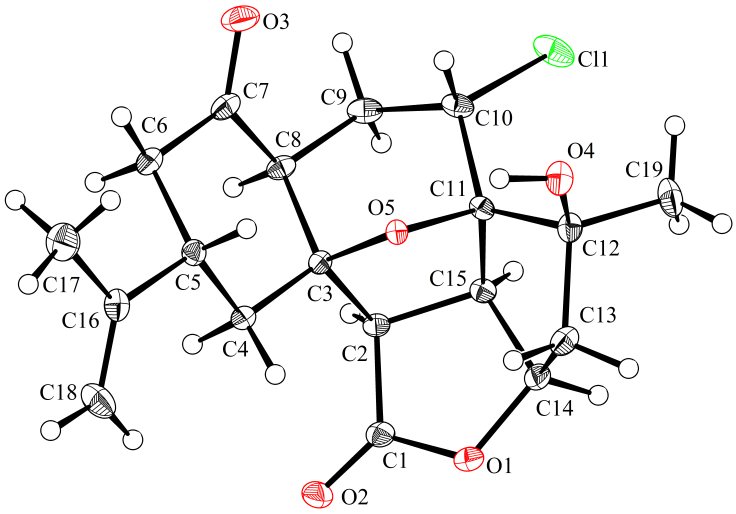

Table A8.7.1.1. Experimental Details for X-Ray Structure Determination of Chloride ***367****.*

Low-temperature diffraction data (ϕ-and ω-scans) were collected on a Bruker AXS KAPPA APEX II diffractometer coupled to a APEX II CCD detector with graphite monochromated Mo K_α radiation (λ = 0.71073 Å) for the structure of chloride **367**. The structure was solved by direct methods using SHELXS[12] and refined against F^2 on all data by full-matrix least squares with SHELXL-2014[13] using established refinement techniques.[14] All non-hydrogen atoms were refined anisotropically. Unless otherwise noted, all hydrogen atoms were included into the model at geometrically calculated positions and refined using a riding model. The isotropic displacement parameters of all hydrogen atoms were fixed to 1.2 times the U value of the atoms they are linked to (1.5 times for methyl groups).

Chloride **367** crystallizes in the orthorhombic space group $P2_12_12_1$ with one molecule in the asymmetric unit. The coordinates for the hydrogen atom bound to O4 was located in the difference Fourier synthesis and refined semi-freely with the help of a restraint on the O-H distance (0.84(4) Å).

*Table A8.7.1.2. Crystal Data and Structure Refinement for Chloride **367**.*

Identification code	rac04	
CCDC Deposition Number	1061354	
Empirical formula	C19 H23 Cl O5	
Formula weight	366.82	
Temperature	100(2) K	
Wavelength	0.71073 Å	
Crystal system	Orthorhombic	
Space group	$P2_12_12_1$	
Unit cell dimensions	a = 7.6863(4) Å	α= 90°.
	b = 9.2978(4) Å	β= 90°.
	c = 23.9062(11) Å	γ = 90°.
Volume	1708.47(14) $Å^3$	
Z	4	
Density (calculated)	1.426 Mg/m^3	
Absorption coefficient	0.251 mm^{-1}	
F(000)	776	
Crystal size	0.300 x 0.150 x 0.100 mm^3	
Theta range for data collection	1.704 to 33.726°.	
Index ranges	$-11 \le h \le 12, -14 \le k \le 14, -37 \le l \le 37$	
Reflections collected	47183	
Independent reflections	6809 [R(int) = 0.0598]	
Completeness to theta = 25.242°	100.0 %	
Absorption correction	Semi-empirical from equivalents	
Max. and min. transmission	0.7473 and 0.6980	
Refinement method	Full-matrix least-squares on F^2	
Data / restraints / parameters	6809 / 1 / 231	
Goodness-of-fit on F^2	1.042	
Final R indices [I>2sigma(I)]	R1 = 0.0379, wR2 = 0.0894	
R indices (all data)	R1 = 0.0472, wR2 = 0.0933	
Absolute structure parameter	-0.01(2)	
Extinction coefficient	n/a	
Largest diff. peak and hole	0.430 and -0.191 $e.Å^{-3}$	

*Table A8.7.1.3. Atomic coordinates (x 10^4) and equivalent isotropic displacement parameters ($Å^2$x 10^3) for Chloride **367**. U(eq) is defined as one third of the trace of the orthogonalized U^{ij} tensor.*

	x	y	z	U(eq)
O(1)	6332(2)	6433(1)	7135(1)	16(1)
C(1)	4809(2)	6305(2)	6854(1)	14(1)
O(2)	3852(2)	7312(1)	6792(1)	19(1)
C(2)	4536(2)	4776(2)	6654(1)	11(1)
C(3)	4993(2)	4542(2)	6022(1)	10(1)
O(5)	6795(1)	4114(1)	6035(1)	9(1)
C(4)	4860(2)	5871(2)	5655(1)	12(1)
C(5)	5379(2)	5568(2)	5049(1)	13(1)
C(16)	5277(2)	6872(2)	4667(1)	16(1)
C(17)	5698(3)	6601(2)	4060(1)	24(1)
C(18)	4888(3)	8182(2)	4847(1)	23(1)
C(6)	4264(2)	4325(2)	4820(1)	16(1)
C(7)	4394(2)	3009(2)	5185(1)	15(1)
O(3)	4772(2)	1830(2)	4999(1)	23(1)
C(8)	3976(2)	3238(2)	5797(1)	13(1)
C(9)	4323(2)	1903(2)	6157(1)	16(1)
C(10)	6252(2)	1729(2)	6304(1)	14(1)
Cl(1)	6423(1)	268(1)	6794(1)	23(1)
C(11)	6990(2)	3162(2)	6512(1)	10(1)
C(12)	8912(2)	3358(2)	6682(1)	13(1)
O(4)	10060(2)	3165(2)	6221(1)	16(1)
C(19)	9565(3)	2355(2)	7138(1)	21(1)
C(13)	8880(2)	4921(2)	6901(1)	16(1)
C(14)	7160(2)	5045(2)	7218(1)	14(1)
C(15)	5913(2)	3905(2)	6965(1)	12(1)

*Table A8.7.1.4. Bond lengths [Å] and angles [°] for Chloride **367**.*

O(1)-C(1)	1.356(2)
O(1)-C(14)	1.453(2)
C(1)-O(2)	1.200(2)
C(1)-C(2)	1.515(2)
C(2)-C(15)	1.526(2)
C(2)-C(3)	1.566(2)
C(2)-H(2)	1.0000
C(3)-O(5)	1.4411(18)
C(3)-C(4)	1.518(2)
C(3)-C(8)	1.539(2)
O(5)-C(11)	1.4509(18)
C(4)-C(5)	1.529(2)
C(4)-H(4A)	0.9900
C(4)-H(4B)	0.9900
C(5)-C(16)	1.520(2)
C(5)-C(6)	1.540(2)
C(5)-H(5)	1.0000
C(16)-C(18)	1.326(3)
C(16)-C(17)	1.508(3)
C(17)-H(17A)	0.9800
C(17)-H(17B)	0.9800
C(17)-H(17C)	0.9800
C(18)-H(18A)	0.9500
C(18)-H(18B)	0.9500
C(6)-C(7)	1.506(2)
C(6)-H(6A)	0.9900
C(6)-H(6B)	0.9900
C(7)-O(3)	1.218(2)
C(7)-C(8)	1.515(2)
C(8)-C(9)	1.533(2)
C(8)-H(8)	1.0000
C(9)-C(10)	1.532(3)
C(9)-H(9A)	0.9900

Table A8.7.1.4. (cont'd)

C(9)-H(9B)	0.9900
C(10)-C(11)	1.532(2)
C(10)-Cl(1)	1.8003(16)
C(10)-H(10)	1.0000
C(11)-C(15)	1.528(2)
C(11)-C(12)	1.543(2)
C(12)-O(4)	1.4234(19)
C(12)-C(19)	1.519(2)
C(12)-C(13)	1.545(2)
O(4)-H(4O)	0.854(19)
C(19)-H(19A)	0.9800
C(19)-H(19B)	0.9800
C(19)-H(19C)	0.9800
C(13)-C(14)	1.528(2)
C(13)-H(13A)	0.9900
C(13)-H(13B)	0.9900
C(14)-C(15)	1.552(2)
C(14)-H(14)	1.0000
C(15)-H(15)	1.0000

C(1)-O(1)-C(14)	111.59(13)
O(2)-C(1)-O(1)	121.53(15)
O(2)-C(1)-C(2)	127.47(16)
O(1)-C(1)-C(2)	110.99(14)
C(1)-C(2)-C(15)	104.38(13)
C(1)-C(2)-C(3)	113.80(13)
C(15)-C(2)-C(3)	103.96(12)
C(1)-C(2)-H(2)	111.4
C(15)-C(2)-H(2)	111.4
C(3)-C(2)-H(2)	111.4
O(5)-C(3)-C(4)	107.57(12)
O(5)-C(3)-C(8)	106.16(12)
C(4)-C(3)-C(8)	113.88(12)
O(5)-C(3)-C(2)	103.46(12)

Table A8.7.1.4. (cont'd)

C(4)-C(3)-C(2)	115.42(12)
C(8)-C(3)-C(2)	109.39(12)
C(3)-O(5)-C(11)	106.56(11)
C(3)-C(4)-C(5)	112.36(13)
C(3)-C(4)-H(4A)	109.1
C(5)-C(4)-H(4A)	109.1
C(3)-C(4)-H(4B)	109.1
C(5)-C(4)-H(4B)	109.1
H(4A)-C(4)-H(4B)	107.9
C(16)-C(5)-C(4)	114.19(13)
C(16)-C(5)-C(6)	110.85(13)
C(4)-C(5)-C(6)	109.28(14)
C(16)-C(5)-H(5)	107.4
C(4)-C(5)-H(5)	107.4
C(6)-C(5)-H(5)	107.4
C(18)-C(16)-C(17)	120.90(17)
C(18)-C(16)-C(5)	123.33(16)
C(17)-C(16)-C(5)	115.75(15)
C(16)-C(17)-H(17A)	109.5
C(16)-C(17)-H(17B)	109.5
H(17A)-C(17)-H(17B)	109.5
C(16)-C(17)-H(17C)	109.5
H(17A)-C(17)-H(17C)	109.5
H(17B)-C(17)-H(17C)	109.5
C(16)-C(18)-H(18A)	120.0
C(16)-C(18)-H(18B)	120.0
H(18A)-C(18)-H(18B)	120.0
C(7)-C(6)-C(5)	111.48(13)
C(7)-C(6)-H(6A)	109.3
C(5)-C(6)-H(6A)	109.3
C(7)-C(6)-H(6B)	109.3
C(5)-C(6)-H(6B)	109.3
H(6A)-C(6)-H(6B)	108.0
O(3)-C(7)-C(6)	122.39(15)

Table A8.7.1.4. (cont'd)

O(3)-C(7)-C(8)	121.98(16)
C(6)-C(7)-C(8)	115.60(14)
C(7)-C(8)-C(9)	113.04(14)
C(7)-C(8)-C(3)	109.90(13)
C(9)-C(8)-C(3)	110.71(13)
C(7)-C(8)-H(8)	107.7
C(9)-C(8)-H(8)	107.7
C(3)-C(8)-H(8)	107.7
C(10)-C(9)-C(8)	112.47(13)
C(10)-C(9)-H(9A)	109.1
C(8)-C(9)-H(9A)	109.1
C(10)-C(9)-H(9B)	109.1
C(8)-C(9)-H(9B)	109.1
H(9A)-C(9)-H(9B)	107.8
C(11)-C(10)-C(9)	109.96(13)
C(11)-C(10)-Cl(1)	114.68(11)
C(9)-C(10)-Cl(1)	107.42(11)
C(11)-C(10)-H(10)	108.2
C(9)-C(10)-H(10)	108.2
Cl(1)-C(10)-H(10)	108.2
O(5)-C(11)-C(15)	103.01(12)
O(5)-C(11)-C(10)	103.68(12)
C(15)-C(11)-C(10)	115.00(13)
O(5)-C(11)-C(12)	103.57(12)
C(15)-C(11)-C(12)	106.17(13)
C(10)-C(11)-C(12)	122.91(14)
O(4)-C(12)-C(19)	105.87(14)
O(4)-C(12)-C(11)	111.96(12)
C(19)-C(12)-C(11)	115.66(14)
O(4)-C(12)-C(13)	113.00(14)
C(19)-C(12)-C(13)	109.87(14)
C(11)-C(12)-C(13)	100.66(13)
C(12)-O(4)-H(4O)	111.7(17)
C(12)-C(19)-H(19A)	109.5

Table A8.7.1.4. (cont'd)

C(12)-C(19)-H(19B)	109.5
H(19A)-C(19)-H(19B)	109.5
C(12)-C(19)-H(19C)	109.5
H(19A)-C(19)-H(19C)	109.5
H(19B)-C(19)-H(19C)	109.5
C(14)-C(13)-C(12)	104.62(13)
C(14)-C(13)-H(13A)	110.8
C(12)-C(13)-H(13A)	110.8
C(14)-C(13)-H(13B)	110.8
C(12)-C(13)-H(13B)	110.8
H(13A)-C(13)-H(13B)	108.9
O(1)-C(14)-C(13)	112.20(14)
O(1)-C(14)-C(15)	106.47(13)
C(13)-C(14)-C(15)	106.84(12)
O(1)-C(14)-H(14)	110.4
C(13)-C(14)-H(14)	110.4
C(15)-C(14)-H(14)	110.4
C(2)-C(15)-C(11)	105.65(12)
C(2)-C(15)-C(14)	104.83(13)
C(11)-C(15)-C(14)	104.48(13)
C(2)-C(15)-H(15)	113.7
C(11)-C(15)-H(15)	113.7
C(14)-C(15)-H(15)	113.7

Symmetry transformations used to generate equivalent atoms:

*Table A8.7.1.5. Anisotropic displacement parameters ($Å^2x10^3$) for Chloride **367**. The anisotropic displacement factor exponent takes the form: $-2\pi^2[h^2a^{*2}U^{11} + ... + 2hka^*b^*U^{12}]$.*

	U^{11}	U^{22}	U^{33}	U^{23}	U^{13}	U^{12}
O(1)	18(1)	14(1)	16(1)	-4(1)	-1(1)	1(1)
C(1)	17(1)	14(1)	10(1)	-1(1)	3(1)	1(1)
O(2)	25(1)	16(1)	16(1)	-3(1)	0(1)	6(1)
C(2)	12(1)	12(1)	10(1)	-2(1)	3(1)	0(1)
C(3)	8(1)	12(1)	10(1)	-1(1)	1(1)	0(1)
O(5)	8(1)	11(1)	9(1)	1(1)	1(1)	0(1)
C(4)	14(1)	12(1)	11(1)	-1(1)	-1(1)	0(1)
C(5)	14(1)	14(1)	11(1)	1(1)	0(1)	1(1)
C(16)	14(1)	19(1)	14(1)	3(1)	-1(1)	1(1)
C(17)	32(1)	26(1)	14(1)	5(1)	2(1)	1(1)
C(18)	28(1)	18(1)	23(1)	6(1)	3(1)	6(1)
C(6)	19(1)	17(1)	12(1)	-2(1)	-3(1)	-1(1)
C(7)	13(1)	17(1)	14(1)	-4(1)	-1(1)	-4(1)
O(3)	33(1)	17(1)	18(1)	-6(1)	1(1)	-1(1)
C(8)	12(1)	14(1)	13(1)	-3(1)	2(1)	-3(1)
C(9)	18(1)	12(1)	18(1)	-1(1)	6(1)	-4(1)
C(10)	18(1)	9(1)	14(1)	2(1)	5(1)	-1(1)
Cl(1)	31(1)	12(1)	26(1)	7(1)	9(1)	2(1)
C(11)	12(1)	10(1)	9(1)	2(1)	3(1)	1(1)
C(12)	12(1)	18(1)	10(1)	1(1)	1(1)	1(1)
O(4)	11(1)	24(1)	12(1)	1(1)	3(1)	3(1)
C(19)	20(1)	27(1)	15(1)	6(1)	-1(1)	8(1)
C(13)	14(1)	20(1)	14(1)	-3(1)	-1(1)	-2(1)
C(14)	16(1)	16(1)	11(1)	-2(1)	-1(1)	2(1)
C(15)	13(1)	12(1)	10(1)	0(1)	3(1)	1(1)

*Table A8.7.1.6. Hydrogen coordinates (x10^4) and isotropic displacement parameters (Å^{2}x10^3) for Chloride **367**.*

	x	y	z	U(eq)
H(2)	3336	4427	6742	14
H(4A)	5623	6632	5809	15
H(4B)	3649	6232	5664	15
H(5)	6616	5236	5052	15
H(17A)	4724	6098	3882	36
H(17B)	6749	6009	4033	36
H(17C)	5894	7521	3870	36
H(18A)	4872	8966	4592	28
H(18B)	4626	8337	5230	28
H(6A)	3033	4636	4798	19
H(6B)	4655	4083	4437	19
H(8)	2708	3467	5826	15
H(9A)	3639	1974	6507	19
H(9B)	3923	1038	5952	19
H(10)	6891	1453	5955	17
H(4O)	9640(30)	3520(30)	5920(9)	24
H(19A)	9645	1374	6990	31
H(19B)	8753	2372	7454	31
H(19C)	10716	2672	7264	31
H(13A)	9878	5104	7153	19
H(13B)	8922	5615	6587	19
H(14)	7343	4858	7626	17
H(15)	5419	3227	7248	14

*Table A8.7.1.7. Torsion angles [°] for Chloride **367**.*

C(14)-O(1)-C(1)-O(2)	172.72(15)
C(14)-O(1)-C(1)-C(2)	-6.50(17)
O(2)-C(1)-C(2)-C(15)	-166.79(16)
O(1)-C(1)-C(2)-C(15)	12.37(17)
O(2)-C(1)-C(2)-C(3)	80.5(2)
O(1)-C(1)-C(2)-C(3)	-100.29(15)
C(1)-C(2)-C(3)-O(5)	91.63(15)
C(15)-C(2)-C(3)-O(5)	-21.28(15)
C(1)-C(2)-C(3)-C(4)	-25.58(19)
C(15)-C(2)-C(3)-C(4)	-138.50(14)
C(1)-C(2)-C(3)-C(8)	-155.56(13)
C(15)-C(2)-C(3)-C(8)	91.52(15)
C(4)-C(3)-O(5)-C(11)	162.39(11)
C(8)-C(3)-O(5)-C(11)	-75.35(14)
C(2)-C(3)-O(5)-C(11)	39.79(14)
O(5)-C(3)-C(4)-C(5)	63.33(16)
C(8)-C(3)-C(4)-C(5)	-54.01(18)
C(2)-C(3)-C(4)-C(5)	178.22(13)
C(3)-C(4)-C(5)-C(16)	-179.59(14)
C(3)-C(4)-C(5)-C(6)	55.62(17)
C(4)-C(5)-C(16)-C(18)	4.4(3)
C(6)-C(5)-C(16)-C(18)	128.3(2)
C(4)-C(5)-C(16)-C(17)	-177.23(15)
C(6)-C(5)-C(16)-C(17)	-53.3(2)
C(16)-C(5)-C(6)-C(7)	178.26(14)
C(4)-C(5)-C(6)-C(7)	-55.02(18)
C(5)-C(6)-C(7)-O(3)	-127.34(18)
C(5)-C(6)-C(7)-C(8)	54.3(2)
O(3)-C(7)-C(8)-C(9)	7.9(2)
C(6)-C(7)-C(8)-C(9)	-173.74(14)
O(3)-C(7)-C(8)-C(3)	132.10(17)
C(6)-C(7)-C(8)-C(3)	-49.51(19)
O(5)-C(3)-C(8)-C(7)	-69.48(16)
C(4)-C(3)-C(8)-C(7)	48.68(18)

Table A8.7.1.7. (cont'd)

C(2)-C(3)-C(8)-C(7)	179.48(13)
O(5)-C(3)-C(8)-C(9)	56.09(16)
C(4)-C(3)-C(8)-C(9)	174.25(13)
C(2)-C(3)-C(8)-C(9)	-54.95(17)
C(7)-C(8)-C(9)-C(10)	79.94(17)
C(3)-C(8)-C(9)-C(10)	-43.85(18)
C(8)-C(9)-C(10)-C(11)	47.41(17)
C(8)-C(9)-C(10)-Cl(1)	172.83(11)
C(3)-O(5)-C(11)-C(15)	-41.99(14)
C(3)-O(5)-C(11)-C(10)	78.19(13)
C(3)-O(5)-C(11)-C(12)	-152.46(12)
C(9)-C(10)-C(11)-O(5)	-62.25(15)
Cl(1)-C(10)-C(11)-O(5)	176.59(10)
C(9)-C(10)-C(11)-C(15)	49.42(17)
Cl(1)-C(10)-C(11)-C(15)	-71.74(16)
C(9)-C(10)-C(11)-C(12)	-178.68(13)
Cl(1)-C(10)-C(11)-C(12)	60.15(17)
O(5)-C(11)-C(12)-O(4)	-51.99(16)
C(15)-C(11)-C(12)-O(4)	-160.11(13)
C(10)-C(11)-C(12)-O(4)	64.50(19)
O(5)-C(11)-C(12)-C(19)	-173.37(13)
C(15)-C(11)-C(12)-C(19)	78.50(17)
C(10)-C(11)-C(12)-C(19)	-56.9(2)
O(5)-C(11)-C(12)-C(13)	68.32(13)
C(15)-C(11)-C(12)-C(13)	-39.81(15)
C(10)-C(11)-C(12)-C(13)	-175.19(13)
O(4)-C(12)-C(13)-C(14)	158.93(13)
C(19)-C(12)-C(13)-C(14)	-83.09(16)
C(11)-C(12)-C(13)-C(14)	39.37(14)
C(1)-O(1)-C(14)-C(13)	114.39(15)
C(1)-O(1)-C(14)-C(15)	-2.16(17)
C(12)-C(13)-C(14)-O(1)	-141.54(13)
C(12)-C(13)-C(14)-C(15)	-25.22(16)
C(1)-C(2)-C(15)-C(11)	-122.83(13)

Table A8.7.1.7. (cont'd)

C(3)-C(2)-C(15)-C(11)	-3.28(16)
C(1)-C(2)-C(15)-C(14)	-12.78(15)
C(3)-C(2)-C(15)-C(14)	106.76(13)
O(5)-C(11)-C(15)-C(2)	26.54(15)
C(10)-C(11)-C(15)-C(2)	-85.52(16)
C(12)-C(11)-C(15)-C(2)	135.07(13)
O(5)-C(11)-C(15)-C(14)	-83.75(14)
C(10)-C(11)-C(15)-C(14)	164.18(13)
C(12)-C(11)-C(15)-C(14)	24.78(15)
O(1)-C(14)-C(15)-C(2)	9.60(15)
C(13)-C(14)-C(15)-C(2)	-110.48(14)
O(1)-C(14)-C(15)-C(11)	120.49(13)
C(13)-C(14)-C(15)-C(11)	0.41(16)

Symmetry transformations used to generate equivalent atoms:

*Table A8.7.1.8. Hydrogen bonds for Chloride **367** [Å and °].*

D-H...A	d(D-H)	d(H...A)	d(D...A)	<(DHA)
C(6)-H(6B)...O(4)#1	0.99	2.63	3.453(2)	140.2
C(8)-H(8)...O(4)#2	1.00	2.26	3.177(2)	151.6
O(4)-H(4O)...O(3)#3	0.854(19)	2.22(2)	2.9252(18)	139(2)
C(19)-H(19A)...Cl(1)	0.98	2.72	3.205(2)	110.9
C(15)-H(15)...O(1)#4	1.00	2.60	3.5895(19)	169.8
C(15)-H(15)...O(2)#4	1.00	2.51	3.325(2)	138.4

Symmetry transformations used to generate equivalent atoms:

#1 x-1/2,-y+1/2,-z+1 #2 x-1,y,z #3 x+1/2,-y+1/2,-z+1

#4 -x+1,y-1/2,-z+3/2

A8.7.2 X-Ray Crystal Structure Analysis of Fluoride 369

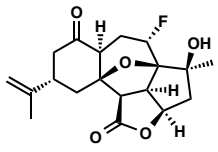

369

Contents

Table A8.7.2.1. Experimental Details

Table A8.7.2.2. Crystal Data

Table A8.7.2.3. Atomic Coordinates

Table A8.7.2.4. Full Bond Distances and Angles

Table A8.7.2.5. Anisotropic Displacement Parameters

Table A8.7.2.6. Hydrogen Atomic Coordinates

Table A8.7.2.7. Torsion Angles

Table A8.7.2.8. Hydrogen Bond Distances and Angles

Figure A8.7.2.1. X-Ray Crystal Structure of Fluoride ***369***

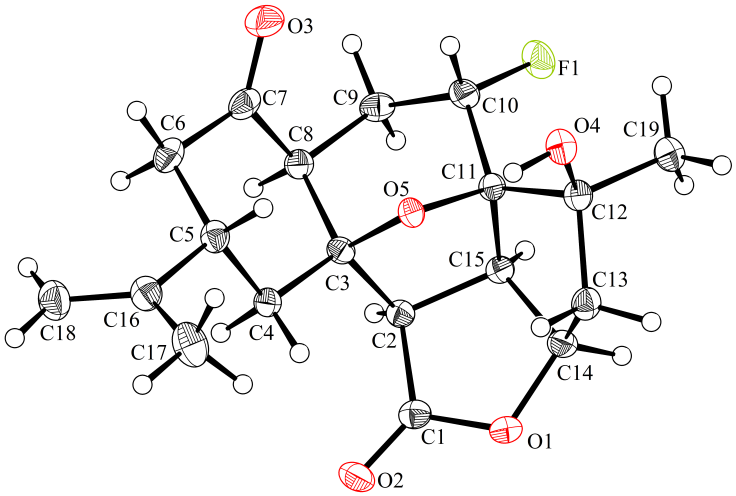

Table A8.7.2.1. Experimental Details for X-Ray Structure Determination of Fluoride ***369****.*

Low-temperature diffraction data (ϕ-and ω-scans) were collected on a Bruker AXS D8 VENTURE KAPPA diffractometer coupled to a PHOTON 100 CMOS detector with Cu K_α radiation (λ = 1.54178 Å) from an IμS micro-source for the structure of fluoride **369**. The structure was solved by direct methods using SHELXS[12] and refined against F^2 on all data by full-matrix least squares with SHELXL-2014[13] using established refinement techniques.[14] All non-hydrogen atoms were refined anisotropically. Unless otherwise noted, all hydrogen atoms were included into the model at geometrically calculated positions and refined using a riding model. The isotropic displacement parameters of all hydrogen atoms were fixed to 1.2 times the U value of the atoms they are linked to (1.5 times for methyl groups).

Fluoride **369** crystallizes in the orthorhombic space group $P2_12_12_1$ with one molecule in the asymmetric unit. The coordinates for the hydrogen atom bound to O4 were located in the difference Fourier synthesis and refined semi-freely with the help of a restraint on the O-H distance (0.84(4) Å).

*Table A8.7.2.2. Crystal Data and Structure Refinement for Fluoride **369**.*

Identification code	P15151	
CCDC Deposition Number	1061353	
Empirical formula	C19 H23 F O5	
Formula weight	350.37	
Temperature	100(2) K	
Wavelength	1.54178 Å	
Crystal system	Orthorhombic	
Space group	$P2_12_12_1$	
Unit cell dimensions	a = 8.1325(2) Å	α= 90°.
	b = 10.5090(3) Å	β= 90°.
	c = 19.6596(5) Å	γ = 90°.
Volume	1680.20(8) $Å^3$	
Z	4	
Density (calculated)	1.385 Mg/m^3	
Absorption coefficient	0.891 mm^{-1}	
F(000)	744	
Crystal size	0.400 x 0.300 x 0.250 mm^3	
Theta range for data collection	4.498 to 74.493°.	
Index ranges	$-9 \le h \le 10, -12 \le k \le 12, -24 \le l \le 24$	
Reflections collected	16744	
Independent reflections	3389 [R(int) = 0.0435]	
Completeness to theta = 67.679°	99.9 %	
Absorption correction	Semi-empirical from equivalents	
Max. and min. transmission	0.7542 and 0.6923	
Refinement method	Full-matrix least-squares on F^2	
Data / restraints / parameters	3389 / 1 / 231	
Goodness-of-fit on F^2	1.055	
Final R indices [I>2sigma(I)]	R1 = 0.0322, wR2 = 0.0713	
R indices (all data)	R1 = 0.0389, wR2 = 0.0745	
Absolute structure parameter	0.06(8)	
Extinction coefficient	n/a	
Largest diff. peak and hole	0.161 and -0.205 $e.Å^{-3}$	

*Table A8.7.2.3. Atomic coordinates (x 10^4) and equivalent isotropic displacement parameters ($Å^2$x 10^3) for Fluoride **369**. U(eq) is defined as one third of the trace of the orthogonalized U^{ij} tensor.*

	x	y	z	U(eq)
O(1)	-520(2)	4008(2)	1300(1)	22(1)
C(1)	323(3)	4685(2)	1766(1)	18(1)
O(2)	-378(2)	5405(2)	2146(1)	25(1)
C(2)	2157(3)	4430(2)	1720(1)	16(1)
C(3)	2851(3)	3668(2)	2336(1)	15(1)
O(5)	2600(2)	2363(1)	2136(1)	15(1)
C(4)	1963(3)	3869(2)	3008(1)	18(1)
C(5)	2652(3)	3039(2)	3584(1)	19(1)
C(16)	1667(3)	3245(2)	4229(1)	22(1)
C(17)	76(3)	2526(2)	4262(1)	31(1)
C(18)	2131(4)	4013(2)	4728(1)	29(1)
C(6)	4502(3)	3301(2)	3661(1)	22(1)
C(7)	5333(3)	3042(2)	2992(1)	21(1)
O(3)	6358(2)	2210(2)	2920(1)	29(1)
C(8)	4734(3)	3845(2)	2395(1)	18(1)
C(9)	5598(3)	3481(2)	1730(1)	20(1)
C(10)	4912(3)	2261(2)	1424(1)	19(1)
F(1)	5530(2)	2168(1)	751(1)	27(1)
C(11)	3049(3)	2285(2)	1425(1)	15(1)
C(12)	2014(3)	1174(2)	1144(1)	18(1)
O(4)	2148(2)	80(1)	1566(1)	21(1)
C(19)	2510(3)	751(2)	432(1)	22(1)
C(13)	281(3)	1763(2)	1138(1)	20(1)
C(14)	545(3)	3147(2)	925(1)	19(1)
C(15)	2320(3)	3502(2)	1120(1)	15(1)

*Table A8.7.2.4. Bond lengths [Å] and angles [°] for Fluoride **369**.*

O(1)-C(1)	1.348(3)
O(1)-C(14)	1.453(3)
C(1)-O(2)	1.206(3)
C(1)-C(2)	1.518(3)
C(2)-C(15)	1.535(3)
C(2)-C(3)	1.558(3)
C(2)-H(2)	1.0000
C(3)-O(5)	1.441(2)
C(3)-C(4)	1.520(3)
C(3)-C(8)	1.547(3)
O(5)-C(11)	1.446(2)
C(4)-C(5)	1.536(3)
C(4)-H(4A)	0.9900
C(4)-H(4B)	0.9900
C(5)-C(16)	1.515(3)
C(5)-C(6)	1.537(3)
C(5)-H(5)	1.0000
C(16)-C(18)	1.324(3)
C(16)-C(17)	1.499(4)
C(17)-H(17A)	0.9800
C(17)-H(17B)	0.9800
C(17)-H(17C)	0.9800
C(18)-H(18A)	0.9500
C(18)-H(18B)	0.9500
C(6)-C(7)	1.504(3)
C(6)-H(6A)	0.9900
C(6)-H(6B)	0.9900
C(7)-O(3)	1.216(3)
C(7)-C(8)	1.525(3)
C(8)-C(9)	1.534(3)
C(8)-H(8)	1.0000
C(9)-C(10)	1.522(3)
C(9)-H(9A)	0.9900

Table A8.7.2.4. (cont'd)

C(9)-H(9B)	0.9900
C(10)-F(1)	1.420(2)
C(10)-C(11)	1.516(3)
C(10)-H(10)	1.0000
C(11)-C(15)	1.531(3)
C(11)-C(12)	1.541(3)
C(12)-O(4)	1.422(3)
C(12)-C(19)	1.524(3)
C(12)-C(13)	1.540(3)
O(4)-H(4O)	0.85(2)
C(19)-H(19A)	0.9800
C(19)-H(19B)	0.9800
C(19)-H(19C)	0.9800
C(13)-C(14)	1.529(3)
C(13)-H(13A)	0.9900
C(13)-H(13B)	0.9900
C(14)-C(15)	1.540(3)
C(14)-H(14)	1.0000
C(15)-H(15)	1.0000

C(1)-O(1)-C(14)	111.72(17)
O(2)-C(1)-O(1)	120.8(2)
O(2)-C(1)-C(2)	127.7(2)
O(1)-C(1)-C(2)	111.48(18)
C(1)-C(2)-C(15)	104.06(17)
C(1)-C(2)-C(3)	113.58(17)
C(15)-C(2)-C(3)	103.84(16)
C(1)-C(2)-H(2)	111.6
C(15)-C(2)-H(2)	111.6
C(3)-C(2)-H(2)	111.6
O(5)-C(3)-C(4)	107.56(17)
O(5)-C(3)-C(8)	105.95(17)
C(4)-C(3)-C(8)	112.82(18)
O(5)-C(3)-C(2)	103.01(16)

Table A8.7.2.4. (cont'd)

C(4)-C(3)-C(2)	115.65(18)
C(8)-C(3)-C(2)	110.84(17)
C(3)-O(5)-C(11)	106.39(15)
C(3)-C(4)-C(5)	112.92(18)
C(3)-C(4)-H(4A)	109.0
C(5)-C(4)-H(4A)	109.0
C(3)-C(4)-H(4B)	109.0
C(5)-C(4)-H(4B)	109.0
H(4A)-C(4)-H(4B)	107.8
C(16)-C(5)-C(4)	110.08(18)
C(16)-C(5)-C(6)	114.20(18)
C(4)-C(5)-C(6)	109.14(18)
C(16)-C(5)-H(5)	107.7
C(4)-C(5)-H(5)	107.7
C(6)-C(5)-H(5)	107.7
C(18)-C(16)-C(17)	121.4(2)
C(18)-C(16)-C(5)	123.7(2)
C(17)-C(16)-C(5)	114.85(19)
C(16)-C(17)-H(17A)	109.5
C(16)-C(17)-H(17B)	109.5
H(17A)-C(17)-H(17B)	109.5
C(16)-C(17)-H(17C)	109.5
H(17A)-C(17)-H(17C)	109.5
H(17B)-C(17)-H(17C)	109.5
C(16)-C(18)-H(18A)	120.0
C(16)-C(18)-H(18B)	120.0
H(18A)-C(18)-H(18B)	120.0
C(7)-C(6)-C(5)	108.75(18)
C(7)-C(6)-H(6A)	109.9
C(5)-C(6)-H(6A)	109.9
C(7)-C(6)-H(6B)	109.9
C(5)-C(6)-H(6B)	109.9
H(6A)-C(6)-H(6B)	108.3
O(3)-C(7)-C(6)	122.7(2)

Table A8.7.2.4. (cont'd)

O(3)-C(7)-C(8)	121.9(2)
C(6)-C(7)-C(8)	115.39(19)
C(7)-C(8)-C(9)	111.84(18)
C(7)-C(8)-C(3)	107.94(18)
C(9)-C(8)-C(3)	111.03(17)
C(7)-C(8)-H(8)	108.7
C(9)-C(8)-H(8)	108.7
C(3)-C(8)-H(8)	108.7
C(10)-C(9)-C(8)	112.27(18)
C(10)-C(9)-H(9A)	109.1
C(8)-C(9)-H(9A)	109.1
C(10)-C(9)-H(9B)	109.1
C(8)-C(9)-H(9B)	109.1
H(9A)-C(9)-H(9B)	107.9
F(1)-C(10)-C(11)	110.88(17)
F(1)-C(10)-C(9)	107.22(17)
C(11)-C(10)-C(9)	110.58(18)
F(1)-C(10)-H(10)	109.4
C(11)-C(10)-H(10)	109.4
C(9)-C(10)-H(10)	109.4
O(5)-C(11)-C(10)	104.74(16)
O(5)-C(11)-C(15)	103.46(16)
C(10)-C(11)-C(15)	113.61(17)
O(5)-C(11)-C(12)	104.58(16)
C(10)-C(11)-C(12)	122.18(18)
C(15)-C(11)-C(12)	106.30(17)
O(4)-C(12)-C(19)	106.25(17)
O(4)-C(12)-C(13)	113.55(18)
C(19)-C(12)-C(13)	110.65(19)
O(4)-C(12)-C(11)	111.19(17)
C(19)-C(12)-C(11)	113.95(19)
C(13)-C(12)-C(11)	101.43(17)
C(12)-O(4)-H(4O)	106.8(19)
C(12)-C(19)-H(19A)	109.5

Table A8.7.2.4. (cont'd)

C(12)-C(19)-H(19B)	109.5
H(19A)-C(19)-H(19B)	109.5
C(12)-C(19)-H(19C)	109.5
H(19A)-C(19)-H(19C)	109.5
H(19B)-C(19)-H(19C)	109.5
C(14)-C(13)-C(12)	104.81(18)
C(14)-C(13)-H(13A)	110.8
C(12)-C(13)-H(13A)	110.8
C(14)-C(13)-H(13B)	110.8
C(12)-C(13)-H(13B)	110.8
H(13A)-C(13)-H(13B)	108.9
O(1)-C(14)-C(13)	111.64(18)
O(1)-C(14)-C(15)	106.35(17)
C(13)-C(14)-C(15)	107.06(18)
O(1)-C(14)-H(14)	110.6
C(13)-C(14)-H(14)	110.6
C(15)-C(14)-H(14)	110.6
C(11)-C(15)-C(2)	105.30(16)
C(11)-C(15)-C(14)	104.98(17)
C(2)-C(15)-C(14)	105.34(17)
C(11)-C(15)-H(15)	113.5
C(2)-C(15)-H(15)	113.5
C(14)-C(15)-H(15)	113.5

Symmetry transformations used to generate equivalent atoms:

*Table A8.7.2.5. Anisotropic displacement parameters ($Å^2x10^3$) for Fluoride **369**. The anisotropic displacement factor exponent takes the form: $-2\pi^2[h^2a^{*2}U^{11} + ... + 2hka^*b^*U^{12}]$.*

	U^{11}	U^{22}	U^{33}	U^{23}	U^{13}	U^{12}
O(1)	16(1)	25(1)	23(1)	-1(1)	-2(1)	4(1)
C(1)	19(1)	19(1)	17(1)	5(1)	1(1)	2(1)
O(2)	28(1)	25(1)	21(1)	0(1)	4(1)	10(1)
C(2)	17(1)	15(1)	16(1)	1(1)	1(1)	1(1)
C(3)	16(1)	13(1)	17(1)	0(1)	1(1)	0(1)
O(5)	17(1)	15(1)	13(1)	0(1)	2(1)	-2(1)
C(4)	19(1)	19(1)	14(1)	0(1)	0(1)	2(1)
C(5)	24(1)	18(1)	16(1)	1(1)	-1(1)	0(1)
C(16)	30(1)	21(1)	16(1)	4(1)	-1(1)	3(1)
C(17)	40(2)	32(1)	21(1)	0(1)	9(1)	-5(1)
C(18)	36(2)	30(1)	20(1)	-3(1)	-1(1)	2(1)
C(6)	25(1)	22(1)	20(1)	3(1)	-7(1)	-1(1)
C(7)	17(1)	18(1)	28(1)	0(1)	-6(1)	-4(1)
O(3)	28(1)	25(1)	35(1)	1(1)	-7(1)	7(1)
C(8)	17(1)	16(1)	20(1)	-1(1)	-1(1)	-1(1)
C(9)	13(1)	22(1)	26(1)	2(1)	2(1)	-2(1)
C(10)	17(1)	24(1)	15(1)	1(1)	5(1)	1(1)
F(1)	26(1)	36(1)	19(1)	-4(1)	8(1)	-2(1)
C(11)	16(1)	18(1)	12(1)	1(1)	1(1)	1(1)
C(12)	19(1)	18(1)	16(1)	1(1)	1(1)	-1(1)
O(4)	27(1)	17(1)	19(1)	1(1)	1(1)	-2(1)
C(19)	25(1)	23(1)	19(1)	-2(1)	2(1)	0(1)
C(13)	17(1)	22(1)	20(1)	-2(1)	0(1)	-5(1)
C(14)	19(1)	22(1)	16(1)	0(1)	1(1)	5(1)
C(15)	14(1)	18(1)	13(1)	2(1)	2(1)	0(1)

*Table A8.7.2.6. Hydrogen coordinates ($x10^4$) and isotropic displacement parameters ($Å^2x10^3$) for Fluoride **369**.*

	x	y	z	U(eq)
H(2)	2792	5230	1639	19
H(4A)	782	3672	2946	21
H(4B)	2054	4775	3140	21
H(5)	2518	2129	3447	23
H(17A)	-533	2782	4670	46
H(17B)	303	1611	4281	46
H(17C)	-581	2716	3857	46
H(18A)	1451	4117	5117	35
H(18B)	3144	4459	4696	35
H(6A)	4681	4198	3796	27
H(6B)	4971	2745	4019	27
H(8)	4970	4760	2495	21
H(9A)	5468	4182	1398	24
H(9B)	6788	3371	1818	24
H(10)	5305	1516	1696	23
H(4O)	1790(30)	290(30)	1956(11)	31
H(19A)	3638	424	441	34
H(19B)	2448	1478	120	34
H(19C)	1763	80	276	34
H(13A)	-438	1316	810	24
H(13B)	-227	1717	1596	24
H(14)	374	3247	424	23
H(15)	2976	3851	733	18

*Table A8.7.2.7. Torsion angles [°] for Fluoride **369**.*

C(14)-O(1)-C(1)-O(2)	-176.52(19)
C(14)-O(1)-C(1)-C(2)	4.8(2)
O(2)-C(1)-C(2)-C(15)	-176.6(2)
O(1)-C(1)-C(2)-C(15)	2.0(2)
O(2)-C(1)-C(2)-C(3)	71.2(3)
O(1)-C(1)-C(2)-C(3)	-110.26(19)
C(1)-C(2)-C(3)-O(5)	87.1(2)
C(15)-C(2)-C(3)-O(5)	-25.2(2)
C(1)-C(2)-C(3)-C(4)	-29.9(3)
C(15)-C(2)-C(3)-C(4)	-142.27(19)
C(1)-C(2)-C(3)-C(8)	-159.93(17)
C(15)-C(2)-C(3)-C(8)	87.7(2)
C(4)-C(3)-O(5)-C(11)	164.65(17)
C(8)-C(3)-O(5)-C(11)	-74.44(19)
C(2)-C(3)-O(5)-C(11)	42.0(2)
O(5)-C(3)-C(4)-C(5)	62.6(2)
C(8)-C(3)-C(4)-C(5)	-53.9(2)
C(2)-C(3)-C(4)-C(5)	177.01(18)
C(3)-C(4)-C(5)-C(16)	-177.60(19)
C(3)-C(4)-C(5)-C(6)	56.3(2)
C(4)-C(5)-C(16)-C(18)	-98.4(3)
C(6)-C(5)-C(16)-C(18)	24.8(3)
C(4)-C(5)-C(16)-C(17)	80.4(2)
C(6)-C(5)-C(16)-C(17)	-156.4(2)
C(16)-C(5)-C(6)-C(7)	179.10(17)
C(4)-C(5)-C(6)-C(7)	-57.2(2)
C(5)-C(6)-C(7)-O(3)	-116.6(2)
C(5)-C(6)-C(7)-C(8)	60.1(2)
O(3)-C(7)-C(8)-C(9)	-1.0(3)
C(6)-C(7)-C(8)-C(9)	-177.74(19)
O(3)-C(7)-C(8)-C(3)	121.4(2)
C(6)-C(7)-C(8)-C(3)	-55.3(2)
O(5)-C(3)-C(8)-C(7)	-67.1(2)
C(4)-C(3)-C(8)-C(7)	50.4(2)

Table A8.7.2.7. (cont'd)

C(2)-C(3)-C(8)-C(7)	-178.14(16)
O(5)-C(3)-C(8)-C(9)	55.8(2)
C(4)-C(3)-C(8)-C(9)	173.27(17)
C(2)-C(3)-C(8)-C(9)	-55.2(2)
C(7)-C(8)-C(9)-C(10)	77.4(2)
C(3)-C(8)-C(9)-C(10)	-43.2(2)
C(8)-C(9)-C(10)-F(1)	167.49(17)
C(8)-C(9)-C(10)-C(11)	46.5(2)
C(3)-O(5)-C(11)-C(10)	77.75(19)
C(3)-O(5)-C(11)-C(15)	-41.5(2)
C(3)-O(5)-C(11)-C(12)	-152.64(17)
F(1)-C(10)-C(11)-O(5)	179.29(15)
C(9)-C(10)-C(11)-O(5)	-61.9(2)
F(1)-C(10)-C(11)-C(15)	-68.5(2)
C(9)-C(10)-C(11)-C(15)	50.3(2)
F(1)-C(10)-C(11)-C(12)	61.0(2)
C(9)-C(10)-C(11)-C(12)	179.84(18)
O(5)-C(11)-C(12)-O(4)	-49.3(2)
C(10)-C(11)-C(12)-O(4)	69.1(2)
C(15)-C(11)-C(12)-O(4)	-158.33(17)
O(5)-C(11)-C(12)-C(19)	-169.30(17)
C(10)-C(11)-C(12)-C(19)	-51.0(3)
C(15)-C(11)-C(12)-C(19)	81.6(2)
O(5)-C(11)-C(12)-C(13)	71.78(19)
C(10)-C(11)-C(12)-C(13)	-169.90(18)
C(15)-C(11)-C(12)-C(13)	-37.3(2)
O(4)-C(12)-C(13)-C(14)	157.13(17)
C(19)-C(12)-C(13)-C(14)	-83.5(2)
C(11)-C(12)-C(13)-C(14)	37.8(2)
C(1)-O(1)-C(14)-C(13)	106.9(2)
C(1)-O(1)-C(14)-C(15)	-9.6(2)
C(12)-C(13)-C(14)-O(1)	-140.96(18)
C(12)-C(13)-C(14)-C(15)	-25.0(2)
O(5)-C(11)-C(15)-C(2)	23.5(2)

Table A8.7.2.7. (cont'd)

C(10)-C(11)-C(15)-C(2)	-89.5(2)
C(12)-C(11)-C(15)-C(2)	133.31(18)
O(5)-C(11)-C(15)-C(14)	-87.47(18)
C(10)-C(11)-C(15)-C(14)	159.57(17)
C(12)-C(11)-C(15)-C(14)	22.4(2)
C(1)-C(2)-C(15)-C(11)	-118.06(18)
C(3)-C(2)-C(15)-C(11)	1.0(2)
C(1)-C(2)-C(15)-C(14)	-7.4(2)
C(3)-C(2)-C(15)-C(14)	111.71(18)
O(1)-C(14)-C(15)-C(11)	121.12(17)
C(13)-C(14)-C(15)-C(11)	1.6(2)
O(1)-C(14)-C(15)-C(2)	10.2(2)
C(13)-C(14)-C(15)-C(2)	-109.25(18)

Symmetry transformations used to generate equivalent atoms:

*Table A8.7.2.8. Hydrogen bonds for Fluoride **369** [Å and °].*

D-H...A	d(D-H)	d(H...A)	d(D...A)	<(DHA)
C(2)-H(2)...O(3)#1	1.00	2.36	3.239(3)	146.7
C(9)-H(9B)...O(1)#2	0.99	2.51	3.315(3)	138.8
C(10)-H(10)...O(3)	1.00	2.66	3.168(3)	111.9
O(4)-H(4O)...O(2)#3	0.85(2)	2.11(2)	2.933(2)	163(3)
C(14)-H(14)...F(1)#4	1.00	2.35	3.310(2)	159.9

Symmetry transformations used to generate equivalent atoms:

#1 -x+1,y+1/2,-z+1/2 #2 x+1,y,z #3 -x,y-1/2,-z+1/2

#4 x-1/2,-y+1/2,-z

A8.8 Notes and References

1. (a) Chen, L.; Deslongchamps, P. *Can. J. Chem.* **2005**, *83*, 728–740. (b) González, M. A.; Ghosh, S.; Rivas, F.; Fischer, D.; Theodorakis, E. A. *Tetrahedron Lett.* **2004**, *45*, 5039–5041. (c) Chen, J.; Marx, J. N. *Tetrahedron Lett.* **1997**, *38*, 1889–1892.

2. See Chapter 3, Section 3.3 for a description of this transformation which produces the ethyl variant of ester **358** and Section 3.9.2 for the associated full experimental details.

3. Malik, H. A.; Taylor, B. L. H.; Kerrigan, J. R.; Grob, J. E.; Houk, K. N.; Du Bois, J.; Hamann, L. G.; Patterson, A. W. *Chem. Sci.* **2014**, *5*, 2352–2361.

4. Fringuelli, F.; Pizzo, F.; Tortoioli, S.; Vaccaro, L. *J. Org. Chem.* **2003**, *68*, 8248–8251.

5. Tentative structural identification of furan **366** was accomplished by 2-dimensional ^{1}H NMR analysis.

6. For a thorough discussion of this attempted transformation, see chapter 3, sections 3.5 and 3.7.

7. Vankar, Y. D.; Arya, P. S.; Rao, C. T. *Synth. Commun.* **1983**, *13*, 869–872.

8. The opening of an epoxide with BF_3•Et_2O has been previously observed, see: Maruoka, K.; Murase, N.; Bureau, R.; Ooi, T.; Yamamoto, H. *Tetrahedron* **1994**, *50*, 3663–3672.

9. (a) Ly, T. W.; Liao, J.-H.; Shia, K.-S.; Liu, H.-J. *Synthesis* **2004**, 271–275. (b) Paisdor, B.; Kuck, D. *J. Org. Chem.* **1991**, *56*, 4753–4759. (c) Paritosh, D.; Byun, H.-S.; Engel, R. *Synth. Commun.* **1986**, *16*, 1343–1346. (d) Mancuso, A. J.;

Swern, D. *Synthesis* **1981**, 165–185. (e) Kornblum, N.; Jones, W. J.; Anderson, G. J. *J. Am. Chem. Soc.* **1959**, *81*, 4113–4114.

10. For full characterization data associated with 1,4-diketone **347**, see Chapter 3, section 3.9.2.

11. Pangborn, A. B.; Giardello, M. A.; Grubbs, R. H.; Rosen, R. K.; Timmers, F. J. *Organometallics* **1996**, *15*, 1518–1520.

12. Sheldrick, G. M. *Acta Cryst.* **1990**, A46, 467–473.

13. Sheldrick, G. M. *Acta Cryst.* **2008**, A64, 112–122.

14. Müller, P. *Crystallography Reviews* **2009**, *15*, 57–83.

CHAPTER 4

Revised Plan for the Synthesis of Ineleganolide: Alternative Advancement Toward the Asymmetric Total Synthesis of Ineleganolide by Late-Stage Oxidation State Manipulation

4.1 Revised Retrosynthetic Analysis – Conjugate Reduction

Having completed an effective synthesis of the carbocyclic core of ineleganolide, yet unable to advance the olefin migration strategy further, we envisioned an alternative completion of the asymmetric total synthesis of *ent*-ineleganolide (***ent*-9**). Our new plan could proceed through the identical late-stage vinylogous diketone **330**, furnishing the natural product following an intramolecular oxa-Michael addition (Scheme 4.1.1). Rather than by olefin isomerization, we envisioned synthesizing endione **330** by the oxidation of saturated 1,4-diketone **370**, which would be formed by a *syn*-facial 1,2-hydride shift from epoxide **371**. Ketone **371** would be synthesized by the sequential conjugate reduction and hydroxyl-directed epoxidation from diene **324**.

Scheme 4.1.1. Adapted Retrosynthetic Analysis of ent-Ineleganolide with Late-Stage Oxidation

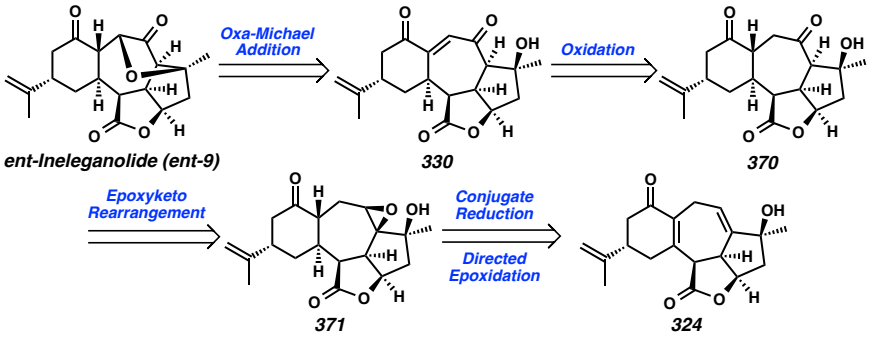

4.2 Exploration of Conjugate Reduction Pathway

The conjugate reduction of the tetrasubstituted enone moiety within tetracyclic triene **324** proved nontrivial. All attempts to reduce the conjugated system using metal hydride sources failed, likely due to the steric environment surrounding the fully-substituted β-position. Alternatively, we were pleased to discover the use of samarium diiodide was a suitable reductant to enable the formation of ketoalcohol **372** (Scheme 4.2.1). The use of water as an additive proved crucial for this transformation. While the absence of an additive or the addition of MeOH, *t*-BuOH, LiCl, or fewer equivalents of H_2O prevented the complete consumption of starting material, the addition of HMPA or the use of additional equivalents of H_2O resulted in diminished yield of tetracycle **372**.

*Scheme 4.2.1. Conjugate Reduction of Diene **324***

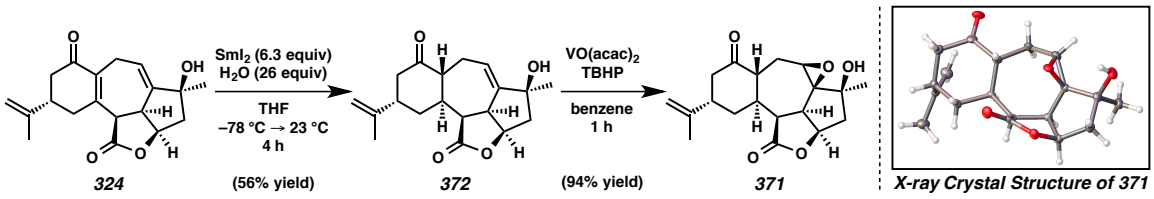

The hydroxyl-directed epoxidation of cycloheptene **372** was then accomplished under vanadium-catalyzed conditions to provide epoxide **371** in 94% yield. Tetracycle **371** proved to be a crystalline white solid, enabling the unambiguous determination of

configuration by single-crystal X-ray diffraction. This crystal structure confirmed the assignment of both the epoxide, being correctly directed to the β-face of the molecule, and also the configuration of the *trans*-fusion at the A,B-ring junction, matching that found in *ent*-ineleganolide (***ent*-9**).

Similar to our experiences with related epoxide 328 (see Chapter 3, Scheme 3.5.2), advancement of epoxide **371** to diketone **373** through an epoxide rearrangement proved unfruitful under a variety of Lewis acidic conditions (Scheme 4.2.2). Thus, we sought alternative access to diketone **373** employing the method used successfully in the synthesis of isoineleganolide C (***ent*-313**, see Chapter 3, Section 3.7). Epoxide **371** was first opened with magnesium(II) bromide to provide bromohydrin **374** in 80% yield (Scheme 4.2.3). Unfortunately, Kornblum oxidation conditions failed to install the desired ketone at C(6).[1,2] This result reenforces our hypothesis that the furan bridge in pentacycle **347** is critical for the efficacy of the Kornblum oxidation of secondary bromide **346** en route to isoineleganolide C (***ent*-313**, see Scheme 3.7.3).

*Scheme 4.2.2. Unsuccessful Epoxide Rearrangement of Epoxide **371***

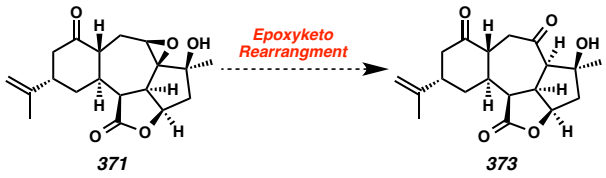

*Scheme 4.2.3. Attempted Kornblum Oxidation of Epoxide **371***

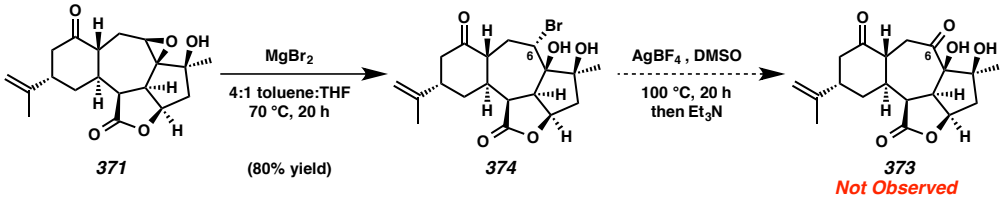

In place of a bromohydrin strategy to access diketone **373**, we began to pursue a reductive epoxide opening strategy employing stoichiometric Cp_2TiCl, which is

generated in situ from $CpTiCl_2$ and a reductant.[3] Initial exploration of this reductive epoxide opening proved immediately successful (Scheme 4.2.4). The use of H_2O as an additive results in the formation of the Cp_2TiCl aquo complex and thereby provides a sacrificial hydrogen atom donor.[3a,4] Subsequent oxidation under optimized conditions using DMP in DCE at elevated temperature provided 2*H*-ineleganolide (**373**) in 33% yield over two steps with the translactonized ketone **375** isolated in equivalent amounts. The structures of both 2*H*-ineleganolide (**373**) and lactone **375** were unambiguously determined by single crystal X-ray diffraction, confirming the relative configuration at C(7) by reductive epoxide.

Scheme 4.2.4. Sequential Reductive Epoxide Opening and Carbinol Oxidation

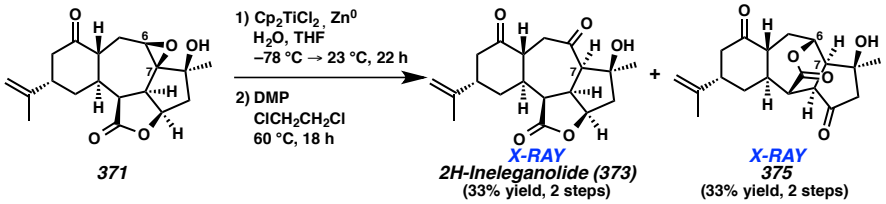

In order to explore the conformational constraints of 2*H*-ineleganolide (**373**), we explored the in vacuo ground state energy (DFT/B3LYP/6-311+G**) of four different conformational isomers: **373**^{ax} and **373**^{equ} and **373A**^{ax} and **373A**^{equ} (Figure 4.2.1).[5] The two conformations in which the cyclohexanone ring adopts a chair conformation, placing the isopropenyl substituent in the axial position (**373**^{ax} and **373A**^{ax}) are calculated to be energetically equivalent in the ground state, within the error of the calculation method (±0.23 kcal/mol), and have the lowest ground state energies of the calculated isomers, mirroring the preferred conformation of *ent*-ineleganolide (***ent*-9**^{ax}, see Figure 3.8.1). The difference in energy between **373**^{ax} and **373A**^{ax} and the corresponding equatorial conformations, **373**^{equ} and **373A**^{equ}, respectively, was calculated to be no more than 1.0

kcal/mol. Complimentarily, the X-ray crystal structure of the isolated 2*H*-ineleganlolide generated through our synthetic pathway shows **373**^{ax} is the preferred conformation. We were optimistic, however, that given the small ground state energy differences among these conformational isomers, we could induce an equilibrium between the isolated **373**^{ax} and one of the conformational isomers **373A**^{ax} or **373A**^{equ} en route the completion of the asymmetric total synthesis of *ent*-ineleganolide (***ent*-9**).

Figure 4.2.1. Computational Evaluation of Conformational Isomers of 2H-Ineleganolide

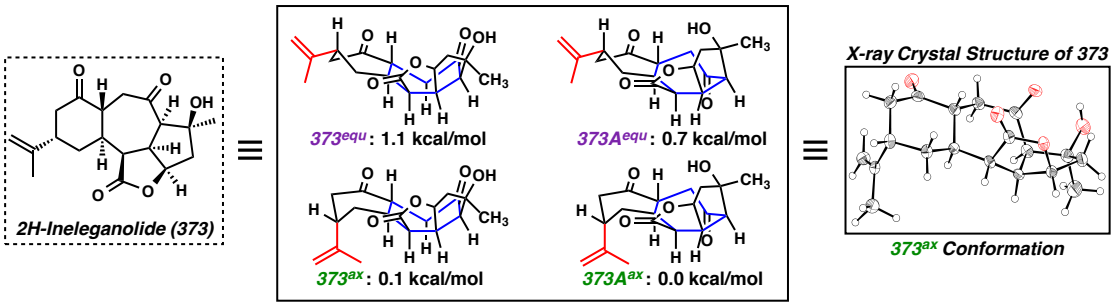

Toward this end, completion of the total synthesis would require the oxidation of 2*H*-ineleganolide (**373**) in order to install the final requisite C–O bond and construct the characteristic furan bridge of *ent*-ineleganolide (***ent*-9**). We envisioned accomplishing this transformation directly by C–H oxidation at C(5) (Scheme 4.2.5). We focused on the application of C–H oxidation methods that were known to accomplish the direct intramolecular formation a C–O bond from a free hydroxyl group. We tested methods based on the Suárez oxidation including the standard reaction conditions ($PhI(OAc)_2$, I_2, hν) and a series of modified Suarez oxidation conditions, which used mixed cyclohexane and dichloromethane solvent systems and exclude light.[6] Additionally, we attempted the oxidation of C(5) using lead(IV) acetate and light as well as with functionalized hypervalent iodine reagents such as PhI(OH)(OTs).[7] Unfortunately, all reaction conditions explored failed to provide any product that was successfully oxidized at C(5).

Scheme 4.2.5. Attempted C(5) Oxidation by C–H Activation

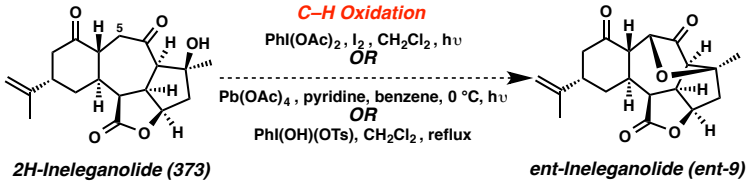

We also explored the potential to access ineleganolide through the oxidation of 2*H*-ineleganolide (**373**), proceeding through vinylogous diketone **330**, which we hypothesize would undergo a spontaneous intramolecular oxa-Michael addition to furnish *ent*-ineleganlide (***ent*-9**, Scheme 4.2.6). Oxidative desaturation could be accomplished through either selective kinetic deprotonation relative to the cycloheptanone carbonyl at C(5) or by "thermodynamic" enolization relative to the cycloheptanone carbonyl at C(4). Complicated by potential enolization at C(2) and C(7), all attempts to accomplish this transformation by direct oxidation using palladium(II) salts (e.g., $Pd(OAc)_2$, $Pd(TFA)_2$),[8] hypervalent iodine reagents (e.g., IBX),[9] or various selenides (e.g., $(PhSeO)_2O$, PhSeCl then H_2O_2) failed to yield any trace of intermediate **330** or *ent*-ineleganolide (***ent*-9**), typically resulting in selective functionalization at C(2).[10] Similar nonproductive reactivity was observed when attempting the C(4)–C(5) oxidation by a Saegusa–Ito oxidation.[11] In order to avoid the undesired functionalization of the cyclohexanone ring, we explored the selective reduction of the C(3) carbonyl. While the selective reduction of the C(3) ketone in the presence of the C(6) carbonyl of 2*H*-ineleganolide (**373**) could not be achieved, we sought to reduced the C(3) ketone at an earlier stage.

Scheme 4.2.6. Representative Reaction Conditions for Attempted C(4)–C(5) Oxidation

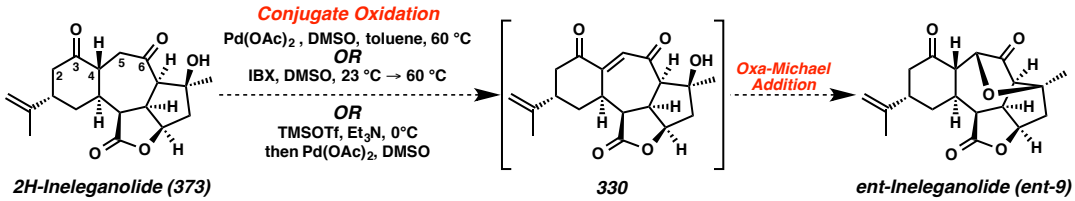

Stereoselective reduction of ketone **372** at C(3) was accomplished using L-selectride at low temperature (Scheme 4.2.7).[12] Subsequent silylation of the intermediate secondary alcohol provided tetracycle **376** in 79% yield over two steps. Epoxidation could then be smoothly accomplished to furnish epoxyalcohol **377** in 80% yield. Reductive epoxide opening of pentacycle **377** under optimized conditions using in situ generated titanium(III) resulted in concomitant translactonization, affording alcohol **378** in 66% yield as the sole product. Unable to manipulate lactone **379** further toward ineleganolide we again revised our retrosynthetic strategy.

*Scheme 4.2.7. Advancement of Tetracycle **372** by Diastereoselective C(3) Reduction*

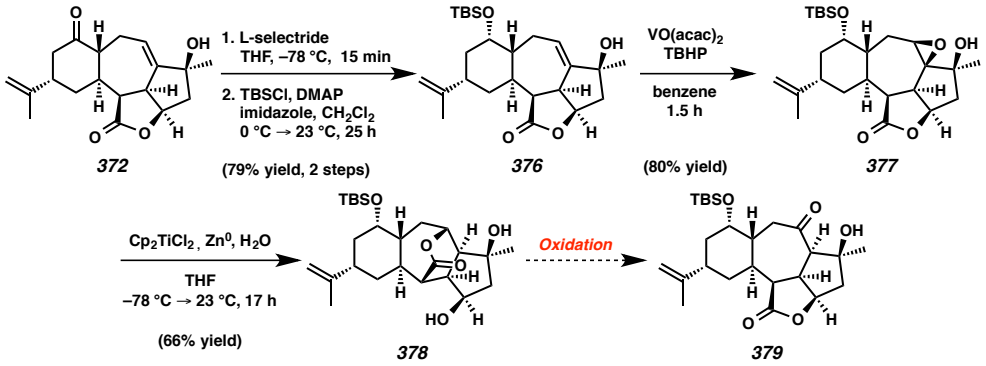

4.3 Revised Retrosynthetic Analysis – 1,2-Reduction

Armed with knowledge that selective late-stage functionalization of the tetracyclic core is complicated by the presence of the ketone functionality at C(3), we revised of our retrosynthetic strategy again. We envisioned accessing *ent*-ineleganolide (***ent*-9**) after oxidation of secondary alcohol **380** and ultimate intramolecular oxa-Michael addition

(Scheme 4.3.1). We anticipated enone **380** would be accessible by the isomerization of olefin **381** into conjugation with the isolated ketone at C(6) followed by deprotection of the masked secondary C(3) hydroxyl group. Ketone **381** would be synthesized after the stereoselective epoxide rearrangement or sequential reductive epoxide opening-oxidation from epoxide **382**, which would be accessible from isoineleganolide A (**328**) after selective 1,2-reduction of the conjugated system and subsequent protection.

Scheme 4.3.1. Retrosynthetic Analysis of ent-Ineleganolide Employing a 1,2-Reduction

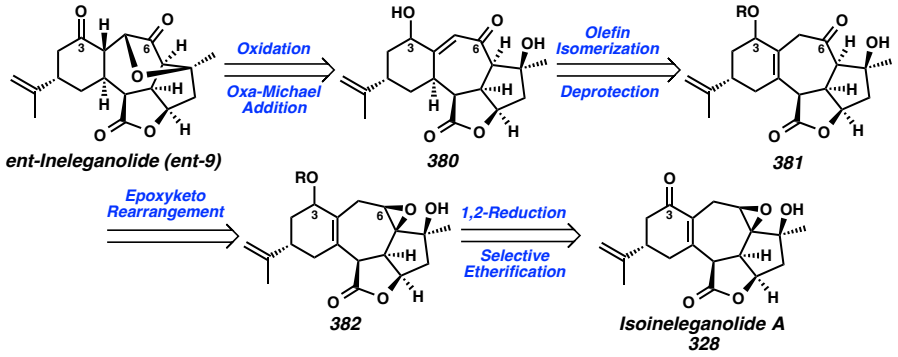

4.4 Exploration of 1,2-Reduction Pathway

Exploration of the revised synthetic route began with the development of conditions that could accomplish the chemoselective 1,2-reduction of cyclohexenone **328**. We were gratified to find that we could accomplish this transformation chemoselectively and diastereoselectively using sodium borohydride in a mixed CH_2Cl_2 and MeOH solvent system at low temperature to provide allylic alcohol **383** in quantitative yield as the sole product (Scheme 4.4.1).[13]

Scheme 4.4.1. 1,2-Reduction of Enone ***328***

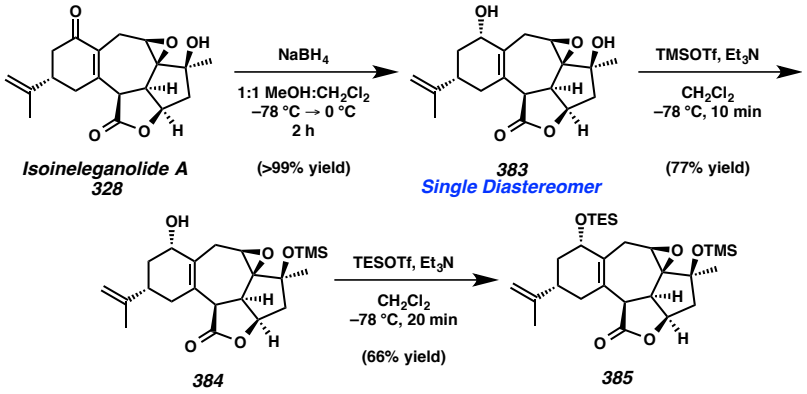

With alcohol **383** in hand, we sought to evaluate the potential to accomplish an epoxide rearrangement on this reduced system. To thoroughly evaluate this desired reactivity, selective protection of the hydroxyl groups on substrate **383** was accomplished, allowing for the isolation of monoprotected allylic alcohol **384** and disilyl ether **385**. Unfortunately, as with all other epoxides containing the [6,7,5,5]-core related to *ent*-ineleganolide, diol **383**, allylic alcohol **384**, and secondary silyl ether **385** all failed to undergo the desired 1,2-hydride shift (Scheme 4.4.2).

Scheme 4.4.2. Attempted Epoxide Rearrangement

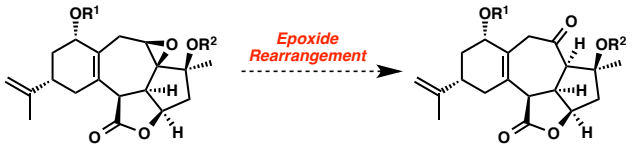

During this investigation, we sought to assess the reactivity of an analog of diol **383** that was functionalized with a silyl ether at solely the allylic secondary alcohol. Under standard imidazole-mediated silylation conditions employing a bulky silyl chloride, we were indeed able to synthesize silyl ether **389** in 26% yield (Scheme 4.4.3). We were surprised, however, to find allylic silyl ether **389** was the minor product. The remaining

portion of diol **383** had been converted to α,β-unstaured lactone **390** to provide unexpected epoxytetracycle **390** as the major product. Under optimized conditions, conjugated lactone **390** was produced in 74% yield.[14]

Scheme 4.4.3. Silyl Ether Formation with Unexpected Olefin Isomerization

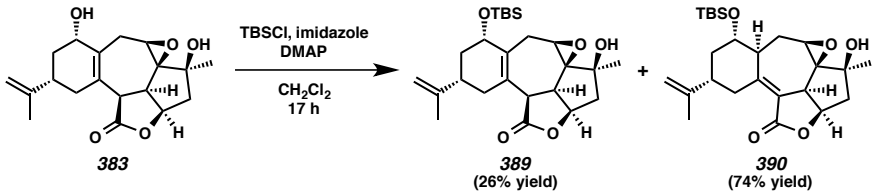

Intrigued by olefin isomerization product **390**, we tested configurational stability of the conjugated lactone. Deprotection of silyl ester **390** using TBAF provided secondary alcohol **391** in quantitative yield (Scheme 4.4.1). Unfortunately, oxidation of secondary alcohol **391** with DMP was accompanied by concomitant olefin migration back into conjugation at the [6,7] ring fusion providing isoineleganolide A (**328**) in 66% yield. No trace of the desired α,β-unsaturated lactone **392** was detected. Although this oxidative route proved unfruitful, simply returning the original enone starting material **328** after 4 synthetic transformations, we continued to investigate the utility of silyl ether isomers **389** and **390** in our synthetic efforts.

Scheme 4.4.4. Assessment of Configurational Stability of Unsaturated Lactone Moiety

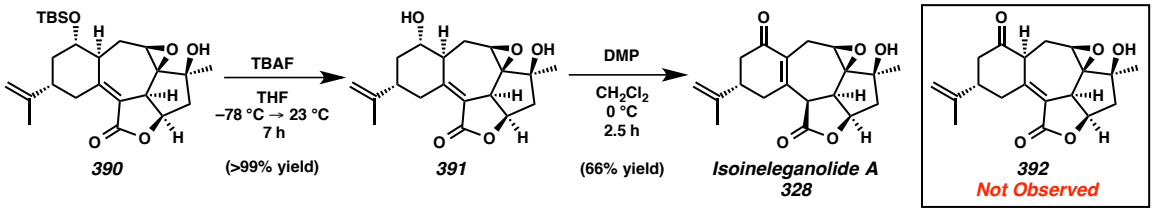

In order to advance allylic ether **389** or unsaturated lactone **390** toward ineleganolide, the epoxide moiety needed to be converted into the requisite C(6) ketone. Although diol **383**, the precursor to these isomer **389** and **390**, proved to be an unsuitable

substrate for titanium(III)-mediated reductive epoxide opening (Scheme 4.4.5.A),[15] both isomers **389** and **390** proved to be competent substrates for this transformation (Scheme 4.4.5).[16] Epoxide opening of allylic silyl ether **389** provided translactonized alcohol **393** as the sole product in 60% yield (Scheme 4.4.5.B). Subsequent oxidation failed to induce the desired retrotranslactontization, furnishing ketone **394** as the sole product that would not be useful for continued advancement toward *ent*-ineleganolide (***ent*-9**), without any trace of desired cycloheptanone **395**.

Scheme 4.4.5. Reductive Epoxide Opening of Isomeric Silyl Ethers

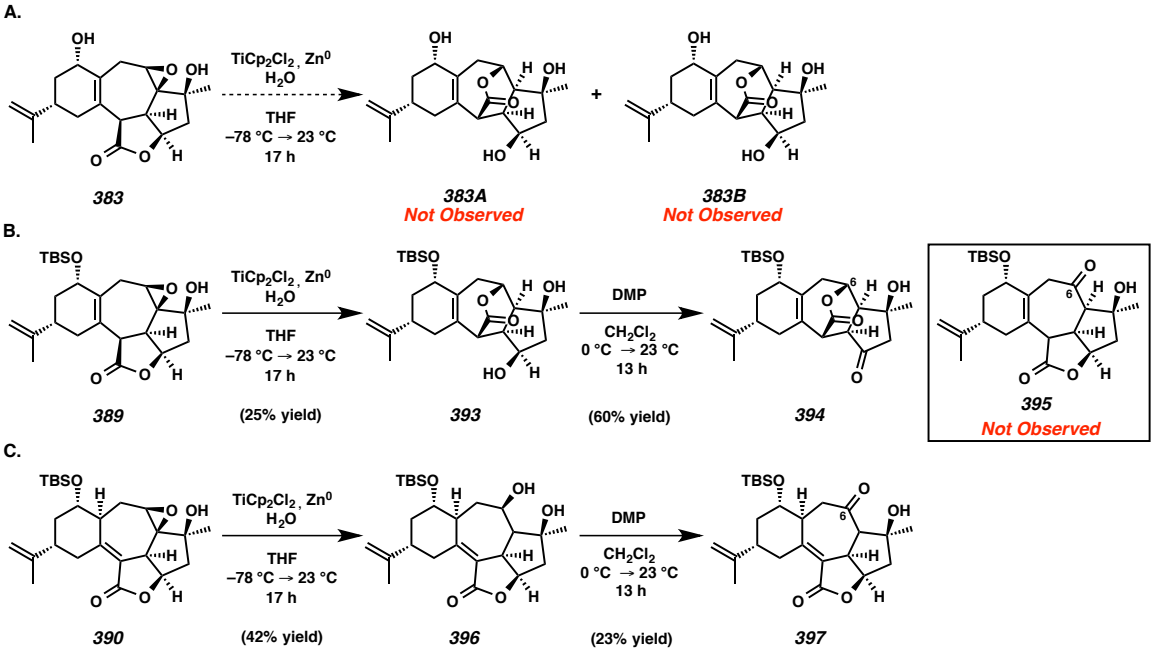

Alternatively, exposure of α,β-unsaturated lactone **390** to identical titanium(III) reductive conditions accomplished the desired epoxide opening while avoiding any translactontization, affording 1,3-diol **396** in 42% yield (Scheme 4.4.5.C).[16] Interestingly, under these reducing and Lewis acidic conditions, the reduction of the conjugated system (i.e., the α,β-unsaturated lactone) was not detected. Advancing diol **396** by oxidation of

the secondary alcohol with DMP smoothly provided ketone **397** in 23% yield as the sole product.

With ketone **397** in hand, we sought to accomplish the installation of the unsaturation required between C(4) and C(5) for the vinylogous diketone system and ultimate oxa-Michael addition to build the desired ketofuran bridge. Using TESOTf and Et_3N, we could indeed access desired enol ether **399**, albeit with undesired concomitant hydration of the α,β-unsaturated lactone (Scheme 4.4.6). Unfortunately, we were unable to advance further toward ineleganolide at this stage as the oxidation of this enol ether **399** could not be accomplished.[17]

*Scheme 4.4.6. Silyl Enol Ether Formation from Ketone **397***

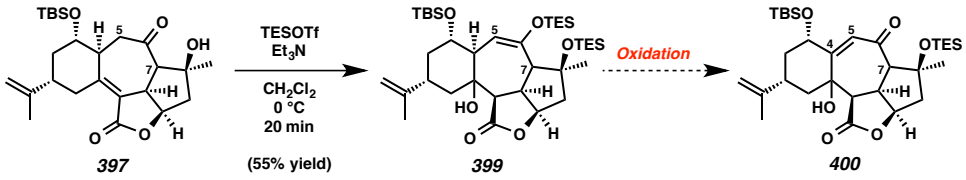

To test if the steric bulk of the disilylated enol ether **399** was preventing the oxidation, we performed the silyl ether formation stepwise. Tertiary alcohol **397** was first protected as TMS ether **401** (Scheme 4.4.7). Surprisingly, when ketone **401** was subjected to silyl enol ether formation conditions, although the starting material was fully consumed, no trace of either desired enol ether **402** or its hydrated analog were detected in the product mixture.[10]

*Scheme 4.4.7. Attempted Formation of TMS Enol Ether of Ketone **401***

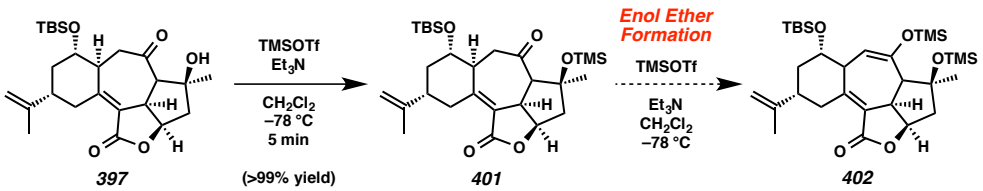

Unfortunately, alternative advancement of ketone **397** or its diol precursor (**396**) by selective conjugate reduction of the unsaturated lactone could not be accomplished. Although the α,β-unsaturated lactone moiety within these compounds had enabled the synthesis of ketone **397**, the inability to advance further toward *ent*-ineleganolide (***ent*-9**) forced another reevaluation of our synthetic strategy.

As such, we began to develop an alternative pathway to avoid the problematic translactontization regularly observed using our titanium(III) epoxide openings. To prevent this undesired isomerization, we investigated the potential to mask the lactone as a lactol by reducing earlier synthetic intermediates. Beginning with either diene tetracycle **324** (Scheme 4.4.8.A) or epoxide **328** (Scheme 4.4.8.B), we could accomplish a completely diastereoselective double reduction in the presence of excess DIBAL at low temperature to afford either allylic alcohol **403** or epoxyalcohol **404**, respectively. The relative stereochemistry of reduction products **403** and **404** was not rigorously assigned. Although the selective reduction of the lactol was desired, reduction of the isolated ketone was the requisite precursor (Scheme 4.4.8.C). Since a late-stage oxidation would be required in this route to regenerate the lactone moiety, the advancement of the observed reduced lactols **403** and **404** could still be employed to advance toward *ent*-ineleganolide (***ent*-9**).

Scheme 4.4.8. Lactol Formation

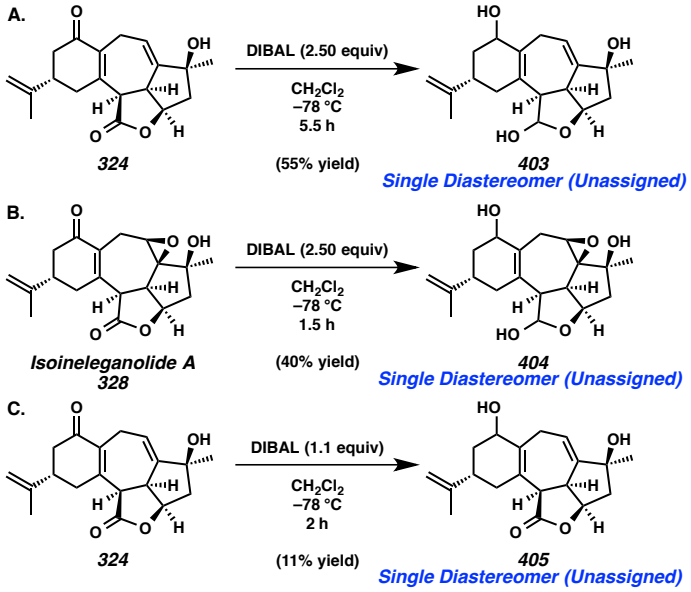

Exploiting the higher yielding reduction of diene **324** compared to epoxide **328**, we chose to advance employing lactol **403**. Disilyl ether formation using TBSCl under standard conditions provided lactol ether **406** in 89% yield (Scheme 4.4.9). Epoxidation of allyl alcohol **406** was then efficiently accomplished in 90% yield to furnish epoxide **407**. Titanium(III)-mediated epoxide opening accomplished the regioselective epoxide opening, smoothly furnishing a single product. Unfortuately, the product observed had undergone an intramolecular tranketalization, furnishing acetal **408** in 89% yield.[12] Yet again, we had produced an intermediate that was not useful for the progression toward *ent*-ineleganolide (***ent*-9**) as opening of the acetal under oxidative conditions could not be achieved. Attempted reactions using SO_3•pyridine in DMSO, DMP in wet CH_2Cl_2, other hypervalent iodine oxidants in wet solvents, and chromium oxidants all proved ineffective, routinely quantitatively returning the starting material after reaction times up to 7 days at elevated temperatures.

Scheme 4.4.9. Advancement of Lactol ***403***

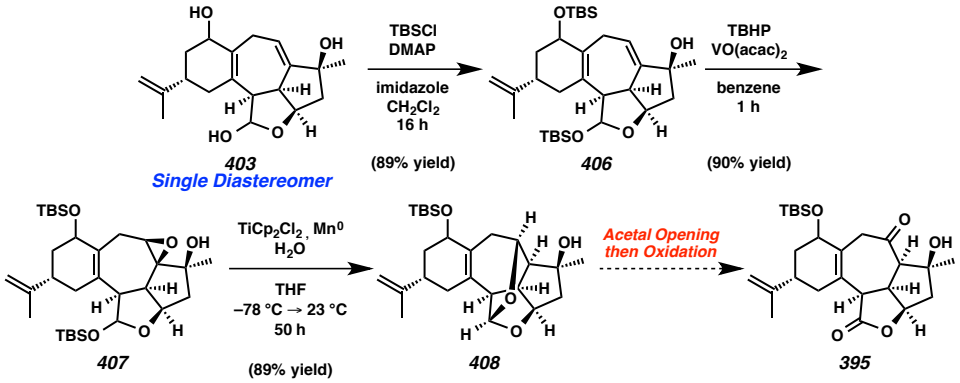

Unable to advance acetal **408** further, we had again encountered an unsuccessful synthetic strategy pairing early-stage reduction with a late-stage oxidation. Thus, we began to design alternative retrosynthetic strategies employing an early-stage oxidation, requiring a late-stage reduction to complete *ent*-ineleganolide.

4.5 Retrosynthetic Analysis — Late-Stage Reduction

We envisioned alternative completion of the asymmetric total synthesis of ineleganolide after dehydration of ketofuran **409** and ultimate conjugate reduction (Scheme 4.5.1). Synthesis of α-alkoxyketone **409** would be accomplished by an intramolecular oxa-Michael addition from vinylogous diketone **410**. Access to enedione **410** was envisioned through the selective reductive opening of furanopentacycle **411**. Access to conjugated dione **411** would be achieved after the oxidation of saturated 1,4-diketone intermediate **347**.

Scheme 4.5.1. Retrosynthetic Analysis of ent-Ineleganolide Employing Late-Stage Reduction

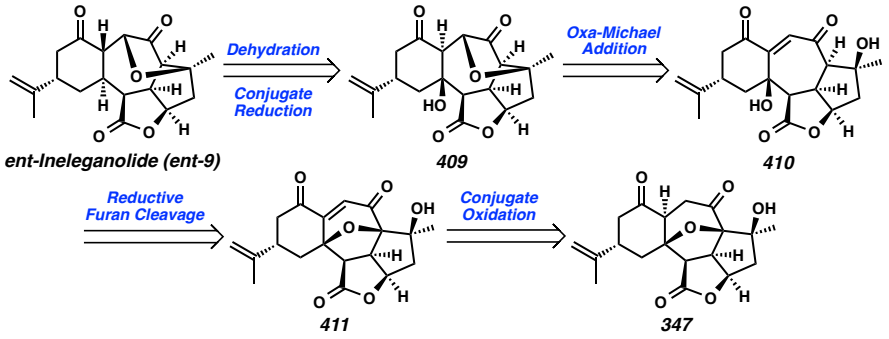

4.6 Exploration of Enedione Synthesis

Evaluation of this synthetic route began with the previously synthesized intermediate furanopentacycle **347** (Scheme 4.6.1). Formation of the thermodynamic trimethylsilyl enol ether at C(3) enabled the subsequent Saegusa-Ito oxidation, smoothly furnishing vinylogous diketone **412** in 56% yield as the major product. Unfortunately, even under optimized conditions, the production of dienone **413** could not be avoided, which can be isolated in 44% yield.[18]

*Scheme 4.6.1. Oxidation of 1,4-Diketone **347***

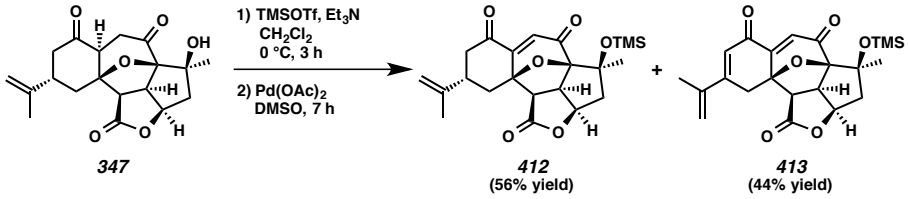

With vinylogous diketone **412** in hand, we began investigating reductive α-alkoxyketone cleavage procedures. These studies focused on the use of samarium diiodide considering that this reagent is known to accomplish related transformations[19] and has been used previously for the α-alkoxyketone cleavage of saturated 1,4-diketone **347**. The use of SmI_2 in the absence of an additive or with H_2O, LiCl, LiBr, HMPA, or *t*-BuOH all failed to provide any trace of enedione **414** (Scheme 4.6.2). Rather, all

conditions selectively reduced the conjugated system. For example, exposure of enone **412** to SmI_2 at low temperature followed sequentially by TBAF-mediated tertiary silyl ether cleavage produced saturated diketone **347** in 75% yield.

*Scheme 4.6.2. Reduction of Vinylogous Diketone **412***

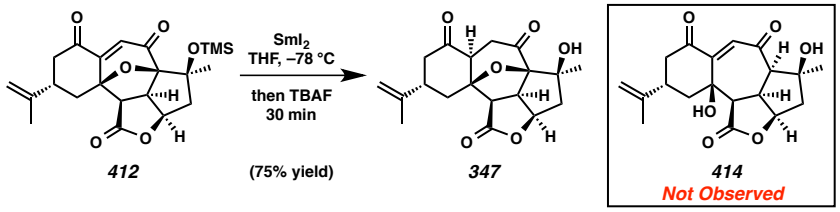

Unable to advance further toward *ent*-ineleganolide (***ent*-9**) using enedione **412**, we regressed further in the synthetic route to find other substrates that could be oxidized in a productive fashion. We were pleased to find that isoineleganolide A (**328**) could be selectively enolized at the γ-position of the conjugated system when DMAP was used as the base (Scheme 4.6.3). Formation of both disilylenol ether **416** (Scheme 4.6.3.A) and dienol acetate **416** (Scheme 4.6.3.B) could be achieved using TESCl and acetic anhydride, respectively. Although TES enol ether **415** could be isolated and purified on small scale, attempts to increase the scale of its production routinely resulted in hydrolysis during purification and reformation of starting material **328**. Although the formation of the analogous TIPS dienol ether could not be accomplished under similar conditions, the TBS analog could be formed using TBSCl in place of TESCl, furnishing a significantly more stable product that was used for further synthetic studies.

Scheme 4.6.3. Dienol Ether Formation

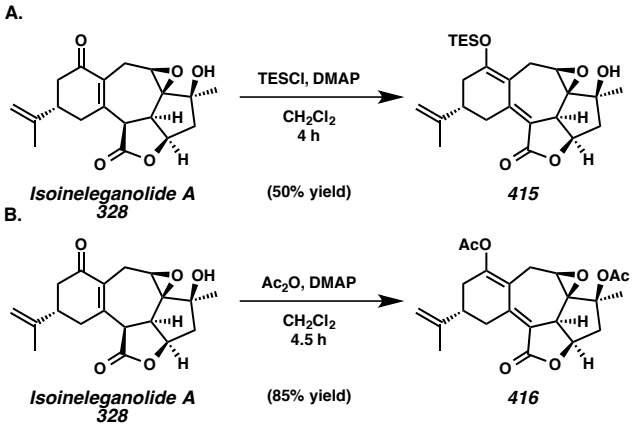

In order to advance the dienol ether substrates toward *ent*-ineleganolide (***ent*-9**), we sought to apply our previously employed titanium(III)-mediated reductive epoxide opening conditions. Isoineleganolide A (**328**) was first converted into the TBS dienol ether **417A** and was subsequently exposed to titanium(III) reductive conditions (Scheme 4.6.4). Not only did we observe hydrolysis of the dienol ether under the reaction conditions, but we observed solely the recovery of starting material **328** without the detection of desired product **417** or epoxide-opened starting material **418**.

*Scheme 4.6.4. Attempted Reductive Epoxide Opening of Disilyl Enol Ether of Enone **328***

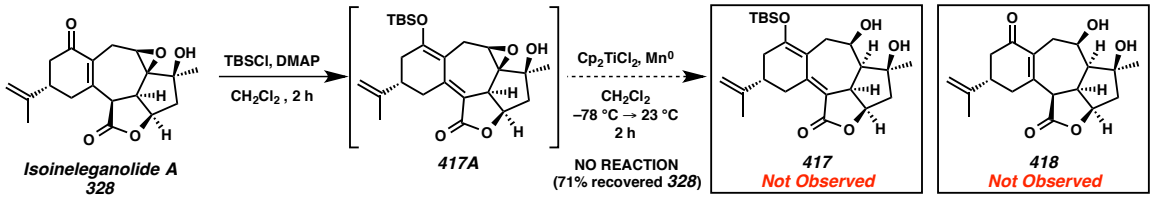

Comparably, dienol acetate **416** proved an incompetent substrate for reductive epoxide opening under the same conditions (Scheme 4.6.5). Rather than producing desired product **419**, we simply observed quantitative return of the staring material.

Scheme 4.6.5. Attempted Reductive Epoxide Opening of Dienol Ether ***416***

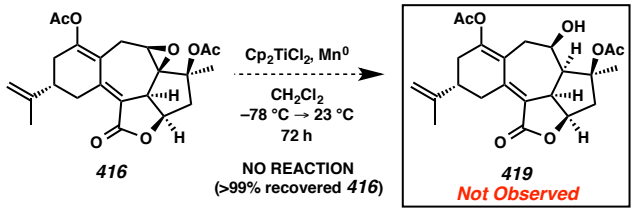

Leaving the epoxide opening for a later stage, we began to investigate the oxidative advancement of these dienol ether intermediates. In an attempt to functionalize isoineleganolide A (**328**) at C(4), we first formed the TBS dienol ether (Scheme 4.6.6). Exposure of this intermediate to NBS in dichloromethane at room temperature afforded solely α-bromolactone **420** rather than α-bromoketone **421**.[20] We did not believe γ-bromide **420** was immediately useful for progression toward *ent*-ineleganolide (***ent*-9**), so we sought alternative oxidative procedures.

Scheme 4.6.6. Construction of α-Bromolactone ***420***

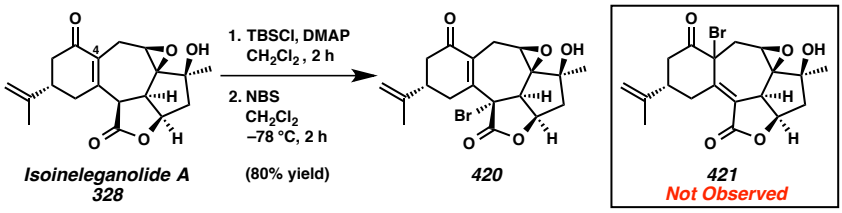

During that investigation, we were gratified to find C(4)–C(5) oxidation of isoineleganolide A (**328**) could indeed be accomplished (Scheme 4.6.7). Beginning again with the formation of the TBS dienol ether from epoxide **328**, oxidation using stoichiometric palladium(II) acetate in DMSO provided dehydroineleganolide (**422**) in 60% yield. Unfortunately, this transformation was plagued by routinely low yields, but afforded enough material to continue our synthetic explorations.

*Scheme 4.6.7. Oxidation of Isoineleganolide A (**328**) to Cycloheptadiene **422***

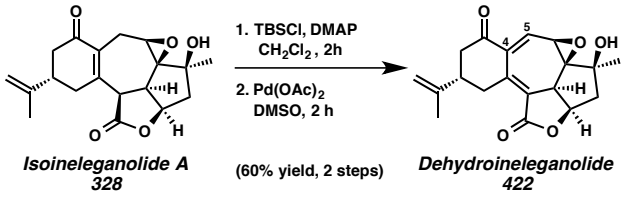

Dehydroineleganolide (**422**) was characterized by unique spectroscopic features, including an unexpected ^{13}C NMR spectrum. For example, consider epoxide **328** and the ^{13}C NMR shifts of C6 and C7 at 54.5 ppm and 70.2 ppm, respectively (Table 4.6.1). These shifts were characteristic with the remaining epoxytetracycles synthesized throughout this study (e.g., **371**, **377**, **383**). In contrast, while the carbon shift of the secondary epoxide carbon C6 of dehydroineleganolide (**422**) is within the expected range at 52.1 ppm, the tertiary epoxide carbon C7 is found at 94.9 ppm. We hoped that the spectral data associated with enone **422** was indicative of a reactivity profile that we could exploit.

*Table 4.6.1. Comparison of ^{13}C NMR Shifts of Enone **328** and Diene **422***

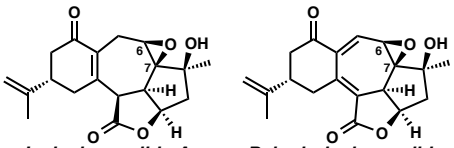

Compound	Carbon	δ (ppm in $CDCl_3$)
328	C6	54.4
422	C6	52.1
328	C7	70.2
422	C7	94.9

Any further advancement toward *ent*-ineleganolide (***ent*-9**) would now require the opening of the epoxide moiety. Unfortunately, dehydroineleganolide (**422**) was extremely reactive under titanium(III)-mediated reductive epoxide opening conditions, largely decomposing upon initiation of the reaction and routinely furnishing a complex mixture of products. Additionally, our attempts to accomplish a Lewis acid-mediated

1,2-hyride shift and generation of the vinylogous diketone **422** were unfruitful. In fact, the only productive reactivity observed during this screen was the production of cycloheptatrienone **423** in 75% yield in the presence of $Yb(OTf)_3$ (Scheme 4.6.8).

*Scheme 4.6.8. Formation of Cycloheptatrienone **423***

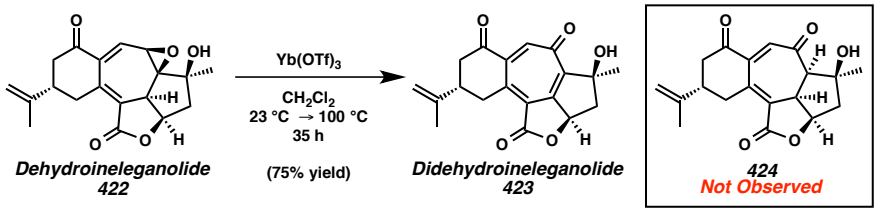

4.7 New Approach toward Ineleganolide

After thorough exploration of the reactivity of a range of [6,7,5,5]-tetracyclic intermediates, without accomplishing the completion of the total synthesis of *ent*-ineleganolide, we revisited and completely redesigned our retrosynthetic strategy. We envisioned completion of *ent*-ineleganolide (***ent*-9**) by an intramolecular cascade from α,β-unsaturated ester **425** (Scheme 4.7.1). Macrocycle **425** would be formed by the intramolecular cyclization of ester **426**. Ketofuran **426** would be constructed by the coupling of ketone **427** and bicycle **428**. Ketone **427** could be formed from known derivatives of (*R*)-(–)-carvone by *Z*-selective olefination. Ketofuran **428** would be accessible after the intramolecular cyclization of previously synthesized methyl ketone **338** by O–H insertion followed by silyl ether cleavage.

*Scheme 4.7.1. Redesigned Retrosynthetic Strategy Toward ent-Ineleganolide (**ent-9**)*

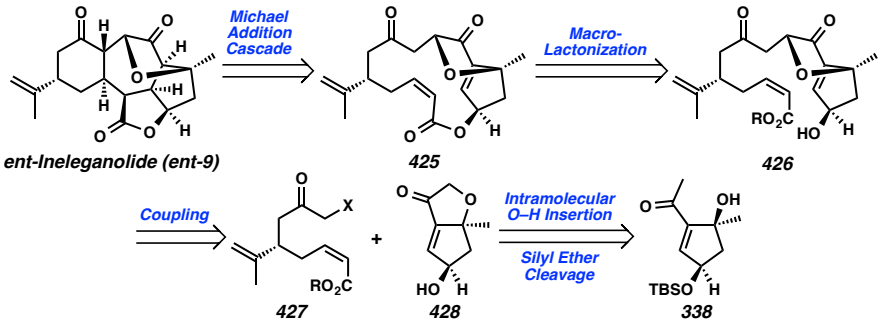

This redesigned strategy was inspired by the biomimetic semisynthesis of ineleganolide[21] as well as the empirical evidence that the late-stage construction of the characteristic ketofuran furan moiety is not feasible. Currently, the investigation of this synthetic strategy toward ent-ineleganolide and the related polycyclic furanobutenolide norcembranoid natural products is ongoing in the Stoltz lab.

4.8. Conclusion

We have disclosed a research program dedicated to developing synthetic access to the core structures of the furanobutenolide norcembranoid diterpene natural products. The synthetic strategy was designed to convergently build the [6,7,5,5]-core tetracycle of ineleganolide (**9**) and then accomplish divergent access to the isomerized carbon skeletons of horiolide (**20**), kavaranolide (**21**), sinulochmodin C (**10**), scabrolide A (**23**), scabrolide B (**24**), and yonarolide (**25**). The convergent assembly of the [6,7,5,5]-core tetracyclic scaffold was accomplished using two independent fragments. The western carboxylic acid fragment was derived from (*R*)-(–)-carvone and contained the requisite enantioenriched remote stereocenter possessing the isopropenyl group that characteristically decorates the norcembranoid diterpenes. The complimentary eastern diol what constructed using a palladium-catalyzed asymmetric allylic alkylation to enantioselectively form a fully substituted tertiary ether center. This stereocenter was

then used to relay chiral information to *all* remaining stereocenters with the [6,7,5,5]-core through a diastereoselective reduction followed by a key cyclopropanation-Cope rearrangement cascade (Scheme 4.8.1).

Scheme 4.8.1. Asymmetric Allylic Alkylation Stereoselectively Determines All Remaining Chiral Information

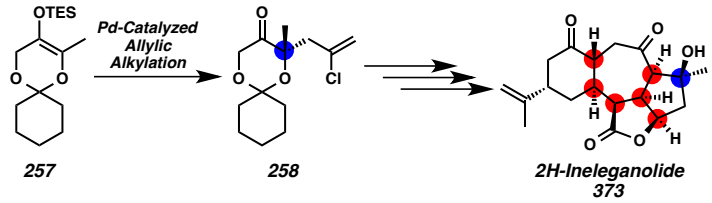

Although the synthesis of the furanobutenolide norcembranoid diterpene natural products themselves has not yet been accomplished, these investigations have provided synthetic access to a large variety of natural product-like "ineleganoloids" (Figure 4.8.1). We are currently in the process of evaluating the biological activity of this class of synthetic, natural product-like compounds in collaboration with Eli Lilly and the City of Hope, as efforts continue toward the completion of the asymmetric total syntheses of the norcembranoid diterpenes natural products. Throughout the course of this research program, we have thoroughly explored the limits of chemical transformation on highly oxygenation cyclopentanediols and complex, constrained fused cycloheptane polycycles. The understanding of this chemistry will not only benefit the derivatization and biological evaluation of the norcembranoid diterpenes, but will be broadly applicable to other total synthetic and semi-synthetic efforts toward the general class of terpenoid natural products. Perhaps then, the greater value in total synthesis is truly derived from the journey taken rather than that simply found at the finish line.

Figure 4.8.1. The Synthetic Natural Product-Like Ineleganoloids

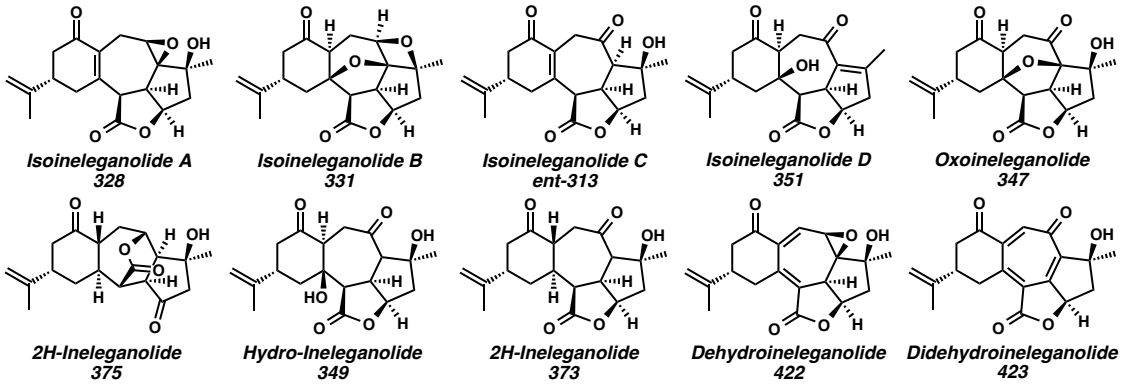

4.9 Experimental Methods and Analytical Data

4.9.1 Materials and Methods

Unless stated otherwise, reactions were performed at ambient temperature (23 °C) in flame-dried glassware under an argon atmosphere using dry, deoxygentated solvents (distilled or passed over a column of activated alumina)[22] stirring with a Teflon®-coated magnetic stirring bar. Commercially available reagents were used as received unless otherwise noted. Et_3N was distilled from calcium hydride immediately prior to use. MeOH was distilled from magnesium methoxide immediately prior to use. Reagent grade acetone was obtained from Sigma-Aldrich and used as received. Purified water was obtained using a Barnstead NANOpure Infinity UV/UF system. Reactions requiring external heat were modulated to the specified temperatures using an IKAmag temperature controller. Thin-layer chromatography (TLC) was performed using E. Merck silica gel 60 F254 precoated plates (250 nm) and visualized by UV fluorescence quenching, potassium permanganate, or *p*-anisaldehyde staining. Silicycle SiliaFlash P60 Academic Silica gel (particle size 40-63 nm) was used for flash chromatography. ^{1}H and ^{13}C NMR spectra were recorded on a Varian Inova 600 (600 MHz and 151 MHz, respectively), Varian Inova 500 (500 MHz and 126 MHz, respectively), Bruker AV III HD spectrometer equipped with a Prodigy liquid nitrogen temperature cryoprobe (400 MHz and 101 MHz, respectively), or a Varian Mercury 300 spectrometer (300 MHz and 76 MHz, respectively) and are reported in terms of chemical shift relative to residual $CHCl_3$ (in $CDCl_3$, δ 7.26 and δ 77.16, respectively) or C_6D_5H (in C_6D_6, δ 7.16 and δ 128.06, respectively). Data for ^{1}H NMR spectra are reported as follows: chemical shift (δ ppm) (multiplicity, coupling constant (Hz), integration). Infrared (IR) spectra were recorded on

a Perkin Elmer Paragon 1000 Spectrometer and are reported in frequency of absorption (cm^{-1}). High resolution mass spectra (HRMS) were obtained from the Caltech Mass Spectral Facility using either a JEOL JMS-600H High Resolution Mass Spectrometer in fast atom bombardment (FAB+) or electron ionization (EI+) mode or an LCT Premier XE TOF mass spectrometer equipped with an electrospray ionization source (ES+) or were acquired using an Agilent 6200 Series TOF mass spectrometer with an Agilent G1978A Multimode source in atmospheric pressure chemical ionization (APCI) or mixed (MultiMode: ESI-APCI) ionization mode. Optical rotations were measured on a Jasco P-2000 polarimeter using a 100 mm path length cell at 589 nm.

4.9.2 Experimental Procedures

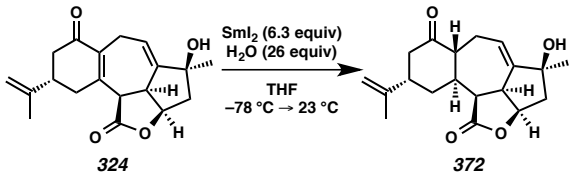

324 *372*

Allylic alcohol 372: Into each of two Schlenk tubes was added freshly filed samarium metal (150 mg, 1.00 mmol, 6.25 equiv). The reaction vessel was then thoroughly flame-dried, backfilled with argon, and allowed to cool to ambient temperature (ca. 23 °C). To each reaction vessel was added THF (10.0 mL) that had previously been sparged with argon for 60 minutes and cooled to 0 °C (ice/H_2O bath) with stirring. EtI_2 (200 mg, 0.71 mmol, 4.44 equiv) was then added to each Schlenk tube in separate 100 mg portions 30 minutes apart. After the addition of the second portion, the Schlenk tubes were removed from the cooling bath, allowed to warm to ambient temperature, and the pale yellow

solution was stirred overnight (ca. 14 h) causing the reaction to become deep blue, indicating formation of SmI_2.

Each Schlenk tube was cooled to –78 °C (*i*-PrOH/dry ice bath) followed by the addition of H_2O (75 μL, 4.16 mmol, 26.0 equiv). After stirring for 5 minutes, the addition of diene **324** (50 mg, 0.16 mmol, 1.00 equiv) as solution in thoroughly sparged THF (1.60 mL) was accomplished quickly dropwise over 4 minutes. After 2 h, the reaction vessel was warmed to 0 °C (ice/H_2O bath). After an additional 2 h, the Schlenk tube was removed from the cooling bath and allowed to warm. After 20 minutes, before warming all the way to ambient temperature, the consumption of starting material was complete as determined by TLC (1:4 EtOAc:CH_2Cl_2 eluent). The dark blue reaction mixture was quenched by the addition of hexanes (10.0 mL) and H_2O (0.10 mL). After stirring for 5 minutes, both reaction mixtures were combined, filtered through a pad of silica gel (50% acetone in hexanes eluent), and concentrated in vacuo. The crude tan solid was purified by silica gel column chromatography (20% acetone in hexanes eluent) to afford allylic alcohol **372** (56 mg, 56% yield) as an amorphous white solid: R_f = 0.21 (1:4 Acetone:Hexanes eluent); ^{1}H NMR ($CDCl_3$, 500 MHz) δ 6.32–6.24 (m, 1H), 4.93–4.86 (m, 1H), 4.74–4.70 (m, 1H), 4.63 (dt, *J* = 1.8, 0.9 Hz, 1H), 3.37 (dq, *J* = 6.0, 2.9 Hz, 1H), 3.12 (ddd, *J* = 15.9, 9.7, 1.7 Hz, 1H), 2.99–2.89 (m, 2H), 2.84 (dq, *J* = 7.8, 4.4 Hz, 1H), 2.68 (ddd, *J* = 15.1, 3.2, 2.3 Hz, 1H), 2.62 (ddd, *J* = 15.2, 6.0, 0.9 Hz, 1H), 2.40–2.29 (m, 2H), 2.19 (tt, *J* = 11.4, 3.8 Hz, 1H), 2.08 (dd, *J* = 15.7, 4.3 Hz, 1H), 2.02 (s, 1H), 1.83 (dtd, *J* = 14.1, 3.8, 2.0 Hz, 1H), 1.74 (dt, *J* = 1.5, 0.7 Hz, 3H), 1.73–1.65 (m, 1H), 1.35 (s, 3H); ^{13}C NMR ($CDCl_3$, 126 MHz) δ 210.3, 174.8, 149.9, 146.2, 128.2, 113.0, 83.1, 79.4, 49.7, 49.4, 48.4, 45.8, 44.5, 40.0, 39.8, 32.4, 30.0, 26.9, 22.5; IR (Neat Film, NaCl) 3479,

2965, 1760, 1699, 1444, 1372, 1224, 1138, 992, 900, 754 cm^{-1}; HRMS (FAB+) *m/z* calc'd for $C_{19}H_{25}O_4$ $[M+H]^+$: 315.1596, found 315.1600; $[\alpha]_D^{25.0}$ –17.7° (*c* 0.400, $CHCl_3$).

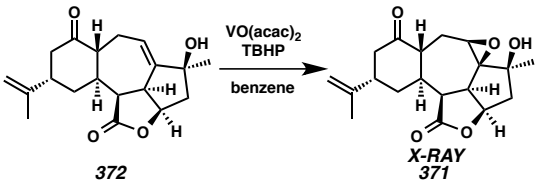

372 *371*

Epoxytetracycle 371: To a pale yellow stirred solution of allylic alcohol **372** (50 mg, 0.16 mmol, 1.00 equiv) in a vial open to air in benzene (5.3 mL) was added $VO(acac)_2$ (0.5 mg, 0.0016 mmol, 0.01 equiv). After 5 minutes, to this dark green solution was added *t*-butyl hydroperoxide (TBHP, 36 μL, 0.018 mmol, 1.10 equiv) as a 5 M solution in decane dropwise causing the reaction to immediately became deep ruby red. After 1 h, the reaction had lost all red color and become pale yellow and the consumption of starting material was complete as determined by TLC (1:4 Acetone:Hexanes eluent). The reaction was concentrated in vacuo and the crude tan solid was purified by silica gel column chromatography (25% acetone in hexanes eluent) to afford epoxide **371** (47 mg, 94% yield) as a white crystalline solid. Colorless, translucent X-ray quality crystals were obtained by slow diffusion of 1% benzene in heptane into a solution of epoxide **371** in EtOAc, mp: 183–185 °C: R_f = 0.15 (1:4 Acetone:Hexanes eluent); ^{1}H NMR ($CDCl_3$, 600 MHz) δ 4.87 (s, 1H), 4.79–4.73 (m, 1H), 4.63–4.57 (m, 1H), 3.34 (d, *J* = 7.1 Hz, 1H), 3.24 (ddd, *J* = 15.9, 7.2, 1.8 Hz, 1H), 3.05 (dd, *J* = 6.0, 4.4 Hz, 1H), 2.97 (ddd, *J* = 13.5, 11.8, 4.5 Hz, 1H), 2.84 (dd, *J* = 6.5, 3.4 Hz, 1H), 2.76 (dd, *J* = 6.0, 3.5 Hz, 1H), 2.67 (m, 2H), 2.63 (dd, *J* = 15.3, 6.0 Hz, 1H), 2.48 (bs, 1H), 2.38 (dd, *J* = 15.8, 6.7 Hz, 1H), 2.18 (d, *J* = 15.8 Hz, 1H), 1.89–1.74 (m, 2H), 1.74 (s, 3H), 1.53 (dd, *J* = 15.8, 10.8 Hz, 1H),

1.31 (s, 3H); ^{13}C NMR ($CDCl_3$, 126 MHz) δ 210.3, 173.8, 146.2, 113.0, 79.2, 75.3, 71.4, 54.4, 46.8, 46.2, 45.3, 44.3, 44.2, 39.7, 38.0, 31.8, 26.3, 25.6, 22.4; IR (Neat Film, NaCl) 3518, 2963, 2931, 1766, 1703, 1442, 1370, 1259, 1131, 985, 893, 758 cm^{-1}; HRMS (FAB+) *m/z* calc'd for $C_{19}H_{25}O_5$ $[M+H]^+$: 333.1702, found 333.1716; $[\alpha]_D^{25.0}$ +13.2° (*c* 0.200, $CHCl_3$).

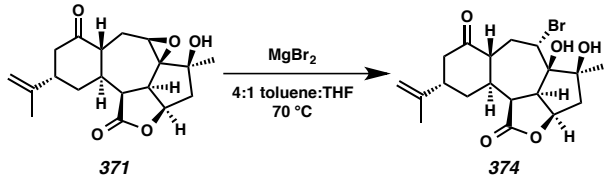

371 *374*

Bromohydrin 374: To a stirred colorless solution of epoxide **371** (8 mg, 0.024 mmol, 1.00 equiv) in a mixture of toluene (1.6 mL) and THF (0.4 mL) in a nitrogen-filled glovebox was added $MgBr_2$ (22 mg, 0.12 mmol, 5.00 equiv) in a single portion. The reaction mixture was then sealed and heated to 70 °C. After 15 h, the consumption of starting material was complete as determined by TLC (3:7 Acetone:Hexanes eluent). The golden yellow solution was removed from the glovebox. The reaction mixture was concentrated in vacuo and the crude tan solid was purified by silica gel column chromatography (20% acetone in hexanes eluent) to afford bromide **374** (8 mg, 80% yield) as an amorphous white solid: R_f = 0.38 (3:7 Acetone:Hexanes eluent); ^{1}H NMR ($CDCl_3$, 600 MHz) δ 4.96 (ddd, *J* = 9.6, 4.1, 2.9 Hz, 1H), 4.89 (dd, *J* = 2.2, 1.1 Hz, 1H), 4.80–4.74 (m, 1H), 4.65 (dt, *J* = 1.7, 0.8 Hz, 1H), 3.17 (d, *J* = 2.6 Hz, 1H), 2.88–2.70 (m, 5H), 2.51 (ddd, *J* = 14.6, 6.5, 1.0 Hz, 1H), 2.39–2.31 (m, 2H), 2.26 (dd, *J* = 12.0, 10.8 Hz, 1H), 2.20 (d, *J* = 9.6 Hz, 1H), 2.15–2.09 (m, 2H), 1.98 (s, 3H), 1.88 (tt, *J* = 12.5, 3.1 Hz, 1H), 1.75 (dt, *J* = 1.4, 0.7 Hz, 3H), 1.61 (dd, *J* = 11.4, 4.4 Hz, 1H); ^{13}C NMR ($CDCl_3$,

126 MHz) δ 209.0, 176.1, 146.1, 113.3, 98.1, 72.5, 69.5, 68.4, 51.0, 49.9, 46.9, 46.8, 44.2, 43.2, 40.4, 33.7, 33.0, 26.1, 22.6; IR (Neat Film, NaCl) 3437, 2926, 1766, 1708, 1444, 1262, 1109, 1014, 799 cm^{-1}; HRMS (FAB+) *m/z* calc'd for $C_{19}H_{26}O_5{}^{79}Br$ $[M+H]^+$: 413.0964, found 413.0965; $[\alpha]_D^{25.0}$ –8.1° (*c* 0.150, $CHCl_3$).

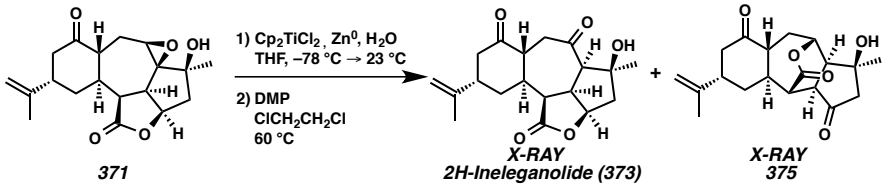

2*H*-Ineleganolide (373) and Lactone 375:

Preparation of a 0.50 M Stock Solution of Titanocene Monchloride (Cp_2TiCl)

Into a thoroughly flame-dried Schlenk tube under an overpressure of argon was charged with zinc(0) dust (647 mg, 9.90 mmol, 3.00 equiv) and titanocene dichloride (Cp_2TiCl_2, 822 mg, 3.30 mmol, 1.00 equiv). The flask was then evacuated and back filled with argon (3 x 5 minute cycles). To the reaction vessel was then added THF (6.6 mL) that had previously been sparged with argon for 60 minutes and stirring commenced. After 1.5 h, the bright red reaction mixture had become dark green and stirring was halted. After 30 minutes, the supernatant was used as a 0.50 M stock solution of Cp_2TiCl.

Epoxide Opening with Cp_2TiCl

A stirred solution of epoxide **371** (26 mg, 0.078 mmol, 1.00 equiv) in THF (2.5 mL) was sparged with argon for 1 h, resulting in a reaction volume of 1.5 mL. The homogeneous, off-white reaction mixture was then cooled to –78 °C (*i*-PrOH/dry ice bath) followed by the addition of H_2O (108 μL, 6.00 mmol, 76.9 equiv). After stirring for 5 minutes, Cp_2TiCl (1.50 mmol, 0.50 M in THF, 19.2 equiv) was added dropwise over 8

minutes. After 2 h, the reaction vessel was warmed to 0 °C (ice/H_2O bath). After an additional 1.5 h, the Schlenk tube was removed from the cooling bath and allowed to warm to ambient temperature (ca. 23 °C). After an additional 18.5 h, the consumption of starting material was complete as determined by TLC (3:7 Acetone:Hexanes eluent). The reaction was quenched by the addition of saturated NaH_2PO_4 (1.0 mL) and brine (1.0 mL), sparged with compressed air for 5 minutes, and allowed to stir for an additional 15 minutes. The reaction mixture was then filtered through a Celite® plug, washing with 50% acetone in hexanes eluent. The combined organics were concentrated in vacuo and immediately purified by silica gel column chromatography (50% EtOAc in CH_2Cl_2 eluent), furnishing a mixture of diol products (21 mg, 81% yield) that was directly carried on without further purification.

Oxidation of Intermediate Diol Products

To a portion of the diol products (8 mg, 0.024 mmol, 1.00 equiv) in wet DCE (3.0 mL) was added DMP (60 mg, 0.14 mmol, 5.82 equiv) at ambient temperature with stirring. The reaction vessel was then sealed and heated to 65 °C. After 18 h, the consumption of starting material was complete as determined by TLC (1:1 EtOAc:CH_2Cl_2 eluent). The reaction vessel was removed from the heating bath and allowed to cool to ambient temperature. The reaction mixture was then quenched by the addition of saturated NaS_2O_3 (3.0 mL) and saturated $NaHCO_3$ (3.0 mL). After stirring to 10 minutes, the reaction mixture was diluted with H_2O (10 mL) and extracted with CH_2Cl_2 (3 x 10 mL). The combined organics were then dried over $MgSO_4$, filtered, and concentrated in vacuo. The crude brown solid was purified by silica gel column

chromatography (25% acetone in hexanes eluent) to furnish 2*H*-ineleganolide (**373**, 4 mg, 50% yield) and lactone **375** (4 mg, 50% yield), both as crystalline white solids.

2*H*-Ineleganolide (373): Colorless, translucent X-ray quality crystals were obtained by slow diffusion of 1% benzene in heptane into a solution of ketone **373** in EtOAc, mp: 218–220 °C: R_f = 0.23 (3:7 Acetone:Hexanes eluent); ^{1}H NMR ($CDCl_3$, 500 MHz) δ 4.96–4.92 (m, 1H), 4.80 (ddd, *J* = 7.2, 6.2, 3.8 Hz, 1H), 4.68 (dt, *J* = 1.7, 0.8 Hz, 1H), 3.62 (q, *J* = 1.3 Hz, 1H), 3.21 (td, *J* = 9.3, 6.2 Hz, 1H), 3.08 (d, *J* = 9.6 Hz, 1H), 3.03 (dd, *J* = 9.0, 1.7 Hz, 1H), 2.96 (dd, *J* = 11.6, 3.8 Hz, 1H), 2.89–2.78 (m, 3H), 2.73 (dt, *J* = 14.7, 2.3 Hz, 1H), 2.67 (ddd, *J* = 14.7, 6.1, 1.0 Hz, 1H), 2.51–2.37 (m, 3H), 2.24–2.15 (m, 1H), 1.91 (ddd, *J* = 10.9, 6.0, 2.6 Hz, 1H), 1.78–1.74 (m, 3H), 1.28 (t, *J* = 1.0 Hz, 3H).; ^{13}C NMR ($CDCl_3$, 126 MHz) δ 213.8, 208.2, 174.1, 145.7, 113.7, 80.9, 80.4, 61.8, 48.0, 46.4, 46.3, 46.1, 44.0, 43.2, 40.3, 37.0, 34.0, 28.7, 22.6; IR (Neat Film, NaCl) 3501, 2965, 2925, 1761, 1698, 1440, 1368, 1318, 1262, 1160, 1081, 1030, 1003, 800, 758 cm^{-1}; HRMS (FAB+) *m/z* calc'd for $C_{19}H_{25}O_5$ $[M+H]^+$: 333.1702, found 333.1714; $[\alpha]_D^{25.0}$ – 32.6° (*c* 0.150, $CHCl_3$).

Lactone 375: Colorless, translucent X-ray quality crystals were obtained by slow diffusion of 1% benzene in heptane into a solution of ketone **375** in EtOAc, mp: 230–232 °C: R_f = 0.14 (3:7 Acetone:Hexanes eluent); ^{1}H NMR ($CDCl_3$, 600 MHz) 5.28 (d, *J* = 9.2 Hz, 1H), 4.90 (d, *J* = 1.8 Hz, 1H), 4.66 (s, 1H), 3.02 (d, *J* = 1.8 Hz, 1H), 2.87 (d, *J* = 10.8 Hz, 1H), 2.84 (d, *J* = 5.6 Hz, 1H), 2.72–2.62 (m, 2H), 2.58–2.49 (m, 2H), 2.45 (d, *J* = 16.9 Hz, 1H), 2.41 (d, *J* = 10.8 Hz, 1H), 2.27 (td, *J* = 12.5, 5.4 Hz, 1H), 2.13–2.07 (m, 2H), 1.90 (s, 1H), 1.82–1.70 (m, 4H), 1.71 (dd, *J* = 15.0, 12.1 Hz, 1H), 1.49 (s, 3H); ^{13}C NMR ($CDCl_3$, 126 MHz) δ 211.5, 208.9, 170.4, 146.3, 113.4, 75.0, 73.6, 53.1, 51.2, 50.1,

49.8, 47.5, 44.1, 41.7, 40.8, 34.4, 31.8, 28.7, 22.7; IR (Neat Film, NaCl) 3449, 2943, 1742, 1661, 1451, 1378, 1260, 1103, 1041, 801 cm^{-1}; HRMS (EI+) *m/z* calc'd for $C_{19}H_{24}O_5$ $[M\bullet]^+$: 332.1624, found 332.1620; $[\alpha]_D^{25.0}$ +7.8° (*c* 0.100, $CHCl_3$).

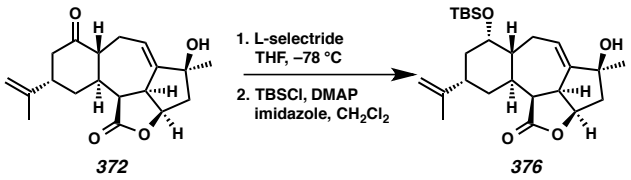

Silyl Ether 376: To a stirred colorless solution of ketone **372** (10 mg, 0.032 mmol, 1.00 equiv) in THF (2.50 mL) at –78 °C (*i*-PrOH/dry ice bath) was added L-Selectride® (100 μL, 1.0 M in THF, 3.00 equiv) slowly dropwise over 2 minutes. After 15 minutes, the consumption of starting material was complete as determined by TLC (3:7 Acetone:Hexanes eluent). The light yellow reaction mixture was quenched by the addition of saturated NH_4Cl (2.00 mL), removed from the cooling bath, and allowed to warm to ambient temperature (ca. 23 °C). The reaction mixture was then diluted with H_2O (10 mL) and extracted with EtOAc (3 x 8 mL). The combined organics were then dried over $MgSO_4$, filtered, and concentrated in vacuo to afford an amorphous white solid that was carried on without further purification, assuming quantitative yield.

To a solution of the crude white solid in CH_2Cl_2 (0.65 mL) were added imidazole (22 mg, 0.32 mmol, 10.0 equiv) and DMAP (0.7 mg, 0.006 mmol, 0.20 equiv) at ambient temperature (ca. 23 °C). The pale yellow reaction mixture was the cooled to 0 °C (ice/H_2O bath) at which time TBSCl (15 mg, 0.096 mmol, 3.00 equiv) was added as a solution in CH_2Cl_2 (0.25 mL) quickly dropwise. After 15 minutes, the reaction was removed from the cooling bath and allowed to warm to ambient temperature (ca. 23 °C).

After 18 h, additional imidazole (50 mg, 0.74 mmol, 23.1 equiv), DMAP (10 mg, 0.082, 2.56 equiv), and TBSCl (30 mg, 0.20 mmol, 6.35 equiv) were added sequentially as solids, each in a single portion. After 6 h, the consumption of starting material was complete as determined by TLC (3:7 Acetone:Hexanes eluent). The reaction mixture was concentrated in vacuo and the resultant crude white solid was purified by silica gel column chromatography (15% acetone in hexanes eluent) to provide silyl ether **376** (79% yield, 2 steps) as an amorphous white solid: R_f = 0.19 (3:17 Acetone:Hexanes eluent); ^{1}H NMR ($CDCl_3$, 400 MHz) δ 6.30 (ddd, *J* = 8.8, 5.0, 2.9 Hz, 1H), 4.77–4.64 (m, 3H), 3.86 (dt, *J* = 4.9, 2.6 Hz, 1H), 3.36 (tt, *J* = 5.9, 2.6 Hz, 1H), 2.97 (dd, *J* = 5.7, 3.9 Hz, 1H), 2.77–2.66 (m, 1H), 2.45–2.32 (m, 2H), 2.14–2.00 (m, 4H), 1.99–1.82 (m, 3H), 1.74 (dt, *J* = 1.2, 0.6 Hz, 3H), 1.73–1.66 (m, 1H), 1.61 (tt, *J* = 11.0, 3.1 Hz, 1H), 1.37 (s, 3H), 0.88 (s, 9H), 0.07 (s, 3H), 0.03 (s, 3H); ^{13}C NMR ($CDCl_3$, 101 MHz) δ 175.4, 149.7, 149.0, 129.9, 108.3, 83.0, 79.4, 73.1, 50.3, 50.2, 45.9, 39.7, 36.6, 36.5, 35.2, 33.4, 32.8, 29.7, 26.1, 21.9, 18.2, –3.9, –4.5; IR (Neat Film, NaCl) 3501, 2927, 2855, 1767, 1444, 1360, 1256, 1151, 1069, 1003, 959, 836, 807, 773 cm^{-1}; HRMS (FAB+) *m/z* calc'd for $C_{25}H_{39}O_4Si$ $[(M+H)–H_2]^+$: 431.2618, found 431.2611; $[\alpha]_D^{25.0}$ –8.1° (*c* 0.250, $CHCl_3$).

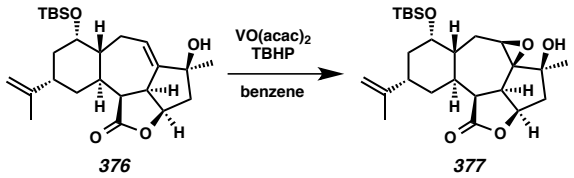

376 ***377***

Epoxide 377: To a pale yellow stirred solution of allylic alcohol **376** (5 mg, 0.012 mmol, 1.00 equiv) in a vial open to air in benzene (2.0 mL) was added $VO(acac)_2$ (0.6 mg, 0.0024 mmol, 0.2 equiv). After 5 minutes, to this dark green solution was added *t*-butyl

hydroperoxide (TBHP, 3 μL, 0.014 mmol, 1.10 equiv) as a 5 M solution in decane dropwise causing the reaction to immediately become deep ruby red. After 1.5 h, the reaction had lost all red color and become pale yellow and the consumption of starting material was complete as determined by TLC (3:17 Acetone:Hexanes eluent). The reaction was concentrated in vacuo and the crude tan solid was purified by silica gel column chromatography (15% acetone in hexanes eluent) to afford epoxide **377** (4 mg, 80% yield) as an amorphous white solid: R_f = 0.19 (3:17 Acetone:Hexanes eluent); ^{1}H NMR ($CDCl_3$, 400 MHz) δ 4.74 (ddd, *J* = 6.6, 4.5, 1.3 Hz, 1H), 4.68 (qt, *J* = 1.9, 0.9 Hz, 2H), 3.87 (dt, *J* = 5.0, 1.7 Hz, 1H), 3.28 (d, *J* = 6.8 Hz, 1H), 3.04 (dd, *J* = 6.0, 4.5 Hz, 1H), 2.79 (dd, *J* = 6.2, 2.7 Hz, 2H), 2.53 (d, *J* = 1.2 Hz, 1H), 2.37 (dd, *J* = 15.7, 6.6 Hz, 1H), 2.17 (d, *J* = 15.7 Hz, 1H), 2.11 (dd, *J* = 13.5, 6.9 Hz, 1H), 2.03–1.83 (m, 6H), 1.76–1.69 (m, 3H), 1.64 (ddd, *J* = 14.3, 7.8, 2.1 Hz, 1H), 1.35–1.30 (m, 3H), 0.88 (s, 9H), 0.07 (s, 3H), 0.04 (s, 3H); ^{13}C NMR ($CDCl_3$, 101 MHz) δ 174.3, 149.7, 108.3, 79.0, 77.4, 75.4, 73.6, 71.5, 55.4, 48.4, 45.5, 44.8, 36.6, 36.4, 35.4, 33.5, 32.7, 32.3, 26.1, 25.6, 21.7, 18.1, –3.9, –4.5; IR (Neat Film, NaCl) 3521, 2928, 2856, 1771, 1645, 1463, 1361, 1257, 1163, 1069, 986, 963, 878, 836, 774 cm^{-1}; HRMS (FAB+) *m/z* calc'd for $C_{25}H_{39}O_5Si$ $[(M+H)–H_2]^+$: 447.2567, found 447.2572; $[\alpha]_D^{25.0}$ +19.9° (*c* 0.200, $CHCl_3$).

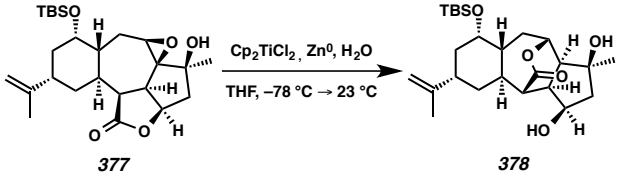

377 ***378***

Diol 378:

Preparation of a 0.50 M Stock Solution of Titanocene Monchloride (Cp_2TiCl)

Into a thoroughly flame-dried Schlenk tube under an overpressure of argon was charged with zinc(0) dust (647 mg, 9.90 mmol, 3.00 equiv) and titanocene dichloride (Cp_2TiCl_2, 822 mg, 3.30 mmol, 1.00 equiv). The flask was then evacuated and back filled with argon (3 x 5 minute cycles). To the reaction vessel was then added THF (6.6 mL) that had previously been sparged with argon for 60 minutes and stirring commenced. After 1.5 h, the bright red reaction mixture had become dark green and stirring was halted. After 30 minutes, the supernatant was used as a 0.50 M stock solution of Cp_2TiCl.

Epoxide Opening with Cp_2TiCl

A stirred solution of epoxide **377** (5 mg, 0.013 mmol, 1.00 equiv) in THF (1.5 mL) was sparged with argon for 1 h, resulting in a reaction volume of 0.5 mL. The homogeneous, off-white reaction mixture was then cooled to –78 °C (*i*-PrOH/dry ice bath) followed by the addition of H_2O (18 μL, 1.00 mmol, 76.9 equiv). After stirring for 5 minutes, Cp_2TiCl (0.25 mmol, 0.50 M in THF, 19.2 equiv) was added dropwise over 3 minutes. After 2 h, the reaction vessel was warmed to 0 °C (ice/H_2O bath). After an additional 2.5 h, the Schlenk tube was removed from the cooling bath and allowed to warm to ambient temperature. After an additional 12 h, the consumption of starting material was complete as determined by TLC (3:17 Acetone:Hexanes eluent). The reaction was quenched by the addition of saturated NaH_2PO_4 (0.25 mL) and brine (0.25

mL), sparged with compressed air for 5 minutes, and allowed to stir for an additional 15 minutes. The reaction mixture was then filtered through a Celite® plug, washing with 50% acetone in hexanes eluent. The combined organics were concentrated in vacuo and immediately purified by silica gel column chromatography (40% EtOAc in CH_2Cl_2 eluent) to furnish diol **378** (4 mg, 66% yield) as an amorphous white solid: R_f = 0.42 (1:1 EtOAc:CH_2Cl_2 eluent); ^{1}H NMR ($CDCl_3$, 400 MHz) δ 4.92 (d, *J* = 8.7 Hz, 1H), 4.69 (t, *J* = 1.8 Hz, 1H), 4.67 (q, *J* = 1.6 Hz, 1H), 4.33 (q, *J* = 4.3 Hz, 1H), 3.72 (q, *J* = 2.8 Hz, 1H), 3.20 (s, 1H), 2.67–2.58 (m, 2H), 2.50 (d, *J* = 5.1 Hz, 1H), 2.28–2.20 (m, 1H), 2.19–2.05 (m, 2H), 2.05–1.91 (m, 4H), 1.75–1.66 (m, 5H), 1.64–1.52 (m, 2H), 1.34 (dddd, *J* = 12.1, 9.0, 6.0, 2.9 Hz, 1H), 1.28 (s, 3H), 0.80 (s, 9H), 0.00 (d, *J* = 3.0 Hz, 3H), –0.06 (s, 3H); ^{13}C NMR ($CDCl_3$, 101 MHz) 174.76, 148.41, 108.35, 81.39, 76.21, 74.16, 70.00, 52.77, 50.22, 48.81, 48.35, 42.47, 37.26, 36.95, 35.81, 34.91, 34.69, 27.47, 25.95, 23.23, 18.18, –3.84, –4.81.; IR (Neat Film, NaCl) 3391, 2927, 2855, 1726, 1444, 1386, 1252, 1173, 1081, 1056, 881 838, 774 cm^{-1}; HRMS (FAB+) *m/z* calc'd for $C_{25}H_{43}O_5Si$ $[M+H]^+$: 451.2880, found 451.2890; $[\alpha]_D^{25.0}$ –2.9° (*c* 0.200, $CHCl_3$).

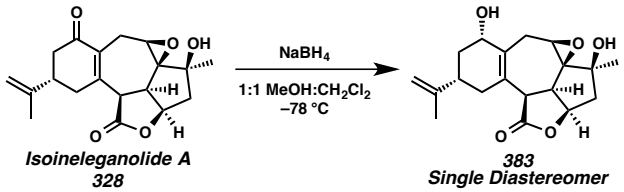

Allylic alcohol 383: To a stirred solution of enone **328** (11 mg, 0.033 mmol, 1.00 equiv) in MeOH (0.3 mL) and CH_2Cl_2 (0.3 mL) at –78 °C (*i*-PrOH/dry ice bath) was added $NaBH_4$ (4 mg, 0.10 mmol, 3.00 equiv) as a solid in single portion. After 1 h, the homogenous colorless reaction mixture was warmed to 0 °C (ice/H_2O bath). After an

additional 1 h, the consumption of starting material was complete as determined by TLC (1:4 EtOAc:CH_2Cl_2 eluent). The reaction was quenched by the addition of saturated aqueous $NaHCO_3$ (80 μL), removed from the cooling bath, and allowed to warm to ambient temperature (ca. 23 °C). The reaction mixture was then filtered through a silica gel plug, eluting with EtOAc. The combined organics were concentrated in vacuo. The crude white solid was purified by silica gel column chromatography (95% EtOAc in hexanes eluent) to provide allylic alcohol **383** (11 mg, >99% yield) as an amorphous white solid: R_f = 0.17 (19:1 EtOAc:Hexanes eluent); ^{1}H NMR ($CDCl_3$, 600 MHz) δ 4.79–4.68 (m, 3H), 4.21 (t, *J* = 8.3 Hz, 1H), 3.35 (dd, *J* = 6.1, 4.5 Hz, 1H), 3.32 (d, *J* = 5.2 Hz, 1H), 3.21 (d, *J* = 6.1 Hz, 1H), 3.01–2.93 (m, 1H), 2.92–2.84 (m, 2H), 2.42–2.32 (m, 2H), 2.29 (d, *J* = 16.0 Hz, 1H), 2.22–2.15 (m, 1H), 1.79–1.70 (m, 4H), 1.42 (td, *J* = 12.3, 9.7 Hz, 1H), 1.33 (s, 3H); ^{13}C NMR ($CDCl_3$, 126 MHz) δ 173.8, 148.4, 129.7, 126.8, 109.4, 79.6, 75.2, 73.8, 70.4, 55.5, 48.8, 45.7, 44.1, 38.5, 38.1, 37.2, 28.0, 26.5, 21.0; IR (Neat Film, NaCl) 3441, 2930, 1771, 1645, 1436, 1373, 1234, 1140, 986, 890, 757 cm^{-1}; HRMS (FAB+) *m/z* calc'd for $C_{19}H_{25}O_5$ $[M+H]^+$: 333.1702, found 333.1695; $[\alpha]_D^{25.0}$ +0.5 ° (*c* 0.550, $CHCl_3$).

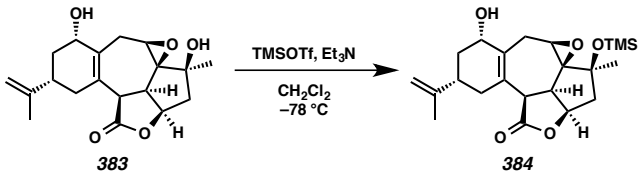

383 *384*

Silyl Ether 384: To a stirred solution of allylic alcohol **383** (11 mg, 0.033 mmol, 1.00 equiv) in CH_2Cl_2 (0.7 mL) at –78 °C (*i*-PrOH/dry ice bath) was added Et_3N (92 μl, 0.66 mmol, 20.0 equiv) dropwise. After 5 minutes, TMSOTf (31 μL, 0.10 mmol, 3.00 equiv)

was added slowly dropwise. After an additional 10 minutes, the consumption of starting material was complete as determined by TLC (19:1 EtOAc:Hexanes eluent). The reaction was quenched by the addition of saturated aqueous $NaHCO_3$ (80 μL), removed from the cooling bath, and allowed to warm to ambient temperature (ca. 23 °C). The reaction mixture was then filtered through a silica gel plug, eluting with 100% EtOAc. The combined organics were concentrated in vacuo. The crude white solid was purified by silica gel column chromatography (40% EtOAc in hexanes eluent) to furnish silyl ether **384** (10 mg, 77% yield) as an amorphous white solid: R_f = 0.36 (1:1 EtOAc:Hexanes eluent); ^{1}H NMR ($CDCl_3$, 600 MHz) δ 4.83–4.67 (m, 3H), 4.33–4.22 (m, 1H), 3.35–3.30 (m, 2H), 3.17 (d, *J* = 6.2 Hz, 1H), 3.00–2.90 (m, 1H), 2.83 (ddt, *J* = 16.6, 4.0, 2.1 Hz, 1H), 2.68 (dd, *J* = 19.7, 5.5 Hz, 1H), 2.55 (bs, 1H), 2.44–2.25 (m, 3H), 2.13–2.04 (m, 1H), 1.83–1.69 (m, 4H), 1.48–1.38 (m, 1H), 1.33 (s, 3H), 0.18 (s, 9H); ^{13}C NMR ($CDCl_3$, 126 MHz) δ 173.8, 148.4, 129.8, 127.0, 109.4, 79.6 (d, *J* = 4.1 Hz), 75.2, 74.8, 70.4, 55.6, 48.8, 45.7, 44.2, 38.6, 38.4, 37.3, 28.5, 26.5, 20.8, 0.6; IR (Neat Film, NaCl) 3429, 2959, 1764, 1371, 1250, 1142, 1056, 887, 841 cm^{-1}; HRMS (FAB+) *m/z* calc'd for $C_{22}H_{33}O_5Si$ $[M+H]^+$: 405.2097, found 405.2088; $[\alpha]_D^{25.0}$ +60.4° (*c* 0.250, $CHCl_3$).

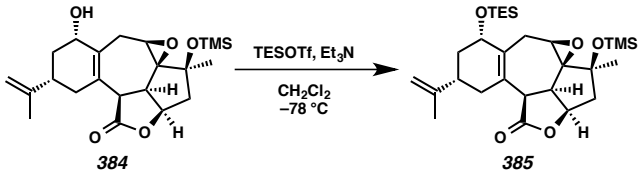

384 ***385***

Silyl Ether 385: To a stirred solution of allylic alcohol **384** (5 mg, 0.012 mmol, 1.00 equiv) in CH_2Cl_2 (0.3 mL) at –78 °C (*i*-PrOH/dry ice bath) was added Et_3N (35 μl, 0.25 mmol, 20.8 equiv) dropwise. After 5 minutes, TESOTf (15 μL, 0.060 mmol, 5.00 equiv)

was added slowly dropwise. After an additional 20 minutes, the consumption of starting material was complete as determined by TLC (1:1 EtOAc:Hexanes eluent). The reaction was quenched by the addition of saturated aqueous $NaHCO_3$ (80 μL), removed from the cooling bath, and allowed to warm to ambient temperature (ca. 23 °C). The reaction mixture was then filtered through a silica gel plug, eluting with EtOAc. The combined organics were concentrated in vacuo. The crude white solid was purified by silica gel column chromatography (10% EtOAc in hexanes eluent) to afford silyl ether **385** (4 mg, 66% yield) as an amorphous white solid: R_f = 0.14 (1:9 EtOAc:Hexanes eluent); ^{1}H NMR ($CDCl_3$, 600 MHz) δ 4.84–4.72 (m, 2H), 4.70 (s, 1H), 4.33–4.21 (m, 1H), 3.25 (dd, *J* = 6.4, 4.7 Hz, 1H), 3.20 (d, *J* = 5.4 Hz, 1H), 3.10 (d, *J* = 6.4 Hz, 1H), 2.93–2.84 (m, 2H), 2.65 (dd, *J* = 19.5, 5.5 Hz, 1H), 2.41–2.32 (m, 2H), 2.28 (dd, *J* = 15.0, 6.5 Hz, 1H), 2.10–2.03 (m, 1H), 1.76–1.70 (m, 4H), 1.41 (td, *J* = 12.7, 10.0 Hz, 1H), 1.31 (s, 3H), 0.93 (t, *J* = 7.9 Hz, 9H), 0.68–0.54 (m, 6H), 0.18 (s, 9H); ^{13}C NMR ($CDCl_3$, 126 MHz) δ 173.7, 148.6, 130.0, 127.0, 109.3, 79.3, 77.0, 74.9, 69.6, 53.8, 48.6, 44.5, 43.4, 38.6, 38.5, 37.2, 29.7, 28.7, 20.8, 7.2, 6.5, 0.6; IR (Neat Film, NaCl) 3464, 2956, 1766, 1665, 1451, 1376, 1249, 1143, 1047, 890, 841, 795, 744 cm^{-1}; HRMS (FAB+) *m/z* calc'd for $C_{28}H_{47}O_5Si_2$ $[M+H]^+$: 519.2962, found 519.2959; $[\alpha]_D^{25.0}$ +53.6° (*c* 0.100, $CHCl_3$).

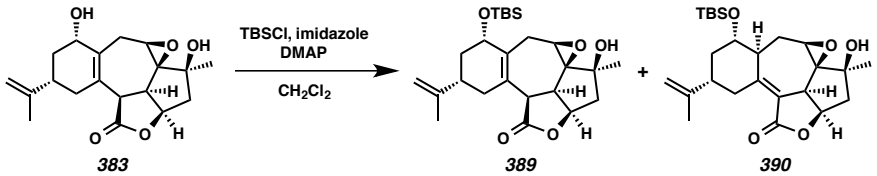

383 389 390

Allylic Silyl Ether 389 and Unsaturated Lactone 390: To a stirred solution of allylic alcohol **383** (65 mg, 0.20 mmol, 1.00 equiv) in CH_2Cl_2 (20 mL) were added imidazole

(2.72 g, 40.0 mmol, 200.0 equiv) and DMAP (98 mg, 0.80 mmol, 4.00 equiv) as solids sequential, each in a single portion. After 5 minutes, to the resulting homogenous, pale yellow solution was added TBSCl (3.01 g, 20.0 mmol, 100.0 equiv) as a solution in CH_2Cl_2 (7.5 mL) quickly dropwise over 5 minutes. After 17 h, the consumption of starting material was complete as determined by TLC (19:1 EtOAc:Hexanes eluent). The reaction mixture was then filtered through a Celite® plug, washing with CH_2Cl_2 eluent. The combined organics were concentrated in vacuo and purified by silica gel column chromatography (15% acetone in hexanes eluent) to furnish diol allylic silyl ether **389** (23 mg, 26% yield) as an amorphous white solid and unsaturated lactone **390** (66 mg, 74% yield) as an amorphous white solid.

Allylic Silyl Ether 389: R_f = 0.20 (3:17 Acetone:Hexanes eluent); ^{1}H NMR ($CDCl_3$, 400 MHz) δ 4.78–4.67 (m, 3H), 4.26 (bt, *J* = 8.0 Hz, 1H), 3.35 (dd, *J* = 6.1, 4.5 Hz, 1H), 3.31 (d, *J* = 5.4 Hz, 1H), 3.17 (dd, *J* = 5.8, 1.9 Hz, 1H), 2.97–2.78 (m, 2H), 2.78–2.67 (m, 1H), 2.55 (bs, 1H), 2.42–2.24 (m, 3H), 2.06 (ddt, *J* = 12.2, 6.3, 2.3 Hz, 1H), 1.79–1.69 (m, 4H), 1.40 (ddd, *J* = 13.5, 12.4, 10.3 Hz, 1H), 1.34 (s, 3H), 0.92 (s, 9H), 0.13 (s, 3H), 0.11 (s, 3H); ^{13}C NMR ($CDCl_3$, 101 MHz) δ 173.9, 148.6, 130.5, 126.5, 109.4, 79.7, 75.3, 75.0, 70.5, 55.8, 48.9, 45.8, 44.3, 38.7, 38.5, 37.4, 28.6, 26.6, 26.2, 20.9, 18.4, –3.5, –4.6; IR (Neat Film, NaCl) 3465, 2930, 2857, 1771, 1463, 1370, 1256, 1140, 1102, 1056, 988, 972, 883, 836, 774 cm^{-1}; HRMS (FAB+) *m/z* calc'd for $C_{25}H_{39}O_5Si$ $[M+H]^+$:447.2567, found 447.2552; $[\alpha]_D^{25.0}$ +87.5 ° (*c* 0.400, $CHCl_3$).

Unsaturated Lactone 390: R_f = 0.29 (3:17 Acetone:Hexanes eluent); ^{1}H NMR ($CDCl_3$, 400 MHz) δ 4.80 (ddd, *J* = 9.3, 7.8, 7.2 Hz, 1H), 4.75 (dt, *J* = 1.8, 0.9 Hz, 1H), 4.73 (s, 1H), 4.16–4.07 (m, 1H), 3.88 (ddd, *J* = 10.1, 9.0, 4.3 Hz, 1H), 3.81 (dt, *J* = 9.3, 2.5 Hz,

1H), 3.37 (ddd, *J* = 5.4, 2.0, 0.7 Hz, 1H), 2.61–2.51 (m, 2H), 2.41 (dtd, *J* = 9.3, 4.7, 2.4 Hz, 1H), 2.38–2.32 (m, 1H), 2.14 (tt, *J* = 11.7, 4.1 Hz, 1H), 2.08–1.97 (m, 2H), 1.97–1.90 (m, 1H), 1.86 (ddd, *J* = 13.7, 11.1, 2.5 Hz, 1H), 1.74 (dd, *J* = 1.5, 0.8 Hz, 3H), 1.43 (td, *J* = 12.5, 10.2 Hz, 1H), 1.32 (d, *J* = 0.9 Hz, 3H), 0.93 (s, 9H), 0.13 (s, 3H), 0.12 (s, 3H); ^{13}C NMR ($CDCl_3$, 101 MHz) δ 169.7, 158.8, 148.2, 116.1, 109.6, 74.5, 73.5, 73.3, 70.9, 54.3, 51.6, 48.1, 41.5, 41.0, 40.4, 32.6, 26.0, 23.5, 22.7, 20.6, 18.2, –3.9, –4.7; IR (Neat Film, NaCl) 3494, 2929, 2857, 1742, 1645, 1455, 1360, 1259, 1176, 1121, 1078, 1053, 957, 918, 898, 837, 775 cm^{-1}; HRMS (FAB+) *m/z* calc'd for $C_{25}H_{39}O_5Si$ $[M+H]^+$: 447.2567, found 447.2577; $[\alpha]_D^{25.0}$ +56.1° (*c* 0.600, $CHCl_3$).

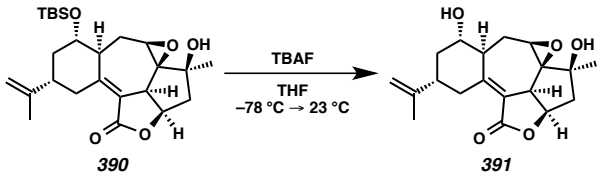

390 ***391***

Epoxyalcohol 391: To a stirred solution of silyl ether **390** (4 mg, 0.009 mmol, 1.00 equiv) in THF (0.6 mL) at –78 °C (*i*-PrOH/dry ice bath) was added TBAF (11 mL, 1 M in THF, 1.22 equiv) slowly dropwise. After 3 h, the reaction was introduced to a 0 °C bath (ice/H_2O). After a further 4 h, the consumption of starting material was complete as determined by TLC (1:4 Acetone:Hexanes eluent). The reaction was removed from the cooling bath and immediately concentrated in vacuo. The crude dark brown oil was purified by silica gel column chromatography (EtOAc eluent) to provide diol **391** (3 mg, >99% yield) as an amorphous white solid: R_f = 0.31 (EtOAc eluent); ^{1}H NMR ($CDCl_3$, 400 MHz) δ 4.83 (dt, *J* = 9.2, 7.4 Hz, 1H), 4.77 (dt, *J* = 1.7, 0.9 Hz, 1H), 4.75 (q, *J* = 1.5 Hz, 1H), 3.96 (dd, *J* = 14.0, 4.7 Hz, 1H), 3.93–3.86 (m, 1H), 3.84 (dt, *J* = 9.2, 2.5 Hz,

1H), 3.43 (dd, *J* = 4.8, 2.2 Hz, 1H), 2.63–2.52 (m, 2H), 2.42 (dddd, *J* = 8.3, 6.2, 4.3, 2.2 Hz, 1H), 2.32 (bs, 1H), 2.26–2.03 (m, 4H), 1.93 (dd, *J* = 13.3, 7.3 Hz, 1H), 1.75 (t, *J* = 1.1 Hz, 3H), 1.44 (ddd, *J* = 12.4, 11.7, 10.5 Hz, 1H), 1.33 (t, *J* = 0.8 Hz, 3H); ^{13}C NMR ($CDCl_3$, 101 MHz) δ 169.6, 158.0, 148.0, 116.9, 109.8, 74.6, 73.5, 72.7, 70.4, 54.3, 50.8, 48.0, 41.6, 40.8, 40.1, 31.9, 23.5, 23.0, 20.8; IR (Neat Film, NaCl) 3418, 2964, 2925, 2855, 1732, 1644, 1446, 1372, 1260, 1177, 1103, 1048, 1029, 911, 802, 732 cm^{-1}; HRMS (FAB+) *m/z* calc'd for $C_{19}H_{25}O_5$ $[M+H]^+$: 333.1702, found 333.1688; $[\alpha]_D^{25.0}$ +14.3° (*c* 0.150, $CHCl_3$).

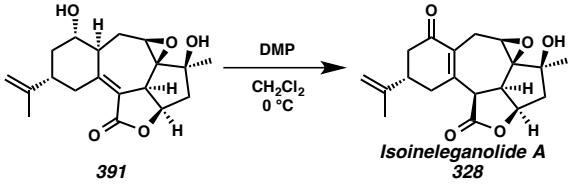

Enone 328: To a stirred solution of unsaturated lactone **391** (3 mg, 0.009 mmol, 1.00 equiv) in wet CH_2Cl_2 (1.3 mL) at 0 °C (ice/H_2O bath) was added Dess–Martin periodinane (DMP, 8 mg, 0.018 mmol, 2.00 equiv) as a solid in a single portion. After 2.5 h, the consumption of starting material was complete as determined by TLC (EtOAc eluent). The reaction was quenched by the addition of saturated aqueous $Na_2S_2O_3$ (2 mL) with vigorous stirring. After 15 minutes, the reaction was diluted with CH_2Cl_2 (5 mL) and poured onto saturated aqueous $NaHCO_3$ (2 mL). The organics were separated and the aqueous was extracted with CH_2Cl_2 (3 x 2 mL). The combined organics were concentrated in vacuo. The crude golden solid was purified by silica gel column chromatography (85% EtOAc in hexanes eluent) to provide enone **328** (2 mg, 66% yield)

as a crystalline white solid: characterization match those reported above (see chapter 3, section 3.9.2).

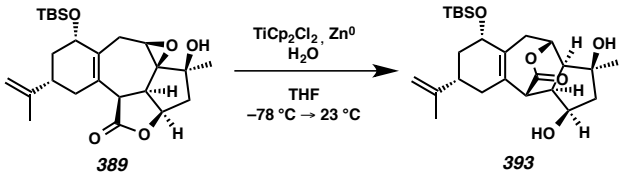

Diol 393:

Preparation of a 0.50 M Stock Solution of Titanocene Monchloride (Cp_2TiCl)

Into a thoroughly flame-dried Schlenk tube under an overpressure of argon was charged with zinc(0) dust (647 mg, 9.90 mmol, 3.00 equiv) and titanocene dichloride (Cp_2TiCl_2, 822 mg, 3.30 mmol, 1.00 equiv). The flask was then evacuated and back filled with argon (3 x 5 minute cycles). To the reaction vessel was then added THF (6.6 mL) that had previously been sparged with argon for 60 minutes and stirring commenced. After 1.5 h, the bright red reaction mixture had become dark green and stirring was halted. After 30 minutes, the supernatant was used as a 0.50 M stock solution of Cp_2TiCl.

Epoxide Opening with Cp_2TiCl

A stirred solution of epoxide **389** (8 mg, 0.018 mmol, 1.00 equiv) in THF (2.0 mL) was sparged with argon for 1 h, resulting in a reaction volume of 0.8 mL. The homogeneous, off-white reaction mixture was then cooled to –78 °C (*i*-PrOH/dry ice bath) followed by the addition of H_2O (27 μL, 1.50 mmol, 55.6 equiv). After stirring for 5 minutes, Cp_2TiCl (0.38 mmol, 0.50 M in THF, 14.1 equiv) was added dropwise over 3 minutes. After 2 h, the reaction vessel was warmed to 0 °C (ice/H_2O bath). After an additional 2.5 h, the Schlenk tube was removed from the cooling bath and allowed to

warm to ambient temperature. After an additional 12.5 h, the consumption of starting material was complete as determined by TLC (3:17 Acetone:Hexanes eluent). The reaction was quenched by the addition of saturated NaH_2PO_4 (0.25 mL) and brine (0.25 mL), sparged with compressed air for 5 minutes, and allowed to stir for an additional 15 minutes. The reaction mixture was then filtered through a Celite® plug, washing with 50% acetone in hexanes eluent. The combined organics were concentrated in vacuo and purified *twice* by silica gel column chromatography (first column: 45% EtOAc in CH_2Cl_2 eluent, second column: 40% EtOAc in CH_2Cl_2 eluent) to furnish diol **393** (2 mg, 25% yield) as an amorphous white solid: R_f = 0.40 (1:1 EtOAc:CH_2Cl_2 eluent); ^{1}H NMR ($CDCl_3$, 400 MHz) δ 5.00 (dd, *J* = 4.5, 2.6 Hz, 1H), 4.74 (p, *J* = 1.7 Hz, 1H), 4.71 (dd, *J* = 1.9, 0.9 Hz, 1H), 4.33 (tt, *J* = 4.9, 2.1 Hz, 1H), 4.14 (td, *J* = 6.3, 3.0 Hz, 1H), 3.55 (s, 1H), 3.16 (d, *J* = 5.3 Hz, 1H), 3.06 (d, *J* = 1.6 Hz, 1H), 2.98 (ddd, *J* = 12.3, 5.0, 1.6 Hz, 1H), 2.84–2.71 (m, 1H), 2.60–2.47 (m, 1H), 2.35–2.15 (m, 3H), 2.06–1.91 (m, 2H), 1.74–1.70 (m, 3H), 1.67 (dd, *J* = 14.0, 3.7 Hz, 1H), 1.44 (td, *J* = 13.3, 12.8, 10.2 Hz, 1H), 1.34 (s, 3H), 0.90 (s, 9H), 0.09 (s, 3H), 0.08 (s, 3H); ^{13}C NMR ($CDCl_3$, 101 MHz) δ 173.3, 148.2, 132.7, 129.4, 109.7, 81.4, 76.0, 74.0, 71.6, 51.5, 49.6, 48.4, 47.7, 39.7, 38.1, 37.6, 36.8, 27.4, 26.1, 20.6, 18.3, -4.0, -4.7; IR (Neat Film, NaCl) 3365, 2927, 2855, 1733, 1454, 1386, 1259, 1081, 1060, 876, 836, 775 cm^{-1}; HRMS (FAB+) *m/z* calc'd for $C_{25}H_{41}O_5Si$ $[M+H]^+$: 449.2723, found 449.2735; $[\alpha]_D^{25.0}$ +31.3° (*c* 0.100, $CHCl_3$).

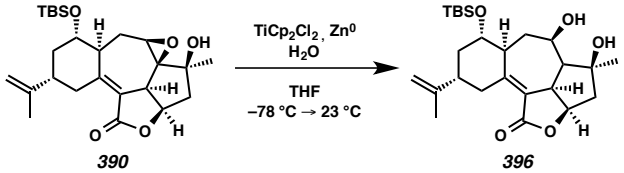

Diol 396:

Preparation of a 0.50 M Stock Solution of Titanocene Monchloride (Cp_2TiCl)

Into a thoroughly flame-dried Schlenk tube under an overpressure of argon was charged with zinc(0) dust (647 mg, 9.90 mmol, 3.00 equiv) and titanocene dichloride (Cp_2TiCl_2, 822 mg, 3.30 mmol, 1.00 equiv). The flask was then evacuated and back filled with argon (3 x 5 minute cycles). To the reaction vessel was then added THF (6.6 mL) that had previously been sparged with argon for 60 minutes and stirring commenced. After 1.5 h, the bright red reaction mixture had become dark green and stirring was halted. After 30 minutes, the supernatant was used as a 0.50 M stock solution of Cp_2TiCl.

Epoxide Opening with Cp_2TiCl

A stirred solution of epoxide **390** (12 mg, 0.027 mmol, 1.00 equiv) in THF (2.0 mL) was sparged with argon for 1 h, resulting in a reaction volume of 0.8 mL. The homogeneous, off-white reaction mixture was then cooled to –78 °C (*i*-PrOH/dry ice bath) followed by the addition of H_2O (27 μL, 1.50 mmol, 55.6 equiv). After stirring for 5 minutes, Cp_2TiCl (0.38 mmol, 0.50 M in THF, 14.1 equiv) was added dropwise over 3 minutes. After 2 h, the reaction vessel was warmed to 0 °C (ice/H_2O bath). After an additional 2.5 h, the Schlenk tube was removed from the cooling bath and allowed to warm to ambient temperature. After an additional 12.5 h, the consumption of starting material was complete as determined by TLC (3:17 Acetone:Hexanes eluent). The reaction was quenched by the addition of saturated NaH_2PO_4 (0.25 mL) and brine (0.25

mL), sparged with compressed air for 5 minutes, and allowed to stir for an additional 15 minutes. The reaction mixture was then filtered through a Celite® plug, washing with 50% acetone in hexanes eluent. The combined organics were concentrated in vacuo and purified *twice* by silica gel column chromatography (25% EtOAc in CH_2Cl_2 eluent) to furnish diol **396** (5 mg, 42% yield) as an amorphous white solid: R_f = 0.19 (1:4 EtOAc:CH_2Cl_2 eluent); ^{1}H NMR ($CDCl_3$, 400 MHz) δ 4.89 (ddd, *J* = 8.3, 6.3, 2.2 Hz, 1H), 4.77–4.73 (m, 1H), 4.69 (q, *J* = 1.5 Hz, 1H), 4.53 (q, *J* = 4.2 Hz, 1H), 3.89 (ddd, *J* = 9.4, 7.6, 4.2 Hz, 1H), 3.86–3.80 (m, 1H), 3.79–3.69 (m, 1H), 3.44–3.34 (m, 1H), 2.76 (ddt, *J* = 19.1, 10.6, 5.3 Hz, 2H), 2.60 (dt, *J* = 8.7, 7.0 Hz, 1H), 2.42 (ddt, *J* = 14.7, 11.9, 4.4 Hz, 1H), 2.20 (dd, *J* = 14.6, 2.1 Hz, 1H), 2.17–1.92 (m, 5H), 1.71 (dd, *J* = 1.4, 0.7 Hz, 3H), 1.43 (s, 3H), 1.37 (ddd, *J* = 13.2, 11.2, 9.2 Hz, 1H), 0.90 (s, 9H), 0.09 (app d, *J* = 0.9 Hz, 6H); ^{13}C NMR ($CDCl_3$, 101 MHz) δ 169.8, 158.2, 148.9, 122.7, 109.7, 81.7, 78.6, 74.6, 68.3, 52.8, 48.4, 47.4, 44.3, 38.8, 37.7, 34.2, 29.6, 26.9, 26.0, 20.1, 18.1, –3.9, –4.5; IR (Neat Film, NaCl) 3359, 2928, 2856, 1727, 1661, 1463, 1360, 1311, 1257, 1230, 1110, 1073, 1034, 887, 836, 775 cm^{-1}; HRMS (FAB+) *m/z* calc'd for $C_{25}H_{41}O_5Si$ $[M+H]^+$: 449.2723, found 449.2721; $[\alpha]_D^{25.0}$ +46.4° (*c* 0.250, $CHCl_3$).

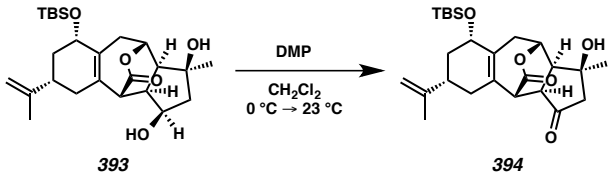

393 *394*

Ketone 394: To a stirred solution of diol **393** (10 mg, 0.022 mmol, 1.00 equiv) in wet CH_2Cl_2 (2.0 mL) at 0 °C (ice/H_2O bath) was added Dess–Martin periodinane (DMP, 30 mg, 0.071 mmol, 3.23 equiv) was a solid in a single portion. After 3 h, the white

suspension was removed from the cooling bath and allowed to warm to ambient temperature (ca. 23 °C). After an additional 10 h, the consumption of starting material was complete as determined by TLC (1:1 EtOAc:CH_2Cl_2 eluent). The reaction was quenched by the addition of saturated aqueous $Na_2S_2O_3$ (3 mL) with vigorous stirring. After 15 minutes, the reaction was diluted with CH_2Cl_2 (10 mL) and poured onto saturated aqueous $NaHCO_3$ (3 mL). The organics were separated and the aqueous was extracted with CH_2Cl_2 (4 x 2 mL). The combined organics were concentrated in vacuo. The crude golden solid was purified by silica gel column chromatography (15% EtOAc in hexanes eluent) to provide ketone **394** (6 mg, 60% yield) as an amorphous white solid: R_f = 0.27 (3:17 EtOAc:CH_2Cl_2 eluent); ^{1}H NMR ($CDCl_3$, 400 MHz) δ 5.25 (ddd, *J* = 5.0, 2.3, 0.8 Hz, 1H), 4.75 (p, *J* = 1.5 Hz, 1H), 4.72 (dd, *J* = 1.7, 0.9 Hz, 1H), 4.19–4.11 (m, 1H), 3.26 (d, *J* = 2.0 Hz, 1H), 3.22 (ddt, *J* = 10.8, 2.0, 0.9 Hz, 1H), 2.86 (dd, *J* = 18.5, 2.6 Hz, 1H), 2.69–2.38 (m, 4H), 2.33–2.16 (m, 3H), 2.04–1.95 (m, 1H), 1.72 (dd, *J* = 1.5, 0.8 Hz, 3H), 1.48 (s, 3H), 1.47–1.38 (m, 1H), 0.92 (s, 9H), 0.10 (s, 3H), 0.10 (s, 3H); ^{13}C NMR ($CDCl_3$, 101 MHz) δ 212.0, 169.9, 147.8, 133.3, 129.3, 109.9, 75.1, 74.0, 71.6, 53.3, 52.9, 47.8, 47.4, 39.6, 37.5, 37.5, 36.7, 29.1, 26.1, 20.5, 18.3, –3.9, –4.7; IR (Neat Film, NaCl) 3447, 2927, 2856, 1750, 1378, 1257, 1185, 1063, 872, 836, 777 cm^{-1}; HRMS (FAB+) *m/z* calc'd for $C_{25}H_{39}O_5Si$ $[M+H]^+$: 447.2567, found 447.2551; $[\alpha]_D^{25.0}$ +35.4° (*c* 0.300, $CHCl_3$).

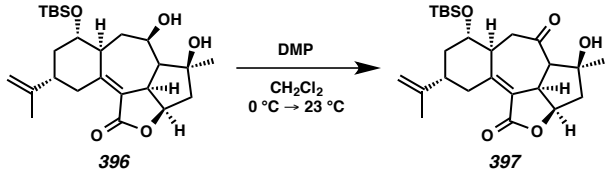

396 *397*

Ketone 397: To a stirred solution of diol **396** (49 mg, 0.11 mmol, 1.00 equiv) in wet CH_2Cl_2 (2.2 mL) at 0 °C (ice/H_2O bath) was added Dess–Martin periodinane (DMP, 140 mg, 0.33 mmol, 3.00 equiv) was a solid in a single portion. After 30 minutes, the white suspension was removed from the cooling bath and allowed to warm to ambient temperature (ca. 23 °C). After 2 h, additional DMP (140 mg, 0.33 mmol, 3.00 equiv) was added in a single portion. After an additional 10.5 h, the consumption of starting material was complete as determined by TLC (1:4 EtOAc:CH_2Cl_2 eluent). The reaction was quenched by the addition of saturated aqueous $Na_2S_2O_3$ (4 mL) with vigorous stirring. After 15 minutes, the reaction was diluted with CH_2Cl_2 (10 mL) and poured onto saturated aqueous $NaHCO_3$ (4 mL). The organics were separated and the aqueous was extracted with CH_2Cl_2 (4 x 2 mL). The combined organics were concentrated in vacuo. The crude golden brown solid was purified by silica gel column chromatography (8% EtOAc in hexanes eluent) to provide ketone **397** (10 mg, 23% yield) as an amorphous white solid: R_f = 0.27 (1:19 EtOAc:CH_2Cl_2 eluent); ^{1}H NMR ($CDCl_3$, 400 MHz) δ 4.94 (ddd, *J* = 8.2, 7.4, 0.9 Hz, 1H), 4.76–4.70 (m, 2H), 4.37 (ddd, *J* = 14.4, 3.9, 2.0 Hz, 1H), 4.17 (tt, *J* = 8.5, 2.8 Hz, 1H), 3.73 (ddd, *J* = 10.6, 9.2, 4.5 Hz, 1H), 3.13 (dd, *J* = 12.2, 6.8 Hz, 1H), 3.08 (d, *J* = 8.9 Hz, 1H), 2.82 (dd, *J* = 12.2, 3.8 Hz, 1H), 2.68 (ddt, *J* = 9.9, 6.6, 3.2 Hz, 1H), 2.58 (d, *J* = 2.4 Hz, 1H), 2.28 (d, *J* = 15.2 Hz, 1H), 2.11–1.95 (m, 2H), 1.87 (ddd, *J* = 15.2, 7.4, 2.5 Hz, 1H), 1.81–1.70 (m, 4H), 1.51–1.40 (m, 4H), 0.91 (s, 9H), 0.18 (s, 3H), 0.14 (s, 3H); ^{13}C NMR ($CDCl_3$, 101 MHz) δ 209.3, 169.7, 153.6, 148.1, 123.9,

109.6, 78.5, 73.1, 67.6, 50.5, 47.3, 43.8, 40.5, 40.4, 40.0, 32.3, 29.9, 27.2, 26.1, 20.8, 18.2, –3.9, –4.5; IR (Neat Film, NaCl) 3542, 2929, 2857, 1733, 1634, 1456, 1362, 1256, 1182, 1147, 1090, 1033, 891, 838, 777 cm^{-1}; HRMS (FAB+) *m/z* calc'd for $C_{25}H_{39}O_5Si$ $[M+H]^+$: 447.2567, found 447.2553; $[\alpha]_D^{25.0}$ +94.3° (*c* 0.750, $CHCl_3$).

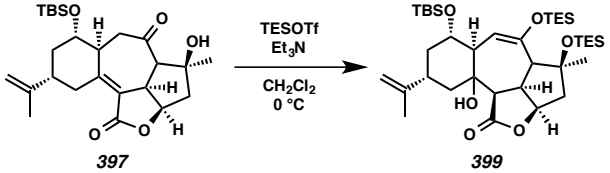

397 ***399***

Silyl Enol Ether 399: To a stirred solution of ketone **397** (13 mg, 0.029 mmol, 1.00 equiv) in CH_2Cl_2 (1.0 mL) at 0 °C (ice/H_2O bath) was added Et_3N (0.20 mL, 1.45 mmol, 50.0 equiv) dropwise. After 5 minutes, TESOTf (66 μL, 0.29 mmol, 10.0 equiv) was added slowly dropwise. After an additional 20 minutes, the consumption of starting material was complete as determined by TLC (1:19 EtOAc:CH_2Cl_2 eluent). The reaction was quenched by the addition of saturated aqueous $NaHCO_3$ (50 μL) and immediately removed from the cooling bath and allowed to warm to ambient temperature (ca. 23 °C). The reaction mixture was then filtered through a silica gel plug, eluting with 10% EtOAc in hexanes. The combined organics were concentrated in vacuo. The crude tan solid was purified by silica gel column chromatography (5% EtOAc in hexanes eluent) to provide enol ether **399** (11 mg, 55% yield) as an amorphous white solid: R_f = 0.50 (1:9 EtOAc:Hexanes eluent); ^{1}H NMR ($CDCl_3$, 400 MHz) δ 5.48 (t, *J* = 2.5 Hz, 1H), 4.91 (td, *J* = 8.3, 6.0 Hz, 1H), 4.72 (q, *J* = 1.2 Hz, 2H), 3.61 (ddd, *J* = 11.6, 8.3, 3.4 Hz, 1H), 3.13–3.04 (m, 1H), 2.68–2.53 (m, 3H), 2.45–2.33 (m, 2H), 2.26 (ddd, *J* = 13.1, 8.1, 1.3 Hz, 1H), 1.97–1.87 (m, 1H), 1.66 (t, *J* = 1.1 Hz, 3H), 1.60–1.46 (m, 4H), 1.15 (d, *J* = 1.2 Hz,

3H), 0.95 (td, *J* = 8.0, 5.4 Hz, 18H), 0.92 (s, 9H), 0.68–0.57 (m, 12H), 0.10 (s, 6H); ^{13}C NMR ($CDCl_3$, 101 MHz) δ 174.7, 147.8, 138.3, 124.2, 110.7, 88.6, 82.3, 80.2, 74.9, 59.6, 56.4, 48.1, 47.4, 47.0, 45.0, 44.2, 38.1, 29.9, 25.9, 20.2, 18.2, 7.4, 7.2, 6.9, 6.8, –4.0, –4.5; IR (Neat Film, NaCl) 2954, 2876, 1767, 1463, 1373, 1353, 1332, 1251, 1157, 1116, 1090, 1028, 871, 836, 775, 743 cm^{-1}; HRMS (ES+) *m/z* calc'd for $C_{37}H_{69}O_6Si_3$ $[M+H]^+$: 693.4402, found 693.4422; $[\alpha]_D^{25.0}$ +34.9° (*c* 0.250, $CHCl_3$).

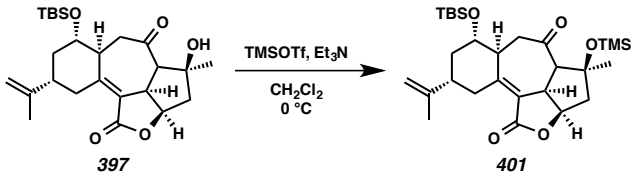

397 *401*

Silyl ether 401: To a stirred solution of ketone **397** (4 mg, 0.009 mmol, 1.00 equiv) in CH_2Cl_2 (1.0 mL) at 0 °C (ice/H_2O bath) was added Et_3N (126 μl, 0.90 mmol, 100.0 equiv) dropwise. After 5 minutes, TMSOTf (20 μL, 0.11 mmol, 12.2 equiv) was added slowly dropwise. After an additional 5 minutes, the consumption of starting material was complete as determined by TLC (1:19 EtOAc:CH_2Cl_2 eluent). The reaction was quenched by the addition of saturated aqueous $NaHCO_3$ (1.5 mL) and immediately removed from the cooling bath and allowed to warm to ambient temperature (ca. 23 °C). The reaction was diluted with Et_2O (2 mL) and poured onto H_2O (3 mL). The organics were separated and the aqueous was extracted with Et_2O (3 x 2 mL). The combined organics were dried over $MgSO_4$, filtered, and concentrated in vacuo. The crude white solid was purified by silica gel column chromatography (18% EtOAc in hexanes eluent) to provide enol ether **401** (4 mg, >99% yield) as an amorphous white solid: R_f = 0.28 (1:4 EtOAc:Hexanes eluent); ^{1}H NMR (C_6D_6, 400 MHz) δ 5.05–4.97 (m, 1H), 4.94 (dt, *J* = 1.9, 0.9 Hz, 1H),

4.84 (p, *J* = 1.5 Hz, 1H), 4.18 (t, *J* = 7.8 Hz, 1H), 3.73 (ddd, *J* = 10.7, 9.6, 4.4 Hz, 1H), 3.13 (tt, *J* = 8.1, 2.9 Hz, 1H), 2.86 (dd, *J* = 11.5, 3.6 Hz, 1H), 2.62 (dd, *J* = 11.5, 5.4 Hz, 1H), 2.41 (ddt, *J* = 9.0, 6.0, 3.3 Hz, 1H), 2.28–2.16 (m, 2H), 1.90 (d, *J* = 14.9 Hz, 1H), 1.83 (dd, *J* = 1.5, 0.8 Hz, 3H), 1.70 (d, *J* = 8.0 Hz, 1H), 1.68–1.49 (m, 2H), 1.39 (s, 3H), 1.08 (s, 9H), 1.03 (dd, *J* = 14.9, 7.6 Hz, 1H), 0.40 (s, 3H), 0.20 (s, 3H), 0.15 (s, 9H) ; ^{13}C NMR (C_6D_6, 101 MHz) δ 204.9, 169.9, 150.1, 148.5, 124.5, 109.5, 81.3, 76.5, 73.3, 68.3, 50.9, 48.5, 43.6, 41.2, 41.2, 40.3, 33.3, 26.4, 26.0, 21.1, 18.5, 2.4, –4.1, –4.3; IR (Neat Film, NaCl) 2928, 2856, 1738, 1716, 1635, 1455, 1362, 1251, 1184, 1149, 1093, 1017, 886, 837, 778 cm^{-1}; HRMS (FAB+) *m/z* calc'd for $C_{28}H_{47}O_5Si_2$ $[M+H]^+$: 519.2962, found 519.2954; $[\alpha]_D^{25.0}$ +61.8° (*c* 0.200, benzene).

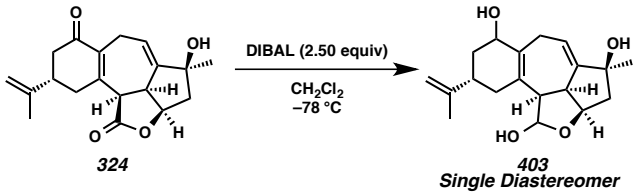

324 ***403***
Single Diastereomer

Lactol 403:[23] To a stirred solution of enone **324** (5 mg, 0.016 mmol, 1.00 equiv) in CH_2Cl_2 (0.70 mL) at –78 °C (*i*-PrOH/dry ice bath) was added DIBAL (48 μL, 1.00 M in CH_2Cl_2, 3.00 equiv) slowly dropwise. After 5.5 h, the consumption of starting material was complete as determined by TLC (1:4 EtOAc:CH_2Cl_2 eluent). The reaction was quenched by the addition of saturated aqueous NH_4Cl (0.5 mL) and saturated aqueous Rochelle salt (0.5 mL) and immediately removed from the cooling bath and allowed to warm to ambient temperature (ca. 23 °C). After stirring for 1 h, the reaction was diluted with CH_2Cl_2 (2.0 mL) and poured onto H_2O (3.0 mL). The organics were separated and the aqueous was extracted with CH_2Cl_2 (4 x 1.5 mL). The combined organics were dried

over $MgSO_4$, filtered, and concentrated in vacuo. The crude off-white solid was purified by silica gel column chromatography (50% EtOAc in hexanes eluent) to provide lactol **403** (11 mg, 55% yield) as an amorphous white solid: R_f = 0.21 (1:1 EtOAc:CH_2Cl_2 eluent); ^{1}H NMR ($CDCl_3$, 400 MHz) δ 6.19 (ddd, *J* = 8.6, 4.5, 3.0 Hz, 1H), 5.55 (d, *J* = 5.2 Hz, 1H), 4.77 (p, *J* = 1.7 Hz, 1H), 4.73 (dt, *J* = 2.0, 1.0 Hz, 1H), 4.61 (t, *J* = 4.7 Hz, 1H), 4.28–4.17 (m, 1H), 3.66–3.58 (m, 1H), 3.06 (d, *J* = 17.5 Hz, 1H), 3.01–2.93 (m, 1H), 2.83 (dd, *J* = 17.2, 8.6 Hz, 1H), 2.40 (d, *J* = 15.1 Hz, 1H), 2.37–2.20 (m, 2H), 2.16 (dddd, *J* = 12.6, 6.1, 2.9, 1.8 Hz, 1H), 2.02–1.92 (m, 2H), 1.76 (t, *J* = 1.1 Hz, 3H), 1.65–1.59 (m, 1H), 1.41 (s, 3H); ^{13}C NMR ($CDCl_3$, 101 MHz) δ 151.6, 149.0, 134.05, 129.7, 126.9, 109.8, 100.7, 85.1, 79.0, 72.9, 52.1, 48.8, 47.7, 38.8, 37.9, 36.2, 27.9, 27.3, 21.0; IR (Neat Film, NaCl) 3316, 2923, 1658, 1442, 1373, 1260, 1107, 1023, 925, 888, 806, 754 cm^{-1}; HRMS (ES+) *m/z* calc'd for $C_{19}H_{26}O_4$ $[M\bullet]^+$: 318.1831, found 318.1780; $[\alpha]_D^{25.0}$ +27.1° (*c* 0.200, $CHCl_3$).

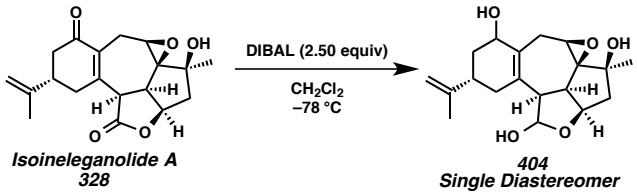

Lactol 404:[24] To a stirred solution of enone **328** (5 mg, 0.015 mmol, 1.00 equiv) in toluene (0.70 mL) at –78 °C (*i*-PrOH/dry ice bath) was added DIBAL (45 μL, 1.00 M in toluene, 3.00 equiv) slowly dropwise. After 1.5 h, the consumption of starting material was complete as determined by TLC (1:4 EtOAc:CH_2Cl_2 eluent). The reaction was quenched by the addition of saturated aqueous NH_4Cl (0.5 mL) and saturated aqueous Rochelle salt (0.5 mL) and immediately removed from the cooling bath and allowed to

warm to ambient temperature (ca. 23 °C). After stirring for 1 h, the reaction was diluted with CH_2Cl_2 (2.0 mL) and poured onto H_2O (3.0 mL). The organics were separated and the aqueous was extracted with CH_2Cl_2 (4 x 1.5 mL). The combined organics were dried over $MgSO_4$, filtered, and concentrated in vacuo. The crude off-white solid was purified by silica gel column chromatography (EtOAc eluent) to provide lactol **404** (2 mg, 40% yield) as an amorphous white solid: R_f = 0.23 (EtOAc eluent); ^{1}H NMR ($CDCl_3$, 400 MHz) δ 5.47 (dd, *J* = 12.1, 5.6 Hz, 1H), 5.39 (d, *J* = 12.1 Hz, 1H), 4.82–4.77 (m, 1H), 4.72 (dt, *J* = 1.8, 0.9 Hz, 1H), 4.58–4.51 (m, 1H), 4.22–4.13 (m, 1H), 3.55 (dd, *J* = 5.5, 1.1 Hz, 1H), 3.19 (ddd, *J* = 7.7, 6.2, 3.8 Hz, 1H), 3.14–3.05 (m, 1H), 3.01–2.92 (m, 2H), 2.47 (dd, *J* = 14.6, 6.8 Hz, 1H), 2.37 (s, 1H), 2.36–2.23 (m, 2H), 2.21–2.13 (m, 2H), 1.91 (ddt, *J* = 14.1, 10.3, 5.1 Hz, 1H), 1.78 (s, 3H), 1.55–1.43 (m, 1H), 1.35 (s, 3H); ^{13}C NMR ($CDCl_3$, 101 MHz) δ 148.7, 129.7, 128.1, 109.9, 99.4, 80.3, 76.0, 73.9, 71.4, 57.6, 53.2, 48.9, 43.4, 38.5, 38.0, 36.6, 27.8, 25.7, 21.0; IR (Neat Film, NaCl) 3388, 2925, 1660, 1445, 1260, 1098, 1027, 888, 800, 759 cm^{-1}; HRMS (ES+) *m/z* calc'd for $C_{19}H_{26}O_5$ [M•]$^+$: 334.1780, found 334.2023; $[\alpha]_D^{25.0}$ +36.2° (*c* 0.250, $CHCl_3$).

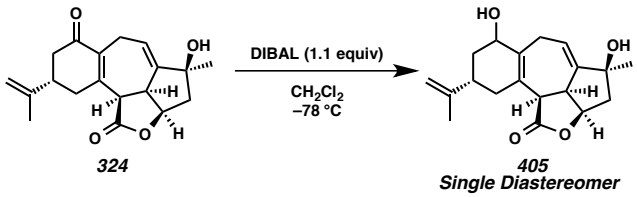

324 ***405***
Single Diastereomer

Allylic Alcohol 405: To a stirred solution of enone **324** (35 mg, 0.11 mmol, 1.00 equiv) in CH_2Cl_2 (4.5 mL) at –78 °C (*i*-PrOH/dry ice bath) was added DIBAL (121 μL, 1.00 M in toluene, 1.10 equiv) slowly dropwise. After 2 h, the reaction was quenched before the complete consumption of starting material, as determined by TLC (1:4 EtOAc:CH_2Cl_2

eluent), by the addition of saturated aqueous NH_4Cl (6.0 mL) and saturated aqueous Rochelle salt (6.0 mL) and immediately removed from the cooling bath and allowed to warm to ambient temperature (ca. 23 °C). After stirring for 1 h, the reaction was diluted with CH_2Cl_2 (10 mL) and poured onto H_2O (30 mL). The organics were separated and the aqueous was extracted with CH_2Cl_2 (4 x 20 mL). The combined organics were dried over $MgSO_4$, filtered, and concentrated in vacuo. The crude off-white solid was purified by silica gel column chromatography (60% EtOAc in hexanes eluent) to provide allylic alcohol **405** (4 mg, 11% yield) as an amorphous white solid: R_f = 0.28 (1:1 EtOAc:CH_2Cl_2 eluent); ^{1}H NMR ($CDCl_3$, 400 MHz) δ 6.22 (dt, *J* = 8.2, 3.3 Hz, 1H), 4.83–4.69 (m, 3H), 4.20 (q, *J* = 7.0, 6.5 Hz, 1H), 3.73 (dq, *J* = 6.0, 2.9 Hz, 1H), 3.36 (dd, *J* = 6.9, 3.0 Hz, 1H), 3.27–3.14 (m, 1H), 2.95–2.78 (m, 2H), 2.43 (d, *J* = 15.4 Hz, 1H), 2.40–2.31 (m, 1H), 2.25–2.14 (m, 1H), 2.02 (dd, *J* = 15.5, 4.1 Hz, 1H), 1.97 (s, 1H), 1.87 (ddt, *J* = 14.2, 10.6, 3.2 Hz, 1H), 1.77 (s, 3H), 1.53 (dd, *J* = 12.2, 9.4 Hz, 1H), 1.41 (s, 3H); ^{13}C NMR ($CDCl_3$, 101 MHz) δ 174.7, 148.7, 148.3, 133.2, 128.0, 127.1, 109.6, 82.3, 78.6, 73.0, 49.1, 47.8, 46.0, 38.7, 38.1, 37.0, 28.9, 28.4, 21.1; IR (Neat Film, NaCl) 3379, 2925, 2855, 1761, 1442, 1373, 1283, 1225, 1151, 1102, 1048, 987, 963, 890, 849, 805, 756 cm^{-1}; HRMS (ES+) *m/z* calc'd for $C_{19}H_{25}O_4$ $[M+H]^+$: 317.1753, found 317.1759; $[\alpha]_D^{25.0}$ +62.5° (*c* 0.200, $CHCl_3$).

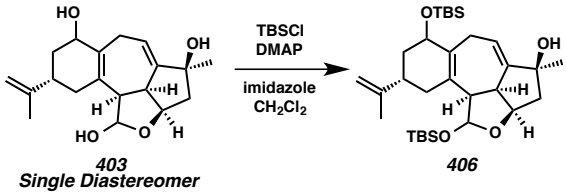

403 ***Single Diastereomer*** ***406***

Silyl Ether 406: To a stirred solution of diol **403** (11 mg, 0.035 mmol, 1.00 equiv) in CH_2Cl_2 (2.0 mL) were added imidazole (181 mg, 2.66 mmol, 76.0 equiv) and DMAP (26 mg, 0.21 mmol, 6.00 equiv) sequentially, each as a solid in a single portion. After 2 minutes, to the colorless homogeneous solution was added TBSCl (80 mg, 0.53 mmol, 15.1 equiv) as a solid in one portion. After 16 h, the consumption of starting material was complete as determined by TLC (1:1 EtOAc:CH_2Cl_2 eluent). The reaction mixture was diluted with hexanes (6.0 mL) and the white suspension was filtered over Celite®, washing with 30% EtOAc in hexanes eluent. The combined organics were concentrated in vacuo. The crude white solid was purified by silica gel column chromatography (5% EtOAc in hexanes eluent) to afford silyl ether **406** (17 mg, 89% yield) as an amorphous white solid: R_f = 0.43 (1:19 EtOAc:Hexanes eluent); ^{1}H NMR ($CDCl_3$, 400 MHz) δ 6.13 (dt, *J* = 8.5, 3.4 Hz, 1H), 5.27 (d, *J* = 5.4 Hz, 1H), 4.71 (q, *J* = 1.7 Hz, 1H), 4.69 (d, *J* = 1.7 Hz, 1H), 4.66 (t, *J* = 3.2 Hz, 1H), 4.27 (d, *J* = 8.8 Hz, 1H), 3.47–3.34 (m, 2H), 3.05–2.92 (m, 1H), 2.80 (t, *J* = 6.1 Hz, 1H), 2.66 (dd, *J* = 18.5, 8.5 Hz, 1H), 2.28 (d, *J* = 17.6 Hz, 1H), 2.22–2.11 (m, 2H), 2.03 (ddt, *J* = 11.3, 6.4, 2.4 Hz, 1H), 1.89–1.76 (m, 2H), 1.74–1.66 (m, 3H), 1.52–1.39 (m, 1H), 1.35 (s, 3H), 0.92 (s, 9H), 0.87 (s, 9H), 0.13 (s, 3H), 0.10 (s, 3H), 0.09 (s, 3H), 0.06 (s, 3H); ^{13}C NMR ($CDCl_3$, 101 MHz) δ 150.8, 148.8, 132.5, 129.7, 126.7, 109.3, 104.0, 83.7, 78.6, 74.2, 55.8, 50.5, 46.3, 39.6, 38.7, 36.3, 28.2, 26.2, 25.9, 25.8, 20.5, 18.4, 17.9, –3.4, –3.6, –4.7, –4.9; IR (Neat Film, NaCl) 2928, 2856, 1461, 1256, 1103, 1066, 1026, 1002, 885, 837, 778 cm^{-1}; HRMS (FAB+) *m/z*

calc'd for $C_{31}H_{53}O_4Si_2$ $[(M+H)–H_2]^+$: 545.3482, found 545.3474; $[\alpha]_D^{25.0}$ +94.6° (*c* 0.200, $CHCl_3$).

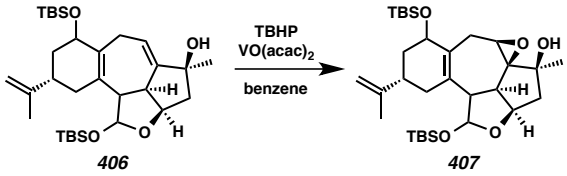

406 *407*

Epoxide 407: To a colorless stirred solution of allylic alcohol **406** (20 mg, 0.036 mmol, 1.00 equiv) in a vial open to air in benzene (2.0 mL) was added $VO(acac)_2$ (1.0 mg, 0.0036 mmol, 0.01 equiv). After 5 minutes, to this dark green solution was added *t*-butyl hydroperoxide (TBHP, 20 μL, 0.10 mmol, 2.78 equiv) as a 5 M solution in decane dropwise causing the reaction to immediately become deep ruby red. After 1 h, the reaction had lost all red color and become pale yellow and the consumption of starting material was complete as determined by TLC (1:19 EtOAc:Hexanes eluent). The reaction was concentrated in vacuo and the crude tan solid was purified by silica gel column chromatography (10% EtOAc in hexanes eluent) to afford epoxide **407** (18 mg, 90% yield) as an amorphous white solid: R_f = 0.17 (1:19 EtOAc:Hexanes eluent); ^{1}H NMR ($CDCl_3$, 400 MHz) δ 5.27 (d, *J* = 5.0 Hz, 1H), 4.71 (t, *J* = 1.6 Hz, 1H), 4.68 (dt, *J* = 1.9, 0.9 Hz, 1H), 4.53 (td, *J* = 4.0, 2.0 Hz, 1H), 4.23 (t, *J* = 8.0 Hz, 1H), 3.22–3.17 (m, 1H), 2.96 (dd, *J* = 6.0, 3.6 Hz, 1H), 2.82–2.65 (m, 3H), 2.62 (s, 1H), 2.43 (d, *J* = 17.0 Hz, 1H), 2.25–2.09 (m, 3H), 2.02 (ddt, *J* = 11.3, 6.4, 2.2 Hz, 1H), 1.79–1.71 (m, 1H), 1.70 (t, *J* = 1.1 Hz, 3H), 1.39 (ddd, *J* = 13.1, 12.1, 10.0 Hz, 1H), 1.28 (s, 3H), 0.92 (s, 9H), 0.87 (s, 9H), 0.13 (s, 3H), 0.11 (s, 3H), 0.10 (s, 3H), 0.08 (s, 3H); ^{13}C NMR ($CDCl_3$, 101 MHz) δ 148.8, 130.4, 126.1, 109.3, 103.3, 80.2, 75.6, 75.2, 71.0, 57.6, 54.8, 46.7, 46.6, 39.1, 38.7,

36.5, 28.2, 27.2, 26.2, 25.9, 20.5, 18.4, 17.9, –3.5, –3.6, –4.7, –4.9.; IR (Neat Film, NaCl) 3441, 2955, 2928, 2856, 1471, 1257, 1093, 1066, 1018, 957, 878, 833, 776 cm^{-1}; HRMS (FAB+) *m/z* calc'd for $C_{31}H_{53}O_5Si_2$ $[(M+H)–H_2]^+$: 561.3432, found 561.3441; $[\alpha]_D^{25.0}$ +88.4° (*c* 0.150, $CHCl_3$).

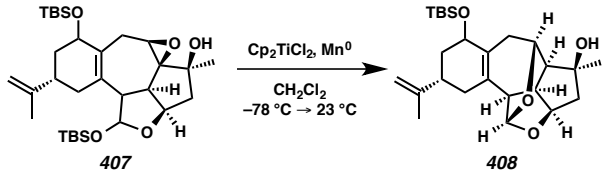

407 ***408***

Ketal 408:

Preparation of a 0.50 M Stock Solution of Titanocene Monchloride (Cp_2TiCl)

Into a thoroughly flame-dried Schlenk tube under an overpressure of argon was charged with manganese(0) dust (543 mg, 9.90 mmol, 3.00 equiv) and titanocene dichloride (Cp_2TiCl_2, 822 mg, 3.30 mmol, 1.00 equiv). The flask was then evacuated and back filled with argon (3 x 5 minute cycles). To the reaction vessel was then added THF (6.6 mL) that had previously been sparged with argon for 60 minutes and stirring commenced. After 1.5 h, the bright red reaction mixture had become yellow-green and stirring was halted. After 30 minutes, the supernatant was used as a 0.50 M stock solution of Cp_2TiCl.

Epoxide Opening with Cp_2TiCl

A stirred solution of epoxide **407** (18 mg, 0.042 mmol, 1.00 equiv) in THF (3.0 mL) was sparged with argon for 1 h, resulting in a reaction volume of 2.0 mL. The homogeneous, off-white reaction mixture was then cooled to –78 °C (*i*-PrOH/dry ice bath) followed by the addition of H_2O (63 μL, 3.50 mmol, 83.3 equiv). After stirring for

5 minutes, Cp_2TiCl (0.88 mmol, 0.50 M in THF, 21.0 equiv) was added dropwise over 3 minutes. After 2.5 h, the reaction vessel was warmed to 0 °C (ice/H_2O bath). After an additional 5.5 h, the Schlenk tube was removed from the cooling bath and allowed to warm to ambient temperature. After an additional 42 h, the consumption of starting material was complete as determined by TLC (3:17 Acetone:Hexanes eluent). The reaction was quenched by the addition of saturated NaH_2PO_4 (0.25 mL) and brine (0.25 mL), sparged with compressed air for 5 minutes, and allowed to stir for an additional 15 minutes. The reaction mixture was then filtered through a Celite® plug, washing with 50% acetone in hexanes eluent. The combined organics were concentrated in vacuo and immediately purified by silica gel column chromatography (8% acetone in hexanes eluent) to furnish ketal **408** (16 mg, 89% yield) as an amorphous white solid: R_f = 0.22 (3:17 Acetone:Hexanes eluent); ^{1}H NMR ($CDCl_3$, 400 MHz) δ 5.46 (dd, *J* = 3.7, 1.0 Hz, 1H), 4.80–4.69 (m, 2H), 4.44 (ddd, *J* = 6.0, 1.9, 0.8 Hz, 1H), 4.27–4.15 (m, 2H), 3.27 (d, *J* = 1.3 Hz, 1H), 3.14 (dt, *J* = 9.9, 3.3 Hz, 1H), 2.65–2.56 (m, 1H), 2.50–2.41 (m, 1H), 2.39 (d, *J* = 9.9 Hz, 1H), 2.35–2.27 (m, 2H), 2.24 (dd, *J* = 14.9, 1.1 Hz, 1H), 2.17 (dddd, *J* = 16.1, 11.3, 5.5, 2.3 Hz, 1H), 1.98 (dddt, *J* = 13.4, 7.5, 4.7, 2.3 Hz, 2H), 1.87 (ddd, *J* = 14.5, 3.2, 1.1 Hz, 1H), 1.73 (t, *J* = 1.1 Hz, 3H), 1.48 (ddd, *J* = 13.1, 12.3, 10.2 Hz, 1H), 1.33 (d, *J* = 1.1 Hz, 3H), 0.91 (s, 9H), 0.09 (app s, 6H); ^{13}C NMR ($CDCl_3$, 101 MHz) δ 148.7, 133.6, 126.9, 109.5, 103.6, 84.9, 82.1, 72.4, 65.8, 54.3, 51.0, 50.0, 48.3, 40.2, 39.8, 39.5, 37.8, 29.9, 26.1, 20.5, 18.4, –3.9, –4.6; IR (Neat Film, NaCl) 3440, 2928, 2856, 1463, 1367, 1258, 1211, 1068, 1046, 958, 869, 836, 776 cm^{-1}; HRMS (FAB+) *m/z* calc'd for $C_{25}H_{39}O_4Si$ $[(M+H)–H_2]^+$: 431.2618, found 431.2622; $[\alpha]_D^{25.0}$ +44.3° (*c* 0.150, $CHCl_3$).

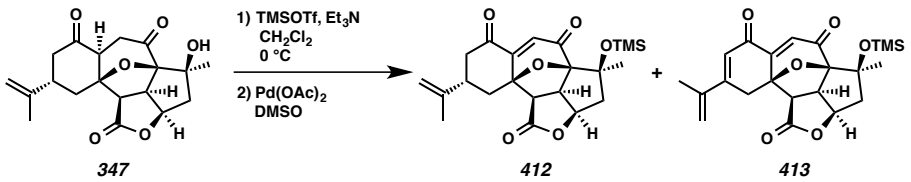

347 *412* *413*

Vinylogous Diketone 412 and Dienone 413: To a stirred solution of diketone **347** (15 mg, 0.043 mmol, 1.00 equiv) in CH_2Cl_2 (0.4 mL) at 0 °C (ice/H_2O bath) was added Et_3N (0.12 mL, 0.87 mmol, 20.0 equiv) dropwise. After 2 minutes, TMSOTf (24 μL, 0.13 mmol, 3.00 equiv) was added slowly dropwise. After 1.5 h, TMSOTf (24 μL, 0.13 mmol, 3.00 equiv) was added slowly dropwise. After an additional 1.5 h, the consumption of starting material was complete as determined by TLC (1:1 EtOAc:CH_2Cl_2 eluent). The reaction was quenched by the addition of saturated aqueous $NaHCO_3$ (1.5 mL) and the biphasic mixture was immediately removed from the cooling bath and allowed to warm to ambient temperature (ca. 23 °C). The reaction mixture was diluted with Et_2O (2 mL) and poured onto H_2O (3 mL). The organics were separated and the aqueous was extracted with Et_2O (5 x 2 mL). The combined organics were dried over $MgSO_4$, filtered, and concentrated in vacuo. The crude amorphous white solid was carried on without further purification.

To a stirred solution of the crude white solid in DMSO (1.5 mL) was added $Pd(OAc)_2$ (30 mg, 0.13 mmol, 3.11 equiv) as a solid in single portion. After 7 h, the consumption of starting material was complete as determined by TLC (3:3 EtOAc:Hexanes eluent). The dark brown reaction mixture was diluted with H_2O (8 mL) and the aqueous was extracted with CH_2Cl_2 (5 x 10 mL) followed by EtOAc (2 x 5 mL). The combined organics were dried over $MgSO_4$, filtered, and concentrated in vacuo. The

crude brown solid was purified by semi-preparative HPLC (Agilent ZORBAX RX-SIL silica gel column, 5 μm mesh, 9.4 mm x 250 mm, mobile phase: 20% EtOAc in hexanes, flow rate: 7.00 mL/min) to provide vinylogous diketone **412** (retention time 9.9 minutes, 10 mg, 56% yield) as an amorphous white solid and dienone **413** (retention time 11.4 minutes, 8 mg, 44% yield) as an amorphous white solid.

Vinylogous Diketone 412: R_f = 0.37 (3:7 EtOAc:Hexanes eluent); ^{1}H NMR ($CDCl_3$, 600 MHz) δ 6.26 (q, *J* = 0.7 Hz, 1H), 4.93 (dddd, *J* = 9.4, 8.3, 6.8, 1.5 Hz, 1H), 4.89 (s, 1H), 4.84–4.82 (m, 1H), 3.35 (td, *J* = 8.8, 1.5 Hz, 1H), 3.15 (dd, *J* = 8.8, 1.5 Hz, 1H), 2.77–2.61 (m, 3H), 2.49–2.38 (m, 2H), 2.31 (ddd, *J* = 12.6, 7.7, 1.4 Hz, 1H), 2.19 (dtd, *J* = 15.1, 2.6, 1.6 Hz, 1H), 1.81 (m, 3H), 1.66 (s, 3H), 0.11 (s, 9H); ^{13}C NMR ($CDCl_3$, 126 MHz) δ 199.8, 194.3, 173.4, 156.2, 145.2, 127.7, 111.6, 96.7, 86.1, 81.2, 77.8, 54.0, 49.9, 47.1, 44.9, 37.8, 35.3, 27.1, 20.9, 2.4; IR (Neat Film, NaCl) 2960, 2928, 1765, 1702, 1252, 1193, 1069, 1046, 869, 841 cm^{-1}; HRMS (FAB+) *m/z* calc'd for $C_{22}H_{29}O_6Si$ $[M+H]^+$: 417.1733, found 417.1741; $[\alpha]_D^{25.0}$ –16.9 ° (*c* 0.100, $CHCl_3$).

Dienone 413: R_f = 0.37 (3:7 EtOAc:Hexanes); ^{1}H NMR ($CDCl_3$, 400 MHz) δ 6.64 (d, *J* = 0.7 Hz, 1H), 6.44 (d, *J* = 2.5 Hz, 1H), 5.75 (s, 1H), 5.57 (dd, *J* = 1.9, 1.0 Hz, 1H), 4.93 (tdd, *J* = 9.5, 8.6, 7.7, 3.4 Hz, 1H), 3.45–3.36 (m, 2H), 3.26 (dd, *J* = 8.8, 0.6 Hz, 1H), 3.01 (dd, *J* = 17.0, 2.6 Hz, 1H), 2.48–2.38 (m, 1H), 2.37–2.30 (m, 1H), 2.08 (d, *J* = 1.3 Hz, 3H), 1.68 (d, *J* = 1.2 Hz, 3H), 0.16–0.08 (m, 9H); ^{13}C NMR ($CDCl_3$, 101 MHz) δ 193.8, 185.0, 173.2, 157.2, 151.4, 141.1, 127.0, 124.9, 122.9, 95.6, 86.5, 80.8, 78.0, 52.8, 50.2, 47.2, 30.3, 26.8, 20.6, 2.4; IR (Neat Film, NaCl) 2959, 1770, 1702, 1660, 1611, 1378, 1252, 1179, 1066, 1036, 870, 842, 759 cm^{-1}; HRMS (FAB+) *m/z* calc'd for $C_{22}H_{27}O_6Si$ $[M+H]^+$: 415.1577, found 415.1588; $[\alpha]_D^{25.0}$ +70.9° (*c* 0.100, $CHCl_3$).

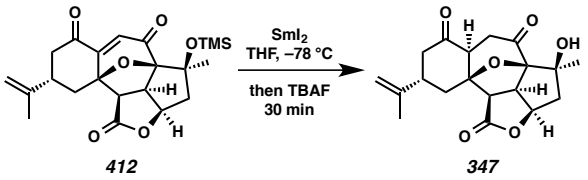

Diketone 347:

Preparation of a 0.07 M Stock Solution SmI_2

Into a Schlenk tube was added freshly filed samarium metal (150 mg, 1.00 mmol, 1.41 equiv). The reaction vessel was then thoroughly flame-dried, backfilled with argon, and allowed to cool to ambient temperature (ca. 23 °C). To the reaction vessel was then added THF (10.0 mL) that had previously been sparged with argon for 60 minutes and cooled to 0 °C (ice/H_2O bath) with stirring. EtI_2 (200 mg, 0.71 mmol, 1.00 equiv) was then added in separate 100 mg portions 30 minutes apart. After the addition of the second portion, the Schlenk tube was removed from the cooling bath, allowed to warm to ambient temperature, and the pale yellow solution was stirred overnight (ca. 14 h) causing the reaction to become deep blue, indicating to formation of SmI_2.

*Reduction of Vinlyogous Diketone **412***

A stirred solution of vinylogous diketone **412** (4 mg, 0.0010 mmol, 1.00 equiv) in THF (1.5 mL) was sparged to 1.5 h, leaving a reaction volume of 0.25 mL. The resultant colorless reaction mixture was then cool to –78 °C (*i*-PrOH/dry ice bath) at which time SmI_2 (0.010 mmol, 0.07 M in THF, 10.0 equiv) was added dropwise. After 20 minutes, the consumption of starting material was complete as determined by TLC (1:4 EtOAc:CH_2Cl_2 eluent). To the reaction mixture was then added TBAF (0.01 mmol, 1.0 M in THF, 10.0 equiv). After 10 minutes, the reaction was quenched by addition of H_2O (50 μL), removed from the cooling bath, and allowed to warm to ambient temperature. The

dark yellow reaction mixture was then filtered through a pad of silica gel (50% EtOAc in CH_2Cl_2 eluent), and concentrated in vacuo. The crude dark gold solid was purified by silica gel column chromatography (20% EtOAc in CH_2Cl_2 eluent) to afford saturated diketone **347** (3 mg, 75% yield) as a crystalline white solid: characterization data match those reported above (see chapter 3, Section 3.9.2).

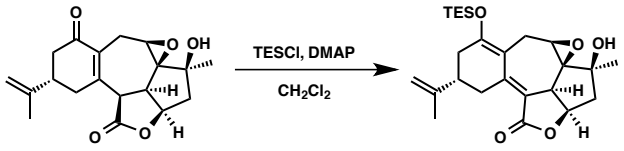

Isoineleganolide A
328

415

Dienol ether 415: To a stirred solution of enone **328** (5 mg, 0.015 mmol, 1.00 equiv) in CH_2Cl_2 (0.5 mL) was added DMAP (7 mg, 0.057 mmol, 3.83 equiv) as a solid in one portion. After 2 minutes, the reaction mixture had become a completely homogenous pale yellow solution, and TESCl (25 μL, 0.15 mmol, 10.0 equiv) was added quickly dropwise. After 4 h, the consumption of starting material was complete as determined by TLC (1:4 EtOAc:CH_2Cl_2 eluent). The reaction was quenched by the addition of saturated aqueous $NaHCO_3$ (50 μL). After 5 minutes, the white suspension was filtered through a pad of silica gel (20% EtOAc in CH_2Cl_2 eluent). The combined organics were concentrated in vacuo and the resultant crude white solid was purified by silica gel column chromatography (30% EtOAc in hexanes eluent) to provide intermediate enol ether **415** (1.5 mg, 50% yield) as an amorphous white solid: R_f = 0.24 (3:7 EtOAc:Hexanes eluent); ^{1}H NMR ($CDCl_3$, 400 MHz) δ 4.82–4.70 (m, 3H), 4.04–3.95 (m, 1H), 3.91–3.85 (m, 1H), 3.68 (dd, *J* = 16.0, 6.6 Hz, 1H), 3.49 (dd, *J* = 6.5, 0.7 Hz, 1H), 2.57 (dd, *J* = 12.9, 7.0 Hz, 1H), 2.51–2.24 (m, 6H), 1.97 (dd, *J* = 12.9, 8.2 Hz, 1H), 1.76 (dd, *J* = 1.5, 0.8 Hz, 3H),

1.31 (d, *J* = 1.0 Hz, 3H), 1.02 (t, *J* = 7.9 Hz, 6H), 0.75 (qd, *J* = 7.9, 0.8 Hz, 9H); ^{13}C NMR ($CDCl_3$, 101 MHz) δ 171.0, 160.7, 154.7, 147.2, 114.7, 110.5, 110.2, 73.8, 72.9, 71.5, 53.9, 48.8, 42.4, 39.9, 36.8, 30.7, 23.6, 23.0, 21.2, 6.8, 5.9; IR (Neat Film, NaCl) 3478, 2960, 1728, 1586, 1449, 1345, 1192, 1112, 1046, 961, 937, 889, 790, 764 cm^{-1}; HRMS (FAB+) *m/z* calc'd for $C_{25}H_{37}O_5Si$ $[M+H]^+$: 445.2410, found 445.2419; $[\alpha]_D^{25.0}$ +229.2° (*c* 0.100, $CHCl_3$).

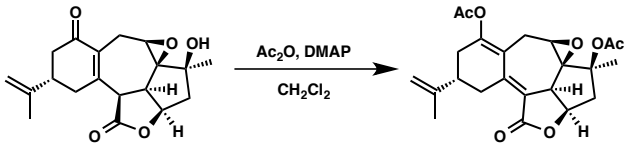

Isoineleganolide A* 328** ***416

Enol Acetate 416: To a stirred solution of enone **328** (10 mg, 0.030 mmol, 1.00 equiv) in CH_2Cl_2 (1.0 mL) was added DMAP (14 mg, 0.11 mmol, 3.67 equiv) as a solid in one portion. After 2 minutes, the reaction mixture had become a completely homogenous pale yellow solution, and Ac_2O (30 μL, 0.32 mmol, 10.7 equiv) was added quickly dropwise. After 2 h, the consumption of starting material was complete as determined by TLC (1:4 EtOAc:CH_2Cl_2 eluent). The reaction was diluted with CH_2Cl_2 (3 mL) and poured onto saturated aqueous $NaHCO_3$ (3 mL). The organics were separated and the aqueous was extracted with CH_2Cl_2 (2 x 5 mL). The combined organics were dried over MgSO4, filtered, and concentrated in vacuo. The crude golden solid was purified by silica gel column chromatography (50% EtOAc with 0.5% Et_3N in hexanes eluent) to provide enol acetate **416** (11 mg, 85% yield) as an amorphous white solid: R_f = 0.42 (1:1 EtOAc:Hexanes eluent); ^{1}H NMR ($CDCl_3$, 400 MHz) δ 4.84 (ddd, *J* = 9.4, 7.9, 7.2 Hz, 1H), 4.80–4.76 (m, 2H), 3.96 (d, *J* = 13.0 Hz, 1H), 3.84 (d, *J* = 9.1 Hz, 1H), 3.71 (dd, *J* =

6.5, 0.7 Hz, 1H), 3.24 (dd, *J* = 16.1, 6.5 Hz, 1H), 3.01 (dd, *J* = 13.2, 7.2 Hz, 1H), 2.57–2.24 (m, 6H), 2.23 (s, 3H), 1.98 (s, 3H), 1.77–1.72 (m, 3H), 1.61 (d, *J* = 1.0 Hz, 3H); ^{13}C NMR ($CDCl_3$, 101 MHz) δ 170.2, 170.0, 168.1, 156.0, 152.4, 146.7, 122.2, 115.1, 110.6, 80.9, 73.1, 69.7, 53.2, 46.3, 42.8, 39.7, 34.2, 30.5, 23.6, 21.9, 21.7, 21.1, 21.0; IR (Neat Film, NaCl) 2925, 1740, 1615, 1440, 1372, 1241, 1204, 1153, 1118, 1043, 968, 934, 899, 792, 754 cm^{-1}; HRMS (FAB+) *m/z* calc'd for $C_{23}H_{27}O_7$ $[M+H]^+$: 415.1757, found 415.1737; $[\alpha]_D^{25.0}$ +241.6° (*c* 0.100, $CHCl_3$).

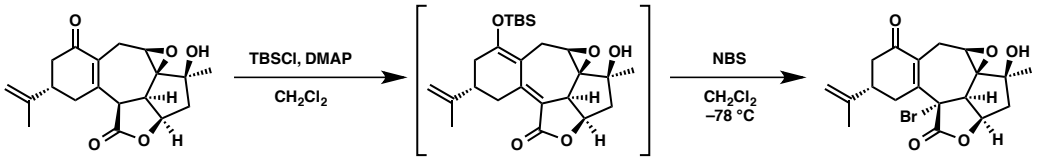

Bromide 420: To a stirred solution of enone **328** (15 mg, 0.047 mmol, 1.00 equiv) in CH_2Cl_2 (3.0 mL) was added DMAP (25 mg, 0.20 mmol, 4.36 equiv) as a solid in one portion. After 2 minutes, the reaction mixture had become a completely homogenous pale yellow solution, and TBSCl (70 mg, 0.46 mmol, 9.79 equiv) was added as a solution in CH_2Cl_2 (0.7 mL) quickly dropwise over 2 minutes. After 2 h, the consumption of starting material was complete as determined by TLC (1:4 EtOAc:CH_2Cl_2 eluent). The reaction was quenched by the addition of Et_3N (0.30 mL, 2.15 mmol, 45.7 equiv) in hexanes (3.0 mL) with stirring. After 5 minutes, the white suspension was loaded directly onto a silica gel column and purified by silica gel column chromatography (30% EtOAc with 0.5% Et_3N in hexanes eluent, silica gel deactivated by wet loading with eluent prior to purification) to provide intermediate enol ether **429** (20 mg, >99% yield), which was immediately carried on to the next transformation.

To a clear, colorless stirred solution of a portion of enol ether **429** (5 mg, 0.011 mmol, 1.00 equiv) in CH_2Cl_2 (0.6 mL) at –78 °C (*i*-PrOH/dry ice bath) was added *N*-bromosuccinimide (NBS, 3.4 mg, 0.019 mmol, 1.73 equiv) as a solid in a single portion to provide a homogenous, colorless reaction mixture. After 2 h, the consumption of starting material was complete as determined by TLC (1:1 EtOAc:Hexanes eluent). The reaction was quenched by the addition of saturated aqueous $Na_2S_2O_3$ (0.5 mL) and the reaction vessel was immediately removed from the cooling bath and allowed to warm to ambient temperature (ca. 23 °C). The biphasic solution was then diluted with CH_2Cl_2 (4.0 mL) and poured onto saturated aqueous $NaHCO_3$ (3.0 mL). The organics were separated and the aqueous was extracted with CH_2Cl_2 (3 x 2 mL). The combined organics were dried over $MgSO_4$, filtered, and concentrated in vacuo. The crude white solid was purified by silica gel column chromatography (50% EtOAc in hexanes eluent) to afford bromide **420** (4 mg, 80% yield) as an amorphous white solid: R_f = 0.32 (1:1 EtOAc:Hexanes eluent); ^{1}H NMR ($CDCl_3$, 400 MHz) δ 5.18 (ddd, *J* = 5.1, 4.2, 2.2 Hz, 1H), 4.88–4.83 (m, 1H), 4.77 (q, *J* = 1.0 Hz, 1H), 3.96 (dd, *J* = 17.3, 6.7 Hz, 1H), 3.68 (ddt, *J* = 16.8, 3.5, 1.9 Hz, 1H), 3.62 (d, *J* = 4.2 Hz, 1H), 3.36 (d, *J* = 6.6 Hz, 1H), 2.80–2.65 (m, 2H), 2.62–2.49 (m, 1H), 2.49–2.42 (m, 2H), 2.39 (dd, *J* = 3.5, 1.3 Hz, 2H), 2.37–2.32 (m, 1H), 1.82 (s, 3H), 1.35 (s, 3H); ^{13}C NMR ($CDCl_3$, 101 MHz) δ 198.8, 169.3, 150.2, 146.4, 129.0, 110.8, 80.7, 75.1, 69.8, 62.1, 54.3, 52.4, 45.1, 43.1, 40.6, 35.6, 27.4, 21.1, 20.8; IR (Neat Film, NaCl) 3508, 2965, 1774, 1668, 1443, 1367, 1260, 1168, 1100, 973, 894, 789, 759 cm^{-1}; HRMS (FAB+) *m/z* calc'd for $C_{19}H_{22}O_5{}^{81}Br$ $[M+H]^+$: 411.0630, found 411.0634; $[\alpha]_D^{25.0}$ +141.1° (*c* 0.200, $CHCl_3$).

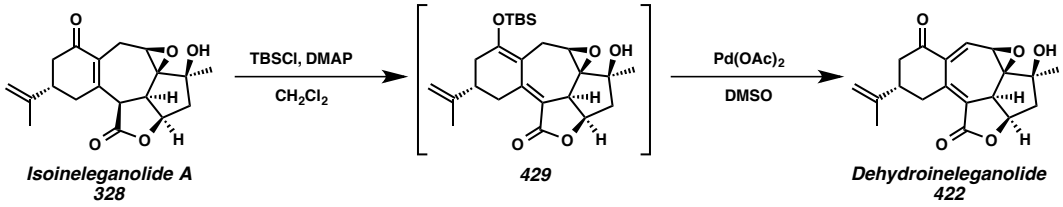

Diene 422: To a stirred solution of enone **328** (46 mg, 0.14 mmol, 1.00 equiv) in CH_2Cl_2 (6.0 mL) was added DMAP (85 mg, 0.70 mmol, 5.00 equiv) as a solid in one portion. After 2 minutes, the reaction mixture had become a completely homogenous pale yellow solution, and TBSCl (210 mg, 1.39 mmol, 10.0 equiv) was added as a solution in CH_2Cl_2 (2.1 mL) quickly dropwise over 2 minutes. After 2 h, the consumption of starting material was complete as determined by TLC (1:4 EtOAc:CH_2Cl_2 eluent). The reaction was quenched by the addition of Et_3N (0.97 mL, 7.0 mmol, 50.0 equiv) in hexanes (6.0 mL) with stirring. After 5 minutes, the white suspension was loaded directly onto a silica gel column and purified by silica gel column chromatography (30% EtOAc with 0.5% Et_3N in hexanes eluent, silica gel deactivated by wet loading with eluent prior to purification) to provide intermediate enol ether **429** (62 mg, >99% yield), which was immediately carried on to the next transformation.

To a clear, colorless stirred solution to enol ether **429** (62 mg, 0.14 mmol, 1.00 equiv) in DMSO (3.0 mL) was added $Pd(OAc)_2$ (35 mg, 0.016 mmol, 1.14 equiv) as a solid in a single portion. After 2 h, the golden yellow homogeneous reaction mixture had become dark brown and the consumption of starting material was complete as determined by TLC (3:7 EtOAc:Hexanes eluent). The reaction was then diluted with EtOAc (10 mL) and poured onto H_2O (30 mL). The organics were separated and the aqueous was extracted with EtOAc (3 x 20 mL). The combined organics were washed with H_2O (30 mL), dried over $MgSO_4$, filtered through a pad of silica gel (EtOAc eluent), and

concentrated in vacuo. The crude brown solid was purified by silica gel column chromatography (55% EtOAc in hexanes eluent) to afford diene **422** (27 mg, 60% yield) as an amorphous white solid: R_f = 0.25 (1:1 EtOAc:Hexanes eluent); ^{1}H NMR ($CDCl_3$, 400 MHz) δ 7.19 (d, *J* = 4.6 Hz, 1H), 4.98 (ddd, *J* = 8.4, 7.5, 6.8 Hz, 1H), 4.83 (h, *J* = 1.5 Hz, 1H), 4.72–4.65 (m, 1H), 3.72 (d, *J* = 4.6 Hz, 1H), 3.59–3.47 (m, 2H), 3.18–3.05 (m, 1H), 2.73–2.60 (m, 3H), 2.56–2.46 (m, 1H), 2.15 (d, *J* = 1.0 Hz, 1H), 1.87 (ddd, *J* = 13.7, 7.0, 1.2 Hz, 1H), 1.79 (dt, *J* = 1.2, 0.6 Hz, 3H), 1.41 (t, *J* = 1.0 Hz, 3H); ^{13}C NMR ($CDCl_3$, 101 MHz) δ 197.5, 169.5, 146.3, 145.9, 140.5, 137.7, 119.6, 111.5, 94.9, 74.6, 74.5, 52.1, 47.1, 44.0, 43.7, 37.9, 31.7, 23.8, 21.3; IR (Neat Film, NaCl) 3459, 2923, 2852, 1742, 1706, 1634, 1449, 1377, 1259, 1173, 1090, 1026, 798 cm^{-1}; HRMS (FAB+) *m/z* calc'd for $C_{19}H_{21}O_5$ $[M+H]^+$: 329.1389, found 329.1373; $[\alpha]_D^{25.0}$ –40.2° (*c* 0.075, $CHCl_3$).

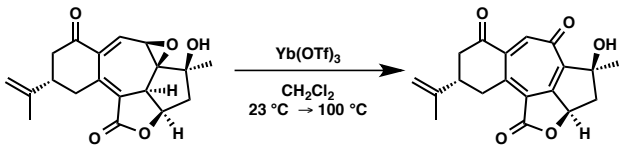

Cycloheptatrienone 423: To a reaction vessel in a nitrogen-filled glovebox was charged $Yb(OTf)_3$ (8 mg, 0.013 mmol, 1.08 equiv). The reaction vessel was sealed, removed from the glovebox, and introduced to an argon atmosphere. To the white solid was added diene **422** (4 mg, 0.012 mmol, 1.00 equiv) as a solution in toluene (1.0 mL) with stirring. The white suspension was then introduced to a preheated 50 °C bath. After 7 h, the reaction was further heated to 80 °C. After an additional 17 h, the reaction was heated to 100 °C. After 11 h, the consumption of starting material was complete as determined by TLC (1:1

EtOAc:Hexanes eluent). The golden yellow heterogeneous reaction mixture was removed from the heating bath and allowed to cool to ambient temperature (ca. 23 °C). The reaction was then concentrated in vacuo. The crude golden brown solid was purified by silica gel column chromatography (40% EtOAc in hexanes eluent) to provide cycloheptatrienone **423** (3 mg, 75% yield) as an amorphous white solid: R_f = 0.09 (3:7 EtOAc:Hexanes eluent); ^{1}H NMR ($CDCl_3$, 400 MHz) δ 8.85 (s, 1H), 5.54 (dd, *J* = 12.8, 5.5 Hz, 1H), 4.94–4.91 (m, 1H), 4.86 (dd, *J* = 1.8, 0.9 Hz, 1H), 3.95 (ddd, *J* = 18.4, 4.0, 2.0 Hz, 1H), 3.57 (s, 1H), 3.18 (dd, *J* = 18.5, 10.2 Hz, 1H), 2.99–2.80 (m, 3H), 2.72 (dd, *J* = 16.0, 11.7 Hz, 1H), 2.20 (t, *J* = 12.3 Hz, 1H), 1.89–1.79 (m, 3H), 1.59 (s, 3H); ^{13}C NMR ($CDCl_3$, 101 MHz) δ 197.4, 195.4, 168.1, 158.5, 151.0, 145.3, 135.9, 131.7, 124.6, 123.8, 112.2, 75.2, 73.8, 43.8, 42.6, 41.0, 30.4, 25.7, 20.8; IR (Neat Film, NaCl) 3366, 2923, 2853, 1775, 1692, 1603, 1441, 1332, 1261, 1202, 1090, 1046, 988, 891, 801 cm^{-1}; HRMS (ES+) *m/z* calc'd for $C_{19}H_{19}O_5$ $[M+H]^+$: 327.1232, found 327.1236; $[\alpha]_D^{25.0}$ +22.7° (*c* 0.150, $CHCl_3$).

4.10 Notes and References

1. (a) Ly, T. W.; Liao, J.-H.; Shia, K.-S.; Liu, H.-J. *Synthesis* **2004**, 271–275. (b) Paisdor, B.; Kuck, D. *J. Org. Chem.* **1991**, *56*, 4753–4759. (c) Paritosh, D.; Byun, H.-S.; Engel, R. *Synth. Commun.* **1986**, *16*, 1343–1346. (d) Mancuso, A. J.; Swern, D. *Synthesis* **1981**, 165–185. (e) Kornblum, N.; Jones, W. J.; Anderson, G. J. *J. Am. Chem. Soc.* **1959**, *81*, 4113–4114.

2. The only products observed from the attempted oxidation of bromide **374** were dehydration products.

3. (a) Gansäuer, A.; Brändle, G. M. Bis(cyclopentadienyl)titanium dichloride: Zinc Metal. In *e-EROS Encyclopedia of Reagents for Organic Synthesis*. 2012. (b) Jiménez, T.; Campaña, A. G.; Bazdi, B.; Paradas, M.; Arráez-Román, D.; Segura-Carretero, A.; Fernández-Gutiérrez, A.; Oltra, J. E.; Robles, R.; Justicia, J.; Cuerva, J. M. *Eur. J. Org. Chem.* **2010**, 4288–4295. (c) Gansäuer, A.; Barchuk, A.; Fielenbach, D. *Synthesis* **2004**, 2567–2573. (d) Gansäuer, A.; Rinker, B. *Tetrahedron* **2002**, *58*, 7017–7026. (e) Gansäuer, A.; Pierobon, M.; Bluhm, H. *Angew. Chem., Int. Ed.* **1998**, *37*, 101–103.

4. 1,4-Cyclohexadiene was also screened as a hydrogen atom donor, but was not as effective as the Cp_2TiCl aquo complex. Mn^0 and Zn^0 were both screened as reductants.

5. Calculations were performed with Spartan '10 (Wavefunction, Inc., Irvine, CA). The in vacuo equilibrium geometry for each structure was calculated by a series of sequential calculations as follows: Hartree–Fock computation (equilibrium geometry, 3-21G basis set), DFT (equilibrium geometry, B3LYP/6-31G basis

set), DFT (energy, B3LYP/6-311+G** basis set), DFT (equilibrium geometry, B3LYP/6-311+G** basis set). The error from these calculations is ±0.23 kcal/mol, thus all energy differences larger than 0.46 kcal/mol were considered significant. Except for molecular mechanics and semi-empirical models, the calculation methods used in Spartan have been documented in: Shao, Y.; Molnar, L. F.; Jung, Y.; Kussmann, J.; Ochsenfeld, C.; Brown, S. T.; Gilbert, A. T. B.; Slipchenko, L. V.; Levchenko, S. V.; O'Neill, D. P.; DiStasio, Jr., R. A.; Lochan, R. C.; Wang, T.; Beran, G. J. O.; Besley, N. A.; Herbert, J. M.; Lin, C. Y.; Van Voorhis, T.; Chien, S. H.; Sodt, A.; Steele, R. P.; Rassolov, V. A.; Maslen, P. E.; Korambath, P. P.; Adamson, R. D.; Austin, B.; Baker, J.; Byrd, E. F. C.; Dachsel, H.; Doerksen, R. J.; Dreuw, A.; Dunietz, B. D.; Dutoi, A. D.; Furlani, T. R.; Gwaltney, S. R.; Heyden, A.; Hirata, S.; Hsu, C-P.; Kedziora, G.; Khalliulin, R. Z.; Klunzinger, P. Lee, A. M.; Lee, M. S.; Liang, W. Z.; Lotan, I.; Nair, N.; Peters, B.; Proynov, E. I.; Pieniazek, P. A.; Rhee, Y. M.; Ritchie, J.; Rosta, E; Sherrill, C. D.; Simmonett, A. C.; Subotnik, J. E.; Woodcock, III, H. L.; Zhang, W.; Bell, A. T.; Chakraborty, A. K.; Chipman, D. M.; Keil, F. J.; Warshel, A.; Hehre, W. J.; Schaefer, H. F.; Kong, J.; Krylov, A. I.; Gill, P. M. W.; Head-Gordon M. *Phys. Chem. Chem. Phys.* **2006**, *8*, 3172–3191.

6. (a) Betancor, C.; Freire, R.; Pérez-Martín, I.; Prangé, T.; Suárez, E. *Tetrahedron* **2005**, *61*, 2803–2814. (b) Cornella, I.; Sestelo, J. P.; Mouriño, A.; Sarandeses, L. A. *J. Org. Chem.* **2002**, *67*, 4707–4714. (c) Paquette, L. A.; Sun, L.-Q.; Friedrich, D.; Savage, P. B. *J. Am. Chem. Soc.* **1997**, *119*, 8438–8450. (d) Dorta, R. L.; Francisco, C. G.; Hernández, R.; Salazar, J. A.; Suárez, E. *J. Chem. Res. (S)* **1990**,

240–241. (e) Concepción, J. I.; Francisco, C. G.; Hernández, R.; Salazar, J. A.; Suárez, E. *Tetrahedron Lett*. **1984**, *25*, 1953–1956.

7. (a) Moriarty, R. M.; Vaid, R. K.; Hopkins, T. E.; Vaid, B. K.; Prakash, O. *Tetrahedron Lett*. **1990**, *31*, 201–204. (b) Koser, G. F.; Relenyi, A. G.; Kalos, A. N.; Rebrovic, L.; Wettach, R. H. *J. Org. Chem*. **1982**, *47*, 2487–2489.

8. (a) Diao, T.; Stahl, S. S. *J. Am. Chem. Soc*. **2011**, *133*, 14566–14569. (b) Trost, B. M.; Dong, G.; Vance, J. A. *Chem. Eur. J*. **2010**, *16*, 6265–6277.

9. (a) Nicolaou, K. C.; Montagnon, T.; Baran, P. S.; Zhong, Y. L. *J. Am. Chem. Soc*. **2002**, *124*, 2245–2258. (b) Nakajima, R.; Ogino, T.; Yokoshima, S.; Fukuyama, T. *J. Am. Chem. Soc*. **2010**, *132*, 1236–1237.

10. Determined by ^{1}H NMR studies of the crude reaction product.

11. For examples of Saegusa–Ito oxidations within cycloheptanones, see: (a) Pandey, G.; Adate, P. A.; Puranik, V. G. *Org. Biomol. Chem*. **2012**, *10*, 8260–8267. (b) Ohmori, N. *J. Chem. Soc., Perkin Trans. 1* **2002**, 755–767. (c) Degrado, S. J.; Mizutani, H.; Hoveyda, A. H. *J. Am. Chem. Soc*. **2001**, *123*, 755–756.

12. The relative stereochemistry at carbinol C(3) of tetracycle **376** was assigned by analogy to the relative stereochemistry of allylic alcohol **383** and by the observed oxidation of alcohol **II** to diepoxide **III** as an inseparable 1:1 mixture of diastereomers as determined by ^{1}H NMR. The directed epoxidation of the dihomoallylic isopropenyl group could only be accomplished with (*S*)-configuration at C(3).

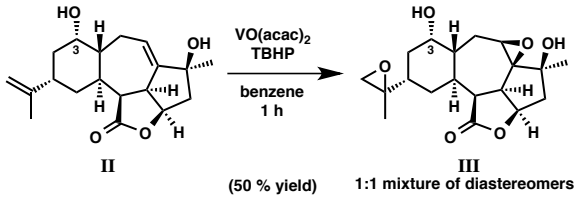

II III
1:1 mixture of diastereomers

13. The C(3) configuration of allylic alcohol **383** was determined by two-dimensional ^{1}H NOE studies and the positive NOE correlation between the methine protons at C(1) and C(3).

14. Reexposure of isolated silyl ethers **389** and **390** to the reaction conditions did not result in any detectable interconversion between the two products.

15. Under titanium(III)-mediated reductive epoxide opening conditions as employed in Scheme 4.4.5, diol **383** failed to furnish any expected product. Rather, dehydration of the secondary alcohol at C(3) was routinely observed under the acidic reaction conditions, as determined by crude ^{1}H NMR.

16. The relative stereochemistry of products **394** and **397** was assigned by analogy to ketones **373** and **375**, whose configurations were established unambiguously by single crystal X-ray diffraction.

17. Attempts to oxidize enol ether **399** focused on reaction conditions employing stoichiometric palladium(II) (e.g., $Pd(OAc)_2$/DMSO) and halogenation reagents (e.g., NBS/CH_2Cl_2).

18. In solution, the *s-trans* conformation of extended enone **413** is preferred and was determined by two-dimensional ^{1}H NOE studies and the positive NOE correlation between the methyl group of the isopropenyl substituent and the vinyl proton at C(2).

19. (a) Szostak, M.; Spain, M.; Procter, D. J. *J. Org. Chem.* **2014**, *79*, 2522–2537. (b) Egger, J.; Bretscher, P.; Freigang, S.; Kopf, M.; Carreira, E. M. *Angew. Chem., Int. Ed.* **2013**, *52*, 5382–5385. (c) Shoji, M.; Uno, T.; Kakeya, H.; Onose, R.; Shiina, I.; Osada, H.; Hayashi, Y. *J. Org. Chem.* **2005**, *70*, 9905–9915. (d) Yamaguchi, J.; Kakeya, H.; Uno, T.; Shoji, M.; Osada, H.; Hayashi, Y. *Angew. Chem., Int. Ed.* **2005**, *44*, 3110–3115. (e) Ready, J. M.; Reisman, S. E.; Hirata, M.; Weiss, M. M.; Tamaki, K.; Ovaska, T. V.; Wood, J. L. *Angew. Chem. Int. Ed.* **2004**, 43, 1270–1272. (f) Fuchs, J. R.; Mitchell, M. L.; Shabangi, M.; Flowers, R. A. *Tetrahedron Lett.* **1997**, *38*, 8157–8158. (g) Molander, G. A.; Hahn, G. *J. Org. Chem.* **1986**, *51*, 1135–1138. (h) Molander, G. A.; Hahn, G. *J. Org. Chem.* **1986**, *51*, 2596–2599.

20. The relative stereochemistry of bromide **420** was assigned by analogy to the unambiguous assignment of the relative stereochemistry of diene **324** by single crystal X-ray diffraction (see Chapter 3 and Figure 3.4.1).

21. (a) Li, Y.; Pattenden, G. *Nat. Prod. Rep.* **2011**, *28*, 1269–1310. (b) Li, Y.; Pattenden, G. *Nat. Prod. Rep.* **2011**, *28*, 429–440. (c) Li, Y.; Pattenden, G. *Tetrahedron* **2011**, *67*, 10045–10052.

22. Pangborn, A. B.; Giardello, M. A.; Grubbs, R. H.; Rosen, R. K.; Timmers, F. J. *Organometallics* **1996**, *15*, 1518–1520.

23. No clean HRMS peak for the parent mass of lactol **403** could be observed, despite screening all instruments and ionization sources available to us. The acid required for most ionization methods is likely causing decomposition of the free lactol.

The major mass peaks observed for this compound by ES+ were: 253.1585, 299.1633, 317.1746, 318.1780.

24. No clean HRMS peak for the parent mass of lactol **404** could be observed, despite screening all instruments and ionization sources available to us. The acid required for most ionization methods is likely causing decomposition of the free lactol. The major mass peaks observed for this compound by ES+ were: 281.1531, 282.1579, 322.1805, 334.2023, 335.2060.

APPENDIX 9

Synthetic Summary for Chapter 4:

Revised Plan for the Synthesis of Ineleganolide:

Alternative Advancement Toward the Asymmetric Total Synthesis

of Ineleganolide by Late Stage Oxidation State Manipulation

*Scheme A9.1. Synthesis of 2H-Ineleganolide (**373**) Through Conjugate Reduction of Diene **324***

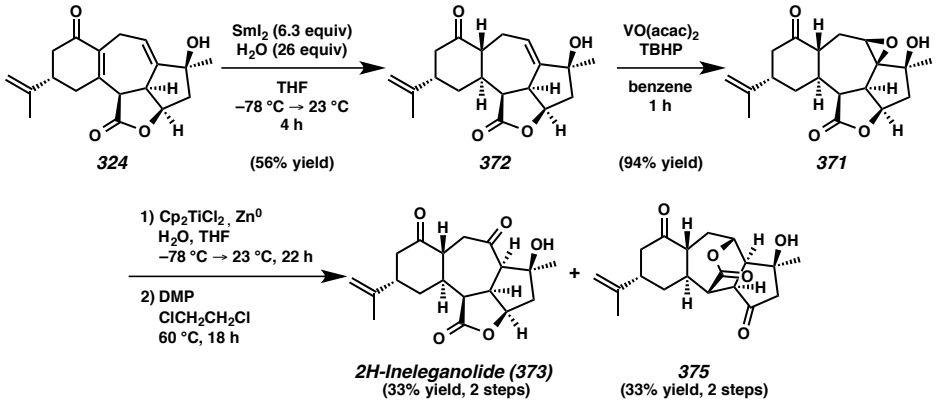

*Scheme A9.2. Formation of Translactonized Polycycle **378***

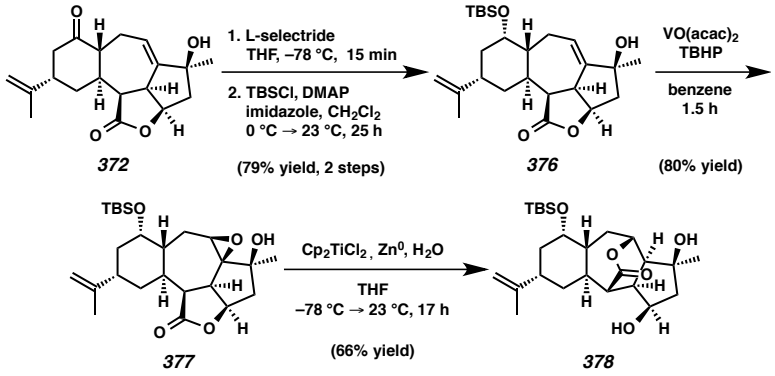

*Scheme A9.3. 1,2-Reduction of Isoineleganolide A (**328**) and Subsequent Silyl Ether Formation with Concomitant Olefin Isomerization*

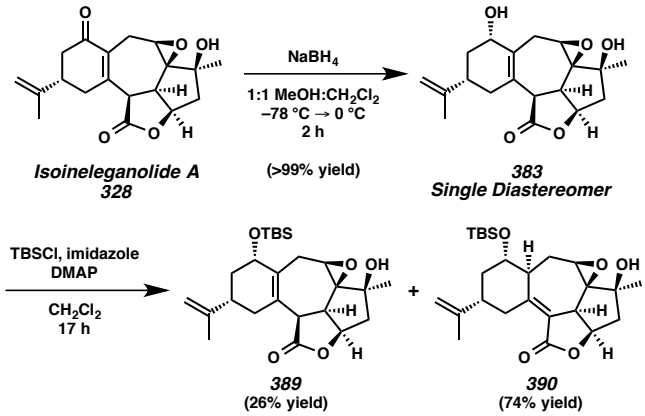

*Scheme A9.4. Advancement of Isomeric Allylic Silyl Ether **389** and Unsaturated Lactone **390***

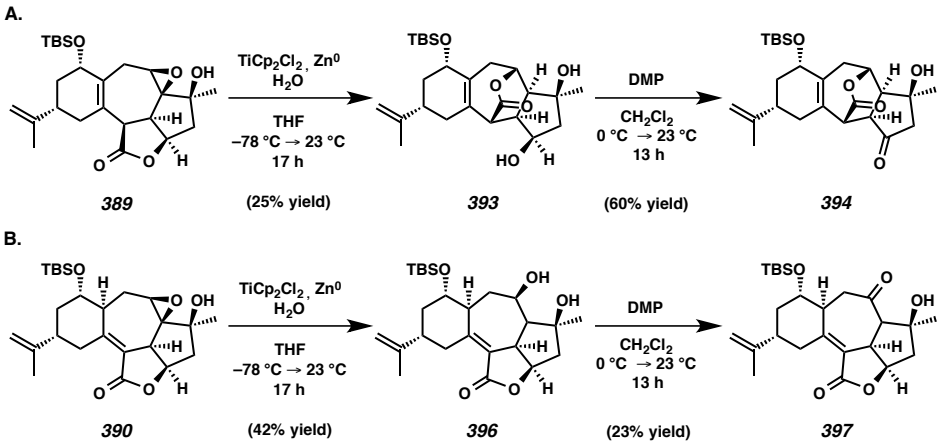

*Scheme A9.5. Construction and Transformation of Lactol **403***

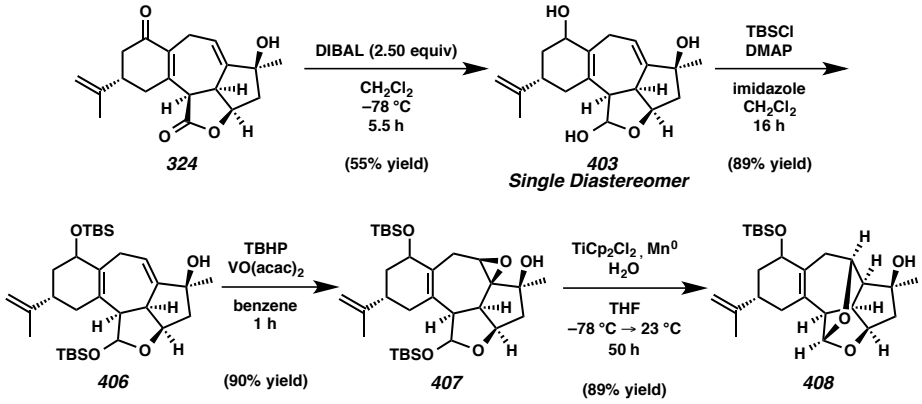

*Scheme A9.6. Oxidative Desaturation of Isoineleganolide A (**328**)*

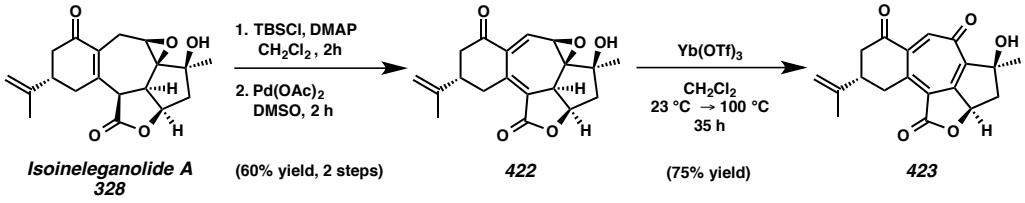

Figure A9.1. Characteristic Examples of the Synthetic Natural Product-Like Ineleganoloids

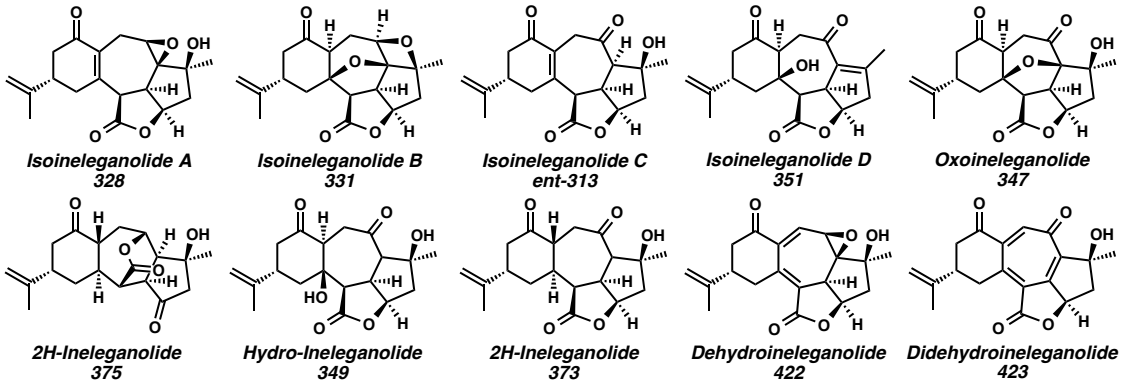

APPENDIX 10

Spectra Relevant to Chapter 4:

Revised Plan for the Synthesis of Ineleganolide:

Alternative Advancement Toward the Asymmetric Total Synthesis

of Ineleganolide by Late Stage Oxidation State Manipulation

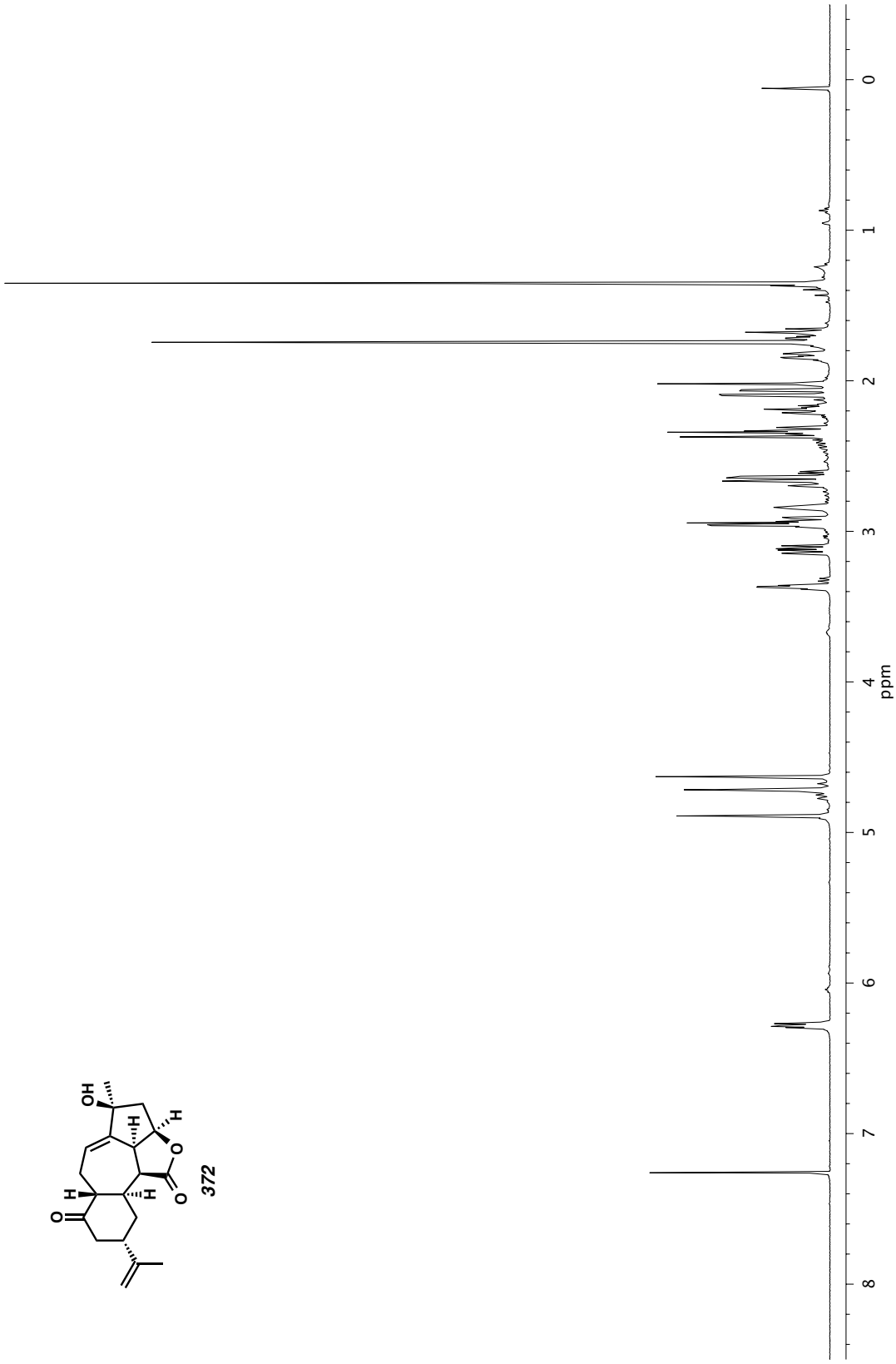

Figure A10.1. ^{1}H NMR (500 MHz, $CDCl_3$) of compound **372**.

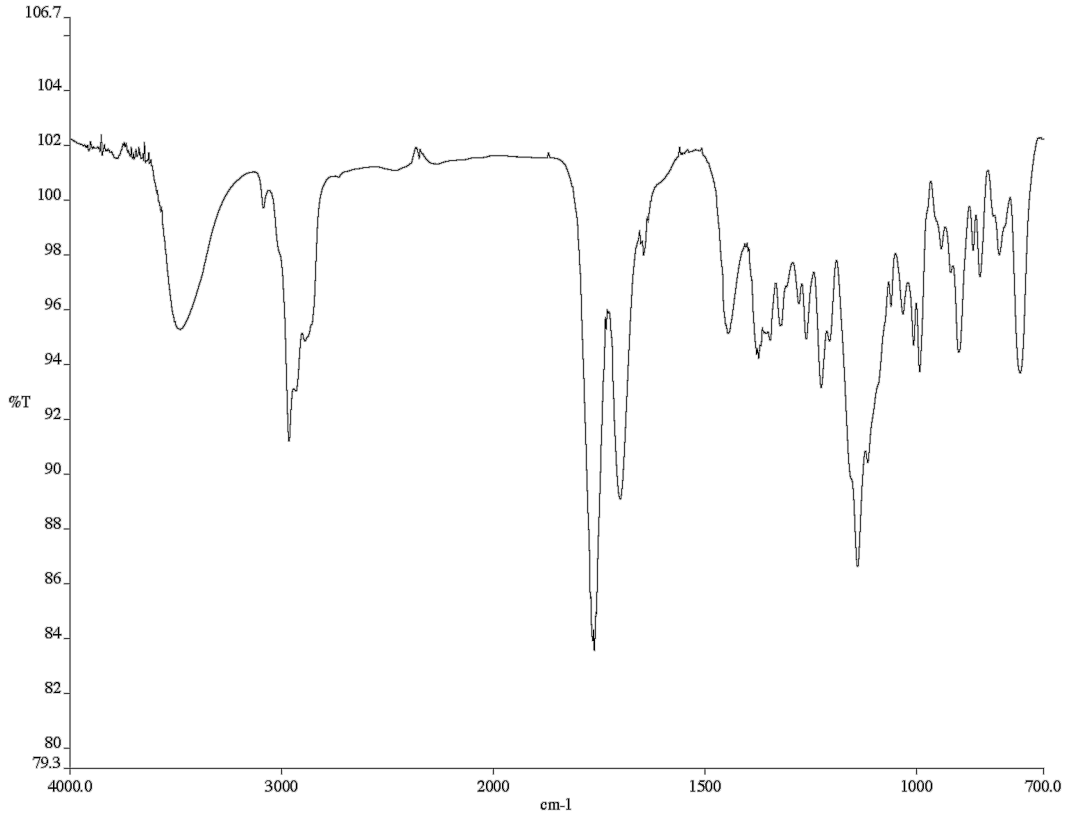

Figure A10.2. Infrared spectrum (Thin Film, NaCl) of compound **372**.

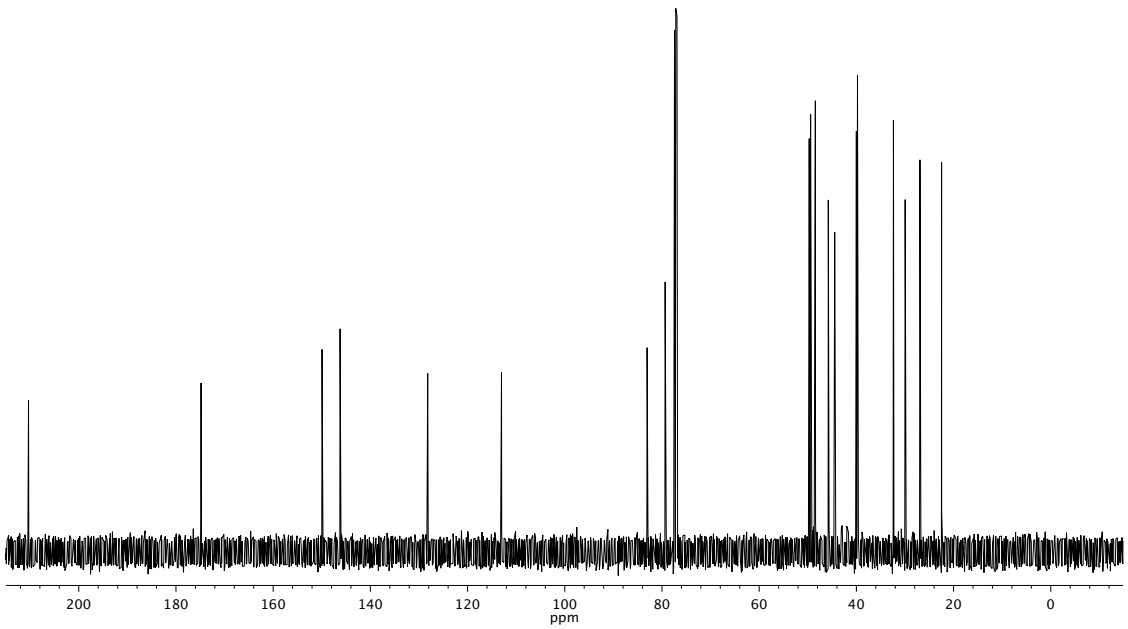

Figure A10.3. ^{13}C NMR (126 MHz, $CDCl_3$) of compound **372**.

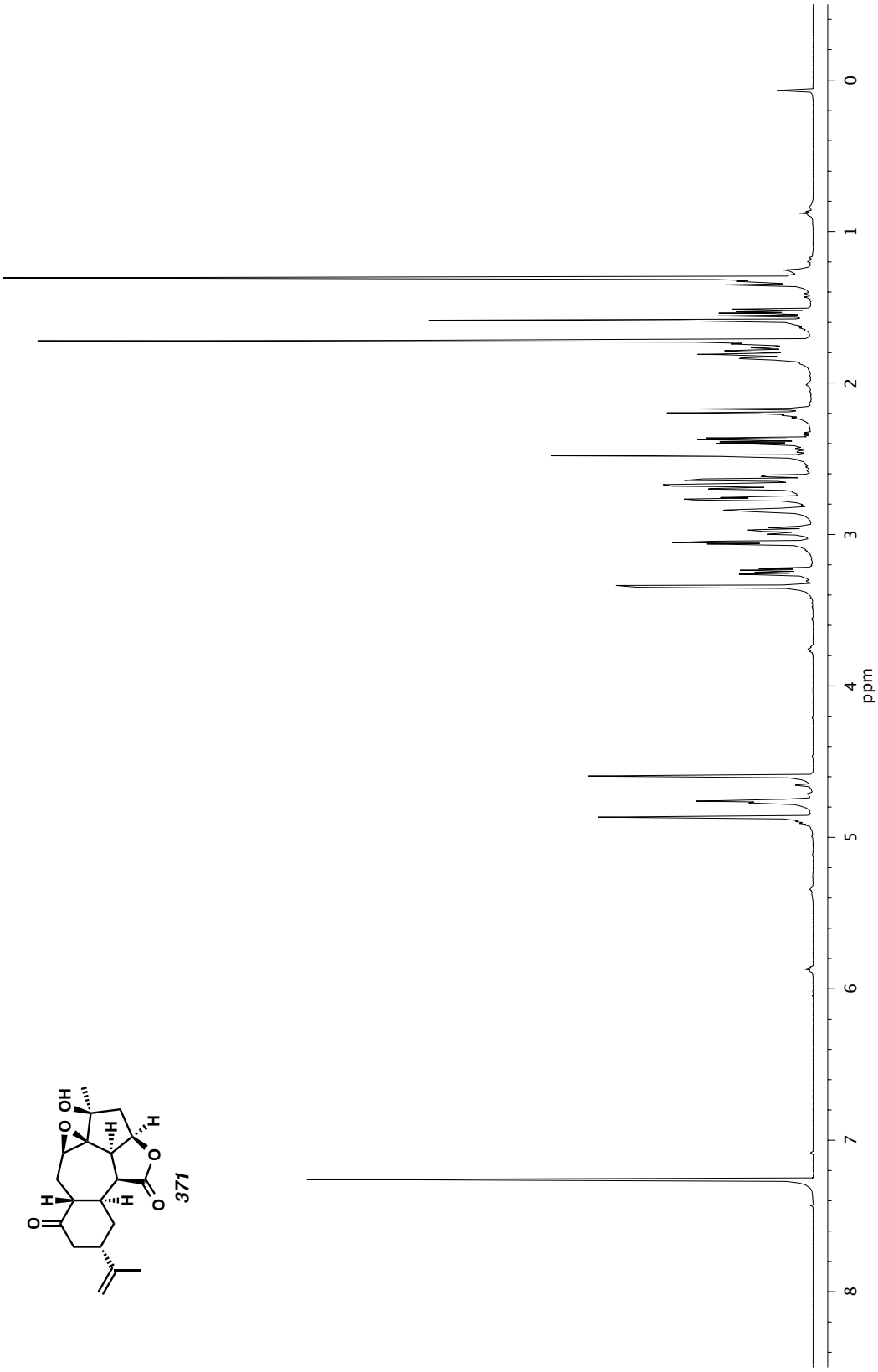

Figure A10.4. ^{1}H NMR (600 MHz, $CDCl_3$) of compound **371**.

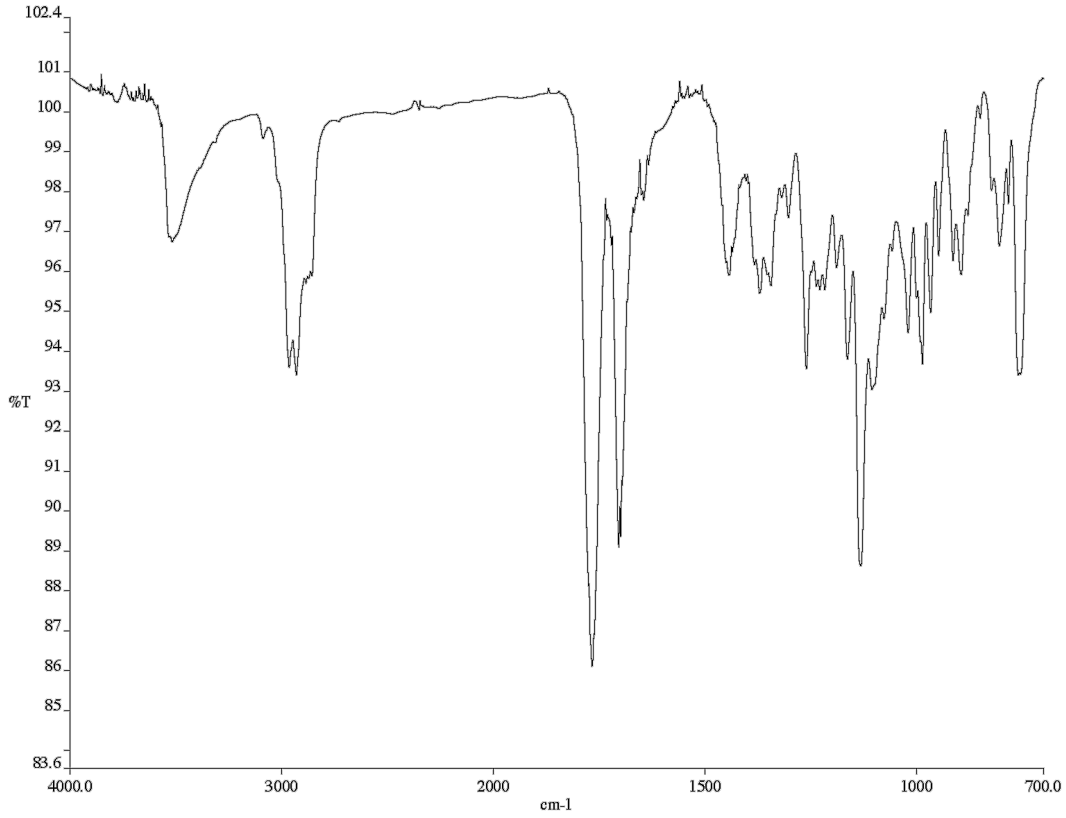

Figure A10.5. Infrared spectrum (Thin Film, NaCl) of compound **371**.

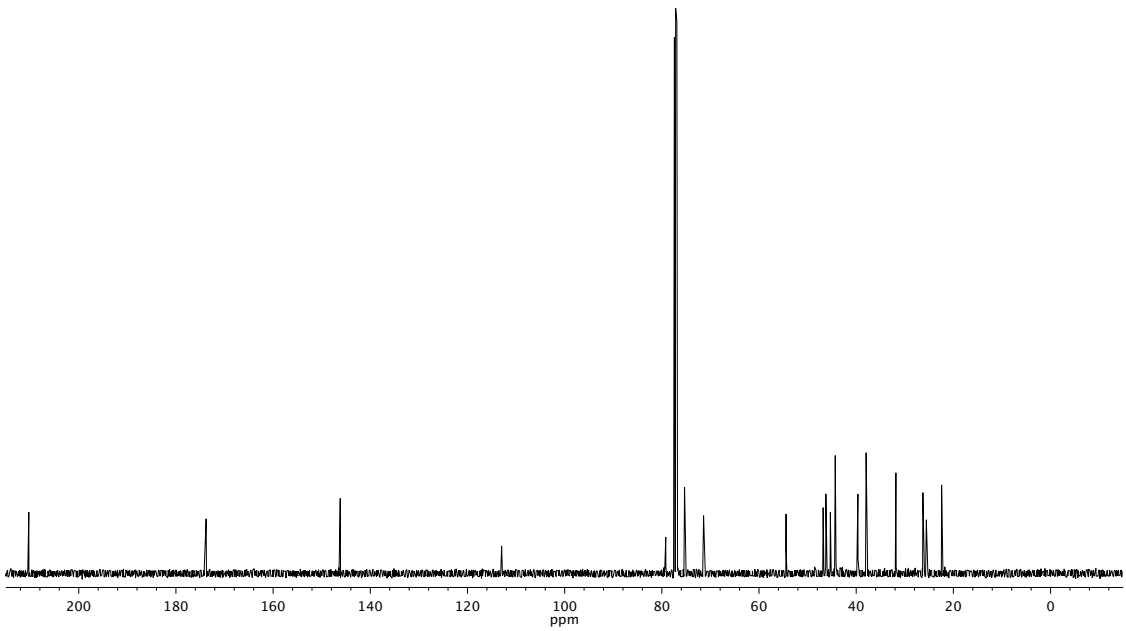

Figure A10.6. ^{13}C NMR (126 MHz, $CDCl_3$) of compound **371**.

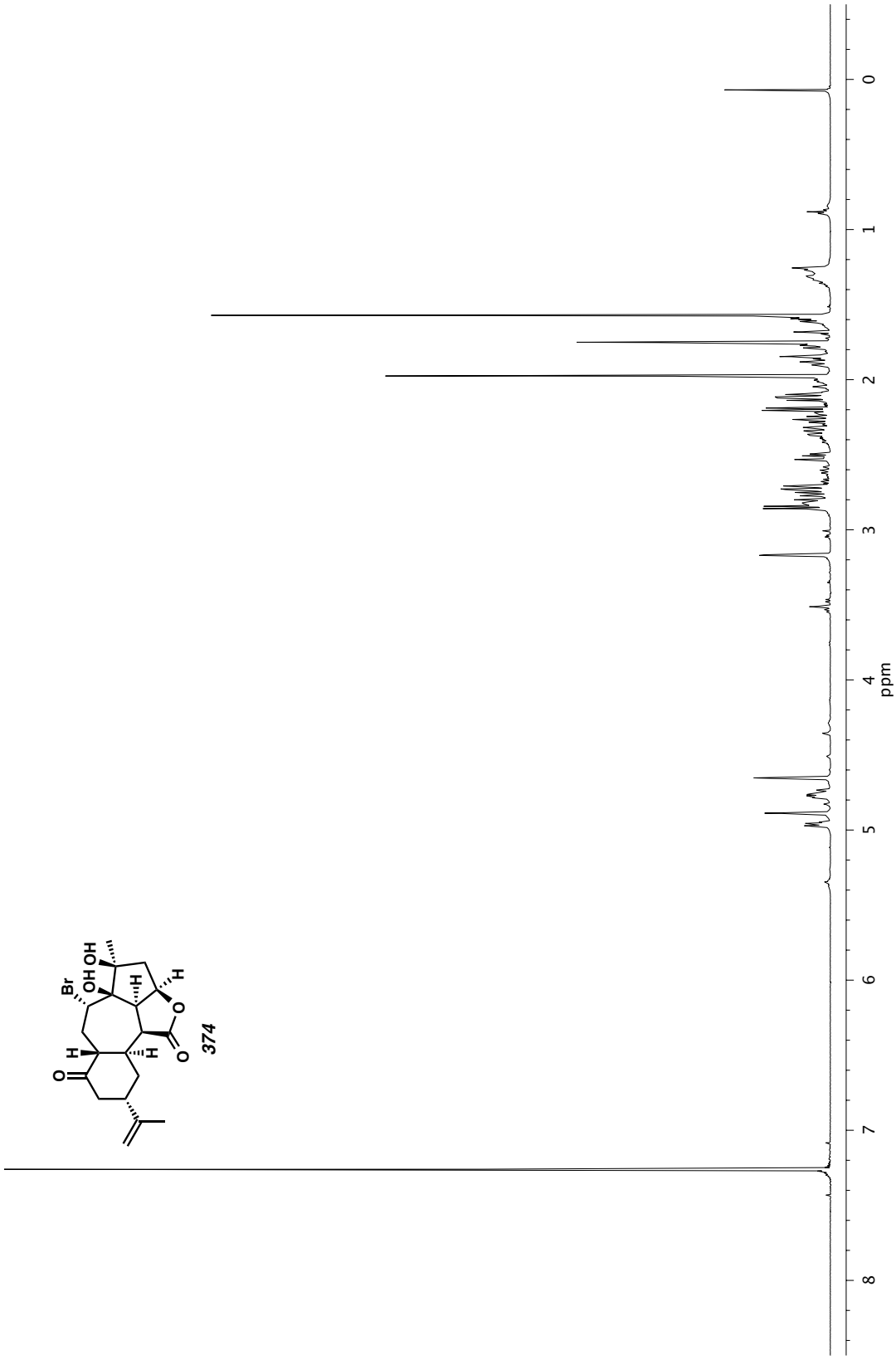

Figure A10.7. ^{1}H NMR (600 MHz, $CDCl_3$) of compound **374**.

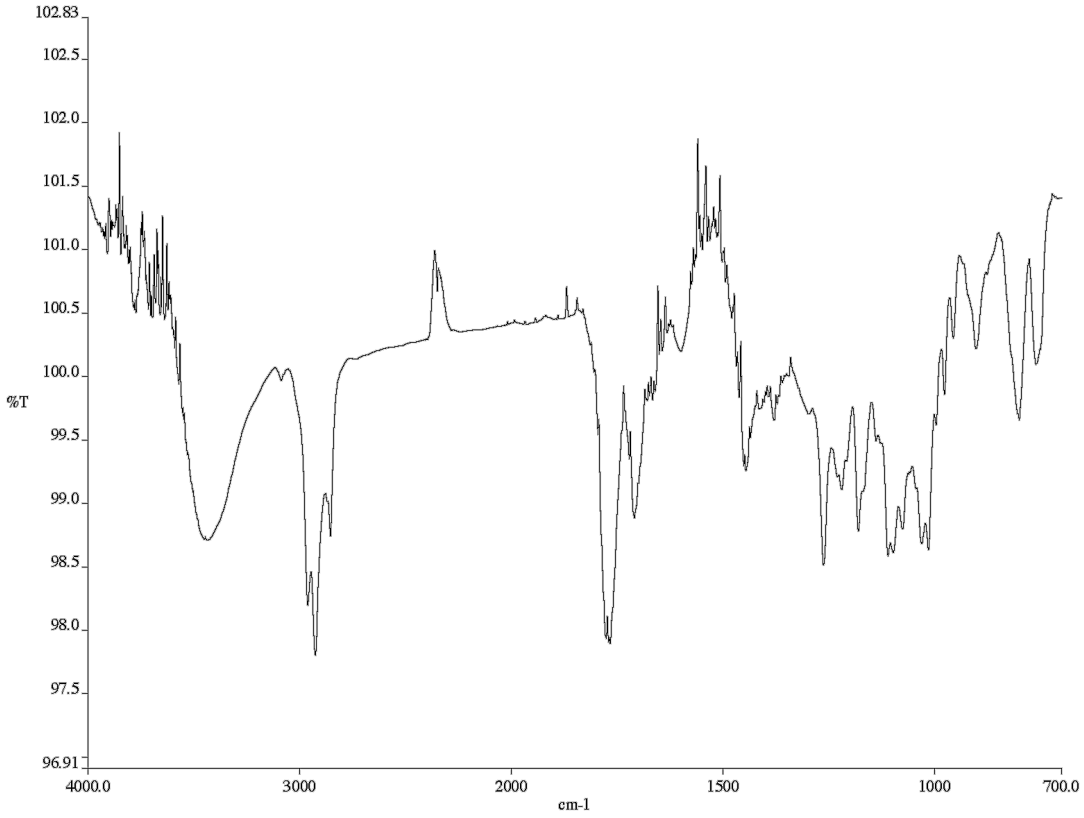

Figure A10.8. Infrared spectrum (Thin Film, NaCl) of compound **374**.

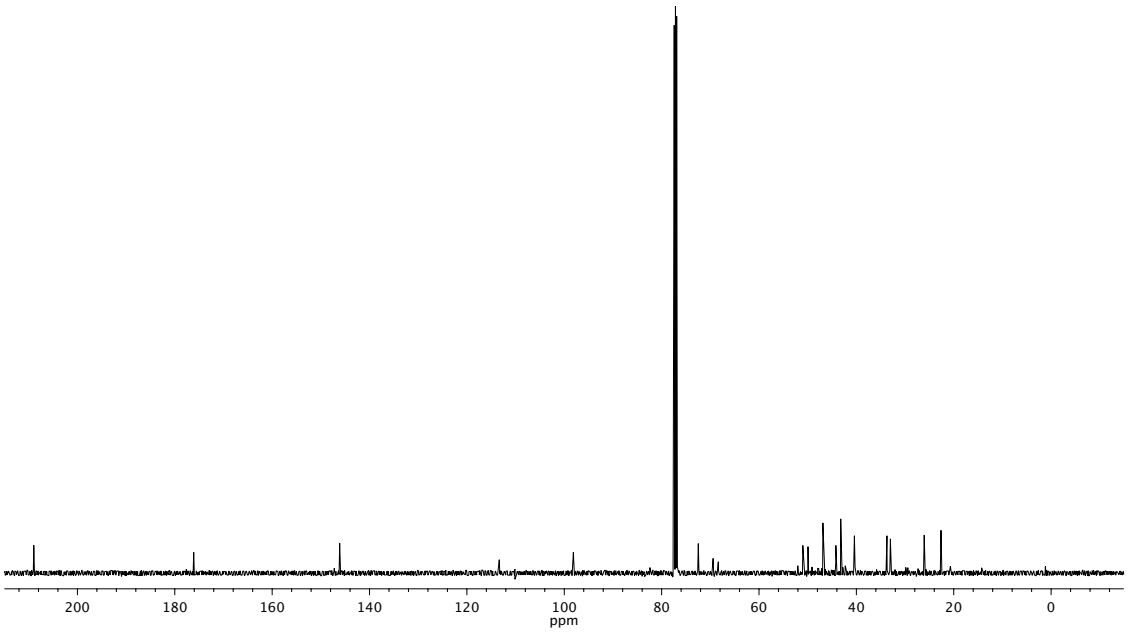

Figure A10.9. ^{13}C NMR (126 MHz, $CDCl_3$) of compound **374**.

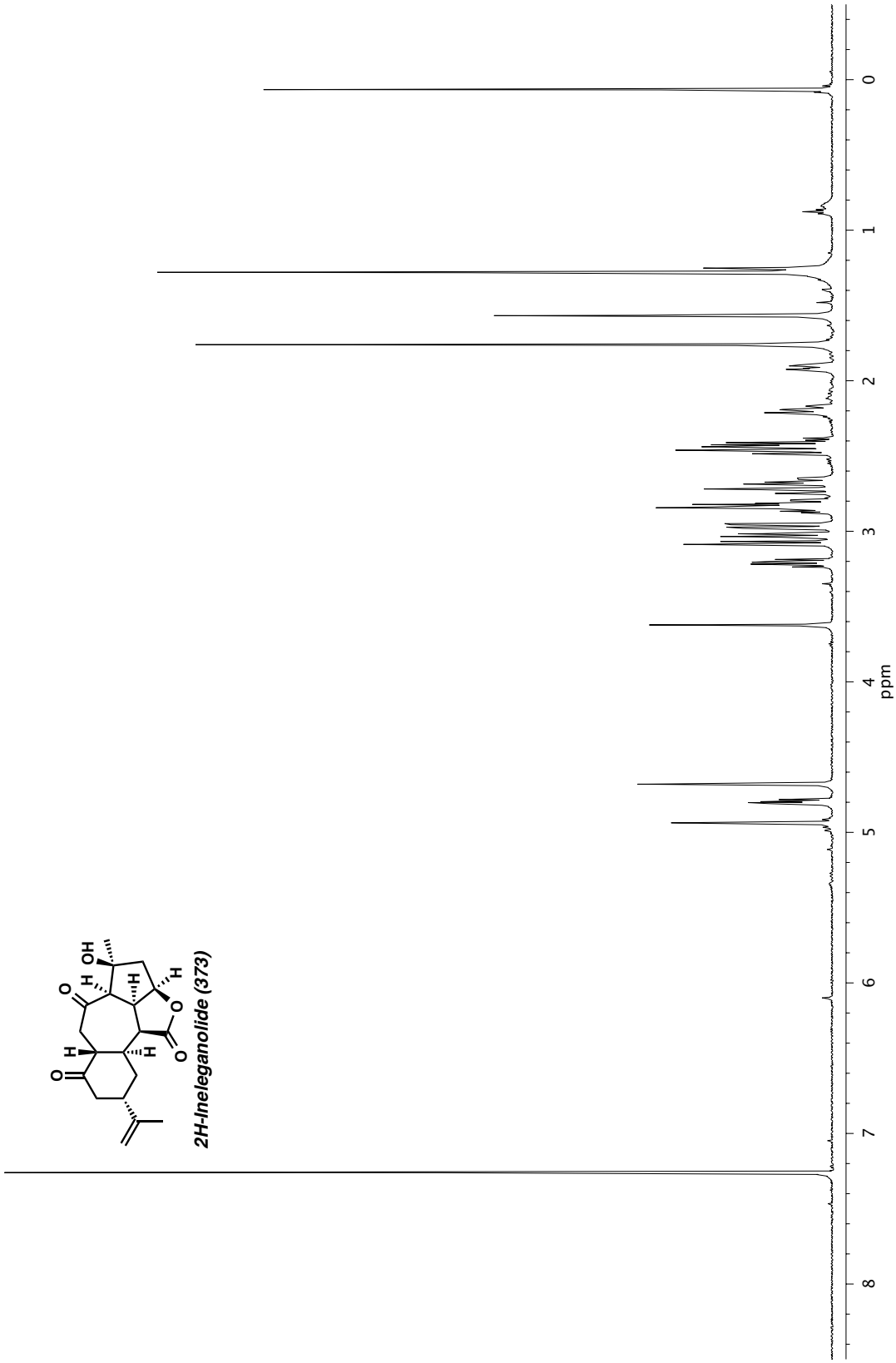

Figure A10.10. ^{1}H NMR (500 MHz, $CDCl_3$) of compound **373**.

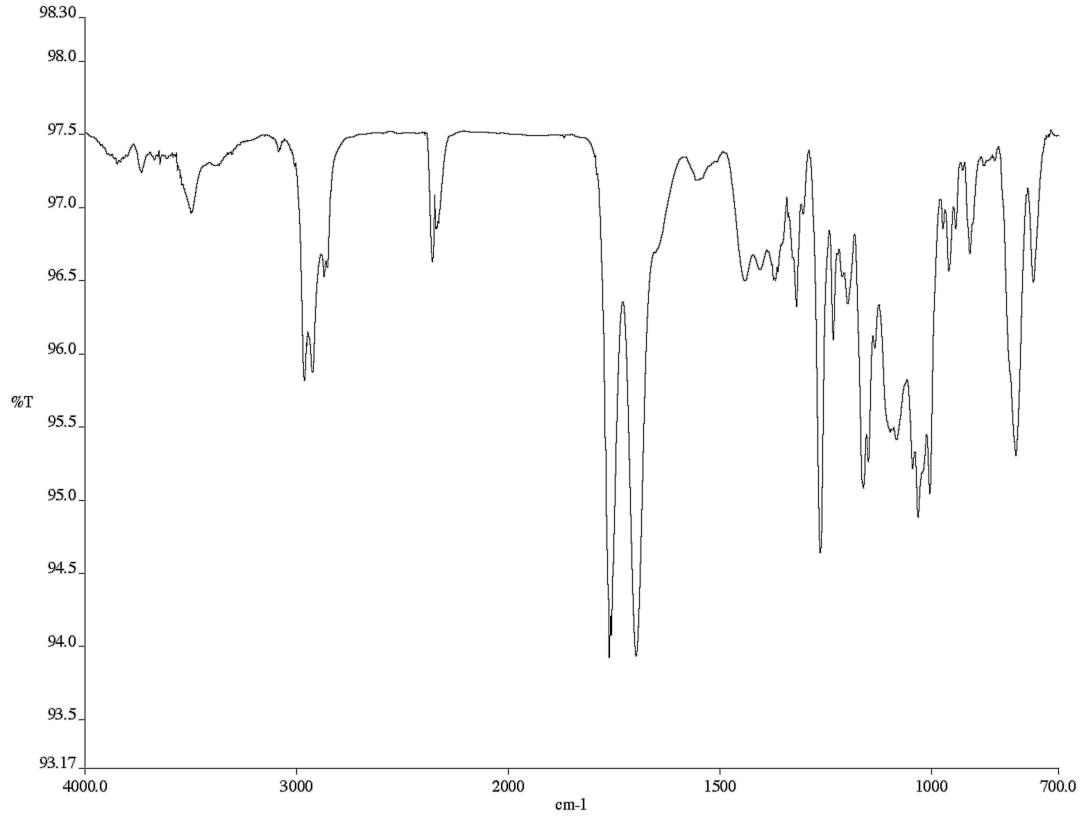

Figure A10.11. Infrared spectrum (Thin Film, NaCl) of compound **373**.

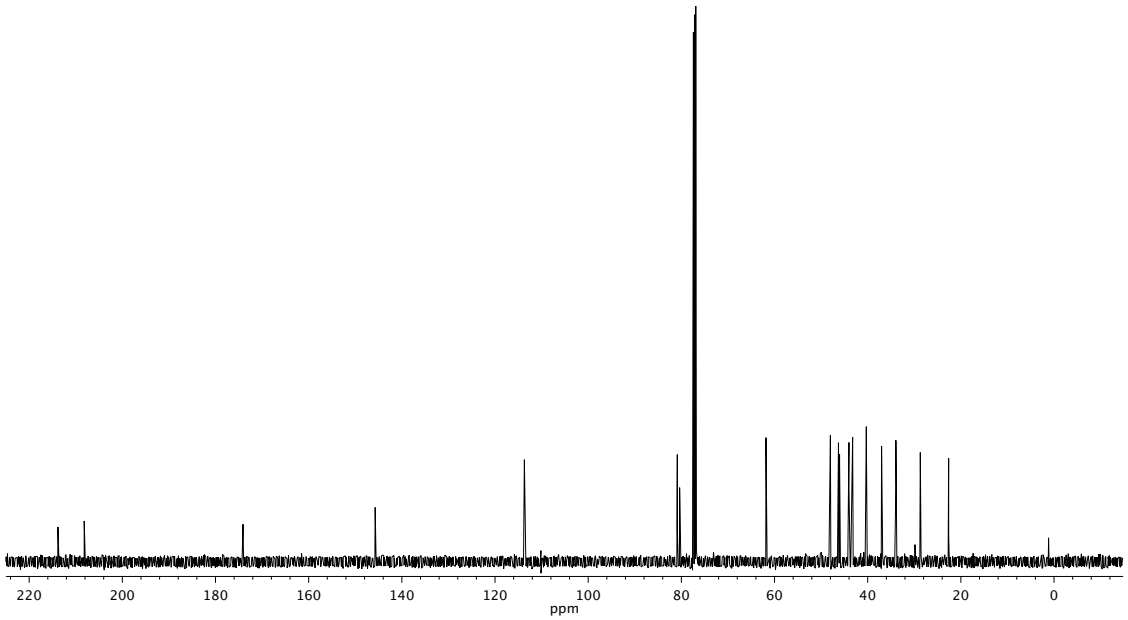

Figure A10.12. ^{13}C NMR (126 MHz, $CDCl_3$) of compound **373**.

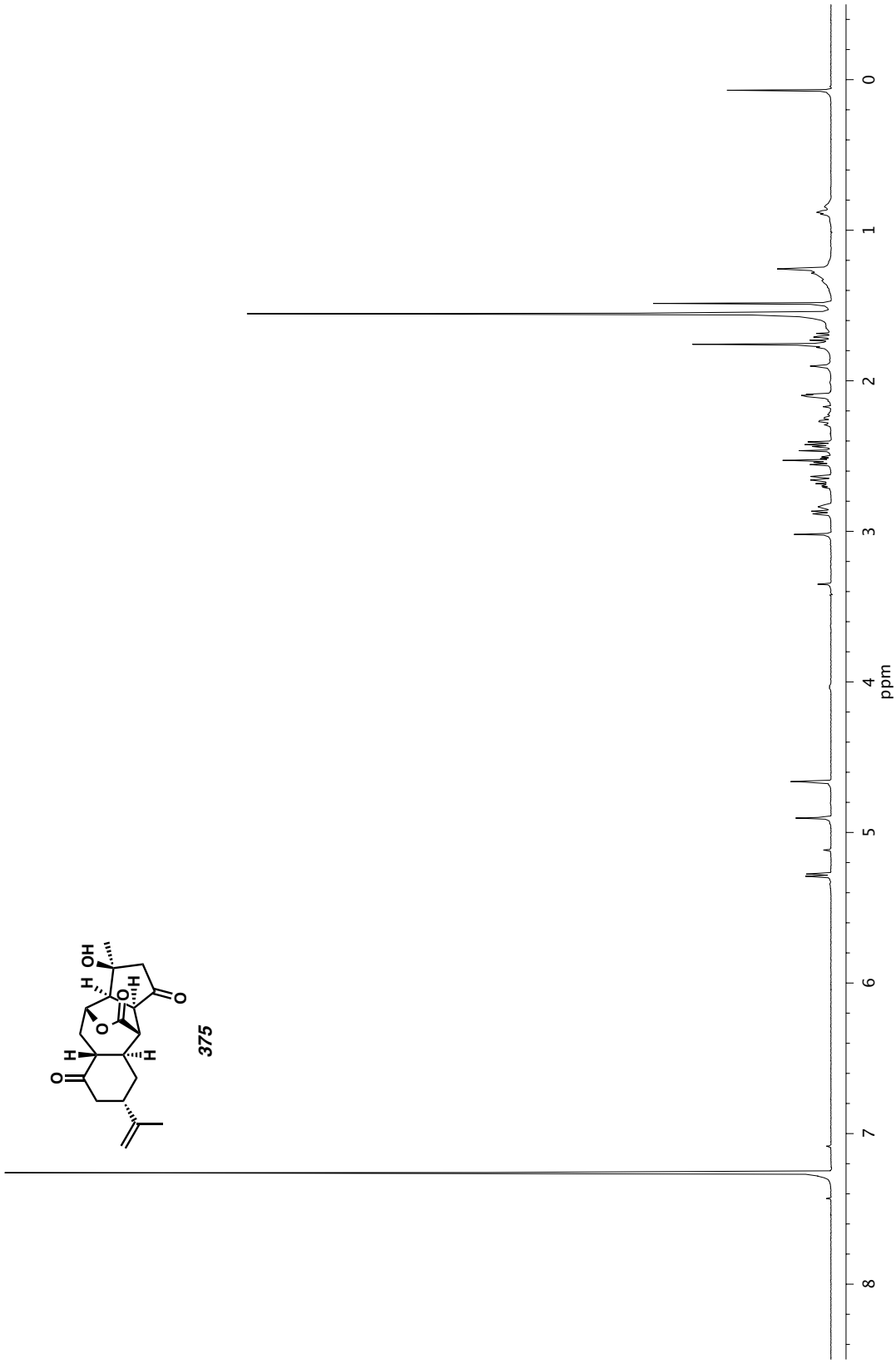

Figure A10.13. ^{1}H NMR (600 MHz, $CDCl_3$) of compound **375**.

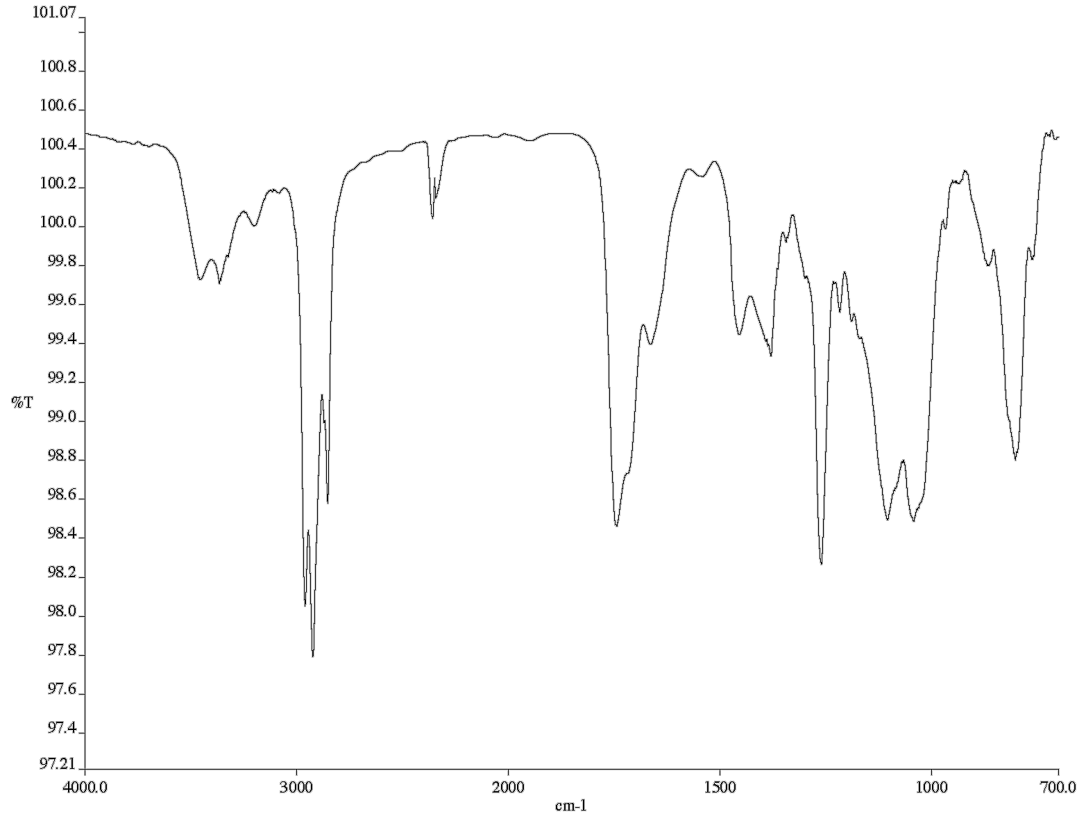

Figure A10.14. Infrared spectrum (Thin Film, NaCl) of compound **375**.

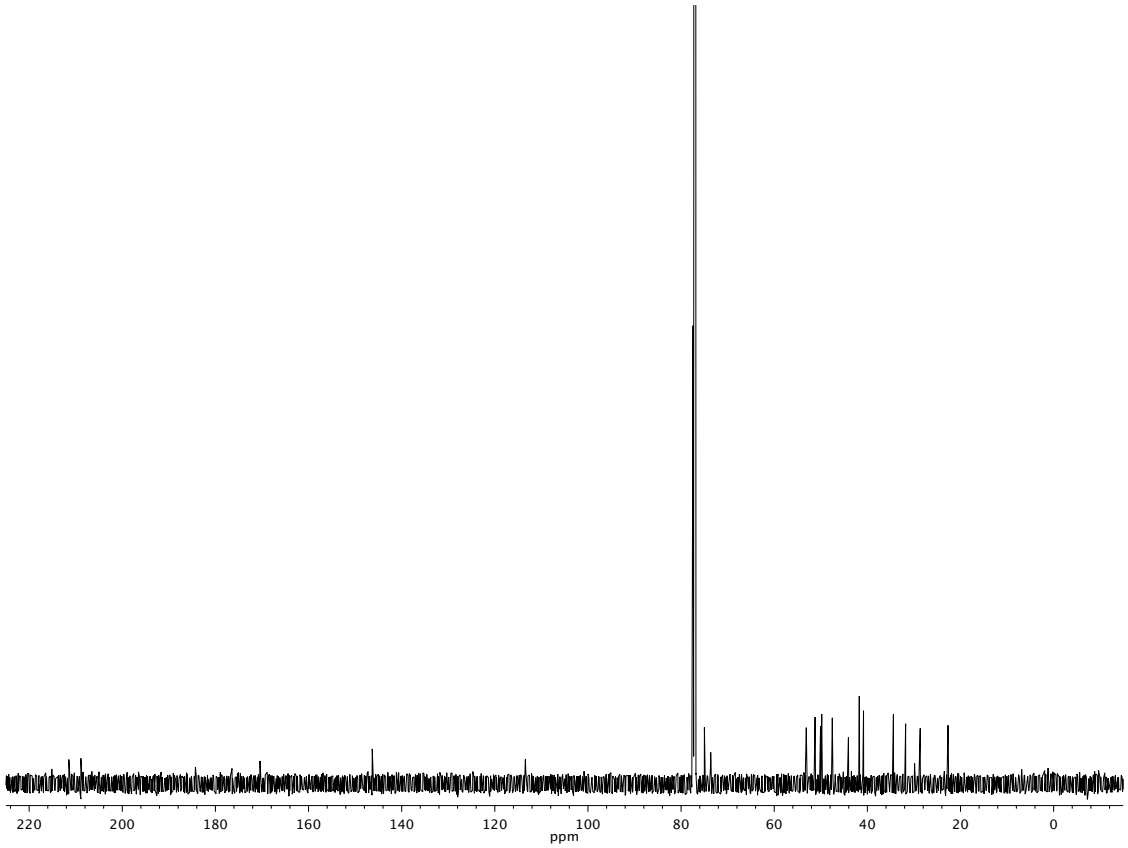

Figure A10.15. ^{13}C NMR (126 MHz, $CDCl_3$) of compound **375**.

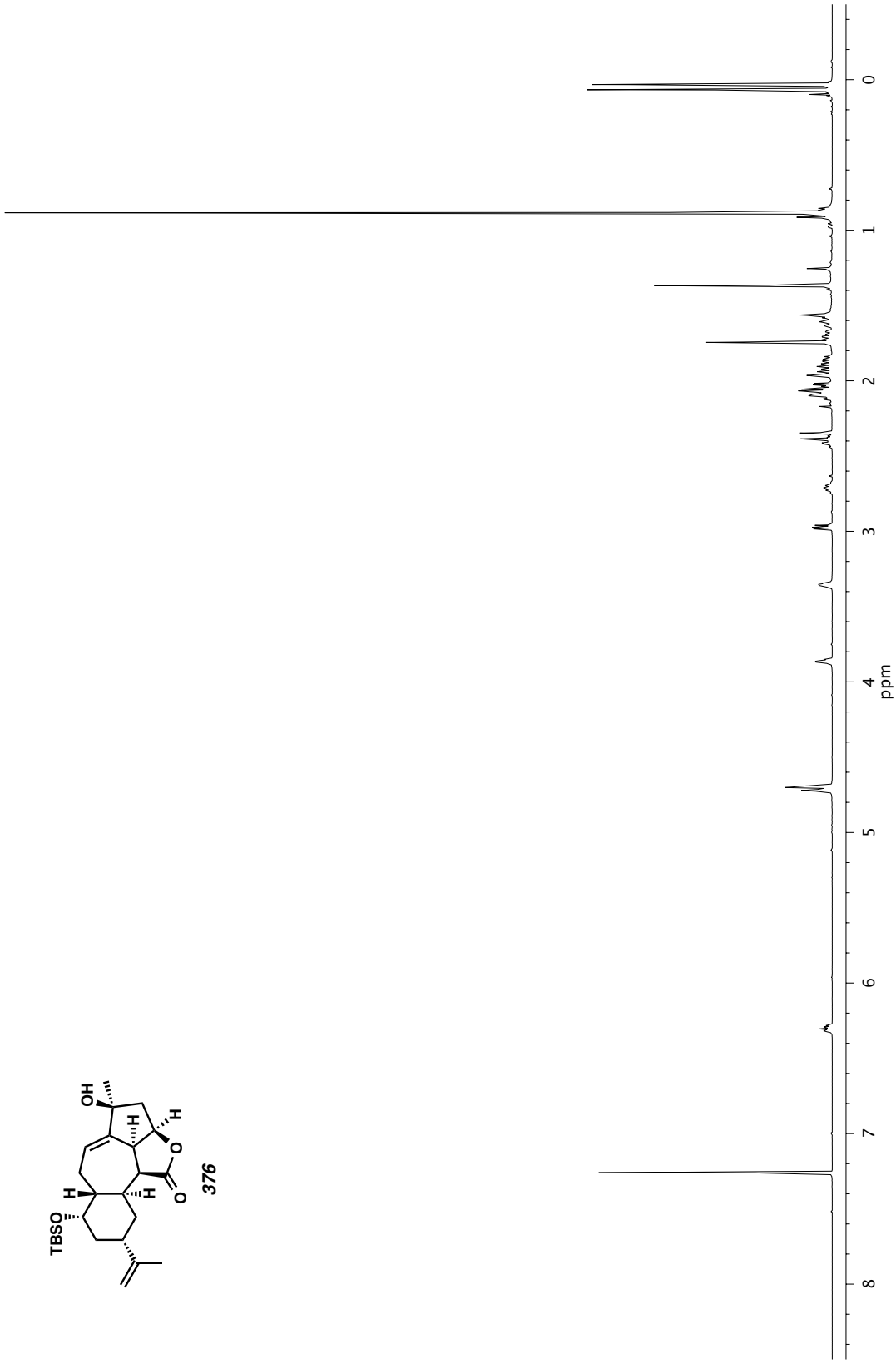

376

Figure A10.16. ^{1}H NMR (400 MHz, $CDCl_3$) of compound **376**.

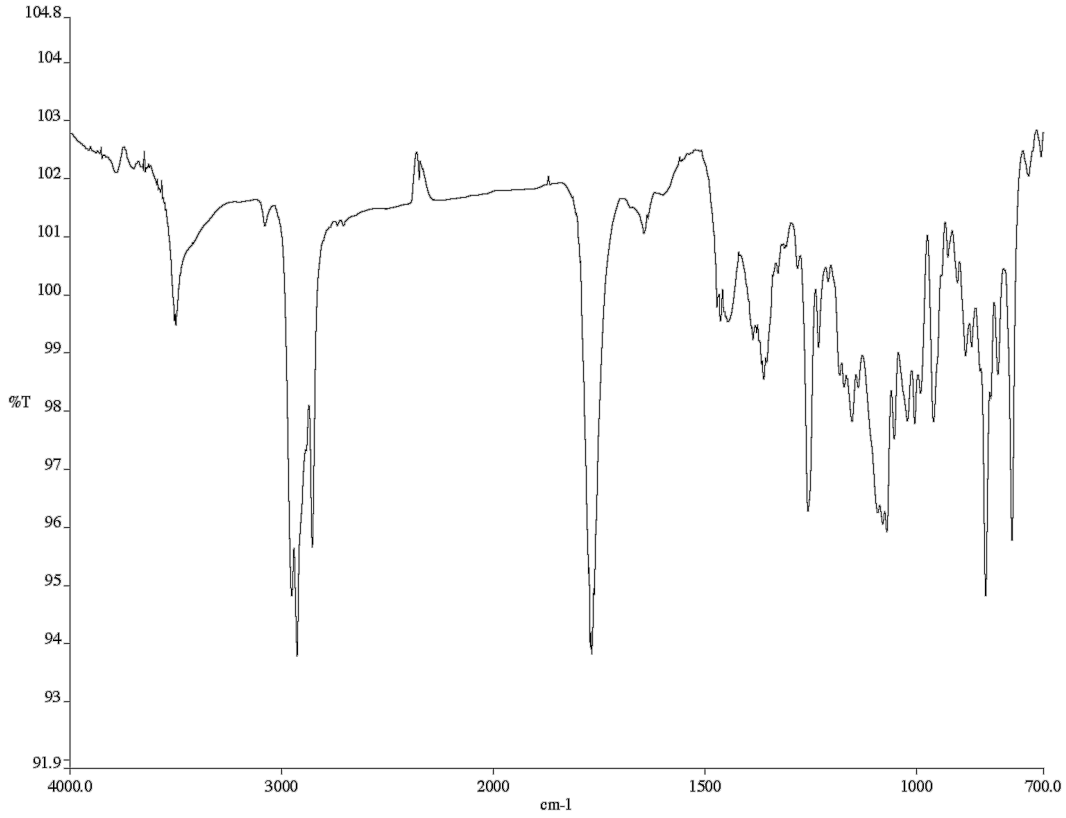

Figure A10.17. Infrared spectrum (Thin Film, NaCl) of compound **376**.

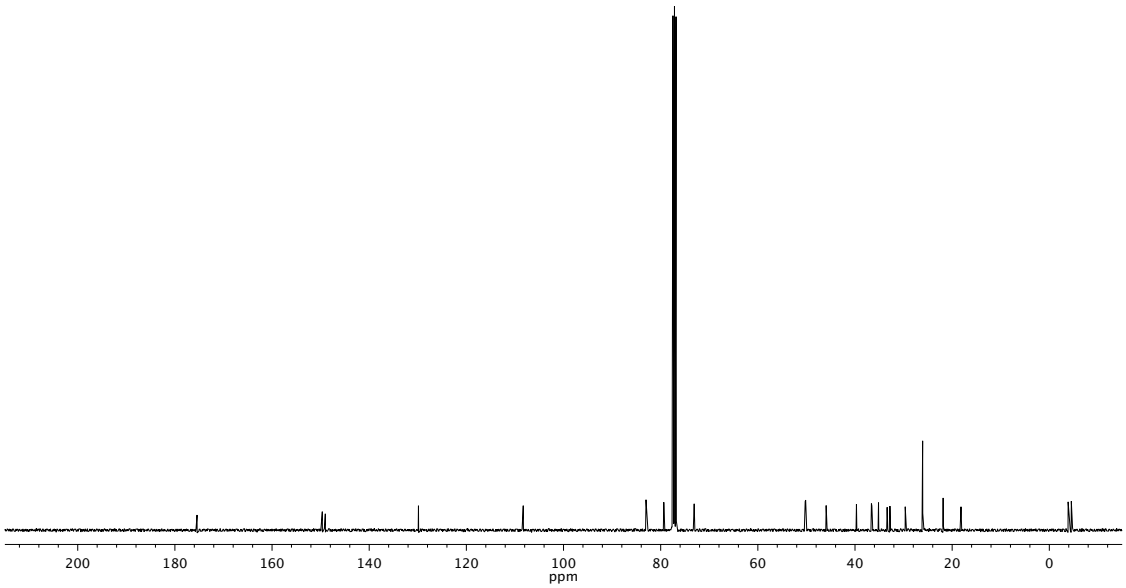

Figure A10.18. ^{13}C NMR (101 MHz, $CDCl_3$) of compound **376**.

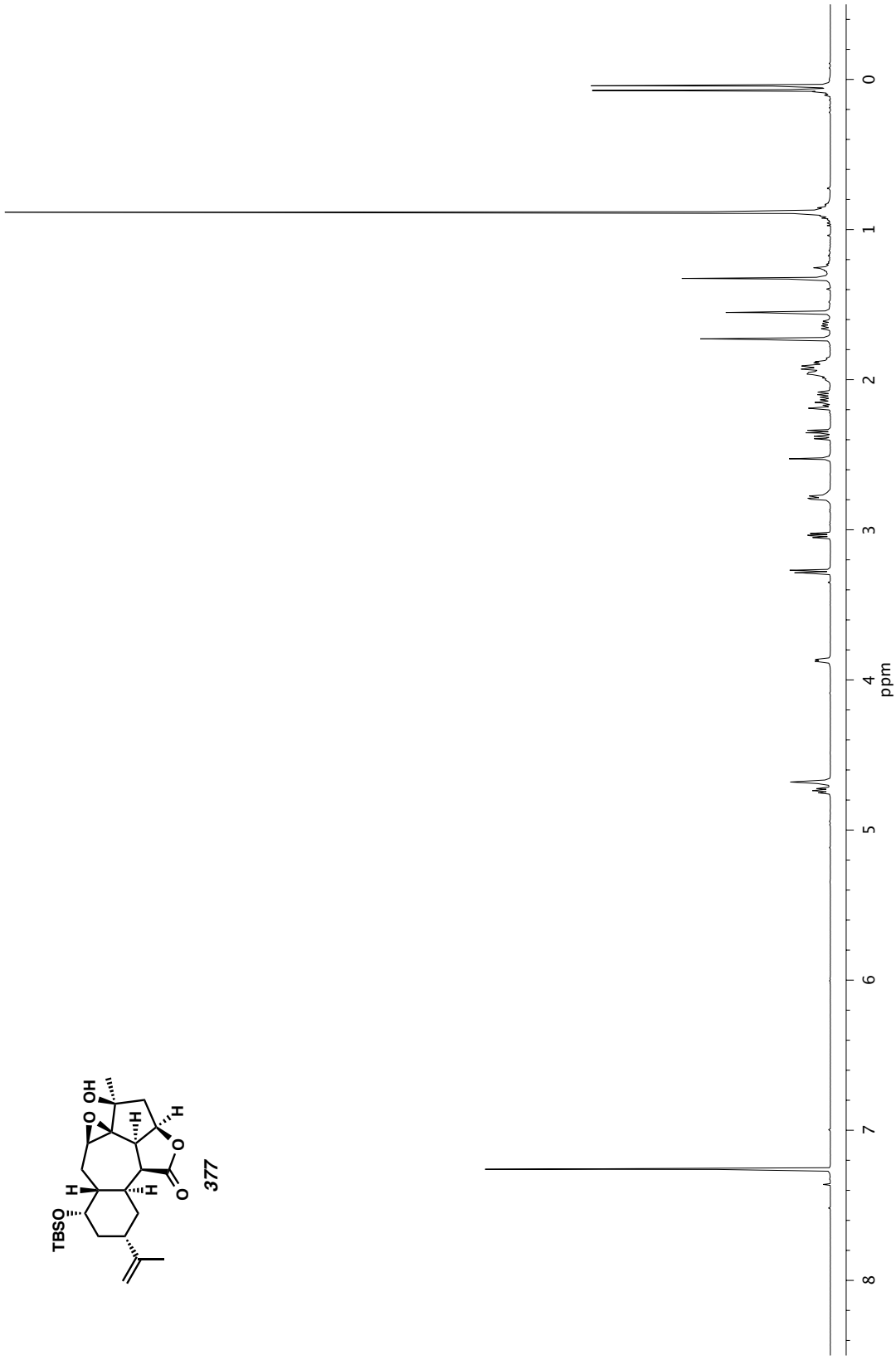

Figure A10.19. ^{1}H NMR (400 MHz, $CDCl_3$) of compound **377**.

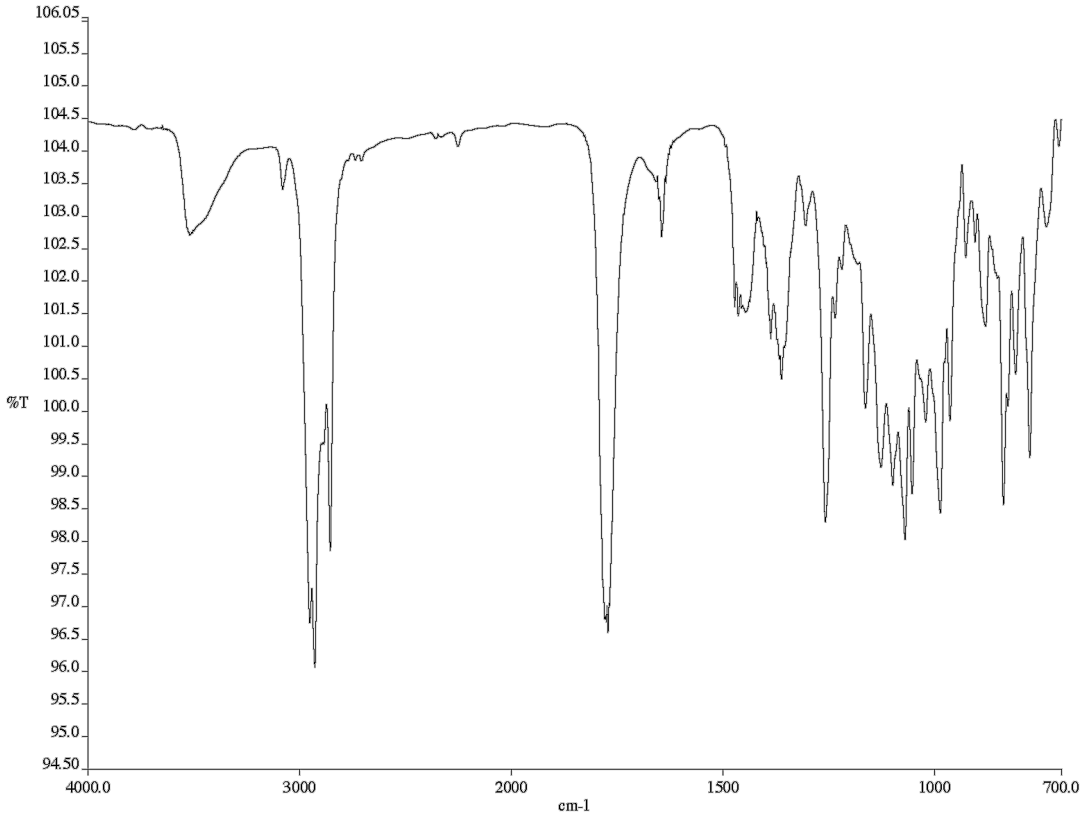

Figure A10.20. Infrared spectrum (Thin Film, NaCl) of compound **377**.

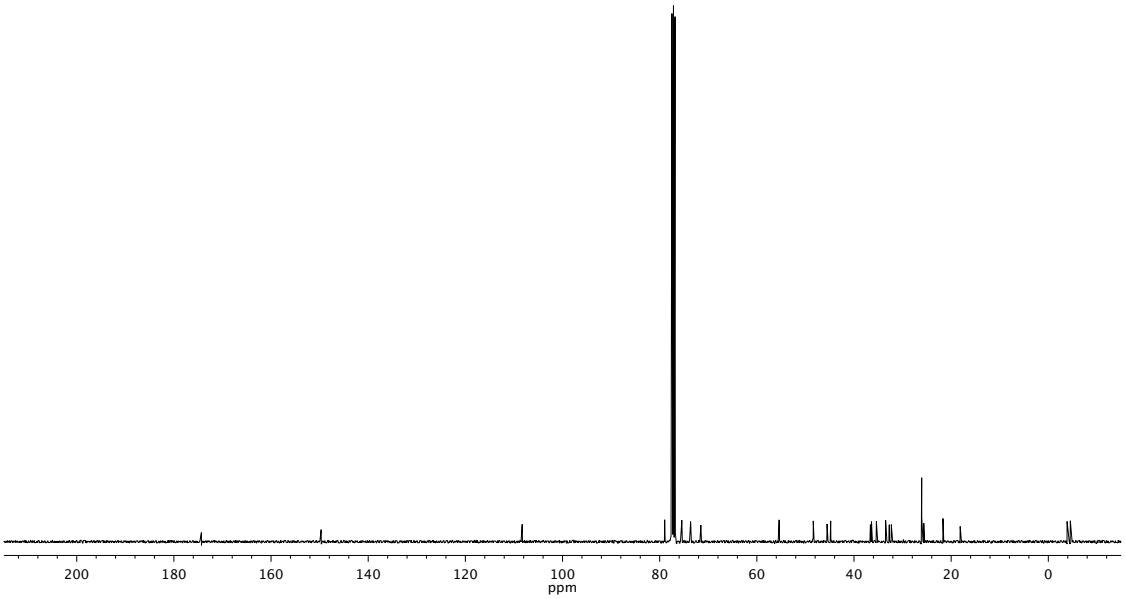

Figure A10.21. ^{13}C NMR (101 MHz, $CDCl_3$) of compound **377**.

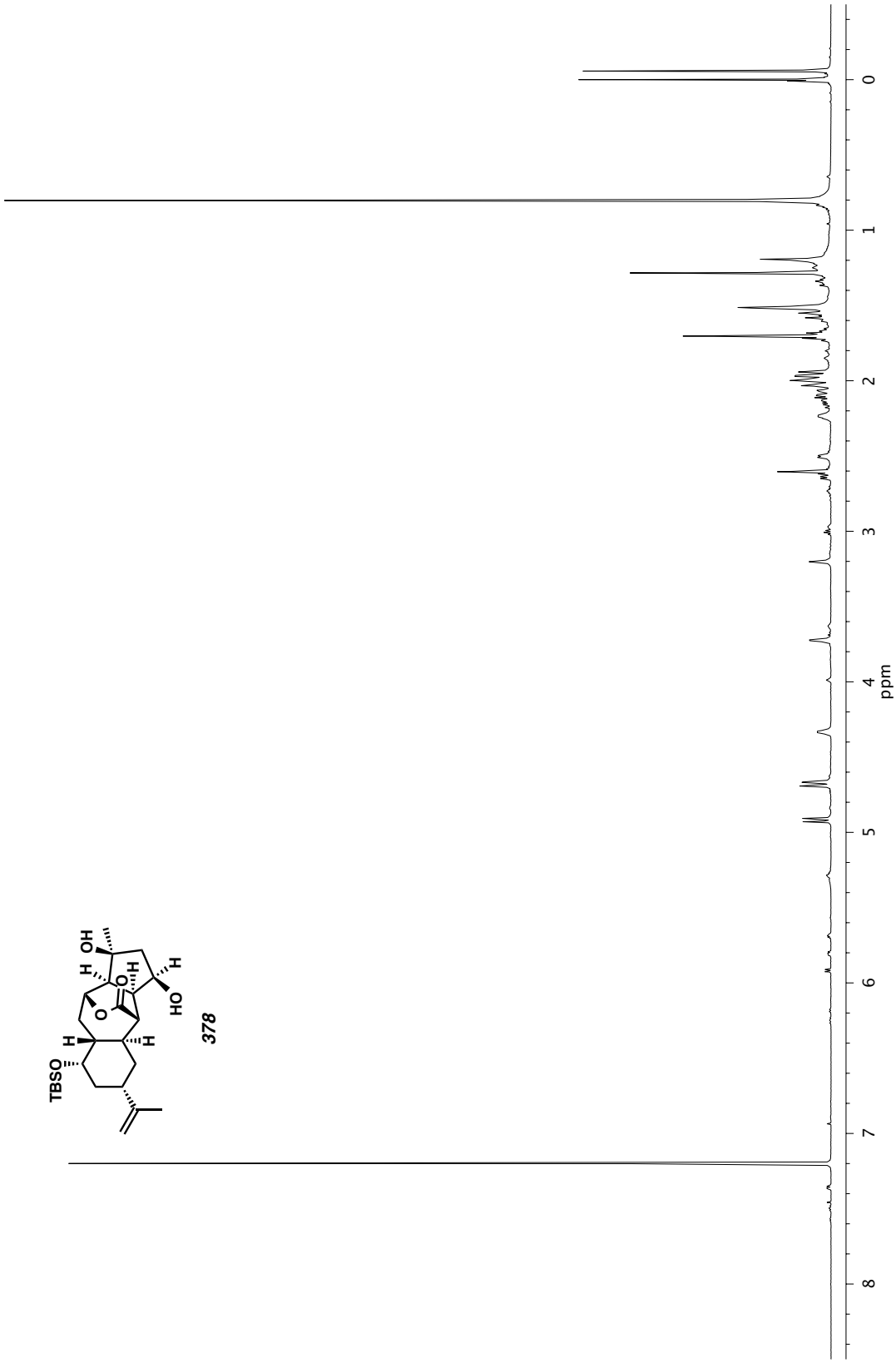

Figure A10.22. ^{1}H NMR (400 MHz, $CDCl_3$) of compound **378**.

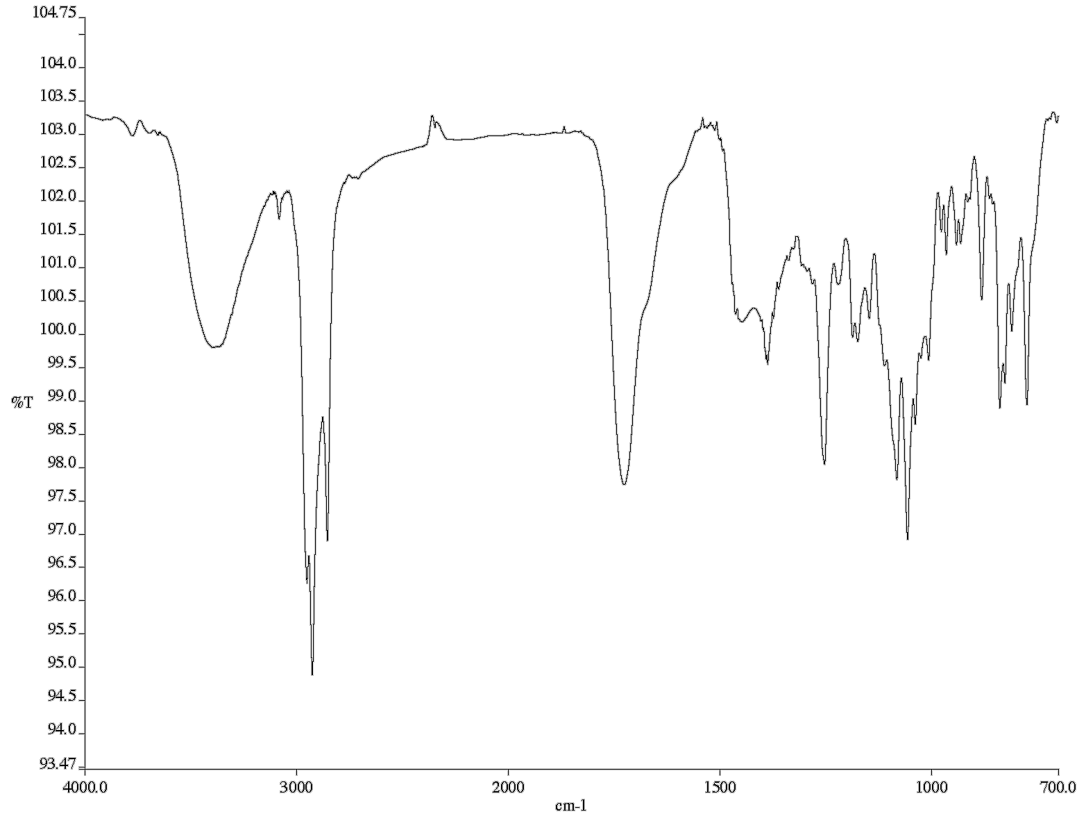

Figure A10.23. Infrared spectrum (Thin Film, NaCl) of compound **378**.

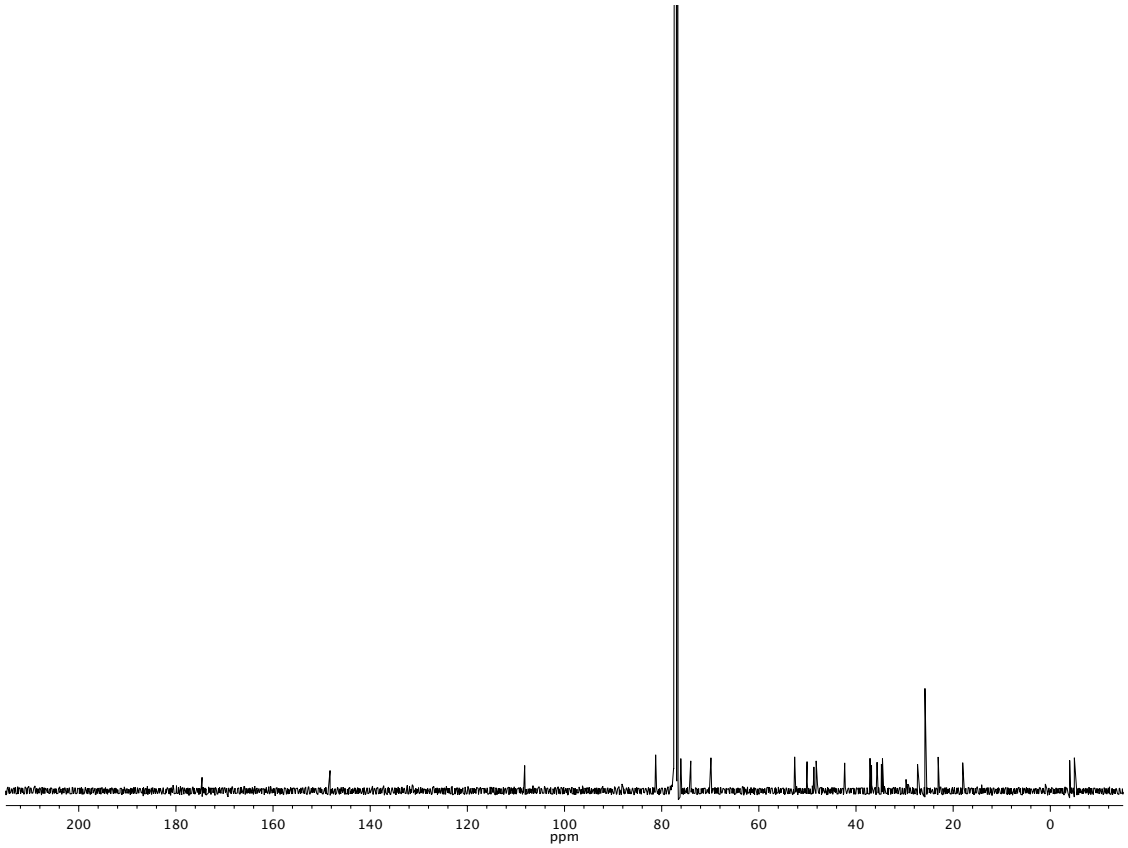

Figure A10.24. ^{13}C NMR (101 MHz, $CDCl_3$) of compound **378**.

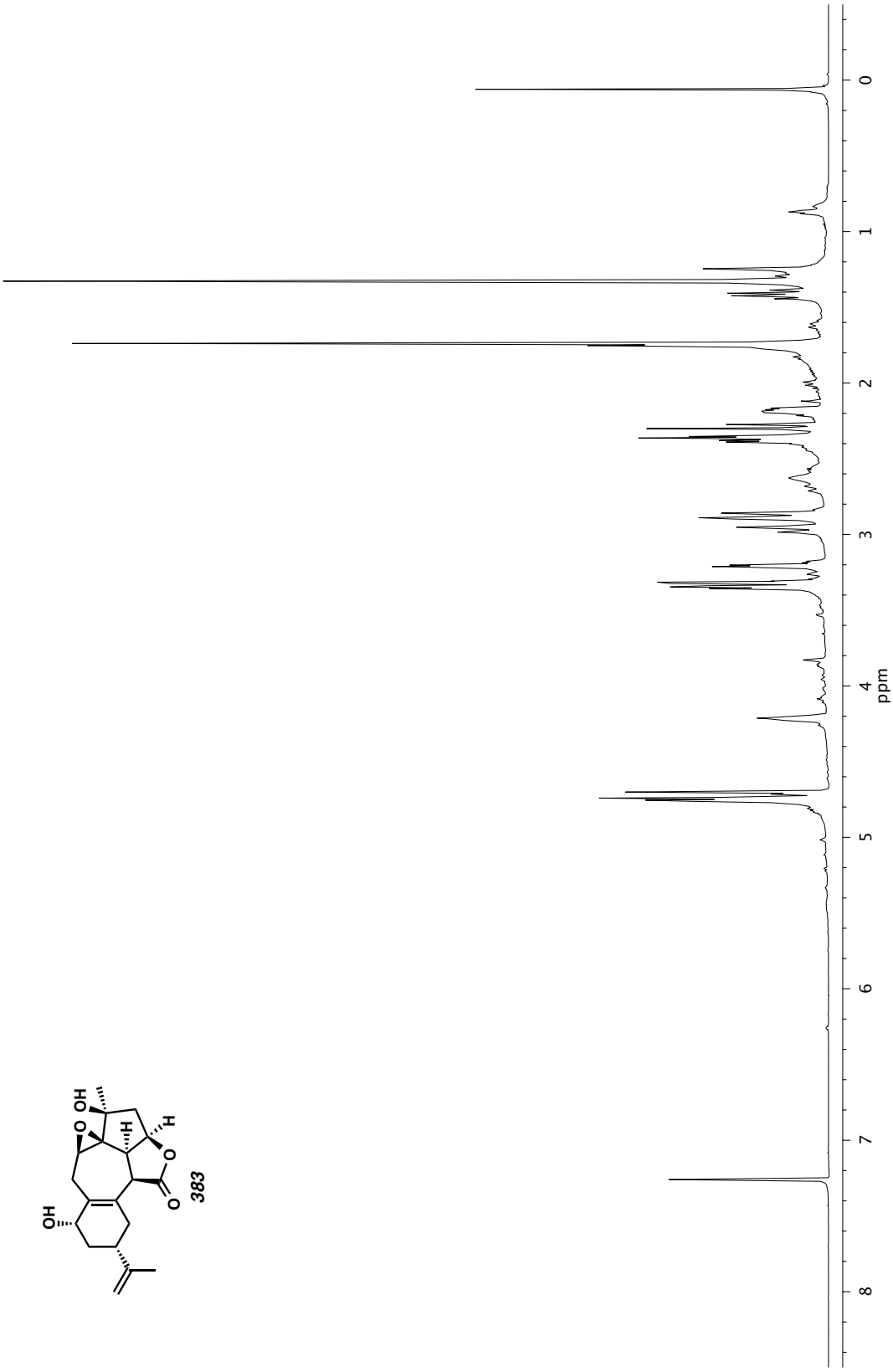

Figure A10.25. ^{1}H NMR (600 MHz, $CDCl_3$) of compound **383**.

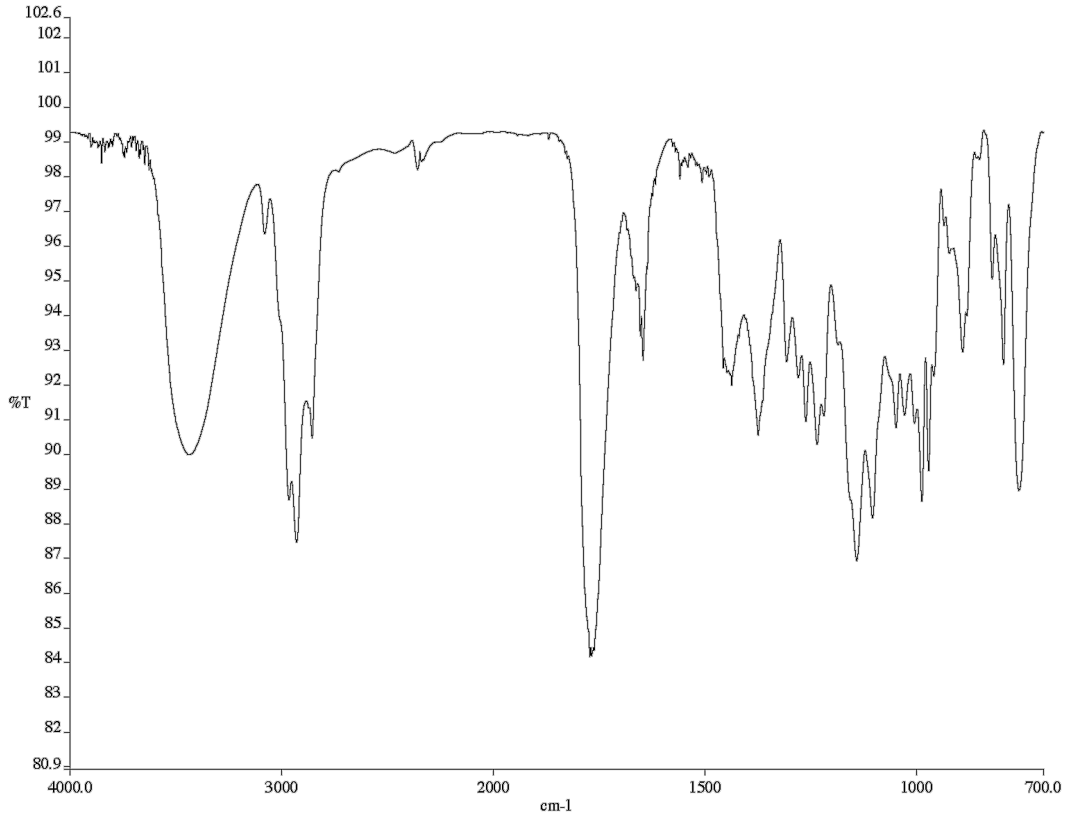

Figure A10.26. Infrared spectrum (Thin Film, NaCl) of compound **383**.

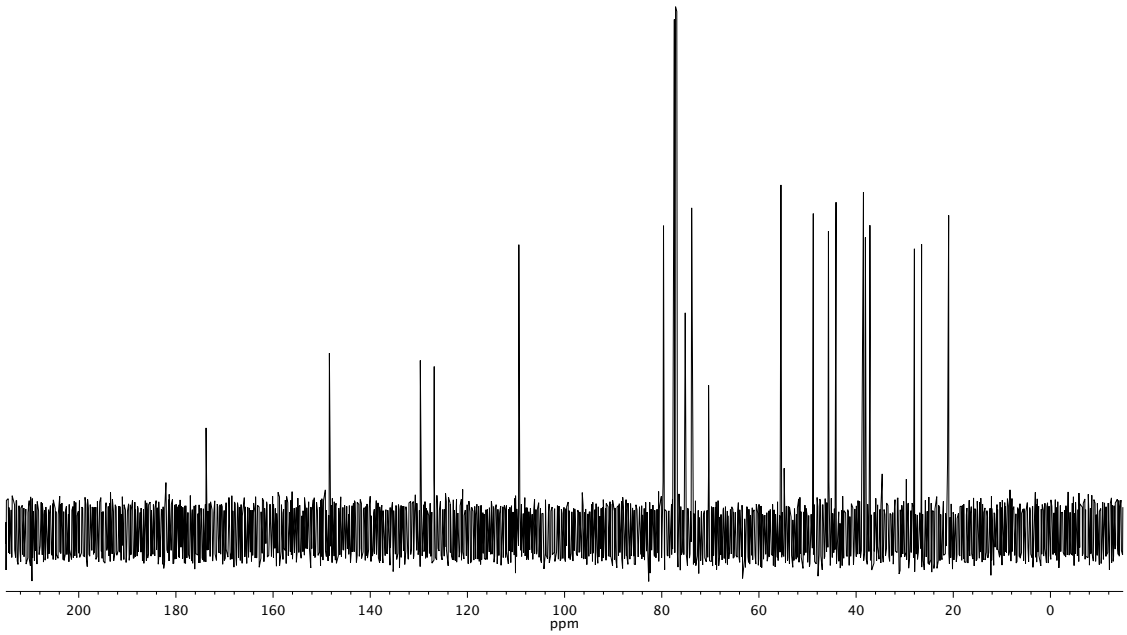

Figure A10.27. ^{13}C NMR (126 MHz, $CDCl_3$) of compound **383**.

Figure A10.28. ^{1}H NMR (600 MHz, $CDCl_3$) of compound **384**.

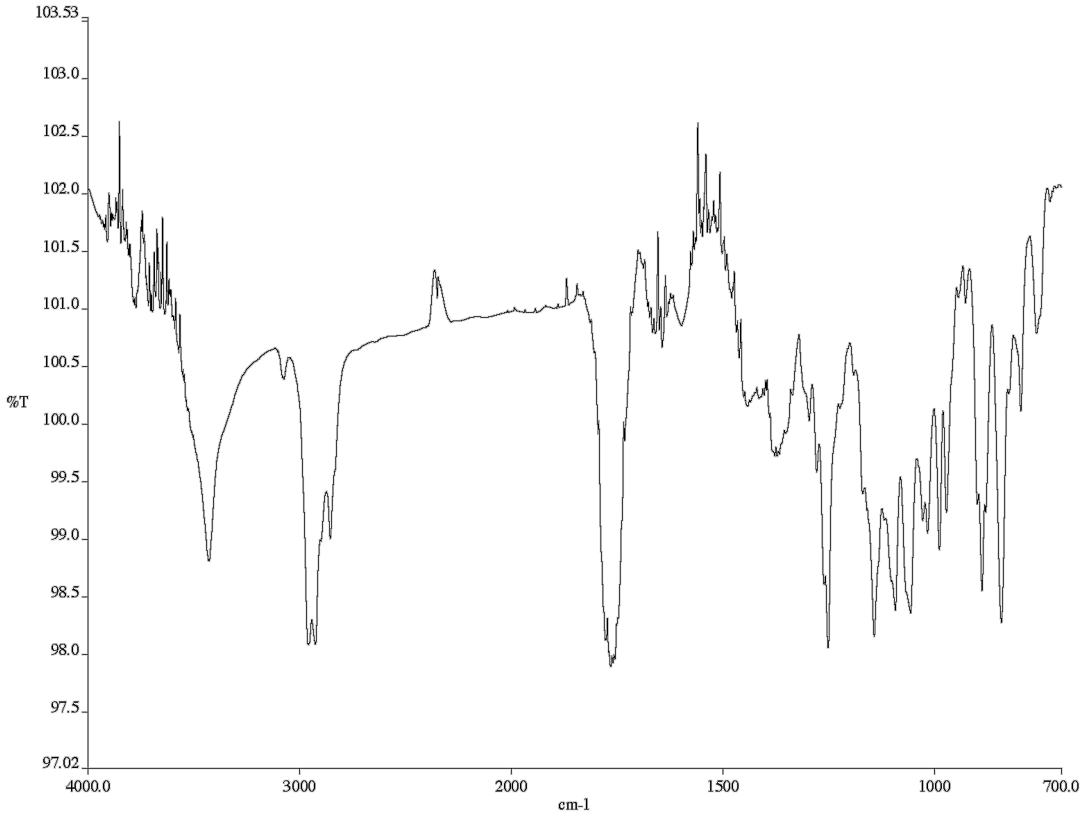

Figure A10.29. Infrared spectrum (Thin Film, NaCl) of compound **384**.

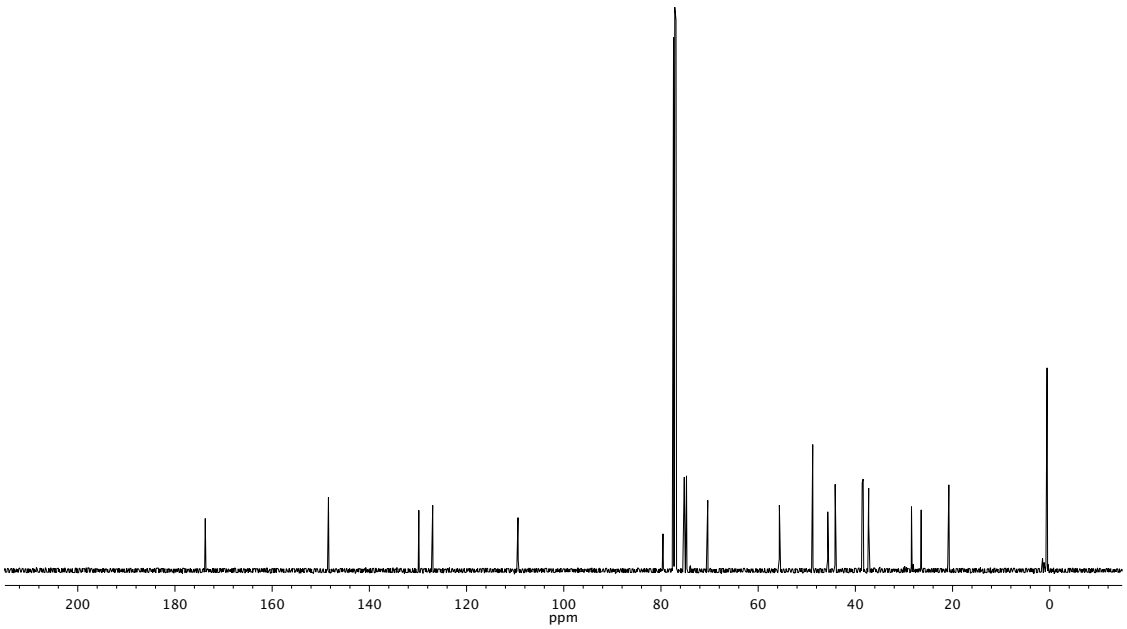

Figure A10.30. ^{13}C NMR (126 MHz, $CDCl_3$) of compound **384**.

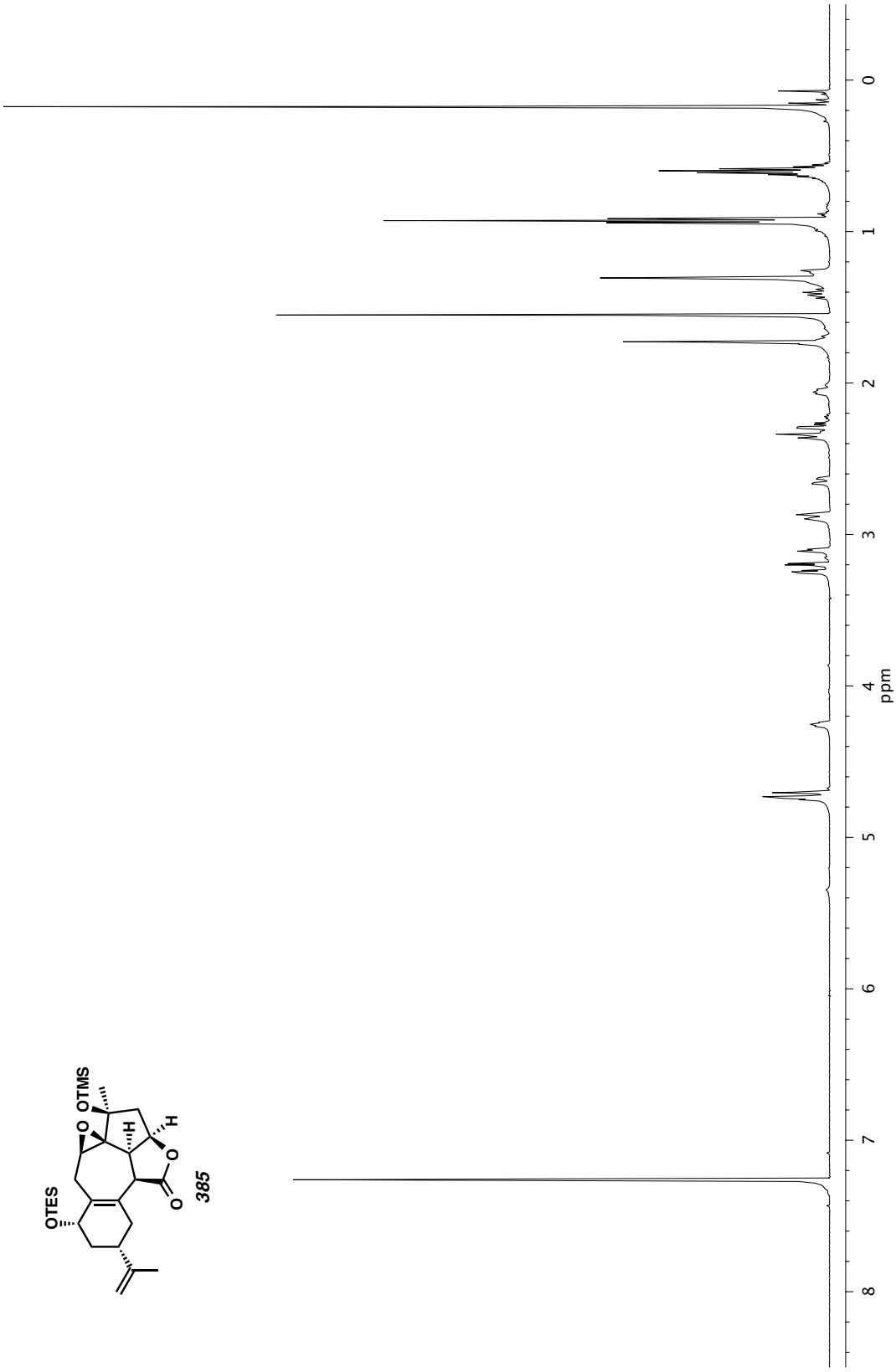

Figure A10.31. ^{1}H NMR (600 MHz, $CDCl_3$) of compound **385**.

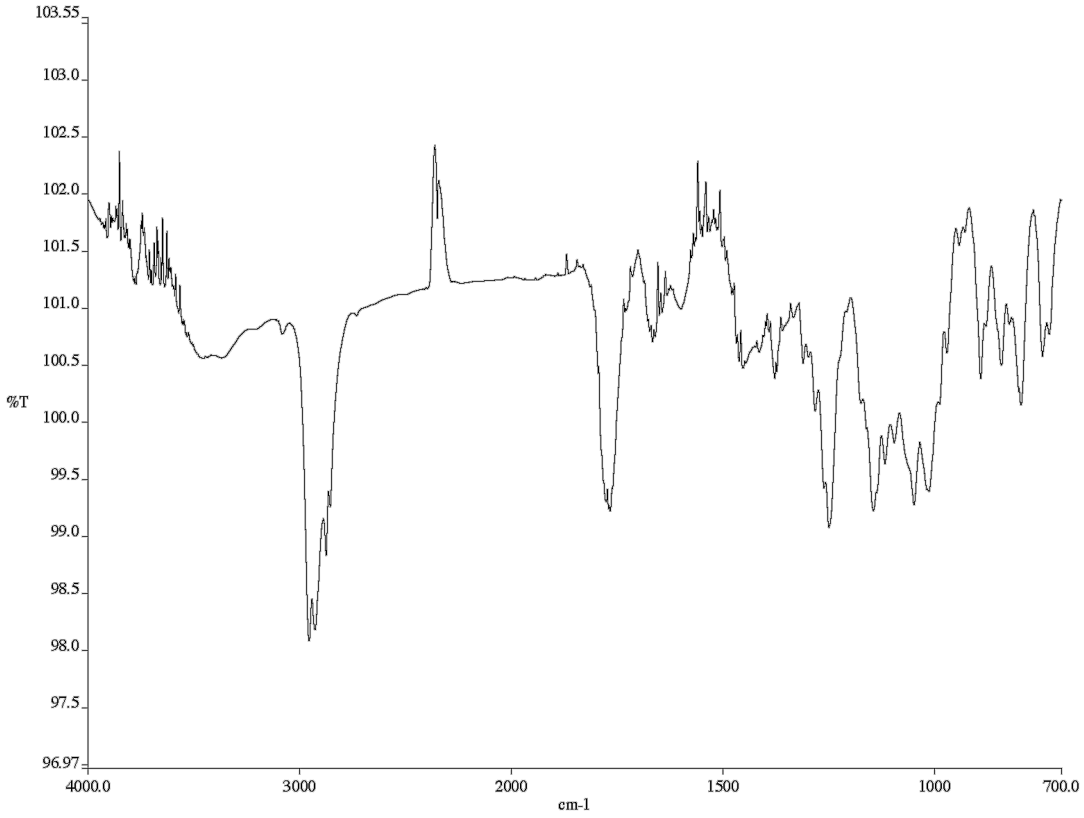

Figure A10.32. Infrared spectrum (Thin Film, NaCl) of compound **385**.

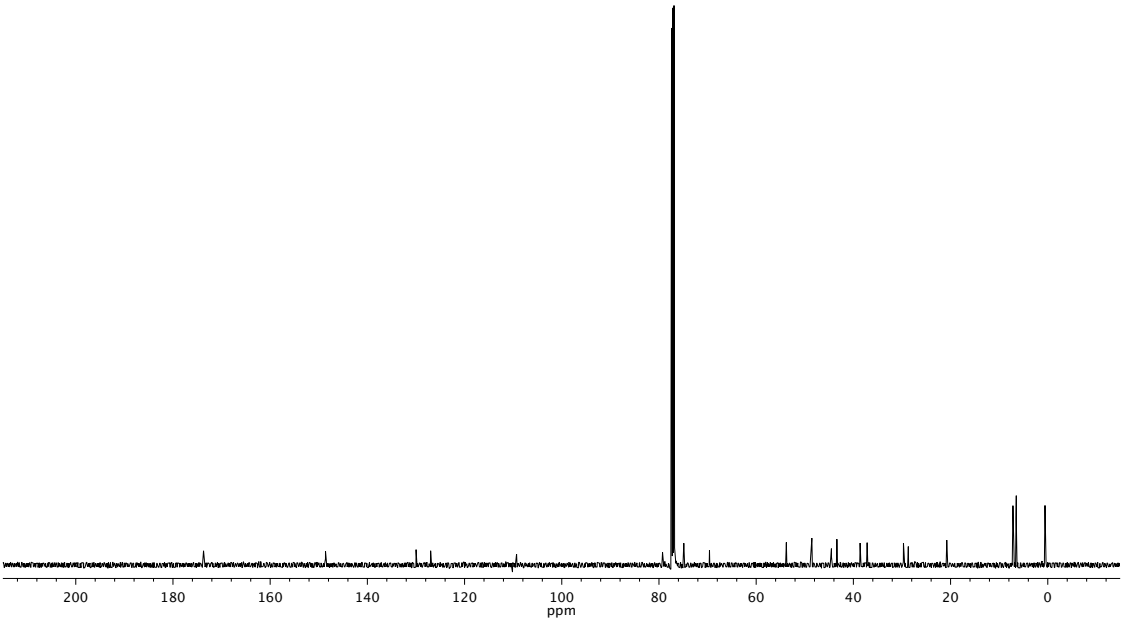

Figure A10.33. ^{13}C NMR (126 MHz, $CDCl_3$) of compound **385**.

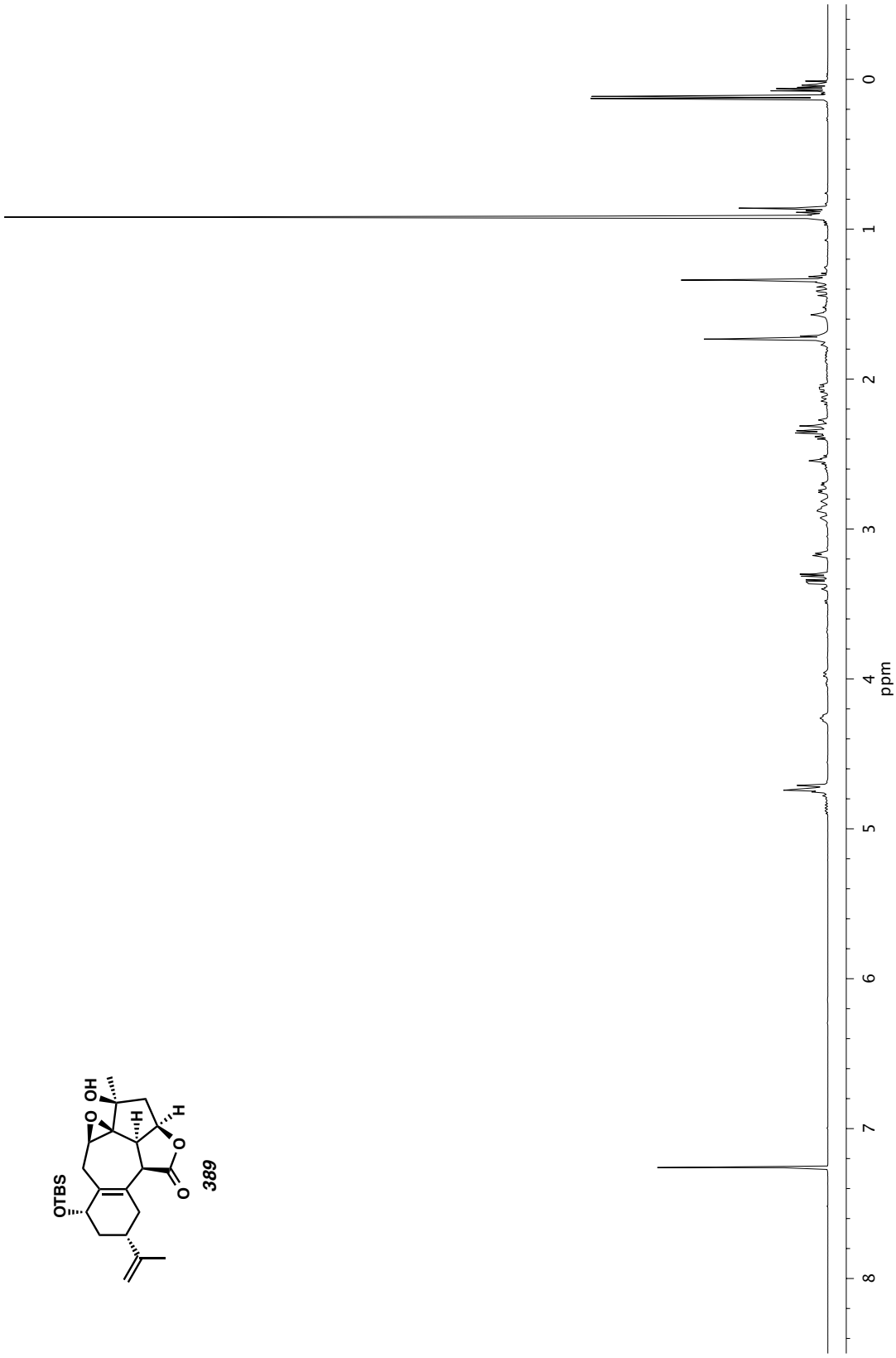

Figure A10.34. ^{1}H NMR (400 MHz, $CDCl_3$) of compound **389**.

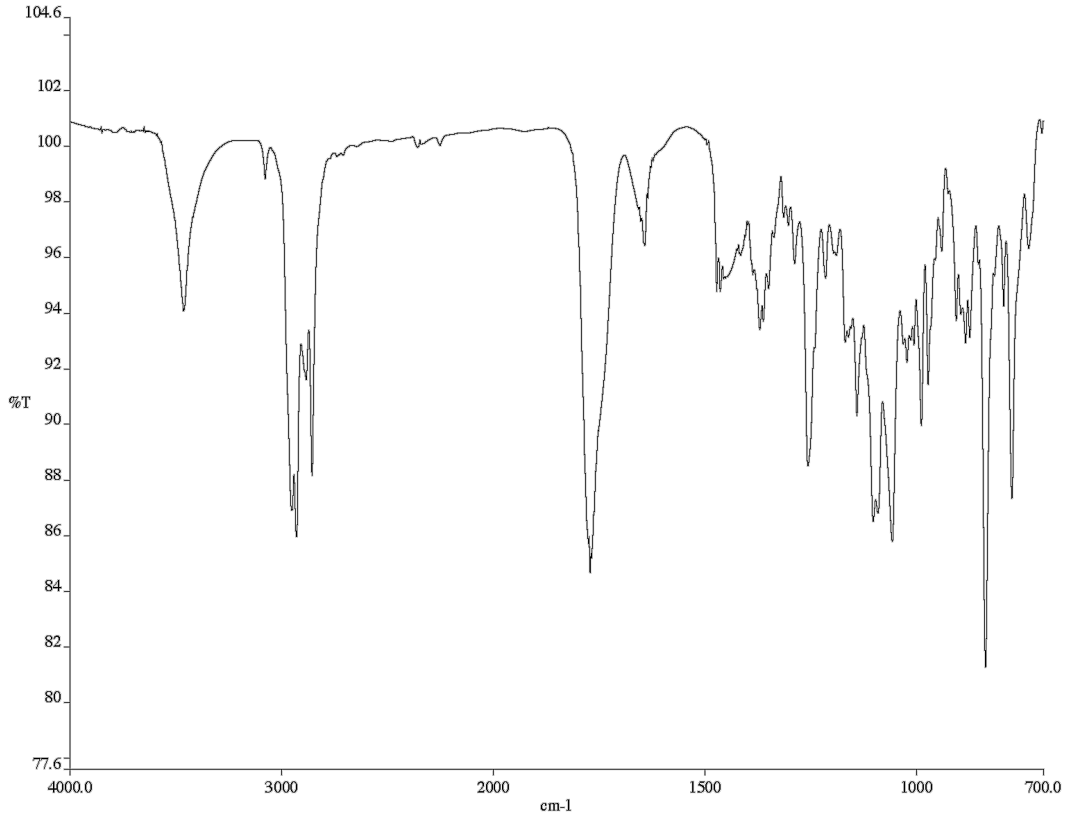

Figure A10.35. Infrared spectrum (Thin Film, NaCl) of compound **389**.

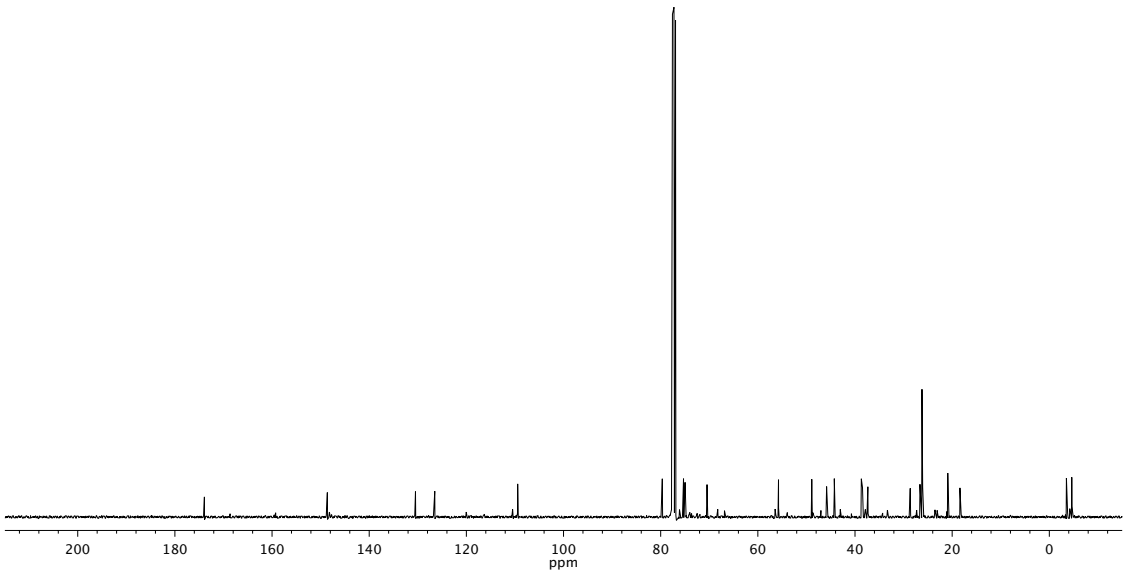

Figure A10.36. ^{13}C NMR (101 MHz, $CDCl_3$) of compound **389**.

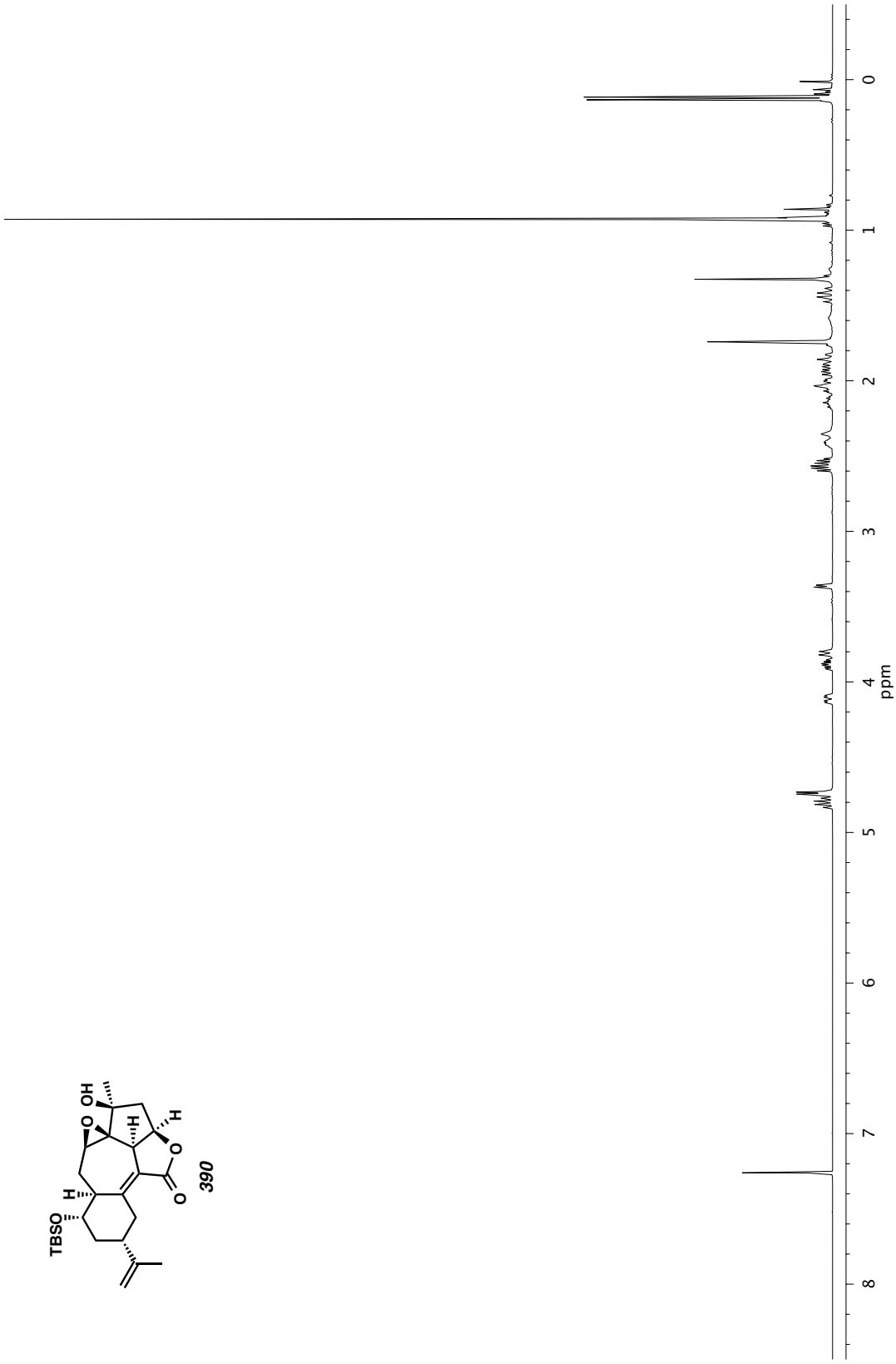

390

Figure A10.37. ^{1}H NMR (400 MHz, $CDCl_3$) of compound **390**.

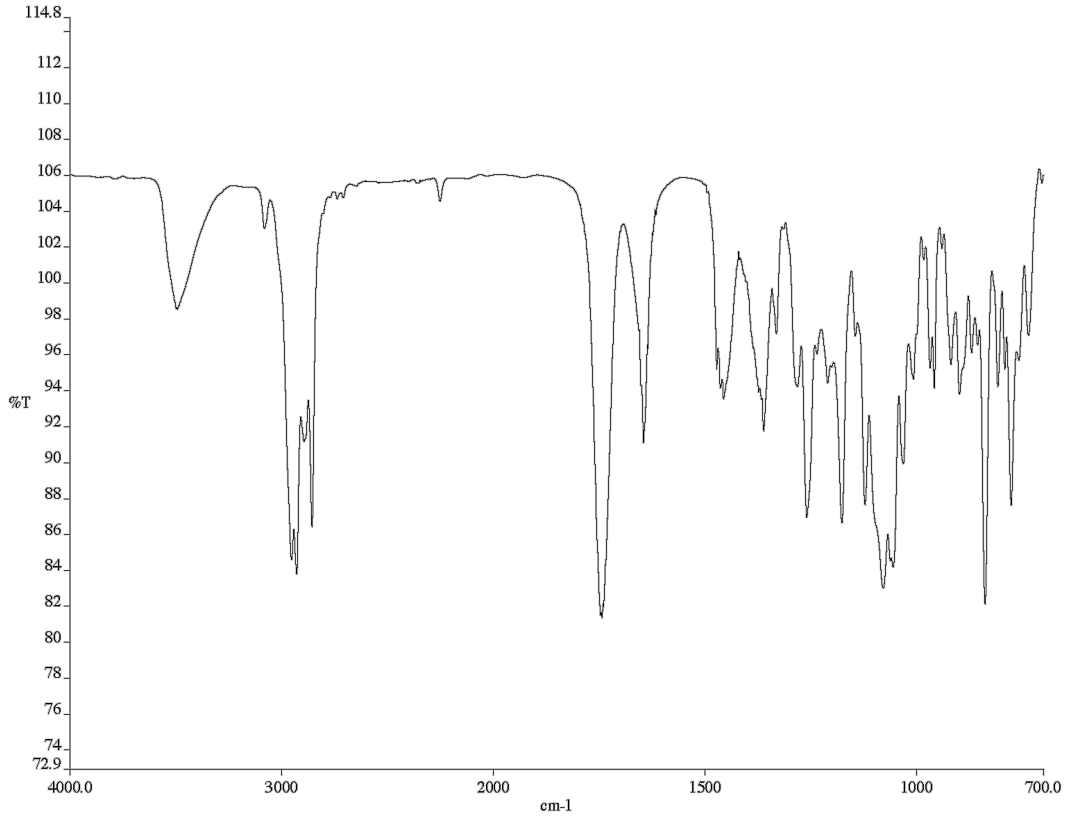

Figure A10.38. Infrared spectrum (Thin Film, NaCl) of compound **390**.

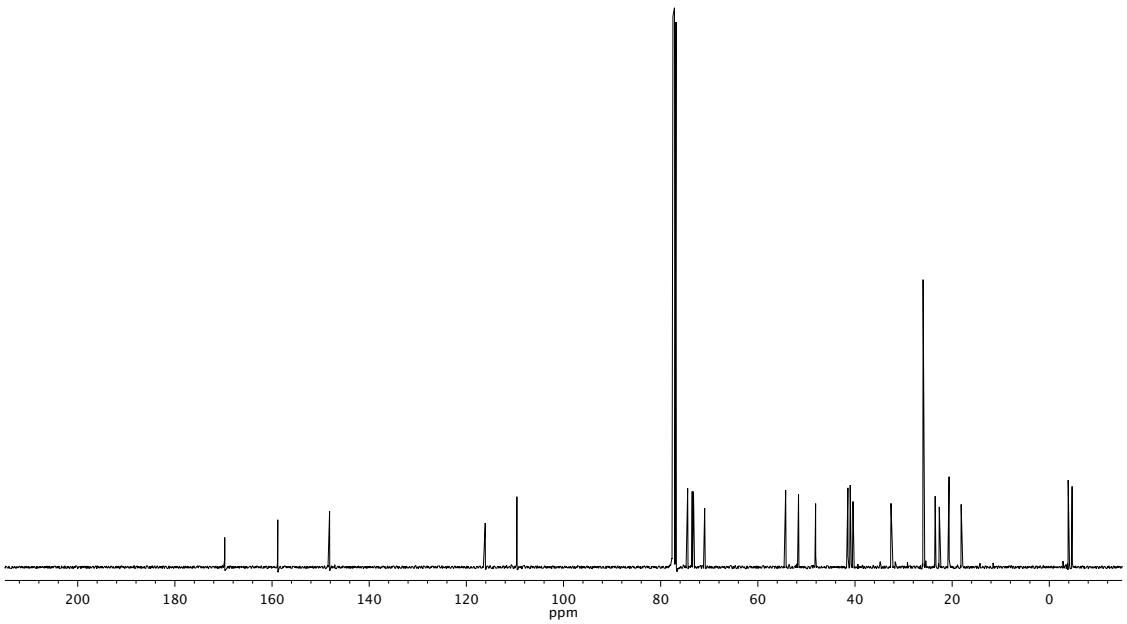

Figure A10.39. ^{13}C NMR (101 MHz, $CDCl_3$) of compound **390**.

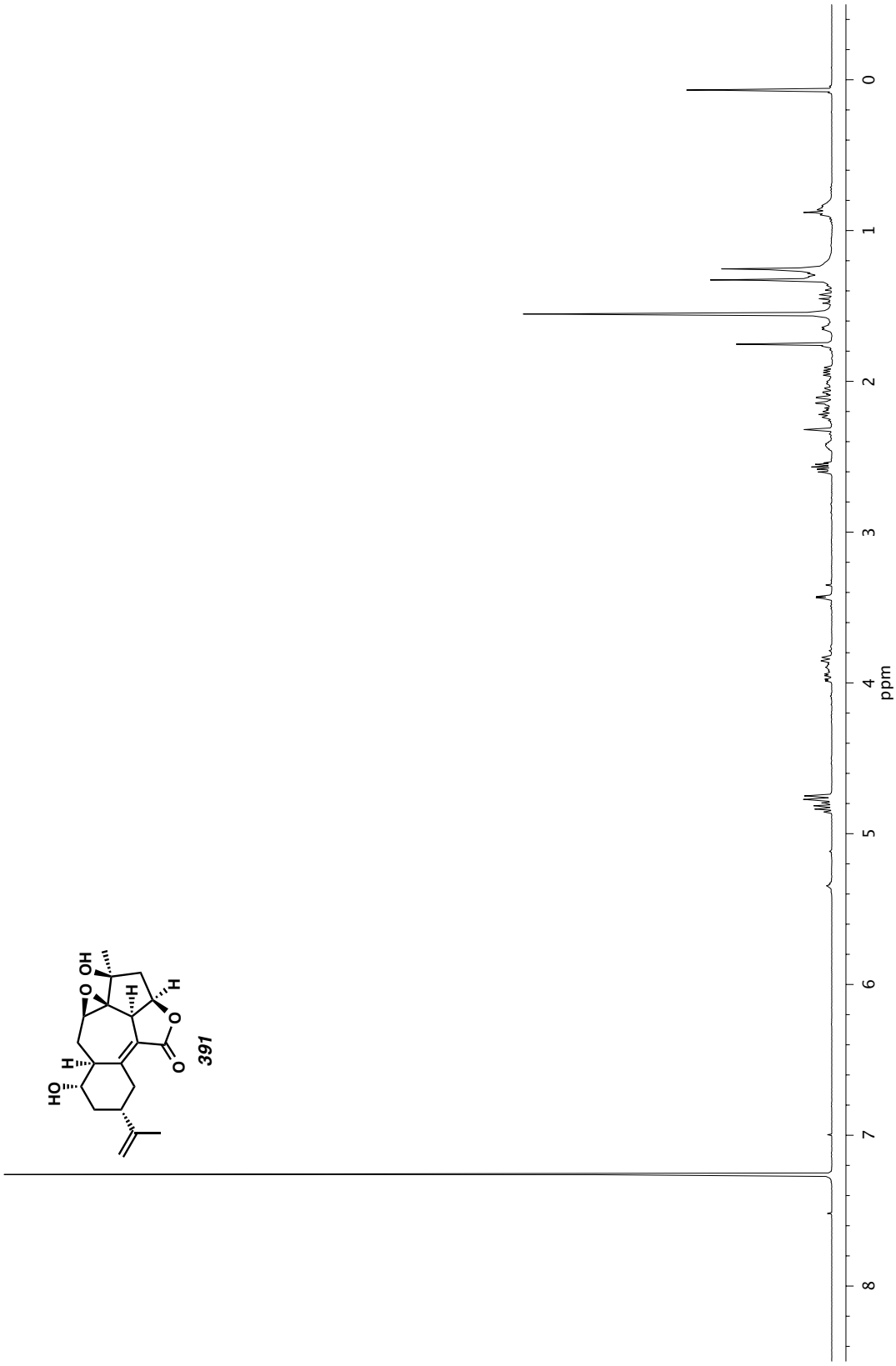

Figure A10.40. ^{1}H NMR (400 MHz, $CDCl_3$) of compound **391**.

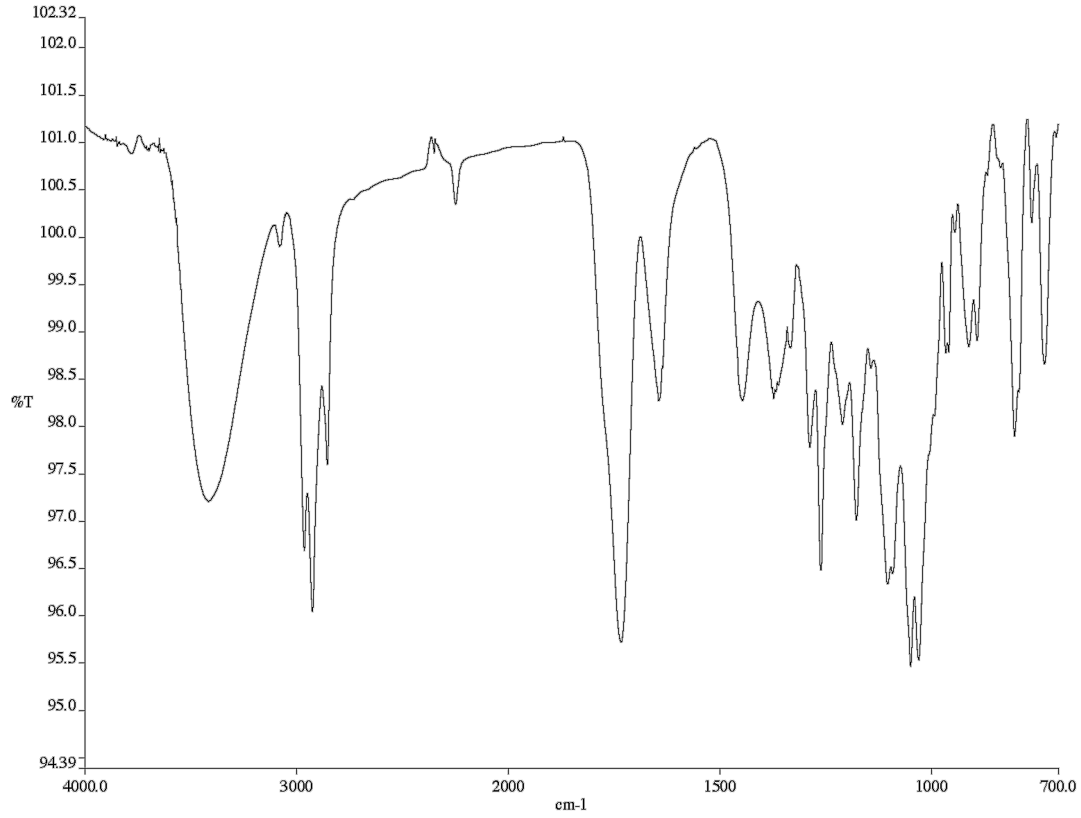

Figure A10.41. Infrared spectrum (Thin Film, NaCl) of compound **391**.

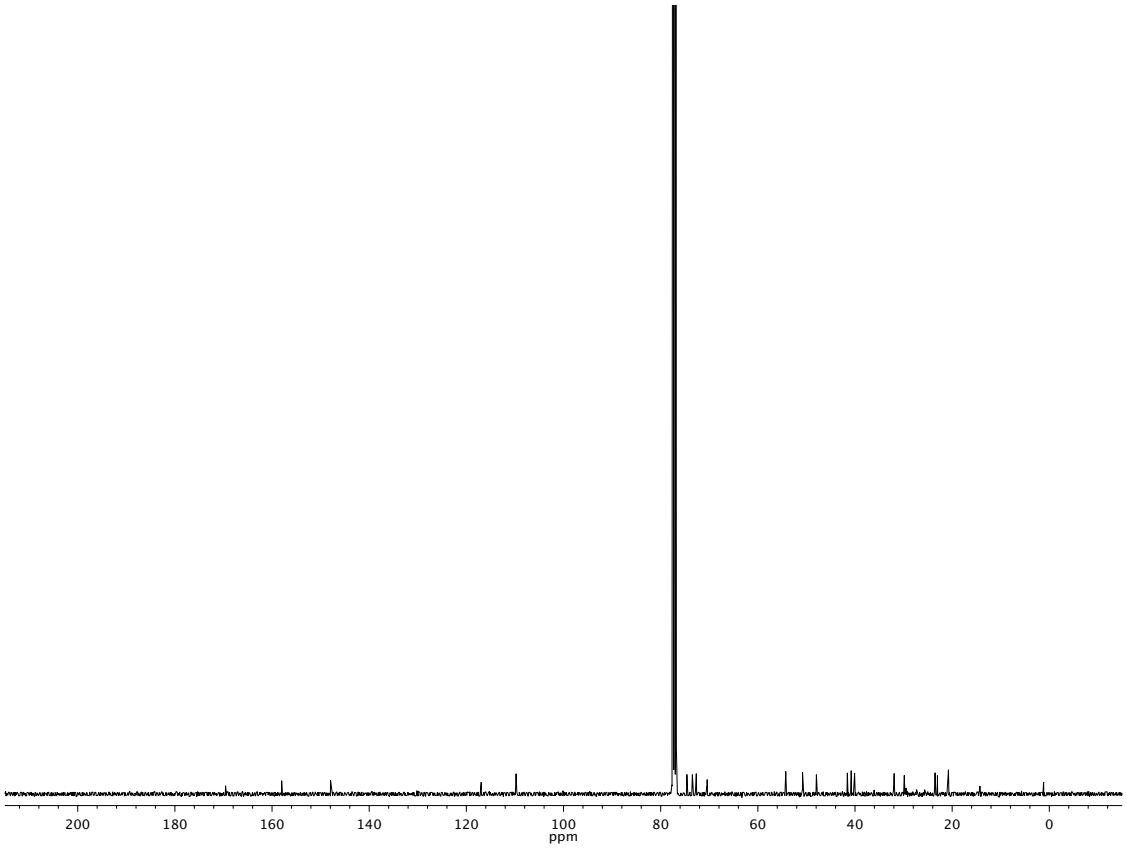

Figure A10.42. ^{13}C NMR (101 MHz, $CDCl_3$) of compound **391**.

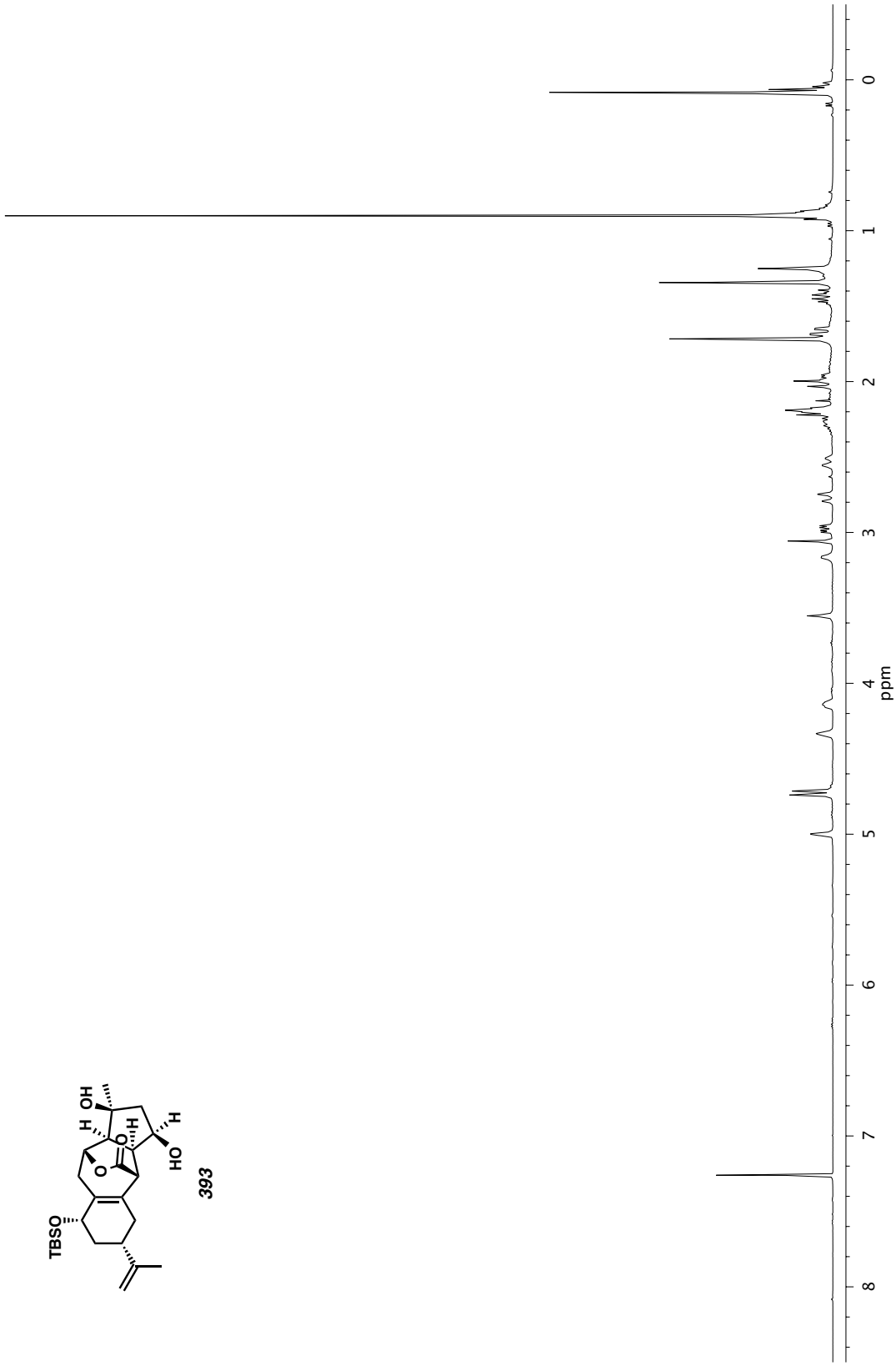

Figure A10.43. ^{1}H NMR (400 MHz, $CDCl_3$) of compound **393**.

393

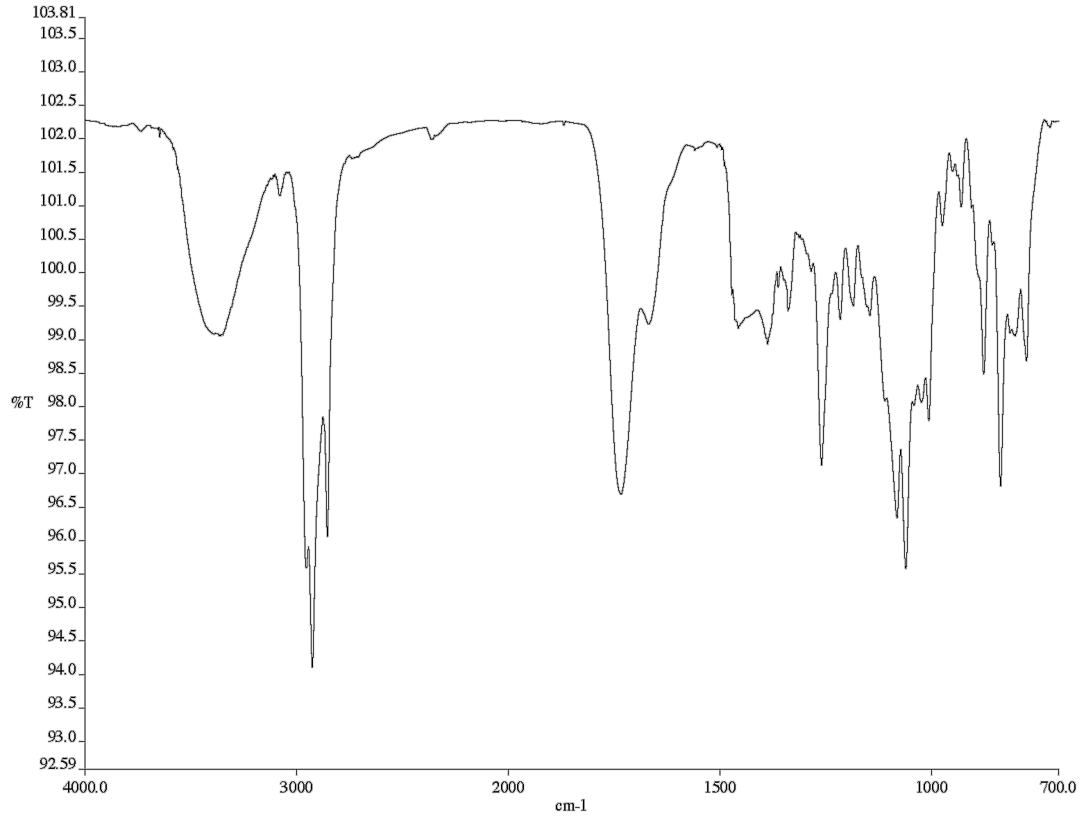

Figure A10.44. Infrared spectrum (Thin Film, NaCl) of compound **393**.

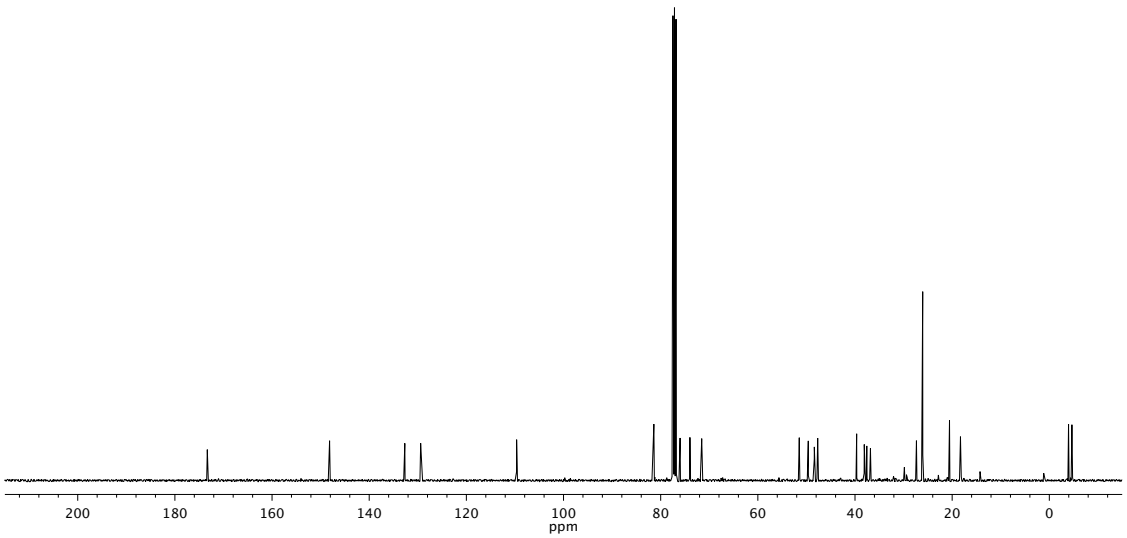

Figure A10.45. ^{13}C NMR (101 MHz, $CDCl_3$) of compound **393**.

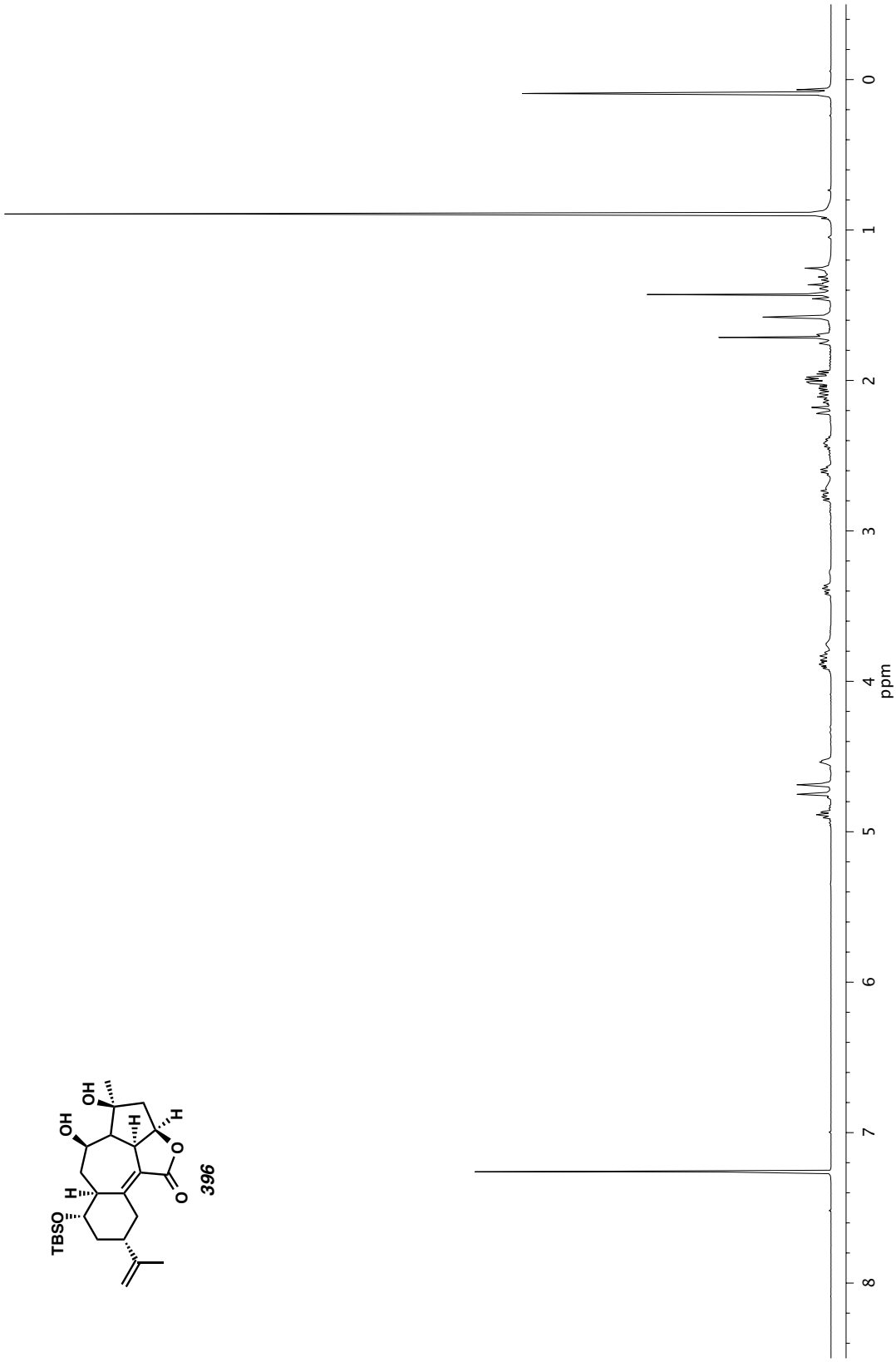

Figure A10.46. ^{1}H NMR (400 MHz, $CDCl_3$) of compound **396**.

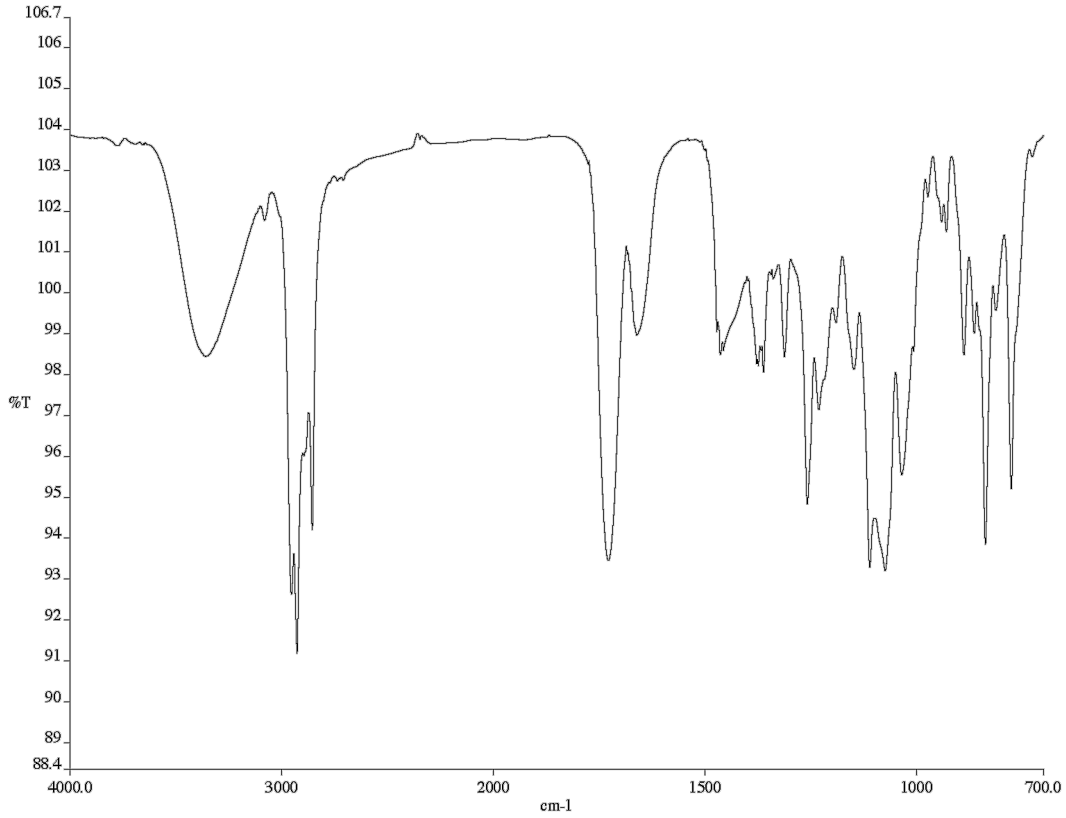

Figure A10.47. Infrared spectrum (Thin Film, NaCl) of compound **396**.

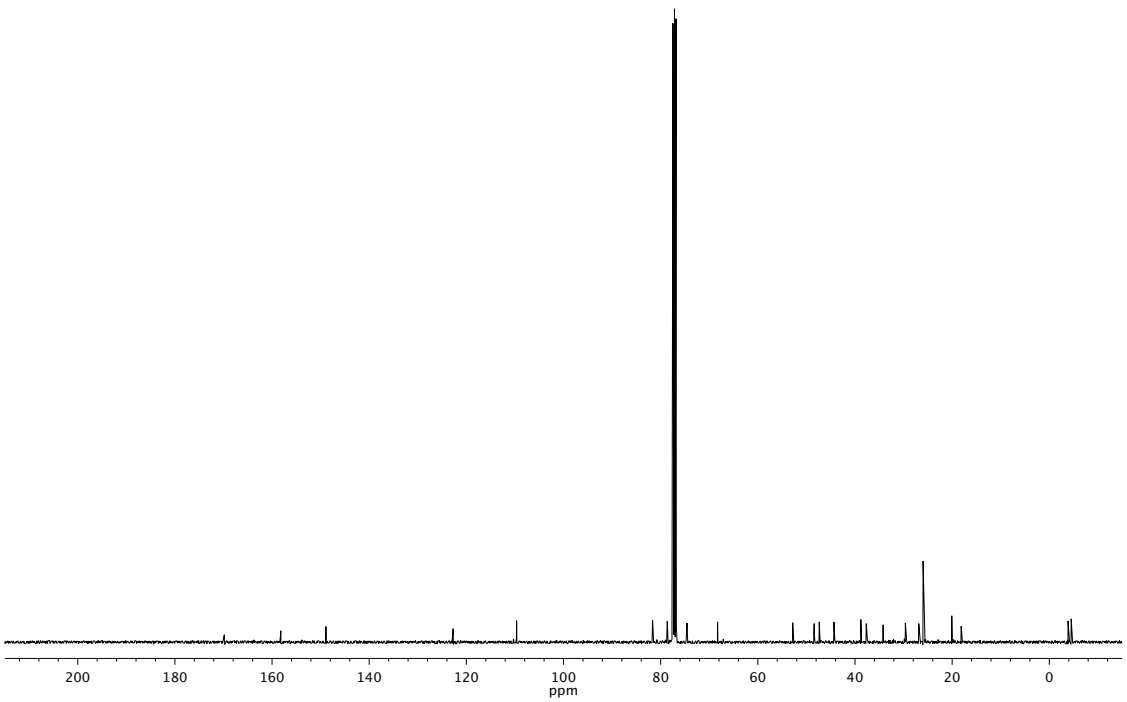

Figure A10.48. ^{13}C NMR (101 MHz, $CDCl_3$) of compound **396**.

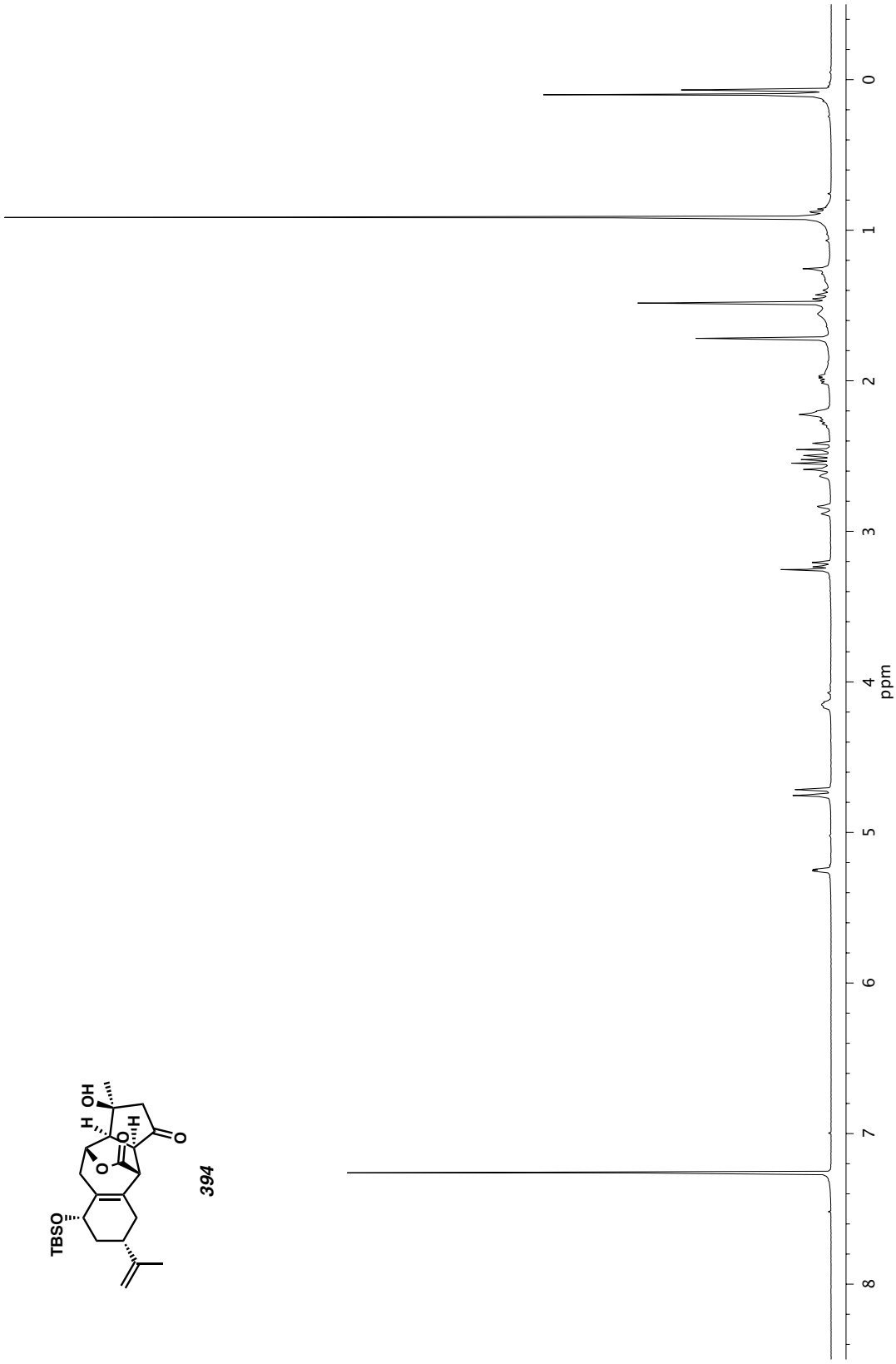

Figure A10.49. ^{1}H NMR (400 MHz, $CDCl_3$) of compound **394**.

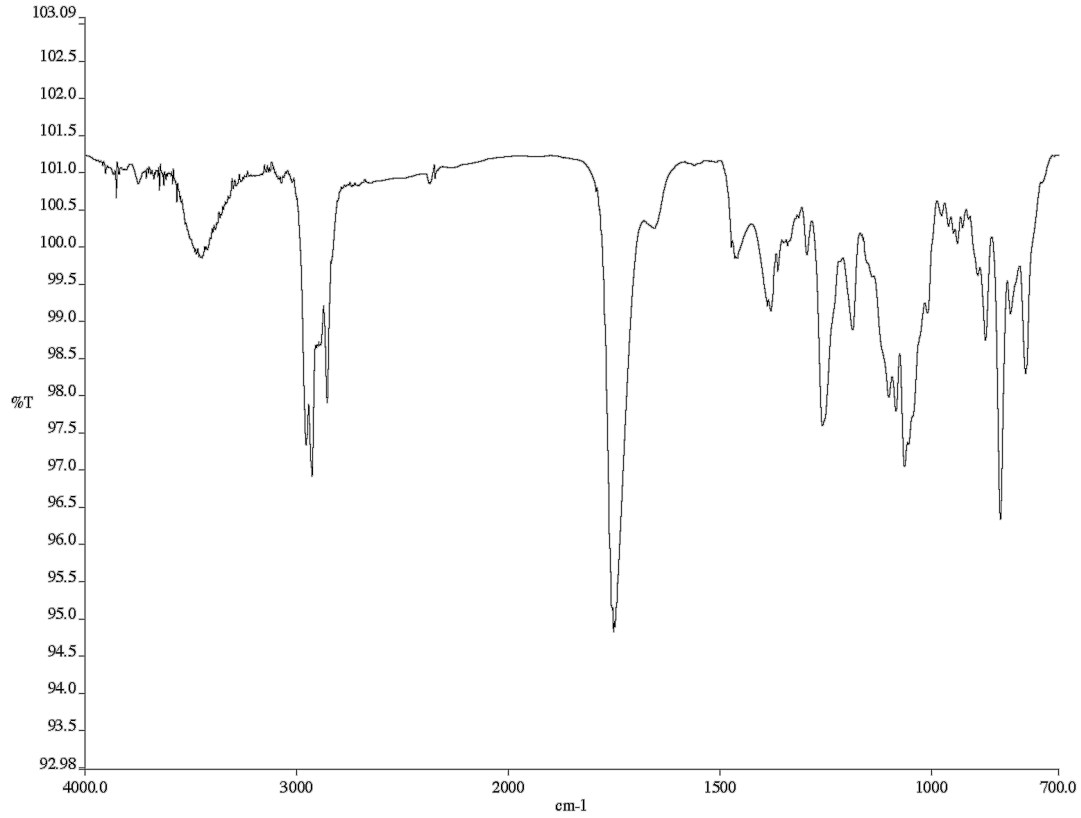

Figure A10.50. Infrared spectrum (Thin Film, NaCl) of compound **394**.

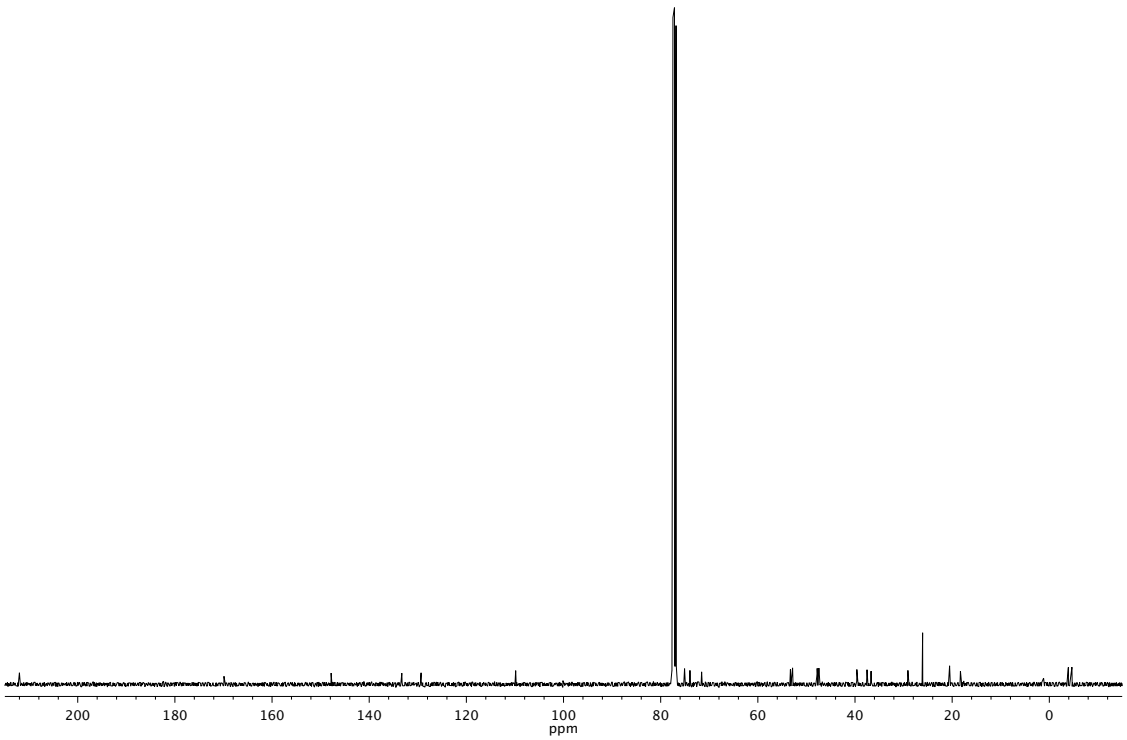

Figure A10.51. ^{13}C NMR (101 MHz, $CDCl_3$) of compound **394**.

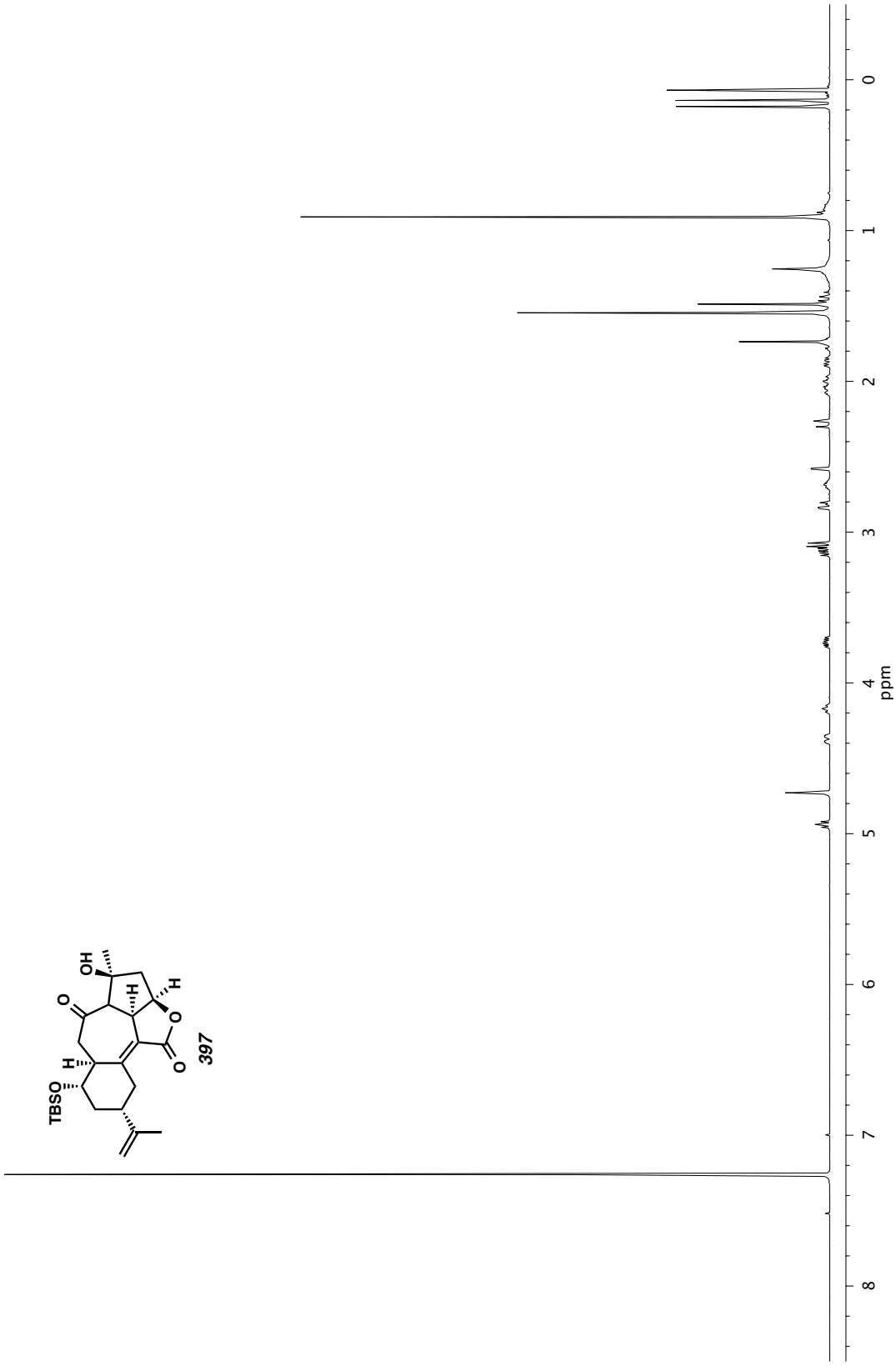

Figure A10.52. ^{1}H NMR (400 MHz, $CDCl_3$) of compound **397**.

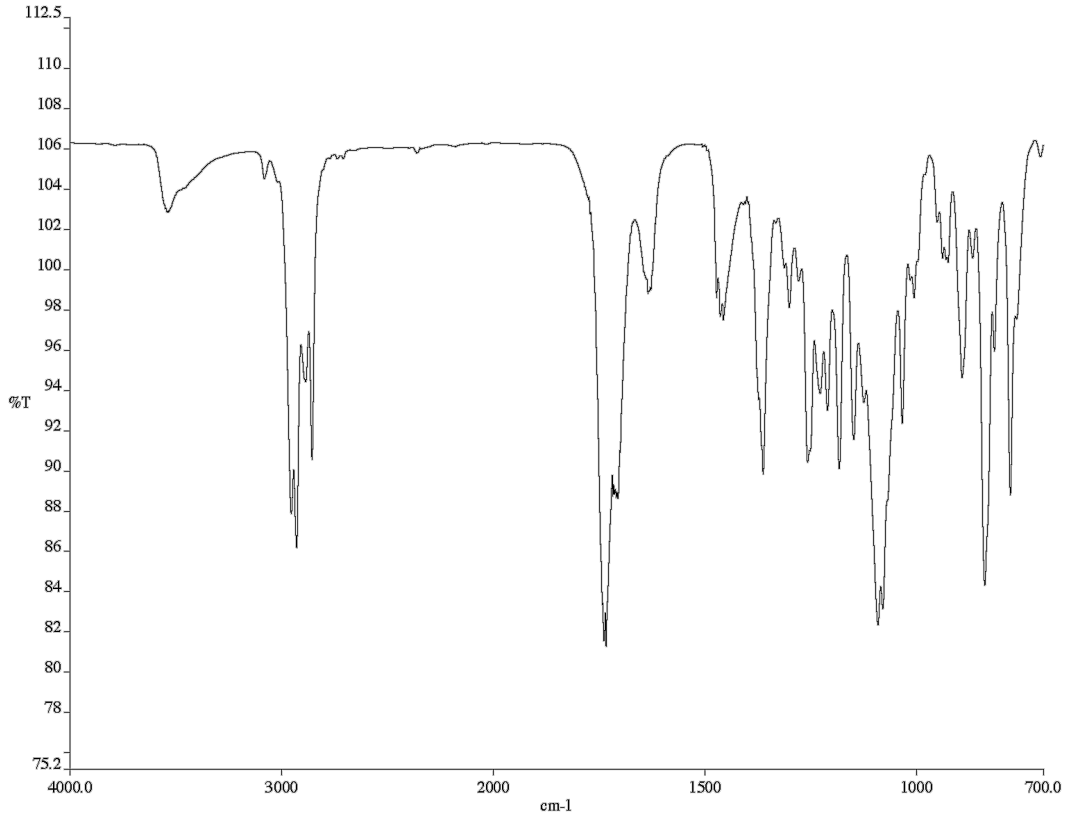

Figure A10.53. Infrared spectrum (Thin Film, NaCl) of compound **397**.

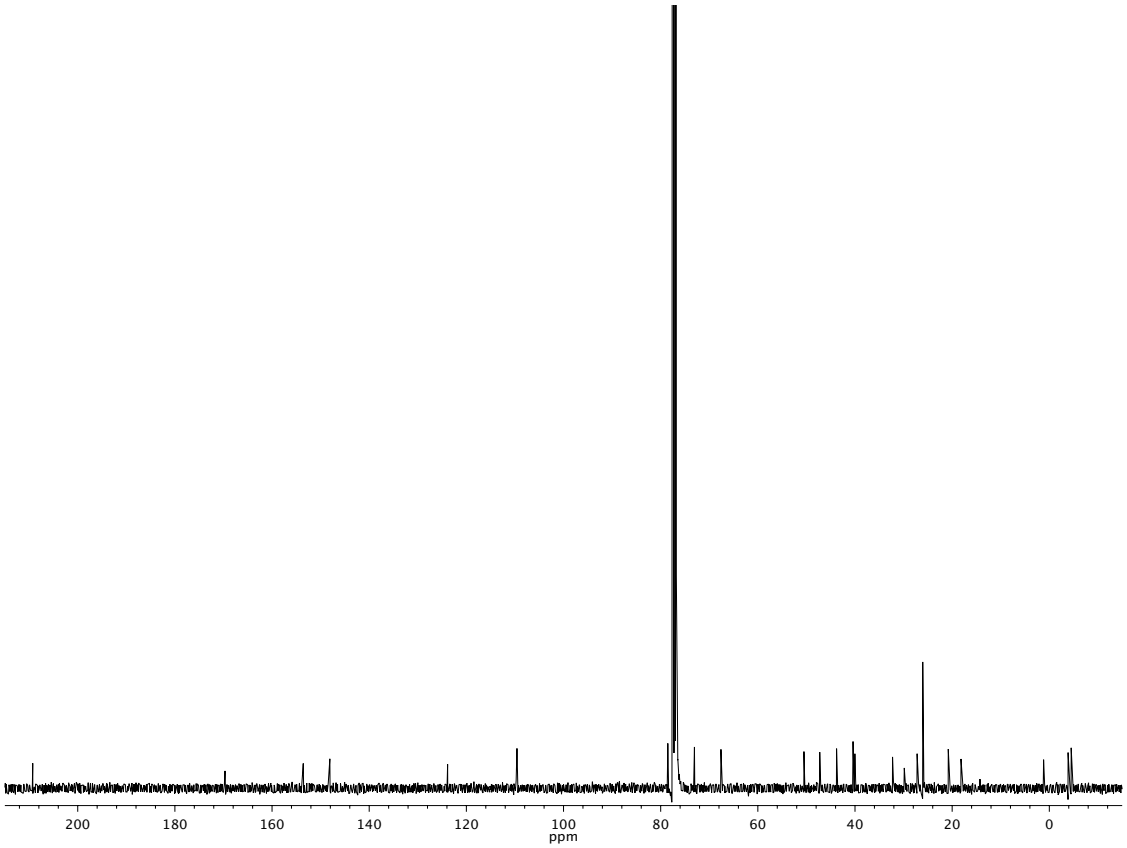

Figure A10.54. ^{13}C NMR (101 MHz, $CDCl_3$) of compound **397**.

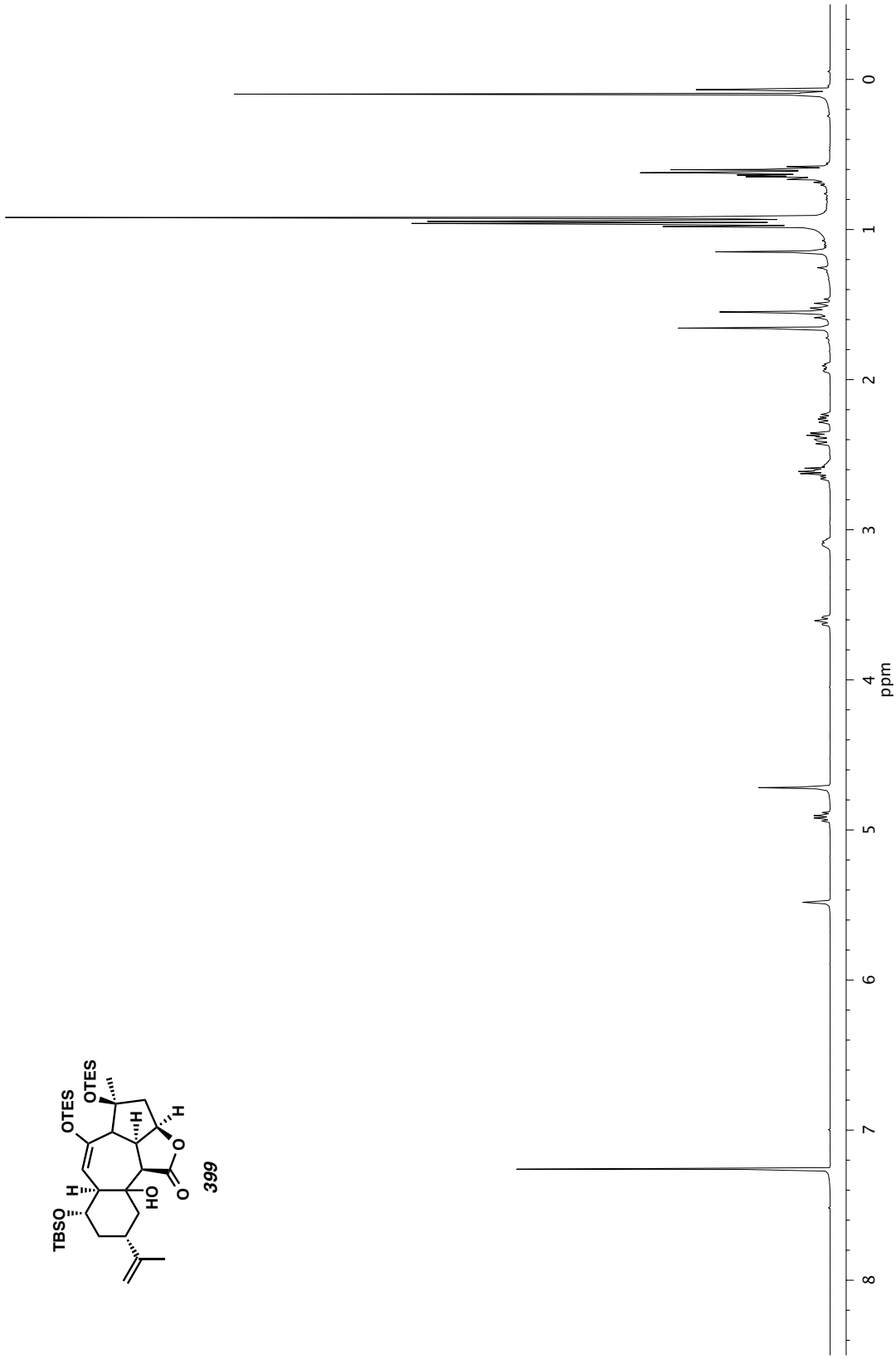

Figure A10.55. ^{1}H NMR (400 MHz, $CDCl_3$) of compound **399**.

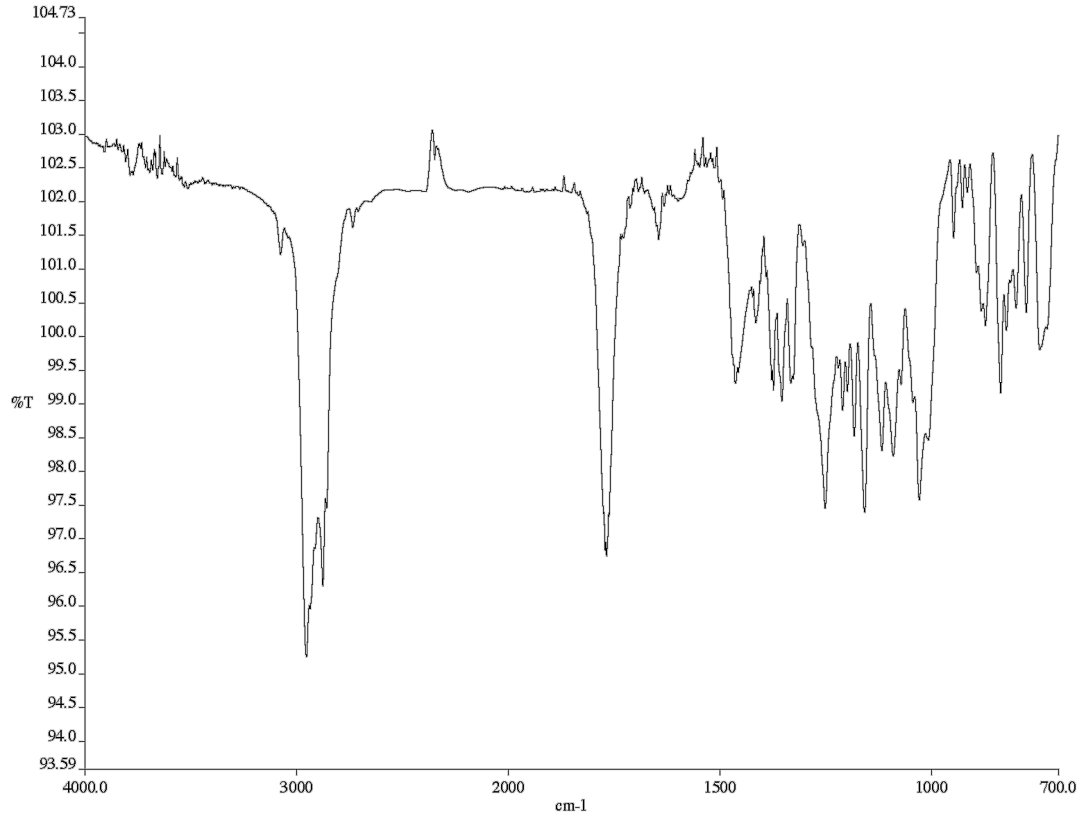

Figure A10.56. Infrared spectrum (Thin Film, NaCl) of compound **399**.

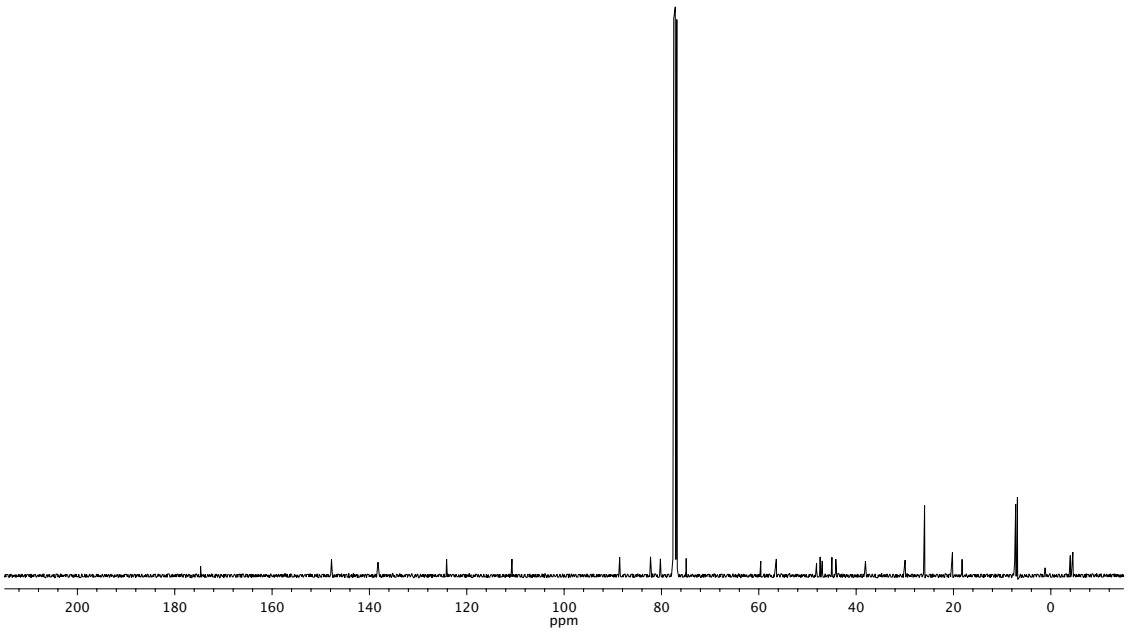

Figure A10.57. ^{13}C NMR (101 MHz, $CDCl_3$) of compound **399**.

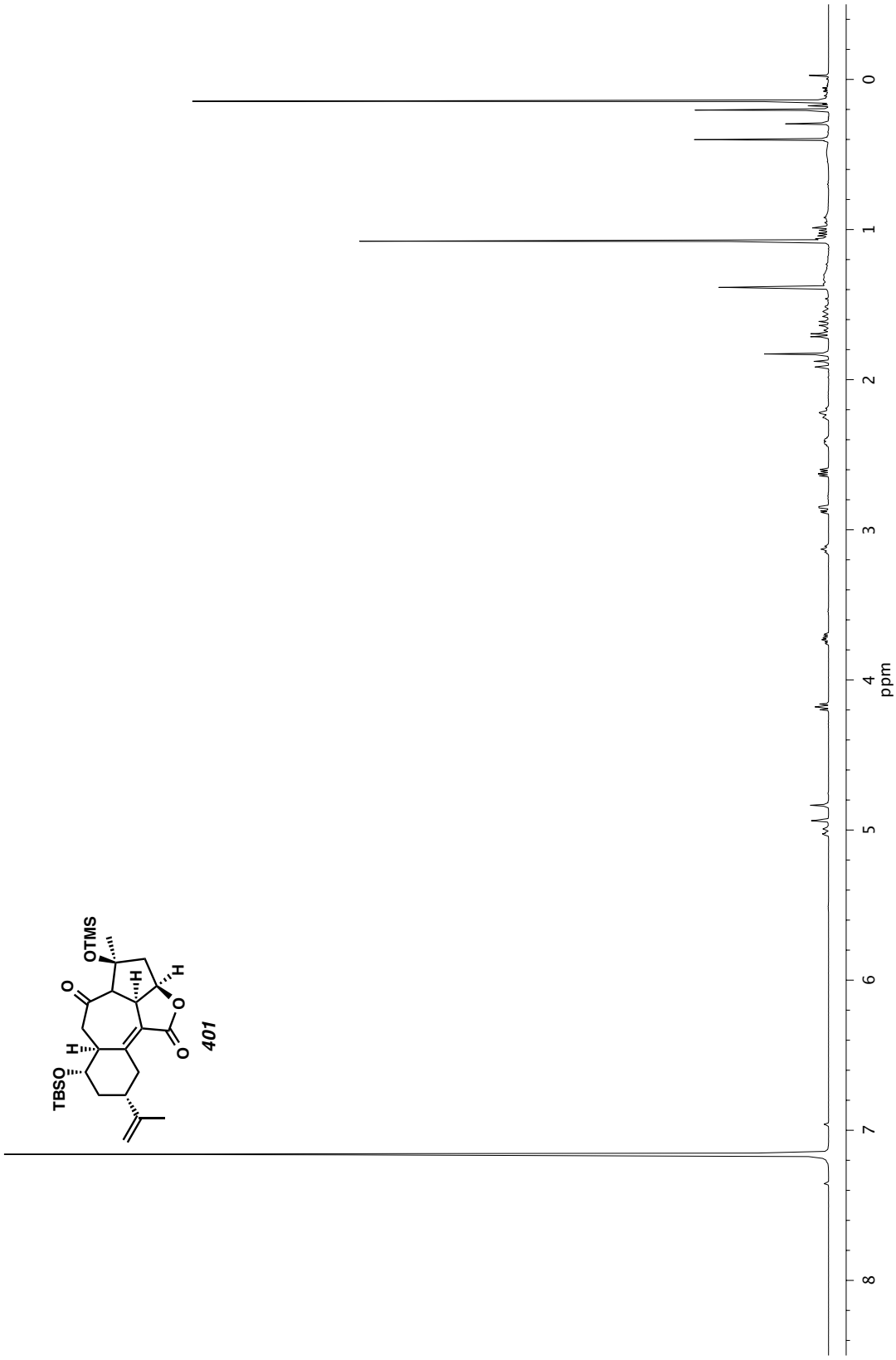

Figure A10.58. ^{1}H NMR (400 MHz, C_6D_6) of compound **401**.

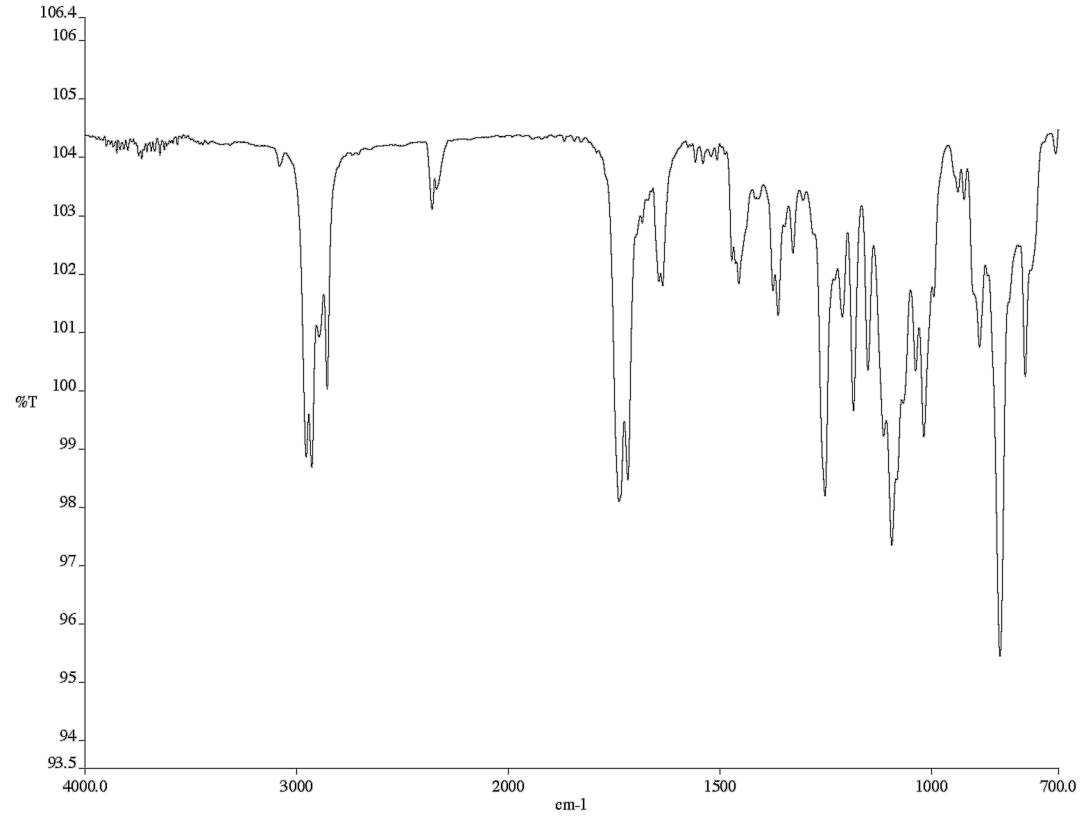

Figure A10.59. Infrared spectrum (Thin Film, NaCl) of compound **401**.

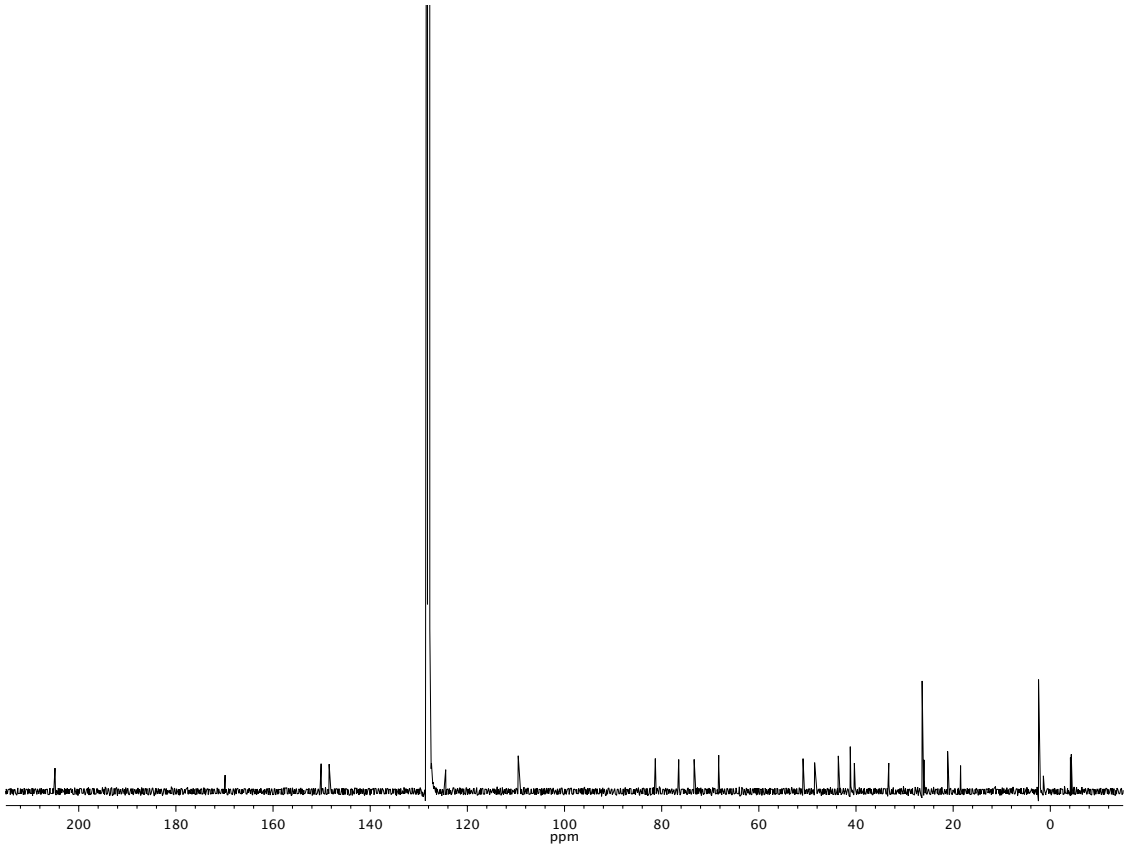

Figure A10.60. ^{13}C NMR (101 MHz, C_6D_6) of compound **401**.

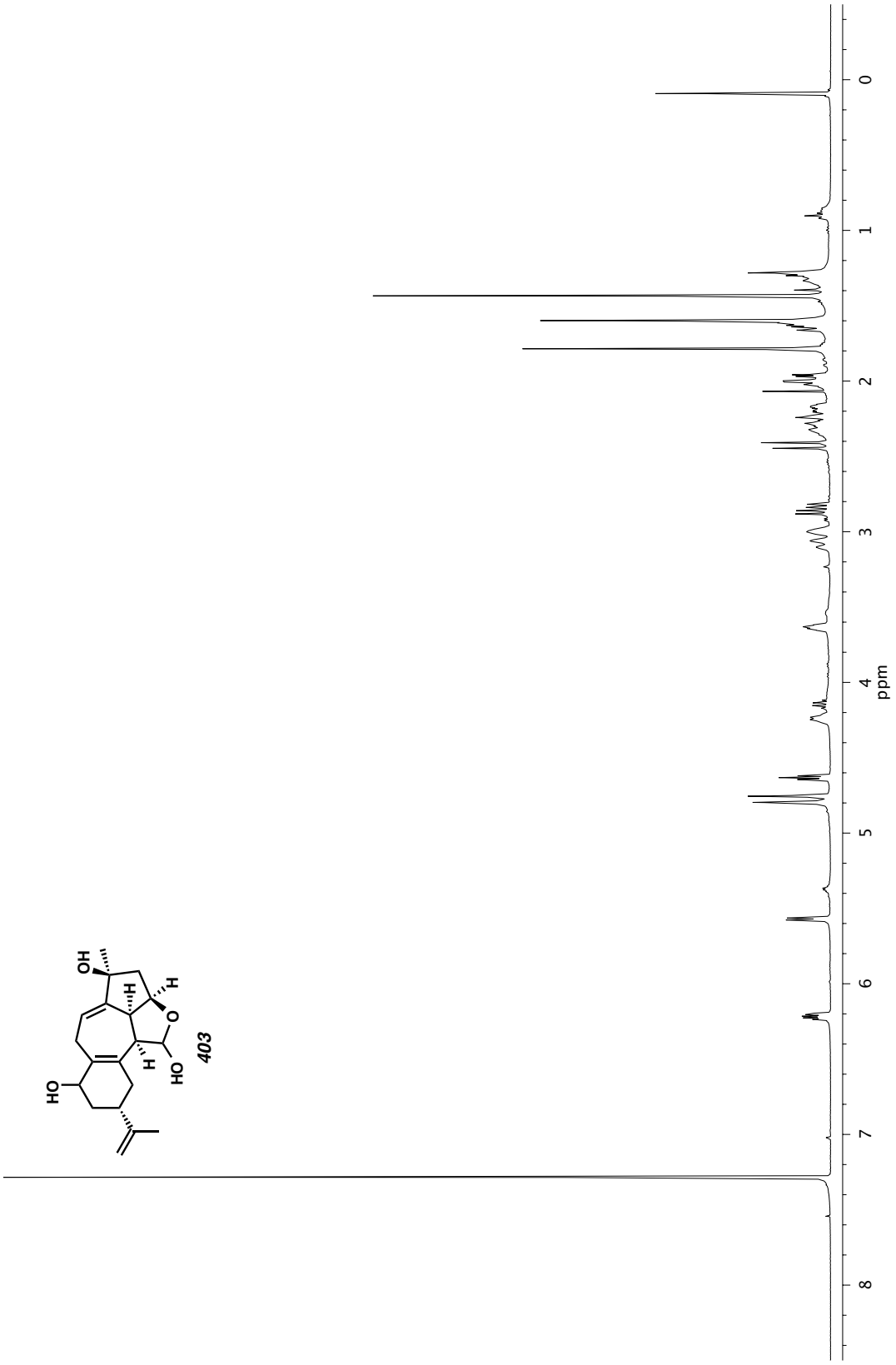

Figure A10.61. ^{1}H NMR (400 MHz, $CDCl_3$) of compound **403**.

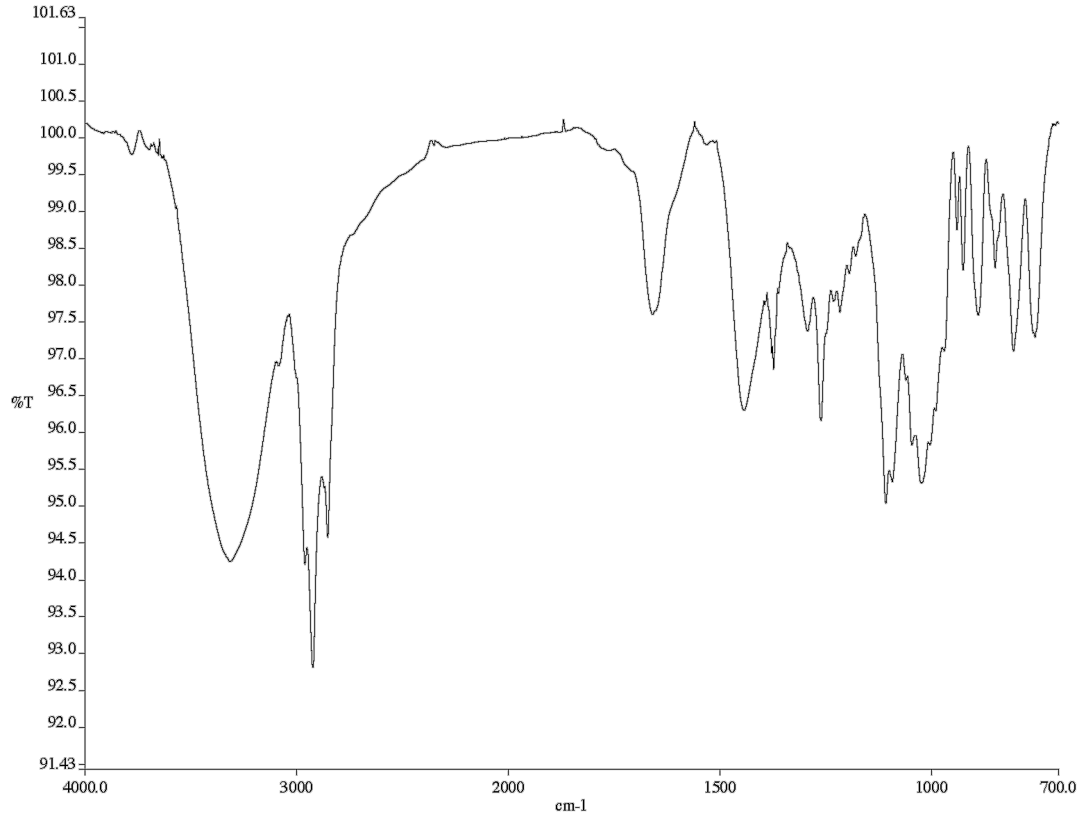

Figure A10.62. Infrared spectrum (Thin Film, NaCl) of compound **403**.

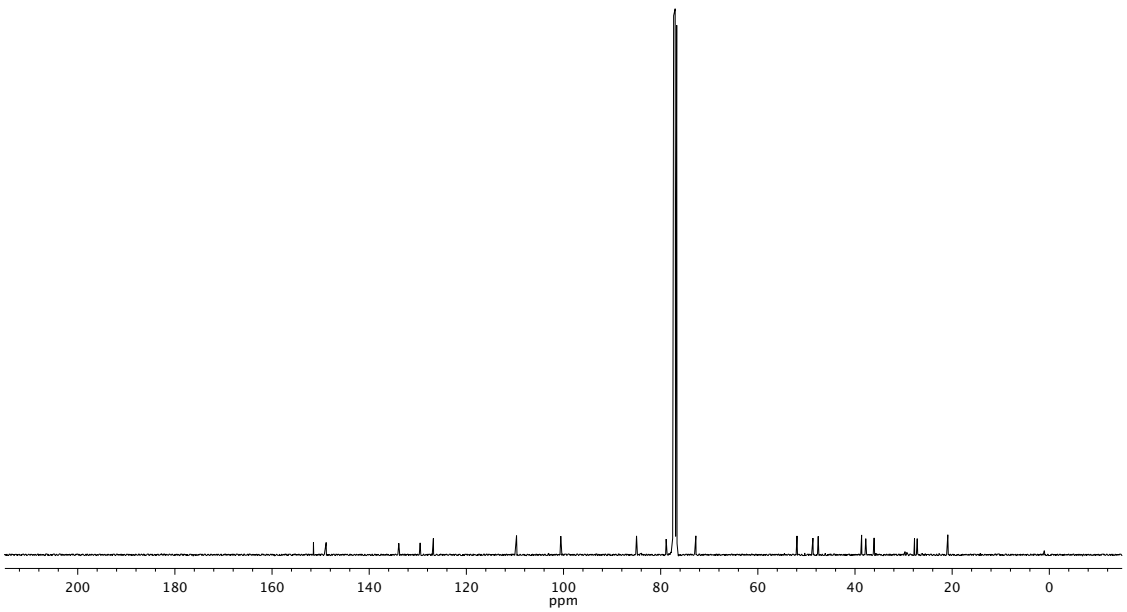

Figure A10.63. ^{13}C NMR (101 MHz, $CDCl_3$) of compound **403**.

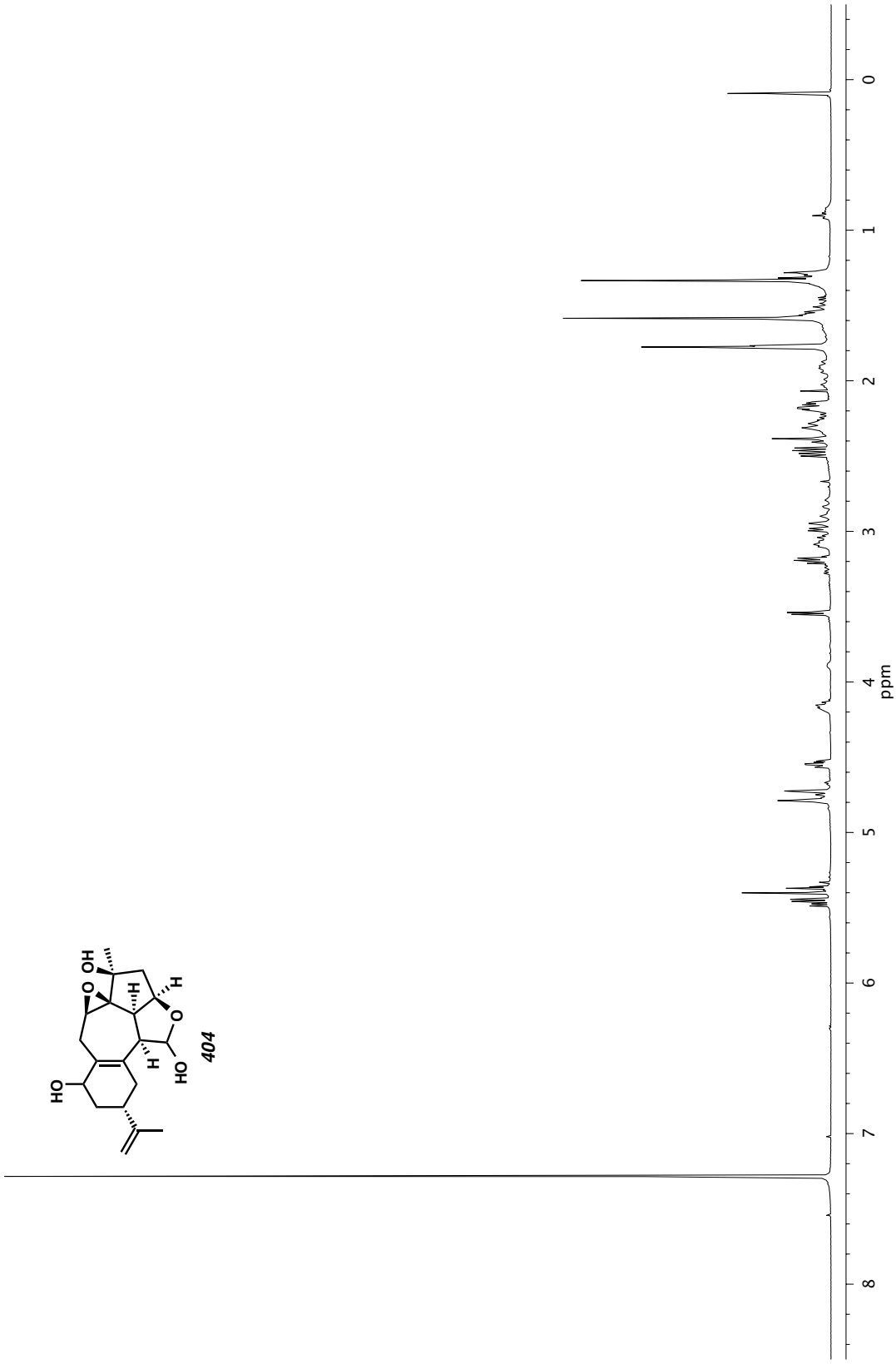

Figure A10.64. ^{1}H NMR (400 MHz, $CDCl_3$) of compound **404**.

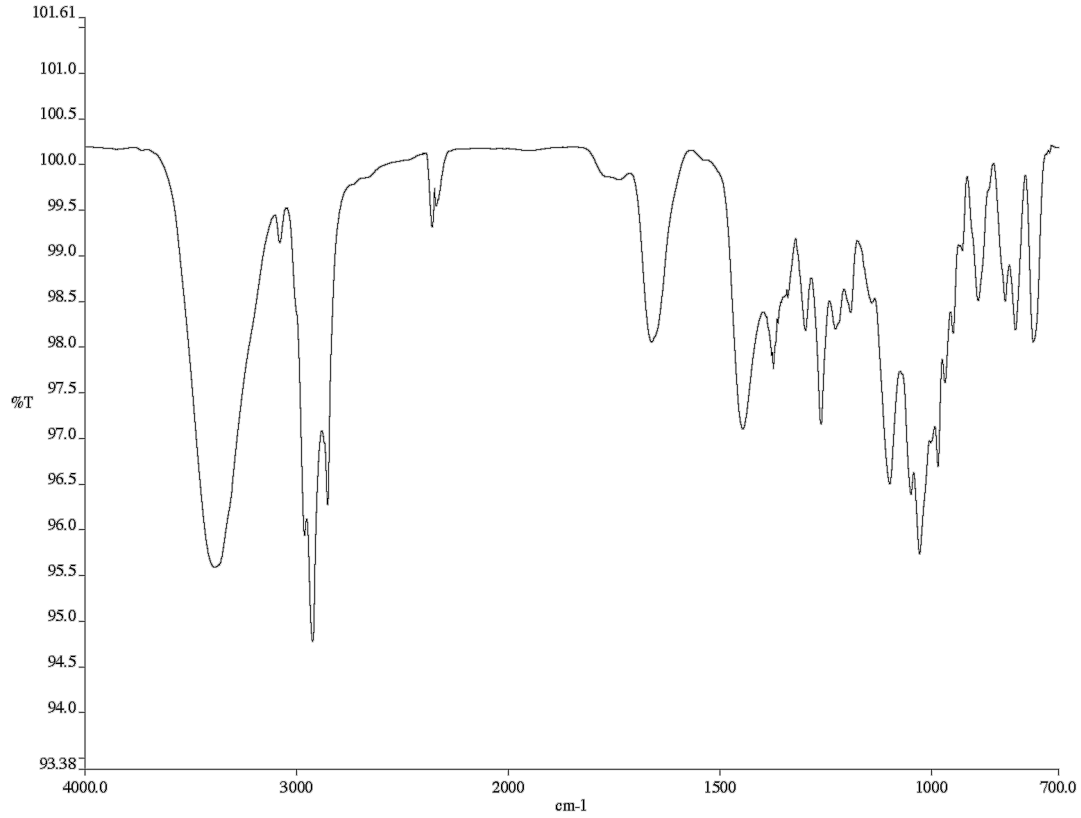

Figure A10.65. Infrared spectrum (Thin Film, NaCl) of compound **404**.

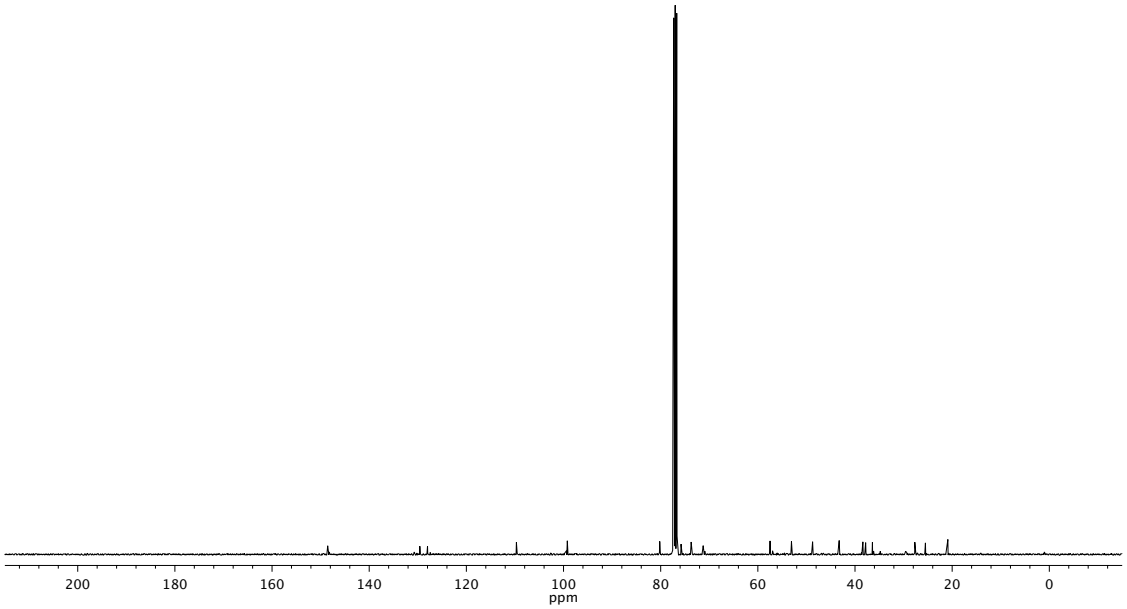

Figure A10.66. ^{13}C NMR (101 MHz, $CDCl_3$) of compound **404**.

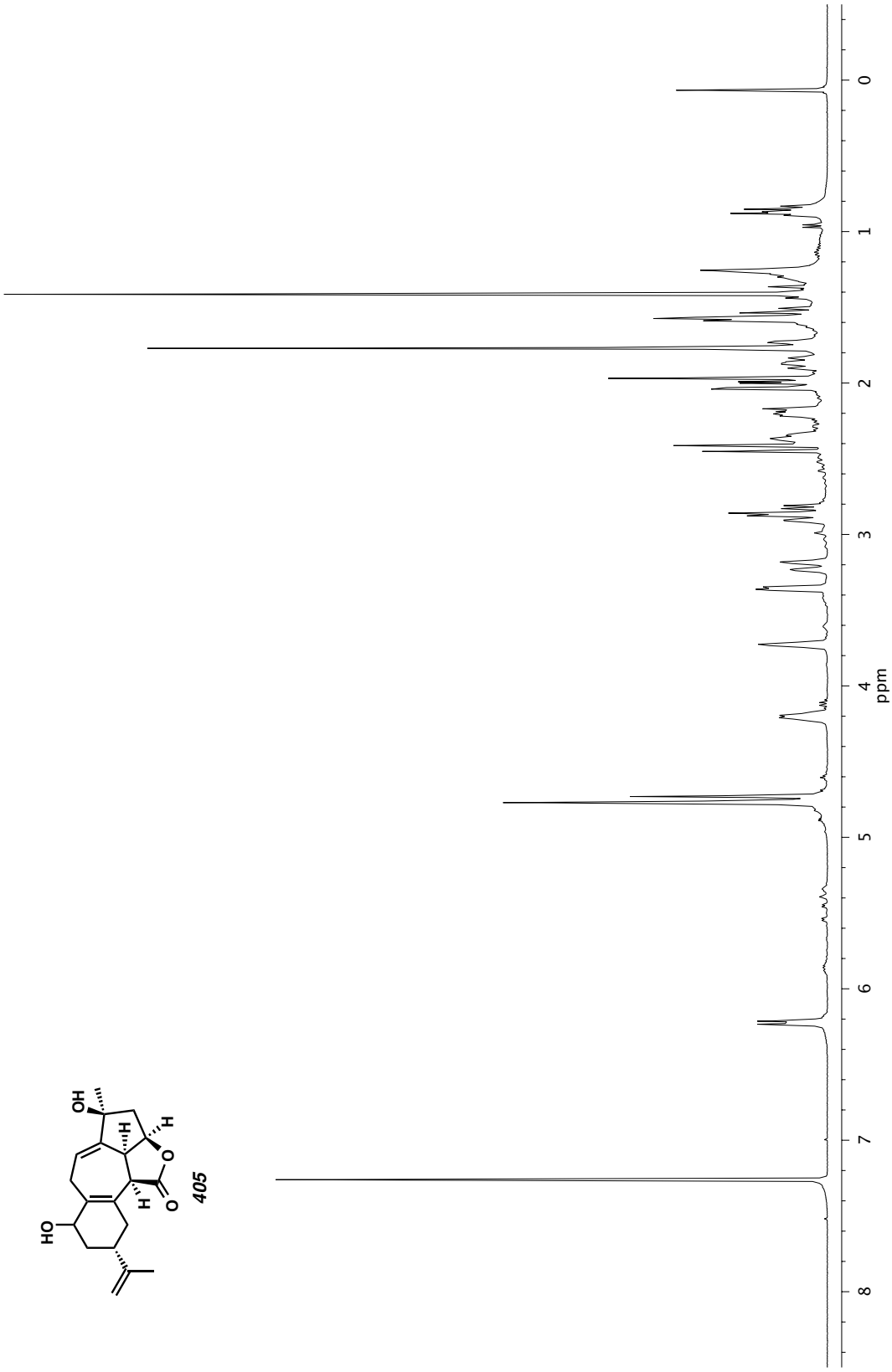

Figure A10.67. ^{1}H NMR (400 MHz, $CDCl_3$) of compound **405**.

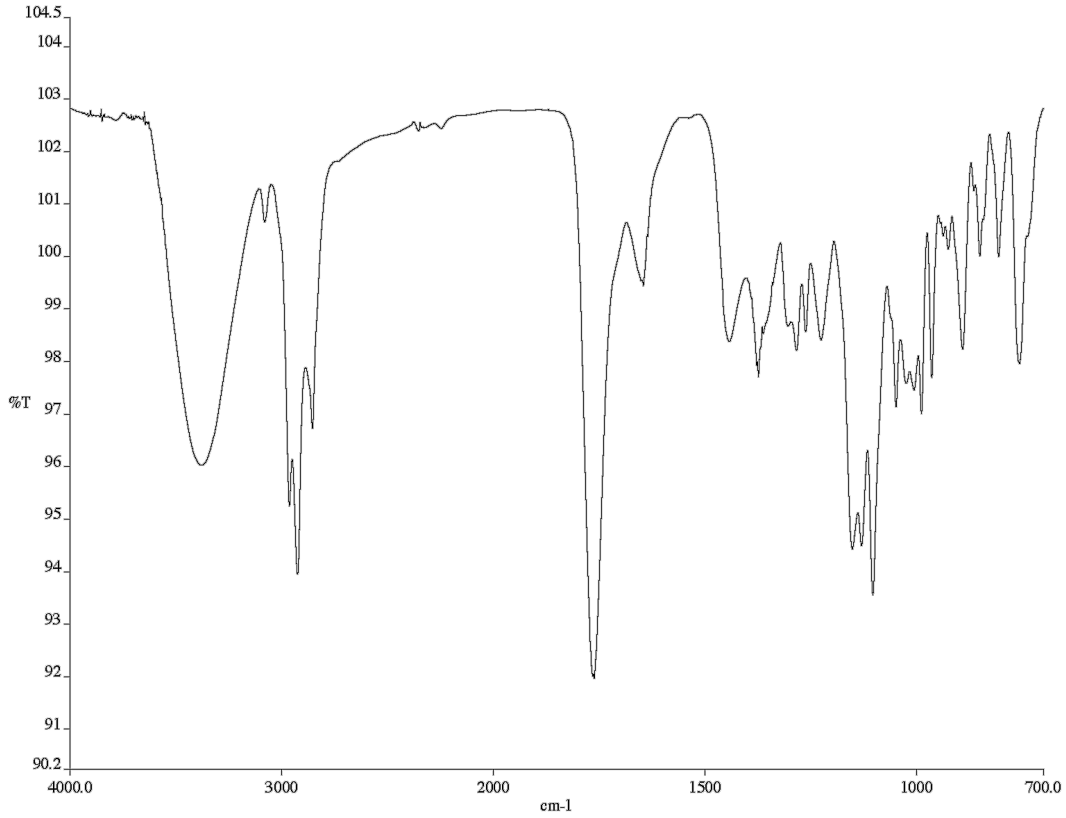

Figure A10.68. Infrared spectrum (Thin Film, NaCl) of compound **405**.

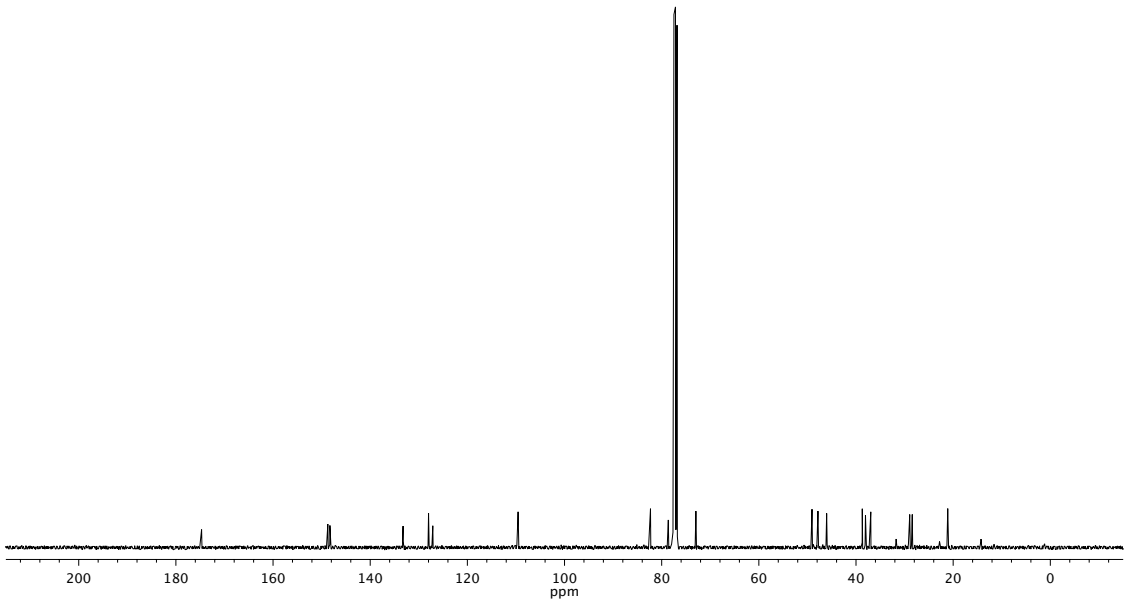

Figure A10.69. ^{13}C NMR (101 MHz, $CDCl_3$) of compound **405**.

Figure A10.70. ^{1}H NMR (400 MHz, $CDCl_3$) of compound **406**.

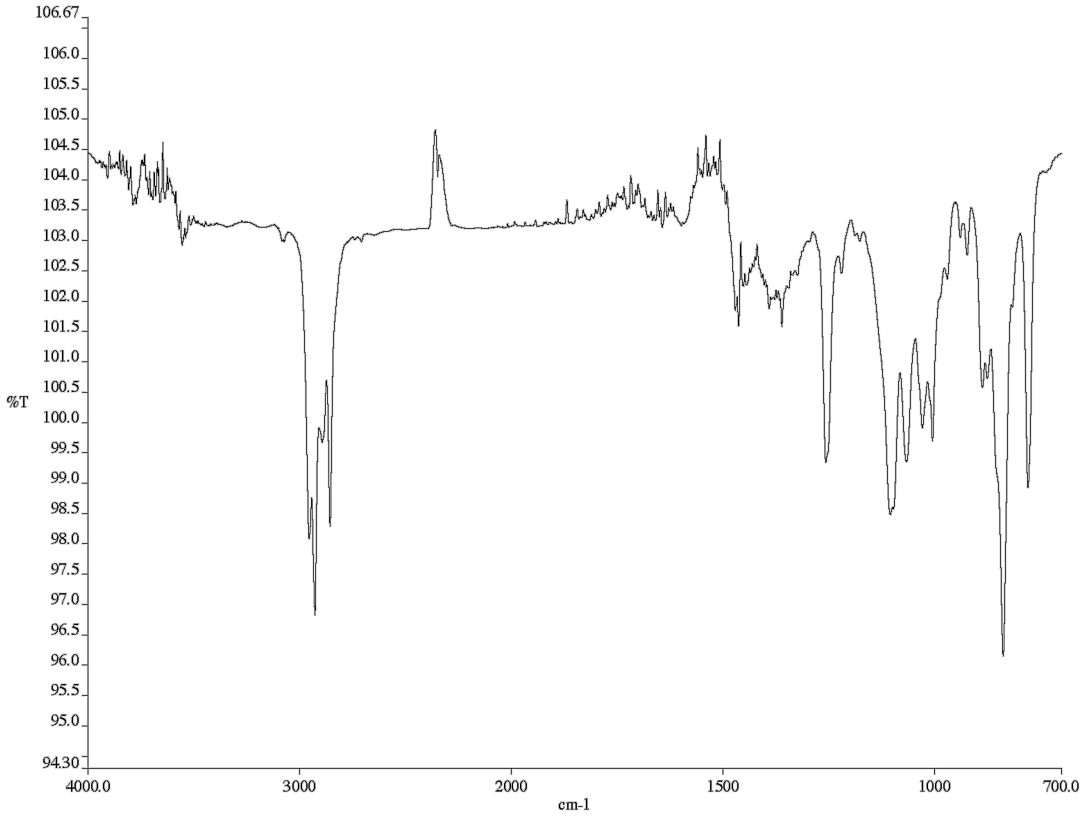

Figure A10.71. Infrared spectrum (Thin Film, NaCl) of compound **406**.

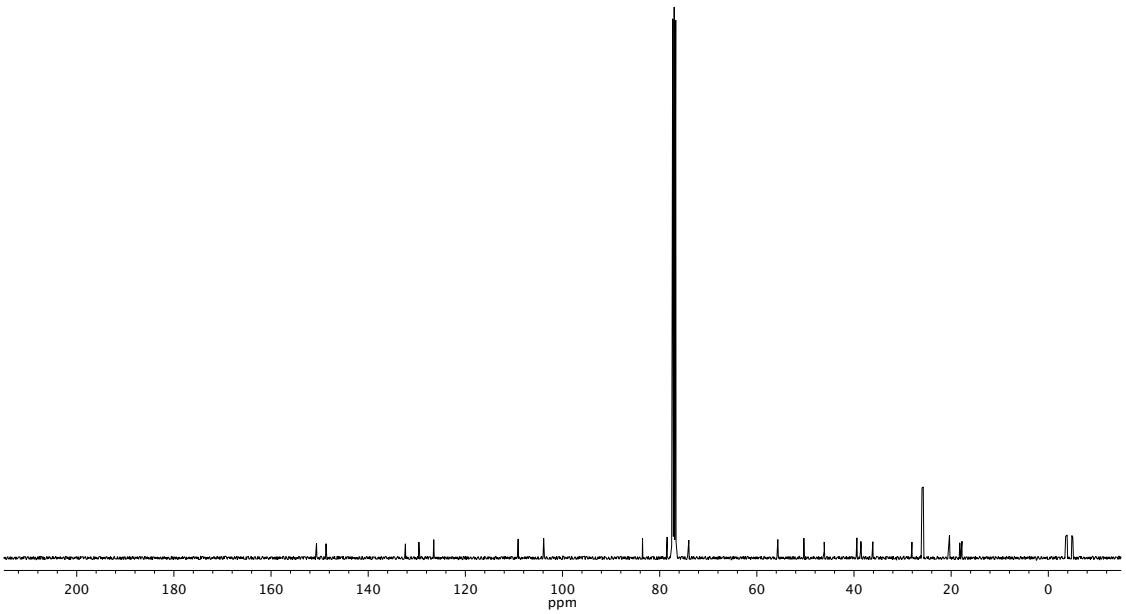

Figure A10.72. ^{13}C NMR (101 MHz, $CDCl_3$) of compound **406**.

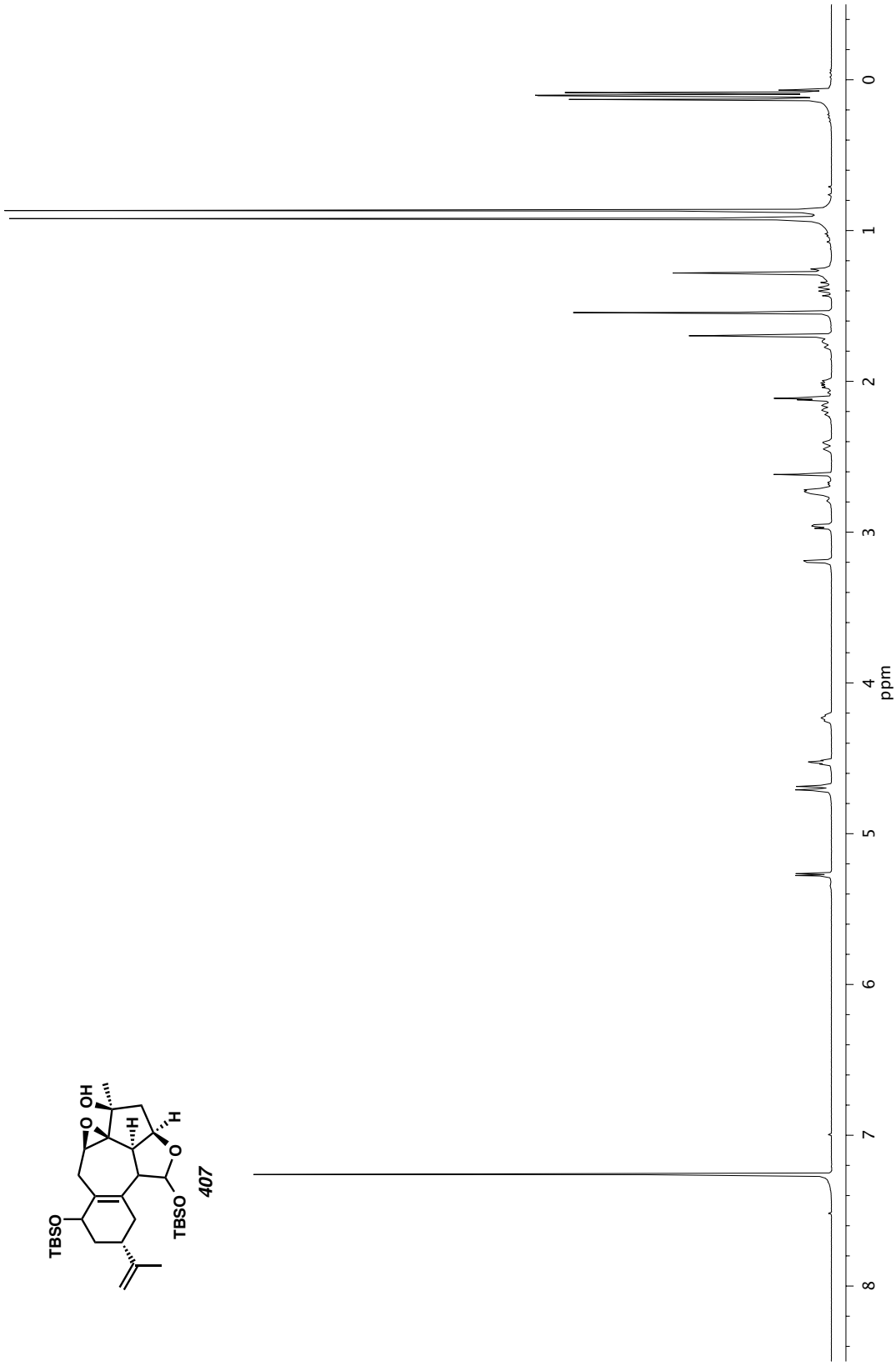

Figure A10.73. ^{1}H NMR (400 MHz, $CDCl_3$) of compound **407**.

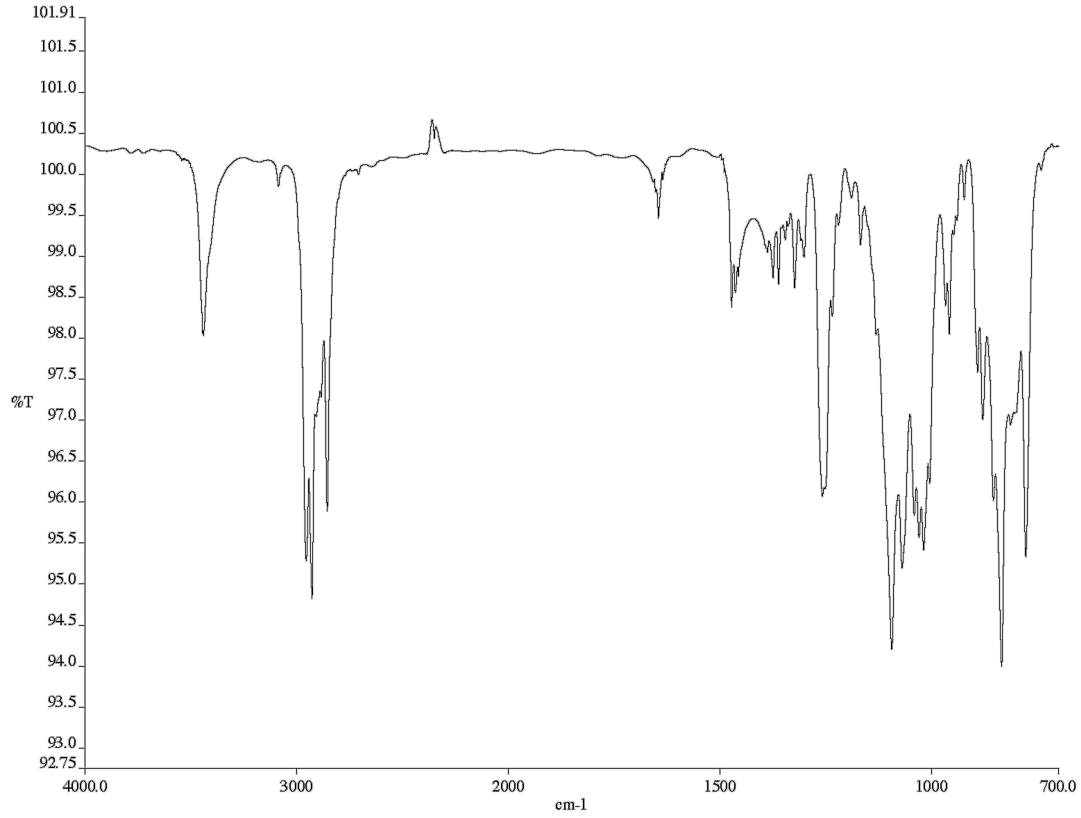

Figure A10.74. Infrared spectrum (Thin Film, NaCl) of compound **407**.

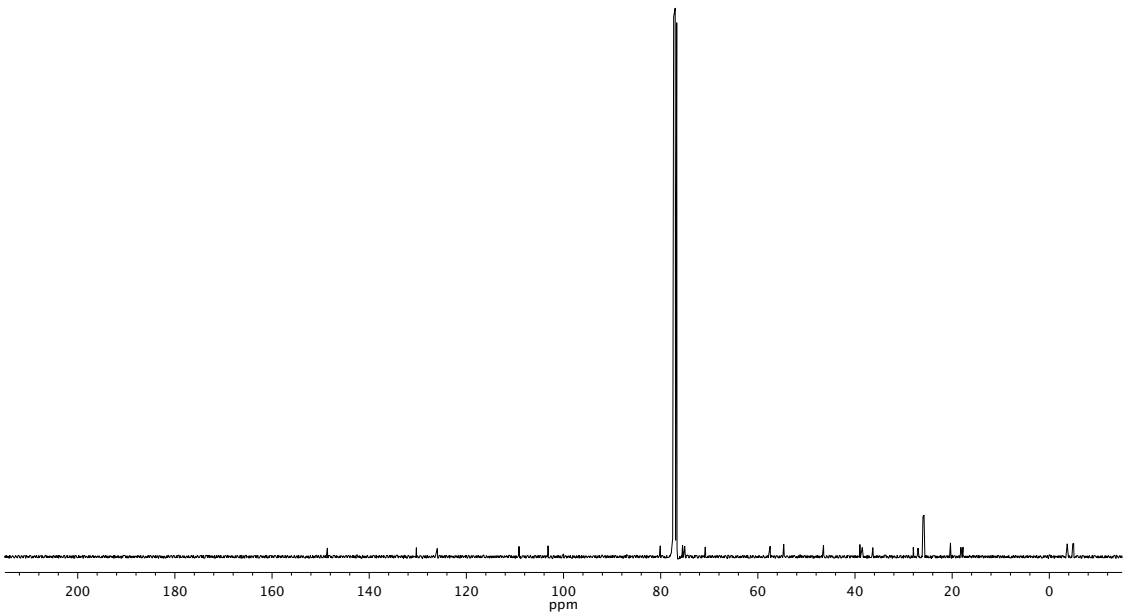

Figure A10.75. ^{13}C NMR (101 MHz, $CDCl_3$) of compound **407**.

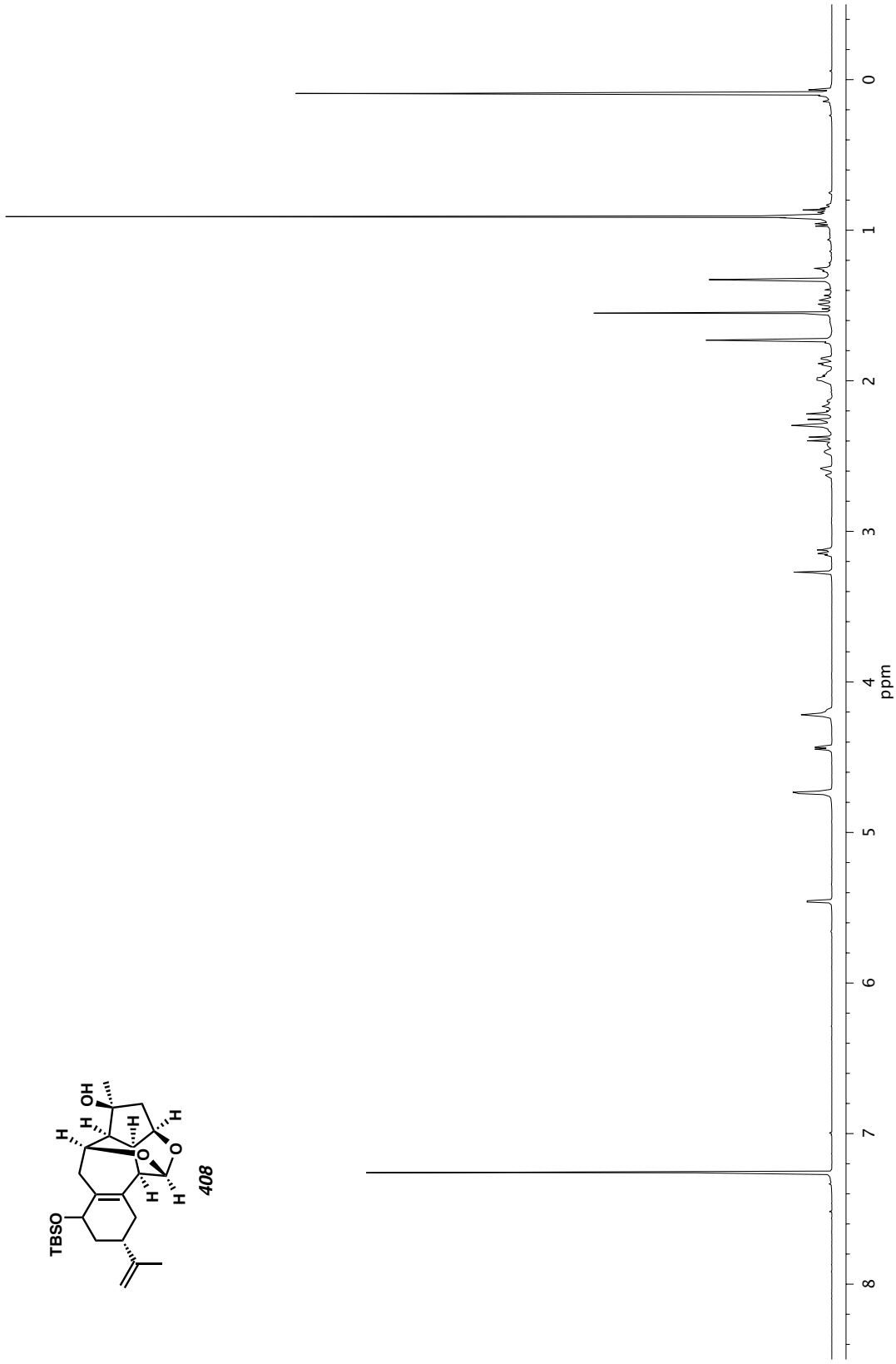

Figure A10.76. ^{1}H NMR (400 MHz, $CDCl_3$) of compound **408**.

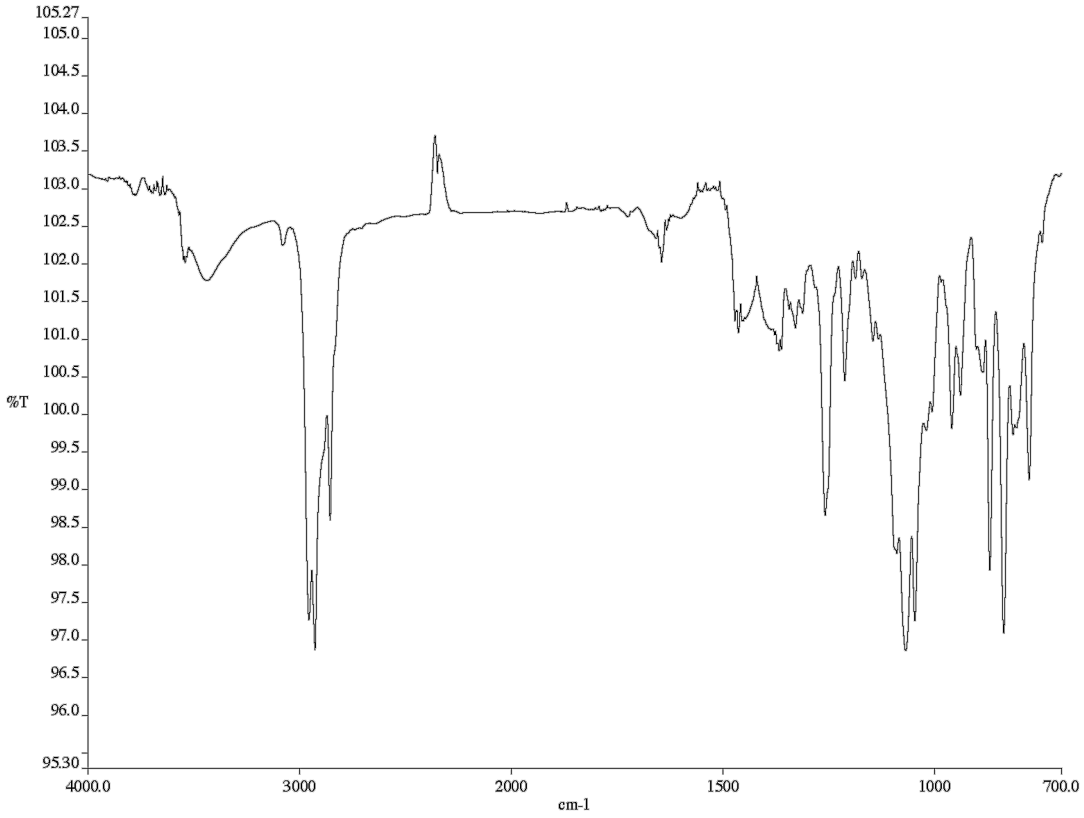

Figure A10.77. Infrared spectrum (Thin Film, NaCl) of compound **408**.

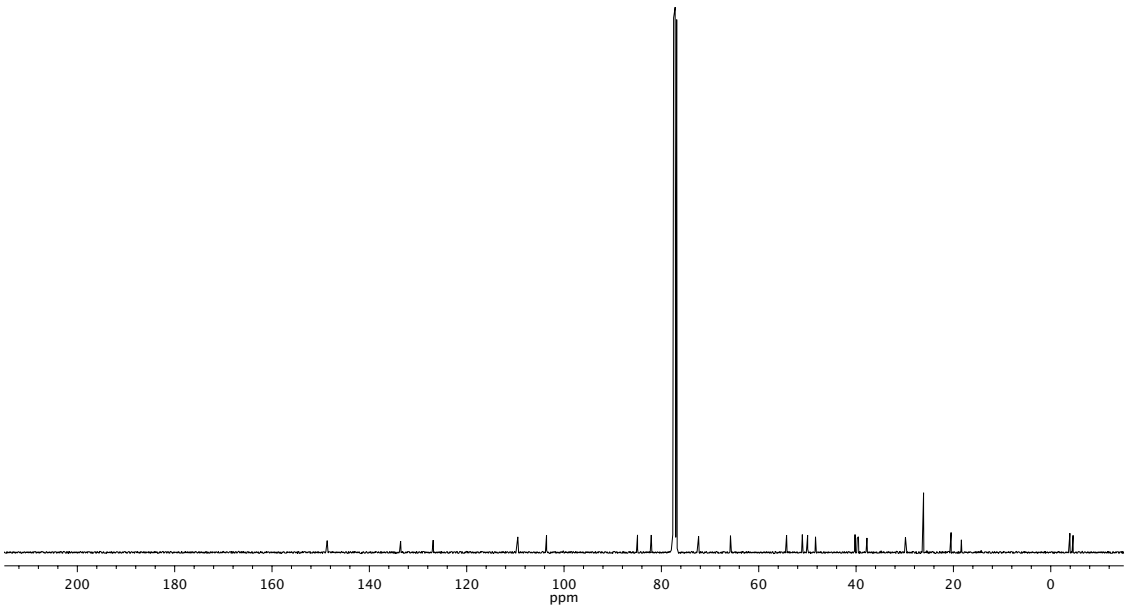

Figure A10.78. ^{13}C NMR (101 MHz, $CDCl_3$) of compound **408**.

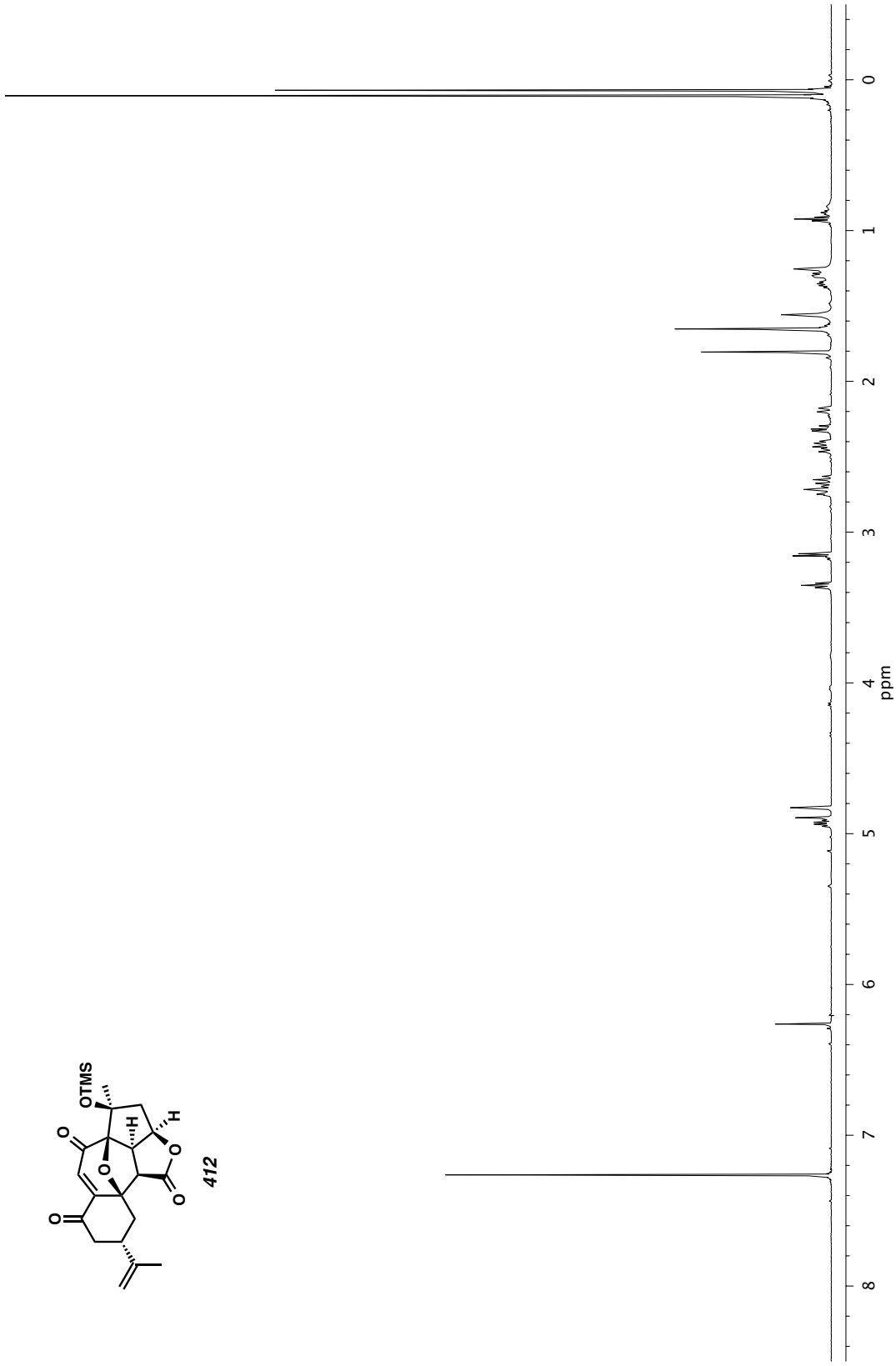

Figure A10.79. ^{1}H NMR (600 MHz, $CDCl_3$) of compound **412**.

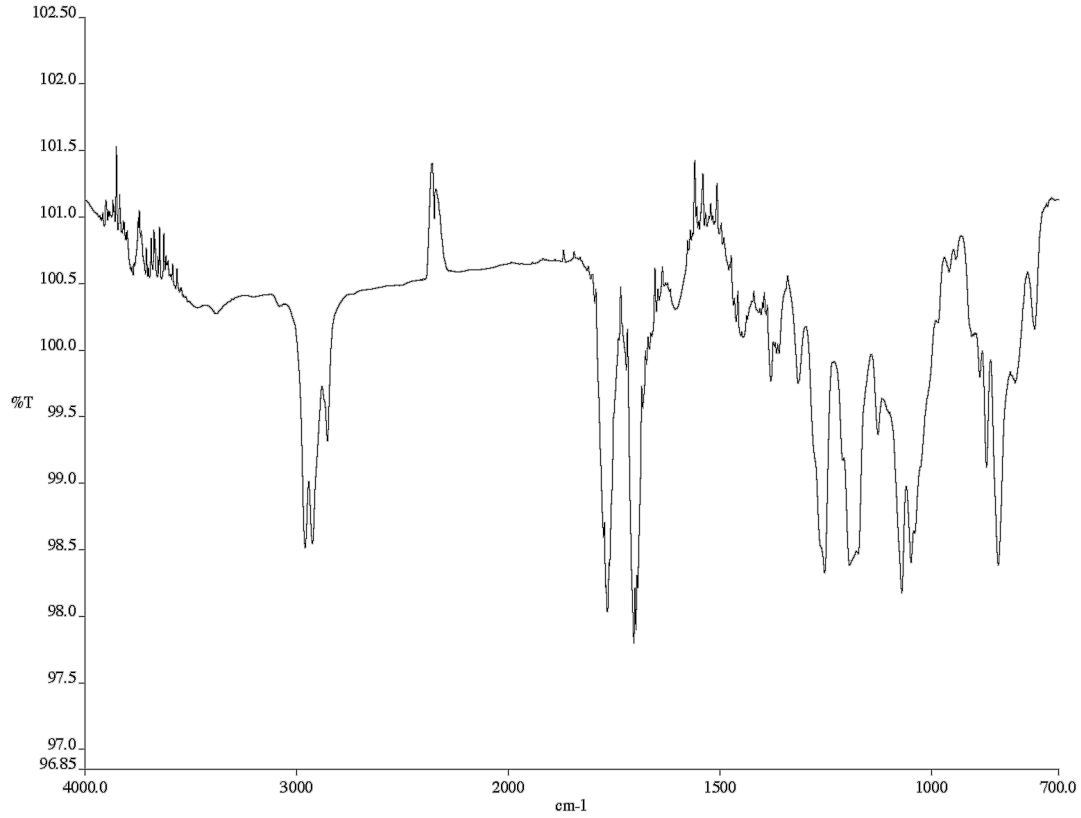

Figure A10.80. Infrared spectrum (Thin Film, NaCl) of compound **412**.

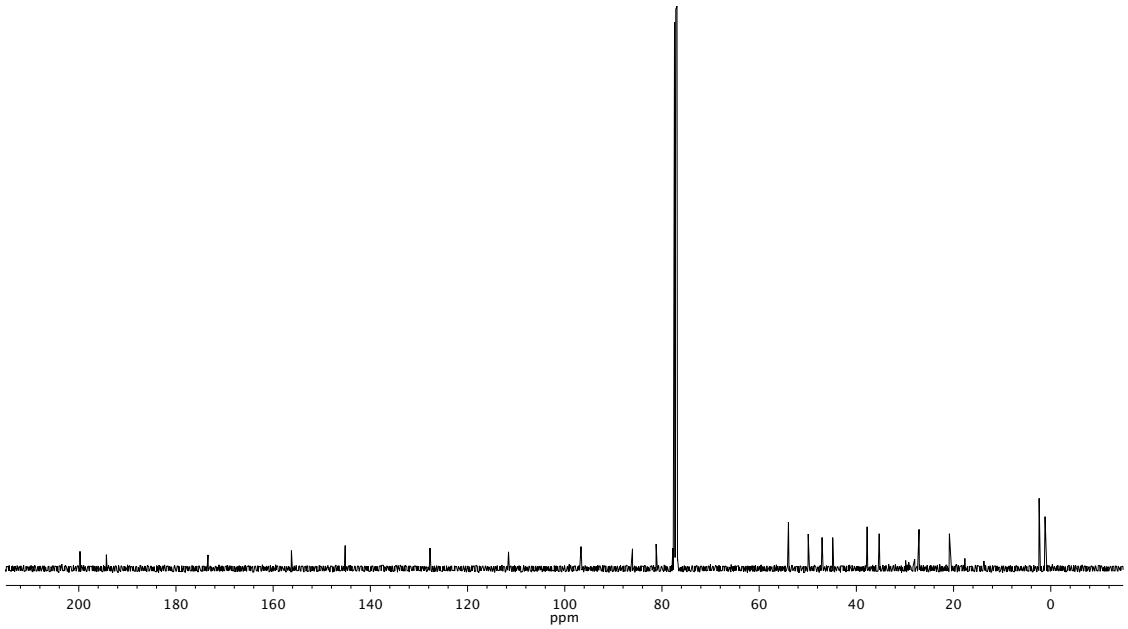

Figure A10.81. ^{13}C NMR (126 MHz, $CDCl_3$) of compound **412**.

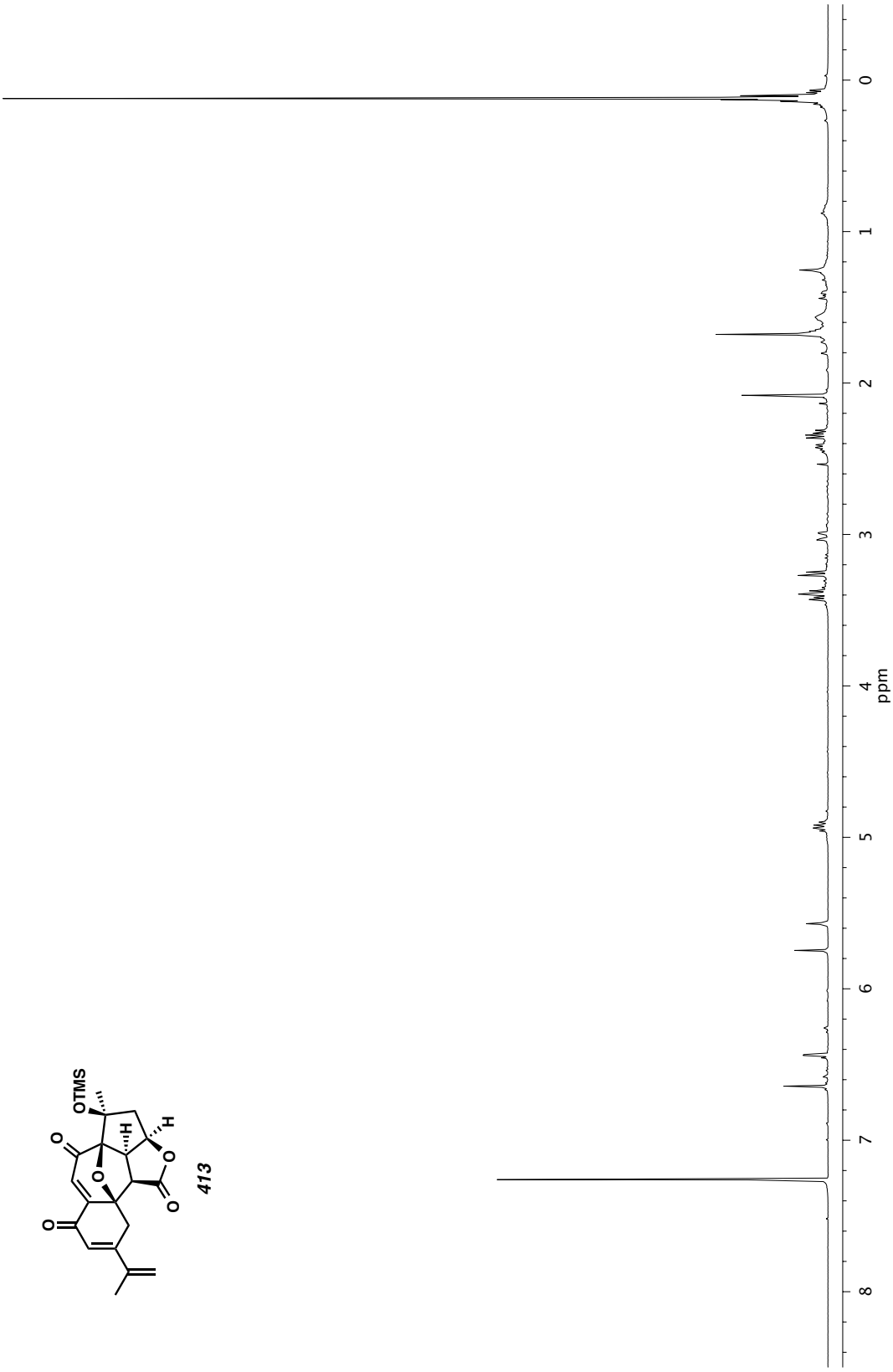

Figure A10.82. ^{1}H NMR (400 MHz, $CDCl_3$) of compound **413**.

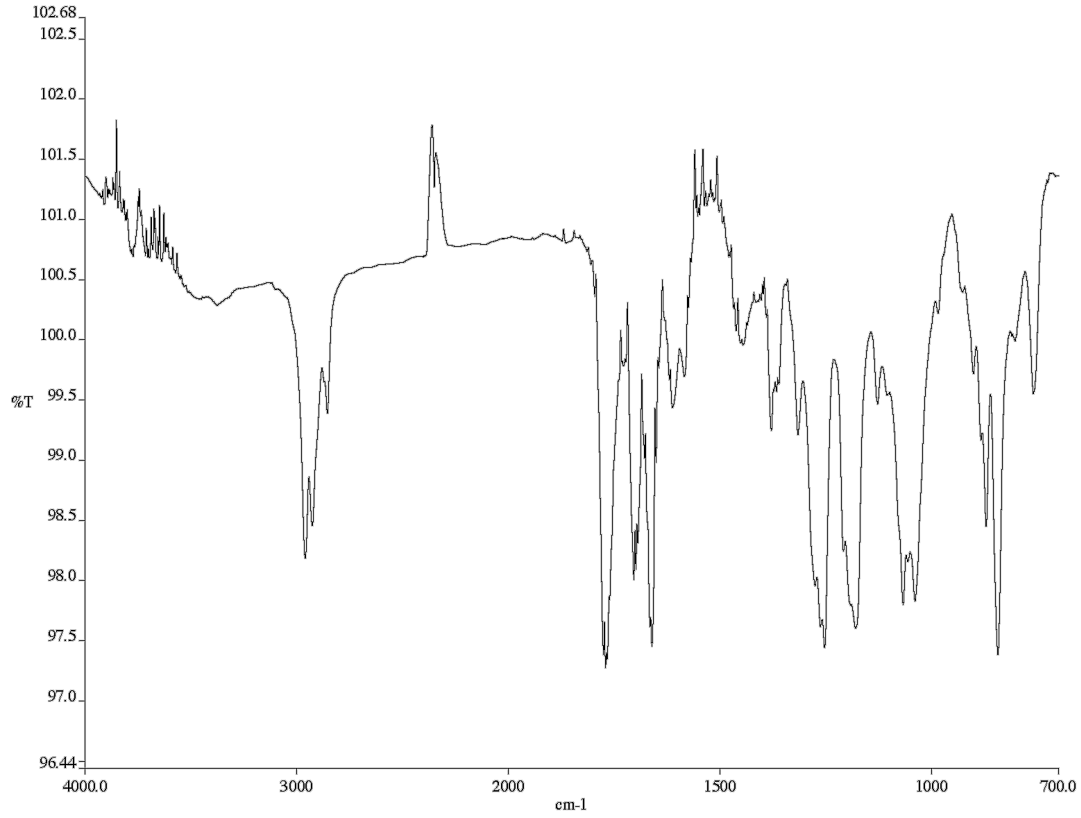

Figure A10.83. Infrared spectrum (Thin Film, NaCl) of compound **413**.

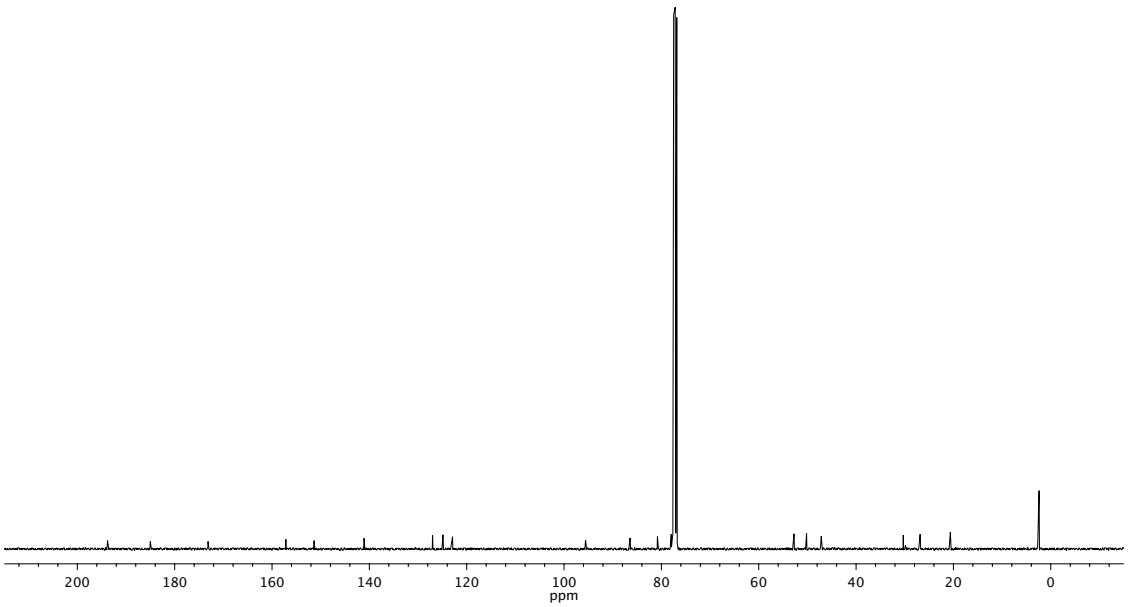

Figure A10.84. ^{13}C NMR (101 MHz, $CDCl_3$) of compound **413**.

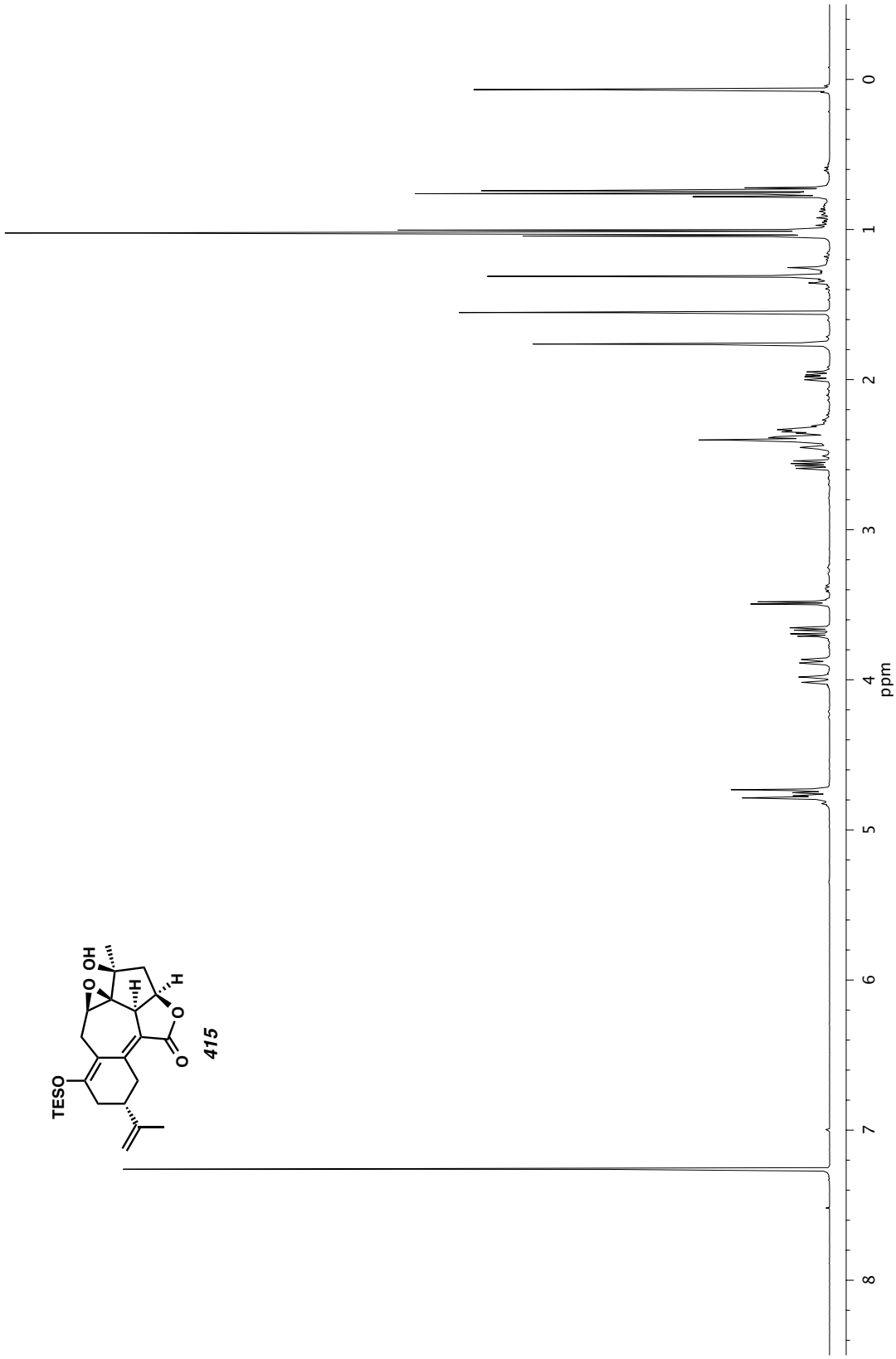

Figure A10.85. ^{1}H NMR (400 MHz, $CDCl_3$) of compound **415**.

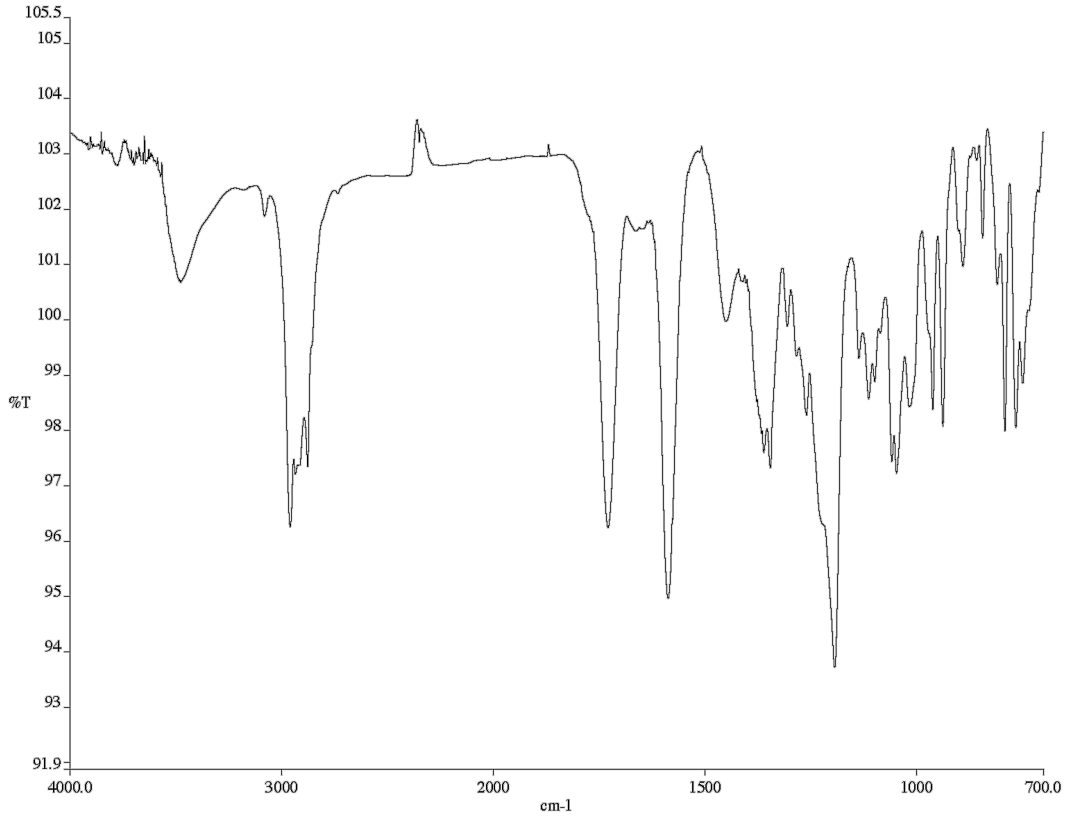

Figure A10.86. Infrared spectrum (Thin Film, NaCl) of compound **415**.

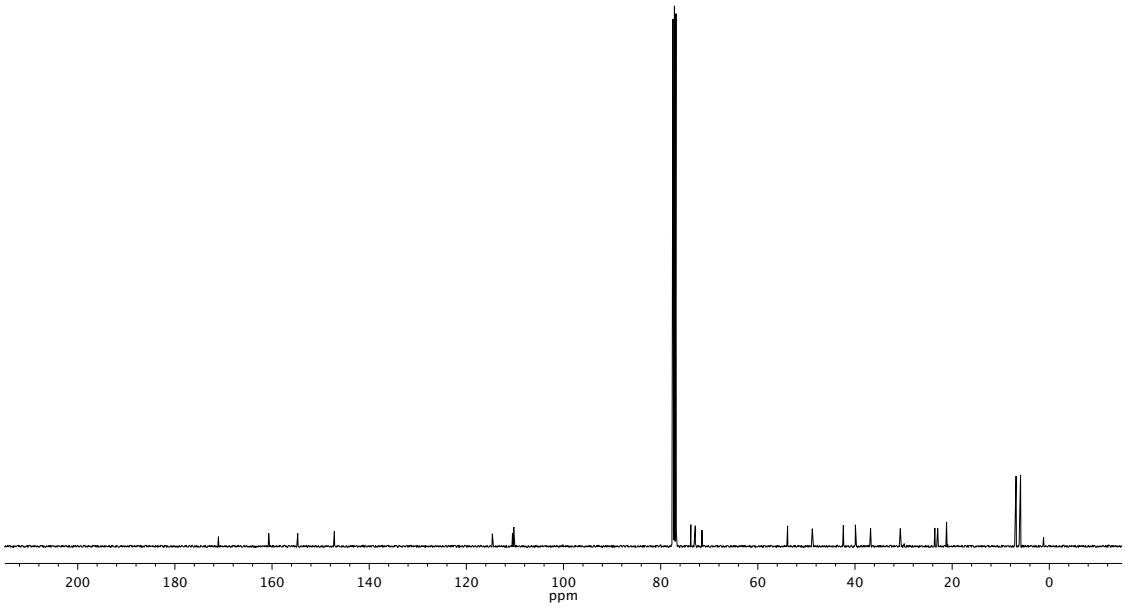

Figure A10.87. ^{13}C NMR (101 MHz, $CDCl_3$) of compound **415**.

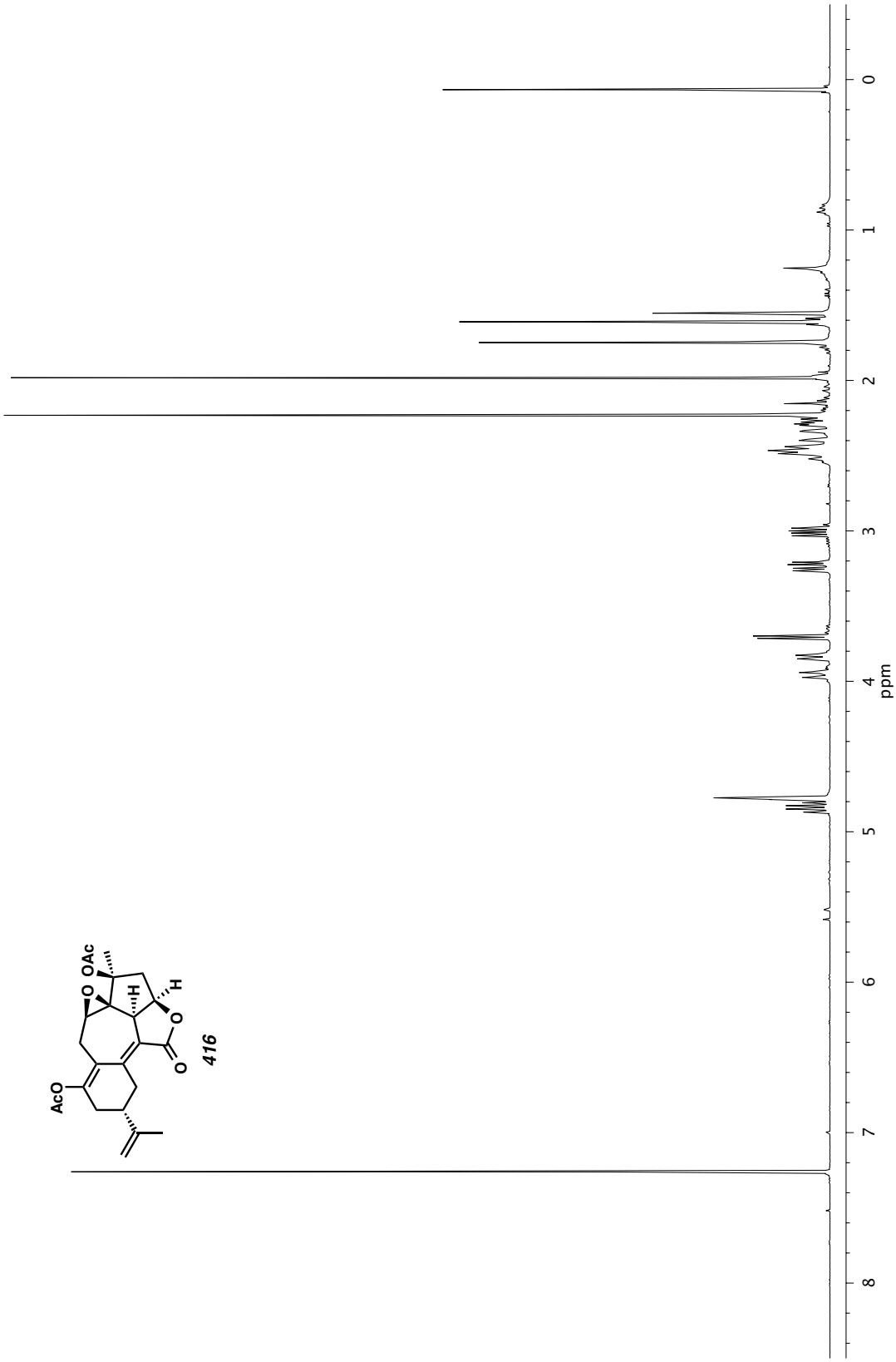

Figure A10.88. ^{1}H NMR (400 MHz, $CDCl_3$) of compound **416**.

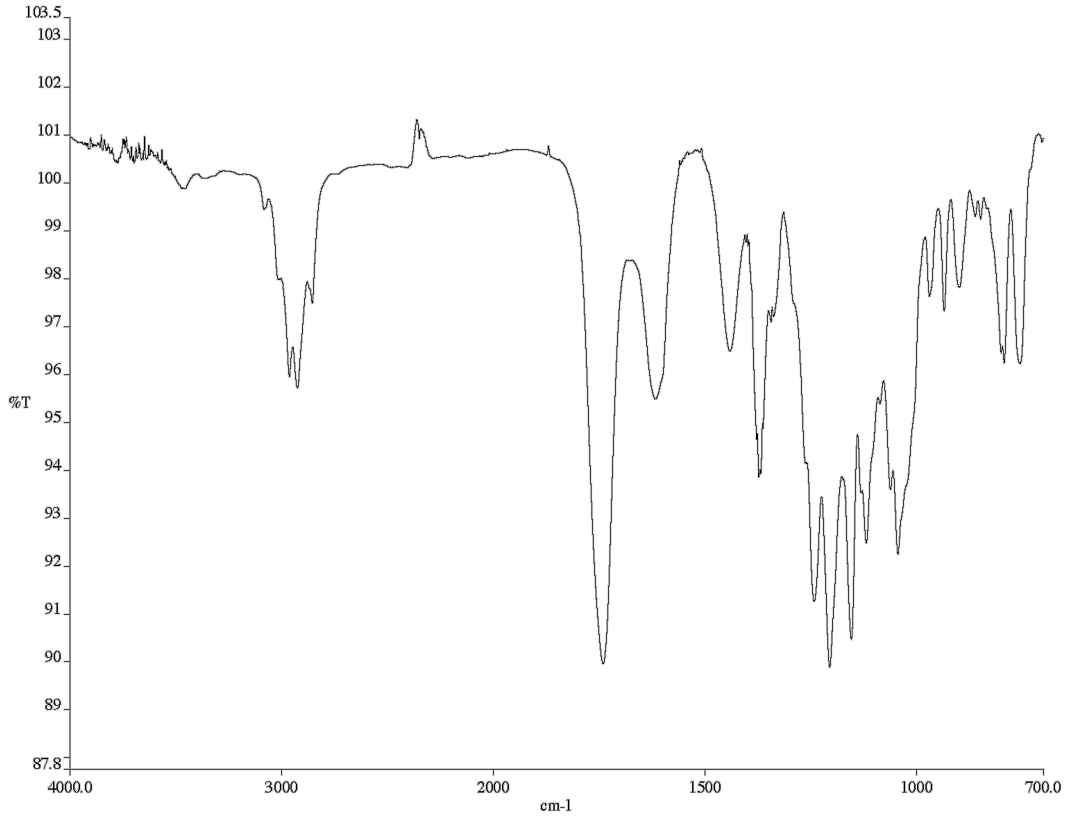

Figure A10.89. Infrared spectrum (Thin Film, NaCl) of compound **416**.

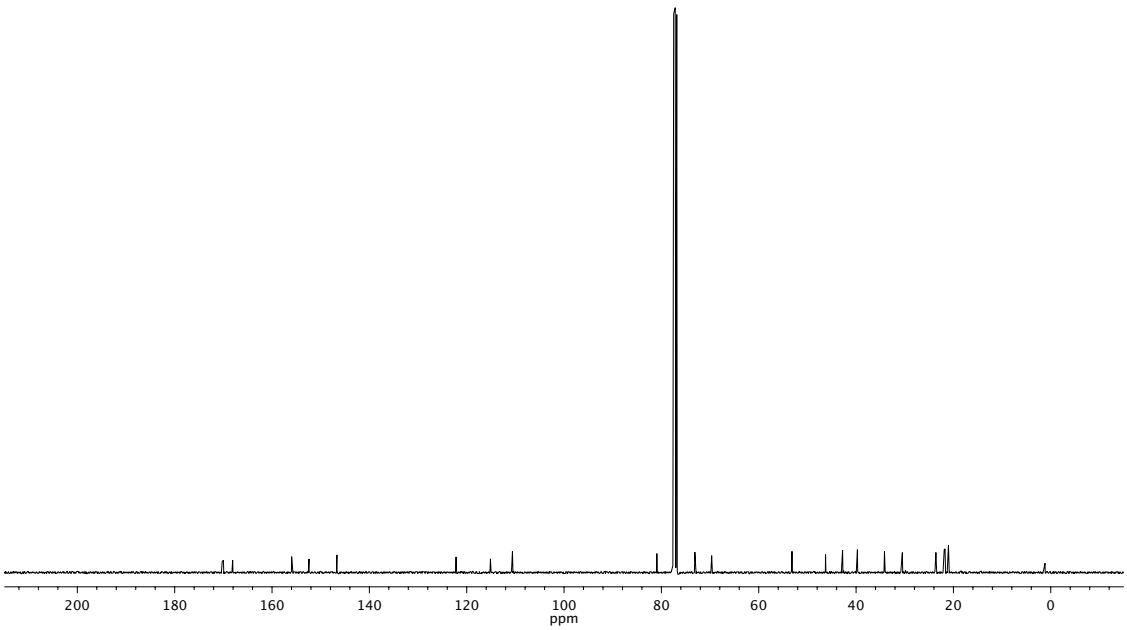

Figure A10.90. ^{13}C NMR (101 MHz, $CDCl_3$) of compound **416**.

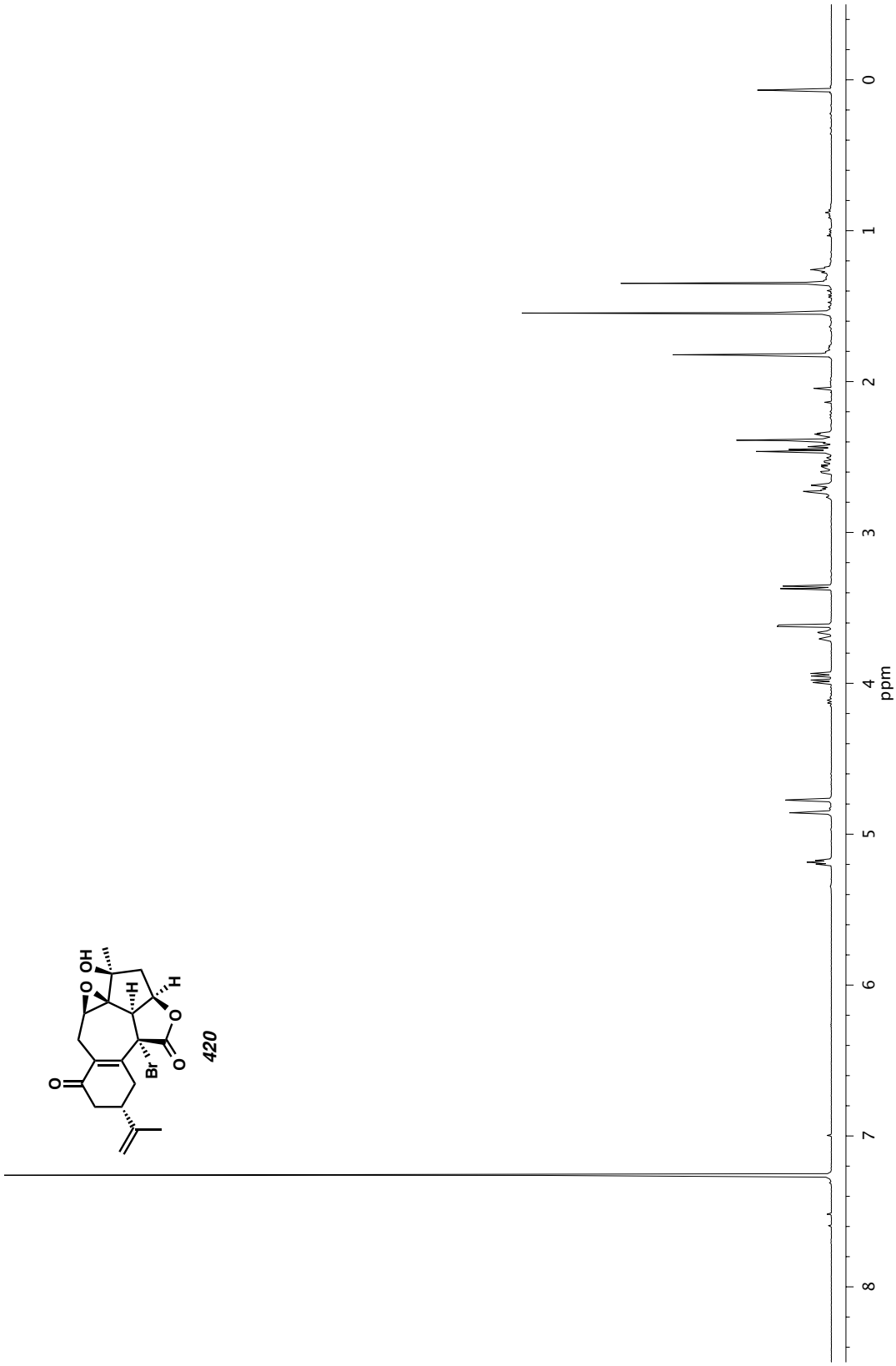

Figure A10.91. ^{1}H NMR (400 MHz, $CDCl_3$) of compound **420**.

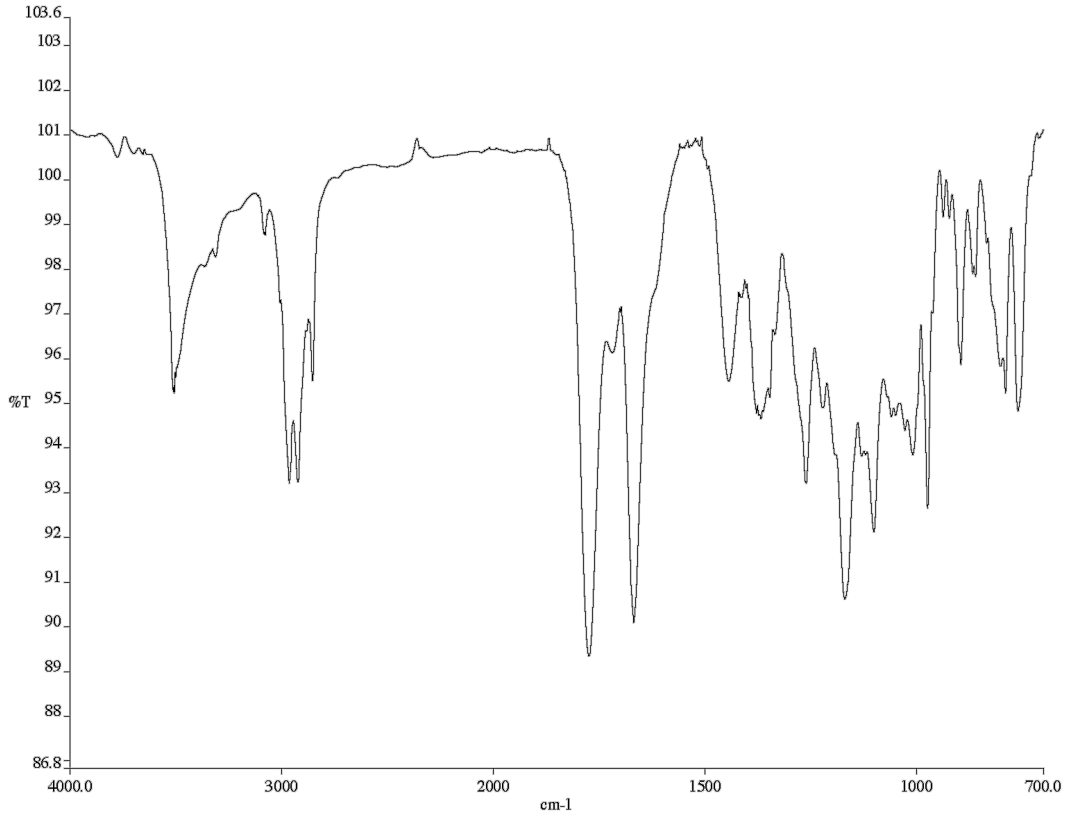

Figure A10.92. Infrared spectrum (Thin Film, NaCl) of compound **420**.

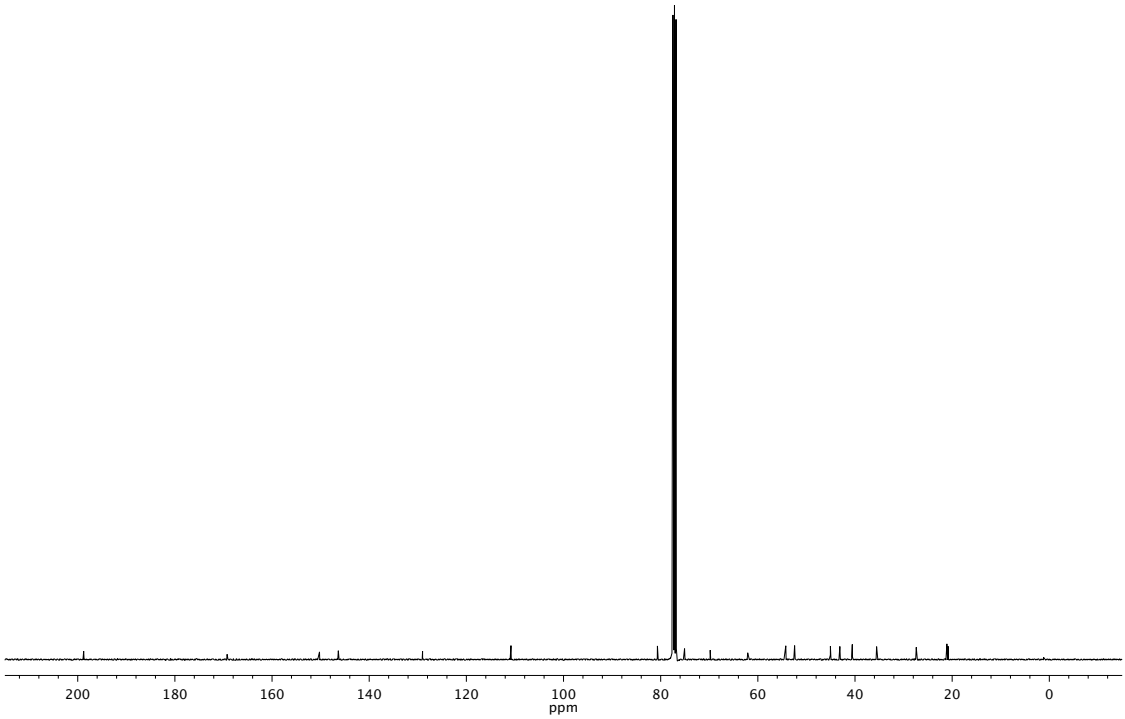

Figure A10.93. ^{13}C NMR (101 MHz, $CDCl_3$) of compound **420**.

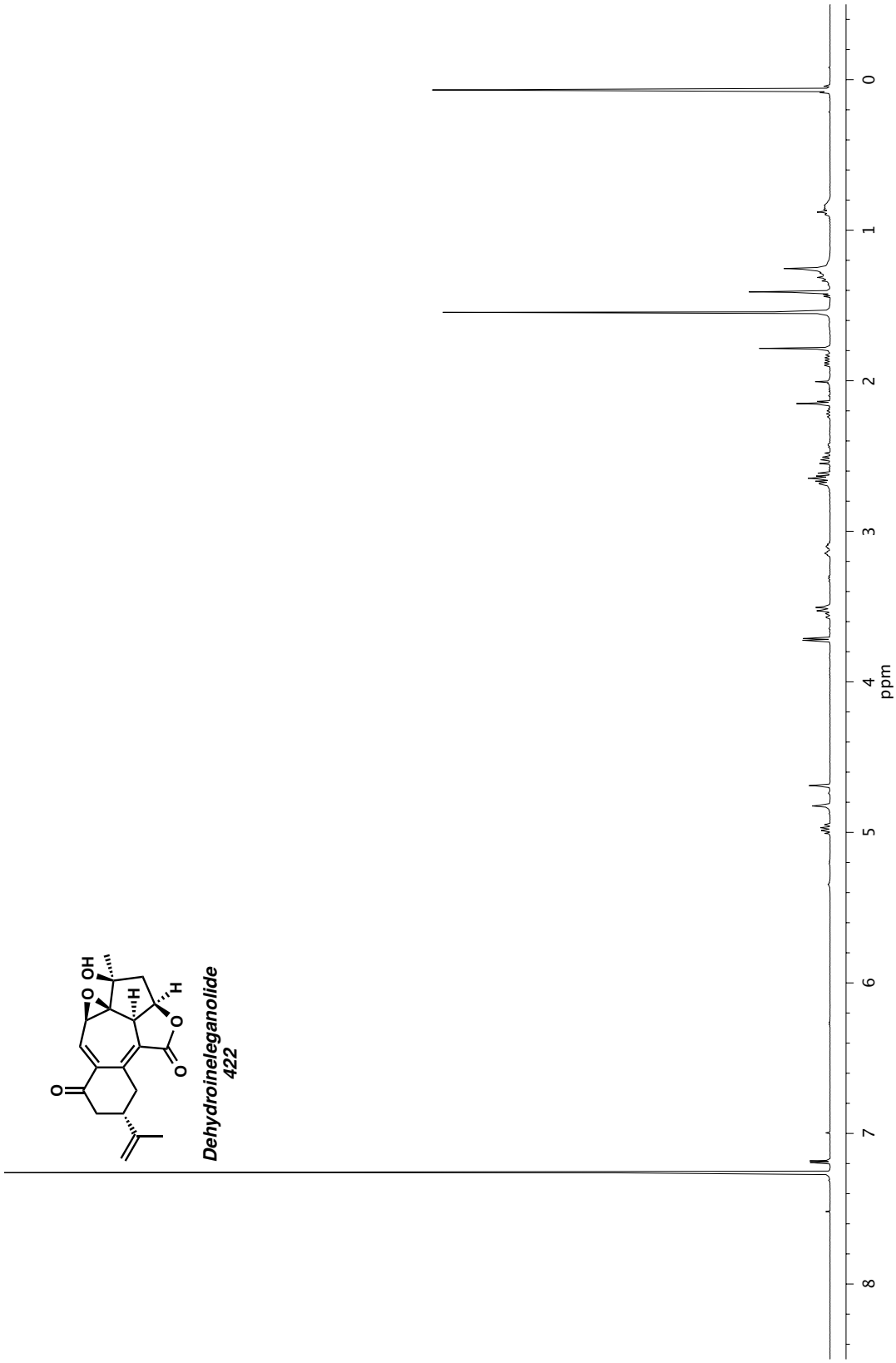

Figure A10.94. ^{1}H NMR (400 MHz, $CDCl_3$) of compound **422**.

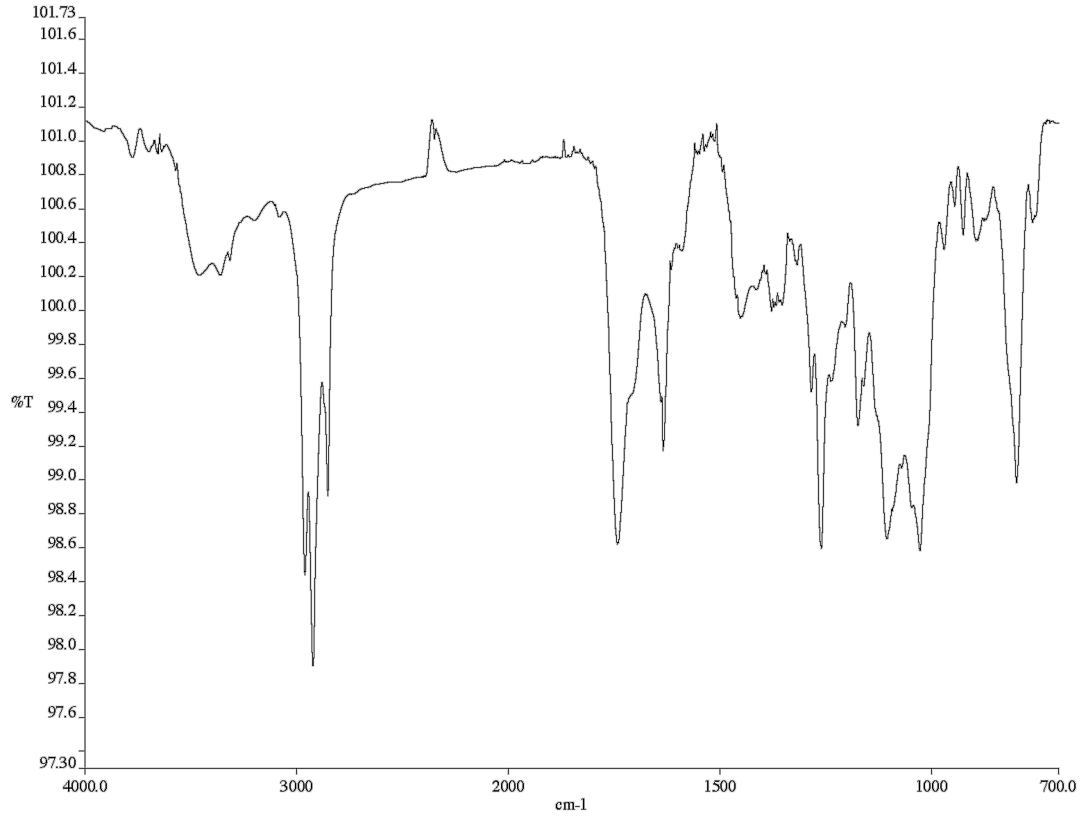

Figure A10.95. Infrared spectrum (Thin Film, NaCl) of compound **422**.

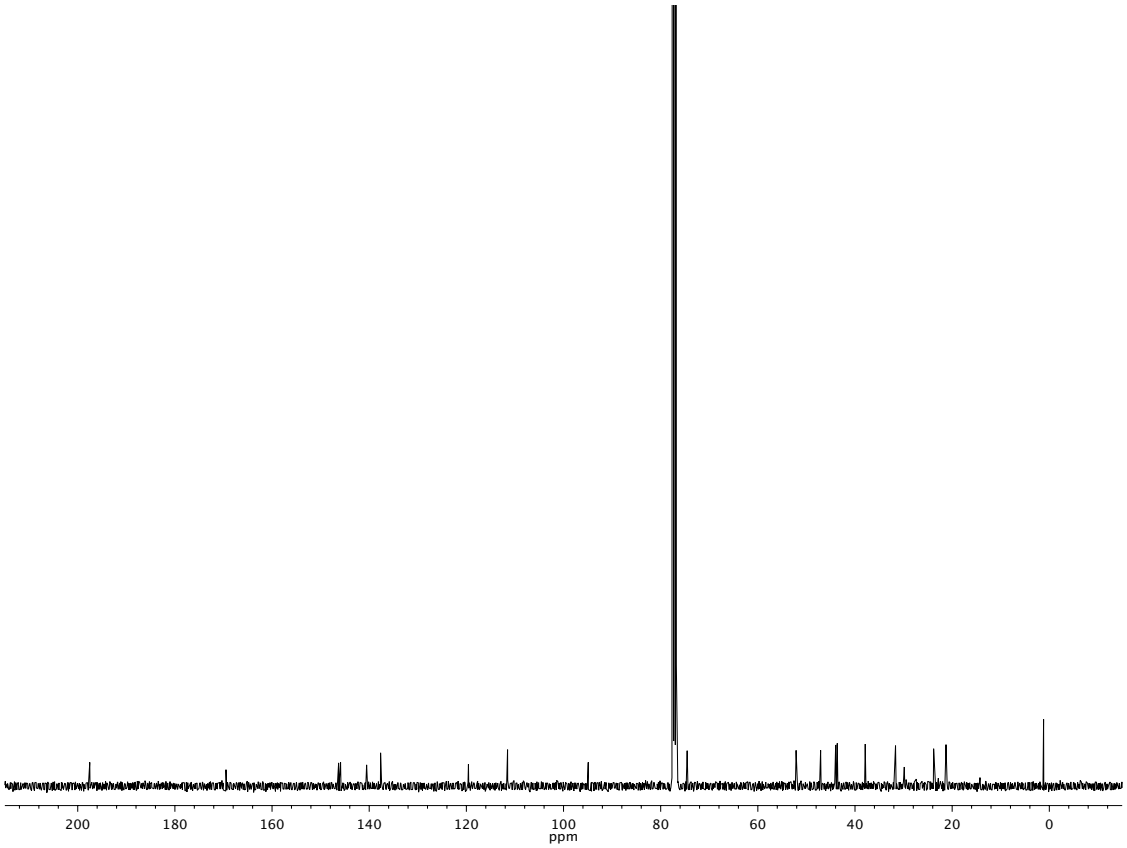

Figure A10.96. ^{13}C NMR (101 MHz, $CDCl_3$) of compound **422**.

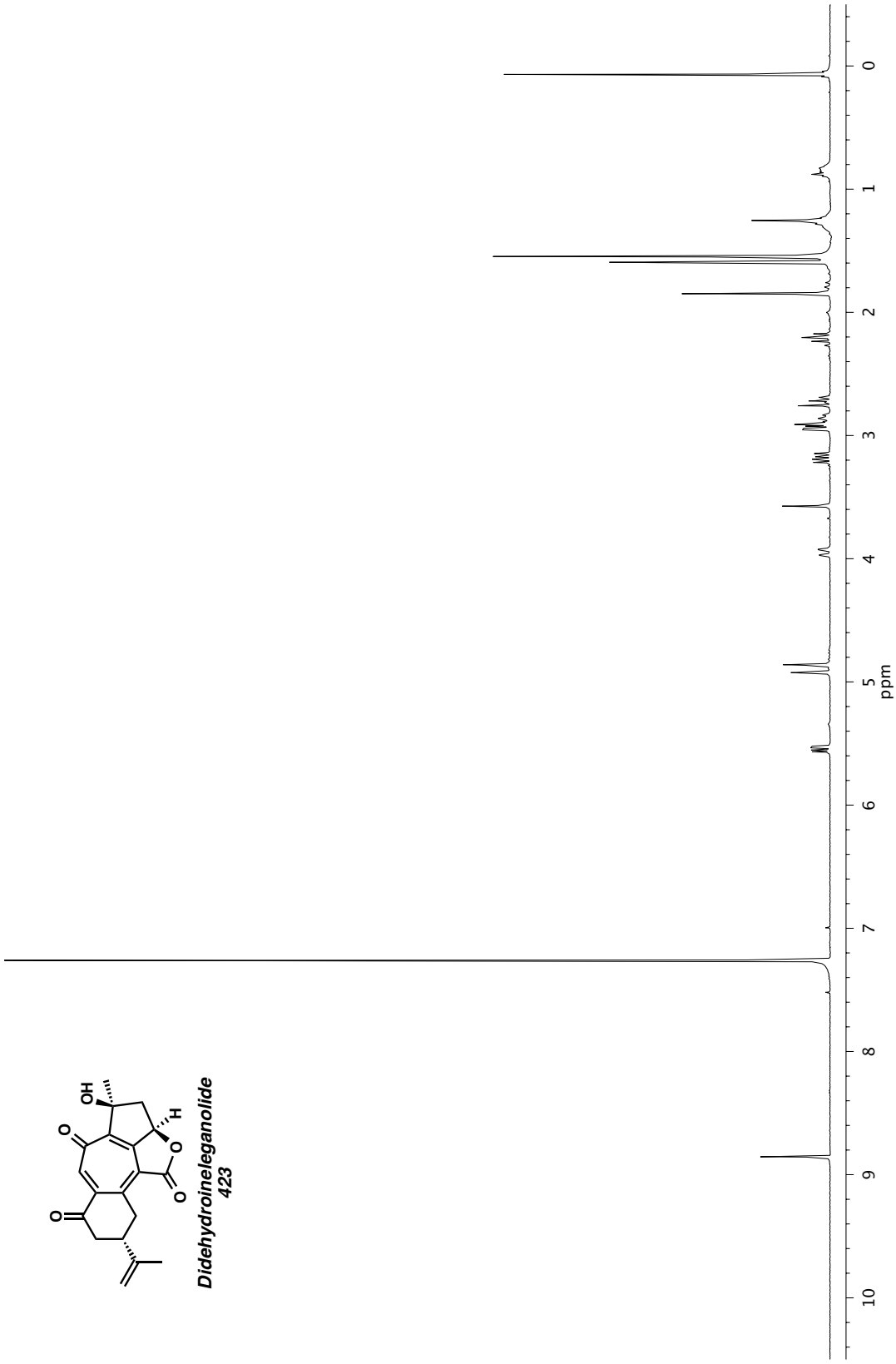

Figure A10.97. ^{1}H NMR (400 MHz, $CDCl_3$) of compound **423**.

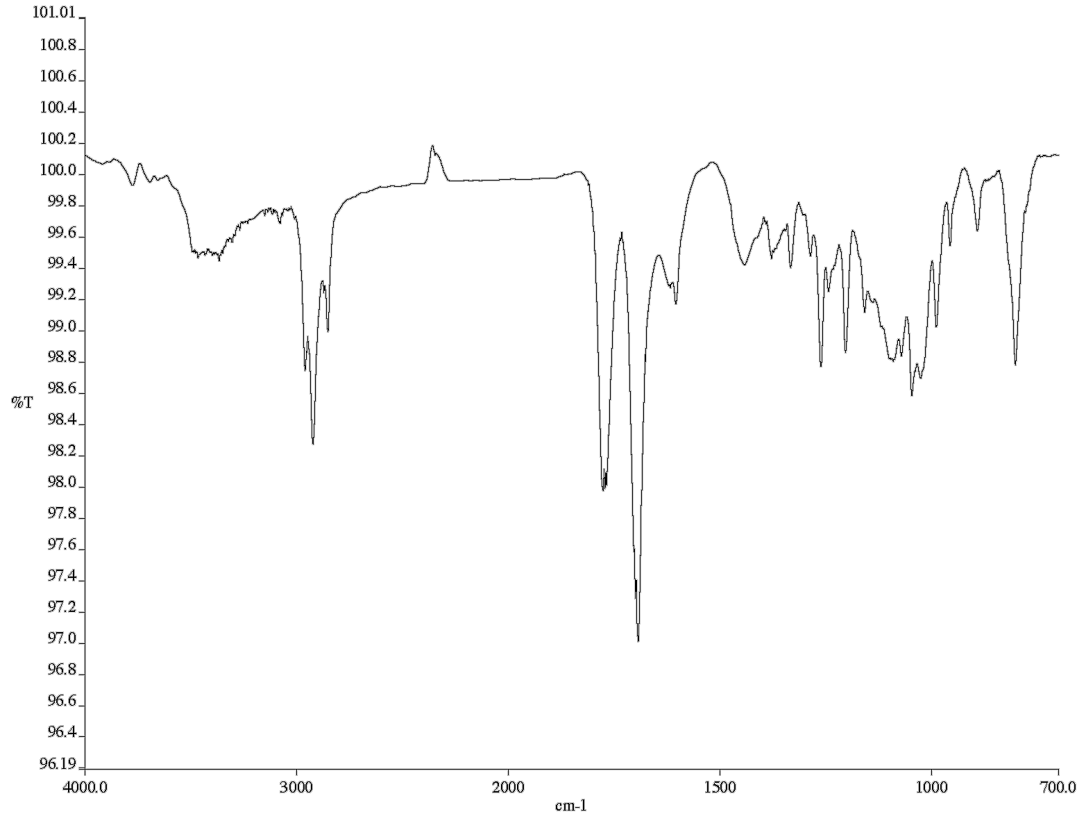

Figure A10.98. Infrared spectrum (Thin Film, NaCl) of compound **423**.

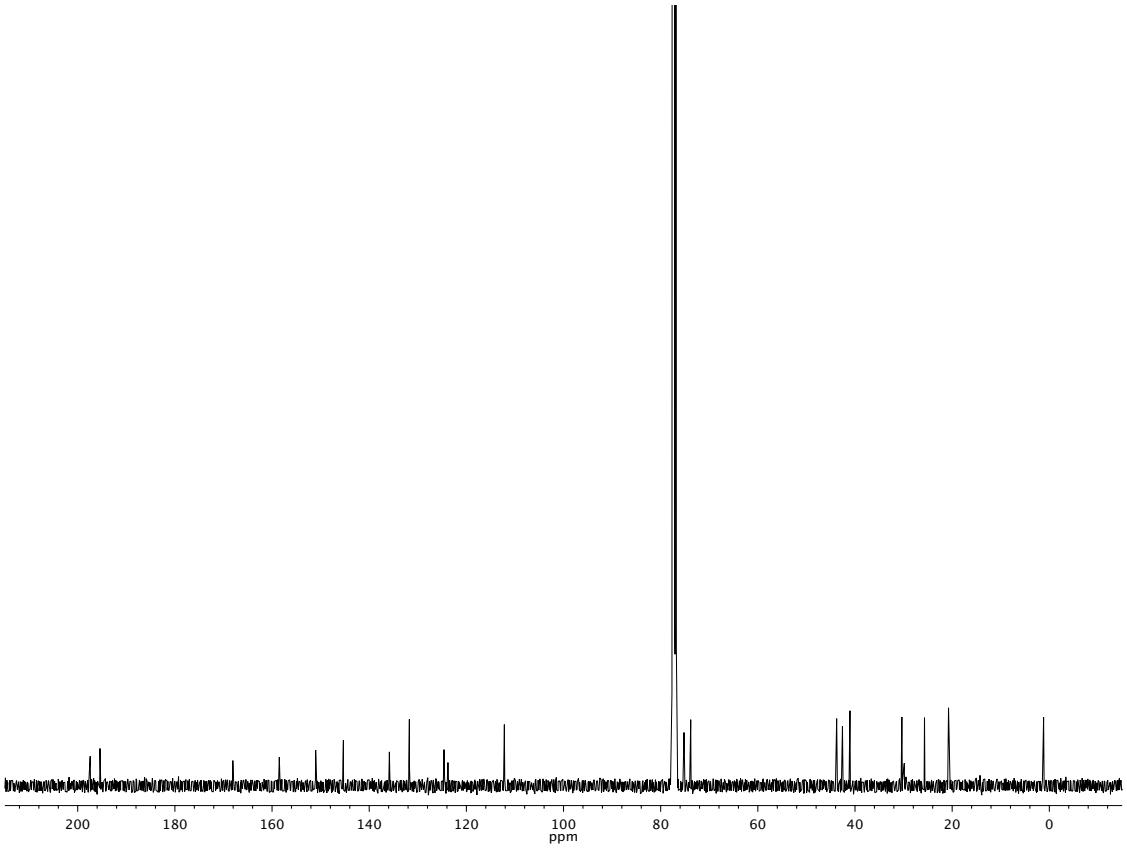

Figure A10.99. ^{13}C NMR (101 MHz, $CDCl_3$) of compound **423**.

APPENDIX 11

X-Ray Crystallography Reports Relevant to Chapter 4:

Revised Plan for the Synthesis of Ineleganolide:

Alternative Advancement Toward the Asymmetric Total Synthesis

of Ineleganolide by Late Stage Oxidation State Manipulation

A11.1 X-Ray Crystal Structure Analysis of Epoxide 371

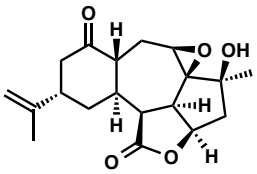

371

Contents

Table A11.1.1. Experimental Details

Table A11.1.2. Crystal Data

Table A11.1.3. Atomic Coordinates

Table A11.1.4. Full Bond Distances and Angles

Table A11.1.5. Anisotropic Displacement Parameters

Table A11.1.6. Hydrogen Atomic Coordinates

Table A11.1.7. Torsion Angles

Table A11.1.8. Hydrogen Bond Distances and Angle

Figure A11.1.1. X-Ray Crystal Structure of Epoxide ***371***

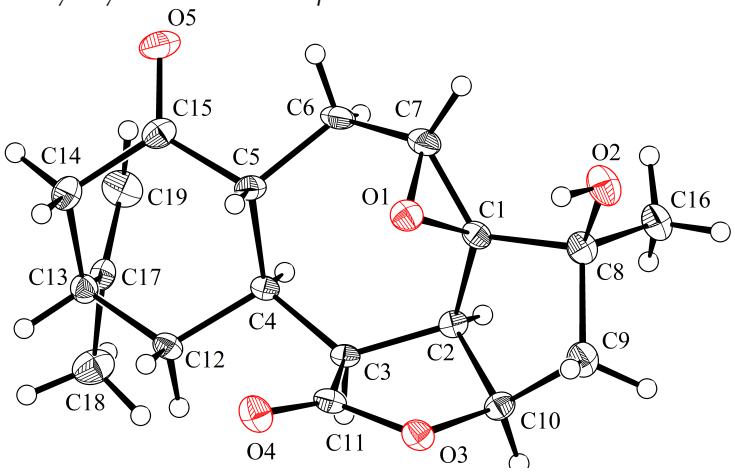

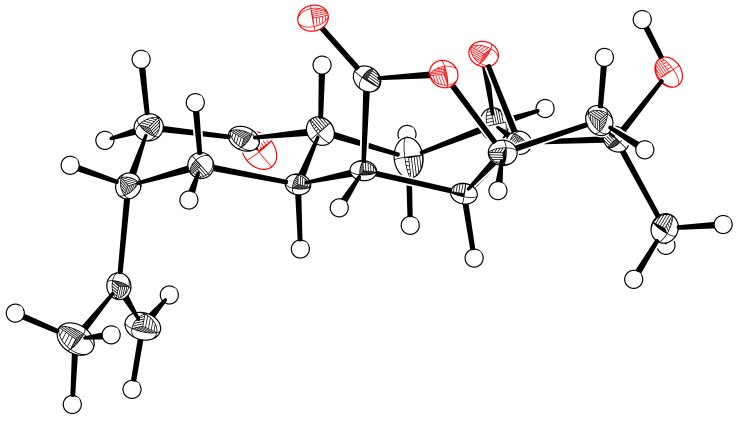

*Table A11.1.1. Experimental Details for X-Ray Structure Determination of Epoxide **371**.*

Low-temperature diffraction data (ϕ-and ω-scans) were collected on a Bruker AXS KAPPA APEX II diffractometer coupled to a APEX II CCD detector with graphite monochromated Mo K_α radiation (λ = 0.71073 Å) for the structure of epoxide **371** and on a Bruker AXS D8 VENTURE KAPPA diffractometer coupled to a PHOTON 100 CMOS detector with Cu K_α radiation (λ = 1.54178 Å) from an IμS micro-source for the structure of compound P15149 and P15156. The structure was solved by direct methods using SHELXS[1] and refined against F^2 on all data by full-matrix least squares with SHELXL-2014[2] using established refinement techniques.[3] All non-hydrogen atoms were refined anisotropically. Unless otherwise noted, all hydrogen atoms were included into the model at geometrically calculated positions and refined using a riding model. The isotropic displacement parameters of all hydrogen atoms were fixed to 1.2 times the U value of the atoms they are linked to (1.5 times for methyl groups).

Epoxide **371** crystallizes in the orthorhombic space group $P2_12_12_1$ with one molecule in the asymmetric unit. The coordinates for all hydrogen atoms were located in the difference Fourier synthesis and refined freely.

*Table A11.1.2. Crystal Data and Structure Refinement for Epoxide **371**.*

Caltech Identification code	a14286	
CCDC Deposition Number	1061014	
Empirical formula	C19 H24 O5	
Formula weight	332.38	
Temperature	100 K	
Wavelength	0.71073 Å	
Crystal system	Orthorhombic	
Space group	P 21 21 21	
Unit cell dimensions	a = 6.2703(9) Å	α= 90°
	b = 11.2931(16) Å	β= 90°
	c = 23.177(4) Å	γ = 90°
Volume	1641.2(4) $Å^3$	
Z	4	
Density (calculated)	1.345 Mg/m^3	
Absorption coefficient	0.097 mm^{-1}	
F(000)	712	
Crystal size	0.57 x 0.25 x 0.03 mm^3	
Theta range for data collection	1.757 to 33.933°.	
Index ranges	$-9 \le h \le 9, -17 \le k \le 17, -36 \le l \le 35$	
Reflections collected	42176	
Independent reflections	6378 [R(int) = 0.0463]	
Completeness to theta = 25.000°	100.0 %	
Absorption correction	Semi-empirical from equivalents	
Max. and min. transmission	1.0000 and 0.8611	
Refinement method	Full-matrix least-squares on F^2	
Data / restraints / parameters	6378 / 0 / 313	
Goodness-of-fit on F^2	1.447	
Final R indices [I>2sigma(I)]	R1 = 0.0413, wR2 = 0.0809	
R indices (all data)	R1 = 0.0538, wR2 = 0.0831	
Absolute structure parameter	-0.6(2)	
Extinction coefficient	n/a	
Largest diff. peak and hole	0.392 and -0.199 e.$Å^{-3}$	

*Table A11.1.3. Atomic coordinates (x 10^4) and equivalent isotropic displacement parameters ($Å^2$x 10^3) for Epoxide **371**. U(eq) is defined as one third of the trace of the orthogonalized U^{ij} tensor.*

	x	y	z	U(eq)
O(1)	60147(17)	38434(9)	46552(5)	183(2)
O(2)	76160(20)	34388(10)	35657(5)	243(3)
O(3)	43551(17)	62722(10)	44133(4)	179(2)
O(4)	26855(17)	58723(10)	52373(5)	212(2)
O(5)	82780(20)	28834(10)	65931(5)	252(3)
C(1)	78760(20)	45191(12)	44797(6)	146(3)
C(2)	78900(20)	57950(12)	46746(6)	134(2)
C(3)	66120(20)	60975(12)	52169(5)	121(2)
C(4)	71270(20)	55487(12)	58083(6)	124(2)
C(5)	69870(20)	41806(12)	58441(6)	161(3)
C(6)	86020(30)	35128(14)	54757(7)	229(3)
C(7)	81550(30)	34815(13)	48377(6)	202(3)
C(8)	81980(20)	45267(13)	38266(6)	175(3)
C(9)	67800(30)	55912(15)	36501(6)	203(3)
C(10)	65480(20)	63631(13)	41907(6)	161(3)
C(11)	43420(20)	60300(12)	49886(6)	153(3)
C(12)	57290(20)	61462(13)	62695(6)	153(3)
C(13)	62610(20)	57484(13)	68893(6)	156(3)
C(14)	59610(30)	44006(14)	69216(6)	192(3)
C(15)	72060(30)	37435(13)	64686(6)	179(3)
C(16)	105320(30)	47240(15)	36731(7)	214(3)
C(17)	84150(20)	61913(14)	70905(6)	161(3)
C(18)	85030(30)	74981(15)	72048(8)	263(3)
C(19)	101020(30)	55096(17)	71833(8)	247(3)

*Table A11.1.4. Bond lengths [Å] and angles [°] for Epoxide **371**.*

O(1)-C(1)	1.4523(18)
O(1)-C(7)	1.465(2)
O(2)-H(2)	0.87(3)
O(2)-C(8)	1.4172(18)
O(3)-C(10)	1.4725(18)
O(3)-C(11)	1.3611(17)
O(4)-C(11)	1.2015(18)
O(5)-C(15)	1.2160(19)
C(1)-C(2)	1.5101(19)
C(1)-C(7)	1.446(2)
C(1)-C(8)	1.527(2)
C(2)-H(2A)	0.97(2)
C(2)-C(3)	1.5290(19)
C(2)-C(10)	1.542(2)
C(3)-H(3)	0.970(17)
C(3)-C(4)	1.5385(19)
C(3)-C(11)	1.5205(19)
C(4)-H(4)	0.987(18)
C(4)-C(5)	1.5497(19)
C(4)-C(12)	1.5383(19)
C(5)-H(5)	1.010(19)
C(5)-C(6)	1.524(2)
C(5)-C(15)	1.5356(19)
C(6)-H(6A)	1.00(2)
C(6)-H(6B)	0.944(19)
C(6)-C(7)	1.505(2)
C(7)-H(7)	0.990(18)
C(8)-C(9)	1.550(2)
C(8)-C(16)	1.522(2)
C(9)-H(9A)	0.970(19)
C(9)-H(9B)	0.95(2)
C(9)-C(10)	1.533(2)
C(10)-H(10)	0.952(18)

Table A11.1.4. (cont'd)

C(12)-H(12A)	0.961(19)
C(12)-H(12B)	0.97(2)
C(12)-C(13)	1.542(2)
C(13)-H(13)	0.981(18)
C(13)-C(14)	1.536(2)
C(13)-C(17)	1.514(2)
C(14)-H(14A)	0.991(18)
C(14)-H(14B)	1.05(2)
C(14)-C(15)	1.504(2)
C(16)-H(16A)	0.96(2)
C(16)-H(16B)	0.98(2)
C(16)-H(16C)	0.93(2)
C(17)-C(18)	1.500(2)
C(17)-C(19)	1.326(2)
C(18)-H(18A)	0.96(2)
C(18)-H(18B)	1.00(2)
C(18)-H(18C)	0.99(2)
C(19)-H(19A)	0.95(2)
C(19)-H(19B)	0.93(2)

C(1)-O(1)-C(7)	59.43(9)
C(8)-O(2)-H(2)	109.1(16)
C(11)-O(3)-C(10)	111.27(11)
O(1)-C(1)-C(2)	114.97(11)
O(1)-C(1)-C(8)	112.77(12)
C(2)-C(1)-C(8)	106.88(11)
C(7)-C(1)-O(1)	60.74(10)
C(7)-C(1)-C(2)	126.92(12)
C(7)-C(1)-C(8)	123.85(13)
C(1)-C(2)-H(2A)	108.7(13)
C(1)-C(2)-C(3)	117.13(11)
C(1)-C(2)-C(10)	100.15(11)
C(3)-C(2)-H(2A)	112.2(13)
C(3)-C(2)-C(10)	102.68(11)

Table A11.1.4. (cont'd)

C(10)-C(2)-H(2A)	115.6(13)
C(2)-C(3)-H(3)	106.1(10)
C(2)-C(3)-C(4)	122.18(11)
C(4)-C(3)-H(3)	105.1(10)
C(11)-C(3)-C(2)	101.12(11)
C(11)-C(3)-H(3)	100.8(10)
C(11)-C(3)-C(4)	119.10(12)
C(3)-C(4)-H(4)	107.0(9)
C(3)-C(4)-C(5)	115.93(11)
C(5)-C(4)-H(4)	106.2(10)
C(12)-C(4)-C(3)	108.83(11)
C(12)-C(4)-H(4)	106.7(9)
C(12)-C(4)-C(5)	111.58(12)
C(4)-C(5)-H(5)	106.1(10)
C(6)-C(5)-C(4)	115.19(13)
C(6)-C(5)-H(5)	110.2(10)
C(6)-C(5)-C(15)	108.03(12)
C(15)-C(5)-C(4)	111.45(11)
C(15)-C(5)-H(5)	105.4(10)
C(5)-C(6)-H(6A)	108.0(11)
C(5)-C(6)-H(6B)	107.6(12)
H(6A)-C(6)-H(6B)	107.5(16)
C(7)-C(6)-C(5)	115.99(14)
C(7)-C(6)-H(6A)	109.5(11)
C(7)-C(6)-H(6B)	107.8(12)
O(1)-C(7)-C(6)	116.57(13)
O(1)-C(7)-H(7)	109.1(10)
C(1)-C(7)-O(1)	59.83(9)
C(1)-C(7)-C(6)	124.54(13)
C(1)-C(7)-H(7)	115.0(10)
C(6)-C(7)-H(7)	117.0(10)
O(2)-C(8)-C(1)	112.57(12)
O(2)-C(8)-C(9)	114.32(13)
O(2)-C(8)-C(16)	105.96(13)

Table A11.1.4. (cont'd)

C(1)-C(8)-C(9)	100.95(11)
C(16)-C(8)-C(1)	111.10(12)
C(16)-C(8)-C(9)	112.09(13)
C(8)-C(9)-H(9A)	111.3(11)
C(8)-C(9)-H(9B)	110.2(13)
H(9A)-C(9)-H(9B)	105.8(17)
C(10)-C(9)-C(8)	106.24(11)
C(10)-C(9)-H(9A)	113.4(11)
C(10)-C(9)-H(9B)	110.0(13)
O(3)-C(10)-C(2)	103.03(11)
O(3)-C(10)-C(9)	109.59(12)
O(3)-C(10)-H(10)	107.0(10)
C(2)-C(10)-H(10)	114.8(10)
C(9)-C(10)-C(2)	107.82(12)
C(9)-C(10)-H(10)	113.9(10)
O(3)-C(11)-C(3)	109.00(12)
O(4)-C(11)-O(3)	120.33(13)
O(4)-C(11)-C(3)	130.53(13)
C(4)-C(12)-H(12A)	109.4(11)
C(4)-C(12)-H(12B)	109.7(11)
C(4)-C(12)-C(13)	113.34(12)
H(12A)-C(12)-H(12B)	105.9(16)
C(13)-C(12)-H(12A)	109.8(11)
C(13)-C(12)-H(12B)	108.5(11)
C(12)-C(13)-H(13)	107.1(10)
C(14)-C(13)-C(12)	107.93(12)
C(14)-C(13)-H(13)	106.9(10)
C(17)-C(13)-C(12)	112.57(12)
C(17)-C(13)-H(13)	106.9(11)
C(17)-C(13)-C(14)	114.95(13)
C(13)-C(14)-H(14A)	110.5(11)
C(13)-C(14)-H(14B)	107.1(12)
H(14A)-C(14)-H(14B)	108.6(16)
C(15)-C(14)-C(13)	113.04(12)

Table A11.1.4. (cont'd)

C(15)-C(14)-H(14A)	110.0(11)
C(15)-C(14)-H(14B)	107.4(12)
O(5)-C(15)-C(5)	122.00(13)
O(5)-C(15)-C(14)	121.02(13)
C(14)-C(15)-C(5)	116.94(13)
C(8)-C(16)-H(16A)	112.6(13)
C(8)-C(16)-H(16B)	112.6(12)
C(8)-C(16)-H(16C)	109.2(12)
H(16A)-C(16)-H(16B)	102.8(17)
H(16A)-C(16)-H(16C)	110.6(17)
H(16B)-C(16)-H(16C)	108.9(16)
C(18)-C(17)-C(13)	114.35(14)
C(19)-C(17)-C(13)	124.73(15)
C(19)-C(17)-C(18)	120.88(16)
C(17)-C(18)-H(18A)	110.7(13)
C(17)-C(18)-H(18B)	110.1(12)
C(17)-C(18)-H(18C)	109.0(14)
H(18A)-C(18)-H(18B)	107.1(18)
H(18A)-C(18)-H(18C)	107.8(18)
H(18B)-C(18)-H(18C)	112.1(17)
C(17)-C(19)-H(19A)	118.4(14)
C(17)-C(19)-H(19B)	122.6(15)
H(19A)-C(19)-H(19B)	119(2)

Symmetry transformations used to generate equivalent atoms:

*Table A11.1.5. Anisotropic displacement parameters ($Å^2x10^3$) for Epoxide **371**. The anisotropic displacement factor exponent takes the form: $-2\pi^2[h^2a^{*2}U^{11} + ... + 2hka^*b^*U^{12}]$.*

	U^{11}	U^{22}	U^{33}	U^{23}	U^{13}	U^{12}
O(1)	194(5)	141(5)	216(5)	-23(4)	1(4)	-37(4)
O(2)	261(6)	241(6)	228(5)	-109(4)	20(5)	-44(5)
O(3)	135(5)	224(5)	176(5)	-14(4)	-40(4)	36(4)
O(4)	115(5)	294(6)	226(5)	-25(4)	-17(4)	11(4)
O(5)	362(7)	157(5)	238(5)	21(4)	-73(5)	38(5)
C(1)	123(6)	145(6)	169(6)	-27(5)	-3(5)	3(5)
C(2)	111(6)	138(6)	152(6)	0(5)	-26(5)	-14(5)
C(3)	98(5)	99(6)	167(6)	-5(5)	-20(5)	1(5)
C(4)	103(6)	115(6)	154(6)	-11(5)	-19(5)	2(5)
C(5)	197(7)	118(6)	170(6)	2(5)	-23(6)	17(5)
C(6)	309(9)	172(7)	207(7)	3(5)	-1(6)	128(7)
C(7)	244(8)	148(6)	213(7)	-27(5)	10(6)	50(6)
C(8)	176(7)	186(7)	164(6)	-39(5)	-15(5)	-15(6)
C(9)	192(7)	265(8)	152(6)	-20(5)	-33(6)	16(6)
C(10)	154(6)	159(7)	170(6)	21(5)	-20(5)	-6(5)
C(11)	146(6)	131(6)	183(6)	-29(5)	-34(5)	31(5)
C(12)	130(6)	161(6)	168(6)	-19(5)	-10(5)	29(5)
C(13)	139(6)	177(7)	153(6)	1(5)	5(5)	10(5)
C(14)	195(7)	201(7)	179(6)	19(6)	4(6)	-37(6)
C(15)	210(7)	128(6)	199(6)	-1(5)	-32(6)	-49(6)
C(16)	177(7)	264(8)	202(7)	-39(6)	23(6)	4(6)
C(17)	186(7)	178(7)	119(5)	6(5)	6(5)	-23(6)
C(18)	330(9)	184(7)	276(8)	-7(6)	-68(7)	-44(7)
C(19)	185(7)	263(9)	294(8)	-41(7)	-57(6)	-7(6)

*Table A11.1.6. Hydrogen coordinates (x10^4) and isotropic displacement parameters (Å^{2}x10^3) for Epoxide **371**.*

	x	y	z	U(eq)
H(2)	6290(50)	3280(20)	3652(11)	50(7)
H(2A)	9360(40)	6063(19)	4700(10)	37(6)
H(3)	6760(30)	6945(15)	5272(7)	13(4)
H(4)	8620(30)	5757(15)	5899(7)	8(4)
H(5)	5490(30)	3966(16)	5724(8)	18(5)
H(6A)	10040(30)	3871(16)	5545(8)	21(5)
H(6B)	8650(30)	2724(17)	5610(8)	24(5)
H(7)	8570(30)	2753(16)	4627(7)	14(4)
H(9A)	7380(30)	6011(17)	3323(8)	24(5)
H(9B)	5420(40)	5320(19)	3527(9)	29(5)
H(10)	6820(30)	7182(16)	4126(7)	13(4)
H(12A)	5870(30)	6992(17)	6239(8)	18(4)
H(12B)	4240(30)	5975(16)	6195(8)	20(5)
H(13)	5190(30)	6103(15)	7144(7)	14(4)
H(14A)	6340(30)	4104(16)	7310(8)	19(4)
H(14B)	4330(40)	4230(20)	6848(10)	40(6)
H(16A)	11450(40)	4137(19)	3839(9)	31(5)
H(16B)	11090(30)	5461(18)	3832(8)	24(5)
H(16C)	10680(30)	4740(16)	3273(9)	23(5)
H(18A)	8190(30)	7938(19)	6859(10)	36(6)
H(18B)	9970(40)	7730(18)	7331(10)	34(6)
H(18C)	7410(40)	7700(20)	7496(10)	42(6)
H(19A)	11370(40)	5870(20)	7323(9)	35(5)
H(19B)	10090(40)	4700(20)	7118(9)	36(6)

*Table A11.1.7. Torsion angles [°] for Epoxide **371**.*

O(1)-C(1)-C(2)-C(3)	25.82(17)
O(1)-C(1)-C(2)-C(10)	-84.19(13)
O(1)-C(1)-C(7)-C(6)	-103.18(18)
O(1)-C(1)-C(8)-O(2)	-35.68(17)
O(1)-C(1)-C(8)-C(9)	86.65(14)
O(1)-C(1)-C(8)-C(16)	-154.33(12)
O(2)-C(8)-C(9)-C(10)	143.34(13)
C(1)-O(1)-C(7)-C(6)	116.27(15)
C(1)-C(2)-C(3)-C(4)	61.50(17)
C(1)-C(2)-C(3)-C(11)	-73.68(14)
C(1)-C(2)-C(10)-O(3)	89.58(12)
C(1)-C(2)-C(10)-C(9)	-26.26(15)
C(1)-C(8)-C(9)-C(10)	22.25(15)
C(2)-C(1)-C(7)-O(1)	100.62(16)
C(2)-C(1)-C(7)-C(6)	-2.6(3)
C(2)-C(1)-C(8)-O(2)	-162.97(12)
C(2)-C(1)-C(8)-C(9)	-40.64(14)
C(2)-C(1)-C(8)-C(16)	78.38(15)
C(2)-C(3)-C(4)-C(5)	-59.89(17)
C(2)-C(3)-C(4)-C(12)	173.39(12)
C(2)-C(3)-C(11)-O(3)	-27.05(14)
C(2)-C(3)-C(11)-O(4)	157.47(15)
C(3)-C(2)-C(10)-O(3)	-31.42(13)
C(3)-C(2)-C(10)-C(9)	-147.27(12)
C(3)-C(4)-C(5)-C(6)	64.81(17)
C(3)-C(4)-C(5)-C(15)	-171.66(12)
C(3)-C(4)-C(12)-C(13)	-174.53(12)
C(4)-C(3)-C(11)-O(3)	-163.99(11)
C(4)-C(3)-C(11)-O(4)	20.5(2)
C(4)-C(5)-C(6)-C(7)	-75.40(18)
C(4)-C(5)-C(15)-O(5)	-137.70(15)
C(4)-C(5)-C(15)-C(14)	44.60(18)
C(4)-C(12)-C(13)-C(14)	-58.76(16)
C(4)-C(12)-C(13)-C(17)	69.16(16)

Table A11.1.7. (cont'd)

C(5)-C(4)-C(12)-C(13)	56.30(15)
C(5)-C(6)-C(7)-O(1)	-13.7(2)
C(5)-C(6)-C(7)-C(1)	56.5(2)
C(6)-C(5)-C(15)-O(5)	-10.2(2)
C(6)-C(5)-C(15)-C(14)	172.10(14)
C(7)-O(1)-C(1)-C(2)	-119.91(14)
C(7)-O(1)-C(1)-C(8)	117.21(14)
C(7)-C(1)-C(2)-C(3)	-45.2(2)
C(7)-C(1)-C(2)-C(10)	-155.26(15)
C(7)-C(1)-C(8)-O(2)	33.4(2)
C(7)-C(1)-C(8)-C(9)	155.75(15)
C(7)-C(1)-C(8)-C(16)	-85.23(18)
C(8)-C(1)-C(2)-C(3)	151.80(12)
C(8)-C(1)-C(2)-C(10)	41.79(14)
C(8)-C(1)-C(7)-O(1)	-99.12(15)
C(8)-C(1)-C(7)-C(6)	157.70(15)
C(8)-C(9)-C(10)-O(3)	-109.06(13)
C(8)-C(9)-C(10)-C(2)	2.41(16)
C(10)-O(3)-C(11)-O(4)	-176.63(13)
C(10)-O(3)-C(11)-C(3)	7.35(15)
C(10)-C(2)-C(3)-C(4)	170.06(12)
C(10)-C(2)-C(3)-C(11)	34.87(13)
C(11)-O(3)-C(10)-C(2)	15.50(14)
C(11)-O(3)-C(10)-C(9)	130.07(12)
C(11)-C(3)-C(4)-C(5)	67.78(16)
C(11)-C(3)-C(4)-C(12)	-58.94(15)
C(12)-C(4)-C(5)-C(6)	-169.87(12)
C(12)-C(4)-C(5)-C(15)	-46.34(16)
C(12)-C(13)-C(14)-C(15)	53.98(16)
C(12)-C(13)-C(17)-C(18)	71.11(16)
C(12)-C(13)-C(17)-C(19)	-111.20(17)
C(13)-C(14)-C(15)-O(5)	132.62(15)
C(13)-C(14)-C(15)-C(5)	-49.66(18)
C(14)-C(13)-C(17)-C(18)	-164.76(13)

Table A11.1.7. (cont'd)

C(14)-C(13)-C(17)-C(19)	12.9(2)
C(15)-C(5)-C(6)-C(7)	159.27(14)
C(16)-C(8)-C(9)-C(10)	-96.06(15)
C(17)-C(13)-C(14)-C(15)	-72.57(16)

Symmetry transformations used to generate equivalent atoms:

*Table A11.1.8. Hydrogen bonds for Epoxide **371** [Å and °].*

D-H...A	d(D-H)	d(H...A)	d(D...A)	<(DHA)
O(2)-H(2)...O(5)#1	0.87(3)	2.37(3)	3.1244(19)	145(2)
C(2)-H(2A)...O(4)#2	0.97(2)	2.44(2)	3.2790(18)	144.5(17)
C(3)-H(3)...O(3)#3	0.970(17)	2.688(17)	3.5378(17)	146.5(13)
C(6)-H(6B)...O(1)#4	0.944(19)	2.39(2)	3.0758(19)	129.3(15)
C(16)-H(16B)...O(3)#2	0.98(2)	2.61(2)	3.427(2)	140.8(16)

Symmetry transformations used to generate equivalent atoms:

#1 x-1/2,-y+1/2,-z+1 #2 x+1,y,z #3 x+1/2,-y+3/2,-z+1

#4 x+1/2,-y+1/2,-z+1

A11.2 X-Ray Crystal Structure Analysis of 2*H*-Ineleganolide (373)

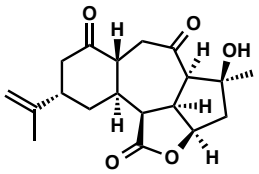

2H-Ineleganolide (373)

Contents

Table A11.2.1. Experimental Details

Table A11.2.2. Crystal Data

Table A11.2.3. Atomic Coordinates

Table A11.2.4. Full Bond Distances and Angles

Table A11.2.5. Anisotropic Displacement Parameters

Table A11.2.6. Hydrogen Atomic Coordinates

Table A11.2.7. Torsion Angles

Table A11.2.8. Hydrogen Bond Distances and Angles

*Figure A11.2.1. X-Ray Crystal Structure of 2H-Ineleganolide (**373**)*

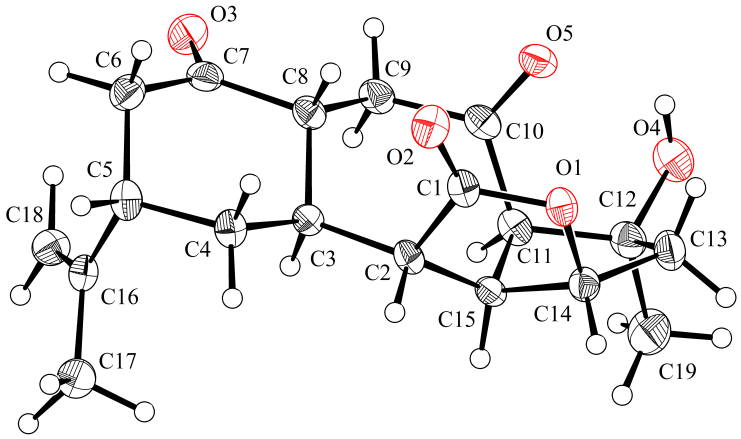

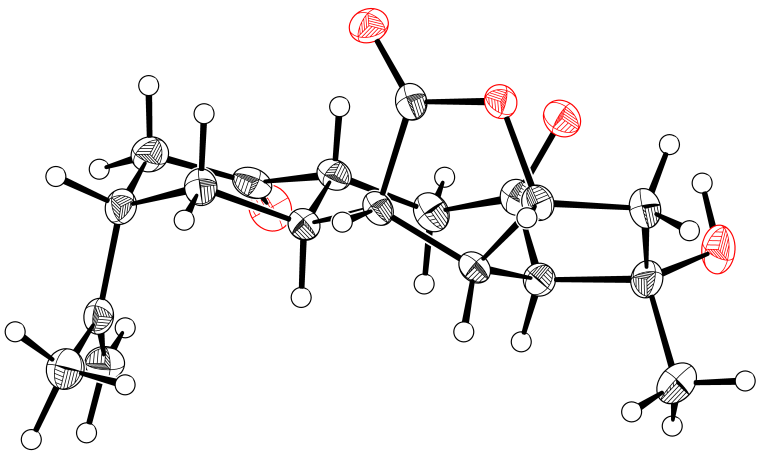

*Table A11.2.1. Experimental Details for X-Ray Structure Determination of 2H-Ineleganolide (**373**).*

Low-temperature diffraction data (ϕ-and ω-scans) were collected on a Bruker AXS KAPPA APEX II diffractometer coupled to a APEX II CCD detector with graphite monochromated Mo K_α radiation (λ = 0.71073 Å) for the structure of 2*H*-ineleganolide (**373**) and on a Bruker AXS D8 VENTURE KAPPA diffractometer coupled to a PHOTON 100 CMOS detector with Cu K_α radiation (λ = 1.54178 Å) from an IμS micro-source for the structure of compound P15149 and P15156. The structure was solved by direct methods using SHELXS[1] and refined against F^2 on all data by full-matrix least squares with SHELXL-2014[2] using established refinement techniques.[3] All non-hydrogen atoms were refined anisotropically. Unless otherwise noted, all hydrogen atoms were included into the model at geometrically calculated positions and refined using a riding model. The isotropic displacement parameters of all hydrogen atoms were fixed to 1.2 times the *U* value of the atoms they are linked to (1.5 times for methyl groups).

2*H*-Ineleganolide (**373**) crystallizes in the orthorhombic space group $P2_12_12_1$ with two molecules in the asymmetric unit. The coordinates for all hydrogen atoms were located in the difference Fourier synthesis and refined freely.

*Table A11.2.2. Crystal Data and Structure Refinement for of 2H-Ineleganolide (**373**).*

Caltech Identification code	p15149	
CCDC Deposition Number	1061016	
Empirical formula	C19 H24 O5	
Formula weight	332.38	
Temperature	100 K	
Wavelength	1.54178 Å	
Crystal system	Orthorhombic	
Space group	$P2_12_12_1$	
Unit cell dimensions	a = 10.4079(3) Å	α= 90°
	b = 14.7042(4) Å	β= 90°
	c = 21.8592(6) Å	γ = 90°
Volume	3345.33(16) $Å^3$	
Z	8	
Density (calculated)	1.320 Mg/m^3	
Absorption coefficient	0.776 mm^{-1}	
F(000)	1424	
Crystal size	0.11 x 0.10 x 0.05 mm^3	
Theta range for data collection	3.623 to 79.108°.	
Index ranges	$-12 \le h \le 13, -18 \le k \le 18, -27 \le l \le 27$	
Reflections collected	46504	
Independent reflections	7174 [R(int) = 0.0796]	
Completeness to theta = 66.500°	100.0 %	
Absorption correction	Semi-empirical from equivalents	
Max. and min. transmission	0.9591 and 0.8890	
Refinement method	Full-matrix least-squares on F^2	
Data / restraints / parameters	7174 / 0 / 625	
Goodness-of-fit on F^2	1.059	
Final R indices [I>2sigma(I)]	R1 = 0.0395, wR2 = 0.0780	
R indices (all data)	R1 = 0.0533, wR2 = 0.0832	
Absolute structure parameter	0.00(9)	
Extinction coefficient	n/a	
Largest diff. peak and hole	0.164 and -0.204 e.$Å^{-3}$	

*Table A11.2.3. Atomic coordinates (x 10^4) and equivalent isotropic displacement parameters ($Å^2$x 10^3) for 2H-Ineleganolide (**373**). U(eq) is defined as one third of the trace of the orthogonalized U^{ij} tensor.*

	x	y	z	U(eq)
O(5)	-3492(18)	56047(13)	60617(9)	257(4)
O(2)	5550(20)	41629(12)	48143(9)	272(5)
O(1)	15419(18)	40753(12)	57144(8)	224(4)
O(4)	8710(20)	60085(16)	71685(10)	344(5)
O(3)	-5710(20)	77121(13)	43577(10)	317(5)
C(15)	26550(30)	54941(17)	57380(12)	186(5)
C(11)	18080(30)	61455(18)	61256(12)	217(6)
C(10)	4620(30)	61450(18)	58779(12)	215(6)
C(9)	1640(30)	67917(19)	53641(13)	239(6)
C(8)	4060(30)	63525(18)	47397(13)	209(6)
C(3)	17970(30)	60187(17)	46347(12)	183(5)
C(2)	22450(30)	52704(17)	50825(11)	189(5)
C(1)	13390(30)	44637(17)	51635(12)	205(5)
C(14)	25330(30)	45637(18)	60602(12)	216(5)
C(13)	20580(30)	47320(20)	67087(13)	270(6)
C(12)	19300(30)	57710(20)	67840(12)	253(6)
C(19)	31090(40)	61710(30)	70917(15)	386(8)
C(7)	-280(30)	70064(19)	42368(13)	236(6)
C(6)	2140(30)	67000(20)	35906(13)	258(6)
C(5)	16110(30)	63940(18)	34952(12)	228(6)
C(4)	19450(30)	56703(18)	39723(12)	225(6)
C(16)	25680(30)	71734(18)	34857(12)	216(6)
C(18)	22410(30)	80350(20)	35596(13)	255(6)
C(17)	39360(30)	69060(20)	33625(15)	283(6)
O(5B)	59070(20)	50022(12)	60452(9)	262(4)
O(2B)	40407(18)	34681(13)	49667(9)	239(4)
O(1B)	48604(18)	29282(13)	58299(8)	230(4)
O(4B)	76480(20)	44953(14)	70004(9)	308(5)

Table A11.2.3. (cont'd)

O(3B)	73160(20)	59914(14)	40281(9)	348(5)
C(15B)	71090(30)	30487(17)	56261(12)	189(5)
C(11B)	76280(30)	39347(18)	59232(12)	207(5)
C(10B)	68140(30)	47391(17)	57380(12)	214(5)
C(9B)	71380(30)	51781(19)	51349(13)	257(6)
C(8B)	64360(30)	47390(18)	45923(12)	197(5)
C(3B)	67320(30)	37204(18)	44942(12)	196(5)
C(2B)	63390(30)	30974(17)	50267(12)	184(5)
C(1B)	49680(30)	31980(16)	52432(12)	198(5)
C(14B)	61090(30)	26871(18)	60892(13)	216(6)
C(13B)	63060(30)	31860(20)	66917(13)	237(6)
C(12B)	75770(30)	37126(18)	66164(12)	224(6)
C(19B)	87110(30)	31200(20)	68043(15)	315(7)
C(7B)	67240(30)	52828(18)	40098(12)	232(6)
C(6B)	61770(30)	49090(20)	34202(13)	250(6)
C(5B)	64620(30)	38920(20)	33323(12)	247(6)
C(4B)	60490(30)	33846(19)	39122(13)	229(6)
C(16B)	78200(30)	36610(20)	31480(12)	292(7)
C(18B)	87410(30)	42570(30)	30882(16)	402(8)
C(17B)	80480(40)	26660(20)	30363(15)	382(8)

*Table A11.2.4. Bond lengths [Å] and angles [°] for 2H-Ineleganolide (**373**).*

O(5)-C(10)	1.227(3)
O(2)-C(1)	1.201(3)
O(1)-C(1)	1.349(3)
O(1)-C(14)	1.467(3)
O(4)-H(4)	0.94(5)
O(4)-C(12)	1.429(3)
O(3)-C(7)	1.211(3)
C(15)-H(15)	0.96(3)
C(15)-C(11)	1.553(4)
C(15)-C(2)	1.531(4)
C(15)-C(14)	1.544(3)
C(11)-H(11)	0.97(3)
C(11)-C(10)	1.503(4)
C(11)-C(12)	1.546(4)
C(10)-C(9)	1.504(4)
C(9)-H(9A)	1.00(4)
C(9)-H(9B)	0.96(3)
C(9)-C(8)	1.531(4)
C(8)-H(8)	0.94(3)
C(8)-C(3)	1.545(4)
C(8)-C(7)	1.529(4)
C(3)-H(3)	1.00(3)
C(3)-C(2)	1.545(3)
C(3)-C(4)	1.544(4)
C(2)-H(2)	0.96(3)
C(2)-C(1)	1.526(4)
C(14)-H(14)	0.97(3)
C(14)-C(13)	1.522(4)
C(13)-H(13A)	0.99(3)
C(13)-H(13B)	0.96(3)
C(13)-C(12)	1.542(4)
C(12)-C(19)	1.518(4)
C(19)-H(19A)	0.98(4)

Table A11.2.4. (cont'd)

C(19)-H(19B)	1.02(4)
C(19)-H(19C)	0.98(4)
C(7)-C(6)	1.504(4)
C(6)-H(6A)	1.03(4)
C(6)-H(6B)	0.94(4)
C(6)-C(5)	1.536(4)
C(5)-H(5)	1.03(3)
C(5)-C(4)	1.530(4)
C(5)-C(16)	1.519(4)
C(4)-H(4A)	1.00(3)
C(4)-H(4B)	1.00(3)
C(16)-C(18)	1.322(4)
C(16)-C(17)	1.501(4)
C(18)-H(18A)	0.98(3)
C(18)-H(18B)	1.02(3)
C(17)-H(17A)	1.03(4)
C(17)-H(17B)	1.07(4)
C(17)-H(17C)	0.99(4)
O(5B)-C(10B)	1.221(3)
O(2B)-C(1B)	1.206(3)
O(1B)-C(1B)	1.347(3)
O(1B)-C(14B)	1.461(3)
O(4B)-H(4BA)	0.90(4)
O(4B)-C(12B)	1.426(3)
O(3B)-C(7B)	1.211(3)
C(15B)-H(15B)	0.96(3)
C(15B)-C(11B)	1.552(4)
C(15B)-C(2B)	1.538(4)
C(15B)-C(14B)	1.547(4)
C(11B)-H(11B)	0.91(3)
C(11B)-C(10B)	1.510(4)
C(11B)-C(12B)	1.551(4)
C(10B)-C(9B)	1.506(4)
C(9B)-H(9BA)	0.95(3)

Table A11.2.4. (cont'd)

C(9B)-H(9BB)	0.99(3)
C(9B)-C(8B)	1.535(4)
C(8B)-H(8B)	0.97(3)
C(8B)-C(3B)	1.544(4)
C(8B)-C(7B)	1.533(4)
C(3B)-H(3B)	1.00(3)
C(3B)-C(2B)	1.537(4)
C(3B)-C(4B)	1.539(4)
C(2B)-H(2B)	0.99(3)
C(2B)-C(1B)	1.511(4)
C(14B)-H(14B)	0.98(3)
C(14B)-C(13B)	1.522(4)
C(13B)-H(13C)	1.02(3)
C(13B)-H(13D)	1.02(3)
C(13B)-C(12B)	1.541(4)
C(12B)-C(19B)	1.523(4)
C(19B)-H(19D)	0.92(4)
C(19B)-H(19E)	0.98(4)
C(19B)-H(19F)	1.00(3)
C(7B)-C(6B)	1.512(4)
C(6B)-H(6BA)	1.00(3)
C(6B)-H(6BB)	1.00(4)
C(6B)-C(5B)	1.537(4)
C(5B)-H(5B)	0.98(3)
C(5B)-C(4B)	1.532(4)
C(5B)-C(16B)	1.508(4)
C(4B)-H(4BB)	0.94(3)
C(4B)-H(4BC)	1.05(3)
C(16B)-C(18B)	1.305(5)
C(16B)-C(17B)	1.503(5)
C(18B)-H(18C)	1.03(4)
C(18B)-H(18D)	0.89(3)
C(17B)-H(17D)	1.07(3)
C(17B)-H(17E)	1.00(4)

Table A11.2.4. (cont'd)

C(17B)-H(17F)	1.02(4)
C(1)-O(1)-C(14)	111.3(2)
C(12)-O(4)-H(4)	104(3)
C(11)-C(15)-H(15)	108.3(17)
C(2)-C(15)-H(15)	111.4(17)
C(2)-C(15)-C(11)	119.0(2)
C(2)-C(15)-C(14)	102.3(2)
C(14)-C(15)-H(15)	110.6(17)
C(14)-C(15)-C(11)	104.5(2)
C(15)-C(11)-H(11)	108.4(18)
C(10)-C(11)-C(15)	109.4(2)
C(10)-C(11)-H(11)	107.4(18)
C(10)-C(11)-C(12)	114.3(2)
C(12)-C(11)-C(15)	104.0(2)
C(12)-C(11)-H(11)	113.1(17)
O(5)-C(10)-C(11)	121.6(2)
O(5)-C(10)-C(9)	120.8(3)
C(11)-C(10)-C(9)	117.4(2)
C(10)-C(9)-H(9A)	110.1(19)
C(10)-C(9)-H(9B)	109.0(18)
C(10)-C(9)-C(8)	111.4(2)
H(9A)-C(9)-H(9B)	108(3)
C(8)-C(9)-H(9A)	109(2)
C(8)-C(9)-H(9B)	109.5(18)
C(9)-C(8)-H(8)	109.7(18)
C(9)-C(8)-C(3)	114.9(2)
C(3)-C(8)-H(8)	105.4(17)
C(7)-C(8)-C(9)	109.1(2)
C(7)-C(8)-H(8)	105.7(18)
C(7)-C(8)-C(3)	111.7(2)
C(8)-C(3)-H(3)	108.9(16)
C(2)-C(3)-C(8)	114.5(2)
C(2)-C(3)-H(3)	105.2(16)

Table A11.2.4. (cont'd)

C(4)-C(3)-C(8)	109.8(2)
C(4)-C(3)-H(3)	109.1(16)
C(4)-C(3)-C(2)	109.1(2)
C(15)-C(2)-C(3)	121.6(2)
C(15)-C(2)-H(2)	106.2(16)
C(3)-C(2)-H(2)	106.0(16)
C(1)-C(2)-C(15)	103.3(2)
C(1)-C(2)-C(3)	116.2(2)
C(1)-C(2)-H(2)	101.4(16)
O(2)-C(1)-O(1)	121.2(2)
O(2)-C(1)-C(2)	129.2(2)
O(1)-C(1)-C(2)	109.6(2)
O(1)-C(14)-C(15)	104.9(2)
O(1)-C(14)-H(14)	105.5(17)
O(1)-C(14)-C(13)	109.3(2)
C(15)-C(14)-H(14)	113.0(17)
C(13)-C(14)-C(15)	107.9(2)
C(13)-C(14)-H(14)	115.6(18)
C(14)-C(13)-H(13A)	111.3(18)
C(14)-C(13)-H(13B)	111.8(19)
C(14)-C(13)-C(12)	106.8(2)
H(13A)-C(13)-H(13B)	106(3)
C(12)-C(13)-H(13A)	112.3(18)
C(12)-C(13)-H(13B)	109.0(19)
O(4)-C(12)-C(11)	113.4(2)
O(4)-C(12)-C(13)	111.8(2)
O(4)-C(12)-C(19)	105.5(2)
C(13)-C(12)-C(11)	105.1(2)
C(19)-C(12)-C(11)	109.9(2)
C(19)-C(12)-C(13)	111.2(3)
C(12)-C(19)-H(19A)	108(2)
C(12)-C(19)-H(19B)	113(2)
C(12)-C(19)-H(19C)	108(2)
H(19A)-C(19)-H(19B)	109(3)

Table A11.2.4. (cont'd)

H(19A)-C(19)-H(19C)	110(3)
H(19B)-C(19)-H(19C)	109(3)
O(3)-C(7)-C(8)	121.3(3)
O(3)-C(7)-C(6)	122.7(3)
C(6)-C(7)-C(8)	115.9(2)
C(7)-C(6)-H(6A)	110(2)
C(7)-C(6)-H(6B)	108(2)
C(7)-C(6)-C(5)	112.0(2)
H(6A)-C(6)-H(6B)	107(3)
C(5)-C(6)-H(6A)	111(2)
C(5)-C(6)-H(6B)	109(2)
C(6)-C(5)-H(5)	109.8(17)
C(4)-C(5)-C(6)	109.0(2)
C(4)-C(5)-H(5)	106.5(17)
C(16)-C(5)-C(6)	113.7(2)
C(16)-C(5)-H(5)	104.9(17)
C(16)-C(5)-C(4)	112.7(2)
C(3)-C(4)-H(4A)	107.4(17)
C(3)-C(4)-H(4B)	109.2(17)
C(5)-C(4)-C(3)	112.7(2)
C(5)-C(4)-H(4A)	111.0(17)
C(5)-C(4)-H(4B)	108.6(17)
H(4A)-C(4)-H(4B)	108(2)
C(18)-C(16)-C(5)	123.6(3)
C(18)-C(16)-C(17)	121.1(3)
C(17)-C(16)-C(5)	115.3(2)
C(16)-C(18)-H(18A)	121.9(19)
C(16)-C(18)-H(18B)	122.2(18)
H(18A)-C(18)-H(18B)	116(3)
C(16)-C(17)-H(17A)	110(2)
C(16)-C(17)-H(17B)	113(2)
C(16)-C(17)-H(17C)	113(2)
H(17A)-C(17)-H(17B)	105(3)
H(17A)-C(17)-H(17C)	110(3)

Table A11.2.4. (cont'd)

H(17B)-C(17)-H(17C)	105(3)
C(1B)-O(1B)-C(14B)	111.5(2)
C(12B)-O(4B)-H(4BA)	102(2)
C(11B)-C(15B)-H(15B)	107.5(16)
C(2B)-C(15B)-H(15B)	111.5(15)
C(2B)-C(15B)-C(11B)	119.9(2)
C(2B)-C(15B)-C(14B)	102.9(2)
C(14B)-C(15B)-H(15B)	110.1(15)
C(14B)-C(15B)-C(11B)	104.4(2)
C(15B)-C(11B)-H(11B)	109.2(18)
C(10B)-C(11B)-C(15B)	110.5(2)
C(10B)-C(11B)-H(11B)	110.0(18)
C(10B)-C(11B)-C(12B)	114.1(2)
C(12B)-C(11B)-C(15B)	102.7(2)
C(12B)-C(11B)-H(11B)	110.1(18)
O(5B)-C(10B)-C(11B)	122.3(3)
O(5B)-C(10B)-C(9B)	121.2(3)
C(9B)-C(10B)-C(11B)	116.4(2)
C(10B)-C(9B)-H(9BA)	110.0(17)
C(10B)-C(9B)-H(9BB)	107.7(18)
C(10B)-C(9B)-C(8B)	112.9(2)
H(9BA)-C(9B)-H(9BB)	110(3)
C(8B)-C(9B)-H(9BA)	108.2(18)
C(8B)-C(9B)-H(9BB)	107.7(18)
C(9B)-C(8B)-H(8B)	111.1(17)
C(9B)-C(8B)-C(3B)	114.9(2)
C(3B)-C(8B)-H(8B)	106.2(17)
C(7B)-C(8B)-C(9B)	109.2(2)
C(7B)-C(8B)-H(8B)	104.4(17)
C(7B)-C(8B)-C(3B)	110.6(2)
C(8B)-C(3B)-H(3B)	109.2(16)
C(2B)-C(3B)-C(8B)	114.8(2)
C(2B)-C(3B)-H(3B)	107.6(16)
C(2B)-C(3B)-C(4B)	108.2(2)

Table A11.2.4. (cont'd)

C(4B)-C(3B)-C(8B)	109.5(2)
C(4B)-C(3B)-H(3B)	107.3(16)
C(15B)-C(2B)-H(2B)	105.6(18)
C(3B)-C(2B)-C(15B)	122.3(2)
C(3B)-C(2B)-H(2B)	107.1(17)
C(1B)-C(2B)-C(15B)	103.3(2)
C(1B)-C(2B)-C(3B)	115.5(2)
C(1B)-C(2B)-H(2B)	100.5(18)
O(2B)-C(1B)-O(1B)	120.5(2)
O(2B)-C(1B)-C(2B)	129.1(2)
O(1B)-C(1B)-C(2B)	110.4(2)
O(1B)-C(14B)-C(15B)	105.2(2)
O(1B)-C(14B)-H(14B)	107(2)
O(1B)-C(14B)-C(13B)	109.8(2)
C(15B)-C(14B)-H(14B)	111(2)
C(13B)-C(14B)-C(15B)	108.0(2)
C(13B)-C(14B)-H(14B)	115(2)
C(14B)-C(13B)-H(13C)	114.2(18)
C(14B)-C(13B)-H(13D)	109.1(16)
C(14B)-C(13B)-C(12B)	105.4(2)
H(13C)-C(13B)-H(13D)	108(2)
C(12B)-C(13B)-H(13C)	111.9(18)
C(12B)-C(13B)-H(13D)	108.0(15)
O(4B)-C(12B)-C(11B)	113.8(2)
O(4B)-C(12B)-C(13B)	112.7(2)
O(4B)-C(12B)-C(19B)	105.2(2)
C(13B)-C(12B)-C(11B)	103.9(2)
C(19B)-C(12B)-C(11B)	110.9(2)
C(19B)-C(12B)-C(13B)	110.4(2)
C(12B)-C(19B)-H(19D)	110(2)
C(12B)-C(19B)-H(19E)	114(2)
C(12B)-C(19B)-H(19F)	108.8(18)
H(19D)-C(19B)-H(19E)	109(3)
H(19D)-C(19B)-H(19F)	108(3)

Table A11.2.4. (cont'd)

H(19E)-C(19B)-H(19F)	108(3)
O(3B)-C(7B)-C(8B)	121.4(2)
O(3B)-C(7B)-C(6B)	122.2(3)
C(6B)-C(7B)-C(8B)	116.4(2)
C(7B)-C(6B)-H(6BA)	106.7(17)
C(7B)-C(6B)-H(6BB)	107.4(19)
C(7B)-C(6B)-C(5B)	112.8(2)
H(6BA)-C(6B)-H(6BB)	110(3)
C(5B)-C(6B)-H(6BA)	114.7(17)
C(5B)-C(6B)-H(6BB)	105.2(19)
C(6B)-C(5B)-H(5B)	106.9(19)
C(4B)-C(5B)-C(6B)	108.4(2)
C(4B)-C(5B)-H(5B)	108.1(19)
C(16B)-C(5B)-C(6B)	115.7(3)
C(16B)-C(5B)-H(5B)	105(2)
C(16B)-C(5B)-C(4B)	112.0(2)
C(3B)-C(4B)-H(4BB)	108.3(19)
C(3B)-C(4B)-H(4BC)	107.6(15)
C(5B)-C(4B)-C(3B)	113.4(2)
C(5B)-C(4B)-H(4BB)	109.7(18)
C(5B)-C(4B)-H(4BC)	109.8(15)
H(4BB)-C(4B)-H(4BC)	108(2)
C(18B)-C(16B)-C(5B)	124.3(3)
C(18B)-C(16B)-C(17B)	121.4(3)
C(17B)-C(16B)-C(5B)	114.2(3)
C(16B)-C(18B)-H(18C)	123(2)
C(16B)-C(18B)-H(18D)	124(2)
H(18C)-C(18B)-H(18D)	112(3)
C(16B)-C(17B)-H(17D)	111.6(18)
C(16B)-C(17B)-H(17E)	112(2)
C(16B)-C(17B)-H(17F)	110(2)
H(17D)-C(17B)-H(17E)	107(3)
H(17D)-C(17B)-H(17F)	112(3)

Table A11.2.4. (cont'd)

H(17E)-C(17B)-H(17F)	104(3)

Symmetry transformations used to generate equivalent atoms:

*Table A11.2.5. Anisotropic displacement parameters ($Å^2x10^3$) for 2H-Ineleganolide (**373**). The anisotropic displacement factor exponent takes the form: $-2\pi^2[h^2a^{*2}U^{11} + ... + 2hka^*b^*U^{12}]$.*

	U^{11}	U^{22}	U^{33}	U^{23}	U^{13}	U^{12}
O(5)	208(10)	281(10)	281(10)	1(9)	44(8)	2(8)
O(2)	355(12)	181(9)	278(11)	-13(8)	-41(8)	-37(8)
O(1)	284(10)	179(9)	208(9)	7(8)	18(8)	-22(8)
O(4)	364(13)	446(13)	222(11)	-58(10)	89(9)	54(11)
O(3)	312(12)	266(11)	373(13)	61(9)	22(9)	104(9)
C(15)	167(13)	185(12)	207(13)	15(10)	36(10)	-4(10)
C(11)	259(15)	191(13)	201(13)	-42(11)	42(11)	-20(11)
C(10)	226(13)	200(12)	219(13)	-58(11)	74(10)	30(11)
C(9)	229(16)	221(13)	267(15)	8(11)	64(11)	47(12)
C(8)	213(14)	176(12)	237(14)	7(11)	27(10)	-22(11)
C(3)	190(13)	155(11)	203(13)	3(10)	21(10)	12(10)
C(2)	219(13)	148(11)	199(13)	3(10)	63(10)	15(10)
C(1)	265(15)	150(11)	201(13)	-12(10)	52(11)	37(10)
C(14)	227(14)	211(12)	210(13)	29(11)	10(11)	12(11)
C(13)	305(16)	301(15)	204(14)	39(12)	26(11)	-14(13)
C(12)	255(15)	309(15)	196(13)	-45(11)	31(11)	-8(12)
C(19)	410(20)	480(20)	267(17)	-45(16)	-71(14)	-89(17)
C(7)	167(13)	232(13)	310(15)	41(12)	3(11)	-26(11)
C(6)	252(16)	263(14)	260(16)	21(12)	-45(11)	-15(12)
C(5)	317(16)	183(12)	183(13)	-16(11)	6(11)	-8(12)
C(4)	283(15)	185(12)	207(13)	1(11)	24(11)	20(11)
C(16)	254(15)	227(13)	166(13)	19(10)	-11(11)	6(11)
C(18)	252(16)	218(13)	296(15)	1(12)	-19(11)	-21(12)
C(17)	300(16)	279(15)	272(16)	-15(13)	8(12)	30(14)
O(5B)	318(11)	205(9)	264(10)	-40(8)	20(8)	50(8)
O(2B)	179(10)	255(9)	282(10)	-41(8)	-45(7)	-18(8)
O(1B)	200(10)	267(10)	223(10)	1(8)	10(8)	-25(8)
O(4B)	413(13)	305(11)	205(10)	-40(8)	-60(9)	-18(10)
O(3B)	443(13)	300(11)	299(11)	48(9)	18(9)	-128(10)
C(15B)	189(13)	167(12)	210(13)	-19(11)	18(10)	33(11)

Table A11.2.5. (cont'd)

C(11B)	163(13)	241(13)	216(13)	-12(10)	17(10)	-11(11)
C(10B)	256(14)	170(12)	217(13)	-59(11)	-29(11)	-55(11)
C(9B)	333(17)	211(13)	227(14)	-1(11)	-21(12)	-72(12)
C(8B)	194(13)	189(13)	208(13)	-5(11)	-12(10)	-21(11)
C(3B)	192(14)	205(13)	192(13)	-16(10)	2(10)	6(11)
C(2B)	217(14)	153(12)	181(13)	-30(10)	-5(10)	9(10)
C(1B)	232(14)	142(11)	220(13)	-56(10)	16(11)	-44(11)
C(14B)	224(14)	189(13)	234(14)	22(11)	-6(11)	9(11)
C(13B)	258(15)	260(14)	194(14)	26(11)	23(11)	4(12)
C(12B)	226(14)	249(13)	198(13)	-24(11)	-9(10)	4(11)
C(19B)	254(17)	402(19)	289(17)	34(15)	-36(12)	43(14)
C(7B)	228(14)	224(13)	244(14)	19(11)	11(11)	5(11)
C(6B)	296(16)	275(15)	180(14)	4(12)	-2(11)	50(13)
C(5B)	256(15)	307(15)	179(13)	-24(12)	-49(11)	43(12)
C(4B)	287(16)	213(14)	188(13)	-33(11)	-34(11)	-2(11)
C(16B)	313(16)	423(17)	139(13)	-7(12)	-26(11)	107(14)
C(18B)	336(19)	520(20)	347(18)	-35(17)	49(14)	9(17)
C(17B)	460(20)	449(19)	240(16)	-29(14)	-45(15)	209(17)

*Table A11.2.6. Hydrogen coordinates (x10^4) and isotropic displacement parameters (Å^{2}x10^3) for 2H-Ineleganolide (**373**).*

	x	y	z	U(eq)
H(4)	170(40)	5710(30)	6990(20)	75(15)
H(15)	3530(30)	5708(19)	5753(13)	17(7)
H(11)	2140(30)	6760(20)	6082(13)	23(8)
H(9A)	700(30)	7350(20)	5401(15)	36(9)
H(9B)	-720(30)	6980(20)	5393(14)	26(8)
H(8)	-110(30)	5833(19)	4697(13)	19(7)
H(3)	2400(30)	6536(19)	4701(12)	18(7)
H(2)	2970(30)	4986(18)	4893(12)	14(7)
H(14)	3310(30)	4190(20)	6025(13)	21(7)
H(13A)	2650(30)	4460(20)	7015(14)	26(8)
H(13B)	1240(30)	4460(20)	6779(14)	29(9)
H(19A)	3000(30)	6830(20)	7103(15)	38(9)
H(19B)	3940(40)	6020(30)	6863(19)	54(12)
H(19C)	3160(30)	5920(20)	7510(17)	42(10)
H(6A)	-30(40)	7210(30)	3291(17)	54(12)
H(6B)	-330(40)	6210(20)	3506(16)	38(10)
H(5)	1700(30)	6090(20)	3072(14)	24(8)
H(4A)	2850(30)	5460(20)	3924(13)	20(7)
H(4B)	1360(30)	5130(20)	3910(14)	23(8)
H(18A)	2870(30)	8530(20)	3529(14)	28(8)
H(18B)	1310(30)	8230(20)	3630(14)	28(8)
H(17A)	4340(40)	6650(30)	3753(18)	56(12)
H(17B)	4540(40)	7470(20)	3236(16)	44(10)
H(17C)	4030(40)	6470(30)	3024(18)	51(11)
H(4BA)	6990(40)	4840(30)	6858(18)	50(12)
H(15B)	7820(30)	2630(17)	5594(11)	10(6)
H(11B)	8460(30)	4023(19)	5804(13)	18(7)
H(9BA)	8040(30)	5140(19)	5062(13)	21(8)
H(9BB)	6870(30)	5820(20)	5157(14)	29(8)
H(8B)	5510(30)	4784(19)	4640(13)	19(7)

Table A11.2.6. (cont'd)

H(3B)	7680(30)	3641(19)	4428(12)	18(7)
H(2B)	6320(30)	2470(20)	4867(13)	24(8)
H(14B)	6150(30)	2020(20)	6113(15)	37(9)
H(13C)	6320(30)	2770(20)	7065(15)	29(9)
H(13D)	5590(30)	3649(18)	6748(12)	12(7)
H(19D)	9470(40)	3410(20)	6706(15)	34(9)
H(19E)	8710(40)	2510(30)	6616(17)	45(11)
H(19F)	8690(30)	3040(20)	7259(15)	28(8)
H(6BA)	6500(30)	5310(20)	3082(14)	25(8)
H(6BB)	5220(40)	4950(20)	3449(15)	37(9)
H(5B)	5920(30)	3680(20)	2994(15)	32(9)
H(4BB)	6220(30)	2760(20)	3867(13)	23(8)
H(4BC)	5050(30)	3464(19)	3980(12)	19(7)
H(18C)	9650(40)	4090(30)	2945(18)	59(12)
H(18D)	8630(30)	4860(20)	3113(14)	21(8)
H(17D)	8130(30)	2300(20)	3454(15)	39(9)
H(17E)	8870(40)	2560(20)	2804(16)	35(9)
H(17F)	7350(40)	2410(20)	2756(17)	50(11)

*Table A11.2.7. Torsion angles [°] for 2H-Ineleganolide (**373**).*

O(5)-C(10)-C(9)-C(8)	-86.1(3)
O(1)-C(14)-C(13)-C(12)	-115.2(2)
O(3)-C(7)-C(6)-C(5)	131.8(3)
C(15)-C(11)-C(10)-O(5)	89.7(3)
C(15)-C(11)-C(10)-C(9)	-86.3(3)
C(15)-C(11)-C(12)-O(4)	-155.9(2)
C(15)-C(11)-C(12)-C(13)	-33.5(3)
C(15)-C(11)-C(12)-C(19)	86.2(3)
C(15)-C(2)-C(1)-O(2)	162.0(3)
C(15)-C(2)-C(1)-O(1)	-19.2(3)
C(15)-C(14)-C(13)-C(12)	-1.6(3)
C(11)-C(15)-C(2)-C(3)	45.8(3)
C(11)-C(15)-C(2)-C(1)	-86.9(3)
C(11)-C(15)-C(14)-O(1)	97.4(2)
C(11)-C(15)-C(14)-C(13)	-19.1(3)
C(11)-C(10)-C(9)-C(8)	90.0(3)
C(10)-C(11)-C(12)-O(4)	-36.7(3)
C(10)-C(11)-C(12)-C(13)	85.7(3)
C(10)-C(11)-C(12)-C(19)	-154.5(3)
C(10)-C(9)-C(8)-C(3)	-58.9(3)
C(10)-C(9)-C(8)-C(7)	174.8(2)
C(9)-C(8)-C(3)-C(2)	61.9(3)
C(9)-C(8)-C(3)-C(4)	-175.0(2)
C(9)-C(8)-C(7)-O(3)	-5.7(4)
C(9)-C(8)-C(7)-C(6)	176.6(2)
C(8)-C(3)-C(2)-C(15)	-77.8(3)
C(8)-C(3)-C(2)-C(1)	49.4(3)
C(8)-C(3)-C(4)-C(5)	57.8(3)
C(8)-C(7)-C(6)-C(5)	-50.5(3)
C(3)-C(8)-C(7)-O(3)	-133.8(3)
C(3)-C(8)-C(7)-C(6)	48.5(3)
C(3)-C(2)-C(1)-O(2)	26.3(4)
C(3)-C(2)-C(1)-O(1)	-155.0(2)
C(2)-C(15)-C(11)-C(10)	23.1(3)

Table A11.2.7. (cont'd)

C(2)-C(15)-C(11)-C(12)	145.6(2)
C(2)-C(15)-C(14)-O(1)	-27.4(3)
C(2)-C(15)-C(14)-C(13)	-143.9(2)
C(2)-C(3)-C(4)-C(5)	-176.0(2)
C(1)-O(1)-C(14)-C(15)	16.8(3)
C(1)-O(1)-C(14)-C(13)	132.3(2)
C(14)-O(1)-C(1)-O(2)	-179.6(2)
C(14)-O(1)-C(1)-C(2)	1.5(3)
C(14)-C(15)-C(11)-C(10)	-90.2(3)
C(14)-C(15)-C(11)-C(12)	32.3(3)
C(14)-C(15)-C(2)-C(3)	160.3(2)
C(14)-C(15)-C(2)-C(1)	27.7(3)
C(14)-C(13)-C(12)-O(4)	145.3(2)
C(14)-C(13)-C(12)-C(11)	21.9(3)
C(14)-C(13)-C(12)-C(19)	-97.0(3)
C(12)-C(11)-C(10)-O(5)	-26.4(4)
C(12)-C(11)-C(10)-C(9)	157.6(2)
C(7)-C(8)-C(3)-C(2)	-173.2(2)
C(7)-C(8)-C(3)-C(4)	-50.1(3)
C(7)-C(6)-C(5)-C(4)	53.9(3)
C(7)-C(6)-C(5)-C(16)	-72.7(3)
C(6)-C(5)-C(4)-C(3)	-59.3(3)
C(6)-C(5)-C(16)-C(18)	0.8(4)
C(6)-C(5)-C(16)-C(17)	-177.1(2)
C(4)-C(3)-C(2)-C(15)	158.7(2)
C(4)-C(3)-C(2)-C(1)	-74.1(3)
C(4)-C(5)-C(16)-C(18)	-123.9(3)
C(4)-C(5)-C(16)-C(17)	58.2(3)
C(16)-C(5)-C(4)-C(3)	67.9(3)
O(5B)-C(10B)-C(9B)-C(8B)	-89.2(3)
O(1B)-C(14B)-C(13B)-C(12B)	-124.2(2)
O(3B)-C(7B)-C(6B)-C(5B)	133.4(3)
C(15B)-C(11B)-C(10B)-O(5B)	92.9(3)
C(15B)-C(11B)-C(10B)-C(9B)	-84.2(3)

Table A11.2.7. (cont'd)

C(15B)-C(11B)-C(12B)-O(4B)	-162.8(2)
C(15B)-C(11B)-C(12B)-C(13B)	-39.8(3)
C(15B)-C(11B)-C(12B)-C(19B)	78.9(3)
C(15B)-C(2B)-C(1B)-O(2B)	161.2(3)
C(15B)-C(2B)-C(1B)-O(1B)	-19.2(3)
C(15B)-C(14B)-C(13B)-C(12B)	-10.0(3)
C(11B)-C(15B)-C(2B)-C(3B)	42.2(4)
C(11B)-C(15B)-C(2B)-C(1B)	-90.0(3)
C(11B)-C(15B)-C(14B)-O(1B)	102.5(2)
C(11B)-C(15B)-C(14B)-C(13B)	-14.7(3)
C(11B)-C(10B)-C(9B)-C(8B)	88.0(3)
C(10B)-C(11B)-C(12B)-O(4B)	-43.2(3)
C(10B)-C(11B)-C(12B)-C(13B)	79.8(3)
C(10B)-C(11B)-C(12B)-C(19B)	-161.6(2)
C(10B)-C(9B)-C(8B)-C(3B)	-60.4(3)
C(10B)-C(9B)-C(8B)-C(7B)	174.7(2)
C(9B)-C(8B)-C(3B)-C(2B)	62.1(3)
C(9B)-C(8B)-C(3B)-C(4B)	-175.9(2)
C(9B)-C(8B)-C(7B)-O(3B)	-6.6(4)
C(9B)-C(8B)-C(7B)-C(6B)	176.2(2)
C(8B)-C(3B)-C(2B)-C(15B)	-75.4(3)
C(8B)-C(3B)-C(2B)-C(1B)	51.7(3)
C(8B)-C(3B)-C(4B)-C(5B)	59.9(3)
C(8B)-C(7B)-C(6B)-C(5B)	-49.3(3)
C(3B)-C(8B)-C(7B)-O(3B)	-133.9(3)
C(3B)-C(8B)-C(7B)-C(6B)	48.8(3)
C(3B)-C(2B)-C(1B)-O(2B)	25.0(4)
C(3B)-C(2B)-C(1B)-O(1B)	-155.3(2)
C(2B)-C(15B)-C(11B)-C(10B)	25.7(3)
C(2B)-C(15B)-C(11B)-C(12B)	147.7(2)
C(2B)-C(15B)-C(14B)-O(1B)	-23.4(2)
C(2B)-C(15B)-C(14B)-C(13B)	-140.6(2)
C(2B)-C(3B)-C(4B)-C(5B)	-174.3(2)
C(1B)-O(1B)-C(14B)-C(15B)	12.6(3)

Table A11.2.7. (cont'd)

C(1B)-O(1B)-C(14B)-C(13B)	128.6(2)
C(14B)-O(1B)-C(1B)-O(2B)	-176.1(2)
C(14B)-O(1B)-C(1B)-C(2B)	4.2(3)
C(14B)-C(15B)-C(11B)-C(10B)	-88.7(2)
C(14B)-C(15B)-C(11B)-C(12B)	33.3(3)
C(14B)-C(15B)-C(2B)-C(3B)	157.4(2)
C(14B)-C(15B)-C(2B)-C(1B)	25.2(2)
C(14B)-C(13B)-C(12B)-O(4B)	154.6(2)
C(14B)-C(13B)-C(12B)-C(11B)	30.9(3)
C(14B)-C(13B)-C(12B)-C(19B)	-88.1(3)
C(12B)-C(11B)-C(10B)-O(5B)	-22.2(4)
C(12B)-C(11B)-C(10B)-C(9B)	160.7(2)
C(7B)-C(8B)-C(3B)-C(2B)	-173.7(2)
C(7B)-C(8B)-C(3B)-C(4B)	-51.7(3)
C(7B)-C(6B)-C(5B)-C(4B)	51.5(3)
C(7B)-C(6B)-C(5B)-C(16B)	-75.3(3)
C(6B)-C(5B)-C(4B)-C(3B)	-58.7(3)
C(6B)-C(5B)-C(16B)-C(18B)	3.0(4)
C(6B)-C(5B)-C(16B)-C(17B)	-177.2(2)
C(4B)-C(3B)-C(2B)-C(15B)	162.0(2)
C(4B)-C(3B)-C(2B)-C(1B)	-70.9(3)
C(4B)-C(5B)-C(16B)-C(18B)	-121.9(3)
C(4B)-C(5B)-C(16B)-C(17B)	57.9(3)
C(16B)-C(5B)-C(4B)-C(3B)	70.1(3)

Symmetry transformations used to generate equivalent atoms:

*Table A11.2.8. Hydrogen bonds for 2H-Ineleganolide (**373**) [Å and °].*

D-H...A	d(D-H)	d(H...A)	d(D...A)	<(DHA)
O(4)-H(4)...O(5)	0.94(5)	2.11(5)	2.796(3)	129(4)
C(15)-H(15)...O(3)#1	0.96(3)	2.52(3)	3.227(3)	131(2)
C(8)-H(8)...O(2)	0.94(3)	2.57(3)	3.228(3)	128(2)
C(2)-H(2)...O(2B)	0.96(3)	2.50(3)	3.253(3)	136(2)
C(14)-H(14)...O(1B)	0.97(3)	2.50(3)	3.450(3)	164(2)
O(4B)-H(4BA)...O(5B)	0.90(4)	2.12(4)	2.863(3)	139(3)
C(15B)-H(15B)...O(2B)#2	0.96(3)	2.39(3)	3.270(3)	151(2)
C(8B)-H(8B)...O(2B)	0.97(3)	2.57(3)	3.222(3)	125(2)
C(2B)-H(2B)...O(2)#2	0.99(3)	2.62(3)	3.440(3)	140(2)
C(2B)-H(2B)...O(1)#2	0.99(3)	2.61(3)	3.588(3)	169(2)
C(13B)-H(13D)...O(5B)	1.02(3)	2.54(3)	3.049(3)	110.7(18)
C(6B)-H(6BA)...O(4B)#3	1.00(3)	2.54(3)	3.449(4)	150(2)

Symmetry transformations used to generate equivalent atoms:

#1 x+1/2,-y+3/2,-z+1 #2 x+1/2,-y+1/2,-z+1 #3 -x+3/2,-y+1,z-1/2

A11.3 X-Ray Crystal Structure Analysis of Diketone 375

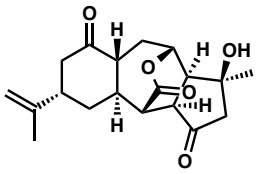

375

Contents

Table A11.3.1. Experimental Details

Table A11.3.2. Crystal Data

Table A11.3.3. Atomic Coordinates

Table A11.3.4. Full Bond Distances and Angles

Table A11.3.5. Anisotropic Displacement Parameters

Table A11.3.6. Hydrogen Atomic Coordinates

Table A11.3.7. Torsion Angles

Table A11.3.8. Hydrogen Bond Distances and Angles

*Figure A11.3.1. X-Ray Crystal Structure of Diketone **375***

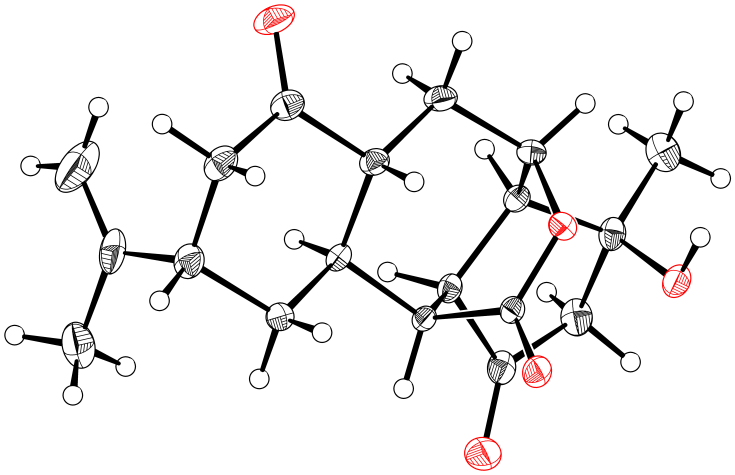

*Table A11.3.1. Experimental Details for X-Ray Structure Determination of Diketone **375**.*

Low-temperature diffraction data (ϕ-and ω-scans) were collected on a Bruker AXS D8 VENTURE KAPPA diffractometer coupled to a PHOTON 100 CMOS detector with Mo K_α radiation (λ = 0.71073 Å) or Cu K_α radiation (λ = 1.54178 Å) from an IμS micro-source for the structure of diketone **375**. The structure was solved by direct methods using SHELXS[1] and refined against F^2 on all data by full-matrix least squares with SHELXL-2014[2] using established refinement techniques.[3] All non-hydrogen atoms were refined anisotropically. All hydrogen atoms were included into the model at geometrically calculated positions and refined using a riding model. The isotropic displacement parameters of all hydrogen atoms were fixed to 1.2 times the U value of the atoms they are linked to (1.5 times for methyl groups).

Diketone **375** crystallizes in the orthorhombic space group $P2_12_12_1$ with one molecule in the asymmetric unit. The carbon atom C18 was refined a mixture of CH_3 and CH_2Cl. The ratio of the components was refined freely and converged to 757(3):0.243(3). The coordinates for the hydrogen atom bound to O4 was located in the difference Fourier synthesis and refined semi-freely with the help of a restraint on the O-H distance (0.84(4) Å).

*Table A11.3.2. Crystal Data and Structure Refinement for Diketone **375**.*

Caltech Identification code	P14028	
CCDC Deposition Number	1061015	
Empirical formula	C19 H23.76 Cl0.24 O5	
Formula weight	340.56	
Temperature	100(2) K	
Wavelength	1.54178 Å	
Crystal system	Orthorhombic	
Space group	$P2_12_12_1$	
Unit cell dimensions	a = 6.6417(3) Å	α= 90°.
	b = 10.7582(5) Å	β= 90°.
	c = 22.9878(11) Å	γ = 90°.
Volume	1642.54(13) $Å^3$	
Z	4	
Density (calculated)	1.377 Mg/m^3	
Absorption coefficient	1.151 mm^{-1}	
F(000)	727	
Crystal size	0.350 x 0.150 x 0.050 mm^3	
Theta range for data collection	3.846 to 74.625°.	
Index ranges	$-8 \le h \le 7, -13 \le k \le 11, -28 \le l \le 28$	
Reflections collected	18385	
Independent reflections	3362 [R(int) = 0.0393]	
Completeness to theta = 67.679°	99.9 %	
Absorption correction	Semi-empirical from equivalents	
Max. and min. transmission	0.7538 and 0.6487	
Refinement method	Full-matrix least-squares on F^2	
Data / restraints / parameters	3362 / 1 / 232	
Goodness-of-fit on F^2	1.002	
Final R indices [I>2sigma(I)]	R1 = 0.0336, wR2 = 0.0822	
R indices (all data)	R1 = 0.0351, wR2 = 0.0831	
Absolute structure parameter	0.042(17)	
Extinction coefficient	n/a	
Largest diff. peak and hole	0.223 and -0.189 $e.Å^{-3}$	

*Table A11.3.3. Atomic coordinates (x 10^4) and equivalent isotropic displacement parameters ($Å^2$x 10^3) for Diketone **375**. U(eq) is defined as one third of the trace of the orthogonalized U^{ij} tensor.*

	x	y	z	U(eq)
O(1)	6910(2)	2659(1)	4395(1)	14(1)
C(1)	8571(3)	3120(2)	4143(1)	13(1)
O(2)	10204(2)	2731(2)	4290(1)	19(1)
C(2)	8248(3)	4076(2)	3670(1)	13(1)
C(3)	7555(3)	3408(2)	3103(1)	14(1)
C(4)	9356(3)	2968(2)	2745(1)	18(1)
C(5)	8713(3)	2419(2)	2154(1)	21(1)
C(16)	7921(4)	3408(3)	1745(1)	28(1)
C(17)	6089(5)	3400(3)	1508(1)	47(1)
C(18)	9323(4)	4471(3)	1626(1)	34(1)
Cl(1)	11943(4)	4100(2)	1619(1)	27(1)
C(6)	7236(3)	1342(2)	2258(1)	22(1)
C(7)	5511(3)	1689(2)	2657(1)	19(1)
O(3)	3773(2)	1466(2)	2540(1)	27(1)
C(8)	6152(3)	2287(2)	3228(1)	16(1)
C(9)	4353(3)	2574(2)	3621(1)	18(1)
C(10)	4943(3)	3148(2)	4212(1)	14(1)
C(11)	4959(3)	4564(2)	4214(1)	14(1)
C(12)	5086(3)	5184(2)	4830(1)	17(1)
O(4)	6490(2)	4544(2)	5196(1)	20(1)
C(20)	3034(4)	5305(2)	5117(1)	23(1)
C(13)	6126(4)	6418(2)	4707(1)	21(1)
C(14)	7684(3)	6082(2)	4255(1)	18(1)
O(5)	9351(3)	6511(2)	4192(1)	28(1)
C(15)	6758(3)	5076(2)	3867(1)	14(1)

*Table A11.3.4. Bond lengths [Å] and angles [°] for Diketone **375**.*

O(1)-C(1)	1.341(2)
O(1)-C(10)	1.470(2)
C(1)-O(2)	1.210(3)
C(1)-C(2)	1.513(3)
C(2)-C(15)	1.530(3)
C(2)-C(3)	1.558(3)
C(2)-H(2)	1.0000
C(3)-C(4)	1.527(3)
C(3)-C(8)	1.551(3)
C(3)-H(3)	1.0000
C(4)-C(5)	1.541(3)
C(4)-H(4A)	0.9900
C(4)-H(4B)	0.9900
C(5)-C(16)	1.514(3)
C(5)-C(6)	1.537(3)
C(5)-H(5)	1.0000
C(16)-C(17)	1.333(4)
C(16)-C(18)	1.500(4)
C(17)-H(17A)	0.9500
C(17)-H(17B)	0.9500
C(18)-Cl(1)	1.786(4)
C(18)-H(18A)	0.9800
C(18)-H(18B)	0.9800
C(18)-H(18C)	0.9800
C(18)-H(18D)	0.9900
C(18)-H(18E)	0.9900
C(6)-C(7)	1.515(3)
C(6)-H(6A)	0.9900
C(6)-H(6B)	0.9900
C(7)-O(3)	1.210(3)
C(7)-C(8)	1.522(3)
C(8)-C(9)	1.529(3)
C(8)-H(8)	1.0000

Table A11.3.4. (cont'd)

C(9)-C(10)	1.544(3)
C(9)-H(9A)	0.9900
C(9)-H(9B)	0.9900
C(10)-C(11)	1.523(3)
C(10)-H(10)	1.0000
C(11)-C(15)	1.539(3)
C(11)-C(12)	1.567(3)
C(11)-H(11)	1.0000
C(12)-O(4)	1.432(3)
C(12)-C(20)	1.520(3)
C(12)-C(13)	1.523(3)
O(4)-H(4O)	0.86(2)
C(20)-H(20A)	0.9800
C(20)-H(20B)	0.9800
C(20)-H(20C)	0.9800
C(13)-C(14)	1.510(3)
C(13)-H(13A)	0.9900
C(13)-H(13B)	0.9900
C(14)-O(5)	1.208(3)
C(14)-C(15)	1.531(3)
C(15)-H(15)	1.0000

C(1)-O(1)-C(10)	118.41(14)
O(2)-C(1)-O(1)	119.33(18)
O(2)-C(1)-C(2)	124.22(18)
O(1)-C(1)-C(2)	116.41(17)
C(1)-C(2)-C(15)	110.88(16)
C(1)-C(2)-C(3)	109.30(17)
C(15)-C(2)-C(3)	112.41(16)
C(1)-C(2)-H(2)	108.0
C(15)-C(2)-H(2)	108.0
C(3)-C(2)-H(2)	108.0
C(4)-C(3)-C(8)	109.22(17)
C(4)-C(3)-C(2)	111.23(16)

Table A11.3.4. (cont'd)

C(8)-C(3)-C(2)	112.35(16)
C(4)-C(3)-H(3)	108.0
C(8)-C(3)-H(3)	108.0
C(2)-C(3)-H(3)	108.0
C(3)-C(4)-C(5)	112.09(17)
C(3)-C(4)-H(4A)	109.2
C(5)-C(4)-H(4A)	109.2
C(3)-C(4)-H(4B)	109.2
C(5)-C(4)-H(4B)	109.2
H(4A)-C(4)-H(4B)	107.9
C(16)-C(5)-C(6)	113.8(2)
C(16)-C(5)-C(4)	111.98(19)
C(6)-C(5)-C(4)	109.20(18)
C(16)-C(5)-H(5)	107.2
C(6)-C(5)-H(5)	107.2
C(4)-C(5)-H(5)	107.2
C(17)-C(16)-C(18)	119.8(3)
C(17)-C(16)-C(5)	124.5(3)
C(18)-C(16)-C(5)	115.7(2)
C(16)-C(17)-H(17A)	120.0
C(16)-C(17)-H(17B)	120.0
H(17A)-C(17)-H(17B)	120.0
C(16)-C(18)-Cl(1)	115.9(2)
C(16)-C(18)-H(18A)	109.5
C(16)-C(18)-H(18B)	109.5
H(18A)-C(18)-H(18B)	109.5
C(16)-C(18)-H(18C)	109.5
H(18A)-C(18)-H(18C)	109.5
H(18B)-C(18)-H(18C)	109.5
C(16)-C(18)-H(18D)	108.3
Cl(1)-C(18)-H(18D)	108.3
C(16)-C(18)-H(18E)	108.3
Cl(1)-C(18)-H(18E)	108.3
H(18D)-C(18)-H(18E)	107.4

Table A11.3.4. (cont'd)

C(7)-C(6)-C(5)	113.00(19)
C(7)-C(6)-H(6A)	109.0
C(5)-C(6)-H(6A)	109.0
C(7)-C(6)-H(6B)	109.0
C(5)-C(6)-H(6B)	109.0
H(6A)-C(6)-H(6B)	107.8
O(3)-C(7)-C(6)	122.5(2)
O(3)-C(7)-C(8)	122.9(2)
C(6)-C(7)-C(8)	114.55(18)
C(7)-C(8)-C(9)	112.05(17)
C(7)-C(8)-C(3)	109.66(17)
C(9)-C(8)-C(3)	114.96(17)
C(7)-C(8)-H(8)	106.5
C(9)-C(8)-H(8)	106.5
C(3)-C(8)-H(8)	106.5
C(8)-C(9)-C(10)	113.71(17)
C(8)-C(9)-H(9A)	108.8
C(10)-C(9)-H(9A)	108.8
C(8)-C(9)-H(9B)	108.8
C(10)-C(9)-H(9B)	108.8
H(9A)-C(9)-H(9B)	107.7
O(1)-C(10)-C(11)	110.52(16)
O(1)-C(10)-C(9)	109.54(16)
C(11)-C(10)-C(9)	113.85(17)
O(1)-C(10)-H(10)	107.6
C(11)-C(10)-H(10)	107.6
C(9)-C(10)-H(10)	107.6
C(10)-C(11)-C(15)	111.24(16)
C(10)-C(11)-C(12)	115.38(17)
C(15)-C(11)-C(12)	105.93(16)
C(10)-C(11)-H(11)	108.0
C(15)-C(11)-H(11)	108.0
C(12)-C(11)-H(11)	108.0
O(4)-C(12)-C(20)	111.73(17)

Table A11.3.4. (cont'd)

O(4)-C(12)-C(13)	103.46(17)
C(20)-C(12)-C(13)	114.36(18)
O(4)-C(12)-C(11)	111.15(16)
C(20)-C(12)-C(11)	112.38(18)
C(13)-C(12)-C(11)	103.15(16)
C(12)-O(4)-H(4O)	108(2)
C(12)-C(20)-H(20A)	109.5
C(12)-C(20)-H(20B)	109.5
H(20A)-C(20)-H(20B)	109.5
C(12)-C(20)-H(20C)	109.5
H(20A)-C(20)-H(20C)	109.5
H(20B)-C(20)-H(20C)	109.5
C(14)-C(13)-C(12)	103.32(17)
C(14)-C(13)-H(13A)	111.1
C(12)-C(13)-H(13A)	111.1
C(14)-C(13)-H(13B)	111.1
C(12)-C(13)-H(13B)	111.1
H(13A)-C(13)-H(13B)	109.1
O(5)-C(14)-C(13)	128.3(2)
O(5)-C(14)-C(15)	124.6(2)
C(13)-C(14)-C(15)	107.10(18)
C(2)-C(15)-C(14)	114.18(17)
C(2)-C(15)-C(11)	113.82(16)
C(14)-C(15)-C(11)	105.26(16)
C(2)-C(15)-H(15)	107.8
C(14)-C(15)-H(15)	107.8
C(11)-C(15)-H(15)	107.8

Symmetry transformations used to generate equivalent atoms:

*Table A11.3.5. Anisotropic displacement parameters ($Å^2x10^3$) for Diketone **375**. The anisotropic displacement factor exponent takes the form: $-2\pi^2[h^2a^{*2}U^{11} + ... + 2hka^*b^*U^{12}]$.*

	U^{11}	U^{22}	U^{33}	U^{23}	U^{13}	U^{12}
O(1)	14(1)	13(1)	16(1)	2(1)	1(1)	2(1)
C(1)	15(1)	14(1)	12(1)	-2(1)	0(1)	0(1)
O(2)	15(1)	24(1)	17(1)	4(1)	-2(1)	4(1)
C(2)	14(1)	14(1)	12(1)	0(1)	-2(1)	-2(1)
C(3)	15(1)	15(1)	12(1)	-1(1)	-3(1)	1(1)
C(4)	16(1)	22(1)	15(1)	-2(1)	1(1)	-2(1)
C(5)	22(1)	24(1)	16(1)	-6(1)	2(1)	2(1)
C(16)	42(1)	31(1)	12(1)	-5(1)	-1(1)	1(1)
C(17)	66(2)	38(2)	37(2)	5(1)	-28(2)	-7(2)
C(18)	40(1)	39(2)	24(1)	7(1)	4(1)	1(1)
Cl(1)	33(1)	26(1)	22(1)	-1(1)	10(1)	-12(1)
C(6)	24(1)	24(1)	20(1)	-8(1)	-2(1)	2(1)
C(7)	20(1)	17(1)	21(1)	-4(1)	-2(1)	-1(1)
O(3)	21(1)	33(1)	29(1)	-13(1)	-4(1)	-5(1)
C(8)	15(1)	17(1)	17(1)	-3(1)	-1(1)	-1(1)
C(9)	14(1)	20(1)	21(1)	-6(1)	0(1)	-3(1)
C(10)	12(1)	14(1)	17(1)	0(1)	0(1)	0(1)
C(11)	14(1)	14(1)	14(1)	0(1)	-2(1)	1(1)
C(12)	23(1)	14(1)	14(1)	-1(1)	-1(1)	1(1)
O(4)	24(1)	19(1)	16(1)	1(1)	-4(1)	-2(1)
C(20)	26(1)	19(1)	24(1)	-2(1)	6(1)	4(1)
C(13)	31(1)	14(1)	19(1)	-3(1)	2(1)	-1(1)
C(14)	27(1)	12(1)	16(1)	3(1)	-2(1)	-2(1)
O(5)	31(1)	26(1)	25(1)	-6(1)	2(1)	-12(1)
C(15)	17(1)	13(1)	12(1)	2(1)	-2(1)	1(1)

*Table A11.3.6. Hydrogen coordinates ($x10^4$) and isotropic displacement parameters ($Å^2x10^3$) for Diketone **375**.*

	x	y	z	U(eq)
H(2)	9568	4489	3589	16
H(3)	6785	4021	2863	17
H(4A)	10101	2329	2968	21
H(4B)	10277	3677	2678	21
H(5)	9945	2058	1970	25
H(17A)	5676	4066	1264	57
H(17B)	5197	2729	1582	57
H(18A)	8930	4881	1263	51
H(18B)	10703	4157	1591	51
H(18C)	9252	5069	1948	51
H(18D)	9093	5118	1925	41
H(18E)	8964	4836	1245	41
H(6A)	6681	1068	1879	27
H(6B)	7978	632	2429	27
H(8)	6986	1657	3438	19
H(9A)	3596	1796	3692	22
H(9B)	3443	3156	3415	22
H(10)	3925	2870	4505	17
H(11)	3695	4858	4022	16
H(4O)	5980(40)	3830(20)	5286(13)	29
H(20A)	2460	4476	5179	35
H(20B)	2138	5789	4865	35
H(20C)	3180	5729	5492	35
H(13A)	5162	7038	4553	25
H(13B)	6768	6753	5062	25
H(15)	6215	5492	3511	17

*Table A11.3.7. Torsion angles [°] for Diketone **375**.*

C(10)-O(1)-C(1)-O(2)	179.77(18)
C(10)-O(1)-C(1)-C(2)	-2.5(2)
O(2)-C(1)-C(2)-C(15)	-134.3(2)
O(1)-C(1)-C(2)-C(15)	48.1(2)
O(2)-C(1)-C(2)-C(3)	101.2(2)
O(1)-C(1)-C(2)-C(3)	-76.4(2)
C(1)-C(2)-C(3)-C(4)	-86.4(2)
C(15)-C(2)-C(3)-C(4)	150.00(17)
C(1)-C(2)-C(3)-C(8)	36.4(2)
C(15)-C(2)-C(3)-C(8)	-87.2(2)
C(8)-C(3)-C(4)-C(5)	61.0(2)
C(2)-C(3)-C(4)-C(5)	-174.41(17)
C(3)-C(4)-C(5)-C(16)	69.8(2)
C(3)-C(4)-C(5)-C(6)	-57.3(2)
C(6)-C(5)-C(16)-C(17)	2.6(3)
C(4)-C(5)-C(16)-C(17)	-121.9(3)
C(6)-C(5)-C(16)-C(18)	-179.3(2)
C(4)-C(5)-C(16)-C(18)	56.2(3)
C(17)-C(16)-C(18)-Cl(1)	-148.6(3)
C(5)-C(16)-C(18)-Cl(1)	33.2(3)
C(16)-C(5)-C(6)-C(7)	-75.0(2)
C(4)-C(5)-C(6)-C(7)	50.9(3)
C(5)-C(6)-C(7)-O(3)	131.4(2)
C(5)-C(6)-C(7)-C(8)	-51.1(3)
O(3)-C(7)-C(8)-C(9)	-0.5(3)
C(6)-C(7)-C(8)-C(9)	-178.03(19)
O(3)-C(7)-C(8)-C(3)	-129.4(2)
C(6)-C(7)-C(8)-C(3)	53.1(2)
C(4)-C(3)-C(8)-C(7)	-56.8(2)
C(2)-C(3)-C(8)-C(7)	179.28(17)
C(4)-C(3)-C(8)-C(9)	175.88(17)
C(2)-C(3)-C(8)-C(9)	52.0(2)
C(7)-C(8)-C(9)-C(10)	178.35(18)
C(3)-C(8)-C(9)-C(10)	-55.6(2)

Table A11.3.7. (cont'd)

C(1)-O(1)-C(10)-C(11)	-48.9(2)
C(1)-O(1)-C(10)-C(9)	77.3(2)
C(8)-C(9)-C(10)-O(1)	-31.9(2)
C(8)-C(9)-C(10)-C(11)	92.4(2)
O(1)-C(10)-C(11)-C(15)	51.7(2)
C(9)-C(10)-C(11)-C(15)	-72.0(2)
O(1)-C(10)-C(11)-C(12)	-68.9(2)
C(9)-C(10)-C(11)-C(12)	167.27(17)
C(10)-C(11)-C(12)-O(4)	41.7(2)
C(15)-C(11)-C(12)-O(4)	-81.8(2)
C(10)-C(11)-C(12)-C(20)	-84.3(2)
C(15)-C(11)-C(12)-C(20)	152.11(17)
C(10)-C(11)-C(12)-C(13)	152.00(18)
C(15)-C(11)-C(12)-C(13)	28.5(2)
O(4)-C(12)-C(13)-C(14)	77.13(19)
C(20)-C(12)-C(13)-C(14)	-161.11(18)
C(11)-C(12)-C(13)-C(14)	-38.8(2)
C(12)-C(13)-C(14)-O(5)	-145.3(2)
C(12)-C(13)-C(14)-C(15)	35.4(2)
C(1)-C(2)-C(15)-C(14)	80.4(2)
C(3)-C(2)-C(15)-C(14)	-156.88(17)
C(1)-C(2)-C(15)-C(11)	-40.5(2)
C(3)-C(2)-C(15)-C(11)	82.2(2)
O(5)-C(14)-C(15)-C(2)	37.9(3)
C(13)-C(14)-C(15)-C(2)	-142.81(17)
O(5)-C(14)-C(15)-C(11)	163.4(2)
C(13)-C(14)-C(15)-C(11)	-17.3(2)
C(10)-C(11)-C(15)-C(2)	-7.5(2)
C(12)-C(11)-C(15)-C(2)	118.63(18)
C(10)-C(11)-C(15)-C(14)	-133.24(18)
C(12)-C(11)-C(15)-C(14)	-7.1(2)

Symmetry transformations used to generate equivalent atoms:

*Table A11.3.8. Hydrogen bonds for Diketone **375** [Å and °].*

D-H...A	d(D-H)	d(H...A)	d(D...A)	<(DHA)
C(18)-H(18E)...O(4)#1	0.99	2.52	3.498(3)	169.0
C(6)-H(6B)...Cl(1)#2	0.99	2.74	3.576(3)	142.2
C(8)-H(8)...Cl(1)#2	1.00	2.84	3.671(3)	140.5
C(10)-H(10)...O(2)#3	1.00	2.52	3.184(2)	123.2
O(4)-H(4O)...O(2)#4	0.86(2)	2.01(2)	2.849(2)	164(3)
C(20)-H(20A)...O(1)#4	0.98	2.52	3.462(3)	160.2
C(20)-H(20B)...O(5)#3	0.98	2.53	3.491(3)	165.2
C(20)-H(20C)...Cl(1)#5	0.98	2.60	3.512(3)	155.1
C(15)-H(15)...O(3)#6	1.00	2.63	3.580(2)	158.1

Symmetry transformations used to generate equivalent atoms:

#1 -x+3/2,-y+1,z-1/2 #2 -x+2,y-1/2,-z+1/2 #3 x-1,y,z

#4 x-1/2,-y+1/2,-z+1 #5 -x+3/2,-y+1,z+1/2 #6 -x+1,y+1/2,-z+1/2

A11.4 Notes and References

1. Sheldrick, G. M. *Acta Cryst*. **1990**, A46, 467–473.

2. Sheldrick, G. M. *Acta Cryst*. **2008**, A64, 112–122.

3. Müller, P. *Crystallography Reviews* **2009**, *15*, 57–83.